

REPORT DOCUMENTATION PAGE

Form Approved OMB No. 0704-0188

Public reporting burden for this collection of information is estimated to average 1 hour per response, including the time for reviewing instructions, searching existing data sources, gathering and maintaining the data needed, and completing and reviewing the collection of information. Send comments regarding this burden estimate or any other aspect of this collection of information, including suggestions for reducing this burden to Washington Headquarters Services, Directorate for Information Operations and Reports, 1215 Jefferson Davis Highway, Suite 1204, Arlington, VA 22202-4302, and to the Office of Management and Budget, Paperwork Reduction Project (0704-0188), Washington, DC 20503.

1. AGENCY USE ONLY (Leave blank)		2. REPORT DATE 31 May 2004	3. REPORT TYPE AND DATES COVERED Conference Proceedings, 20-22 April 2004
4. TITLE AND SUBTITLE New Trends in Research of Energetic Materials			5. FUNDING NUMBERS FA8655-04-1-5001
6. AUTHOR(S) Prof Zvatopluk Zeman, editor			
7. PERFORMING ORGANIZATION NAME(S) AND ADDRESS(ES) University of Pardubice CZ-532 10 Pardubice Czech Republic			8. Performing Organization Report Number
9. SPONSORING/MONITORING AGENCY NAME(S) AND ADDRESS(ES) EOARD PSC 802 Box 14 FPO 09499-0014			10. SPONSORING/MONITORING AGENCY REPORT NUMBER CSP-04-5001
11. SUPPLEMENTARY NOTES Copyright 2004 held by the University Pardubice available from: University Pardubice, Studenska Str., 95, CZ-532 10 Pardubice, Czech Republic. The Department of Defense has permission to use for government purposes only. All other rights are reserved by the copyright holder.			
12a. DISTRIBUTION/AVAILABILITY STATEMENT Approved for public release; distribution is unlimited. (approval given by local Public Affairs Office)			12b. DISTRIBUTION CODE A
ABSTRACT (Maximum 200 words) The Final Proceedings for New Trends in Research of Energetic Materials, 20 April – 22 April 2004 The seventh consecutive Seminar on new trends in research of energetic materials is intended to be a world meeting of young people and university teachers working in the field of teaching, research, development, processing, analyzing and application of all kinds of energetic materials. Topics include explosions of gaseous, dispersing and condensed systems.			
14. SUBJECT TERMS EOARD, Energetic materials			15. NUMBER OF PAGES
			16. PRICE CODE
17. SECURITY CLASSIFICATION OF REPORT UNCLASSIFIED	18. SECURITY CLASSIFICATION OF THIS PAGE UNCLASSIFIED	19. SECURITY CLASSIFICATION OF ABSTRACT UNCLASSIFIED	20. LIMITATION OF ABSTRACT UL

NSN 7540-01-280-5500

Standard Form 298 (Rev. 2-89)
Prescribed by ANSI Std. Z39-18
298-102

UNIVERSITY OF PARDUBICE

Faculty of Chemical Technology

and

**EUROPEAN OFFICE
OF AEROSPACE RESEARCH AND DEVELOPMENT**



**NEW TRENDS IN RESEARCH
OF ENERGETIC MATERIALS**

PROCEEDINGS OF THE VII. SEMINAR

CD version



Pardubice, Czech Republic

April 20 - 22, 2004



AUSTIN DETONATOR



Indet Safety Systems



OZM Research Ltd.

UNIVERSITY OF PARDUBICE
Faculty of Chemical Technology
Department of Theory & Technology of Explosives
CZ-532 10 Pardubice

EUROPEAN OFFICE OF AEROSPACE RESEARCH AND DEVELOPMENT
London NW1 5TH United Kingdom

PROCEEDINGS
of the seventh Seminar

„NEW TRENDS IN RESEARCH OF ENERGETIC MATERIALS“

CD version

held at the University of Pardubice,
Pardubice, the Czech Republic

April 20 – 22, 2004

*intended as a meeting of students, postgraduate students, university
teachers and young research and development workers concerned
from the whole world*

NOTICE

This publication has not been submitted to language corrections and contributions have not been reviewed.

Formatting of the contributions has been checked by editor.

The only distributor of the present publication is the
Department of Theory & Technology of Explosives, University of Pardubice,
CZ-532 10 Pardubice,
where the publication can be ordered or gained by exchange of similar publications.
Contributions of the Proceedings will be quoted in the Chemical Abstracts.

March 11th, 2004

Close

Editor:
Jiří Vágenknecht

Edition 1st, Limited, 50 pcs Original Copies, Unprotected CD-R
Published by the University of Pardubice

Document designed by J. Vágenknecht at DTTX by Adobe Acrobat 5.0.5.0 CZ

© University of Pardubice, 2004

ISBN (for printed version)

part I. 80-7194-651-6

part II. 80-7194-652-4

Seminar is supported by:

***European Office of Aerospace Research and Development of the USAF,
Austin Detonator, Inc., Vsetín,
Indet Safety Systems, Inc., Vsetín,
Dr. Oldrich Machacek, president of UTeC Corp., LLC, Dallas,
OZM Research, Ltd., Hrochův Týnec***

Chairman of the Seminar:

Prof. Svatopluk Zeman, D.Sc.

Scientific Committee:

Chairman: Dr. Adam Cumming (*DSTL, Sevenoaks, U.K.*)

Members: Prof. Ang How-Ghee	(<i>National Univ. of Singapore</i>)
Dr. Anthony J. Bellamy	(<i>Cranfield Univ, UK</i>)
Prof. Anatolii N. Dremin	(<i>RAS Chernogolovka, Russia</i>)
Dr. Stanislaw Cudzilo	(<i>Military Univ. Technol., Warsaw, Poland</i>)
Prof. Thomas Klapoetke	(<i>Ludwig-Maximilians-Universität München</i>)
Prof. Michel Lefevre	(<i>Royal Military Academy, Belgium</i>)
Prof. František Ludvík	(<i>Military Academy Brno, Czech Rep.</i>)
Prof. Andrzej Maranda	(<i>Military Univ. Technol., Warsaw, Poland</i>)
Prof. Hans J. Pasman	(<i>Delft Univ., The Netherlands</i>)
Assoc. Prof. Shu Yuanjie	(<i>Inst. of Chem. Materials, CAEP, Sichuan, China</i>)
Dr. Muhamed Sućeska	(<i>Brodarski Inst., Zagreb, Croatia</i>)
Prof. Waldemar A. Trzciński	(<i>Military Univ. Technol., Warsaw, Poland</i>)
Assoc. Prof. Pavel Vávra	(<i>Univ. of Pardubice, Czech Rep.</i>)
Dr. Fred Volk	(<i>ICT Pfinztal, Germany</i>)
Dr. Woodward Waesche	(<i>Office of Naval Res. Int. Field Office, USA</i>)

Organizing Committee:

Chairman:	Jiří Vágenknecht, Ph.D.	(<i>Univ. Pardubice</i>)
Members:	Gabriela Hurtosová, M.Sc.	(<i>Univ. Pardubice</i>)
	Zdeněk Jalový, Ph.D.	(<i>Univ. Pardubice</i>)
	Assoc. Prof. Břetislav Janovský	(<i>Univ. Pardubice</i>)
	Marcela Jungová, M.Sc.	(<i>Univ. Pardubice</i>)
	Miloslav Krupka, Ph.D.	(<i>Univ. Pardubice</i>)
	Richard Kuracina, M.Sc.	(<i>Univ. Pardubice</i>)
	Robert Matyáš, M.Sc.	(<i>Univ. Pardubice</i>)
	Jiří Pachmáň, M.Sc.	(<i>Univ. Pardubice</i>)
	Radovan Skácel, Mgr.	(<i>Univ. Pardubice</i>)
	Jakub Šelešovský, M.Sc.	(<i>Univ. Pardubice</i>)
	Jaroslav Švihovský, M.Sc.	(<i>Univ. Pardubice</i>)
	Róbert Varga, M.Sc.	(<i>Univ. Pardubice</i>)
	Pavel Valenta, MSc.	(<i>Austin Detonator</i>)
	Dr. Jan Jakubko	(<i>Indet Safety Systems</i>)

CONTENT

CD version

PREFACE	12
----------------	-----------

INVITED LECTURES

A.N. Dremin Institute of Problems of Chemical Physics, Chernogolovka, Moscow Region, 142432, Russia	
ON MATERIALS' CAPABILITY TO DETONATE	13
T.M. Klapötke*, G. Holl**, J. Geith*, A. Hammerl* and J. Weigand* * Department of Chemistry, University of Munich, Butenandtstr. 5-13 (D), D-81377 Munich Germany) ** Bundeswehr Research Institute for Materials, Fuels and Lubricants, Swisttal-Heimertsheim; Großes Cent, D-53913 Swisttal (Germany)	
NEW HIGH EXPLOSIVES AND PROPELLANTS BASED ON BIURET SAND TETRAZOLE COMPOUNDS	23
H.J. Pasman and J.F. Zevenbergen Delft University of Technology, Faculty of Applied Sciences, Explosion Group, Julianalaan 136, 2628 BL Delft, Netherlands	
NEW SAFETY THINKING APPLICABLE TO EM SYNTHESIS AND MANUFACTURE	35

LECTURES

Z. Akštein and L. Říha Research Institute Of Industrial Chemistry, Explosia a.s., 532 17 Pardubice-Semtín, Czech Republic	
INFLUENCE OF TAMPING ON PERFORMANCE OF LINEAR SHAPED CHARGES	51
D. Bahulayan*, C.P.Joshua** and H.G.Ang* * HEDM Research Laboratory, Faculty of Science, National University of Singapore, Science Drive 2, Singapore 117543 ** Department of Chemistry, University of Kerala, Kariyavattom, Trivandrum, Kerala, India	
LIQUID PHASE AND SOLID PHASE NITRATION OF AROMATIC COMPOUNDS: GREEN SYNTHETIC ROUTES	61
S. Beaucamp*, D. Mathieu* and V. Agafonov** * Commissariat à l'Energie Atomique, Centre du Ripault, BP16, F-37260 Monts, France ** Laboratoire de Chimie Physique, EA PIMIR 2098, Faculté de Pharmacie, 31 Avenue Monge F-37200 Tours, France	
DEVELOPMENT OF ENERGETIC SALTS FOR PROPELLANTS	68
A.J. Bellamy*, N.V. Latypov** and P. Goede** * Cranfield University, Royal Military College of Science, Shrivenham, Swindon SN6 8LA, UK ** Swedish Defence Research Agency (FOI), SE-147 25 Tumba, Sweden	
STUDIES ON THE NITRATION OF NEW POTENTIAL PRECURSORS FOR FOX-7	74
A.J. Bellamy and T.P. Price Cranfield University, Royal Military College of Science, Shrivenham, Swindon SN6 8LA, UK	
1:1 HNS-DIOXAN COMPLEX	82
J. Błądek, S. Pietrasiak and S. Cudziło Institute of Chemistry, Military University of Technology, Kaliskiego 2, 00–908 Warsaw, PL	
DETERMINATION OF RESIDUE OF EXPLOSIVES IN ENVIRONMENTAL SAMPLES	89
S. Cudziło*, W. Kiciński*, J. Błądek*, A. Arciszewska* and A. Huczko** * Institute of Chemistry, Military University of Technology, Kaliskiego 2, 00–908 Warsaw, PL ** Department of Chemistry, Warsaw University, Pasteura 1, 02-093, Warsaw, PL	
CHARACTERIZATION OF THE CARBONACEOUS PRODUCTS OF HALOGENOCARBONS REDUCTION IN COMBUSTION WAVE	94

V.Y. Egorshhev, V.P. Sinditskii and M.V. Berezin

Mendeleev University of Chemical Technology 9 Miusskaya Square, 125047, Moscow, Russia

STUDY ON COMBUSTION OF LIQUID AND GELATINIZED GLYCIDYL AZIDE OLIGOMERS 100

N.V. Garmasheva, I.V. Chemagina, V.P. Filin, M.B. Kazakova and B.G. Loboiko

Zababakhin Russian Federal Nuclear Centre – VNIITF, P.O. Box 245, Snezhinsk, Chelyabinsk region, 456770, Russia

INVESTIGATION OF DIAMINODINITROETHYLENE (DADNE) 115

S. Gheorghian

Academia Tehnică Militară, George Coșbuc bd. nr. 81-83, 050141 București, România

ESTIMATION OF THE THERMODYNAMIC PROPERTIES OF SOLID PROPELLANTS 122

J. Hamid, T. Griffiths, R. Claridge and T. Jordan

QinetiQ Ltd., Energetic Materials Dept., MOD Fort Halstead, Sevenoaks, Kent, UK

APPLICATION OF NOVEL ENERGETIC MATERIALS FOR INITIATORS AND EXPLOSIVE TRAINS 132

Peng-wan CHEN*, Feng-lei HUANG*, Yan-sheng DING**

* National Key Laboratory of Explosion and Safety Science, Beijing Institute of Technology, Beijing 100081, China

** Institute of Mechanics, Chinese Academy of Sciences, Beijing 100080, China

MICROSTRUCTURE, MECHANICAL PROPERTIES AND MECHANICAL FAILURE OF POLYMER BONDED EXPLOSIVES 141

H. S. Jadhav*, M. B. Talawar*, D. D. Dhavale*, S. N. Asthana*** and V. N. Krishnamurthy****

* Department of Chemistry, Garware Research Centre, University of Pune, Pune 411 007, INDIA

** DRDO/ISRO Cell, University of Pune, Pune 411 007, INDIA

*** High Energy Material Research Laboratory, Sutarwadi Pashan, Pune 411 021, INDIA

SYNTHESIS AND CHARACTERISATION OF NITROGUANIDINE BASED NITRATE AND PERCHLORATE SALTS OF -5-NITRO-2-NITROIMINOHEXAHYDRO-1,3,5-TRIAZINE 149

V. Ježová*, J. Skládál, A. Eisner*, L. Gollová* and K. Ventura***

* Department of Analytical Chemistry, University of Pardubice, 53210, Pardubice, Czech Republic

** Research Institute of Industrial Chemistry, Explosia a.s., 53217, Pardubice - Semtín, Czech Republic

DETERMINATION OF LOW CONCENTRATION TRINITROTOLUENE CONTENT IN WATER SAMPLES 157

M.H. Lefebvre, B. Falmagne and B. Smedts

Laboratory of Energetic Materials, Royal Military Academy, Brussels – Belgium

SENSITIVITIES AND PERFORMANCES OF NON-REGULAR EXPLOSIVES 164

K. Lipińska*, M. Lipiński*, A. Maranda and J. Sobala*****

* Institute of Industrial Organic Chemistry, 6 Annopol St., 03-236 Warszawa, Poland

** Military University of Technology, 2 Kaliskiego St., 00-908 Warszawa, Poland

*** Central Mining Institute, 1 Gwarków Sq., Katowice, Poland

RESEARCH ON THE INFLUENCE OF AMMONIUM NITRATE PRILL PROPERTIES ON DETONATION PARAMETERS OF ANFO AND THEIR MIXTURES WITH DOUBLE BASE PROPELLANTS 174

D. Mathieu, J.-P. Becker and E. Theerlynck

Commissariat à l’Energie Atomique, Centre d’Etudes du Ripault, BP 16, 37260 Monts, France

BEYOND THE GROUP CONTRIBUTION APPROACH TO FLUID PROPERTIES: NEW MODELS FOR THE DENSITY AND THERMAL STABILITY OF ENERGETIC COMPOUNDS 183

Y.M. Milyokhin*, A.N. Klyuchnikov*, A. V. Fedorychev*, S.V. Gunin*, V.V. Serushkin, V.P. Sinditskii** and S.A. Filatov****

* Federal Center of Dual-Use Technologies “Soyuz”, Academician Zhukov St. 42, 140090, Dzerzhinsky, Moscow region, Russia

** Mendeleev University of Chemical Technology, 9 Miusskaya Square, 125047 Moscow, Russia

IDENTIFICATION OF SOLID PROPELLANT COMBUSTION DYNAMIC CHARACTERISTICS FROM THE RESULTS OF EXPERIMENTS WITH REGISTRATION OF THE CURRENT BURNING FRONT POSITION 190

H. Muthurajan*, R. Sivabalan, M.B. Talawar** and S.N. Asthana****

* Armament Research and Development Establishment, Pashan, Pune-411021, India

** High Energy Materials Research Laboratory, Sutarwadi, Pune-411 021, India

DEVELOPMENT OF COMPUTER CODE FOR QUALITATIVE PREDICTION OF HEAT OF FORMATION OF HIGH ENERGETIC MATERIALS; Part I

202

A. Nepovím*, R. Podlipná*, S. Zeman, Z. Jalový**, A. Gerth*** and T. Vaněk***

* Institute of Organic Chemistry and Biochemistry, Flemingovo nám. 2, CZ-166 10 Praha 6

** University of Pardubice, CZ-532 10 Pardubice

*** Bioplanta GmbH, Benndorfer Landstraße 2, D-04509 Leipzig

STUDY OF TNT METABOLISM IN PLANTS AND ITS PRACTICAL APPLICATION FOR ENVIRONMENT DECONTAMINATION

224

T. Piotrowski, T. Salaciński, M. Frączak and D. Buczkowski

Instytut Przemysłu Organicznego, Annopol 6, 03-236 Warszawa, Poland

TEMCLEV-EX.

ADAPTATION OF TEMCLEV SYSTEM TO FIRE AND EXPLOSION HAZARD ASSESSMENT IN MANUFACTURING OF EXPLOSIVES

227

H. J. Prentice and W. G. Proud

Cavendish Laboratory, University of Cambridge, Cambridge, UK

EXPERIMENTAL INVESTIGATION OF IGNITION MECHANISMS IN CONFINED ENERGETICS

234

Fritz van Rooyen

National Institute for Explosives Technology (NIXT) South Africa PO Box 32544, Glenstantia 0010, Pretoria, Republic of South Africa

THE ETHICS OF ANALYSIS AND MEASUREMENT - IS YOUR ANSWER THE CORRECT ANSWER?

243

P. Shishkov, T. Tzvetkoff, I. Glavchev and R. Ganev

University of Chemical Technology and Metallurgy, 8. Ohridski Str. Kl., 1756 Sofia, Bulgaria

THERMAL AND THERMO-MECHANICAL INVESTIGATIONS OF LONG TIME STORED PROPELLANTS

262

M. Šimáček*, V. Kuttelwascher* and P. Stojan**

* Military Academy in Brno, Faculty of Airforces and Air Defence, Kounicova 65, CZ-602 00, Brno, Czech Republic

** Explosia a.s., Research Institute for Industrial Chemistry, CZ-532 17, Pardubice - Semtin, Czech Republic

INFLUENCE OF VELOCITY OF GAS FLUX TO THE BURNING SURFACE

268

C.R. Siviour, S.G. Grantham, D.M. Williamson, W.G. Proud,

S.M. Walley and J.E. Field

PCS Group, Cavendish Laboratory, Cambridge, CB3 0HE, United Kingdom

HIGH RESOLUTION OPTICAL ANALYSIS OF DYNAMIC EXPERIMENTS ON PBXs

276

M. Sućeska, S. Matečić Mušanić and M. Rajić Linarić

Brodarski Institute, Av. V. Holjevca 20, 10000 Zagreb, Croatia

INFLUENCE OF NC PROPELLANT SAMPLE SELF-HEATING ON ARRHENIUS KINETIC CONSTANTS DERIVED FROM NON-ISOTHERMAL DSC MEASUREMENTS

284

U. Teipel, U. Förter-Barth and H. Krause

Fraunhofer Institute for Chemical Technology (ICT), P.O. Box 1240, 76318 Pfinztal, Germany

MECHANICAL PROPERTIES OF GEL-PROPELLANTS WITH NANOPARTICLES

298

I.A. Ugryumov, M.A. Ilyushin, I.V. Tselinsky, A.S. Kozlov, V.Yu. Dolmatov, I.V. Shugalei and A.N. Golovchak

St.-Petersburg State Institute of Technology (Technical University), 190013, St.-Petersburg, Russia

STUDY OF SUB-MICRON STRUCTURED PHOTOSENSITIVE PRIMARY EXPLOSIVES FOR LASER INITIATION SYSTEMS

306

T. Vasile, C. Barbu and D. Safta

Military Technical Academy, 81-83 George Cosbuc Avenue, Bucharest, Romania

STUDIES AND RESEARCHES REGARDING THE UTILIZING OF RESULTS OBTAINED AT THE BURNING OF POWDER IN CLOSE BOMB FOR SOLVING OF FUNDAMENTAL PROBLEM OF INTERIOR BALLISTICS

317

R. Wild

PBX-Center Maasberg, Diehl Munitionssysteme GmbH & Co KG, Karl-Diehl-Straße 1, D-66620 Nonnweiler, Germany

EFFECTS OF THE COATING PROCESS OF HE MOULDING POWDERS ON SAFETY AND IM CHARACTERISTICS

325

S. Wilker*, P. Guillaume, M.H. Lefebvre***, S. Chevalier**** and Laurence Jeunieu*****

* WIWEB ASt Heimerzheim, Großes Cent, 53913 Swisttal (DE)

** PB Clermont S.A., Rue de Clermont 176, 4480 Engis (BE)

*** Ecole Royale Militaire, Avenue de la Renaissance 30, 1000 Bruxelles (BE)

**** SME – Centre de Recherches Le Bouchet, Boîte Postale N° 2, 91710 Vert-le-Petit (FR)

BALLISTICAL AND CHEMICAL STABILITY OF ROLLED BALL PROPELLANTS

333

D. Williamson, S. Palmer, J. Field and W. Proud

University of Cambridge, Cavendish Laboratory, Physics and Chemistry of Solids Group, Madingley Road, Cambridge, CB3 0HE, United Kingdom

DEFORMATION AND FRACTURE OF ENERGETIC MATERIALS AND THEIR SIMULANTS

348

Shu Yuanjie, Cai Huaqiang, Huanghui and Cheng Bibo

Institute of Chemical Materials CAEP, 621900, Mianyang, Sichuan, China

ON THE REACTIONS OF 2-(DINITROMETHYLENE) -4,5-IMIDAZOLIDINEDIONE WITH ALKALINE AGENTS

359

PRESENTED ONLY IN PROCEEDINGS

A. A. Astratev, D.V. Dashko, A. I. Mershin and A. I. Stepanov,

Special Design and Construction Bureau SDCB, "Technolog " of the Saint-Petersburg State Institute of Technology 190013, , Saint-Petersburg, Moskovskiy pr.26; Russia

MECHANISTIC STUDIES OF DESTRUCTIVE NITRATION OF 2-ALKYL SUBSTITUTED 4,6-DIHYDROXY PYRIMIDINES

365

Zhou Renbin*, Xie Tiebang* and Xiang Weixiang**

* Huazhong University of Science and Technology, School of Mechanical Science and Engineering, Wuhan, Hubei, 430074, P.R.China

** Wuhan Ordnance Noncommissioned Officer Academy of PLA, Department of artillery, Wuhan, Hubei, 430075, P.R.China

SIMULATION STUDY ON ARMOUR-PIERCING EFFECT OF ARMOUR-PIERCING BOMB

373

POSTERS

V. Adamík*, J. Vágenknecht, P. Vávra** and W.A. Trzeciński*****

* External Consultant of the DTTX on Continuum Dynamics

** Department of Theory and Technology of Explosives (DTTX), University of Pardubice, 532 10 Pardubice, Czech Republic

*** Military University of Technology, Kaliskiego 2, 00 980 Warsaw, Poland

***EFFECT OF TNT CHARGES ORIENTATION ON GENERATED AIR BLAST WAVES
- NUMERICAL SIMULATION USING LS-DYNA***

380

V. Adamík*, B. Janovský and A. Tkáč*****

* External Consultant of the DTTX on Continuum Dynamics, CZ

** Department of Theory and Technology of Explosives, University of Pardubice, 532 10 Pardubice, Czech Republic

*** Nuclear Power Plants Research Institute, Okružná 5, 918 64 Trnava, Slovak Republic

DETERMINATION OF THE CONSEQUENCES OF POSSIBLE INDUSTRIAL ACCIDENTS

390

B.P. Aducev*, V.P. Filin, E.V. Tupitsin*, G.M. Belokurov*, D.E. Aluker* and A.S. Pashpekin***

Kemerovo State University, 650043, Kemerovo, Russia

* Russian Federal Nuclear Center, All-Russia Research Institute of Technical Physics (RFNC-VNIITF)

456770, PO Box 245, Snezhinsk, Chelyabinsk region, Russia

***TOPOGRAPHY OF REACTION ORIGINATION OF SILVER AZIDE EXPLOSION DECOMPOSITION
UNDER INITIATION BY ELECTRON ACCELERATOR PULSE***

401

B.P. Aducev*, G.M. Belokurov*, N.V. Garmasheva, S.S. Grechin*, E.V. Tupitsin*
and V.N. Shvayko****

* Kemerovo State University, 650043, Kemerovo, Russia

** Russian Federal Nuclear Center, All-Russia Research Institute of Technical Physics (RFNC-VNIITF)

456770, PO Box 245, Snezhinsk, Chelyabinsk region, Russia

***SPECTRAL-KINETIC CHARACTERISTIC OF PETN LUMINESCENCE UNDER INITIATION
BY ELECTRON BEAM***

404

N.I. Akinin*, S.V. Arinina*, G.D. Kozak*, I.N. Ponomarev**

* Mendelev University of Chemical Technology, 125047, Miusskaja sq. 9, Moscow, Russia.

** Joint-stock company "POLION-P", 125047, Miusskaja sq. 9, Moscow, Russia

THE EXPLOSION PARAMETERS OF BENZOYL AND CYCLOHEXANONE PEROXIDES

409

E.D. Aluker*, A.G. Krechetov*, A.Yu. Mitrofanov*, B.G. Loboiko, D.R. Nurmuhametov*
and E.V. Tupitsin***

* Kemerovo State University, 650043, Kemerovo, Russia,

** Russian Federal Nuclear Center, All-Russia Research Institute of Technical Physics (RFNC-VNIITF)

456770, PO Box 245, Snezhinsk, Chelyabinsk region, Russia

***AN EXPERIMENTAL CHECKING OF A DIVACANCY MODEL OF INICIATING HEAVY METAL
AZIDES***

419

A.M. Astachov, V.A. Revenko and E.S. Buka

Siberian State Technological University, Prosp. Mira 82, 660049 Krasnoyarsk, Russia

***EXPLOSIVES: 4-NITRO-5-NITRIMINO-1H-1,2,4-TRIAZOLE
AND 3-NITRO-5-NITRIMINO-1,4H-1,2,4-TRIAZOLE***

424

J. Błądek, R. Kowalczyk and S. Cudzilo

Institute of Chemistry, Military University of Technology, Kaliskiego 2, 00–908 Warsaw, PL

APPLICATION OF TLC FOR AN ANALYSIS OF INITIATING EXPLOSIVES

433

J. Błądek, A. Arciszewska, S. Cudzilo and W. Kiciński

Institute of Chemistry, Military University of Technology, Kaliskiego 2, 00–908 Warsaw, PL

***APPLICATION OF CARBONACEOUS PRODUCTS OF HALOGENOCARBONS REDUCTION
FOR SOLID PHASE EXTRACTION***

437

M. Cieślukowska, M. Moskalewicz and T. Wolszakiewicz

Institute of Organic Industrial Chemistry, Annopol 6, 03 – 236 Warsaw, Poland

***THE EXAMINATION OF CHOSEN BALLISTIC PARAMETERS OF IGNITER CHARGE BKNO₃
FOR IGNITERS OF SOLID PROPELLANT ROCKET MOTORS***

443

K. Dudek*, P. Mareček*, J. Skládal* and Z. Jalový**	
* Explosia a.s. Research Institute of Industrial Chemistry (VÚPCH), CZ-532 17, Pardubice-Semtín, Czech Republic	
** Department of Theory and Technology of Explosives, University of Pardubice, CZ-532 10 Pardubice, Czech Republic	
SYNTHESIS AND SOME PROPERTIES OF BU-NENA	451
A. Eisner*, M. Adam*, K. Ventura*, V. Ježová* and J. Skládal*	
* Department of Analytical Chemistry, Faculty of Chemical – Technology, University of Pardubice, Nám. Čs. Legií 565, Pardubice 532 10, CZ	
** Research Institute of Industrial Chemistry, Explosia a.s., Pardubice – Semtín 532 17, CZ	
ANALYSIS AFTER COMBUSTION OF PROPELLANTS	459
J. Geith, K. Karaghiosoff, T.M. Klapötke, P. Mayer and J. Weigand	
Department of Chemistry and Biochemistry, University of Munich, Butenandtstr. 5-13 (D), D-81377 Munich (Germany)	
DINITROBIURET AND ITS SALTS	463
V.I. Grozev*, R.H. Ganey** and Z. S. Grozeva***	
* Konstantin Preslavsky University of Shumen, University str.115, 9712 Shumen, Bulgaria (BG)	
** University of Chemical Technology and Metallurgy, Kliment Ohridski blvd. 8, 1756 Sofia, Bulgaria (BG)	
*** Konstantin Preslavsky University of Shumen, University str. 115, 9712 Shumen, Bulgaria (BG)	
EFFECTS ON ENFRGETIC MATERIALS PROCESSED WITH POWER ULTRASOUND	467
Cai Hua-Qiang, Shu Yuan-Jie, Huang Hui and Cheng Bi-Bo	
Institute of Chemical Materials, China Academy of Engineering Physics, 621900, Mianyang, China	
STUDY ON RING CLEAVAGE AND ADDUCTIVE PROPERTY OF 2-(DINITROMETHYLENE)-4,5-IMIDAZOLIDINEDIONE	472
M. Chovancová, P. Očko, M. Lazar and A. Pechová	
VTSÚ (Military Technical and Testing Institute) Zahorie, 905 24 Senica, SK	
AGEING INFLUENCE ON STABILITY AND SENSITIVITY OF PETN EXPLOSIVES	479
B. Janković, D. Vrkljan and Z. Ester	
Faculty of Mining, Geology and Petroleum Engineering, Pierottijeva 6, 10-000 Zagreb, Croatia	
EXPLOSIVE TYPE SELECTION WITH RESPECT TO THE VENTILATION CYCLE DURATION	487
B. Janovský	
Dept. of Theory and Technology of Explosives, University of Pardubice, 532 10 Pardubice, CZ	
DISSOLVER VER. 1.1 HELPS CENTRAL MINING RESCUE STATION	493
Chen Jun and Sun Chengwei	
Laboratory for Shock Wave and Detonation Research, Southwest Institute of Fluid, CAEP, PO Box 919-103, Mian Yang, Sichuan 621900, P.R.China	
EXPANSION OF METALLIC TUBES DRIVEN BY HEAD-ON GRAZING DETONATION	505
I.L. Kovalenko, V.P. Kuprin and A.V. Kuprin	
Ukrainian State University of Chemical Technology, "ECCOM Ltd", 49000, Dnepropetrovsk, UA	
NONAERATIONS SENSIBILIZATION OF EMULSIVE EXPLOSIVES	512
G.D. Kozak* and Z. Lin**	
* Mendelev University of Chemical Technology Miusskaya Sq.9, Moscow, 125190	
** Beijing Institute of Technology, P O Box 327, Beijing 100081, China	
THE CONDENSED EXPLOSIVE SYSTEMS CAPABLE OF PROPAGATING DETONATION IN THE SPIN-PULSATING REGIME	516
G.D. Kozak, V.M. Raikova and V.V. Potapov	
Mendelev University of Chemical Technology, 125047, Miusskaja sq. 9, Moscow, Russia	
DETONATION ABILITY OF SOLUTIONS OF AROMATIC NITROCOMPOUNDS IN NITRIC ACID	524
R. Kuracina, B. Janovský and M. Ferjenčík	
Department of Theory and Technology of Explosives, University of Pardubice, Czech Republic	
FAULT TREE ANALYSIS IN THE PROCESS SAFETY INCIDENT INVESTIGATION	530

K. Leinweber and J. Petržilek

Explosia a.s., 532 17, Pardubice - Semtín, CZ

INTERNAL BALLISTIC ANALYSIS OF THE 20 × 102 CARTRIDGE 541

M. Lipiński, K. Lipińska, B. Florczak and W. Witkowski

Institute of Industrial Organic Chemistry, 6 Annopol St., 03-236 Warszawa, Poland

UNSATURATED POLYESTER INHIBITION SYSTEM FOR DOUBLE BASE PROPELLANTS 546

P. Mareček*, K. Dudek* and F. Liška**

* Explosia a.s. Research Institute of Industrial Chemistry (VÚPCH), CZ-532 17, Pardubice-Semtín, Czech Republic

** Institute of Chemical Technology, Faculty of Chemical Technology, Department of Organic Chemistry, CZ-166 28 Prague, Czech Republic

SYNTHESIS OF DI(1H-TETRAZOLE-5-YL)AMINE (BTA) 553

S. Matečić Mušanić, M. Sućeska, M. Rajić Linarić, B. Sanko and R. Čuljak

Brodarski institut–Marine Research & Special Technologies, Av. V. Holjevca 20, 10020 Zagreb, Croatia

CHANGES OF DYNAMIC MECHANIC PROPERTIES OF DOUBLE BASED ROCKET PROPELLANT DURING ARTIFICIAL AGEING 557

P. Nesvadba

Explosia a.s., Research Institute of Industrial Chemistry, 532 17 Pardubice -Semtín, Czech Republic

APPLICATION OF SHEET EXPLOSIVE FOR METAL HARDENING 571

A. Orzechowski*, D. Powała*, A. Maranda and J. Nowaczewski****

* Institute of Industrial Organic Chemistry, 6 Annopol St, 03-236 Warszawa, PL

** Military University of Technology, 2 Kaliskiego St, 00-908 Warszawa 49, PL

INFLUENCE OF INSENSITIVE ADDITIVES ON DETONATION PARAMETERS OF PBX 576

J. Paszula*, A. Maranda*, B. Gołabek and J. Kasperski****

* Military University of Technology, 00-908 Warszawa, ul. Kaliskiego 2, Poland

** Blastexpol, Duninów, Poland

AN UNDERWATER TEST FOR LWC EMULSION EXPLOSIVES 584

D.V. Pleshakov and Y.M. Lotmentsev

Mendeleyev University, Department of Chemical Engineering, 125047 Miusskaya pl.9, Moscow, Russia

PREDICTION OF THERMODYNAMIC CONDITIONS FOR NITROESTER VAPOR CONDENSATION ON THE SURFACES OF PROCESS APPARATUS DURING THE PRODUCTION OF ENERGETIC MATERIALS 591

M. Pospíšil* and P. Vávra**

* Charles University, Faculty of Mathematics and Physics, Ke Karlovu 3, 12116 Prague 2, Czech Republic

** University of Pardubice, Department of Theory and Technology of Explosives, Studentská 95, 53210 Pardubice, Czech Republic

STUDY OF ELECTRON DENSITY OF MOLECULES, INTERMOLECULAR FORCES AND IMPACT SENSITIVITY OF EXPLOSIVES 600

D. Powała*, A. Orzechowski*, A. Maranda and J. Nowaczewski****

* Institute of Industrial Organic Chemistry, 6 Annopol St, 03-236 Warszawa, PL

** Military University of Technology, 2 Kaliskiego St, 00-908 Warszawa 49, PL

SPHERICAL NITROGUANIDINE AS COMPONENT OF HIGH EXPLOSIVES 606

V.M. Raikova and E.A. Likhlatov

Mendelev University of Chemical Technology, Miusskaya sq. 9, Moscow A-47, Russia

THE CHEMICAL KINETIC AT DETONATION OF AROMATIC NITROCOMPOUNDS – NITRIC ACID MIXTURES 614

M. Rajić Linarić, M. Sućeska, S. Matečić Mušanić and R. Čuljak

Brodarski institut–Marine Research & Special Technologies, Av. V. Holjevca 20, 10020 Zagreb, Croatia

INITIAL STAGE DECOMPOSITION KINETICS OF NITROCELLULOSE PROPELLANT 621

Fritz van Rooyen

National Institute for Explosives Technology (NIXT) South Africa, PO Box 32544, Glenstantia 0010, Pretoria, Republic of South Africa

DETERMINATION OF THE RELATIVE DENSITY OF MOLTEN EXPLOSIVES 630

V.P. Sinditskii, A.I. Levshenkov, V.Yu. Egorshv and V.V. Serushkin Mendeleev University of Chemical Technology, 9 Miusskaya Square, 125047, Moscow, Russia	
COMBUSTION OF DINITRAMIDE SALTS	636
R. Smileski, O. Popovski and J. Naumoski Military Academy "General Mihailo Apostolski" Skopje, Republic of Macedonia	
DETERMINATION OF CHEMICAL STABILITY OF GUNPOWDERS BY QUALITATIVE AND QUANTITATIVE METHODS	646
R. Špásová Explosia a. s., Research Institute for Industrial Chemistry, Safety Engineering Laboratory, 532 17 Pardubice-Semtín, CZ	
DETERMINATION OF EXPLOSIVE PROPERTIES	653
R.S. Stepanov, L.A. Kruglyakova and A.M. Astachov Siberian State Technological University, 660049, Krasnoyarsk, prosp. Mira 82, Russia	
GEMINAL DINITROCOMPOUNDS THERMAL DECOMPOSITION UNDER NON-ISOTHERMAL CONDITIONS	659
W. A. Trzciński, and L. Szymańczyk Military University of Technology, Kaliskiego 2, 00 908 Warsaw, Poland	
DETONATION PERFORMANCES OF LOW-SENSITIVITY NTO/HMX EXPLOSIVES	667
R. Varga*, P. Ulbrich**, M. Koložvári** and M. Fuknová** * Department of Theory and Technology of Explosives, University of Pardubice, 532 10 Pardubice, Czech Republic ** Institute of Forensic Science of the Slovak Police Corps, Sklabinská 1, Bratislava 812 72, Slovak Republic	
TRACE ANALYSIS OF EXPLOSIVES BY LC-MSD TECHNIQUE	676
J. Vávra* and P. Vávra** * Department of Economy and Management of Chemical and Food Industry, Faculty of Chemical Technology, University of Pardubice, 53210 Pardubice, Czech Republic ** Department of Theory and Technology of Explosives, Faculty of Chemical Technology, University of Pardubice, 53210 Pardubice, Czech Republic	
LIFE-CYCLE-ANALYSIS AND "GREEN" ENERGETIC MATERIALS	687
L. Velehradský, J. Petržílek and V. Puš Explosia a.s., Research Institute for Industrial Chemistry (VÚPCH), CZ-532 17, Pardubice - Semtín, Czech Republic	
MODERN PROPELANTS FOR 30 MM AMMUNITION APPLICATIONS	694
Z.A. Walenta*, A. Teodorczyk** and W. Witkowski*** * Institute of Fundamental Technological Research, Polish Academy of Sciences, Swietokrzyska 21, 00-049 Warszawa, Poland ** Institute of Heat Engineering, Warsaw University of Technology, Nowowiejska 25, 00-665 Warszawa, Poland *** Institute of Industrial Organic Chemistry, Annopol 6, 03-236 Warszawa, Poland	
DIRECT MONTE – CARLO SIMULATION OF DETONATION PROCESS IN A GAS	699
V.L. Zbarsky, D. M Stepashkow and N.V. Yudin Mendeleev University of Chemical Technology, 9 Miusskaya Square, 125047, Moscow, Russia	
SYNTHESIS OF 4,6-DINITROBENZOFUROXAN	704
S. Zeman and E. Zemanová Department of Theory & Technology of Explosives, University of Pardubice, CZ-532 10 Pardubice, Czech Republic	
APPLICATION POSSIBILITIES OF POLAROGRAPHY IN STUDIES OF CHEMICAL MICRO-MECHANISM OF INITIATION OF POLYNITRO ARENES	708
S. Žganec*, E. Zvonimir** and M. Dobrilović** * Minervo Ltd, Ljubljana, Slovenia ** Faculty of Mining, Geology and Petroleum Engineering, University of Zagreb, Croatia	
IN SITU MEASUREMENT OF VELOCITY OF DETONATION AND COMPARISON OF HEAVY ANFO PRODUCED IN THE FIELD OF USAGE AND CARTRIDGE EXPLOSIVES	717

PREFACE

This is the seventh seminar “New Trends in Research of Energetic Materials” and the sixth international one in the series organized by the Department of Theory and Technology of Explosives (DTTX) at the University of Pardubice. The original purpose of these meetings was to teach young research workers how to present their results in front of scientific audience. With regard to economic situation of the middle European countries, Balkan and former Soviet Union, no fee was and is asked from the participants.

The fourth seminar in 2001 was already conceived as a worldwide meeting of young research workers and university teachers. The original aim of these meetings was thus complemented by not only the exchange of findings and experience but in particular making friendly contacts between the members of the beginning young generation of experts in the area of energetic materials coming from many countries all over the world.

Starting with the third seminar, the papers presented at these meetings are quoted in the Chemical Abstracts. The interest in these meetings has been gradually growing: the development in the attendance at the seminars can be seen from the following survey:

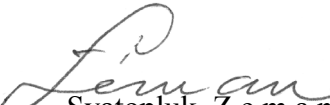
Seminar		Number of		
No.	year	countries	papers	participants
3	2000	6	32	88
4	2001	11	41	106
5	2002	19	51	116
6	2003	18	60	129
7	2004	20	84	ca 150

One of the decisive factors enabling realization of these seminars has been the financial assistance of well-wishers of this activity. In the last three years a very significant financial support has been regularly provided by the European Office of Aerospace Research & Development of the USAF in London, by Austin Detonator Comp. (Vsetín), by Indet Safety Systems Comp. (a member of Nippon Kayaku group in Vsetín) and by the Czech company OZM Ltd. in Hrochův Týnec. Almost traditionally, some financial support has been provided by Dr. Oldrich Machacek, president of the Universal Tech. Corporation, Dallas, who (as chance would have it) is one of the first PhD graduates from DTTX. Also our Faculty of Chemical Technology markedly contributed towards the costs of the seventh Seminar. The efficient help in ensuring smooth and successful course of the meeting obtained from all these institutions and individuals is gratefully acknowledged. We greatly appreciate it that thanks to this sponsoring all the above-mentioned specifics of the previous seminars can be maintained.

Finally, I wish to thank the members of the Scientific Committee, the authors of all the seminar papers and, last but not least, you, the participants of this seminar, for its success and its influence on the continued success and growth of all future meetings at our University of *young* people and university teachers working in the field of all kinds of energetic materials.

Allow me to use this opportunity for inviting you in the name of my co-workers and myself: we are looking forward to meet you at the seventh seminar on April 19-21, 2005 in the Aula Magna of our University.

Pardubice, March 10th, 2004


Svatopluk Z e m a n

ON MATERIALS' CAPABILITY TO DETONATE

A.N. Dremín

Institute of Problems of Chemical Physics
Chernogolovka, Moscow Region, 142432, Russia

Abstract:

The idea of how to determine the composition of mixtures of liquid explosives with inert diluents and solutions of solid explosives in inert solvents which are still capable to detonate has been introduced. It has been demonstrated experimentally with nitromethane/acetone mixtures and diethanolnitramine/dinitrat/acetone/nitril solutions that the most weak composition still capable to detonate is that which detonation's CJ pressure is still larger than the minimum shock pressure necessary to initiate the detonation. Considerations have been proposed on conditions at which so called gasless detonation could be realized theoretically.

Keywords: *detonation, limit of concentration, gasless detonation.*

1. INTRODUCTION

Detonation theory based on the theory of shock waves was proposed by Michelson^[1], Chapman^[2] and Jouguet^[3,4]. Detonation wave was represented as a shock wave with energy release inside the wave front. However, the Michelson-Chapman-Jouguet (MCJ) hydrodynamic theory does not take into account explosive's decomposition kinetics. For the reason the theory is unable to interpret any detonation limits (initiation, stability and propagation).

Appreciable improvements of the MCJ theory have been made by Grib^[5], Zeldovich^[6], Von Neuman^[7] and Döring^[8]. The Grib-Zeldovich-Von Neuman-Döring (GZND) theory is based on the same premise as the MCJ theory. In both theories detonation is a combined propagation of shock wave compression and chemical reaction. However, there is a substantial difference as well. It is tacitly suggested in the MCJ theory that explosive compression and its chemical transformation into detonation products proceed simultaneously within the detonation wave shock front. And in the GZND theory explosive does not change chemically at all within the wave's shock discontinuity zone; it is only compressed inside this zone. In this case selfignition and combustion of the shock-compressed and heated explosive take place in some induction time behind the zone. In that way the GZND theory predicted existence in the front of detonation waves some space of increased pressure (so called chemical spike), the spike's pressure profile being presented of a convex shape. Chemical spikes were observed experimentally in the front of detonation waves of many explosives (see, for example, ^[9-15]). However, nobody has observed yet the spike of a convex shape as it would have to be according to the GZND theory; in all cases chemical spikes of only a concave downward profile were observed. Moreover detonation waves without any chemical spike have been found (see, for example, ^[16-18]).

The profile of chemical spikes of a concave shape and especially detonation waves without any chemical spikes strongly testify in favour of the explosives' nonequilibrium athermal decomposition within the shock front of detonation waves ^[19]. In this case the chemical spike's absence means the explosive's complete transformation into detonation products within its detonation wave shock front ^[19,20].

The concave shape of detonation waves' chemical spike means that the shock-compressed explosive's selfignition takes place at the very top of the chemical spike. It is quite probable that it takes place for the origin of some critical concentration of active particles due to the explosive partial decomposition within the detonation waves' shock front ^[19].

It should be mentioned that the detonation front with the foregoing regularities of explosive's energy release (so called "fast kinetics") is kinetically stable ^[19]. On the other hand detonation waves with unstable (pulsating) fronts have been observed as well ^[10]. It means that the concentration of active particles originated within their shock front is insufficient for the shock-compressed explosive's selfignition. In this case the shock-compressed explosive should continue to be activated during some additional time (induction time). However, it is well-known that the detonation front with such regularities of explosive's energy release (so called "slow kinetics") is kinetically unstable ^[10, 19]. The instability manifest itself in the following. First, the one-dimensional detonation wave chemical spike is broken down and, second, the explosive's shock-compressed layer approximately CJ pressure appears in the pulsating detonation front. In this case explosive's transformation into detonation products proceeds through a numerous local adiabatic explosions (LAE) of the shock-compressed explosive ^[19, 20].

It is obvious that no material whatever can detonate if its hypothetical CJ detonation wave's maximum pressure is smaller than a critical (minimum) shock pressure P_{CR} necessary to initiate the detonation. Taking into account the foregoing the chemical spike's pressure should be considered in the capacity of the detonation maximum pressure for kinetically stable detonation; and for kinetically unstable detonation – the wave's CJ pressure.

2. DETONATION LIMITS ON CONCENTRATION OF NITROMETHANE/ACETONE MIXTURE AND DIETHANOLNITRAMIN – DINITRAT/ACETONITRIL SOLUTION

2.1 Nitromethane/Acetone mixture

In Table 1 data on detonation parameters (ρ_0 – initial density, D_{CJ} – Chapman-Jouguet detonation velocity, P_{CJ} – pressure), critical (minimum) pressure to initiate the detonation P_{CR} and the detonation's failure diameter d_f are presented for some mixtures of nitromethane and acetone NM/A ^[10, 21].

Table 1. *Parameters of detonation of Nitromethane/Acetone mixtures.*

Mixtures [Vol. %]	ρ_0 [g.cm ⁻³]	D_{CJ} [km.s ⁻¹]	P_{CJ} [Gpa]	d_f [mm]	P_{CR} [Gpa]
NM	1.14	6.3	13.5	18	8
NM/A 84/16	1.08	6.0	10.9	80	8
NM/A 75/25	1.05	5.75	9.1	280	8

The same data are shown in Fig.1. One can see that the P_{CR} 's value does not depend on the mixtures' composition and equals to 8 GPa. And P_{CJ} decreases linearly with the increase of acetone's content in the mixtures, so that at acetone's content more than ~ 31 Vol % the value of P_{CJ} of the mixtures' hypothetical detonation turns out to be smaller than the P_{CR} 's value.

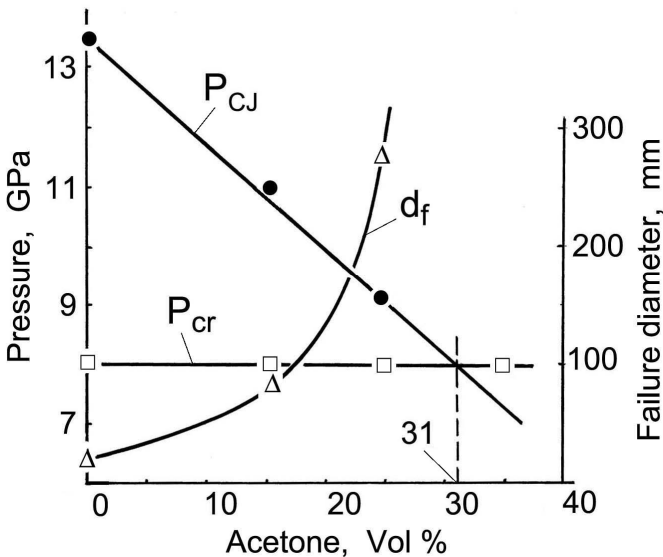


Fig 1. Nitromethane/Acetone mixture. Dependences of the mixture detonation's pressure P_{CJ} , failure diameter d_f and critical shock pressure P_{CR} to initiate the detonations on the mixture's composition.

It follows from the foregoing, that any mixture's detonation has to discontinue if its P_{CR} is larger than P_{CJ} . Data on the shock initiation of detonation of NM/A mixtures of acetone's contents of near 31 Vol % clearly demonstrate the statement. To substantiate the statement, at first, it should be reminded that under the effect of shock of P_{CR} intensity homogeneous explosives' selfignition originates always in some induction time [10, 19, 22]. It follows that the explosive's selfignition should appear in the front of detonation wave close to its limit on concentration also in some induction time. However, as it has been already mentioned, the front of detonation of any explosive with such regularities of energy release is unstable. For this reason the front of any homogenous explosive's detonation in the

vicinity of its propagation on concentration has to be always unstable. Second. It should be reminded also that CJ detonation of any homogeneous explosive always originates from its strong detonation ^[10, 19]. And it has been shown experimentally that strong detonation turns gradually into its CJ regime in all NM/A mixtures if their acetone's content is smaller than 31 Vol %. During the process of the strong detonation transition to the CJ detonation the quantity of LAEs of the shock-compressed mixture in the wave front decreases gradually to some one corresponding to the CJ detonation. However, if acetone's content in a NM/A mixture is larger than 31 Vol % LAEs disappear all over the wave's front and the detonation discontinuates at some stage of the process of the mixture's strong detonation pressure decrease. It follows from the foregoing that it takes place as soon as the pressure's value becomes smaller than the P_{CR} 's value.

In accordance with the notion that no material can detonate if its hypothetical detonation wave's maximum pressure is smaller than a minimum shock pressure necessary to initiate the detonation the value of mixtures' detonation failure diameter dramatically increases with the increase of acetone's content in the mixtures. For example, the value of detonation failure diameter for the NM/A 75/25 Vol % is as large as 280 mm.

It should be mentioned that percentage of an inert diluent in a mixture of a liquid explosive at which the value of failure diameter of the mixture's detonation tends to infinity is bound to be smaller than the diluent's percentage content in the liquid explosive's mixture corresponding to its detonation limit on concentration. Principal features of the mechanism of liquid explosive's unstable detonation failure diameter ^[19, 23, 24] should be reminded to substantiate the statement. According to the mechanism a break-down (BD) of LAEs takes place in the detonation wave's front under the effect of lateral rarefaction waves from the charge's open surface. The BD propagating over the front 1 (see Fig. 2) to the charge's axis

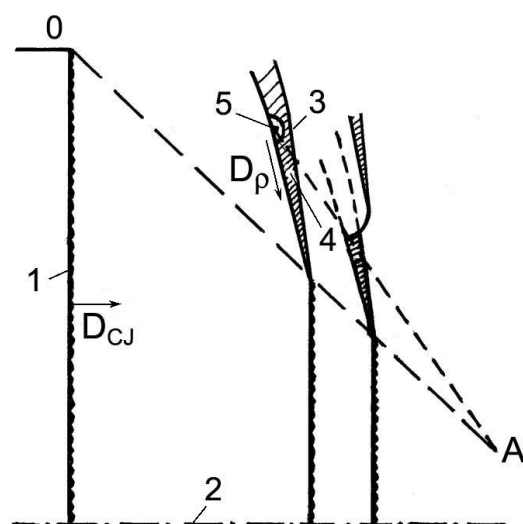


Fig 2. Schematic diagram of failure wave origin to illustrate failure diameter of liquid explosive's unstable detonation.

- 1 – detonation wave front, 2 – the charge's axis,
- 3 – adjoined shock wave with shock-compressed explosive, 4 – behind its front,
- 5 – point of the shock-compressed explosive's selfignition and detonation origin,
- 0A – the locus of the failure wave front's motion, D_{CJ} – CJ detonation velocity,
- D_p – velocity of shock-compressed explosive's detonation.

2 in the form of a failure wave results in the origin of adjoint shock wave 3 with a shock-compressed explosive 4 behind its front. At sufficiently large diameter of the charge the shock-compressed explosive selfignition originates at some point 5. It leads to the appearance of the explosive's detonation. In its propagation to the charge's axis with D_p velocity it overtakes the failure wave front and prevents the further BD of LAEs in the basic detonation's front 1. In this case the detonation front 1 continues its motion along the charge's axis with its CJ velocity. However, if the shock-compressed detonation fails to overcome the failure wave's front, that is if the failure waves have chance to shut down the whole cross section of the charge, the charge's detonation will discontinue.

It follows from the foregoing that, on the one hand, for selfignition of the shock-compressed explosive 4 (see Fig. 2) behind the adjoint shock wave front 3, the front's 3 intensity P_{AD} does not have to be weaker than the initial explosive's P_{CR} . And, on the other hand, it is obvious that the adjoint shock wave intensity is always smaller than that of the basic detonation wave's P_{CJ} . Just for the reason the diluent's content in the mixture which detonation failure diameter tends to infinity has to be smaller than in the mixture which is close to the limit of detonation on concentration.

In connection with the just mentioned finding some misunderstanding can arise. Really, on the one hand, it is argued that a mixture's (or solvent's) detonation can not propagate as its failure diameter tends to infinity, and, on the other hand, it is added there and then that even more weak mixture's of the same components can detonate. One can apprehend it as some contradiction. But the fact is that there is no here any contradictions. The matter is that the BD of LAEs in the front of unstable detonation waves under the effect of lateral rarefaction waves from the charge' open surface governs the detonation's failure diameter. However, it is possible to prevent the BD's origin at all. It is easy to do by using for charges some metal confinement of a proper thickness ^[19, 25]. If the BD's origin is prevented the detonation can propagate along charges of even far smaller diameter than its failure diameter ^[10, 19, 25]. In this case the detonation's possibility will be governed by the BD of LAEs in the detonation's front under the effect of rarefaction waves not from the charge's open surface but from the detonation wave's rear. As at detonation of the failure diameter charge the basic detonation wave front's intensity P_{CJ} is larger than the detonation's P_{CR} , it is obvious that all mixtures which detonation's P_{CJ} (in its dependence on concentration) is larger than the detonation's P_{CR} will detonate steadily in charges of metal confinement mentioned ^[19, 25].

It should be mentioned that the determination of the limit of detonation on concentration of liquid mixtures and solutions through comparison of the detonation's P_{CJ} and P_{CR} contains some uncertainty. The matter is that the shock-to-detonation process depends not only on the shock's amplitude but also on its pressure's time profile. The profile depends on the active charge's characteristic size. The values of P_{CJ} and P_{CR} presented in Table 1 have been measured with the use of charges of 70 – 80 mm diameter and about a 100 mm height. In this case it has been shown that even a slight change of the initiating shock amplitude leads to a tremendous change of the explosives' selfignition time. It is obvious that it takes place due to the strong exponential dependence of explosives' selfignition time on their conditions. It follows from the foregoing that it would need to increase tremendously the active charge's size to initiate the explosive with a somewhat weaker shock. At the same time it means that the uncertainty mentioned above does not have to be significant.

2.2 Diethanolnitramindinitrat/Acetonitril solution.

Transparent solutions of solid diethanolnitramindinitrat (DINA, $C_4H_8N_3O_6$, monocrystal density $\rho_0 = 1.67 \text{ g/cm}^3$) in liquid acetonitril (C_2H_3N , $\rho_0 = 0.783 \text{ g/cm}^3$) have been investigated in ^[26], DINA's content in the D/A solutions being varied from its maximum value (68.5 wt %) capable to be dissolved at room temperature till down to its minimum value (61 wt %) at which the solution's detonation was able no longer to propagate. It has been found out that P_{CR} 's value as in the case of NM/A mixtures does not depend on the solution's composition. In this case the value of P_{CR} is equal to 7.4 GPa. The CJ detonation velocity D_{CJ} and pressure P_{CJ} of the most concentrated solution (D/A 68.5/31.5 wt %, $\rho_0 = 1.20 \text{ g/cm}^3$) turned out to be equal to 5.78 km/s and 8.7 GPa, correspondingly. Data on the initiation of detonation by the shock of the P_{CR} intensity clearly demonstrate that strong detonations of solutions of 68.5 and 65 wt % DINA content turn gradually into their CJ detonation regimes (see, for example, Fig. 3) ^[26]. However, at 61 wt % of DINA's content (see Fig. 4) ^[26] LAEs disappear and detonation discontinuates all over the pulsating wave's front at some stage of the solution's strong detonation pressure decrease. It should be mentioned that in this case the shock-compressed solution's detonation has not been registered for its faint luminescence.

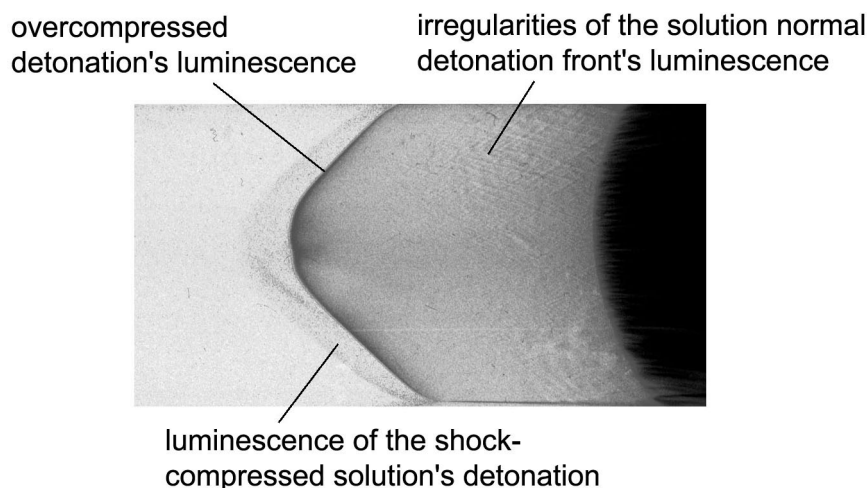


Fig 3. Schematic view of the experimental streak-camera negative photograph of D/A 65/35 wt % solution's detonation origin under the effect of 7.4 GPa shock wave.

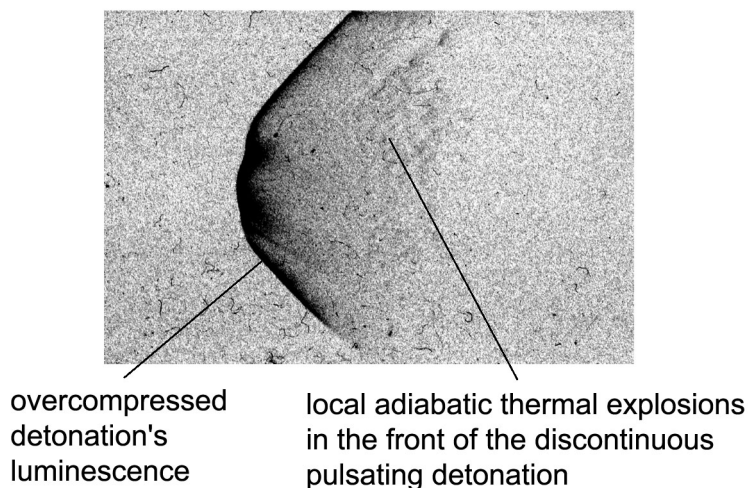


Fig 4. Schematic view of the experimental streak-camera negative photograph of D/A 61/39 wt % solution's initiation by the 7,4 GPa shock wave.

As for failure diameter of DINA/A solutions' detonation, an attempt has been undertaken to measure it only for the solution of maximum (68.5 wt %) DINA's content ^[27]. As a result it has been shown that the value of the detonation failure diameter even for this most powerful solution is rather large (somewhat larger than 150 mm). It follows that the solution in its DINA's content is close to that one which detonation failure diameter tends to infinity.

3. ON THE PROBABILITY OF GASLESS DETONATION

Some ineffective attempts (see, for example ^[28-31]) are known to observe so called gasless detonation (self-propagating high-temperature synthesis, SHS). On the other hand a large body of research has been performed in the former Branch of the Institute of Chemical Physics on chemical reactions in condensed matter under the effect of shock waves. In particular, phase formation in systems of titanium, zirconium and hafnium oxides with oxides of rare-earth elements as well as in the system of germanium and silicon oxides under the effect has been investigated in detail ^[32, 33]. In this case it was shown that compounds (rather often in metastable forms) of the components in recovering devices were originated in the form of well-crystallized single-crystals. The data made it possible to propose the overall mechanism of phase formation under the effect of shock waves. According to the mechanism under the effect of shock wave of proper for each system intensity some melt of components and their fast reaction take place simultaneously within the wave's front, compounds originated being thermodynamically equilibrium at the front's state. Due to the extremely fast cooling of the melt behind the shock wave front under the effect of rarefaction waves liquid compounds turn to be in and crystallize from a highly overcooled state. In this case those of them which do not exist in thermodynamically equilibrium form at the conditions appearing after the passage of rarefaction waves crystallize in the form of metastable compounds.

Starting from the foregoing mechanism and taking into account the notion presented above on the capability of any material (system) to detonate it is possible to state conditions at which gasless detonation could be realized theoretically. To start with the problem, first, it is necessary to calculate (or to measure experimentally) the components mixture's shock Hugoniot and the intensity of shock wave P_{mt} under the effect of which if only one (but

better both) component is in its melted state under the conditions of the shock compression. Second. It is necessary to calculate the detonation Hugoniot of the mixture's reaction products (on the assumption that the reaction is complete). Third. With the use of the detonation Hugoniot as well as the shock Hugoniot of the components' mixture it is necessary to calculate the value of the maximum pressure P_m in the front of the hypothetical detonation wave. The probability of the system's detonation will be governed by the relation of the two calculated pressures: P_m and P_{mt} . The probability will be good if the value of the (P_m/P_{mt}) 's relation is larger than unity. And vice versa, it is obvious that the detonation will be improbable at all if the relation is smaller than unity.

4. CONCLUSION

The notion has been stated and confirmed experimentally that the front of detonation of any liquid explosive mixtures with inert diluents as well as solutions of any solid explosive in inert solvents in the vicinity of the detonation's limit on concentration is always unstable, pulsating.

The experimental technique has been proposed to evaluate the explosive's minimum concentration in the mixtures and solutions which are still capable to detonate. The technique has its origin in registration of the shock-to-detonation process with the help of high speed streak cameras. It has been shown that the minimum concentration is that below which local adiabatic explosions in the front of strong attenuating detonations always originated during the process disappear and detonation discontinuates.

It has been stated, on the ground of the previously discovered mechanism of liquid explosives unstable detonation's failure diameter ^[23], that the minimum explosive's concentration in the mixtures and solutions which detonation's failure diameter tends to infinity is larger than that at which they are still capable to detonate in principle. The statement has been confirmed experimentally for NM/A's mixtures and D/A's solutions.

Considerations have been proposed on conditions at which so called gasless detonation could be realized theoretically.

REFERENCES

- [1] V.A. Michelson: *On the normal ignition velocity of explosive gaseous mixtures*, Scientific Transactions of Imperial Moscow University on Mathematics and Physics, 10:1-93, 1893
- [2] D.L. Chapman: *On the rate of explosions in gases*, Philos. Mag., 47:90-104, 1899
- [3] E. Jouguet: *On the propagation of chemical reaction in gases*. J. de Mathématiques Pures et Appliquées, 7:347-425, 1905 continued in [Jou06]
- [4] E. Jouguet: *On the propagation of chemical reaction in gases*, J. de Mathématiques Pures et Appliquées, 2:5-85, 1906
- [5] A.A. Grib: Thesis, Tomsk Univ., 1939, publ. in Prikl. Mathem. Mech., Vol. 8, N 4, p. 273 (in Russian), 1944
- [6] Ya.B. Zeldovich: *On the theory of the propagation of detonation in gaseous systems*, Sov. Phys. JETP, 10(5):542-568, 1940
- [7] J. Von Neumann: *Report on "theory of detonation waves" (OD-02)*, Technical report, National Defense Research Committee of the Office of Scientific Research and Development, Division B, Section B-1, Serial # 238, 1942
- [8] W. Döring: *Über der detonation vergang in gasen*, Ann. Phys., 43(5):421-436, 1943
- [9] R.E. Duff and E. Houston: *Measurement of the Chapman-Jouguet pressure and reaction time in a detonating high explosive*, J. Chem. Phys., 23:1268-1273, 1955
- [10] A.N. Dremin, S.D. Savrov, V.S. Trofimov, and K.K. Shvedov: *Detonatsionnye Volny v Kondensirovannykh Sredakh (Detonation Waves in Condensed Media)*, Izd-vo Nauka, Moscow, 1970. (Translated from Russian by Foreign Technology Division, Wright-Patterson Air Force Base, O.H., FTD-HT-23-1889-71), Aug. 1972
- [11] C.M. Traver, R.D. Breithaupt, J.W. Kury: *Detonation waves in Pentaerythritol Tetranitrate*, J. Appl. Phys., V. 81, # 11, pp. 7193-7202, 1997
- [12] C.M. Traver, J.W. Kury, R.D. Breithaupt: *Detonation waves in Triaminotrinitrobenzene*, J. Appl. Phys., V. 82, # 8, pp. 3771-3781, 1997
- [13] A.V. Fedorov, A.V. Menshikh, N.B. Yagodin: *On detonation wave front structure of condensed high explosives*, In Proc. Shock Compr. of Condensed Matter – 1997, edited by Schmidt/Dandekar/Forbes. American Inst. of Physics, pp. 735-738, 1998
- [14] A.V. Fedorov, A.V. Menshikh, N.B. Yagodin: *Heterogeneous explosives detonation front structure*, Chem. Phys., V. 18, N 11, pp. 64-68, 1999
- [15] S.N. Lubyatinsty, B.G. Loboiko: *Density effect on detonation reaction zone length in solid explosive*, Shock Compression of Condens. Matter – 1997, edited by Schmidt/Dandekar/ Forbes. American Inst. of Physics, pp. 743-746, 1998
- [16] V.K. Ashaev, G.S. Doronin, A.D. Levin: *On the structure of detonation front in condensed explosives*, FGV (russian), V. 24, N 1, pp. 95-99, 1988
- [17] B.G. Loboiko, S.N. Lubyatinsty: *Chemical reaction zone of detonating explosives*, FGV (russian), V. 36, N 6, pp. 45-64, 2000
- [18] A.V. Utkin, A.S. Kolesnikov, V.E. Fortov: *The structure of steady-state detonation wave of pressed RDX*, Dokl. Acad. Nauk, Russia, V. 381, N 6, 2001
- [19] A.N. Dremin: *Toward detonation theory*, Springer, N.Y., 1999
- [20] A.N. Dremin: *Discoveries in detonation of molecular explosives in the 20th century*, Comb., Expl., and Shock waves, V. 36, N 6, pp. 704-715, 2000
- [21] O.K. Rozanov: *Investigation of liquid explosives detonation mechanism*, Candidate of Science Thesis, Institute of Problems of Chemical Physics, Russian Academy of Sci., Chernogolovka, 1965, Russia
- [22] R.F. Chaiken: *Comments of hypervelocity wave phenomena in condensed explosives*, Journal Chemical Physics, 33:760-768, 1960

- [23] A.N. Dremin: *The critical detonation diameter of liquid explosives*, Dokl. Akad. Nauk SSSR, 147:870-873, 1962.
- [24] A.N. Dremin and V.S. Trofimov: *On the nature of the critical diameter*, In Proc. 10th Symposium (Int.) on Compustion, 839-843, Pittsburgh, USA, The Combustion Institute. , 1965
- [25] A.N. Dremin: *On the reality of chemical changes of molecular condensed explosives during the process of their compression within the shock front of detonation waves*, Proc. XIth Symp. on Comb. and Expl., Chernogolovka, Russia, V. II, Chemical Physics of Combustion's and Explosion's processes, pp. 41-43, 1996
- [26] A.N. Dremin, A.V. Ananin, V.A. Garanin, L.T. Eremenko, S.A. Koldunov, D.A. Nesterenko: *The unlooked for result of DINA/Acetonitril solutions detonation study*, Proc. Fifth Intern. Symp. High Dynamic Pressures, Saint-Malo, France, V. 1, pp. 125-133, 2003
- [27] A.N. Dremin, A.V. Ananin, V.A. Garanin, L.T. Eremenko, S.A. Koldunov, Yu. M. Litvinov, D.A. Nesterenko: *On the detonation failure diameter of the DINA/Acetonitril solution*, Proc. of the 12th Symp. (Int.) on Detonation, San-Diego, USA, to be published, 2002
- [28] M.B. Boslogh: *A thermochemical model for shock-induced reaction (heat detonation) in solids*, J. Chem. Phys., V. 92, N 3, pp. 1839-1848, 1990
- [29] A.S. Shteinberg, V.A. Knjasik, V.E. Fortov: *On possibility of gasless detonation of condensed systems*, Dokl. Acad. Nauk SSSR, V. 336, N 1, pp. 71-73, 1994
- [30] A.G. Merzhanov, Yu.A. Gordopolov, V.S. Trofimov: *On the possibility of gasless detonation in condensed systems. Shock Waves*, V. 6, N 3, pp. 157-159, 1996
- [31] E.A. Dobler, A.N. Grjadunov, A.S. Shteinberg, A.V. Utkin, V.E. Fortov.: *Shock compressebility of CuO-B system capable – of – reaction*, Chem. Phys., V. 19, N 5, pp. 43-49, 2000
- [32] A.V. Kolesnikov: Thesis, *Phase formation in systems of titanium, zirconium and hafnium oxides with oxides of rare-earth elements under the effect of shock waves*, Inst. of Chem. Phys., USSR Academy of Sci., Chernogolovka, 1981.
- [33] A.V. Kolesnikov, A.V. Lebedev, S.S. Nabatov. A.N. Dremin: *Investigation of phase formation in $GeO_2 - SiO_2$ system under the effect of shock waves*, Chem. Phys., V. 16, N 11, pp. 92-98, 1997

NEW HIGH EXPLOSIVES AND PROPELLANTS BASED ON BIURET AND TETRAZOLE COMPOUNDS

T.M. Klapötke*, G. Holl**, J. Geith*, A. Hammerl* and J. Weigand*

* Department of Chemistry, University of Munich,
Butenandtstr. 5-13 (D), D-81377 Munich Germany)

** Bundeswehr Research Institute for Materials, Fuels and Lubricants,
Swisttal-Heimertsheim; Großes Cent, D-53913 Swisttal (Germany)

Abstract:

The synthesis of energetic, non-nuclear materials for possible military application has been a long term goal in our research group. Modern high-energy-density materials (HEDM) derive most of their energy either (i) from oxidation of the carbon backbone, as with traditional energetic materials or (ii) from their very high positive heat of formation. Examples for the first class are traditional explosives such as TNT, RDX and HMX. Modern nitro compounds such as CL-20, TEX or the recently reported hepta- and octanitrocubanes possess very high densities and have enhanced energies due to substantial cage strain. The most recent and most exciting members of the second class of compounds are 3,3'-azobis(6-amino-1,2,4,5-tetrazine) and various salts which are based on the 5,5'-azotetrazolate dianion, which derive most of their energy from their very high positive heats of formation. The heavy metal salts of 5,5'-azotetrazolate, particularly lead 5,5'-azotetrazolate dihydroxide, have been investigated for use as initiators. The ammonium, guanidinium and triaminoguanidinium salts of 5,5'-azotetrazolate were found to be powerful, yet smokeless gas generators.

Since in general, tetrazole derivatives are very useful building blocks in the chemistry of highly nitrogen-rich compounds, in this contribution we report on the synthesis and characterization of several tetrazole based energetic materials with up to and over 90% nitrogen.

The synthesis, NMR spectroscopic characterization and structure determination of highly explosive tetrazole azide, a very nitrogen-rich material (88.3% N) is reported. The computed electrostatic potential suggests a pronounced shock and friction sensitivity which was confirmed experimentally. Quantitative valence bond (VB) calculations were performed for the most important 21 VB structures in order to obtain the structural weights and to obtain an assessment for the importance of the various individual VB structures considered.

The synthesis, reactivity and physical properties of new nitrogen-rich, highly energetic materials is presented.

Examples of nitrogen-rich compounds with up to 95% nitrogen content by weight include hydrazinium azide hydrazinate, $N_2H_5^+N_3^- \cdot N_2H_4$ (91.5 % N) and trinitrotriazidobenzene, $C_6(N_3)_3(NO_2)_3$. Also presented are new, highly energetic tetrazole derivatives and derivatives of tetrazene.

The heats of combustion (ΔH_{comb}) of dinitrobiuret (DNB) and diaminotetrazole nitrate (HDAT- NO_3) were determined experimentally using oxygen bomb calorimetry: $\Delta H_{comb}(DNB) = 5195 \pm 200 \text{ kJ kg}^{-1}$, $\Delta H_{comb}(DAT-NO_3) = 7900 \pm 300 \text{ kJ kg}^{-1}$. The standard heats of formation (ΔH_f°) of DNB and HDAT- NO_3 were obtained on the basis of quantum chemical computations: $\Delta H_f^\circ(DNB) = -353 \text{ kJ mol}^{-1}$, -1829 kJ kg^{-1} ; $\Delta H_f^\circ(HDAT-NO_3) = +254 \text{ kJ mol}^{-1}$, $+1558 \text{ kJ kg}^{-1}$. The detonation velocities (D) and detonation pressures (P) of DNB and HDAT- NO_3 were calculated semiempirically:

$D(\text{DNB}) = 8.66 \text{ mm } \mu\text{s}^{-1}$, $P(\text{DNB}) = 33.9 \text{ GPa}$; $D(\text{DAT-NO}_3) = 8.77 \text{ mm } \mu\text{s}^{-1}$, $P(\text{HDAT-NO}_3) = 33.3 \text{ GPa}$.

Integral to this research are investigations concerning the explosive nature and safe-handling of such compounds. The sensitivity of the compounds towards heat, friction and electrostatic shock have been both experimentally (drop hammer, steel sleeve and firing tests) and theoretically investigated (calculation of electrostatic potential surfaces).

Possible applications for these energetic materials will be highlighted, in particular with respect to new detonators and rocket propulsion systems.

Keywords: Azides, Azotetrazole compounds, Dinitrobiuret, Explosives, High energy density materials, Tetrazole compounds

1. INTRODUCTION

The synthesis of energetic, non-nuclear materials for possible military application has been a long term goal in our research group. Modern high-energy-density materials (HEDM) derive most of their energy either (i) from oxidation of the carbon backbone, as with traditional energetic materials or (ii) from their very high positive heat of formation. Examples for the first class are traditional explosives such as TNT, RDX and HMX. Modern nitro compounds such as CL-20 or the recently reported hepta- and octanitrocubanes possess very high densities and enhance the energies utilizing substantial cage strain. The most recent and most exciting member of the second class of compounds is 3,3'-azobis(6-amino-1,2,4,5-tetrazine) which shows the desired remarkable insensitivity to electrostatic discharge, friction and impact while having a very high heat of formation of $\Delta H_f^\circ = 206 \text{ kcal mol}^{-1}$ ($936.7 \text{ kcal kg}^{-1}$). In this contribution we report on the synthesis and characterization of $[\text{N}_2\text{H}_5]^+_2[\text{N}_4\text{C-N=N-CN}_4]^{2-}$ (**1**), $[\text{N}_2\text{H}_5]^+_2[\text{N}_4\text{C-N=N-CN}_4]^{2-} \cdot 2 \text{ H}_2\text{O}$ (**2**) and $[\text{N}_2\text{H}_5]^+_2[\text{N}_4\text{C-N=N-CN}_4]^{2-} \cdot 2 \text{ N}_2\text{H}_4$ (**3**), which are new members of the second family which derive most of their energy from their very high positive heats of formation.

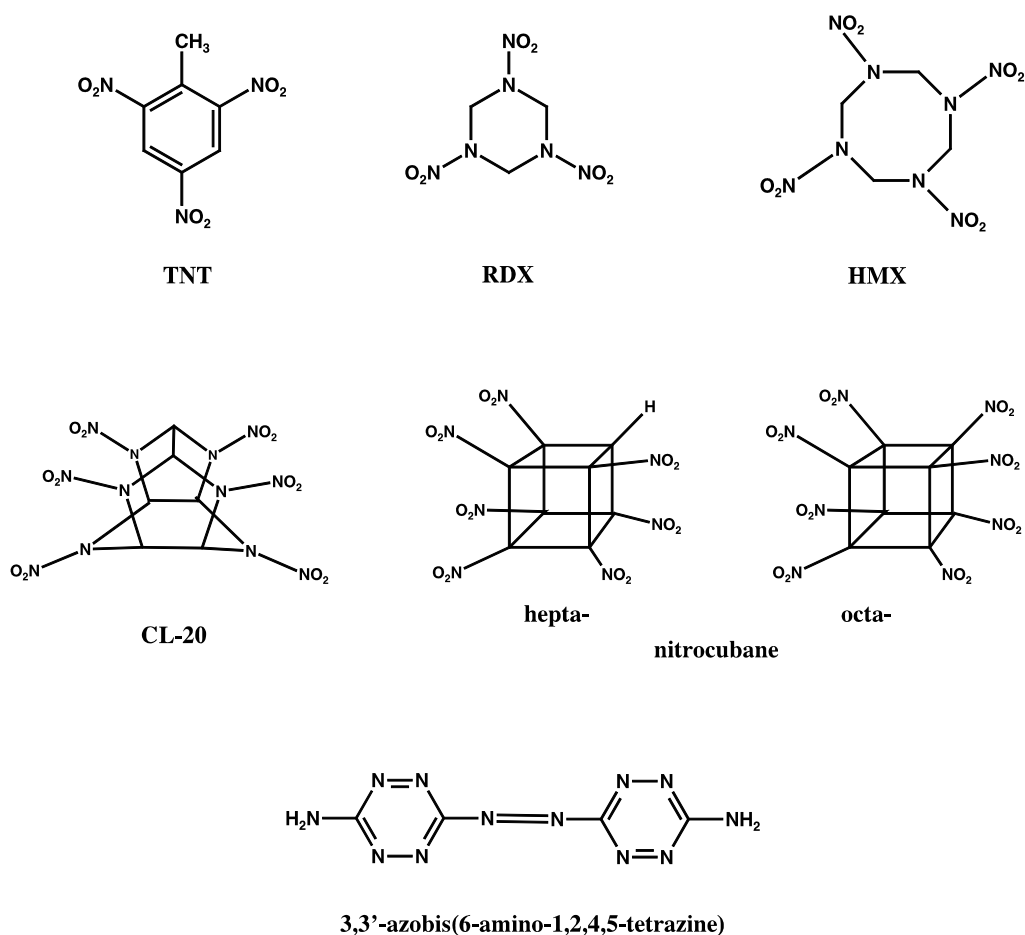


Fig 1. Structures of TNT, RDX, HMX, CL-20, hepta and octanitrocubane, 3,3'-azobis (6-amino-1,2,4,5-tetrazine).

After the first synthesis of 5,5'-azotetrazolate salts by Thiele, who investigated some alkali, alkaline earth and heavy metal salts as well as the $[\text{NH}_4]^+$, $[\text{N}_2\text{H}_6]^{2+}$ and the $[\text{NH}_3\text{OH}]^+$ salts, the 5,5'-azotetrazolate dianion has often been considered for practical use. Covalent 1,1-diphenyl, 1,1-dimethyl derivatives and several other 1,1'-disubstituted aromatic derivatives of 5,5'-azotetrazolate were studied by Stolle et al. The heats of combustion were determined for 1,1'- and 2,2'-dimethylated derivatives of 5,5'-azotetrazolate. The heavy metal salts of 5,5'-azotetrazolate, particularly lead 5,5'-azotetrazolate dihydroxide, have been investigated for use as initiators.

Among others, the guanidinium, dimethylammonium, and semicarbazide salts of 5,5'-azotetrazolate were tested as gas generators in combination with the oxidizers KNO_3 and KClO_4 . The ammonium, guanidinium and triaminoguanidinium salts of 5,5'-azotetrazolate were found to be powerful yet smokeless gas generators. Compared to HMX in composite propellants these compounds gave comparable performance and cooler, less reactive and less visible gases. 5,5'-azotetrazolate decomposes in acidic medium under nitrogen evolution to 1-hydrazinotetrazole. We therefore replaced the more acidic $[\text{N}_2\text{H}_6]^{2+}$ ion with the more basic $[\text{N}_2\text{H}_5]^+$ ion.

2. HYDRAZINIUM AZOTETRAZOLATE COMPOUNDS ^[1]

The reaction of $[\text{N}_2\text{H}_5]^+\text{[SO}_4\text{]}^{2-}$ with barium-5,5'-azotetrazolate gave new high-energy-density materials (HEDM) based on the 5,5'-azotetrazolate dianion. The dihydrazinium salt of $[\text{N}_4\text{C-N=N-CN}_4]^{2-}$ **1**, its dihydrate **2** and its dihydrazinate **3** were prepared in high yield. Synthesis in water afforded yellow needles with two coordinated molecules of water: $[\text{N}_2\text{H}_5]_2^+[\text{N}_4\text{C-N=N-CN}_4]^{2-} \cdot 2 \text{ H}_2\text{O}$ (**2**): *monoclinic*, $P2_1/c$, $a = 8.958(2)$, $b = 3.6596(7)$, $c = 16.200(3)$, $\beta = 96.834(3)$, $V = 527.3(2) \text{ \AA}^3$, $Z = 2$; synthesis in anhydrous hydrazine gave yellow needles with two coordinated molecules of hydrazine: $[\text{N}_2\text{H}_5]_2^+[\text{N}_4\text{C-N=N-CN}_4]^{2-} \cdot 2 \text{ N}_2\text{H}_4$ (**3**): *triclinic*, $P-1$, $a = 4.6208(6)$, $b = 8.585(1)$, $c = 9.271(1) \text{ \AA}$, $\alpha = 108.486(2)$, $\beta = 95.290(2)$, $\gamma = 102.991(2)^\circ$, $V = 334.51(8) \text{ \AA}^3$, $Z = 1$. The compounds were characterized by elemental analysis, vibrational (IR, Raman) and multinuclear NMR spectroscopy (^1H , ^{13}C , ^{14}N , ^{15}N). The new compounds represent new high-nitrogen HEDMs with one of the highest nitrogen contents reported to date ($[\text{N}_2\text{H}_5]_2^+[\text{N}_4\text{C-N=N-CN}_4]^{2-}$: 85.2 %; $[\text{N}_2\text{H}_5]_2^+[\text{N}_4\text{C-N=N-CN}_4]^{2-} \cdot 2 \text{ H}_2\text{O}$: 73.3 %; $[\text{N}_2\text{H}_5]_2^+[\text{N}_4\text{C-N=N-CN}_4]^{2-} \cdot 2 \text{ N}_2\text{H}_4$: 85.7 %). The standard heat of formation of the solvate free compound **1** was computed at MP2(FULL)/6-311+G(d,p) level of theory to be $\Delta H_f^\circ = 264 \text{ kcal mol}^{-1}$ which translates to $1147 \text{ kcal kg}^{-1}$ and is one of the highest ever reported. The compounds are stable at room temperature ($T_{\text{dec}} = 194 \text{ }^\circ\text{C}$ (**1**), $192 \text{ }^\circ\text{C}$ (**2**) and $185 \text{ }^\circ\text{C}$ (**3**)) and are almost insensitive to friction and impact but detonate violently when the explosion is initiated.

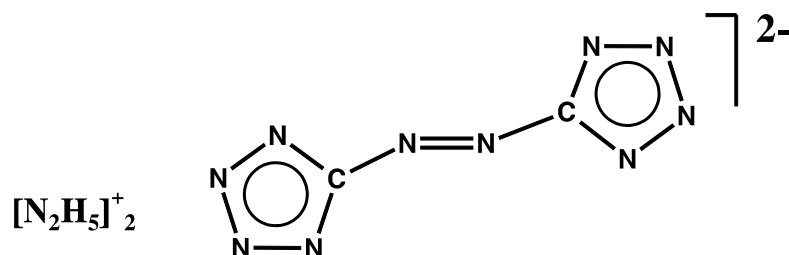


Fig 2. Structure of $[\text{N}_2\text{H}_5]^+_2[\text{N}_4\text{C-N=N-CN}_4]^{2-}$, (**1**).

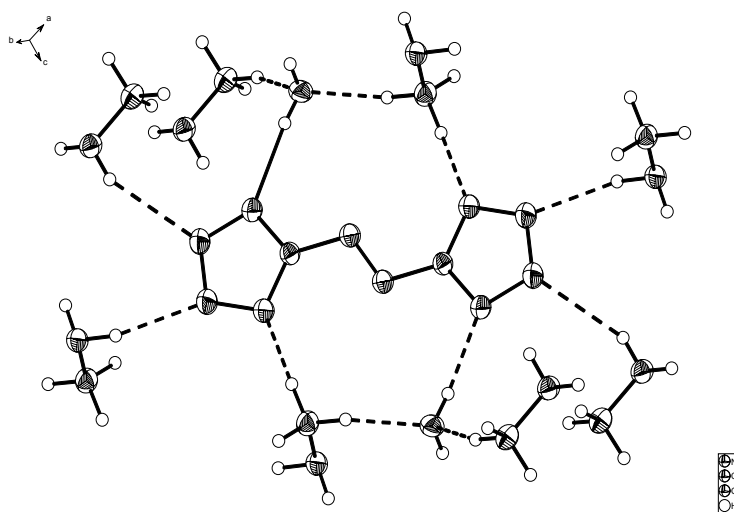


Fig 3. Hydrogen bonds of the azotetrazolate dianion of **2** as ORTEP plot (thermal ellipsoids represent 25% probability).

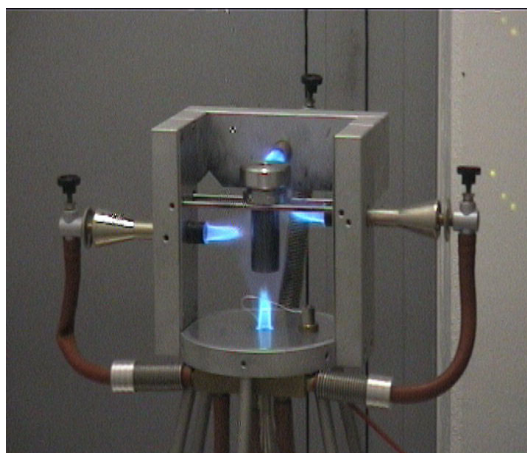
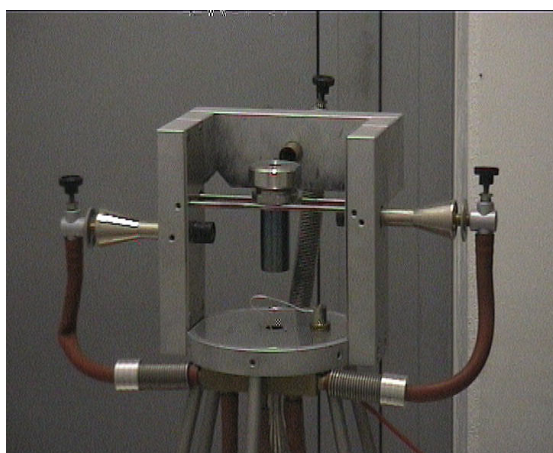
3. DINITROBIURET AND DIAMINOTETRAZOLE NITRATE ^[2]

We recently prepared and determined the molecular structures of dinitrobiuret (DNB) (Fig. 6) and diaminotetrazole nitrate (HDAT-NO₃) (Figs. 7, 8). The high chemical and thermal stability of both compounds and the previously determined critical diameters of the steel sleeve test of 8 mm for HDAT-NO₃ and 6 mm for DNB (Figs. 4, 5) which are comparable to the values reported for HMX (8 mm), RDX (8 mm) or PETN (6 mm) prompted us to obtain the thermodynamic data and detonation pressures and velocities for both compounds in a combined experimental and theoretical study.

The heats of combustion ($\Delta H_{\text{comb.}}$) of dinitrobiuret (DNB) and diaminotetrazole nitrate (HDAT-NO₃) were determined experimentally using oxygen bomb calorimetry: $\Delta H_{\text{comb.}}(\text{DNB}) = 5195 \pm 200 \text{ kJ kg}^{-1}$, $\Delta H_{\text{comb.}}(\text{HDAT-NO}_3) = 7900 \pm 300 \text{ kJ kg}^{-1}$. The standard heats of formation (ΔH_f°) of DNB and HDAT-NO₃ were obtained on the basis of quantum chemical computations at the electron-correlated ab initio MP2 (second order Møller-Plesset perturbation theory) level of theory using a correlation consistent double-zeta basis set (cc-pV-DZ): $\Delta H_f^\circ(\text{DNB}) = -353 \text{ kJ mol}^{-1}$, -1829 kJ kg^{-1} ; $\Delta H_f^\circ(\text{HDAT-NO}_3) = +254 \text{ kJ mol}^{-1}$, $+1558 \text{ kJ kg}^{-1}$. The detonation velocities (D) and detonation pressures (P) of DNB and HDAT-NO₃ were calculated using the empirical equations by Kamlet and Jacobs: $D(\text{DNB}) = 8.66 \text{ mm } \mu\text{s}^{-1}$, $P(\text{DNB}) = 33.9 \text{ GPa}$; $D(\text{HDAT-NO}_3) = 8.77 \text{ mm } \mu\text{s}^{-1}$, $P(\text{HDAT-NO}_3) = 33.3 \text{ GPa}$.

From this combined experimental and theoretical study the following conclusions could be drawn:

- (i) Dinitrobiuret (DNB) and diaminotetrazole nitrate (HDAT-NO₃) are very powerful and promising new explosives.
- (ii) Whereas DNB has a slightly positive oxygen balance (+4.1%), the oxygen balance of HDAT-NO₃ is negative (-29.4%).
- (iii) Both compounds show detonation velocities and detonation pressures similar to well established energetic materials such as PETN, RDX or HMX.



t = 0

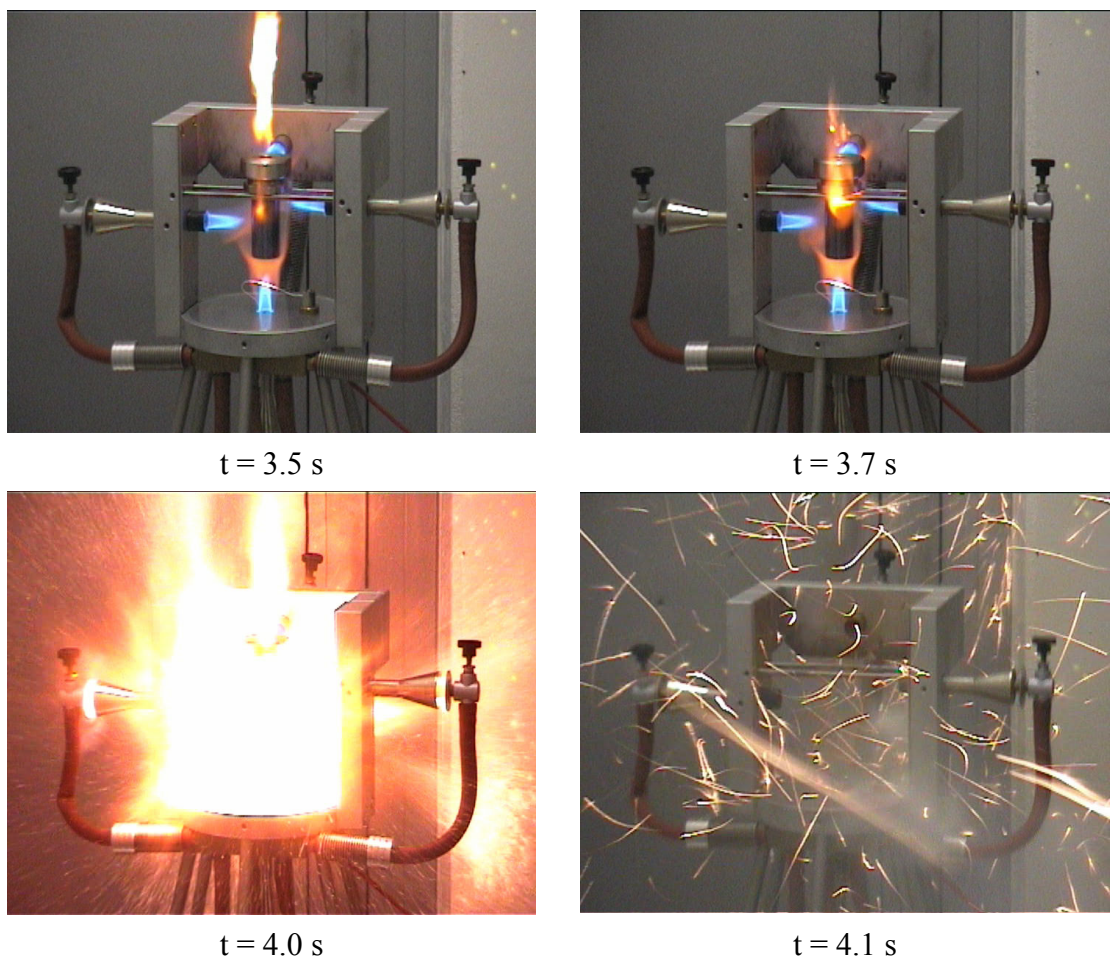


Fig 4. Steel sleeve test of DNB (10 g, 6 mm).



Fig 5. Steel sleeve test of DNB (10 g, 6 mm); before (left) and after test (right).

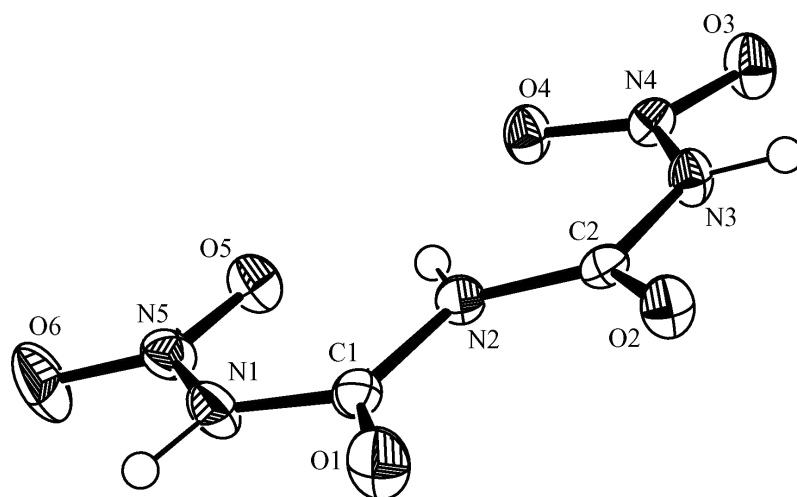


Fig 6. Molecular structure of DNB in the crystalline state.

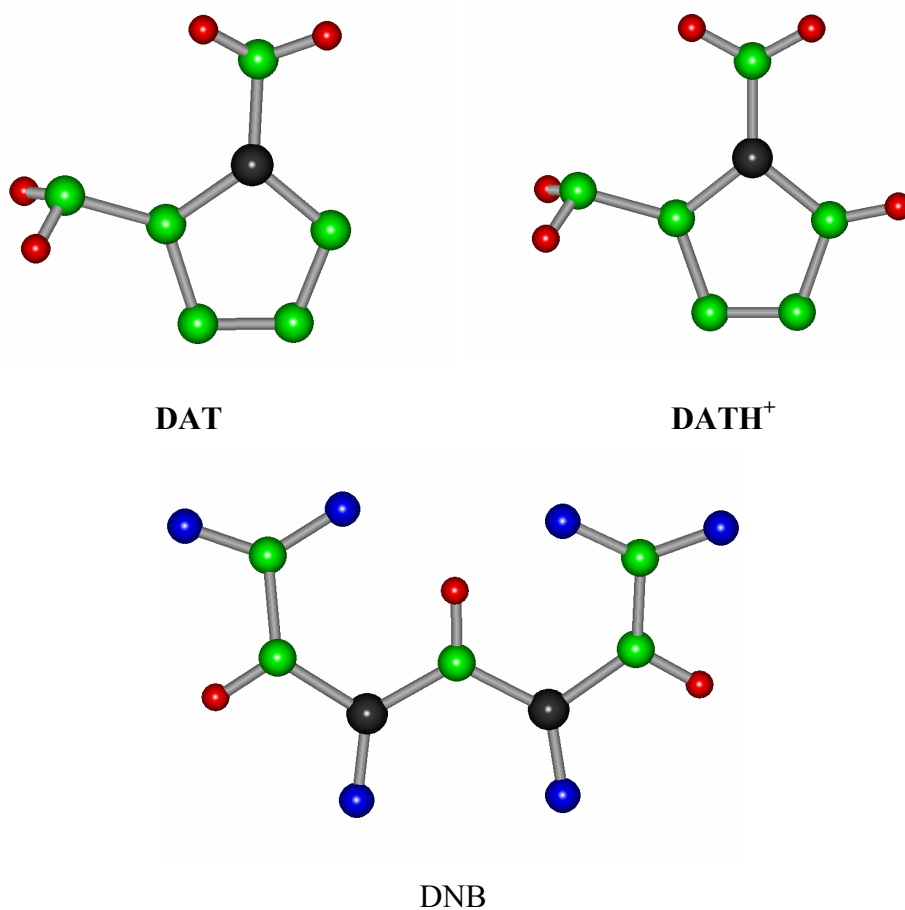


Fig 7. Ab initio (MP2/cc-pVDZ) computed molecular structures of DAT, DATH⁺ and DNB.

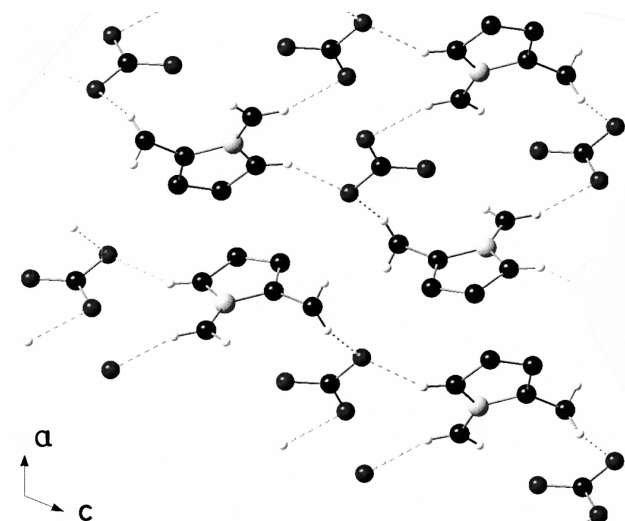


Fig 8. Molecular structure of HDAT-NO₃ in the crystalline state, View along the [010] axis.

4. SYNTHESIS, STRUCTURE AND MO CALCULATIONS FOR TETRAZOLE AZIDE, CHN₇ ^[3]

Modern high-energy-density materials (HEDM) derive most of their energy either (i) from oxidation of the carbon backbone, as with traditional energetic materials or (ii) from their very high positive heat of formation. Examples for the first class are traditional explosives such as TNT, RDX and HMX. Modern nitro compounds such as CL-20, TEX or the recently reported hepta- and octanitrocubanes possess very high densities and have enhanced energies due to substantial cage strain. The most recent and most exciting members of the second class of compounds are 3,3'-azobis(6-amino-1,2,4,5-tetrazine) and various salts which are based on the 5,5'-azotetrazolate dianion, which derive most of their energy from their very high positive heats of formation. The heavy metal salts of 5,5'-azotetrazolate, particularly lead 5,5'-azotetrazolate dihydroxide, have been investigated for use as initiators. The ammonium, guanidinium and triaminoguanidinium salts of 5,5'-azotetrazolate were found to be powerful, yet smokeless gas generators.

Since in general, tetrazole derivatives are very useful building blocks in the chemistry of highly nitrogen-rich compounds, in this contribution we report on the synthesis and characterization of another tetrazole based highly energetic material, namely tetrazole azide, CHN₇, which has a very high nitrogen content of over 88%.

The synthesis, NMR spectroscopic characterization and structure determination of highly explosive tetrazole azide, a very nitrogen-rich material (88.3% N) is reported. Tetrazole azide was prepared in high yield from the diazotation reaction of aminotetrazole, followed by treatment of the formed diazonium salt with sodium azide. Synthesis in diethylether/methanol and recrystallization from diethylether afforded colorless cubes: CHN₇ (**4**): *monoclinic*, *P1* 2₁/n₁, *a* = 1346.6(5), *b* = 499.6(2), *c* = 1360.9(5) pm, *β* = 105.14(1)°, *V* = 0.884(2) nm³, *Z* = 8, *ρ* = 1.670 g cm⁻³. The observed structural parameters (X-ray) are in good accordance with the results from molecular orbital (MO) calculations. The computed electrostatic potential (B3LYP) suggests a pronounced shock and friction sensitivity which was confirmed experimentally.



(4)

Recrystallization of the crude product from anhydrous diethylether yielded colorless crystals in 65% yield.

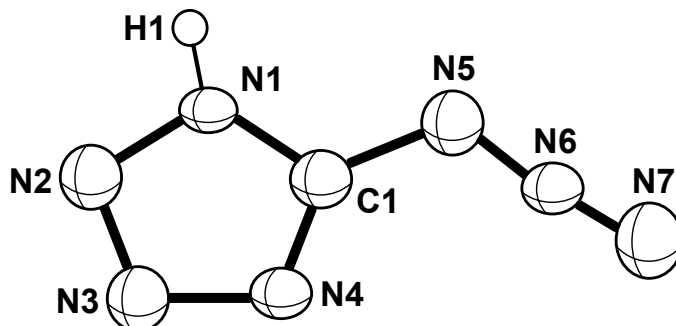


Fig 9. Molecular structure of tetrazole azide, CHN_7 (**4**) as ORTEP plot.

The ^{14}N NMR spectrum clearly indicated that the material (**4**) was pure and no impurities originating from the starting material (aminotetrazole), the diazonium salt or sodium azide were detected. In the ^{14}N NMR spectrum, compound **4** shows in addition to the two tetrazole resonances at -27 (N_α) and -4 ppm (N_β) three resonances typical for a covalent azide at -253 (N_α), -135 (N_β) and -144 (N_γ) ppm (rel. to $\text{CH}_3\text{-NO}_2$).

In order to get an appreciation for the initial decomposition behavior of tetrazole azide (**4**), three initial dissociation pathways were calculated at B3LYP/6-31G(d,p) level of theory (Fig. 10). In the first possible dissociation step, a N_2 molecule is given off from the azide group in a symmetry-allowed process. If the symmetry is constrained to C_s , an endothermic (188 kJ mol^{-1}) dissociation occurs into N_2 and tetrazole nitrene (Fig. 10, eq. 3a). If a breaking of the symmetry to C_1 is allowed, the dissociation occurs through an activation energy barrier ($E_A = 159 \text{ kJ mol}^{-1}$; changing the symmetry from C_s to C_1) yielding $\text{N}\equiv\text{C-N(H)-N}$ nitrene (singlet state) and two equivalents of N_2 (eq. 3b). In a third possible mechanism (retro 2+3 dipolar cycloaddition reaction, C_s symmetry), compound **4** dissociates again through an activation barrier ($E_A = 234 \text{ kJ mol}^{-1}$) into hydrogen azide, HN_3 , and cyanogen azide (eq. 4). From the B3LYP/6-31G(d,p) computed total energies of **4**, HN_3 and NC-N_3 it can be concluded that reaction (4) is energetically unfavorable by $\Delta E^{\text{el}} = 139 \text{ kJ mol}^{-1}$. On the other hand, reaction (3b) is thermodynamically favorable by $\Delta E^{\text{el}} = -56 \text{ kJ mol}^{-1}$. From the computational results shown in Fig. 10, it can be seen that both the dissociation of **1** into two equivalents of N_2 and $\text{N}\equiv\text{C-N(H)-N}$ (eq. 3) and the dissociation of **4** into HN_3 and NC-N_3 (eq. 4) are kinetically both possible.

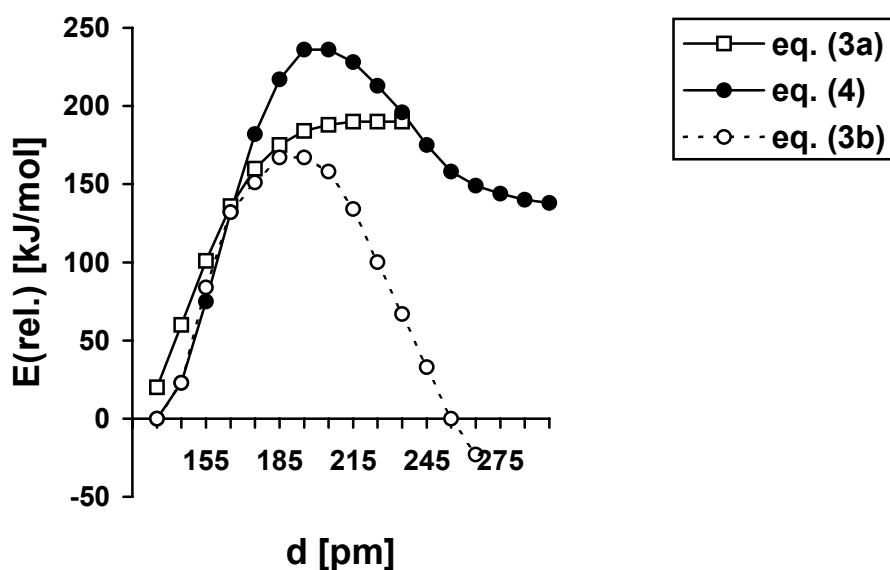
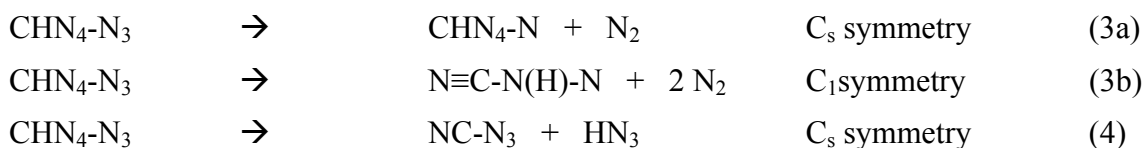


Fig 10. Two-dimensional energy hypersurface (B3LYP/6-31G(d,p)) showing the dissociation of **4** into N_2 and $\text{CHN}_4\text{-N}$ (C_s , eq. 3a, \square), the dissociation of **4** into 2N_2 and $\text{N}\equiv\text{C-N(H)-N}$ (C_1 , eq. 3b, \circ) and the dissociation of **4** into HN_3 and NC-N_3 (eq. 4, \bullet); x-direction: distances in pm, y-direction: rel. energy in kJ mol^{-1} .)



It has recently been found by Politzer et al. and extensively used by Rice et al. that the pattern of the computed electrostatic potential (eq. 5) on the surface of a molecule can in general, be related to the sensitivity of the bulk material. The electrostatic potential at any point r , is given by eq. (5), in which Z_A is the charge on nucleus A, located at R_A .

$$V(r) = \sum \{Z_A / (|R_A - r|)\} - \int (\rho(r') dr') / (|r' - r|) \quad (5)$$

While in many energetic systems the regions of positive potential are almost always larger in area, they are also stronger (in terms of average magnitudes) than the negative areas, in contrast to the situation in usual non-energetic organic compounds. This atypical contrast between stronger positive regions and weaker negative ones can be related to the impact sensitivities.

Typically, for organic molecules in general, the negative regions cover a smaller portion of the total surface area but are significantly stronger (in terms of average magnitudes) than the positive ones. On the other hand, in the case of energetic molecules, the positive regions are still larger but now also stronger in magnitude than the negative. Politzer et al. were able to show that impact sensitivities can be expressed as a function of the extent of this anomalous reversal of the strengths of the positive and negative surface potentials. Figure 11 shows the calculated electrostatic potentials of tetrazole azide (**4**) and of aminotetrazole, methylamino tetrazole and phenyltetrazole azide for comparison. Comparing

methylaminotetrazole with the more impact sensitive aminotetrazole and the extremely sensitive tetrazole azide (Fig. 11), the most obvious feature of the ESPs in Fig. 11 appears in the region over the aromatic CN₄ ring. Molecules that are more sensitive to impact have a larger electron deficiency in this region than molecules that are less sensitive. There also appears to be some deficiency of electron density over the C-N bonding regions, as observed by Rice and Murray et al. Additionally, it seems that the less evenly the electron density is distributed over the surface of the molecule (excluding extrema of charge localized over atoms of the electron-donating or electron-withdrawing substituents) the more sensitive the molecule. For phenyltetrazole azide (Fig. 11) the electron density seems to be distributed more evenly over the surface of the molecule than is the case for the unsubstituted tetrazole azide. This would account for a lower impact sensitivity of phenyltetrazole azide in comparison with tetrazole azide.

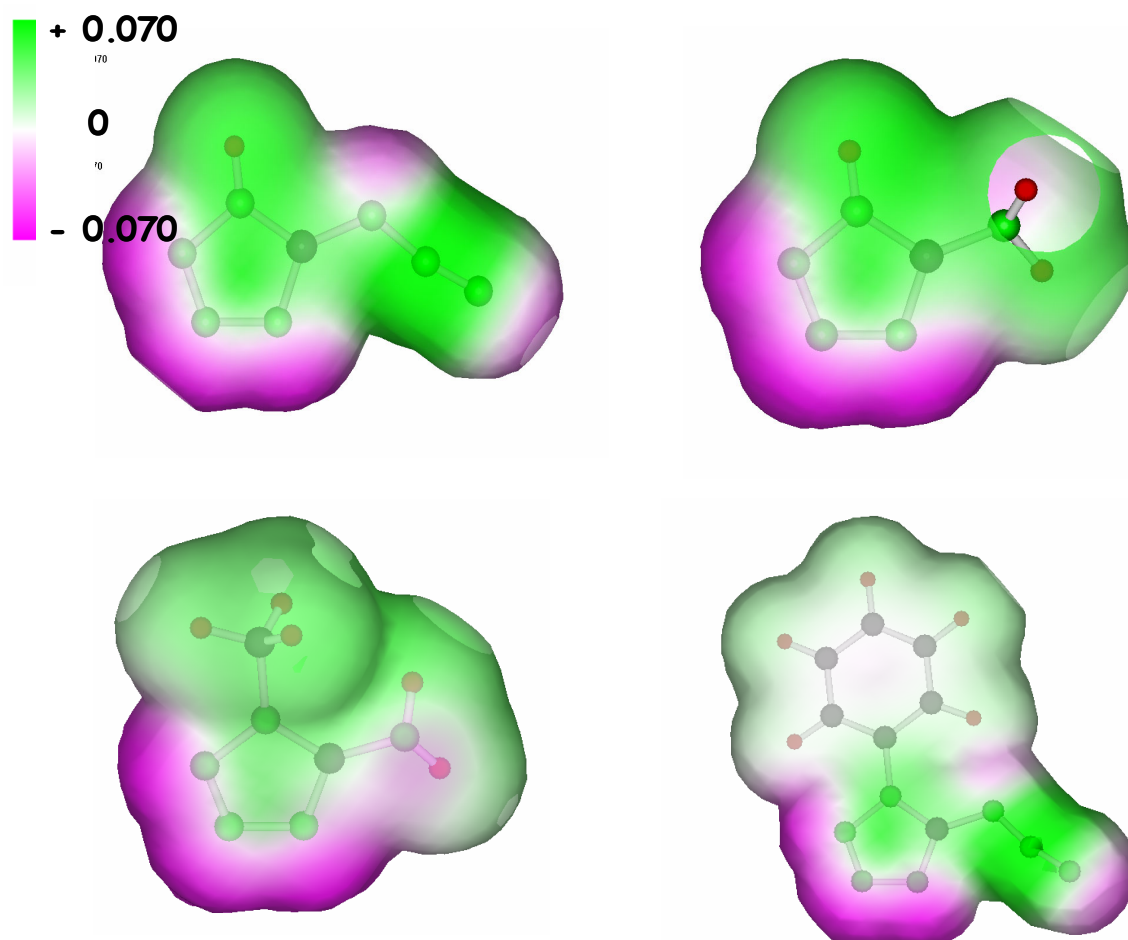
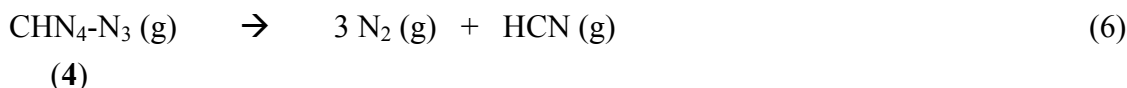


Fig 11. Electrostatic potential of tetrazole azide (**4**) (top left), aminotetrazole (top right), methylaminotetrazole (bottom left) and phenyltetrazole azide. Legends for the color ranges of the ESPs are given above (top left corner) and range from -0.07 to $+0.07$ hartrees (a.u.); element colors: H - red, carbon - black, nitrogen - green.

In order to calculate the heat of detonation (Q), and the standard heat of formation (ΔH_f°), the reaction energy for reaction 6 was calculated ab initio at B3LYP/6-31G(d,p) level of theory.



From the computed total energies, (4, and N₂ see Tab. 2; HCN -93.424581 a.u., *zpe* = 43 kJ mol⁻¹) the electronic reaction energy $\Delta E^{\text{el}}(6)$ was calculated to be:

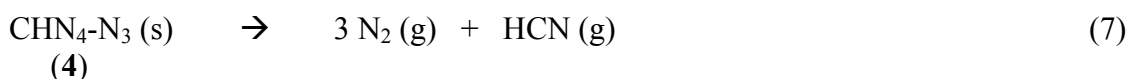
$$\Delta E^{\text{el}}(6) = -407 \text{ kJ mol}^{-1}.$$

After corrections for the zero point energies, the work term ($p\Delta V = 3 \text{ RT}$), the translational energy ($\Delta U^{\text{tr}} = 4.5 \text{ RT}$) and the rotational energy ($\Delta U^{\text{rot}} = 2.5 \text{ RT}$) this value was converted into the reaction enthalpy $\Delta H^{\circ}(6)$ at room temperature.

$$\Delta H^{\circ}(6) = -427 \text{ kJ mol}^{-1}.$$

With an estimated heat of sublimation for tetrazole azide (4) of $\Delta H_{\text{sub}}(4) = 105 \text{ kJ mol}^{-1}$ and the heat of vaporization for HCN of $\Delta H_{\text{vap}}(\text{HCN}) = 26 \text{ kJ mol}^{-1}$ ($\Delta H^{\circ}_{\text{f}}(\text{HCN}(\text{g})) = +135 \text{ kJ mol}^{-1}$) the standard enthalpy of formation of 4 ($\Delta H^{\circ}_{\text{f}}(4)$) and the heat of detonation (Q) for 4 according to eq. (7) can be stated as:

$$\Delta H^{\circ}_{\text{f}}(4) = +458 \text{ kJ mol}^{-1} = +4121 \text{ kJ kg}^{-1}.$$



$$Q(4) = -323 \text{ kJ mol}^{-1} = -2905 \text{ kJ kg}^{-1}.$$

In order to assess more quantitatively the expected detonation properties of compound 4, we calculated the expected detonation pressure (*P*) and detonation velocity (*D*) using the semi-empirical equations suggested by Kamlet and Jacobs (eq. 8 and 9).

$$P [10^8 \text{ Pa}] = K \rho^2 \phi \quad (8)$$

with: $K = 15.58$; ρ density in g cm^{-3}

$$\Phi = 0.49 N M^{0.5} Q^{0.5} \quad \text{with: } N = \text{moles of gas per g of explosive;}$$

$M = \text{g of gas per mol of gas;}$
 $Q = \text{estimated or guessed heat of detonation (cf. eq. 7) (in kJ kg}^{-1}\text{)}$

$$D [\text{mm } \mu\text{s}^{-1}] = A \phi^{0.5} (1 + B \rho) \quad (9)$$

with: $A = 1.01$; $B = 1.30$

For compound 4 we calculated a detonation pressure of $P = 21.7 \text{ GPa}$ and a detonation velocity of $7.16 \text{ mm } \mu\text{s}^{-1}$ (7160 ms^{-1}), which compares nicely with nitroglycerine (7600 m.s^{-1}).

REFERENCES

(please note that all the references cited in the references below are also relevant)

- [1] A. HAMMERL, T. M. Klapötke, H. NÖTH AND M. WARCHHOLD, G. HOLL, M. KAISER: *Inorg. Chem.*, 40, 3570 – 3575, 2001
- [2] J. GEITH, T. M. Klapötke, J. WEIGAND, G. HOLL: *Propellants Explosives and Pyrotechnics*, (in press), 2004
- [3] A. HAMMERL, T. M. Klapötke, H. NÖTH, M. WARCHHOLD, G. HOLL: *Propellants Explosives and Pyrotechnics*, 28(4), 165 – 173, 2003

NEW SAFETY THINKING APPLICABLE TO EM SYNTHESIS AND MANUFACTURE

H.J. Pasman and J.F. Zevenbergen

Delft University of Technology, Faculty of Applied Sciences, Explosion Group
Julianalaan 136, 2628 BL Delft, Netherlands

Abstract:

The occurrence of major accidents in the chemical process industry has over the years stimulated world wide safety thinking. This resulted also rather recently in interesting new concepts in the approach to design and the control of operation of processes with hazardous materials. A practical concept applicable in many situations is the layer of protection analysis. This kind of top down barrier thinking encompasses both technical and organisational measures and is very suited for risk control both in the laboratory and in the case of industrial installations. It involves the user and his management and can optimise cost-benefit. It can be used in new design, but also for installations that have been operated already for years. Thinking starts of course with the question what are the risks and can these be prevented. The inherent safer approach offers a number of check list items which can be checked off. Improvements can semi-quantitatively be measured by indexing. Of course with energetic materials inherent safer working has its limitations, but sometimes by selecting different solvents, other installation lay-out etc. considerable improvements can be made. Subsequently independent layers of protection are defined. Independence is not easy to realise, but is a crucial condition. In a second part specific hazards of energetic materials are highlighted. This is covering the initiation and explosion severity of energetic materials themselves, the process run-away risk when manufacturing them and the health hazards solvents may present.

Keywords: hazards and risks, process safety, layers of protection, energetic materials

1. INTRODUCTION

The activity of making new energetic materials is a challenging one and requires much dedication and persistence. One that survived the first trials without too many scars is however concerned about safety. Safety in synthesizing on small scale is relatively simple in the sense that quantities involved are usually small and where effects of a mishap always decrease in intensity with range, they are brought to small proportion over relatively small distance. In manufacturing things may be different and many plants have been already blasted by their own product. However mastership is craftsmanship: When one understands the safety first principle, one will master the situation more easily, which will translate in better product. Safety is not a matter of signing forms or proving a point to safety committees which do not have the expertise to judge a situation!

2. HAZARDS AND RISKS IN GENERAL

2.1 Definitions

When talking about safety, first a few unavoidable definitions have to be given in a language as simple as possible. It is necessary since the English language contains the words hazard, danger and risk, while most other languages only have danger and risk. Here the words will be used in the following context.

Hazard is a potential of a physical, often energetic phenomenon or a material in contact to do harm to people or the environment. The potential can break loose in a certain situation. Such a situation presents a *danger*. When having such a dangerous situation there is a *risk*. Risk has two elements, the chance or probability it will occur and the effect or the consequence when it happens.

A hazard manifests itself in an accident situation. Therefore we should consider an accident situation as it can occur in an environment of a laboratory or process plant. In Figure 1 we see the elements of an accident situation with a cause-consequence pair. A contained material with hazardous properties, e.g. a flammable liquid constitutes the potential leading to the consequence. Somewhere a trigger, e.g. overpressure, is present that initiates a fracture of the tank and causes loss of containment. The trigger may be hold back by a barrier, because the tank wall remains strong as it is well preserved by paint. Over the years the preservation may degrade, corrosion starts to do its work and all of a sudden, e.g. in a filling operation, the tank bursts open. This is the enabling condition and event. The physical effects can produce damage to exposed “targets” or “responsive subjects” like people, property and other. Often the physical effects are retained or mitigated by safeguards or layers of protection. These may be physical, hence technical, or procedural. The whole setting of an accident is called the *scenario*. The model can be called a hazard-barrier-target or HBT-model ^[1].

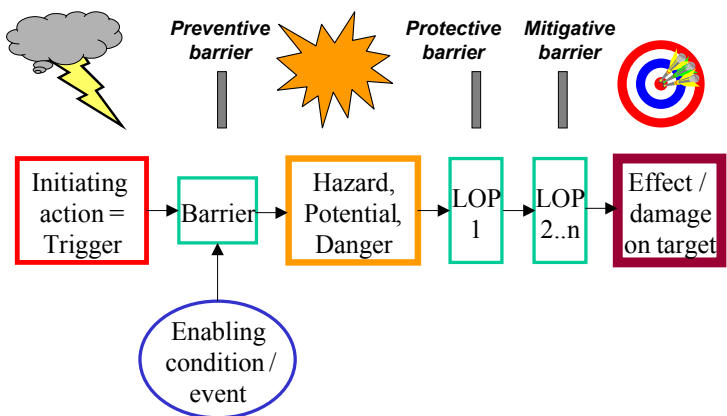


Fig 1. Elements in an accident situation: potential, trigger and various types of barriers, which form together a scenario; LOP stands for Layer of Protection. The enabling condition can be built up itself as a cause-consequence chain with barriers.

In case of explosive material the trigger can be often of some thermal nature: hot spot ignition by spark, friction, impact etc. We shall see this in the next chapter in more detail.

So far the problem is simple. The treacherous point is the enabling condition that takes the preventive barrier away and triggers the initiating action. In fact there may be an underlying recursive mechanism active, which can be seen as a series of other HBT chains, in which each “hazard” attacks a barrier as its “target”. The enabling condition can therefore be quite complex to unravel, also because the time

of failing of underlying barriers need not to be close to the moment of the accident, but can have taken place in the past. Also not all barriers are physical, they may be procedural.

Sometimes decisions by designers or management of twenty years ago may lead to a failing underlying barrier, which in the end causes an accident. Systematic approaches have been developed to try to surface these mechanisms such as MORT: Management Oversight and Risk Tree ^{12]}.

2.2 Hazard and risk assessment

When having a set-up either on bench scale or as a large scale plant the question will come up: “How safe is safe enough”. In very brief statements some general experience in trying to answer that question will be given.

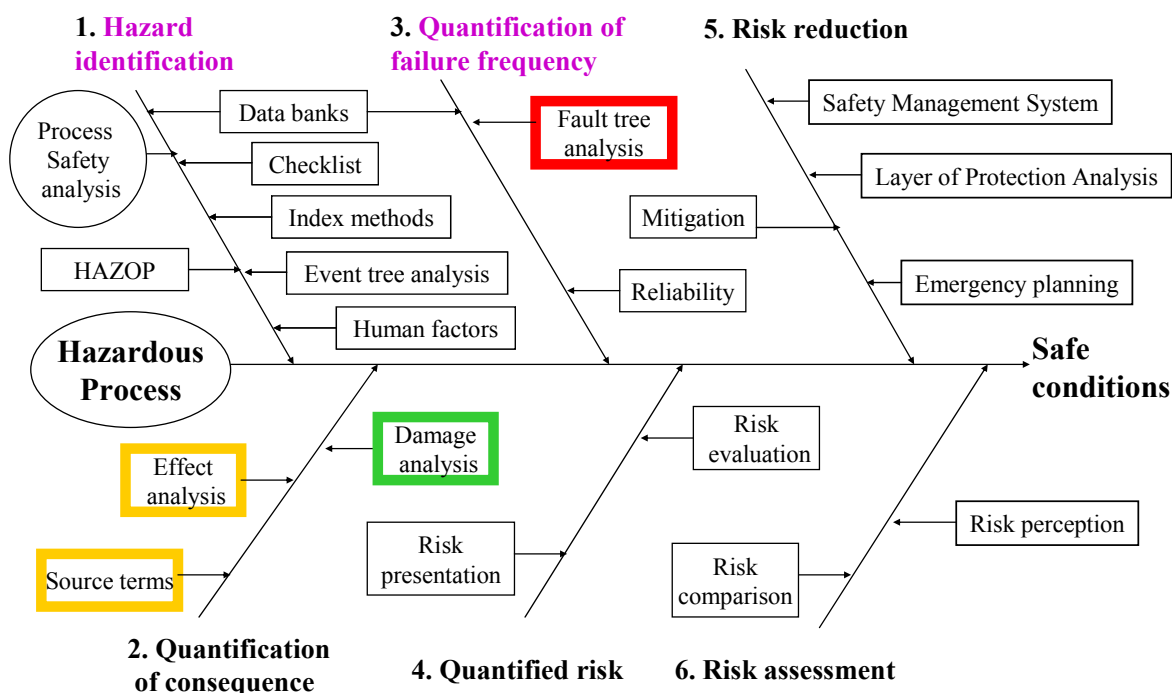


Fig 2. Risk assessment scheme, starting with identification.

The scheme does not need to be quantified, but it certainly sharpens the mind if an attempt is undertaken.

First is the notion of a formal risk assessment. In Figure 2 the stages of an analysis are shown. Essential is the first step of identification of the source hazards and the scenarios in which risks occur. This is highly decisive for the success of the assessment. The human mind does not like to think what can go wrong. One is focused on the result of the work.

By making an inventory of all substances involved, retrieving from literature (e.g. Sax^{13]}, <http://hazard.com/msds/>, and Bretherick^{14]}) information on their properties and given their quantity, the potential can be estimated. To further stimulate the thinking various tools have been developed. The most known ones are Index methods and HAZOP. An index method like the Dow Fire & Explosion Index^{15]} is in the chemical industry very common and provides in simple calculation on the basis of the materials involved an impression of the risk level of the operation. Hazard & Operability^{16]} is a qualitative approach by a team of experts of different disciplines under experienced chairmanship. It tries to identify the hazards and it examines the operability of the process, whether it is difficult to control or not. The team examines a set-up by generating questions about it in a systematic manner. For this purpose a number of "guide-words" are used that question the effect on process behaviour of

a deviation of a process parameter from the design intention. Commonly used guide-words are given in Table 1. Process parameters can be chosen from a wide variety, but the first five of the set mentioned here are the most frequently used: Flow, pressure, temperature, mixing, stirring, control, pH, level, sequence, viscosity, signal, reaction, start/stop, composition, addition, separation, services, operate, maintain, time, communication. Meaningful combinations are shown in Table 2.

Table 1. *Standard guide-words and their generic meanings.*

<i>Guide-word</i>	<i>Meaning</i>
No (not, none)	None of the design intent is achieved
More (more of, higher)	Quantitative increase in a parameter
Less (less of, lower)	Quantitative decrease in a parameter
As well as (more than)	An additional activity occurs
Part of achieved	Only some of the design intention is
Reverse intention occurs	Logical opposite of the design
Other than (other)	
activity takes place	Complete substitution - another

Table 2. *Examples of meaningful combinations of parameters and guide-words.*

<i>Parameter combination</i>	<i>Guide-words that can give a meaningful</i>
Flow	None; more of; less of; reverse; elsewhere; as well as
Temperature	Higher; lower
Pressure	Higher; lower, reverse
Level	Higher; lower; none
Mixing	Less; more; none
Reaction	Higher (rate of); lower (rate of); none; reverse; as well as/other than; part of
Phase	Other; reverse; as well as
Composition	Part of; as well as
Communication	None; part of; more of; less of; other, as well as

When producing chemicals this technique is very useful. It has proven itself all over the world. Not only the hazard presented by an explosive, will be considered, but also that by the solvents, the cooling medium etc. The activity is however tedious and labor intensive.

Other sources of information of what can go wrong are colleagues and data bases telling you what happened to others. The explosives industry branch has already many years a co-operative exchange of information. In the process industry it became a culture to investigate not only accidents to reveal the most hidden combination of causes, but also to look at near misses quite profoundly to identify root causes. This developed for continuous processes to monitoring all process deviations and malfunctioning of equipment. This appeared to be a rich source of identifying potential precursors of more serious incidents. At the same time it helps to save costs by eliminating future process interruption.

Although quantification is not an always necessary step, it is useful to try it. Consequences are in itself probabilistic: In other words in making an estimate of a person

getting killed or injured by some effect from the threatening source, the outcome is a chance. Given the intensity of a load such as fire radiation, blast overpressure, or toxic concentration, at the location of the exposed person a probit relation will predict the probability of fatality or injury. The same holds for the fire and blast load on structures, see e.g. the Green Book^[7]. With respect to failure frequency matters are more complex. Yet for an overall risk analysis an estimate of failure probability is essential. Fault tree analysis may help.

2.3 Risk reduction

The thinking about risk reduction shall be hierarchical as is schematically shown in Figure 3. It means that when the hazards are identified, one should try to eliminate these all together in the first place. If one is free to choose, as at the initial stage of design, it is often very valuable to rethink the process and the chemical substances involved. This is in order to eliminate risks either by the course of the reaction, by the conditions applied or by the properties of intermediates, solvents etc. This concerns too preparatory steps and product refinement steps. The last few years much has been written about making processes inherently safer and cleaner.

Improvement is not only possible at plant level for new and renovated plants, but also at equipment level. By good design a number of hazards occurring in rotating equipment like in pumps can be avoided or minimised. This pertains to avoiding contamination, leakage, inclusion of air in liquids, local overheating and such like. So, technical equipment safety and integrity contributes much to safer and cleaner production.

The concept of minimizing hazards or fostering inherent safety was strongly promoted by Trevor Kletz^[8a-d] starting already in the 1980s. The eleven principles for making processes inherently safer are given in Table 3.

Intensification or minimisation means creating conditions by which reaction or other operations like centrifuging or extraction go faster, so that volumes involved to produce a certain amount of product per unit of time are smaller and as a net result the hazard is much lower. It also means a tendency toward replacing batch processes by continuous ones, since the latter can be operated economically with a much smaller reaction volume. A known old example of this is the manufacture of nitro-glycerine.

Table 3. *Principles of Inherent Safety* ^[8a-d]

1. <i>Intensification</i>	5. <i>Simplification (change early-on)</i>	9. <i>Tolerance</i>
2. <i>Substitution</i>	6. <i>Avoiding knock-on effects</i>	10. <i>Ease of Control</i>
3. <i>Attenuation</i>	7. <i>Making incorrect assembly impossible</i>	11. <i>Ease of Administrative Controls /Procedures</i>
4. <i>Limitation of effects</i>	8. <i>Make Status Clear</i>	

Substitution is replacing in a process, hazardous materials by less risky ones. This can pertain to solvents like water based paints versus products on the basis of organic solvents, but it can also mean that the whole chemistry of a process is changed.

Attenuation or moderation means using materials with hazardous properties under conditions, which make them less hazardous, e.g. in dilution (sulfuric acid instead of oleum) or “packaged” in porous grains or cryogenic instead of under pressure as propene. This should of course not be in conflict with the principle of intensification. *Limitation of effects* is also brought under *moderation*: It comprises the kind of measures that come under the heading of passive protection as placing walls and dikes as well as isolation by siting, which

means taking sufficient distance between locations where hazardous materials are handled or stored.

Further keywords can be summarised under the headings *simplify* and make things easier: the Keep It Simple and Safe or KISS principle. This has much to do with “human factors”.

Hierarchical approach in reducing safety and environmental risks

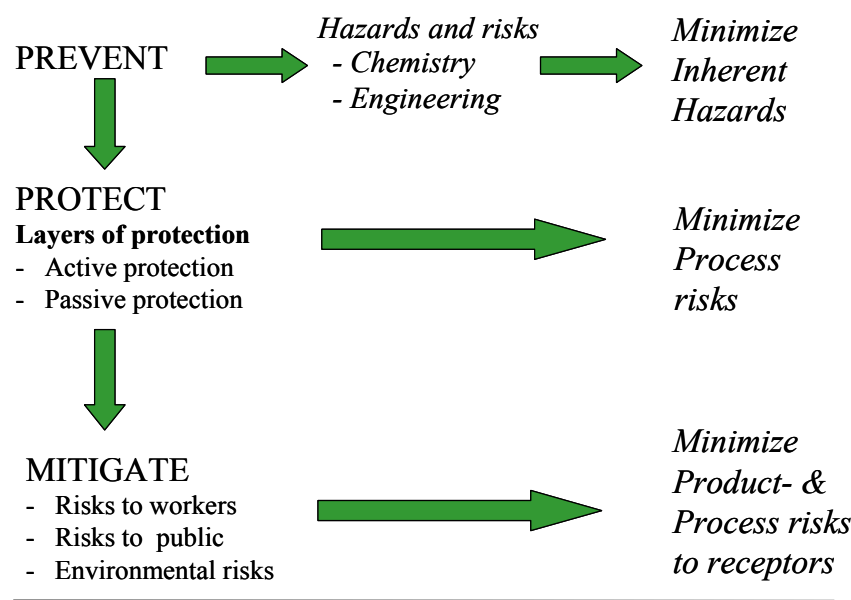


Fig 3. When considering risk reduction, start with rethinking fundamentally the process. Can there be inherent improvements? Subsequently the question can be asked which protective measures can be taken and finally what mitigation is possible.

Protection can be active and passive. Active protection applies to a device that functions to restore a safe state in case a deviation of the normal process conditions threatens to arise. In passive protection the hazard is eliminated or minimised by design features that reduce mostly the consequence. Both types can be by technical provisions or organisational /procedural by rules. Protective measures come usually in a series of one acting after the other. This is called layers of defence, barriers or layers of protection. The concept of *Layers of Protection Analysis, LOPA*, shall be examined together with procedural measures of protection below.

Mitigation is reducing the risk to people and environment by e.g. rapidly dispersing and diluting a toxic or explosive cloud by applying steam or water “curtains”.

2.4 Layers of Protection Analysis

Layer Of Protection Analysis (LOPA) which was put forward and promoted by the Center for Chemical Process Safety of the AIChE in New York^[9], starts by defining a scenario and analysing which *independent* protection layers (IPL's) are in place. The concept of LOPA can be depicted as in Figure 4. The independence is not easy to guarantee. It means that whatever happens, the layer will be still there to protect when the previous one has failed. There is of course a finite probability that also this layer will fail under the impact of the incident effects.

As we have seen protection can be *active* or *passive*. Examples of active protection are controls, safety interlocks or emergency shutdown systems and measures like rupture disks. In passive protection, however, nothing needs to actively function. Equipment is designed such that it can withstand effects of unwanted incidents. For example, a reactor wall can be designed such that it is strong enough to withstand the pressure generated by a (thermal) explosion or the reactor can be placed in a strong concrete cubicle.

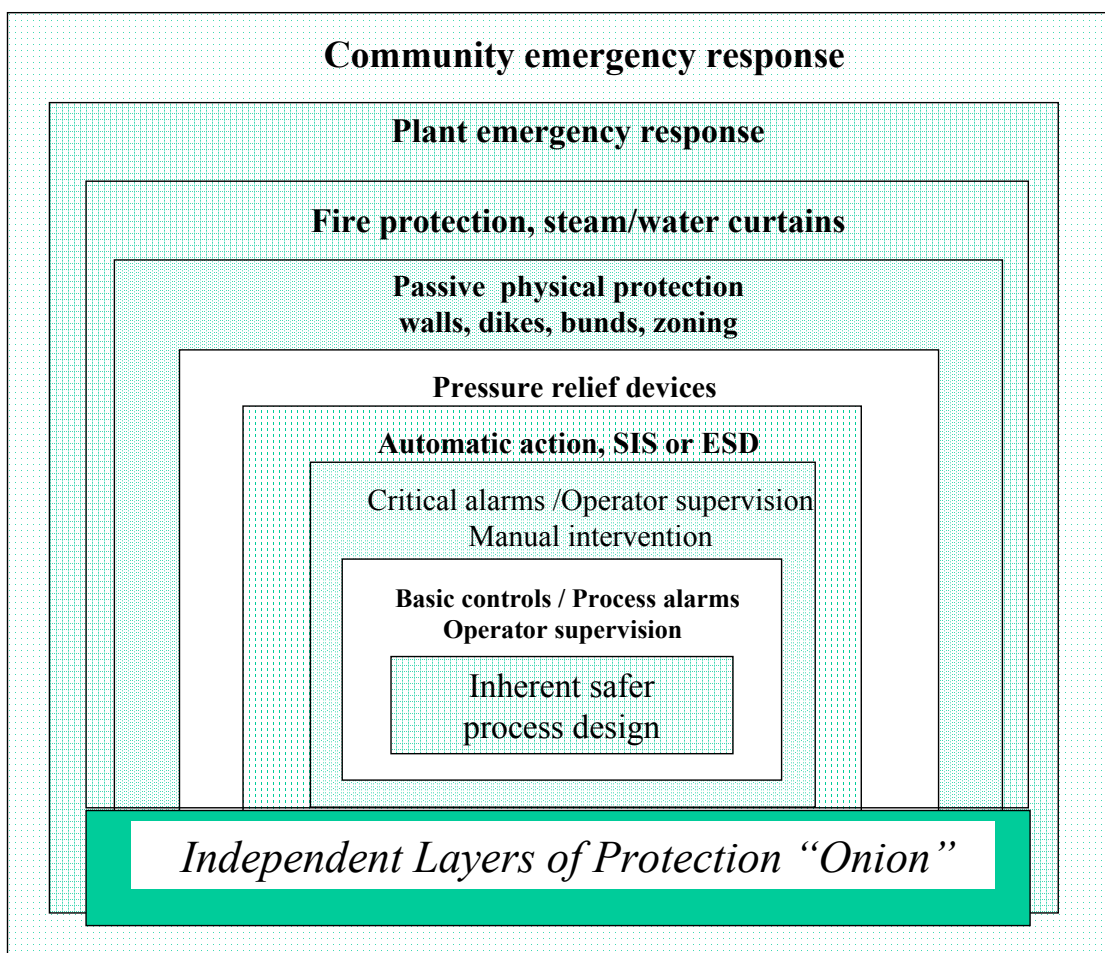


Fig 4. Layer of Protection concept in which the various layers are portrayed as the concentric peels of an onion.

Protective measures are usually designed in a hierarchical series and such that each measure acts consecutively to the former one, thus backing it up. The layers can also include mitigation measures. These start functioning as soon as damage occurs and either reduce or limit the final damage or injury, or enable fast recovery, e.g. the fire brigade.

The innermost core of the concept is inherently safer process design. Good design, however, requires further robust engineering. It also includes an organisational safety system with effective procedures: a Safety Management System, and the availability of high quality operators and maintenance personnel. As a first layer of active protection, a basic control system should be installed with one or more sensors, logic controllers, and actuators, with process alarms and operator supervision. The next layer consists of critical alarms and manual intervention. The probability of human error leading to a hazardous situation can be lowered by an additional layer consisting of an automatic action, high integrity safety instrumented system (SIS), which can take several forms as for example the safety interlock system or emergency shutdown (ESD), but which usually are costly.

A further, additional layer can be obtained by mounting e.g. an emergency pressure relief. Subsequently, also a passive structural safety system can be built, like a concrete bunker, safe haven (off-shore), fire and blast wall, and suitable lay-out and zoning (hazardous area classification with zones 0, 1 and 2 for flammable gas/vapour-air or 20, 21, and 22 in case of combustible dust-air mixtures). The size of zoning depends on the flammable or explosive class, which in turn is determined by properties such as flash point, etc. Zoning also determines the level of explosion safety of electrical apparatus. Fire protection can be installed (smoke detection, sprinklers, fire resistant materials) and mitigation means can be applied, such as water sprays or steam curtains when toxic or flammable vapours may escape. As mitigating layers, an emergency response should be organised both for inside the plant and the community outside.

As in a Hazard and Operability study, a multidisciplinary team with e.g. representation of operations, maintenance, management, process and chemical engineering, instrumentation and electrical engineering performs a LOPA. The team is completed with a risk analyst. On the basis of a HAZOP or another potential incident identification analysis or cause-consequence analysis, the frequency and severity of an initiating event for a given scenario are determined. Then Independent Protection Layers (IPLs) (or Layers of Protection: LOPs) are defined and their Probability of Failure on Demand (PFD) determined. The latter includes not only equipment reliability, but also human error. The team can quantify the probabilities of the incident and those of failure of the layers and hence determine a residual risk.

2.5 Safety Management System

The organisation of safety has become at least as important as technical safety of equipment. Attention of management to safety matters has proved to be of utmost importance. It is a major improvement in the past ten years that this has been understood in top management of many large companies. SHE (Safety, Health and Environment) shall be no less important than production, quality, cost and personnel^[10]. It shall reflect in installing a safety management system in production as well as in trans-shipment or storage facilities.

The critical ingredient is management leadership directed towards the desired level of safety performance. Management systems are comprehensive sets of policies, procedures and practices designed to ensure that barriers to major incidents are in place, in use and effective. The functions to be distinguished are planning, organising, implementing and control with feed back: *Plan, do, check and act*. An SMS is therefore a true management system. According to an early CCPS publication ^[11] on this topic a SMS contains twelve elements:

1. *Accountability*, i.e. clarity in objectives, (who is responsible for what, which lines of communication, how to report and audit),
2. *Process knowledge and documentation*, records of design criteria and management decisions,
3. *Critical project review* and design procedures for new or existing plants, expansion and acquisition,
4. *Process risk management*, incl. encouragement of clients and suppliers to conform,
5. *Management of change* of technology, facility or organisation, both temporary and permanent,
6. *Process and equipment integrity* (reliability, materials, installation, inspection, maintenance, alarms),
7. *Human factors* (error assessment, task design, man-machine interface, ergonomics),
8. *Training and performance* (development of programs, design of procedures, manuals),
9. *Incident investigation* (near-miss reporting, accidents, follow-up),
10. *Standards*, codes and laws (in-and external),
11. *Audits* and corrective actions,
12. Enhancement of process safety knowledge by *research* and improvement of predictive techniques.

Fig. 5 depicts the “institutionalization” of “lessons learned” and the “ploughing back of experience” by three feedback loops with increasing time constant: *Control, correction and improvement*. In fact, if the culture of a team and company would welcome openness, talk about things that can go wrong, carry out near-miss reporting and audit at various levels and in an organised way, most of the advantages would be realised.

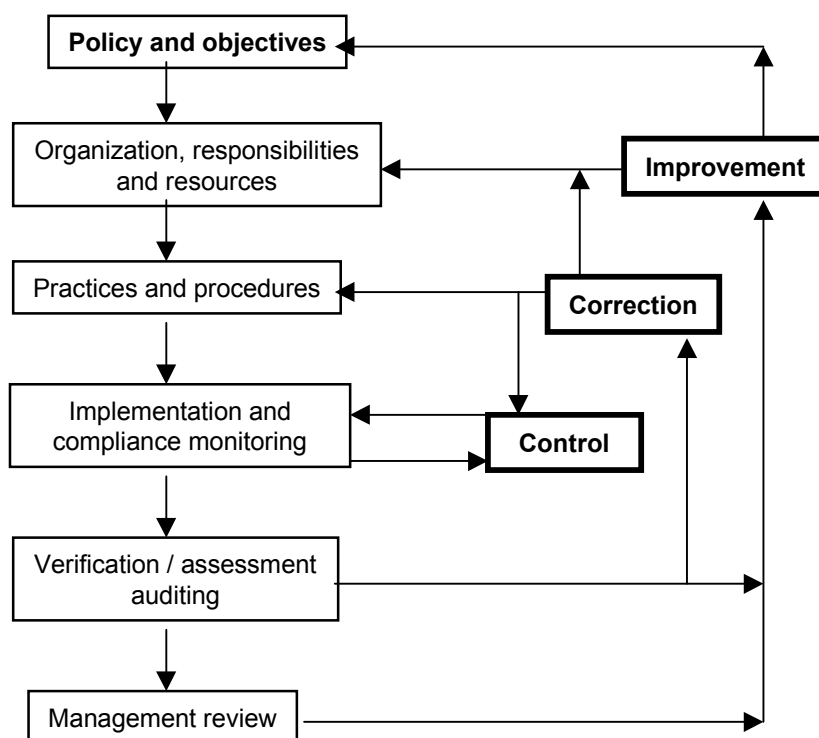


Fig 5. Typical structure of key elements in a safety management system; source Fröhlich EPSC Safety Management Systems, IChemE publ. 1994 ^[9].

A brief word on Human factor: Yes, we can make errors. Even I can do it myself. I can do things in a routine activity, which I never would think I could do wrong. Make it therefore easy and simple.

There has been done much to provide techniques for improving human behaviour with respect to motivation, social climate and environment, personnel management, instructions (not too lengthy) and procedures (clear), avoiding stress and alcohol or drugs, adequate training, quality of provided information, discipline, checking performance. Then there is a five-step method for short-term *behaviour modification*, on the same principle as the control loop:

1. Find concentrations of accidents
2. Revise safety rules and working procedures
3. Develop a plan of action
4. Realise the plan
5. Install efficiency controls.

In general four types of *unsafe human acts* are distinguished: Slips (of the mind), lapses (of the memory, something not carried out), mistakes (the wrong thing done by lack of knowledge or bad procedure), and circumvention (because "I am better, it will not happen to me" –attitude).

Fundamental to safety thinking is to systematically plough back experience with accidents and near-misses. "Lessons learned" and case histories are also basic to education and training.

Education and training should also ensure that the operator has the right mental model of the process. Errors of representation have been quite common in the control room: the operator thinking the process functions a certain way, but reality being different. This can include non-identified risks. Process control is also often not optimal; too many alarms installed leading to alarm avalanches in case of process upset, too many false alarms occurring, insufficient overview, and where it is necessary, insufficient detail; unclear instruction manuals, too much stress when the process really jams. For training purposes simulation of a running-out-of-hand scenario by computer is helpful.

Although most human factor work has been centred around the individual, more attention is given to teamwork. Safety culture has become a topic: team spirit, positive attitude, and discipline.

Many accidents showed as a precursor minor deviations from normal routine, and small defects in combination with a less-safety conscious attitude. The defects in itself have nothing to do with the coming event, but these require attention and therefore distract concentration from the main error. Wagenaar and Reason developed a predictive tool to detect latent, or dormant failures and negative attitude in a team like in the project called *Tripod* by Wagenaar & Reason c.s., Leiden/Manchester,^[12] for Shell. This has developed to a tool for Human Factor assessment by measuring performance through the scores in a Basic Risk Factor (BRF) -profile of a team or even a company in a so called Tripod condition review, reflecting the effectiveness of a SMS. The BRF's are in prevention (Design, Tools & equipment, Maintenance, Housekeeping, Error enforcing conditions, Procedures, Training, Communication, Incompatible goals, Organisation) or mitigation (defences). The information is collected by means of a questionnaire and the answers treated statistically.

The scores run from 0 to 100. A version of the method has been developed for investigating incident causation called TRIPOD Beta. The three “feet” of the method are the incident itself, active failures and latent failures. Active failures are physically noticeable and appear usually shortly before the accident. They consist of breached system barriers and unsafe acts. Barriers, also called layers of protection or defences, are systems or devices like (active) control systems, and overpressure vents, which act in case of an incident. These have a finite reliability, already because of infrequent use. So they may fail due to local technical faults, atypical conditions, and severe environmental conditions. Latent failures cause preconditions for the accident. Preconditions are conditions, which determine how readily an error is committed, e.g. a state of stress, poor motivation, or ignorance. Line management can influence them. The causes may have been in the organisation already for a long time and may be attributed to wrong decisions of designers and planners. Even further in the past may be scene setting for fallible decisions of top-level decision-makers. Unsafe acts are by personnel in direct contact with the equipment or structure, which lead up to the accident. The whole sequence is illustrated in Figure 6.

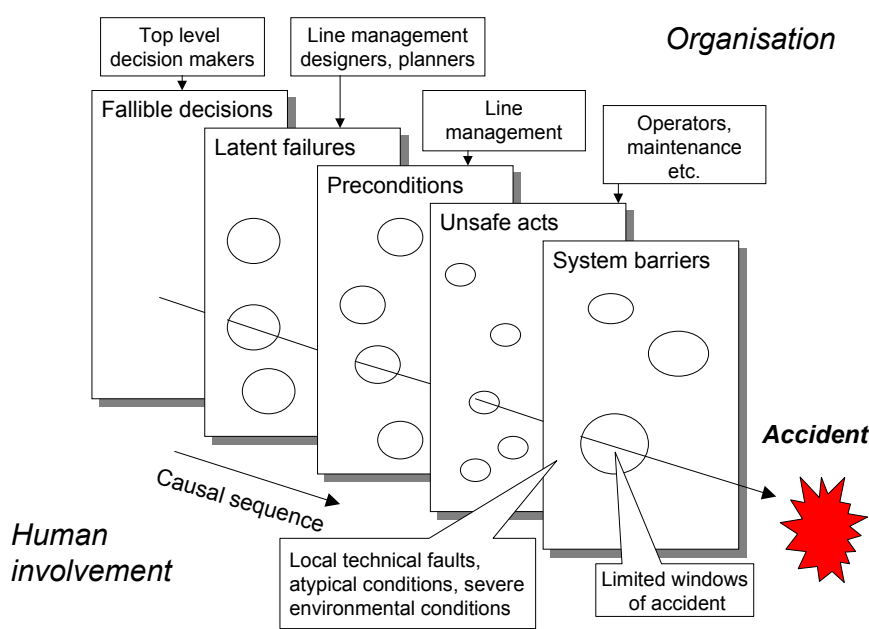


Fig 6. Accident causation sequence as seen in the Tripod model ^[13].

3. SPECIFIC HAZARDS ENERGETIC MATERIALS

3.6 Properties of EM

About explosive potential little has to be said. There is a mass of knowledge available. Each country which has a manufacturing capability will have had an author writing his own compendium on explosive performance. Sometimes the thought may come up, we have seen it all. However there is still much unexplored terrain, so there will be new surprises. Low vulnerability explosives may not behave so low vulnerable when applied in masses and new more powerful explosives may be developed.

From a hazard point of view initiation is more interesting. It still is despite the many investigations rather unpredictable when the question is asked, is initiation possible in this particular situation? The standard tests for impact, friction, and spark initiation produce figures which give a ranking order but do not say very much when they would be translated to a particular situation. The hot spot theory will now be 60 years old and indeed there is some correlation between initiation sensitiveness and the thermal reactivity, but physics and chemistry interact also in this domain sometimes rather unpredictable.

About toxic properties of explosives much less is known. For acute toxicity there is not that much to fear. Many cyclic nitro-compounds and aromatic amines are carcinogenic though. Strong carcinogenicity is often related with an easily oxidisable amino-group or reducible nitro-group. In particular the latter is suspect. Some explosives are allergenic to some people. Tetryl is an example. The SIRI MSDS (Material Safety Data Sheets), data base, <http://hazard.com/msds/> and RTECS (Registry of Toxic Effects of Chemical Substances), <http://ccinfoweb.ccohs.ca/rtecs/search.html> may give information.

3.7 Cook-off; Run away processes

Thermal explosion theory is assumed to be known and the Semenov and Frank-Kamenetskii models will not be explained here. Cook off is basically a test to investigate the behaviour of an EM in a fire. It sets off a thermal explosion under input of heat and confinement of the material. The heat input makes the substance to start decomposing exothermally at a sufficiently high temperature, the confinement by e.g. a steel wall makes the effect of blast and fragments at the end of the reaction much worse. The temperature and the amount of confinement depend on the properties of the specific EM involved. Some start at a relatively low temperature and have a moderate effect; some others a violent, others decompose only at much higher temperature, but in the end all go. The larger the diameter of the mass, the less steel confinement is necessary to get the effect. The slower the heating is the more violent the effect. Some EM's can pass from a local thermal explosion into a deflagration, which can even transit into a detonation. All these processes can be quantified to some extent.

The strength of the blast can be characterised and expressed in peak shock pressure and impulse at a certain distance from the explosion point and translated into a TNT-equivalent. The effect of the blast on "targets", such as structures can fairly well be calculated, given peak pressure and impulse. For the fragments prediction is more problematic, since the initial fragment distribution and the initial fragment speed have to be known. Estimates can be made on the basis of the TNT-equivalent. So, in general protective structures can be designed quite well. It is however recommendable to test a mock-up prototype with a real charge to see whether a protection really works.

The next part will be on run-away of a synthesis process, a frequently occurring type of accident. Basically this is also an exothermal decomposition and usually is considered as a Semenov type of thermal explosion, since the temperature gradients in a stirred reactor vessel remain small. There is a great variety of causes of run-away:

- *chemical*: run-away can typically occur in polymerisations (almost 50% of reactor accidents), nitrations, sulfonations, Grignard diazotation reactions, and (Friedel and Craft) alkylations. Further there are runaways found in aminations, halogenizations, oxidations, hydrolyses. Aside from polymerisations, it is often not the reaction desired that is causing the trouble, but a decomposition reaction or oxidation starting at a higher than usual temperature and having a higher energy of activation than the intended reaction. The runaway starts with self-

heating after decomposition is initiated by a chemical effect. This can be the addition of wrong reactant into the reactor or by dosing in the wrong sequence, an overdose of e.g. catalyst or many other causes like undue delay in start of reaction and accumulation of reactant by too cold a mixture or too slow a dosing. Also by initial decomposition autocatalytic products may have formed or the reaction mix got contaminated because the remains from previous batches have not been cleaned out in advance or otherwise.

- *physical*: stratification, a sudden lack of cooling, or faulty control of temperature may cause runaway. The heater may have been on unnoticed or the reactor is exposed to fire, the stirrer drive may have failed, the stirring was not switched on, or switched on too late. There might have been a lack of maintenance: leaking of materials, plugging of pipes, water remains after cleaning etc.

Since batch reactor mishaps can have many causes, such a reactor has to be safeguarded by a control system and emergency measures. As regards the chemical nature of the batch a practical safety criterion parameter has been developed that characterizes the dynamic performance of the reaction. This is the *Barklev number*: $B = E \Delta T_{ad} / RT^2$, in which E is activation energy of the reaction, ΔT_{ad} the adiabatic temperature rise of the reaction, R is gas constant and T is the operating temperature. It means that the hazard of runaway increases when the energy of activation is high, the maximum, hence adiabatic temperature rise high, or the reactor temperature low. (In the latter case it is more sensitive to failure of cooling) Batch processes with B -values < 5 are non-critical and semi-batch with $B < 10$ are non-problematic^[14]. In other cases the reactions should be studied further by additionally examining the *Damköhler* and *Stanton* number, see also ^[15, 16].

In case a secondary reaction is possible it is important to determine the temperature, T_{sec} , at which the secondary reaction becomes noticeable. This temperature should be compared with the maximum possible temperature that the mix can achieve by the *primary* reaction:

$$T_{sec} > T_{max,prim} = T_{reaction} + \Delta T_{ad,prim}$$

If this condition cannot be fulfilled risk reducing measures have to be installed.

It makes sense to perform screening tests with the unstable substances involved. Chemistry and chemical thermodynamics (ASTM E27.07 CHETAH code version 7.0, 1994) can predict the possible occurrence of exothermic reactions and quantify their magnitudes. But whether this potential reaction will in reality occur and its rate of occurrence - both critical to the occurrence of an explosion - is a matter of chemical kinetics. Chemical rates as a function of temperature and other factors (e.g. catalytic effects!) are notoriously difficult to predict. Since prediction from first principles is usually not possible, many empirical techniques have been developed using small quantities. A widely applied test method is Differential Thermal Analysis (DTA). Or DSC, Differential Scanning Calorimeter. DTA is normally done at constant pressure, i.e. in an open system. Not surprisingly, it is also possible to test in a closed system and thus also measure pressure and sample the gas phase evolved. A screening test that has become quite popular the last few years is the Adiabatic Rate Calorimeter or ARC. For descriptions, see the CCPS Guideline on Reactive Chemical Hazards^[17].

When laboratory experiments are carried out to determine the values of various reaction parameters it is important to be able to measure the heat generation rate in a test environment, which is as close to adiabatic as possible. The Adiabatic Rate Calorimeter, ARC, produces in many cases a fair approximation, but for initially low heat productions it is too insensitive. In Bench Scale Reactors, BSR, the reaction patterns can be studied more reliably and the heats of reaction measured. However, there remains always a scaling-up problem, since in an industrial scale reactor temperature equalisation is limited despite efficient stirring.

3.8 Risk reduction

There are several possibilities to prevent, protect and mitigate. In the first place to prevent cook-off it is important to store flammable liquids separately and have means of fire fighting available. A deflagration can only be stopped by massive cooling. Oxygen depletion does not help. With respect to a run-away detection in a very early stage is very helpful, but not easy to realise. Run-away can come “as a thief at night”. Because many industrial reactor systems are multi-purpose, protection should be general and therefore much work has been done on emergency relief venting in particular in the industrial co-operation DIERS: Design Institute for Emergency Relief Systems. For a recent overview, see ^[18].

As a further measure one can go from batch to continuous operation. The chance of run-away and its effects are in that case much less.

3.9 Toxics and other hazards of solvents

Beside the EMs there are the solvents to pay attention too^[19]. Take-in can be by inhalation and through the skin (percutane). By now everyone will know that toluene replaces benzene and di-chloro-methane replaces chloroform and tetra-chloro-carbon, although the MAC-value (maximum allowed concentration for the 8 hour per day worker) of the latter is still 40 ppm. Acetone and diethylether are the safest to use from a toxic point of view although the latter one can develop over time as known an EM itself – a peroxide, if in contact with air. Modern solvents are (polar) acetonitril, (polar) dimethylformamide (DMF), (dipolar) dimethylsulfoxide, (in all mixture ratios miscible with water) 1,4-dioxane, (dipolar) hexamethyl-phosphoric acid-triamide (HMPA), and (as a replacement of di-ethylether in various organic synthesis, also at higher temperature) tetrahydrofurane. All of these have MAC-values which are quite low (10-50 ppm), except DMSO, HMPA and THF. The latter has a MAC-value of 100 ppm and is possibly carcinogenic, while HMPA is suspect carcinogenic. Acetonitril and DMF can react violently in some situations; DMSO can be flammable at higher temperature; and dioxane and THF are auto-oxidising and form peroxides even more rapid than di-ethylether.

In general the advice is to have sufficient ventilation, at least 5 times per hour, to work with gloves and to pay attention to the peroxide formation in THF and dioxane.

3.10 Protective structures and personal protection

To just mention a few key words:

- Separate and compartmentalise both operation and storage.
- Don't expose more people than is strictly necessary
- Maintain good housekeeping, order and cleanliness
- Have sufficient means for personal protection (face mask, gloves, protective clothing) and fire protection
- Obey the gas explosion safety zoning and corresponding equipment requirements
- Write an emergency procedure and practice it, including extinguishing a laboratory fire.

4. CONCLUSION

1. Safety is investing in one's own future. Cutting curves is tempting and in the short term an advantage. With EM's some day by some trigger not understood, the potential gets loose. Hence protect against the possible effects
2. By simple risk analysis and scenario thinking incidents may be identified as a possibility before they actually happen. Risk reduction measures can be considered.
3. By layer of protection approach one can systematically invest in protective provisions and be able to make cost-benefit analysis.
4. With EM thermal stimuli direct or indirect are to be avoided, since these are the common trigger. Solvents have to be given careful attention. Potential explosion effects can better once be simulated in some kind of mock-up.

REFERENCES

- [1] SCHUPP, B.A., S.M. LEMKOWITZ, L.H.J. GOOSSENS, A.R. HALE, and H.J. PASMEN: Modeling safety in a distributed technology management environment for more cost-effective conceptual design of chemical process plants, in European Symposium on Computer Aided Process Engineering – 12, ELSEVIER SCIENCE BV: Amsterdam. p. 337, 2002
- [2] JOHNSON, W.G.: "MORT - The Management Oversight and Risk Tree", Journal of Safety Research, March, Vol. 7, No. 1, 4 – 15. b) JOHNSON, W.G., 1980, "MORT Safety Assurance Systems", Marcel Dekker, New York, 1975,
- [3] LEWIS, R.J., Sax's dangerous properties of industrial materials, 8th ed, Van Nostrand Reinhold, New York, 1992
- [4] URBEN, P. (editor): Bretherick's Reactive Chemical Hazards, 5th Edition Handbook (and Software Version 2.0 on disk or CD-ROM), Butterworth Heinemann, Standard reference, ca. 2100 (!) pages, 1995

- [5] Dow's Fire and Explosion Index Hazard Classification Guide, F&EI, and Dow Chemical Exposure Index, CEI, AIChE Technical Manual LC 80-29237, New York, 1994.
- [6] F. CRAWLEY, M. PRESTON and B. TYLER, "HAZOP: Guide to best practice, guidelines to best practice for the process and chemical industries" European Process Safety Centre, to be obtained from IChemE, 165-189 Railway Terrace, Warwickshire CV21 3HQ, U.K, ISBN 0 85295 427 1, 2000
- [7] "Methods for the Determination of Possible Damage to People and Property by the Release of Dangerous Substances", (the "Green Book"), CPR 16E, SDU Uitgevers Den Haag, the Netherlands, First edition, ISSN 021-9633;16, 1990
- [8] KLETZ, T., 1989, "Friendly plants", Chem. Engrg. Progr., July, 18-26; b) KLETZ, T., 1991, "Inherently safer Plants, an Update", Plant Operations Progress, 10, No.2, April, 18-26; c) KLETZ, T., 1991, "Plant Design for Safety", Hemisphere Publ. Corp., N.Y.; d) KLETZ, T., 1998, "Process Plants: A Handbook for Inherently Safer Design", Taylor & Francis, Philadelphia, PA.
- [9] "Layer of Protection Analysis: Simplified Process Risk Assessment", Guideline CCPS, AIChE, New York, ISBN 0-8169-0811-7, 2001
- [10] FRÖHLICH, B. et al., *"Safety management Systems"*, IChemE, Davis Building, 165-189 Railway Terrace, Rugby, Warwickshire CV21 3HQ, UK, ISBN 0 85295 356 9, 1994
- [11] *"Guidelines for Technical Management of Chemical Process Safety"*, Center for Chemical Process Safety (AIChE), 345 East 47th Street, New York, NY 10017, ISBN 0-8169-0423-5, 1989
- [12] HUDSON, P.T.W., GROENEWEG, J., REASON, J.T., WAGENAAR, W.A., Van der MEEREN, R.J.W. and VISSER, J.P.: *"Application of TRIPOD to Measure Latent Errors in North Sea Gas Platforms: Validity of Failure State Profiles"*, First Int'l Conf. on Health, Safety and Environment, Soc. Petr. Eng., The Hague, NL, 10-14 November, 725 – 730, 1991
- [13] Van der WANT, P.G.D., "Tripod incident analysis methodology", Safety Performance Measurement, Conf. European Process Safety Centre, Paris, October, 99 – 109, ISBN 0 85295 382 8, 1996
- [14] GREWER, T. et al.: "Determination and assessment of the characteristic values for the evaluation of the thermal safety of chemical processes", J.Loss Prev. Proc. Ind., Vol 2, 215-223, 1989
- [15] STEENSMA, M. and WESTERTERP, K.R.: "Thermally Safe Operations of a Semibatch Reactor for Liquid-Liquid Reactions. Slow Reactions", Ind. Eng. Chem. Res., Vol. 29, No. 7, 1259-1270, 1990
- [16] STEENSMA, M. and WESTERTERP, K.R.: "Thermally Safe Operations of a Semibatch Reactor for Liquid-Liquid Reactions - Fast Reactions", Chem. Eng. Technol., 14, 367-375, , 1991
- [17] CCPS, 1995, *"Guideline on Reactive Chemical Hazards"*.
- [18] FAUSKE, H.K.: *Emergency relief system design for reactive and non-reactive systems: extension of the DIERS methodology*", Plant/Operations Progr., 7, (3), 153 - 158, 1988
- [19] As can be found in textbooks on laboratory safety. Citation here from Zwaard, W. et al., "Gevaren in het laboratorium", ten Hagen & Stam, Den Haag, the Netherlands, ISBN 90-71694-46-1, 1990

INFLUENCE OF TAMPING ON PERFORMANCE OF LINEAR SHAPED CHARGES

Z. Akštein and L. Říha

Research Institute Of Industrial Chemistry
Explosia a.s., 532 17 Pardubice-Semtín, Czech Republic

Abstract:

Nowadays we are often confronted with limitation of quantity of explosives in terms of protection of surroundings, hygienic standards etc. Linear shaped charges (LSC) as such represent significant reduction in quantity of explosives (when compared with open charges) at blasting work, especially at demolitions of metal structures. Further decrease in quantity of explosives is achieved by tamping. This report deals with finding of relationship (represented by cavity depth produced by jet of LSC in steel plate with 30 mm thickness) between tamped and open LSC of the same performance.

Keywords: linear shaped charge, tamped charge

1. INTRODUCTION

It is a well-known fact from blasting profession that tamped charge delivers higher performance than equal open charge. This fact is also known in the field of LSC.

The basis of this work was comparing the performance of prepared open LSCs and their tamped equivalents, which were prepared by following the calculations of Gurney equations for the mass accelerated by explosive. Performance was defined as a cavity depth produced by LSC jet in steel plate with 30 mm thickness.

As already mentioned, the basis of this work was the study of R.W.Gurney about the mass accelerated by explosive at different arrangements, or, more precisely, his empiric equations. Equation for asymmetrical sandwich and its subsequent modification were used for our arrangement.

$$\frac{v}{\sqrt{2E}} = \left[\frac{1 + A^3}{3 \cdot (1 + A)} + \frac{N}{C} \cdot A^2 + \frac{M}{C} \right]^{-\frac{1}{2}} \quad A = \frac{1 + 2 \cdot \frac{M}{C}}{1 + 2 \cdot \frac{N}{C}} \quad (1, 2)$$

Where v - velocity of plate M,
 $\sqrt{2E}$ - Gurneyho velocity,
 M - weight of accelerated plate,
 C - weight of explosive,
 N - weight of tamping layer.

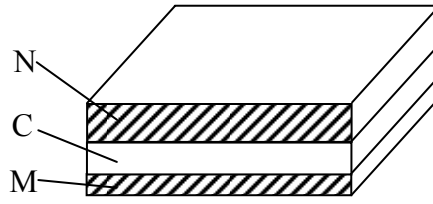


Fig 1. Asymmetrical sandwich: M - accelerated plate; C - explosive; N - tamping layer.

Open face sandwich

Equation for open face sandwich was used to calculate parameters of open LSC. We obtain this equation after modification of equations (1) and (2), where $N = 0$.

$$\frac{v}{\sqrt{2E}} = \left[\frac{\left(1 + 2 \cdot \frac{M}{C}\right)^3 + 1}{6 \cdot \left(1 + \frac{M}{C}\right)} + \frac{M}{C} \right]^{-\frac{1}{2}} \quad (3)$$

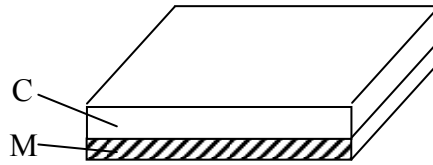


Fig 2. Open face sandwich: M - accelerated plate; C - explosive.

Dependence of $v/\sqrt{2E}$ on M/C ratio according to equation (3) is presented on Fig.3. It is evident, that at reducing the quantity of accelerated mass M acceleration becomes higher, but only up to the limit value $v/\sqrt{2E} = 1/\sqrt{3}$ (for $M/C \rightarrow 0$).

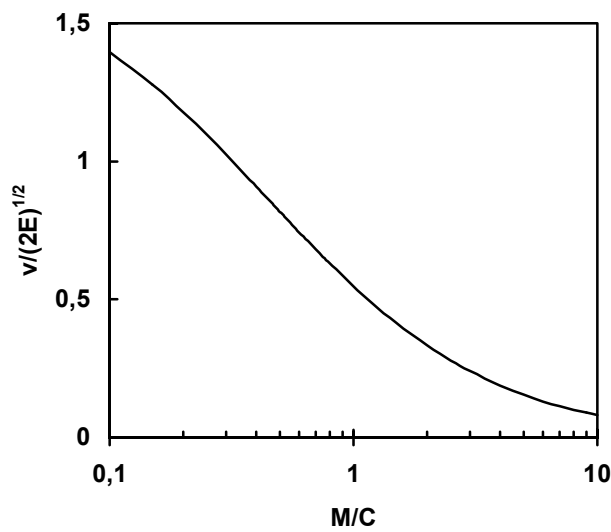


Fig 3. Dependence of mass acceleration on M/C ratio for open face sandwich.

Dependence of kinetic energy E_K of accelerated material on M/C ratio at constant quantity of explosive C is shown at Fig.4. The maximum is evident for value $M/C = 0.5$. The M/C value area 0,3 - 0,7 is usually the starting point for construction of LSC.

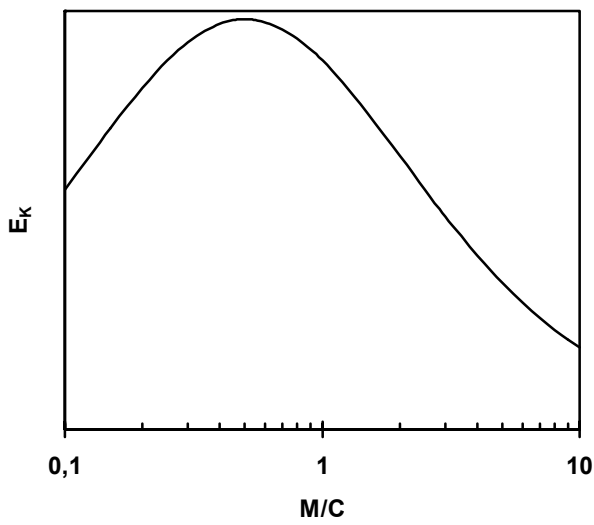


Fig 4. Dependence of kinetic energy E_K of accelerated material on M/C ratio at constant quantity of explosive C for open face sandwich.

Symmetrical sandwich

This arrangement was used for tamped LSC’s design. In case that mass of tamping layer N is similar to the mass of accelerated material M we obtain simpler equation:

$$\frac{v}{\sqrt{2E}} = \left[\frac{1}{3} + 2 \cdot \frac{M}{C} \right]^{\frac{1}{2}} \tag{4}$$

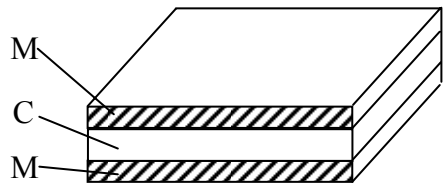


Fig 5. Symmetrical sandwich: M - accelerated material, tamping layer; C - explosive.

Dependences of $v/\sqrt{2E}$ and kinetic energy E_K of accelerated material on M/C ratio at constant quantity of explosive C are compared with the same dependences for open face sandwich (dotted line) on Figs. 6 and 7. The course of function (4) is similar to that of open face sandwich (3). A difference is evident only when comparing kinetic energy E_K of accelerated material. It is evident here, that the tamping layer of symmetrical sandwich is worth using for M/C values higher than 0.25 only.

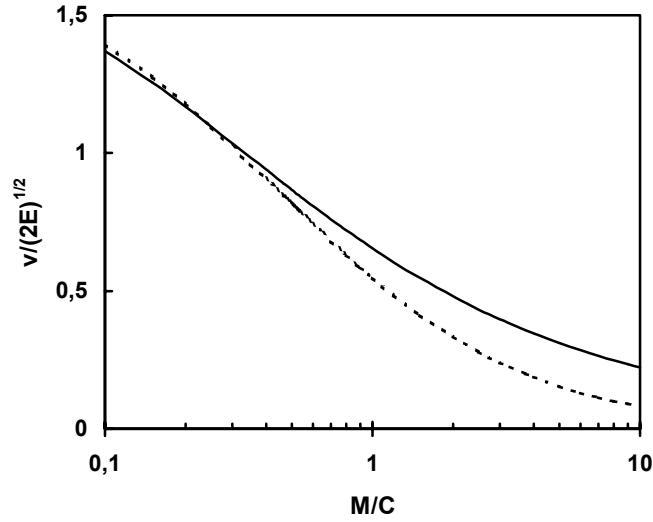


Fig 6. Dependence of mass acceleration on M/C ratio: full line - symmetrical sandwich; dotted line - open face sandwich.

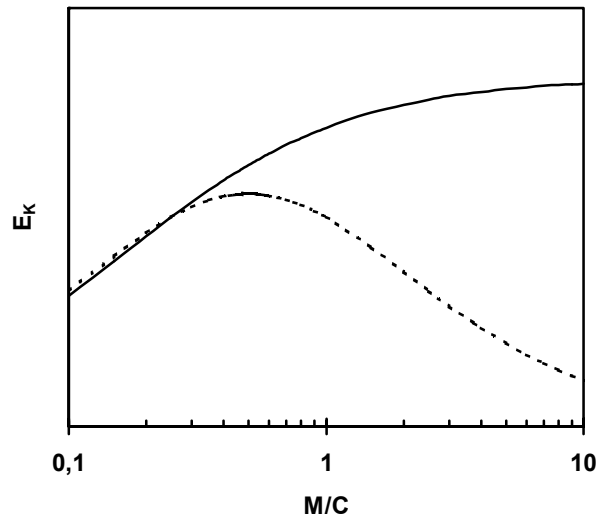


Fig 7. Dependence of kinetic energy E_K of accelerated material on M/C ratio at constant quantity of explosive C : full line - symmetrical sandwich; dotted line - open face sandwich.

Asymmetrical sandwich

If we keep increasing tamping ratio N/M , the velocity and kinetic energy of accelerated material will increase too. This can be seen at Figs. 8 and 9. Dependences of $v/\sqrt{2E}$ and kinetic energy E_K of accelerated material on M/C ratio at constant quantity of explosive C and tamping ratio $N/M = 2$ are compared with the same dependences for symmetrical sandwich (dotted line) and for asymmetrical sandwich with tamping ratio $N/M = 4$ (dashed line).

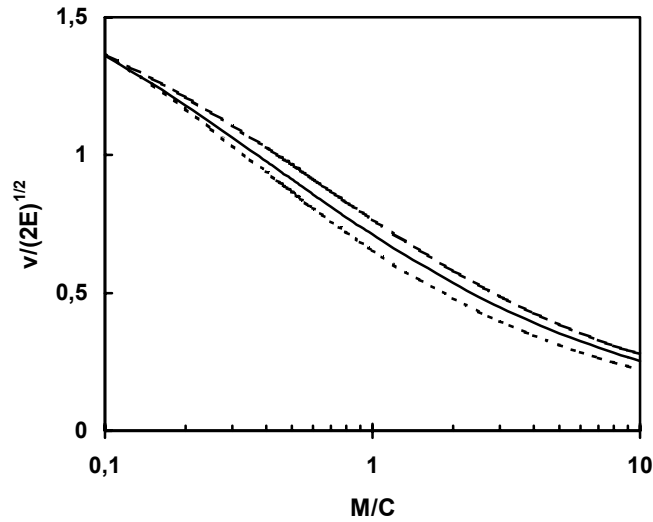


Fig 8. Dependence of mass acceleration on M/C ratio: full line - $N/M = 2$; dashed line - $N/M = 4$; dotted line - symmetrical sandwich ($N/M = 1$).

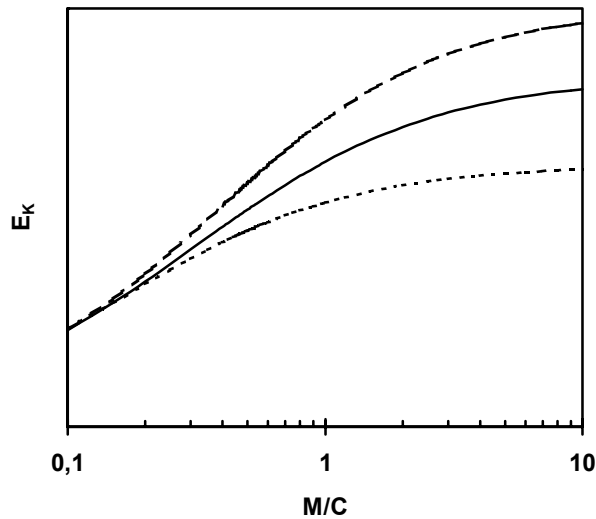


Fig 9. Relation of kinetic energy E_K of accelerated material on M/C ratio with constant quantity of explosive C solid line - $N/M = 2$; dashed line - $N/M = 4$; dotted line - symmetrical sandwich ($N/M = 1$).

2. EXPERIMENTAL

Design of LSC

3 types of LSC were designed for our experiments.

Open charges were designed with ballistic ratio ($C/M!$) 1.5.

Tamped charges were designed with tamping ratio $N/M = 1$. Height of explosive layer was designed so that the final velocity of liner responds with the liner velocity of open

charge liner. In our case the following equation obtained after modification of equations (3) and (4) was used:

$$C_T = \frac{2M}{\frac{\left(1 + 2 \cdot \frac{M}{C}\right)^3 + 1}{6 \cdot \left(1 + \frac{M}{C}\right)} + \frac{M}{C} - \frac{1}{3}} \tag{5}$$

where C - weight of explosive layer of open charge
 C_T - weight of explosive layer of tamped charge
 M - weight of liner

A - LSC with constant thickness of explosive layer

	Open variant	Tamped variant
Thickness of liner	1.0 mm (M = 7.80)	1.0 mm (M = 7.80)
Thickness of explosive layer x	7.5 mm (C = 11.63)	5.9 mm (C _T = 9.15)
Thickness of tamping layer	-	1.65 mm (N = 7.76)
Length of side of explosive layer L	15 mm	
Stand-off distance	11 mm	

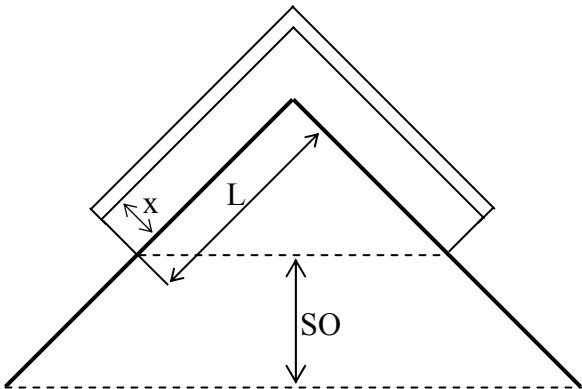


Fig 10. LSC type A: x - thickness of explosive layer; L - length of side of explosive layer; SO - stand-off distance.

B - LSC with decreasing thickness of explosive layer

	Open variant	Tamped variant
Thickness of liner	1.0 mm (M = 7.80)	1.0 mm (M = 7.80)
Thickness of explosive layer x ₁	8.5 mm (C ₁ = 13.18)	6.9 mm (C _{T1} = 10.70)
Thickness of explosive layer x ₂	6.5 mm (C ₂ = 10.08)	4.8 mm (C _{T2} = 7.44)
Thickness of tamping layer	-	1.65 mm (N = 7.76)
Length of side of explosive layer L	15 mm	
Stand-off distance	11 mm	

C - LSC with decreasing thickness of explosive layer

	Open variant	Tamped variant
Thickness of liner	1.0 mm (M = 7.80)	1.0 mm (M = 7.80)
Thickness of explosive layer x_1	9.5 mm ($C_1 = 14.73$)	8.0 mm ($C_{T1} = 12.40$)
Thickness of explosive layer x_2	5.5 mm ($C_2 = 8.53$)	3.8 mm ($C_{T2} = 5.89$)
Thickness of tamping layer	-	1.65 mm (N = 7.76)
Length of side of explosive layer L	15 mm	
Stand-off distance	11 mm	

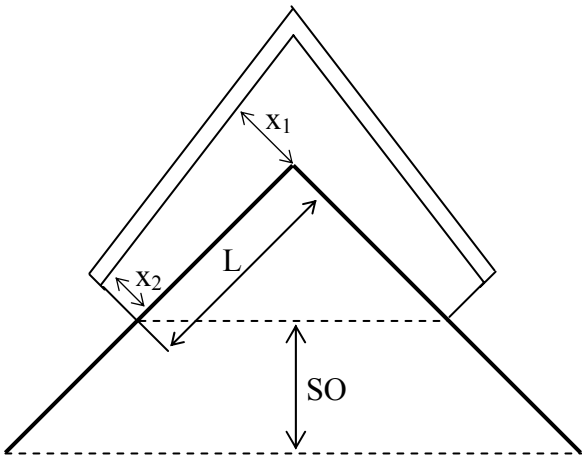


Fig 11. LSC type B (C): x_1 , x_2 - thickness of explosive layer; L - length of side of explosive layer; SO - stand-off distance.

Used material

Rollled plastic explosive containing 88 % RDX with detonation velocity $7,800 \text{ m.s}^{-1}$ at density 1.55 g.cm^{-3} was used for LSC manufacturing.

Liners with internal angle 90° were made of deep-ductile metal sheet with thickness 1.0 mm.

Mixture of powdered copper and polyisobutylene was used for preparation of tamping layer. This mixture was rolled to thickness 1.65 mm with density 4.7 g.cm^{-3} .

Performance of prepared LSCs was tested on the plate of steel of Class 11373 with dimensions $1200 \times 320 \times 30 \text{ mm}$.

Manufactured LSCs

Unified liner made of deep-ductile metal sheet with thickness 1.0 mm ($M = 7.80$) was used for preparation of all LSCs. Chosen length of the liner was 300 mm. Length of liner side 30 mm also ensured stand-off distance 11 mm.

Table 1. *Prepared LSCs*

Charge No.		Length of explosive layer L (mm)	Thickness of explosive layer x_1 (mm)	C_1	Thickness of explosive layer x_2 (mm)	C_2	Explosive content (g.m^{-1})	Thickness of tamping layer (mm)	N
A	1	15	7.5	11.55	-	-	415	-	-
	2	15	7.5	11.55	-	-	415	-	-
	3T	15	5.8	8.93	-	-	309	1.65	7.76
	4T	15	5.8	8.93	-	-	306	1.65	7.76
B	1	15	8.6	13.33	6.5	10.08	436	-	-
	2	15	8.6	13.33	6.5	10.08	440	-	-
	3T	15	6.9	10.7	4.8	7.44	323	1.65	7.76
	4T	15	6.9	10.7	4.8	7.44	317	1.65	7.76
C	1	15	9.7	15.04	5.5	8.53	458	-	-
	2	15	9.7	15.04	5.5	8.53	446	-	-
	3T	15	8.2	12.79	4.0	6.24	351	1.65	7.76
	4T	15	8.2	12.79	4.0	6.24	361	1.65	7.76

3. OBTAINED RESULTS

Middle part of steel plate was cut out after experiments to facilitate measuring of overall dimensions of cavity including penetrated slug. Introduced values are average values from two measurements done on opposite sides of the cut.

Table 2. *Measured values of cavities dimensions*

Charge No.		Depth (mm)	Average depth (mm)	Input width (mm)
A	1	21.75	21.60	9.75
	2	21.45		9.50
	3T	17.30	18.43	8.65
	4T	19.55		8.35
B	1	17.10	17.60	8.35
	2	18.10		8.35
	3T	16.25	16.83	6.40

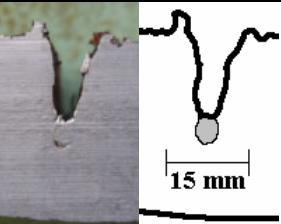
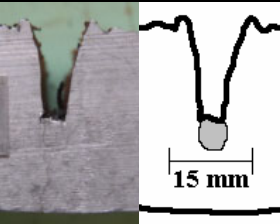
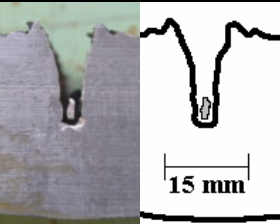
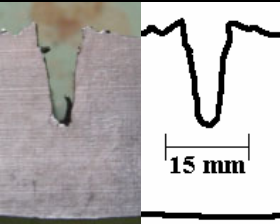
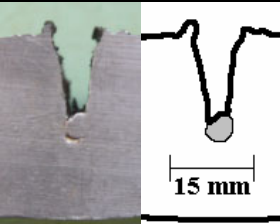
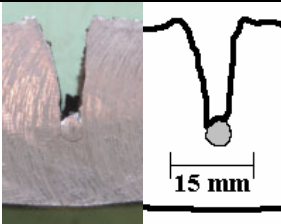

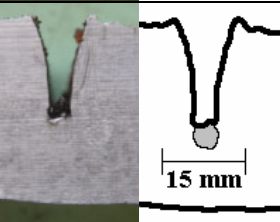
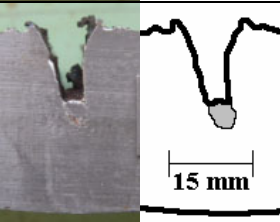
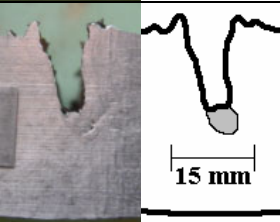
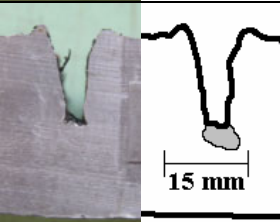
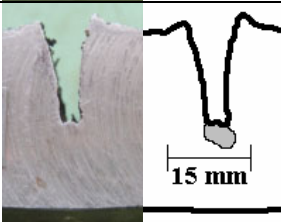
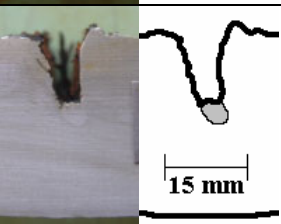
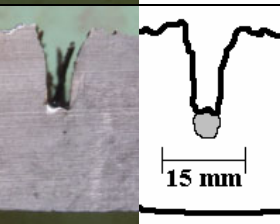
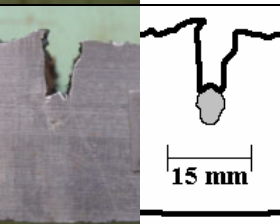
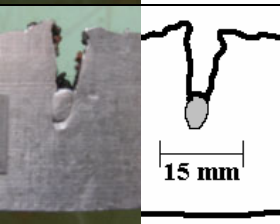
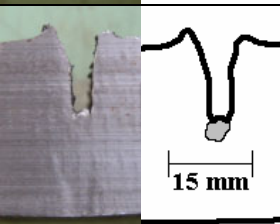
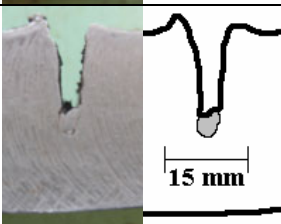
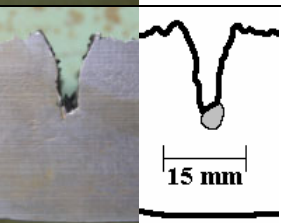
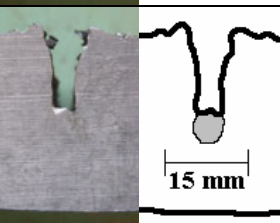
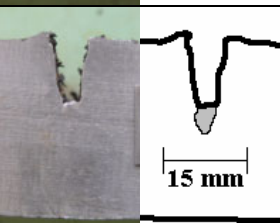
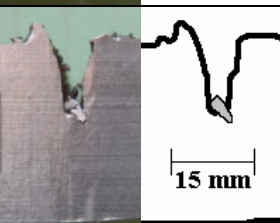
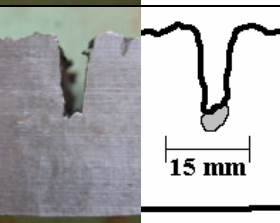
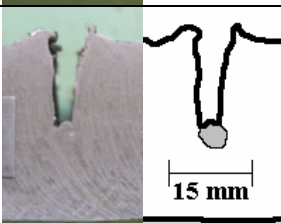
Charge No.		Depth (mm)	Average depth (mm)	Input width (mm)
	4T	17.40		7.05
C	1	21.50	20.83	9.10
	2	20.15		8.35
	3T	19.55	19.93	7.30
	4T	20.30		6.85

4. CONCLUSION

The values measured confirm, that at LSC with constant thickness of explosive layer (type A) the performance decreased by 15 % when the quantity of explosive was reduced by approximately 25 %. On the contrary, at LSC with variable explosive layer thickness (types B, C) the decrease in performance was by 5 % only, when the quantity of explosive was reduced by approximately 25 %.

These experiments also proved the applicability of powder material in polymere matrix for tamping of charges. On detonation of a charge complete disintegration to fine particles occurs that rapidly decelerate and the surroundings is not exposed to fragments dispersion.

Table 3. *Comparison of LSC performances*

	A		B		C	
	cut 1	cut 2	cut 1	cut 2	cut 1	cut 2
1						
2						
3T						
4T						

LIQUID PHASE AND SOLID PHASE NITRATION OF AROMATIC COMPOUNDS: GREEN SYNTHETIC ROUTES

D. Bahulayan*, C.P. Joshua** and H.G. Ang*

* HEDM Research Laboratory, Faculty of Science, National University of Singapore, Science Drive 2, Singapore 117543

** Department of Chemistry, University of Kerala, Kariyavattom, Trivandrum, Kerala, India

Abstract

*Selective mono- and di-nitration of aromatic hydrocarbons with various nitrating agents are discussed. Nitration of hindered diamines with potassium nitrate in conc. sulfuric acid yielded 80-95 % di-nitro derivatives. Nitration using 40% nitric acid with montmorillonite K10 and ferric nitrate supported on montmorillonite K10 showed high *p*-selectivity for mono-substituted substrates and also avoids the use of sulfuric acid. The total omission of sulfuric acid and the reduction of nitric acid concentration to 40% considerably reduce the emission of environmental pollutants. The montmorillonite K10 used as the solid support and catalyst is reusable by removing the water formed in the reaction followed by washing with acetone and subsequent drying in an air oven at 110 °C.*

Keywords: green synthesis, nitration, montmorillonite K10

1. INTRODUCTION

Nitro compounds represent an important class of compounds as potential energetic molecules, pharmaceutical intermediates and precursors for azo-dyes. C-Nitrocompounds are usually prepared by direct nitration of aromatic and aliphatic hydrocarbons under specific conditions ^[1]. In the laboratory, aromatic compounds are usually been nitrated by using a mixture of conc. HNO₃ and conc. H₂SO₄ ^[2, 3]. This totally “ungreen” process creates severe environmental pollution caused by the evolution of gaseous nitrogen oxides from oxidative degradation. The disposal of used acids and waste water is another serious issue. In the industrial process, a large excess of H₂SO₄ is required for compensating the retarding effect caused by water molecules formed as the by product, which dilutes the acid during nitration. In addition to that the reactions under high acidic conditions would inevitably cause corrosion and occupational hazards.

In recent years many alternative methods are reported for the ecofriendly synthesis of C- nitrocompounds which included the use of clays ^[4] and zeolites ^[5] as solid support. Similarly, a number of methods have been reported in the literature on the synthesis of nitramines involving the direct nitration of primary and secondary amines with acetone cyanohydrin nitrate ^[6a], CF₃CMe₂ONO₂ ^[6b], N₂O₅ ^[6c], HNO₃ ^[6d], NH₄NO₃ ^[6d], NO₂OSO₂CF₃ ^[6e], n-butyl nitrate with organomagnesium bromide ^[6f] and with 4-chloro-5-methoxy-2-nitropyridazin ^[6g]. These reagents are also not user-friendly because of their inherent

explosive and polluting character. In this context, the development of new green synthesis of nitro compounds is highly important. In continuation of our on-going programs in the area of energetic molecules, we herein report the results of solid phase and liquid phase nitration studies involving nitrate salts and nitric acid.

2. RESULTS AND DISCUSSION

2.1 C-Nitration with potassium nitrate in concentrated sulfuric acid

We have tested the C-nitration capability of the reagent by conducting the nitration of various 4, 4'-diaminodiphenylmethane derivatives. The reagent is prepared by the dissolution of anhydrous potassium nitrate in 95% sulfuric acid. Nitration was carried out by adding the reagent to an ice-cold solution of amine dissolved in conc.sulfuric acid. During the reaction, no gas evolution was observed. The progress of the reaction was monitored by TLC examination at regular intervals. After 6 hours of stirring at 0-5°C, the reaction was found to complete and the dinitro product obtained was recovered by pouring the reaction mixture on to crushed ice and subsequent neutralization with dilute ammonia solution (Equation 1).

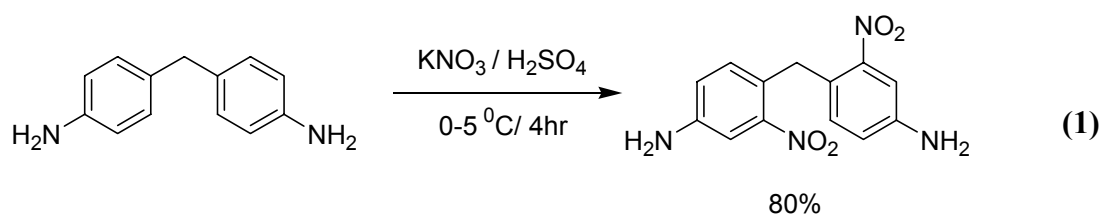
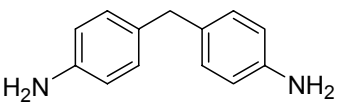
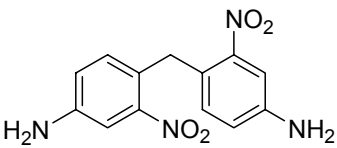
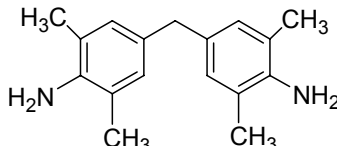
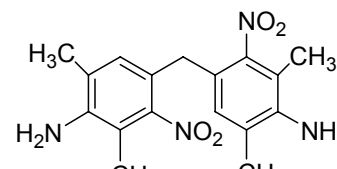
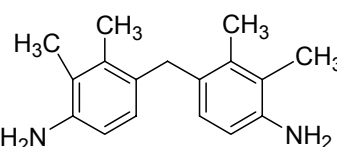
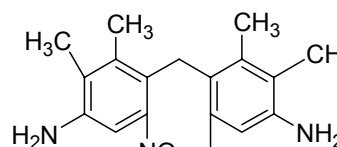
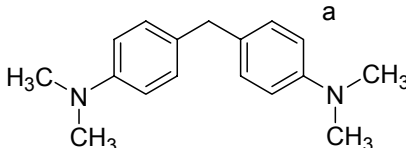
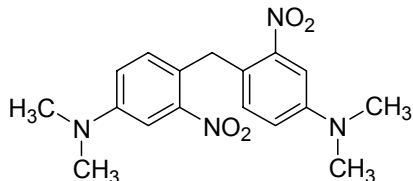
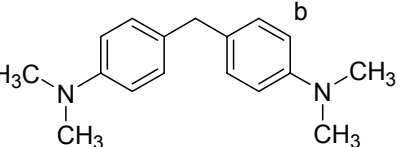
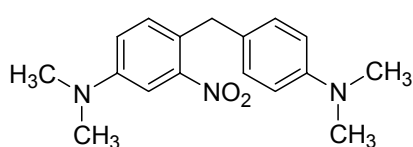


Table 1: *C-Nitration of aromatic amines using KNO₃/H₂SO₄ system*

Entry	Starting material	Product	% Yield
1.	 1	 1a	80
2.	 2	 2a	95
3.	 3	 3a	82
4.	 4	 4a	92
5.	 4	 4b	88

^a Dinitro product obtained by using two equivalent of potassium nitrate
^b Mono nitro product obtained by using one equivalent of potassium nitrate

We have carried out the nitration of selected sterically hindered di-amines and have obtained good results give yields in excess of 80%. We could not isolate any mono-nitro products in the nitration of amines **1**, **2** and **3** when carried out with one equivalent of nitrating agent. However, the nitration of the N-substituted amine **4** yielded the mono- and di-nitro derivatives when the nitration was undertaken with one and two equivalents of the nitrating agent respectively. The results are summarized in Table 1.

2.2 C-Nitration with nitrate salt supported on Montmorillonite K10 clay

In order to develop a more economical and eco-friendly process for nitration that would lead to the synthesis of high-energy compounds, we have focused our attention towards nitrating agents supported on solid acids (Equation 2). We have prepared ferric nitrate supported on montmorillonite K10 clay following the procedure of Laszlo et al ^[7]. The reagent is prepared by dissolution of ferric nitrate monohydrate in acetone, resulting in a muddy, light brown suspension, to which Mont. K10 is added and stirred well. The evaporation of the solvent under reduced pressure yielded the powdered reagent and used for the nitration of aromatic hydrocarbons.

All the reactions were carried out in hexane medium. The substrate molecule was uniformly mixed with the supported nitrating agent and then hexane was added to it. The R.B.flask is then fitted with Dean-Stark water separator and refluxed at the boiling temperature of hexane. The progress of the reaction was monitored by TLC analysis at regular intervals. After the completion of the reaction, the solid clay residue was filtered off and the work-up of the filtrate by alumina column chromatography yielded pure nitro products in good to excellent yield. The generality of the reactions was established by performing the reaction with different aromatic substrates. The nitration of benzene yielded 92% *p*-nitrobenzene, whereas toluene gave a mixture of 75% *p*-nitro and 10% dinitro derivative. The nitration of anisole yielded 91% *p*-nitro anisole as the single product. The results are summarized in Table 2

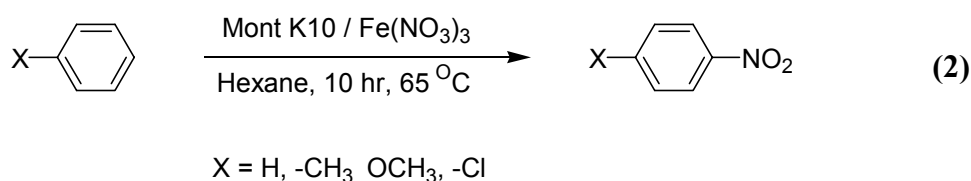

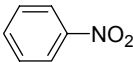
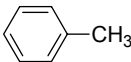
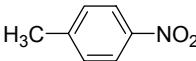
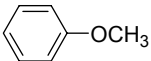
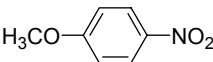
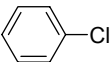
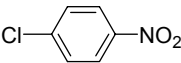
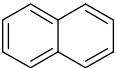
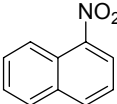
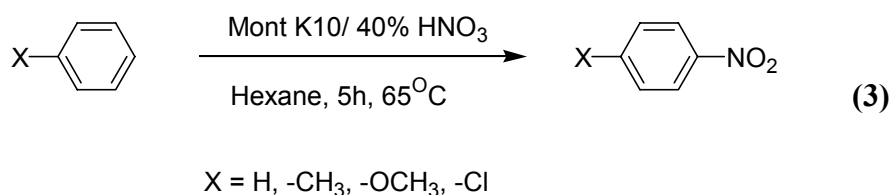


Table 1. C-Nitration with nitrate salt supported on Montmorillonite K10 clay

Entry	Starting material	Product	Time, hr	% Yield
1			10	92
2			10	75
3			10	91
4			10	90
5			24	85

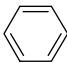
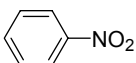
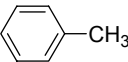
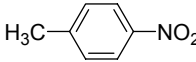
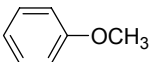
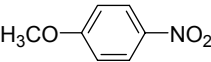
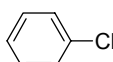
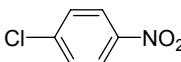
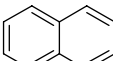
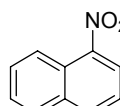
2.3 C- Nitration with 40% nitric acid / Montmorillonite K10 system

We have also carried out the nitration reaction over montmorillonite K10 clay using 40% nitric acid as the nitrating agent.



The methodology was the same as that described for C-nitration with ferric nitrate supported on montmorillonite K10 clay. The only difference is the use of 40 % nitric acid as the nitrating agent. In this case the reaction was found to complete around 5 hr which was only half of the time compared to the ferric nitrate case. Here the substrate also showed *p*-selectivity with good-to-excellent yields.

Table 3: Nitration of aromatic hydrocarbons using 40% HNO₃ / Montmorillonite K10 system

Entry	Starting material	Product	Time,hr	% Yield
1			5	99
2			5	81
3			5	90
4			5	35
5			24	91

3. REGENERABILITY OF THE SOLID ACID CATALYST MONT K10

The catalyst filtered from the reaction mixture was thoroughly washed with acetone and dried at 110 °C for 3 hr in an air oven. This was then directly used in a fresh reaction. The process was repeated in five cycles and no considerable change was observed in the activity of the catalyst.

3.1 Experimental

General procedure for the C- nitration of aromatic amines with potassium nitrate

Nitration of the 4, 4'-diaminodiphenylmethane was accomplished in the following way. In a typical experiment, to an ice cold solution of 4, 4'-diaminodiphenylmethane (0.05M, 9.9 g) in concentrated sulfuric acid (18M, 40 ml), was added a solution of potassium nitrate (10.1 g) in conc.sulfuric acid (18M,15ml) over a period of 1 hr. Stirring was continued for another 3 hr, keeping the reaction mixture below 5 °C. The reaction mixture was then poured into crushed ice and neutralized with ice-cold ammonia solution. The yellow solid was collected on a filter and washed with water and dried. Crystallization of this product from dioxane-alcohol mixture afforded 4,4'-diamino-2,2'-dinitrodiphenylmethane as yellow flakes, (mp. 206-208 °C). Analysis: found C 54.11, H 4.18, N 19.33%; required for C₁₃H₁₂N₄O₄: C 54.16, H 4.16, N 19.44%.

4, 4'-Diamino-3, 5,3', 5'-tetramethyl-2, 2'-dinitrodiphenylmethane: (mp. 226°C). Analysis: found, C 59.33, H 5.62, N 16.34%; required for C₁₇H₂₀N₄O₄: C 54.16, H 4.16, N 19.44%.

3.2 Preparation of Montmorillonite K10 clay supported ferric nitrate

The reagent was prepared by the procedure reported by Laszlo et al. In a typical preparation, ferric nitrate monohydrate (22.5g) was added to acetone (375ml) and the mixture was stirred well. Montmorillonite K10 clay (30g) was then added to it in small amounts and stirring was continued for another 5 minutes. The solvent was removed by distillation under reduced pressure and water is removed by placing it on a water bath at 50°C for 30 minutes. The dry solid thus obtained was again heated on a waterbath for another 30 minutes and the reagent thus obtained (~ 50g) was used for the nitration.

3.3 General procedure for the nitration with Clay supported ferric nitrate.

The following procedure for the preparation of nitrobenzene is representative. A dry 250ml round bottomed flask was fitted with a Dean – Stark apparatus and was charged with benzene (7.8 g. 0.1 mol) and 10 g of clay supported ferric nitrate. To this 100 ml of dry hexane was added and the setup was fitted with a water-cooled reflux condenser and refluxed for 10 hr. Then the clay supported reagent residue was filtered off and the solvent was removed under reduced pressure. Vacuum distillation of the left over mixture yielded pure mono-nitrobenzene (39.5%)

REFERENCES

- [1] (a) GIZIEWICZ J., WNUK S.F., ROBINS M.J.: J.Org.Chem.1999, 64, 2149, (b) GORCHS O., HERNANDEZ M., GARRIGA L., PDROSO E., GRANDAS A., FARRAS J.: Org. Lett. 2002, 4, 1827. (c) ONO N: The Nitro Group in Organic Synthesis, Wiley-VCH, New York, 2001. (d) FEUER H., NIELSON A.T.: Nitro Compounds: Recent Advances in Synthesis and Chemistry, VCH, New York, 1990.
- [2] SCHOFIELD K: Aromatic Nitrations, Cambridge University Press, Cambridge, 1980.
- [3] OLAH G.A, MALHOTRA R., NARANG S.C: Nitration: Methods and Mechanisms, VCH, New York, 1989.
- [4] (a) DELAUDE L., LASZLO P., SMITH K: Acc.Chem.Res. 1993, 26, 607. (b) BAHULAYAN D., NARAYAN G., SREEKUMAR V., LALITHAMBIKA M.: Synth.Comm., 2002, 32, 3565.
- [5] CHOUDHARY B.M., SATHEESH M., KANTAM M.L., RAO K.K., PRASAD K.V.R., RAGHAVAN K.V., SARMA J.A.R.P.: Chem Commun. 2000,1,25.
- [6] (a) EMMONS W.D., FREEMAN J.P.: J.Am.Chem.Soc.1955,77, 4387. (b) BOTTARO J.C., SCHMITT R.J., BEDFORD C.D.: J.Org.Chem. 1987, 52, 2292. (c) GOLDING P., MILLER R.W., PAUL N.C., RICHARDS D.H.: Tetrahedron Lett. 1988, 29, 2735. (d) SURI S.C., CHAPMAN R.D.: Synthesis, 1988, 743. (e) ADAMS C.M., SHARTS C.M., SCHAKELFORD S.A., Tetrahedron Lett. 1993, 34, 6669. (f) DASZKIEWICZ Z., DOMANSKI A., KYZIOL, J.B.: Org. Prep. Proced. Int. 1994, 26, 337. (g) PARK, Y.-D., KIM, H.-K., KIM, J.J., CHO S.-D., KIM S.-K., SHIRO M., YOON Y.-J.: J.Org.Chem, 2003, 68, 9113.
- [7] LASZLO P., CORNELIS A.: Synthesis, 1980, 849."

DEVELOPMENT OF ENERGETIC SALTS FOR PROPELLANTS

S. Beaucamp*, D. Mathieu* and V. Agafonov**

* Commissariat à l'Energie Atomique, Centre du Ripault, BP16, F-37260 Monts, France

** Laboratoire de Chimie Physique, EA PIMIR 2098, Faculté de Pharmacie,
31 Avenue Monge F-37200 Tours, France

Abstract:

The development of new energetic salt compounds composed by an ammonium cation fixed on an energetic nitrogen heterocycle and a nitrate anion are presented here. On one hand, these materials are more stable than their counterpart with nitro groups because of ionic charges which increase the cohesive energy. Despite the latter reduces the solid state heat of formation, the presence of ammonium and nitro groups on the energetic backbone decreases this effect. On the other hand, the nitrate group provides the oxygen necessary to generate stable reaction products. Moreover, the synthesis of these compounds requires methods to estimate their performances which depend on the density and the heat of formation. This provides information to lead chemists to promising components. A contribution groups method to estimate the density and semi-empirical methods to evaluate the heat of formation of salts have been developed because of the lack of suitable methods for ionic species.

Keywords: *molecular modeling, molecular mechanics, crystal packing, ionic crystal*

1. INTRODUCTION

The design of materials environmentally friendly and with low sensibility is presented here. The development of salts composed by an heterocycle bearing an ammonium nitrate group (N^+ , NO_3^-) could be facilitated and accelerated by computational models to determine their energetic properties which lead chemists to identify promising components. The first part emphasizes the interest of energetic salts. In the second part, we examine models to determine energetic properties as density or solid state heat of formation (ΔH_f) for energetic salts materials.

2. INTEREST OF SALTS

Ammonium salts as ammonium perchlorate, nitrate or dinitramide salts have applications potential for propulsion^[1,2,3,4]. Their performances strongly depend on their densities, their stoichiometries and solid-state heats of formation. Some of these have interesting thermal stability, a low mechanical sensibility, a low toxicity and may be produced economically^[6]. Moreover, salts have low vapour pressures eliminating the risk of inhalation^[5] and a satisfactory thermal stability.

Among ammonium salts, ammonium nitrate compounds are those which have a fair stability as shows the table 1. This interesting feature is especially due to electrostatic energy

created by atomic charges interactions present in their crystal structure ^[7]. Indeed, the coulombic contribution of salts dominates the lattice energy and increases the cohesion of the materials ^[8].

Table 1. *Example of energetic salts and their major properties.*
a : at 75 °C
b : kg.cm

Salt name	Density ^a ^[5]	T _{dec} ^[5]	Melting point ^a ^[5]	Impact ^b ^[5]
4-amino-1,2,4-triazolium nitrate	1.6	180°C	69°C	>200
1,2,4-triazolium nitrate	1.64	182°C	137°C	>200
1,2,3-triazolium nitrate	1.57	110°C	110°C	>200
4-amino-1,2,4-triazolium dinitramide	-	20°C	146°C	<5
1,2,4-triazolium dinitramide	1.66	75°C	12°C	98
1,2,3-triazolium dinitramide	1.66	61°C	80°C	-

As shows the figure 1 salts may exhibit high densities (because of their crystalline state) and quite equilibrated oxygen balances (because of availability of oxygen rich ions, like nitrate) necessary for the formation of stable decomposition products. These features could make up for the very negative contribution to the solid-state heat of formation associated with the cohesive energy.

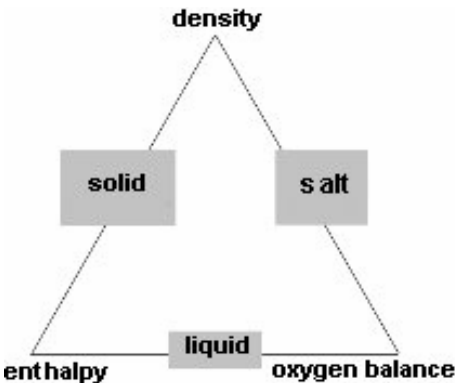


Fig 1. Scheme illustrating the trade-off between relevant properties of different kinds of energetic materials. Liquids tend to have poor densities, salts often have low enthalpies, while it is difficult to get molecular crystals with optimized the oxygen balance.

In addition, the heat of formation may be enhanced by high value of gas phase contribution. For instance, the ammonium nitrate groups contributes positively to the energy content of the compounds, as shown in figure 2. A drawback of the $-\text{NH}_3^+$ ammonium is the low density ^[9] associated with the hydrogen atoms. However, this negative effect on the density can be mitigated by the use of high density backbone. In fact, the best performances should results from a trade-off between the fair stability and relative ease of synthesis of salts and the high density and enthalpy of energetic compounds. In addition the another goal of the backbone is to increase the distances between charges and hence reducing the cohesive energy and increasing $\Delta H_f(s)$.

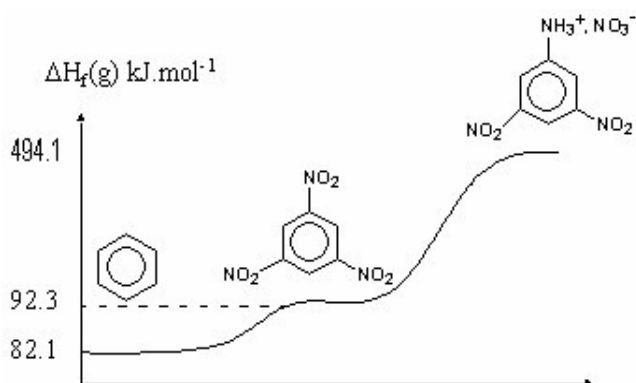


Fig 2. Gas phase enthalpy for benzene, trinitrobenzene and aminodinitrobenzene nitrate

Two reasons have motivated the design of ammonium nitrate salts. First, for the most energetic compounds, oxygen is provided by the explosive $-\text{NO}_2$ group. Nevertheless, the add of too many groups affect the stability of molecules. Their replacement by nitrate is easier and put ionic charges in materials which increase the cohesion and form ordered and dense lattice structure. Second, ammonium nitrate salts are more stable than other salts composed by dinitramide anion as shown in the table 1. So their synthesis is easier because they require only an acid-base reaction between an amine and hydrochloric acid ^[5]. In other respect, the use of such materials avoid the environmental problem associated with the formation of HCl during the combustion of ammonium perchlorate.

Therefore, the design of such compound (X-N^+ , NO_3^-) is more efficient if relevant properties as density and ΔH_f can be calculated ab initio i.e. before their synthesis. These determination lead chemists to select promising components.

3. COMPUTATIONAL METHOD

3.1 Density

The density can be evaluated by group contribution methods ^[10,11], empirical methods based on van der Waals volumes ^[12] or molecular descriptors ^[13]. Volume additivity has the advantage of speed and simplicity. An accurate group contribution method have been derived for neutral organic compounds containing only C, H, O, N, F atoms ^[10]. Recently this method has been extended to salts by deriving standard volumes for charges groups containing C, H, O, N, Br and Cl atoms ^[9]. With this new group volumes, the density of organic salts is obtained with an average error of 2.5% ^[9] and some results obtained are presented in the table 3. This method adapted for organic salts is useful to select promising components.

3.2 Solid-state enthalpy

Solid-state heats of formation are more difficult to obtain with accuracy needed for thermochemical calculation i.e. with an error of 0.5 kJ.g^{-1} . $\Delta H_f(s)$ of energetic compounds can be estimated from gas phase heat of formation $\Delta H_f(g)$ and their sublimation enthalpy [14]. But methods applied to neutral compounds using semi-empirical, analytical expressions [14] to evaluate sublimation enthalpy is though not applicable to salts. Long range interactions (electrostatic energy) [9] present in salts structures require molecular packing constructions or semi empirical expression to evaluate the cohesive energy. $\Delta H_f(s)$ is estimated from gas phase enthalpy $\Delta H_f(g)$ and cohesive energy E_{coh} of salts structure according to the following equation [8]:

$$\Delta H_f(s) = \Delta H_f(g) - E_{\text{coh}} - 2RT \quad (1)$$

where T is the temperature and R the ideal gas constant. Using this model, a method has been developed to determinate the solid state heat of formation. $\Delta H_f(s)$ may be estimated using standard quantum chemical methods [8]. E_{coh} is represented by a point charges model with CHELPG charges computed from crystal structures [8]. Its application to known salts yields satisfactory results [8]. However, the design of salts requires estimations of performances before their synthesis i.e the determination of the cohesive energy without crystal structure.

3.3 Cohesive energy

To predict the cohesive energy, we have developed a semi-empirical model which predict the cohesive energy of salts from ab initio data crystals extracted from CSD database [15] and containing C, H, O, N and S atoms. We have developed a model to predict the cohesive energy with no need of RX salt structures. This method computes the lattice energy from atomic charges and geometry of isolated ions which composed an organic salts as shows the equation 2. In addition to terms depending on charges parameters and interatomic distances, an another term which depends on the size of the system should be included. Indeed, as shown in the figure 3, we can see that the crystals cohesive energies depend on the average number of atoms in the constitutive compounds N (for instance, if the crystal is made only of anions (A) and cations (C) then $N = \frac{1}{2} * (N_A + N_C)$).

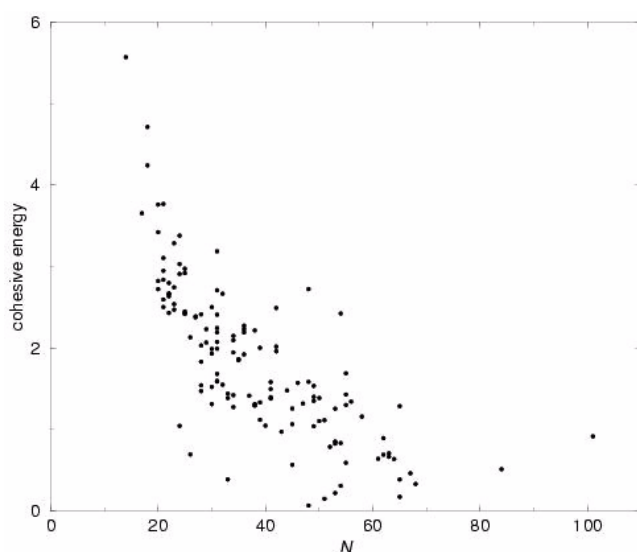


Fig 1. Graph of the crystals cohesive energies (kJ.g^{-1}) versus the average number of atoms (N) in the constitutive compounds

Cohesive energy has been computed from point charges (PC) model with atomic charges derived from CHELP procedure at B3LYP/6-31G* level [9]. From isolated ions optimized at B3LYP/6-31G*, atomic charges derived from CHELP procedure at B3LYP/6-31G* and geometries of ions allow to calculated parameters for our calibration. The expression obtained by the calibration procedure is the following equation (2) :

$$E_{coh}=\frac{Q_{moy}}{R_{inter}}*\left(A_1+\frac{A_2}{N^2}\right)+\frac{Q_{moy}^{+}*Q_{moy}^{-}}{R_{inter}}*\left(A_3+\frac{A_4}{N^2}\right)+(\delta_{+}*\delta_{-})*\left(A_5+\frac{A_6}{N}\right)+\left(\frac{\delta_{+}+\delta_{-}}{2}\right)^p*\left(A_7+\frac{A_8}{N}\right) \tag{2}$$

Q_{moy} is the average of the absolute charges of anion and cation, Q_{moy}^{+} and Q_{moy}^{-} are the average charge of the positive and negative charges respectively, R_{inter} is the average of the interatomic distances between atoms of ionic molecules. The second moment δ_{+} and δ_{-} are moments of positive (Q^{+}) and negative (Q^{-}) charges with respect to their respective means Q_{moy}^{+} and Q_{moy}^{-} . N is the average number of atoms in the constitutive compounds.

Table 1. Definition of parameters contained in equation 2. (N_{at} is the number of atoms in the constitutive compounds)

variables	expressions
Q_{moy}	$\sqrt{\frac{1}{N_{at}}*\sum_i Q_i^2}$
Q_{moy}^{+}	$\sqrt{\frac{1}{N_{at}}*\sum_i Q_i^{+2}}$
Q_{moy}^{-}	$\sqrt{\frac{1}{N_{at}}*\sum_i Q_i^{-2}}$
δ_{+}	$\sqrt{\frac{1}{N_{at}}*\sum_i [Q_i-Q_{moy}^{+}]^2}$
δ_{-}	$\sqrt{\frac{1}{N_{at}}*\sum_i [Q_i-Q_{moy}^{-}]^2}$

This method yields an average calibration error of 0.40 kJ.g⁻¹ for 300 crystal salts and a validation procedure obtained from 123 compounds yields a average error of 0.50 kJ.g⁻¹. This method has been assessed to determine the solid-states enthalpy via the equation 1. This results will be shown in the oral presentation.

4. CONCLUSION

Ammonium nitrate salts exhibit interesting features as energetic compounds. Moreover, computational methods developed to determine densities and solid-state enthalpies should be useful for the design of new energetic salts as components of propellants.

REFERENCES

- [1] M.A. PETRIE, J.A. SHEEHY, J.A. BOATZ, G. RASUL, G.K.S. PRAKASH, G.A. OLAH and K.O. CHRISTE: *J. Am. Chem. Soc.*, **119**, pp. 8802-8808, 1997
- [2] P. POLITZER, J.M. SEMINARIO AND M.C. CONCHA: *Journal of Molecular Structure (Theochem)*, **427**, pp. 123-129, 1998
- [3] P. POLITZER AND P. LANE: *Journal of Molecular Structure (Theochem)*, **454**, pp. 229-235, 1998
- [4] C. OOMMEN AND S.R. JAIN: *Journal of Hazardous Materials*, **A67**, pp. 253-281, 1999
- [5] G. DRAKE, T. H. A. BRAND, L. HALL AND M. MCKAY: *Propellants, Explosives, Pyrotechnics*, **28(4)**, pp. 174-180, 2003
- [6] J. P. AGRAWAL: *Prog. Energy. Combust. Sci.*, **24**, pp. 1-30, 1998
- [7] P. VERWER AND F. J. J. LEUSEN: *Rev. Comput. Chem*, **12**, pp. 327-364, 1998
- [8] S. BEAUCAMP, A. BERNAND-MANTEL, D. MATHIEU AND V. AGAFONOV: *Mol. Phys.*, in press
- [9] S. BEAUCAMP, N. MARCHET, D. MATHIEU AND V. AGAFONOV: *Acta Cryst. B*, **B59**, pp. 498-504, 2003
- [10] H. AMMON AND S. MITCHELL: *Propellant, Explosive, Pyrotechnics*, **23**, pp. 260-265, 1998
- [11] J.R. Stine, Prediction of crystal, *Densities of Organic Explosive by group additivity*, Report LA-8920. LANL, Los Alamos, NM, USA, 1981
- [12] G.PIACENZA, G. LEGSAI, B. BLAIVE AND R.GALLO: *J. Phys. Org*, **86**, pp. 8595-8599, 1989
- [13] S.G. CHO, E.M. GOH AND J.K. KIM: *Bull. Kor. Chem. Soc*, **22**, pp. 775-778, 2001
- [14] D. MATHIEU AND P. SIMONETTI: *Thermochimica acta*, **384**, pp. 369-375, 2002
- [15] *Cambridge Structural Database version 5.23.*, Cambridge Crystallographic Data Centre, Cambridge, UK, 2002
- [16] ICT Thermochemical Database, *Institut of Chemical Technology*, Pfingsttal, Germany, 2002

STUDIES ON THE NITRATION OF NEW POTENTIAL PRECURSORS FOR FOX-7

A.J. Bellamy*, N.V. Latypov** and P. Goede**

* Cranfield University, Royal Military College of Science,
Shrivenham, Swindon SN6 8LA, UK

** Swedish Defence Research Agency (FOI), SE-147 25 Tumba, Sweden

Abstract:

FOX-7 is commonly produced by the nitration of 2-methylpyrimidine-4,6(3H,5H)-dione. However this method forms dinitromethane as an unwanted by-product since the nitrated intermediate has been nitrated at C-5 as well as in the required methyl group. We have now studied the nitration of several related 2-methylpyrimidinedione and methyl-1,3,5-triazine systems in the hope that their nitrated products would also give FOX-7 on hydrolytic decomposition, but without forming unwanted by-products. Unfortunately, this expectation was not realised. Whilst nitration in the methyl group did occur in all cases, reaction did not stop at the required dinitromethyl stage. In most cases the trinitromethyl derivative was formed, and in some cases this underwent C-C bond cleavage.

Keywords: 1,1-Diamino-2,2-dinitroethene, FOX-7, nitration

1. INTRODUCTION

1,1-Diamino-2,2-dinitroethene (I), also known as FOX-7, has generated considerable interest in recent years as an explosive with relatively high performance and low sensitivity to both friction and impact^[1]. It was originally synthesised via nitration of 2-methylimidazole^[2], but more recently nitration of 2-methylpyrimidine-4,6(3H,5H)-dione (II) has been shown to be the method of choice^[3,4,5]. However, nitration of 2-methylpyrimidine-4,6(3H,5H)-dione has a significant disadvantage. Nitration occurs not only on the desired methyl group, but also on the C-5 methylene group (Fig. 1). Nitrating agent is thereby wasted and dinitromethane is an unwanted by-product.

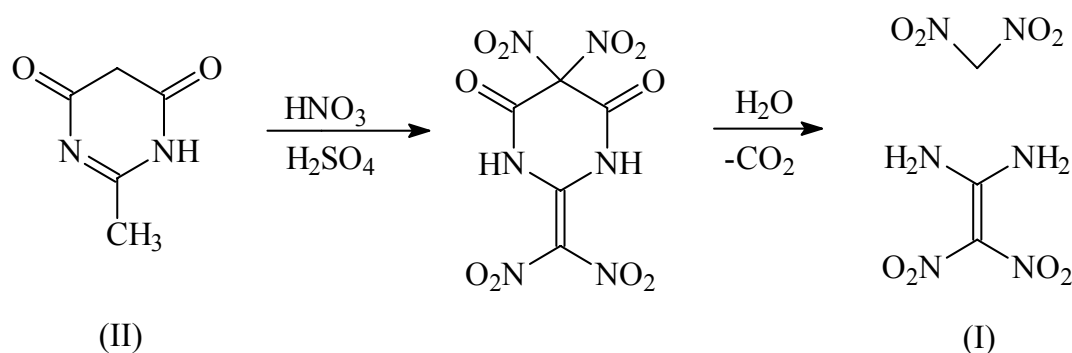


Fig 1. Formation of FOX-7 (I) from II.

It was envisaged that the use of heterocyclic precursors that were unable or unlikely to nitrate at position 5 (relative to N atoms at positions 1 and 3) might furnish 1,1-diamino-2,2-dinitroethene via nitration of the methyl group without concomitant nitration in other parts of the molecule.

2. RESULTS AND DISCUSSION

2.1 Nitration of 2-methylpyrimidine-4,6(3H,5H)-dione (II)

The optimum yield of FOX-7 is obtained when II is nitrated with mixed acid containing around 5 equivalents of HNO_3 , 4 equivalents being required to form the tetranitro intermediate. When less than 4 equivalents of HNO_3 are used, the yield of FOX-7 is reduced and it is accompanied by only one nitrated pyrimidine, the 5-nitro derivative III (Fig. 2). The latter is formed within minutes of the addition of the HNO_3 to the H_2SO_4 solution of the substrate. Taken together, these results indicate that nitration to the mono-nitro derivative is relatively fast, nitration to a di-nitro derivative is slow (allowing isolation of the mono-nitro derivative) and further nitration is fast (preventing the isolation of any other intermediate before the tetra-nitro derivative is formed). The relatively slow rate of the second nitration is probably a consequence of the destruction of the aromatic system when the 5,5-dinitro derivative is formed. This also probably facilitates enolisation onto the methyl group and further nitration at that centre.

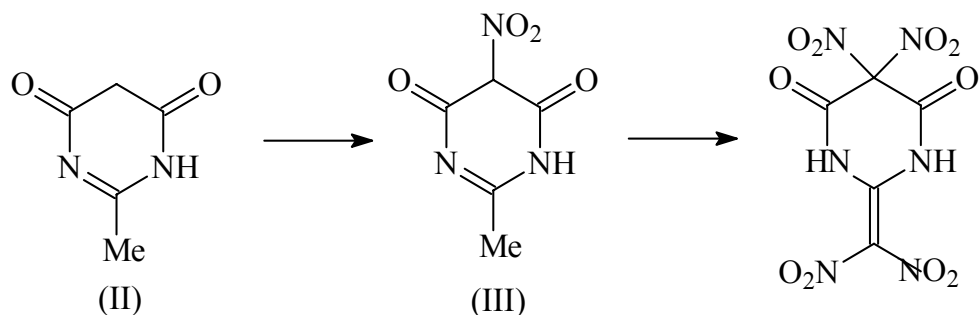


Fig 2. Nitration of II.

2.2 Nitration of 6-methyl-1,3,5-triazine-2,4(1H, 3H)-dione (IV)

It had been demonstrated ^[6], via deuterium exchange, that under acidic conditions, the hydrogen atoms in the methyl group of 6-methyl-1,3,5-triazine-2,4(1H, 3H)-dione (IV) are labile, and a species with an exocyclic methylene group was suggested to be involved. It therefore seemed likely that this molecule would undergo nitration at the methyl group (Fig. 3).

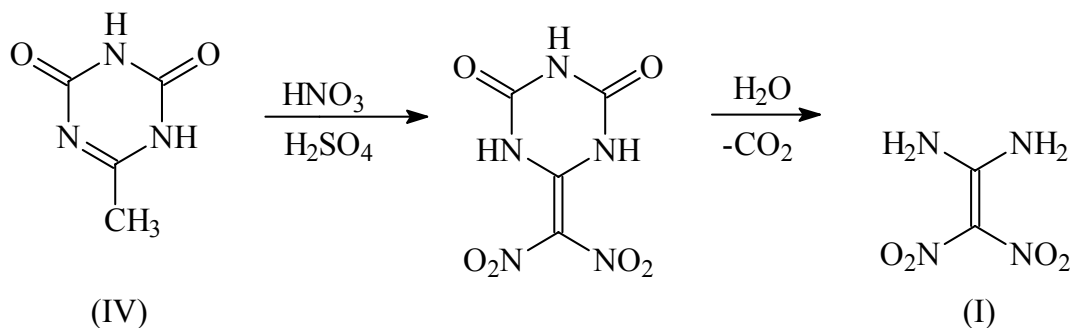


Fig 3. Anticipated nitration of IV.

The nitration of 6-methyl-1,3,5-triazine-2,4(1H, 3H)-dione (IV) was initially performed under identical conditions to those used for the nitration of 2-methylpyrimidine-4,6(3H, 5H)-dione (II) viz. $\text{HNO}_3/\text{H}_2\text{SO}_4$ at 25°C . Under these conditions no colour developed, no solid separated and no precipitate was formed on addition of the reaction mixture to water. It was subsequently discovered that there was no evidence of nitration even after 118h at 25°C . When the temperature was raised to 80°C , nitration did occur, but not to give the anticipated product. After 20h at 80°C , the products were 2,4,6-trihydroxy-1,3,5-triazine (V) and tetranitromethane (VI) (Fig. 4). This suggested that the nitration had occurred as anticipated, but that the intermediate had then undergone further nitration with cleavage of the original C- CH_3 bond. It is possible that 2-methylpyrimidine-4,6(3H, 5H)-dione (II) does not undergo an analogous cleavage process under normal conditions due to precipitation of the tetra-nitrated intermediate. Indeed, when the normal nitration (25°C) of 2-methylpyrimidine-4,6(3H, 5H)-dione (II) was followed by heating at 80°C , degradation of the tetra-nitrated intermediate occurred. Nitration of IV with concentrated HNO_3 alone also gave 2,4,6-trihydroxy-1,3,5-triazine (V), even at room temperature (60% after 46h, and 84% after 166h).

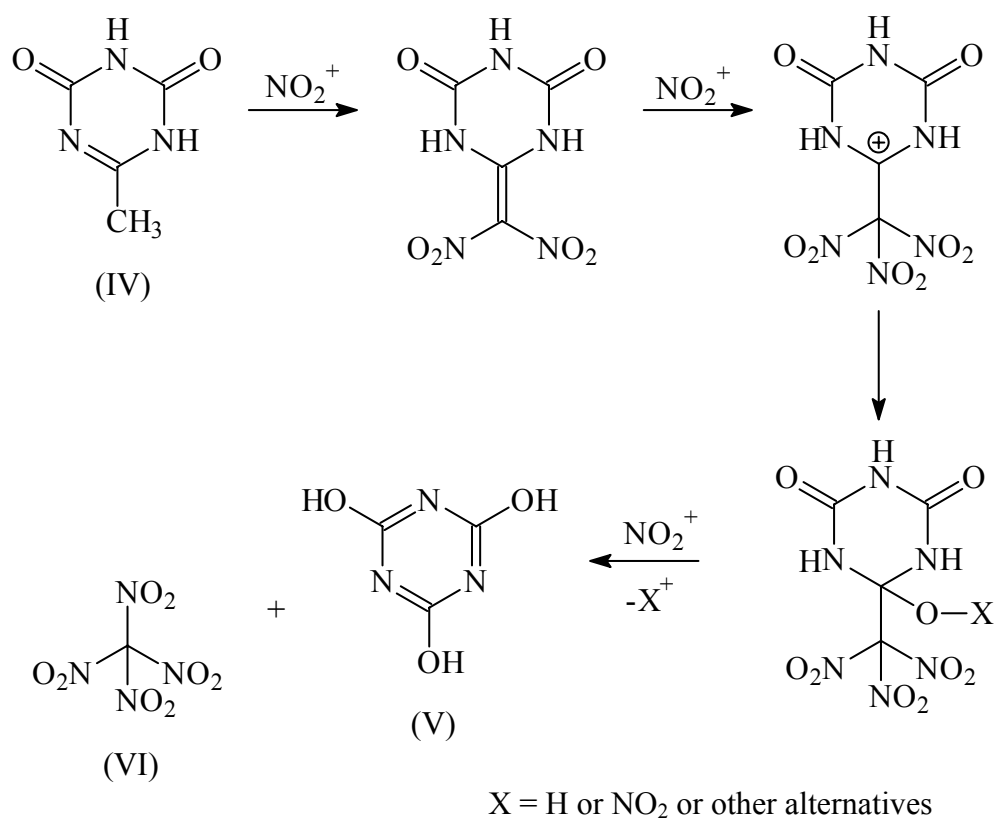


Fig 4. Observed nitration of IV.

2.3 Nitration of 2,4-dimethoxy-6-methyl-1,3,5-triazine (VII)

Nitration of 2,4-dimethoxy-6-methyl-1,3,5-triazine (VII), an intermediate in the synthesis ^[7] of IV, using $\text{HNO}_3/\text{H}_2\text{SO}_4$ gave a clean conversion to the known ^[8] 2,4-dimethoxy-6-trinitromethyl-1,3,5-triazine (VIII) in moderate yield (57%) (Fig. 5).

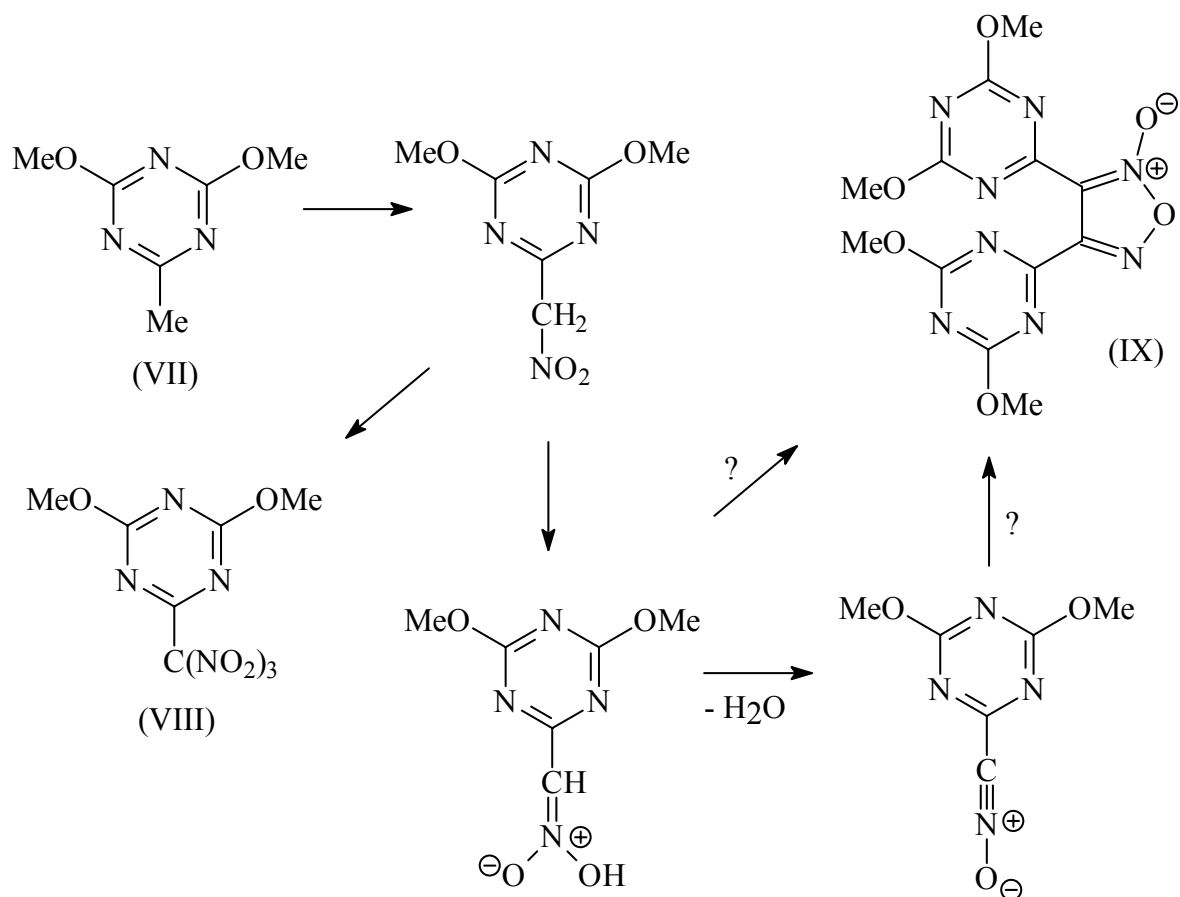


Fig 5. Nitration of VII.

However when 2,4-dimethoxy-6-methyl-1,3,5-triazine (VII) was nitrated with nitric acid alone, the product (~60%) was 3,4-bis(3',5'-dimethoxy-s-triazinyl)-1,2,5-oxadiazole 2-oxide (IX), a furazan N-oxide derivative, together with a small amount of the former trinitromethyl derivative (VIII) (Fig. 5). Neither product could be converted to the other by treatment under the alternative nitration conditions. Furazan N-oxides are commonly formed ^[9] by uncatalysed dimerisation of nitrile oxides. In this case it is probable that mono-nitration of the methyl group leads, via tautomerisation and loss of water, to a nitrile oxide which then dimerises. Under the more forcing conditions of mixed acid nitration, the mono-nitro derivative is further nitrated before it can convert to the nitrile oxide and thence dimer (Fig. 5).

Although VIII was not the desired product, it was hoped that selective removal of one of the nitro groups followed by hydrolytic removal of the methoxy groups might furnish 1,1-diamino-2,2-dinitroethene (I). Treatment of VIII with methanolic KI using the method of Glover and Kamlet^[10] did produce the potassium salt of 2,4-dimethoxy-6-dinitromethyl-1,3,5-triazine (X). However hydrolysis of X under conditions used ^[7] for the hydrolysis of VII to IV (5M HCl) gave 2,4,6-trihydroxy-s-triazine (V, cyanuric acid) (Fig. 6).

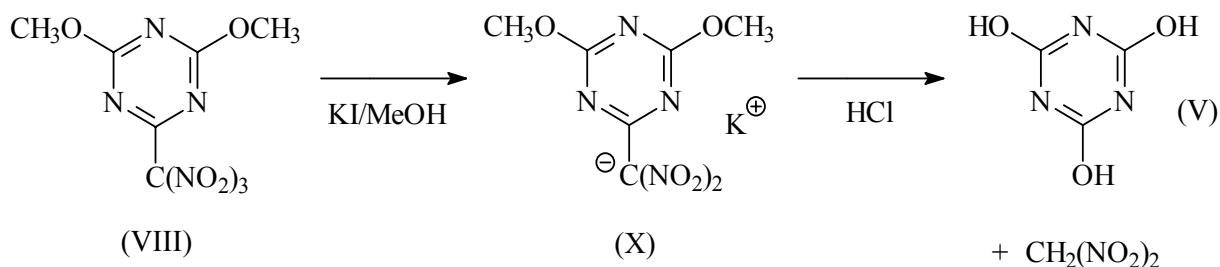


Fig 6. Cleavage of VIII.

2.4 Nitration of 2,5-dimethylpyrimidine-4,6(3H,5H)-dione (XI)

Nitration of 2,5-dimethylpyrimidine-4,6(3H,5H)-dione (XI) with mixed acid (4 equivalents of HNO_3) did not give the expected trinitro derivative XII but nitroform (isolated as its potassium salt) (Fig. 7). This was still the only isolated product when only 1 equivalent of HNO_3 was used.

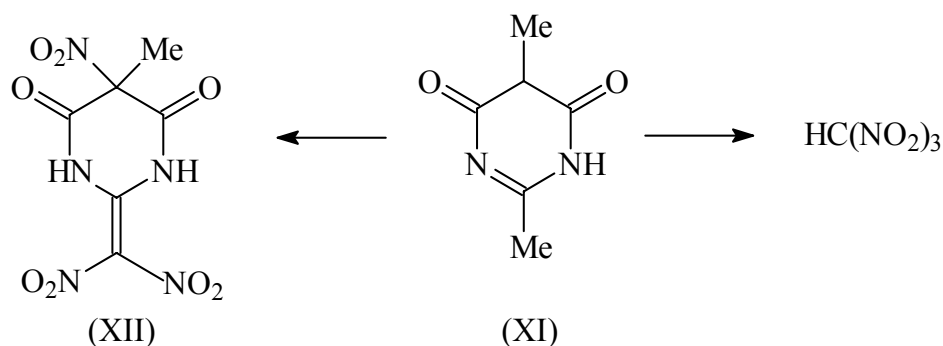


Fig 7. Anticipated vs observed nitration of XI.

2.5 Nitration of 5,5-dialkyl-2-methylpyrimidine-4,6(3H,5H)-dione (XIII)

Two 5,5-dialkyl derivatives ($\text{R} = \text{Me}, \text{Et}$) were synthesised and their nitration studied. Nitration of the diethyl derivative, using either mixed acid or HNO_3 alone, required the more severe conditions that were required for the triazine IV. The only isolated product was 5,5-diethylpyrimidine-2,4,6-trione (5,5-diethylbarbituric acid) (Fig. 8). The dimethyl derivative behaved similarly, but in this case the initially precipitated product re-dissolved and the final product was 2,2-dimethylmalonic acid (Fig. 8).

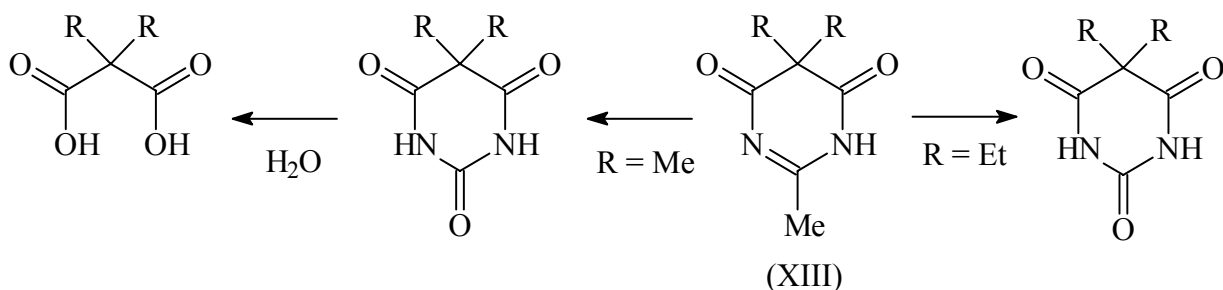


Fig 8. Nitration of XIII.

3. CONCLUSIONS

We conclude that those systems viz. 6-methyl-1,3,5-triazine-2,4(1*H*, 3*H*)-dione (IV) and the 5,5-dialkyl-2-methylpyrimidine-4,6(3*H*,5*H*)-diones (XIII), which we considered would be forced to nitrate in the methyl group, did in fact do so, but nitration in this position was less controlled than in the case of 2-methylpyrimidine-4,6(3*H*,5*H*)-dione (II) and led to the elimination of the methyl group (as a polynitromethane) and its replacement by a carbonyl function. The selectivity in the case of 2-methylpyrimidine-4,6(3*H*,5*H*)-dione (II) may be due, as least in part, to the insolubility of its tetranitro derivative.

4. WARNING

1,1-Diamino-2,2-dinitroethene and various nitrated derivatives described here are potentially explosive and should be treated with appropriate precautions e.g. use protective shielding and avoid friction, impact and vigorous heating.

REFERENCES

- [1] H. ÖSTMARK, H. BERGMAN, U. BEMM, P. GOEDE, E. HOLMGREN, M. JOHANSSON, A. LANGLET, N.V. LATYPOV, A. PETTERSSON, M-L. PETTERSSON, N. WINGBORG, C. VÖRDE, H. STENMARK, L. KARLSSON and M. HIIKIÖ, *2,2-Dinitro-ethene-1,1-diamine (FOX-7) - properties, analysis and scale-up*, ICT Conference on Energetic Materials, Karlsruhe, Germany, 26-1 to 26-21, July 2001
- [2] N. V. LATYPOV, J. BERGMAN, A. LANGLET, U. WELLMAR and U. BEMM, *Synthesis and reactions of 1,1-diamino-2,2-dinitroethylen*, Tetrahedron, **54**, 11525-11536, 1998.
- [3] N. V. LATYPOV, A. LANGLET and U. WELLMAR, *Synthesis of diaminodinitroethylene explosive by nitration and hydrolysis of intermediates*, PCT Int. Appl., WO 9903818 A1, 1999.
- [4] A. A. ASTRAT'EV, D. V. DASHKO, A. Y. MERSHIN, A. I. STEPANOV and N. A. URAZGIL'DEEV, *Some specific features of acid nitration of 2-substituted 4,6-dihydroxypyrimidines. Nucleophilic cleavage of the nitration products*, Russian J.Org.Chem., **37**, 729-733, 2001 (Zhur.org.Khim., **37**, 766-770, 2001)
- [5] I. J. LOCHERT, *FOX-7, a new insensitive explosive*, Australian Department of Defence DSTO Report No. TR-1238, November 2001
- [6] M. SAFTA, F. CHIRALEU, A. T. BALABAN and G. OSTROGOVICH, s-Triazine field (new series). VI. *Quantitative study of active methyl groups in C-methyl-s-triazines. I. Hydrogen exchange kinetics of 6-methyl-s-triazine-2(1H), 4(3H)-dione and its N-methyl derivatives*, Revue Roumaine de Chemie, **17(12)**, 2055-2065, 1972
- [7] G. REMBARZ, E. FISCHER, M. KOBOW, M. MICHALIK and R. OHFF, *Reactions of 2-alkyl(aryl)-4,6-dialkoxy-1,3,5-triazines*, Wiss.Z.Univ.Rostock, Math.-Naturwiss.Reihe, **21(2)**, 113-117, 1972
- [8] A. V. SHASTIN, T. I. GODDOVIKOVA, S. P. GOLOVA, L. I. KHMEL'NITSKII and B. L. KORSUNSKII, *Nucleophilic substitution reactions of 2,4,6-tris(trinitromethyl)-1,3,5-triazine. 1. Reaction of 2,4,6-tris(trinitromethyl)-1,3,5-triazine with alcohols, diols, ammonia and secondary amines*, Khim.Geterotsikl. Soedin, 674-678, 1995
- [9] G. BARBARO, A. BATTAGLIA and A. DONDONI, *Kinetics and mechanism of dimerization of benzonitrile N-oxides to furazan N-oxides*, J.Chem.Soc.(B), 588-592, 1970
- [10] D. J. GLOVER and M. J. KAMLET, *Reaction of trinitromethyl compounds with potassium iodide*, J.Org.Chem., **26**, 4734-4735, 1961

A 1:1 HNS-DIOXAN COMPLEX

A.J. Bellamy and T.P. Price

Department of Environmental and Ordnance Systems, Cranfield University,
Royal Military College of Science, Shrivenham, Swindon SN6 8LA, UK

Abstract:

HNS IV is commonly produced by crash precipitation of a DMF or NMP solution into water. The product usually contains 0.5-1.5 wt% of solvent trapped inside the HNS crystals. This residual solvent may be removed by washing with methanol containing dioxan. However this also causes a dramatic change in particle shape and size, and, unless further washed with pure methanol, the product will contain a considerable amount of dioxan. We have found that this dioxan-containing HNS is in fact a 1:1 complex with a different crystal structure to that of pure HNS. The dioxan may be removed from the complex by either heating above the boiling point of dioxan or washing with methanol. This does not significantly change the outward appearance of the crystals, but it does change the inner structure to that of normal HNS.

Keywords: hexanitrostilbene, HNS IV, dioxan, complex

1. INTRODUCTION

The finely divided form of hexanitrostilbene, commonly known as HNS IV, is usually prepared by the addition of a solution of HNS in an organic solvent e.g. DMF (N,N-dimethylformamide) or NMP (N-methylpyrrolidin-2-one), to water (crash precipitation). The product typically has a specific surface area of 15-30 m²g⁻¹. HNS IV prepared by this method has been found to contain 0.5-1.5 wt% of the original solvent ^[1,2] and this cannot be removed by washing with water. Since the HNS IV may be required for incorporation into a slapper detonator system, it is deemed necessary to remove this occluded solvent. A method for removing the solvent has already been described ^[1]. This involves washing the HNS IV with methanol containing dioxan. Unfortunately this also causes a dramatic change in particle shape and size, and, unless further washed with pure methanol, the product contains a considerable amount of dioxan.

2. RESULTS AND DISCUSSION

The initial product from crash precipitation consists of fine particles of ill-defined shape (see Figure 1). When these are washed with methanol:dioxan (80:20), the particles undergo a dramatic 'recrystallisation' to form needle-shaped crystals (see Figure 2). [This change occurs within <5s when observed under an optical microscope (x1000).] Our study of this washed material using ¹H NMR spectroscopy, differential scanning calorimetry (DSC),

thermogravimetric analysis (TG), FTIR spectroscopy, scanning electron microscopy (SEM) and X-ray crystallography, has shown that it is in fact a 1:1 complex of HNS and dioxan.

^1H NMR spectroscopy (DMSO-d_6) showed 3 singlets integrating for Ar (δ 9.11ppm, 3.84H), $\text{CH}=\text{CH}$ (δ 7.14ppm, 2.00H) and dioxan (δ 3.57ppm, 7.34H) (see Figure 3). DSC analysis showed an endotherm at 112°C , whilst TG analysis showed a mass loss of 16.4% between 40 and 120°C (see Figure 4; theoretical for a 1:1 complex 16.37%). The SEM picture of the sample after loss of dioxan through heating (TG) still showed crystals of needle-like appearance, but the surface of the crystals appeared porous (Figure 5).

The FTIR (KBr) spectrum of HNS IV containing residual NMP (Figure 6) was identical to that of HNS I, but after washing with methanol:dioxan the spectrum had changed significantly (Figure 7). Superficially it had become a combination of the spectra of HNS and dioxan (Figure 8), but with shifts in peak positions. The spectrum of the sample after heating to 140°C in a TG experiment viz. after loss of the dioxan, was again identical to that of HNS I. X-ray powder analysis also showed changes (see Figure 9) that indicated the washed material was morphologically different from HNS IV. The original HNS IV exhibited the same lines as HNS I and HNS II, but with different intensities, the methanol:dioxan washed material exhibited many new lines, but on heating (TG) the pattern reverted to that of HNS IV.

The same complex may also be prepared by rapidly adding a saturated NMP solution of HNS to dioxan (equal volumes), although in this case the particles are very much larger.

A range of charge-transfer complexes of HNS with, for the most part, substituted anilines and phenols has been reported ^[3] but this does not include dioxan. In most cases there were 2 molecules of complexing agent per HNS molecule. A 1:1 charge-transfer complex of HNS with tetrathiafulvalene has also been reported ^[4]. As with HNS-dioxan and HNS itself when recrystallised from NMP ^[5], this is also needle-like in appearance. Both HNS ^[6] and HNS-tetrathiafulvalene are monoclinic. A full crystal structure of HNS-dioxan is not yet complete.

3. CONCLUSIONS

Removal of occluded solvent (NMP or DMF) from HNS IV by washing with methanol:dioxan produces a 1:1 complex of HNS and dioxan which is needle-like in appearance. The dioxan may be removed from this complex by either further washing with methanol, or heating above the boiling point of dioxan. Either treatment leaves the crystals in the needle form, with a porous appearance.

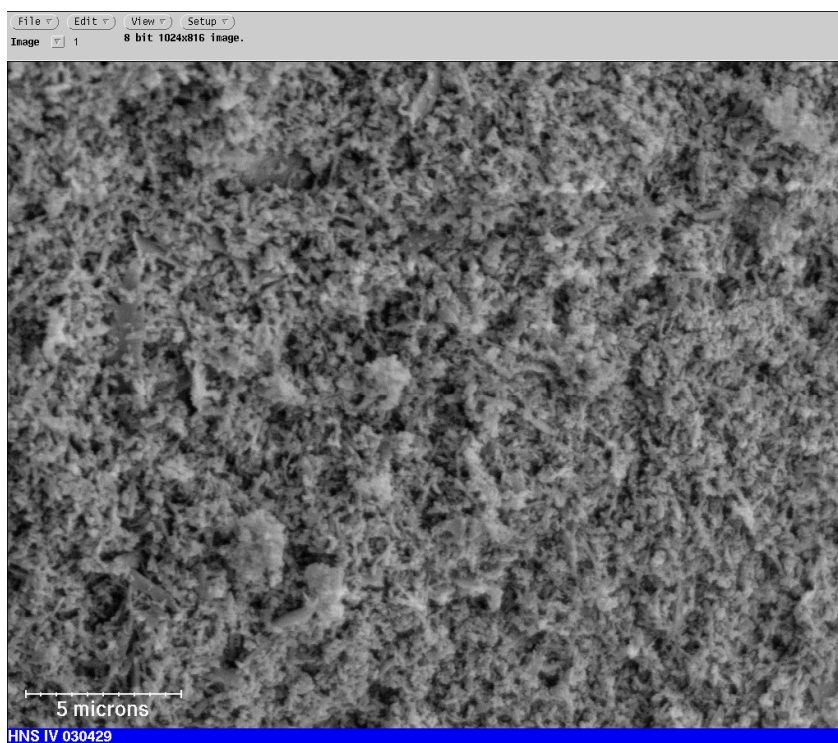


Fig 1. HNS IV

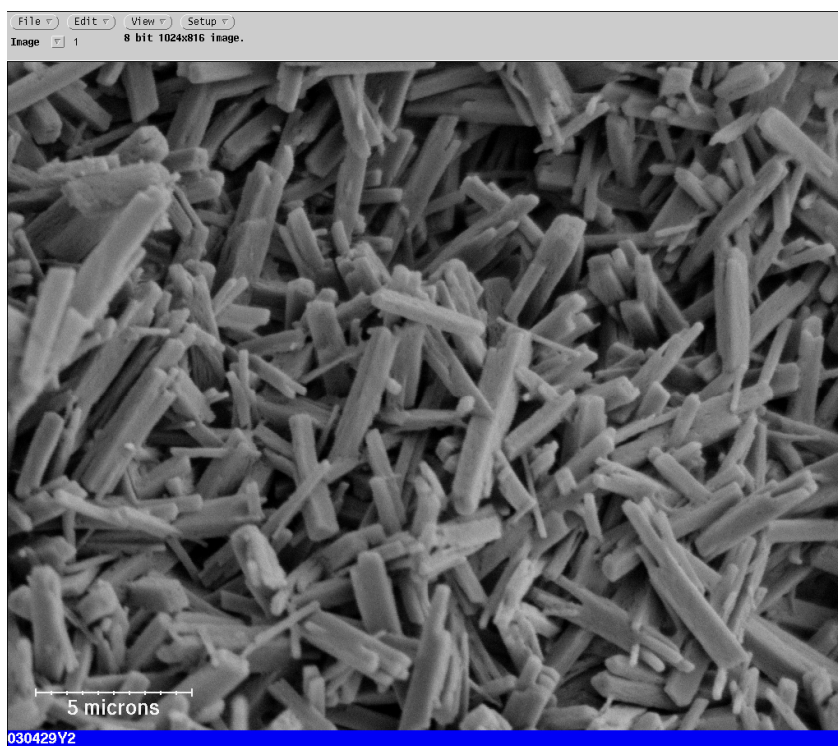


Fig 2. HNS IV after washing with methanol:dioxan

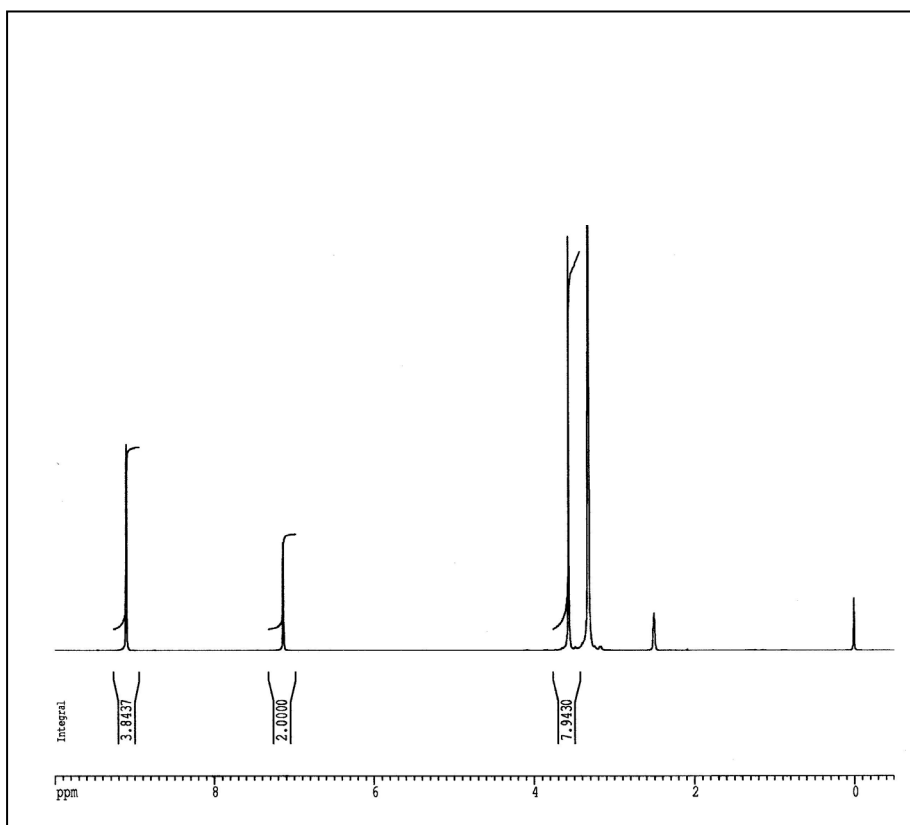


Fig 3. ^1H NMR spectrum (DMSO-d_6) of HNS-dioxan

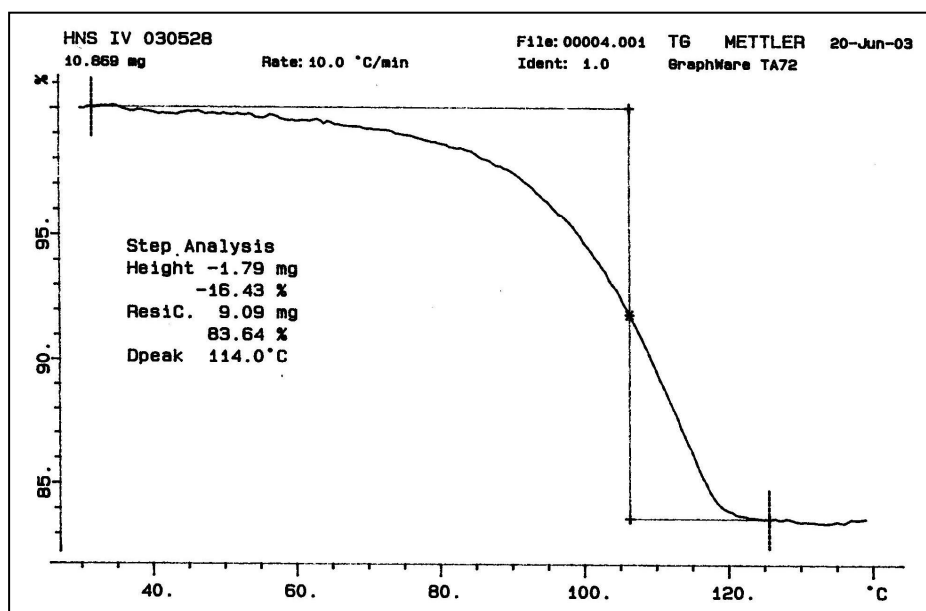


Fig 4. Thermogravimetric analysis (TG) of HNS-dioxan

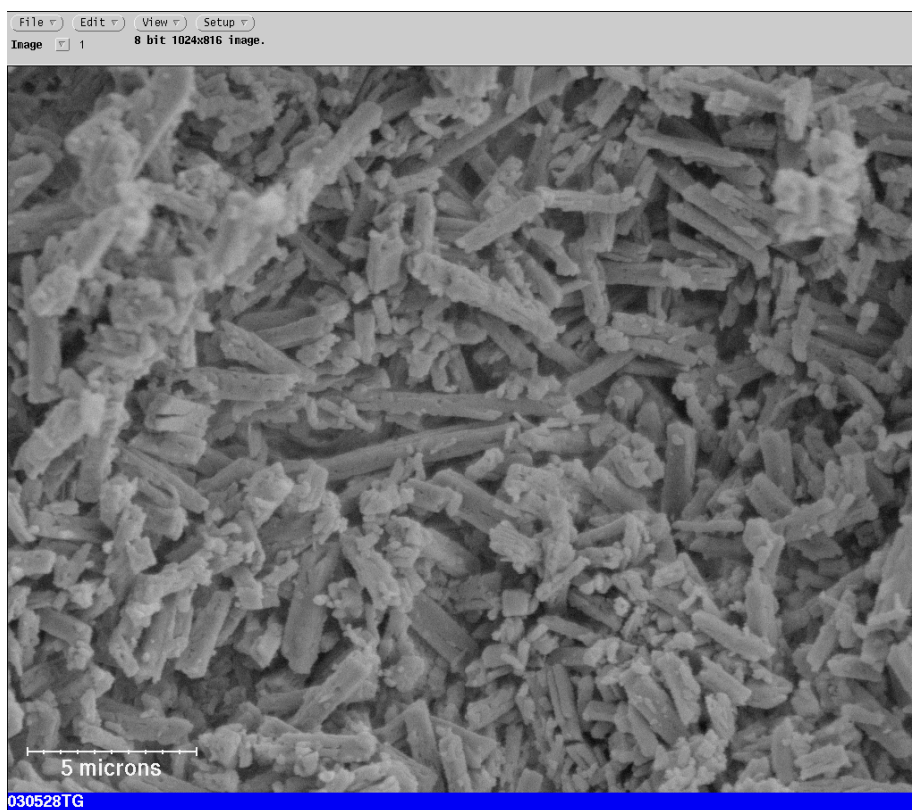


Fig 5. SEM of HNS-dioxan after heating to 140°C

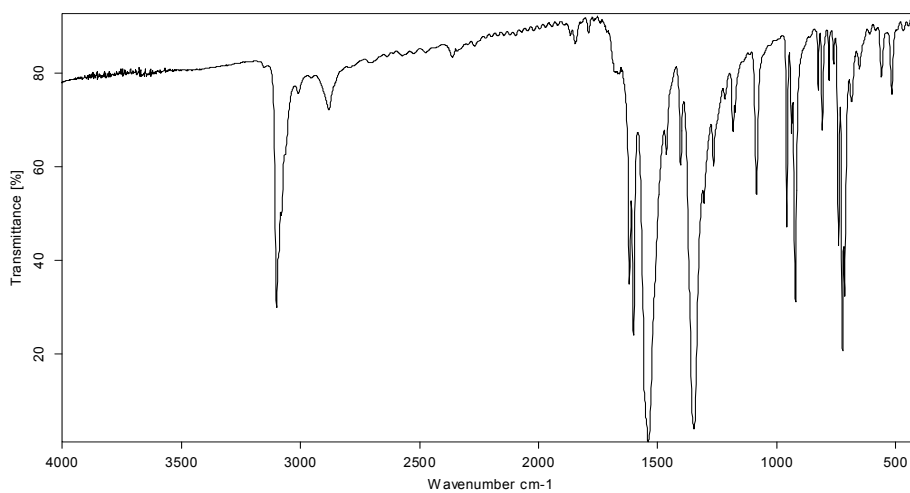


Fig 6. FTIR spectrum of HNS IV (KBr disc)

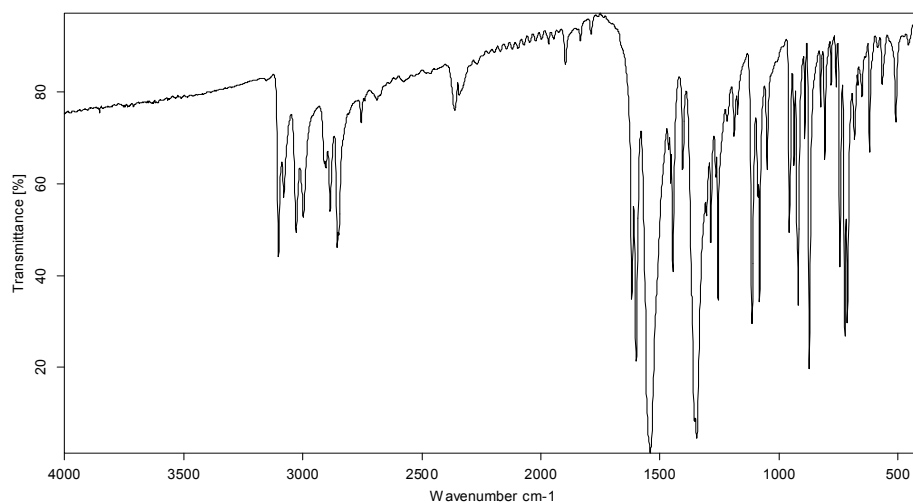


Fig 7. FTIR spectrum of HNS-dioxan (KBr disc)

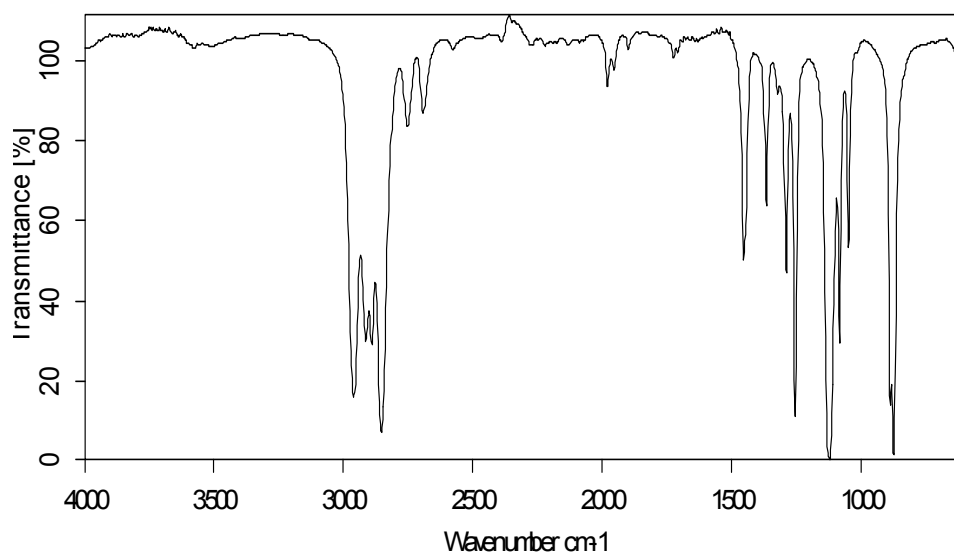


Fig 8. Dioxan (film)

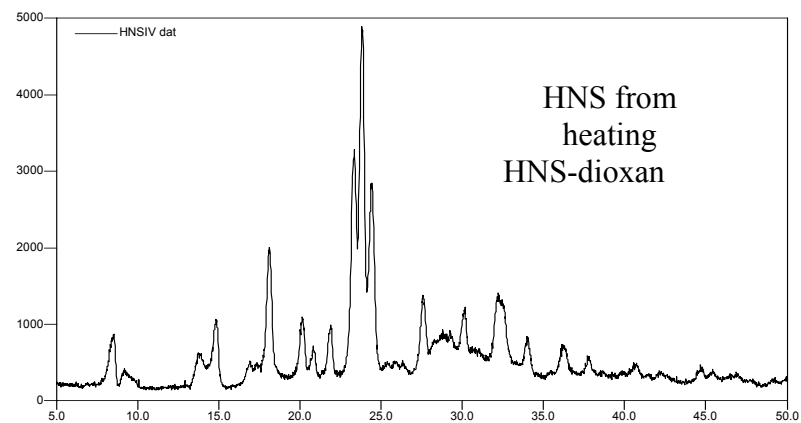
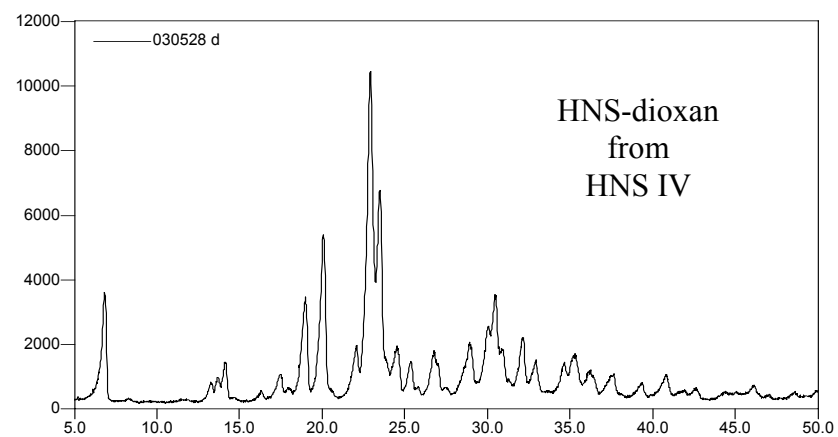
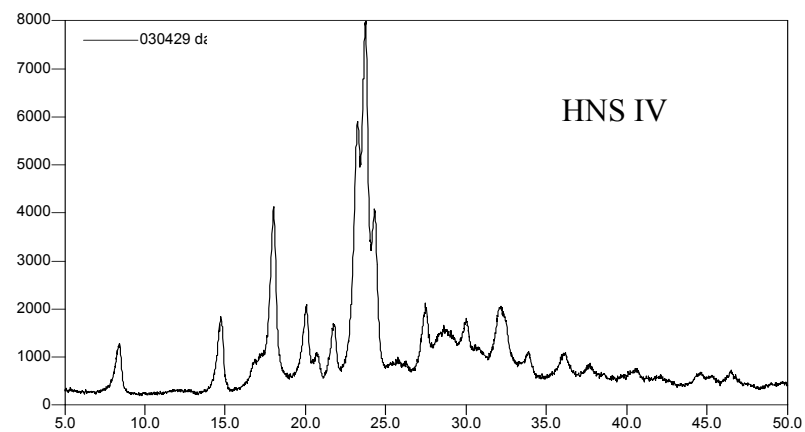
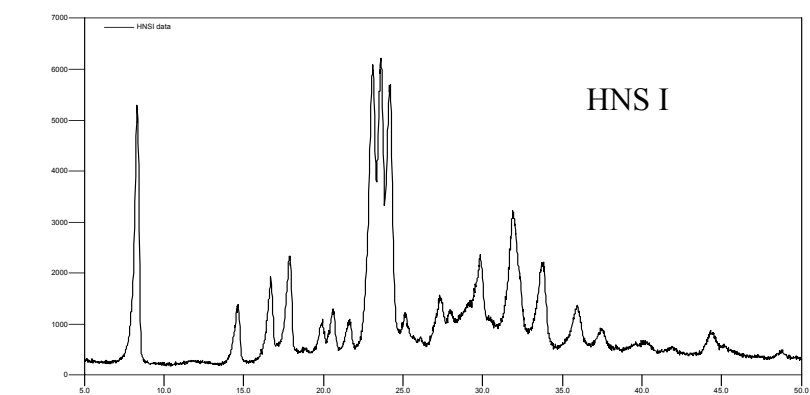


Fig 9. X-ray powder data for various HNS samples.

DETERMINATION OF RESIDUE OF EXPLOSIVES IN ENVIRONMENTAL SAMPLES

J. Bładek, S. Pietrasiak and S. Cudzilo

Institute of Chemistry, Military University of Technology,
Kaliskiego 2, 00–908 Warsaw, PL

Abstract:

Modern TLC equipment was used for determination of 1,3,5-trinitro-1,3,5-triazacyclohexane (RDX, hexogen) post-detonation residues in environmental samples. Chromatographic system suitable for the analyte separation from matrix components and method of densitometric determination of RDX was proposed. A linear dependence of densitometric peak areas A on the analyte mass c [ng] in the chromatographic band was received ($A = 26.302 \cdot c - 484$). A limit detection (150 ng) and maximal range of linear measurements (1800 ng) were determined. Methods of extraction were specified and recoveries of RDX were estimated (they were about 70 %).

Keywords: RDX, detection, analysis, TLC, densitometry

1. INTRODUCTION

Post-detonation analyses of explosive residues are directly associated with combat, and criminal or terrorist activity. Results of such analyses may give information about the type, and sometimes also about the source of explosives. Only a few works devoted to measurements of after-detonation residues of an explosive can be found ^[1, 2]. Unfortunately, a quantitative characterization of this process (for example the mass of an explosive which does not change during detonation or determination of the influence of matrix type on the recovery and quantity of the explosive residue) is not recognized and that is why we concentrated our attention on estimation of these parameters. In this paper result of RDX analyses are presented.

Analyses were carried out by thin layer chromatography (TLC). The method is the oldest, one of the well-known and widespread techniques for the analysis of explosives ^[3]. Most of the works concerning selection of the chromatographic systems and techniques of visualization were realized at the end of the XX century. These early studies were performed on home made chromatographic plates and involved the separation of classical high explosives such as TNT, RDX, HMX and PETN ^[4]. Recently, more sophisticated methods such as spectrophotometry, thermal analysis and column gas or liquid chromatography are commonly used in many laboratories, but TLC is still applied (especially in the instrumental version) to indicate and analyze explosives or as a clean-up technique.

2. EXPERIMENTAL

The possibility of identification and determination of RDX residue getting into matrixes (sand, bricks or concrete) located in the direct neighborhood of explosion of a RDX charge was investigated. The results obtained were also used for estimation of the mass fraction of RDX that did not react in the detonation wave. Experimental part of this work consisted in: (i) – selection of chromatographic systems which are necessary for separation of the analyte from other matrix components which are in a solution, (ii) – estimation of quantitative relations in densitometric measurements, (iii) – evaluation of the efficiency of different extraction methods from the point of view of maximization of recovery and purity of a sample and (iv) – measurements of post-detonation explosive residues.

Apparatus and materials. Applicator LINOMAT IV (CAMAG); horizontal chromatographic chamber DS; densitometer CS-9000 (SHIMADZU); solid phase extraction set (J. T. Baker); chromatoplates with silica gel 60 F₂₅₄ HPLC (MERCK, catalog number 5548) or silica gel with chemically bounded octadecyl (MERCK, catalog number 5559); organic solvents (J. T. Backer, MERCK); explosive standards (Department of Explosives, Military University of Technology).

Selection of chromatographic system. Experiments to select the chromatographic systems were carried out with the standard solution in acetone with concentration of 10 ng/μl. The solution was sprayed (LINOMAT) on the start line of chromatoplates in the form of bands 4 mm in width. The chromatograms were developed to the length of 6 cm in the horizontal chamber DS. The correctness of separation was determined on the basis of observation of fluorescence quenching. The best separation conditions were gained in the case of the following chromatographic system: stationary phase – high-performance silica gel, mobile phase – carbon tetrachloride:acetonitrile 8:1 (v/v).

The determination of quantitative relation $A = f(c)$ (where A – the area of a densitometric peak in relative units of the apparatus, c – mass [ng] of the analyte in the chromatographic band) was also conducted using the standard RDX solution (10 ng/μl). First, absorption spectrum of RDX was measured in order to find the wavelength corresponding to the absorbance maximum λ_{max} . Next, by scanning of a chromatogram (*zig-zag* technique), at the characteristic value of λ_{max} , the amounts of the analyte were determined. To measure the detection limit a quantity of the analyte was chosen for which the densitometric peak area was 5 times larger than the largest noise peak. The average results from five measurements enabled us to specify the equation of the standardization curve and evaluate the limit of detection and the maximum range of linearity of detector indications (Tab. 1).

Table 1. *Analytical parameters of RDX*

R _F	λ_{max} [nm]	Calibration curve $A = f(c)^*$	Correlation coefficient, R ²	Maximum range of linearity, [ng]	Detection limit, [ng]
0.28	226	$A = 26.302 \cdot c - 484$	0.9877	1800	150

* A – surface area of the densitometric peak, c – mass of the analyte in the chromatographic band [ng]

These parameters were also used for an assessment of the RDX recovery in extraction processes and for determination of post-detonation residues.

Extraction. Samples of bricks, concrete and sand of 20 g in mass each were powdered and contaminated with 150 µg of RDX. The analyte was extracted with two portions of acetone, 12 ml each, in an ultrasonic water bath (30°C, 25 minutes) or in Soxhlet apparatus (150 ml of acetone, 5 exchanges). Extracts were dried with anhydrous magnesium sulfate, filtered and concentrated to about 5 ml in an evaporator and then in nitrogen stream to 500 µl. A 5-µl portions of the obtained solutions were placed at the start line of chromatoplates. After developing of chromatograms the masses of the analyte in bands were evaluated (conditions of chromatographic analysis and scanning were the same as during standardization curve measurements). Results of the analyses are presented in Tab. 2.

Table 2. Recoveries of the analyte from different matrixes

Matrix	Recovery, [%]*/standard deviation, [%]	
	Soxhlet apparatus	LSE, ultrasonic
Sand	68.2/4.5	69.2/4.6
Concrete	71.3/5.3	71.8/4.8
Brick	72.0/6.3	72.9/4.9

* – an average value from 5 experimental results

Measurements of after-detonation residues of RDX. Explosive experiments were conducted in a steel tube with inside diameter of 120 mm, wall thickness of 30 mm and length of 800 mm. The tube was placed on a steel plate of 10 mm thick which was used as the tube lock, Fig. 1.

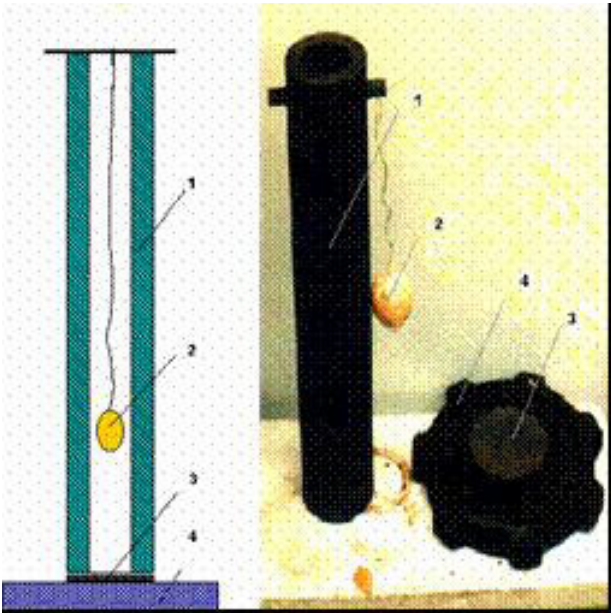


Fig 1. A scheme and a view of the experimental stand: 1 – steel tube, 2 – explosive charge and matrix, 3 – bottom lock of the tube, 4 – tube base

An RDX charge of 25 g in mass surrounded by the matrix material was positioned axially inside the tube at a distance of 1/3 tube length measured from the bottom. Matrixes were placed in paper containers or foil bags and then fused with blasting cap, Fig. 2.

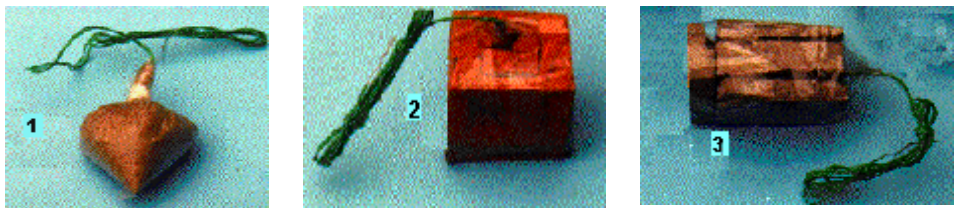


Fig 2. Photos of fused RDX charges immersed in matrixes:
1 – sand, 2 – brick, 3 – concrete

After detonation the internal tube walls were swept with a bore brush, the tube was taken off the base and some matrix fragments that remained on it (treated like representative samples) were analyzed. Exemplary results of densitometric measurement are presented in Fig. 3.

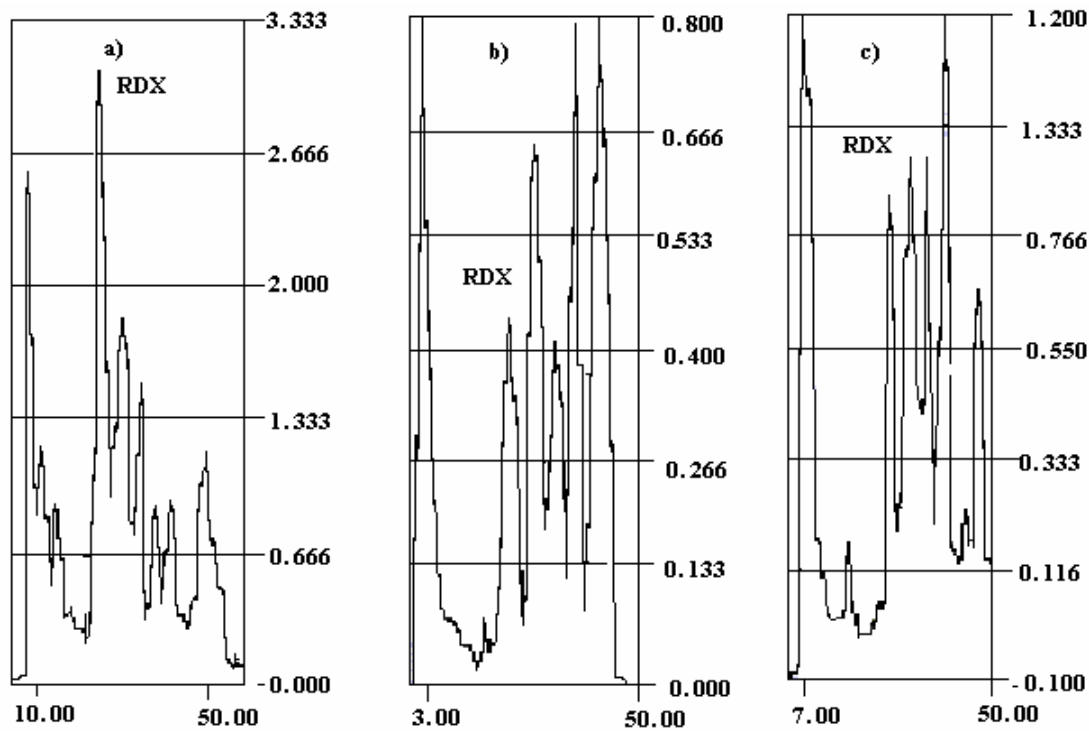


Fig 3. Results of densitometric measurements of chromatograms of RDX post-detonation extracts from different matrixes: a) – brick, b) – concrete, c) – sand, abscissa – distance of elution, ordinate – absorbance

In each case, i.e. regardless of the matrix type and the analytical purpose, explosive experiments and consecutive analyses were repeated five times in order to get the possibility to assess the method's repeatability and measuring errors. Results of the analyses are presented in Tab. 3.

Table 3. *Residues of RDX in matrixes after detonation of a 25-g charge*

Matrix	Results of analyses	
	Mass [µg]	Standard deviation [%]
Sand	1134	4.7
Concrete	676	5.3
Brick	497	4.7

3. CONCLUSIONS

The performed experiments have shown the possibility of the application of the modern instrumental TLC for an analysis of RDX residues in environmental samples. The developed method allows qualitative and quantitative analysis of RDX in samples taken from the close vicinity of the explosive charge. One should emphasize the high reliability of such analyses, because in the case of densitometric measurements it is possible not only to compare the *R_F* value but also the UV spectra of the analyte.

An analysis of the experimental results enables us to state that after detonation of a small explosive charge only a slight amount of the explosive remains in environmental samples taken from the place of explosion. The mass fraction of unreacted RDX calculated as a ratio of RDX mass found in a matrix to the mass of RDX charge equals $10^{-6} \div 10^{-5}$. This value is much smaller than that found by T. Baran ^[2] who detonated big explosive charges.

The mass of RDX residue depends on the type of matrix and it increases in series: bricks<concrete<sand. The observed differences in the amount of unreacted RDX may be caused by different density of the materials surrounding the RDX charge.

Acknowledgment:

This research was supported by the State Committee of Scientific Research through Military University of Technology, Grant PBS 700.

REFERENCES

[1] W. H. GRIEST, C. GUZMAN, B. DEKKER: J. Chromatogr., No. 467, p. 423, 1989
 [2] T. BARAN: Prob. Krym., No. 123, p. 562, 1976
 [3] J. BŁĄDEK: Explosives; Thin Layer Chromatography, In: Encyclopedia of Separation Science. Ed.: I. Wilson, C. Cooke and C. Poole, Academic Press Ltd., London, pp. 2782-2789, 2000
 [4] J. YINON AND S. ZITRIN: The Analysis of Explosives, Pergamon Press, Oxford, 1981

CHARACTERIZATION OF THE CARBONACEOUS PRODUCTS OF HALOGENOCARBONS REDUCTION IN COMBUSTION WAVE

S. Cudzilo*, W. Kiciński*, J. Błądek*, A. Arciszewska* and A. Huczko**

* Institute of Chemistry, Military University of Technology,
Kaliskiego 2, 00–908 Warsaw, PL

** Department of Chemistry, Warsaw University,
Pasteura 1, 02-093, Warsaw, PL

Abstract:

In the paper a method of synthesis of carbonaceous materials in self-propagating heat waves is described and results of some physical and chemical investigations of the materials are presented. The chemical (ultimate analysis) and phase (XRD) composition as well as the microstructure (SEM) of the solid reaction products were determined. Next the relation between reactant composition and heats of reaction as well as the amount, type and structure of the reaction products was established. It was shown that some of the obtained materials are characterized by unique structural and surface properties.

Keywords: combustion synthesis, carbon materials, nitrogen adsorption, XRD, SEM

1. INTRODUCTION

Combustion synthesis ^[1] is a self-sustaining chemical process leading to the creation of new compounds and structures as a result of thermally initiated chemical reactions in a mixture of substrates. Chemical reactions occur in a narrow high temperature zone propagating in the initial mixture at a velocity ranging from a few mm/s to several m/s. This zone separates the substance, which has not reacted yet, from the reaction products, and its propagation in a medium capable of exothermic chemical reactions is called combustion wave ^[2]. Due to high temperature gradients in the combustion wave, chemical reactions do not reach equilibrium and therefore the combustion process generates compounds and structures that are difficult to make (or even unattainable) using other methods of synthesis. For example, combustion of mixtures of silicon and its compounds with calcium or iron with polytetrafluoroethene (PTFE) leads to synthesis of silicon carbide monocrystals in the form of nanofibers, and spherical multi-walled carbon nanoparticles ^[3, 4].

Recently published results ^[5] have shown that some other fluorocarbons, e.g. decafluorobiphenyl (DFBF, C₁₂F₁₀) and chlorocarbons, such as hexachlorobenzene (HCB, C₆Cl₆), hexachloroethane (HCE, C₂Cl₆) or chlorinated polyvinyl chloride (SPVC, -C₄H₅Cl₃-) can be used as oxidizing agents. These oxidizers react very vigorously with powdered metals, their alloys and compounds generating large quantities of carbonaceous materials with completely unknown structure, compositions and properties. Continuing this research an attempt to determine their elemental and phase compositions as well as microstructure and surface properties was undertaken.

2. EXPERIMENTAL

Synthesis conditions. The starting mixtures (Tab. 1) were prepared by mixing powders of sodium azide (NaN_3) or calcium silicide (CaSi_2) with organic fluorine or chlorine compounds (PTFE, DFBF, HCB, HCE and SPVC) that act as oxidizers and carbon sources. Some of the mixtures contained ferrocene or diamond powder as additives catalyzing creation of carbon particles, e.g. fullerenes or nanotubes. The reactants were pelleted into cylindrical samples of 10 g in mass. The sample was placed in a graphite crucible and ignited by an electrically heated igniter attached to the top of the pellet. The combustion synthesis was carried out in argon atmosphere (0.5 MPa) in a calorimetric bomb in order to monitor the heat of reaction. Compositions of the mixtures tested and results of measurements of the heat effects accompanying their combustion are collected in Table 1.

Table 1. *Composition of the studied mixtures and results of calorimetric measurement*

Lp.	Mixture composition [wt %]	Additive and its contents [wt %]	Heat of reaction Q [kJ/kg]
1.	$\text{NaN}_3/\text{PTFE} = 62.2/37.8$	-	3460
2.	$\text{NaN}_3/\text{PTFE} = 72.2/27.8$	Ferrocen – 20%	3410
3.	$\text{NaN}_3/\text{C}_{12}\text{F}_{10} = 66.1/33.9$	Diamond – 2%	2630
4.	$\text{NaN}_3/\text{C}_{12}\text{F}_{10} = 66.1/33.9$	Ferrocene – 10%	3220
5.	$\text{NaN}_3/\text{C}_6\text{Cl}_6 = 57.8/42.2$	-	2630
6.	$\text{NaN}_3/\text{C}_6\text{Cl}_6 = 57.8/42.2$	Ferrocene – 10%	2860
7.	$\text{NaN}_3/\text{C}_6\text{Cl}_6 = 57.8/42.2$	Ferrocene – 20%	2780
8.	$\text{NaN}_3/\text{C}_6\text{Cl}_6 = 57.8/42.2$	Diamond – 2%	-
9.	$\text{NaN}_3/\text{C}_2\text{Cl}_6 = 52.2/47.8$	-	2590
10.	$\text{NaN}_3/\text{C}_2\text{Cl}_6 = 62.2/37.8$	Ferrocene – 20%	2810
11.	$\text{NaN}_3/\text{C}_2\text{Cl}_6 = 62.2/37.8$	Diamond – 2%	2320
12.	$\text{NaN}_3/\text{C}_2\text{Cl}_6/\text{C}_6\text{Cl}_6 = 60/18.9/21.1$	-	2430
13.	$\text{NaN}_3/\text{SPVC} = 55.0/45.0$	-	2700
14.	$\text{CaSi}_2/\text{C}_{12}\text{F}_{10} = 37.7/62.3$	-	5030
15.	$\text{CaSi}_2/\text{C}_6\text{Cl}_6 = 16.85/83.15$	-	2430
16.	$\text{CaSi}_2/\text{C}_2\text{Cl}_6 = 39.6/60.4$	-	3100
17.	$\text{CaSi}_2/\text{SPVC} = 43.2/56.8$	-	1970

The solid products of combustion were washed out from the reactor with water. The obtained suspension was filtered off and the deposit was washed with ethanol. After drying, the reaction products were analyzed using elemental analysis, X-ray diffraction and scanning electron microscopy to characterize their chemical composition and structural features.

Elemental and phase analyses. The elemental analyses of recovered solid products were carried out in order to determine the total carbon content. All the result reported here were obtained using Perkin-Elmer Analyser CHNS/O Model 2400. The runs were performed applying an elongated time of combustion. X-ray diffraction (XRD) spectra were measured using a Simens Diffractometer D500 in conjunction with $\text{CuK}\alpha$ radiation. Measurements were done in the range of 2Θ from 20° to 70° with a step of 0.02° . The XRD data were calcu-

lated and the phase analysis performed utilizing an in-house program, XRAYAN. Results of the analyses are presented in Table 2.

Table 2. *Results of elemental and phase analyses of products of combustion*

Lp.	Mixture composition [wt %]	Additive and its contents [wt %]	Carbon con- tents [wt %]	Phases identi- fied (XRD analysis)
1.	NaN ₃ /PTFE = 62,2/37,8	-	60.3	C, NaF
2.	NaN ₃ /PTFE = 72,2/27,8	Ferrocene – 20%	52.1	C, NaF
3.	NaN ₃ /C ₁₂ F ₁₀ = 66,1/33,9	Diamod – 2%	83.9	C, NaF
4.	NaN ₃ /C ₁₂ F ₁₀ = 66,1/33,9	Ferrocene – 10%	57.6	C, NaF
5.	NaN ₃ /C ₆ Cl ₆ = 57,8/42,2	-	79.8	C
6.	NaN ₃ /C ₆ Cl ₆ = 57,8/42,2	Ferrocene – 10%	65.0	-
7.	NaN ₃ /C ₆ Cl ₆ = 57,8/42,2	Ferrocene – 20%	61.1	-
8.	NaN ₃ /C ₆ Cl ₆ = 57,8/42,2	Diamond – 2%	77.1	C
9.	NaN ₃ /C ₂ Cl ₆ = 52,2/47,8	-	71.3	C
10.	NaN ₃ /C ₂ Cl ₆ = 62,2/37,8	Ferrocene – 20%	51.7	-
11.	NaN ₃ /C ₂ Cl ₆ = 62,2/37,8	Diamod – 2%	71.6	C
12.	NaN ₃ /C ₂ Cl ₆ /C ₆ Cl ₆ = 60/18.9/21.1	-	75.0	C
13.	NaN ₃ /SPVC = 55,0/45,0	-	79.0	-
14.	CaSi ₂ /C ₁₂ F ₁₀ = 37,7/62,3	-	-	-
15.	CaSi ₂ /C ₆ Cl ₆ = 16,85/83,15	-	64.3	C, Si, SiC, Fe ₂ C
16.	CaSi ₂ /C ₂ Cl ₆ = 39,6/60,4	-	17.2	C, Si, SiC, FeSi ₂
17.	CaSi ₂ /SPVC = 43,2/56,8		22.7	C, SiC, Si, FeSi ₂

Structural analysis. Solid reaction products were examined by scanning electron microscopy (SEM, LEO 5000, operating at 20 kV). Carbon in the form of spherical particles with diameters ranging from 30 to 100 nm was found in every sample (Figs 1÷2).

In Fig. 1 there are shown SEM images of the combustion products of NaN₃/C₆Cl₆ mixture with addition of diamond or ferrocene. In both cases the structure is similar so that the kind of the additive does not affect the structure of combustion products.

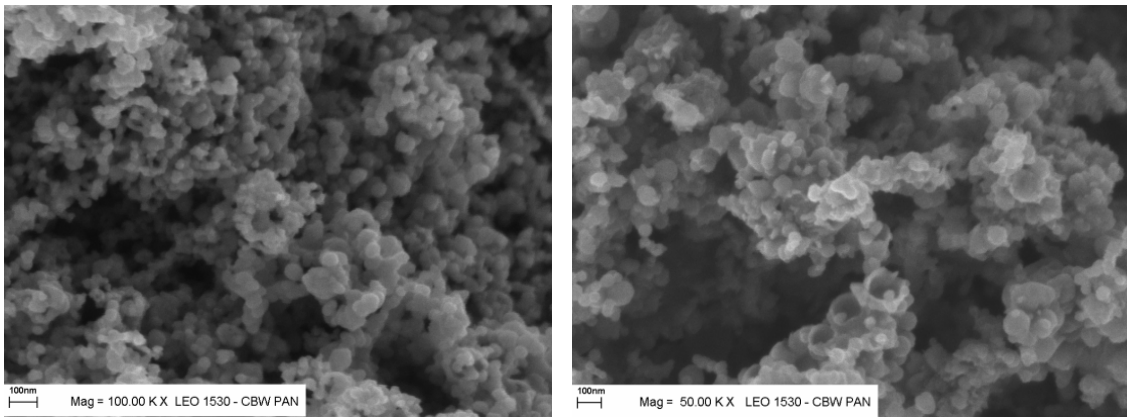


Fig 1. SEM images of combustion products of NaN₃/C₆Cl₆ = 57,8/42,2 mixture with diamond (left side) and ferrocene (right side)

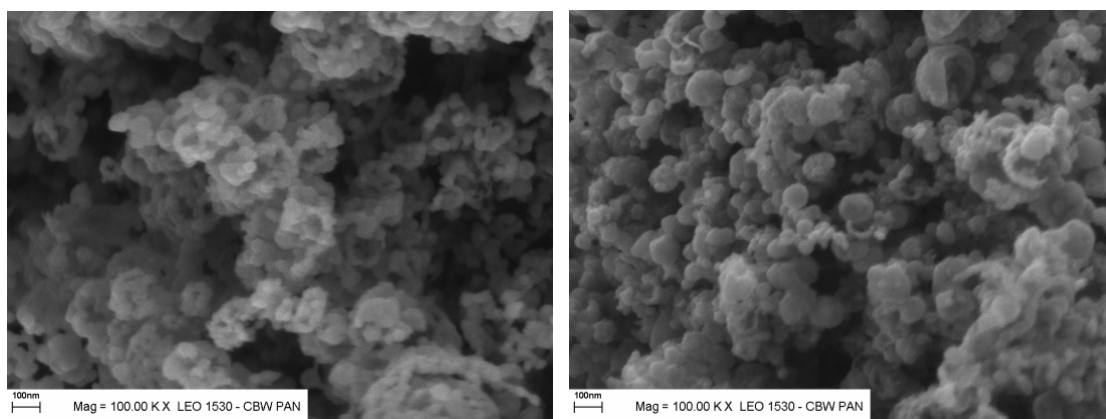


Fig 2. SEM images of combustion products of $\text{NaN}_3/\text{C}_2\text{Cl}_6 = 62,2/37,8$ mixture without additives (left side) and with 20% of ferrocene (right side)

The combustion products are also very similar when C_2Cl_6 is used as an oxidizing agent. This implies that even such an essential change in composition of the starting mixture as replacement of aromatic carbon with aliphatic carbon does not cause a dramatic change in the structure of combustion products.

Adsorption measurements. Low temperature nitrogen adsorption was used to characterize the porous structure of chosen combustion products. Nitrogen adsorption isotherms for all samples studied were measured at 77 K on a Micromeritics ASAP 2010 volumetric adsorption analyzer (Norcross, GA, USA). A high purity nitrogen was used to measure the amount adsorbed as a function of the equilibrium pressure. Before each adsorption measurement the sample was outgassed under vacuum at 200 °C for at least 2 h.

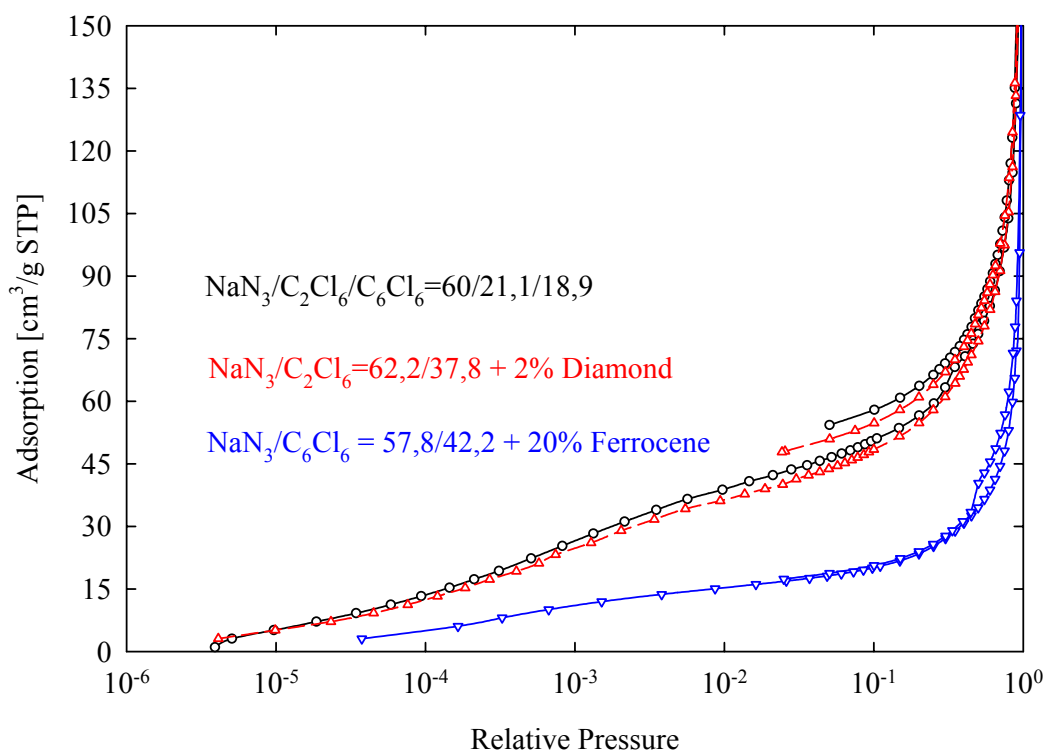


Fig 3. Nitrogen adsorption-desorption isotherms at 77K for combustion products of sodium azide – chlorocarbons mixtures with additives

Exemplary nitrogen adsorption isotherms at 77 K on combustion products of $\text{NaN}_3/\text{C}_2\text{Cl}_6 = 62.2/37.8$ with 2% of diamond, $\text{NaN}_3/\text{C}_6\text{Cl}_6 = 57.8/42.2$ with 20% of ferrocene and $\text{NaN}_3/\text{C}_2\text{Cl}_6/\text{C}_6\text{Cl}_6 = 60/21.1/18.9$ compositions are shown in Fig. 3. The amount adsorbed expressed in cm^3 STP per gram is plotted as a function of the logarithm of the relative pressure.

The specific surface area S_{BET} and the volume of nitrogen necessary to cover unit mass of the adsorbent with a monomolecular layer V_{m} were determined according to the well-known BET method [6]. The total pore volume was estimated by converting the volume adsorbed at the relative pressure of 0.99 to the volume of liquid nitrogen. Results of the analyses are shown in Tab. 3.

Table 3. Adsorption parameters evaluated on the basis of nitrogen isotherms

Composition of the starting mixture	$p/p_{0\text{BET}}$	S_{BET} [m^2/g]	V_{c} [cm^3/g]	V_{m} [$\text{cm}^3/\text{g STP}$]
$\text{NaN}_3/\text{C}_2\text{Cl}_6 = 62,2/37,8 + 2\%$ Diamond	$0.043 \div 0.300$	193	0.64	43.3
$\text{NaN}_3/\text{C}_6\text{Cl}_6 = 57,8/42,2 + 20\%$ Ferrocene	$0.037 \div 0.251$	84	0.28	19.2
$\text{NaN}_3/\text{C}_2\text{Cl}_6/\text{C}_6\text{Cl}_6 = 60/21,1/18,9$	$0.043 \div 0.300$	189	0.54	44.5

$p/p_{0\text{BET}}$ – the relative pressure range used for S_{BET} evaluation, S_{BET} – BET specific surface area, V_{c} – total pore volume at the relative pressure $p/p_0 = 0.99$, V_{m} – the volume of adsorbed nitrogen in the monomolecular layer.

3. DISCUSSION

Results of calorimetric measurement show, that the reaction heats reach most frequently its maximum value in the cases when the composition of the starting mixture corresponds to the stoichiometry of reaction leading to creation of carbon and fluoride of a reductant at its highest oxidation number. The heats of reactions vary considerably – from ca. 2000 kJ/kg to about 5000 kJ/kg. Such significant changes of this parameter are accompanied by proportional big changes in the temperature in combustion wave so that by significant changes in synthesis conditions. It was noticed that an addition of 10 or 20% of ferrocene to a mixture increases the heat of combustion. It means that the products of ferrocene decomposition react exothermically with fluorine and chlorine. However a small addition of diamond does not cause noticeable changes in the heat effects.

The contents of carbon in reaction products depends on the starting mixture composition and ranges from ca. 17 to about 80%. The highest yields of carbon were obtained from mixtures of sodium azide with chlorinated hydrocarbons because of NaCl good solubility in water (combustion products were washed out using water). The fact that carbon is not the only combustion product of NaN_3/HCB and NaN_3/HCE mixtures implies that the dechlorination is not complete. Elemental analyses have also shown that alongside chlorine, the samples contain significant amount of oxygen (even up to 10% by weight) and small amount of hydrogen and nitrogen (1÷1,5%). It is undoubtedly a result of adsorption of the atmosphere components on the tested materials. As expected a reduction of the share of carbon precursors in the starting mixtures causes a decrease in the amount of this element in the reaction products. However the influence of ferrocene presence in a mixture on contents of carbon is rather surprising – in each case this additive caused a decrease in the amount of carbon in the combustion products.

XRD analyses showed that alongside expected products, i.e. carbon and fluorides or chlorides of a reductant, the tested samples contained a considerable amount of carbides and silicides. Turbostratic graphite phase was identified in all products with the strongest peak at 2Θ in the $26.50\div 26.65$ range. More phases appeared when CaSi_2 was used as a reductant. In this case silicides and carbides were created in a considerable amount, regardless of the kind of oxidizer.

Spherical carbon particles with outer diameters of $30\div 100$ nm were found in each sample. In many cases these particles had open pores. This means that the porous structure of the carbon materials is formed at least by mesopores ($2\div 50$ nm in diameter) and macropores (diameters above 50 nm). It was also noticed that an addition of ferrocene or diamond to the starting mixtures does not cause noticeable structure changes of the obtained carbons.

A qualitative comparison of the nitrogen adsorption isotherms (Fig. 3) shows that combustion products of two compositions, namely $\text{NaN}_3/\text{C}_2\text{Cl}_6 = 62.2/37.8$ with diamond and $\text{NaN}_3/\text{C}_2\text{Cl}_6/\text{C}_6\text{Cl}_6 = 60/21.1/18.9$ possess almost identical adsorption characteristics. Thus a partial replacement of the aliphatic carbon precursor (C_2Cl_6) with an aromatic one (C_6Cl_6) does not change the porous structure and surface properties of the reaction products. As can be seen in Fig. 3, carbonaceous material obtained from the composition containing ferrocene differs significantly from that measured on the two other samples. Its adsorption capacity is much lower within the entire range of the relative pressure. This may be caused by the fact that the sample contained much less carbon than the two other tested materials.

The volume of nitrogen covering the adsorbent surface with monolayer equals merely to $19\div 45$ cm^3/g STP, whereas the total pore volumes filled with liquid nitrogen at $p/p_0 = 0.99$ are quite high and range from 0.28 to 0.64 cm^3/g . Comparatively high ratio of volume to surface area implies that porous structure of the tested samples includes mainly large mesopores ($20\div 50$ nm in diameter) and macropores (more than 50 nm in diameter). Consecutively, the BET specific surface area does not exceed 200 m^2/g , regardless of the composition of the starting mixture. However, these values of S_{BET} are large enough for some analytic applications of the studied materials, e.g. they can be used as adsorbents for solid phase extraction [7].

Acknowledgment:

This research was supported by the State Committee of Scientific Research through Military University of Technology, Grant PBS 700.

REFERENCES

- [1] A. VARMA, S. ROGACHEV, A. MUKASYAN, S. HWANG: *Combustion synthesis of advanced materials: Principles and applications*, Advances in Chemical Engineering, **24**, p. 79, 1998.
- [2] A. P. HARDT: *Pyrotechnics*, Pyrotechnica Publications, Post Falls, Idaho 2001.
- [3] A. HUCZKO, H. LANGE, G. CHOJECKI, S. CUDZIŁO, Y. QIU ZHU, H. W. KROTO, D. R. M. WALTON: *Synthesis of novel nanostructures by metal-polytetrafluoroethene thermolysis*, J. Phys. Chem. B, **107**, p. 32519, 2003.
- [4] S. CUDZIŁO: *Analiza procesu spalania mieszanin reduktor-politetrafluoroeten*, WAT, Warszawa 2003.
- [5] S. CUDZIŁO, A. HUCZKO, W. KICIŃSKI: *Synteza materiałów węglowych i ceramicznych w fali spalania i badanie ich właściwości*, Biul. WAT, **LII**, p. 145, 2003.
- [6] H. JANKOWSKA, A. ŚWIĄTKOWSKI, J. CHOMA: *Active Carbon*, Ellis Horwood, New York, 1991.
- [7] J. BŁĄDEK, S. CUDZIŁO, A. ARCISZEWSKA: Application of carbonaceous products of halogeno-carbons reduction for solid phase extraction, This Proceedings.

STUDY ON COMBUSTION OF LIQUID AND GELATINIZED GLYCIDYL AZIDE OLIGOMERS

V.Y. Egorshhev, V.P. Sinditskii and M.V. Berezin

Mendeleev University of Chemical Technology
9 Miusskaya Square, 125047, Moscow, Russia

Abstract

Effect of the molecular weight of glycidyl azide oligomers on the burning rate and effect of gelatinization have been examined. It has been shown that combustion of uncured GAP obeys usual rules of monopropellant burning of liquid energetic materials with all resulting consequences (turbulization, unusual burn rate-pressure dependence, etc.). Small additives of PMMA, used as a gelatinizing agent to GAP oligomers appeared to influence drastically their burning behavior through alteration of the viscosity. Data on combustion of uncured neat azide oligomers and their compositions with the polymer as well as data of temperature measurements in the combustion wave have been used to propose the combustion mechanism of azide energetic materials.

Keywords: *glycidyl azide oligomers, burning rate, temperature profiles*

1. INTRODUCTION

Aliphatic polyethers having alkyl azide substituents are of particular interest as energetic binders and plasticizers for solid rocket propellants and gun powders. These compounds have an advantage of not only high energetic performance, but also are capable of affecting the burning rate of propellants. However, the general principle of the modifier action remains to be solved. It may include either a physical contribution at the expense of high burning rate of modifier and prompt heat release in the combustion zone, or a chemical one at the cost of increasing the leading reaction rate in the flame. High-reactive intermediate nitrenes are known to be initial products in the decomposition of azides which reactions with nitrogen oxides can be expected to proceed very fast.

For the most part combustion studies of azide polymers dealt with crosslinked and cured samples.^[1-4] At the same time data on combustion of uncured azide oligomers («as received») coupled with temperature measurements in combustion wave are thought to present considerable interest for generating combustion mechanism of energetic azide polymers and binders.

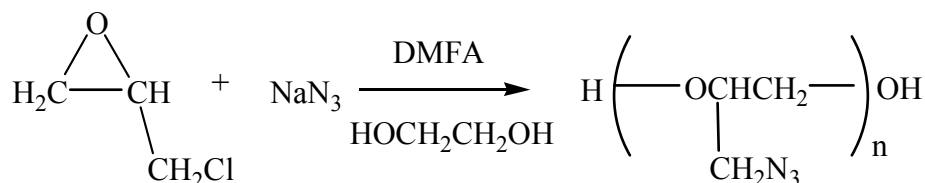
This paper presents a study of the burning behavior and flame structure of glycidyl azide oligomers of low molecular weights as well as compositions gelatinized with polymethylmethacrylate.

2. EXPERIMENTAL

2.1 Sample preparation

Synthesis of low molecular weight GAP directly from epichlorohydrin

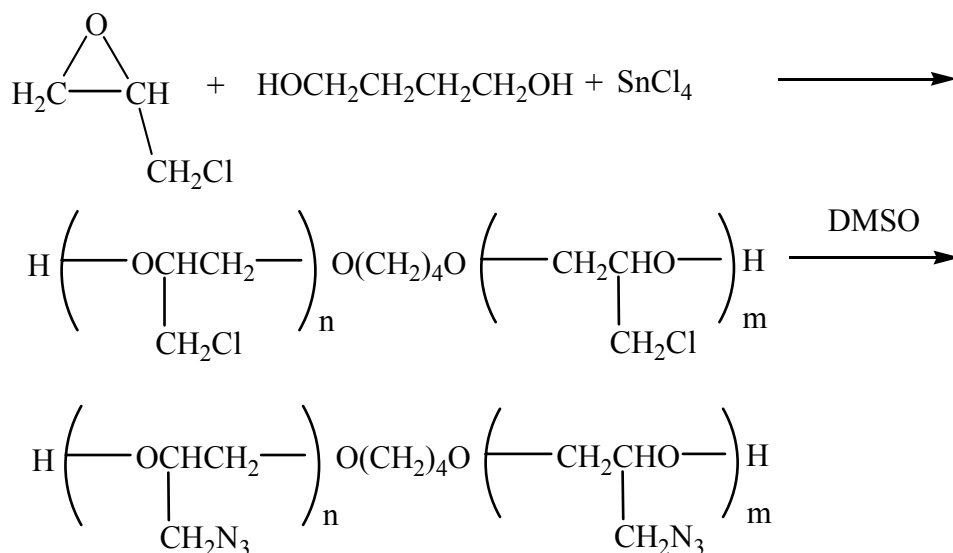
GAP has been prepared by the following reaction scheme:^[5]



Sodium azide 60 g is gradually added to a mixture of epichlorohydrin (ECH) 60 g, dimethylformamide (DMF) 120 g, and ethyleneglycol (EG) 6 g, heating at approximately 70°C and agitation are started. Because of initial exothermic reaction, the temperature is controlled during the first 30 minutes (approx.) of the synthesis. Once the addition of sodium azide is over and no sudden rise in temperature is observed, then the reaction mixture is heated to 90°C and the agitation is carried out at this temperature for about 15 hours. Heating and agitation are stopped and the reaction mixture is allowed to cool. The polymer is given three 300 ml hot water (60°C) washes to remove DMF, EG and the salts (sodium azide and sodium chloride). The polymer is dissolved in 400 ml methylene chloride (MC). The MC solution is dried over magnesium sulfate and then is passed through a column containing 30 g of silica gel. The resultant solution is heated to 50°C to remove MC and then stripped in vacuum to yield 30 g of the GAP polymer: a viscous liquid with an amber color.

Synthesis of GAP diol of molecular weight around 1000 from polyepichlorohydrin

GAP has been synthesized by the following reaction scheme:^[6]



Polymerisation of EPH in the presence of 1,4-butylenediol as initiator and SnCl₄ as catalyst was carried out using procedure described elsewhere in literature. 3 ml (0.033 mole) of 1,4-butylenediol and 9 ml dichloroethane were placed in 250 ml three-necked flask fitted with stirrer, dropping funnel, thermometer, and condenser. 0.2 ml of SnCl₄ was added to the mixture at continuous stirring followed by dropwise addition of 70 ml (0.08 mole) of ECH within 3 hours at temperature of 65°C. To remove the catalyst, the reaction mixture was

treated with water (5x50 ml), then 125 ml of dichloroethane was added and organic layer was dried over CaCl_2 , and remaining solvent was distilled off under vacuum. Yield of light yellow viscous liquid was 61.5 g (75%).

A mixture of 79 g (~0.85 mole) of PECH diol and sodium azide (79 g, 1.21 mole) in 165 ml of DMSO was stirred at 80°C for 24 hr. The precipitated NaCl and unreacted NaN_3 were filtered off, mother liquor poured into an equal volume of water and heated at 80°C for 2 hours. 100 ml of dichloroethane were added and layers were allowed to separate. Organic layer was washed with water (5x80 ml), dried over CaCl_2 , light brown solution was passed through a column containing 40 g of silica gel. The dichloroethane was removed from resultant solution under a reduced pressure to yield 56 g (~70%) of light yellow viscous liquid.

2.2 Structure determinations

Number average molecular weights were determined by cryoscopic method with naphthalene as a solvent. The molecular weight of GAP synthesized directly from epichlorohydrin was measured to be 450-480 (hereinafter called GAP500). The second GAP sample obtained in two-step process *via* polyepichlorohydrin had $\text{MW} = 900\text{-}1500$ (hereinafter called GAP1000).

The ^1HMR -spectra of GAP500 and GAP1000 were obtained at 60 MHz with a HITACHI-1500 spectrometer. Spectra were collected at room temperature in a solution of CDCl_3 with internal standard of tetramethylsilane. The IR-spectra of GAP samples were recorded with SPECORD IR-75 spectrometer.

Differential thermal analysis (DTA) and thermogravimetry analysis (TG) were conducted by using a derivatograf “Paulik, Paulik and Erdey” at a heating rate of 10 K/min.

2.3 Burn rate and temperature measurements

Burn rate measurements were carried out in a window constant pressure bomb of 1.5 liter volume. The pressure range studied was 0.1-36 MPa. A slit camera was used to determine a character of the combustion process as well as burning rate values.

GAP specimens were filled into transparent acrylic tubes of 4 or 7 mm i.d. and ignited with electrically heated nichrome wire.

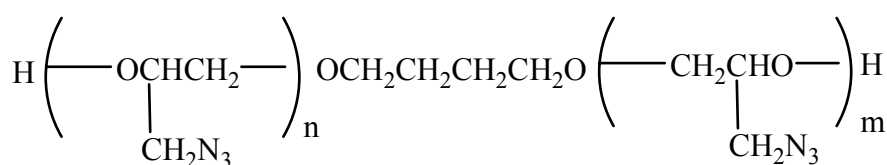
Temperature profiles in the combustion wave of GAP were measured using flat tungsten-rhenium microthermocouples of 7 μm bead size. The thermocouple was embedded across an acrylic tube of 7 mm i.d. filled with GAP, so that the thermocouple bead was placed at the center of the tube. The signal from the thermocouple was recorded with TDS 210 digital oscilloscope.

3. RESULTS AND DISCUSSION

3.1 Structure and analysis data

IR spectra measured for both GAP500 and GAP1000 were almost identical and indicated broad band of absorbance at 3400 cm^{-1} (νOH), and strong absorbance at 2080 cm^{-1} (νN_3), and also absorbances of C-H, C-O and C-N bonds.

Structure formula for GAP1000 presented below was confirmed by elemental analysis data for $n + m = 8$ (Table 1).

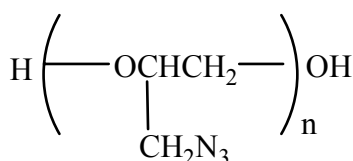


This structure conforms well with ¹HMR-spectroscopy data. The ¹HMR-spectrum of GAP1000 exhibits four groups of peaks corresponding to methylene protons of two central carbon atoms of the butylglycol fragment -CH₂CH₂- (1.6-1.7 ppm), the other protons of CH₂ and CH groups (3.38-3.48 and 3.6-3.8 ppm), and the terminal protons of two diol groups (3.95-4.05 ppm). The proton intensity ratio N_{OH} : N_{-CH₂CH₂-} : N_{CH, CH₂} calculated for GAP1000 structure with m + n = 8 is equal to 2 : 4 : 44. The ratio found from ¹HMR-spectrum is about 2 : 3.8 : 43.

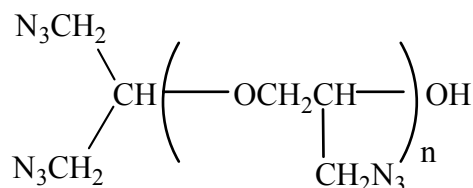
Table 1. *Elemental analysis data for GAP1000.*

Item	Found	Calculated for structure with m + n = 8
MW _n	850-900	882
C, %	38.26	38.10
H, %	5.77	5.67
N, %	39.16	38.10

Structure formula for GAP500 (structure I) proposed by E. Ahad ^[5] appeared to lack support from elemental analysis data. Because of this, another structure has been set forth for GAP500 (structure II), which is consistent with the analysis data (Table 2).



GAP500 structure I ^[5]



GAP500 structure II (proposed)

Table 2. *Elemental analysis data for GAP500.*

Item	Found	Reported in ^[5] for structure (I) with n = 4	Calculated for structure(II) with n = 3
MW _n	450-480	400	439
C, %	32.18	35.7	32.80
H, %	4.93	5.0	4.78
N, %	47.61	39.9	47.84

The ¹HMR-spectrum of GAP500 exhibits only three groups of peaks corresponding to protons of CH₂ groups (3.38-3.48), CH groups (3.6-3.8 ppm), and the terminal proton of the OH group (3.95-4.05 ppm). The found proton intensity ratio N_{OH} : N_{CH, CH₂} is about 1 : 16 and supports generally structure (II), since the theoretical proton intensity ratio for structure (II) is about 1 : 20, and no more than 1 : 10 for structure (I).

0.1% chlorine was determined by elemental analysis for GAP1000 and 0.5% Cl for GAP500.

Exothermic peaks of decomposition were determined by means of DTA to be at 220-250°C for both GAP500 and GAP1000 and corresponded to the temperature of first-stage decomposition for cured and crosslinked GAP (GAP propellant). DG analyses showed, however, that this decomposition of uncured GAP500 and GAP1000 was accompanied by considerably larger weight-loss (95 and 80%, respectively) as compared to GAP propellant (approximately 40%).^[1]

Some properties of the GAP samples, including IR, DTA, and TG data are summarized in Table 3.

Table 3. *Properties of GAP500 and GAP1000.*

GAP500	GAP1000
$\begin{array}{c} \text{N}_3\text{CH}_2 \\ \diagup \\ \text{CH} \left(\text{---} \text{OCH}_2\text{CH} \text{---} \right)_n \text{OH} \\ \diagdown \\ \text{N}_3\text{CH}_2 \end{array}$	$\text{H} \left(\text{---} \text{OCHCH}_2 \text{---} \right)_n \text{OCH}_2\text{CH}_2\text{CH}_2\text{CH}_2\text{O} \left(\text{---} \text{CH}_2\text{CHO} \text{---} \right)_m \text{H}$
MW _n = 450-480	MW _n = 850-900
ΔH _f ^o (calc.) = 197 kcal/mole	ΔH _f ^o (calc.) = 145 kcal/mole
IR: 3430br (νOH), 2080s (νN ₃)	IR: 3440br (νOH), 2080s (νN ₃)
DTA: T exotherm = 220-250°C	DTA: T exotherm = 220-250°C
TG: Weight loss 95%	TG: Weight loss 80%
Density: 1.27 g/cc	Density: 1.27 g/cc

3.2 Combustion behavior of GAP samples of different molecular weights

Uncured samples of GAP500 were found to be capable of sustained burning only at pressures above 200 atm. Burning occurs at a turbulent regime at rather high speeds of the order of tens of centimeters per second. More viscous GAP1000 starts burning at subatmospheric pressures. After a local maximum of the burning rate, combustion is damped out at 6 atm and, at approximately 180 atm it revives again. There exists a region (6-180 atm) within which burning is not sustained (Fig 1).

Data of Kubota and Sonobe,^[1] Hori and Kimura^[3] obtained for cured and crosslinked samples of GAP fall just on the interval, where combustion process for uncured specimens is not sustained.

Liquid alkyl azides easily change their combustion from laminar to turbulent regime as the pressure increases. Laminar combustion of the azides has been observed in the subatmospheric pressure region^[7,8]. Ceasing monopropellant combustion of many liquid explosives (nitroglycerine, for example) is known to be owing to transition from steady-state to turbulent regime, resulting in surface layer heat disbalance and stopping the process^[9]. The noted behavior is conditioned by Landau instability effect,^[10] when disturbance of the liquid-vapor interface (turbulization of the burning surface) appears and progresses until some critical burn rate value is attained, depending on viscosity of the liquid.

The growth of GAP1000 burning rate observed in the low-pressure region is connected with expansion of the burning surface. According to Andreev,^[11] turbulization exerts a double effect: on the one hand it increases the apparent burning rate because of growing burning surface, and on the other hand it can inhibit combustion and lead to extinction because of destroying the preheated layer in the condensed phase. It is likely ambivalent action of turbulization that is responsible for the local maximum of the burning rate on the $b_r(p)$ curve observed for GAP 1000 in low-pressure region. As pressure grows until a certain value, the size of disturbances decreases, resulting in revival of turbulent burning.

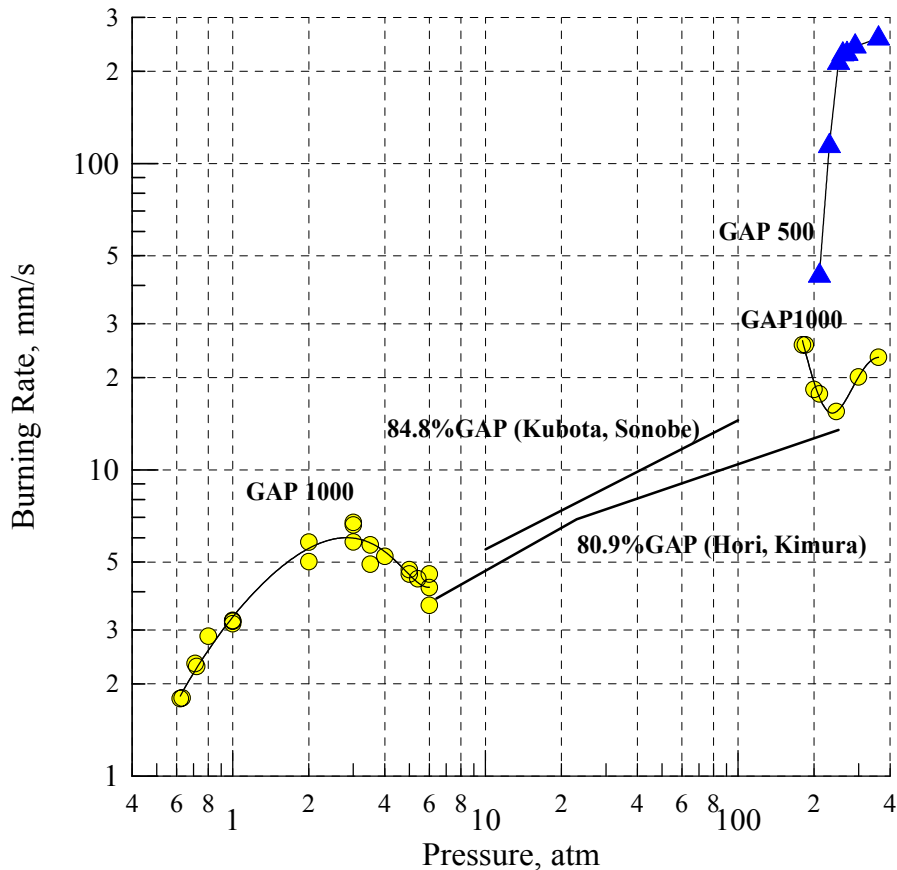


Fig 1. Burning rate vs. pressure for GAP500 and GAP1000, and comparison with literature data for cured and crosslinked GAP specimens.

3.3 Combustion behavior of GAP samples gelatinized with polymethylmethacrylate

Viscosity of GAP oligomers can be also increased by means of thickening with another high-molecular polymer, for example polymethylmethacrylate (PMMA). Gelatinizing liquid GAP500 with PMMA leads to increasing viscosity, which, due to suppressing perturbations on the surface of the liquid, makes it possible to get combustion over larger pressure region. The burning rate decreases, and as little as 5% of PMMA added allows laminar burning at low pressures starting with subatmospheric one (Fig 2).

The formation of light carbonaceous skeleton is observed at low pressures and is not the case at increased ones. The distinguishing feature of combustion of the gelatines is that there also exist pressure regions (3.5-40 atm for 5% gelatine and 5-20 atm for 8% gelatine) within which burning is not sustained. It should be noted that the more PMMA content, the smaller the pressure range of lack of burning. Burning rate vs. pressure dependences for gelatinized

GAP500 also have local maximums at low pressures before extinction as was the case of GAP1000.

Gelatinizing more viscous GAP1000 with 5%PMMA fully remove the pressure region within which burning is not sustained (Fig 3). The fitting line through the experimental burn rate data proves to be parallel to the dependence obtained for cured and crosslinked samples of GAP.^[1] In the low- and high-pressure regions burning behavior of gelatinized GAP1000 is somewhat representative of combustion of the uncured oligomer.

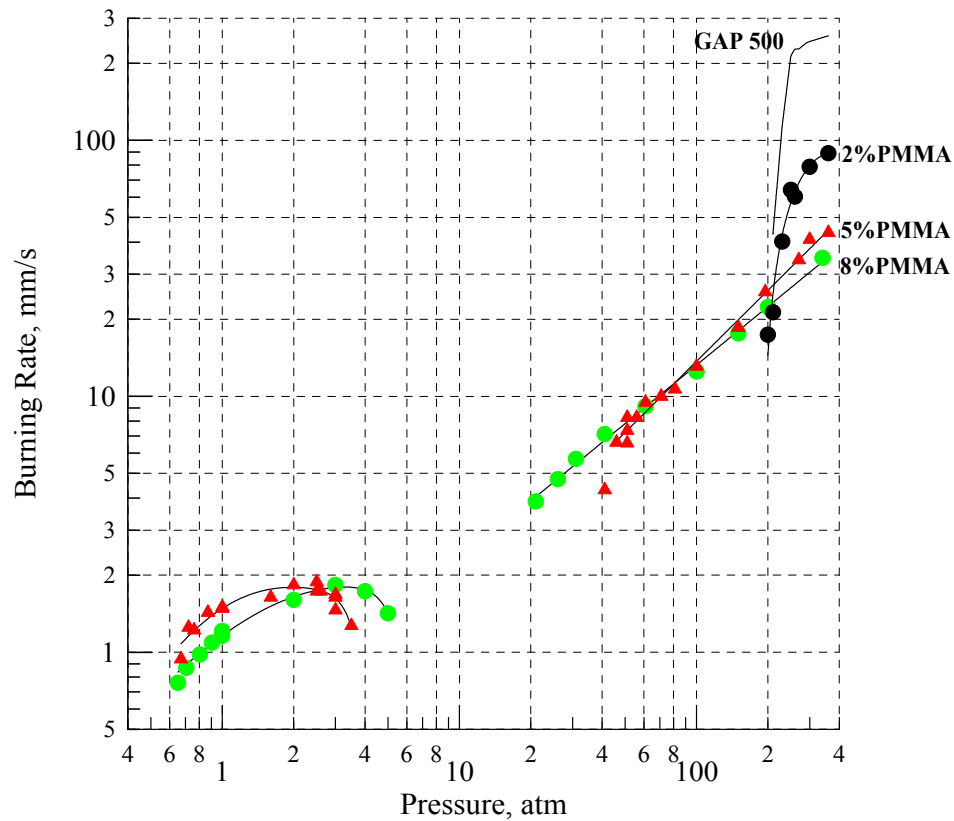


Fig 2. Burning rate vs. pressure for GAP500 gelatinized with PMMA.

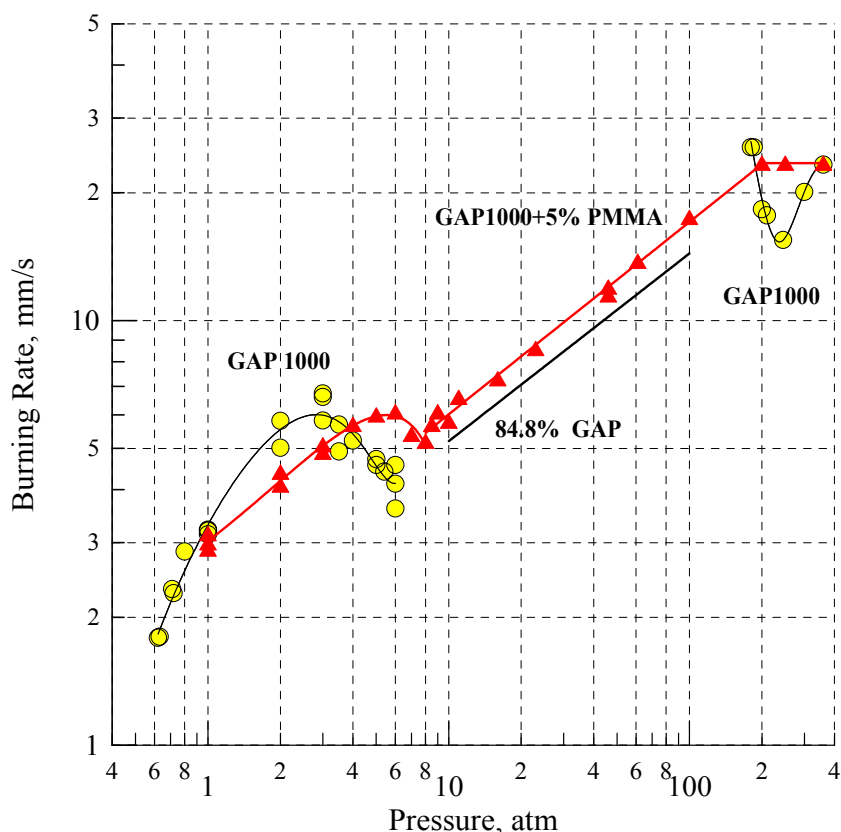


Fig 3. Burning rate vs. pressure for GAP1000 (circles) and GAP1000 gelatinized with 5%PMMA (triangles).

3.4 Temperature measurements in the combustion wave of GAP500 and GAP1000

Flame structure of GAP500 and GAP1000 gelatinized with 5%PMMA has been investigated with 5- μ m-thick Π -shaped tungsten-rhenium tape thermocouples. The pressures tested for GAP500 gelatinized with 5%PMMA were: 1 atm that corresponded to stable burning of the gelatine, 3 atm - in the close vicinity of the burning failure, and 45 atm - immediately after revival of the burning process. These boundary pressure values were chosen also with the aim of getting information about flame structure at critical conditions of GAP burning. Temperature profiles for GAP500 with 5%PMMA are presented in Fig 5 – Fig 6.

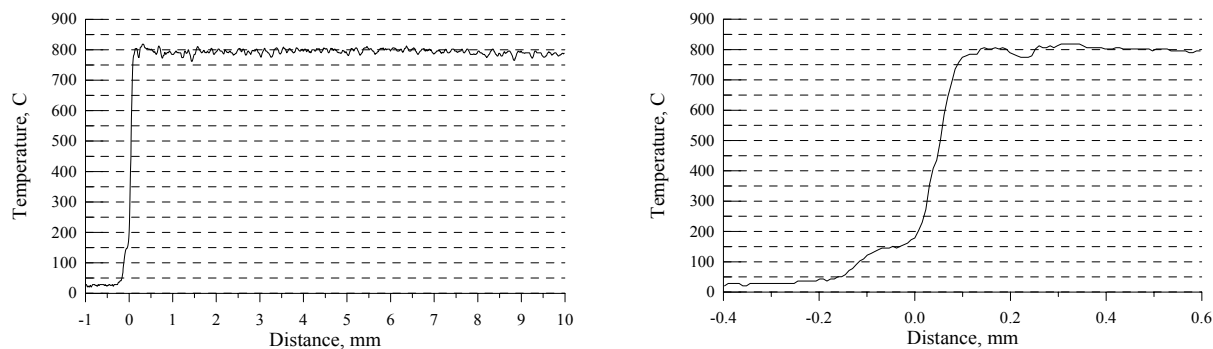


Fig 4. Temperature profiles for GAP500+5%PMMA at atmospheric pressure.

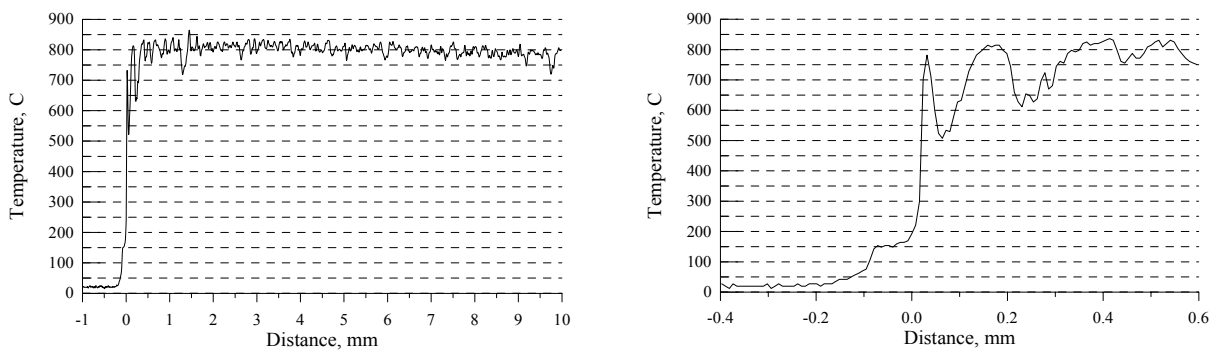


Fig 5. Temperature profiles for GAP500+5%PMMA at 3 atm.

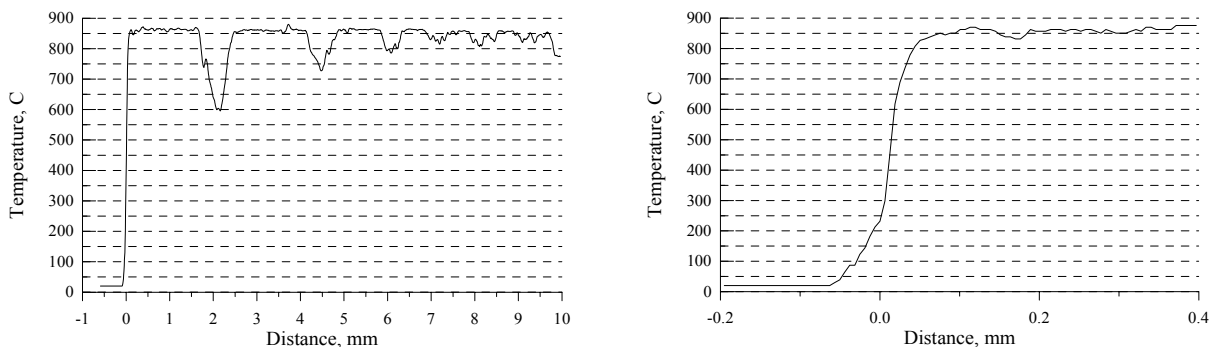


Fig 6. Temperature profiles for GAP500+5%PMMA at 45 atm.

Temperature profiles of GAP500 have revealed very low temperatures at the surface as well as large values of the heat flux transferred back from the gas to the condensed phase. The right part of Fig 4-Fig 6 represents the profiles extended close to the surface. The surface temperature is sharply defined at these profiles. An increase in the surface temperature is not observed at going from atmospheric pressure to 3 atm, but at 45 atm it is significantly higher. At the “critical” values of pressure (3 and 45 atm) the profiles exhibit large fluctuations of temperature in the gas phase. At 3 atm, these fluctuations occur mainly just above the burning surface, whereas the temperature drops take place over full length of the flame at 45 atm (see Fig 5 and Fig 6). Sometimes such temperature drops led to the complete stopping of combustion.

Temperature profiles of GAP1000 were measured at 1 atm for the liquid oligomer and 1, 3, and 8 atm for GAP1000 gelatinized with 5%PMMA. Pressures 1 and 3 atm were taken as previous to the local maximum at the $b_r(p)$ curve, 8 atm as corresponding to the local minimum on the $b_r(p)$ curve, and 45 atm at which burning of uncured GAP1000 oligomer was not sustained. Temperature profiles for GAP1000 and GAP1000 with 5%PMMA are presented in Fig 7-Fig 8.

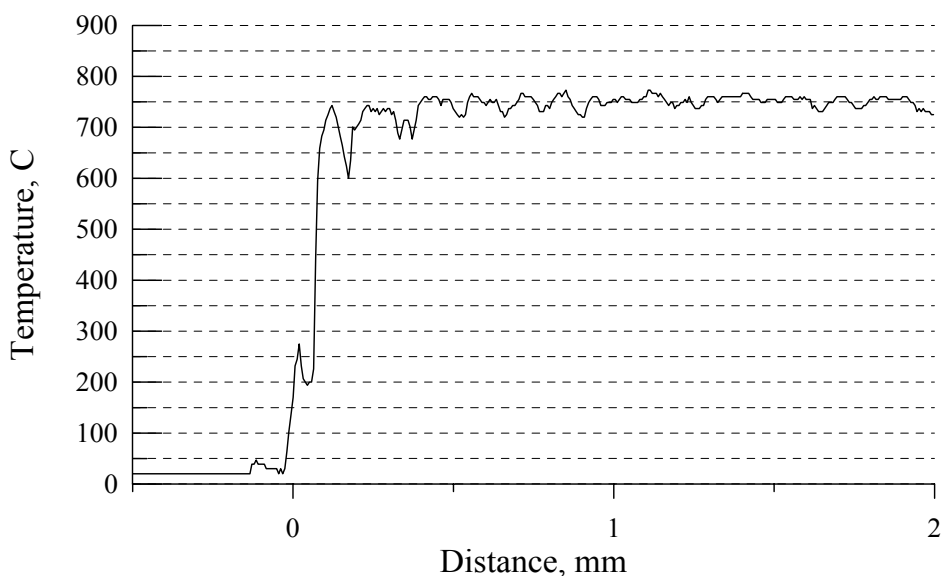


Fig 7. Temperature profiles for uncured GAP1000 at atmospheric pressure.

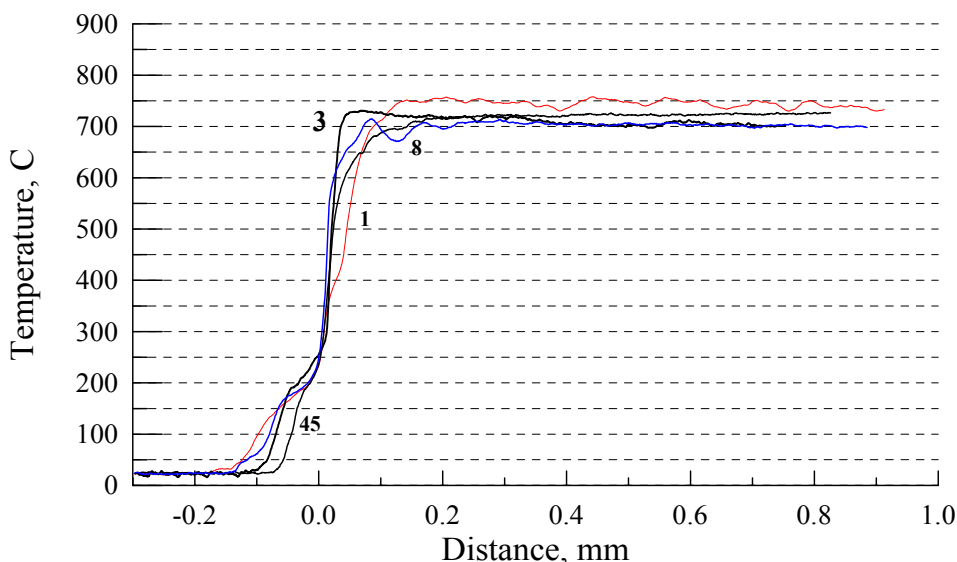


Fig 8. Temperature profiles for gelatinized GAP1000 at different pressures. Numbers at the profiles are pressures in atm.

Burning of uncured GAP1000 at atmospheric pressure is accompanied by strong perturbation of the surface, drop formation and carry-over the drops into the gas phase. This situation is reflected in the appearance of strong temperature fluctuations on temperature profiles (Fig 7). Unfortunately, because of this the surface temperature turns out to be undetectable on these profiles.

Gelatinizing GAP1000 with 5%PMMA eliminates large fluctuations of temperature in the gas phase (Fig 8). The surface temperature is sharply defined at these profiles. At low pressures, the surface temperature of gelatinized GAP1000 oligomer is appreciably higher than that of GAP500, but still much lower than the surface temperature of cured and crosslinked GAP samples.^[1] The surface temperatures are surprisingly weakly dependent on pressure, growing from 230 to 300°C only when pressure increases from 1 to 45 atm.

The surface temperatures of GAP oligomers seem to be too low to correspond to the boiling points of compounds with the molecular weight of 500 and higher. However, it may well correspond to the boiling point of a low-boiling fraction necessarily present in the oligomers.

Results of temperature measurements are summarized in Table 4 and compared with those for cured and crosslinked GAP propellant ^[1].

Table 4. *Results of thermocouple-aided measurements and calculations for combustion of GAP500+5%PMMA, GAP1000, GAP1000+5%PMMA, and GAP propellant.*

Pressure, atm	Experimental				Calculation	
	Surface Tempe- rature T _s , °C	Flame Tempe- rature, T _f , °C	Heat Flux Transferred Back, cal/cm ² s	Heat Feedback from the Gas Phase cal/g	Adiabatic Flame Tempera- ture T _f , °C	Flame Temperatur e if HCN unreacted T _{HCN} , °C
GAP 500 + 5%PMMA						
1	180	800	13±1	71	1365	780
3	180	850	40±2	210	1370	820
45	280	870	-	-	1400	955
GAP 1000						
1	-	750	-		1005	700
GAP 1000+ 5%PMMA						
1	230	725-735	22±2	56		
3	250	725-735	50±6	79		
8	255-260	725-735	60±12	91		
45	265-300	725-735	-	-		
GAP 2000 cured and crosslinked with HMDI and TMP ^[1]						
4 – 8	400-450	730	3.8-6.4		960-990	740-775

As seen from Table 4, the surface temperatures for uncured GAP are considerably lower than those for the cured and crosslinked GAP propellant. At the same time, heat flux transferred back from the gas to the condensed phase is almost ten times greater. Calculations at 1, 3, and 8 atm show that this amount of heat is sufficient for heating-up the condensed phase and, presumably, following evaporation. At pressure of 45 atm, the measurements of the temperature gradient were not made because of too high burning rate and, as a sequence, very narrow burning zones.

Therefore, one may assume that GAP oligomers behave at low pressures as common volatile aliphatic azides, with the gas-phase chemistry being dominated in the combustion process. One can show, using data on decomposition kinetics,^[12] that proportion of GAP which might decompose for the time of consumption (burning out) of the warmed-up layer at the surface temperature of GAP500 and GAP1000 is negligible.

Another point to be mentioned is the flame temperature. Measured values are well below calculated adiabatic flame temperatures for both GAP500 and GAP1000, and for GAP propellant. If the flame temperature is calculated on the assumption that each azide group produces a molecule of HCN as a final product of its transformation, thus saving some energy stored in it, the resulting temperatures T_{HCN} will be in a good agreement with

experimental T_f (Table 4). The formation of nitrile-moiety was proposed in many works, and HCN was experimentally determined as one of the main products of rapid decomposition of GAP and other azidopolymers.^[12,13]

3.5 Combustion mechanism of glycidyl azide oligomers

Thermal decomposition mechanism of organic azides, including glycidyl azide oligomers, is known to involve elimination of the nitrogen molecule to form nitrene intermediate, RN , which reacts further by C-H and C-C bonds first to produce imines and nitriles.^[12,14,15] The secondary reactions of nitrene RN are considered to take place very fast; a rearrangement of the nitrene skeleton has been even suggested to proceed concurrently with liberation of the nitrogen molecule.^[14] Alkyl radical chemical structure has only a slight effect on the decomposition kinetics of alkyl azides,^[15] available decomposition data are quite close together.

Analysis of combustion of organic azides made in work^[16] has shown that the burning rate of volatile alkyl azides is determined by the rate of decomposition reaction at the flame temperature. Experimental data on surface temperatures for GAP and BAMO/THF were used to calculate rate constants from a combustion model based on a dominant role of the condensed-phase chemistry^[17] and the results derived were in a satisfactory agreement with the kinetics of azide polymer slow thermal decomposition.

The results of the present work suggest that glycidyl azide oligomers behave as common volatile aliphatic azides, with the gas-phase chemistry dominated in the combustion process. A comparison between burning behaviors of GAP oligomers of different molecular weights gelatinized with PMMA (Fig 9) shows that gelatinized GAP500 has significantly less burning rates than GAP1000, in spite of close combustion temperatures (Table 4). The pressure exponent in the burning rate low for gelatinized GAP1000 in the 100-200 atm pressure interval is close to 0.5, that is in a good agreement with the first order of the leading reaction on combustion in the gas phase at flame temperature.

At the same time, the pressure exponent for gelatinized GAP500 in this pressure interval is appreciably bigger. The thermocouple measurements indicate to strong perturbation of the surface, drop formation and carry-over the drops into the gas phase. Heat losses caused by these effects are likely responsible for the observed combustion behavior of GAP500.

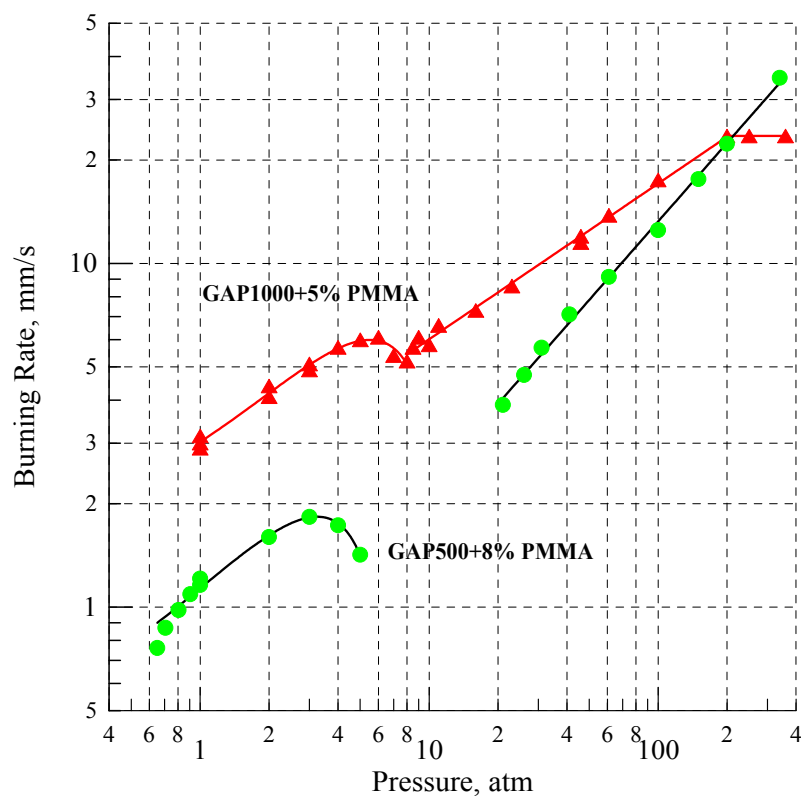


Fig 9. Comparison of burning rates of gelatinized GAP500 and GAP1000

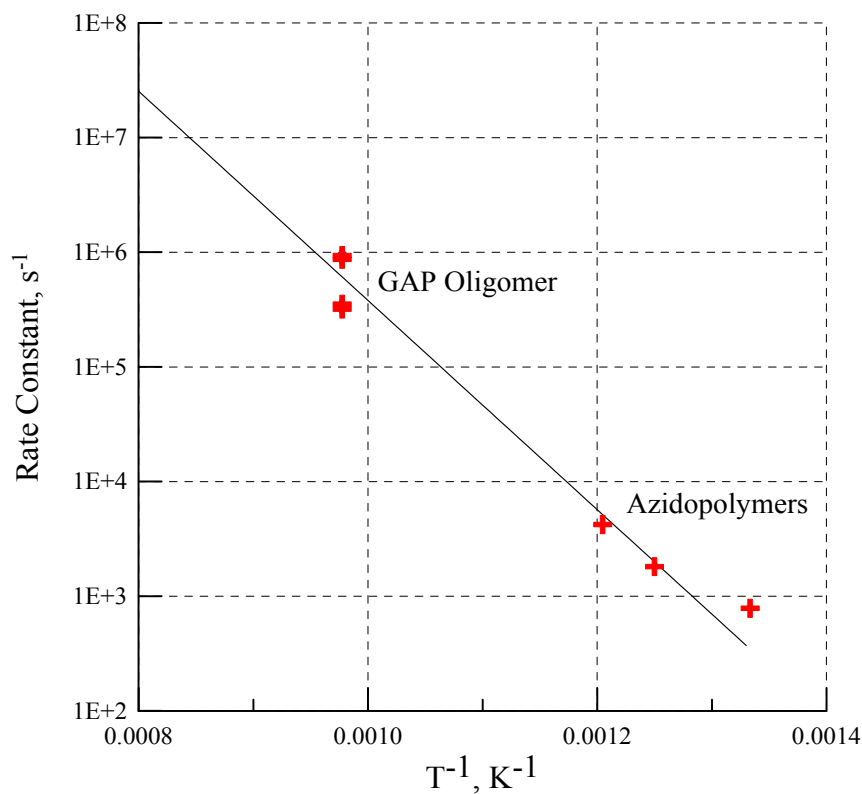


Fig 10. Arrhenius plot of apparent first-order rate constants for the decomposition reaction of GAP (solid line) and rate constants of the leading reaction on combustion of GAP1000 oligomers and polymers (GAP and BAMO) derived from the combustion models.

Rate constants for the leading gas-phase reaction on combustion of GAP1000 gelatinized with 5% PMMA at 1, 3, 8 and 45 MPa have been calculated from the gas-phase combustion model and compared with Arrhenius plot of first-order rate constants for the GAP decomposition reaction^[12] (Fig 10).

In the figure are also presented rate constants for the leading reaction on combustion of GAP and BAMO/THF polymers found previously^[16] from the assumption of the condensed phase priority. As can readily be observed, the burning rate of all the considered azides is governed by the kinetics of the decomposition, irrespective of whether it occurs in the condensed or gas phase.

4. CONCLUSION

Experiments with uncured GAP samples of different molecular weight and structure have shown that the burning behavior is dependent on the molecular weight and physical state of GAP sample. In general, combustion of uncured GAP obeys usual rules of monopropellant combustion of liquid energetic materials with all resulting consequences (turbulization, unusual burn rate-pressure dependence, etc.).

Small additives of PMMA to GAP oligomers appeared to influence drastically their burning behavior through alteration of viscosity. GAP oligomers studied burn seemingly in the gas phase, since any significant decomposition of the azide is impossible in the condensed phase because of very low surface temperature. The burning rate of GAP1000 gelatinized with 5% PMMA is determined by the rate of azide decomposition reaction at the flame temperature.

Incomplete release of energy stored in the azide groups during their decomposition to form HCN molecules is suggested to be responsible for lower measured flame temperature as compared to the calculated adiabatic one.

The burning rate of all the considered azides is governed by the kinetics of the decomposition, irrespective of whether it occurs in the condensed or gas phase.

REFERENCES

- [1] N. KUBOTA AND T. SONOBE: Combustion of GAP Propellants, Proc.19th Int. Ann. Conf. of ICT, paper 2, pp. 1-12, 1988
- [2] G. NAKASHITA AND N. KUBOTA: Energetics of Nitro/Azide Propellants, Propellants, Explosives, Pyrotechnics, Vol. 16, pp.177-181, 1991.
- [3] K. HORI AND M. KIMURA: Combustion Mechanism of Glycidyl Azide Polymer, Propellants, Explosives, Pyrotechnics, Vol. 21, pp.160-165, 1996
- [4] A.N. NAZARE, S.N. ASTHANA AND H. SINGH: Glycidyl Azide Polymer (GAP) - an Energetic Component of Advanced Solid Rocket Propellants - a Review, J. Energetic Materials, Vol. 10, pp.43-63, 1992
- [5] E. AHAD: Direct Conversion of Epichlorohydrin to Glycidyl Azide Polymer, U.S. Patent No 4,891,438, Jan.2, 1990
- [6] S.P. PANDA, S.K. SAHU, J.V. THAKUR, S.G. KUKARNI, C.G. KAMBHAR AND D.S. SADAFULE: Synthesis and Characterisation of Hydroxy Terminated Polyepichlorohydrin and Polyglycidylazide, Defence Science Journal, Vol. 46, No. 5, pp. 399-403, 1996
- [7] V.V. SERGEEV AND M.S. KOZHUKH: On Combustion of 1,3-diazidopropanol-2, Fizika Goreniya i Vzryva (Detonation and Shock Waves), Vol. 11, No 3, pp. 403-412, 1975
- [8] M.S. KOZHUKH AND V.V. SERGEEV: Limit Burning Conditions of Some Organic Azides, Fizika Goreniya i Vzryva (Detonation and Shock Waves), Vol. 13, No 5, pp. 690-698, 1977
- [9] K.K ANDREEV: Book of Articles on the Theory of Explosives, Oborongiz, Moscow, 1940.
- [10] L.D.LANDAU AND E.M. LIVSHITS: Mechanics of Continuous Mediums, Gostechteorizdat, Moscow, 1953
- [11] K.K ANDREEV: "Thermal Decomposition and Combustion of Explosives," Nauka, Moscow, 346p, 1968
- [12] J.K.CHEN AND T.B.BRILL: Thermal Decomposition of Energetic Materials 54. Kinetic and Near-Surface Product of Azide Polymers AMMO, BAMO, and GAP in Simulated Combustion, Combustion and Flame, Vol. 87, pp.157-168, 1991
- [13] Y. OYUMI AND T.B. BRILL: Thermal Decomposition of Energetic Materials 12. Infrared Spectral and Thermolysis Studies of Azide-Containing Monomers and Polymers, Combustion and Flame, Vol. 65, pp.127-135, 1986
- [14] D. BARTON AND W.D. OLLIS: Nitrogen Compounds, Comprehensive Organic Chemistry, Vol. 2, Pergamon Press, New York, 1979
- [15] G.B. MANELIS, G.M. NAZIN, YU.I. RUBTSOV AND V.A. STRUNIN: Thermal Decomposition and Combustion of Explosives and Propellants, Nauka, Moscow, 1996
- [16] V.P. SINDITSKII, A.E. FOGELZANG, V.YU.EGORSHEV, V.V.SERUSHKIN, V.I. KOLESOV: Effect of Molecular Structure on Combustion of Polynitrogen Energetic Materials (Solid Propellant Chemistry, Combustion, and Motor Interior Ballistics, edited by V.Yang, T. B. Brill, and W. Z. Ren), Vol. 185, Progress in Astronautics and Aeronautics, AIAA, Reston, VA, pp.99-128, July 2000
- [17] YA.B ZELDOVICH: Theory of Combustion of Propellants and Explosives, Z. Eksperimental'noy i Teoreticheskoy Fiziki (J.Exper.Theor.Phys.), Vol. 12, pp.498-524, 1942

INVESTIGATION OF DIAMINODINITROETHYLENE (DADNE)

N.V. Garmasheva, I.V. Chemagina, V.P. Filin, M.B. Kazakova and B.G. Loboiko

Zababakhin Russian Federal Nuclear Centre – VNIITF,
P.O. Box 245, Snezhinsk, Chelyabinsk region, 456770, Russia

Abstract:

DADNE (FOX-7 or 1,1-diamine-2,2-dinitroethylene) is investigated by methods of differential-thermal (DTA) and thermo-gravimetric (TGA) analyses. Two exothermal peaks that, presumably, correspond to transitions between polymorphic modifications of this HE, are registered on DTA curve. Heat of low-temperature polymorphic transition ($\sim +113^{\circ}\text{C}$) is estimated as ~ 25 J/g. Heat of high-temperature transition ($\sim +158^{\circ}\text{C}$) is ~ 20 J/g. Presence of two exothermic peaks ($+207^{\circ}\text{C}$ and $+277^{\circ}\text{C}$ under the heating rate of $2^{\circ}\text{C}/\text{min}$) on DTA of DADNE is confirmed. It is shown, that DADNE decomposes in two stages at heating over $+210^{\circ}\text{C}$. The product of the first stage of decomposition of DADNE is new explosive (DADNE-T). The DTA, TGA, FTIR of DADNE-T are carried. The endothermic processes in DADNE-T in the temperature range $+20^{\circ}\text{C} - 400^{\circ}\text{C}$ are not founded. The beginning of exothermic decomposition of DADNE-T is recorded. By results of FTIR it is supposed that DADNE-T is the product of chemical transformation of two molecules of DADNE with participation of the part of amino and nitro groups. The crystals of three types (tetrahedral prisms, crystals of the trimetric form and hexahedral prisms) are received at crystallization of DADNE from acetone, water and water-acetone mixes. Received crystals are investigated by methods of FTIR, DTA and TGA.

Keywords: DADNE (FOX-7), DADNE-T, DTA, TGA, FTIR

1. INTRODUCTION

1.1 DADNE – 1,1-dinitroacetamidine (or 1,1-diamine-2,2-dinitroethylene, or FOX-7).

DTA for FOX-7 have two exothermic peaks instead of one as for the majority of HE ^[1]. The similar results have been received in our researches ^[2] which were carried out on Perkin Elmer devices: thermogravimetric analyzer TGA-7NT, differential - thermal analyzer DTA-7. DTA-curves of DADNE in comparison with HMX are given on Fig.1.

Two exothermic peaks on DTA of DADNE can be observed if:

- DADNE represents the mix of several substances – isomers of DADNE or DADNE and impurities (first peak corresponds to the least thermally stable ingredients decomposition, second one corresponds to the decomposition of more thermally stable ingredients);
- DADNE decomposes in two stages

2. SAMPLES PREPARATION

Samples prepared by DADNE double crystallization from water, acetone and water-acetone mixes.

Crystals of three types have been obtained after crystallization of DADNE: tetrahedral prisms, crystals of the trimetric form and hexahedral prisms.

DTA, TGA, FTIR have been made for different types of DADNE crystals.

DTA, TGA – curves of DADNE samples after crystallization from water-acetone mix in comparison with initial HE is shown on Fig.2 (heating rate is 2 °C /min). The review of received results is given in the Table 1.

Table 1. *DTA results for different samples of DADNE ¹⁾*

Agents for crystallization of DADNE	The kind of crystals	Endothermic peaks ²⁾ , °C		Exothermal peaks ²⁾ , °C	
		1 st peak	2 nd peak	1 st peak	2 nd peak
-	-	113	178	207	277
Water ³⁾	Mix of crystals	115	158	213	279
Acetone ³⁾	Mix of crystals	111	159	223	274
Acetone ⁴⁾	tetrahedral prisms	112	160	226	273
water-acetone mix ³⁾	Tetrahedral prisms	115	158	213	278
	Trimetric crystals	114	155	213	279

Notes:

1) at 2°C /min heating rate; 2) temperatures correspond to the beginning of peaks;

3) double crystallization; 4) single crystallization

Crystalline density for initial and crystallized DADNE have been obtained by pycnometric technique using of hexane as a supplementary fluid. The density of initial DADNE was $\rho_{in}=1,877\pm0,005$ g/cm³. The density of DADNE crystallized from acetone was $\rho_{ac}=1,881\pm0,005$ g/cm³.

FTIR spectra of initial DADNE, tetrahedral prisms and the trimetric crystals received as a result of crystallization of DADNE from acetone. Spectra are received on Fourier transform IR spectrometer SPECTRUM-2000, Perkin Elmer, in the range of 4000 – 370 cm⁻¹ (tablets with KBr). The basic characteristic lines of all samples coincide, that gives the basis for conclusion that initial DADNE and one have been crystallized have an identical molecular structure.

3. ENDOTHERMIC PROCESSES IN DADNE

The endothermic processes taking place initial and crystallized DADNE have been investigated under the heat rate of 2⁰/min.

Table 2. Description of the Test 1

Step number	Heating (max, °C)	Cooling (min, °C)	Step number	Heating (max, °C)	Cooling (min, °C)
1	180		5	180	-
2	-	75	6	-	20 ¹⁾
3	180		7	320	
4	-	100			

Notes: 1) Sample are hold 1 hour

Two endothermic peaks in the ranges of +113 - +120 °C and +155- +161 °C were recorded during initial heating (step 1). During cooling (step 2) in the same temperature range the exothermic signals have not been recorded. This fact allows excluding the assumption about correspondence of endothermic peaks on DTA of DADNE to reversible phase transitions such as, for example, melting.

At reheating (step 3) the endothermic peaks of essentially smaller intensity (in comparison with step 1) have been recorded (Fig.3). The endothermic peaks have not been recorded at cooling down to +100 °C (step 4) and consequent heating up to +180°C (step 5). Two endothermic peaks of initial intensity have been observed after holding of DADNE at ambient temperature within one hour (step 6) and consequent heating up to +320 °C (step 7).

The comparative analysis of received results gives the basis for the supposition about presence at DADNE of several (at least, three) polymorphic modifications, transitions between which have endothermic character and are observed at temperatures ~ 113 °C, ~158°C .

4. EXOTHERMIC PROCESSES IN DADNE

The following experiments were carried out for study of the nature of the exothermic processes in DADNE at heating up (exothermic peaks on DTA).

One of DADNE samples crystallized from water-acetone mix has attacked under the following script (heating rate – 2⁰/min):

Table 3. Description of Test 2

Step number	Heating (max, °C)	Cooling (min, °C)
1	2400	
2	-	50
3	350	

Two endothermic peaks (temperature range +113°C and +156°C) and one exothermic peak at T = +212°C, finished to +240 °C, were recorded at initial heating (step 1). At the next heating (step 3) endothermic signals and the first exothermic peak have not been observed. At T=+277°C only one exothermic peak have been registered on DTA-curve.

The results of the carried out experiment have allowed forming the supposition that during the heating up to +250°C the irreversible processes have taken place in DADNE and as a result the new explosive called by us as DADNE-T was formed.

For checkout of given supposition DADNE (both initial and crystallized) has been thermally treated at T = +210–215 °C during ~1 hour. The compounds of light brown color have been received and the loss of mass was ~ 35 % from the mass of initial sample of DADNE.

TGA- and DTA-curves of DADNE and DADNE-T, received after thermal treatment at temperature +210 °C in 1 hour are shown on Fig.4.

Comparative analysis of FTIR of DADNE and DADNE-T has shown that changes have affected the areas of wave numbers, connected with groups -NH₂ and -NO₂. At the same time, the areas of the complete coincidence of FTIR of DADNE and DADNE-T also include wave numbers of these groups. These circumstances allow to support that transformation of DADNE in DADNE-T takes place with modification of molecular structure of DADNE in which the part of amino- and the part of nitro groups participate. The reaction between amino- and nitro groups of two adjacent molecules of DADNE with formation of heterocyclic compound can be one of possible processes.

5. CONCLUSIONS

The following conclusions can be made on the basis of carried out experiments.

DADNE has several (at least, three) polymorphic modifications, transitions between them have reversible character. At heating of DADNE the polymorphic transitions occur with endothermic effect and have the specific heat ~ 25 J/g for low-temperature (at ~ +113 °C) polymorphic transition and ~20 J/g for high-temperature (~ +158 °C) ones.

The mixes of crystals of three types after crystallization of DADNE from water, acetone and water-acetone mixes are received: tetrahedral prisms, crystals of the trimetric form and hexahedral prisms. By methods of FTIR the differences of the molecular structure of received crystals are not registered.

DADNE decomposes in two stages under the heating higher than +210°C . The product of the first stage of DADNE decomposition is explosive (DADNE-T) which, presumably, is the product of chemical transformation of two DADNE molecules with participation of the part of amino- and nitro groups.

REFERENCES

- [1] H.QSTMAR, A.LANGLLET, N.WINGBORD, U.WELLMAR AND U.BEMM: *FOX-7 – a New Explosive With Low Sensitivity and High Performance*, 11. Symp. On Det (Int.), pp.807-812, 31 Aug – 1 Sep, Snowmass, Colorado, USA, 1998
- [2] I.V. CHEMAGINA, V.P. FILIN, N.V. GARMASHEVA, M.B. KAZAKOVA, YU.A. SHAKHTORIN, N.P. TAIBINOV, B.G. LOBOIKO” *Investigation of Diaminodinitroethylene (DADNE)* 7th Zababakhin Scientific Talking, 8 – 12 Sep, Snezhinsk, Russia, 2003

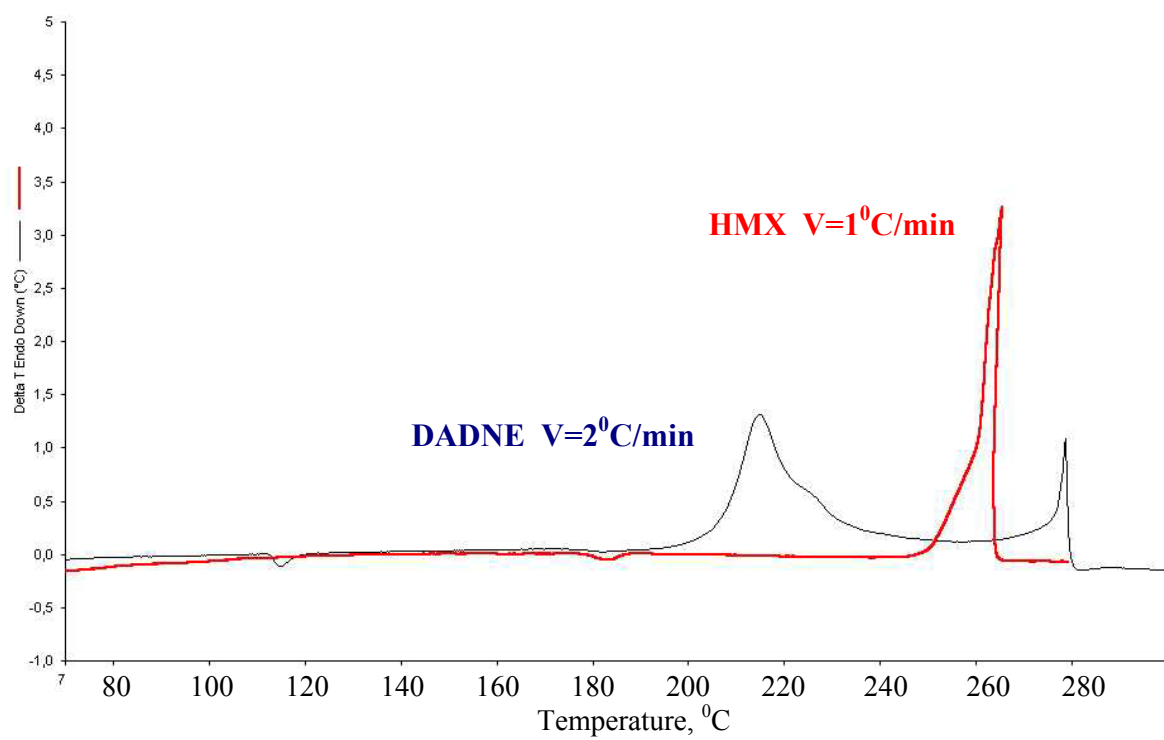
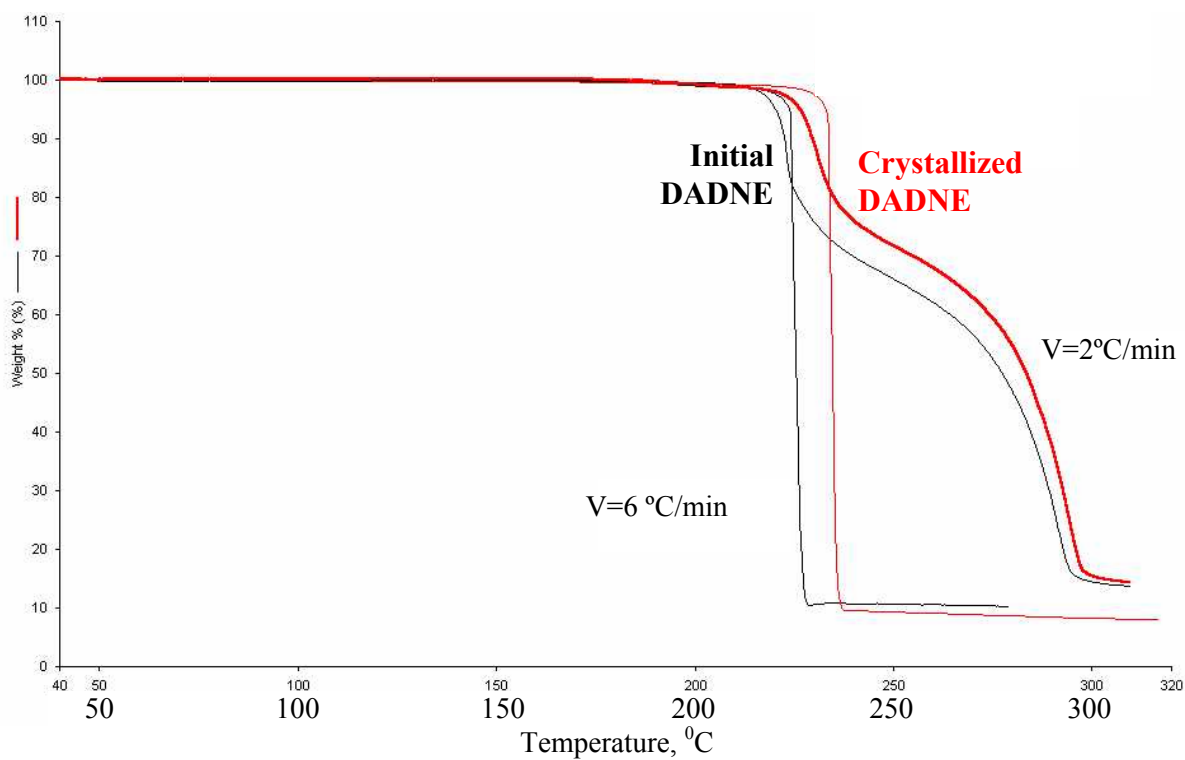
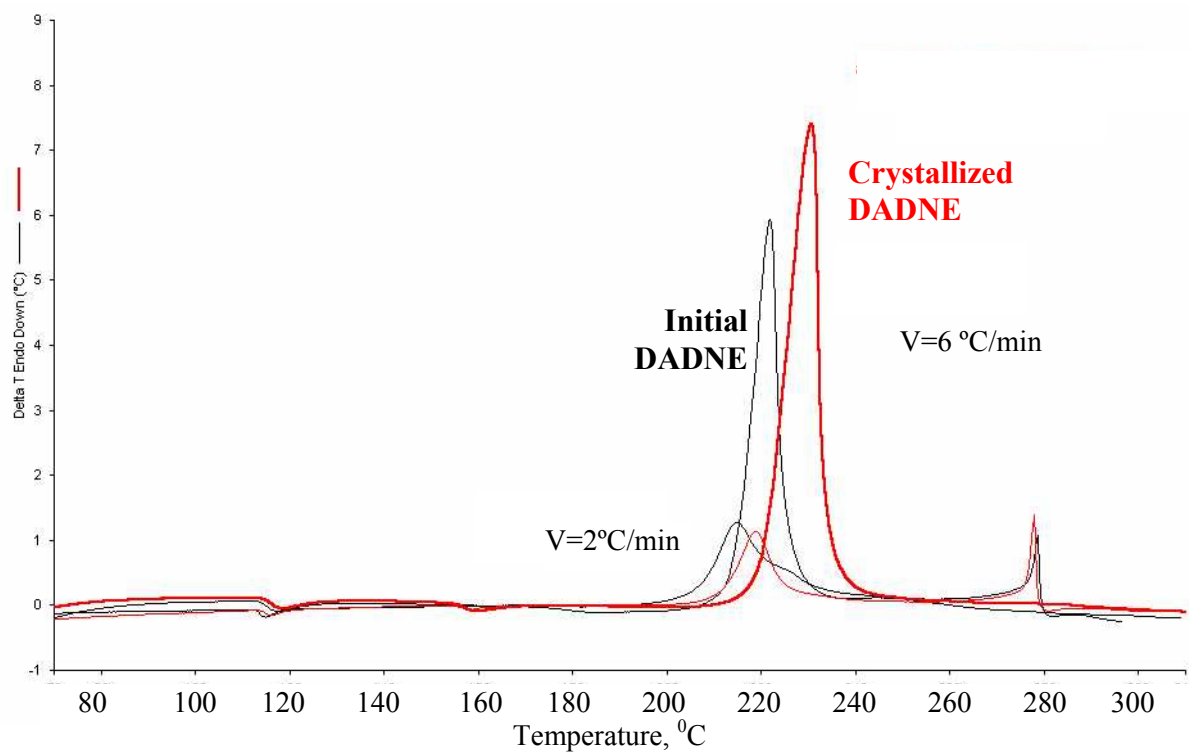


Fig 1. DTA-curves of DADNE and HMX



a) TGA curves



b) DTA curves

Fig 2. TGA curves (a) and DTA curves (b) of initial DADNE and after crystalization one form water acetone mix

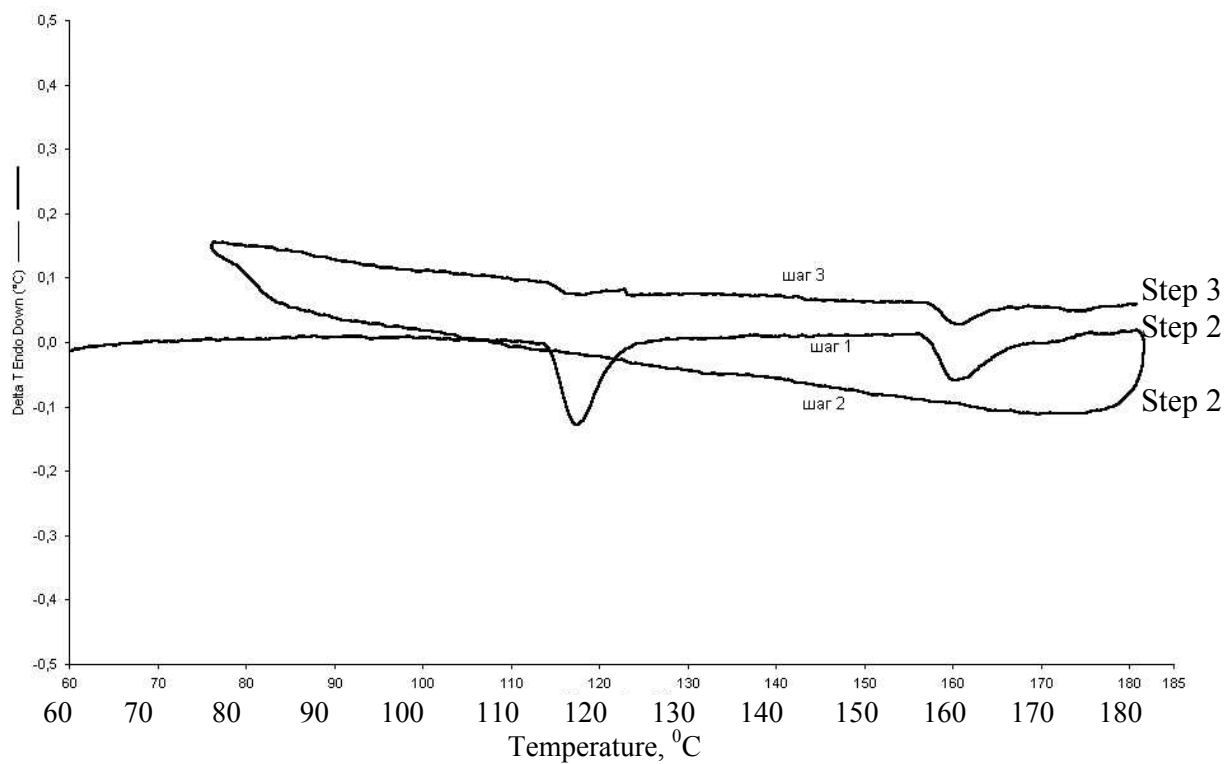


Fig 3. DTA-curves of polymorphic transitions of DADNE (Test 1)

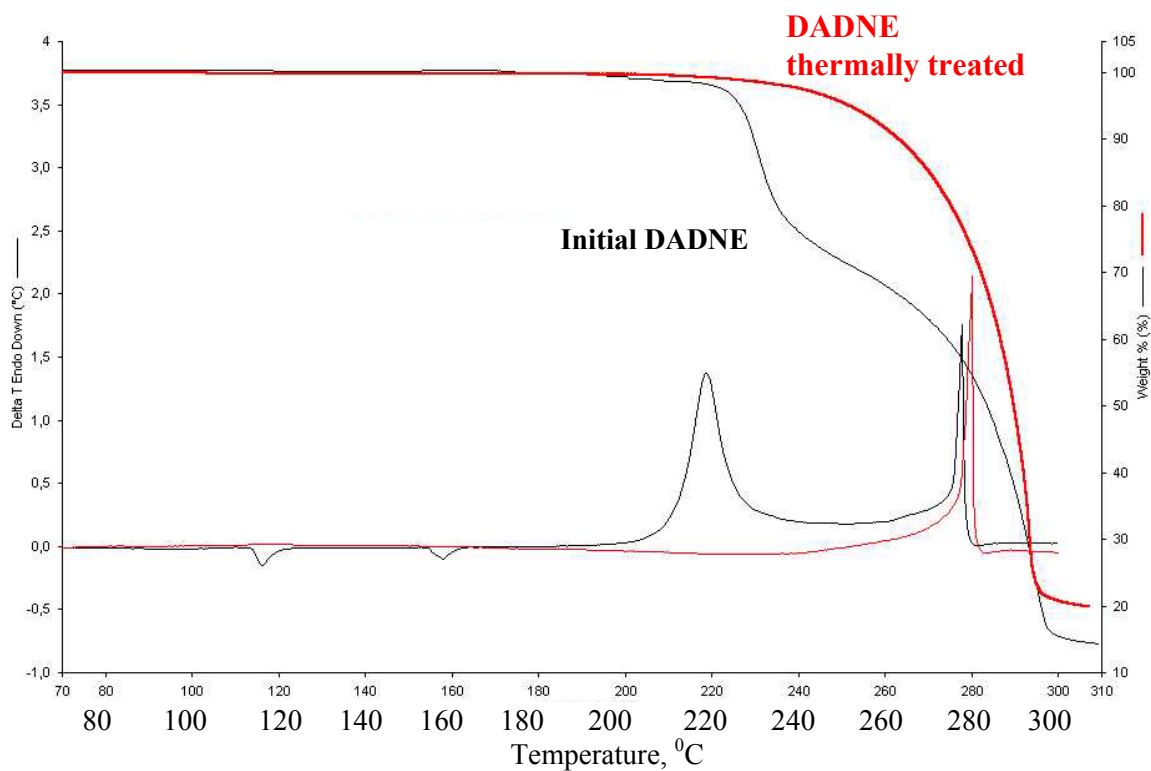


Fig 4. TGA-, DTA-curves of initial and thermally treated DADNE with heat rate 2 °/min

ESTIMATION OF THE THERMODYNAMIC PROPERTIES OF SOLID PROPELLANTS

S. Gheorghian

Academia Tehnică Militară,
George Coșbuc bd. nr. 81-83, 050141 București, România

Abstract:

The paper presents a theoretical method, based on Corner's method, for the estimation of the thermodynamic properties of solid propellants. The mathematical model contains the truncated virial equation of state, the equilibrium constant equation for each chemical reaction, the mass and energy conservation equations. The virial coefficients were calculated from the intermolecular forces using the Lennard-Jones 6,12 potential function. Based on this model, a computer program, called REAL, has been written. At the end, one presents some results obtained with this program for three gun propellants.

Keywords: chemical equilibrium, propellants

1. INTRODUCTION

The thermodynamic properties of solid propellants are those properties which define the final state of the gases resulted after combustion at constant volume, in certain conditions. Accurate estimation of thermodynamic properties of propellants is very important for interior ballistic trajectory simulation of artillery projectiles. The adiabatic flame temperature, the force, the covolume and the ratio of specific heats are the main thermodynamic properties of propellants.

There are different methods of calculating the properties, three of which are Hirschfelder - Sherman ^[5], Corner ^[1] and BLAKE ^[2]. Further on it is presented a method based on Corner's method. This method applied only to the propellant containing four elements at maximum: carbon, hydrogen, oxygen and nitrogen. The assumptions made are:

- the products of combustion are in thermochemical equilibrium and there is no heat loss during combustion;
- the virial equation of state, truncated after the third term, is used to describe the products of combustion;
- the thermochemical equilibrium is obtained through equilibrium constants.

The truncated virial equation of state is ^[1]

$$\frac{PV}{nRT} = 1 + \frac{nB}{V} + \frac{n^2C}{V^2}, \quad (1)$$

where P [Pa], V [cm³/g], T [K] are the pressure, the volume and the temperature of the gas, n [mole/g] - number of moles of gas per gram; $R = 8,31451$ [J/(mole K)] - universal gas constant and B [cm³/mol] and C [cm⁶/mol²] - the second and the third virial coefficients. The virial coefficients are dependent on gas temperature and its composition and are not influenced by pressure.

2. CALCULATION OF SECOND AND THIRD VIRIAL COEFFICIENTS

For non-polar gases (i.e. CO₂, N₂, CO, etc.), the Lennard-Jones 6,12 potential function ^[4] is used. This function takes into account the mutual attractions between molecules at greater distance and the repulsion associated with close distance. The equation is

$$\Phi(r) = 4\varepsilon \left[\left(\frac{\sigma}{r} \right)^{12} - \left(\frac{\sigma}{r} \right)^6 \right] \quad [\text{J}] \quad (2)$$

where ε [J] is the maximum energy of attraction, or the depth of the potential well, and occurs at $r = 2^{1/6} \sigma$ [nm]. σ is that value of r for which the potential function is zero. The values of ε and σ for some gases are given in Table 1.

Table 1. *Potential Parameters for the Lennard-Jones 6,12 Potential and Stockmayer Potential*

Gas	σ [nm]	ε/k [K]	μ (Debye)	Gas	σ [nm]	ε/k [K]	μ (Debye)
CO ₂	0.407	205	-	H ₂	0.293	37	
N ₂	0.370	95	-	H ₂ O	0.252	775	1.85
CO	0.376	100	-				

Further on we will use the following reduced variables: the temperature $T^* = \frac{kT}{\varepsilon}$, the second virial coefficient $B^* = \frac{B}{b_0}$ and the third virial coefficient $C^* = \frac{C}{b_0^2}$, where $b_0 = \frac{2}{3} \pi N \sigma^3$ [cm³/mole], $k=1.380658 \cdot 10^{-23}$ J/K is the Boltzmann constant and $N=6.022137 \cdot 10^{23}$ mole⁻¹ – the Avogadro constant.

The second virial coefficient for gases is:

$$B^* = \sum_{j=0}^{\infty} b^{(j)} \left(T^* \right)^{\frac{2j+1}{4}}, \quad (3)$$

where $b^{(j)} = -\frac{2^{j+\frac{1}{2}}}{4j!} \Gamma\left(\frac{2j-1}{4}\right)$. Usually, the sum in (3) is done up to $j=40$.

Similar, the third virial coefficient is given by

$$C^* = \sum_{j=0}^{\infty} c^{(j)} \left(T^* \right)^{\frac{j+1}{2}}, \quad (4)$$

where $c^{(j)}$ are tabulated below.

Table 2. $c^{(j)}$ values

j	0	1	2	3	4	5	6	7	8
$c^{(j)}$	1.729	-3.203	1.519	0.958	0.429	0.059	-0.140	-0.210	-0.205
j	9	10	11	12	13	14	15	16	17
$c^{(j)}$	-0.168	-0.168	-0.084	-0.059	-0.035	-0.020	-0.011	-0.006	-0.004

For polar gases, the Stockmayer potential function ^[4] is used, which takes into account dipole-dipole interactions. The function is

$$\Phi(r, \theta_1, \theta_2, \phi_2 - \phi_1) = 4\epsilon \left[\left(\frac{\sigma}{r} \right)^{12} - \left(\frac{\sigma}{r} \right)^6 \right] - \frac{\mu^2}{r^3} g(\theta_1, \theta_2, \phi_2 - \phi_1) \quad [\text{J}] \quad (5)$$

where $g(\theta_1, \theta_2, \phi_2 - \phi_1) = 2 \cos(\theta_1) \cos(\theta_2) - \sin(\theta_1) \sin(\theta_2) \cos(\phi_2 - \phi_1)$, μ [Debye] is the dipole moment and $\theta_1, \theta_2, \phi_1, \phi_2$ - the angles of orientation of the molecules. The parameters ϵ and σ have a slightly different interpretation here than in the Lennard-Jones potential. Note that the consideration of polarities necessitates using a third parameter (the dipole moment), which is a new source of uncertainty. Values of μ for H₂O is given in Table 1.

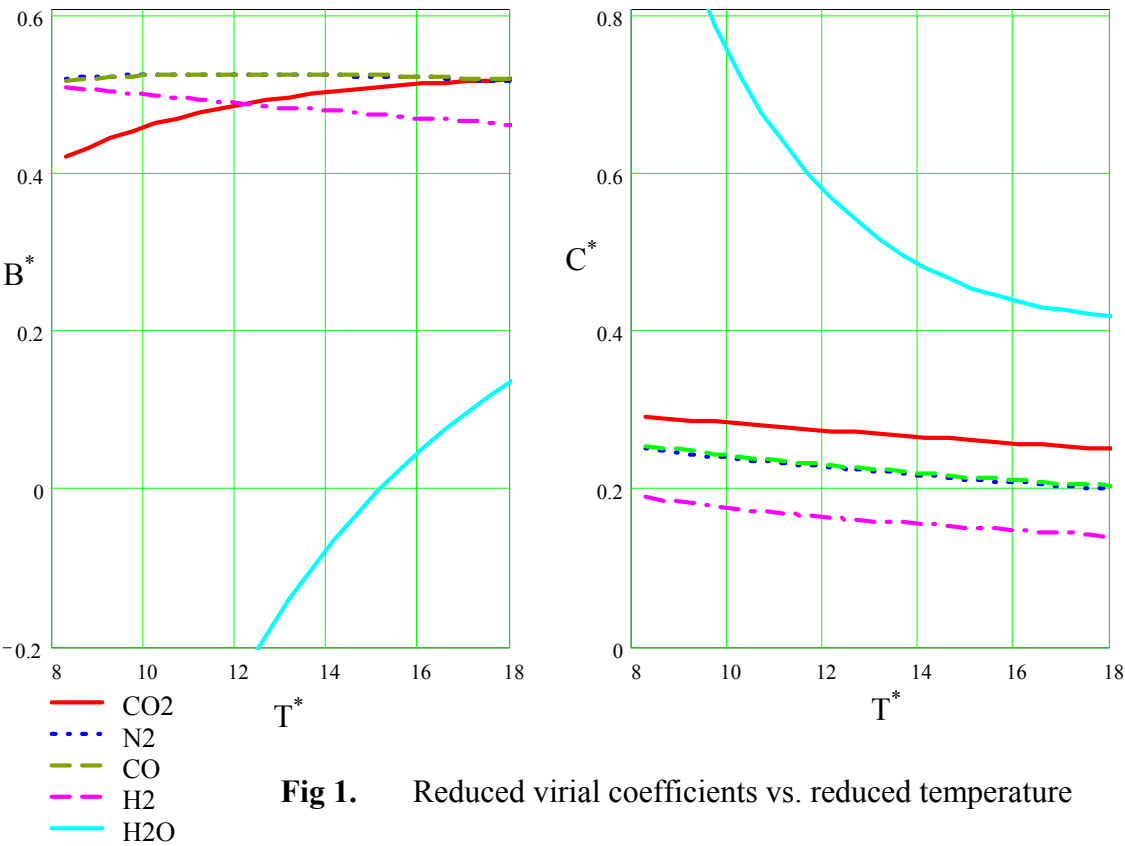


Fig 1. Reduced virial coefficients vs. reduced temperature

The equations for B and C for polar gases are very complicated. Because of this, they are calculated by interpolation, using the values of B and C tabulated in ^[4] for various values

of T and $t = \frac{\left(\mu^*\right)^2}{\sqrt{8}}$, where $\mu^* = \frac{\mu}{\sqrt{\epsilon\sigma^3}}$ is the reduced dipole moment.

Based on the above equations, the virial coefficients of the gases nominated in Table 1 were calculated. The results are presented in Table 3, for temperatures from 2000 K up to 3500 K. The variation of the virial coefficients versus temperature is presented in Figure 1. It can be seen that the second virial coefficients of the gases rise within the temperature range. The rise of the temperature increase the collisions between molecules, being influenced not much by the weak mutual attraction, but affected by the repulsion associated with close distance. An exception occurs at H_2 . The collisions between its molecules become so strong that the molecules interfere as their volume becomes smaller. The curve of the polar gas (H_2O) lay below the curves of the non-polar gases, showing a greater compressibility of the polar gases. This behavior owes to mutual attractions induced by the dipole moments into the interaction potential between molecules.

Table 3. The virial coefficients, B [cm^3/mol] and C [cm^6/mol^2] for various gases

T [K]	B_{CO_2}	B_{N_2}	B_{CO}	B_{H_2}	$B_{\text{H}_2\text{O}}$	C_{CO_2}	C_{N_2}	C_{CO}	C_{H_2}	$C_{\text{H}_2\text{O}}$
2000	38.81	33.65	35.22	16.00	-11.37	2072	991	1106	181	322
2100	39.54	33.70	35.31	15.91	-9.77	2055	978	1092	178	298
2200	40.18	33.74	35.37	15.82	-8.26	2039	966	1078	175	277
2300	40.75	33.76	35.40	15.74	-6.93	2023	954	1065	172	260
2400	41.24	33.77	35.43	15.66	-5.73	2007	942	1053	170	245
2500	41.69	33.76	35.43	15.57	-4.66	1991	931	1041	167	233
2600	42.08	33.74	35.43	15.49	-3.7	1976	920	1029	165	221
2700	42.42	33.72	35.42	15.42	-2.83	1961	910	1018	162	212
2800	42.73	33.68	35.39	15.34	-2.03	1946	900	1007	160	203
2900	43.01	33.64	35.36	15.27	-1.3	1932	890	996	158	196
3000	43.25	33.60	35.33	15.19	-0.64	1918	881	986	156	191
3100	43.47	33.55	35.29	15.12	-0.03	1904	872	976	154	186
3200	43.66	33.50	35.24	15.05	0.53	1890	863	966	152	182
3300	43.84	33.44	35.19	14.98	1.05	1877	855	957	150	179
3400	43.99	33.38	35.14	14.92	1.53	1864	847	948	148	176
3500	44.13	33.32	35.08	14.85	1.98	1851	839	939	147	174

For a mixture of CO_2 , CO , H_2O , H_2 and N_2 , the virial coefficients can be determined assuming a certain combining law. The simplest one neglects interactions between molecules of different types and was proposed by Corner ^[1]

$$nB = n_{\text{CO}_2}B_{\text{CO}_2} + n_{\text{CO}}B_{\text{CO}} + n_{\text{H}_2\text{O}}B_{\text{H}_2\text{O}} + n_{\text{H}_2}B_{\text{H}_2} + n_{\text{N}_2}B_{\text{N}_2} \quad [\text{cm}^3/\text{mol}] \quad (6)$$

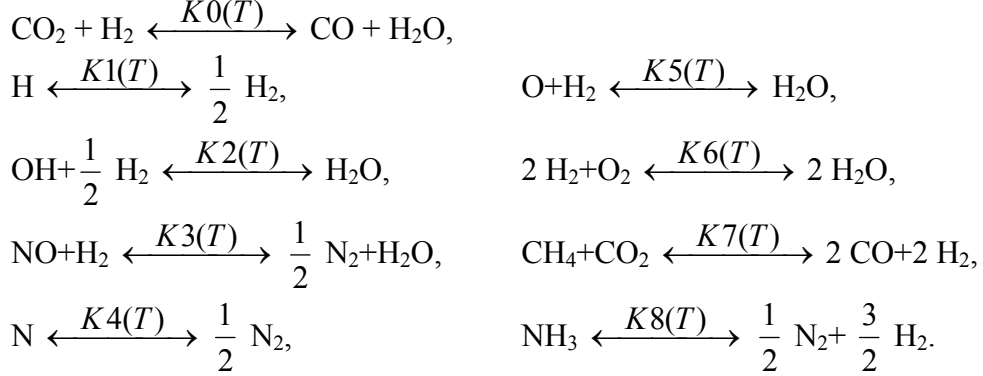
$$nC = n_{\text{CO}_2}C_{\text{CO}_2} + n_{\text{CO}}C_{\text{CO}} + n_{\text{H}_2\text{O}}C_{\text{H}_2\text{O}} + n_{\text{H}_2}C_{\text{H}_2} + n_{\text{N}_2}C_{\text{N}_2} \quad [\text{cm}^6/\text{mol}^2] \quad (7)$$

where $n = n_{\text{CO}_2} + n_{\text{CO}} + n_{\text{H}_2\text{O}} + n_{\text{H}_2} + n_{\text{N}_2}$ [mole/g].

The use of a law that considers the interactions between polar and non-polar molecules necessitates taking into account the polarisability of the non-polar molecules, thus giving an additional source of uncertainty. The rigorous calculation method increases enormously the complexity for a very small gain in accuracy.

3. CALCULATION OF COMPOSITION AT A GIVEN TEMPERATURE

Let a propellant composed of carbon, hydrogen, oxygen and nitrogen atoms. The products can be divided, based on their amounts, in major products: CO₂, CO, H₂O, H₂, N₂ and minor products: H, OH, NO, N, O, O₂, CH₄, NH₃. At temperature T , between this products take place the following chemical reactions



Writing for each chemical reaction the Guldberg - Waage law, we find

$$\left\{ \begin{aligned}
 &\frac{n_{\text{CO}} n_{\text{H}_2\text{O}}}{n_{\text{CO}_2} n_{\text{H}_2}} = K0, \\
 &\frac{(n_{\text{H}_2})^{\frac{1}{2}}}{n_{\text{H}}} = \left(\frac{R T}{V}\right)^{-\frac{1}{2}} K1, & \frac{n_{\text{H}_2\text{O}}}{n_{\text{O}} n_{\text{H}_2}} = \left(\frac{R T}{V}\right)^{-1} K5, \\
 &\frac{n_{\text{H}_2\text{O}}}{n_{\text{OH}} (n_{\text{H}_2})^{\frac{1}{2}}} = \left(\frac{R T}{V}\right)^{-\frac{1}{2}} K2, & \frac{(n_{\text{H}_2\text{O}})^2}{(n_{\text{H}_2})^2 n_{\text{O}_2}} = \left(\frac{R T}{V}\right)^{-1} K6, \\
 &\frac{(n_{\text{N}_2})^{\frac{1}{2}} n_{\text{H}_2\text{O}}}{n_{\text{NO}} n_{\text{H}_2}} = \left(\frac{R T}{V}\right)^{-\frac{1}{2}} K3, & \frac{(n_{\text{CO}} n_{\text{H}_2})^2}{n_{\text{CH}_4} n_{\text{CO}_2}} = \left(\frac{R T}{V}\right)^2 K7, \\
 &\frac{(n_{\text{N}_2})^{\frac{1}{2}}}{n_{\text{N}}} = \left(\frac{R T}{V}\right)^{-\frac{1}{2}} K4, & \frac{(n_{\text{N}_2})^{\frac{1}{2}} (n_{\text{H}_2})^{\frac{3}{2}}}{n_{\text{NH}_3}} = \frac{R T}{V} K8.
 \end{aligned} \right. \quad (8)$$

where n_{CO_2} , n_{CO} , $n_{\text{H}_2\text{O}}$... [mole/g] are the amount of CO₂, CO, H₂O ... and $K0$, $K1$, ..., $K8$ - the equilibrium constants of the chemical reactions. The equilibrium constants are functions of temperature and are given, at zero density, in [1]. Because the combustion of gun propellants occurs at high pressures, usually between 100 and 500 [MPa], it is necessary to correct the equilibrium constants. In order to simplify the calculations without significantly affect the accuracy, only three constants were corrected $K0$, $K2$ and $K3$. Those were replaced in (8) by

$$K0 \exp\left(-\frac{n\Delta B}{V} - \frac{n^2 \Delta C}{2V^2}\right), \quad K2 \exp\left(-\frac{n\Delta B2}{V}\right), \quad K3 \exp\left(-\frac{n\Delta B3}{V}\right) \quad (9)$$

where n is the amount of products participating in the corresponding reaction and

$$\begin{cases} \Delta B = B_{CO} + B_{H_2O} - B_{CO_2} - B_{H_2}, & \Delta B_2 = 20 [\text{cm}^3/\text{mol}], \\ \Delta C = C_{CO} + C_{H_2O} - C_{CO_2} - C_{H_2}, & \Delta B_3 = 20 [\text{cm}^3/\text{mol}]. \end{cases} \quad (10)$$

The coefficients B [cm^3/mol] and C [cm^6/mol^2] are the second and the third virial coefficients of the products. Their values for CO_2 , CO , H_2O , H_2 and N_2 at 2000, 2100, ..., 3500 [K] are given in Table 3.

Because there are thirteen unknowns, n_{CO_2} , n_{CO} , n_{H_2O} , ..., four more equations are needed. Those are supplied by the mass conservation equation for each atomic species

$$\begin{cases} n_{CO_2} + n_{CO} + n_{CH_4} = C, \\ 2n_{H_2O} + 2n_{H_2} + n_H + n_{OH} + 4n_{CH_4} + 3n_{NH_3} = H, \\ 2n_{CO_2} + n_{CO} + n_{H_2O} + n_{OH} + n_{NO} + n_O + 2n_{O_2} = O, \\ 2n_{N_2} + n_{NO} + n_N + n_{NH_3} = N, \end{cases} \quad (11)$$

where C , H , O și N are the amounts in g-atoms of carbon, hydrogen, oxygen and nitrogen contained into one gram of propellants.

The calculation of composition at a given temperature T is iterative as given below:

1. the initial composition is calculated without pressure corrections and neglecting all the minor products;
2. the number of gram atoms per gram of propellant is reduced according to the minor products;
3. the new composition is calculated tacking into account the pressure corrections and the minor products;
4. the new major products are compared with the previous ones; if the required accuracy is not acquired, the calculation proceed with step 2.

This algorithm was written in *MATHCAD* (see Figure 2). The main procedure *CP* returns the composition n_{CO_2} , n_{CO} , n_{H_2O} , ..., n_{NH_3} [mole/g] at a temperature index i ($i=0, 1 \dots 14$, $T_0=2000$ K, $T_1=2100$ K, ... $T_{14}=3500$ K). *CP* calls the procedure *CO2* that computes the amount of CO_2 . For example, consider the propellant X containing $C=2238$, $H=3014$, $N=1044$, $O=3468$, all in 10^{-5} [mole/g]. At $V = 5 [\text{cm}^3/\text{g}]$ and $T_{11}=3000$ K the computed composition is $n_{CO_2}=318$, $n_{CO}=1920$, $n_{H_2O}=909$, $n_{H_2}=592$, $n_{N_2}=521$, $n_H=5.4$, $n_{OH}=2.6$, $n_{NO}=0.3$, all in 10^{-5} [mole/g]. The convergence criteria $err < 10^{-9}$ [mole/g] was fulfilled after five iterations.

4. CALCULATION OF EQUILIBRIUM TEMPERATURE

The equilibrium temperature or adiabatic flame temperature is computed from the condition, that the energy required to heat the products equals the heat of combustion.

The energy required to heat the products at constant volume and zero density, from the reference temperature $T_r=300$ [K] to T [K] is

$$E_0 = (n_{CO_2} \bar{C}_{v_{CO_2}} + n_{CO} \bar{C}_{v_{CO}} + \dots + n_{N_2} \bar{C}_{v_{NH_3}}) (T - T_r) [\text{J/g}] \quad (12)$$

where $\bar{C}_{v_{CO_2}}$, $\bar{C}_{v_{CO}}$, ..., $\bar{C}_{v_{NH_3}}$ [J/(mole K)] are the mean specific heats of CO_2 , CO , ..., NH_3 , from T_r to T . The values of \bar{C}_v , for each product, at constant volume and zero density, are given in [1]. Because the density of products differ from zero, it is necessary to add terms proportional to the first and second powers of the density.

$CO2(C, H, O, N, K) :=$	$\left \begin{array}{l} a \leftarrow K - 1 \\ b \leftarrow K \cdot (0.5 \cdot H + C - O) + O \\ c \leftarrow C \cdot (C - O) \\ x \leftarrow \frac{1}{2 \cdot a} \cdot \left(-b + \sqrt{b^2 - 4 \cdot a \cdot c} \right) \\ x \end{array} \right $	
$CP(i) :=$	$\left \begin{array}{l} n'CO2 \leftarrow CO2(C, H, O, N, K0_i) \\ n'CO \leftarrow C - n'CO2 \\ n'H2O \leftarrow O - C - n'CO2 \\ n'H2 \leftarrow 0.5 \cdot H - O + C + n'CO2 \\ n'N2 \leftarrow 0.5 \cdot N \\ n'H \leftarrow 0 \cdot mole \cdot gm^{-1} \\ n'OH \leftarrow 0 \cdot mole \cdot gm^{-1} \\ n'NO \leftarrow 0 \cdot mole \cdot gm^{-1} \\ n'N \leftarrow 0 \cdot mole \cdot gm^{-1} \\ n'O \leftarrow 0 \cdot mole \cdot gm^{-1} \\ n'O2 \leftarrow 0 \cdot mole \cdot gm^{-1} \\ n'CH4 \leftarrow 0 \cdot mole \cdot gm^{-1} \\ n'NH3 \leftarrow 0 \cdot mole \cdot gm^{-1} \\ \text{while } 1 \\ \quad \left \begin{array}{l} C \leftarrow C - n'CH4 \\ H \leftarrow H - n'H - n'OH - 4 \cdot n'CH4 - 3 \cdot n'NH3 \\ O \leftarrow O - n'OH - n'NO - n'O - 2 \cdot n'O2 \\ N \leftarrow N - n'NO - n'N - n'NH3 \\ n \leftarrow n'CO + n'H2O + n'CO2 + n'H2 \\ \Delta \quad B \leftarrow B_CO_i + B_H2O_i - B_CO2_i - B_H2_i \\ \Delta \quad C \leftarrow C_CO_i + C_H2O_i - C_CO2_i - C_H2_i \\ K \leftarrow K0_i \cdot e^{\frac{-n \cdot \Delta B}{V} - \frac{n^2 \cdot \Delta C}{2 \cdot V^2}} \\ nCO2 \leftarrow CO2(C, H, O, N, K) \\ nCO \leftarrow C - nCO2 \\ nH2O \leftarrow O - C - nCO2 \\ nH2 \leftarrow 0.5 \cdot H - O + C + nCO2 \\ nN2 \leftarrow 0.5 \cdot N \\ nH \leftarrow nH2^{\frac{1}{2}} \cdot \left(\frac{V}{R \cdot T_i} \right)^{\frac{1}{2}} \cdot K1_i \\ n \leftarrow n'OH + nH2O + \frac{1}{2} \cdot nH2 \\ nOH \leftarrow \frac{nH2O}{nH2^{\frac{1}{2}}} \cdot \left(\frac{V}{R \cdot T_i} \right)^{\frac{1}{2}} \cdot K2_i \cdot e^{\frac{-n \cdot \Delta B2}{V}} \\ n \leftarrow n'NO + nH2O + \frac{1}{2} \cdot nN2 + nH2 \end{array} \right \end{array} \right $	$\left \begin{array}{l} nNO \leftarrow \frac{nH2O \cdot nN2^{\frac{1}{2}}}{nH2} \cdot \left(\frac{V}{R \cdot T_i} \right)^{\frac{1}{2}} \cdot K3_i \cdot e^{\frac{-n \cdot \Delta B3}{V}} \\ nN \leftarrow nN2^{\frac{1}{2}} \cdot \left(\frac{V}{R \cdot T_i} \right)^{\frac{1}{2}} \cdot K4_i \\ nO \leftarrow \frac{nH2O}{nH2} \cdot \left(\frac{V}{R \cdot T_i} \right) \cdot K5_i \\ nO2 \leftarrow \frac{nH2O^2}{nH2^2} \cdot \left(\frac{V}{R \cdot T_i} \right) \cdot K6_i \\ nCH4 \leftarrow \frac{nCO^2 \cdot nH2^2}{nCO2} \cdot \left(\frac{R \cdot T_i}{V} \right)^2 \cdot K7_i \\ nNH3 \leftarrow nN2^{\frac{1}{2}} \cdot nH2^{\frac{3}{2}} \cdot \frac{R \cdot T_i}{V} \cdot K8_i \\ n \leftarrow nCO2 + nCO + nH2O + nH2 + nN2 \dots \\ \quad + nH + nOH + nNO + nN + nO + nO2 \dots \\ \quad + nCH4 + nNH3 \\ \text{if } \left \begin{array}{l} nCO2 - n'CO2 \\ + \quad nH2O - n'H2O \\ + \quad nN2 - n'N2 \end{array} \right + \left \begin{array}{l} nCO - n'CO \\ + \quad nH2 - n'H2 \end{array} \right \dots > err \\ \quad \left \begin{array}{l} n'CO2 \leftarrow nCO2 \\ n'CO \leftarrow nCO \\ n'H2O \leftarrow nH2O \\ n'H2 \leftarrow nH2 \\ n'N2 \leftarrow nN2 \\ n'H \leftarrow nH \\ n'OH \leftarrow nOH \\ n'NO \leftarrow nNO \\ n'N \leftarrow nN \\ n'O \leftarrow nO \\ n'O2 \leftarrow nO2 \\ n'CH4 \leftarrow nCH4 \\ n'NH3 \leftarrow nNH3 \end{array} \right \\ \text{break} \quad \text{otherwise} \end{array} \right $
		$\left[\begin{array}{l} nCO2 \\ nCO \\ nH2O \\ nH2 \\ nN2 \\ nH \\ nOH \\ nNO \\ nN \\ nO \\ nO2 \\ nCH4 \\ nNH3 \\ n \end{array} \right]$

Fig 2. MATHCAD procedure for the calculation of the products composition at a given temperature

It can be shown that the internal energy of the products of 1 g of propellants is

$$E = E0 - \frac{nR}{V} T \left(n_{CO_2} T \frac{d}{dT} B_{CO_2} + n_{CO} T \frac{d}{dT} B_{CO} + \dots \right) - \frac{n^2 R}{2V^2} T \left(n_{CO_2} T \frac{d}{dT} C_{CO_2} + n_{CO} T \frac{d}{dT} C_{CO} + \dots \right) \quad [J/g] \quad (13)$$

where $\frac{d}{dT} B_{CO_2}$, $\frac{d}{dT} C_{CO_2}$, ... are the first derivatives of the virial coefficients B_{CO_2} , C_{CO_2} , This equation may be written in the easier form

$$E = E0 + \frac{n}{V} (n_{CO_2} E1_{CO_2} + n_{CO} E1_{CO} + \dots) + \left(\frac{n}{V} \right)^2 (n_{CO_2} E2_{CO_2} + n_{CO} E2_{CO} + \dots) [J/g] \quad (14)$$

where $E1_{CO_2}$, $E1_{CO}$, ..., $E2_{CO_2}$, $E2_{CO}$, ... are the corrections to internal energy for CO_2 , CO , These corrections were calculated for the major products and are given in Table 4.

Table 4. Corrections to internal energies,
 $E1 / 100 [(J \text{ cm}^3)/\text{mol}^2]$, $E2 / 1000 [(J \text{ cm}^6)/\text{mol}^3]$

$T [K]$	$E1_{CO_2}$	$E1_{N_2}$	$E1_{CO}$	$E1_{H_2}$	$E1_{H_2O}$	$E2_{CO_2}$	$E2_{N_2}$	$E2_{CO}$	$E2_{H_2}$	$E2_{H_2O}$
2000	-2594	-229	-320	291	-6068	282	220	239	54	458
2100	-2504	-170	-257	317	-5561	305	233	254	56	412
2200	-2415	-111	-194	343	-5809	328	246	268	59	372
2300	-2327	-52	-132	368	-5491	352	258	282	61	346
2400	-2240	6	-71	393	-5417	376	271	296	63	330
2500	-2153	64	-9	418	-5266	401	283	310	65	313
02600	-2067	122	52	443	-5155	425	295	324	67	293
2700	-1982	179	112	468	-5045	450	308	338	69	271
2800	-1897	236	173	493	-4945	474	319	351	71	248
2900	-1813	293	233	517	-4850	499	331	364	73	223
3000	-1729	350	293	541	-4764	524	343	377	75	197
3100	-1646	406	352	565	-4681	548	354	390	77	172
3200	-1563	462	411	590	-4603	573	366	403	79	149
3300	-1480	518	470	613	-4529	597	377	416	81	126
3400	-1398	574	529	637	-4460	621	388	428	83	107
3500	-1316	629	588	661	-4394	646	399	440	85	92

From Table 4 it can be seen that the corrections $E1$ have opposite signs, and, accordingly, the summation over all constituents tends to be small. Reference to the previous example, $E=3472$ [J/g], and of this about -33 [J/g] comes from $E1$ terms and about 9 [J/g] from the $E2$ terms.

The variation of the energy of formation is

$$\Delta EF = EF_{products} - EF_{propellant} \quad [J/g]. \quad (15)$$

The energy of formation of products is

$$EF_{products} = n_{CO_2} EF_{CO_2} + n_{CO} EF_{CO} + \dots + n_{NH_3} EF_{NH_3} \quad [J/g]. \quad (16)$$

where $EF_{CO_2}, EF_{CO}, \dots, EF_{NH_3}$ [J/mole] is the standard energy of formation of CO_2, CO, \dots, NH_3 . The values of the energy of formations of products from carbon (s), hydrogen (g), nitrogen (g) and oxygen (g), at constant volume and standard conditions, are given in [1].

At equilibrium $E = \Delta EF$. As a matter of fact, the calculation of equilibrium temperature, is as follows:

1. two successive temperature, between we presume the equilibrium temperature lies, are chosen from the row 2000, 2100, ... 3500 [K];
2. the compositions at these two temperatures are computed according to § 3;
3. the variable $\zeta = E - \Delta EF$ is calculated for each of two temperatures;
4. if the signs of two ζ are the same (both of them are positive or both are negative), the equilibrium temperature do not lie between the two chosen temperatures; the calculation must be resume from step 1;
5. if the signs of two ζ are different (one of them is positive and the other is negative) the temperature corresponding to $\zeta = 0$ are computed by linear interpolation; this is just the equilibrium temperature or adiabatic flame temperature, Tf ; the composition at Tf is then calculated by interpolation between the two compositions from step 2.

For the propellant X previously used as an example, it was presumed that the equilibrium temperature lies between 3000 [K] and 3100 [K]. After the compositions were calculated, it was found for ζ the values -133.43 [J/g] and 27.46 [J/g]. The temperature for which $\zeta = 0$ is $Tf = 3082.9$ [K]. The internal energy of products at equilibrium is $E = 3597.3$ [J/g]. The composition at Tf is $n_{CO_2} = 315$, $n_{CO} = 1923$, $n_{H_2O} = 911$, $n_{H_2} = 590$, $n_{N_2} = 522$, $n_H = 6.9$, $n_{OH} = 3.6$, $n_{NO} = 0.4$, total number of moles $n = 4271.9$, all in 10^{-5} [mole/g].

5. CALCULATION OF THERMODYNAMIC PROPERTIES

The pressure at equilibrium is calculated from (1), using the combining laws (6) and (7). The virial coefficients of the products at Tf are calculated by interpolation in Table 3.

By definition, the force and covolume can be expressed as

$$f = n\Re Tf \quad [J/g] \quad (17)$$

$$\eta = V - \frac{f}{P} \quad [cm^3/g] \quad (18)$$

The molecular mass and the ratio of specific heats of the products are

$$M = \frac{1}{n} \quad [mol/g], \quad (19)$$

$$\gamma = 1 + \frac{n\Re}{\bar{C}_v} \quad (20)$$

where $\bar{C}_v = \frac{E(Tf) - E(0.7Tf)}{0.3Tf}$ [J/(g K)], is the mean C_v over the range Tf to $0.7 Tf$ and $E(T)$ is the internal energy, at temperature T [1].

For example, the thermodynamic properties of the above-mentioned propellant X are: $Tf = 3082.9$ [K], $f = 1095.1$ [J/g], $\eta = 1.067$ [cm³/g], $M = 23.406$ [g/mole], $\gamma = 1.235$.

6. COMPUTER PROGRAM *REAL*

The above-described method was used to write a computer program called *REAL*. The input data required for the calculation of thermodynamic properties are: composition of propellant, and specific volume.

Using *REAL*, there were calculated the thermodynamic properties of three propellants at $V=5$ [g/cm³]. The results were summarized in Table 5. For comparison, Table 5 includes the results obtained with Corner's method and *BLAKE* [3].

Table 5. *Thermodynamic properties of three propellants*

Method	T_f [K]	M [g/mole]	P [MPa]	f [J/g]	η [cm ³ /g]	γ [-]
M1A1						
<i>CORNER</i>	2262	21.762	216.3	864.0	1.006	1.280
<i>REAL</i>	2266	21.744	225.8	866.5	1.162	1.276
<i>BLAKE</i>	2283	21.764	224.6	872.3	1.118	1.273
M14						
<i>CORNER</i>	2722	23.061	243.6	981.3	0.971	1.246
<i>REAL</i>	2731	23.061	252.4	984.6	1.099	1.246
<i>BLAKE</i>	2743	23.085	251.3	988.0	1.069	1.254
M26E1						
<i>CORNER</i>	3106	23.868	267.0	1082	0.948	1.234
<i>REAL</i>	3116	23.867	274.8	1085	1.051	1.233
<i>BLAKE</i>	3125	23.889	274.2	1087	1.034	1.239

It can be seen that compared with *BLAKE*, *REAL* computes f and γ with an error less than 0.5 %, T_f , P and M with an error less than 1 % and η with an error less than 5 %. As a general rule, the error lowers as the temperature increases.

7. CONCLUSIONS

The presented method allows a better estimation of the thermodynamic properties of solid propellants than Corner's method. This is due only to the recalculation of the virial coefficients and the corrections of the internal energy, using the Lennard-Jones 6,12 and Stockmayer potential functions.

REFERENCES

[1] CORNER, J.: Theory of Interior Ballistics of Guns, Wiley, New York, 1950.

[2] FREEDMAN, E.: BLAKE - A Thermodynamics Code Based on TIGER: User's Guide and Manual, BRL Technical Report ARBRL-TR-02411, BRL, Aberdeen Proving Ground 21005, July 1982.

[3] FREEDMAN, E.: Thermodynamic Properties of Military Gun Propellants, Progress in Astronautics and Aeronautics: Gun Propulsion Technology, Vol. 109, New York, 1988

[4] HIRSCHFELDER, J. O., CURTISS C. F., BIRD R. B.: Molecular Theory of Gases and Liquids, Wiley, New York, 1954

[5] HIRSCHFELDER, J. O., SHERMAN, J.: Simple Calculation of Thermochemical Properties for Use in Ballistics, National Defense Research Committee, Rept. A-101, (OSRD Rept. 935), Oct. 1942.

APPLICATION OF NOVEL ENERGETIC MATERIALS FOR INITIATORS AND EXPLOSIVE TRAINS

J. Hamid, T. Griffiths, R. Claridge and T. Jordan

QinetiQ Ltd., Energetic Materials Dept.,
MOD Fort Halstead, Sevenoaks, Kent, UK

Abstract:

As well as improving the survivability of weapons and platforms, Insensitive Munitions (IM) reduce both casualty rates and mission losses. Their use also leads to improved safety during storage and transportation. For a munition to completely fulfil IM criteria each of its energetic sub-systems must be IM compliant.

The initiator and explosive train are the most critical of these sub-systems; their safety and reliability are paramount if the weapon is to be suitable for service use. They are generally the most difficult part of a weapon system to protect from inadvertent initiation since their primary function is initiation of the main charge explosive.

In the last decade, a number of new high temperature compounds with improved power outputs and potential for both exploding foil initiator (EFI) and explosive train applications have been reported. Several of the more promising materials based on pyrazine, pyridine and polynitro- aromatic systems have been successfully synthesised and characterised.

Keywords: *explosive train, exploding foil initiator, IM, pyrazine, polynitro-, initiators*

1. INTRODUCTION

Insensitive munitions (IM) improve the survivability of weapon systems and their associated platforms from accident or enemy action. This can lead to a reduction in casualties, mission losses and whole of life costs while still giving equivalent performance. For this reason the UK armed forces include IM in their weapons buying policies and research programmes.

Research into the technologies that make the energetic subsystems of a weapon insensitive will contribute to allowing the whole system to become an IM. The initiator and explosive train systems (Fig.1) are the most difficult to protect since their primary function is the initiation of the main charge explosive. Improved initiatory systems are required for IM weapons. They must reliably initiate IM booster explosives in the design mode but not when they are accidentally initiated by external threats. Exploding foil initiators (EFIs) are high voltage detonators that can fulfil IM criteria for initiatory systems. They do not require mechanical safety and arming unit and can therefore be used ‘in-line’.

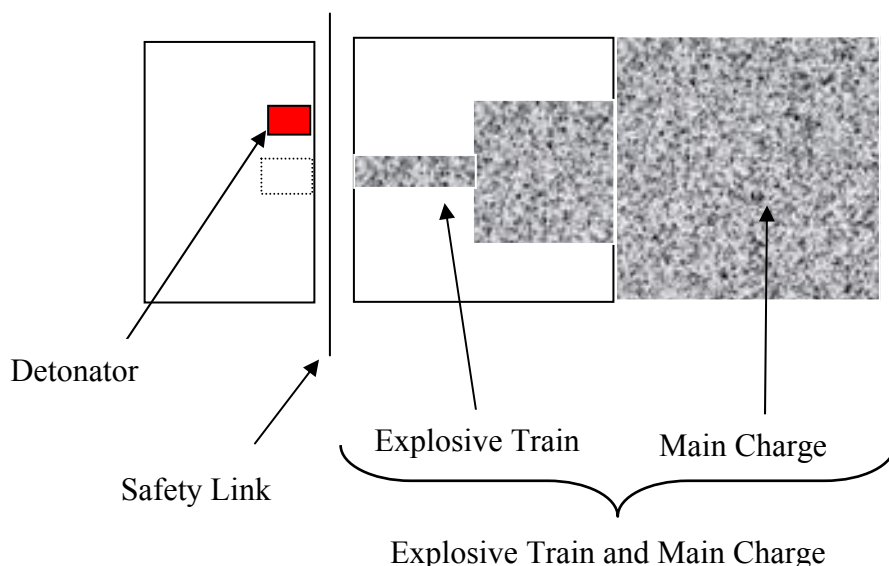
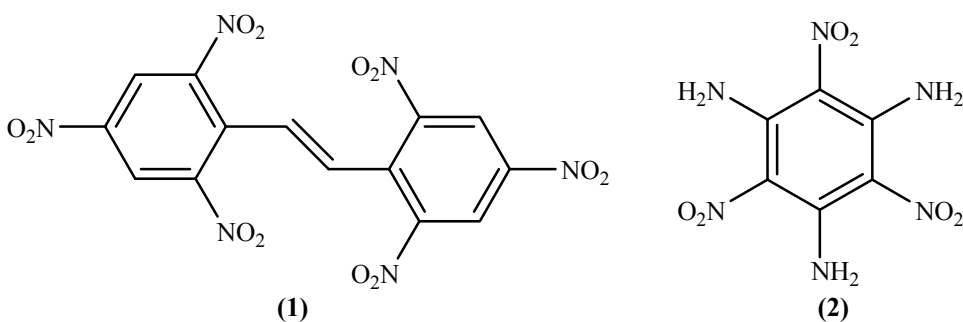


Fig 1.

Hexanitrostilbene (HNS) (**1**) has been used recently in the UK for achieving detonation transfer and as a booster explosive ^[1]. Although not completely IM compliant its high thermal stability (318°C) and insensitiveness make it ideal for low vulnerability weapon applications. However, it has low power output as well as poor handling and pressing characteristics. The low power output is due to its low density (1.74 g cm⁻³) and aromatic structure which does not provide optimum energy release. As a result of this its use in such devices is limited.

1,3,5-Triamino-2,4,6-trinitrobenzene (TATB) (**2**) is another insensitive explosive with good thermal characteristics, but its use is limited by its critical diameter of 4mm (density 1.86 g cm⁻³) when unconfined. This prevents the transmission of detonation when it is pressed into narrow channels.



In the last decade many new high temperature insensitive heterocyclic and carbocyclic compounds have been reported with improved power output, which may have potential for EFIs and explosive train applications.

2,6-Diamino-3,5-dinitropyrazine (ANPZ) (**3**), 2,6-diamino-3,5-dinitropyrazine-1-oxide (PZO) (**4**), 2,6-diamino-3,5-dinitro pyridine-1-oxide (DADNPO) (**5**), nonanitro m-terphenyl (NONA) (**6**), [(3-picrylamino)-1,2,4-triazole] (PATO) (**7**), and 5,7-diamino-4,6-dinitrobenzofuroxan (CL-14) (**8**) are just several novel compounds which have been selected as potential replacements for HNS and TATB (Fig 2).

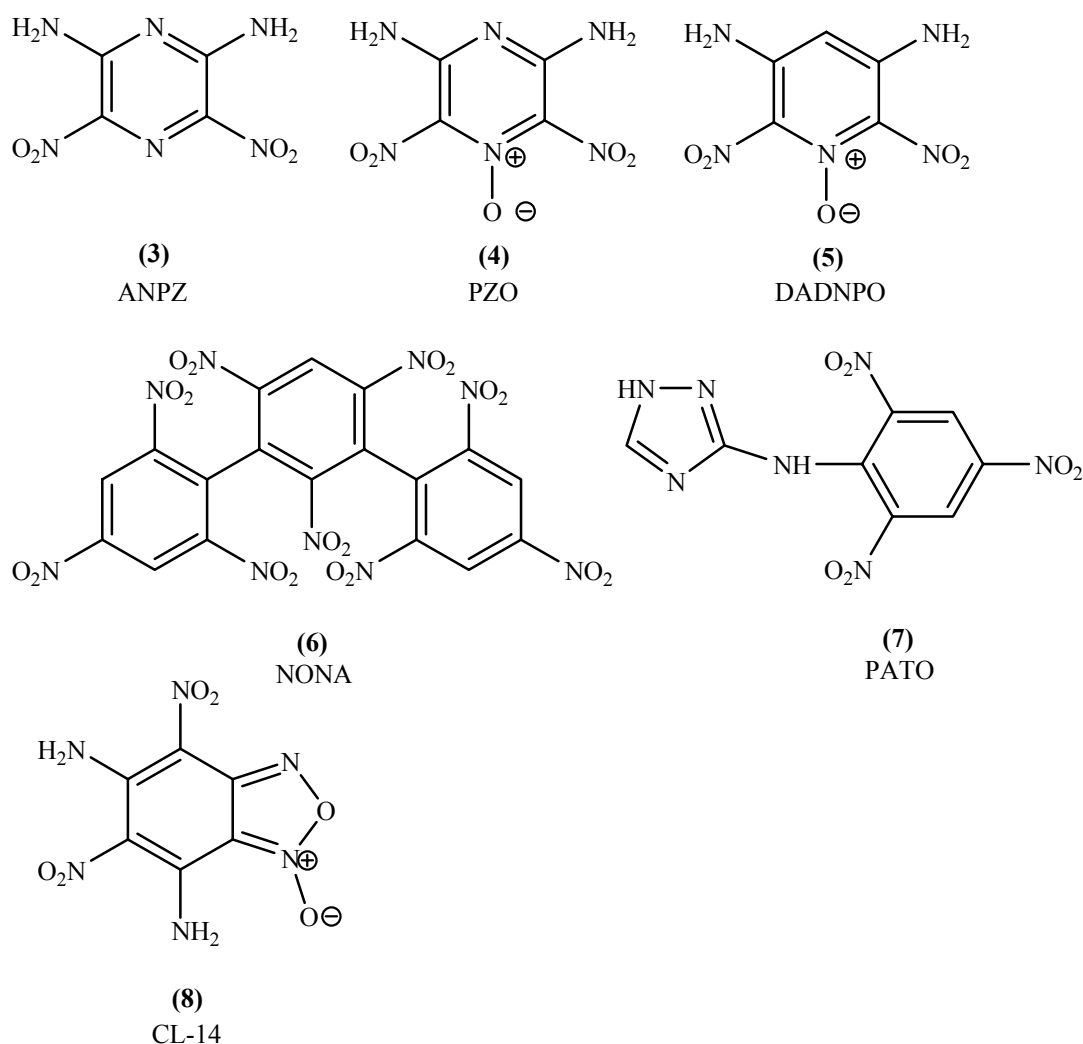


Fig 2.

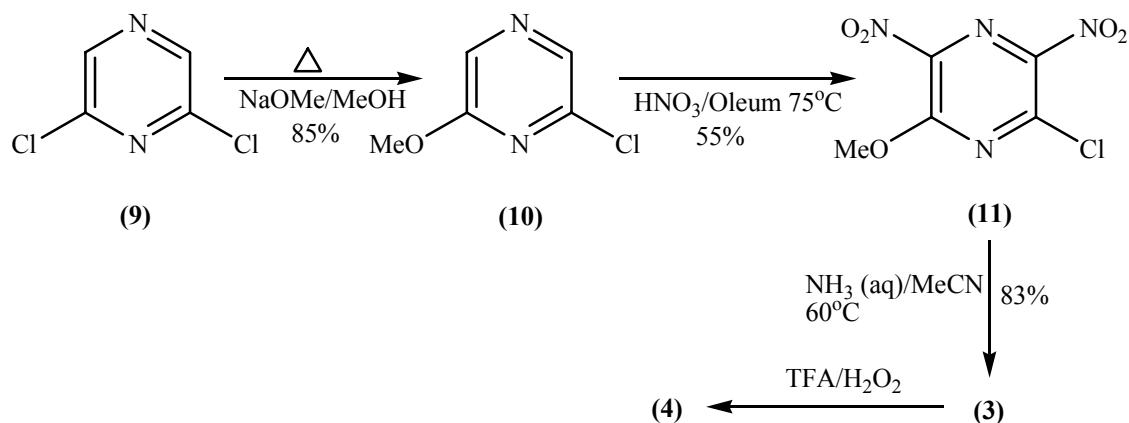
The selection criteria were ease of synthesis, thermal stability (Mpt. > 300°C) and explosive power output (P_{c-j} calculated) which should be at least 10% in excess of that of HNS i.e. a minimum of 240 kbar. Most of the aforementioned compounds are based on nitrogen heterocycles (with the exception of NONA). The substitution of carbon by nitrogen gives them improved thermochemistry, it also increases their oxygen balance and reduces their aromatic stabilisation energy. Both of these factors contribute to an overall increase in explosive power output ^[2]. In addition, these classes of compounds have strong intermolecular interactions in the crystal structure. These interactions result from the dipolar nature of the constituents (e.g. amino groups) which can participate in hydrogen bonding interactions and as a result of the polar nature of the ring nuclei as compared to carbocyclic nuclei. As a result of these interactions a high melting point is observed for such compounds.

The compounds selected have high densities (1.8 g cm⁻³ with the exception of NONA) which has the effect of increasing explosive output since P_{c-j} increases with the square of the density ^[2]. NONA is the exception to the list and was selected on the basis of its high melting point (> 400°C) and is reportedly being used in a number of commercial devices ^[3].

The above mentioned compounds were synthesised in 50 g quantities to undertake an independent evaluation and characterise their hazard properties. This evaluation would provide the basis for whether such compounds could be used as TATB and HNS replacements for IM sub-systems.

2. RESULTS AND DISCUSSION

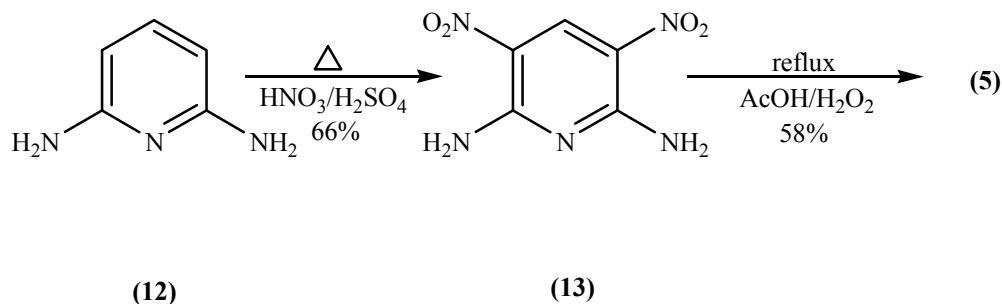
Several methods ^[4-6] have been reported for the synthesis of PZO and ANPZ. The Route disclosed in the Russian Patent ^[6] starts from the commercially available 2,6-dichloro pyrazine (**9**) (Scheme 1) which upon methoxylation using sodium methoxide in refluxing methanol afforded the 2-chloro-6-methoxy pyrazine (**10**) in 85% yield. Nitration of this with 30% oleum and 100% nitric acid gave the 2-chloro-6-methoxy-3,5-dinitro pyrazine (**11**) in 55% yield. Subsequent treatment of this material with aqueous ammonia in acetonitrile at 60°C gave ANPZ (as a yellow/orange powder in 83% yield. Oxidation with 30% hydrogen peroxide in trifluoroacetic acid afforded PZO in 90% yield. Characterisation and hazard data for all the aforementioned compounds are given in Table 1.



Scheme 1

ANPZ is found to be insensitive to impact and friction with good thermal stability. PZO has also good thermal stability but the material was found to have similar sensitivity to HMX. This was unexpected since earlier reports ^[4-6] suggest a much higher value for insensitivity. Analysis of the material could only detect small amounts of ANPZ precursor which would be unlikely to result in a higher sensitivity since this material is known to be very insensitive. Further work to identify the higher sensitivity issues are still under investigation.

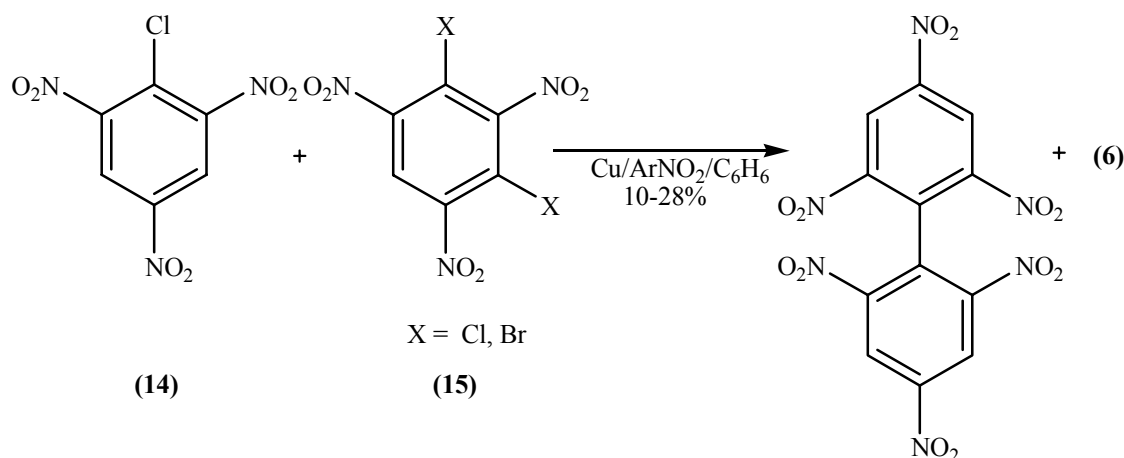
DADNPO has been reported in the mid 90s ^[7,8] and can be easily prepared by nitration of 2,6-diaminopyridine (**12**) followed by oxidation of the dinitro- derivative (**13**) using acetic acid/hydrogen peroxide in 58% yield (Scheme 2).



Scheme 2

This material is found to be insensitive to both impact and friction and is likely to be a promising candidate for future investigations.

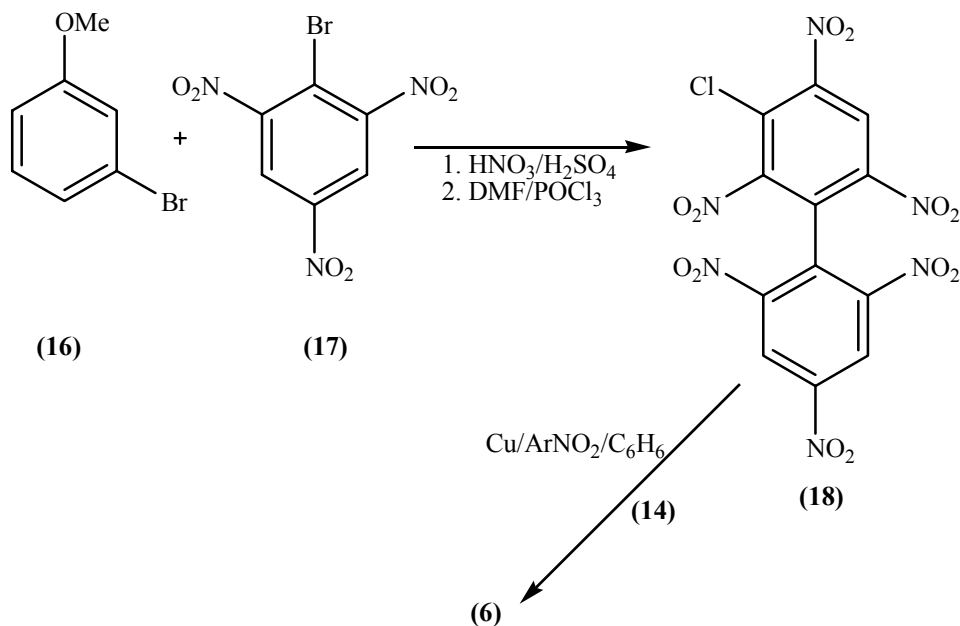
NONA is an explosive of the polynitropolyaryl class which possesses excellent thermal stability (Mpt. 440-450°C). The material was developed for space applications in the 1960's by NOL^[9]. The original synthesis involved high temperature Ullmann coupling of picryl chloride (**14**) with 1,3-dichloro-2,4,6-trinitrobenzene (**15**) in the presence of copper powder using a mixture of benzene and nitrobenzene solvent system (Scheme 3)



Scheme 3

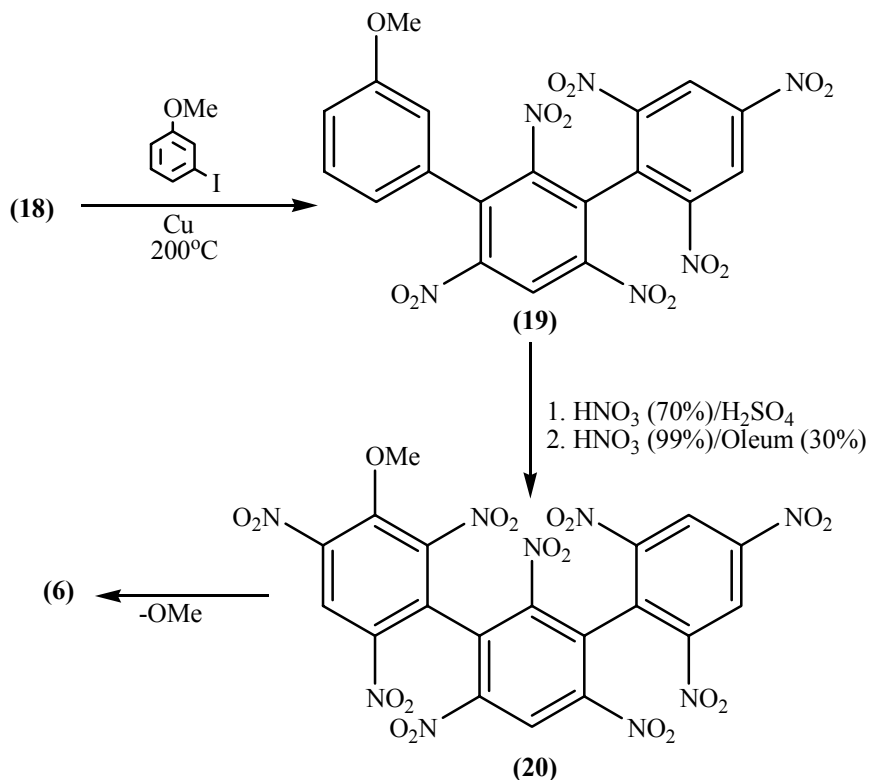
The reaction is low yielding and the workup is complex and laborious due to the similar solubilities of the hexanitrobiphenyl by-product and NONA. The use of the dibromo-precursor was found to give higher yields and cleaner reactions.

An alternative route^[10] utilising bipicryl chloride (**18**) was also investigated (Scheme 4) as this compound was potentially a key precursor in the synthesis of NONA. The reaction of bromoanisole (**16**) with picryl bromide (**17**) followed by nitration and dehalogenation gave **(18)**. This was subsequently coupled with **(14)** to give NONA.



Scheme 4

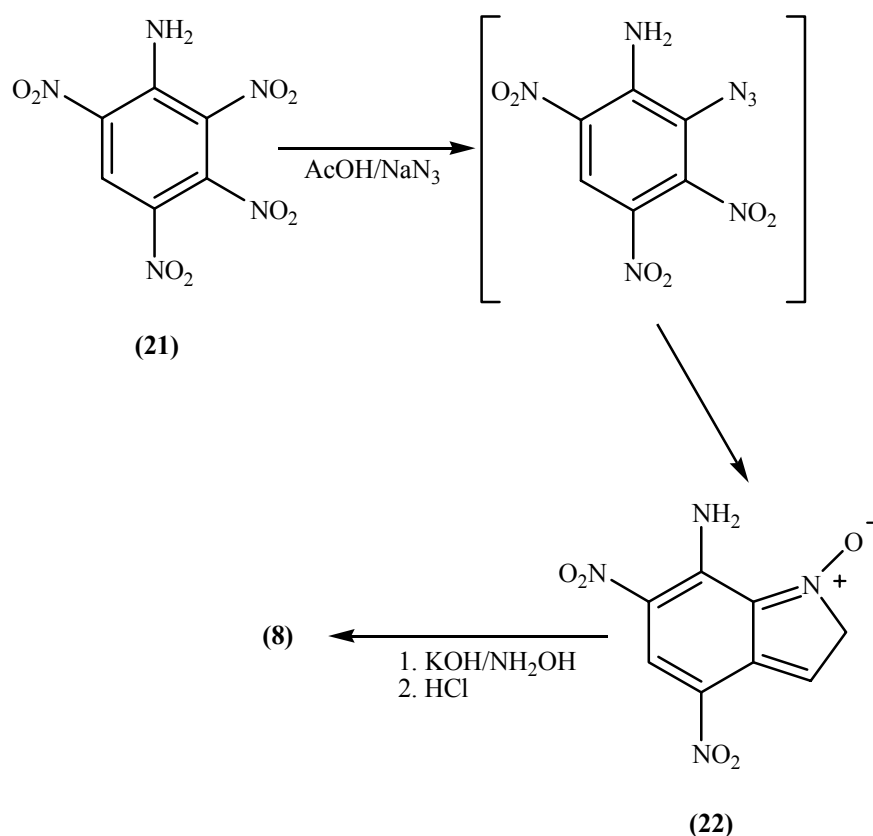
The approach by Bellamy ^[11] (Scheme 5) utilised a series of low temperature Ullmann coupling reactions with associated nitrations and halogenations. This gave access to the penultimate methoxy-NONA precursor **(20)**. However in our hands this procedure proved troublesome and despite activation by the methoxy group only the octanitro- derivative could be obtained reliably.



Scheme 5

A sample of NONA was prepared via the original and bipicryl route for characterisation and hazard evaluation. The material was found to be more sensitive than anticipated having a sensitivity similar to that of PETN. This high sensitivity was unexpected for this material and coupled with the complex and laborious work-up may preclude this material from further assessment.

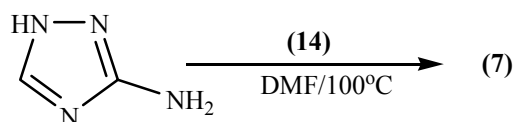
5,7-Diamino-4,6-dinitrobenzofuroxan (CL-14) has been studied extensively in the US by several organizations ^[12-16]. The synthesis of CL-14 (Scheme 6) involves azidation of tetranitroaniline (**21**) followed by ring closure to give 7-amino-4,6-dinitrobenzofuroxan (**22**). Amination in the presence of potassium hydroxide furnished the potassium salt which was subsequently acidified to give CL-14.



Scheme 6

Sufficient quantities of CL-14 were prepared by this route for evaluation, however the material upon hazard assessment was found to exhibit high sensitiveness to impact (similar to PETN). The increased sensitivity was traced to the presence of <2% of an unknown impurity. The impurity was found to be a phenolic compound arising from a competing hydrolysis reaction during the workup procedure employed in the synthesis of the tetranitroaniline intermediate. Careful workup reduced the amount significantly and this was borne out by the hazard data from a second batch of CL-14. The sensitiveness had been reduced to HMX levels but was still undesirable. The insolubility of CL-14 in virtually most solvents made recrystallisation difficult. Attempts to recrystallise from solvents such as DMF and DMSO resulted in decomposition of the compound. Alternative methods to prepare CL-14 also met with failure or gave impure material.

[(3-Picrylamino)-1,2,4-triazole] (PATO) was prepared using the method outlined by Coburn^[17]. This involved condensation of 3-amino-1,2,4-triazole with (14) (Scheme 7). Li and co-workers^[18] reported a modified procedure using tetryl instead of (14).



Scheme 7

The material has excellent thermal properties, is very insensitive to stimuli and does not suffer the detonability problems associated with TATB. PATO has been successfully pressed into pellets, however later batches of PATO did not press well. This was found to result from a change in crystal habit when compared to earlier batches. The needle-like crystals from the later batches were found to be the cause of the poor pressing.

Table 1.

Compound	Melting Point ^a (°C)	Density (g cm ⁻³)	P _{c-j} ^b (kbar)	Rotary Friction (F of I)	Rotter Test (F of F)
ANPZ	338.5	1.84	296	>6	145
PZO	333.5	1.91	330	4.5	54
DADNPO	322.5	1.88	303	5.9	93
NONA	440 ^c	1.78	255	2.1	37
PATO	315.6	1.82	307 ^d	>6	>168
CL-14	287.7	1.94	337	4.5	58

a) DSC onset value

b) Calculated by Detonics Modelling Group, QinetiQ.

c) NOL data

d) Based on density of 1.94 ^[11]

3. CONCLUSIONS

A number of high-energy heterocyclic and carbocyclic compounds have been prepared and characterised as potential replacements for TATB and HNS in initiators and explosive trains.

ANPZ is an attractive candidate due to its high insensitivity and high power output. The ease of synthesis and the possibility to obtain PZO from ANPZ result in an overall more economical process since two compounds could in theory be obtained from the same starting materials. The only disadvantage at present to this material is the high price and availability of the starting material (9).

DADNPO is another high-energy compound showing promise as preliminary hazard assessments have demonstrated it to be quite insensitive. The ease of synthesis from readily available and relatively low cost starting materials make it an ideal candidate for booster applications.

The first batch of CL-14 was found to be extremely sensitive (similar to PETN) due to a minor amount of unknown impurity, which was believed to be carried through from the initial preparation of the tetranitroaniline starting material. Although this impurity could not be totally eliminated its amount could be reduced. This was borne out by later hazard data which showed a decrease in sensitivity to HMX levels. The main problem of purification arose from the insolubility of CL-14 in common solvent systems and its ease of decomposition in certain solvents during attempted recrystallisation. In order to consider this material for further evaluation, alternative purification procedures would need to be developed for the final product or even the starting tetranitroaniline precursor.

NONA is a promising material due to its very high thermal stability. Problems with its synthesis have been identified and its high sensitiveness to impact.

PATO is showing great promise and has been successfully pressed into pellets. Surprisingly in some of the later batches, needle-like crystals were obtained after purification which was found to be difficult to press. The addition of pressing agents and further investigation into the purification method may be required to overcome this problem.

PZO, a leading candidate was unexpectedly found to be more sensitive than the same material synthesised at LLNL in the US. At present the reason for this is unclear as the only identifiable impurity is ANPZ.

Acknowledgements

The authors would like to thank the UK MOD's Corporate Research Programme for financial support.

REFERENCES

- [1] T. ROGERS AND M. WASKO: DERA report 'Unpublished results, 1998.
- [2] M. J. KAMLETT AND S. JACOBS: *J. Chem. Phys.* 48, 23, 1968.
- [3] J. BARKER, M. FREAK, J. MOONEY AND T. RAYNE: *Explosive Engineering*, Sept 1999.
- [4] D. S. DONALD: US Patent 3,808,209 (30/4/74).
- [5] E. C. TAYLOR, C. K. CAIN AND H. M. LOUX: *J. Am. Chem. Soc.*, 76, 1874, 1954. E. C. TAYLOR, H. M. LOUX, E. A. FALCO AND G. H. HITCHINGS: *J. Am. Chem. Soc.*, 77, 2243, 1955.
- [6] V. A. TARTAKOVSKII, O. P. SHITOV, I. L. YUDIN AND V. A. MAYASNIKOV: Russian Patent SU 1,703,645.
- [7] R. A. HOLLINS, L. H. MERWIN, R. A. NISSAN AND W. S. WILSON: *J. Het. Chem.*, 33, 895, 1996.
- [8] LICHT AND RITTER: *Proc. ICT* 1993.
- [9] J. C. DACONS, J. C. HOFFSOMMER AND F. TAYLOR JNR.: NOL report 'Heat Resistant Explosives XIX – An Improved Synthesis of 2,2',2'',4',4'',6,6',6'' – Nonanitroterphenyl, NONA', (3/5/1965)
- [10] A. J. BELLAMY AND P. N. HUDSON: *J. Chem. Res. (Synop)*, 4, 180, 1996.
- [11] W. P. NORRIS, M. P. KRAMER AND D. J. VANDERAH: NAWC Tech. Paper, 6955, (1989).
- [12] W. P. NORRIS, M. P. KRAMER AND D. J. VANDERAH: US Stat. Invent. Regist. 1078H1, (7/7/92).
- [13] W. P. NORRIS: US Patent 5039812 (13/8/91).
- [14] B. CHEN, AND Z. LIAO: *Proc. 21st Ann. Conf. ICT, Karlsruhe*, presentation no. 58, 1990.
- [15] A. P. CHAFIN AND R. L. ATKINS: US Patent 475040 (28/6/88).
- [16] M. CHAYKOVSKY AND H. G. ADOLF: *J. Het. Chem.*, 28, (6), 1491-5, 1991.
- [17] M. D. COBURN, H.H. HAYDEN, C. L. COON AND A. R. MITCHELL: *Synthesis*, (6), 490-2, 1999.
- [18] J. LI, B. CHEN AND Y. OU: *Propellants, Explosives and Pyrotechnics*, 24, 95, 1999.

MICROSTRUCTURE, MECHANICAL PROPERTIES AND MECHANICAL FAILURE OF POLYMER BONDED EXPLOSIVES

Peng-wan CHEN*, Feng-lei HUANG*, Yan-sheng DING**

* National Key Laboratory of Explosion and Safety Science,
Beijing Institute of Technology, Beijing 100081, China

** Institute of Mechanics, Chinese Academy of Sciences, Beijing 100080, China

Abstract:

The initial microstructure of hot pressed polymer bonded explosives and its evolution under thermal and mechanical aggressions were studied. The thermal aggressions include low temperature freezing and frozen combustion. Mechanical aggressions include tension, compression, ultrasonic wave insult and long-pulse low-velocity impact. The mechanical properties under tension and compression were studied and compared. Brazilian test was used to study the tensile properties. The failure mechanisms of polymer bonded explosives under different loading conditions were analyzed.

Keywords: *polymer bonded explosive, microstructure, mechanical properties, mechanical failure*

1. INTRODUCTION

The study of the microstructure, mechanical properties and mechanical failure is of crucial importance for the design, safety evaluation, and life prediction of energetic materials. Energetic materials may submit to different external stimuli, e.g. compression, tension and impact, resulting in the change of microstructure and even mechanical failure. Damage caused by external stimuli influences not only the mechanical properties, but also the sensitivity, combustion and even detonation behavior of energetic materials. Numerous studies have shown that the presence of defects, such as pores or cracks, can greatly increase the sensitivity of the energetic materials because they are potential hot spots where chemical reactions are likely to happen and also because they increase the specific area available for combustion.

Polymer bonded explosives (PBXs) are highly particle filled composite materials comprised of crystals of a secondary explosive and a polymer binder. They are used in both civil and military applications when very high performance is required. The study of the mechanical properties and failure mechanisms of PBXs has drawn tremendous attention in recent years ^[1,2]. Low strengths and safety concerns bring additional difficulties in preparing samples and conducting mechanical tests of PBXs. Optical and electronic microscopic examinations are effective methods to study the microstructure and its evolution and to reveal the mesomechanical deformation and failure mechanisms of explosive materials. Different microscopic methods including scanning electronic microscopy (SEM), environmental scanning electronic microscopy (ESEM) ^[3] and polarized light microscopy

(PLM) ^{14]} have been successfully used in this regard. Brazilian test, or diametrical compression, in which a disc of material is loaded diametrically in compression, has been used to generate tensile stress and evaluate the tensile failure stress of a material without the inconvenience of uniaxial dumbbell testing. Due to its low cost, ease of preparing samples and operation, Brazilian test has been widely used to evaluate the tensile properties of explosives ^{15, 6]}. The present paper presents the study of the microstructure, mechanical properties and mechanical failure of polymer bonded explosives conducted in our laboratory.

2. EXPERIMENTS

Hot pressed HMX-based PBXN-5 was used in the experiments. PBXN-5 contains HMX 94.5%-95.0% and fluorin rubber 5.0%-5.5% by weight. Molding powder was pressed into different sizes of samples in steel dies. The pressing temperature was 100 ° and the time duration of pressing was 1.5 h. To generate different microstructure, different pressure was used, ranging from 25 MPa to 400 MPa. For mechanical test samples, the pressure was fixed to 200 MPa.

To examine the evolution of microstructure under different stimuli, pressed PBXN-5 samples were subjected to different thermal and mechanical aggressions. The thermal aggressions included low temperature freezing and frozen combustion. Mechanical aggression included Brazilian test, uniaxial compression, ultrasonic wave test and long-pulse low-velocity impact. To evaluate the influences of freezing, low temperature freezing tests were conducted by keeping samples in dry ice and liquefied nitrogen for 5 minutes. In frozen combustion test, samples were ignited by a flame, and after a few seconds, were dropped in a water bucket where it was instantly cooled and extinguished. Ultrasonic waves are basically a mechanical aggression which is very different from shocks or impacts. In ultrasonic test, samples were submitted to ultrasonic waves in a bath with distilled water for 5 minutes. A long-pulse low-velocity gas gun with a gas buffer was also developed and used to apply dynamic compression, through which the time duration of dynamic compression can be extended to several milliseconds ^{17, 8]}. The explosive samples were confined in a steel tube during impact.

SEM and optical microscopy were used to examine the microstructure of the explosive. Low toughness and safety concerns bring additional difficulties in preparing PBX samples for microscopic examination. In microscopic examination, samples were first ground using standard fine silicon carbide papers (800 grid) to obtain a flat surface. Final polishing was carried out in an automatic polishing machine using 1 μm alpha alumina powder, at a load of 50 g, while being lubricated with distilled water. To avoid bringing additional unexpected damage to the samples, especially the damaged or fractured samples, during polishing, samples were first potted in commercial low-viscosity epoxide mounts with traditional amine hardening agent and then cured. To better reveal the details of the microstructure, isomethyl butyl ketone was selected to etch the surface.

A Brazilian test apparatus was developed to study the tensile properties of PBXs, in which a CCD camera was attached to conduct real time microstructural examination of the explosive sample during loading. In general failure occurs along the vertical axis in Brazilian test, which brings convenience for real time examination of the microstructural evolution. Uniaxial compression was also conducted to evaluate the compression properties of the explosives. Different strain rates were used in both Brazilian test and compression. The sample sizes were $\phi 10\text{mm} \times 12\text{mm}$ for compression and $\phi 20\text{mm} \times 10\text{mm}$ for Brazilian test and low velocity impact respectively.

3. RESULTS AND DISCUSSION

The pressing pressure greatly influenced the microstructure of pressed PBXN-5. At low pressing pressure, a lot of intergranular voids were still present. With the increase of pressure, the intergranular voids decreased, however crystal fractures also occurred. When the pressing pressure reached 100 MPa, extensive crystal fractures can be observed. Fig.1 shows a micrograph of PBXN-5 with a porosity of 2.5% pressed under 100 MPa. It is clearly shown that various forms of defects are present in pressed PBXN-5, including intergranular voids, debonding of the binder from crystals, and crystal fractures. In addition, deformation twinning can also be observed on large crystals in some cases. To further examine the microstructure of HMX crystals, pressed PBXN-5 was kept in a selected solution for enough time to totally remove the binder and leave the explosive particles alone, and then the obtained explosive particles were examined by SEM. Fig.2 shows the microstructure of the recovered HMX crystals after pressing at 100 MPa, showing the presence of extensive fracture of particles and a lot of microcracks. Crystal fractures are mainly associated with particle-to-particle contacts due to an extremely high concentration (over 90 %) of explosive crystals in PBX. Another important phenomenon in pressed PBX was the presence of deformation twinning, an evidence of plastic deformation of explosive crystals during pressing. The above results also reveal that considerable initial damage is present in hot pressed PBX. Pressing not only consolidates the molding powder, but also induces new damage to explosive crystals.

When PBXN-5 was subjected to freezing in dry ice for 5 minutes, no visible cracks were observed. However when PBXN-5 was subjected to freezing in liquefied nitrogen for 5 minutes, cracks were initiated. Some small cracks were linked together and formed larger ones. The cracks propagated mainly along the crystal boundaries. The results show that the interfacial strength of PBXN-5 is low. Recent thermal shock experiments also showed that cracking can be initiated when PBX sample was transferred from a lower temperature water environment (2°) to a higher temperature water environment (25°~ 30°) ^[9]. Due to the large difference of thermal expansion properties between explosive and binder, PBX has poor resistance to thermal shock.

Macroscopically the recovered sample subjected to frozen combustion had an undulating, gooey appearance and was brown in color compared with the pristine white of unburned PBXN-5. Cross sectional views showed the presence of three characteristic zones including fusion zone, heat affected zone and base material. The fusion zone was characterized by uneven edges and internal void regions which resembled bubbles. This may be the result of decomposition gases trapped in the melt as it solidified. The heat affected zone was dominated by extensive interfacial debonding. The zone of base material resembled unheated, original materials. Fig.3 shows a plan view of recovered sample. Because part of binder has been destroyed by combustion, HMX crystals are exposed. The plan view is dominated by pits and pocks, especially for HMX crystals. At high resolution, some of the pits and pocks reveal ordered, columnar crystal growth, indicating possible phase transition from β -HMX to δ -HMX. More experiments are needed to investigate the possible phase transition.

Fig.4 shows a plan view of PBXN-5 damaged by ultrasonic waves for 5 minutes. A lot of pull-outs can be observed and some of them are very large and involve many grains. The balls of the initial molding powder may have an influence on that process. The grains do not seem to be broken and no intragranular cracks can be detected. Besides, nearly all the contacts between the grains are debonded. The above results show that ultrasonic waves are able to seriously damage pressed PBXN-5. Ultrasonic waves are frequently used in polishing

process to clean the samples before microscopic examination, however it seems to be inappropriate for PBX materials.

Real time microscopic examination of Brazilian test revealed that the failure first started at several independent sites, usually around the boundaries of the larger HMX filler particles and formed microcracks. These microcracks linked up into larger cracks and finally induced the rupture of the samples. The initial damage such as debonding and uncoating generated during hot pressing are the origins of failure. Fig.5 shows that a crack is extending along the boundaries of larger particles. Fig.6 shows some extended binder filaments bridging the crack surfaces, demonstrating that the binder undergoes considerable deformation. Plan views of the fracture routes showed that crystal fracture was very rare, but may appear due to the orientation of some larger particles perpendicular to an advancing crack path.

The fracture surfaces in Brazilian test were rough, with some particles completely pulled out. Larger particles exhibited clean crystal faces due to the debonding of binder from particles. In contrast, the finer particles appeared rough having binder fibrils fractured due to extensive deformation. Fig.7 shows a typical fractograph of PBXN-5 under quasi-static Brazilian test, in which both clean crystal surfaces and binder filaments can be observed. Examination of fracture surfaces also showed that the failure predominantly followed the boundaries of the explosive fillers due to interfacial debonding with few fractured crystals. Some microcracks can also be observed on some particles (see fig.7). Due to the low stress amplitude applied in Brazilian test, it is reasonably to assume that these microcracks were caused during pressing.

Microscopic examination of PBX samples fractured under higher strain rates in quasi-static Brazilian test showed that with the increase of strain rates more crystal fractures occurred. To further investigate the influence of even higher strain rates, dynamic Brazilian test was conducted, in which the sample disc was loaded by a drop weight and the corresponding strain rate was estimated as $0.3 \times 10^2 \text{ s}^{-1}$. Fig.8 shows a typical fractograph of PBX under dynamic Brazilian test, demonstrating the presence of extensive crystal fractures. To further investigate the mesomechanical deformation and failure of PBXs, we are using high resolution moiré interferometry in Brazilian test. The results will be discussed elsewhere.

Fig.9 shows a typical fractograph of PBXN-5 in quasi-static compression test. Extensive crystal fractures can be observed, causing the formation of a large number of smaller particles. The corresponding tensile failure stress in Brazilian test and the compressive failure stress in compression test were estimated as 0.8 MPa and 8.8 MPa respectively, revealing that explosive particles with initial microcracks caused by pressing may not fracture under a tensile stress of 0.8 MPa, while may fracture under a compressive stress of 8.8 MPa. Determination of the critical failure tensile and compressive stresses of explosive crystals is crucial to understand the mesomechanical phenomena of PBXs. Unfortunately the data of mechanical properties of explosive crystals are very scarce at present due to the difficulties in experiments.

Fig.10 shows a plan view of PBXN-5 damaged by a steel projectile at an impact velocity of 108 m/s. Impact direction is from the right of the figure. The impact induced a large number of microcracks in explosive crystals. A vertical crack across explosive crystals can also be observed. Particle size distribution analysis showed that before impact the average particle size of HMX was $130.8 \mu\text{m}$, however after impact the average particle size decreased to $114.5 \mu\text{m}$ due to the extensive particle fractures. At this impact velocity, no fragments were observed in PBXN-5 samples; however at the same velocity, Composition B (containing TNT 40 % and RDX 60 % by weight) was severely fragmented. This

demonstrates that despite the low concentration of binder, PBXN-5 exhibits better resistance to impact loading than Composition B.

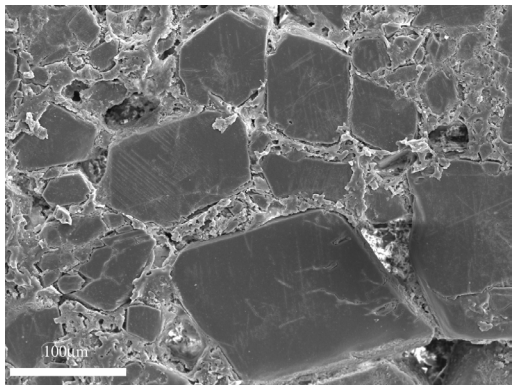


Fig 1. Micrograph of pressed PBX

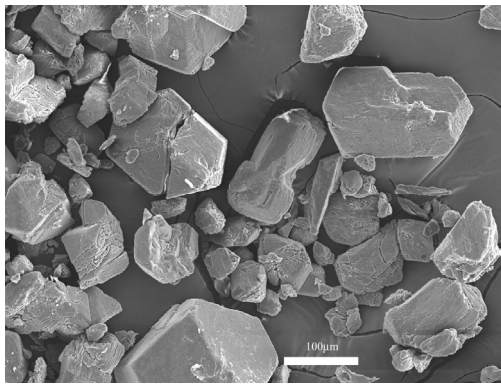


Fig 2. Microstructure of HMX crystals in pressed PBX

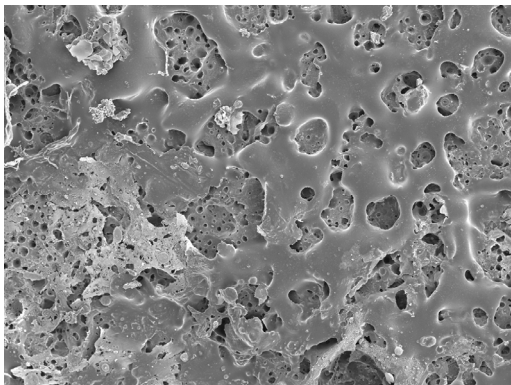


Fig 3. Microstructure of PBX subjected to frozen combustion

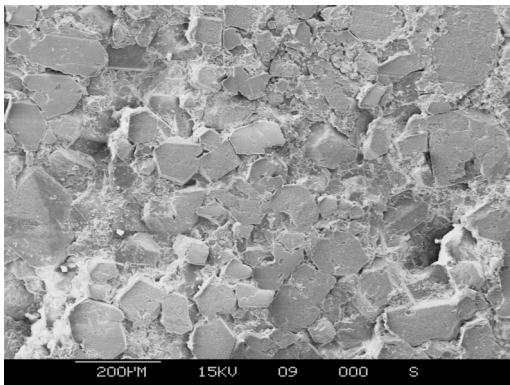


Fig 4. Microstructure of PBX subjected to ultrasonic waves

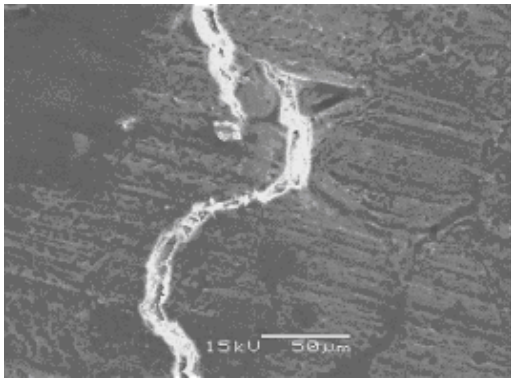


Fig 5. Cracking along particle boundaries

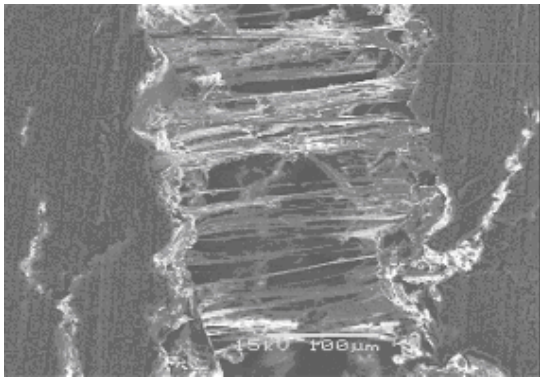


Fig 6. Binder filaments bridging crack walls

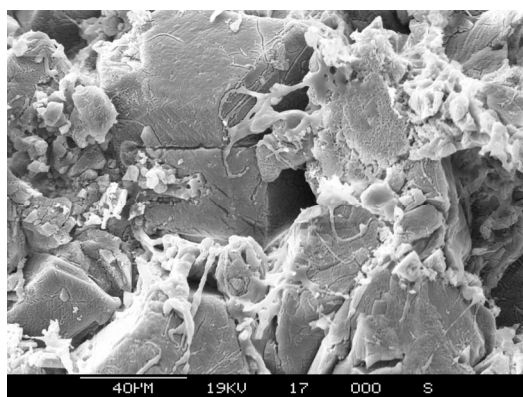


Fig 7. A typical fractograph of PBX under quasi-static Brazilian test

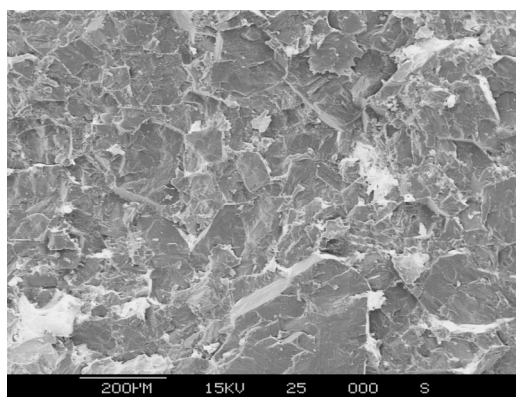


Fig 8. A typical fractograph of PBX under dynamic Brazilian test

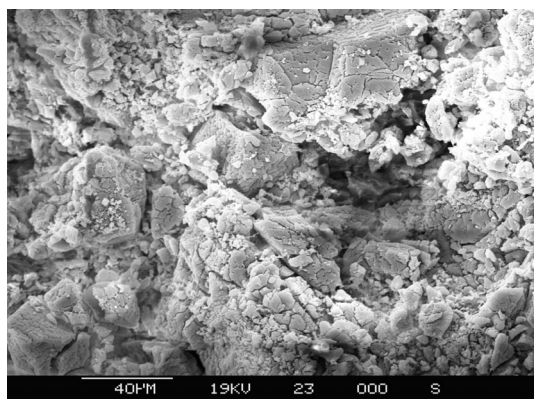


Fig 9. Fractograph of PBX under compression

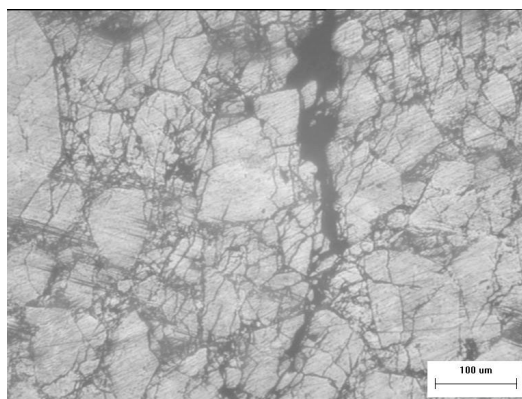


Fig 10. Impact damaged PBX

Fig.11 shows some tensile stress-strain curves obtained by Brazilian test under different strain rates, demonstrating that the tensile properties of PBXs are influenced by strain rates. At a strain rate of $8.33 \times 10^{-5} \text{ s}^{-1}$, the tensile failure stress and failure strain at the sample center are 0.85 MPa and 3.52×10^{-3} respectively. While at a strain rate of $8.33 \times 10^{-4} \text{ s}^{-1}$, the failure stress and failure strain are 1.16 MPa and 2.85×10^{-3} . In indirect tensile creep tests (Brazilian test), instantaneous elastic-plastic response, steady creep development and final rupture can be observed. The creep of PBX is mainly due to the contribution of the binder, demonstrating that PBX still exhibits viscoelastic properties despite a low concentration of binder. Fig.12 shows some compressive stress strain curves of PBXN-5, demonstrating that the compressive properties of PBXs are also influenced by strain rates. The maximum stresses in the curves correspond to uniaxial compressive strengths. The compressive strengths increase with strain rates. At a strain rate of $6.94 \times 10^{-4} \text{ s}^{-1}$, the compressive strength is 9.8 MPa; while at a strain rate of $6.94 \times 10^{-2} \text{ s}^{-1}$, the compressive stress increases to 19.8 MPa. It is also shown that the strains corresponding to the maximum stresses do not change noticeably. Wiegand ^[10] reported similar results in the study of the compressive properties of PBXs and other explosives and proposed a failure criterion of constant critical strains for explosives and propellants.

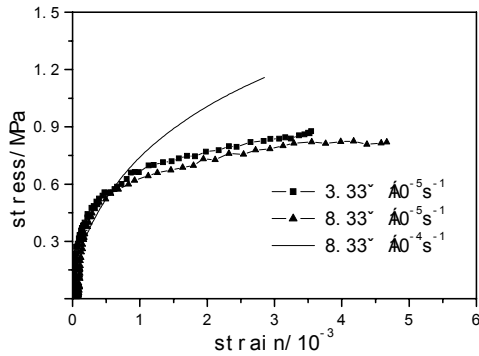


Fig 11. Tensile stress strain curves

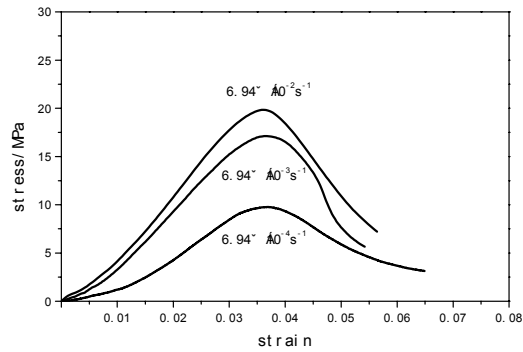


Fig 12. Compressive stress strain curves

Table 1 lists the tensile and compressive strengths of PBXN-5 obtained in the experiments, demonstrating that the tensile strengths are much lower than the compressive strengths, less than one tenth of the compressive strengths. The microstructure of PBXs can account for this result. The explosive particles are separated in tension, so the binder plays a predominant role during deformation. While in compression the explosive particles are pressed and contacted with each other due to the extremely high volume fraction of explosive crystals, so the explosive particles play a more important role during deformation. The above results demonstrate that PBXs have low strengths and low failure strains and their mechanical properties are strain rate dependent.

Table 1. Tensile strengths and compressive strengths of PBXN-5.

strain rates/s ⁻¹	tensile strengths/MPa	strain rates/s ⁻¹	compressive strengths/MPa
3.33×10^{-5}	0.82	6.94×10^{-4}	9.8
8.33×10^{-5}	0.85	6.94×10^{-3}	17.1
8.33×10^{-4}	1.16	2.78×10^{-2}	18.1
--	--	6.94×10^{-2}	19.8

4. CONCLUSIONS

The characteristic initial damage modes present in pressed PBX include intragranular voids, crystal fractures, interfacial debonding and deformation twinning. The high concentration of explosive crystals results in extensive particle-to-particle contacts, which in return causes extensive fractures during pressing. When PBXN-5 is submitted to low temperature freezing, cracks can be initiated. When PBXN-5 is subjected to frozen combustion, extensive debonding occurs. Ultrasonic waves may induce severe damage to PBX, causing extensive debonding and even pull-outs.

PBXs are brittle materials with low strengths and low fracture strains. The tensile strengths of PBXs are much lower than the compressive strengths, less than one tenth of the compressive strengths. Different failure modes correspond to different loading conditions. Interfacial debonding is the predominant failure mode in quasi-static Brazilian test, and crystal fracture is very rare. In Brazilian test, initial failure tends to start around the edges of larger filler particles and often occurs at several independent sites simultaneously. The

increase of strain rates causes more explosive crystals to fracture. In dynamic Brazilian test, the predominant failure mode is crystal fracture. Extensive crystal fractures are also present in compression. Low velocity impact also induces extensive crystal fractures.

Acknowledgements

The authors of this paper acknowledge the financial support from the National Natural Science Foundation of China under contract number 10002022 and Joint foundation of Chinese National Natural Science Committee and Chinese Academy of Engineer Physics under contract number 10076021.

REFERENCES

- [1] D. A. WIEGAND: *Mechanical properties and mechanical failure of composite plastic bonded explosives and other energetic materials* - J. M. Short and J. E. Kennedy. Paper Summaries-Eleventh International Detonation Symposium, Snowmass, 1998. 85-88.
- [2] G. T. GRAY III, D. J. IDAR, W. R. BLUMENTHAL, ET AL.: *High- and low- strain rate compression properties of several energetic material composites as a function of strain rate and temperature* - J. M. Short and J. E. Kennedy. Paper Summaries-Eleventh International Detonation Symposium, Snowmass, 1998. 229-231.
- [3] P. J. RAE, H. T. GOLDREIN, S. J. P. PALMER, ET AL.: Studies of the failure mechanisms of polymer-bonded explosives by high resolution moiré interferometry and environmental scanning electron microscopy - J. M. Short and J. E. Kennedy. Paper Summaries-Eleventh International Detonation Symposium, Snowmass, 1998. 235-239.
- [4] C. B. SKIDMORE, D. S. PHILLIPS, N. B. CRANE: Microscopical examination of plastic-bonded explosives. *Microscope*, 1997, 45(4): 127-136.
- [5] H. D. JOHNSON: Diametric disc and standard tensile test correlation study. MHSMP-81-22, 1981.
- [6] P. J. RAE, H. T. GOLDREIN, S. J. P. PALMER, ET AL.: Quasi-static studies of the deformation and failure of β - HMX based polymer bonded explosives. *Proc. R Soc. Lond. A*, 2002, 458: 743-762.
- [7] PENGWAN CHEN, FENGLEI HUANG AND YANSHENG DING: An experimental study on the impact damage of explosives - Ping Huang, Yajun Wang, Shengcai Li, Xinming Qian *Progress in Safety Science and Technology* (vol. III), Taian, 2002. 1417-1422.
- [8] PENGWAN CHEN, FENGLEI HUANG, KAIDA DAI, YANSHENG DING: Detection and characterization of long-pulse low-velocity impact damage in plastic bonded explosives. *International Journal of Impact Engineering* (in press).
- [9] YONG TIAN, SHUN-HUO LUO, WEI-BIN ZHANG: Water-bathed thermal shock damage of PBX JOB-9003 and its Ultrasonic Characteristics. *Chinese Journal of Explosives and Propellants*, 2002, 25(3): 17-19
- [10] D. A. WIEGAND: Constant critical strain for mechanical failure of several particulate polymer composite explosives and propellants and other explosives. AD-E402 775, 1997.

SYNTHESIS AND CHARACTERISATION OF NITROGUANIDINE BASED NITRATE AND PERCHLORATE SALTS OF -5-NITRO-2-NITROIMINOHEXAHYDRO-1,3,5-TRIAZINE

H. S. Jadhav*, M. B. Talawar***, D. D. Dhavale*, S. N. Asthana***
and V. N. Krishnamurthy**

* Department of Chemistry, Garware Research Centre, University of Pune,
Pune 411 007, INDIA

** DRDO/ISRO Cell, University of Pune, Pune 411 007, INDIA

*** High Energy Material Research Laboratory,
Sutarwadi Pashan, Pune 411 021, INDIA

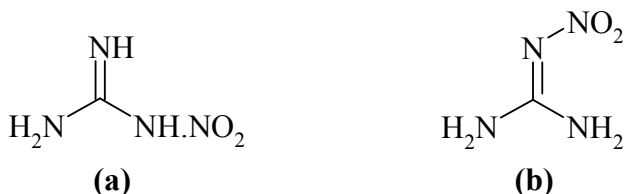
Abstract:

The condensation of nitroguanidine, formaldehyde and amine followed by nitration afforded 5-nitro-2-nitroiminohexahydro-1,3,5-triazine (2). Compound 2 on nitric acid and perchloric acid treatment afforded the nitrate and perchlorate salts of 2.

Keywords: *high energy materials, nitro compounds, energetic salts*

1. INTRODUCTION

Nitroguanidine, also known as picrite, is an aliphatic nitramine. It exists in two tautomeric forms (a) and (b) shown below^[1].



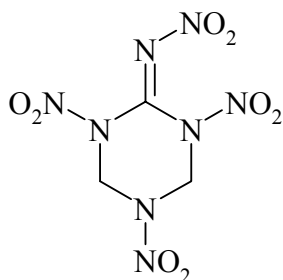
Nitroguanidine is a well-known nitro compounds. It has been used not only in tribasic propellants for many years but also as a potential insensitive explosive recently^[2]. The physical properties and detonation data of nitroguanidine have been studied extensively but its chemical reactivity on using it to synthesize high explosive has rarely been explored. The only published work concerned with this area is by McKay and Wright^[3], who studied the reaction of a nitroguanidine with alkylamines in basic mediums and obtained some derivatives of nitroguanidine^[4, 5]. The hydrazinolysis of nitroguanidine was investigated by Henry^[6] and the research work on chemical reaction of nitroguanidine was reviewed by McKay^[7] in 1952. Afterward, some reports involving the use of nitroguanidine as a component to prepare heterocyclic nitrogen compounds appeared, but none of these compounds are explosives.

Since there are two amino groups, one nitroimino groups and one carbon atom in the molecule of nitroguanidine, which may be used as a ideal element to form a desired explosive molecule. It does seem, however a little surprising that the reaction of nitroguanidine with urotropine or formaldehyde have been ignored for many years. Inspired by the fact as stated above we made an attempt to examine some reaction concerned with nitroguanidine, which are described below.

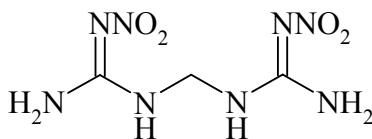
The reaction of nitroguanidine with urotropine or formaldehyde has been studied. The following compounds are synthesized from nitroguanidine.

- (i) 6-nitroimino-1,3,5-trinitro-1,3,5-triazacyclohexane (c) and a number of its derivatives
- (ii) *bis* (nitroguanidino) methane (d), a valuable intermediate for preparing some high explosives.
- (iii) 1,5-dinitro-2,4-dinitroimino-1,3,5-triazacyclohexane (e) and some of its derivatives via intramolecular cyclization of (d)
- (iv) 2-nitroimino-1,3-diaza-5-oxacyclohexane (f), 1-(nitroguanidinomethyl)-2-nitroimino-1,3-diaza-5-oxacyclohexane (g), and bis (2-nitroimino-1,3-diaza-5-oxacyclohexyl)methane (h) by reaction of (d) with formaldehyde.

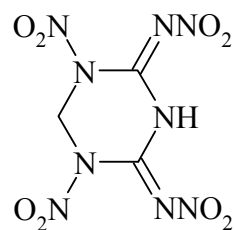
Literature survey ^[2] shows some detonation data of these compounds in which compounds **c** and **e** are powerful explosives but very unstable thermally and easily hydrolysed. However compound **f-h** possesses a better stability than triazacyclic polynitrocompounds containing nitroimino groups such as **c** and **e**.



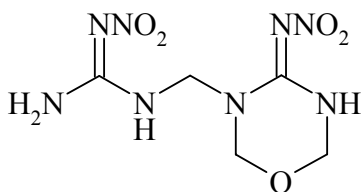
(c)



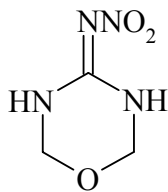
(d)



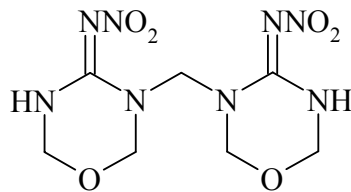
(e)



(f)



(g)



(h)

Nitroguanidine has been used to some extent as an industrial explosive. It has not been used as a military explosive because of its relatively low energy content and difficulty of initiation. Attention has been paid to Nitroguanidine as an explosive since the gases from the decomposition of other explosives of comparable power, which is because of its low temperature of explosion ^[8-11]. Nitroguanidine ignites with difficulty and undergoes incomplete explosive decomposition and may be regarded as an explosive, which is powerful, but difficult to detonate. Although its detonation rate at comparable densities is almost as high as that of RDX it has an anomalously low detonation energy and pressure, indicating a decomposition mechanism different from that of conventional explosives. One of the crystal forms of Nitroguanidine is fiber or feather like and this enables the crystal to mechanically interlock with large void spaces left between them. This property enables Nitroguanidine to maintain fairly decent mechanical properties at low density makes

Nitroguanidine a useful laboratory explosive where some experiments require controlled low detonation velocity and pressure. The high nitrogen content of the products of combustion and lower flame temperature per unit of energy accounts for the wide spread use of Nitroguanidine in multi base gun propellants to reduce barrel wear, muzzle blast and flash. Many guanidine derivatives have been prepared as possible substitutes for nitroguanidine in propellants including triaminoguanidine, nitroaminoguanidine and trinitroethylguanidnidine. Nitroguanidine is less sensitive than TNT to impact, friction and shock. Its brisance and blast characteristics are similar to that of TNT.

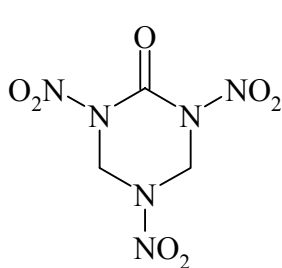
Nitroguanidine composition used in the air bags:

Literature survey indicates that the nitroguanidine-based composition is used as for inflation of vehicle airbags [12-18]. The thermally stable gas generating compositions especially for inflation of vehicle airbags, consist of nonazide based mixture containing nitroguanidine, at least one nonazide high nitrogen fuel selected from guanidines, tetrazole and triazoles and salt of tetrazole and triazoles, and potassium nitrate stabilized ammonium nitrate. These composition having melting point $>115^{\circ}\text{C}$, these composition have a reduced yield of solid combustion products, acceptable burn rates thermal stability and ballistic properties. Metal salt of nitroguanidine propellants are used for airbags, metal salt of the nitroguanidine showing excellent ignition properties [12-16].

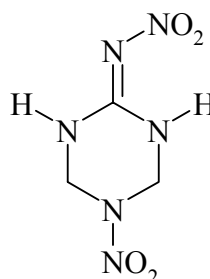
Astachov *et al.* [17] synthesized 1,2,4-trizolyl and tetrazolyl derivatives of nitroguanidine and he presented MO calculation of synthesized nitroguanidine based compounds. The gas-generating agent comprises ≤ 45 wt.% phase-stabilized ammonium nitrate, nitroguanidine, and oxygen-containing potassium salt. The oxygen-containing potassium salt is selected from potassium nitrate, potassium perchlorate, potassium sulfate, potassium chlorate, potassium chromate, potassium dichromate, potassium permanganate, and potassium oxalate. The agent is used in a gas generator for inflating airbags with high-gas evolution efficiency [11-13].

The nitroguanidine compositions are also used as a gas generating pellets, gas generators and air bags apparatus.

A method for the preparation of 2,4,6-trinitro-2,4,6-triazacyclohexanone (**i**, TNTC) yielding a product with a low concentrations of impurities and improved thermal stability is reported. The product is advantageous compared with RDX and HMX since it is more energetic and has a higher density. The reaction of 2-nitroimino-5-nitrohexahydro-1,3,5-triazine (NNHT) with $(\text{CF}_3\text{CO})_2\text{O}$ / ammonium nitrate gave 62.2% TNTC (**i**). Impact test of TNTC indicated shock sensitivity corresponding to a height of 9 cm for a 2 kg wt. and an exothermic onset at 183.9°C with an exothermic peak at 206.3°C .



(i)



(j)

2. EXPERIMENTAL

2.1 General methods

Melting points were recorded with Thomas Hoover melting point apparatus and are uncorrected. IR spectra (ν , cm^{-1}) were recorded on a Shimadzu FTIR - 8400 spectrometer. ^1H NMR (300 MHz) spectra were recorded in DMSO- d_6 as a solvent unless otherwise noted. NMR chemical shifts are reported in δ (ppm) downfield from TMS. Elemental analyses were carried out on a Hosli C, H-analyser. As and when required, the reactions were carried out in oven-dried glassware under dry N_2 . Thin layer chromatography was performed on pre-coated plates (0.25mm, silica gel 60 F₂₅₄). The detonation velocity is estimated based on empirical calculations on molecular structure developed by L.R. Rothstein^[19]. Detonation pressure was calculated by Chapman-Jouguet (CJ) method^[19]. Density (ρ) values were calculated by L. T. Eremenko method^[19]. The results are summarized in Table-1. The oxygen balance values calculated are given in Table-1. The thermal analysis (with about 2 mg samples) experiments were performed on Mettler Toledo star system at a heating rate of $10^\circ\text{C} / \text{min}$ in nitrogen atmosphere (at a flow rate of 80 ml/min) and the results are summarized in Table-2. Energy of Activation and frequency factor calculated using the Madhusudnan, Ninan and Krishnan method^[20] and the results are given in Table-3. The Impact test was conducted using an impact tester similar to that used in Naval Ordnance Laboratory (NOL) U.S.A. Test specimens (30-35 mg of powder) were kept between two hardened anvils and a 3 kg drop weight was allowed to fall freely from different heights. Both open and aluminum foil encapsulated specimens were used. The 50% ignition height (cm) in each case was evaluated using Bruceton method. Ten samples were tested for each compound. The results are presented in Table-4. The friction test was conducted in a test set up similar to the one employed by NOL. The sample was kept between a fixed corrugated (rough) stainless steel plate and a movable stainless steel plate. Pulling the movable plate at varying lever loads causes friction. The sample size and evaluation procedure was the same as followed for impact testing. The data are given in Table-4. All the chemicals used were from Aldrich, recrystallisation of the compounds was done based on the solubility in the solvent.

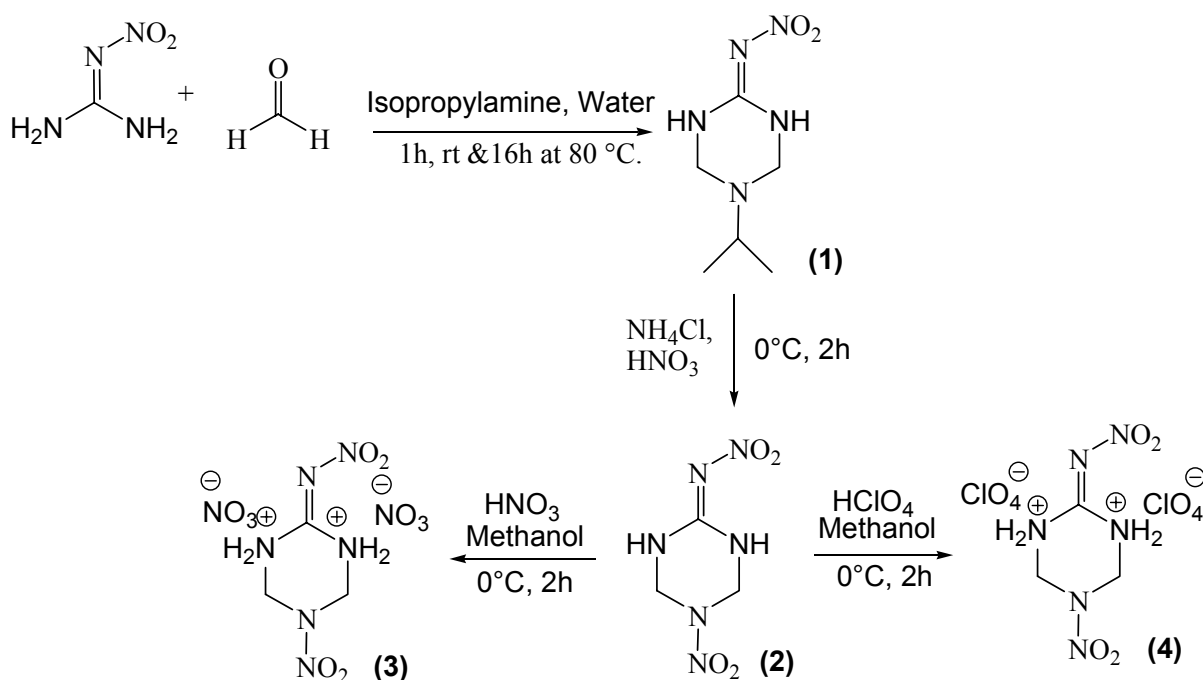
2.2 Preparation of 5-isopropyl-2-nitroimino-hexahydro-1,3,5-triazine(1)

To a slurry of nitroguanidine (5.0 g, 48 mmol) in water (20ml) was added a 37-45% aqueous formaldehyde solution (8.8 ml, 82 mmol) and the mixture stirred for 30 minutes at room temperature. Isopropyl amine (3.4 g, 57.5 mmol) was then added slowly and the mixture stirred for 1 hr at room temperature and 16 h at 80°C . The slurry was cooled to room temperature, filtered and the solid washed with cold water and dried to give a white powder. Recrystallisation from acetone gave the title compound as white crystalline plates **1** (6.8 g, 89%) having melting point at $190\text{-}192^\circ\text{C}$, (reported $191\text{-}192^\circ\text{C}$).

IR in cm^{-1} (ν max): 820 (ring), 1529 ($\text{C}=\text{N}$), 1586 ($-\text{N}-\text{NO}_2$), 3460 ($-\text{NH}$ stretching).

^1H NMR (300 MHz, DMSO- d_6): 1.05 (6H, d), 2.85 (1H, m), 4.3 (4H, s), 8.8 (2H, bs, 2 x -NH). Elemental Analysis calculated for $\text{C}_6\text{H}_{13}\text{N}_5\text{O}_2$: C:40.22(40.35); H:7.26(7.12); N:39.10(39.14).

Scheme 1.



2.3 Preparation of 5-nitro-2-nitroimino-1,3,5-triazine (2)

To 98% nitric acid (3.0 ml) at 0 °C was added **1** (500 mg, 2.67 mmol) over a 10 min period. Ammonium chloride (150 mg, 2.80 mmol) was then added and the resulting yellow solution was stirred at 0 °C for 2h and then poured onto crushed ice. The precipitated solid was filtered, washed with cold water and dried *in vacuo* to give pure **2** as a white solid (360 mg 76%), mp: 203-205 °C (reported.205-206).

IR in cm^{-1} (v max): 835 (ring), 1540 (C=N), 1575 (-N-NO₂), ¹H NMR (300 MHz, DMSO-d₆): 5.02 (2H, s), 5.7 (2H,s), 9.1 (1H, bs, -NH), 9.8 (1H, bs, -NH).

Elemental Analysis calculated for C₃H₆N₆O₄: C:18.94(19.00); H: 3.15(3.12); N:44.21(44.24).

2.4 Preparation of nitrate salt of 5-nitro-2-nitroimino-1,3,5-triazine (3).

Compound 5-Nitroimino-1,3,5-triazine (1 g, 5.26 mmol) **2** was dissolved in dry methanol (10 ml) and nitric acid was added slowly upto neutralization at 0 °C. The reaction mixture was stirred at 0°C for 1-2 h. The yellow precipitate obtained was filtered on a buchner funnel and washed with cold methanol gave compound **3** (Yield 0.980 g. 59 %), having the melting point at 260-262 °C.

IR in cm^{-1} (v max): 835 (ring), 1540 (C=N), 1575 (-N-NO₂), 2850 (-NH₂).

Elemental Analysis calculated for C₃H₈N₈O₁₀: C:11.39(11.35); H:2.53(2.40); N: 35.44(35.39)

2.5 Preparation of perchlorate salt of 5-nitro-2-nitroiminohexahydro - 1,3,5-triazine (4).

Compound 5-Nitroiminohexahydro-1,3,5-triazine (1g, 5.26 mmol) was dissolved in dry methanol (10 ml) perchloric acid was added slowly upto neutralization at 0°C. The reaction mixture was stirred at 0°C for 1-2 h. The yellow precipitate thus obtained was filtered on a buchner funnel and washed with cold methanol afforded compound **4**. (Yield 1.2 g, 58.5 %), which shows the melting point at 328-330 °C.

IR in cm^{-1} (v max): 835 (ring), 1540 (C=N), 1575 (-N-NO₂) 1600, 2950 (salt).

Elemental Analysis calculated for C₃H₈N₆O₁₂Cl₂: C:9.2(10.0); H:2.04(2.10); N:21.48(21.53).

3. RESULTS AND DISCUSSION

The melting point matches with the reported values wherever it is applicable, while for the new compounds elemental analysis confirms the synthesis.

For compound **2**, melting point shows 203-205°C, matches with the reported values.^[9] The IR data show the 3400 peak for the tertiary amine formation in addition to its nitramine functional group at 1580 cm^{-1} and the 3300 cm^{-1} for -NH stretching frequency and these data clearly indicate the synthesis of compound. The NMR spectrum shows the broad singlet is at 9.1 and 9.8 δ due to -NH protons and this secondary amine proton exchanges in deuterated water. Elemental analysis for the compound is matches with the theoretical one. Thermogravimetric data shows compound **2** decomposes in single step. The decomposition temperature is between at 207- 210°C, 92% weight loss is there while the maximum decomposition is at 209°C.

Compound **3** shows melting point at 235°C. The elemental analysis for compound **3** is matches with theoretical value. IR spectral data shows the peak at 2850, 2868 cm^{-1} indicates the formation of salts in addition to its compound shows the peak at 1575 cm^{-1} for (-N-NO₂) groups. Compound **3** shows positive oxygen balance while shows density 1.7 g/cm^3 . Thermogravimetric data shows two stage decomposition first stage starts at 210-310°C, with 40% weight loss the maximum weight lost is at 270°C, while second stage starts at 310-450°C, with 10% mass loss may be due to the evaporation of residue.

Compound **4** shows the melting point at 260°C, the elemental analysis for compound **4** is matches with the theoretical one while IR data confirms the salt formation. Due to the positive oxygen balance (+8.11%) compound shows high detonation velocity (9.42 Km/s) and detonation pressure 51.46 (GPa).The TG data of the **4** shows the high stability of the compound it decomposes in single stage. The compound is stable upto 250°C; the weight loss is between 260 -360°C with 82% weight loss while the maximum weight loss is at 348°C. Sensitivity data of the nitrate and perchlorate salts shows insensitive to impact. The order of the energetic performance of compound is **4** > **3** > **2**.

4. TABLES

Table 1. Theoretical performance of the compound 2-4

Compound	Mole. Form.	Density	Oxygen balance	Detonation velocity	Detonation pressure
		g/cm ³	%	Km/s	GPa
2	C ₃ H ₆ N ₆ O ₄	1.70	-21.61	8.94	33.98
3	C ₃ H ₈ N ₈ O ₁₀	1.72	5.06	9.65	40.25
4	C ₃ H ₈ N ₆ O ₁₂ Cl ₂	1.80	8.18	7.74	27.067

Table 2. Thermal data of the compound 2-4

Compound	Decomposition Temp. (°C)		Tmax	Weight loss in
	1 st step	2 nd step	°C	%
2	207-210	-	209	92
3	210-310	310-450	270, 330	50
4	260-360	-	348	82

Table 3. Kinetic data of the compound 2-4

Compound	Energy of activation	Frequency Factor	Correlation Coefficient
	(Ea)	(A)	(r)
2	323.69	30.87	0.914
3	135.98	17.27	0.956
4	155.01	9.43	0.995

Table 4. Sensitivity data of the compound 2-4

Compound	Direct impact test Ignition values (h50 %) cms Drop weight 3 Kg
2	>100
3	75
4	65

5. CONCLUSION

The present investigation demonstrates the synthesis and characterisation of two new energetic salts of -5-nitro-2-nitroimino-hexahydro-1,3,5-triazine. The thermal analysis, theoretical calculation of detonation velocity and detonation pressure establishing their candidature as high energy materials.

Aacknowledgement

Authors are thankful to Dr. Haridwar Singh, outstanding Scientist and Director, High Energy Materials Research Laboratory, Pune, India for his constant encouragement and motivation.

REFERENCES

- [1] S. KRISHNAN, S. R. CHAKRAVARTHY, S. K. ATHITHAN: Propellants and Explosive Technology, Course notes of the Professional Development Short Term Course conducted at IIT madras, India, Dec. 6-7, 1998
- [2] YU YONGZHONG AND SU ZHUANG: *Propellants, explosive, Pyrotechnics*, **14**, 150, 1989
- [3] A. F. MCKAY, AND G. W. WRIGHT: *J. Am. Chem. Soc.* 1948
- [4] A. F. MCKAY: *J. Am. Chem. Soc.*, **71**, 1968, 1949
- [5] R. H. HALL, A. F. MCKAY, AND G. F. WRIGHT: *J. Am. Chem. Soc.*, **72**, 2015, 1951
- [6] R. A. HENRY, H. D. LEWIS, AND G. B. L. SMITH: *J. Am. Chem. Soc.*, **72**, 2015, 1950
- [7] A. F. MCKAY: *Chem. Rev.*, **51**, 304, 1952
- [8] SAMUEL DELVIN: *Explosives*, **1st** edition, 2000
- [9] MATTHEW D. CLIFF: *Heterocycles*, **48 (4)**, 657, 1998
- [10] ASHLEY, KENNETH D: *American Cyanamid Co*, CAN 40:7548, 1945
- [11] P. F. PAGORIA, ALEXANDER R. MITCHELL AND EDWARD S. JESSOP: *Propellants, Explosive, Pyrotechnics* **21**, 14, 1996
- [12] KHANDHADIA, PARESH S, BURNS, SEAN P: *Automotive Systems Laboratory*, (USA). U.S. CAN:135:320147, 2001
- [13] HISKEY, MICHAEL A, NAUD, DARREN L.: (USA). *U.S. Pat. Appl. Publ.* 5 pp. CAN 137:297032, 2002
- [14] KUNIKATA, KENJI, SATO, EIJI, KUBO, HIROMICHI, IKEDA, KENJIRO (Nippon Kayaku Co., Ltd., Japan): *Jpn. Kokai Tokkyo Koho*, 8 pp. CAN:136:403890, 2002
- [15] KUBO, HIROMICHI, SATO, EISHI, SAKO, KENJI, IKEDA, KENJIRO (Nippon Kayaku Co., Ltd., Japan): *Jpn. Kokai Tokkyo Koho* 7 pp. CAN: 133: 45734, 2000
- [16] MINOGUCHI, SUSUMU, YOSHIKAWA, EIICHIRO, ITO, HIROJI, TANAKA, AKIHIKO, SATO, EISHI, IWASAKI, MAKOTO, KUBO, HIROMICHI (Nippon Kayaku Co., Ltd. Japan): Sensor Technology Inc, 5 pp, CAN:128:232458. *Jpn. Kokai Tokkyo Koho*, 1998
- [17] Astachov Alexander M, Gelmurzina, Irina V., Valiliev, Alexander D., Nefedov, Andrey A. Kruglyakova, Ludmila A., Stepanov, Rudolf S. (Siberian State Technology University, Krasnoyarsk, Russia): *32nd Energetic Materials, International Conf. of ICT*, Paper 139, 2001.
- [18] HUANG DER SHING (Gencorp Aerojw, USA): CAN:122: 265405, U. S. Patent 1995
- [19] PAUL W. COOPER, "Explosive Engineering", U.S. of America, 24 & 70; 1997
- [20] P. M. MADHUSUNAN, K. KRISHNAN AND K. N. NINAN: *Thermochim. Acta.*, **97**, 189; 1986

DETERMINATION OF LOW CONCENTRATION TRINITROTOLUENE CONTENT IN WATER SAMPLES

V. Ježová*, J. Skládal**, A. Eisner*, L. Gollová* and K. Ventura *

* Department of Analytical Chemistry, University of Pardubice,
53210, Pardubice, Czech Republic

** Research Institute of Industrial Chemistry, Explosia a.s.,
53217, Pardubice - Semtín, Czech Republic

Abstract

Polynitroaromatic organic explosives (2,4,6-trinitrotoluene) are typical labile and environmental that can transform with soil indigenous microorganisms, photodegrade by sunlight and migrate through subsurface soil to cause groundwater contamination. To be able to determine the type and concentration of explosives and their (bio)transformation products in different soil environments, a comprehensive analytical methodology of sample preparation, separation and detection is thus required. This present paper describes the use of solid-phase microextraction (SPME) and solid-phase extraction (SPE) for the extraction of nitroaromatic explosives for subsequent analysis by either GC/MS or HPLC/UV.

The two techniques are examined in terms of procedure, chromatographic analysis and method performance.

The adsorption temperature and adsorption times were examined by the using SPME fiber. SPE extraction was done by variable columns and microcolumns and was examined the columns with high efficiency and with short sorption time.

Keywords: *solid-phase microextraction (SPME), solid-phase extraction (SPE), explosives in water, nitroaromatic compounds*

1. INTRODUCTION

Over the past few decades site investigations of past and present military installations confirmed the presence of nitroaromatic explosives and their metabolites caused by extensive manufacturing, storage or even leakage from unexploded ordnance. Explosives are moderately to weakly soluble in water and thus can migrate through subsurface soil to cause groundwater contamination. In addition, unexploded ordinances left in the ocean following various military exercises are known to release a signature plume containing toxic levels (ng/l to µg/l range) of 2,4,6-trinitrotoluene (TNT) and 2,4-dinitrotoluene (DNT) ^[3]. High levels of TNT constitute a health hazard, as it is a suspected mutagen and was demonstrated to be toxicity to aquatic and terrestrial life. The biodegradation and photolytical by-products of TNT introduce highly reactive compounds often greater polarity and water solubility, which may constitute an even environmental concern than TNT itself. The US Environmental Protection Agency (EPA) has determined, for example, that TNT is toxic at levels above 2 µg/l ^[2].

The present study thus describes the use of different extraction techniques, including SPME and SPE to extract explosives and their degradation products from samples for subsequent analysis GC/MS and HPLC/UV.

1.1 Solid-phase extraction

Solid-phase extraction (SPE) ^[1] was developed from classical chromatography, which is historically marked from 1906. SPE was developed with sorbents for LC and as extraction technique is called from 1980s. In present, SPE has become routine.

The term "solid-phase" or "sorbent extraction", frequently abbreviated to "SPE", simply implies a physical extraction process involving a liquid and a solid phase. In practice, it is a sample preparation technique and has come to mean the use of commercial pre-packed columns containing stationary phases related to those used widely in high-performance liquid chromatography (HPLC), that may be adsorbents such as silica gel, reversed-phase materials or ion-exchange media. The packing material is held in a place within a plastic column by porous frits, also constructed of a plastic material, and the column ends in a Luer tip to facilitate connection to a vacuum manifold, to a needle or to a collection vessel.

Normal-phase sorbent consists of a stationary phase that is more polar than the solvent or sample matrix that is applied to the SPE sorbent. This means that water is not usually a solvent is normal phase SPE because is too polar. Also moderately polar to polar analytes are extracted from nonpolar solutions onto polar sorbents. The sorbents used for normal phase SPE is used Silica Gel (SiOH); Kieselguhr (SiO_n); Florisil® (Mg₂SiO₃) and Alumina (Al₂O₃).

The reversed phases are commonly used in SPE when aqua samples are involved. Nonpolar to moderately polar analytes are extracted from polar solutions onto nonpolar sorbents. The sorbents used for reversed phase SPE is use Octadecyl (C₁₈); Octyl (C₈); Cyclohexyl (C₆H₁₁); Phenyl (C₆H₅); Ethyl (C₂H₅); Cyano (CN); WP Butyl (C₄).

The objective of the analyst is ideally to isolate a component of interest from a more complex sample in a pure concentrated state. This might be achieved by choosing conditions so that the required analyte is retained on the column while the impurities pass straight through, or conversely by allowing the analyte to elute through while the impurities are retained.

Sorbent and solvent are optimized to effect a separation. In solid phase extraction these interactions are optimized to effect retention or elution. Solid phase extraction is performed in the following steps:

1. Column Conditioning

Condition column with 1-2 column volumes of methanol. Other water miscible solvents such as ethanol, isopropanol, or acetonitrile may be used.

Condition column with 1-2 column volumes of polar solvent similar to the sample solution (water, buffer, etc.). Keep sorbent bed wet during conditioning.

2. Sample Addition

If the analyte is to be retained by the sorbent, the sample solution should be a polar solvent in which the analyte has limited solubility.

If the analyte is to be passed through the column and nonpolar interferences remain, the sample solution should be a polar solution in which the polar analytes are very soluble.

3. Column Wash

Wash with polar solvent as required.

4. Sample Elution

Elute the retained analyte with two (2) or more void volumes of a nonpolar to moderately polar solvent. Basic analytes strongly retained by unbonded silanols can be eluted with solvents modified with an acid or an amine, such as diethylamine or triethylamine.

Explosives are extracted usually only on the reversed phase SPE columns. Typical solvent for conditioning SPE columns is methanol.

1.2 Solid-phase mikroextraction

Solid-phase mikroextraction (SPME) ^[5] is fast, simple, solventless method and it was developed by Pawliszyn and Belardi in 1992. It is based on extraction using a thin polymeric-coated fused-silica fiber, fitted in a special syringe-type holder for protection and sampling. When the fiber coated with stationary phase is exposed to an aqueous solution or to the headspace above it, organic compounds are extracted from their matrix to the stationary phase until equilibrium is achieved. One sampling is completed, the fiber is transferred to the heated injection port a GC system where the analytes are thermally desorbed. The whole extraction and transfer process usually takes only a few minutes, and can be easily automated. SPME was applied to the determination of a large variety of volatile and semi-volatile analytes in several types of environmental matrices ^[4]. SPME is an increasingly popular method for the extraction of organic analytes as it is rapid, solvent-free, easily automated and filed usable. But the SPME fiber is expensive and their lifetime is limited as they degrade with increased usage.

SPME fibers are a 1 or sometimes 2cm long fused silica fibre coated with a polymeric phase. The polymeric phases available are:

- polydimethylsiloxane (PDMS); polydimethylsiloxane/divinylbenzene (PDMS/DVB)
- polyacrylate (PA)
- carbowax/divinylbenzene (CW/DVB)
- polydimethylsiloxane/carboxen (PDMS/CAR)
- polydimethylsiloxane/divinylbenzene/carboxen1006 (PDMS/DVB/CAR)
- carbowax/Templated resin (CW/TPR)

The fibres are available in differing stationary phases film thickness from 7µm to 100 µm. The differing thickness will alter the amounts of analyses absorbed or adsorbed on to the surface of the polymeric phase.

The number of surface sites on a fibre where adsorption can take place is limited, when all these sites are filled no further adsorption can take place, unless the analyte can condense into the pores by capillary condensation mechanisms as in CAR fibres. Adsorption is a competitive process where an analyte with a higher affinity for the surface can displace one with a lower

affinity; this leads to the amount of an analyte being significantly affected by the type of surface matrix used in the fibre.

Each of the fibre coatings has different pore sizes that will attract differing sizes of molecules. To choose a fibre for a particular application the types of volatiles to be extracted must be known, 'Like prefers like', careful consideration to the sample matrix of the fibre used must be given as the amount of analyte extracted by the different fibres could affect the results.

SPME fibres can be used for both direct (two-phase system) or Head space (three-phase system).

2. EXPERIMENTAL

2.1 SPE procedure

SPE procedure was tested on different types of columns - STRATA C₁₈ (Phenomenex) 3 ml, SEPARONTM SGX C₁₈ (Tessek) 1 ml, DISCOVERY SUPELCO - 18 and DISCOVERY SUPELCO - 18LT (Supelco) both 6 ml. The packing materials were chosen specially because they are reversed phase, which are used for analyses of explosives.

The condition of SPE columns was made with 10 ml of methanol and then with 10 ml of distilled water. It was extracted 500 ml water standard with concentration of TNT 0,72 µg/ml. This volume was applied to all kinds of columns and the column with the best efficiency was searched. The extraction time was between 1 and 7 hours. (The extraction time depended on the used SPE column). The 4th step of SPE extraction was not done. The elution of analytes was made with 5 ml or 10 ml of methanol. The extracted samples were analysed with using the HPLC/UV system.

2.2 SPME procedure

It was used a manual 65 µm polydimethylsiloxane-divinylbenzene (PDMS-DVB) fiber and a SPME fiber holder assembly all purchased from Supelco, Sigma-Aldrich. It was prepared solution with concentration 10 µg/ml TNT in 500 ml distilled water. It was chosen the direct immersion sampling of the salt and aqueous sample solution. 4 ml of the solution were placed to 5 ml glass vial. Magnetic stirring was used at all temperatures and times. It was not used any internal standard.

The SPME fiber holder assembly was then clamped at a fixed location above the glass vial containing the stirred spiked sample solution. The SPME fiber was exposed to the salt and aqueous sample solution and after 15 min the fiber was retracted and transformed to the heated injection port of the GC/MS system for 5 min. Time and temperature aqueous sample solution were optimized to efficiency. The temperature was optimized from 30-70 °C and the sorption time was optimized from 10 to 40 min.

2.3 HPLC/UV method

Hewlett-Packard series HP 1050 system with diode array detection was used to separate the extracted compounds by SPE and integrate the resolved peaks. For the determination of TNT was used high performance liquid chromatography coupled to UV spectrometry. Separation was made on SEPARON SGX C18 column. TNT was eluted with an isocratic mobile phase of acetonitrile : methanol : water (35,5:29:35,5 v/v/v) and for detection was used wavelength 230 nm (Fig. 1).

The quantitative analysis was made by external standard of TNT. The concentration of calibration standards was 4 µg/ml; 8 µg/ml; 16 µg/ml; 80 µg/ml and 200 µg/ml.

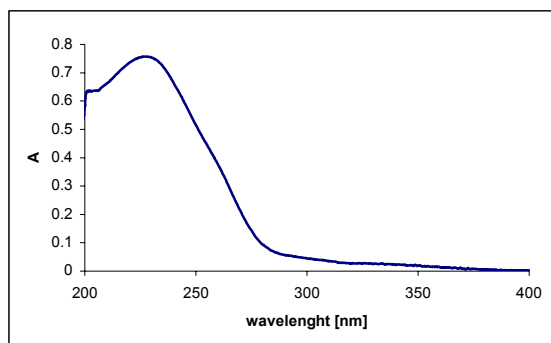


Fig 1. UV spectrum of TNT

2.4 GC/MS method

A Shimadzu GC-17A, Version 3, QP-5050A GC/MS system (Shimadzu, Japan) equipped with a 30 m x 5 µm HP-5MS capillary column (Hewlett-Packard, USA) was used for analyses extracted compounds with SPME. A low-volume inlet liner, special for SPME, was used (Supelco). The system operated using helium as a carrier gas at a flow-rate 0,6 ml/min. The injection temperature was 260 °C, the column temperature was 200 °C and the interface temperature was 230 °C. Split ratio 1:100 was used.

The MS ionization mode was electron ionization (70 eV) and the data were acquired in the SIM (m/z: 63, 89, 210).

3. RESULTS AND DISCUSSION

3.1 SPE procedure with HPLC/UV analysis

First of all the best SPE column was found for analyses water samples. The best column had to have short extraction time and high efficiency of extraction.

The best column was DISCOVERY SUPELCO - 18 (6 ml, Supelco). Columns characteristic are shown in the table 1.

The analytes were eluted on the column DISCOVERY SUPELCO - 18 (6 ml) with 5 ml or 10 ml of methanol. The elution with 5 ml of methanol had the efficiency of extraction about 89,60 % and the elution with 10 ml of methanol had the efficiency of extraction about 93,75 %. Also the elution with 10 ml of methanol was better than 5 ml (from views of efficiency).

Table 1. *The comparison of different SPE columns used by extraction samples with concentration 0,72 µg/ml and sample volume 500 ml.*

Column	Sorbent	Sorbent quantity [mg]	Column volume [ml]	Extraction time [hours]	Extraction efficiency [%]
STRATA C ₁₈	C ₁₈	100	3	4	37,30
SEPARON SGX C ₁₈	C ₁₈	520	1	6,5	63,60
DISCOVERY SUPELCO - 18	C ₁₈	1000	6	2	93,75
DISCOVERY SUPELCO - 18 LT	C ₁₈	1000	6	2	69,40

3.2 SPME procedure with GC/MS analysis

SPME extraction was made with 65 µm polydimethylsiloxane-divinylbenzene (PDMS-DVB), it was used the stirring during the whole sorption time. Sorption time and temperature were optimized. It was found the best temperature between 45-50 °C (Fig. 2).

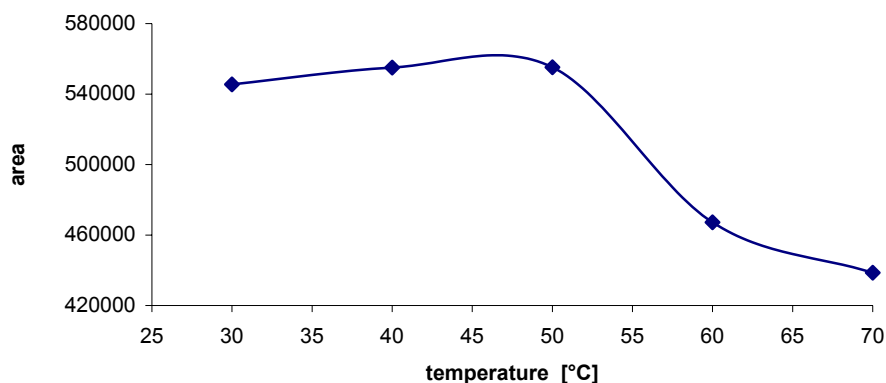


Fig. 2 Temperature effect for extraction recovery

The temperature for the sorption was chosen 50 °C and the sorption time was optimized between 10 to 40 min. The highest efficiency was discovered with 35 min (Fig. 3).

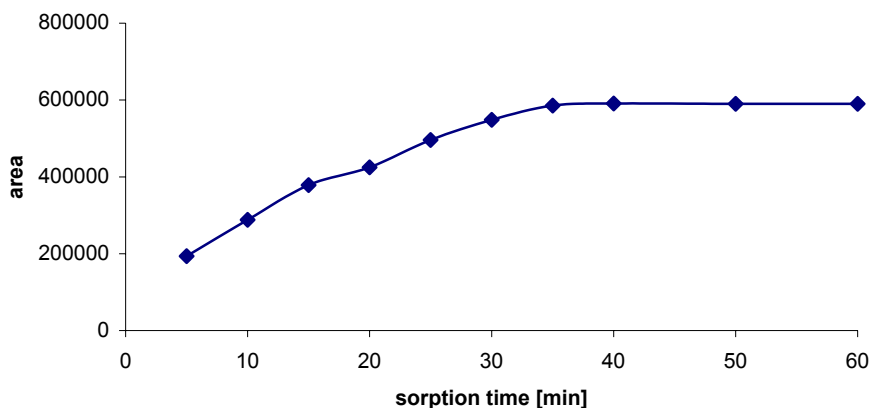


Fig. 3 Sorption time for extraction recovery

4. CONCLUSION

Several SPE columns were tested in this study. The SPE column DISCOVERY SUPELCO - 18 had the highest efficiency. The extracts were analysed with HPLC/UV.

The water sample was measured with SPME (polydimethylsiloxane-divinylbenzene). The best conditions for analyses of low concentration trinitrotoluene from water samples were found temperature 50°C and sorption time 35 min.

Acknowledgement

Experiments were performed thanks to financial support from the Ministry of Education, Youth and Sports of the Czech Republic (Project MSM 253100002), from the Grant Agency of the Czech Republic (Project 203/02/0023).

REFERENCES

- [1] E. M. THURMAN, M. S. MILLS: *Solid-Phase Extraction, Principles and Practice*, Wiley, New York 1998
- [2] Environmental Protection Agency, Health Advisory for TNT, Criteria and Standard Division, Office of Drinking Water, 1989
- [3] M. SMITH, G. E. COLLINS, J. WANG, J.: *of Chromatogr. A* 991 159 (2003)
- [4] E. PSILLIKAKIS, N. KALOGERAKIS J.: *of Chromatogr. A* 938 113 (2001)
- [5] <https://www.science.uwaterloo.ca/chemistry/pawliszyn>, download 5.2. 2004

SENSITIVITIES AND PERFORMANCES OF NON-REGULAR EXPLOSIVES

M.H. Lefebvre, B. Falmagne and B. Smedts

Laboratory of Energetic Materials, Royal Military Academy, Brussels – Belgium

Abstract:

Some chemical characteristics, safety properties and explosive performances of two explosives are investigated, namely tri-aceton-tri-peroxide (TATP) and hexa-methyl-triperoxyde-diamine (HMTD). Production is relatively easy to perform with quite easily available materials, but the purity, the quality and the properties of the explosive crystals are quite dependent on the synthesis process. Pure and unpurified compounds are tested for both their sensitivities and performances. The sensitivity to friction and to impact is determined and compared with values of other energetic materials.

The performances of small explosive charges (up to a few grams) are evaluated: brisance and initiation capability. The detonability and brisance of the compounds are observed and characterized using standard aluminum witness plates. The study shows that TATP can be used efficiently – at own and great risk of the technician – as secondary as well as primary explosive, accounting for a good versatility of the compound.

This work shows the great risks associated with these two peroxides but also why some of their characteristics make these explosives popular among certain groups.

Keywords: TATP, HMTD, explosive sensitivity, brisance, performance

1. INTRODUCTION

Recently, it became quite popular to use various chemical formulations to produce “irregular” explosives, i.e. non-commercial and non-military explosives. People performing such manufacturing are driven by a variety of reasons ranging from carefree attitude to juvenile delinquency and international terrorism. Many recipes do exist on publicly available sources like commercial literature or internet. It is well known from experts that these sources are often unreliable and one must act with great care when using data from such uncontrolled sources.

Two peroxides are investigated for their explosive characteristics: the triacetone-triperoxide (TATP) and the hexamethyl-triperoxide-diamine (HMTD). The structures of these compounds are given in Fig. 1. These explosive compounds are allegedly ‘home made’ by several groups and/or international organisations.

First, we shall shortly describe the synthesis and the chemical analysis of these compounds. They are relatively easy to perform with quite readily available material.

Secondly, impact and friction sensitivities and performances of these compounds are determined. The evaluated performances are brisance and initiation capability on TNT.

2. SYNTHESIS

2.1 HMTD

The HMTD synthesis is performed by reaction of hydrogen peroxide and hexamethylene-tetramine (HMTA) in acetic acid solution. After the addition, done at low temperature (Fig. 2), the solution crystallises. After filtration and acid neutralisation, final wash with solvent is performed. The crystals are placed in a desiccator. This synthesis provides pure HMTD in good yields and is reproducible.

2.2 TATP

The TATP synthesis is performed by the action of an acid on a mixture of acetone and hydrogen peroxide at low temperature (Fig. 3). After the addition, the solution is covered by a parafilm and crystallises. After filtration and acid neutralisation, the formed TATP dried in a desiccator.

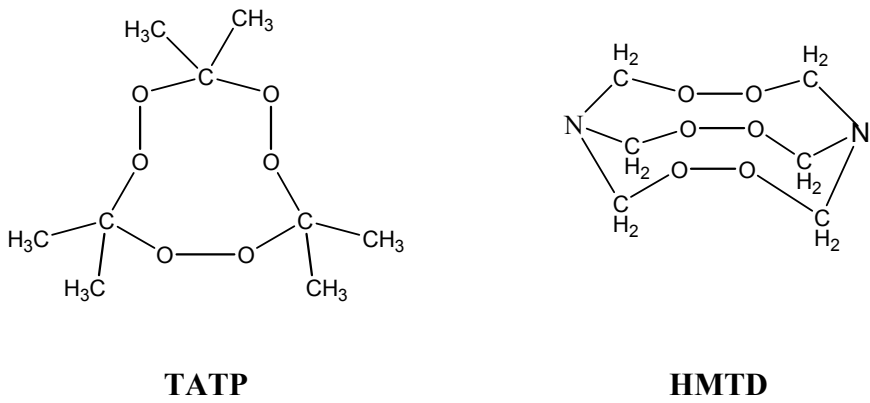


Fig 1. Chemical structures of HMTD and TATP

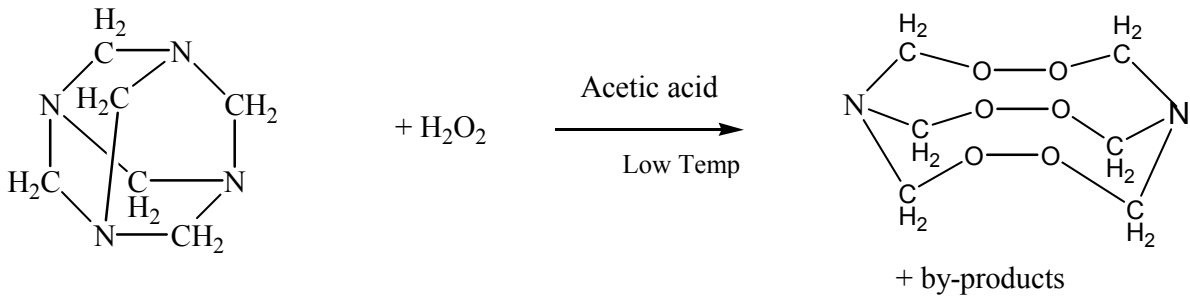


Fig 2. HMTD formation reaction

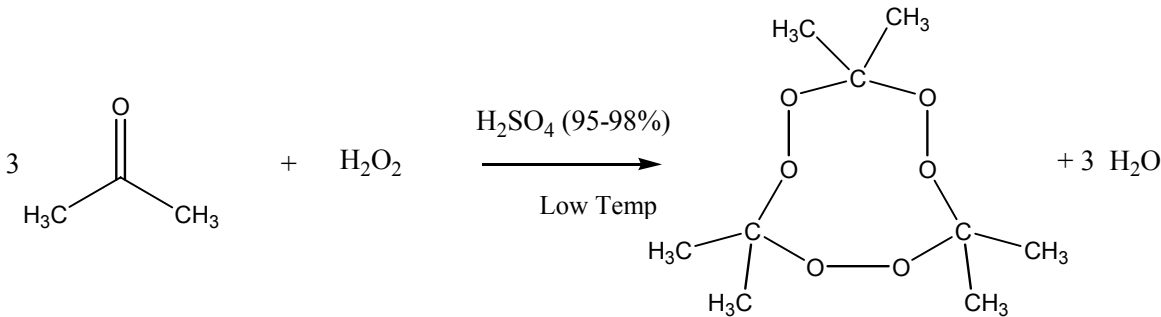


Fig 3. Reaction of TATP formation

Different acid solutions were tried: HCl, H₂SO₄, acetic acid, citric acid. With organic acids no proper crystallisation could be achieved and the TATP could not be extracted with any solvent. When HCl is used, the produced TATP is not stable and decomposes quickly.

The synthesis provides TATP with various levels of quality in variable yields and is no reproducible. When the operating conditions are optimised, 5 ml of acetone and 5 ml of hydrogen peroxide provides 2 g of TATP. The control of the temperature is important to obtain good quality and yields: when the temperature is too high, the reaction is too vigorous; when the temperature is too low, the synthesised product is not TATP. Note that the presence of by-products is important for the sensitivities and the performances of the formed peroxides.

3. CHARACTERISATION

The thermal and chemical characterisations are performed by differential scanning calorimeter (DSC) and by infrared spectroscopy (FTIR). These techniques enable us to assess the purity of the product.

3.1 HMTD

The DSC analysis is performed between 50 and 400 °C at 20°C/min. The thermogram shows no fusion peak and a characteristic exothermic peak at about 170°C. A typical DSC curve is given in Fig 4.

The IR-scans are performed directly on crystals between 650 and 4000 cm⁻¹. A typical spectrum is given in Fig 5.

3.2 TATP

Different DSC-curves are obtained dependent on the different synthesis processes. Pure (good quality) TATP shows an endothermic peak around 80°C and an exothermic reaction at about 120 °C (Fig. 6). The characteristic DSC curve is largely dependent on the purity of the manufactured explosive and therefore on the manufacturing process. TATP samples show endothermic peak ranging from 80 to 140°C and exothermic peak ranging from 120 to 240°C.

Similar discrepancies depending on the purity of the peroxide are also noticeable on the FTIR spectrums.

Typical DSC result and FTIR spectrum are given in Figs. 6 and 7, respectively.

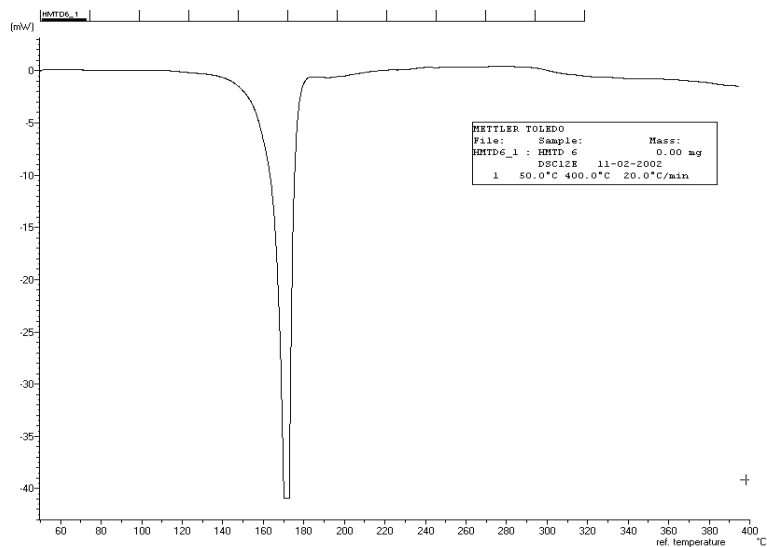


Fig 4. HMTD DSC-curve

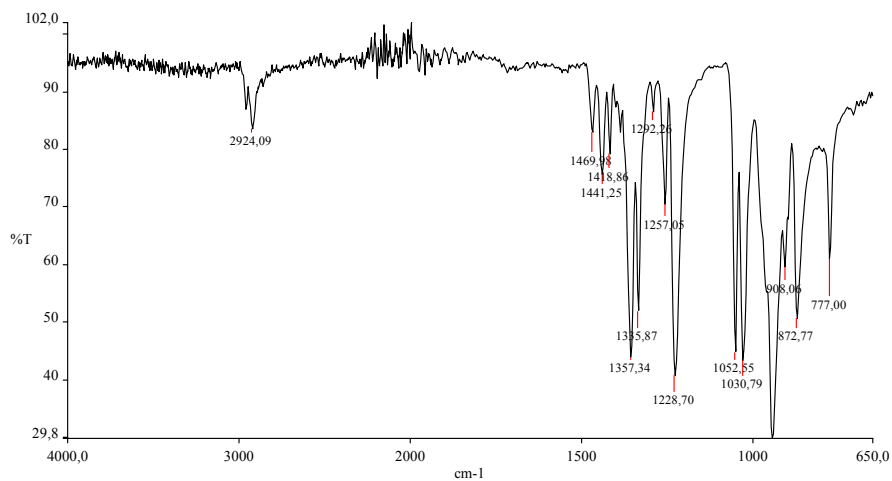


Fig 5. HMTD FTIR spectrum

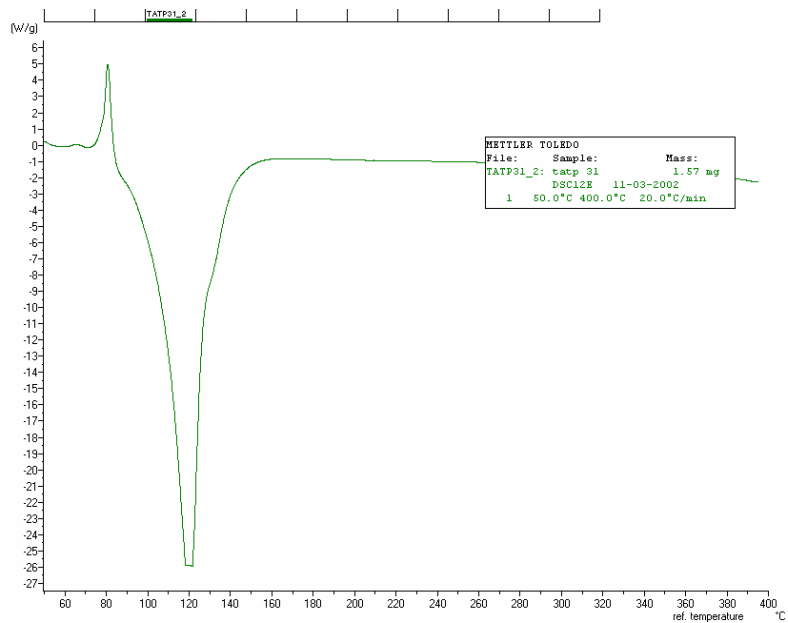


Fig 6. TATPDSC-curve

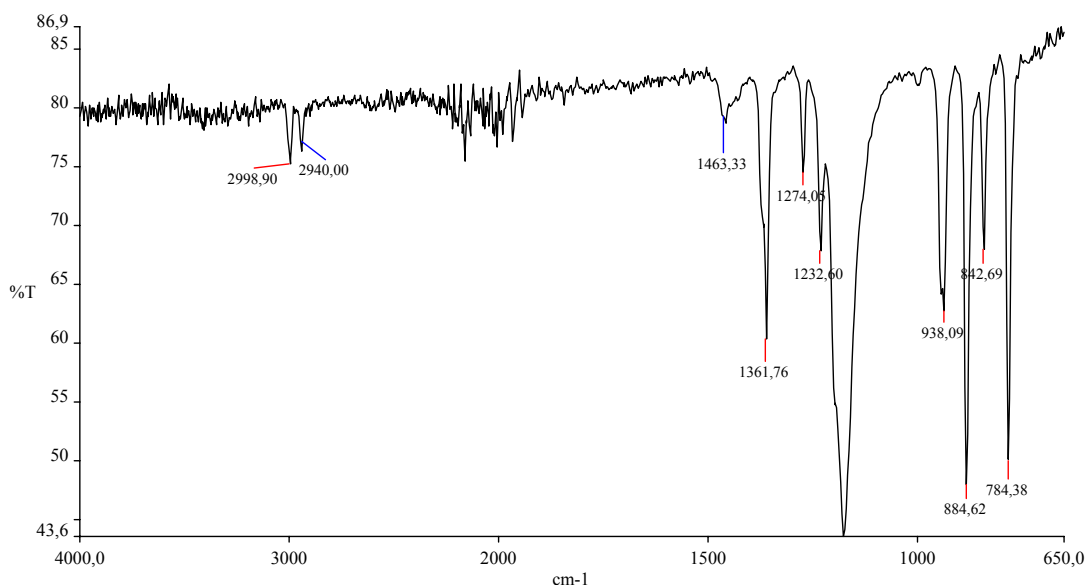


Fig 7. TATP FTIR spectrum

4. SENSITIVITY

4.1 Friction sensitivity

The friction test is performed with a standard friction BAM apparatus, according to the usual standard procedures. The load on the pistil may vary between 0.5 kgf and 36 kgf. The test is performed until 6 negative results occur. The latter is considered positive when reaction occurs, i.e. colour changing, smell or smoke formation, crackle or explosion.

The test is performed with HMTD, TATP, RDX, TNT and PETN, for comparison purpose. Moreover, results from this work are compared in Table 1 with results from the literature.

HMTD and TATP are so sensitive that they react even without weight applied. These two explosives are below the detection limit of our experimental set-up. In the case of TATP, the friction sensitivity is obviously related to the purity of the explosive. A low-grade sample is not as sensitive as a pure one.

Table 1. *Results from friction sensitivity test. The experimental values obtained during this investigation are compared with values from the literature.*

	(kgf)	HMTD	TATP	PbN ₆	TNT	RDX	PETN
Reference							
[1]		0.01	0.01	0.01	No react up to 36	12	6
[2]					29.5	11.5	4.5
This work		< 0.5	< 0.5		> 36	11.2	4.2

4.2 Impact sensitivity

The sensitivity to impact is tested with the BAM fallhammer apparatus. By decreasing the high of falling till 6 negative results are observed, one determines the lowest impact energy for initiation of the tested explosive.

The test is performed with HMTD, TATP, RDX and PETN and results are compared with literature references (Table 2). Both HMTD and TATP are within the limit of the test apparatus.

Table 2. *Results from impact sensitivity tests (in kgm). The experimental values obtained during this investigation are compared with values from the literature and of other typical explosives*

	(kgm)	HMTD	TATP	PbN ₆	TNT	RDX	PETN
Reference							
[1]		0.06	0.03	0.75	1.5	0.75	0.3
[2]					1.8-1.9	0.45	0.31
This work		0.015	0.03			0.65	0.21

5. PERFORMANCES

The performances are evaluated for 2 aspects: (1) the brisance and (2) the capability to initiate an high explosive charge. The two tests are performed with similar experimental set-up (Fig. 8). A stainless steel confinement (cylinder) of 10 mm inner diameter and 35 mm high is placed on an aluminium witness plate. The assembly is kept in place with insulating foam. The tested explosive composition is pressed in the steel confinement to a given density. This test set-up is analogue to the one described in the standard prEN 13763-15 (Determination of equivalent initiating capability of detonators).

5.1 Brisance

When the brisance is tested, the TATP is initiated with a #8 detonator and the thickness of the witness plate is 30 mm. The brisance is evaluated by measuring the depth of the dent made in the aluminium witness plate and by visual investigation of the fragmentation of the confining steel cylinder. The assembly is shown on Fig. 8(a).

The brisance is a function of the density of the explosive sample. The correlation between the brisance and the density is usually linear and an increasing density means usually an increasing brisance. In some specific cases high density does not imply high brisance. The brisance of HMTD has not been evaluated because of its extreme sensitivity, which didn’t enable us to press it safely. For TATP, the test has been performed at a density equal to 1.26. The same test is performed with TNT and RDX to compare the performance of TATP with well-known high explosives (Table 3).

These results indicate that TATP is definitely a high explosive, but somehow less powerful than TNT. Tests with TATP at density lower than 1.26 have not been carried out. But according to the results mentioned in the next paragraph, one may speculate and expect that the brisance at low density could be higher, even higher than the one of TNT.

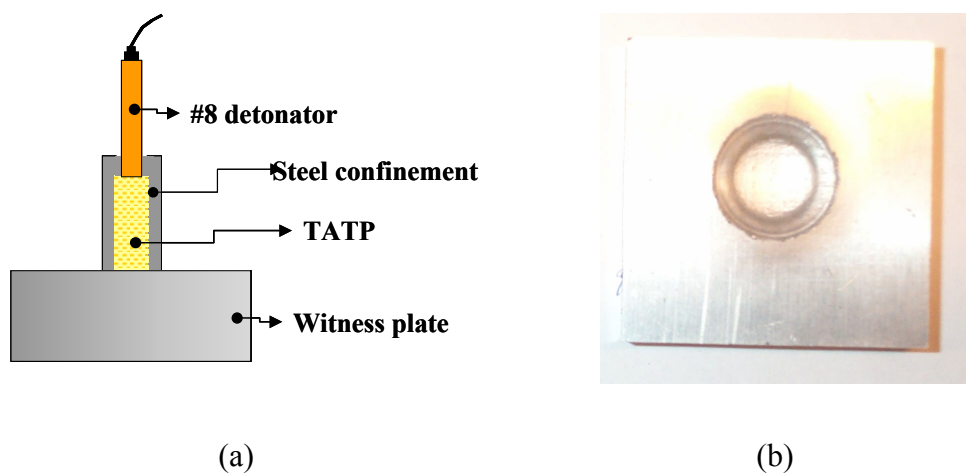


Fig 8. (a) Assembly for testing the brisance of TATP
 (b) Example of imprint in the witness plate
 (test with TATP at 1.26 density)

Table 3. *Qualitative comparison of the brisance (dent depth in witness plate) of TATP with values obtained with other explosives*
Each explosive charge has been initiated with a #8 detonator

Explosive (X)	TNT		RDX	HMTD	TATP
Manufacturing pressure (bar)	1440	50		Spontaneous explosion during sample preparation	720
Mass of explosive charge (g)	3.25	2.7			2.27
Diameter of expl. charge (mm)	10	10	7		10
Density of explosive	1.55	1.3	1.4		1.26
Dent depth (mm)	6.84	5.43	5.9	Not tested	3.65

5.2 Initiation capability

In a first experimental setting, a TATP charge is initiated by a fusehead. The full detonation and the initiation capability of the charge are evaluated by measuring the dent depth in the aluminium witness plate and by comparing it with the imprint of regular detonators (Fig 9a). This experimental procedure is quite similar to the one described in the CEN prEN 13763-15 for the determination of the initiation capability of detonators. The thickness of the witness plate is equal to 10 mm. Figure 9(a) shows a schematic of the assembly and Table 4 gives the experimental conditions and the test results. The initiation capability of TATP is surprisingly inversely proportional to its density. Figure 10 gives the dent depth as function of the TATP density.

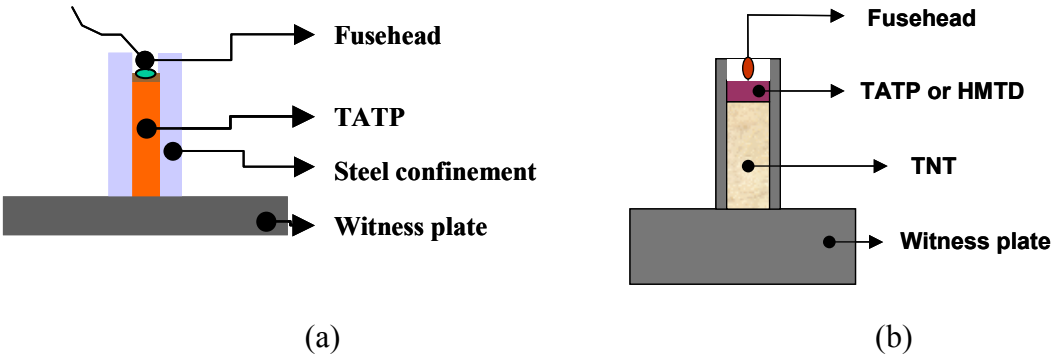


Fig 9. Assembly for testing the initiating capability:
(a) set-up similar to the CEN standard prEN 13763-15 for detonators
(b) set-up for testing direct initiation of a small TNT charge by a TATP or HMTD pellet

Table 4. *Initiating capability of TATP (dent depth in witness plate) at different initial densities*
The TATP charge is initiated by a fusehead

Density	Mass (g)	Diameter (mm)	Manufacturing pressure (bar)	Effect	Dent depth (mm)
0.86	1.14	7.62	Manually	Detonation	2.5
1.03	1.54	7.65	303.5	Detonation	2.03
1.18	1.35	7.7	~425	Low order detonation	0.26
1.18	1.69	7.65	607	Low order detonation	0.3
1.25	2.29	10.20	720	Deflagration (burn)	
Standard #8 detonator					1.96

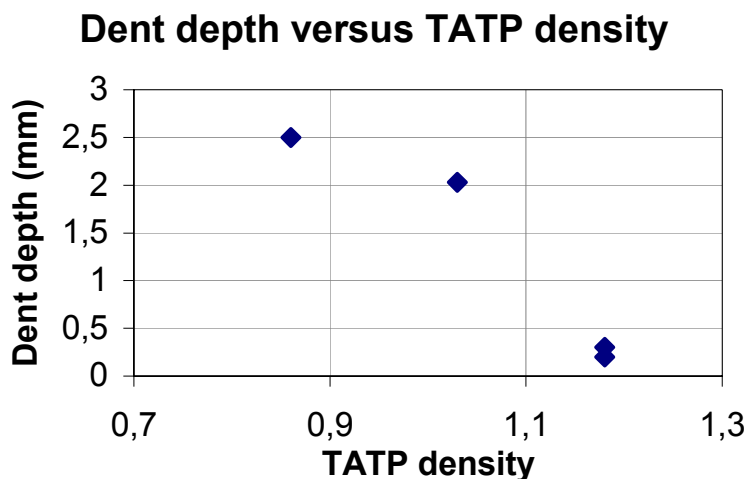


Fig 10. Dent depth versus TATP density

A second experimental set-up consists in directly initiating a secondary TNT charge with a small compressed pellet of TATP or HMTD and witnessing the full detonation of TNT on the Al-witness plate (Fig. 9b). The HMTD or TATP initiating charge is ignited with a fusehead, like in any standard electric detonator. 270 mg of HMTD compressed at +/- 70 bars make TNT easily detonating. The obtained dent is 6.085 mm depth (Table 5), which corresponds to a fully detonated TNT charge. The TATP pellet must be somehow larger to achieve full detonation of the TNT. Moreover, the experiments show the same tendency than that observed in previous experiments: the initiation capability of TATP is inversely proportional to its density.

These tests show the very good initiation capability of both HMTD and TATP.

Table 5. *Witness of the full detonation of the TNT secondary charges, initiated by TATP or HMTD*
The TATP / HMTD primary charge is ignited by a fusehead

Primary Initiating Charge	Secondary charge (TNT) and effect on witness plate					
TATP/HMTD	density (g/cm ³)	mass (g)	Diameter (mm)	Length (mm)	Effect	Dent depth (mm)
0.880 g TATP	1.55	4.39	10	43.08	TNT detonates	7.1
0.270 g HMTD	1.55	3.3	10	26.95	TNT detonates	6.085

6. CONCLUSION

The risks associated with these two peroxides are demonstrated. HMTD and TATP are both very sensitive, but HMTD seems much more dangerous than TATP when handled and manipulated. Both explosive compounds can be used successfully as primary initiating charges.

The synthesis of these compounds is reasonably easy. For TATP, the efficient synthesis is more complicated due to the temperature influence on the quality of the produced explosive. It is important to note that even when the synthesis is not optimised, the formed explosive product remains useable but with diverse sensitivity and performances.

The brisance of HMTD could not be evaluated due to its high sensitivity. TATP exhibits a brisance ranging approximately from 60% to 100% of the one of TNT.

The risks associated with these two compounds require specific safety precautions to work with and their use is not recommended.

REFERENCES

- [1] R. MEYER: Explosives, *Weinheim-Chemie*, 1977
- [2] T. URBANSKI: Chemistry and technology of explosives, *Pergamon Press*, 1984

RESEARCH ON THE INFLUENCE OF AMMONIUM NITRATE PRILL PROPERTIES ON DETONATION PARAMETERS OF ANFO AND THEIR MIXTURES WITH DOUBLE BASE PROPELLANTS

K. Lipińska*, M. Lipiński*, A. Maranda** and J. Sobala***

* Institute of Industrial Organic Chemistry, 6 Annopol St., 03-236 Warszawa, Poland

** Military University of Technology, 2 Kaliskiego St., 00-908 Warszawa, Poland

*** Central Mining Institute, 1 Gwarków Sq., Katowice, Poland

Abstract:

Properties of ammonium nitrate prills determine the physical stability and detonation characteristics of ANFO. Some physical characteristics of ammonium nitrate prills (apparent density, specific surface area and structure examinations by scanning electron microscopy) were determined. We investigated the influence of commercial ammonium nitrate prill properties on detonation velocities of some explosives. They included commercial ANFO explosives and their mixtures with demilitarized double base propellants of different nitroglycerine content. Results suggest that double base rocket propellants can increase detonation parameters of mining explosives.

Keywords: waste energetic materials, ANFO, demilitarized double base propellant, ammonium nitrate prills

1. INTRODUCTION

Ammonium nitrate (AN), which is intended for use as an oxidizer in explosives, is manufactured in the form of porous prills. The prills can absorb liquid carbonaceous fuel to produce ANFO (ammonium nitrate and fuel oil). ANFO is one of the most popular industrial explosives because it is safe and easy to handle. It is also relatively inexpensive. Properties of AN prills determine the physical stability and detonation parameters of ANFO ^[1,2]. The low-density ANFO has the improved detonation characteristics, such as detonation velocity, in comparison with the conventional one.

In our study we attempted to show some correlation between the physical properties of porous prilled AN and the detonation characteristics of ANFO and their mixtures with demilitarized double base propellants. Waste rocket propellants are a growing disposal problem. Demilitarized double base propellants may be economically and efficiently utilized in industrial explosives ^[3-5]. ANFO is one of the industrial explosives, which is suitable for double base propellant incorporation. Our research is to support the development of methods of double base propellant disposal.

2. EXPERIMENTAL

2.1 Materials

2.1.1. Commercial ammonium nitrate prills and ANFO

Two different kinds of commercial ammonium nitrate prills were chosen. They were both products targeted for use as an oxidizer in explosives. They were commercial prills with additives, but the type and the amount of the additives were not known. The first sample, identified as AN 1 is a conventional porous prilled AN type. The second one, AN 2, is a low-density porous AN.

Two types of commercial ANFO were used in this study. The first one, designated as ANFO 1, was made of AN 1. The second one, ANFO 2, was made of AN 2. Both AN prills and ANFO were received from Polish producers.

2.1.2. Double base propellants

We used two different kinds of double base propellants, identified as propellant A and propellant B. They were in the form of squares of 2×2 mm, having a thickness of 0,25 mm. The propellants differed primarily in nitroglycerine content. Propellant A contained 40 % of nitroglycerine. The nitroglycerine content in propellant B was only 26 %, but dinitrotoluene (9 %) was present. Propellant content in investigated mixtures was 20 and 40 %.

2.2 Measurements of ammonium nitrate properties

We determined some physical characteristics of prilled ammonium nitrate. They included bulk density, apparent density, specific surface, size distribution and oil absorption.

The bulk density refers to the density of prills including pores and inter-prills spaces. The apparent density means the mass of AN divided by its apparent volume (volume excluding open pores but including closed pores). The apparent density of AN was established by gas (helium) pycnometer. This provides a more accurate determination of void volumes than can be obtained via liquid displacement.

The determination of specific surface was based on a low-temperature gas adsorption process analysed with the algorithm introduced by Brunauer, Emmett and Teller (BET method).

The size distribution was determined by sorting the prills through sieves with various sizes. The prills were sifted in seven size ranges.

For oil absorption test only prills over diameter of 1 mm were used. Method of oil absorption test involved measuring the percentage of fuel oil that could only be absorbed into the AN prills.

The external and internal structure of AN prills was examined by scanning electron microscopy. The sample preparation was a standard procedure.

2.3 Velocity of detonation

The detonation velocity tests were conducted in steel pipes having an inside diameter of 36 mm, an outer diameter of 42 mm and a length of 210 mm. The explosives were loaded into pipes with moderate tamping. Detonation velocity was determined by the measurement of the time of detonation wave transition through three sections; each of them was 40 mm long. Every explosive was initiated by RDX/Al booster with a detonator. Measurements of time were done by short circuit sensor method.

3. RESULTS

3.1 Physical characteristics of ammonium nitrate prills

The bulk density, apparent density, specific surface area, prill size distribution and oil absorption test values of two different AN are summarized in Table 1. The size distribution test data are given in Table 2.

Table 1. Physical characteristics of AN prills

Type	Bulk density [g/cm ³]	Apparent density [g/cm ³]	Density ratio	Surface area [m ² /g]	Oil absorption [%]
AN 1	0,82	1,61	0,5	0,01	4,0
AN 2	0,69	1,70	0,4	0,08	10,5

Table 2. Size distribution of AN prills

Type	mass with prill diameter [%]						
	>2,50	2,00-2,50	1,60-2,00	1,25-1,60	1,00-1,25	0,80-1,00	<0,80
AN 1	2,7	15,1	81,5	0,2		0,5	
AN 2	1,1	7,3	75,8	8,6	4,9	1,4	0,9

When a solid material is in granular or powdered form, the bulk contains three types of void: open pores, cavities with no access to an external surface and interparticle space. The total volume of interparticle voids depends on the size and shape of the individual particles and how well the particles are packed. There is a significant difference in bulk density and apparent density of AN 1 and AN 2. Although AN 1 bulk density is higher, its apparent density is lower. That means that there are more closed pores in AN 1. The volume of closed cavities in the case of AN 2 is small, as the density of ammonium nitrate is 1,73 g/cm³.

The two types of AN also differ in size distribution of prills that is wider in the case of AN 2. Neither of the AN samples proved to contain a significant amount of fine material. The type AN 1 have about 16 % of prills with smaller dimensions. Specific surface area for both AN types is rather small. The desorption process were done at low temperature (because of AN phase transitions) but the results of the test were repeatable. However, the results of specific surface area and oil absorption tests are in agreement with the size distribution of the AN samples. The development of specific surface of AN 2 influences the bigger value in oil absorption test.

3.2 Structure Examination by Scanning Electron Microscopy

The external and internal structure of AN prills was examined by scanning electron microscopy. Although we can only examine the sample surface with a small viewing area it is sufficient for evaluating the differences in prill structure. We investigated the external and internal surface of AN prills. As presented in Fig. 1 the external surface of AN prills is not smooth. The internal structure of the prills is more interesting. As depicted in Fig. 2 and 5 both AN prills have an internal central hollow, but AN 2 also have some smaller hollows around the central one. The internal structure of AN 2, as shown in Fig. 3 and 4, consists of interconnected grains. The internal structure of AN 1 is different [Fig. 6 and 7]. There are lots of small pores and the structure of AN resembles pumice-stone. These small pores have no connection with the external surface of the prills and that is why AN 1 prill has lower apparent density.

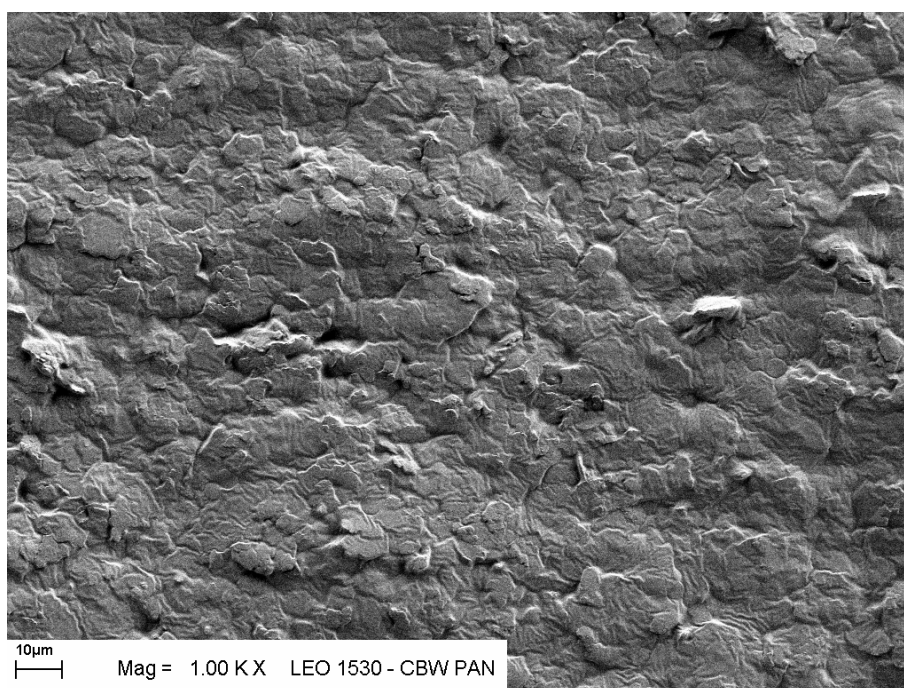


Fig 1. SEM micrograph on the external surface of AN 2 prill

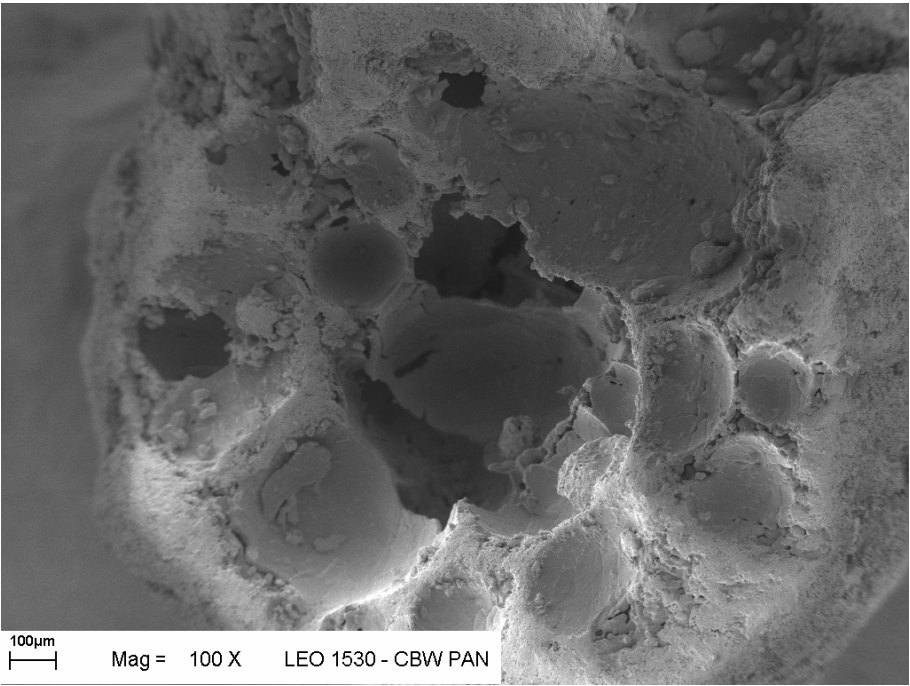


Fig 2. SEM micrograph on the cross-section of AN 2 prill

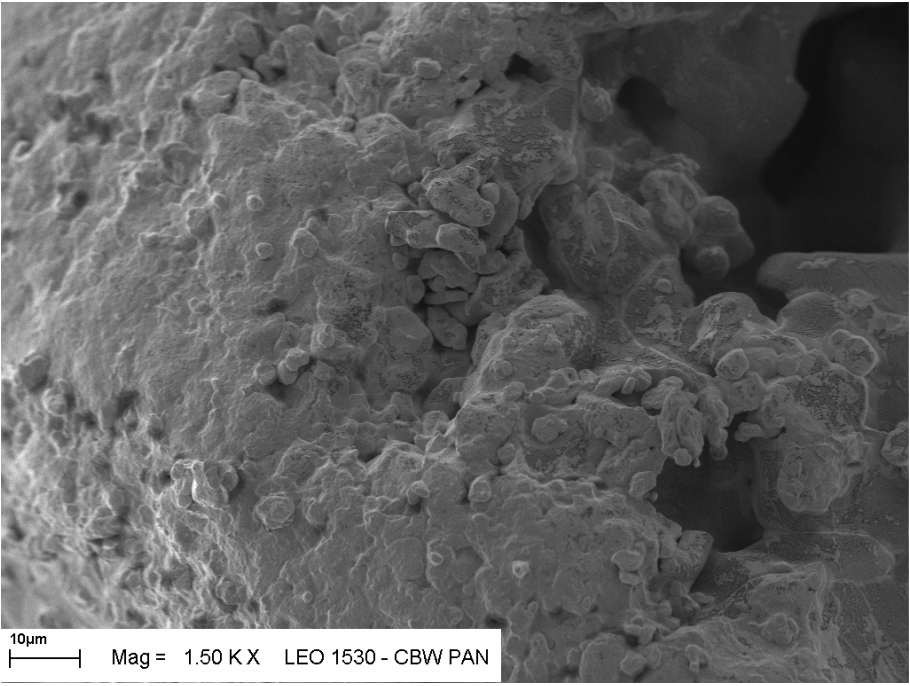


Fig 3. SEM micrograph on the internal surface of AN 2 prill

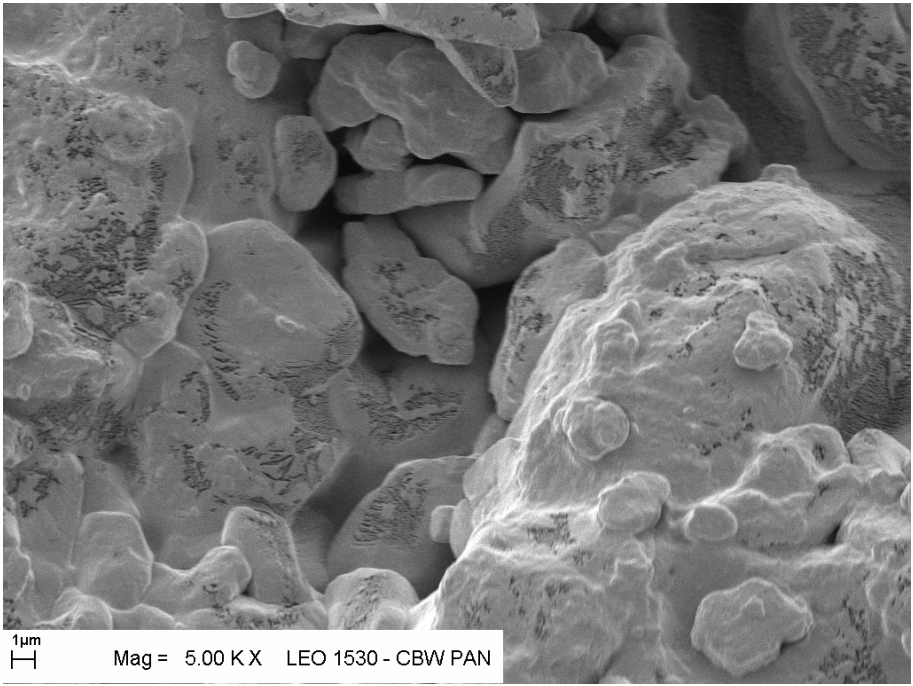


Fig 4. SEM micrograph on the internal surface of AN 2 prill

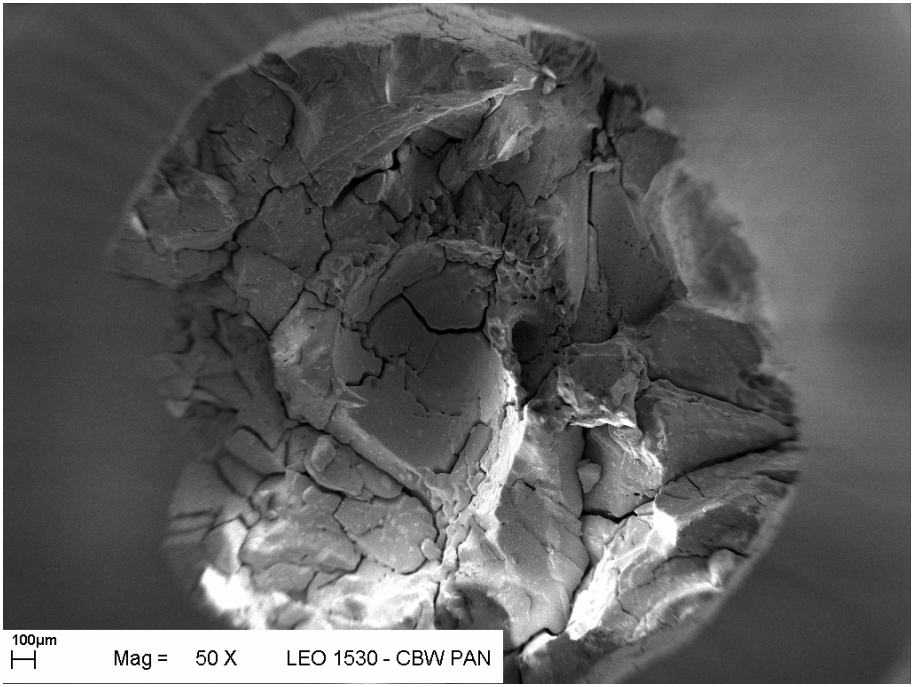


Fig 5. SEM micrograph on the cross-section of AN 1 prill

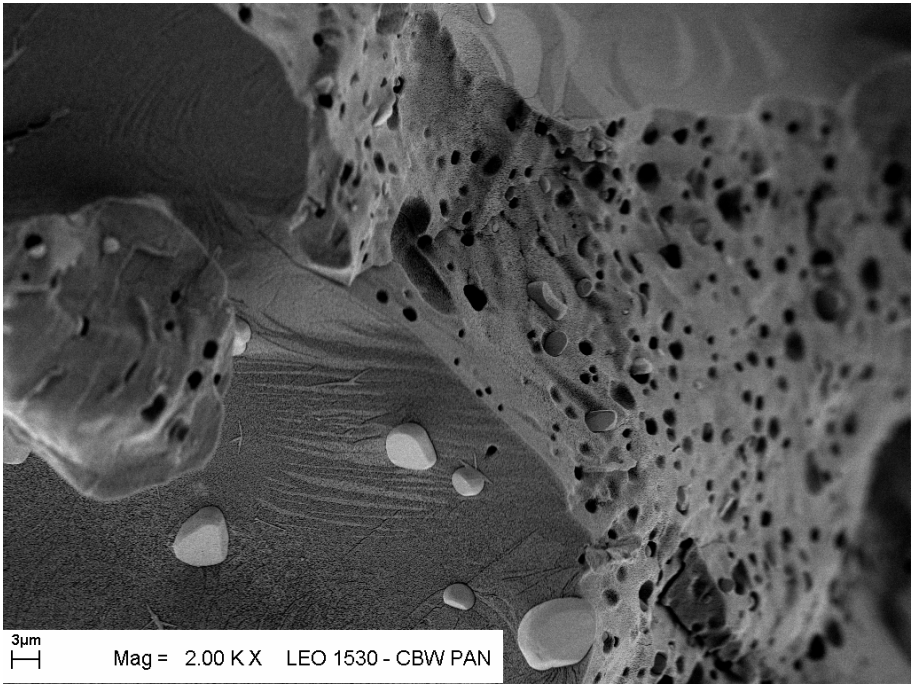


Fig 6. SEM micrograph on the internal surface of AN 1 prill

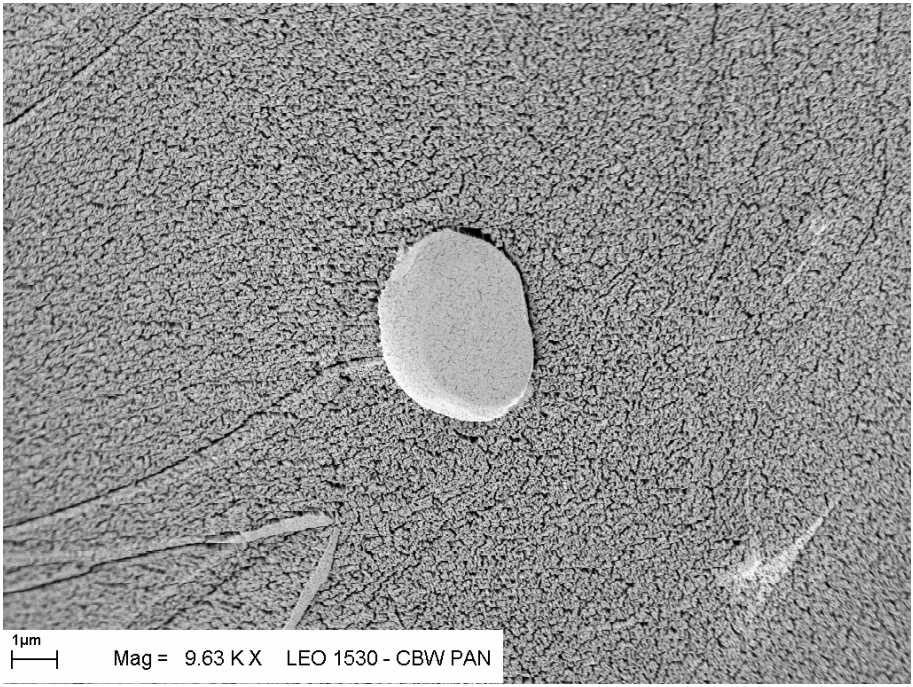


Fig 7. SEM micrograph on the internal surface of AN 1 prill

3.3 Velocity of detonation

Compositions of investigated mixtures and results of detonation velocity measurements are presented in Table 3 and 4.

Table 3. *Detonation velocities of ANFO and ANFO/double base propellant A*

Explosive	Tap density [kg/m ³]	VOD [m/s]
ANFO 1	972	2000
ANFO 2	761	2560
ANFO 1/ propellant 80/20	942	3050
ANFO 1/ propellant 60/40	848	3540
ANFO 2/ propellant 80/20	782	3280
ANFO 2/ propellant 60/40	775	3610

Table 4. *Detonation velocities of ANFO and ANFO/double base propellant B*

Explosive	Tap density [kg/m ³]	VOD [m/s]
ANFO 1	972	2000
ANFO 2	761	2560
ANFO 1/ propellant 80/20	975	1800
ANFO 1/ propellant 60/40	970	2140
ANFO 2/ propellant 80/20	781	2790
ANFO 2/ propellant 60/40	779	3120

The measured VOD values of the ANFO appeared to coincide with the densities of the explosives, with the lower density product producing higher detonation velocity. The results show that the addition of double base propellant A increases detonation velocities of both ANFO 1 and ANFO 2. The bigger is propellant content the higher detonation velocity of investigated explosives. That indicates detonation process in investigated mixtures propagates mainly between grains of propellant A. However the increase in detonation

velocities of ANFO 2 with 20 % of propellant A is not significant. Explosives with 40 % of double base propellant A have the most favorable detonation parameters. There is no clear detonation velocity increase in the case of double base propellant B. ANFO 1 with 20 % of propellant B detonates at lower velocity than ANFO 2.

4. CONCLUSIONS

This study confirmed that physical characteristics of AN prills influenced detonation parameters of ANFO and they mixtures with double base propellants. Double base rocket propellants can be used as ingredients of ANFO, increasing their detonation parameters. The increase of detonation velocity depended on the ANFO type. Two types of ANFO were investigated – conventional ANFO 1 and low-density ANFO 2. The most significant increase in detonation velocity we observed in the case of ANFO 1 with propellant A containing higher amount of nitroglycerine. That means that conventional ANFO can improve its detonation characteristics by the addition of propellant of high detonation velocity. Detonation parameters of ANFO were not significantly influenced by propellant B of lower detonation velocity and lower nitroglycerine content. The increase in detonation velocities was rather low.

REFERENCES

- [1] H. SUGIHARA, Y. SATO, A. INOUE: *Correlation between physical properties of PPAN and detonation characteristics of ANFO*, *Explosives and Blasting Technique*, Holmberg (ed.), Sweets&Zeitlinger, Lisse, p. 277-281, 2003
- [2] Q. KWOK, D. JONES, P. KRUUS: *Investigation of the wettability of ammonium nitrate prills*, Proc. of the VI Seminar New Trends In Research Of Energetic Materials, Pardubice, p. 183-195, 1997
- [3] E. F. OKHRIMENKO, N. G. IBRAGIMOV, E. KH. AFIATULLOV, L. S. LUKIN, YU. M. YUKOV, I. P. IVANOVA: *Use of Powders in National Economy*, (Conversion Concepts for Commercial Applications and Disposal Technologies of Energetic Systems, Kluwer Academic Publishers), Dordrecht, 1997
- [4] G. ECK, O. MACHACEK, K. TALLENT: *The Use of Surplus Smokeless Powder Propellants As Ingredients In Commercial Explosive Products in the United States*, (Application of Demilitarized Gun and Rocket Propellants in Commercial Explosives, Kluwer Academic Publishers), Dordrecht, 2000
- [5] K. LIPÍŃSKA, M. LIPÍŃSKI, A. MARANDA: *Influence of double base propellants on detonation velocity of mining blasting agents*, *Polish Journal of Applied Chemistry* XLVII 3, 221-225, 2003

BEYOND THE GROUP CONTRIBUTION APPROACH TO FLUID PROPERTIES: NEW MODELS FOR THE DENSITY AND THERMAL STABILITY OF ENERGETIC COMPOUNDS

D. Mathieu, J.-P. Becker and E. Theerlynck

Commissariat à l'Energie Atomique, Centre d'Etudes du Ripault, BP 16
37260 Monts, France

Abstract:

Many properties of molecular fluids may only be estimated using group contribution methods. Some of them lend themselves naturally to such an additive scheme (e.g. the density) while this is not the case for others (e.g. the thermal stability). Alternative models are presented to calculate the density and decomposition temperature of molecular liquids. For the density, the accuracy of the new scheme is similar to that of the most reliable available methods, despite a drastic reduction of the number of empirical parameters. For thermal stability, a simple kinetic model is shown to be a better basis to develop predictive tools than any group contribution schemes.

Keywords: *thermostability, density, molecular modelling,
group contribution methods*

1. INTRODUCTION

The group contribution approach is a very simple method to estimate the properties of molecular solids or liquids. In this scheme, the system under study is viewed as a mixture of chemical groups. It is especially suited for extensive properties X , that scale with the number of atoms in the system. In that case, X is simply expressed as the sum of contributions X_i associated with the various groups i . The result is exact if there is no interaction between the groups. For instance, the mass M of a compound is exactly the sum of the masses M_i of its atoms. In contrast, its molar volume V in a condensed phase is only approximately obtained as the sum of atomic volumes V_i . In practice, the contribution X_i to property X is often assumed to depend on the environment of atom i . Alternatively, i stands for a chemical group (such as nitro $-\text{NO}_2$, methylene $-\text{CH}_2-$, amine $-\text{NH}_2\ldots$) rather than for an atom. Furthermore, many extensive properties do not easily lend themselves to such an additive decomposition. For instance, satisfactory estimates of formation enthalpies $\Delta_f H^\circ$ may be derived using group contribution schemes provided a very large number of groups and *ad hoc* terms accounting for inter-groups interactions are introduced, thus restricting the scope of the method.^[1]

On the other hand, an intensive property x , such as the density ρ or the decomposition temperature T_{dec} , cannot be obtained as a sum of group contributions. In many cases, intensive properties may be derived from intensive ones, suitable for a group contribution approach. For instance, the density ρ is usually obtained as the ratio M/V where M is the mass of the system and V its volume, both derivable from additive group contributions. The surface tension γ of a liquid is related to the molar volume V and to the so-called parachor P through $\gamma = (P/V)^4$ (neglecting the density of the vapor wrt the density of the liquid). P turns

out to be an additive quantity. Thus, γ is often estimated from values of P and V obtained from group contribution models. However, such simple relationships between intensive and extensive properties are not always straightforward. For instance, transition temperatures (T_m for melting, T_g for glass transition or T_{dec} for decomposition) are not so simply related to additive properties. Such properties x are usually estimated as an average over group values x_i . The weighting scheme for this average is arbitrarily. In most cases, to estimate x , the extensive quantity $X=M.x$ is introduced. In other words, the contribution of chemical groups i are weighted according to the group masses M_i . Indeed, in that case, $x_i = X_i/M_i$ represents the value of x for group i . Curiously, this widely accepted approach has been used also to estimate liquid densities through the $M.\rho$ product, rather than from the molar volume.^[2]

This paper focusses on very simple models as alternatives to group contribution approaches. Two properties are addressed. The first is the density ρ , for which the use of group contributions (via the molar volume V) is quite natural. The second property investigated is the decomposition temperature T_{dec} for which the model based on a weighted average over group decomposition temperatures T_i , although quite reasonable, appears deficient.

2. NORMAL LIQUID DENSITIES

2.1 Motivation

Density is one of the condensed-phase properties for which group contribution approaches are most successful. For crystals, recent schemes taking advantage of the availability of extensive databases yield an average accuracy of 2%. For liquids, versatile models are less numerous. A popular one is the group contribution scheme commercialized by ACD.^[3] Typical errors, although maybe more significant than for crystals, are mostly within a few percents. However, this fair accuracy relies on a large number of adjustable parameters. The present scheme examines to what extent the use of 3D structures could afford a reduction of these parameters, or an extension of the scope of group contributions schemes.

2.2 The van der Waals model

While the molar volume V of solids and liquids scales linearly with the van der Waals volume V_w of the constitutive molecules, it is well-known that the simple expression $V=(1/k)V_w$ yields poor results. In an attempt to improve over this procedure, Piacenza et al. used overestimated van der Waals volumes (calculated using molecular atomic radii, larger than the standard van der Waals radii) and introduced an additional constant in the linear expression above, expressing the molar volume as $V= (1/k)V_w-b$.^[4]

In fact, a more natural approach consists in seeking to account for the variation of the inverse compacity $1/k$, instead of assuming a constant value. The most obvious reason for variations of $1/k$ among different compounds is hydrogen bonding, which brings about enhanced overlap between the van der Waals volumes of neighbouring molecules. Thus, hydrogen bonds contribute negatively to the reduced volume $1/k$.

On the other hand, considering van der Waals molecular models, empty space between molecules in condensed phases occur at the molecular surfaces. Therefore, it is natural to assume that for a given value of the van der Waals volume V_w , the empty volume between molecules increases which the van der Waals surface area A_w .

To account for the influence of these factors on molar volumes of liquids, the following expression for $1/k$ is introduced:

$$\frac{1}{k} = \frac{1}{V_w} \sum_i A_i l_i - g \sqrt{h} \quad (1)$$

where A_i is the contribution of atom i to A_w , l_i is the rate of change of the molar volume as A_i is varied, h is a parameter measuring the number of hydrogen bonds in the fluid and g is the rate of change of the molar volume with h . The adjustable parameters are l_i and g . Considering a liquid with small concentrations C_D and C_A of proton donors and acceptors, the concentration of hydrogen bonds would be $K_e.C_D.C_A$ where K_e is the equilibrium constant for hydrogen bond formation. In fact, the protons donors and acceptors are more or less available for hydrogen bonding. Therefore, $C_D.C_A$ is replaced with $h=A_D.A_A / A_w^2$ where A_D and A_A stand for the available surface area of proton donors and proton acceptors on the molecule.

Table 1. Values of the l_i parameters for common chemical elements, in Å.

H	C	N	O	F	S	Cl	Br
1.135	1.277	1.170	0.957	1.508	1.126	1.312	1.307

The l_i coefficients (lengths) are assumed to depend only on the atomic number of atom i . They were fitted against the normal densities of 138 compounds with no hydrogen bond. Their values are listed in Table 1. Then, g was fitted against the densities of 64 hydrogen-bonded liquids, using the l_i coefficients previously derived. A value of 2.918 was found.

2.3 Results

The present scheme was applied to 35 organic molecules not included in the calibration set. The average absolute error obtained is 3.4% versus 4.0% for the ACD additive scheme. For an additional dozen of heavy compounds (perhalogenated or heavily nitrated) both schemes exhibited average absolute error of 10%. In fact, the densities calculated using the present van der Waals approach and the ACD group contribution method are quite similar and fail in the same cases. More parameters are needed for the group contribution approach in order to account for the overlap of neighbouring atoms within chemical groups. This overlap is naturally taken into account by the van der Waals approach. Because of this dramatic reduction of the number of empirical parameters needed, the scope of the present scheme is enhanced. For instance, it may be applied to liquid azides that lie beyond the scope of the ACD parameterization. Predicted densities thus obtained are reported in Table 2. The average absolute deviation from experiment is 3.2%.

Table 1. *Experimental and calculated (using the present van der Waals model) normal liquid densities of azide compounds (g/cc).*

Compound	ρ_{calc}	ρ_{obs}
1-Azidohexane	0.962	0.979
1-Azidopentane	0.963	0.985
4-Azidotoluene	1.061	1.053
1,5-Diazidobutane	1.005	1.060
2-Azidotoluene	1.071	1.065
Azidomethylbenzene	1.059	1.066
1,4-Diazidobutane	1.033	1.079
Azidobenzene	1.094	1.086
2-Azidoethanol	1.176	1.149
1-2bis,2-Azidoethyl-diaziridine	1.072	1.170
Bis-1,3-Diazidoisopropyladipate	1.311	1.254
1,3-Diazidopropanol	1.293	1.260
1,2,4-Triazidobutane	1.164	1.266

3. DECOMPOSITION TEMPERATURES

3.4 Motivation

To date, no theory is available to predict decomposition temperatures T_{dec} . In fact, this quantity is not well-defined as it depends on details of the measurement technique. To estimate T_{dec} for polymers, a group contribution approach is available,^[5] which has been subsequently extended using topological indexes.^[6] For energetic materials, no such scheme is available. In fact, experimental values are lacking to develop such procedures.

In this context, a standard criterion for thermostability is the bond dissociation energy D_e for the weakest bond in the compound. For nitro compounds, this weakest bond is usually an explosophore X-NO₂ bond. For some compounds, this criterion works very well, as illustrated on Figure 1. This is all the more surprising as some of the materials reported on Figure 1 decompose in the solid state, while most of them decompose in the melt. In the latter case, the molecules in crystals do not have as many degrees of freedom as in the melt for reacting together. The procedure based on D_e values (calculated on isolated molecules) does not account for the additional constraints induced by solid-state decomposition. Therefore, in such cases, as for HMX, decomposition temperatures should be underestimated. Since T_{dec} is in fact overestimated for HMX, the excellent results of Figure 1 are a matter of chance. Indeed, for nitroalkanes and nitric esters, no such good results were obtained, hence the interest of alternative approaches.

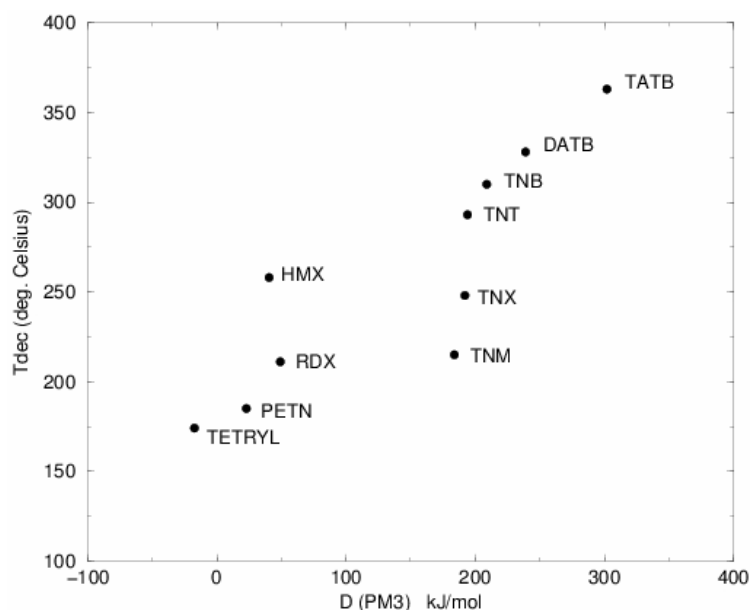


Fig 1. Decomposition temperatures of some nitro compounds (in °C) as a function of the dissociation energy (in kJ/mol) of the weakest X-NO₂ bond in the compound, calculated using the semi-empirical PM3 method. Tetryl is found to be unstable at this level.

3.2 Influence of the number of trigger linkages

The previous procedure based on D_e focusses on one bond (the weakest one). In fact, it may be expected that the more trigger bonds are present in a given amount of material, the easier it is for it to decompose. This is especially clear when several weak bonds have the same energy (by symmetry). Therefore, in addition to the energy of individual bonds, the distribution of trigger linkages with different dissociation energies should be considered. It is expected that the larger the concentration n of trigger linkages, the lower the decomposition temperature. This is actually the case, as illustrated in Figure 2 for compounds that decompose in the melt, and are listed elsewhere.^[7]

A simple group contribution approach might assign decomposition temperatures $T_{dec}^{(ii)}$ and $T_{dec}^{(i)}$ to trigger linkages and other moities, respectively. Then, T_{dec} should decrease linearly with n . In fact, Figure 2 rather suggests a concave function $T_{dec}(n)$.

To account for this concavity, a simple analytic model may be easily derived from kinetic considerations. The critical step is the proper definition of T_{dec} at the microscopic level. We start from the number N of chemical bonds not yet damaged by the decomposition process. The reaction rate is defined as:

$$k = \frac{1}{N} \frac{dN}{dt} = \frac{1}{N} \sum_i N_i A_i \exp(-E_i/kBT) \quad (2)$$

with N_i the number of trigger bonds of type i , A_i and E_i kinetic parameters associated with rupture of i bonds. In this model, k depends on temperature, the possibility of chain reactions is disregarded. In that case, it is natural to define T_{dec} as the temperature for which k reaches a critical value k_c .

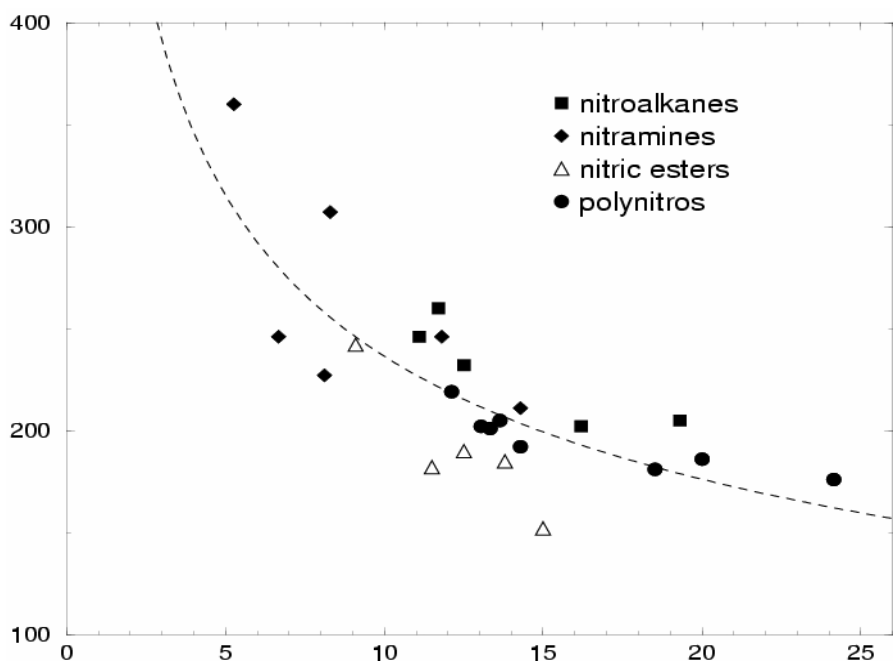


Fig 2. Decomposition temperatures of nitro compounds (in °C) as a function of the trigger linkage (X-NO₂) concentration (in %).

In that case, T_{dec} is a solution of a simple algebraic equation, involving a pair (a_i, E_i) of kinetic parameters for every kind i of trigger linkages (a_i stands for a reduced pre-exponential factor equal to A_i/k_c). These parameters may be obtained from adjustments against observed decomposition temperatures. In principle, it is necessary to introduce several pairs of kinetic parameters according to the type of trigger bond (N-NO₂, C-NO₂, O-NO₂). This has been done in a previous work. In fact, a single pair (a_i, E_i) allows to derive an analytic expression for T_{dec} :

$$\frac{1}{kBT_{dec}} = \frac{1}{E_i} \ln \left(\frac{N_i}{N} a_i \right) \quad (3)$$

This simple analytic expression fits the data on Figure 2 reasonably well, as illustrated by the dashed line. In contrast to the group contribution approach which would predict a linear dependence, it accounts for the concavity of the function. Therefore, it might provide a useful starting point for new models to estimate thermostability of materials that decompose in the melt. For instance, N_i is an extensive parameter that could be estimated using a group contribution scheme. A more physical approach might aim at improving the model or the evaluation of the kinetic parameters.

REFERENCES

- [1] K. K. IRIKURA and D. J. FRURIP: *Computational Thermochemistry*, American Chemical Society, 1998
- [2] C. H. TU and Y. Y. LAY: *J. Chi. I. Ch. E.* 21, p. 275, 1990
- [3] Advanced Chemistry Development website: http://www.acdlabs.com/products/phys_chem_lab/liquid_prop
- [4] G. PIACENZA, G. LEGSAI, B. BLAIVE and R. GALLO: *J. Phys. Org. Chem.* 9, p. 427, 1996
- [5] D. W. VAN KREVELEN: *Polymer Properties*, Elsevier, Amsterdam, 1990
- [6] J. BICERANO: *Prediction of Polymer Properties*, Marcel Dekker, New York, 1996
- [7] E. THEERLYNCK, D. MATHIEU, P. SIMONETTI : *Proceedings of the 31st North American Thermal Analysis Society Conference (NATAS) Albuquerque, NM, USA, Sept. 22-24, 2003*, p. 69, 1-10, edited by M. J. Rich, Omnipress, Madison, WI, 2003

IDENTIFICATION OF SOLID PROPELLANT COMBUSTION DYNAMIC CHARACTERISTICS FROM THE RESULTS OF EXPERIMENTS WITH REGISTRATION OF THE CURRENT BURNING FRONT POSITION

Y.M. Milyokhin*, A.N. Klyuchnikov*, A. V. Fedorychev*, S.V. Gunin*,
V.V. Serushkin**, V.P. Sinditskii ** and S.A. Filatov **

* Federal Center of Dual-Use Technologies “Soyuz”,
Academician Zhukov St. 42, 140090, Dzerzhinsky, Moscow region, Russia

** Mendeleev University of Chemical Technology,
9 Miusskaya Square, 125047 Moscow, Russia

Abstract:

A stable algorithm of structural and parametric identification of combustion dynamic characteristics from the results of experiments with registration of the current burning front position has been developed, which allows prediction of current values of burning rate $u(\tau)$ and its frequency response with accuracy acceptable to practice. The proposed approach has been tested by simulation calculations with harmonic input signals, including superimposed noise of different intensity, to determine the accuracy of identification of the amplitude and phase frequency characteristics of burning. The approach has been used to study dynamic combustion characteristics of a model propellant under oscillating pressure. The transfer and response functions have been determined for a low frequency area. It has been shown that the approach is favorably distinguished from other procedures by higher accuracy and authenticity of estimations.

Keywords: *combustion, dynamic characteristic, solid propellants,
transfer functions, response functions*

1. INTRODUCTION

Study of non-stationary combustion processes of solid propellants is of large importance when creating propulsion systems with automatic regulation of pressure (mass flow, thrust) in the combustion chamber. In such systems, solid propellant combustion dynamic characteristics largely determine areas of steady work, output parameters and design of the systems. Accuracy of prediction of dynamic characteristics determines available stability margin of the systems. In this connection, problems of the prediction of these characteristics with accuracy acceptable to practice gain in paramount importance.

Differential equations, transfer functions, amplitude-phase responses, referred as dynamic characteristics of combustion, are generally used for the description of processes of non-stationary combustion. The preset form of combustion dynamic characteristics should imply opportunity for analyzing system stability both in time and frequency domains. The combustion dynamic characteristics allow calculating the current values of the burning rate, $u(\tau)$, from known dependence of pressure on time, $p(\tau)$, in the time domain, and amplitude - frequency and phase-frequency responses of burning rate in the frequency domain.

The combustion dynamic characteristics can be specified in the form of either mathematical models of non-stationary combustion or relations smoothing results of a direct experimental determination of burning rate (or some characteristic parameters) under altering pressure conditions.^[1]

The mathematical models of non-stationary combustion are relative to either Zel'dovich-Novozhilov's phenomenological theory (ZN-model),^[2] or to a class of models with concrete kinetics^[3] (FM-models). All of them require primary informational supply obtained from experiments. Unfortunately, the experimental estimations of many parameters are characterized by a wide scatter of values. This property at once calls in question an opportunity of achievement of acceptable accuracy at predicting of dynamic characteristics of burning rate using FM-models, since all of them, as a rule, contain a lot of parameters determined experimentally, even in the case of description of simplest monopropellant steady-state burning of cyclic nitramines.^[4, 5] Using FM-models practically excludes the opportunity of system stability analysis in the frequency domain.

Among parameters used in ZN-models, the biggest scatter of experimental estimations ($3 \div 5$ % for double-based propellants and HMX^[6]) is typical for determination of temperature of burning surface (T_s). As a result, finding derivatives of T_s on pressure ($r_N = dT_s/dp$) and initial temperature (dT_s/dT_0) is attended with large errors. Therefore, as shown in work,^[6] the standard error in determination of response function reaches $20 \div 50\%$, even for such relatively simple systems as monopropellants. In the case of heterogeneous propellants characterized by much greater scatter of experimental estimations of initial parameters, the standard error in determination of the response function of burning rate will obviously exceed the above values. To compute frequency responses within the framework of ZN-models, the transfer functions of burning rate on pressure are used, containing transcendental and irrational expressions in their structure. Such transfer functions should be transformed into partial differential equations at transition to time domain that essentially complicates mathematical model of propulsion system. Combined with a large error of determination of model parameters, it makes difficult to find steady work areas, select structure and parameters of control algorithm, and identify mathematical model of the system by test results.

The most reliable information on dynamic characteristics of solid propellant combustion, from the practical point of view, can be recovered from results of direct experiment, in which the synchronous registration of pressure $p(\tau)$ and the current burning front position $x(\tau)$ is carried out in some way or another.

The determination of the current burning front position of propellant can be carried out, for example, with use of video-recording method, microwave and ultrasonic techniques.^[7] The task of parametric identification of burning rate dynamic characteristics by results of such type of experiments was considered by the authors of the present article in work.^[8] A model of non-stationary burning was accepted as a typical discrete transfer function, $W_{xp}(z)$, with constant factors linking directly measured parameters: pressure and the burning front position. The error of prediction of burning rate dynamic characteristics in the vicinity of base pressure, p^0 , using this approach was comparable with error of determination of the initial data (burning front position, $x(\tau)$) and did not exceed 10 %.

Use of structurally simple mathematical expressions gives the acceptable accuracy of burning rate prediction only in the vicinity of p^0 . For the adequate description of $u(p(\tau))$ dependence in a wide range of pressure, the factors of the differential equations must change with pressure.

In the present work, a task of structural and parametrical identification of non-stationary combustion model from family of differential equations (which factors generally depend on pressure) is examined:

$$\sum_{i=1}^2 \left(T_{i+1}(p) \cdot \frac{d^i u}{d\tau^i} \right) + u = T_1(p) \cdot \frac{du_s}{d\tau} + u_s, \quad (1)$$

where u_s – burning rate in stationary conditions; T_1, T_2, T_3 – parameters to be identified from experimental data.

2. RESULTS AND DISCUSSIONS

2.1 Problem statement

The task of structural identification of the model of non-stationary combustion consists in determination of the best model from the models-candidates of the family of differential equations (1). A model that satisfies the condition of adequacy at minimum number of parameters is admitted as the best one. The similar approach was successfully applied by the authors at identification of experimental stationary-state dependence of burning rate on pressure with the use of exponential functions.^[9]

The task of parametric identification of each of the models-candidates consists in determination of a vector of model factors, at which calculated output value would differ from the measured one as small as possible. In the given statement the problem belongs to a class of reverse tasks, and the presence of errors at determination of initial dependences $p(\tau)$ and $x(\tau)$ makes it incorrect in the mathematical sense. The incorrectness, as a rule, shows itself in the absence of the unique solution, or in its instability. Therefore, is an urgent task to develop a numerical algorithm, which allows obtaining a steady solution of the parametric identification with acceptable-to-practice accuracy.

2.2 Algorithm of the solution

Let us define a set of models-candidates in the form of the differential equations (1) and consider a classic case when the pressure changes in the vicinity of p^0 and the factors of the equation are independent from pressure. Then the family (1) can be transformed into the following form:

$$\sum_{i=1}^2 \left(T_{i+1} \cdot \frac{d^i \bar{u}}{d\tau^i} \right) + \bar{u} = \nu \cdot \left(T_1 \cdot \frac{d\bar{p}}{d\tau} + \bar{p} \right), \quad (1a)$$

where $\bar{p} = p/p^0 - 1$ and $\bar{u} = u/u^0 - 1$ – dimensionless deviations of burning rate and pressure, respectively; p^0, x^0 – the base magnitudes relative to which the deviations are considered; ν – sensitivity of the burning rate to pressure (pressure exponent); T_1, T_2, T_3 parameters of the transfer function. The each element of the set of the models-candidates is defined by a vector of parameters $T = \{T_1 T_2 T_3\}$ and represents a concrete model.

In the frequency domain, expression (1a) is identical to the family of continuous rational transfer functions. Written for $i=2$ it is as follows:

$$W_{up}(s) = \nu \frac{T_1 s + 1}{T_3 s^2 + T_2 s + 1} \quad (2)$$

Expression (2) at $s=i\omega$ (where $i=\sqrt{-1}$, ω – the circular frequency) gives amplitude of the response of burning rate and its phase shift. This expression covers all forms of the equations of typical transfer functions. If $T_3=0$ the described process has forcing (differentiating) properties at $T_1>T_2$, delay (integration) properties at $T_1<T_2$, and we have a static unit with amplification factor ν at $T_1=T_2$. At $T_3\neq 0$, it is an oscillatory or aperiodic unit of the second order.

Introduction of component with the second-order derivative on pressure in the right part of equation (1) or using the second degree polynomial in numerator of the transfer function (2) is inexpedient, since finding the second derivative of noise discrete input signal $p(\tau)$ is a mathematically incorrect operation, that amplifies effect of disturbance interferences and results in the large errors of parameter identification.

Let us consider an algorithm of parameter identification of the non-stationary combustion model (2). To avoid differentiation procedure with experimental array $x(\tau)$, the propagation of the burning front rather than the burning rate (as was done in work [8]) has been adopted as output value. Then the construction of the dynamic combustion model consists in finding a continuous transfer function, $W_{xp}(s)$, linking directly measured experimental values: pressure and the burning front position. The following relation connects the transfer functions $W_{xp}(s)$ and $W_{up}(s)$:

$$W_{xp}(s) = \frac{1}{s} \cdot W_{up}(s) \quad (3)$$

In view of expression (2), the transfer function of position x on pressure p assumes the form:

$$W_{xp}(s) = \frac{1}{s} \cdot \nu \frac{T_1 s + 1}{T_3 s^2 + T_2 s + 1} \quad (4)$$

To determine factors of the transfer function $W_{xp}(s)$, we describe dynamics of combustion in the vicinity of p^0 in the differential form:

$$T_3 \bar{x}''' + T_2 \bar{x}'' + \bar{x}' = \nu \cdot (T_1 \bar{p}' + \bar{p}), \quad (5)$$

with initial conditions $\bar{x}(\tau_0) = \bar{x}_0$, $\bar{x}'(\tau_0) = \bar{u}_0$, $\bar{x}''(\tau_0) = \bar{u}_0'$, where $\bar{x} = x/u^0 - \tau$. Parameters $T = \{T_1 T_2 T_3\}$ of this equation are ones of transfer function (4) and define dynamics of non-stationary combustion.

From the equation (5) the expected magnitude of output signal, \hat{x} , can be found using methods of numerical integration of the differential equations, for example, the Runge-Kutta method.^[10]

The parameters of the model T_1, T_2, T_3 are generally so determined that value \hat{x} calculated from the equation (5) differs from the corresponding measured value \bar{x} as small as possible. For this purpose it is necessary to minimize criterion function:

$$S(T) = \sum_{k=1}^N (x_k - \hat{x}_k)^2, \quad (6)$$

where x_k – experimental values of the burning surface position at the moment of time τ_k , $\hat{x}_k = (\hat{x}_k + \tau_k) \cdot u^0$, \hat{x}_k – calculated from the equation (5), N – number of measurements. The

function (residual) characterizes the deviation of the burning surface positions calculated from the experimentally measured values by the model (5)

In the task of structural identification of a non-stationary burning model from the family (1a) it is impossible to preset dimension of the vector of model parameters, since some T_i can be equal to zero. In this case the task is reduced to determination of such a vector $T^* = \{T_1^* T_2^* T_3^*\}$ that

$$S(T^*) = \inf S(T), \quad (7)$$

where $T \in E^3$ – three-dimensional Euclidean space.

Inasmuch as the dimension of vectors T is not specified and it is impossible to assert that function (6) has the only minimum, then the task (7) is incorrectly formulated in the mathematical sense. Transformation to a correctly stated task can be done by application of regularization procedure.^[11] Construct a parametric function:

$$\Phi(T) = S(T) + \alpha \cdot \Omega(T), \quad (8)$$

where $\alpha > 0$, Ω – stabilizing functional, for example, $\Omega(T) = \|T\|_n^2$, α – regularization parameter, $\|\cdot\|_n$ – norm of the vector in n -dimensional space, $1 \leq n \leq 3$. If $S(T)$ is a convex function, and Ω is a uniformly convex one, then the function Φ will be also a uniformly convex function at any $\alpha > 0$. In this case the task of determination of the vector $T_\alpha^* \in E^n$ satisfying expression:

$$\Phi(T_\alpha^*) = \inf \Phi(T), \quad (9)$$

is formulated correctly and its solution T_α^* is the only one for every fixed α .

To determination T_α^* let us assume an ascending sequence of integers, n , $n = 1, 2, 3, \dots$ and determine vector T^* for every n in steady Euclidean (E^n) space. For selection of the regularization parameter, a residual principle can be used. For this purpose let us construct an auxiliary function of one variable α :

$$\psi(\alpha) = [S(T) - N \cdot \sigma^2]^2, \quad (10)$$

where σ^2 – noise dispersion in experimental values x .

Sequence of operations to find values of function (10) is as following:

- T_α^* is found by the solution of an extreme task (9) with fixed α and n ;
- the equation (5) is integrated at T_α^* ;
- $S(T_\alpha^*)$ is found, substituted in (10), and $\psi(\alpha)$ is calculated.

The optimal regularization parameter α^* is selected to meet the condition:

$$\psi(\alpha^*) = \inf \psi(\alpha) = 0, \quad \alpha > 0 \quad (11)$$

If $\inf \psi$ does not attained zero, the dimension of E^n is to be increased until the condition (11) is met. The increase in E^n dimension from $n=1$ to $n=3$ means consecutive complication

of the model (5) structure from $T = \{T_1\}$ to $T = \{T_1, T_2, T_3\}$. The extreme tasks (9), (11) were solved by the methods of the steepest descent and golden section, respectively.^[12]

Now let us consider the identification algorithm of combustion dynamic characteristics for the case when the pressure varies in a rather wide range and the parameters of the family (1) are pressure dependent. Parameters of the family (1) can be presented as:

$$T_1(p) = \sum_{k=1}^{l_1} a_k \varphi_{1k}(p), \quad T_2(p) = \sum_{k=1}^{l_2} b_k \varphi_{2k}(p), \quad T_3(p) = \sum_{k=1}^{l_3} c_k \varphi_{3k}(p), \quad (12)$$

where $\{\varphi_{jk}(p)\}$ ($k=1, \dots, l_j$, $j=1, \dots, 3$) – specified system of basic functions, for example $\varphi_k = p^{k-1}$. After that a total vector of unknown parameters $m = [m_1, m_2, \dots, m_L]$, $L = \sum_{j=1}^3 l_j$, can be generated. The task of parametric identification, as previously, is reduced to minimization of residual:

$$S(m) = \sum_{k=1}^N (x_k - \hat{x}_k)^2 \quad (13)$$

The task of structural identification of non-stationary combustion model from the family (1) is reduced to find the vector $m^* = [m_1^*, m_2^*, \dots, m_L^*]$ so that:

$$S(m^*) = \inf S(m), \quad (14)$$

$m \in E^L$ – Euclidean space of L variables.

The task (14) is incorrectly formulated in the mathematical sense. The transformation of it into a correctly formulated task is carried out with the use of a regularization procedure. Algorithm of the regularization and solution of the correctly formulated task is similar to the above one.

2.3 Algorithm testing

The proposed algorithm of parametric identification of burning rate dynamic characteristics has been tested on a model example. For this purpose a model of non-stationary burning (5) with parameters $T_1=0.0882$, $T_2=0.0133$, $T_3=0$; $\nu=0.745$ was accepted as the "true" model. The alteration of pressure p was set by the harmonic law

$$p = p^0(1 + \bar{p}(\tau)), \quad \bar{p}(\tau) = \sin(2 \cdot \pi \cdot \Omega \cdot \tau)$$

where, $p^0=1.567$ MPa is the base pressure, $\Omega=1$ Hz – frequency of the input signal, $\tau_1=0$ – initial time, $\tau_N=6$ – final time. The value base burning rate u^0 was accepted to be 1.56 mm/s. Then, the "true" curve $x(\tau)$ was computed by the model (5), on which the white noise $z(\tau)$ with zero mathematical expectation and dispersion $\sigma^2=0.0075$ was additively imposed. The accepted value of σ^2 was close to dispersion of experimental error of measuring current values $x(\tau)$ by the method of video registration.^[13] In doing so, the natural disorder of experimental values $x_k^e = x(\tau_k) + z(\tau_k)$ around the true $x(\tau)$ was simulated. Dependences of the position of the burning surface on time calculated in this way were used as the initial data in the parametric identification task. Hereafter x_k^e values are called pseudo-experimental.

To solve the task of parametric identification the interval of time $1 \leq \tau_k \leq 5$ s, containing more than 80 pseudo-experimental values of burning surface positions, was chosen. Input

$(p(\tau_k))$ and output (x_k^e) signals were processed within the selected time interval by algorithm (5) ... (11). The results of identification are presented in Table 1 and Figure 1.

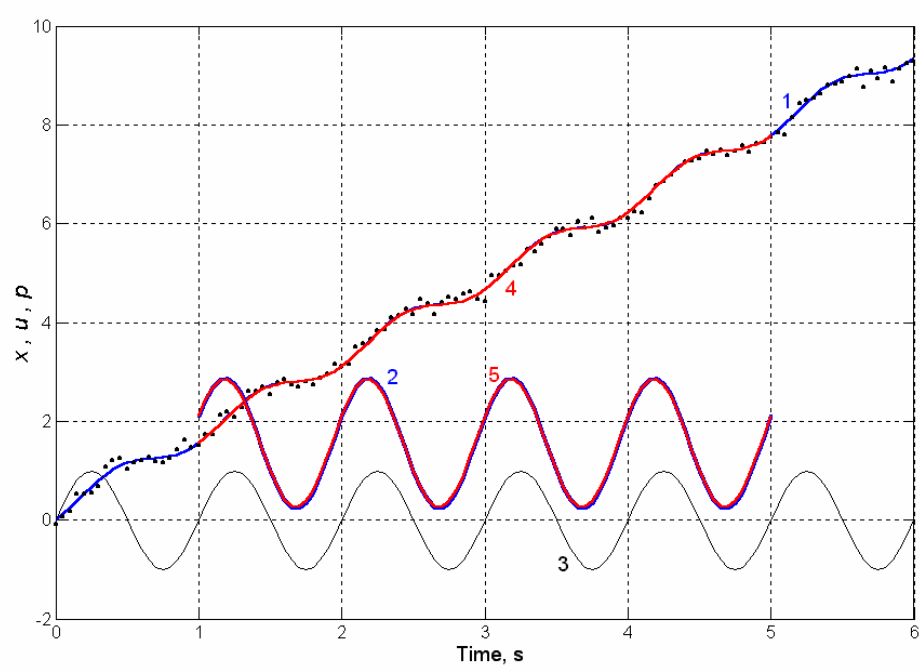


Fig 1. Dependences of burning surface position, burning rate, and relative change of pressure $\bar{p}(\tau)$ on time (numerical experiment):
1, 2 – initial non-perturbed position of the burning surface, $x(\tau)$, and burning rate, $u(\tau)$, respectively; \bullet – perturbed "experimental" position x_k^e ;
3 – relative change of pressure with time, $\bar{p}(\tau)$;
4, 5 - calculated dependences of the burning surface position, $x_c(\tau)$, and burning rate, $u_c(\tau)$.

Table 1. Results of identification of the model example

Characteristic values	T_1	T_2	A	φ
“True” values	0.0882	0.0133	0.8487	24.22
Identification by the model (5)...(11)	0.0815	0.0087	0.8356	23.97
Error of identification, %	7.58	34.24	1.54	1.01

A, φ – amplitude and phase responses at $\Omega = 1$ Hz

With the use of the identified values of parameters the time dependences of the burning surface position, $x_c(\tau)$, and burning rate, $u_c(\tau)$, as well as frequency responses of the burning rate were calculated, showing influence of error of determination of dynamic parameters, T_1, T_2 .

In Figure 1 the "true" curve $x(\tau)$, pseudo-experimental x_k^e values, true burning rate $u(\tau)$, and burning rate identified by the model (5) $u_c(\tau)$ are presented.

In Figure 2 "true" and calculated by identified model (5) frequency responses are presented. The values of frequency responses and error of their determination are presented in Table 1.

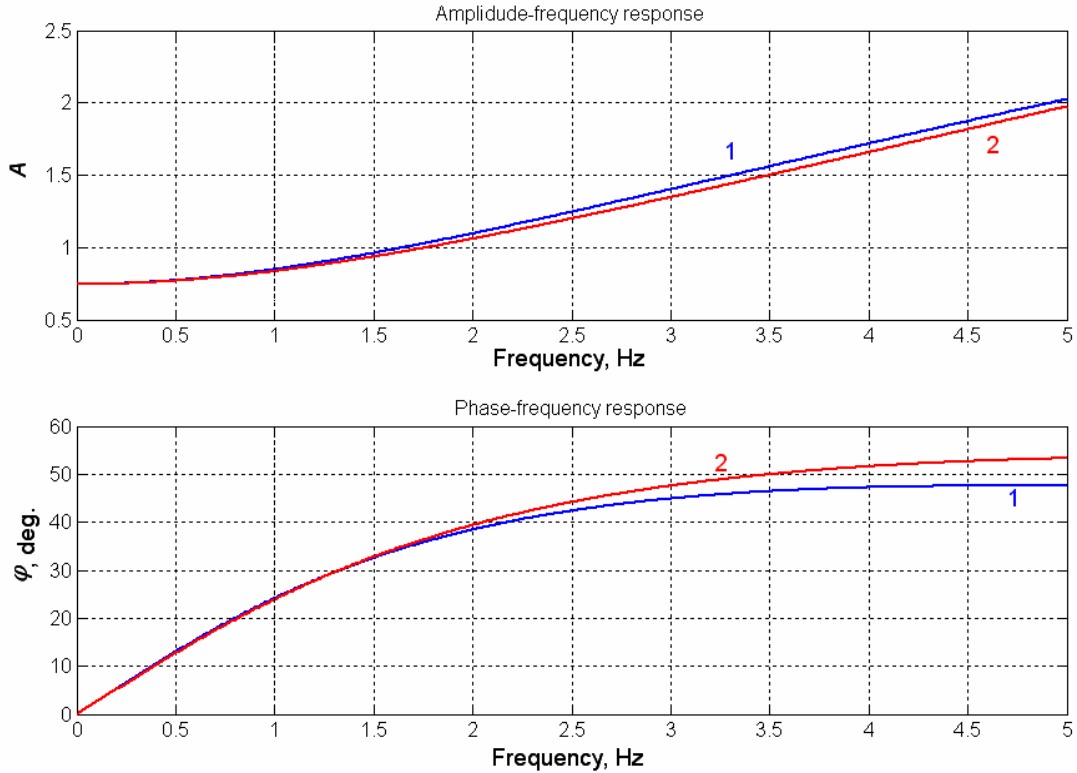


Fig 2. Frequency responses of the burning rate (numerical experiment):
1 - true responses, 2 – responses calculated from the identified model (5).
Frequency of input signal – 1Hz.

As shown in Figure 1, the true and computed dependences practically coincides with each other, testifying to stability of the proposed algorithm of parametric identification. In the frequency domain, a good agreement of "true" and calculated dependences in the range of frequencies $\Omega = 0 \dots 1$ Hz (see Figure 2) is also observed.

Residual dispersion between the identified position $x_c(\tau)$ and pseudo-experimental values x_k^e amounts to 0.0094, that practically coincides with the error of the initial data $\sigma^2=0.01$ and indicates to adequacy of the identified model to pseudo-experimental data.

2.4 Experimental examination of the proposed approach

The proposed approach has been used to study the dynamic combustion characteristics of a model solid propellant with a low burning rate (~ 1 mm/s at pressure 10 atm) and high pressure exponent ($\nu > 0.7$). The experimental data required for evaluation of combustion dynamic characteristics were obtained by using a technique based on video recording of combustion process under oscillating pressure conditions.^[8] The range of pressures below 30 atmospheres was investigated, in which the appearance of non-stationary combustion is most probable even at low frequencies of pressure oscillation. A typical video recording time diagram demonstrating change of parameters at burning of model propellant samples under

conditions of harmonic pressure oscillations has been presented in the work.^[8] It is practically the same as the diagram in the Figure 1.

Figure 3 presents frequency responses of burning rate for the model propellant composition obtained from experimental data with the use of algorithm (5) - (11). In the Figure also are shown frequency responses calculated by ZN-model.^[12]

$$W_{up}(s) = \frac{\nu + \delta\sigma}{1 - k + (r - k/s)\sigma} \quad (15)$$

where s – complex variable; ν , r , μ and $k = \beta(T_s - T_0)$ – parameters of ZN-model;

$$\delta = \nu r - \mu k; \quad \sigma = \sqrt{s + \frac{1}{4}} - \frac{1}{2}.$$

The dependence $T_s(p)$ necessary for calculation by ZN-model was obtained from data of microthermocouple measurements. To decrease errors of determination of derivatives dT_s/dp , du/dp and du/dT_0 the experimental data were smoothed out. The accuracy of determination of ZN-model parameters approximately corresponded to that previously reported in the work.^[6] The dependence of steady-state burning rate on pressure was obtained with the use of algorithm described in the work.^[9] For calculation of ZN-model parameters (ν , β and μ) the following expressions were used:

$$\nu = \left(\frac{\partial \ln u}{\partial \ln p} \right)_{T_0}, \quad \beta = \left(\frac{\partial \ln u}{\partial T_0} \right)_{p^0}, \quad \mu = \frac{1}{T_s - T_0} \cdot \left(\frac{\partial T_s}{\partial \ln p} \right)_{T_0}, \quad (16)$$

where p^0 and T_0 – values of base pressure and initial temperature. The derivative dT_s/dT_0 (r parameter) was determined from the expression:

$$r = (T_s - T_0) \cdot \mu \cdot \frac{\beta}{\nu} \quad (17)$$

As it is seen from Figure 3, response functions obtained from the experimental data with the use of the proposed algorithm and calculated by ZN-model are characterized by smooth increase in both amplitude and phase characteristics and demonstrate a qualitative agreement with each other. The presence of the advancing phase shift as well as increase in the amplitude response with frequency testify unequivocally to a non-stationary character of the model propellant burning rate under oscillatory conditions at low pressure. This is in a good agreement with the theory, which predicts differentiating properties of the burning rate at low frequencies of pressure oscillations.

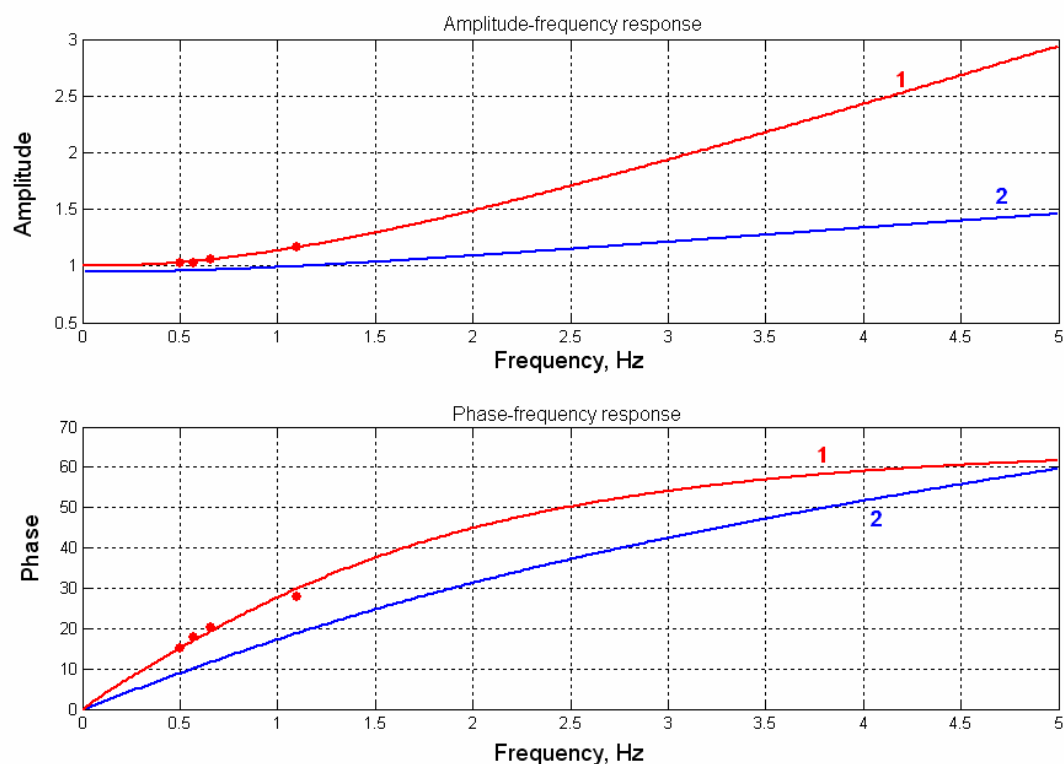


Fig 3. Frequency responses of the model propellant burning rate:
 1 – processing of experimental data with the use of algorithm (5)...(11);
 2 – responses calculated with ZN-model;
 Points – data on phase shift and amplitude characteristic determined from separate experiments at different frequencies of pressure oscillation.
 Base pressure value – 30 atmospheres.

It is necessary, however, to note that appreciable quantitative divergence between response functions obtained from the experimental data with the use of proposed algorithm and calculated by ZN-model is observed. The experimental values of the amplitude and phase characteristics obtained in separate experiments at various frequencies of pressure oscillations are much better described if using the proposed algorithm (see Figure 3). It allows making a conclusion that the method for determination of combustion dynamic characteristics developed in the present work has the higher accuracy in both time and frequency domains as compared with estimations by ZN - model.

3. CONCLUSIONS

A stable algorithm of structural and parametric identification of combustion dynamic characteristics from the results of experiments with registration of current burning front position at any character of pressure change has been developed, which allows predicting the current values of burning rate $u(\tau)$ and its frequency response with acceptable-to-practice accuracy. Unfortunately, the application of this algorithm in combination with technique of video registration has essential restrictions. Shortcoming of the technique is in that it allows obtaining initial experimental data used for determination of combustion dynamic characteristics only in the low range of frequencies of pressure oscillations ($0.5 \div 10$ Hz). Non-stationary phenomena (phase shifts and amplitude deviations) on combustion of practicable propellants and their components (such as HMX), which possess higher burning rates than the investigated model one, can take place at higher frequencies. However, the developed procedure can be applied in combination with all other techniques of higher sampling frequency and accuracy which allow continuous registration of the burning front. Such a technique can be created, for example, on the basis of microwave method, which allows measuring the burning front position averaged by the area of a waveguide. Combination of the microwave method and video registration technique, used in this for controlling the burning surface shape, enable studying combustion dynamic characteristics in considerably wider (tens of hertz) frequency range. In this case the algorithm to determinate the combustion dynamic characteristics will remain fully the same. The accuracy of dynamic characteristics thus obtained will correspond to the accuracy of burning front position measurements.

The proposed algorithm can also be used for determination of combustion dynamic characteristics in a half-closed volume, when the output signal is the burning rate derived, for example, from the solution of inverse problem of interior ballistics using results of propulsion systems tests.

REFERENCES

- [1] O. YA. ROMANOV, V.S. TARKHOV. *Dynamic Parameters of Mass Combustion Rate of a Condensed Matter*. Combustion Explosion and Shock Waves, **Vol. 22, No 1**, p.3-11, 1986.
- [2] B.V. NOVOZHILOV. *Non-stationary Combustion of Solid Propellants*. Moscow: Nauka, 1973.
- [3] L. DE LUKA. *Theory of Burning and Combustion Stability of Solid Propellants by Flame Models*. Nonsteady Burning and Combustion Stability of Solid Propellants. (Progress in Astronautics and Aeronautics; **Vol. 43**). L. De Luka, E.W. Price, and M. Summerfield (Eds.), Washington, AIAA, p. 519-600, 1992.
- [4] Y.C. LIAY, V. Yang. *Analysis of RDX Monopropellant Combustion with Two-Phase Subsurface Reactions*. JPP, **Vol. 11, No. 4**, p. 729-739, 1995.
- [5] B. ERIKSON, M.W. BECKSTEAD. *A numerical Model of Monopropellant Deflagration under unsteady conditions*. AIAA Paper, 96-0652.
- [6] A.A. ZENIN, S.V. FINJAKOV. *Burning-Rate Response Function of Nitramine-Based Propellants and HMX from Microthermocouple Data Measurements*. Combustion Explosion and Shock Waves, **Vol. 36, No 1**, p. 10-20, 2000.
- [7] V.E. ZARKO and K.K. KUO. *Critical review of methods for registration rate measurements of condensed phase systems*. Non-Intrusive Combustion Diagnostics, K.K. Kuo and T.P. Parr (Eds.). New York: Begell House, p. 600-623, 1994.
- [8] V.V. SERUSHKIN, V.P. SINDITSKII, S.A. FILATOV, YU.M. MILYOKHIN, A.N. KLYUCHNIKOV, A.V. FEDORYCHEV, S.V. GUNIN. *Procedure for Determination of Solid Propellant Combustion Dynamic Characteristics*. Proceedings of 34th Annual International Conference of ICT, Karlsruhe, Germany, paper 143, p. 1-12, 2003.
- [9] YU.M. MILYOKHIN, A.N. KLYUCHNIKOV, A.V. FEDORYCHEV, S.V. GUNIN, V.V. SERUSHKIN. *Identification of Experimental Dependences of Propellant Burning Rate on Pressure*. Proceedings of 34th Annual International Conference of ICT, Karlsruhe, Germany, paper 142, pp. 1-11, 2003.
- [10] S.K. GODUNOV, V.S. RYABEN'KIY. *Differented schemes*. Moscow: Nauka, 1973.
- [11] V.S. BALAKIREV, V.M. VOLODIN, A.M. TSIRLIN. *Optimum Control of Processes of Chemical Technology*. Moscow: Khimiya, 1978.
- [12] B.T. POLYAK. *Introduction into optimization*. Moscow: Nauka, 1983.
- [13] L. Galfetti, G. COLOMBO, A. MENALLI, G. BENZONI, C. GALLY. *Experimental Study of Solid Propellant Ignition Transient and Flame Spreading under Convective Flows*. Combustion Explosion and Shock Waves, **Vol. 36, No 1**, pp. 108-118, 2000.

DEVELOPMENT OF COMPUTER CODE FOR QUALITATIVE PREDICTION OF HEAT OF FORMATION OF HIGH ENERGETIC MATERIALS

Part I

H. Muthurajan*, R. Sivabalan**, M.B. Talawar** and S.N. Asthana**

* Armament Research and Development Establishment, Pashan, Pune-411021, India

** High Energy Materials Research Laboratory, Sutarwadi, Pune-411 021, India

Abstract

A computer code has been developed to predict heat of formation based on two methodologies. In first methodology, the logic of Stine and Kramer method of predicting heat of formation has been used and extended to terminal functional groups such as -OH, -NH, -NH₂, -NO₂, -H and C=O. In the second methodology, a new equation for heat of formation has been derived by merging the equations of Stine et al and Rothsetien et al, which are being used for the theoretical prediction of velocity of detonation. The linear regression coefficient $R^2 = 0.9387$ and 0.8358 are obtained for heat of formation predicted by this code and compared with those reported in literature, using methodology I and II respectively. This new technique of predicting heat of formation from elemental composition of HEM's has been successfully appended in a windows based user-friendly software code named LOTUSES (Linear Output Thermodynamic User-friendly Software for Energetic Systems) developed by our team. The LOTUSES code also simultaneously predicts properties such as molecular weight, oxygen balance, velocity of detonation, C-J pressure, density, heat of explosion, relative strength of an explosive in comparison to 2,4,6-trinitro toluene (TNT) as well as the possible explosive decomposition products after explosion, volume of explosion products and air blast effects has been reported recently by authors. The predicted heat of formation by LOTUSES can be stored in various formats such as .txt, .html, .doc, .pdf and can be saved either in hard disk or even in floppy diskettes/compact diskette. The predicted output can also be copied into RAM, which can be pasted in other softwares such as microsoft word/powerpoint etc.,. Also output of the predicted heat of formation can be heard/listen from speakers attached to the PC through multimedia sound card.

Keywords: heat of formation, predicting explosives performance parameters, computational modelling, high energetic materials

1. INTRODUCTION

One of the new trends in research of explosive is to predict the performance parameters of high energy materials (HEMs) before their synthesis which saves lot of time, energy and other resources for the individuals working in search of HEMs with highest possible performance. It is useful in effective screening of newly proposed target molecules. The theoretically predicted performance parameters give an idea to the HEMs scientists and technologists about the possible performance level of the unknown HEM in comparison to benchmark known explosive

in the event of its synthesis. Based on the performance parameters obtained one can decisively undertake programme on synthesis of new HEMs.

One of the well-known code currently used for predicting explosive performance parameters of any unknown or known HEM is BKW (Becker-Kistiakowsky-Wilson) CODE. The input parameters for BKW code are molecular formula, molecular weight, density and heat of formation. Authors have recently developed ^[1,2] a code named LOTUSES which can simultaneously predict a wide range of HEMs performance parameters such as molecular weight, oxygen balance, velocity of detonation, C-J pressure, density, heat of explosion, relative strength of an explosive in comparison to 2,4,6-trinitro toluene (TNT) as well as the possible explosive decomposition products after explosion, volume of explosion products and air blast effects. Therefore an attempt was made to develop computer code, which can predict heat of formation based on two methodologies. In the first methodology the logic of Stine and Kramer was used and in second methodology an equation for predicting heat of formation has been derived by merging the standard Rothstein et al and Stine methods. The code developed based on the above logics has been successfully interfaced / appended with the existing LOTUSES code to make it more versatile and user friendly in the explosive performance prediction of known / unknown HEMs. Hence, the new methodology of predicting ΔH_f from elemental composition and the software code LOTUSES will be of immense value for the scientists, researchers, academicians and technologists working in the field of HEMs to optimise desired performance parameters. The menu bar and tool bar with brief action of each tools of LOTUSES is illustrated in figure-1.

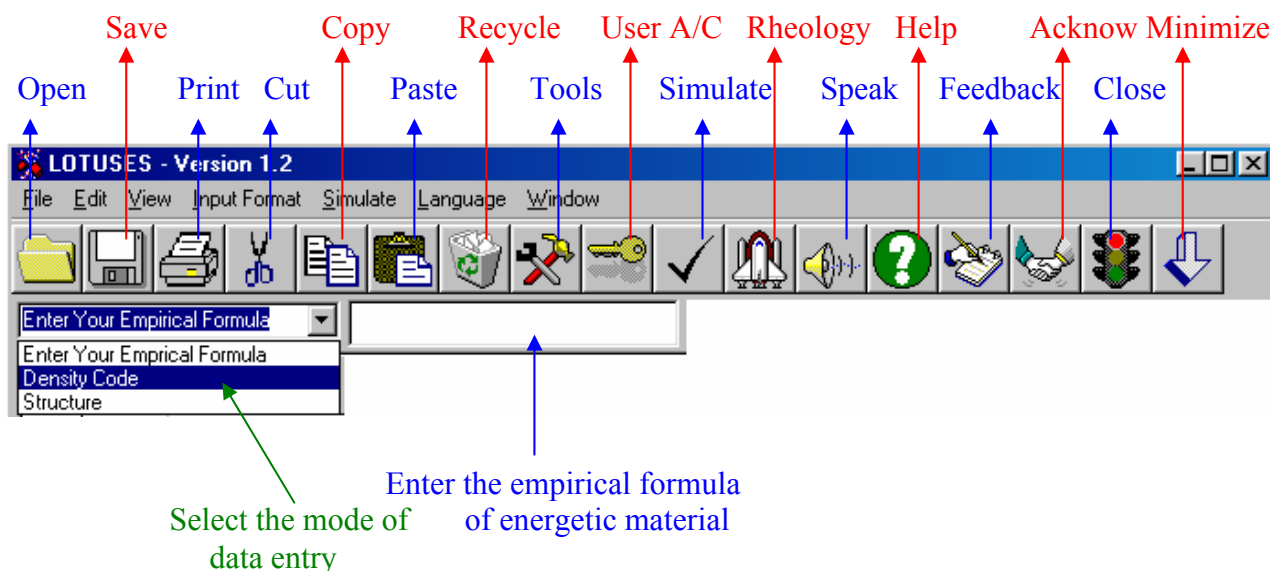


Fig 1. Menu bar and tool bar of newly developed LOTUSES code

Heat of formation of a compound is defined as “the heat evolved or absorbed when 1 gram mole of the compound is formed from its elements in the standard state”. In many instances it is not possible or not convenient to determine the heat of formation of a compound experimentally ^[3]. In most of the cases, it is not possible to form a compound from its elements. For example, it

is not possible to synthesise NG (Nitroglycerine – figure 2) from its elements of C,H,N and O as shown in the equation 1. This is quite common in HEMs research where an estimate of the heat of formation may be desirable for performance evaluation before an extended effort is made to synthesize the compound or before sufficient material is available to make the experimental measurements involved. Even when the compound is available, a scheme by which the heat of formation may be determined may not have been formulated.

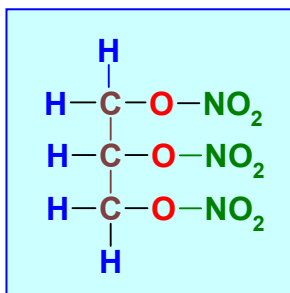
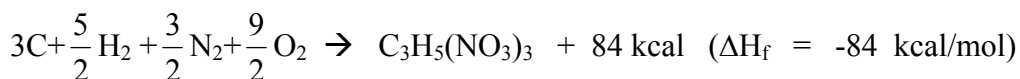


Fig 2. Nitroglycerine

2. METHODOLOGY - I

J.R.Stine and J.F.Eramer of Los Alamos National Laboratory have proposed a method based on the structure of the molecule to estimate the heat of formation^[4]. This method does not account for the terminal functional groups such as –OH, C=O, –NH, –NO₂ groups and hydrogen attached to aromatic / nonaromatic carbon. Authors have introduced empirical constants for the above groups to obtain heat of formation and the entire logic was converted in to a window based computer programme and incorporated in to the same software ‘LOTUSES’.

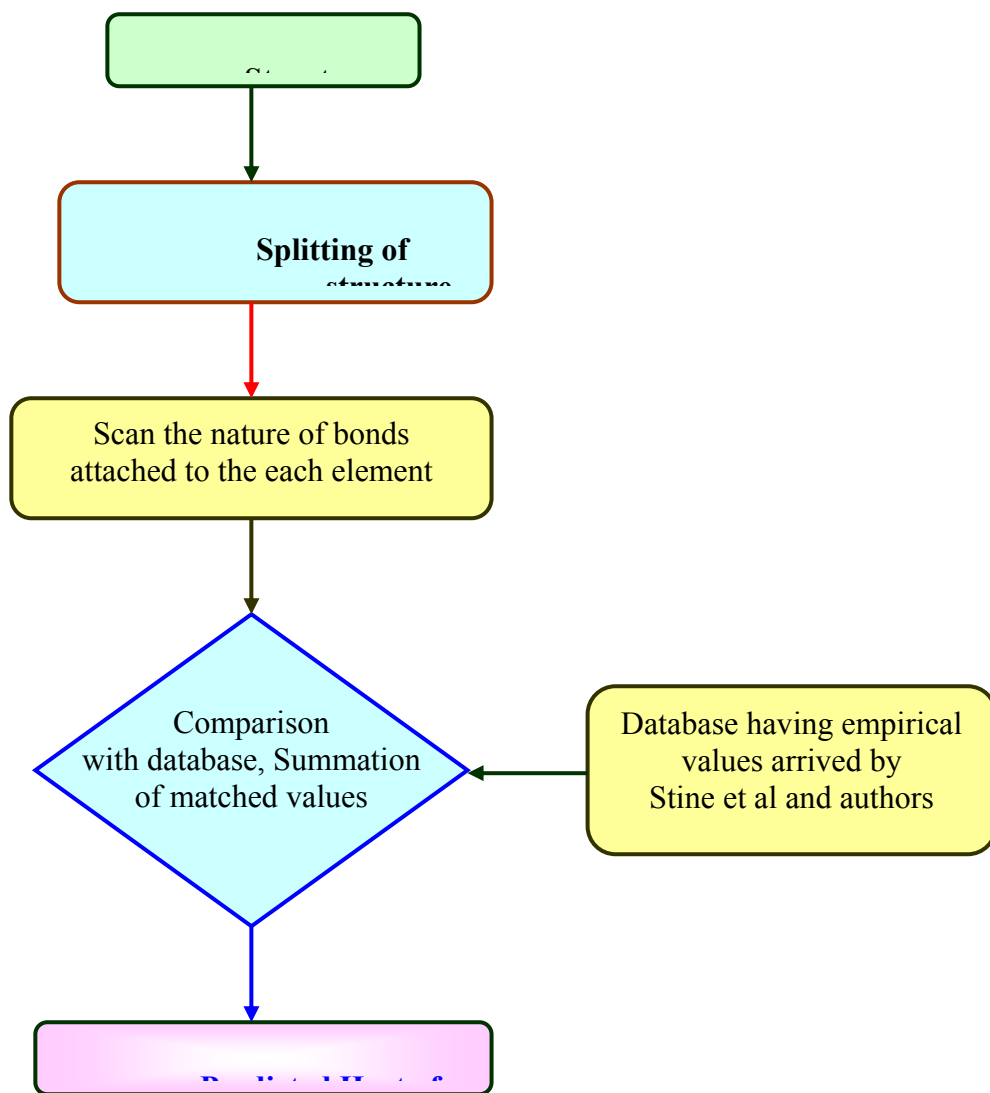


Fig 3. Logic tree used in computer programming in the estimation of heat of formation by Methodology I

Initially database containing empirical values of Stine& Kramer and that of authors was created. In Stine & Kramer method, structure of unknown / known HEMs was split into individual elements and the nature of the bond present in the molecule was keyed into LOTUSES code and consequently heat of formation was computed. The logic tree for Stine and Kramer method is depicted in figure 3.

3. METHODOLOGY - II

The proper use of theoretical estimation of velocity of detonation by Rothstein et al and Stine provides a new method of estimating the heat of formation of a HEMs. We have derived preliminary empirical equation by merging the above two methods to estimate the heat of formation. The merging of two methods is illustrated in figure 4.

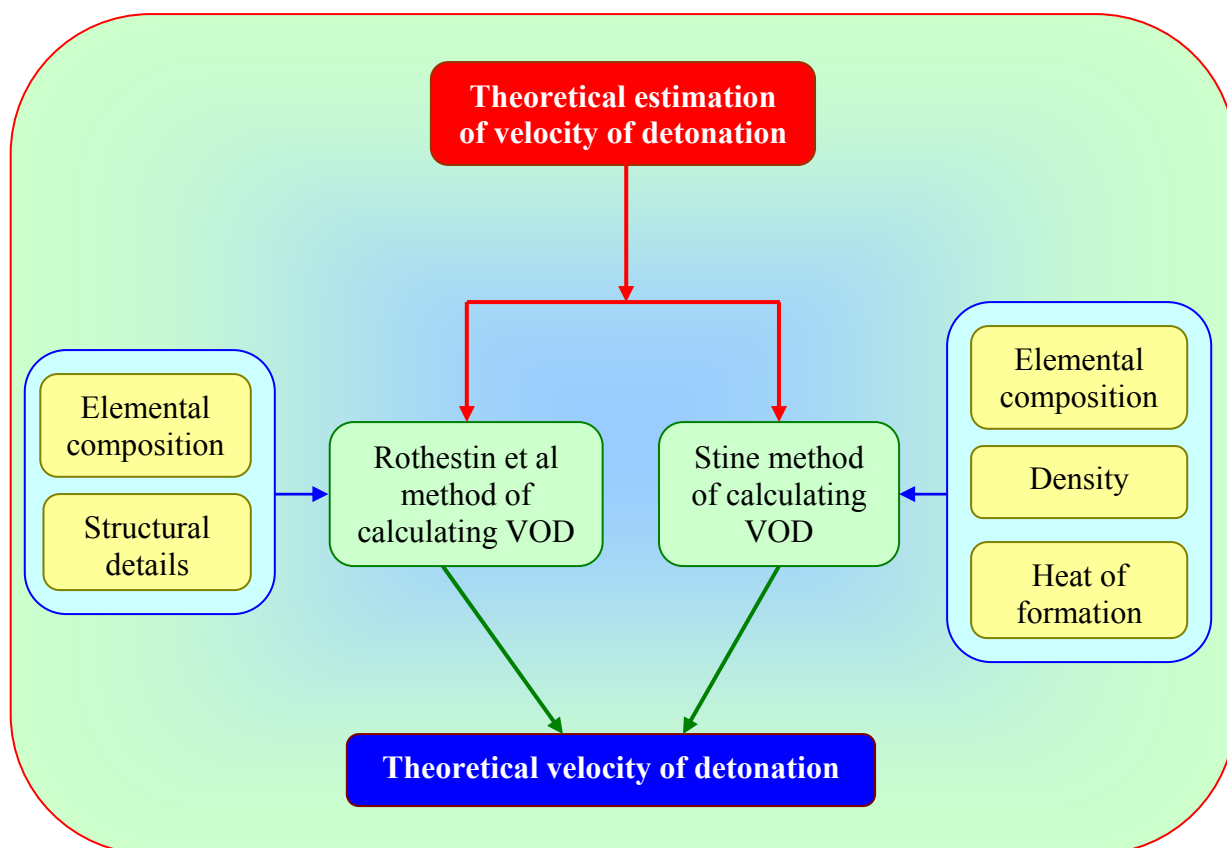


Fig 4. Block diagram representing the methodology II for estimating heat of formation

3.1 Rothstein and Petersen method

One method that relies only on the chemical structure is Rothstein and Petersen method (1979,1981). It yields values for D' (D at the theoretical maximum density)^[5]. A simple, empirical linear relationship between detonation velocity at theoretical maximum density and factor F that is dependent solely upon chemical composition and structure is postulated for a gambi of ideal C,H,N,O type explosives by L.R.Rothstein and R.Petersen^[6,7]. The factor F is expressed as

$$F = 100x \frac{nO + nN - \frac{nH}{2nO} + \frac{A}{3} - \frac{nB}{1.75} - \frac{nC}{2.5} - \frac{nD}{4} - \frac{nE}{5}}{MW} - G \quad (1)$$

$$D = \frac{F - 0.26}{0.55} \quad (2)$$

where nH, nN, nO are number of Hydrogen, Nitrogen and Oxygen atoms in a molecule (users need not to enter separately in or software, it will be taken from the empirical formula entered by the user), nB is number of oxygen atoms in excess of those already available to form CO₂ and H₂O (users need not to enter this value, our software automatically predicts this value), nC number of oxygen atoms doubly bonded directly to carbon as in carbonyl, nD number of oxygen atoms singly bonded directly to carbon, nE number of nitro groups existing either as in a nitrate ester configuration or as a nitric acid salt such as hydrazine mononitrate, A = 1 if the compound is aromatic otherwise A = 0, G = 0.4 for liquid explosive, G = 0 for solid explosive, F = factor and D = Detonation velocity (km/s)

3.2 Stine method

A relative accurate method of estimating detonation velocities for CHNO explosives only (Stine, 1990) is based upon using the atomic composition of either a pure or mixed explosive, along with the explosive's density and heat of formation^[5,8]. In this method the explosive composition is defined as C_aH_bN_cO_d, where a, b, c and d are atomic fractions (i.e., a is the number of carbon atoms in the molecular formula divided by the total number of all atoms in the molecular formula, etc.,)

$$D = 3.69 + (-13.85a + 3.95b + 37.74c + 68.11d + 0.6917\Delta H_f) \left(\frac{\rho}{M} \right) \quad (3)$$

where D is detonation velocity (km/s), ρ is initial HEMs density (g/cm³), ΔH_f is the heat of formation of the explosive (kcal/mol) and M is the molecular or gram formula weight.

3.3 Derivation of equation for computing Heat of formation

Based on the above two equations authors attempted the feasibility of deriving an equation for calculating heat of formation by merging equations (2) and (3). The various steps involved in the derivation are as follows: -

On rearranging equation (3)

$$D - 3.69 = (-13.85a + 3.95b + 37.74c + 68.11d + 0.6917\Delta H_f) \left(\frac{\rho}{M} \right)$$

$$\begin{aligned}
D - 3.69 \left(\frac{M}{\rho} \right) &= (-13.85a + 3.95b + 37.74c + 68.11d + 0.6917\Delta H_f) \\
\left[(D - 3.69) \left(\frac{M}{\rho} \right) \right] + (13.85a - 3.95b - 37.74c - 68.11d) &= +0.6917\Delta H_f \\
\Delta H_f &= \frac{\left[(D - 3.69) \left(\frac{M}{\rho} \right) \right] + (13.85a - 3.95b - 37.74c - 68.11d)}{0.6917} \quad (4)
\end{aligned}$$

Substituting (1) in (2), we get

$$D = \frac{\left[100x \frac{nO + nN - \frac{nH}{2nO} + \frac{A}{3} - \frac{nB}{1.75} - \frac{nC}{2.5} - \frac{nD}{4} - \frac{nE}{5} - G}{MW} \right] - 0.26}{0.55} \quad (5)$$

on substitution of D in equation (4), we get

$$\Delta H_f = \frac{\left[\left(\frac{\left[100x \frac{nO + nN - \frac{nH}{2nO} + \frac{A}{3} - \frac{nB}{1.75} - \frac{nC}{2.5} - \frac{nD}{4} - \frac{nE}{5} - G}{MW} \right] - 0.26}{0.55} \right) - 3.69 \left(\frac{M}{\rho} \right) + (13.85a - 3.95b - 37.74c - 68.11d) \right]}{0.6917} \quad (6)$$

The above equation (6) is incorporated in the software code of LOTUSES and the way of incorporation of above logic in the computer programme is illustrated in a flow chart form in figure 5.

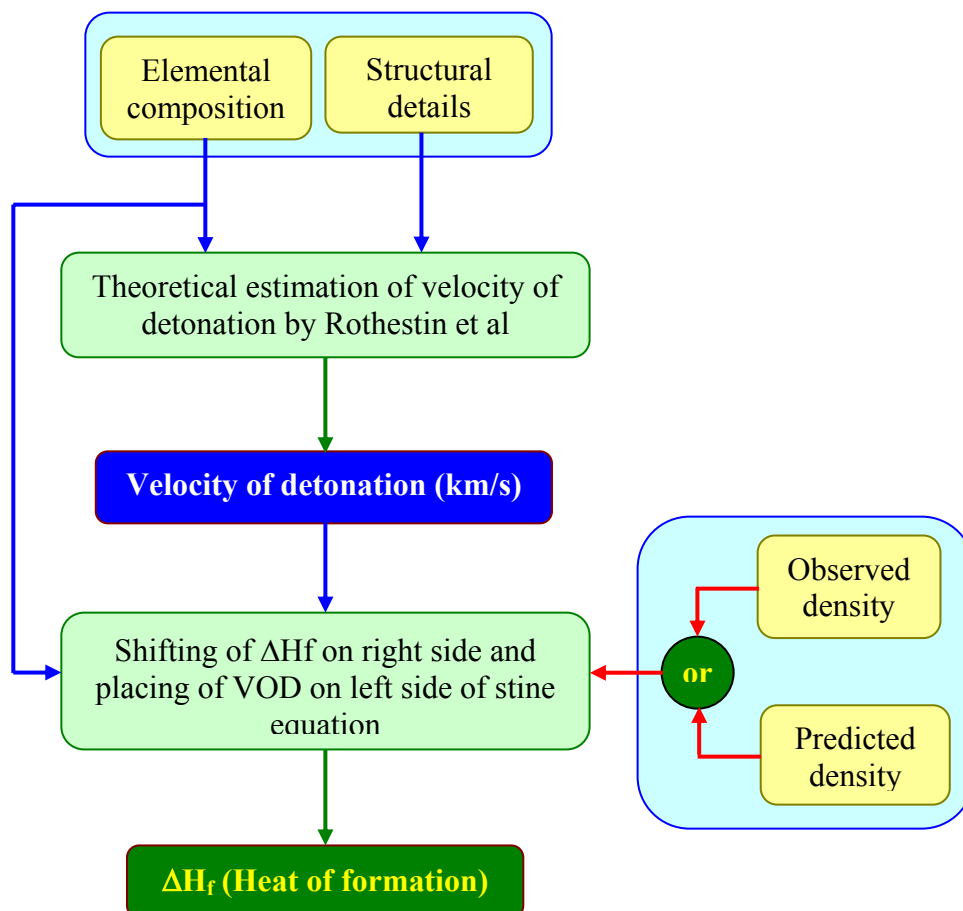


Fig 5. Logic tree behind the computer programming in estimation of heat of formation by methodology II

Since the software code of LOTUSES could predict the density and molecular weight of the HEM's, the users need not to enter these values to the LOTUSES. At the same time, if the user wishes to know the heat of formation of HEM's for particular required density, then the user can also give the density directly as input to LOTUSES. Hence from the equation (6) it is possible to estimate the heat of formation from elemental composition of the HEMs by LOTUSES.

4. RESULTS AND DISCUSSION

The validity of Stine and Kramer method extended to terminal functional groups such as –OH, C=O, –NH, –NO₂ groups and hydrogen attached to aromatic / nonaromatic carbon by authors (methodology I) was tested with 88 HEMs and the results are tabulated in Table 1. A linear straight line having R^2 as 0.9387 with straight-line equation of $y = 0.9559x + 1.1472$ was obtained on plotting (Figure 6) heat of formation reported in literature^[9,10] along the x-axis and predicted heat of formation by LOTUSES along the y-axis. The heat of formation specified in Table 1 and 2 are at 25°C and under constant volume condition. It is very clear from the bar

graph (Figure 7) that nearly 35, 16, 10, 8, 2, 9, 8 of test candidates gave heat of formation within the error limit of $\pm 10\%$, $\pm 20\%$, $\pm 30\%$, $\pm 40\%$, $\pm 50\%$, ± 50 to $\pm 100\%$ and above $\pm 100\%$.

The results obtained by combination of Rothstein et al and Stine (methodology II), which purely depends on the empirical formula of the molecule are compared with the reported literature values ^[9,10] and are tabulated in Table 2. A linear straight line having R^2 as 0.8358 with straight-line equation of $y = 1.2136x - 20.244$ was obtained on plotting (Figure 8) heat of formation reported in literature along the x-axis and predicted heat of formation by LOTUSES along the y-axis.

The compounds such as picric acid, trinitrobenzoic acid, styphnic acid, diazido dinitrophenol (DDNP), trinitropyridine (TNP) gave predicted heat of formation with error limit of $\pm 11 - \pm 34\%$. This method needs further exhaustive studies by considering large number of compounds having a wide variety of functional groups to arrive at a concrete conclusion.

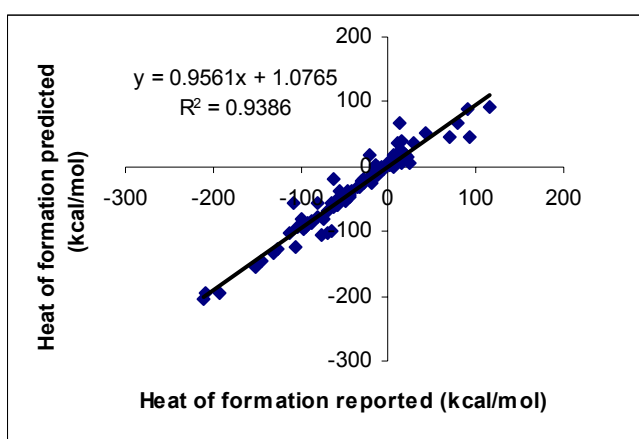


Fig 6. Experimental vs Predicted heat of formation derived by methodology I

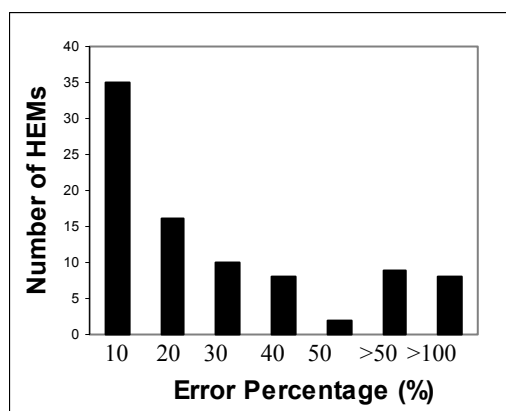


Fig 7. Error Percentage vs Number of HEMs

In view of the scanty reports on the availability of user friendly computer programmes for heat of formation prediction, this work is an humble beginning towards the quantitative prediction of heat of formation. Further work is in progress and will be reported elsewhere.

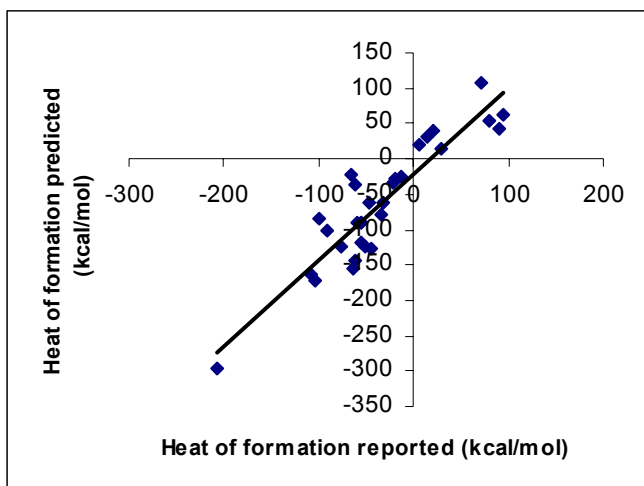
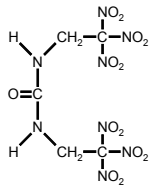
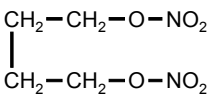
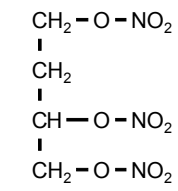
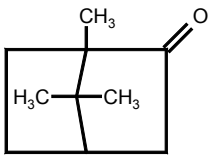
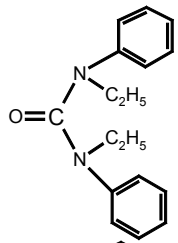
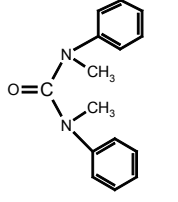
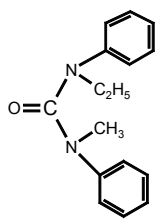
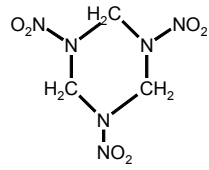
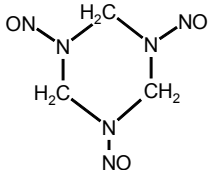
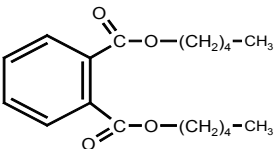
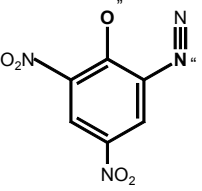
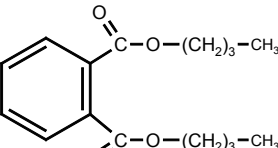
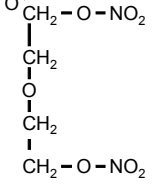
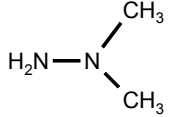
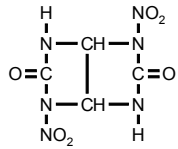
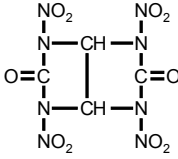
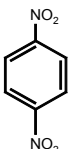


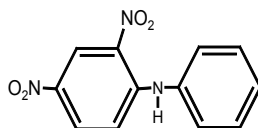
Fig 8. Experimental vs Predicted heat of formation derived by methodology II

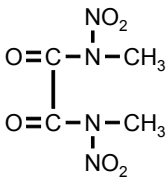
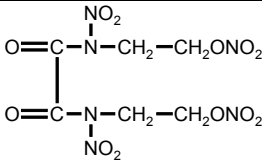
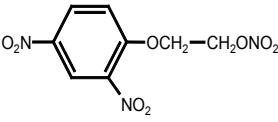
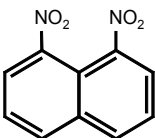
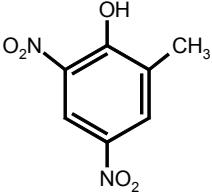
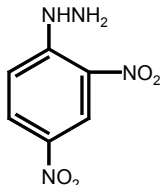
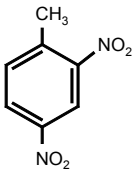
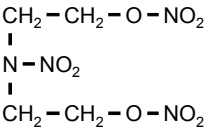
Table 1. Comparison of heat of formation predicated by LOTUSES and reported in literature based on methodology I

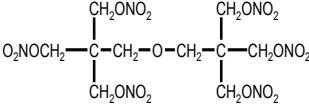
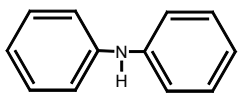
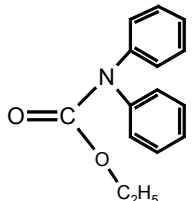
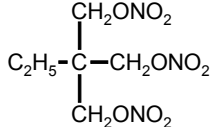
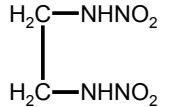
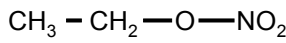
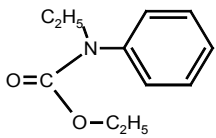
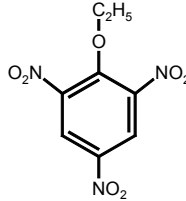
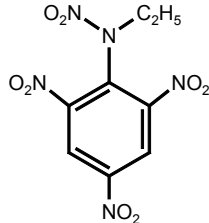
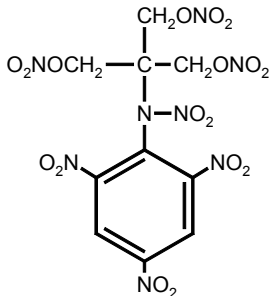
Sl No.	Name	Empirical formula	Structure	Heat of formation (kcal/mole)		
				Predicted	literature	Error%
1	Akardite - I (Diphenylurea)	$C_{13}H_{12}N_2O$		-17.18	-22.3	22.82
2	Akardite - II (Methyldiphenylurea)	$C_{14}H_{14}N_2O$		-13.68	-17.7	22.58
3	Akardite - III (Ethyldiphenylurea)	$C_{15}H_{16}N_2O$		-19.71	-27.9	29.31
4	Bi-trinitro ethyl nitramine (BTNENA)	$C_4H_4N_8O_{14}$		1.481	1.2	-23.43

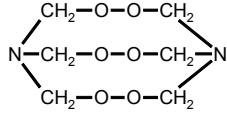
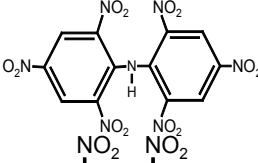
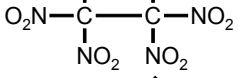
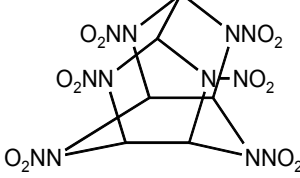
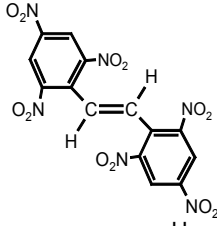
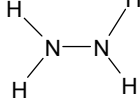
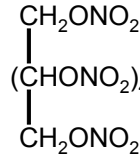
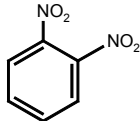
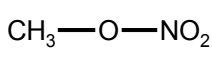
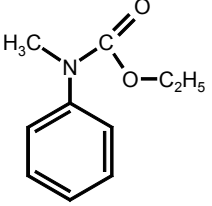
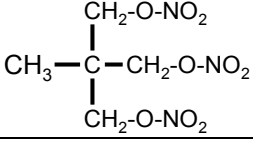
SI No.	Name	Empirical formula	Structure	Heat of formation (kcal/mole)		
				Predicted	literature	Error%
5	Bi-trinitroethylurea (BTNEU)	$C_5H_6N_8O_{13}$		-55.04	-64.9	15.2
6	Butanediol dinitrate	$C_4H_8N_2O_6$		-69.17	-70	1.224
7	Butanetriol trinitrate, BTTN	$C_4H_7N_3O_9$		-84.56	-88.5	4.428
8	Camphor	$C_{10}H_{16}O$		-79.62	-73.1	-8.967
9	Centralite I (Diethyl diphenyl urea)	$C_{17}H_{20}N_2O$		-23.98	-29.1	17.56
10	Centralite II (Dimethyl diphenyl urea)	$C_{15}H_{16}N_2O$		-11.93	-11.9	-0.403
11	Centralite III (Diethyl diphenyl urea)	$C_{16}H_{18}N_2O$		-17.95	-18.4	2.313
12	Cyclonite (RDX)	$C_3H_6N_6O_6$		16.41	19.73	16.82

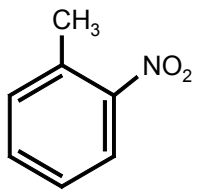
SI No.	Name	Empirical formula	Structure	Heat of formation (kcal/mole)		
				Predicted	literature	Error%
13	Cyclotrimethylene trinitrosamine	$C_3H_6N_6O_3$		45.51	70.44	35.4
14	Diamyl phthalate	$C_{18}H_{26}O_4$		-205.1	-210	2.369
15	Diazido dinitrophenol (DDNP)	$C_6H_2N_4O_5$		67.84	79.66	14.84
16	Dibutyl phthalate	$C_{16}H_{22}O_4$		-193.9	-194	-0.118
17	Diethyleneglycol dinitrate (DBP)	$C_4H_8N_2O_7$		-93.8	-94.4	0.606
18	Dimethylhydrazine (DMH)	$C_2H_8N_2$		9.399	14.63	35.75
19	Dingu	$C_4H_4N_6O_6$		-104.4	-77	-35.6
20	Sorguyl	$C_4H_2N_8O_{10}$		-98.37	-63.8	-54.17
21	Dinitrobenzene	$C_6H_4N_2O_4$		7.853	11.74	33.11

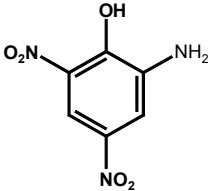
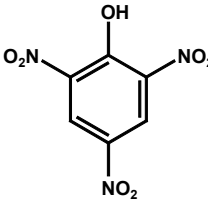
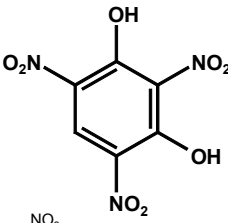
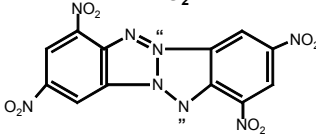


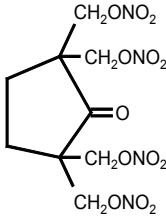
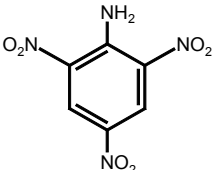
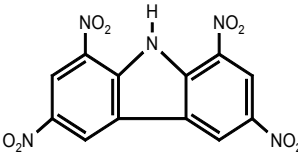
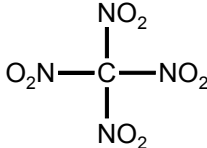
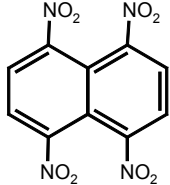
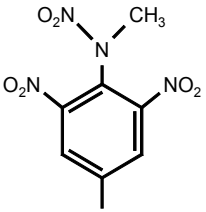
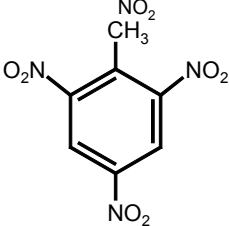
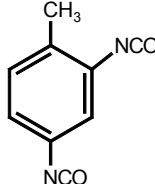
Sl No.	Name	Empirical formula	Structure	Heat of formation (kcal/mole)		
				Predicted	literature	Error%
22	Dinitro diphenylamine	$C_{12}H_9N_3O_4$		36.89	10.14	-263.8
23	Dinitrodimethyloxamide (DNDMOA)	$C_4H_6N_4O_6$		-101.1	-68.4	-47.95
24	Dinitrodioxy ethyloxamide dinitrate (NENO)	$C_6H_8N_6O_{12}$		-55.67	-108	48.6
25	Dinitrophenoxy ethyl nitrate	$C_8H_7N_3O_8$		-59.41	-61.1	2.72
26	Dinitronaphthalene	$C_{10}H_6N_2O_4$		23.78	14.65	-62.34
27	Dinitro orthocresol	$C_7H_6N_2O_5$		-43.88	-44	0.151
28	2,4-dinitrophenyl hydrazine	$C_6H_6N_4O_4$		39.34	16.08	-144.6
29	Dinitrotoluene, DNT	$C_7H_6N_2O_4$		-0.798	-6.95	88.52
30	Dioxyethylnitramine dinitrate, DINa	$C_4H_8N_4O_8$		-50.06	-55.6	9.963

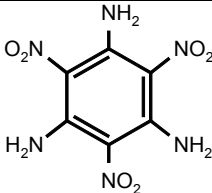
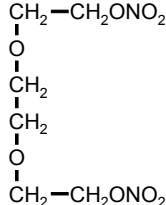
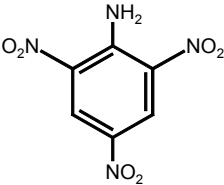
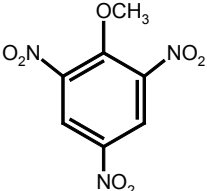
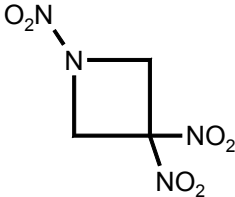
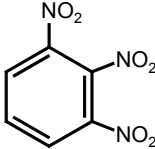
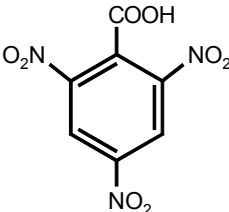
SI No.	Name	Empirical formula	Structure	Heat of formation (kcal/mole)		
				Predicted	literature	Error%
31	Dipentaerythrol hexanitrate, DPEHN	$C_{10}H_{16}N_6O_{19}$		-194.1	-208	6.638
32	Diphenylamine, DPA	$C_{12}H_{11}N$		50.64	42.75	-18.46
33	Diphenyl urethane	$C_{15}H_{15}NO_2$		-18.47	-61.8	70.1
34	Ethriol trinitrate (TMPTN)	$C_6H_{11}N_3O_9$		-94.15	-104	9.721
35	Ethylenedinitramine (EDNA)	$C_2H_6N_4O_4$		16.71	-20.5	181.6
36	Ethyl nitrate	$C_2H_5NO_3$		-38.41	-41.6	7.75
37	Ethyl phenyl urethane	$C_{11}H_{15}NO_2$		-124	-105	-17.59
38	Ethyl picrate	$C_8H_7N_3O_7$		-47.75	-43.9	-8.869
39	Ethyl tetryl	$C_8H_7N_5O_8$		18.02	5.92	-204.4
40	Heptryl	$C_{10}H_8N_8O_{17}$		-59.64	-57.3	-4.024

SI No.	Name	Empirical formula	Structure	Heat of formation (kcal/mole)		
				Predicted	literature	Error%
41	Hexamethylene triperoxide diamine	$C_6H_{12}N_2O_6$		-56.44	-80.1	29.54
42	Hexanitro diphenyl amine (HEXYL)	$C_{12}H_5N_7O_{12}$		6.483	14.01	53.73
43	Hexanitroethane (HNE)	$C_2N_6O_{12}$		4.027	24.33	83.45
44	Hexanitro hexaaza isowurtzitane (CL20)	$C_6H_6N_{12}O_{12}$		89.03	89.91	0.98
45	Hexanitrostilbene (HNS)	$C_{14}H_6N_6O_{12}$		14.25	20.9	31.8
46	Hydrazine	H_4N_2		24.52	13.88	-76.65
47	Mannitol hexanitrate (MHN)	$C_6H_8N_6O_{18}$		-154.4	-152	-1.567
48	orthodinitrobenzene	$C_6H_4N_2O_4$		4.125	4.11	-0.358
49	Methyl nitrate	CH_3NO_3		-31.11	-34.8	10.68
50	Methyl phenyl urethane	$C_{10}H_{13}O_2N$		-97.81	-96.5	-1.4
51	Metriol trinitrate (MTN)	$C_5H_9N_3O_9$		-88.54	-86.7	-2.151

SI No.	Name	Empirical formula	Structure	Heat of formation (kcal/mole)		
				Predicted	literature	Error%
52	Nitroaminoguanidine	$\text{CH}_5\text{N}_5\text{O}_2$	$\begin{array}{c} \text{NH}-\text{NH}_2 \\ \diagup \\ \text{HN}=\text{C} \\ \diagdown \\ \text{NHNO}_2 \end{array}$	8.869	8.85	-0.215
53	Nitroethane	$\text{C}_2\text{H}_5\text{NO}_2$	$\text{CH}_3-\text{CH}_2-\text{NO}_2$	-21.74	-30.8	29.4
54	Nitroglycerine (NG)	$\text{C}_3\text{H}_5\text{N}_3\text{O}_9$	$\begin{array}{c} \text{H}_2\text{C}-\text{O}-\text{NO}_2 \\ \\ \text{HC}-\text{O}-\text{NO}_2 \\ \\ \text{H}_2\text{C}-\text{O}-\text{NO}_2 \end{array}$	-78.95	-79.9	1.146
55	Nitroglycol (EGDN)	$\text{C}_2\text{H}_4\text{N}_2\text{O}_6$	$\begin{array}{c} \text{H}_2\text{C}-\text{O}-\text{NO}_2 \\ \\ \text{H}_2\text{C}-\text{O}-\text{NO}_2 \end{array}$	-48.64	-50.8	4.329
56	Nitroguanidine (NQ)	$\text{CH}_4\text{N}_4\text{O}_2$	$\begin{array}{c} \text{NH}_2 \\ \diagup \\ \text{HN}=\text{C} \\ \diagdown \\ \text{NHNO}_2 \end{array}$	-24.38	-19.6	-24.24
57	Nitroisobutyl glycerol trinitrate (NIBTN)	$\text{C}_4\text{H}_6\text{N}_4\text{O}_{11}$	$\begin{array}{c} \text{H}_2\text{C}-\text{O}-\text{NO}_2 \\ \\ \text{O}_2\text{N}-\text{C}-\text{CH}_2-\text{O}-\text{NO}_2 \\ \\ \text{H}_2\text{C}-\text{O}-\text{NO}_2 \end{array}$	-54.57	-48.4	-12.78
58	Nitromethane	CH_3NO_2	$\begin{array}{c} \text{H} \\ \\ \text{H}-\text{C}-\text{NO}_2 \\ \\ \text{H} \end{array}$	-15.72	-19.5	19.4
59	Nitrotoluene	$\text{C}_7\text{H}_7\text{NO}_2$		2.932	2.56	-14.55
60	Nitrourea	$\text{CH}_3\text{N}_3\text{O}_3$	$\begin{array}{c} \text{NHNO}_2 \\ \diagup \\ \text{O}=\text{C} \\ \diagdown \\ \text{NH}_2 \end{array}$	-60.42	-61.5	1.761
61	Octogen, HMX	$\text{C}_4\text{H}_8\text{N}_8\text{O}_8$	$\begin{array}{c} \text{H}_2\text{C}-\text{N}-\text{CH}_2 \\ \quad \quad \\ \text{O}_2\text{N}-\text{N} \quad \quad \text{N}-\text{NO}_2 \\ \quad \quad \\ \text{H}_2\text{C}-\text{N}-\text{CH}_2 \\ \quad \quad \\ \quad \quad \text{NO}_2 \end{array}$	37.5	28.68	-30.74

SI No.	Name	Empirical formula	Structure	Heat of formation (kcal/mole)		
				Predicted	literature	Error%
62	Pentaerythritol trinitrate (PETRIN)	$C_5H_9N_3O_{10}$	$ \begin{array}{c} \text{CH}_2\text{-O-NO}_2 \\ \\ \text{HO-CH}_2\text{-C-CH}_2\text{-O-NO}_2 \\ \\ \text{CH}_2\text{-O-NO}_2 \end{array} $	-127.5	-127	-0.006
63	Pentaerythritol tetrainitrate (PETN)	$C_5H_8N_4O_{12}$	$ \begin{array}{c} \text{CH}_2\text{-O-NO}_2 \\ \\ \text{O}_2\text{N-O-CH}_2\text{-C-CH}_2\text{-O-NO}_2 \\ \\ \text{CH}_2\text{-O-NO}_2 \end{array} $	-103.9	-114	8.75
64	Picramic acid	$C_6H_5N_3O_5$		-36.28	-55.6	34.7
65	Picric acid	$C_6H_3N_3O_7$		-38.96	-47.4	17.77
66	Propylene glycol dinitrate	$C_3H_6N_2O_6$	$ \begin{array}{c} \text{CH}_3 \\ \\ \text{CH-O-NO}_2 \\ \\ \text{CH}_2\text{-O-NO}_2 \end{array} $	-63.57	-62.2	-2.162
67	Propyl nitrate	$C_3H_7NO_3$	$ \begin{array}{c} \text{CH}_3 \\ \\ \text{CH}_2 \\ \\ \text{CH}_2 \\ \\ \text{O} \\ \\ \text{NO}_2 \end{array} $	-44.02	-47.8	7.984
68	Styphnic acid	$C_6H_3N_3O_6$		-81.69	-99.7	18.09
69	Tetranitrobenzo-1,3a,4,6a-tetrazapentalene (Tacot)	$C_{12}H_4N_8O_8$		93.34	115.7	19.34

SI No.	Name	Empirical formula	Structure	Heat of formation (kcal/mole)		
				Predicted	literature	Error%
70	Tetramethylolcyclopentanone tetranitrate	$C_9H_{12}N_4O_{13}$		-144.7	-144	-0.202
71	2,3,4,6-Tetranitroaniline (TNA)	$C_6H_3N_5O_8$		-1.369	-13.7	89.98
72	Tetranitrocarbazole (TNC)	$C_{12}H_5N_5O_8$		7.378	9.83	24.95
73	Tetranitromethane (TNM)	CN_4O_8		19.6	16.55	-18.42
74	Tetranitronaphthalene (TNN)	$C_{10}H_4N_4O_8$		16.32	15.84	-3.047
75	Tetryl	$C_7H_5N_5O_8$		65.81	13.43	-390
76	2,4,6-Trinitotoluene (TNT)	$C_7H_5N_3O_6$		-4.528	-6.06	25.27
77	2,4-Toluene Diisocyanate (TDI)	$C_9H_6N_2O_2$		7.192	0.96	-649.2

SI No.	Name	Empirical formula	Structure	Heat of formation (kcal/mole)		
				Predicted	literature	Error%
78	1,3,5-Triamino-2,4,6-trinitrobenzene (TATB)	$C_6H_6N_6O_6$		-1.162	-12.5	90.72
79	Triethyleneglycol dinitrate (TEGN)	$C_6H_{12}N_2O_8$		-133.8	-132	-1.367
80	Trinitroaniline (TNA)	$C_6H_4N_4O_6$		2.361	-13.7	117.3
81	Trinitroanisole	$C_7H_5N_3O_7$		-32.7	-32.2	-1.659
82	1,3,3-Trinitroazetidine (TNAZ)	$C_3H_4N_4O_6$		-1.591	6.24	125.5
83	1,3,5-Trinitrobenzene	$C_6H_3N_3O_6$		4.123	4.85	14.99
84	Trinitrobenzoic acid	$C_7H_2N_3O_7$		-88.24	-92.2	4.254

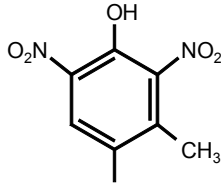
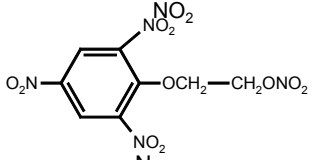
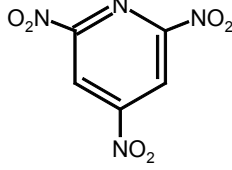
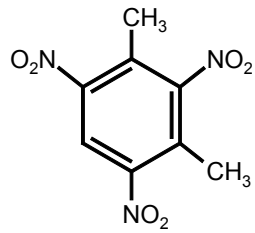
SI No.	Name	Empirical formula	Structure	Heat of formation (kcal/mole)		
				Predicted	literature	Error%
85	2,4,6-Trinitrocresol	$C_7H_5N_3O_7$		-47.61	-55.9	14.75
86	Trinitrophenoxethylnitrate	$C_8H_6N_4O_{10}$		-55.4	-60.4	8.255
87	Trinitropyridine (TNP)	$C_5H_2N_4O_6$		46.42	93.56	50.38
88	2,4,6-Trinitroxylene (TNX)	$C_8H_7N_3$		-13.18	-19	30.49

Table 2 Comparison of heat of formation predicated by LOTUSES and reported in literature based on methodology II

SI No	Name	Formula	Density (g/cm ³)	Heat of formation (kcal/mole)		
				Predicted	literature	Error%
1	1,3,5-Triamino-2,4,6-trinitrobenzene (TATB)	$C_6H_6N_6O_6$	1.93	-25.68	-12.5	-105.17
2	Trinitroanisole	$C_7H_5N_3O_7$	1.61	-62.27	-32.2	-93.56
3	Ethylenedinitramine (EDNA)	$C_2H_6N_4O_4$	1.75	-33.56	-20.5	-63.99
4	Ethriol trinitrate (TMPTN)	$C_6H_{11}N_3O_9$	1.48	-170.97	-104	-63.94
5	2,4,6-Trinitrocresol	$C_7H_5N_3O_7$	1.68	-90.56	-55.9	-62.15
6	Dioxyethylnitramine dinitrate, DINA	$C_4H_8N_4O_8$	1.67	-89.85	-55.6	-61.60
7	Dingu	$C_4H_4N_6O_6$	1.98	-123.87	-77	-60.87
8	Dinitrodioxy ethyloxamide dinitrate (NENO)	$C_6H_8N_6O_{12}$	1.72	-164.29	-108	-51.70
9	Trinitrophenoxethylnitrate	$C_8H_6N_4O_{10}$	1.68	-91.48	-60.4	-51.52
10	Cyclotrimethylene trinitrosamine	$C_3H_6N_6O_3$	1.5	106.27	70.44	-50.87

SI No	Name	Formula	Density (g/cm ³)	Heat of formation (kcal/mole)		
				Predicted	literature	Error%
11	Dipentaerythrol hexanitrate (DPEHN)	C ₁₀ H ₁₆ N ₆ O ₁₉	1.63	-295.32	-208	-42.07
12	Nitroguanidine (NQ)	CH ₄ N ₄ O ₂	1.76	-27.14	-19.6	-38.35
13	Picric acid	C ₆ H ₃ N ₃ O ₇	1.767	-62.18	-47.4	-31.24
14	Trinitrobenzoic acid	C ₇ H ₂ N ₃ O ₇	1.54	-102.42	-92.2	-11.14
15	Styphnic acid	C ₆ H ₃ N ₃ O ₆	1.83	-83.54	-99.7	16.22
16	Diazido dinitrophenol	C ₆ H ₂ N ₄ O ₅	1.63	54.88	79.66	31.09
17	Trinitropyridine (TNP)	C ₅ H ₂ N ₄ O ₆	1.77	61.47	93.56	34.29
18	Nitrourea	CH ₃ N ₃ O ₃	1.69	-37.09	-61.5	39.68
19	Octogen, HMX	C ₄ H ₈ N ₈ O ₈	1.902	15.11	28.68	47.29
20	Hexanitro hexaaza isowurtzitane (CL20)	C ₆ H ₆ N ₁₂ O ₁₂	2.04	43.31	89.91	51.82
21	Bi-trinitroethylurea (BTNEU)	C ₅ H ₆ N ₈ O ₁₃	1.861	-22.50	-64.9	65.32

5. CONCLUSION

In the HEMs community there is considerable interest to design exotic high-performance molecules. This paper presents, one aspect of estimating the heat of formation of HEMs to predict performance level. A method to predict the heat of formation of CHNO type HEMs as a function of elemental composition has been developed and appended in a windows based software code. The Stine et al method of predicting heat of formation as a function of structural information has been extended to terminal group such as -OH, -NH, -NH₂, -NO₂, -H, C=O in the present work. The linear regression coefficient $R^2 = 0.9387$ and 0.8358 are obtained for heat of formation predicted by LOTUSES vs reported in literature, using methodology I and II respectively. It reflects that the predicted values by methodology I are in close agreement with heat of formation as reported in literature. However further refinement of computer code is in progress to achieve higher accuracy in the prediction of heat of formation. The estimation of heat of formation using LOTUSES will be useful for designing possible high-energy molecules based on the constituent values. That is, constituents with highly negative heat of formation can be ruled out early on in the design stage of the molecule, and hence substantially reduce the number of molecular possibilities that must be further examined.

Acknowledgement

Authors are highly grateful to Shri AS Rajagopal, Director, Armament Research & Development Establishment, Pune and Dr. Haridwar Singh, Outstanding Scientist and Director, High Energy Material Research Laboratory, Pune for providing infrastructure and permission to present this paper. Authors express their deep sense of gratitude to Shri S.R. Madhavan, Scientist 'E', OSD-to-Director, ARDE for his inspiration and constant motivation.

REFERENCE

- [1] H. MUTHURAJAN, R. SIVABALAN, N. VENKATESAN, M.B.TALAWAR AND S.N.ASTHANA: *Computational approaches for performance prediction of High energy Materials*, pp.470-486, Proceedings of 4th International High Energy Materials Conference, India, 2003
- [2] H. MUTHURAJAN, SIVABALAN.R, M.B.TALAWAR AND S.N.ASTHANA: *Artificial Intelligence methodology for Thermodynamic Analysis of High Energetic Materials*, pp.225-228, Proceedings of 14th National Symposium on Thermal Analysis, India, 2004
- [3] STANLEY F SARNER: *Propellant Chemistry*, Reinhold publishing corporation, New York, 1966
- [4] J.R. STINE AND J.F. ERAMER: *Estimation of Heats of formation and the development of chemical databases useful for energetic materials*, pp.53-56, 26th JANNAF Combustion meeting, Jet Propulsion Laboratory, Pasadena, California, CPIA Publication, Vol. II, 1989
- [5] PAUL W. COOPER: *Introduction to Detonation Physics*", Chapter 4 of "*Explosive Effects and Applications*", pp.115-135, edited by Jonas A. Zukas and William P. Walters, Springer-Verlag, New York, United States of America, 1997
- [6] L.R. ROTHSTEIN AND R.PETERSEN: *Predicting High Explosive Detonation Velocities from their Composition and Structure*, Propellants and Explosive 4, pp.56-60, 1979
- [7] L.R. ROTHSTEIN: *Predicting High Explosive Detonation Velocities from their Composition and Structure (II)*, Propellants and Explosive 6, pp.91-93, 1981
- [8] J.R. STINE: *On predicting properties of explosives – detonation velocity*, Journal of Energetic Materials, Vol 8, pp.41-73, 1990
- [9] ICT DATABASE OF THERMOCHEMICAL VALUES, Version 3.0: Fraunhofer Institut Chemische Technologie, 2001
- [10] RUDOLF MEYER, JOSEF KOHLER, AXEL HOMBURG: *Explosives*, fifth edition, Wiley-Vch publications, Germany, 2002

STUDY OF TNT METABOLISM IN PLANTS AND ITS PRACTICAL APPLICATION FOR ENVIRONMENT DECONTAMINATION

A. Nepovím*, R. Podlipná*, S. Zeman**, Z. Jalový**, A. Gerth*** and T. Vaněk*

* Institute of Organic Chemistry and Biochemistry, Flemingovo nám. 2, CZ-166 10 Praha 6

** DTTX, University of Pardubice, CZ-532 10 Pardubice

*** Bioplanta GmbH, Benndorfer Landstraße 2, D-04509 Leipzig

Abstract:

*Although a contamination of sites by TNT is an environmental problem all over the world, the fate of its degradation products claims attention as well. A study of metabolism of TNT in plants was focused on degradation of 4-amino-2,6-dinitrotoluene (4-ADNT), a stable degradation product. Two plant species *Senecio jacobea* and *Buphthalmum salicifolium* cultivated under in vitro conditions in the presence of different concentration of 4-ADNT for 3 weeks. The highest concentration 50 mg/l of 4-ADNT was degraded by plants within two weeks but any major degradation product was not detected in the medium. The IC_{50} was not determined in the range of used concentration therefore a linear regression was used for prediction of the IC_{50} and 61,8 mg/l and 70,2 mg/l were calculated for *S. jacobea* and *B. salicifolium*, respectively.*

Keywords: TNT, ADNT, phytoremediation, biodegradation, plant metabolism

1. INTRODUCTION

As a result of munitions production and storage, 2,4,6-trinitrotoluene (TNT) and its byproducts are widespread and persistent contaminants of soil and groundwater at a number of government facilities. Since it is toxic and poses a serious environmental risk ^[1], contaminated soil and water are currently being remediated. During the evaluation of remediation processes, phytoremediation has been identified as a viable low-cost option for the cleanup of TNT-contaminated media ^[2, 3]. The TNT is covalently bound in the soil and TNT transformation products to plant derived organic matter is mediated by alkylation and acetylation reactions, rather than by 1,4 addition of TNT-derived nitrogenous groups to quinones of the humic material. The mechanisms for the formation of amide bonds during the transformation of TNT in soils lead to accumulation of macromolecular polyamide-type structures ^[4].

A metabolism of TNT is intensively studied to better understand degradation processes in plants ^[5-7]. Phytoremediation of TNT represents an alternative technology for cleaning of the environment at sites contaminated by nitroaromatic compounds. The efficiency of degradation of TNT is affected by toxicity of TNT and its degradation products to plant itself and by bioavailability.

In our study we focused on the degradation of one of the first stable identified degradation product – 4-aminodinitrotoluene by two plant species widely growing in sandy or nutrient/humus poor soil typical for the areas of ammunition factories.

2. MATERIAL AND METHODS

2.1 Plant material

The plant material was collected on the base of Czech – Germany cooperation. The species of *Senecio jacobea* (ragweed) and *Buphthalmum salicifolium* (ox eye) were found at a site of former ammunition factory contaminated by TNT and the seeds were harvested. The seeds of both plant species were surface sterilized and sown on the agar-solidified Murashige and Skoog ^[8] medium cultivated on liquid medium prepared according to and supplemented with phytohormone 6-benzylaminopurine (BAP, 5 mg/l). The formation of roots was initiated on a hormone-free medium. The plants were subcultured every 4-5 weeks on a fresh medium.

2.2 HPLC analysis

The content of TNT and its degradation products was analyzed by High Performance Liquid Chromatography (HPLC). The sample of 20 µl was separated on stainless steel column (250x4 mm) packed by reverse phase Si-C₁₈ (size: 7 µm; Biosphere, Labio Praha, CZ) using a linear gradient of mobile phases (10→100% methanol in 40 min). The concentration of known compounds was calculated from particular peak areas integrated from chromatogram at 230 nm ^[4].

3. RESULTS AND DISSCUSION

The selected plant species of *S. jacobea* and *B. salicifolium* degraded 4-amino-2,6-dinitrotoluene (4-ADNT) of concentration of 50 mg/l *in vitro* within 2 weeks (Fig. 1). 4-ADNT is less soluble than the parent TNT in water. The concentration inhibiting the growth in 50% (IC₅₀) was not reached therefore IC₅₀ was predicted according to a linear regression from values shown in the Table 1. 4-ADNT inhibited growth of *S. jacobea* and *B. salicifolium* at concentration of 61,8 mg/l and 70,2 mg/l, respectively.

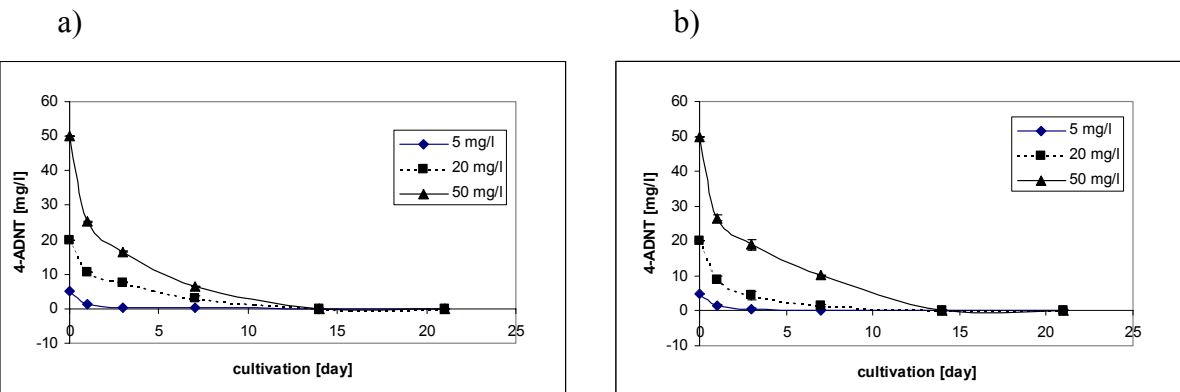


Fig 1. Degradation of 4-ADNT by ragweed (*S. jacobea*) and ox eye (*B. salicifolium*) *in vitro*. A decrease of 4-ADNT in the medium was determined by HPLC.

Table 1. The effect of 4-ADNT at different concentration on the biomass production. Growth values (GV) were calculated according to equation $GV=(w_t-w_0)/w_0$ where w_0 is inoculum and w_t is biomass in 3 weeks.

ADNT [mg/l]	GV (<i>B. salicifolium</i>)	GV (<i>S. jacobea</i>)
0	4,99	17,72
5	7,15	6,80
20	11,22	15,66
50	8,64	10,38

The ability of selected wild plants to degrade 4-ADNT can be used up for searching of responsible enzymes participating degradation of TNT and its subsequent degradation products. The genes encoding appropriate participating enzymes can be further used up for construction of genetically modified plants naturally having higher biomass production capacity than shrub as *S. Jacobea* and *B. Salicifolium* appears.

Acknowledgment:

Thank to Prof. Ing. Svatopluk Zeman, Dr.Sc. and Ing. Zdeněk Jalový, Ph.D. for synthesis and preparation of degradation products of TNT.

The work was supported by GAČR project no. 206/02/P065, COST 837.1, MŠMT project Kontakt no: CZ 01/024 and Research project no: Z4 055 905.

REFERENCES

- [1] M. SIMINI, R. S. WENSTEL, R. T. CHECKAI, C. T. PHILLIPS, N. A. CHESTER, M. A. MAJOR, J. C. AMOS: Environ. Toxicol. Chem., **14**, 623-630, 1995
- [2] J. L. SCHNOOR, L. A. LICHT, S. C. MCCUTCHEON, N. L. WOLFE, L. H. CARREIRA: Environ. Sci. Technol., **29**, 318-323, 1995
- [3] A. J. PALAZZO, D. C. J. LEGGETT: Environ. Qual., **15**, 49-52, 1986.
- [4] H. KNICKER: Sci Total Environ., **308**, 211-220, 2003
- [5] T. VANĚK, A. NEPOVÍM, R. PODLIPNÁ, S. ZEMAN: Water, Air & Soil Poll.: Focus **3**, 259-267.
- [6] R. BHADRA, D. WAYMENT, J. B. HUGHES, J. V. SHANKS: Environ. Sci. Technol., **33**, 446-452, 1999
- [7] SNELLINX Z., NEPOVÍM A., TAGHAVI S., VANGRONSVELD J., VANEK T., VAN DER LELIE D.: Environ. Sci. Poll. Res., **9**, 48-61, 2002
- [8] T. MURASHIGE and F. SKOOG: Physiol. Plant., **15**, 473-497, 1962

TEMCLEV-EX.

ADAPTATION OF TEMCLEV SYSTEM TO FIRE AND EXPLOSION HAZARD ASSESSMENT IN MANUFACTURING OF EXPLOSIVES

T. Piotrowski, T. Sałaciński, M. Frączak and D. Buczkowski

Instytut Przemysłu Organicznego, Annopol 6, 03-236 Warszawa, Poland

Abstract:

The main assumptions of a new research-technical project have been presented, which aim is to adapt the system of evaluation and classification the process hazards in chemical industry, called shortly Temclev, to the specificity of manufacturing of explosives. A brief description of the original Temclev system has been given as well as a direction of its transformation into a new version – Temclev-Ex.

Keywords: explosion-fire hazard ranking, risk assessment, explosives manufacturing

1. INTRODUCTION

The problems connected with an assurance of industrial production safety are growing up with development of technology, which parameters of run are coming closer and closer to the critical conditions. It is particularly important on the area of manufacturing of explosives (HE).

This project is dedicated to enlarging “The system of identification, evaluation and classification the process hazards in chemical industry” called shortly from its English name Temclev [1-5], with problems connected to identification, evaluation and classification the process hazards in manufacturing explosives and pyrotechnics. It is a very specific industrial branch, exposed to risk of explosions and fires on every stage of manufacturing process as well as during storage the final products. The original Temclev method, elaborated at the frames of research project PBZ 03807 sponsored by the State Committee for Scientific Research in the years 1996-1998, did not covered such problems. However the requirements of environmental protection and labor protection, which dictate a risk assessment of the operated processes, effect a need of an individual and collective hazard assessment at work process as well as an assessment of risk level caused by the given plant for its surroundings [6-10].

It has been assumed, that for doing such an assessment, the new, specific for HE, indices of the process hazards should be elaborated. Such indices should take into account material properties, types of technological processes, apparatuses and devices used, safety measures, supervising and organizational actions. In practice it will be a quite new subsystem connected with the standardized methods of explosives testing, a way of evaluation their physicochemical and functional properties as well as with legislation (national and EU) regarding manufacturing,, storage, handling and using HE on the civil and military area.

2. A BRIEF DESCRIPTION OF TEMCLEV SYSTEM

Fire and explosive properties of processed substances (media) are in Temclev system the basic criteria for hazard evaluation. They give an elementary level of potential hazard accumulated in those materials, which may cause a fire or explosion hazard on a process plant. This has been expressed by the mathematic formula below, given for a conventional description of the process hazard level of a “process unit” being evaluated.

$$ZP = [(W + P)] \cdot S \cdot (T/T_{ZAB}) \quad (1)$$

where **P** - fire index, **W** - explosion index, **T** - technological index,
S - specific material properties index, **T_{ZAB}** - protection index.

The value of ZP index is a resultant of two parts coming from dangerous media properties and process conditions. Proposed mathematical equation is easy and shows clearly all the elements of process hazard.

The equation (1) is based on, coming from calculus of probability, so called „logical product” of two components. Material component of hazard [(P+W)S] and process component (T/T_{ZAB}). To occur a potential hazard state in a given industrial process both of the components mentioned above must be present simultaneously. That means: dangerous media (combustible substances, explosive atmospheres, oxidizing agents, etc.) and generated by a process itself the strong enough stimuli, which activate the properties of media used. Using the proposed formula (1) it is easy to realize and proof mutual interactions of the process components and to take satisfactory corrective and protective measures for all elements of danger.

Decreasing a ZP value may be effected by decreasing the material indices values (exchanging media into less dangerous, adding inert materials not changing the final properties of a product) and/or decreasing the process hazard indices (changes of process conditions, devices, using more or better safety measures, process monitoring, computer control etc.).

2.1 Material hazard indices

The fire index, P, has been constructed with taking into account the heat of combustion of a substance and a certain, characteristic temperature. For combustible gases it is self-ignition temperature, for combustible liquids – its flash point and for combustible solids in dust, powder or granular form – ignition temperature of their volatile thermal decomposition products.

The explosion index, W, has been constructed with taking into account a minimum ignition energy and a range of explosibility (UEL – LEL, expressed in v/v%) of given gas or vapour. For dust-air mixtures only the lower explosion limits (LEL, expressed in g/m³) have been used.

The sum of indices P and W has been enlarged of a value of specific material index S. This index has been constructed with taking into account thermal stability (s₁) of substances, their reactivity (s₂) and oral toxicity on inhalation (s₃). It shows the influence of those properties on increasing the fire-explosion hazard level and on troubles in brake-down fighting. The construction of all indices has been described in details in [1-3].

2.2 Process hazard indices

An assumption has been made that processing a substance causes hazard increasing. Dangerous properties of processed media may be activated in running process. In the given equation (1) that role plays technological index T . It has been constructed using numerical notes given for:

- I. **General characteristics of a process (operation) – TO.** In this group the information about dangerous material, process/operation type, a way of acting, devices/apparatuses used and process/operation parameters have been taken into account.
- II. **Detailed characteristics such unit operations – TF,** as: storage, transport, supplying, emptying, dosage, mixing, distribution, sorting, pumping, compression, heating, mass transfer operations and others.
- III. **Chemical process characteristics – TP.** In this group all chemical processes have been divided in the respect of thermal effect, system homogeneity, catalytic agent presence and reaction phase (gaseous, liquid, solid, mono and multi-phase).
- IV. **Specific hazards characteristics – TS.** In this group such information have been taken into account as: plant area, apparatuses height, potential emission sources, corrosion, static electricity, extremely difficult processes, fire and/or explosion zone presence, processes in explosive range and many others.

The use of protective measures decreases process hazard level. According to equation (1) resultant note is diminished T_{ZAB} note. The index T_{ZAB} is very important in the system. It shows the areas where a hazard should be reduced and helps acting in that direction. In the range of using protective measures, which may be technical, technological and organizational, any selected unit should be analyzed in 4 thematic groups:

- I. **Monitoring emergency states – KS.** In this group checking of fixed values of process parameters, sensors presence, alarm systems, automatic block systems, computer control and others have been taken into account.
- II. **Failure's preventive measures – ZA,** including: automatic control, protective atmosphere, fire extinguishing agents, construction material used, apparatuses design and so.
- III. **Emergency systems and control – SA,** including: cut-off valves, draining valves, safety valves, explosion suppression systems, fire fighting systems, flame arrestors, water supplying systems, water sprinklers and curtains, cooling systems, safety shut down systems, smoke ventilation and many others.
- IV. **Organization and safety management - DO.** In this group operating instructions, safety management, safety audits and training, plant supervision, cooperation with fire-brigade and others have been taken into account.

3. ASSUMPTIONS TAKEN FOR TEMCLEV-EX

An assumption has been taken that, keeping former segment construction of the system, the new material indices and above described types of process indices for HE shall be created. A new evaluation path for HE technologies shall be elaborated, giving a subsystem called Temclev-Ex. All the indices shall be computed in the same way as in original Temclev system using tables with notes. A new "Evaluation manual" for different kinds of HE manufacturing processes shall be prepared and edited

The authors of this paper foresee an addition a fully new segment to the subsystem, concerning a risk level assessment in HE manufacturing. They are going to use for this purpose the modified “Risk Score” method – adopted to the process conditions, called “PRAM”^[11]. The well known foreign ranking systems used in western industrialized countries^[12,13] have not such a segment.

One of the very important parts of the project is a software for rapid evaluation of process hazards. Such a functional tool is required by industrial technical staff and without it any – even the best – evaluation system has no chance for practical application in modern industry. A basis for such a complex software shall be “Temclev-Ocena”^[4]. This is a software written for Temclev system, but for new applying it needs many changes and a new line of approach. The new software has to be “user-friendly” and offer the user useful “system help” and links to important data bases.

4. PROPOSED DIRECTIONS OF TEMCLEV SYSTEM TRANSFORMATION

Primary proposal for transformation the equation describing a hazard level of a process unit ZP in Temclev-Ex for manufacturing and processing explosives presents as follow:

$$ZP_{Ex} = [(A_{Rw} + B_{Rz}) \cdot S_{Ex}] \cdot (T/T_{ZAB}) \quad (2)$$

where: **A, B** – the notes of $R_{z,w}$ parameters,

$R_{w,z}$ – indices describing explosives parameters according to Polish legislation:

$R_z = 4,71 \times 10^{-4} (Q_w \times V_g)^{1/2}$ - hazard index – computed from chemical reaction equation (Q_w – heat of explosion, V_g – volume of explosion gases),

$R_w = (R_M \times R_{Temp})^{1/2}$ - sensitivity index – computed on the base of tests results

($R_M = 0,076 (R_U \times R_T)^{1/2}$ - mechanical sensitivity index, $R_{Temp} = 39,02 \times \log (T_p/373)$ - thermal sensitivity index (thermal decomposition), T_p – thermal decomposition temperature in the range from +373 K to +673 K, R_U – impact sensitivity in the range from 1J to about 50J (49,1J), R_T - friction sensitivity in the range from 0,1 N to about 360N (353N))

The range of proposed indices are shown below:

$0 < R_z < 1,10$ - the bigger its value- the higher hazard level,

$0 < R_w < 10$ - the bigger its value – the material lower sensitive,

R_M - the bigger its value – the material lower sensitive,

R_{Temp} - the bigger its value – the material lower sensitive,

The values of A and B notes have a discret digital form. They are taken from the tables of evaluation the R_w/R_z indices described above. The evaluation has been established in a range from 1 to 25 units to save a ZP scale from original Temclev system (see equations 1 and 2).

Table 1. *The reference list of explosives illustrating the assumptions of a system (data taken from literature ^[14-17] and Polish standard PN-E-05205:1997)*

Material name	R _Z	R _W	W _{Z, min} [J]
Ammonium Nitrate (AN)	0,59	6,67	1·10 ⁻³
Ammonium nitrate based explosives	0,91	5,35	6,5 - 12
ANFO (94,5/5,5)	0,92	5,73	1·10 ⁻³
Black powder	0,39	7,07	8,0·10 ⁻¹ aerosol 2,3·10 ⁻² dust deposit
Ethylene glycol dinitrate (EGDN)	1,06	1,72	1·10 ⁻³
Hexogen (RDX), pure	1,00	3,23	1,0·10 ⁻² aerosol 1,8·10 ⁻¹ dust deposit
Lead azide	0,29	1,44	4,0·10 ⁻⁶ aerosol 1,0·10 ⁻⁸ dust deposit
Lead trinitroresorcinate (Lead styphnate, TNR-Pb)	0,39	0,97	3,8·10 ⁻⁷
Mercury fulminate	0,29	1,36	1,0·10 ⁻⁴
Nitroglycerine (Ngl)	1,00	1,61	2,0·10 ⁻³
Octogen (HMX)	1,03	4,11	1·10 ⁻³
Picric acid (TNF)	0,77 – 0,90	5,33	1·10 ⁻³
Pentryt (PETN)	1,01	2,05	6,2·10 ⁻¹ dust deposit
Single base propellants (nitrocellulose / difenylamine)	0,87	2,98	9,0·10 ⁻² aerosol 3,0·10 ⁻² dust deposit
Tetrazene	0,81	0,54	1,3·10 ⁻⁴
Tetryl	0,90	2,94	4·10 ⁻³ aerosol
Trinitrotoluene (TNT)	0,83 – 0,86	6,32	3,0·10 ⁻³ aerosol 3,0·10 ⁰ dust deposit

For computing a digital value of a specific material properties index, S_{Ex}, the equation given below has been proposed:

$$S_{Ex} = 1 + \sum (s_i / 10) \quad \text{for } i = 1, 2, \dots, n \quad (3)$$

where: **s_i** – a digital note for every kind of specific material properties evaluation, like: sensitivity for flame, electric/electrostatic spark, toxicity of combustion/decomposition products for humans and environment, HE type, process type (explosion or detonation), a range of acting (projection) and others.

The authors of this paper tried to connect some properties of HE with ADR divisions of class 1. An example has been shown in table 2 below.

Table 2. *An example of some specific material properties evaluation.*

Divisions of class 1 (ADR)	Description of ADR divisions of class 1 / HE type	Proposed note
1.1	Substances and articles which have a mass explosion hazard (which affects almost the entire load virtually instantaneously)	10
1.5	Very insensitive substances which have a mass explosion hazard (for example brisant explosives type B or E)	5
1.2	Substances and articles which have a projection hazard but not a mass explosion hazard	3
1.3	Substances and articles which have a fire hazard and either a minor blast hazard or a minor projection hazard or both, but not a mass explosion hazard	2
1.4 1.6	Substances and articles which present no significant hazard and extremely insensitive articles which do not have a mass explosion hazard	1

5. SOME QUESTIONS AND PROBLEMS TO SOLVE IN THIS PROJECT

1. Should the system cover chemical processes only, that means until manufacturing a raw product or purified product (HE)?
2. Should the system cover other types of processes / operations, for example: shell filling, manufacturing other object containing HE, that means non chemical processes?
3. What a range of notes for hazard indices to use in Temclev-Ex? The same scale as in original Temclev system (used now) or different (extended)?
4. How do the pyrotechnics should be treated in the system? As a part of basic HE assessment or as an independent assessment?

Acknowledgement

This project is sponsored by the State Committee for Scientific Research as a grant number 4 T09B 06325 entitled: “Adaptation of Temclev System to Fire and Explosion Hazard Assessment in Manufacturing of Explosives”.

REFERENCES

- [1] PIOTROWSKI T., HANCYK B., GŁOWIŃSKI J., SEWERYNIAK M.: Materiały II Kongresu Technologii Chemicznej, Wrocław 15 – 18.09.1997, tom IV, 1798-1808, Dolnośląskie Wydawnictwo Edukacyjne, Wrocław, 1998.
- [2] PIOTROWSKI T., HANCYK B., GŁOWIŃSKI J.: Organika - Prace Nauk. Inst. Przem. Org., 1997-98, cz. II, 89-99.
- [3] PIOTROWSKI T.: Przemysł Chemiczny 78/12, 419-421, 1999
- [4] PIOTROWSKI T., HAŁAT A.: Organika – Prace Nauk. Inst. Przem. Org., , 149-163, 1999-2000
- [5] PIOTROWSKI T.: Przemysł Chemiczny 82/8-9, 1318-1321, 2003
- [6] Ustawa „Prawo ochrony środowiska” z 27.04.2001, Dz. U. Nr 62 poz. 627. “Environmental Protection Law”, 20.06.2001
- [7] Council Directive 96/82/EC of 9 December 1996 on the Control of major-accident hazards involving dangerous substances. Official Journal of the European Communities L 10, 14, Vol. 40, 13-33, January 1997
- [8] Rozporządzenie Ministra Gospodarki z dnia 9 kwietnia 2002 r., Dz. U. Nr 58, poz. 535, 2002 r.
- [9] Rozporządzenia Ministra Gospodarki, Pracy i Polityki Społecznej z dnia 29 maja 2003 r., Dz. U. Nr 104 poz. 970, 2003 r.
- [10] Council Directive 93/15/EEC of 5 April 1993 “Placing Explosives on the Market”
- [11] Piotrowski T., Głowiński J. – „Technology&Media Classification and Evaluation System – TEMCLEV. System Construction and Examples of Its Practical Use”. The paper accepted for 11-th International Symposium “Loss Prevention 2004”, 31.05-3.06.2004, Praha, Czech Republic.
- [12] DOW’S Fire & Explosion Index Hazard Classification Guide, Seventh Edition, AIChE Technical Manual, New York, 1994
- [13] THE MOND INDEX, Second Edition 1985, Amended January 1993, Mond Index Services ICI 1993
- [14] S. CUDZIŁŁO, M. MARANDA, J. NOWACZEWSKI, R. TRĘBIŃSKI, W. A. TRZCIŃSKI: "Wojskowe Materiały wybuchowe", Wyd. Wydziału Metalurgii i Inżynierii Materiałowej Politechniki Częstochowskiej, Częstochowa 2000
- [15] R. MEYER, J. KÖHLER, A. HOMBURG: "Explosives" Fifth, Completely Revised Edition Wiley-VCH Verlag GmbH, Weinheim, 2002
- [16] JACQUELINE AKHAVAN: "The Chemistry of Explosives." RSC Paperbacks The Royal Society of Chemistry, 1998
- [17] Karty oceny materiału wybuchowego pod względem bezpieczeństwa. Materiały Instytutu Przemysłu Organicznego, Warszawa

EXPERIMENTAL INVESTIGATION OF IGNITION MECHANISMS IN CONFINED ENERGETICS

H. J. Prentice and W. G. Proud

Cavendish Laboratory, University of Cambridge, Cambridge, UK

Abstract:

Detailed understanding of the response of confined energetic materials to different stimuli is critical to their design. This paper presents an experimental investigation of ignition mechanisms in Detasheet (a polymer-bonded explosive) when confined between copper plates and impacted at normal incidence with copper plates at velocities up to 600 m/s. High-speed photography and optical fibres are used to detect points of ignition and consequent reaction history. PVDF stress gauges are used to relate velocity of impact with pressure generated in the explosive. A Hugoniot curve for detasheet has been plotted.

Keywords: ignition, PBX, impact, Hugoniot

1. INTRODUCTION

The primary use of PBXs is for applications in which high output combined with insensitivity are paramount. They are generally insensitive when compared to pressed explosive pellets ^[1] and have the advantage of being machinable and castable. The importance in determining the sensitivity of the explosive to shock pressures and shear is principal to its manufacture, confinement, transportation and application.

It is possible to initiate PBX systems using relatively low velocity impact ^[2]. In applications with the requirement that response is prompt, given specific stimuli, the threat of ignition by other mechanisms must be minimised. Impact-induced reaction can occur by various mechanisms, such as pinch, shear and cavity collapse. The motivation for this work is to investigate lower order reaction in detasheet produced by impact and to assess the effect of short duration shock properties. This study complements earlier research from this laboratory ^[3] where a technique based on three-dimensional digital speckle photography was developed to look at bulging in targets when impacted. The knowledge of impact deformation combined with that of ignition mechanisms will provide information relevant to modellers.

2. EXPERIMENTAL

A single-stage gas gun was used to fire projectiles up to velocities of 600 m/s (figure 1). The projectile was a copper disk mounted on a nylon sabot to provide stable flight. The target was aligned to give normal impact with the projectile. The target consisted of a disk of detasheet confined by a front plate of copper and rear plate of either copper or glass. The disk of detasheet was of larger diameter than the projectile; the relative diameters of the impactor and the explosive were chosen in order to be able to distinguish between shear and shock pressure as ignition mechanisms. The impacts were conducted in a chamber which was evacuated to below 100 mBar pressure.

Copper was chosen as its Hugoniot is well-documented. The method of punching copper disks from a sheet resulted in some degree of bowing of the metal; the faces were polished with glass-paper to provide flat and smooth surfaces. Thin layers of silicon grease (which is compatible with detasheet) were incorporated between the target layers to eliminate air pockets and ensure good stress transmission. Some targets were constructed with air pockets and the results are compared to those where silicon grease was used.

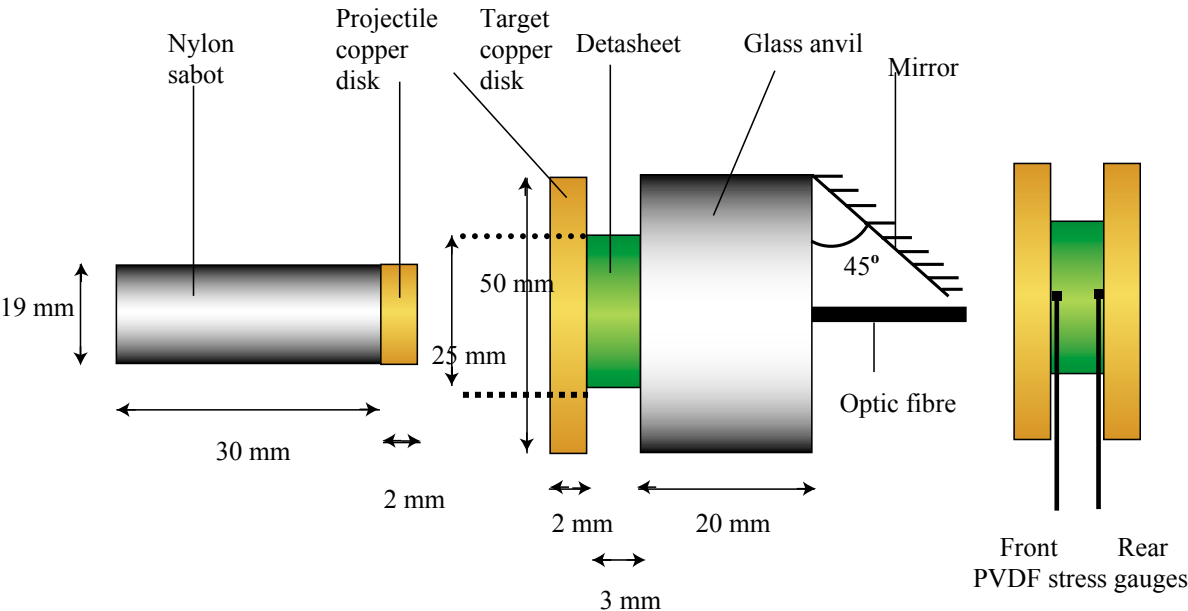


Fig 1. Projectile and target geometries with diagnostics (not to scale). From left to right: projectile; target with glass rear confinement; target with copper rear confinement

Each target was fitted with a variety of diagnostics which included PVDF stress gauges^[4,5], photodiodes and high-speed photography. PVDF gauges are piezoelectric; with appropriate calibration (figure 2) it is possible to interpret stress as a function of time. The gauges were constructed by positioning a small disk (1 mm diameter) of piezoelectric film concentric with the impact axis and between two insulated legs of brass shim. The gauges have a response time of approximately 200 ns. It should be noted that the gauges would give very high output when detonation occurs.

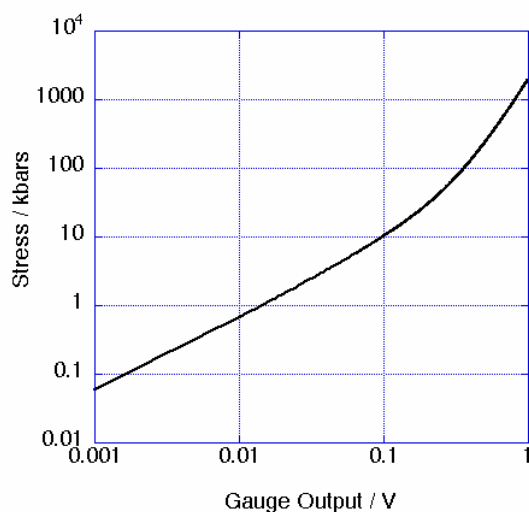


Fig 2. Stress-Voltage PVDF gauge calibration

An optic fibre was positioned to view along the impact axis through the rear glass anvil and the light evolved was fed into the photodiode; the response time of the photodiode is 200 ps. A mirror at 45° to the rear plane allowed high-speed photography of the rear face of the explosive with a DRS Hadland Ultra-8 digital camera, which produces eight frames with $1\mu\text{s}$ interframe time and $1\mu\text{s}$ exposure time.

3. RESULTS

3.1 Photodiode traces for samples with air pockets

For samples with air pockets, the results in figure 3 show photodiode traces over a velocity range between 156 m/s and 622 m/s. Light output indicates that reaction has taken place and such results were accompanied by post-impact indicators of reaction, such as sample damage and smoke. The system was tested with inert samples to ensure that no light was produced from the cell materials. For samples with an explosive filling, there was no light output in the absence of reaction; in this instance the explosive was either shredded and scattered about the gun chamber or, at lower velocities, left intact. The absence of any photodiode response when no reaction took place suggests that, in this regime, both the cell and the fracturing detasheet produce little in comparison to the light produced by reacting detasheet.

Light was recorded from between $1.5\mu\text{s}$ and $2.0\mu\text{s}$ after impact in systems where reaction occurred (525 m/s and 622 m/s). The traces are typical of a burning reaction. In addition, the rise-time to maximum intensity is approximately $2\mu\text{s}$ which is slower than would be expected for a prompt detonation. It can therefore be concluded that the explosive is ignited and deflagrates without a transition to detonation.

The results suggest that there is a go/no-go reaction threshold within an approximate 40 m/s range of impact velocities between 488 m/s and 525 m/s. The output for an impact velocity in the middle of this range shows light but at a significantly lower level. This may be due to an off-centre reaction rather than a lower rate of reaction as the rise-time is similar to that of the higher velocities. Some variation in the magnitude of the maximum light recorded is explained by slight differences in the polishing of the optic fibres. However it is observed that higher impact velocities result in a faster rise of the light pulse.

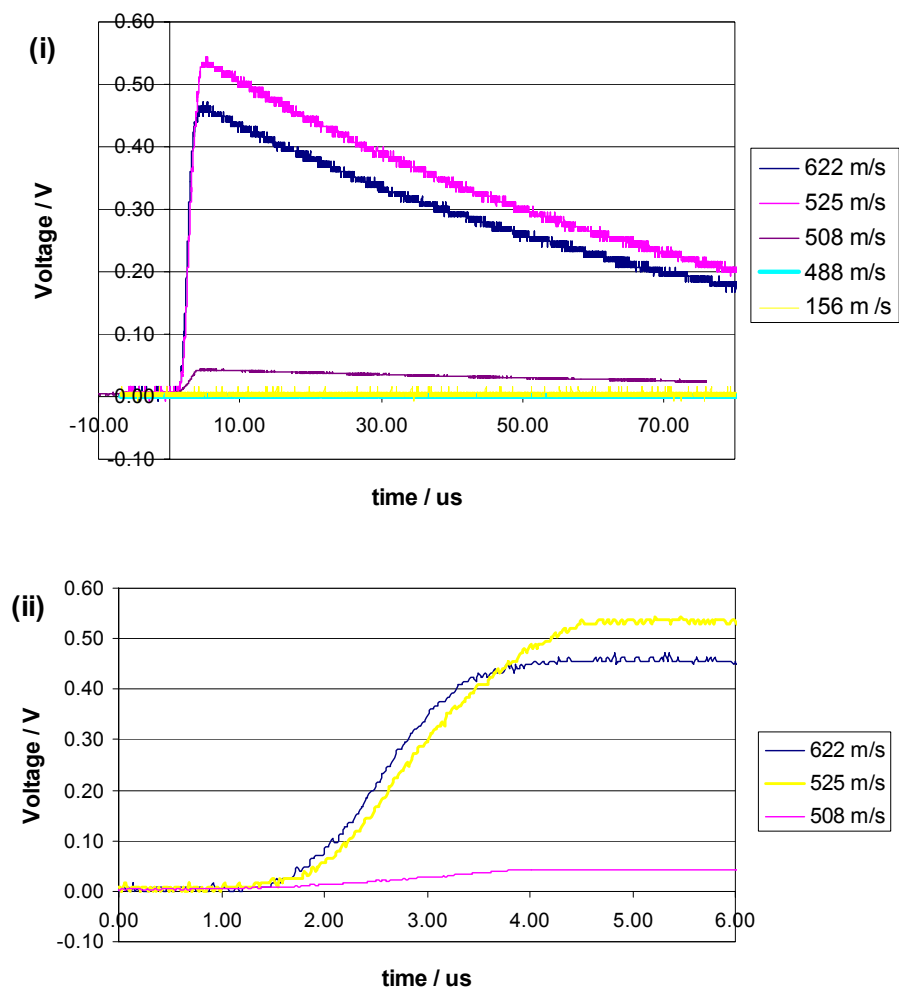


Fig 3. (i) Photodiode traces for the impact velocity range 156 - 622 m/s;
(ii) Photodiode rise-times in reacting detasheet.

3.2 Effect of air pockets

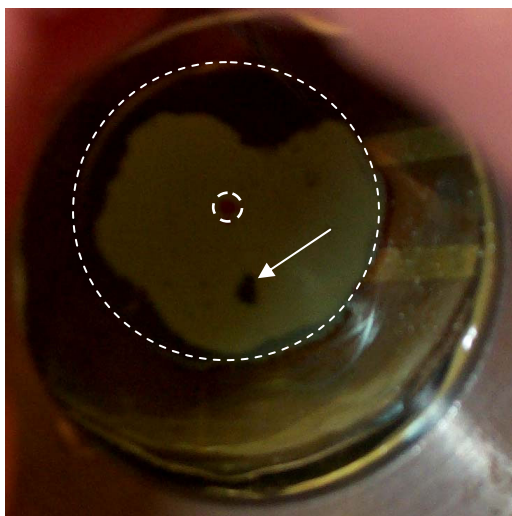


Fig 4. Photograph of air pocket in prepared target: the boundary of the explosive disk is shown by the superimposed outer dashed white circle (25 mm diameter) and the inner circle marks the centre of the detasheet disk. Air pockets are identified by dark patches on the explosive surface where light is scattered (indicated with arrow). The typical size of air pockets vary between 0.5 mm to 4 mm diameter.

Figure 4 shows a typical air pocket trapped between the detasheet and a confining glass anvil. Without explicitly removing such pockets, their presence will clearly affect the response of the explosive to impact, through adiabatic compression of the gas in the pocket and consequential hot spot formation.

High-speed photographs compare the reactions firstly with an air pocket and then with a layer of silicon grease to remove the air pockets (figure 5). The reaction appears to start at an air pocket, noted prior to impact, and spreads out. Micron-sized lines can be identified at the edge of the reaction area in the photograph of the impact without air pockets; these may be lines of shear. A similar pattern of reaction occurs without the air pockets present. Photodiode and PVDF stress traces are also similar in each case (figure 6). Figure 3 shows that pulse rise-times depend on velocity but that the maximum level of light output appears to be largely independent of impact velocity once reaction is successfully induced; hence the different velocities are comparable for the photodiode traces.

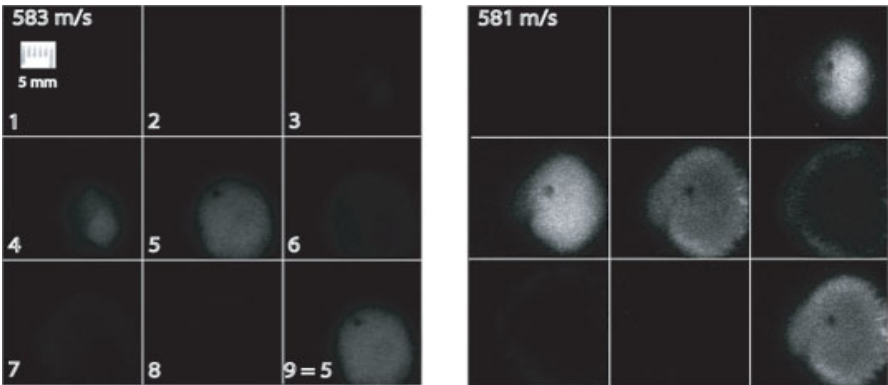
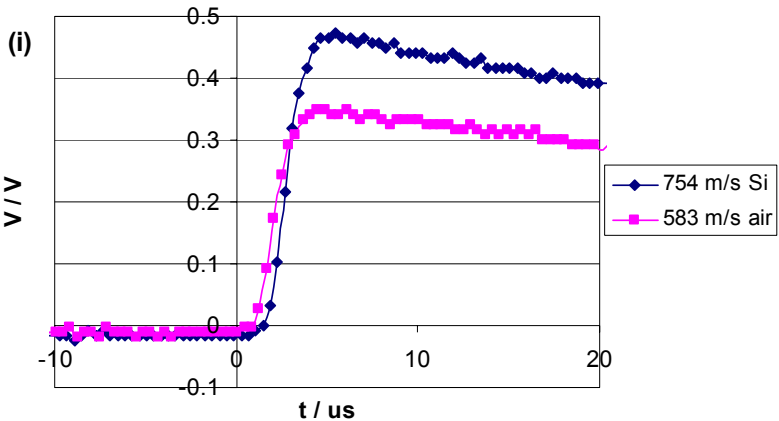


Fig 5. High-speed photographs showing the reaction in targets with and without air pockets for impact velocities of 583 m/s and 581 m/s respectively. The first frame starts at the moment of impact; subsequent frames are for successive microsecond intervals, with 1 μ s exposure. Frame 9 is a repeat of frame 5 owing to the nature of the ultra-8 camera. The black dot indicates the impact axis and the dark spot indicates the centre of the explosive.



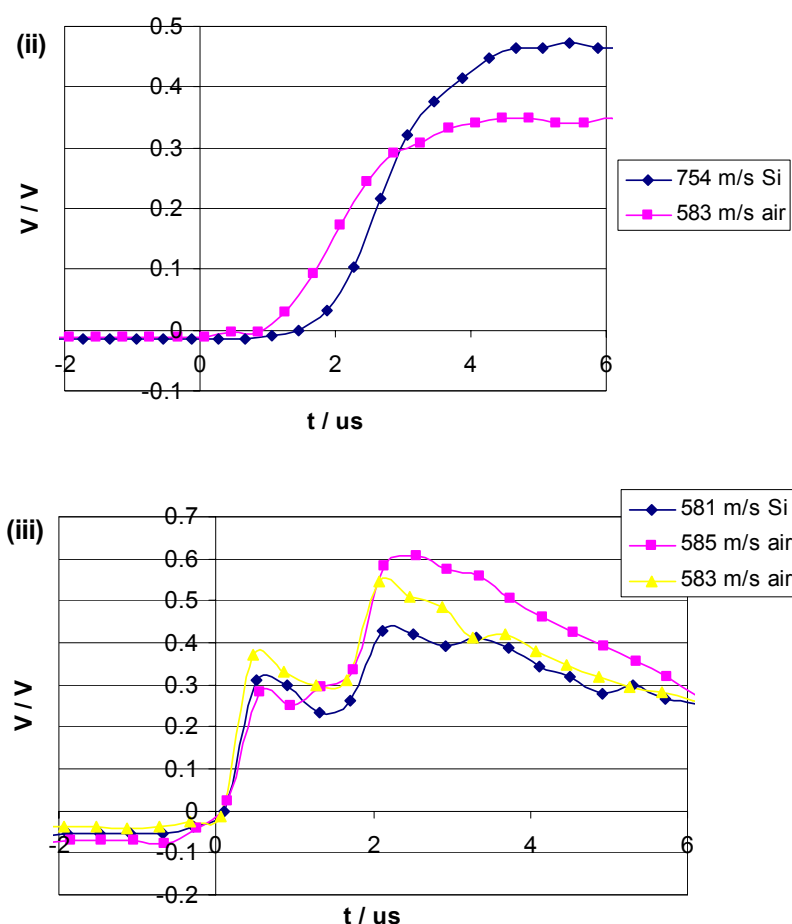


Fig 6. Comparison of results for targets with and without air:
(i) Photodiode traces; (ii) Photodiode rise-times; (iii) PVDF stress pulses

At this level of impact, the presence of visible air bubbles does not significantly affect the apparent mode of reaction. It should be noted that studies have shown smaller air bubbles (micron-sized) to collapse, due to adiabatic compression, far more quickly than larger air pockets (mm sized) and hence smaller pockets are more favourable hot-spot sites ¹⁶¹. Greasing methods do not eliminate such tiny bubbles. It is possible that the larger pockets of air identified do not collapse sufficiently quickly to significantly affect the explosive.

3.3 Targets without air pockets

A series of experiments was undertaken impacting targets, fitted with PVDF stress gauges in front and behind the energetic material, at different velocities. Typical results are shown in figure 7 for cases where no reaction occurs and for the case when there is reaction. Successive peaks represent the stress wave reflecting between the copper plates. The higher velocity impact results in higher pressures than the lower velocity impact. The smoother nature of the 581 m/s trace is due to a slower sampling frequency.

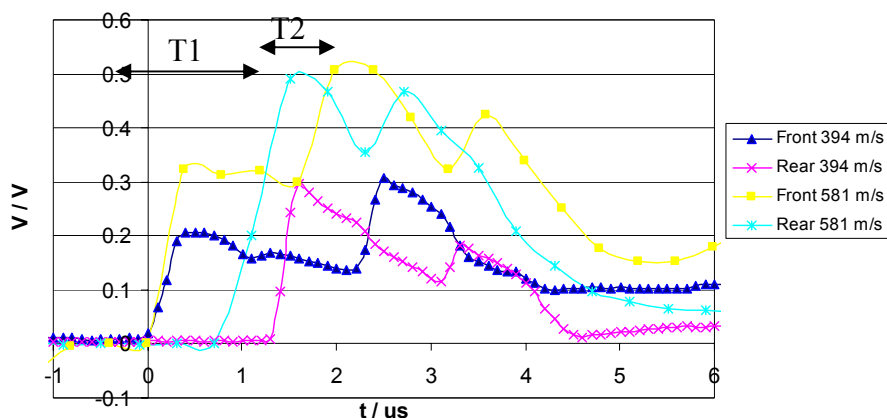


Fig 7. Comparison of typical front and rear PVDF stress gauge responses for impact velocities above and below the critical impact velocity range for reaction (581 m/s and 394 m/s respectively); time zero is approximately 300 ns after impact.

Figure 6 suggests that light from reaction is observed between 1.5 μs and 2 μs after impact. This corresponds to the time between the first peak arriving at the rear gauge and the second peak at the front gauge for the higher velocity impact.

The shock lasts for approximately 600 ns before release is realised due to the finite extent of the projectile; this agrees with the width of the first pulse seen by the front gauge at each velocity. It can be seen that there are a series of steps on the PVDF signals. The time difference between the first pulses recorded by either gauge, T1 is longer than the time difference T2 for the reflected shock to reach the front gauge. This suggests an accelerated stress wave velocity; which can be interpreted either as a consequence of compressed material owing to the impact shock, or as evidence for an reaction. It must be remembered that the sample is deforming along with the gauge during the impact process. However, the trend is clear: higher impact velocity gives a greater stress throughout the system. The large broad peak at the rear PVDF gauge at the higher velocity gives extra support for the idea of reaction occurring. These measurements will be extended by observing the effect of semi-infinite backing of the samples, to reduce bending.

The pressures recorded by the rear gauges often exceed those generated by the copper-copper impact when compared with the appropriate Hugoniot curves. Coupled, these results support reaction and hint at a claim for detonation.

There is a degree of variation from gauge to gauge owing to the method of their construction; impacts at (583 ± 2) m/s give an initial peak in voltage of (0.32 ± 0.04) V. However, using figure 2, we can see that the initial peak in stress at the front gauge increases with impact velocity from approximately (26 ± 1) kbar for 300 m/s to (83 ± 2) kbar for 581 m/s. Using the well-documented Hugoniot of copper^[7], a tentative effort to find the Hugoniot for detasheet is shown in figure 8. However, this will be obtained with greater accuracy using a larger diameter sample for which one-dimensional conditions can be approximated far better.

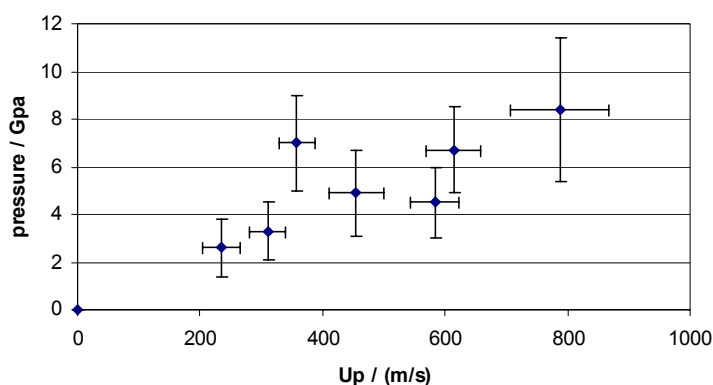


Fig 8. Hugoniot for Detasheet

4. CONCLUSIONS AND DISCUSSION

The process of ignition and initiation in confined energetic materials is a complex process. Mechanisms such as void collapse, pinch, shear and fracture all contribute. In some applications it is possible that gas pockets will develop between the energetic material and the confinement.

This study illustrates that at the impact velocities studied here, the presence or absence of air pockets (0.5 mm – 4 mm diameter) has little overall effect; the extent of reaction, as measured by photodiodes, is similar for both cases. Of more potential concern is that, at lower velocities, the presence of such pockets may provide the hot-spots which result in reaction so sensitising the system. The use of high-speed photography was key in linking reaction sites to air pockets. Finally there is a low velocity threshold below which reaction does not occur.

The PVDF stress pulses show the form of the stress pulses in the system. For experiments in which reaction occurred the stress pulse is broader than when no reaction resulted. This will be pursued in further studies where the backing to the explosive is effectively rigid, so eliminating potential effects caused by flexing of the gauge. Using the initial step on the PVDF traces, an approximate Hugoniot for the system has been constructed. This will be improved upon using thicker samples with a larger diameter where longer duration shocks can be produced and the one-dimensional assumptions for the Copper Hugoniot used may be more effectively transferred.

By combining the knowledge of the processes leading to reaction with the mechanical response of the energetic material and the confining plates, models of greater applicability and accuracy can be produced.

Acknowledgements

The support of EPSRC and Drs N. Lynch and J. Curtis of QinetiQ is acknowledged. Mr. R. Marrah of the Cavendish workshop provided invaluable technical support.

REFERENCES

- [1] C. R. SIVIOUR, S. M. WALLEY, W. G. PROUD AND J. E. FIELD: *Hopkinson Bar Studies on Polymer Bonded Explosives*, Proceedings of New Trends in Research of Energetic Materials, Pardubice, Czech Republic, 22-24 April, publ. University of Pardubice, 2003
- [2] S. K. CHIDESTER, C. M. TARVER, A. H. DEPIERO AND R. G. GARZA: *Single and Multiple Impact Ignition of New and Aged High Explosives in the Steven Impact Test*, Proceedings of Shock Compression of Condensed Matter, 1999
- [3] H. J. PRENTICE, S. G. GRANTHAM, W. G. PROUD AND J. E. FIELD: *Three-dimensional Penetration Measurements using Digital Speckle Photography*, Proceedings of Shock Compression in Condensed Matter, , Portland, Oregon, 20-27 June, publ. American Institute of Physics, 2003
- [4] T. OBARA, N. K. BOURNE AND Y. MEBAR: *The Construction and Calibration of an Inexpensive PVDF Stress Gauge for Fast Pressure Measurements*, Meas. Sci. Technol. **6** 345-348
- [5] A. CHAKRAVARTY, W. G. PROUD AND J. E. FIELD: *Small Scale Gap Testing of Novel Compositions*, Proceedings of Shock Compression in Condensed Matter, Portland, Oregon, 20-27 June, publ. American Institute of Physics, 2003
- [6] M. M. CHAUDHRI AND J. E. FIELD: *The Role of Rapidly Compressed Gas Pockets in the Initiation of Condensed Explosives*, Proceedings of Royal Society, London, **340** 113-128
- [7] S. P. MARSH: *LASL Shock Hugoniot Data*, University of California Press, Berkeley and Los Angeles, 1980

THE ETHICS OF ANALYSIS AND MEASUREMENT

IS YOUR ANSWER THE CORRECT ANSWER?

Fritz van Rooyen

National Institute for Explosives Technology (NIXT) South Africa
PO Box 32544, Glenstantia 0010, Pretoria. Republic of South Africa

Abstract:

In spite of careful analysis and measurement, results are often incorrectly calculated and reported. This may have serious effects on the outcomes of the investigation - products, ammunition and associated systems may not meet the specifications and miss the target, time and materials are wasted and revenue eventually lost.

This paper deals with the necessity for and principles of correct scientific numerical communication. The basic measuring units are initially reviewed followed by a discussion of the proper use of figures and correct handling of measurements. In conclusion the nature of measuring errors is studied and guidelines for its prevention provided. A number of exercises are provided in the text, the answers to be found at the end of the paper. The ultimate aim will be to improve the reliability of the reader as an analyst/researcher.

Keywords: *SI Units, significant figures, reliability, precision, accuracy, analysis of errors*

1. INTRODUCTION

Reliability is a noble human characteristic that should be strived for. It earns esteem from colleagues and even promotion from managers. This not only applies to human relationships but equally to activities as a scientist, engineer, technologist, manager, supervisor or humble worker. Unfortunately, without knowing it, results and findings may be unreliable merely because the principles of correct scientific numerical communication, the avoidance of errors, as well as the visualisation of results have never been mastered. This is unfortunately a shortcoming of some employees that have, for instance, caused factories and mines to be closed, contracts and communication satellites to be lost and products to be withdrawn.

This paper aims to improve the reliability of tests and analysis. As a start it may be of interest to try exercise 3.2. A correct answer at the first attempt will prove mastery of the most important aspects of reliable calculation!

2. THE INTERNATIONAL SYSTEM OF UNITS

Since measurement and control inevitable involves units, the analyst/researcher should have a good grasp of the various measuring units and its conversion into sub- or other units, especially in view of the fact that a degree of confusion exists with respect to some of these. Many reference manuals and books still adhere to the old Imperial units. The variety of pressure and vacuum, for instance, can be quite confusing.

The so-called SI (*System Internationale*) was introduced by the French in order to supply a logical and correct reference framework for all measurements in science, technology, industry and commerce. The system is based on seven basic units and their sub-units. Of these only mass requires a physical unit for its definition. Each basic unit is sub-divided into a number of subsidiary and even smaller units that are used during measurement. The seven SI basic units and their sub-units are listed in Table 1.

Table 1. *The SI Units of Measurement*

1. LENGTH:	<u>Metre</u> (m). A helium-neon laser is used for its accurate calibration. <u>Area</u> : Square metre (m ²). <u>Volume</u> : Cubic metre (m ³). The sub-unit is the cubic decimetre (dm ³). In industry volumes are often expressed in terms of litres.
2. TIME:	<u>Second</u> (s). It is based on the stable oscillations of the Caesium atom. <u>Frequency</u> : Hertz (Hz). One hertz equals one cycle per second. <u>Speed</u> : Meter per second (m/s). Dividing distance by time gives the speed. <u>Acceleration</u> : Meter per second per second (m/s ²). Acceleration is the rate of change in speed
3. MASS:	<u>Kilogram</u> (kg). A physical standard is used which is a cylinder of platinum/iridium alloy kept at the Bureau of Weights and Measures in Paris It is approximately the mass of one cubic decimetre of water at 4 °C.
Force:	<u>Newton</u> (N). A <u>force</u> of one Newton, when applied for one second to a mass of one kilogram, will result in an acceleration of one metre per second per second.
Pressure:	<u>Pascal</u> . 1 <u>newton</u> /m ² = 1 Pa. 1 Atmosphere or 1 Bar = 100 kPa.
Work and Energy:	<u>Joule</u> (J). The weight of an object is the force exerted on it by gravity. Gravity gives mass a downward acceleration of about 9,8 m/s ² . J = 1N x 1m
Power:	<u>Watt</u> (W). 1W = 1J/1s.

5. ELECTRIC CURRENT:

Ampere (A). This is the value of the current that will cause a magnetic force of certain magnitude when flowing through two long parallel wires separated by a certain distance.

Voltage: Volt (V). $1\text{ V} = 1\text{ W} / 1\text{ A}$.

Resistance: Ohm (Ω). $1\Omega = 1\text{ V}/1\text{ A}$
6. LUMINOUS INTENSITY

Candela (cd). A candela is the luminous intensity of 1/600 000 of a square metre of a radiating cavity at the temperature of freezing platinum (2 024 ° K)..

Light flux: Lumen (lm). A source with intensity of 1 candela in all directions radiates a light flux of 4 lumens. A 100 watt light bulb emits about 1 700 lumens.
7. AMOUNT OF SUBSTANCE:

Mole per litre (M). One mole of a substance is equivalent to its molar mass expressed in grams.

The recognised SI multiples, submultiples, prefixes and symbols are listed in Table 2. It should be pointed out that the comma is still the official decimal denominator and not the point. Industry pays little attention to this. However, because of problems experienced in this respect by manufacturers of certain computerized instrumentation that are unable to handle the comma, there is an international movement towards again allowing the point as decimal denominator.

Table 2. *Prefixes for SI units*

Multiples and Submultiples	Prefixes
1 000 000 000 000 = 10 ¹²	tera
1 000 000 000 = 10 ⁹	giga
1 000 000 = 10 ⁶	mega
1 000 = 10 ³	kilo
100 = 10 ²	hecto
10 = 10 ¹	deka
0,1 = 10 ⁻¹	deci
0,01 = 10 ⁻²	centi
0,001 = 10 ⁻³	milli
0,000 001 = 10 ⁻⁶	micro
0,000 000 001 = 10 ⁻⁹	nano
0,000 000 000 001 =10 ⁻¹²	pico
0,000 000 000 000 001 = 10 ⁻¹⁵	femto

3. CORRECT HANDLING OF MEASUREMENTS AND CALCULATIONS

Scientific communication is largely based on the use of figures. In the process measurements and answers are quantitative and refer to some physical property such as mass, density, VOD, heat of explosion, etc. Scientific communication is expected to be correct and intelligible, an aspect that also applies to the use of figures. Unfortunately this is not always the case. This paper intends to provide guidelines in this respect.

3.1 Significant figures

Results are mostly correctly calculated but, because of the incorrect use of significant figures, not correctly expressed. It is important that the answer should always reflect the sensitivity and reliability of the analysis. The weak link in the measuring and hence calculation chain should be identified and the relative uncertainty of this measurement reflected in the final answer, which, however, should not be less than that of the weakest link.

Consider for instance a claim made by the manufacturer of a well-known car who states that the gasoline consumption of the car is 5,475 litres per 100 km. As will be seen, this implies a relative uncertainty of one part per 5 475, a figure which has an uncertainty at least five times better than that obtained in a normal analytical laboratory doing wet analysis. This is absurd in view of the fact that a large measuring cylinder has an error of about 1%. The consumption should therefore be correctly expressed as 5,48 litres per 100 km.

3.2 Basic rules applying to significant figures:

When expressing a quantity the measurements and results are represented by so-called significant figures. Significant figures are those digits in a number that are known with certainty, followed by one digit that appears to be an uncertain or a doubtful digit. This figure is generally considered to be uncertain by ± 1 , for example, a density of 1,475 g/cm³ for cast TNT biscuit can be regarded to be certain as far as the digits 1, 4 and 7 are concerned, but the 5 may possibly be either a 4 or a 6.

In some cases the uncertainty may exceed one digit. The age of a rock may, for instance, be reported as 17,35 \pm 0,05 billion years. Likewise uncertainty about the concentration of a component in a sample may be reported as 17,4 \pm 0,4%. This, as an example, is observed when a number of experts analyse samples intended to form part of a batch of standard samples.

Up to 1971 the value for the atomic mass of hydrogen was given as 1,0079 \pm 0,0001 mass units. New information called for its adjustment to 1,00794 \pm 0,00007 units, increasing the number of significant figures from five to six.

The digit zero should be considered with care. Zero is a significant figure, except when it is the first digit in a number. Thus 715 has three significant figures, 3,78 has three, 0,0378 has three, 0,01490 has four, 0,060110 has five, etc. The leading zeros are not significant but serve to indicate the magnitude of the number, in other words, the position of the decimal comma. As an example a distance of 42 metres may also be expressed as 0,042 km; a concentration of 15,2 mg/dm³ (ppm) as 0,0152 g/dm³. The number of significant figures remains the same even though different measuring units are used and additional zeros introduced.

There is a tendency to ignore terminal zeroes, even if they are significant. When the number 15,30159 has to be rounded off to four significant numbers, it should be written as 15,30 and not 15,3 since, apart from being a significant number, the terminal zero indicates the relative uncertainty of the number. Because of the earth's elliptical orbit the average distance to the sun should not be written as 149 000 000 km but more correctly as 149 million or $1,49 \times 10^8$ kilometres. Avogadro's number, $6,023 \times 10^{23}$, is another good example. Since only four significant figures are available, there is no sense in writing down all the 23 zeroes! Also take note that the volume of a pipette or volumetric flask should be stated as 20,00 cm³ and not just as 20 cm³.

Exercise 1.

Write down the number of significant figures in the following examples:
(Answers for all exercises are provided at the end of the paper):

- | | | |
|-------------------------|----------------------------|----------------------------|
| (a) 460,10 | (b) 400 | (c) 0,0010 |
| (d) 2900 | (e) $7,540 \times 10^{-7}$ | (f) 3050,7 |
| (g) $1,680 \times 10^4$ | (h) 230,006 | (i) $2,620 \times 10^{11}$ |

3.3 Rejection of superfluous figures:

Electronic calculators normally provide more figures than are significant and one should make certain how many figures are to be retained. Keep in mind that the number of significant figures in a number should include one uncertain figure at the end. When the number 27, for instance, is divided by 23, the answer, 1,173913..., obviously has too many figures. As will be explained later, not more than three should be used, providing an answer of 1,71.

Superfluous figures are rejected according to the following standard rules:

1. If a figure beyond the last one to be retained is less than 5, the last figure is retained unchanged, e.g. if 6,4173 is to be rounded to four significant figures, it becomes 6,417.
2. If a figure next beyond the last one to be retained is greater than 5, increase the last figure by 1, e.g. if 5,4376 is to be rounded to four significant figures, it becomes 5,438.
3. If the figure next beyond the last one to be retained is 5 and there is no figure or there are only zeroes beyond the five, it is increased by 1 if it is odd, and left unchanged if it is even, for example, 2,425 or 2,42500 stays 2,42 if three figures are to be retained, while 1,235 or 1,23500 becomes 1,24.
4. The last figure to be retained is increased by one if it is followed by 5, followed by more figures.

As will be pointed out later, it is not necessary to discard figures when a string calculation is conducted on a calculator. This will save time. However, intermediate and final answers should contain the correct number of significant figures.

Exercise 2.

Rewrite the numbers in Exercise 1 to three significant figures. (More examples will follow in the remaining text.)

3.4 Addition and subtraction

During addition or subtraction sufficient figures corresponding to the term having the least number of decimal places should be retained in each number and in the result. Say, for instance, three charges are independently weighed and the following masses obtained: 39,48 kg; 34,51 g; 165 g.

There is no sense in adding the mass of one parcel, weighed to the nearest 10 grams, to that of another, weighed to the nearest 10 milligrams. The same unit, in this case kilograms, must be used and superfluous figures discarded. (It would not be correct to convert the masses to grams or milligrams before addition).

39,48 kg	stays	39,48 kg
34,51 g	becomes	0,03 kg
165 g	becomes	0,16 kg
Total		39,67 kg

During addition and subtraction the decimal comma therefore plays an important role when determining the number of significant figures to be retained. If your final answer has more decimal figures than contained in the measurements, they must be discarded since including them would indicate a precision better than that actually measured. The average value of a series of measurements of the heat of explosion for mercury fulminate serves as an example:

<u>Heat of explosion:</u>	1 486 kJ/kg
	1 484 kJ/kg
	1 488 kJ/kg
	1 485 kJ/kg
Average:	1 485,75 kJ/kg

If 1 485,75 kJ/kg is to be taken as the average value, six significant figures are used implying a relative precision of one part in 148 575 parts. This is obviously unrealistic since the answer should more or less reflect the same relative uncertainty than the least uncertain measurement, which, in the above case, is approximately one part in 1 485. The correct answer for the above calculation is therefore 1 486 kJ/kg.

The agreement between the individual measurements must also be taken into account when stating the final answer. The average of 34,01; 34,35 and 34,17 should be reported as 34,2 and not as 34,18, since the measurements show considerable fluctuation and the third figure is also uncertain. Be careful, however, not to apply the same rule in the following case where the measurements are 34,11; 34,17 and 34,22. The third figure seems to be uncertain which is not the case since the variation of the last figure is less than unity. When in doubt calculate the average deviation (part 5.1). If the average deviation in this case is less than 0,10, only the fourth figure is uncertain. However, if it is above 0,1 and below 1,00, the third figure is uncertain.

Exercise 3.

1. Rewrite the following additions and subtractions, using a vertical column:

(a) $16,1 + 0,0557 + 1,64 + 0,0497 = ?$

(b) $(0,7650 \times 10^6) + (1,75 \times 10^4) + (21,2 \times 10^5) = ?$

2. Calculate the average titres in the following cases:

(a) $25,63; 25,59; 25,61 \text{ cm}^3$

(b) $25,70; 25,57; 25,41 \text{ cm}^3$

3.5 Multiplication and division

When multiplying and dividing numbers only sufficient figures to express a relatively uncertainty as large as that of the number with the largest relative uncertainty should be retained in each term and in the result. For example, during an analysis the readings from instruments with various sensitivities provide measurements that are used for the following calculation:

$$6,7 \times 31,421 \times 0,0581 = 12,2312563$$

As stated before the answer should reflect the relative uncertainty of the least uncertain number. To make things easy the comma is (temporarily) not taken into account. The relative uncertainties of the individual numbers are therefore $1/67$; $1/31421$ and $1/581$. The first number has the largest relative uncertainty, hence qualifies the number of significant figures to be retained in the other terms and in the answer. The factors may be inspected and modified individually according to these and other rules that have been developed before the introduction of the electronic calculator and when the only calculating aids were the slide rule and logarithms, that respectively handle only 3 and 4 significant figures. (Although more sensitive slide-rules and logarithmic tables were available.) Rejection of figures was a necessity when using these tools.

Since numbers are entered with greater speed into a calculator than struggling with rounding off procedures, the above numbers can be used just like they are, provided that the answer is adjusted to reflect the relative uncertainty of the number with the largest uncertainty, 6,7 in this case. The answer (disregarding the comma) should therefore not be less than the number 67 and for the above calculation should therefore be $= 12,2$. ($67 < 122$)

A typical misconception when reporting answers is the belief that the number should consist of four figures after the decimal comma. This may relate to the relative uncertainty of about one part per thousand applicable to the burette as used during volumetric analysis. The restriction to four figures as demanded during the earlier use of logarithms may also be a reason.

It should be remembered that zeroes, like other digits, are only significant if their removal does not change the relative uncertainty of the number, the essential criterion of significance. In the case of a number such as 4 170 it is assumed that the zero is the first significant number which is uncertain. However, if the 7 seems to be the uncertain digit, the number should be expressed in scientific notation, e.g. as $4,17 \times 10^3$.

Exercise 4.

Calculate the following according to the rules for significant figures:

- (a) $(1,263 \times 10,3) \div (3,1614 \times 0,0020) = ?$
- (b) The diameter of a sphere as measured with an ordinary ruler was found to be 2,1 x 102 mm. Calculate the volume in dm³. (Volume of a sphere = $\frac{4}{3} \pi r^3$ where r = diameter/2.)

3.6 Calculators and significant figures

The use of inexpensive calculators has speeded up calculations tremendously. Unfortunately its ease of use created a disregard for the correct use of significant figures. The complete lack of respect for the limitations or experimental measurements of computed results is probably directly attributable to the calculator screen displaying eight or ten digits or even more. This large number is often equated with accuracy and precision. The number of digits, however, has nothing to do with these two terms. This statement, however, does not apply to users of the old-fashioned sliding rules and log books that had to scale all numbers down to four significant figures!

Exercise

+Six students were requested to calculate the volume of a rectangular wooden block by measuring the length, width, and thickness of to the nearest 0,01 cm using a vernier calliper. The results are shown in table 3.

Table 3. *Calculation of the volume of a wooden block*

	Length (cm)	Width (cm)	Thickness (cm)	Volume (cm³)	Adjusted volume
1.	14.88	6.50	1.91	185.01941	185
2.	14.98	6.49	1.82	176.94076	177
3.	15.07	6.48	1.92	187.49491	187
4.	15.02	6.50	1.90	185.49700	185
5.	14.98	6.51	1.84	179.43643	179
6.	14.82	6.53	1.83	177.09752	177
7.	14.96	6.50	1.87	181.91434	182
8.	0.08	0.01	0,04		4
9.	1/187	1/650	1/47		

From the preceding table the following observations may be made:

1. The measurements listed in rows 1 to 6 show unexpected variation in spite of the fact that a reliable vernier calliper was used. Unknown to the students the wooden block was not perfectly symmetrical, the dimensions along the three axes varying by about 1 mm. This simulates a number of samples, for instance, from different batches that are not completely homogenous, a situation often found in commercial analysis.
2. If a perfectly symmetrical block was used it is likely that the answers would be identical, indicating a measuring instrument that is not sensitive enough. A three decimal calliper vernier should be used.
3. A perfectly symmetrical block measured with an ordinary ruler, on the other hand, may once again show variation in the measurements, mainly because of parallax errors that are introduced.
4. The calculated volumes are indicated in the fifth column with all the digits supplied by the calculator. As expressed, these answers indicate a relative uncertainty of about $1/18\ 200\ 000$ which is obviously far-fetched. It should be rounded off, but to what extent?
5. From the table it seems as if the second digit seems to be uncertain, but for safe measure rounding of is initially limited to three digits. The relative average deviation (see part 5.1) of these measurements are shown in row 8. The measurement with the highest uncertainty, thickness, has an average relative deviation of 0,04, which indicates a relative uncertainty of $0,04/1,82 = 1/47$. According to the rules, the answer should be > 47 , in other words, 182. Any further digits after the decimal comma will imply an uncertainty which is not reflected by the least uncertain measurement, that of the width.

This exercise illustrates the necessity for limiting the numbers of digits in order to obtain a sensible answer reflecting the correct degree of uncertainty of the measurement and analysis. It also illustrates the effect of variations in an “imperfect” sample, as for instance when the sampling units taken during the sampling procedure sample was too small resulting in inhomogeneous samples. The same effect is obtained when measuring a supposed to be symmetrical object, e.g. a cartridge that is not perfectly symmetrical. It may also reflect the results obtained by a single analyst using a measuring tool that is too sensitive.

3.7 Practical applications

Mass

Probably the laboratory instrument with the best sensitivity in everyday use is the analytical balance. These balances are normally capable of weighing to one tenth of a milligram, for instance indicating a mass of 25,3524 g. Since the last figure is the first uncertain figure with a value of $\pm 0,0001$, this implies a relative uncertainty of $0,0001 / 25,3524$ which is equal to 1 part in about 250 000. If 100 grams are weighed out, this uncertainty improves to 1 part in 1 million.

Since virtually all other measurements related to an experiment or analysis involving mass have far worse uncertainties, it is often not necessary to use an analytical balance at all, especially if the sample is large. In volumetric analysis the relative uncertainty is seldom better than $1/500$, which means that samples in excess of 10 grams may be weighed on a top loading balance with a read-out of 0,01 grams. Time and investment capital may be saved in this way.

Let us consider the following case history: When determining the relative density of cast TNT biscuits using the Archimedes principle, the analyst was instructed by the laboratory manager to use a five decimal analytical balance. The result of using this over-sensitive balance was that with each measurement he had to wait until the last two figures on the read-out stabilized in the draughty room, or when a reasonable average could be obtained. Each measurement took a few minutes. What none of them realized was that the sample (about 10 grams in size) was measured with an uncertainty of about $1 / 1\,000\,000$, or 0,00001%, which was absolutely unnecessary. A two decimal top loading balance was then used which provided a precision of 0,1%, which, since the listed value for the density of a typical sample of TNT biscuit is about 1,47, is quite acceptable. The analyst was now able to take measurements in about 5 seconds or less!

Measurement of time and its derivatives

Accurate measurement of time and its derivatives such as frequency, speed and acceleration is of great importance in the explosives and military industries, e.g. measuring the speed and acceleration of a projectile. Fortunately timing devices such as the wristwatch and especially scientific timing devices, oscillators, etc employing the absolute stable oscillation of the quartz crystal, provide extremely accurate and stable data. Atomic clocks based on the oscillations of Caesium are of the most accurately available measuring devices, having an error of about one second in 1×10^{13} years. These clocks are now available in credit card sizes!

Length and its derivatives

Length measuring instruments as used by scientists and engineers differ largely with respect to sensitivity and in effect the number of significant figures indicating the measurement. The common ruler, for instance, cannot measure better than about 0,2 mm at the best and an error of the same magnitude is easily made. This means that over a length of 10 mm the relative error is 0,2 per 10 mm, which is equal to $0,2/10 \times 100\% = 2\%$ relative uncertainty. If the length is 100 mm, this relative uncertainty decreases to 0,2%. In the case of a square with 10mm sides, however this uncertainty may increase to 4%, with a value of more than 6% if a cube with 10 mm sides is considered. For greater precision a vernier should be used.

The accurate measurement of line-of-sight velocity and acceleration is greatly facilitated by quartz controlled radar and Doppler radar technology. GPS positioning, also reliant on these techniques, can be done with great accuracy. The distance to the moon, for instance, using radar or laser technology, can be measured accurately to a few centimetres, that to satellites, to a few millimetres. The position, speed, acceleration and even trajectory of shells and missiles (and even tennis and cricket balls) can likewise be measured with great accuracy. Handheld units are also available for short distances. This technology is based on the revolutionary Tellerumeter invented 50 years ago by Dr Trevor Wadley at the South African CSIR, who initiated quartz crystal controlled oscillators.

Other instruments

Many measuring techniques rely on the readout from a pointer/scale or digital display. The former operates on an analogue basis and has the same limitations as that of a ruler. Mechanical failure or fatigue may also result in less accurate readings, for instance the pressure meters on gas cylinder regulators, especially towards the higher and lower ends of the scale where the reading error may be in the order of a few per cent. Digital read-outs are far more accurate. While glass thermometers have limitations similar to those of an ordinary ruler, some digital electronic temperature meters may read to $1/10\,000$ of a degree.

The supplier's specification sheets should be considered if the accuracy and precision of a particular instrument have to be known. It may also be established by experiment by measuring the same parameter a number of times.

Calibration

Reliable analysis depends on the regular calibration of the measuring instruments and the applicable calibration procedures applied on a regular basis. This calls for stringent quality control. Measurements should always be traceable to a country's national standards.

4. BASIC STATISTICS OF ERRORS

Data supplied by quantitative analysis and testing results from the measurement of some parameter such as mass, volume, density, electrical units, explosives properties, etc. Whatever the fields of science and technology, these results are quantitative and should be reliable. The various factors used to define the reliability of measurements and results, namely precision and accuracy will now be discussed. Since there is no sense in science and technology to define values and results in terms of various subjective statements of "good" or "bad", it must be described in absolute terms in numerical format. In order to achieve this, basic statistical analysis and manipulations are used.

4.1 Precision

Precision expresses the reproducibility of a measurement, that is, the agreement among themselves of several measurements of the same substance or property. It is sometimes also known as repeatability. Precision, of course, relates to the resolution of the measurement, which is qualified by the "size" of the smallest division of the measuring tool, in other words, its sensitivity. An ordinary ruler, as an example, normally has a resolution of about one millimetre. The smaller the resolution of the measuring instrument, the better the chance for the introduction of variations and hence an assessment of adequate measuring sensitivity.

To illustrate all the above statements, the analysis of a TNT/RDX brisant charge will be used as an example. Six samples from the same batch were analysed by means of liquid chromatography and the following values for TNT obtained:

61,2; 61,1; 60,8; 61,7; 61,9; 60,6 %

The variation in the results may have different causes, among these:

1. The batch was not homogeneous resulting in samples that were not exactly identical;
2. Preparation of the sample solutions introduced errors such as non-reproducible weighing of the sample, careless use of the volumetric apparatus, etc;
3. The samples were analysed by different analysts;
4. The liquid chromatograph was slightly erratic or not correctly used.

The reproducibility or precision of a measurement is expressed by the deviation, d , of that measurement. The deviation is the difference between the measured value X_i and the arithmetic average, X_a , of all the measurements, in other words, $d = |X_i - X_a|$. The vertical bars indicate that this value is taken without regards to sign.

The arithmetic average of the deviations, d_a , is used to calculate the precision or reproducibility of the measurements. This is an absolute value. Note that additional digits should not be introduced as a result of these calculations.

From the measurements the following results are obtained:

<u>Observed value (X)</u>	<u>Deviation (Xi - X_a)</u>
60,7	0,4
61,2	0,1
61,1	0,0
61,9	0,8
60,9	0,2
60,8	0,3
<hr/> X _a = 61,1	<hr/> d _a = 3d/6 = 0,3

Since absolute deviation is a number that is rather meaningless, the relative deviation is of more practical value. Relative deviation relates d_a with respect to X_a and is expressed as a fraction, d_a/X_a , or as a percentage, $(d_a/X_a) \times 100 \%$. The above average relative deviation is therefore reported as a fraction $0,3/61,1$, or more convenient as a percentage, $(0,3/61,1) \times 100 = 0,5 \%$, or since this value is quite small, as parts per thousand, $(0,3/61,1) \times 1000 = 5 \text{ ‰}$. Care should be taken that superfluous significant figures are not generated in the process.

Laboratory analysis are frequently based on the average of triplicate measurements. In this case no statistical manipulations are possible.

4.2 Range

Range is simply the difference between the largest and the lowest results. It is expressed as:

$$R = X_{\text{largest}} - X_{\text{lowest}}$$

Range can also be expressed in relative terms. In the above example, $R = 61,9 - 60,7 = 1,2$, and the relative range is $(1,2/61,1) \times 1000 = 20 \text{ ‰}$. Range has little value for indicating the spread of a large number or population of measurements. For a smaller number it becomes more meaningful as indicator of the dispersion of results. If $n = 3$ to 10 , for instance, range can be used to express the average deviation since in these cases the average and even the standard deviation are poor estimates of precision. With only two measurements, the range and the average provide all the information about the measurements.

Since the true value of the quantity measured is usually unknown, deviations can be used to express the reliability of measurements.

4.3 Rejection of a Result

In the previous example, one of the values, $61,9$, seems to differ widely from the other. The question now arises whether this value should be accepted. If the cause of its large deviation is known, the value should obviously not be included in the series. However, it may happen that the cause for this unacceptable deviation is unknown. There are statistical rules that can then be used to decide whether the suspected value should be rejected or not. Testing for rejection of a measurement is conducted as follows:

If, in a series of four or more values, one value appears to differ widely from the other values, the suspected value is temporarily rejected, and the mean of the other measurements and the average deviation are computed. If the deviation of the suspected value from the mean of the other values is more than four times the average deviation, the suspected value should be discarded; otherwise it must be retained, and a new average and average deviation computed.

This rather obscure definition will become clear if the previous calculation is considered. A clue to which value (if any) may be suspected is best obtained by rearranging the measurements in a particular order, say from the highest to the lowest, and observing the differences between adjacent values. It should be obvious that either the lowest or the highest measurement in the series will be suspect. The deviation (1,0) of the suspected value (61,9) in the following calculation is more than four times the average deviation of the other values (0,2) and is therefore rejected. The relative average deviation of the remaining results is now = $0,2/60,9$, or 3 ‰.

<u>Observed</u>	<u>Deviation</u>	
[61,9]	[1,0]	Temporarily rejected:
61,2	0,1	
61,1	0,0	
60,9	0,2	
60,8	0,3	
60,7	0,4	
$X_a = 60,9$	$d_a = 0,2$	

4.4 Accuracy

The correctness of a measurement is defined by its accuracy, that is, the agreement of the average value with the “true value”, μ . The true value of the constituents of a commercial sample is not generally known. The value 12,000000 for the atomic mass of the carbon 12 isotope, is an exception. It was arbitrarily chosen as a reference for the relative masses of other atoms as determined experimentally. The value obtained by counting the number of cartridges in a case or the number of drilled holes on a stoping face is a true value since there is no uncertainty about these numbers. Data generated during quantitative analysis, however, is generally obtained not by counting but by measuring parameters such as grams, millilitres, metres per second, kilojoules per kilogram, etc. During such measurement discrepancies may arise as result of one or more errors that may be made at any stage. The “true value” is likely to be the most probable value as derived through the application of statistical methods for the evaluation of data obtained by repeated, careful measurement. Since this paper mainly deals with factors affecting reliability and obtaining correct answers, little attention will be given to these statistical methods.

Standard samples are essential for the accurate calibration of a process or a product. In some cases standard samples such as those issued by the British Bureau of Analysed Samples, Ltd, and provided by many suppliers of laboratory products may be used. These samples represent metal alloys, ores, cement, etc and are issued with certificates reporting the concentrations of components as found by a number of recognised analytical experts. The analytical methods used are also stated on the certificate. The concentrations of the various ingredients are hence regarded as “true” values and can be used to calibrate in-house techniques and samples. Unfortunately no such standard samples exist for many commercial products, especially energetic materials such as explosives. (An exception is vials containing

micrograms per litre standard solutions of explosives that may be used for the calibration of chromatographs.) The main problem is that suppliers are not prepared to incur the cost involved by licensed magazines, apart from problems with legal transport. Since efficient quality control is important, one or other form of reference standard is essential. These may be obtained by selecting samples from a batch of explosives, ammunition or any relevant materials that are deemed to be of high quality or acceptable performance and that conforms to the set specifications. Selection should follow standard sampling procedures. For laboratory purposes it is fairly easy to obtain pure reference samples of, for example, high explosives such as TNT, RDX, PETN, etc. by repeated re-crystallisation of commercial grade materials.

Provided that the measuring tool is sufficiently sensitive to detect the existent level of variability all experimental measurements will be variable. It is, in fact, important that measurements should exhibit a small variability and not be all the same. This enables the analyst to estimate the magnitude of the smallest observable effect, or the quantitative reliability of a measured difference. Students, especially, try to get similar readings in order to boast about their precise abilities!

As a practical example the distance to a nearby magazine may be measured using a car with an odometer not indicating tenths of a kilometre. It is likely that no variation in the reading will be obtained, indicating a non-sensitive measuring unit. On the other hand, using a surveyor's distance measuring wheel may result in too many uncertain figures, indicating a too sensitive measuring device. A normal car will do the trick!

4.5 Error

Accuracy is quantified by the error (E), which is the difference between an observed or measured value, X_i , and the true (most probable) value, μ . In other words: $\mu = X_i - \mu$.

When calculating the error, account should be taken of whether it has a positive or negative value. Referring to the analysis of the TNT/RDX mixture, assume the true value, μ , to be 61,0%. We now have:

<u>Observed (X_i)</u>	<u>Error ($X_i - \mu$)</u>
61,2	+0,2
61,1	+0,1
60,9	-0,1
60,8	-0,2
60,7	-0,3
$X_a = 60,9$	$d_a = -0,1$

The same error, in sign and magnitude, is directly obtained by subtracting the true value from the mean of the retained observed values ($60,9 - 61,0 = -0,1$). This the same as by taking the algebraic average of the individual errors ($- 0,3/5 = -1$).

As for deviations, the absolute error is of little significance. The error relative to the true value, E/μ expressed in suitable units, is of more practical value. This is illustrated in Table 4.

Table 4. *Magnitude or the relative error*

Measured value, X_i	33	303	3003
True value, μ	30	300	3000
Absolute error, E	3	3	3
% Relative error, $(E/\mu) \times 100$	10	1	0,01

Although the absolute error, 3, is the same in each case, the relative errors are widely different

4.6 Reliability and its relation to accuracy, precision and resolution.

An almost constant source of error during measuring may cause the values to be precise without necessarily being accurate. Important is that good precision (small relative deviation) does not necessarily imply good accuracy (small relative error). The well-known example illustrated in Figure 1 will be helpful in distinguishing between precision and accuracy.

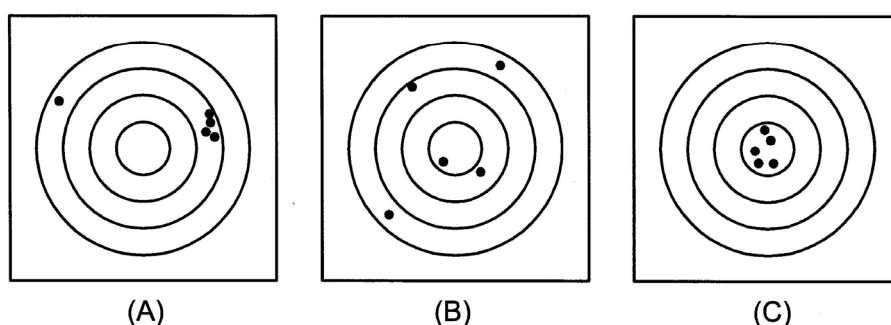


Fig 1. Precision and accuracy as illustrated by target shooting

It represents three targets at each of which five rifle rounds have been fired. In the case of target (a) the shots are precise if the one shot at the “ten o’clock” position is disregarded. Since they are not in the bull’s-eye, they are obviously not accurate. The way-off shot could be due to some determinate equipment error (see part 4.1) such as non-calibration of the rifle’s sight. Otherwise it could be due to a personal error such as not compensating for the wind. It then has to be discarded. If the reason for a large deviation is unknown, testing for rejection in the case of any measuring situation like in analytical chemistry can be conducted by means of statistical methods. On target (b) the hits are neither precise nor accurate since the deviations are both large and random and probably indicate considerable lack of skill of the rifleman. The possible argument that the average location of the shots is in or near the bull’s-eye would certainly not satisfy the general! In (c) the hits are both precise and accurate. This indicates good marksmanship and by the same token, reliability! This candidate will receive top marks. Experience has shown that poor accuracy accompanied by good precision can be rectified in a candidate by proper training methods.

This example may be applied to many analytical and measuring situations. It defines the reliability of the operator and may be used to select candidates, instruments or techniques.

Careful measurements may yield a number of closely related values with a high probability that the true value lies in the middle of a very narrow range. Use of the term's true value, error, and accuracy in their real sense can then be used to evaluate the reliability of measurements and in investigating the kinds and sources of errors.

5. CLASSIFICATION OF ERRORS

Two types of errors are experienced during measurement and analysis:

5.1 Determinate Errors

Determinate errors are errors that may either be avoided or for which corrections can be applied after their magnitude was determined.

An error of the same sign and magnitude during multiplicative measurements is not always revealed by a lack of precision. This is an example of a constant error that is not suspected and that may lead to a false interpretation without the analyst being aware of its presence. Examples are cited below. To prevent its occurrence in new analytical method and without the availability of a suitable calibration standard, it is good practice to conduct the analysis by using an alternative method based upon a completely different physical technique or principle. It is rather unlikely that errors of the same sign and magnitude would be present if widely different methods are used. Any discrepancy in the results of different methods may lead to the source of the error. Measuring the composition of a TNT/RDX charge, for instance, is normally rapidly conducted by means of liquid chromatography. To check this method, a rather lengthy but accurate volumetric or extractive gravimetric method may be used. It is easier, though, to calibrate the liquid chromatograph with pure recrystallised explosives.

In the case of variable determinate errors, also known as systematic errors, it is not only the amount but even the sign that may change if conditions are changed. If the manner of the variation is known, corrections can then be applied. For example, the effect of temperature on the volume of volumetric glassware or on the efficiency of an extractive process can be compensated for.

There are many types or sources of determinate errors during measurement and analysis. Some of the more common ones are mentioned below:

- Errors caused by the equipment being used. These include the use of non-calibrated measuring devices (volumetric apparatus, balances, timers, measuring gages), etc.
- Failure to compensate for all the parameters that affect ballistic performance. (Wind speed, the Coriolis effect, etc).
- Errors due to impure materials, the impurities interfering with the method of analysis. Secondary synthesis products may, for instance, affect the results.
- Personal errors are caused by a limited ability of the analyst to make observations with certainty. Colour blindness may, for instance, cause problems during volumetric analysis. It is difficult to avoid or evaluate the magnitude of these known errors. They may be more or less constant and therefore not revealed by a lack of precision. A tendency, especially among beginners, is to allow prejudice to overcome judgment by adjusting slightly differing measurements to agree with one another in order to obtain an acceptable answer.
- Methodic errors are caused by the physical and/or chemical properties of the system being analysed. The problem is that the magnitude and sign of these

errors are constant if the analytical conditions during a series analysis remain the same. As already pointed out they may be revealed by changing the conditions or using a different method. The necessary corrections may then be applied.

- Operational errors are caused by inexperience, carelessness or failure to follow the prescribed procedures, which, in the case of the explosives industry, may be fatal! Some examples are spillage of materials, incorrect filling of shells, failure to apply known corrections, etc. To this should be added errors that arise during calculations, a weak spot with beginners. Careless errors should not be tolerated. Fortunately operational errors tend to decrease as the skills, experience, and understanding of the analyst improves. What initially appear to be indeterminate errors by the beginner eventually turn into variable determinate errors in the hands of an experienced analyst.

It happens that certain errors experienced during an analysis seem to be constant, both with respect to magnitude and sign if the quantity or magnitude of the component being determined changes. A non-calibrated timing device, for instance, may result in fairly precise but erroneous VOD values. Some errors, in turn, are proportional to the quantity of the sample. The absorption of moisture or retention of mother liquor or impurities during crystallization may serve as examples.

Some errors will always have the same sign. Non-calibrated instruments may introduce constant negative or positive errors. Contamination by impurities is another example. During multiple analysis positive errors arising in one procedure may be more or less cancelled by negative errors in another.

In all instances awareness of possible errors that may arise during an analytical or measuring process should be anticipated and corrected for if the result has to be meaningful. Keep in mind that calibration standards in the explosives industry hardly exist.

5.2 Indeterminate Errors

The identification of and correction for determinate errors may still leave slight variations in the source, magnitude, and sign of the resulting answer. Invariably these differences cannot be predicted nor estimated. They are known as indeterminate errors. They follow the law of chance or probability and are also known as random errors. Since they are indeterminate, no examples can be provided. Their study and quantification calls for more advanced statistical measures that do not fall within the scope of this paper and involve application of the laws of probability that will reveal the reliability of the measurements. These laws are based on the fact that:

1. Very large errors occur only seldom.
2. Small errors occur frequently
3. Positive and negative errors occur with equal frequency with the most probable value provided by the arithmetic mean of the measured values.

These rules apply only to situations involving a very large population or a number of observations or measurements and are represented graphically in the form of the normal error or frequency curve, also known as the Gaussian distribution curve, where the X-axis represents magnitude and the Y-axis frequency.

6. CONCLUSION

In summary it can be stated that ultimate reliability depends on various factors, e.g.:

- The ability of the analyst to take measurements and readings that are both precise and accurate. This calls for thoroughness.
- The ability to correctly calculate the final answer, not forgetting to include the appropriate units. This involves correct conversion between different units of measure and confident handling of calculators or other computing devices.
- The ability to visualise the final answer. Inability to do this may result in answers that, due to one or other miscalculation, are orders out without the analyst seeming to realise the big mistake!
- Finally it should be emphasised that analytical results are as good as the sampling technique. The laboratory sample should be the result of sampling units that have been collected in a systematic way, the correct reduction of the gross sample, a combination of sampling units, and proper care of the material to prevent unnecessary exposure to the atmosphere and heating during grinding procedures. Otherwise the results may be meaningless,

7. ANSWERS TO EXERCISES

Exercise 1: (a) 5, (b) 3, (c) 2, (d) 4, (e) 4, (g) 4, (h) 6, (I) 4.

Exercise 2: 460; (b) 400; (d) $2,90 \times 10^3$; (e) $7,54 \times 10^{-7}$; (f) $3,05 \times 10^3$; (g) $1,68 \times 10^4$; (h) 230; (i) $2,62 \times 10^{11}$.

Exercise 3: 1(a) 17,8; (b) $2,90 \times 10^6$. (if 10^4 is selected, additional uncertain figures will be introduced)
2(a) 25,28; (b) 25,6 (the average deviation is more than 0,1 indicating uncertainty of the first decimal)

Exercise 4: (a) 20,6
(b) $4,8 \text{ dm}^3$

This last calculation has been used by the author for more than three decades to evaluate the calculating skills of students. In the first place it tests the ability to correctly convert a linear dimension measured in millimetres to a volumetric one expressed in cubic decimetres. Secondly it must be noticed that the weak link in the calculation is the diameter, $2,1 \times 10^2$ mm, which must be written in this way since the first decimal is the uncertain one. This is because of the difficulty of measuring the diameter of the ball with a straight ruler. (Of course there are other methods of measure the diameter more accurately!) In the third place the ordinary calculating skills are tested. Fourthly the correct approximation should be performed. The calculator's 4,849677 ... must be converted to indicate the relative uncertainty of the weakest link, which is 1/21. Lastly, visualisation of the answer would prevent silly answers such as $4,8 \times 10^5$ to $4,8 \times 10^{-6} \text{ dm}^3$ presented by students who smilingly believed that their answers are correct. With a little visualisation these microscopic or macroscopic results could have been obviated if the round ball is seen as a box, maybe having a volume between about 3 to 10 dm^3 .)

REFERENCES

This paper is based on the following classical references but was largely further developed over the past three decades.

- [1] R.C. PINKERTON and C.E. GLEIT: J. Chem. Educ., **No. 44**,232, 1967
- [2] H.A. FLASCHKA, A.J. BARNARD and P.E. STURROCK: *Quantitative Analytical Chemistry*, Barnes and Noble Inc., 1969
- [3] G.J. VAN NIEKERK, B.D. VERMEULEN, ET AL; *Quality Guide*, Armscor, Pretoria, 1991

THERMAL AND THERMO-MECHANICAL INVESTIGATIONS OF LONG TIME STORED PROPELLANTS

P. Shishkov, T. Tzvetkoff, I. Glavchev and R. Ganev

University of Chemical Technology and Metallurgy,
8. Ohridski Str. Kl., 1756 Sofia, Bulgaria

Abstract:

Samples of single based propellant (SBP) and double based propellants (DBP) stored a long time in non-heated military store houses were investigated up to 393 K. The dependences temperature / deformation were made by the heating rate 2°C/min. and the values of glass transition temperature (T_g) were determined. With the Flory-Fox-Biky equation the values of $T_{g(\infty)}$ and K were calculated. After measuring the dimensions of the samples in several temperatures were calculated the coefficient of thermal expansion of the propellants. The influence of the time of storage of the propellants on their properties was determined.

Keywords: propellants, thermo mechanical dependence,
coefficient of thermal expansion.

1. INTRODUCTION

The decreasing of the nitrogen content of nitrocellulose (NC) in propellants during their ageing change the configuration and conformation of the macromolecules. The obtaining of –OH groups in the place of –NO₂ groups in different positions in the glucoside rings lead to the possibility of H-bond formation and to change of the crystallinity of the propellants. In the ageing the decreasing of the molecular weight of NC and the increasing of molecular weight distribution take place after the braking of oxygen bonds. All these processes must to change the thermo mechanical properties of NC in propellants, the plastic and elastic deformation and the coefficient of thermal expansion (CTE). Near to glass transition temperature (T_g) CTE, deformation and the dimensions of the sample change their values because the increasing of free volumes and of segmental movement in macromolecules.

In the literature was published the equation

$$(\alpha_L - \alpha_G) \cdot T_g = \text{const} \quad (1)$$

where α_L and α_G are the CTE above and below T_g .

In [1] was given another equation:

$$\Delta = (\alpha_{\max} - \alpha_{\min}) / \alpha_{\max} \quad (2)$$

and this value depend from the hardness of the materials.

From the dependence CTE versus temperature is possible to be determine the value of T_g . The value of T_g is possible to be obtaining and directly from thermo mechanical curves. The aim of the investigation is the determination of the values of CTE, T_g and $T_{g(\infty)}$ of SBP and DBP, their thermo mechanical curves and the dependence of the obtained results from the time of storage in non heated military store houses - the time of ageing of the propellants.

2. EXPERIMENTAL

The samples of pyroxylin, nitrodiglycole/NC (NDG) and nitroglycerine/NC (NG) propellants, produced in Arsenal AD, Bulgaria, stored a different time in non-heated military store houses were investigated. The values of CTE were determined from 254 K to 383 K by measuring the longitude of the samples by accuracy from 0.001 to 0.1 mm. The thermo mechanical curves were determined by apparatus with the heating of the samples from 295 K to 415 K by rate 2 K/min and accuracy of measurement of deformation 0.01 mm.

3. RESULTES AND DISCUSSION

The investigation of SBP by apparatus “Crater” is a standard method for their characterization. In ^[2] was described the modified version - the values of the rates of gas release were differentiated and was obtained a linear dependence with the time of storage of propellants. In our previous investigations of SBP, ageing a different long periods were determined the decreasing of the molecular weight of NC and increasing of its molecular weight distribution ^[3]. In the literature have a lot of information for the investigation of ageing processes by IR spectroscopy. The conformations of molecules of a –NO₂ substituted low molecular carbo-hydrates are the reason for doublets, triplets and quadropletes in the absorbance at 1660 cm⁻¹ in their IR spectra ^[4]. The most of authors confirmed the existence of a doublet at 1660 cm⁻¹ in IR spectra of NC because of a smaller numbers of conformations of the macromolecules. In ^[5] was described a IR spectra of a long stored SBP with triplet in the peak at 1660 cm⁻¹, connected by decreasing of the molecular weight and with H-bond formation shown by the shift of the bands and by the ratios $A_1 = A_{3340} / A_{\max}$ and $A_2 = A_{3314} / A_{\max}$. In this way the IR data confirm the processes during the ageing of propellants.

The values of T_g and melting points of polymers were connected with their molecular weight. According to the equation of Flory-Fox-Biky

$$T_g = T_{g(\infty)} - K/M \quad (3)$$

where K is constant, different in every polymer, the values of T_g increased with increasing of the molecular weight to the limit T_(∞). The reason for this dependence according to some of authors is the decreasing of the concentration of the ends groups. The values for the investigated SBP, calculated by equation (3) are:

$$\begin{aligned} T_{g(\infty)} &= 390 \text{ K} ; & K &= 1630 \cdot 10^3 \text{ (from the data of } M_n \text{)} \\ T_{g(\infty)} &= 416 \text{ K} ; & K &= 1520 \cdot 10^3 \text{ (from the data of } M_w \text{)} \end{aligned}$$

According to ^[6] the value of T_g of NC is 440 K. It is well known, that after 393 K in propellants start the gas release and in this way the obtained results for higher temperatures are no a real one. The stabilizers content in SBP and the low molecular components of DBP change the values of T_g too. I this way the obtained results belong to the analyzed samples.

The dependences longitude/ versus temperature of samples of SBP and DBP stored different time in non-heated military store houses are in figures from 1 to 7.

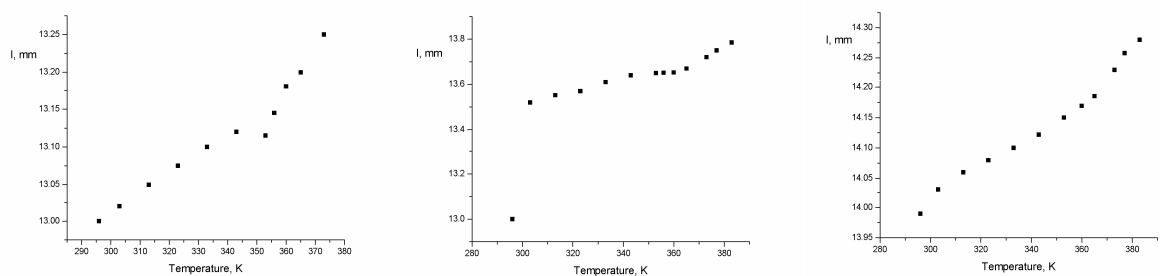


Fig 1,2,3. Dependence of the longitude l , mm of SBP, stored 45 (1), 27(2), 21(3) years from the temperature, K

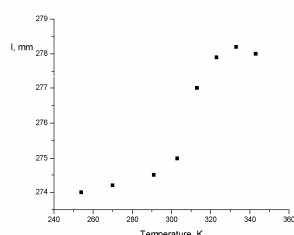


Fig 4. Dependences of the longitude, l [mm] of NDGP stored 21 years

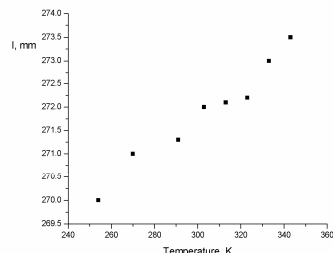
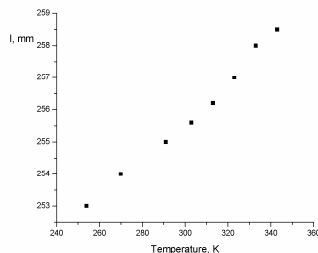
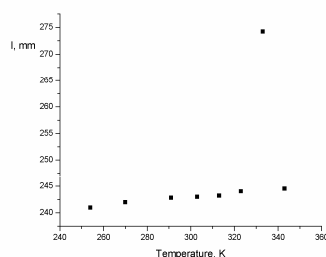


Fig 5,6,7. Dependences of the longitude, l [mm] of NGP stored 50 (5), 30 (6), 21 (7) years

From the points of braking the linear dependences were determined the values of T_g , given in fig. 8.

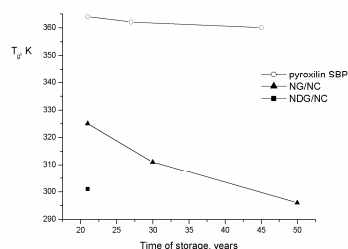


Fig 8. Dependences of T_g from the time of storage of propellants

It is evident that the values of T_g decreased by the increasing of the time of ageing, because the molecular weights decreased too. In this way the values of T_g is possible to characterize the ageing of propellants.

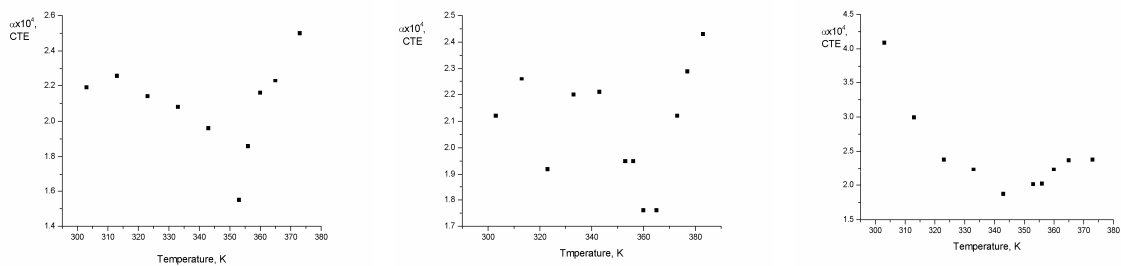


Fig 9,10,11. Dependence of the CTE from the temperature for SBP, stored 45 (9), 27 (10), 21 (11) years

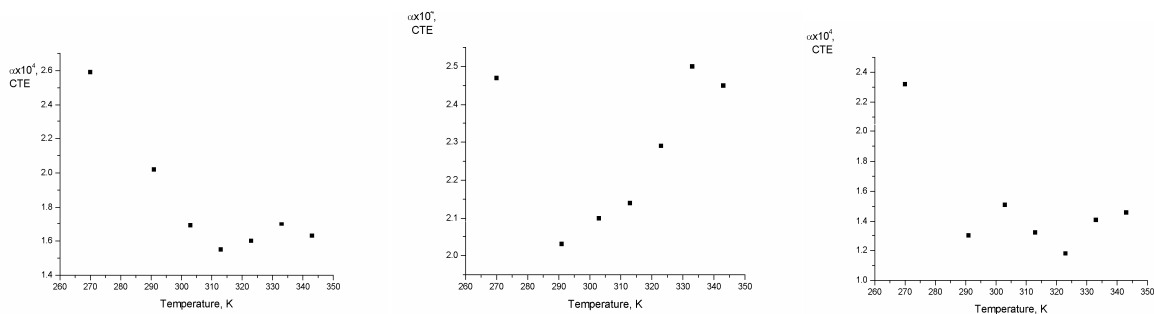


Fig 12,13,14. Dependence of the CTE from the temperature for NG, stored 50 (12), 30 (13), 21 (14) years

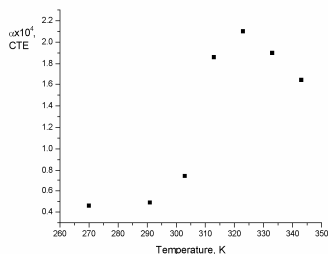


Fig 15. Dependence of the CTE from the temperature for NDG, stored 21 years

From the dependences longitude – temperature were calculated the values of CTE. The obtained results are in figures from 9 to 15. It is evident that in several dependences CTE versus temperature have minimums around T_g , but the calculations by the equation (2) are difficulties. In this way the application of the differences in CTE around T_g for the characterization of the ageing of propellant is no correct.

The thermo-mechanical curves of the samples of propellants are in figures from 16 to 19.

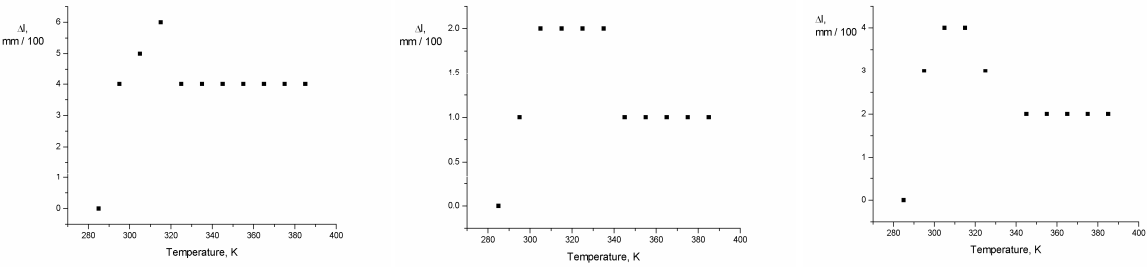


Fig 16,17,18. Thermo-mechanical curve of SBP, stored 60 (16), 45 (17), 21 (18) years

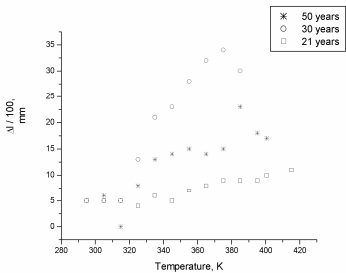


Fig 19. Thermo-mechanical curves of NGP

It is evident that the process of cold crystallization takes place in SBP. For NGP the values of T_g were determined:323 K, 333 K and 345 K for samples stored 50,30 and 21 years. The obtained results confirm the data in fig.8 and the possibility of application of thermo-mechanical curves for characterization of the ageing of propellants.

4. CONCLUSION

By the determination of T_g and thermo-mechanical curves of SBP and DBP is confirmed that these methods are sensitive to the time of storage – the processes of ageing of propellants.

REFERENCES

- [1] I. GLAVCHEV, KR. PETROVA, M. IVANOVA: Determination of the coefficient of thermal expansion of epoxy composites, *Polymer Testing*, 21, 177, 2002
- [2] R. GANEV, I. GLAVCHEV: Research into the ageing of pyroxylin powders for strong periods of over 50 years, III-rd Seminar "New trends in research of energetic materials", april 12-13, 2000, University of Pardubice, Czech Republic, 2000
- [3] R. GANEV, I. GLAVCHEV, P. NOVAKOV: Self extinguishing and high-flammability point coatings based on waste pyroxylin powder blended with halogen-containing polymers, *J. Surface Coat. Int.*, Vol 81, 11, 528, 1998
- [4] L.K. PRIHODKO, T.E. KOLOSOVA: IR krioskopskie issledovanie nizkomolekularnih anaogov nitratoov cellulose, *J. prikladnoi spectroscopii*, 56, 294, 1992 (in Russian)
- [5] R. GANEV, I. GLAVCHEV, TZ. TZVETKOFF, M. IVANOVA, T. TOTEV: Investigation of long-term ageing of single based propellants by IR spectroscopy, *J. of explosives and propellants*, R.O.C., accepted.
- [6] B.V. PRIVALKO, *Svoistva polymerov v blochnom sostoianii*, Kiev, Naukova dumka, p.114 (in Russian), 1984

INFLUENCE OF VELOCITY OF GAS FLUX TO THE BURNING SURFACE

M. Šimáček*, V. Kuttelwascher* and P. Stojan**

* Military Academy in Brno, Faculty of Airforces and Air Defence,
Kounicova 65, CZ-602 00, Brno, Czech Republic

** Explosia a.s., Research Institute for Industrial Chemistry,
CZ-532 17, Pardubice - Semtín, Czech Republic

Abstract:

This paper includes the solution of testing Solid Propellant Rocket Motor with erosive burning part of burning process when gas generator is used for the purpose mentioned. Students of doctor's study programs of Military Academy in Brno and members of Explosia a.s. provided the realisation of these tests.

Keywords: erosive burning, solid propellant, gas generator

1. INTRODUCTION

The Solid Propellant Rocket Motor (SPRM) with high level of specific impulse needs to realize the case of erosive burning of solid propellant. There is the problem with free cross-section of Combusting Chamber (CC). High velocity of gas stream brings very important influence to the surface of propellant and internal surface of chamber (see Fig.1). Mainly when the burning process is starting.

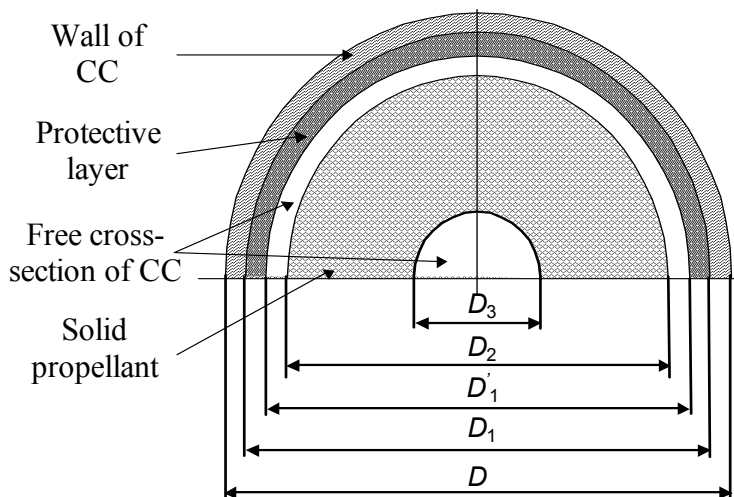


Fig 1. Cross-section of combustion chamber (where D is external diameter of CC, D_1 is internal diameter of CC (with out of protective slide), D_1' is internal diameter of CC (with the protective slide), D_2 is external diameter of mass propellant and D_3 is internal diameter of mass propellant).

The flow of burnt elements passes through the free cross-section of CC. The situation can be described by the coefficient of filling of combustor chamber K_{SK} . At the beginning of burning process the products of burning flow through the channel with the lowest cross-section has the maximum velocity. Then his value goes to lower according to the burning rate. The erosion kind of burning is expired in the first part of mass propellant burning.

There is convenient to pay an attention:

- *Theoretical computation of values of the solution boundary condition,*
- *Drawing and production of parts of testing motor,*
- *Providing of testing place for pressure and thrust measurement,*
- *Realization of experimental tests,*
- *Evaluation of tests results,*
- *Comparing of values from tests with theoretical computation,*
- *Conclusion and discussion of the results,*
- *Giving the results: (i) Tables of values of constants of erosive burning and (ii) Graphical expression of dependence between erosive burning and velocity of gas stream.*

2. THEORY

Values of gas pressure inside of the CC, burning temperature and velocity of gas flow are important parameters to express the function of SPRM. These values determine the rate of burning, which we can be expressed as follows ^[1]

$$u = u_0 f(T_{ph}) g(p) h(w), \quad (1)$$

where u_0 is burning rate constant, function $f(T_{ph})$ includes sensitivity of SP with respect to the temperature of SP surface, $g(p)$ is the pressure function of gasses inside of CC and $h(w)$ determine the function of gas velocity influence regarding erosive burning. The erosive burning rate of rocket motors can be expressed as follows ^[1,4]

$$u_e = u_0 f(T_{ph}) p_{sk}^\alpha K_e, \quad (2)$$

where u_0 is unit burning rate, p_{sk} is pressure of gases inside of CC, α is exponent of burning and $K_e > 1$ is the parameter of erosive burning.

Parameter K_e of erosive burning SP can be expressed from one of next equation ^[1,2]

$$\begin{aligned} K_e &= 1 + K_w (w - w_{mez}), \\ K_e &= 1 + K_\lambda (\lambda - \lambda_{mez}), \\ K_e &= 1 + K_\delta (\delta - \delta_{mez}), \end{aligned} \quad (3)$$

where K_w , K_λ and K_δ are kinds of expressions for coefficients of SP sensitivity towards the erosive burning, $\lambda = w / c_{kr}$ is a dimensionless rate of gas velocity where c_{kr} is critical velocity of sound and $\delta = (\rho w) / (\rho_{cr} c_{cr})$ is a mass velocity of gas velocity with relevant density

ρ , w_{mez} is a critical speed level of erosive burning rate ($w_{mez} \sim (100 - 150) \text{ m.s}^{-1}$) [1,4], λ_{mez} is a critical dimensionless velocity of erosion burning rate ($\lambda_{mez} \sim 0,1$) and δ_{mez} is dimensionless level of mass erosive burning rate increase.

Usual expression of internal ballistics solution can be mentioned in following manner :

1) Solution of long and thick SP grain (see Fig 2).

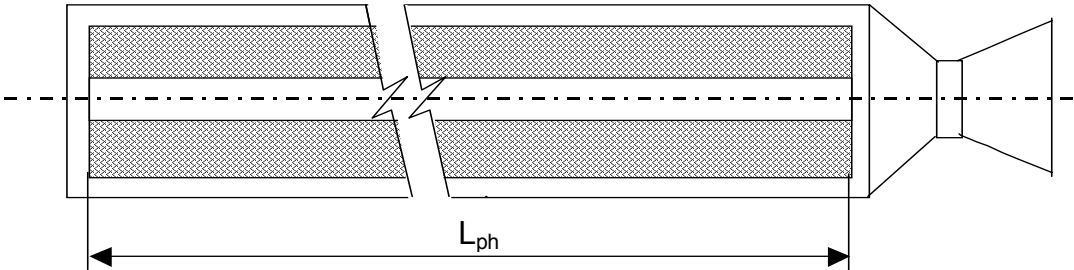


Fig 2. Scheme of rocket motor with a long and thick SP.

2) Solution of SP charge using gas generator (GG) in order to obtain gas stream velocity to be able to increase same conditions as first. There is chance to change the gas velocity through the CC free cross-section, as shown in Fig.3. [4]

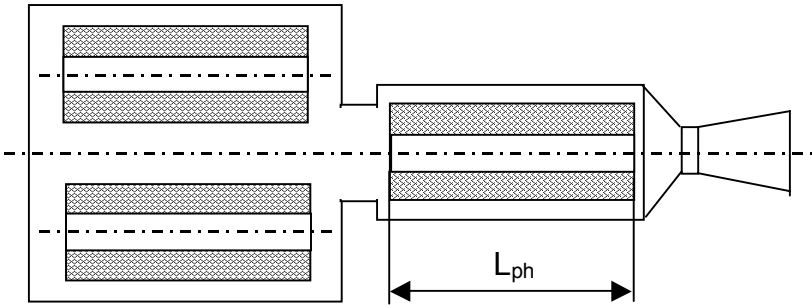


Fig 3. Scheme of rocket motor with the gas generator.

The first solution requires relative big values of the grain length L_{ph} and great numbers of nozzles. Due to the mentioned the costs experiments will be rised. On the other side the second solution allows simulate wide interval of gas velocity whereas the velocity can be changed in several ways (e.g. by changing number of SP grains in GG, by changing value of cross-section of regulator of gas velocity to the main CC, by changing the critical cross-section of the main CC nozzle etc.). In addition the relevant velocity is relatively constant along short SP grain and therefore only two pressure sensors (the first on the GG and the second on the main CC) could be used.

The second solution was chosen with regard to above mentioned. Testing rocket motor was made in the shape as shown Fig. 4, having four main construction parts, i.e.:

- *Gas generator (2)*
- *Regulator of gas flux to the main CC (3)*
- *Main combustng camber (1)*
- *Main CC nozzle (4)*

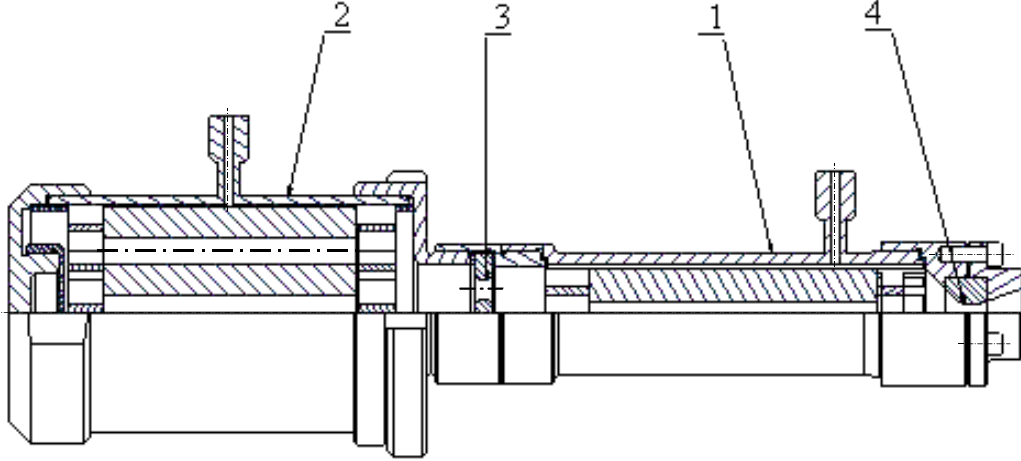


Fig 4. Testing rocket motor (1- main combustng camber, 2- gas generator, 3- regulator of gas flux to the main CC, 4- nozzle of main CC)

General solution ^[2, 3] of the given problem is possible when assuming the following conditions:

- *Adiabatic process is presupposed;*
- *Neutral kind SP burning;*
- *Flow cross-sections are chosen so that total pressures in them are same, as well as dimensionless gas velocities.*

Next system of equations can be applied here:

$$A_{vg} \lambda_g \left(1 - \frac{\kappa - 1}{\kappa + 1} \lambda_g^2 \right)^{\frac{1}{\kappa - 1}} = \varepsilon_r A_r \lambda_r \left(1 - \frac{\kappa - 1}{\kappa + 1} \lambda_r^2 \right)^{\frac{1}{\kappa - 1}}, \quad (4)$$

$$A_{vz} \lambda_z \left(1 - \frac{\kappa - 1}{\kappa + 1} \lambda_z^2 \right)^{\frac{1}{\kappa - 1}} = \varepsilon_v A_{krz} \lambda_{krz} \left(1 - \frac{\kappa - 1}{\kappa + 1} \lambda_{krz}^2 \right)^{\frac{1}{\kappa - 1}}, \quad (5)$$

where A_{vg} is free cross-section of gas generator, A_{vz} is free cross-section of combustion chamber, A_r is cross-section of regulating part, A_{krz} is critical cross-section of nozzle, λ_g , λ_z , λ_r , λ_{krz} are appropriate dimensionless rates of gas velocity, where $\varepsilon_r = \varepsilon_v = 1$ because it is excepted that cross-section edges are rounded.

For the theoretical solution of testing RM can be given parameters of gas velocity passing through the channel between SP and body of combustion chamber. The value of gas

velocity is decreasing during the burning process with respect to increasing of the free cross-section of combustor chamber.

The basic assumption solution is

$$p_{skz} \geq p_{atm} \left(\frac{\kappa + 1}{2} \right)^{\frac{\kappa}{\kappa - 1}}, \quad (6)$$

where p_{atm} is atmospheric pressure, κ is an adiabatic exponent.

Then, dimensionless value of gasses flux in CC is

$$\lambda_z = \frac{w_z}{c_{kr}}, \quad (7)$$

where

$$c_{kr} = \sqrt{\frac{2\kappa}{\kappa + 1} \chi r T_{sk}} \quad (8)$$

is critical sonic sound, χ is parameter of heat losses, r is specific gas constant, T_{sk} is a burning temperature (inside of CC).

Area of critical cross-section can be expressed from eq. (5) as follows :

$$A_{krz} = \frac{A_{vz} \lambda_z \left(1 - \frac{1 - \kappa}{1 + \kappa} \lambda_z^2 \right)^{\frac{1}{\kappa - 1}}}{\left(\frac{2}{\kappa + 1} \right)^{\frac{1}{\kappa - 1}}}. \quad (9)$$

Relation between pressures in the CC and in the GG is

$$\left(\frac{p_{skz}}{p_g} \right) = \frac{A_r}{A_{krz}} \left(\frac{\kappa + 1}{2} \right)^{\frac{1}{\kappa - 1}} \lambda_r \left(1 - \frac{\kappa - 1}{\kappa + 1} \lambda_r^2 \right)^{\frac{1}{\kappa - 1}}. \quad (10)$$

Mass flux can be written as

$$m_{ph} = A_{krz} \frac{\varphi(\kappa)}{\sqrt{\chi r T_{sk}}} \left(\frac{p_{skz}}{p_g} \right) p_g, \quad (11)$$

where $\varphi(\kappa)$ is the function of adiabatic exponent.

Pressure inside of gas generator is given by

$$p_g = \left\{ \frac{u_0 f(T_{ph}) \rho_{ph} \sqrt{\chi r T_{sk}}}{\varphi(\kappa) A_{krz} \left(\frac{p_{skz}}{p_g} \right)} \left[S_{0g} + S_{0z} \left(\frac{p_{skz}}{p_g} \right)^\alpha \right] \right\}^{\frac{1}{1 - \alpha}}. \quad (12)$$

Algorithm of the solution is given by the following set of equations: ^[1,2]

$$\begin{aligned}
 1. \quad A_{krz} &= \frac{A_{vz} \lambda_z \left(1 - \frac{1-\kappa}{1+\kappa} \lambda_z^2 \right)^{\frac{1}{\kappa-1}}}{\left(\frac{2}{\kappa+1} \right)^{\frac{1}{\kappa-1}}}, \\
 2. \quad z(\lambda_z) &= 0,5(\lambda_z + \lambda_z^{-1}), \\
 3. \quad a_z &= 1 - \left(\frac{\kappa-1}{\kappa+1} \right) \left(\frac{A_{vz}}{A_r} - 1 \right), \\
 4. \quad \lambda_r &= \frac{z(\lambda_z)}{a_z} - \sqrt{\left(\frac{z(\lambda_z)}{a_z} \right)^2 - \frac{A_{vz}}{a_z A_r}}, \\
 5. \quad z(\lambda_r) &= 0,5(\lambda_r + \lambda_r^{-1}), \\
 6. \quad \lambda_g &= \frac{A_{vg}}{A_r} z(\lambda_r) - \sqrt{\left(\frac{A_{vg} z(\lambda_r)}{A_r} \right)^2 - 1}, \\
 7. \quad A_{vg} &= A_{skg} \left(1 - \frac{A_{phg}}{A_{skg}} \right), \\
 8. \quad \left(\frac{p_{skz}}{p_g} \right) &= \frac{A_r}{A_{krz}} \left(\frac{\kappa+1}{2} \right)^{\frac{1}{\kappa-1}} \lambda_r \left(1 - \frac{\kappa-1}{\kappa+1} \lambda_r^2 \right)^{\frac{1}{\kappa-1}}, \\
 9. \quad p_g &= \left\{ \frac{u_0 f(T_{ph}) \rho_{ph} \sqrt{\chi r T_{sk}}}{\varphi(\kappa) A_{krz} \left(\frac{p_{skz}}{p_g} \right)} \left[S_{0g} + S_{0z} \left(\frac{p_{skz}}{p_g} \right)^\alpha \right] \right\}^{\frac{1}{1-\alpha}}, \\
 10. \quad p_{skz} &= p_g \left(\frac{p_{skz}}{p_g} \right), \\
 11. \quad m_{ph} &= A_{krz} \frac{\varphi(\kappa)}{\sqrt{\chi r T_{sk}}} \left(\frac{p_{skz}}{p_g} \right) p_g, \\
 12. \quad F &= c_{Fz} p_v \left(\frac{p_{skz}}{p_v} \right) A_{krz}.
 \end{aligned} \tag{13}$$

3. EXPERIMENTS

MA in Brno had made the analysis of burning process and basic computing solution of testing rocket motor. Exploitation and preparation of testing area were made in cooperation between MA in Brno and Research Institute for Industrial Chemistry (Explosia a.s., Pardubice –Semtín), which one is allowed to offer the testing area according to Certificate for accredited testing company in field of internal ballistics to measure thrust and pressure on testing RM (i.e. ballistic tests of rocket motors, etc.).

Experimental measurement on the testing rocket motors involved measures of pressure in gas generator and measure of pressure in main combustion chamber. Testing rocket motor configuration before ignition is shown in Fig 5. ^[3]

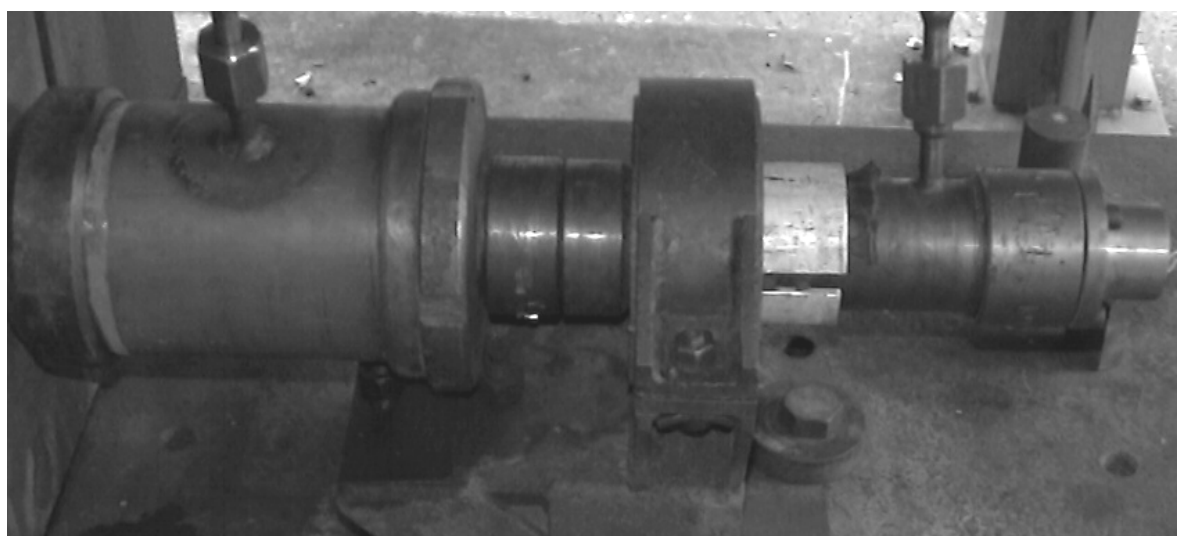


Fig 5. Testing rocket motor before ignition.

The gas velocity of around testing SP grain was controlled by number of SP grains in gas generator and by critical diameter of nozzle of main combustion chamber. Estimated values of gas velocity are shown in the Table 1. These values were chosen as initial boundary conditions as mentioned.

Table 1. *Calculated values of velocities of gas flux (products of combustion) around testing SP grain in experiments.*

Number of SP grains in GG	Diameters of regulator (regulating nozzle) [m]. 10^{-3}	Critical diameter of nozzle of main CC [m]. 10^{-3}	w [ms ⁻¹]
1	4 x 11,5	14,04	120
2	4 x 11,5	16,16	160
2	4 x 11,5	18,00	200
3	4 x 11,5	19,62	240
3	4 x 11,5	21,07	280

4. CONCLUSION

Performed experiments prove, that theoretical part of this work was given correctly. Chosen solid propellant seems to be able to burn according to estimated kind of burning process.

This cooperation between MA in Brno and Research Institute for Industrial Chemistry (Explosia a.s., Pardubice–Semtín) is presupposed to continue also in future. Both partners decided to leap the way with cooperation in the field of practical tests of special testing rocket motors for others students of doctor study programs.

REFERENCES

- [1] F. LUDVÍK and P. KONEČNÝ: Vnitřní balistika raketových motorů na tuhou pohonnou hmotu, Učebnice VA v Brně U-1153/1, Brno, 1999 (in Czech)
- [2] A. A. ŠIŠKOV: Gazodinamika porochovykh raketnykh dvigatělej, Mašinostrojenie, Moscow, 1963
- [3] F. LUDVÍK: Zkušební zařízení pro sledování vlivu rychlosti plynového proudu na rychlost hoření tuhé pohonné hmoty, Sborník VA v Brně, Brno, 1985 (in Czech)
- [4] A. H. KARAM ALLA: The influence of erosive burning of solid propellant on the internal ballistics of solid propellant rocket motors, MA Brno, 1985

HIGH RESOLUTION OPTICAL ANALYSIS OF DYNAMIC EXPERIMENTS ON PBXs

C.R. Siviour, S.G. Grantham, D.M. Williamson, W.G. Proud,
S.M. Walley and J.E. Field

PCS Group, Cavendish Laboratory, Cambridge, CB3 0HE, United Kingdom

Abstract:

Previous research^[1] has provided information on the high strain rate behaviour of energetic systems. This paper outlines developments in the measurement of strain fields and strain localisation. In particular, the conditions for strain localisation in materials are discussed. The application of a photographic technique, digital speckle metrology, allows deformation fields to be measured. Although this does not provide sufficient resolution for strain localisations to be observed in detail, this aspect is being actively pursued.

Keywords: *polymer bonded explosives, PBX, high strain-rate testing,
optical techniques, strain localisation*

1. INTRODUCTION

The split Hopkinson pressure bar is a standard technique for the high strain-rate loading of materials. It allows measurements of a material's stress strain relationship at rates between 500 s^{-1} and $10,000 \text{ s}^{-1}$, and over a range of temperatures. A thorough description of the technique is available elsewhere^[1], but a basic overview follows.

The specimen is a small cylinder (length and diameter between 5 and 10 mm) of material. It sits between two metal rods, called the input and output bars. A gas gun is used to launch a striker bar into the input bar, and this introduces a stress wave into the input bar. The stress wave travels to the specimen, causing the specimen to deform. Because of the impedance mismatch between the bars and specimen some of the input wave is reflected, and some transmitted through the specimen into the output bar. These waves are measured using strain gauges on the bars, and can be used to calculate the stress strain response of the material. There are a number of advantages to using this technique. The first is that the instrumentation is on the bars, which remain elastic even when the specimen undergoes large plastic deformations. The second is that the specimen is small, and easy to prepare. This is a very important consideration when using explosive materials.

Polymer bonded explosives (PBXs) consist of explosive crystals dispersed throughout a soft polymer binder. When the material is loaded most of the deformation is taken up by the binder, which makes the material less sensitive than a pure explosive. The explosive content can be up to 95%, so that the PBX output approximated that of the pure explosive. The mechanical properties of the explosive depend on the temperature, strain rate and crystal loading. In fact, the binder properties have a very strong effect on the overall strength. It is found that a stiffer PBX is more sensitive to ignition than one with a lower modulus, given the behaviour of polymers this suggests that sensitivity increases with decreasing temperature. This means that testing at low temperatures and high strain rates is important since a surprisingly large number of events can cause high strain rate loading.

An important mechanism in hot-spot formation in explosives can be the development of regions of localised deformation (shear bands). In metals, these occur when the strain hardening of the material is not able to compensate for the thermal softening. Since heat is produced during deformation this leads to a local instability which, once it develops, causes strain to localise along bands in the material. Understanding these bands, and the conditions under which they occur is very important for improving explosive safety.

A major disadvantage of the Hopkinson bar, which is shared with other remotely gauged systems, is that the average properties of the specimen are measured. This does not prevent inhomogeneous materials, such as PBXs being tested, however it does mean that the specimen size must be large, compared to the particle size, if the results are to be meaningful. A general rule is that there should be at least 25, and preferably 100, grains in any cross section.

In order to make more useful measurements of PBX properties, it would be useful to be able to measure the specimen deformation field, rather than the average deformation. This is possible using digital speckle metrology (DSM) ^[2,3,4].

The following sections describe the DSM technique, before considering its application to high strain-rate testing. The results describe some of the conditions under which strain localisation appears. Results from optical analysis of high strain rate experiments are discussed.

2. THEORY

The speckle technique works by following the motion of a random pattern on the surface of a specimen. The pattern can be produced due to natural features on the surface, by using spray paint, or by laser speckle. A series of photographs is produced during the deformation (the dynamic image), and these can either be analysed sequentially, or by comparison to a static image taken before the deformation (the reference image)

The analysis, which is fully automated, involves selecting a small area of the reference photograph, and then another smaller region, from within this area, but on the deformed photograph, these are called the reference and deformed subimages. The deformed subimage is smaller than the reference, and is padded with random 'greyscale' speckles. The two subimages are compared, and a 'correlation coefficient' is computed, which is 1 if the two pictures are exactly the same, and 0 if they have no similarity. The deformed subimage is shifted around the reference subimage, and the correlation has a peak at the point where the two images are most similar to each other. This correlation value will not be 1 due to rotations and distortion, but will be clearly defined from the background noise. The position of the subimage at this peak tells us the movement of that point. If a series of subimages from the two photographs are compared, then local displacement maps are produced over the specimen surface. The sequence is shown in figure 1.

The correlation algorithm used in these experiments was developed by Sjö Dahl & Benckert ^[5]. The correlation is not performed in the spatial domain, like other algorithms ^[6], but in the frequency domain. The use of the Fast Fourier Transform (FFT) allows the computational time to be reduced and allows non-integer pixel shifting to be carried out. The cross-correlation is expressed in equation 1.

$$C(p, q) = F^{-1}(H_{s1}^* H_{s2}) \quad (1)$$

where $C(p,q)$ is the discrete two dimensional correlations, F^{-1} is the inverse Fourier transform. H_{s1}^* is the complex conjugate of the Fourier transform of sub-image $s1$ and H_{s2} is the Fourier transform of sub-image $s2$.

Due to the use of the FFT, the sub-image size is chosen to be an integer power of two to optimise the algorithm. An iterative procedure is used to reduce signal-to-noise and create a sharp correlation peak. Non-integer pixel displacements are dealt with using an expansion of the correlation surface to create a continuous surface [8]. This achieves a displacement accuracy of 0.01 pixels of displacement for an optimised speckle system. The spatial resolution is defined by the speckle size, since a finite number of speckles must be present in a sub-image to provide a successful correlation.

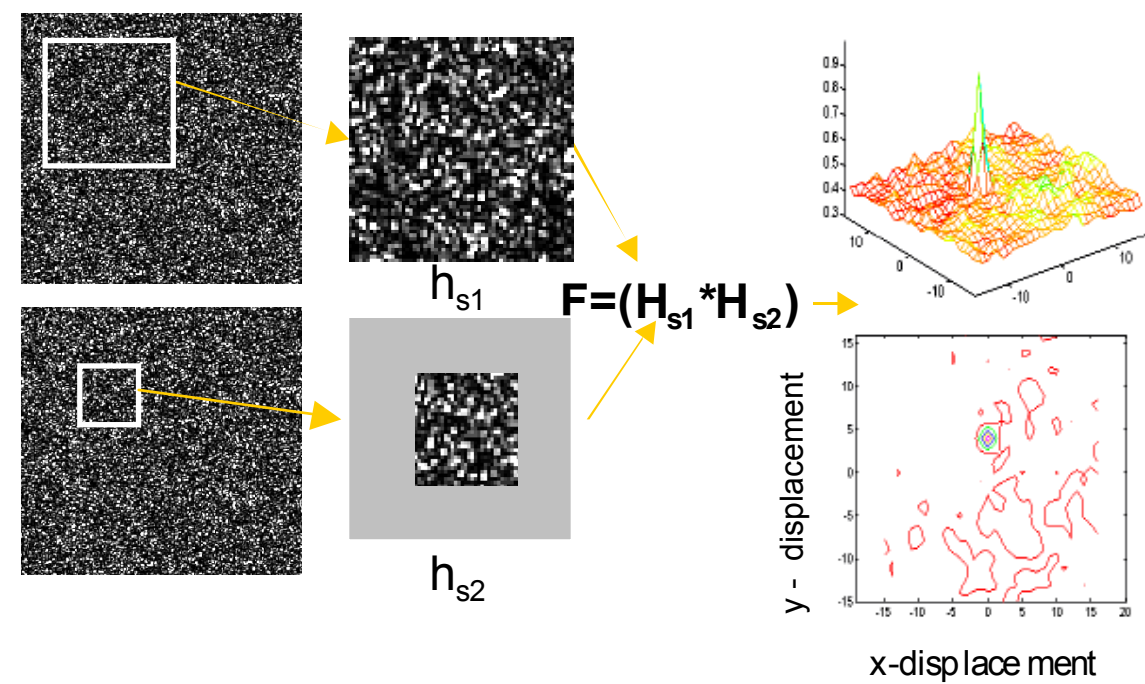


Fig 1. Schematic diagram of speckle analysis, from [7]

3. EXPERIMENT

3.1 Compression tests on PBXs

Mechanical tests were carried out in compression on two explosives and a simulant. Two of these had the same binder (HTPB), but different loading densities; these were PBS 9501 (loading density above 90%), and ‘PBX1’ (loading density 88%). The final material was EDC37, which has a loading density similar to PBS 9501, but a softer binder. PBX1 specimens were of two types, with two particle size distributions, 710 μm (PBX1a) and 160 μm (PBX1b) respectively. EDC37 was the subject of a more detailed study of the effects of strain rate [9], some of the results from that paper are reproduced here for ease of reference, and results from PBX1 are presented in [10].

3.2 Digital Speckle Metrology

The specimens used in the Hopkinson bar are right cylinders, which range in size from 2 mm to 5 mm long, and 5 mm to 10 mm diameter. Initial observations showed that, whilst the surface features in PBXs were distinct enough to produce a speckle pattern for quasi-

static testing, more contrast was needed for high-speed photography. This was applied using an artist's airbrush to produce a fine pattern in black paint.

The photographs were taken using a high-speed camera, the Hadland Ultra-8. Light entering the camera is split by a prism into 8 parts, which fall onto a square array of 8 CCDs. These CCDs are independently triggered, although in this case the photographs were taken at constant time intervals. Illumination was applied using argon flash bulbs, and the whole system was triggered using a make trigger on the front of the input bar, which was made by the impact of the striker. The specimen and bar would be set up, and a static set of photographs taken. A corresponding series of dynamic images was produced during the deformation. There are two ways of analysing the photographs. The first is to compare each dynamic image to the corresponding static image, and produce deformation maps that way. The advantage is that any distortion caused by the camera is immediately removed. Unfortunately the correlation breaks down for very large deformations, and so the results in the later photographs are incomplete. Instead it is possible to produce the maps temporally, comparing the first image on the deformed sequence with the second, and so on. In order to compensate for distortions, the same process is carried out on the static set of images, and any deformations measured are removed. This allows larger deformations to be measured without loss of correlation, because the deformations between each image are small. However, in this case any errors in the measurement add up over time. Ideally, both methods are used and compared, but the results shown are usually from temporal correlations.

4. RESULTS

4.1 Compression tests on PBXs.

Figure 3 shows stress strain curves for EDC37 at a strain rate of about 3900 s^{-1} . The shape of the stress strain curve is typical for cylindrical materials that exhibit strain localisation, and is very different from the elastic, yielding and brittle materials that were shown in last year's seminar. The existence of localisations is confirmed in figure 2, which shows high speed photographs of the deformation. PBS 9501 also exhibits stress strain behaviour indicative of strain localisations, figure 4, PBX 1, however, does not, figure 5. It has stress strain behaviour more similar to that of HTPB, the binder from which it is made, although the PBX is obviously stiffer than the binder. The lower loading density PBX1 is tested at -60°C , figure 6. Here the material with smaller grain size, and therefore separation, does show strain localisations, whereas that with higher separation does not.

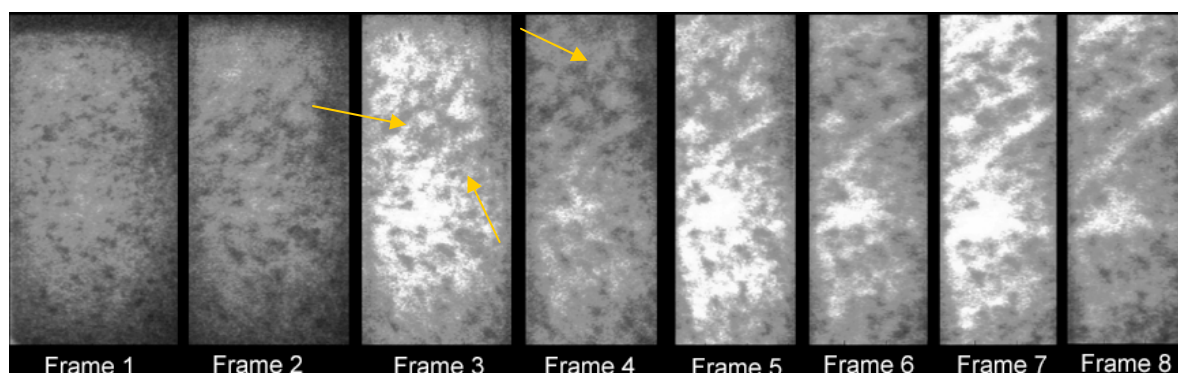


Fig 2. Strain localisations developing in EDC37, initial development is shown by arrows. The interframe and exposure times are $20\mu\text{s}$. The stress pulse reaches the sample between frames 1 and 2^[9].

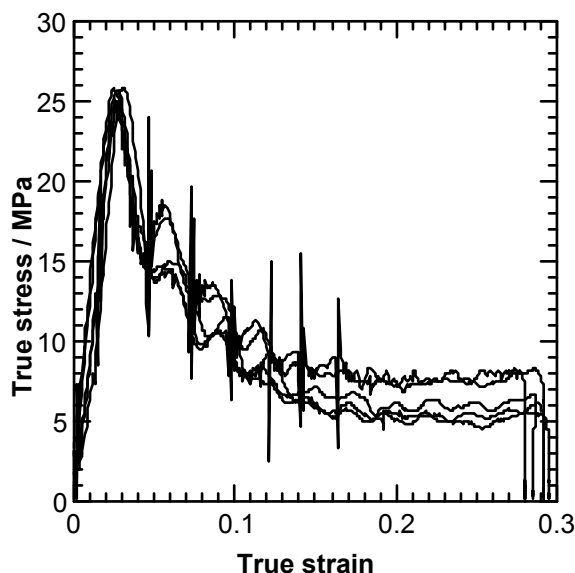


Fig 3. Stress strain curves for EDC37 at $3900 \pm 50 \text{ s}^{-1}$

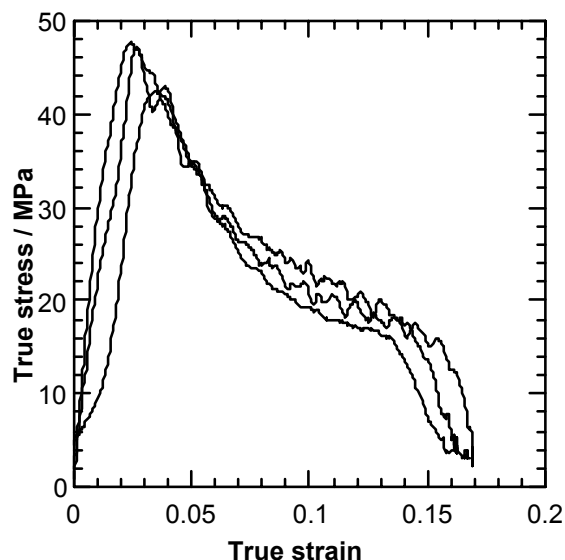


Fig 4. Stress strain curves for PBS 9501 at $1500 \pm 50 \text{ s}^{-1}$

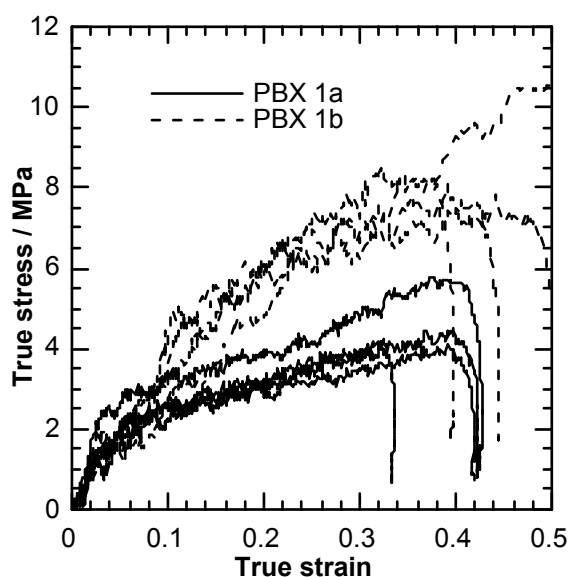


Fig 5. Stress strain curves for PBX1 at room temperature and $5000 \text{ s}^{-1[10]}$

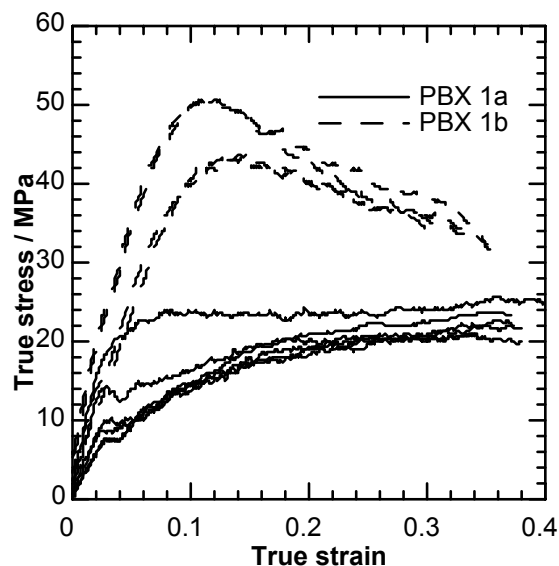


Fig 6. Stress strain curves for PBX1 at $-60 \text{ }^{\circ}\text{C}$ and 3500 s^{-1}

4.2 Speckle results

Figure 7 shows displacement quiver plots for a specimen of PBS 9501 deformed in compression. A strain time plot is shown in figure 8, which is compared to the strain time curves calculate from the Hopkinson bar equations.

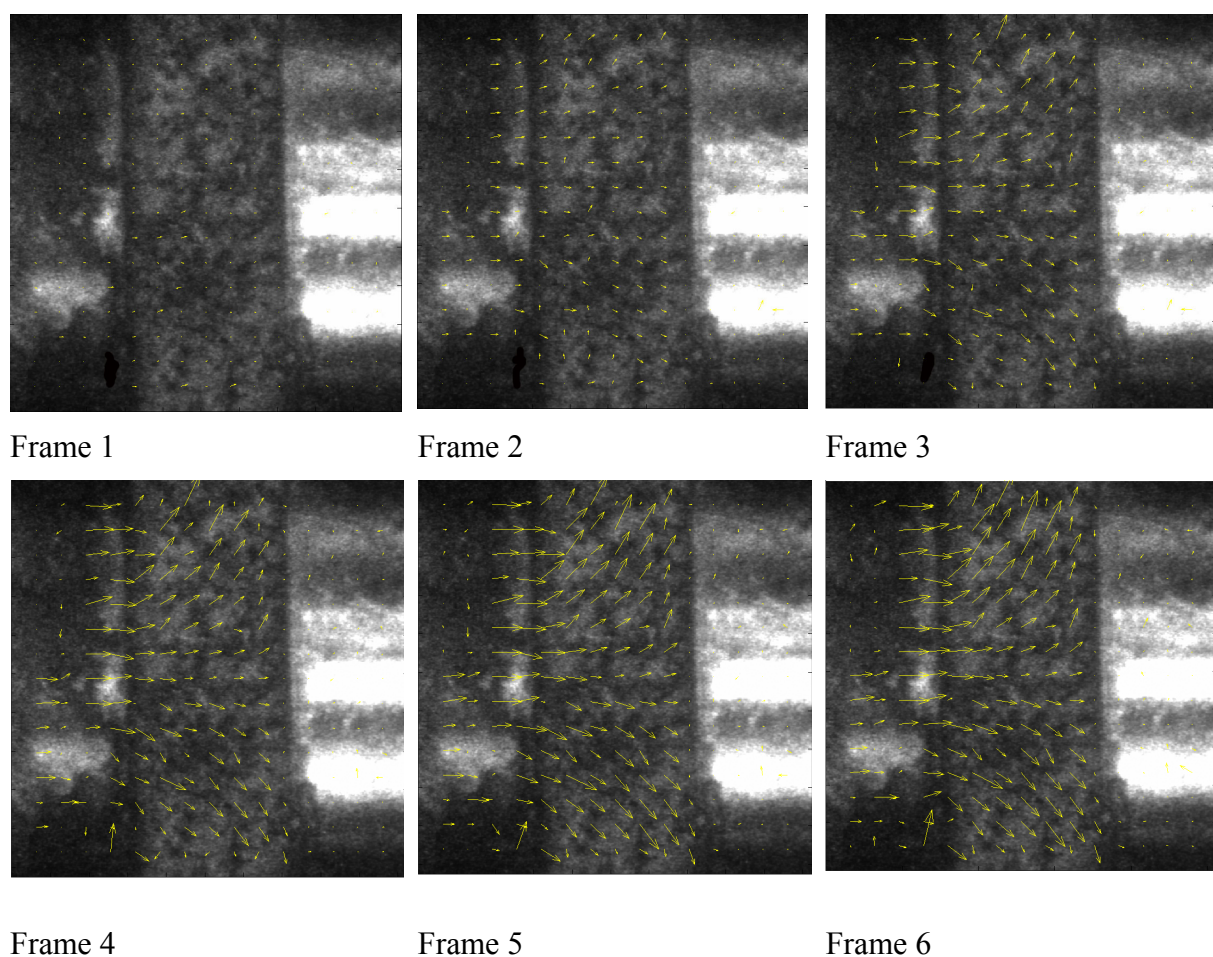


Fig 7. Development of specimen displacement in a Hopkinson Bar experiment on PBS 9501. The interframe and exposure times were both 20 μ s

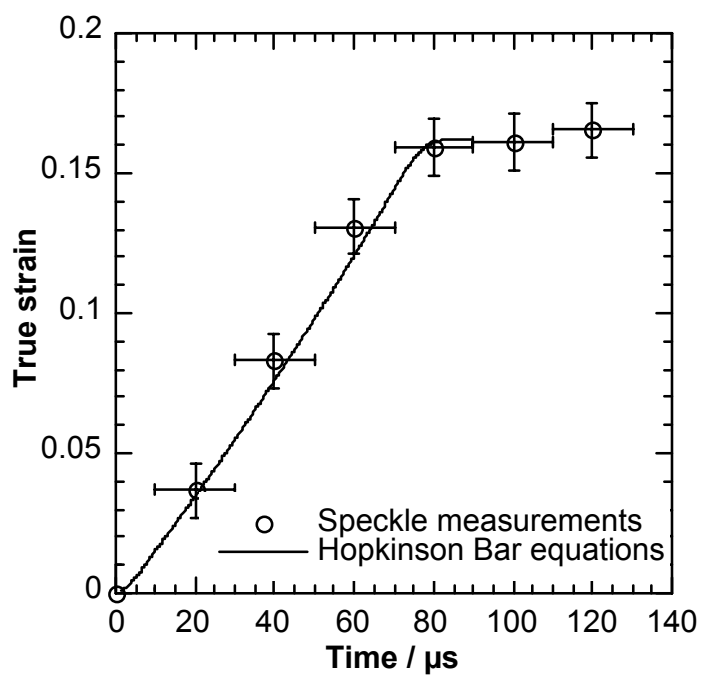


Fig 8. Comparison of strains measured using the speckle displacements and the Hopkinson Bar equations

5. DISCUSSION

At room temperature, two PBX/Ss with a high loading density, but different binders, were observed to show shear bands during compressive deformation. Reducing the loading density, by a few percent, prevented this from occurring at room temperature, even if the binder remained the same. However strain localisation bands were then formed when the temperature was reduced. This demonstrates that strain localisation is dependent on particle-particle interaction within the material, rather than just thermal and strain hardening considerations. If the binder is soft, the particles must be close together for this to take place. As the binder becomes stiffer, i.e. when the temperature is lower, the particles can interact when further apart, although figure 6 shows that there is still a maximum separation. It is important to note that the glass transition temperature of the HTPB binder in PBX1 is below 60 °C, so the binder by itself would neither yield, nor show strain localisations. Of course the same effect would be seen at room temperature if a stiffer binder than HTPB were used.

The most important aspect of the speckle results shown is that the interframe and specifically exposure times on the photographs were very long (20 μ s) on the timescale of the experiment (100 μ s). This was due to inexperience on the part of the operators, and problems with illumination of the specimens. More recent experiments on inert materials have improved the quality of the results obtained, so that exposure times of 1 μ s can be used. Figure 8 showed that the longitudinal strains measured from the speckle photographs agreed with those from the Hopkinson bar equations. We also see that the shape of the speckle plots is consistent with symmetrical deformation of the specimen, with constant longitudinal strain. Unfortunately neither the quality of the photographs, nor the density of speckle measurements, allowed interrogation of these localisations in this case.

Because the specimen is cylindrical, the quality of the photographs decreases towards the edge. This means that the best measurements are made in the centre of the specimen. The shape of the specimen introduces two other important considerations. Firstly, the photograph is a two dimensional projection of a three dimensional movement. Fortunately the y-strain in the projected image is equal to the specimen's radial strain. This means that if more data dense measurements can be made it may be possible to use this technique to find the dynamic Poisson's ratio of a material. The second effect of the radial expansion is to move the specimen closer to the camera. This could cause an apparent strain due to the change in magnification of the image. However, the camera is about 500 mm from the specimen, and the movement towards it is about 1-2 mm, so this is not an important effect.

6. CONCLUSIONS

The appearance of strain localisation in PBXs is shown to be a function of particle separation, and binder stiffness, which combine to allow, or not, the necessary particle-particle interactions. The speckle metrology technique has been applied to energetic materials deforming rapidly in the Split Hopkinson Pressure bar. The technique allows the standard experiment, which measures an average compressive strain within the specimen, to be extended to measure 2D displacement fields. The addition of this technique will allow more accurate measurements of strain fields in inhomogeneous specimens to be measured. Future work will look at producing polymer bonded explosives or stimulants, and examining in detail the combinations of binder stiffness and loading density that produce strain localisation.

Acknowledgements

The authors would like to thank Mr Stewart Palmer for his invaluable assistance. CR Siviour would like to thank EPSRC, [dstl], in particular Richard Biers, QinetiQ, EOARD and Professor Armstrong for their financial and intellectual support. He is also very grateful for a scholarship from the Worshipful Company of Leathersellers. SG Grantham and DM Williamson would both like to thank AWE Aldermaston for their support.

REFERENCES

- [1] C.R. SIVIOUR, S.M. WALLEY, W.G. PROUD AND J.E. FIELD: *Hopkinson bar studies on polymer bonded explosives*, Proc. 6th Seminar on New Trends in Research of Energetic Materials, p. 338-349, University of Pardubice, Czech Republic, April 22-24 2003
- [2] R.S. SIROHI: *Speckle Metrology* 1st ed., Marcel Dekker, New York, 1993
- [3] S.G. GRANTHAM, C.R. SIVIOUR, W.G. PROUD, S.M. WALLEY AND J.E., FIELD, *Speckle measurements of sample deformation in the split Hopkinson pressure bar*, J. Phys. IV France **110**, p.405-410, 2003
- [4] D.M. WILLIAMSON, S.J.P. PALMER, S.G. GRANTHAM, W.G. PROUD, J.E.FIELD, *Mechanical Properties of PBS9501*, Shock Compression in Condensed Matter, 2003, Portland, Oregon, American Institute of Physics, 20-27 June 2003 (In Press)
- [5] M. SJÖDAHL AND L.R. BENCKERT, *Electronic Speckle Photography: Analysis of an Algorithm Giving the Displacement with Subpixel Accuracy*, Applied Optics, **32** p. 2278-2284, 1993.
- [6] M.A., SUTTON, W.J WOLTERS, W.H. PETERS, W.F. RANSOM AND S.R. MCNEILL, *Determination of Displacements Using an Improved Correlation Method*, Image and Vision Computing, **1** p. 133-139, 1983
- [7] P. SYNNEGREN *White Light and X-ray Digital Speckle Photogtaphy*, Doctoral Thesis, Luleå University of Technology, Sweden, 2000
- [8] M. SJÖDAHL, *Systematic and random errors in electronic speckle photography*, Applied Optics, **33** p. 6667-6673, 1994
- [9] C.R. SIVIOUR, D.M. WILLIAMSON, S.G. GRANTHAM, S.J.P. PALMER, W.G. PROUD, J.E.FIELD, *Split Hopkinson pressure bar measurements of PBXs*, Shock Compression in Condensed Matter, 2003, Portland, Oregon, American Institute of Physics, 20-27 June 2003 (In Press).
- [10] C. R. SIVIOUR, M.J. GIFFORD, S.M. WALLEY, W.G. PROUD, J.E. FIELD, *Particle size effects on the mechanical properties of a polymer bonded explosive*, Journal of Materials Science 2004 (In Press)
- [11] S.G. GRANTHAM, C.R. SIVIOUR, W.G. PROUD, S.M. WALLEY, J.E., FIELD *Speckle measurements of sample deformation in the split Hopkinson pressure bar*, J. Phys. IV France **110**, p.405-410, 2003

INFLUENCE OF NC PROPELLANT SAMPLE SELF-HEATING ON ARRHENIUS KINETIC CONSTANTS DERIVED FROM NON-ISOTHERMAL DSC MEASUREMENTS

M. Sućeska, S. Matečić Mušanić and M. Rajić Linarić

Brodarski Institute, Av. V. Holjevca 20, 10000 Zagreb, Croatia

Abstract:

Non-isothermal isoconversional kinetic methods described by Ozawa, and Flynn and Wall are widely used to study kinetics of energetic materials. However, to obtain valuable kinetic constants great care must be taken to ensure proper experimental conditions, as well as data treatment procedure.

In this paper we have discussed the influence of NC propellant sample mass and heating rate during non-isothermal DSC measurements, i.e. the influence of NC propellant sample self-heating on kinetic results derived in accordance with the Ozawa and Flynn and Wall methods.

It was calculated by the Ozawa method that the activation energy equals ~199 kJ/mol in the case when sample self-heating has been avoided, while in the case of sample self-heating existence the activation energy was calculated to be ~191 kJ/mol. Also, it was shown that the activation energy calculated by the Flynn and Wall method depend not only on sample self-heating existence but also on degree of conversion – it ranges between ~145 and 200 kJ/mol.

Keywords: *single base propellants, differential scanning calorimetry, kinetic constants, self-heating*

1. INTRODUCTION

The kinetics and mechanism of thermal decomposition of energetic materials affects many important their properties. From a practical point of view, the most important are that the rate of thermal decomposition affects the quality of an energetic material and its shelf life, as well as its thermal hazard potential ^[1].

In order to be able to predict with required accuracy the shelf-life and the thermal hazard potential of an explosive material, a true decomposition mechanism and true kinetic constants should be known ^[2-9]. The application of an inaccurate decomposition model and inaccurate values of Arrhenius kinetic constants in the calculation of the thermal hazard potential of an explosive may result in highly uncertain and unusable data on the critical conditions of the self-ignition, and on the shelf-life ^[10,11].

Consequently, various experimental techniques and testing conditions have been used in order to determine the kinetic constants as accurately as possible. Various kinetic approaches and data treatment procedures have been also applied, resulting sometimes in considerable disagreement in the values of the kinetic parameters reported in literature ^[12].

Non-isothermal isoconversional kinetic methods described by Ozawa, and Flynn and Wall are widely used to study kinetics of energetic materials ^[13, 14, 15]. However, these methods are used sometime uncritically – that means they are used not taking into account

certain limitations of these methods and possible dependence of experimental data on testing conditions applied. Since these methods were first published more than two decades ago, surprisingly little work has been done to characterise these limitations and to examine the robustness of the methods by measuring the effects of sample mass and heating rate on the activation energy values ^[16].

One more serious problem with the use of isoconversional methods is that variation of Arrhenius constants with the extent of reaction poses difficulties in the interpretation of the kinetic data ^[3, 17, 18, 19].

In our previous papers ^[20, 21] we have reported on the influence of some testing conditions and data treatment method on results of double base propellant Arrhenius kinetic constants determined by the Ozawa non-isothermal isoconversional methods. The results reported have shown that sample self-heating occurs at very slow heating rates and small sample masses (above 2 °C/min for 0.5 mg samples), resulting in 20-30 % lower value of the activation energy.

In this paper we have continued to study the robustness of the Ozawa and Flynn and Wall methods using NC propellant as a test sample.

1.1 Theory of non-isothermal isoconversional method

The so-called “*isoconversional approach*” to non-isothermal kinetics rests upon the principle according to which the reaction rate at a constant conversion is only a function of temperature ^[3, 16]. Several isoconversional methods were suggested in the 1960's. The method developed by Ozawa, and Flynn and Wall ^[13, 14, 15] starts from the fact that the temperature integral in Eq.1 may be calculated by Doyle's equation ^[22] (Eq.2):

$$g(\alpha) = \frac{A}{\beta} \int_{T_0}^T \exp\left(-\frac{E}{RT}\right) dT = \frac{A}{\beta} I(E, T) \quad (1)$$

where T is temperature, β is heating rate, A is pre-exponential factor, E is activation energy, $g(\alpha)$ is a function called the reaction model, and $I(E, T)$ is temperature integral.

The above equation can be derived by the integration of the basic kinetic equation for the special case of non-isothermal experiments in which samples are heated at a constant heating rate: $\beta = dT / dt$.

$$\log[p(x)] \cong -2.315 - 0.4567x \quad (-20 > x > -60) \quad (2)$$

Combining Eqs. 1 and 2 one obtains:

$$g(\alpha) \cong \log \frac{AE}{R} - \log(\beta) - 2.315 - 0.4567 \frac{E}{RT} \quad (3)$$

It follows from Eq. 3 that if series of experiments are performed at heating rates $\beta_1, \beta_2, \beta_3, \dots, \beta_j$ and if $T_{k,j}$ is the temperature at which the fraction of conversion α_k was reached at heating rate β_j , then a plot of $\log(\beta_j)$ vs. $(1/T_{k,j})$ for each of k fractions of conversion $\alpha_1, \alpha_2, \alpha_3, \dots, \alpha_k$ will give k isoconversional lines whose slopes are:

$$slope \cong -0.4567 \frac{E}{R} \quad (4)$$

An accurate value of the activation energy is obtained through an iterative procedure described elsewhere ^[22, 23]. Also, the temperature integral may be nowadays calculated using methods based on numerical integration, or by using more accurate approximations such is, for example, the Senum-Yang approximation ^[3, 24, 25].

Taking that the conversion at the DSC (or DTA) peak maximum temperature (T_m) is constant ($\alpha_m=const.$) and independent on the heating rate, Eq. 3 may be written in the following form:

$$\log(\beta) = -0.4567 \frac{E}{RT_m} - 2.315 + \log \frac{AE}{R} - \log[g(\alpha_m)], \quad (5)$$

where α_m is conversion at the peak maximum temperature, and T_m is the peak maximum temperature.

It follows from the above equation that $\log(\beta)$ vs. $1/T_m$ will give straight line (so-called Ozawa plot) slope of which yields the activation energy. This is the basis of the Ozawa method for the derivation of kinetic parameters from non-isothermal DSC measurements. The Ozawa's method was the basis for the ASTM E 698-79 standard for the determination of Arrhenius kinetic constants for thermally unstable materials ^[23, 26].

It is obvious from the above mentioned that certain preconditions should be fulfilled in order to apply the non-isothermal DSC measurements and the Ozawa method. The most important are:

- the extent of reaction at the peak maximum is constant and independent on the heating rate
- the temperature dependence of the reaction rate constant obeys the Arrhenius equation
- the reaction model should be known in order to calculate the pre-exponential factor.

However, it should be noted that there are also some specific limitations regarding thermal methods that can influence kinetic results. The most important limitation lies in the fact that true kinetic results can be derived only if there is no temperature gradient within the sample ^[27, 28]. To avoid the temperature gradient (which is connected with the heating rate, sample mass and shape, sample self-heating during exothermal reactions, etc.), small and thin samples should be used, as well as slower heating rates.

It seems that the Achilles heel of the Ozawa and Flynn and Wall methods is excess self-heating ^[1, 16, 20, 21, 27]; that is, the tendency of energetic materials to increase the rate of heating of the sample to a greater degree than that of the programmed rate. Energetic materials are capable of considerable self-heating in a DSC instrument. Although the reaction kinetics and enthalpy of reaction are obviously the root cause of self-heating, for a given material the degree of self-heating is also influenced by the heating rate and sample size. The main consequences of self-heating are the following:

- the actual (i.e. instantaneous) heating rate experienced by the sample is greater than the programmed heating rate (see Fig. 1)
- the peak maximum temperature at the same programmed heating rate does not have the same value as the temperature obtained with no self-heating.

The effect of self-heating during the exothermal decomposition is substantial deviation of the $T = f(t)$ curve from linearity, i.e. existence of a pronounced blip visible in Fig. 1. A sufficiently small sample will give an essentially straight line with no evidence of self-heating, while a large sample will show behaviour given in Fig. 2. The larger the sample size (at a given heating rate), the greater self-heating, and consequently, the error in the heating rate (the greater deviation of the actual sample heating rate from the programmed heating rate). The final result of self-heating is a lower value of the calculated activation energy ^[1, 19, 28].

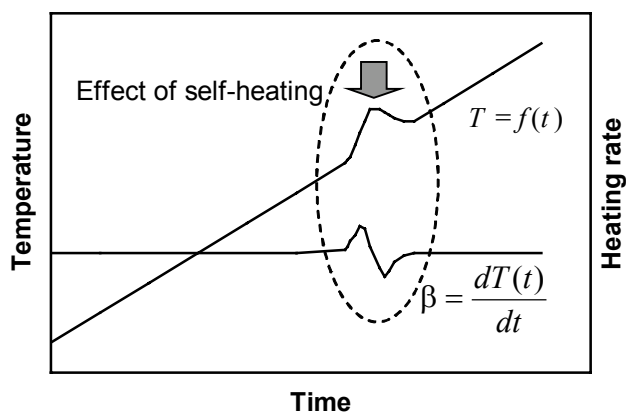


Fig 1. Effect of self-heating on actual heating rate and temperature

It is common in practice to use the non-isothermal isoconversional DSC method applying a *constant sample size method*. The consequence of using a constant sample size for all heating rates may be considerable self-heating at faster heating rates, and consequently in an incorrect value of the activation energy calculated.

To follow and to avoid self-heating in the non-isothermal DSC measurements it is necessary to find a way to measure the degree of sample self-heating and its influence on the kinetic results. In modern DSC instruments this is possible by following the deviation of the actual heating rate from the programmed heating rate. Also, modern DSC instruments enable to follow the change of degree of conversion at the peak maximum temperature, that is also important precondition for the application of the Ozawa method.

2. EXPERIMENTAL

Single base (NC) propellant was used for the study. The samples weighing 0.5; 1.5, and 2.5 mg were cut from propellant grains.

The DSC experiments were carried out using the *TA instruments DSC 2910* apparatus that is based on the heat flux type of the cell. The measurements were done using aluminium sample pans with perforated aluminium cover, and under nitrogen purging with 100 ml/min.

3. RESULTS AND DISCUSSION

In order to analyse the influence of NC propellant sample mass and heating rate on degree of sample self-heating during the exothermal decomposition, i.e. on the kinetic results, a series of non-isothermal DSC experiments were carried out. The mass of samples in three series of experiments was 0.5 mg; 1.5 mg and 2.5 mg. The heating rate was varied from 0.2 °C/min to 25 °/min.

A typical non-isothermal DSC curve of studied NC propellant is given in Fig. 2. Along with the heat flow curve, the heating rate curve and sample conversion curve, which are important for further study, are given. The parameters taken for the kinetic study are assigned on the curves.

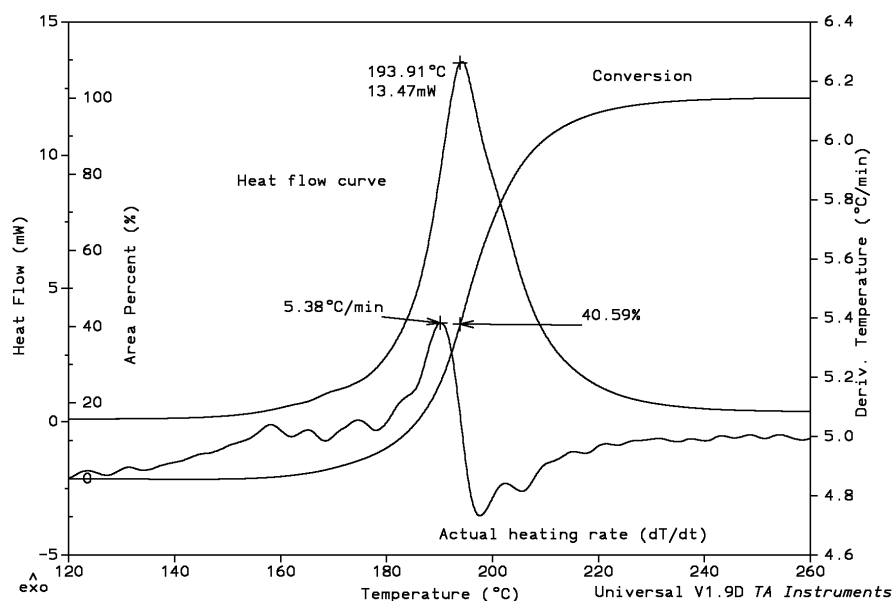


Fig 2. Typical non-isothermal DSC curve of tested NC propellant showing heat flow, heating rat, and sample conversion curves (testing conditions: sample mass 1.5 mg, programmed heating rate 5 °C/min)

Summarised experimental data necessary for studying of the kinetics in accordance with the isoconversional Ozawa method are given in Table 1.

Dependence of conversion at DSC peak maximum on heating rate and sample mass

As it follows from the Ozawa method, the first precondition for the applicability of the method is that the degree of conversion at DSC peak maximum temperature (α_m at T_m , in Eq. 5) is constant and does not depend on the heating rate. Consequently, the first thing to be done should be to check if this precondition is fulfilled.

The conversion at DSC peak maximum was determined from DSC thermogram as a ratio between the peak area until peak maximum and the total peak area (see Fig. 2). The effect of the heating rate and sample mass on conversion at the peak maximum (α_m) is shown graphically in Fig. 3.

It is obvious from Fig. 3 that the conversion decreases strongly with heating rate increase, while the influence of sample mass is not too pronounced. For the heating rates ranging below 2 °C/min the conversion seems to be constant (mean value is 52.3 %), while at heating rates above 2 °C/min the conversion decreases almost linearly with the heating rate increase. On the basis of such results one may conclude that the Ozawa method may be applied only if heating rates are slower than 2 °C/min. At the same time, the results presented in Fig. 4 show that there is no sample self-heating if heating rate is slower than 2 °C/min. Combining Figs. 3 and 4 one may conclude that the conversion at the peak maximum decreases as sample self-heating increases.

Table 1. Summarised experimental data obtained from non-isothermal DSC measurements

Sample mass, mg	$\beta_{\text{programmed}}$, °C/min	Parameters derived from non-isothermal DSC measurements				
		T_m , °C	h_m , mW	α_m , %	β_{max} , °C/min	$\Delta\beta$, °C/min
0.5 ± 0.02	0.2	169.79	0.144	54.94	0.20	0.00
	0.5	177.19	0.304	49.07	0.50	0.00
	1	182.28	0.477	52.49	1.03	0.03
	2	189.59	1.481	51.79	2.03	0.03
	5	196.05	3.274	44.75	5.08	0.08
	10	202.07	7.804	41.09	10.43	0.43
	15	205.89	8.238	46.38	15.76	0.76
	20	207.62	12.970	33.04	21.72	1.72
	25	210.2	12.660	30.84	27.09	2.09
1.5 ± 0.02	0.5	177.94	1.017	56.48	0.50	0.00
	1	182.07	2.134	51.96	1.00	0.00
	2	187.90	5.571	50.75	2.06	0.06
	5	194.16	13.210	41.41	5.43	0.43
	10	201.48	22.720	40.65	11.72	1.72
	15	204.55	30.770	30.61	18.59	3.59
	20	207.22	37.130	36.83	26.56	6.56
	25	208.45	40.410	20.54	34.50	9.50
2.5±0.05	0.2	168.93	0.608	52.42	0.20	0.00
	0.5	175.96	1.897	51.95	0.52	0.02
	1	182.11	4.073	50.87	1.03	0.03
	2	187.10	9.971	51.44	2.15	0.15
	5	194.04	22.950	40.62	5.89	0.89
	10	200.48	39.260	37.24	13.62	3.62
	15	204.44	54.700	33.29	23.76	8.76
	20	207.38	66.300	35.99	34.44	14.44

Legend: T_m – uncorrected peak maximum temperature; h_m – peak height; α_m – degree of conversion at peak maximum temperature; β_{max} – maximum actual heating rate at the peak region; β_{prog} – programmed heating rate at the peak region, $\Delta\beta$ - difference between maximum actual heating rate and programmed ones

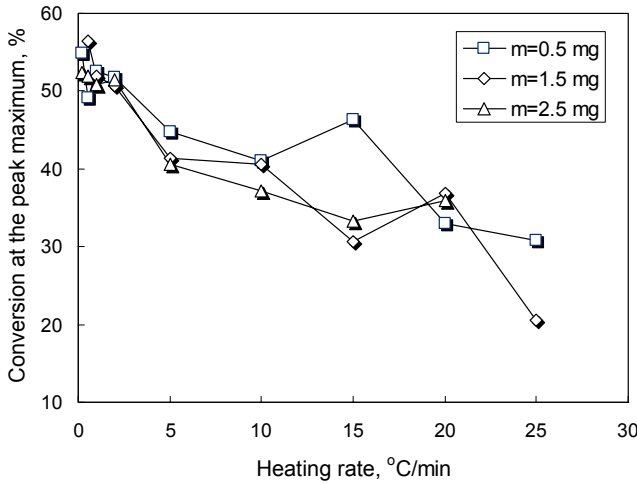


Fig 3. Dependence of NC propellant sample conversion at DSC peak maximum on heating rate and sample mass

Dependence of self-heating degree on heating rate and sample mass

It was reported in several papers [1, 16, 20, 21] that the thermal decomposition of an energetic material sample during DSC measurements may cause considerable sample self-heating if the sample mass is sufficiently large and the heating rate sufficiently high. In our previous papers [20, 21] we have proposed the quantification, i.e. the “measurement” of sample self-heating degree by following an increase of the actual heating rate at the peak region, in respect to the programmed heating rate (see Fig. 2).

As a measure of a sample self-heating degree we have used the difference between the maximum value of actual heating rate (β_{\max}) in the peak region and the programmed heating rate ($\beta_{\text{programmed}}$):

$$\Delta\beta = \beta_{\max} - \beta_{\text{programmed}} \tag{6}$$

The values of $\Delta\beta$ as a function of the heating rate and NC propellant sample size are presented graphically in Fig. 4. This figure shows that at the same sample mass, the degree of self-heating increases exponentially with the heating rate, while at the same heating rate the degree of self-heating increases almost linearly with the sample mass. At the same time, Fig. 4 and results given in Table 1 show that a measurable degree of self-heating exists at higher heating rates, even when a small sample size is used. For example, a sample having 0.5 mg in mass exhibits a measurable degree of self-heating at the heating rates above 2 °C/min, while sample having 2.5 mg in mass exhibits a measurable self-heating even at the 0.5 °C/min heating rate. The results obtained show clearly that self-heating in the case of the NC propellant is quite large – maximum value of actual heating rate can be almost two time greater than the programmed ones in the case of larger samples and higher heating rates. It implies that the experimental conditions during DSC measurements should be selected very carefully in order to derive true kinetic results

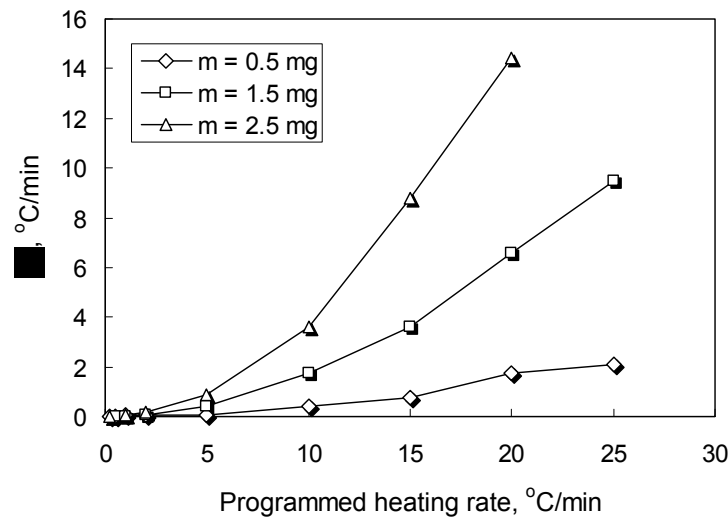


Fig 4. Dependence of NC propellant sample degree of self-heating on programmed heating rate and sample mass

3.1 Kinetic results

Ozawa method

The non-isothermal DSC measurements were carried out in accordance with the common practice in many studies: the sample mass was kept constant while the heating rates were varied. The method is known as *constant sample mass method*. Three series of experiments were carried out using the same sample mass (0.5 mg, 1.5 mg, and 2.5), and applying the heating rates ranging from 0.2 °C/min to 25 °C/min (Table 1). Typical DSC curves obtained in this way are given in Fig. 5.

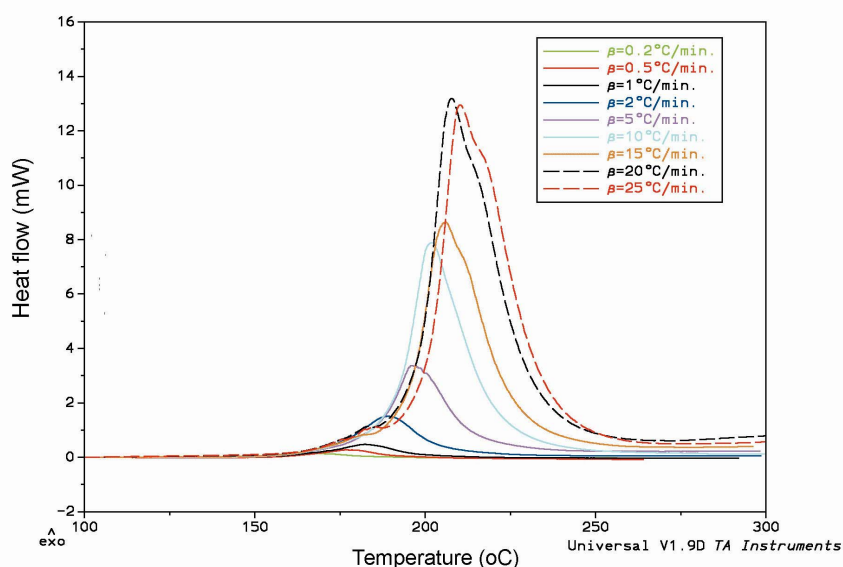


Fig 5. Non-isothermal DSC curves of NC propellant obtained at several different heating rates (sample mass is 0.5 m)

The data given Table 1, obtained experimentally by the non-isothermal DSC measurements, were treated according to the common procedure described elsewhere to evaluate Arrhenius kinetic constants in accordance with the Ozawa isoconversional method [1, 11, 12]. Since the method requires precise measurement of the peak maximum temperature, the uncorrected peak maximum temperatures given in Table 1 (T_m) are corrected for the thermal lag and heating rate in accordance with [12].

The Ozawa plots, i.e. the $\log(\beta)$ vs. $1/T$ curves, for different sample masses are given in Fig. 6. In order follow the degree of self-heating in each measurement, along with the Ozawa plots the $\Delta\beta$ vs. $1/T$ curves are given.

It seems from Fig. 6 that all data points lie on the same straight line. That means that the influence of sample mass on the slope of the Ozawa plot (and value of activation energy) is not too pronounced. At the same time, a detailed analysis has shown that there is certain discontinuity on the Ozawa plot at the region at which self-heating exists. The same behaviour was observed in our previous study conducted on double base propellant [20, 21].

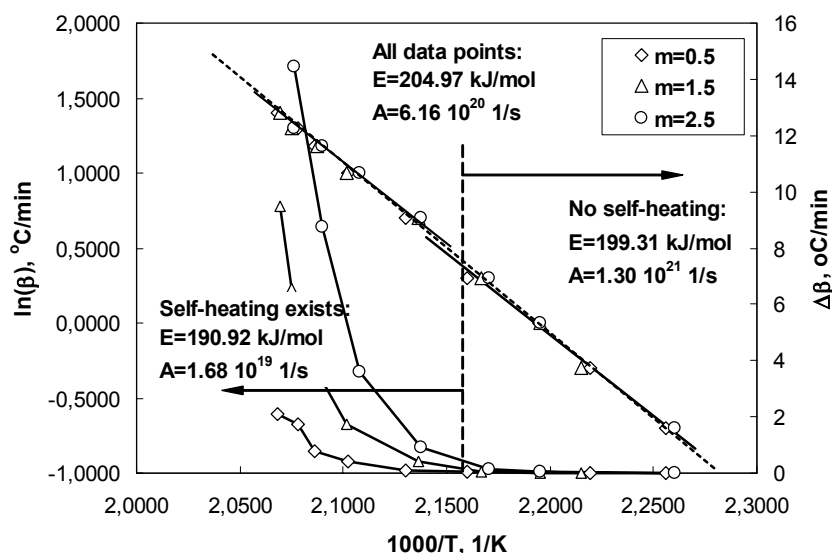


Fig 6. Ozawa plots and $\Delta\beta$ curves for NC propellant samples having different mass

As mentioned earlier, the Ozawa method is applicable only if degree of conversion at DSC peak maximum is constant, i.e. does not depend on heating rate. Fig. 3 clearly shows that this precondition is fulfilled only for the heating rates slower than 2 °C/min. At the same time, it follows from Fig. 4 that there is no sample self-heating for the heating rates lower than 2 °C/min. On the basis of these facts one may conclude that the true kinetic data can be derived only from data points obtained for heating rates slower than 2 °C/min. However, in order to analyse influence of sample self-heating on the kinetic results the activation energies were calculated for the following three regions (Figs. 6 and 7):

- the region at which self-heating does not exists ($\Delta\beta = 0$ °C/min)
- the region at which self-heating exists ($\Delta\beta > 0$ °C/min)
- the whole region (all data points), which includes all data and the regions with and without self-heating.

The activation energies and pre-exponential factors, calculated as the mean values for samples having different mass, are:

- the region at which self-heating does not exist: $E = 199.31$ kJ/mol; $A = 1.30 \cdot 10^{21}$ 1/s
- the region at which self-heating exists: $E = 190.92$ kJ/mol; $A = 1.68 \cdot 10^{19}$ 1/s
- the whole region (all data points), which includes all data and the regions with and without self-heating: $E = 204.97$ kJ/mol; $A = 6.16 \cdot 10^{20}$ 1/s

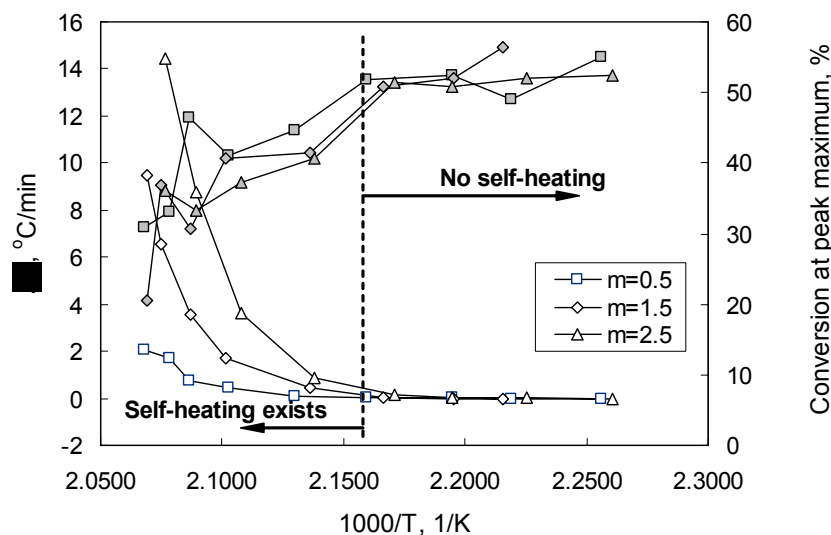


Fig 7. Dependence of degree of NC propellant sample self-heating and conversion at DSC peak maximum on reciprocal peak maximum temperature

It follows from these results that the activation energy for the region at which self-heating exists is lower for about 5 %, while the activation energy calculated from all data points is greater for about 3 % than the activation energy for the region without self-heating (“true” activation energy according to theory). At the same time the difference in values of pre-exponential factors are quite larger (few orders of magnitude).

Flynn and Wall method

In accordance with the Flynn and Wall isoconversional method the activation energies were calculated for different degrees of conversions in the following way. From DSC thermograms obtained at several different heating rates (Fig. 5) the conversions (α), as a function of temperature, were calculated as a ratio between partial and total peak area:

$$\alpha = \frac{A_T}{A_{total}}, \quad (7)$$

where A_T is partial peak area, i.e. area from starting point and given temperature, and A_{total} is total peak area. The curves obtained in this way are given in Fig. 8.

Temperatures at which given conversion was reached at a given heating rate was plotted against logarithm of the heating rate (Fig. 9). In this way a series of isoconversional lines whose slopes (Eq. 4) give the activation energy for a given conversion were obtained.

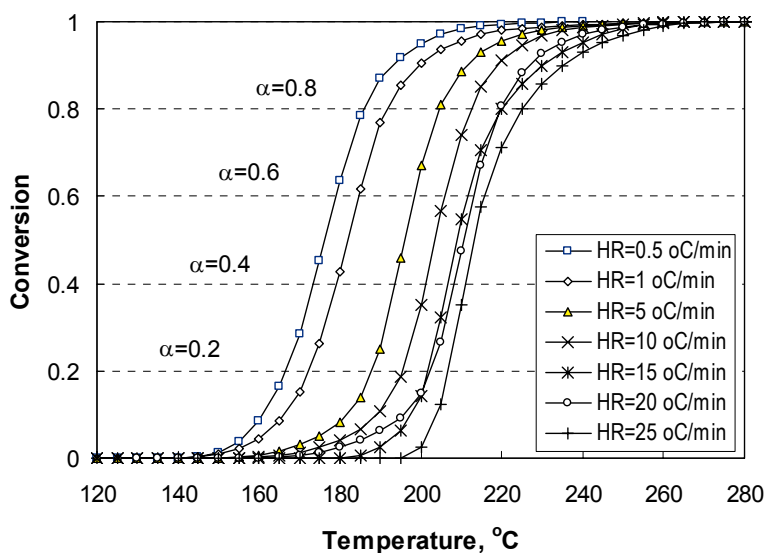


Fig 8. NC propellant conversion at different heating rates as a function of temperature (sample mass is 1.5 mg)

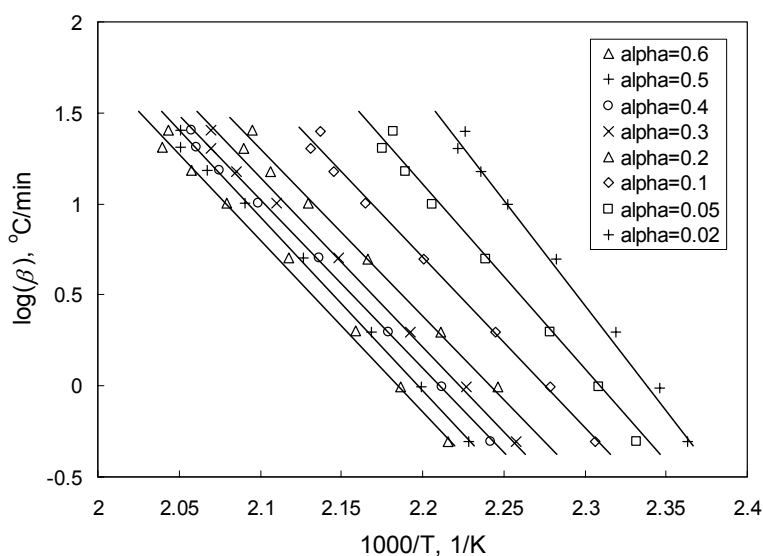


Fig 9. Isoconversional lines for different degrees of NC propellant conversion (sample mass is 1.5 mg)

The activation energies were calculated for different conversions, as well as for different regions – region without self-heating (for heating rates slower than 2 °C/min), region at which self-heating exists (for heating rates above 2 °C/min), and for all data points. The results are given in Table 2 and graphically in Fig. 10.

Table 2. Activation energies at different conversions and different regions

Conversion	Activation energy for region without self-heating ($\beta < 2$ °C/min), kJ/mol	Activation energy for region at which self-heating exists ($\beta > 2$ °C/min), kJ/mol	Activation energy calculated from all data points – whole region ($0.2 < \beta < 25$ °C/min), kJ/mol
0.02	201.1	181.8	187.5
0.55	196.1	165.6	174.0
0.10	180.4	152.6	160.9
0.20	169.7	142.0	151.9
0.30	171.1	139.8	150.7
0.40	176.9	146.1	155.3
0.50	185.3	144.3	156.3
0.60	196.6	140.7	157.8

Note: values of activation energy are the mean vales for three samples having 0.5, 1.5 and 2.5 mg.

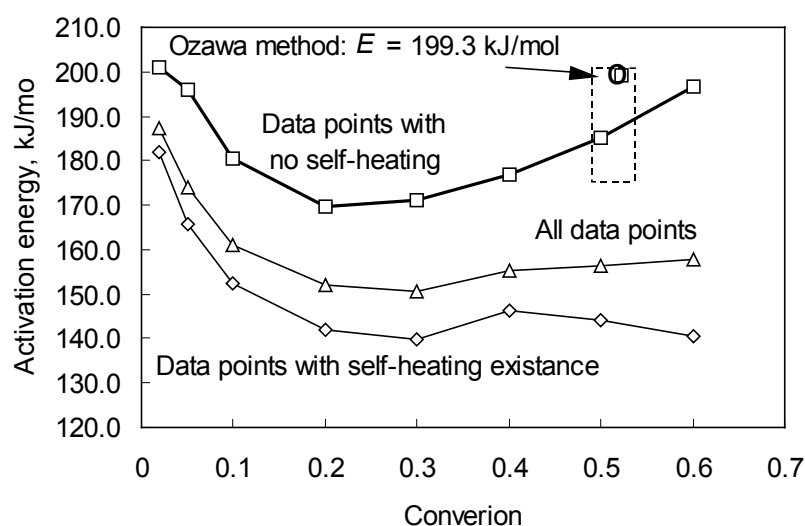


Fig 10. Dependence of activation energy on conversion at different testing conditions

The data given in Table 2 and Fig. 10 clearly show two important things: a) the activation energy changes with conversion, and b) the activation energy for the same degree of conversion decreases in the case of sample self-heating existence.

It should be mentioned that the region of conversions $0 < \alpha < \sim 0.2$ corresponds to the accelerated stage of NC sample decomposition (Fig. 8), the region $\sim 0.2 < \alpha < \sim 0.3$ corresponds to the inflexion point region, while the region $\sim 0.3 < \alpha < 1$ corresponds to the decelerated stage of NC sample decomposition. The lowest value of the activation energy has is in the inflexion point region, and the highest value in the initial stage of decomposition.

The values of the activation energies obtained by the Ozawa method and by the Flynn and Wall method should be comparable in the case of equal degree of conversions. In other

words, if conversion at DSC peak maximum temperature is constant and does not vary with the heating rates, than the Ozawa method, and Flynn and Wall method should give the same value of the activation energy for that conversion. For example, in the case of no self-heating the mean value of conversion equals 0.523 and the activation energy calculated by the Ozawa method equals 199.31 kJ/mol. For the same degree of conversion the Flynn and Wall method gives the activation energy of 188.8 kJ/mol, i.e. $\sim 5.5\%$ lower value. Such difference may be the results of several factors: a) the conversion at DSC peak maximum temperature is not constant and changes to some extent even in the case of very slow heating rates – ranging from 0.2 to 2.0 °C/min; b) the errors due to an inaccurate determination of DSC peak maximum temperature and conversion at the peak maximum, etc.

4. CONCLUSIONS

The results presented in the paper show that the Ozawa method and Flynn and Wall method should be applied for NC propellant kinetic study with great care. The most important for the applicability of the Ozawa method is to adjust testing conditions to give the same degree of conversion at different heating rates and to avoid temperature gradient within sample. To fulfil these preconditions, heating rates should be very slow (below 2 °C/min), and sample mass should be small (up to 2.5 mg), otherwise the values of activation energy will be erroneous.

The results of the Flynn and Wall method have shown that the activation energy of tested NC propellant changes considerable with conversion – the maximum value it has at the initial stage of decomposition (at conversions up to 0.2), and minimum value at the inflexion point region. This method has also shown that the existence of sample self-heating yields considerable lower values of the activation energy for the same degree of conversion, compared to values obtained from data points at which self-heating does not exist.

The Ozawa method and Flynn and Wall method does not give the same value of the activation energy for the conversion corresponding to DSC peak maximum, even in the case of very slow heating rates, which indicates that the conversion at the peak maximum temperature is not constant even in this case.

Since modern DSC instruments have possibility to follow both degree of conversion at the peak maximum temperature and degree of sample self-heating (Fig. 2) it will be good practice not only to follow these parameters in each DSC scan in order to control testing conditions, but also to report them when reporting kinetic results.

REFERENCES

- [1] MCCARTY, J.: Introduction to Differential Scanning Calorimetry (effects of self-heating on kinetics), TLN Systems Inc., Phoenix, Arizona, USA, URL: <http://www.TechLearningNow.com>, 2002
- [2] BOHN, M. A.: Kinetic modelling of the ageing of gun and rocket propellants for the improved and time-extended prediction of their service lifetime, Proc. of 1998 Life Cycles of Energetic Materials, Fullerton, California, USAA, pp.1-38 29 March-1 April, 1998
- [3] VYAZOVKIN, S., WIGHT, W.: International Reviews in Physical Chemistry 17 (3), 407, 1998
- [4] MERZHANOV, A. G., ABRAMOV, V. G.: Propellants and Explosives 6 130, 1981
- [5] ISLER, J., KAYSER, D.: Correlation between kinetic properties and self-ignition of nitrocellulose, Proc. of 6th Symp. Chem. Probl. Connected Stab. Explos, Kungälv, Sweden, , pp. 217, 1982

- [6] SUČESKA, M.: J. Therm. Anal. Cal., 68, 865, 2002
- [7] TICMANIS, U., PANTEL, G., WILD, R., EICH, T., WILKER, S.: Simulation and verification of exothermically reacting systems, Proc. of 33rd Int. Annual Conference of ICT, Karlsruhe (Germany), June 25-June 28, pp.111.1, 2002
- [8] SUČESKA, M.: Influence of thermal decomposition kinetic model on results of propellants self-ignition numerical modeling, Proc. of 5th Seminar "New Trends in Research of Energetic Materials, Pardubice (Czech Republic), pp. 308, 2002
- [9] MCQUIRE, R. R., TARVER, C. M.: Chemical decomposition models for thermal explosion of confined HMX, RDX, and TNT explosives, Report UCRL-84986, Lawrence Livermore Laboratory, Livermore, 1981.
- [10] TICMANIS, U., PANTEL, G., WILKER, S., KAISER, M.: Precision required for parameters in thermal safety simulation, Proc. of 32nd Int. Annual Conference of ICT, Karlsruhe (Germany), July 3 -6, pp.135.1, 2001
- [11] SUČESKA, M., RAJIĆ, M.: Change of critical condition of propellants self-ignition under conditions of artificial ageing at elevated temperature (in Croatian), Report No. 9-2-668, Brodarski institut, Zagreb, 2002.
- [12] STANKOVIĆ, M., KAPOR, V., PETROVIĆ, S.: The thermal decomposition of triple base propellants, Proc. of 7th European Symposium on Thermal Analysis and Calorimetry, Balatonfüred (Hungary), pp. 196. Aug. 30-Sept. 4, 1998
- [13] OZAWA, T.: J. Thermal Anal. 2, 301, 1970
- [14] FLYNN, J.H., WALL, L.A.: Polym. Lett., 4, 323, 1966
- [15] FLYNN, J.H.: J. Thermal Anal. 27, 95, 1983
- [16] BEHME, R., MCCARTY, J.: Self-heating and determination of kinetics using ASTM method E698, Proc. of the 21st Annual Conference of North American Thermal Analysis Society, September 22-24, Albuquerque, NM, 2003.
- [17] VYAZOVKIN, S., WIGHT, C. A.: Annu. Rev. Phys. Chem. 48, 125, 1997
- [18] SANTHOSH, G., VENKATACHALAM, S., FRANCIS, A. U., KRISHNAN, K., CATHERINE, K. B., NINAN, K. N.: Thermal decomposition kinetic studies on ammonium dinitramide (AND) - glycidyl azide polymer (GAP system, Proc. of 33rd Int. Annual Conference of ICT, Karlsruhe (Germany), June 25-June 28, pp. 64.1, 2002
- [19] SUČESKA, M., MIHALIĆ, Ž., RAJIĆ, M.: Applicability of non-isothermal methods and different kinetic approaches for description of thermal decomposition of homogeneous propellants (in Croatian), Report. No. 9-2-250, Brodarski institut, Zagreb, 2000.
- [20] SUČESKA, M., MCCARTY, J., MATEČIĆ-MUŠANIĆ, S., RAJIĆ, M.: Influence of testing conditions on results of Arrhenius constants determination by non-isothermal isoconversional methods, "Forum Explosivstoffe 2002", 3rd International workshop "Thermoanalyse" des WIWEB, October 29-30, pp.65-87, 2002
- [21] SUČESKA, M., MATEČIĆ MUŠANIĆ, S., RAJIĆ, M.: Determination of Arrhenius kinetic constants for double base propellant by non-isothermal DSC measurements. Influence of sample self-heating, Proc. of the 6th seminar "New trends in research of energetic materials", Pardubice, Czech Republic, April 22-24, pp. 374-391, 2003
- [22] DOYLE, C. D.: J. Appl. Polymer Sci., 6, 639, 2003
- [23] Arrhenius kinetic constants for thermally unstable materials, American Society for Testing and Materials (ASTM) standard, E 698-79, 1979.
- [24] VYAZOVKIN, S.: J. Comp. Chem., 18, 393, 1997
- [25] VYAZOVKIN, S.: J. Thermal. Anal. 49, 1493, 1997
- [26] DUSWALT, A. A.: Thermochimica Acta 8, 57, 1974
- [27] MCCARTY, J.: Self-heating errors in using ASTM method E698 for the determination of reaction kinetics, TA Hotlinks, 1984
- [28] ROGERS, R. N.: Private communications, 2002.

MECHANICAL PROPERTIES OF GEL-PROPELLANTS WITH NANOPARTICLES

U. Teipel, U. Förter-Barth and H. Krause

Fraunhofer Institute for Chemical Technology (ICT),
P.O. Box 1240, 76318 Pfinztal, Germany

Abstract:

Gel propellants provide rocket propulsion systems of high specific impulse, low sensitivity and low vulnerability in combination with the capability to control the thrust, i.e., variation of thrust and thrust cut off. The rheological characterization is essential for the development of adequate gel propellant formulations and thus for the design of an applicable propulsion system. In this contribution, the rheological behavior of a gel propellant consisting of nitromethane as fuel and nanoparticles of silicon dioxide as gelling agent was examined. The experiments were conducted under steady state shear flow and oscillatory shear. The nitromethane/silicon dioxide gels exhibit non-Newtonian flow behavior over the whole concentration range examined. Additionally, a yield stress is determined for all the gels. The viscoelastic properties are typically gel-like in that the storage and the loss moduli are both independent of frequency.

Keywords: *gel propellant, rheology, steady state shear flow, oscillatory shear, nitromethane, nanoparticles*

1. INTRODUCTION

In recent years, the challenge of achieving high performance while also improving the safety characteristics of rocket propellants has become an important goal within the industry. Gel propellants offer the potential to satisfy such demands because they combine certain advantages of liquid propellants with other attractive properties typical of solid propellants. Gel propellants can be designed as mono or bi-propellants. When used as a bi-propellant, both the fuel and oxidizer can be prepared as gels. The safety of the system is improved by separating the fuel and oxidizer. In general, gel propellants exhibit a specific impulse comparable to liquid propellants, but their performance can be increased even further through the addition of additives such as metal particles. A significant advantage of gel propellants over solid rocket propellants is the ability to control the thrust by controlling the mass flow of propellant into the combustion chamber. The rocket motor can even be turned on and off or pulse driven as required. Furthermore, gel propellants are less sensitive than liquid propellants and can be handled, stored and transported more securely because of their solid-like properties. This is especially important when, for instance, fissures or leakage sites develop within the combustion chamber of a gel propellant driven rocket motor. The viscoelasticity of the gel propellant significantly reduces the risk that the propellant will leak from the motor and inadvertently ignite.

The rheological properties of a gel propellant significantly affect a number of key operational and production requirements, including the propellant material behavior, casting and spraying operations, and combustion within the rocket motor. The characterization of the mechanical properties of the gel provides basic information critical to the production and

storage of gel propellants, rocket motor casting as well as the design of the entire rocket motor system.

This study examined the mechanical properties of nitromethane gelled with nanometer sized silicon dioxide. In combination with suitable oxidizers and additives, nitromethane exhibits a specific impulse $I_s > 2400 \text{ N}\cdot\text{s}\cdot\text{kg}^{-1}$ and is much less toxic than hydrazine derivatives, thus providing environmental and handling advantages compared to such compounds.

2. EXPERIMENTAL

2.1 Steady State Shear Flow

The rheological behavior of the gels prepared was examined in steady state and oscillatory shear flow using a UDS 200 rotational rheometer manufactured by Physica Meßtechnik GmbH. Cone and plate measurement fixtures were used.

Under steady state shear flow, the characteristic material function can be described as follows:

$$\tau(\dot{\gamma}) = \eta(\dot{\gamma}) \cdot \dot{\gamma} \quad (1)$$

Here $\eta(\dot{\gamma})$ is a characteristic material function that describes the flow properties when the fluid is subjected to a rheometric flow.

Various models are available in the literature ^[1] to describe the material behavior of fluids in stationary shear flow. Examples of several model functions ^[1, 2] that describe nonlinear flow behavior are presented in this section.

The power law function of Ostwald/de Waele can be used to model shear thinning (pseudoplastic) or shear thickening (dilatant) flow behavior:

$$\tau = K_1 \cdot \dot{\gamma}^n \quad (2)$$

K_1 is termed the consistency coefficient and n is called the flow index. Shear thinning behavior corresponds to $n < 1$, while shear thickening behavior exists when $n > 1$. Ideal viscous (Newtonian) behavior corresponds to $n = 1$. This model is unfortunately not effective in describing the flow behavior of many fluids at very small shear rates (near the limiting viscosity at zero shear rate) and at very high shear rates. The viscosity function for such power law fluids is expressed as follows:

$$\eta(\dot{\gamma}) = K_1 \cdot \dot{\gamma}^{n-1} \quad (3)$$

The model presented by Ellis is more suitable for describing flow behavior in the low shear rate region:

$$\eta(\tau) = \eta_0 / (1 + K_2 \cdot \eta_0 \cdot \tau^m) \quad (4)$$

Here, K_2 and m are fitted model parameters.

When the shear stress applied to a fluid must exceed a threshold value (i.e., yield stress) before the onset of irreversible deformation, the material is said to exhibit plastic flow behavior. Below the yield stress the fluid exhibits reversible (elastic) deformation. Highly concentrated disperse systems, in which the solid particulates tend to aggregate, exhibit such

viscoplastic material behavior. Materials that exhibit a linear relationship between the shear stress and shear rate at stresses above the yield stress, τ_0 , are known as Bingham fluids.

If the behavior at shear stresses above the yield stress, τ_0 , is nonlinear, the material can be described by the Herschel-Bulkley equation:

$$\tau = \tau_0 + K \cdot \dot{\gamma}^n \quad (5)$$

This power law equation allows one to describe shear thinning or shear thickening fluids that exhibit a yield stress, τ_0 .

Besides shear rate dependence, non-Newtonian behavior can also manifest itself as shear time dependence. For instance, if a material's viscosity decreases with time at a constant shear rate, it is said to exhibit thixotropic behaviour.

2.2 Oscillatory Shear Flow

In oscillatory shear flow, the fluid is subjected to a periodic (e.g., sinusoidal) deformation $\gamma(t)$ with an amplitude $\hat{\gamma}$ at a radial frequency $\omega = 2 \pi f$ [1]:

$$\gamma(t) = \hat{\gamma} \sin(\omega t) \quad (6)$$

At sufficiently small amplitudes—i.e., in the linear viscoelastic range—subjecting the material to an oscillatory (sinusoidal) shear deformation results in a sinusoidal shear stress $\tau(t)$ output. Viscoelastic material behavior is characterized by the existence of a phase shift δ between the shear stress output $\tau(t)$ and the deformation input $\gamma(t)$:

$$\tau(t) = \hat{\tau} \cdot \sin(\omega t + \delta) \quad (7)$$

By definition, the phase shift, δ , of a perfectly elastic solid is zero and that of a purely viscous fluid is $\pi/2$, whereas for viscoelastic fluids $0 \leq \delta \leq \pi/2$.

The shear stress function can be described in terms of the frequency dependent complex shear modulus $G^*(\omega)$,

$$\tau(t) = \hat{\gamma} |G^*(\omega)| \cdot \sin(\omega t + \delta(\omega)) \quad (8)$$

The complex shear modulus can also be expressed as

$$|G^*(\omega)| = \frac{\hat{\tau}(\omega)}{\hat{\gamma}} \quad (9)$$

The complex shear modulus $G^*(\omega)$ of a viscoelastic material is composed of two material functions, a real and an imaginary component, called the storage modulus, $G'(\omega)$, and the loss modulus, $G''(\omega)$, respectively. The storage modulus $G'(\omega)$ is proportional to the deformation energy stored by the material (the elastic component), while the loss modulus $G''(\omega)$ is proportional to the amount of energy dissipated by the material (the viscous component).

$$|G^*(\omega)| = \sqrt{G'(\omega)^2 + G''(\omega)^2} \quad (10)$$

Oscillatory shear experiments must be conducted at deformations within the material's linear viscoelastic range. In this range, at a constant radial frequency ω , the deformation

amplitude $\hat{\gamma}$ is proportional to the resulting shear stress amplitude $\hat{\tau}$, i.e., $\hat{\tau} \sim \hat{\gamma}$. This is only the case at sufficiently small oscillatory deformations. Within the linear viscoelastic region, the moduli $G'(\omega)$, $G''(\omega)$ and $G^*(\omega)$ are independent of the oscillatory amplitude in tests conducted at a constant frequency.

2.3 Materials

The gel propellants examined consisted of nitromethane as the continuous phase and nanometer sized silicon dioxide particles as the dispersed phase. Nitromethane exhibits Newtonian flow behavior with a dynamic viscosity of $\eta(25^{\circ}\text{C}) = 0.61 \text{ mPas}$. Its density is $\rho = 1139 \text{ kg/m}^3$. The silicon dioxide particles were obtained from Degussa AG, Frankfurt and had a density $\rho = 1.51 \text{ g/cm}^3$ (determined by gas pycnometry) and a specific surface area $S_V = 260 \text{ m}^2/\text{g}$ (determined by gas adsorption). The mean size of the primary particles was $\bar{x} = 7 \text{ nm}$.

3. RESULTS

3.1 Steady State Shear Flow Behavior of the Nitromethane/Silicon Dioxide Gels

Prior to the rheological characterization, the nitromethane/silicon dioxide gels were stirred for several hours to deagglomerate the particles and homogenize the gel. The rheological properties were then determined under steady state shear flow. Figure 1 shows the relative viscosity of the gel as a function of shear rate. The concentration of dispersed particles was varied from 4 to 8 vol. %. Figure 1 also shows the viscosity function of pure nitromethane.

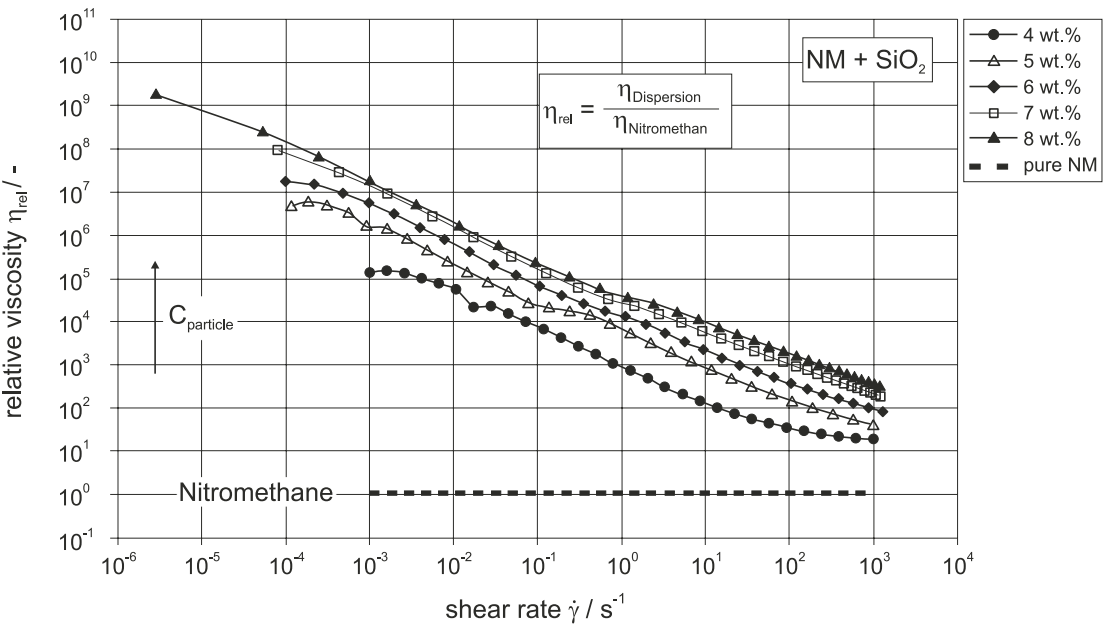


Fig 1. Relative Viscosity of the Nitromethane/Silicon Dioxide Gels as a Function of Shear Rate

The relative viscosity, η_{rel} , is defined as the ratio of the gel viscosity to that of the matrix fluid at a constant shear rate $\dot{\gamma}$.

$$\eta_{rel} = \frac{\eta_{gel}|\dot{\gamma}}{\eta_{nitromethane}} \tag{11}$$

With increasing silicon dioxide concentration, more pronounced shear thinning flow behavior is observed. This nonlinear material behavior of the gel can be attributed to particle-particle interactions as well as the changed hydrodynamics of the multiphase system compared to the single phase fluid. This viscosity increase as a function of concentration is especially pronounced at low shear rates. In this shear rate region the interparticulate interactions dominate compared to the relatively small hydrodynamic forces, so that the rheological properties of the suspension depend very strongly on the solids concentration and structural interactions within the suspension. Increasing the shear rate leads to an increase in the hydrodynamic forces, which in turn results in a shear induced structuring of the nanometer sized particles and a corresponding decrease in the viscosity at a given concentration. The viscosity difference as a function of concentration is therefore much smaller in the high shear rate region than in the low shear rate region, due to the hydrodynamic structuring that occurs in the system at higher shear rates.

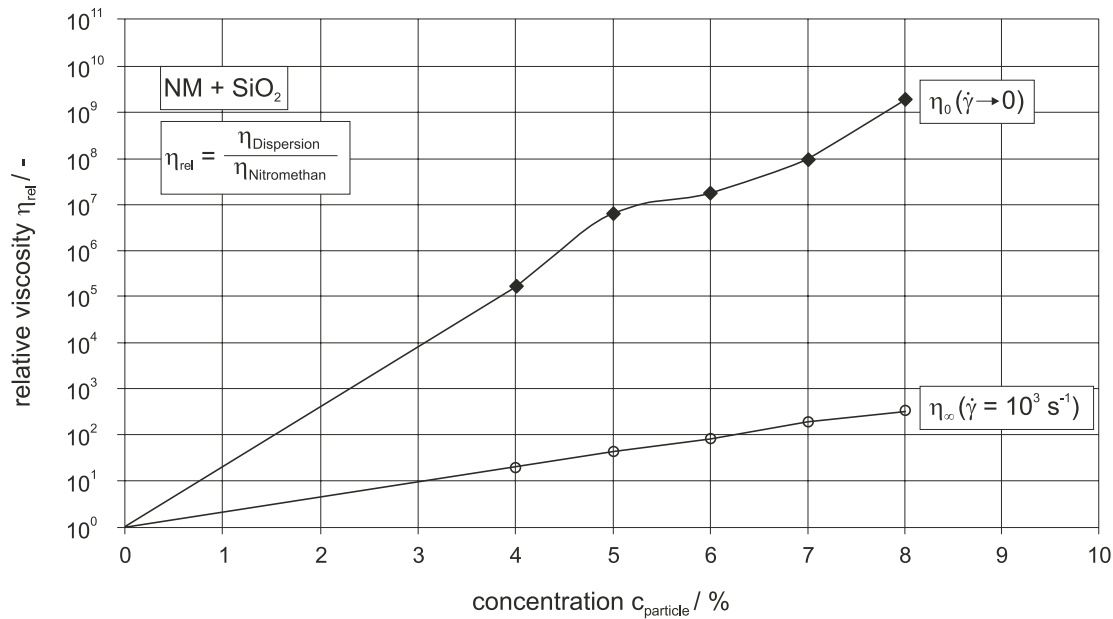


Fig 2. Relative Viscosity of the Nitromethane/Silicon Dioxide Gels as a Function of Particle Concentration

Figure 2 shows how the viscosity of the gel depends on solids concentration at the limiting viscosity at zero shear rate ($\dot{\gamma} \rightarrow 0$) and at a shear rate $\dot{\gamma} = 1000 \text{ s}^{-1}$.

As the silicon dioxide concentration increases, the inner particulate structure of the system becomes ever more pronounced. This inner quiescent structure in the nitromethane/silicon dioxide gel leads to the limiting viscosity at zero shear rate behavior shown in Figure 2. The viscosity difference between the suspension and the pure fluid is $\approx 10^6$ at a solids concentration $c_{particle} = 8 \text{ wt.}\%$. In contrast to the behavior of the limiting viscosity at zero shear rate, the slope of the relative viscosity function at the maximum shear rate is much lower. This relatively small increase in the viscosity of the nitromethane/silicon dioxide gel within this shear rate range arises because hydrodynamic effects are dominant

and lead to development of a shear induced structure within the silicon dioxide particles. The viscosity difference may also indicate that the gel's inner structure undergoes reversible breakdown at such high shear rates [1].

The flow behavior of the nitromethane/silicone dioxide gel can be described using the following equation for the shear stress:

$$\tau = \tau_0 - \eta_\infty \cdot \dot{\gamma} + \eta^* \cdot \dot{\gamma}^\alpha \tag{12}$$

Here τ_0 is the yield stress of the gel, η_∞ is the viscosity at a shear rate $\dot{\gamma} \rightarrow 0$, η^* is the viscosity that characterizes structuring within the disperse system and α is the exponent that characterizes structural changes within the system.

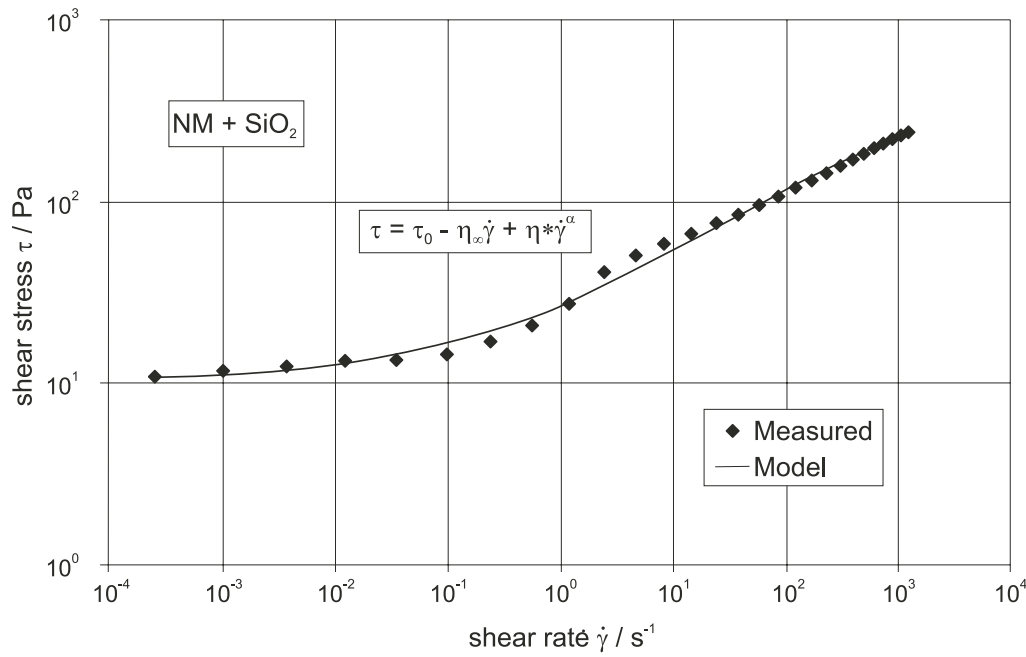


Fig 3. Measured Values and Model for the Shear Stress of a Nitromethane/Silicone Dioxide Gel

Figure 3 shows the measured shear stress values for the nitromethane/silicone dioxide gel with a concentration $c_{\text{particle}} = 8 \text{ wt.}\%$ compared with the shear stress function calculated from equation (12). There is good agreement between the calculated and measured values.

3.2 Viscoelastic properties of the Nitromethane/Silicon Dioxide Gels

Viscoelastic properties can be determined via oscillatory shear experiments. The complex shear modulus determined via dynamic experiments in the linear viscoelastic region can be separated into two material functions as shown in equation (10), the storage modulus $G'(\omega)$ and the loss modulus $G''(\omega)$. Figure 4 shows the storage modulus of the nitromethane/silicon dioxide gel at various solids concentrations.

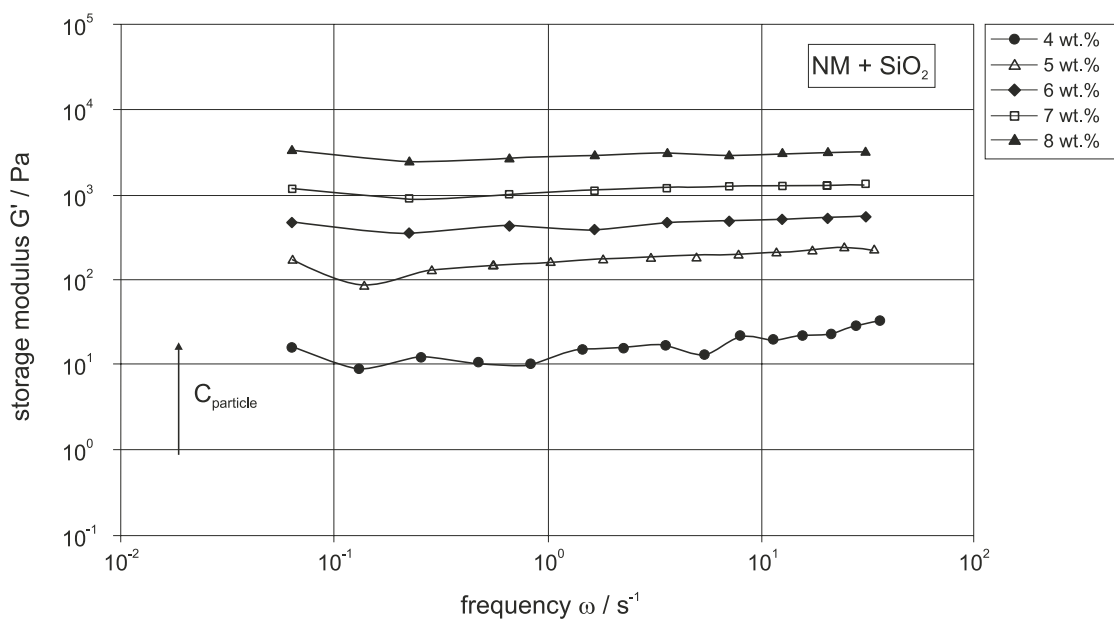


Fig 4. Storage Modulus as Function of Frequency of the Nitromethane/Silicone Dioxide Gels

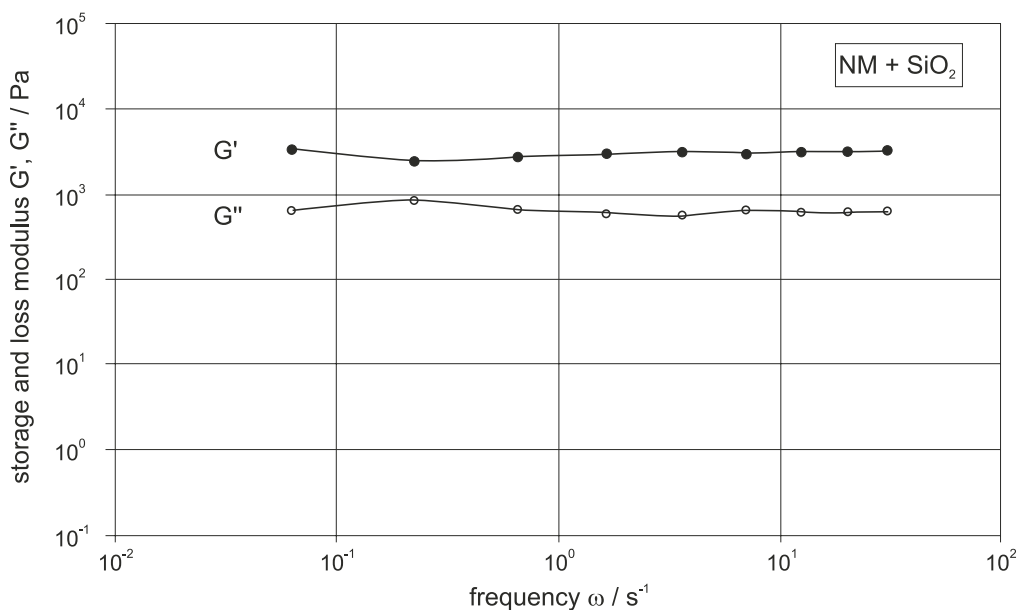


Fig 5. Storage and Loss Modulus as Function of Frequency of a Nitromethane/Silicone Dioxide Gel ($c_{\text{particle}} = 8 \text{ wt.}\%$)

In the concentration region examined, the storage modulus was independent of the radial frequency, indicating the existence of a compact inner structure in the nitromethane/silicone dioxide gel. Figure 5 shows example results of the storage and loss moduli as a function of frequency for the gel with a solids concentration $c_{\text{particle}} = 8 \text{ wt.}\%$. The moduli $G'(\omega)$ and $G''(\omega)$ are independent of frequency, meaning that within this frequency range the nitromethane/silicone dioxide gel exhibits elastic, solid-like behavior.

From this rheological study the following hypothesis concerning the material behavior of gel propellants are proposed:

- A gel propellant must exhibit shear thinning behavior when subjected to stationary shear flow
- The limiting viscosity at zero shear rate (η_0) of a gel propellant should be as high as possible
- The shear viscosity at high shear rate (η_∞) of a gel propellant should be sufficiently small
- A gel propellant should exhibit a yield stress τ_0 .
- The elastic component of the complex modulus must always be higher than the viscous component
- The moduli $G'(\omega)$ and $G''(\omega)$ should be independent (or nearly independent) of the oscillatory frequency ω

4. CONCLUSIONS

The nitromethane/silicone dioxide gels examined in this study exhibited pronounced shear thinning behavior with a yield stress when subjected to stationary shear flow. This behavior is attributable to the inner structure of the gel, which leads it to exhibit solid-like properties. At high shear rates the hydrodynamic forces exceed the interparticle interaction forces, producing flow induced structuring of the nanometer sized silicon dioxide particles and pronounced nonlinear flow behavior. The shear stress equation introduced in this work accounts for the change in the inner particle structure during stationary shear flow and thus provides a good description of the material behavior of this class of nitromethane gel propellants. The oscillatory shear experiments showed that the storage and loss moduli were independent of frequency in the range examined, meaning that the gel exhibits elastic behavior at low frequencies.

REFERENCES

- [1] U. TEIPEL: *Rheologisches Verhalten von Emulsionen und Tensidlösungen*, PhD-Thesis, University of Bayreuth, Scientific Publication of Fraunhofer ICT, **22**, 1999
- [2] C. W. MACOSKO: *Rheology: principles, measurements, and applications*, VCH Publishers Inc., New York, 1994

STUDY OF SUB-MICRON STRUCTURED PHOTOSENSITIVE PRIMARY EXPLOSIVES FOR LASER INITIATION SYSTEMS

I.A. Ugryumov, M.A. Ilyushin, I.V. Tselinsky, A.S. Kozlov, V.Yu. Dolmatov,
I.V. Shugalei and A.N. Golovchak

St.-Petersburg State Institute of Technology (Technical University),
190013, St.-Petersburg, Russia

Abstract:

Synthesis of nano-structures with predetermined characteristics and development of functional materials on their basis have become one of the priority problems in the materials science. Nano-particles possessing the size in the range 1 – 100 nanometers often show in comparison with materials formed by particles of the micron size often possess unusual characteristics. Working out energetic condensed systems, especially photosensitive primary explosives for the systems of laser initiation is one of the primary branches of application of nano-structured materials. We have synthesized and investigated mercury (II) complex perchlorate with 5-hydrazinotetrazole as a ligand (compound (I)) as a potential photosensitive primary explosive. This complex having particles of $1.1 \pm 0.8 \mu\text{m}$ size demonstrated the highest sensitivity to laser irradiation combined with an extremely low initiation threshold. On the basis of compound (I) the photosensitive formulation EC-2 containing ~ 90 % of the complex mercury perchlorate and ~ 10 % of an optically transparent polymer as an inert matrix has been proposed. Formulation EC-2 has externally high sensitivity to Q-switch IR-laser irradiation. Formulation EC-2 with added ultra disperse diamonds (UDD) (<100 nm) has shown lower initiation thresholds in comparison with neat EC-2 or EC-2 with added sub-micron black carbon instead of UDD. To increase the safety, an optical detonator on the basis of EC-2 separated from the high explosive charge (HE) by a metal cup, has also been studied.

Keywords: complex; explosives; initiation systems; laser; pulse, UDD,
optical detonator

1. INTRODUCTION

Synthesis of nanostructures with predetermined characteristics and development of different functional materials on their basis have become one of priority problems in the materials science. Nanoparticles possessing the size in the range 1 – 100 nanometers often show unusual properties in comparison with those of the micron size. Grade of the particles substantially changes macroscopic properties of materials. The high reactivity of nanoparticles is apparently due to the growth in the ratio of the particles' surface to their volume.

From among the numerous applications of nanostructured materials it is expedient to single out the design of energetic condensed systems, for example, photosensitive primary explosives (PE) for the systems of laser initiation.

Laser initiation is currently a widespread means of PE blasting due to its higher safety. In the optical range there are no sporadic energy sources capable of blasting the optical detonator (OD). Laser initiation guarantees a high level of isolation of the OD from occasional pulses transferred along the communication line from a pulsed laser. OD is tolerant both to electromagnetic interference and to discharges of static electricity. A photosensitive energetic compound is one of the basic elements of the laser initiation circuit. As compared to the other means of shock initiation, laser radiation has a number of features. Irradiation of a photosensitive explosive by the laser mono pulse results in a sequence of complicated nonlinear nonequilibrium thermochemical processes that can be divided into several stages, the main ones being: 1) light absorption by the substance, 2) energy and matter transfer, 3) chemical reactions of thermal decomposition.

Laser IR radiation provides high rates of local changes in temperature of the irradiated material approaching to 10^{10} K s^{-1} and forming the gradients of temperature up to 10^7 K cm^{-1} that result in strong interactions of energy, substance, charge and other streams in the sample.. Such parameters can be achieved with no other ways of influence. The modern theory of the initiation of high explosives (HE) under the conditions of pulsed stimuli is based on the concept of "hot spots" - the centers of intense local heating that are responsible for fast reactions of thermal decomposition, including an explosion. Local heating centers are formed owing to the structural heterogeneity of the substance (dot defects, congestions of vacancies, dislocations, interfaces, etc.), chemical impurities, microinclusions occurring due to non-stoichiometric composition of the initial products, presence of various additives and so on. The defects can also arise in the field of an intense light wave. The main hypothesis of warming up the optical dissimilarities resulting in HE ignition has been taken up to rationalize the laser initiation considering short duration and therefore the high power of the laser pulse. Carbon inclusions embedded in organic high explosives, or metal microinclusions present in heavy metal azides can play the role of the nuclei. The smallest size of experimentally found "hot spots" under the action of laser monopulse (Q-switch) ($\lambda = 1064 \text{ nm}$, $\tau_q = 8 \text{ ns}$) depends upon the nature of an explosive. In a covalent-bonded explosive (RDX, hexogen) it equals to $\sim 20 \text{ nm}$. For ionic compounds(viz., ammonium perchlorate, NH_4ClO_4) the size of hot spots is larger and amounts to - $200\text{-}300 \text{ nm}$ or even to 1000 nm . The center of decomposition is most likely located at depth of the substance rather than on its surface. Such location is more favorable for the development of thermal decomposition processes due to minimal scattering of the hot products of explosion from the initiation zone. For the visible and near infra-red regions of electromagnetic spectrum HE behaves as a diffuse-dispersing medium with a closely packed diffuser. On irradiation of a sample a repeated light scattering takes place in its volume that results in the growth of illumination inside the sample and leads to the production of hot spots in the most illuminated zone located in the volume of the irradiated sample.

It was possible to explain regularities of HE initiation with laser monopulse using the hypothesis of "hot spots" as ignition centers. Supersonic cracking in a charge during

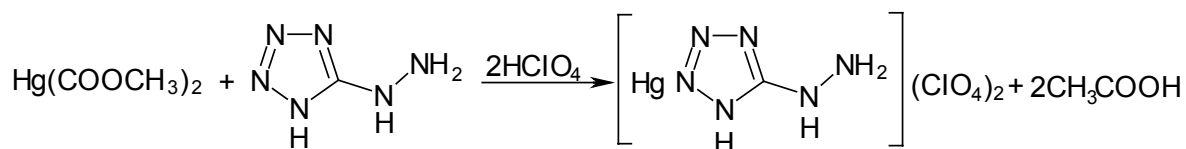
irradiation explains the high sensitivity to laser monopulse of confined HE with partly blocked ways for scattering of the gaseous reaction products. The process of HE cracking may also result in the failure of ignition. The above assumption allowed to explain the significant increase in sensitivity of pressed HE charges having a glass plate near their free surface.

As opposed to HE, the ignition of PE by laser monopulse does not depend on the presence of a barrier at the surface of explosive. It means that the rate of chemical reaction in PE is so high that scattering of gaseous products in free space does not significantly influence the process of ignition under the action of laser IR radiation. Among various energetic compounds inorganic azides show the greatest susceptibility to laser irradiation. Monocrystals of α -lead- and silver azides have a threshold of initiation equal to $4 - 6 \text{ mJ}\cdot\text{cm}^{-2}$. As the size of HE monocrystals is reduced, the critical density of initiation energy grows. There exist the limiting sizes of monocrystals capable of detonation. The samples of smaller dimensions decompose without explosion at any capacity of the initiating laser monopulse. There exists great variability in the sensitivity of pressed charges of lead azide to the monopulse of the Nd-laser (from $\sim 10 \text{ mJ}\cdot\text{cm}^{-2}$ up to $\sim 1 \text{ J}\cdot\text{cm}^{-2}$) according to the data of different authors. Such deviations are apparently connected with dissimilar conditions of the experiments, first of all with variations in the area of the irradiated zone. It has been found that the energy necessary for initiation decreases and approaches its lower limit with the diminution of the area of a light stain. Thus the threshold of the energy density indefinitely grows. As the size of the influence zone grows, the threshold of energy density decreases gradually, reaching the limiting value.

Minding the results of the investigation on the influence of crystal size on the susceptibility of photosensitive PE to the laser pulse, it is possible to suppose that each photosensitive compound has its optimal size of particles possessing the lowest threshold of initiation. Their diameter should be close to the size of "hot spots" Apparently, the size of nanostructures for energetic ionic compounds should be less than 100 nanometers, according to the latest results in the investigation of centers of intense local heating emerging under the laser initiation of PE^[1-6].

2. DISCUSSION

We have synthesized and investigated as potential photosensitive energetic primary explosives a number of complex perchlorates of mercury (II) with hydrazinoazoles as ligands. Our choice is based on the high positive enthalpy of formation of hydrazinoazoles, high oxidizing ability of the perchlorate ion and high ionization potential of the mercury cation. The perchlorate complex of mercury with 5-hydrazinotetrazole as ligand showed the greatest sensitivity to the laser monopulse. A laboratory synthesis of the complex may be carried out by mixing of solutions of a mercury salt (for example, acetate) and the ligand (5-hydrazinotetrazole) in HClO_4 according to the general scheme:



Scheme (I)

The residue was filtered, washed successively with water and alcohol and then dried. Salt I can be prepared on the multipurpose automatic laboratory installation designed for the synthesis of energetic materials (Fig.1).

The perchlorate complex of mercury (**I**) is a white crystalline solid with the following characteristics (Table1):

Table 1. *Characteristics of complex I.*

Property	Value
Molecular weight	499.5
Density of monocrystals (Calc.).	3.45 g / cm ³
Oxygen balance	+12.8 %
Oxygen coefficient	+180 %
Ignition temperature (5 s delay)	186 °C
Onset of thermal decomposition	175 °C
Impact sensitivity (Veller drop hammer)	60 mm /125 mm
Flame sensitivity (100 % ignition / 100 % refusal)	60 mm /150 mm
Detonation velocity at density 3.4 g / cm ⁻³ (Calc.).	6 km/s
Minimum charge of I for RDX in blasting cap №8	~ 0.015 g

Coordination compound I is a nonhygroscopic solid, insoluble in alcohol, acetone, aliphatic, chlorinated and aromatic hydrocarbons and soluble in dimethylsulphoxide. It is decomposed by an alkaline solution of KMnO₄ to produce unexplosive compounds.

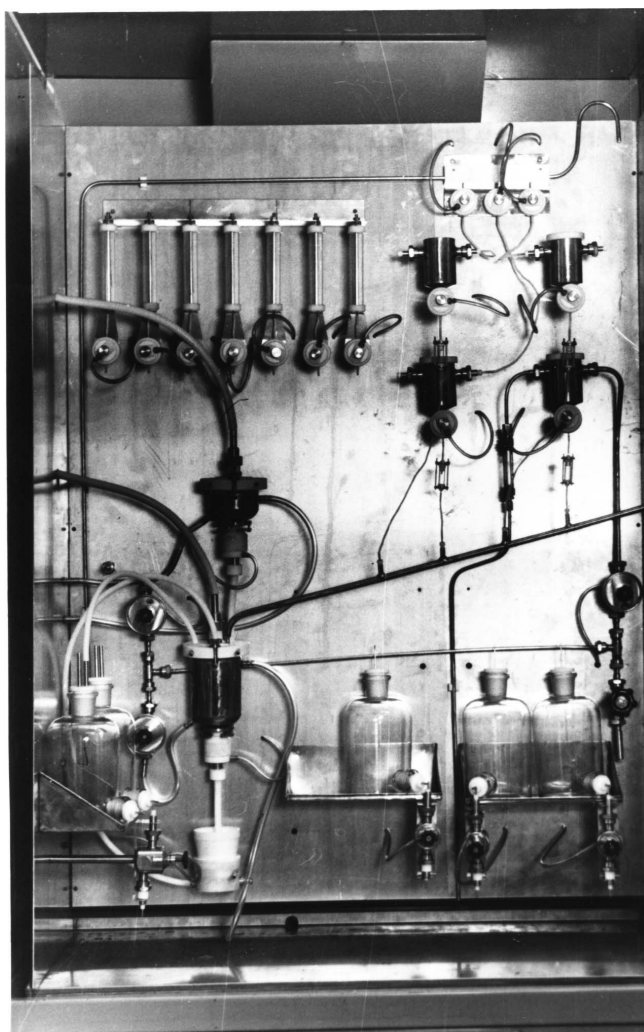


Fig 1. Multipurpose automatic laboratory installation for the synthesis of energetic materials

As was shown by the microscopic dispersion analysis, the synthesized complex contains both fine and coarse crystals (Table 2, Fig. 2 – 3):

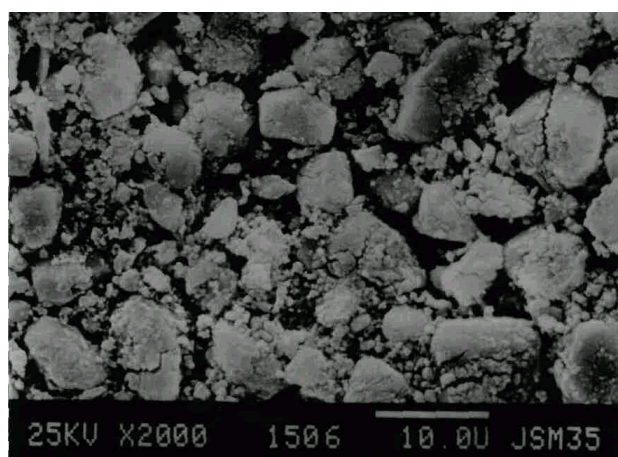


Fig 2. SEM photograph of polydispersion crystals of I

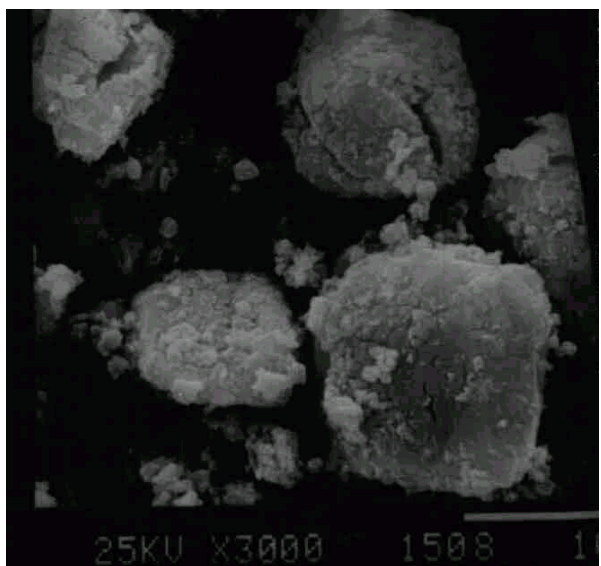


Fig 3. SEM photograph of mixture of fine and coarse crystals of **I** under higher magnification.

Table 2. *Distribution of particle size of complex I*

N	D μm	D min – D max
935	1.1 ± 0.8	0.5-8.1

N – data file, D – average size of crystals.

The microscopic dispersion analysis of complex **I** was carried out on an electronic microscope JSM-35CF (JEOL company, Japan).

Application of complex **I** as photosensitive PE is problematic because of its high sensitivity to mechanical stimuli and propensity to spontaneous aggregation of nanostructures resulting in the increase of the threshold of laser monopulse initiation. The problem of stabilization of ultradispersed powders of energetic compounds is usually solved by preparing composite materials containing sub-micron particles of solids embedded into a chemically inert polymer matrix. Such procedure allows to avoid aggregation of sub-micron particles, protects them from external influences but considerably hinders practical application of such materials. Optically transparent polymers are traditionally used as an inert matrix. Polymer bund samples of mercury complex perchlorate **I** have an increased sensitivity to laser pulse in comparison with the pressed charge of the metal complex. The initiation threshold reduces to $2,3 \text{ mJ/cm}^2$ ($\lambda = 1.06 \mu\text{m}$, $\tau_q = 30 \text{ ns}$, $d_{\text{beam}} = 4 \text{ mm}$), which is smaller than that for the pressed charges of heavy metal azides. The sensitivity to mechanical stimuli for such formulation is reduced to the level of HE making them safe enough for transportation, storage and application.

The photosensitive formulation EC-2 consists of $\sim 90 \%$ of mercury complex perchlorate **I** and $\sim 10 \%$ of an optically transparent polymer. For example, polymethyl vinyl tetrazole **II** can be used as a matrix. Properties of polymer **II** are listed in Table 3.

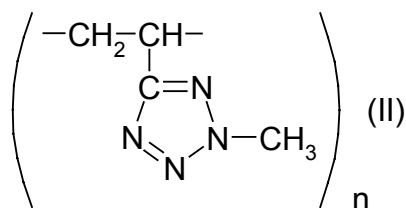


Table 3. *Physical and chemical characteristics of polymer.II.*

N	Property	Value
1	Intrinsic viscosity in DMF, 10 ⁻³ m ³ /kg	0.64
2	Mass fraction of the residual monomer, %	0.09
3	Mass fraction of ashes, %	0.16
4	Mass fraction of moisture, %	1.9
5	Weight average molecular weight	68400
6	Number average molecular weight	27700
7	Polydispersity coefficient	2.5
8	Enthalpy of formation, kJ/kg (Calc.).	1850

A suspension of EC-2 formulation in a volatile solvent was deposited on the substrate surface. Photosensitive film charges were manufactured according to this procedure. These films were used in laboratory experiments for the generation of shaped shock waves, hardening of steel by explosion, development of test models of optical detonators.

Table 4. *Results of derivatographic analysis (rate of heating 5K/min)*

Sample	De-comp. stage	Δ T of the effect, [°C]	T _{max} of the effect, [°C]	Mass loss, [%]	Character of the effect
Complex I	1	170-195	186	30	Exo
	2	195-260	200	40	Exo
Polymer II	1	220-310	275	40	Exo
Complex I – 90% + Polymer II – 10% (Formulation EC -2)	1	170-195	186	30	Exo
	2	195-270	200	70	Exo

The influence of polymer II on salt I decomposition was of great interest. The results of derivatographic analysis are given in Table 4.

From Table 4 it is obvious that salt I decomposition takes place in 2 steps. The 1st step is the ligand oxidation, the 2nd one is the total decomposition of the complex. Table 4 also shows that polymer II decomposes in a single step that involves tetrazole ring destruction. It is also seen that formulation EC -2 decomposes in 2 steps, like salt I. The oxygen balance of EC-2 is near zero so that its destruction produces only gaseous products of decomposition.

The results also show that Polymer II and complex I are compatible.

Since explosives are convenient models for investigating fast reactions in chemically active media, so it seems rather important to test the sensitivity of light-sensitive explosives to laser initiation, though the mechanisms of their low threshold initiation are not yet worked out.

Sheets of light-sensitive EC-2 explosive (thickness ~1.5 mm, diameter ~5 mm) were also prepared and investigated in this respect. Two lasers, viz., Nd-glass laser for the investigation of ignition in a monopulse mode ($\tau_q = 30\text{ ns}$), and a laser with an active element comprising Nd-containing potassium-gadolinium tungstate were used to generate initiation in a free generation mode ($\tau_q = 30\text{ }\mu\text{s}$). Both lasers operate at wavelength 1060 nm. The laser beam illuminates the central area of charges. The thresholds of initiation of the charges were calculated with 50% probability of ignition. The accuracy of calculation of the thresholds of initiation was near 20%. The thresholds of initiation were calculated in terms of the minimum energy, E_o (mJ), or minimum of energy density H_o (mJ/cm²). The results of experiments are listed in Tables 5-7.

Table 5. *The sensitivity of EC-2 explosive as a function of the diameter of illumination zone ($\tau_q = 30\text{ ns}$)*

d, diameter of illuminated zone, [mm]	E_o [mJ]	H_o [mJ/cm ²]
0.48	1.8×10^{-2}	10.14
3.18	0.6	7.48
9.52	1.8	2.57

Table 6. *The thresholds of initiation of EC-2 explosive as a function of exposure*

τ_q , pulse duration [ns]	d, diameter of illuminated zone [mm]	E_o [mJ]	H_o [mJ/cm ²]
30	1.02	6.8×10^{-2}	8.32
30×10^3	1.02	2.52	308.4

Table 7. *Delay of ignition of EC-2 explosive as a function of energy density of the laser beam ($\tau_q = 30 \mu s$)*

H_0 , J/cm^2	Delay, τ , μs
0.26	15
0.35	14.5
1.10	11.5
3.06	1

It was found that the sensitivity of EC-2 explosive depended both on the diameters of the illuminated zone and on the duration of illumination with the laser beam (see Tables 5, 6). The thresholds of initiation of EC-2 explosive are smaller than those published for lead azide. For example, they are $H_0 \sim 10.1 \text{ mJ/cm}^2$ for EC-2 explosive and $H_0 \sim 23.4 \text{ mJ/cm}^2$ for a pressed charge of lead azide (1500 MPa) of $\sim 0.48 \text{ mm}$ [8] in diameter.

The times of ignition delay for EC-2 explosive depended on the energy density of the laser beam, H_0 , and were always smaller than the duration of free generation (see Table 7).

It is known that black particles of carbon of micron size decrease the thresholds of initiation of explosive charges by non-Q-switch IR-laser pulses [7].

But there also exist some unknown effects of other forms of carbon on the sensitivity of explosive charges to laser pulses.

The results of investigation of the influence of black carbon (particle size $\sim 1 \mu m$) and nano-diamonds (ultra disperse diamonds of detonation synthesis, UDD) (particle size $< 100 \text{ nm}$) on the sensitivity of charges of EC-2 to Q-switch IR-laser pulses are presented in Table 8 ($\lambda = 1.06 \mu m$, $\tau_q = 8 \text{ ns}$, $d_{\text{diaphragm}} = 0.86 \text{ mm}$). The diameter of charges of EC-2 equals to 5 mm and its thickness is 2 mm.

Table 8. *Initiation of EC-2 by Q-switch laser pulse.*

Charge	E_0 , μJ	Result of initiation
EC-2	310	Explosion
EC-2 + 1% black carbon	$600 < E_0 < 2000$	Explosion
EC-2 + 0,5% UDD	260	Explosion
EC-2 + 1% UDD	200	Explosion
EC-2 + 3% UDD	190	Explosion
EC-2 + 5% UDD	340	Explosion

The micron size black carbon has been found to be a phlegmatizer, increasing the threshold of initiation of EC-2. Black carbon increases the area of irradiation absorption that results in the growth in the threshold of initiation and increase in the dissipation of laser energy from the surface of the charge.

The influence of UDD on EC-2 differs from that of black carbon. UDD has high enthalpy of formation. The experimental value of ΔH_f^0 of UDD is about 2.56-2.95 MJ/kg and calculated ΔH_f^0 equals to 3.5 MJ/kg [9]. UDD in up to ~3% concentration increases the sensitivity of EC-2 to Q-switch laser pulse. This effect may be the result of increasing of energy absorption inside the EC-2 charge because of an extremely high refractive index of UDD. An increased quantity of UDD decreases the sensitivity of EC-2 to the monopulse of IR-laser, playing the role of an inert substance lowering the sensitivity of EC-2 to laser pulse.

So UDD is the first example of a substance which increases the sensitivity of a light sensitive energetic material to Q-switch laser pulse.

Formulation EC-2 found practical application in some research projects. For example, an optical detonator (OD) in which EC-2 formulation for the sake of increased safety was separated from the secondary high explosive by a metal cap, has been studied. Optical fiber guide 400-600 μm in diameter was used for the laser irradiation of OD. The cap was coated with EC-2 formulation ~1.5 mm thick (Fig. 4).

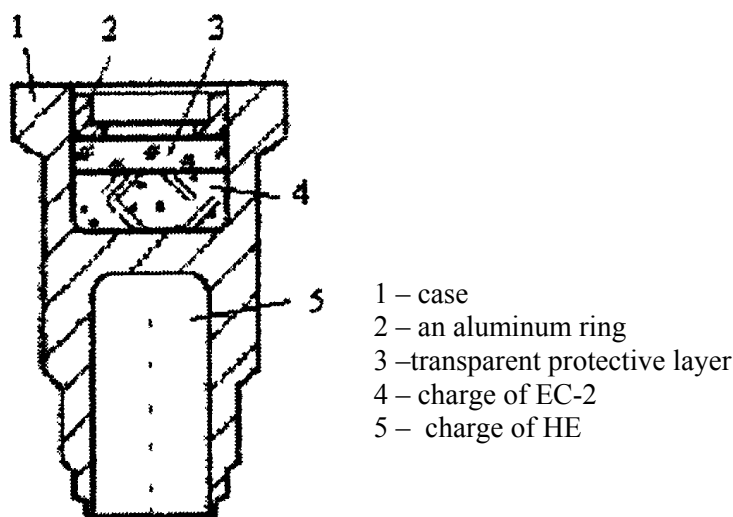


Fig 4. The scheme of OD

Trial tests showed that EC-2 sensitivity to the Q-switch Nd-laser pulse exceeded that of lead azide (~80 μJ). In particular, the 50 % explosion probability of the model OD charged with EC-2 in the mono pulse mode of initiation took place at radiant energy of 20 μJ , while in the free generation mode it comprised 2,5 mJ. Initiation of EC-2 in all cases resulted in the transfer of detonation to the HE charge. Thus, the model of a safe OD of new generation has been developed and successfully tested.

Consequently, a complex perchlorate of mercury with as 5-hydrazinotetrazole as a ligand and formulation EC-2 on its basis are promising energetic materials for the investigation of laser initiation and development of safety initiation systems.

Acknowledgments

The work was financially supported by the Ministry of Education of the Russian Federation in the framework of the Intercollegiate Research and Development Program “Scientific Research of High School in the Field of Chemistry and Chemical Products”.

REFERENCES

- [1] ILYUSHIN M.A., TSELINSKY I.V.: Primary explosives.//Ross. Khim. Zh., v.41, N 4, p. 3 – 13, 1997 (in Russian)
- [2] ILYUSHIN M.A, TSELINSKY I.V., CHERNAY A.V.: Light-sensitive explosives and compositions and there laser initiation. Ross. Khim. Zh, v.41, N 4, p. 81 – 88, 1997 (in Russian)
- [3] ILYUSHIN M.A., TSELINSKY I.V.: Laser initiation of high-energy-capacity compounds in science and technology.//Russ. J. Appl. Chem., v.73, N 8, p. 1305 – 1312, 2000
- [4] ILYUSHIN M.A, TSELINSKY I.V.: Energetic complexes of metals for initiation systems.//Ross. Khim. Zh., v.41, N 1, p. 72 – 78, 2001 (in Russian)
- [5] ILYUSHIN M. A., TSELINSKY I. V., UGRUMOV I. A., ZHILIN A. YU., KOZLOV A. S.: Coordination complexes as inorganic primary explosives// Proceeding of the VI seminar “New trends in research of energetic materials” Pardubice. Czech Republic.. p. 146-152, April 22-24., 2003
- [6] BOURNE N.K.: On the laser ignition and initiation of explosives// Proc. R. Soc. Lond. A., Vol. 457. P. 1401-1426, 2001.
- [7] HANKOMA M., VORMISTO T., MINKIO M., SAIRIALA M.: Laser ignition research of RDX // Proceeding of the Seminar. Levi. Finland. Sept. 5-11. 2002. P.266-271.// Chem Abstr.. v.138. ref.403740., 2003
- [8] ALEXANDROV E.I., TSIPILEV V.P.: The influence of generation regime on properties of dimensional effect under laser initiation of pressed lead azide//Phys. Combust. Explos., v. 19. №6, p.60-62, 1982 (in Russian)
- [9] DOLMATOV V.YU.: Ultra disperse diamonds of detonation synthesis. Saint-Petersburg., p. 300, 2003 (in Russian)

STUDIES AND RESEARCHES REGARDING THE UTILIZING OF RESULTS OBTAINED AT THE BURNING OF POWDER IN CLOSE BOMB FOR SOLVING OF FUNDAMENTAL PROBLEM OF INTERIOR BALLISTICS

T. Vasile, C. Barbu and D. Safta

Military Technical Academy, 81-83 George Cosbuc Avenue, Bucharest, Romania

Abstract:

In this paper it is presented a mathematical model of firing phenomenon, using the results obtained during of the powder burning in close bomb. On the base of the mathematical model was elaborated an interior ballistic soft, which allows to study the variation of the powder gases pressure and the projectile velocity versus its displacement inside of grooved barrel and versus time. For an extant weapon, the theoretical results that was obtained with the aid of this soft and the experimental data are compared.

Keywords: close bomb, powder burning, geometrical law, firing phenomenon

1. INTRODUCTION

The fundamental problem of interior ballistics it is solved, in many cases, accepting a series of simplified assumptions, due to complexity of the firing phenomenon. Thus, in many works of literature ^[1, 2, 3, 4] it is admitted, among others, the geometrical law for powder burning, proposed by French researcher Vieille and a constant index of burning rate law.

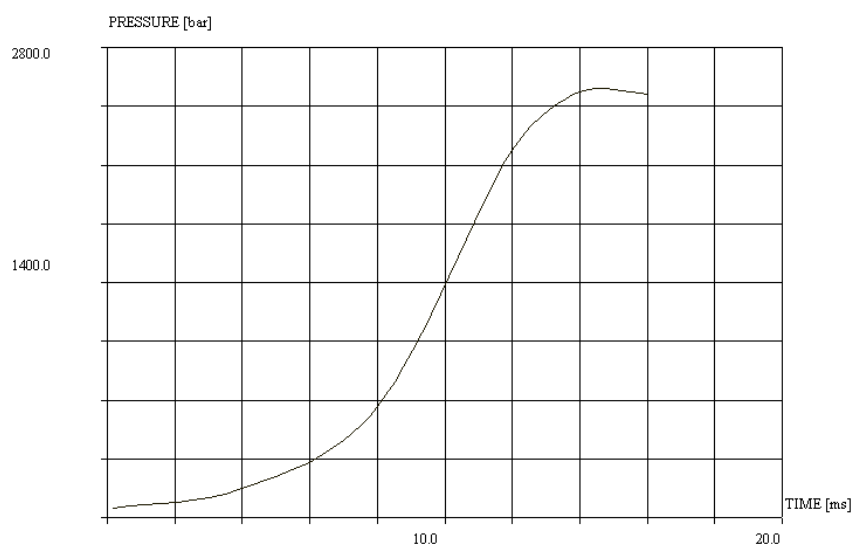


Fig 1. Pressure in close bomb versus time.

In the proposed mathematical model, for the powder burning was utilized the physical law which reflects better the reality of firing phenomenon, and uses the experimental results obtained during the powder burning in the close bomb at densities much bigger than the densities from guns. The index from the burning rate law is variable. It is determined as a function of the pressure using the pressure in close bomb $P(\tau)$, which are presented in Fig. 1.

The elaborated mathematical model is consisted of the differential and algebraic equations. By solving the differential and algebraic equations system, in numerical way with the aid of the computer, it is obtained the variation of gases pressure and projectile velocity versus its displacement within the barrel and versus time since the beginning of powder burning, which defines the content of fundamental problem of interior ballistics.

The signification of the used parameters is that established in literature ^[1, 2, 3, 4].

2. MATHEMATICAL MODEL

The elaborated mathematical model is based on the main differential and algebraical equations of interior ballistics ^[1, 2, 3], thus:

- the fundamental equation of interior ballistics:

$$sp(\ell_{\psi} + \ell) = f\omega \left(\psi + \frac{v^2}{v_{\text{lim}}^2} \right) \quad (1)$$

- the equation of projectile translation motion:

$$\varphi q \frac{dv}{dt} = sp \quad (2)$$

or

$$\varphi q \frac{v dv}{d\ell} = sp \quad (2')$$

- the burning rate law:

$$\frac{de}{d\tau} = AP^{\nu} \quad (3)$$

or

$$\frac{de}{dt} = Ap^{\nu} \quad (3')$$

- the rate of gases forming:

$$\frac{d\psi}{dt} = \frac{\chi}{e_1} \sigma AP^{\nu} \quad (4)$$

or

$$\frac{d\psi}{dt} = \frac{\chi}{e_1} \sigma Ap^{\nu} \quad (5)$$

The differentiyal equation of displacement is obtained with the aid of the fundamental equation of interior ballistics and of the equation of projectile translation motion, thus:

$$\frac{d\ell}{\ell_{\psi} + \ell} = \frac{\varphi q}{f\omega} \frac{v dv}{\psi + \frac{v^2}{v_{\lim}^2}} \quad (6)$$

where:

$$\ell_{\psi} = \ell_0 (a - b\psi); \quad a = 1 - \frac{\Delta}{\delta}; \quad b = \Delta \left(\alpha - \frac{1}{\delta} \right); \quad \psi = \left(\frac{1}{\Delta} - \frac{1}{\delta} \right) \left(\frac{f}{P} + \alpha - \frac{1}{\delta} \right)$$

For the obtaining of velocity differential equation, it is admit that in close bomb and in gun has been burned the same thickens of powder grain and it is took into account the equation of projectile translation motion, thus:

$$\frac{dv}{dt} = \frac{s}{\varphi q} \left(\frac{P}{p} \right)^{\nu-1} \quad (7)$$

The differential equation for time has got the following form:

$$dt = \frac{d\ell}{v} \quad (8)$$

These equations have been adequately transformed in order to allow the utilizing of experimental data, obtained during the powder burning in close bomb, at the solving of fundamental problem of interior ballistics.

So, it is adopted as an independent variable ζ , defined as ratio between impulse value of powder gases pressure at certain moment I and impulse value of powder gases pressure at the fragmentation moment I_s , in the case of multiperforated powders. In the case of simple shape powders, impulse I_s is changed with impulse I_k .

In order to increase level of generality of these equations are utilized following dimensionless variables:

$$\eta = \frac{v}{v_{\lim}}; \quad \lambda = \frac{\ell}{\ell_0}; \quad \varepsilon = \frac{t}{t_{\lim}}$$

where:

$$v_{\lim} = \sqrt{\frac{2f\omega}{\theta\varphi q}}; \quad t_{\lim} = \frac{\varphi q}{s} \frac{v_{\lim}}{P}$$

Utilizing the dimensionless variables, the equation (6) becomes

$$\frac{d\lambda}{d\zeta} = 2 \frac{E}{\theta} \frac{\eta d\eta}{d\zeta} \quad (9)$$

where

$$E = \frac{a - b\psi + \lambda}{\psi - \eta^2}$$

Taking into account that $dI = I_s d\zeta$ and $v = \eta v_{\text{lim}}$, the equation (7) gets the form

$$\frac{d\eta}{d\zeta} = \sqrt{\frac{B\theta}{2}} \left(\frac{P}{p}\right)^{v-1} \quad (10)$$

The differential equation for time (8), after the utilizing of the dimensionless variables and the changing of $\frac{d\lambda}{d\zeta}$ with its expression from equation (9), becomes

$$\frac{d\varepsilon}{d\zeta} = 2 \frac{1}{t_{\text{lim}}} \frac{\ell_0}{v_{\text{lim}}} \frac{E}{\theta} \sqrt{\frac{B\theta}{2}} \left(\frac{P}{p}\right)^{v-1} \quad (11)$$

After the introducing of the dimensionless variables in the equation of projectile translation motion, this gets the form

$$p = \frac{f\Delta}{E} \quad (12)$$

It is eliminated the pressure from equations (9), for displacement, from (10), for velocity, from (11), for time and, finally, it is obtained:

$$\frac{d\lambda}{d\zeta} = \sqrt{\frac{2B}{\theta}} \eta E \left(\frac{EP}{f\Delta}\right)^{v-1} \quad (13a)$$

$$\frac{d\eta}{d\zeta} = \sqrt{\frac{B\theta}{2}} \left(\frac{EP}{f\Delta}\right)^{v-1} \quad (13b)$$

$$\frac{d\varepsilon}{d\zeta} = \frac{1}{t_{\text{lim}}} \frac{I_s}{P} \left(\frac{EP}{f\Delta}\right)^v \quad (13c)$$

$$p = \frac{f\Delta}{E} \quad (13d)$$

For the index v from burning rate law, it was taken a variable value that is calculated on the base of experimental data from close bomb, for two densities of charge, with the aim of relation

$$v = 1 - \frac{\log \frac{dI_2}{dI_1}}{\log \frac{P_2}{P_1}} = \frac{\log \frac{d\tau_1}{d\tau_2}}{\log \frac{P_2}{P_1}} \quad (14)$$

The differential and algebraical equations system (13) can be used in first period and as well as second period of the firing phenomenon.

The differential and algebraic equations system of projectile motion within grooved barrel (13) represents the new mathematical model which allows to study the variation of gases pressure and projectile velocity versus its displacement and versus time in conditions closer of the reality of the firing phenomenon.

3. DETAILS CONCERNING THE INTEGRATION OF DIFFERENTIAL AND ALGEBRAICAL EQUATIONS SYSTEM

The differential and algebraical equations system (13) was integrated using the fourth order Runge-Kutta method, with the aid of following initial conditions:

$$\zeta = \zeta_0 \neq 0; \eta = \eta_0 = 0; \lambda = \lambda_0 = 0; \varepsilon = \varepsilon_0 \neq 0,$$

in which:

$$\zeta_0 = \frac{I_0}{I_s} = \frac{\int_0^{\tau_0} P d\tau}{\int_0^{\tau_s} P d\tau}; \varepsilon_0 = \frac{t_0}{t_{\lim}} = \frac{2.303}{t_{\lim}} \frac{I_k (1 - \alpha \Delta)}{f \Delta} \log\left(\frac{p_0}{p_a}\right)$$

The first period, in the case of multiperforated powder grains has two phases.

In the first phase, from the moment of the inflammation of powder until the moment of breaking of powder grains, when $\psi \leq \psi_s$ and $v \leq 1$, it is integrated equations system (13).

In the second phase, from the moment of powder grains breaking until the moment of the end of powder charge burning, when $\psi_s \leq \psi \leq 1$ and $v = 1$, the system (13) becomes:

$$\frac{d\lambda}{d\zeta} = \sqrt{\frac{2B}{\theta}} \eta E \quad (15a)$$

$$\frac{d\eta}{d\zeta} = \sqrt{\frac{B\theta}{2}} \quad (15b)$$

$$\frac{d\varepsilon}{d\zeta} = \frac{1}{t_{\lim}} \frac{I_s E}{f \Delta} \quad (15c)$$

$$p = \frac{f \Delta}{E} \quad (15d)$$

In the equations of this system is not included the pressure P from close bomb. However, the solving of this system is done with the aid of the curve $P(\tau)$, because the values for ψ from E relation are calculated on the base of experimental data.

In the second period, from the moment of the end of powder charge burning until the moment when projectile leaves the barrel, $\psi = 1$ and $v = 1$, the expression for E becomes

$$E = \frac{a - b + \lambda}{1 - \eta^2}.$$

The initial conditions for the integration of differential and algebraical equations system (15) are just values of ballistic magnitudes at the moment of end of powder burning.

If the solving is effectuated for the powder that burns without breaking and in the conditions of the burning rate law $u = u_1 P$, in which $v = 1$, than it is utilized the system (15), taking into consideration the particularities of the second phase of the powders that burn with the breaking of grains.

4. RESULTS AND CONCLUSIONS

In the Fig.2 and Fig.3 it is presented the variation of gases pressure* and projectile velocity* versus its displacement* and time*, obtained with the aid of the interior ballistics soft that was elaborate on the base of proposed mathematical model, for an extant gun. The magnitudes with index are relative variables that were obtained as the ratio between the value of current variable and its maximum value.

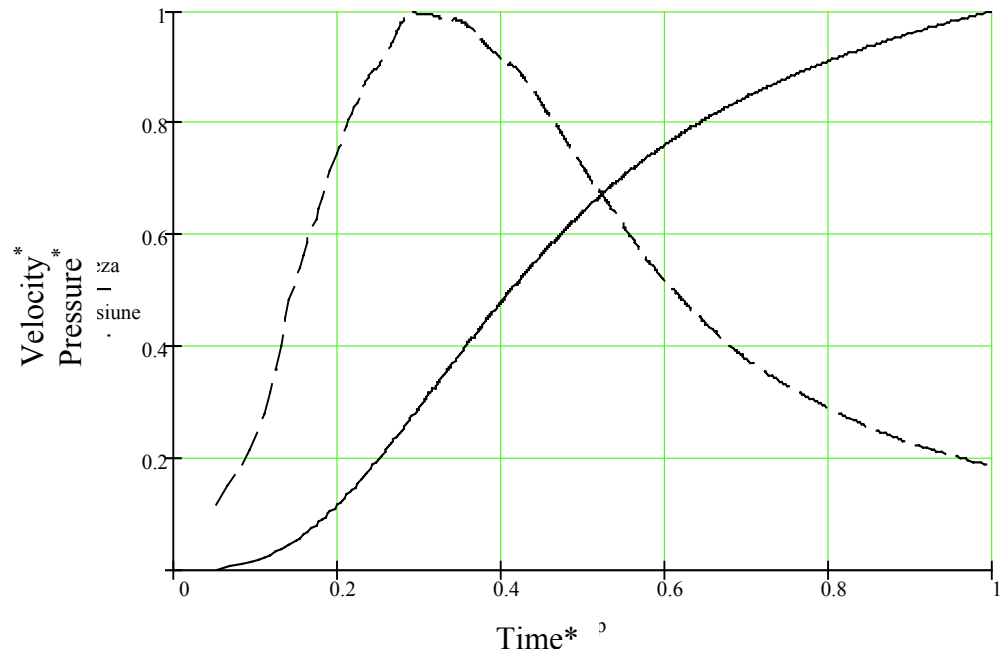


Fig 2. The variation of pressure and velocity versus time

From the analysis of the data, one of them are presented in the diagrams from Fig.2 and Fig.3, can be concluded that this way of the fundamental problem solving of interior ballistics it is closer of firing phenomenon intimacy with guns that use multiperforated powders [5, 6, 7].

It is necessary to remark that the finish of the powder burning takes place after the projectile leaves the barrel of gun.

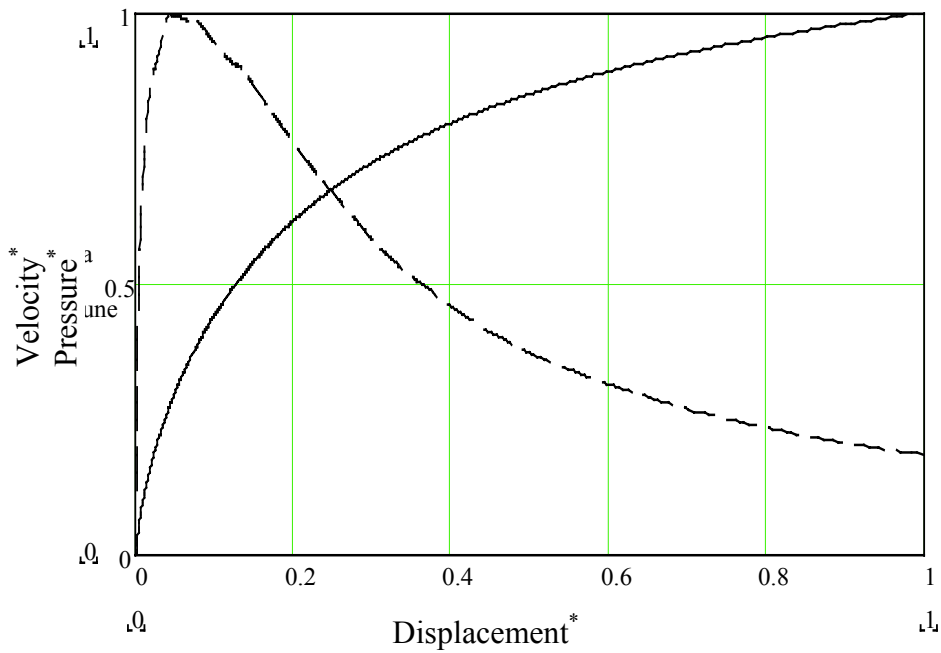


Fig 3. The variation of pressure and velocity versus displacement

The magnitudes with index from graphics are obtained as a ratio between current values of magnitudes and their maximum values.

For an extant gun, the experimental and theoretical data are presented in Table 1.

Table 1. *Experimental and theoretical data*

Type of data Parameters	Experimental data	Theoretical data
Maximum pressure [MPa]	240	256,6
Muzzle velocity [m/s]	840	847,1

From the comparing of the experimental data with the theoretical values obtained in the case of the proposed mathematical model, had resulted that the difference between the muzzle velocities values is approximate 0,5% and between the maximum pressures values is approximate 6%.

The advantages of this manner of the fundamental problem solving comparative with the manner based on geometrical law of the powder burning consist of followings:

- it is utilized whole curve of the pressure $P(\tau)$ that is obtained at the combustion of the powder in close bomb and that takes into account all particularities of powder burning;
- it is used the variable values for index ν from the burning rate law, in the case of the powders that burn with the breaking of the grains, which allow to present all aspects of the powder burning.

REFERENCES

- [1] E.V. CIURBANOV: *Vnutrenniaia Ballistika*, Izdatelstvo VAOLKA, Leningrad, 1975
- [2] M.E. SEREBRIAKOV: Internal ballistics of guns and solid propellant rocket engines, vol. 1 and 2, Military Academy Publishing House, Bucharest, 1970
- [3] T. VASILE: *Internal ballistics of guns, vol.1*, Military Academy Publishing House, Bucharest, 1993
- [4] T. VASILE: *Internal ballistics of guns, vol.2*, Military Academy Publishing House, Bucharest, 1996
- [5] T. VASILE: *Contributions to the fundamental problem solving of interior ballistics*, PROCEEDINGS of the II-nd International Conference "Artillery Barrel Systems, Ammunition, Means of Artillery Reconnaissance and Fire Control", October, 27-29, Kiev, pg.440-445, 1998
- [6] T. VASILE and I. NISTOR: *Mathematical modeling of projectile motion in grooved barrel*, The XXIIIth National Conference of Solides Mechanics, University Buletin, "Petrol-Gaze" Ploiesti, vol.LI nr.1, May, 28-29, Ploiesti, pg.61-66, 1999
- [7] T. VASILE: *Studies and researches regarding the fundamental problem solving of interior ballistics for weapon with grooved barrel*, PROCEEDINGS of III-rd International Armament Conference on Scientific Aspect of Armament Technology, October, 11-13, Waplewo, pg.157-165, 2000

EFFECTS OF THE COATING PROCESS OF HE MOULDING POWDERS ON SAFETY AND IM CHARACTERISTICS

R. Wild

PBX-Center Maasberg, Diehl Munitionssysteme GmbH & Co KG,
Karl-Diehl-Straße 1, D-66620 Nonnweiler, Germany

Abstract:

High performance warheads are very demanding on every component of the whole system.

The HE “low cost” component has to fulfil performance and IM criteria.

Two coating methods, slurry and paste process, promise better results and effectiveness for new moulding powders.

Keywords: *PBX, slurry process, paste process, moulding powder, sensitivity*

1. INTRODUCTION

High performance warheads with IM requirements are very demanding on every component of the whole system.

Desired, but contradictory, properties for the main charge of a warhead can be

- sensitive enough to be easily initiated by the ignition train
- low sensitivity for handling and IM
- high energetic for performance.

This means for the IHE moulding powders, their processing on presses and their properties:

- regular agglomerates, homogeneously coated with binder
- no batch differences in bulk density and flowing behavior

As is well known, the coating process for explosives all over the world is based on a water slurry.

A water free paste process in kneaders is not used so often.

In the last years we had the possibility to test the suitability of similar explosive moulding powders prepared with both preparation methods for the warhead production.

What are the differences in the coating process and how do they affect the product and the safety?

2. COATING PROCESS

The preparation process of explosives has to guarantee, that

- the HE crystal mixtures are homogenized,
- raw material agglomerates, especially fine particles sticking on larger ones, are destroyed,
- the binder is coating the whole surface of all particles,
- additives are regularly distributed.

Relating to these requirements, the results achieved by kneading and suspension processes are different.

2.1 Water Slurry



Fig 1. Slurry process; HMX based moulding powder

In a stirring vessel with water, the water wet crystals are suspended.

High concentrated binder solution is stirred into the suspension.

The solvent is drawn off by temperature and/or vacuum.

The granules are filtered and dried.

The simple and safe process is the main advantage for the slurry process:

- water wet explosive from the crystallization process can directly be used, supporting to destroy raw material agglomerates,
- a minimum of solvent is needed,
- because of the slight mixing stress, the change of particle size and shape during the stirring in the water suspension is negligible,
- size and bulk density of the granules are adjustable,
- upscaling for higher quantities is easy .

To dry the wet agglomerates in a separate step is a necessary evil of the slurry process.

2.2 Paste

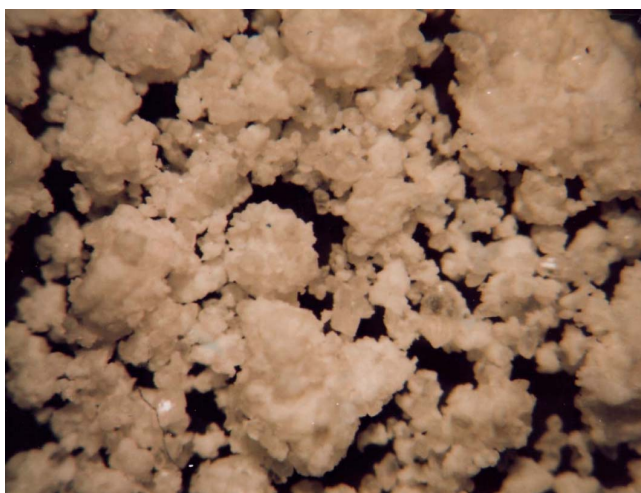


Fig 2. Paste process; HMX based moulding powder

In a separate step, the water wet explosive crystals are dried.

In a kneader with solved binder, the dry crystals are worked into the binder lacquer.

The high viscous mixture is homogenized and kneaded until the final coating is achieved.

Temperature and vacuum are set to draw the solvent off.

The solvent free product is granulated in the kneading bowl.

With this kind of coating a water free process is possible.

Some of the disadvantages of the paste process are:

- the crystals have to be thoroughly dried, thereby building strong agglomerates especially with fine particles,
- a surplus of solvent needs to be added to ensure enough liquid for a sufficient coating of all crystals,
- the shear stress in a kneader is crushing HE crystals and causes a debasement of the coating,
- the granules have on the one hand a high quantity of fine material, even single crystals are present, on the other hand much coarse lumpy portions, what makes e.g. the bulk density varying,
- the quality of the product is very sensitive to process and plant changes. Every change in the filling degree, the size of the mixer or even new mixing blades effect the shear stress and influence the product. This makes upscaling difficult.

3. EFFECTS

3.1 Process Safety

The **slurry process** is a safe process for an explosive moulding powder preparation and needs no remote controlling.

All steps with uncoated materials, work with water: water wet crystals are used in water suspension.

Only after the coating is finished, the compact granules are dried.

For the remote controlled **paste process**, the handling and mixing of dry explosive together with combustible organic solvents at variable shear stresses is very exacting.

The more solvent is drawn off, the higher becomes the viscosity of the paste and the more the kneader works like a mill: the shear stress crushes HE crystals.

Viscosity and stress also increase with higher explosive quantities, when e.g. production batches are manufactured.

Shear stress is disadvantageous for the coating quality in a double sense:

- HE crystals more easily crush at the end of the process. Then the mixture is very high viscous or even “dry”. These “new” surfaces will show a lower coating quality.
- binder layers on the crystals are rubbed off by the material friction, causing a debasement of the coating.

The more complicated method (higher probability for human error), additional measures for safety (which may fail) and coating imponderabilities make the paste process expensive and risky.

3.2 Compacting Moulding Powders



Fig 3. Free flowing moulding powder from a slurry process

With this kind of explosives densities close to TMD (theoretical material density) are obtained at less than 1 kbar compacting pressure.

Samples pressed under these conditions, obtain initiation pressures in the WIWEB water gap test higher than 30 kbar.

Moulding powders supporting these qualities by easy compacting processes are desirable in the warhead production.

The compact granules from the **slurry process** are free of dust, free flowing without segregation and have a high and well defined bulk density, see Figure 3.

This regular and void free granules are good for high speed fill and provide excellent HE charge homogeneity.

With this moulding powder the ammunition production process can be designed safe and effective.

Paste process:

In its packaging the PBX powder is caking together and builds conglomerates, easy to destroy, but unable to flow. So automatically dosing into warhead cases is not possible.

The irregular granules are segregating in coarse and fine material and show varying bulk density, causing variable filling heights in the pressing mould.

Granules full of voids and caking together while poured into the mould are difficult to be evacuated. It needs a longer time and a better vacuum to get acceptable charge homogeneity.

The poor quality of the granules, manufactured in a paste process, makes the compacting process complicated, ineffective and expensive.

3.3 IM Behaviour

In small scale tests the IM behavior of pressed cylinders made of slurry and paste prepared moulding powders were compared.

The granules were compacted to cylinders of 50 mm diameter and 100mm length and assembled into the same steel cylinders as used for the WIWEB IHE tests:

Steel cylinder with an inner diameter of 50 mm and a length of 100 mm, closed on both ends with steel covers. The wall thickness of the metal case and covers is 5 mm.

A cook-off and an impact test were chosen to see possible safety influences in an open fire and by the hard impact stress of a shaped charge jet.

4. RESULTS

For the cook-off test, the closed steel tube with the explosive was fixed on a holding device over a fuel basin.

Figure 4 shows the monitor view of one test sample in the fuel fire:



Fig 4. Cook-off test, test set up

The cook-off tests of the specimen in an open fire showed no differences in the reaction response: both RDX based explosive fillings had type 5 reactions, examples see Figure 5.



Fig 5. Cook-off test: type V reactions

A stronger influence was observed in the shaped charge jet impact (SCJI) tests:

A 38,7 mm bomblet is used together with a 20 mm mild steel barrier, as shown in figure 6, to shoot axial into the filled steel cylinder.



Fig 6. Shaped charge jet impact, test set up

The impact response of the slurry explosives mostly were burning reactions. All tests showed reaction types between IV and V.

The tests with the paste explosives mostly showed partial detonation. All reaction levels were between II and III.

Examples of parts found after the test shows Figure 7:

LEFT SIDE:
Paste Process;
Partial Detonation,
RT 2



RIGHT SIDE:
Slurry Process;
Burning,
RT 5

Fig 7. Shaped charge jet impact, results.
(barrier, explosive, shell fragments, witness plate)

While the resistance to fire for both explosive types is “burning”, the response of a paste explosive to a shaped charge impact is two classes worse than the response of a slurry explosive.

The difference in coating quality is looked upon being the reason for the different sensitivity.

While the slurry process builds up step by step the coating and agglomeration, modeling compact granules, the paste process destroys the coated crystals by friction and the needed vacuum generates voids in the granules.

Paste mixtures tend to produce granules that have void areas which contribute to sensitivity.

5. SUMMARY

On the surface, the explosive one-dish meal of a paste process seems to be better than other methods.

Looking closer on details, expenditure and disadvantages of kneading processes become more and more clear, influencing safety, properties and production costs in a not acceptable way:

Handling dry explosives together with combustible, organic solvents is risky.

The lumpy and inhomogeneous paste explosive is not suitable for high precision warheads.

All desired HE properties are not generated by the process.

Significantly higher product costs will not justify a worse paste explosive.

At the end of the day the kneading process shows no advantages compared with a slurry process.

In all requirements the slurry explosive is superior.

It is worth while spending time and attention to a good coating quality of HE crystals.

BALLISTICAL AND CHEMICAL STABILITY OF ROLLED BALL PROPELLANTS

S. Wilker*, P. Guillaume**, M.H. Lefebvre***,
S. Chevalier**** and Laurence Jeunieu***

* WIWEB ASt Heimerzheim, Großes Cent, 53913 Swisttal (DE)

** PB Clermont S.A., Rue de Clermont 176, 4480 Engis (BE)

*** Ecole Royale Militaire, Avenue de la Renaissance 30, 1000 Bruxelles (BE)

**** SME – Centre de Recherches Le Bouchet, Boîte Postale N°2, 91710 Vert-le-Petit (FR)

Abstract

This paper presents in summary the work of a Belgian-French-German cooperation programme on the chemical and ballistical stability of a ball propellant for the 5.56 · 45 mm ammunition. The programme comprises thermoanalytical, analytical, ballistical and spectroscopical techniques applied on unaged and aged samples of the propellant K 5810.

The propellant K 5810 is chemically stable. This fact is proven by microcalorimetry; the maximum heat flow does not reach the limit values of STANAG 4582. Also the stabilizer content after ageing times which are comparable to a 10 years storage at 25°C is much higher than the limit values given in AOP-48, Ed. 2. The ageing mechanism is strongly dependent on the loading density of the ampoules and the atmosphere above the sample which underlines the big effect oxygen has on the ageing of nitrocellulose based propellants.

The slight energy loss during the ageing periods used here does not affect the ballistic behaviour significantly. In contrast to the 9 mm ammunition tested before there seems to be no incompatibility between the propellant and the Sintox primer because the propellant K 5810 does not contain isopropanol in contrast to the K 6210 propellant in the 9 mm ammunition.

The ballistic life time is limited by the migration of the deterrent. This migration leads to an increased burning rate and thus to an increased pressure in the early phase of the burning reaction. As not all samples are available at the moment a final value for the activation energy of the migration of the DBP can not be given. First estimations lead to a value slightly above the activation energy of the nitrate ester decomposition.

Keywords: *ballistic stability, migration, double base propellants,
activation energy*

1. INTRODUCTION

Ball powders are used in many small calibre applications. They are easy to prepare and can be specially designed for different ammunition types by modification of their surface. This surface modification usually consists of an impregnation by phthalates which are only present along the surface up to a certain depth. This helps to maintain a nearly constant pressure generation during the burning reaction, because the burning rate increases with time which compensates the reducing burning surface area.

The disadvantage of this special design is the possibility of the migration of the deterrents throughout the propellant. In this case the burning rate increases at the beginning of the burning process which may lead to higher pressures which can damage the weapon or give rise to malfunctions of the ammunition. Another disadvantage of ball propellants is the relative incompatibility between the stabilizer diphenylamine (DPA) with nitroglycerin ^[1] which can lower the service life of the propellant.

To determine the effects of migration and decomposition processes in ball propellants on the service life we have started a trilateral investigation programme between Germany, Belgium and France which is a follow-up of the studies on 9 mm ammunition ^[2]. The aims of this study are the determination of the temperature dependence of migration and decomposition processes. In a second step we correlate the migration (made visible through IR microscopy) with the burning behaviour to be able to understand the effects of a decreasing deterrent concentration at the surface on the pressure increase in the weapon.

This study also gives the opportunity to benefit from special analytical methods which are available in only one or two of the participating laboratories. So we have studied the correlation between the stabilizer depletion and the nitrogen oxide content after ageing of the propellant. As well the correlation between characteristic microcalorimetric signals and the stabilizer content has been worked out. Finally we studied the effect of two different primers used for the 5.56 mm ammunition in two different countries. From the previous study ^[2] we know that the incompatibility between a propellant ingredient (solvent) and one component of the primer limitates the service life of the ammunition.

2. PROPELLANT AND AMMUNITION

The **propellant sample** which is used for the investigations is the double base ball propellant K 5810, lot 02MQ. It contains around 10 % of nitroglycerin and it is stabilized with diphenylamine (DPA). The deterrent applied on the surface is dibutylphthalate (DBP). The average concentration of this material is 4,5 %.

Two types of **ammunition** are tested. Both are 5.56·45 mm cartridges, one produced in Germany containing a lead free primer („Sintox“), the other one produced in the UK with a lead containing primer.

3. EXPERIMENTS / WORK PROGRAMME

As mentioned in the introduction many different areas of investigations are covered, namely stability, migration studies, ballistic tests and chemical analysis.

Heat flow measurements (HFC) were conducted with a „Thermal Activity Monitor“ TAM 2277 (Thermometrics AB, Sverige). The measurements were performed in 3 ml glass ampoules. Usually the ampoules are completely filled and sealed. For the determination of the influence of different measuring conditions we varied the standard method by

filling the ampoule from only 5% to 80% (details see in ^[6])

replacing the air in the ampoule by argon (details see in ^[6])

The stabilizer content was analyzed after heat flow measurements. Prior to HPLC analyses around 120 mg of the propellant sample were dissolved in 10 mL of acetonitrile, and then 40 mL methanol are added. The nitrocellulose was precipitated by adding 50 ml of water. The solution was filtered through a filter syringe and directly passed into the HPLC autosampler flasks. The stabilizers were detected with a Gynkotek HPLC system consisting

of a pump M480S, an automatic sampler Gina 50, a column oven and a diode array detector UVD 320S. The detection wavelength was 225 nm. The column (Lichrospher 100RP18 - 5µm; 250·4 mm with a pre-column 20·4 mm) was tempered at 25°C. A methanol/ water mixture (67/33) was used as mobile phase and pumped with a flow rate of 1.2 ml/min.

The stabilizer depletion products N-NO-2-NO₂-DPA, N-NO-4-NO₂-DPA, N-NO-2,4'-DNDPA and N-NO-4,4'-DNDPA were synthesised according to literature methods from 2-NO₂-DPA (resp. 4-NO₂-DPA) and NaNO₂ ^[3] or by nitration of N-NO-2-NO₂-DPA, N-NO-4-NO₂-DPA with HNO₃ and subsequent chromatographic separation of the products. Their chemical structure was verified by FT-IR and NMR spectroscopy.

Chemiluminescence experiments were performed discontinuously after ageing of the propellant sample. Both the atmospheric nitrogen oxides (those which are in the gas phase) as well as those which are liberated by a stream of nitrogen gas out of the propellant grains within one day are detected. The detection occurs for NO alone and for NO + NO₂ together. From these results the NO₂ concentration is calculated. All experiments were performed at a loading density of about 0.6.

Ballistic experiments were performed with unaged and aged ammunition (both German and UK ammunition). The chamber pressure, case mouth pressure, port pressure and the velocity of the projectile were measured. The pressure was measured with a transducer Kistler 6215.

Migration of the deterrent was made visible by IR microscopy. To do this, the propellant grain was placed into an adhesive and cut by a microtome into small slices (thickness 7 µm) which were then analysed by FT IR microscopy. Two IR bands (one typical for nitrocellulose, the second typical for phthalates) were chosen for analysis. Their relation was used to calculate the local content of dibutyl phthalate. The measuring window had an aperture of 10 µm * 50 µm, the step for each data point was 3 µm so neighbouring IR spectra overlap.

The ageing plan of the propellant is presented in table 1. The ageing plan of the cartridges is presented in table 2. Sample abbreviation: Throughout this document K stands for propellant alone, D for German and E for UK ammunition. The two numbers behind the first letter describe the ageing temperature whereas the last letter describes the ageing time (see tables 1 and 2).

Table 1. *Ageing plan of propellant K 5810. The figures refer to the number of ageing days. The last row indicates the energy release at each decomposition stage derived from HFC experiments at 80°C*

<i>T [°C]</i>	<i>A</i>	<i>B</i>	<i>C</i>	<i>D</i>	<i>E</i>	<i>F</i>	<i>G</i>	<i>H</i>
80	1,20	1,81	2,41	3,61	5,41	7,22	9,02	10,83
70	4,83	7,25	9,66	14,50	21,74	29,00	36,23	43,48
65	-	-	-	30,00	-	-	-	-
60	21,06	31,61	42,12	63,22	-	126,4	-	189,6
50	100,7	151,0	201,4	302,0	-	605	-	-
40	532	798	1064	-	-		-	-
<i>Q [J/g]</i>	2,79	3,56	4,28	5,70	8,08	12,43	22,75	33,45

Table 2. Ageing plan of GE and UK ammunition. The figures refer to the number of ageing days. The last row indicates the energy release at each decomposition stage derived from HFC experiments of the propellant at 80°C

$T [^{\circ}\text{C}]$	A	B	C	D	E	F	G	H
80	1,20	1,81	2,41	3,61	5,41	7,22	9,02	10,83
70	4,83	7,25	9,66	14,50	21,74	29,00	36,23	43,48
65	10,00	15,00	20,00	30,00	45,00	60,00	75,00	90,00
60	21,06	31,61	42,12	63,22	94,79	126,4	158,0	189,6
50	100,7	151,0	201,4	302,0	453	605	755	907
40	532	798	1064	-	-		-	-
$Q [\text{J/g}]$	2,79	3,56	4,28	5,70	8,08	12,43	22,75	33,45

The temperature dependence was derived from HFC measurements where an activation energy of around 140 kJ/mole was found (see section 4). This means that all samples in one column have the same decomposition degree. Anyway, slight deviation from 140 kJ/mole especially at low α makes an individual calculation of Q necessary. All evaluations against the released energy are therefore based on the individual energy release of each sample determined by HFC.

4. RESULTS

4.1 HFC measurements

Figure 1 shows HFC curves of the propellant K 5810, lot 02 MQ in comparison with another lot of this propellant type and with K 6210. The curves show the typical behaviour of DPA stabilized double base propellants. The shape of the curve and the chemical reactions are described in ^[4]. Table 3 summarizes the main features of the curves.

Table 3. Summary of HFC results of the samples from Fig 1 at 89°C

Sample	K 5810, lot 02MQ		K 5810, lot 403		K 6210, lot 225	
1 st minimum (t, P)	0,68 d	47,0 $\mu\text{W/g}$	0,76 d	56,2 $\mu\text{W/g}$	0,52 d	67,1 $\mu\text{W/g}$
2 nd maximum (t, P)	2,64 d	231 $\mu\text{W/g}$	2,13 d	226 $\mu\text{W/g}$	1,29 d	266 $\mu\text{W/g}$
highest value within 3,83 days [5]	231 $\mu\text{W/g}$		226 $\mu\text{W/g}$		266 $\mu\text{W/g}$	
heat generation within 3,83 days	43,7 J/g		47,1 J/g		68,4 J/g	

In comparison with K 6210, which has a higher nitroglycerin content (19 %), K 5810 shows a longer first minimum, which is equivalent to a longer time until DPA is consumed. Within the ‘STANAG 4582 time’ (= 3,83 days at 89°C) K 5810 has a lower energy release than K 6210. All three propellants pass the stability criterion of this STANAG ^[5].

P, $\mu\text{W/g}$

T = 89°C

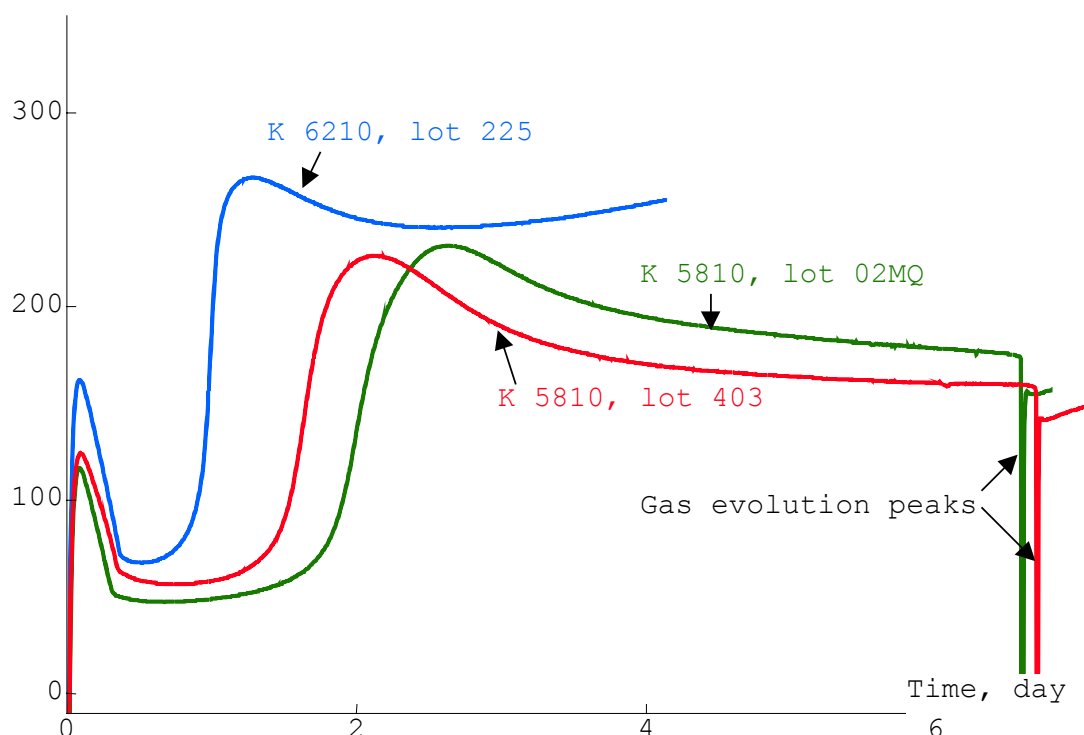


Fig 1. HFC curves of K 5810 (two different lots) and of K 6210.
Completely filled and sealed ampoules; atmosphere = air

HFC measurements were also performed at 80°C, 70°C and 60°C. A double-logarithmic plot shows that all important reactions appear at all temperatures (see Fig 2). Of course the time to reach the 2nd maximum is much longer at lower temperatures.

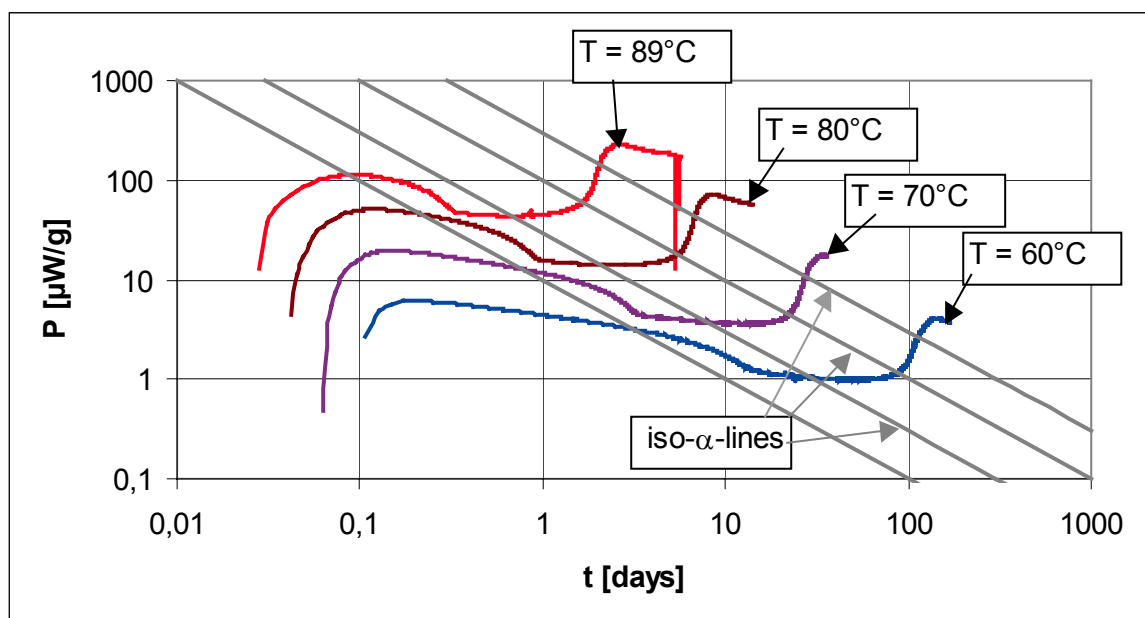


Fig 2. HFC curves of K 5810, lot 02MQ at temperatures between 89°C and 60°C.
Iso- α lines connect the stages of comparable reaction degrees at different temperatures with one another.

HFC experiments were also performed with complete cartridges in a 20 ml ampoule. To improve the heat conduction from the cartridge to the ampoule wall the ampoule was filled with small glass balls. The results are shown in figure 3, the compatibility evaluation is presented in figure 12.

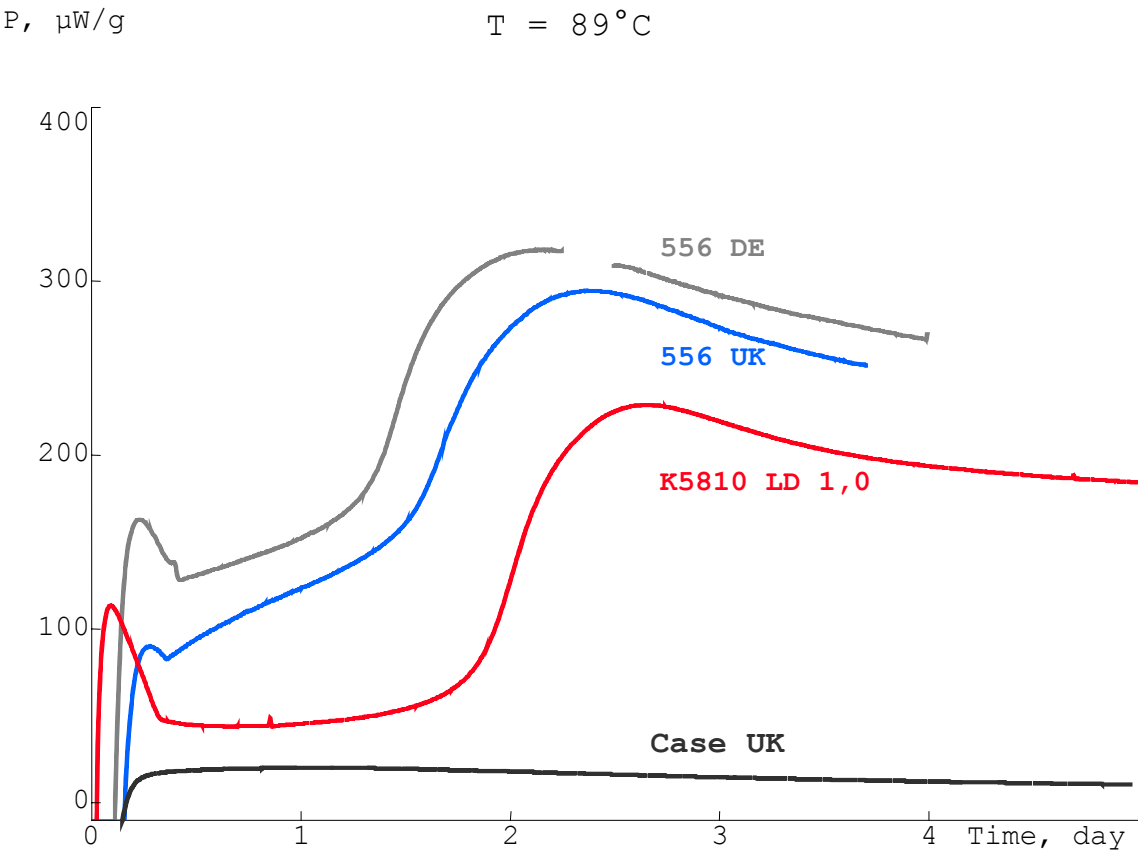


Fig 3. HFC curves of ammunition (UK and GE production) at 89°C in comparison with the propellant and with the empty case alone. Values for the ammunition and the propellant are given in $\mu W/g$ propellant.

4.2 Stabilizer depletion

Stabilizer analysis was performed after HFC measurements. All the ageing took place in hermetically sealed ampoules. The stabilizer depletion was sampled as a function of time (at a constant loading density) as well as a function of loading density (with constant ageing times). Please find detailed results in ^[6].

Stabilizer depletion analyses were also performed in parallel to the chemiluminescence experiments (see fig. 13).

4.3 Chemiluminescence

Chemiluminescence experiments were performed at 80°C and at 70°C. Both series exhibit a low level of NO_x concentration. After 4 days at 80°C (respectively 18 days at 70°C) the value increases rapidly. Figure 4 shows the results of one of the experimental series.

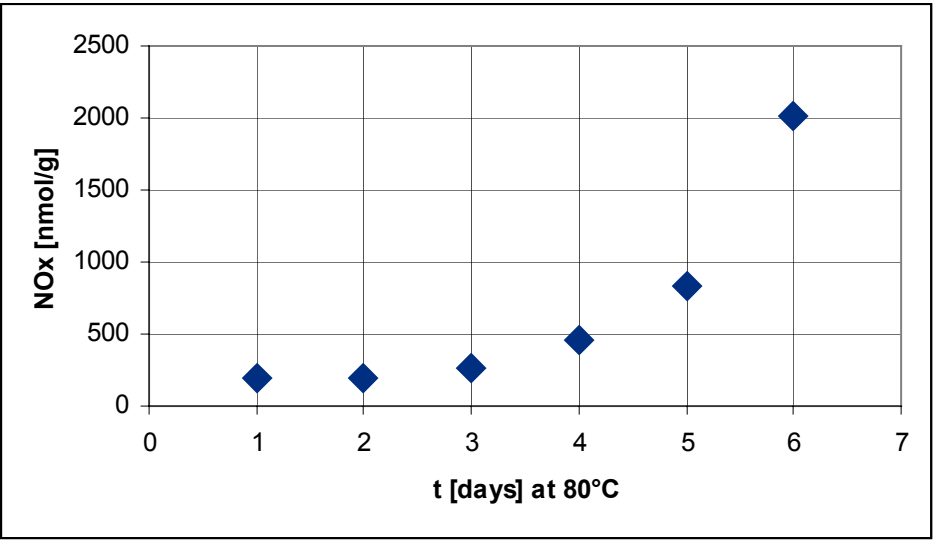


Fig 4. NO_x development of K 5810 at 80°C as a function of time.

4.4 Ballistic studies

The ballistic experiments were performed with aged cartridges. The characteristic values (case mouth pressure (Pm), port pressure (P2) and velocity of the bullet (v)) are determined as a function of ageing. Figures 5-8 show typical examples.

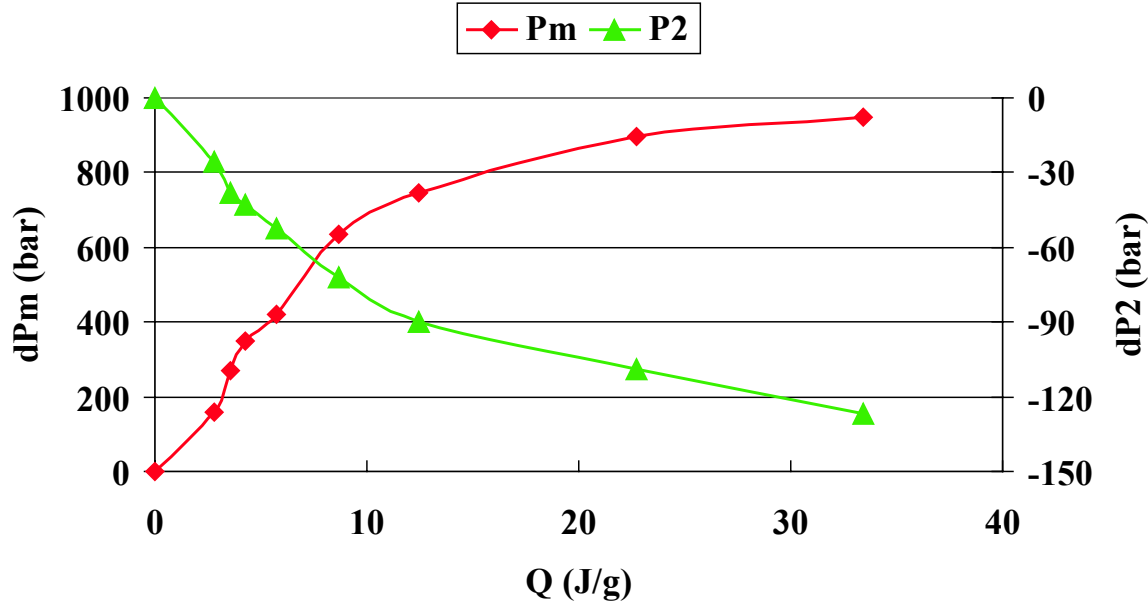


Fig 5. Pressure increase (case mouth (dPm)) and decrease (port (dP2)) of aged sample (UK ammunition; ageing temperature = 70°C)

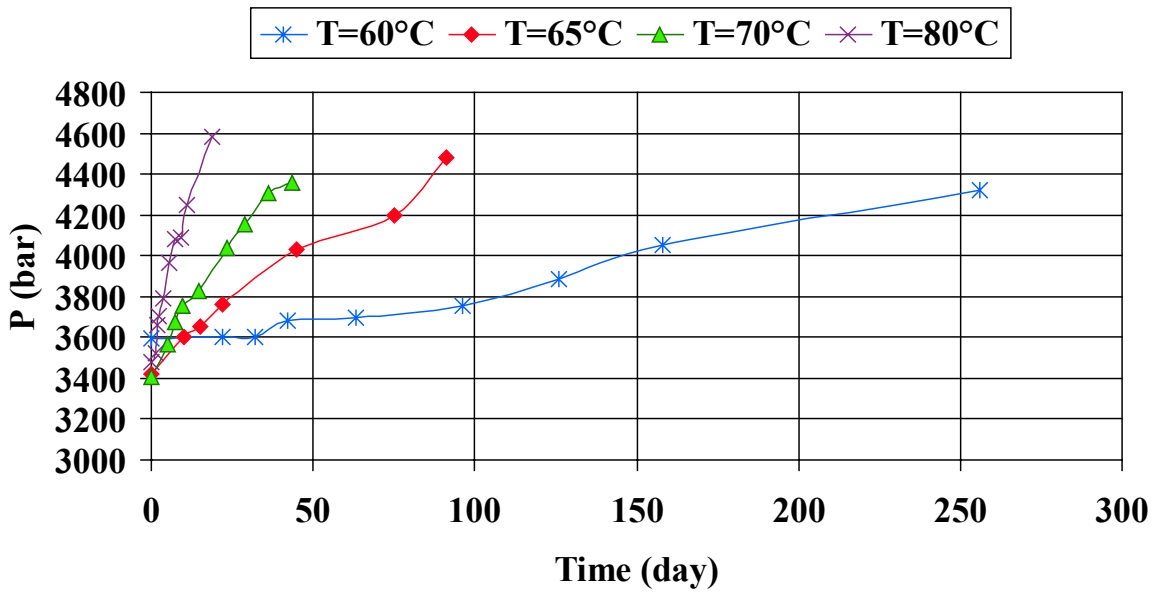


Fig 6. Case mouth pressure of UK ammunition aged at different temperatures as a function of ageing time. The values are not corrected for the day of firing

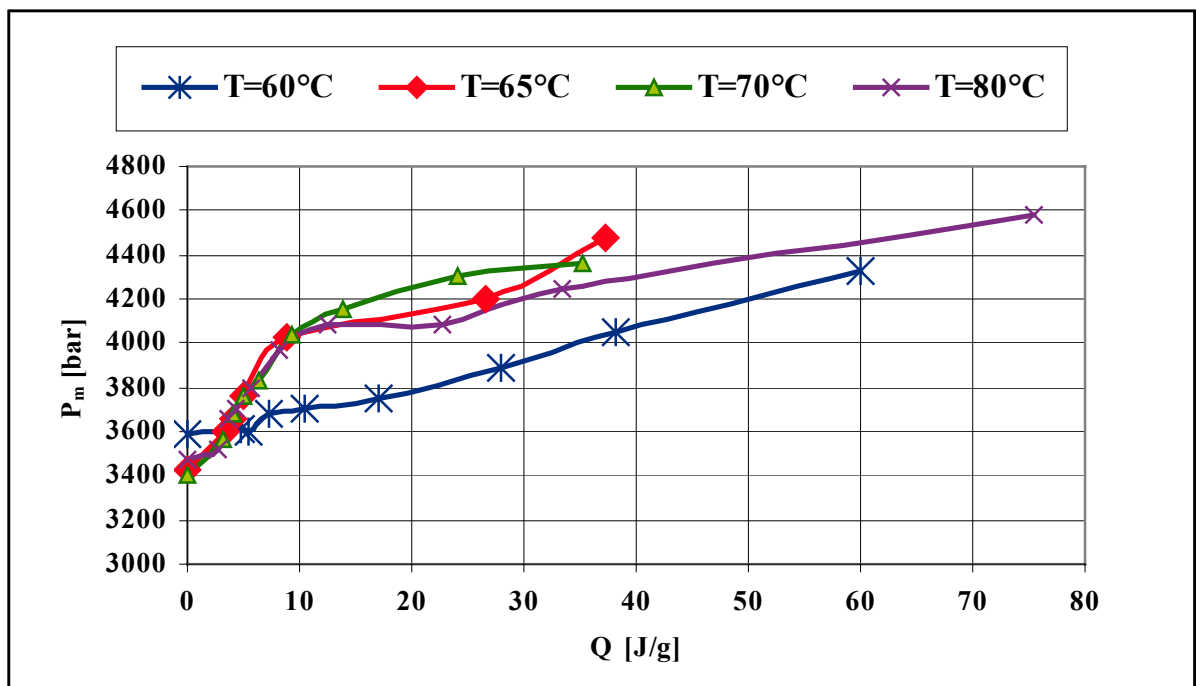


Fig 7. Case mouth pressure of UK ammunition aged at different temperatures as a function of released energy. The values are not corrected for the day of firing.

All ballistic experiments were accompanied with closed vessel tests. Unaged and aged propellant was fired and the pressure/time curve recorded. Like in the ballistical experiments described above a change in burning behaviour was observed (higher burning rate than the unaged propellant in the beginning, slower burning rate in the later part of the experiment).

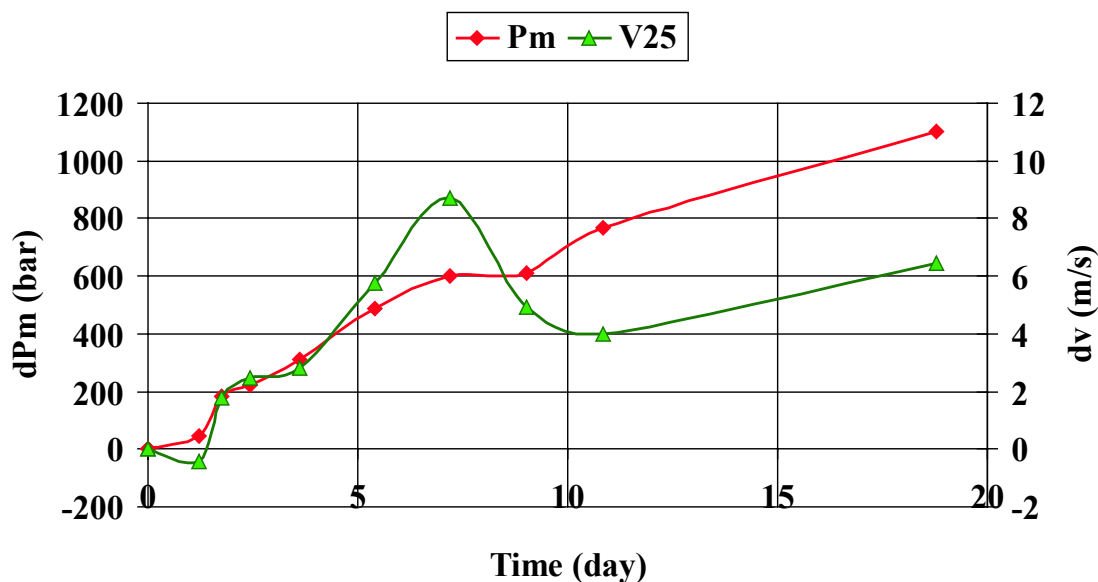


Fig 8. Changes in P_{\max} (dPm) and velocity (dv) after ageing (UK ammunition, ageing temperature = 80°C)

4.5 Deterrent migration

After ageing the propellant grains were cut into thin slices and analysed by FT IR microscopy. Because the concentration profile is dependent on the cutting angle multiple analyses of each ageing state were performed to overcome this uncertainty. The raw results were then mathematically fitted to form an exponential (Gaussian) curve. Fig 9 shows the raw signals and the fitted curve for sample K80B, Fig 10 shows the fitted curves of all samples of the K80 series.

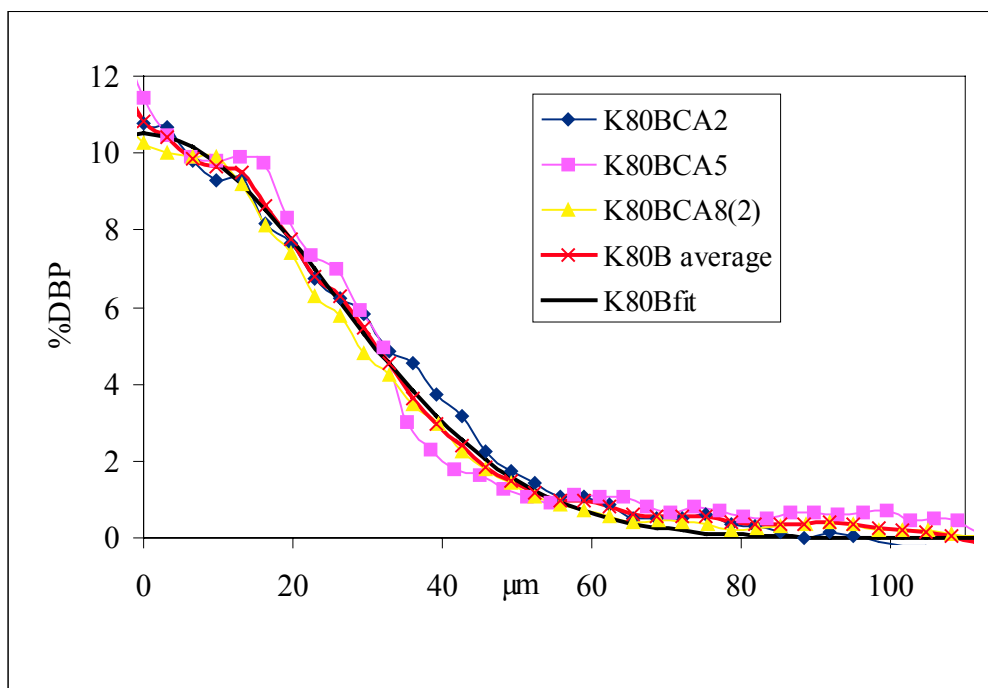


Fig 9. DBP profile in sample K80B

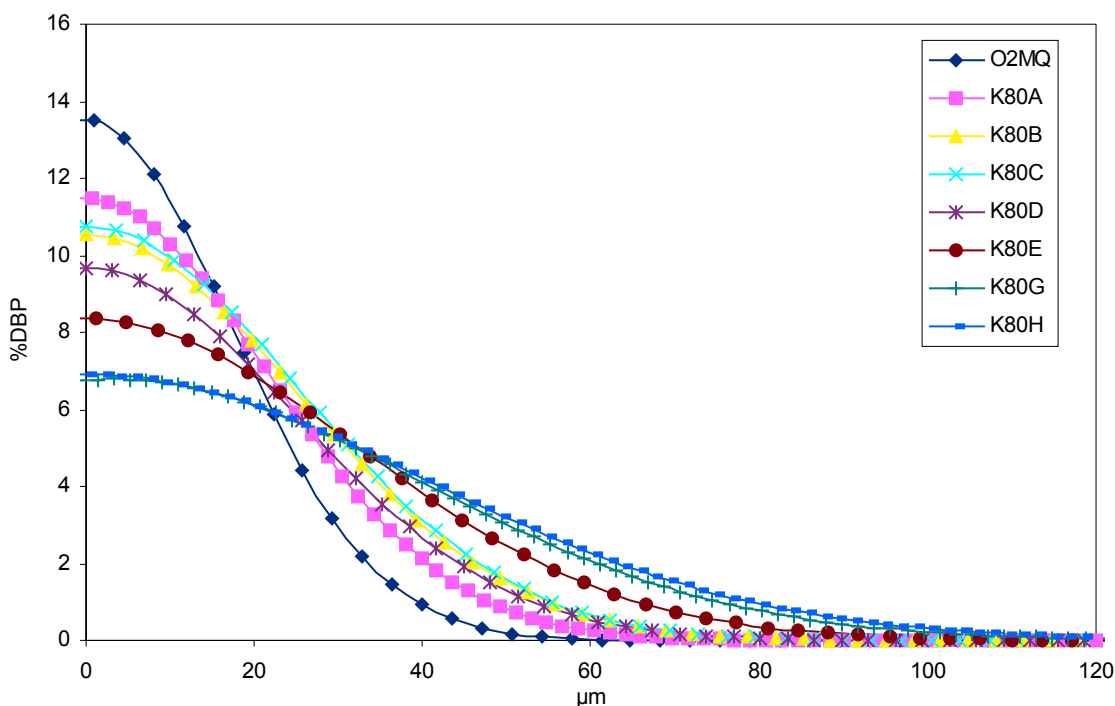


Fig 10. DBP profiles (fits) in aged propellant (80°C series, 02MQ = unaged sample)

5. DISCUSSION

5.1 HFC of propellant and ammunition

Both K 5810 and K 6210 have the typical shape of DPA stabilized propellants with a first maximum (this is the oxidation peak of the nitrocellulose), a broad first minimum and a sharp increase up to a second maximum. This is the point where the DPA is completely consumed. After the second maximum both propellants show a slight decrease of the HFC curve. The endothermic peaks at the end of the measurements are due to gas evolution from the ampoule because the decomposition gases build up a pressure which the PTFE cap of the ampoules can stand only up to about 8 bar. The activation energy of the decomposition were calculated using a model-free iso- α -evaluation (as it was done in ^[4]). Its value lies at around 110-120 kJ/mole in the first minimum (as long as DPA is present). DPA depletion kinetics also show activation energies of 110-120 kJ/mole. After DPA is gone the activation energy increases into the range between 138 and 140 kJ/mole. So this value is very much comparable to the values found in other propellants.

The HFC signal of the two tested cartridges exhibit a comparable pattern (see Fig 3). But – if the HFC value is expressed in $\mu\text{W/g}$ propellant – the level of heat flow is higher and the time to reach the second maximum is significantly shorter. The HFC curve of the empty cartridge (without propellant) shows a signal of 20 $\mu\text{W/g}$ during the first two days. This heat is caused by oxidation reactions of the metal case and the lacquer. Also a small part of the heat may come from decomposition reactions of the primer.

The compatibility of the case with the propellant was evaluated (see fig. 12). A slight incompatibility was detected ($Q_R = 3,1 \text{ J/g}$) which is not relevant concerning the limit values (30 J/g ^[7]).

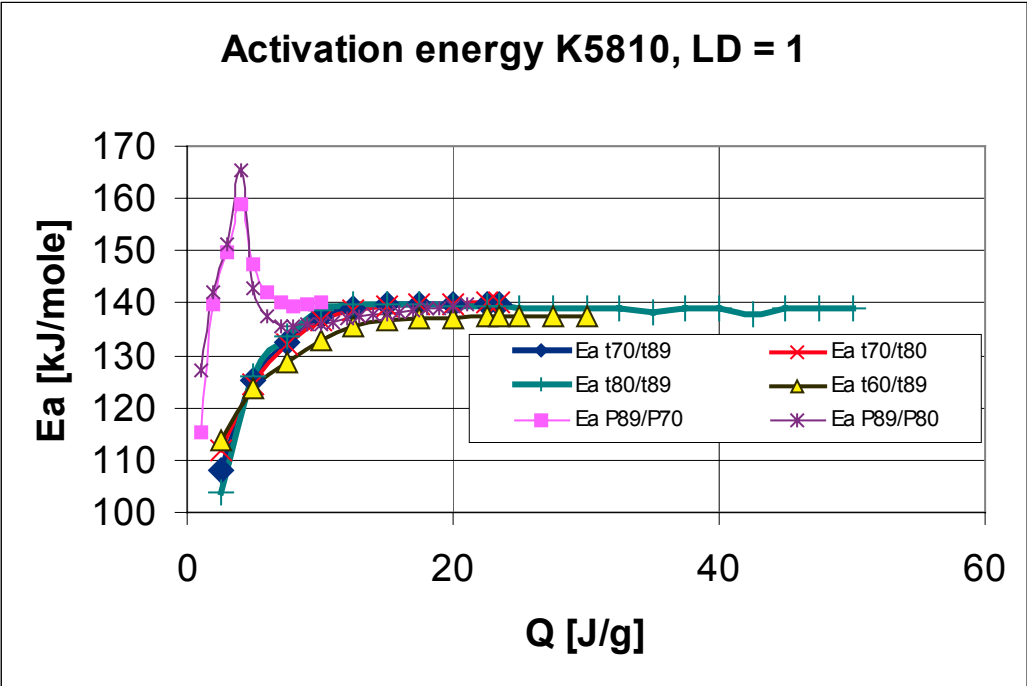


Fig 11. Activation energy of propellant K 5810 as a function of the decomposition degree (α). $E_a(t)$ refers to the time when an iso- α -point is reached, $E_a(P)$ refers to the ratio of heat generation rates at the iso- α -points.

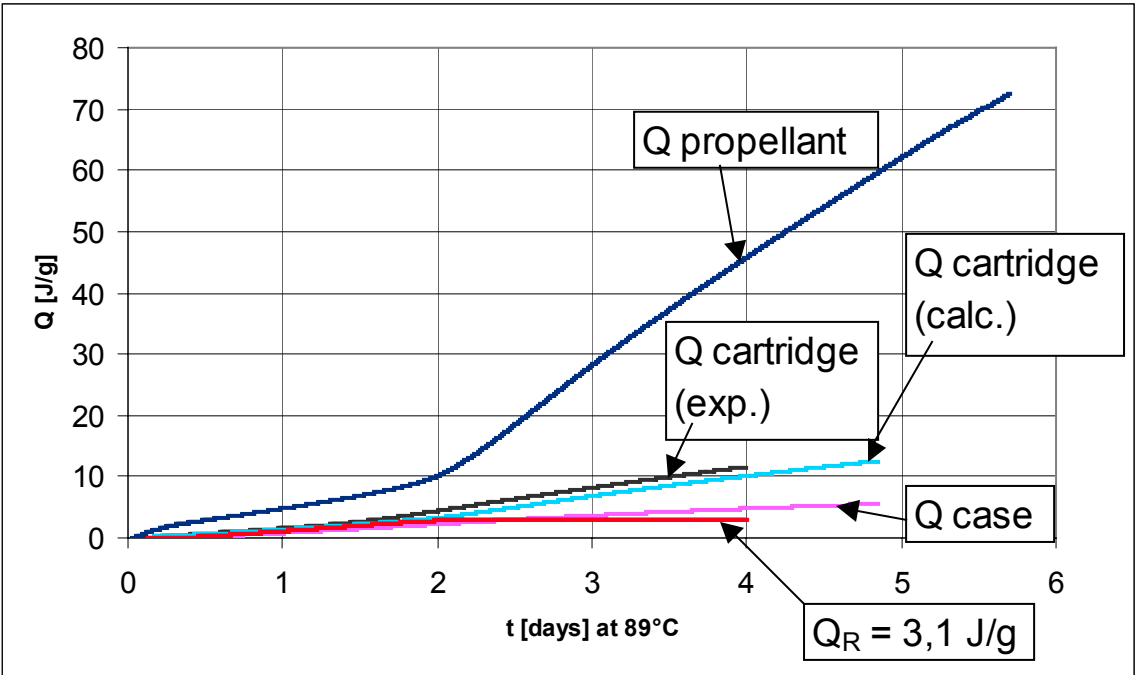


Fig 12. Compatibility evaluation of the 5.56 mm ammunition

5.2 Stabilizer analyses

In completely filled and sealed ampoules the main decomposition product is N-NO-DPA, which is slowly nitrated into the N-NO-4-NDPA and N-NO-2-NDPA. When the storage time is longer than 5 days at 89°C (equivalent to 70 J/g) then dinitro-DPA derivatives appear. The major species of this kind is 2,4'-DNDPA. This distribution of

stabilizer products is typical for ,closed and filled‘ conditions. From the data obtained at different temperatures an average activation energy of 137 kJ/mole was calculated.

5.3 Chemiluminescence

The increase of nitrogen oxides after 4 days at 80°C (resp. 18 days at 70°C) is directly connected with the stabilizer content of the sample. As long as DPA is present, it readily reacts with NO_x to form N-NO-DPA. After DPA has been completely converted into N-NO-DPA the amount of NO_x increases rapidly, because N-NO-DPA only slowly reacts with nitrogen oxides to form N-NO-2-(or 4-)NO₂-DPA. How chemiluminescence and stabilizer depletion this correlate is presented in figure 13.

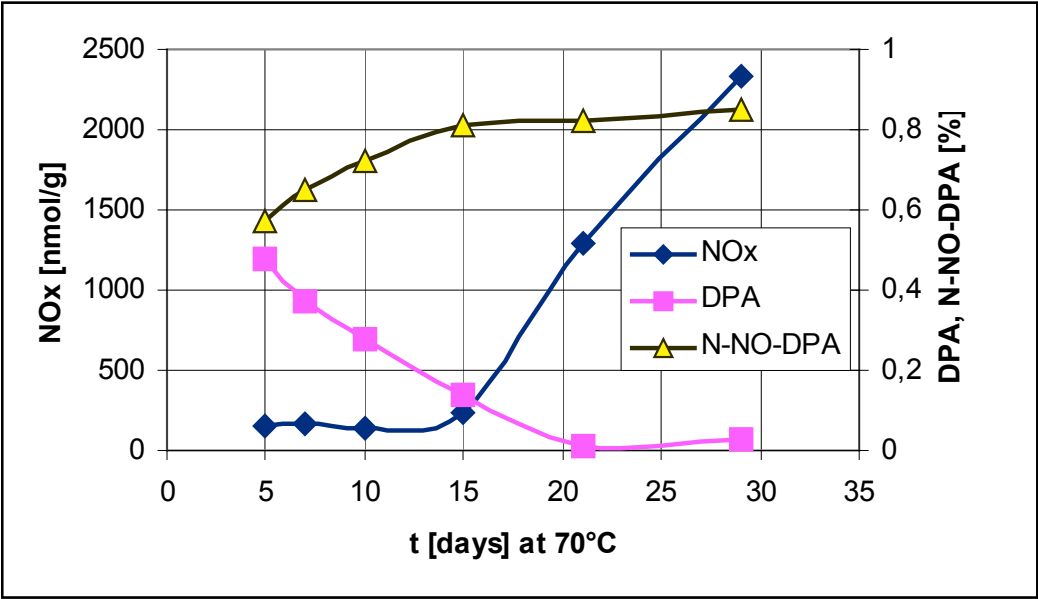


Fig 13. Correlation of NO_x concentration and stabilizer depletion (T = 70°C).

5.4 Ballistic results

Two principal changes of the burning behaviour of aged ammunition should appear. The first is a slow reduction of burning rate due to the energy release during the storage. This effect is usually small, but clearly visible (see ^[2]) when there is no migration of ingredients possible. A second effect comes from the migration of DBP. If its concentration is decreasing in the outer parts of the propellant grain the burning rate increases rapidly. This effect is much bigger in magnitude than the slight reduction due to energy loss.

The results of the ballistic experiments show a rapid pressure increase at the first part of the burning reaction whereas in the later parts the pressure decreases. This pressure increase in the first parts can be easily explained by the migration of the phthalate. This increases the burning rate of the propellant. This pressure increase is visible at all tested temperatures (80, 70, 65 and 60°C; 50°C and 40°C will be available in future). The specification of this weapon defines that P_{mean} must be less than 4050 bar $P_{mean} + 3 \cdot \sigma$ must not exceed the value of 4450 bar. The velocity of the projectile must not decrease by more than 30 m/s within the same time frame.

The results show that the velocity of the projectile is not affected markedly by the ageing of the cartridge. Therefore for this property the limit value is not reached at any temperature.

The last specification ($dP < 450$ bar after 30 days at 65°C) is fulfilled, as depicted in table 4 (entry D at 65°C). All values of these series are presented in table 4.

Table 4. Increase in case mouth pressure (UK ammunition) after ageing at different temperatures. All values in bar. See table 2 for ageing times.

Ageing stage	$T = 60^{\circ}\text{C}$	$T = 65^{\circ}\text{C}$	$T = 70^{\circ}\text{C}$	$T = 80^{\circ}\text{C}$
A	13	179	154	45
B	12	234	266	185
C	89	338	348	224
D	106	242	419	312
E	162	533	631	487
F	294	606	742	603
G	461	778	893	609
H	730	1058	946	768

5.5 Plasticizer migration

The plasticizer migration was observed at different temperatures. As it is very complex to describe the DBP distribution throughout the whole grain we decided to correlate the DBP content on the surface (fitted values were taken; see chapter 4.5) as a measure for the migration progress.

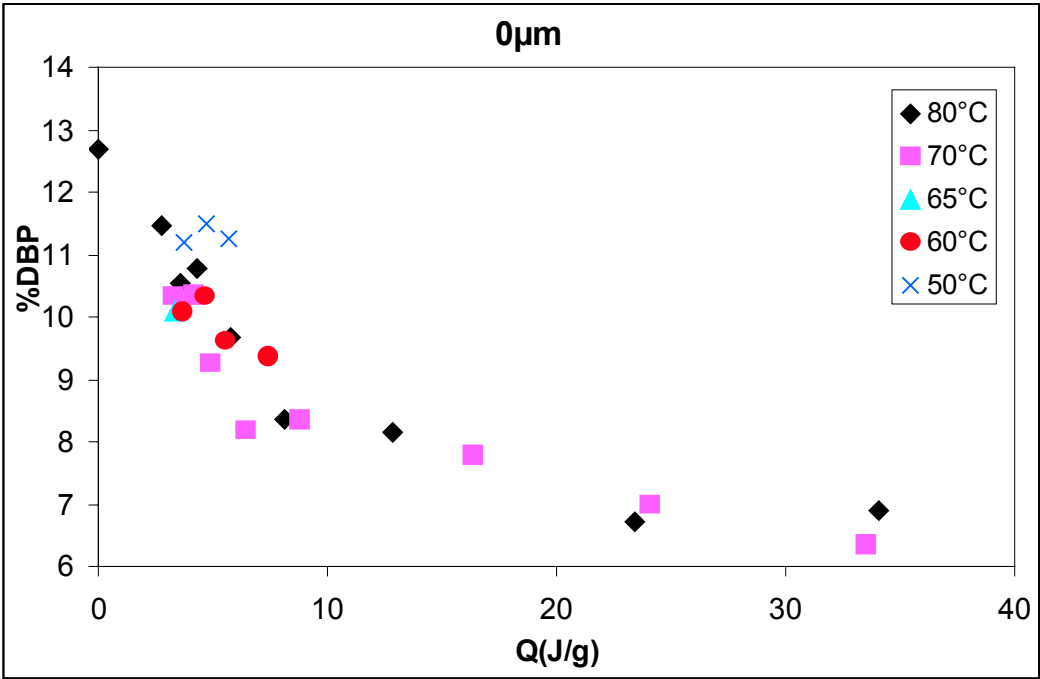


Fig 14. Correlation of energy release and DBP surface concentration (all ageing temperatures)

As a decreasing DBP content on the surface increases the burning rate and makes the inflammation easier it was interesting to see whether there was a correlation between the DBP content on the surface and the ignition time or the burning rate respectively. Fig. 15 clearly shows such a correlation. This correlation is true for all ageing temperatures. A more detailed description of the migration phenomena will be given in ^[8].

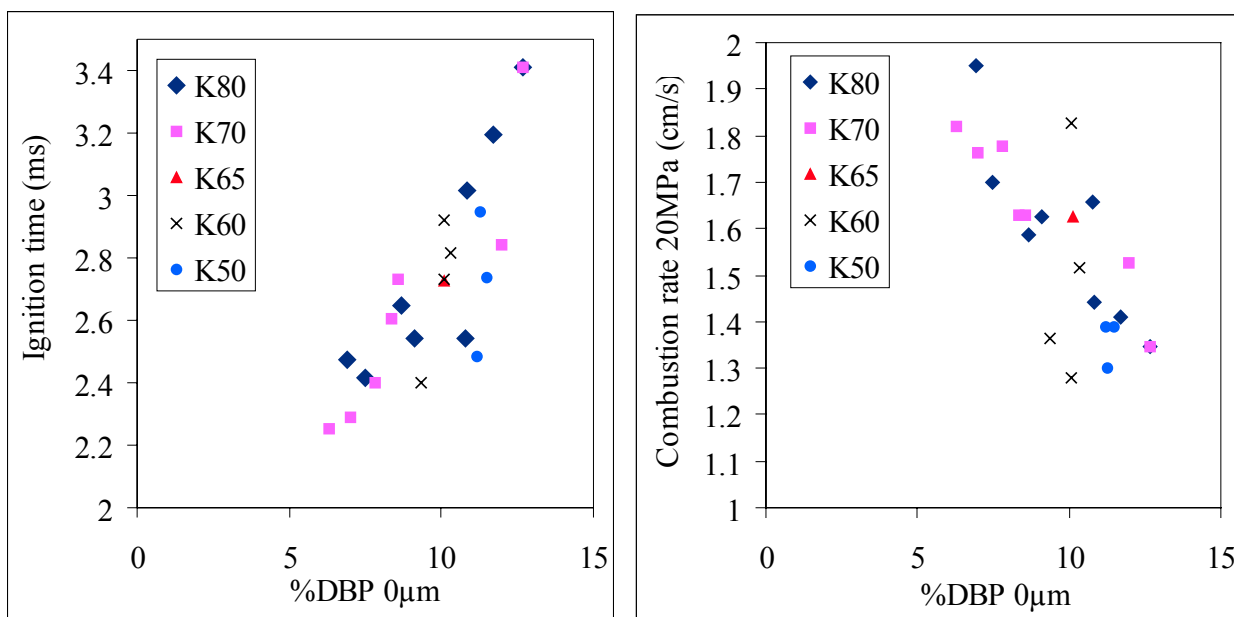


Fig 15. Correlation of DBP surface concentration and ignition time and burning rate

The temperature dependence of the migration process is very expressed. This results in an activation energy of the diffusion rate constants which is higher than the decomposition kinetics of this propellant (see chapters 5.1 and 5.2) and also higher than described in literature (125 kJ/mole in ^[9]). A final value will be given when all samples are measured.

6. CONCLUSION

The propellant K 5810 is chemically stable. This fact is proven by microcalorimetry; the maximum heat flow does not reach the limit values of STANAG 4582. Also the stabilizer content after ageing times which are comparable to a 10 years storage at 25°C is much higher than the limit values given in AOP-48, Ed. 2.

The slight energy loss during the ageing periods used here does not affect the ballistic behaviour significantly. In contrast to the 9 mm ammunition tested before (see^[2]) there seems to be no incompatibility between the propellant and the Sintox primer because the propellant K 5810 does in contrast to the K 6210 propellant in the 9 mm ammunition not contain isopropanol.

The ballistic life time is limited by the migration of the deterrent. This migration leads to an increased burning rate and thus to an increased pressure in the early phase of the burning reaction. The increase is more expressed at higher (80°C) than at lower temperatures (60°C). This assumption is supported by the results of the FT IR microscopy evaluation. As not all samples are available at the moment a final value for the activation energy of the migration of the DBP can not be given. First estimations lead to a value slightly above the activation energy of the nitrate ester decomposition.

Acknowledgements:

The authors would like to thank all participants for their contribution to the success of this work and for their enthusiasm.

REFERENCES

- [1] JAN PETRŽILEK, STEPHAN WILKER, JAN SKLÁDAL, GABRIELE PANTEL and LUTZ STOTTMEISTER: „Stability analyses of spherical propellants in dependence of their stabiliser and nitroglycerin content“, *Symp.Chem.Probl. Connected Stabil.Explos.* **12th**, 2001
- [2] ULDIS TICMANIS, PIERRE GUILLAUME, ANDRÉ FANTIN, GABRIELE PANTEL, JEAN-PIERRE MARCHANDISE and STEPHAN WILKER: „Assessment of the Ballistic Service Lifetime of a Small Caliber Cartridge by Heat Flow Calorimetry“, *3rd International symposium on Heat Flow Calorimetry and it's applications for Energetic materials*, 2002
- [3] STOERMER and HOFFMAN: *Chem.Ber.* **31**, 2535 (1898) [Beilstein XII, page 728].
- [4] PIERRE GUILLAUME, MAURICETTE RAT, GABRIELE PANTEL and STEPHAN WILKER: „Heat Flow Calorimetry of propellants – Effects of sample preparation and Measuring Conditions“, *Propellants, Explosives, Pyrotechnics* **26**, 51-57, 2001
- [5] STANAG 4582, „Explosives, Nitrocellulose Based Propellants, Stability Test Procedures and Requirements Using Heat Flow Calorimetry“, 1st Edition, March 2003; ULDIS TICMANIS, STEPHAN WILKER, GABRIELE PANTEL, MANFRED KAISER, PIERRE GUILLAUME, CORINNE BALÈS and NIELS V.D. MEER: „Principles of a STANAG for the estimation of the chemical stability of propellants by heat flow calorimetry“, *Int. Annu. Conf. ICT* **31**, 2, 2000
- [6] STEPHAN WILKER, PIERRE GUILLAUME, MICHEL H. LEFEBVRE, SAMMY CHEVALIER, LAURENCE JEUNIEAU, GABRIELE PANTEL, ULDIS TICMANIS and LUTZ STOTTMEISTER: “Stability analyses of rolled ball propellants – Part 1: Microcalorimetric studies and stabilizer depletion”, *Int. Annu. Conf. ICT* **34**, 83, 2003
- [7] STANAG 4147: „Explosives – Chemical Compatibility of Ammunition Components with Explosives and Propellants (Non-Nuclear Applications)“, Test 2, Draft Edition 3 (2003).
- [8] LAURENCE JEUNIEAU, PIERRE GUILLAUME, MICHEL H. LEFEBVRE, SEBASTIAN EIBL, STEPHAN WILKER: “Stability analyses of rolled ball propellants – Part 2: Ballistic Stability”, *Int. Annu. Conf. ICT* **35**, 2004
- [9] BEAT VOGELSANGER, BRUNO OSSOLA and ERNST BRÖNNIMANN: „The Diffusion of Deterrents into Propellants Observed by FTIR Microscopy – Quantification of the Diffusion Process“, *Propellants, Explosives, Pyrotechnics* **21**, 330-336, 1996

DEFORMATION AND FRACTURE OF ENERGETIC MATERIALS AND THEIR SIMULANTS

D. Williamson, S. Palmer, J. Field and W. Proud

University of Cambridge, Cavendish Laboratory, Physics and Chemistry of Solids Group,
Madingley Road, Cambridge, CB3 0HE, United Kingdom

Abstract:

A detailed understanding of the deformation and fracture mechanisms of energetic materials is vital to ensure optimum performance and safety. A series of deformation and fracture experiments with optically derived results are being developed on a sugar based energetic simulant with the ultimate aim of transferring the proven experiments to energetic materials. The physical insight and quantitative data these experiments yield are crucial in developing accurate and predictive models of the response of energetic materials to mechanical stimuli. This paper outlines the results taken to date and future research

Keywords: PBXs, fracture toughness, deformation, crack growth, DICC

1. INTRODUCTION

For optimum performance and safety, the explosive compositions in modern munitions must possess structural integrity; deformation and fracture can perturb shaped charge detonations, fracture can sensitise and lead to subsequent inadvertent initiation. It is therefore of crucial importance to obtain a detailed understanding of the deformation and fracture mechanisms of energetic materials.

The types of explosives under consideration are dual phase composites consisting of an explosive crystalline filler material bound in a polymeric matrix and are referred to as Polymer Bonded Explosives (PBXs). The filler loading in a typical PBX composition of interest is of the order of 95 % by weight. The explosive filler has a bimodal particle size distribution with a maximum particle size of the order of several hundred of microns. Safety considerations dictate that experiments on the sample sizes required are not practical in a general-purpose laboratory. To this end an inert simulant has been developed, with similar mechanical properties to an in-service energetic composition, whereby sugar grains are substituted for the explosive.

Of interest to the fracture experimentalist are such parameters as the fracture toughness, energy release rate and crack speed. The fracture toughness of a material is a measure of its resistance to fracture. The energy release rate is a related quantity that describes the amount of energy released from the strain field as a crack propagates. Both these quantities are only truly valid within the Linear Elastic Fracture Mechanics (LEFM) framework, but frequently some degree of flexibility is permitted. Previous work has shown that these quantities are both rate and temperature dependent^[1], this is in keeping with other mechanical properties such as compressive yield strength^[2,3]. The crack speed is also an important parameter when validating computational models of PBX fracture behaviour.

In this paper experiments have been performed to ascertain the value of the mode I critical stress intensity factor for a given rate and temperature using a Compact Tension (CT) geometry following ESIS recommendations. Crack speed measurements have been made by virtue of having the crack break elements of an electrical circuit as it propagated giving a voltage-time history from which the speeds may be deduced. In-plane surface displacements have been measured using the Digital Image Cross-Correlation (DICC) algorithm developed by Sjö Dahl ^[4]. DICC allows displacements to be measured by comparing segments of pre and post-deformation images in Fourier space and locating the position of maximum correlation. Through repetition of this process using sub-images from across the sample, whole-field displacement maps can be generated from which the strain fields can be calculated.

2. THEORETICAL

Linear elastic fracture mechanics is built on the foundations of elasticity theory; that is to say that if body is stressed then the accompanying strain is uniquely associated with that value of stress; there is no degeneracy. Furthermore the strain varies linearly with stress and the two are related through the appropriate modulus. When fracture occurs all energy dissipation is associated with the fracture process.

Of the three modes of fracture, opening (I), in-plane shear (II) and out-of-plane shear (III), mode I is found in general to occur most readily, it is therefore the mode of interest in this paper. The subscript I is used when discussing the stress intensity factor and the energy release rate for samples tested under this condition.

There are two main approaches within LEFM towards fracture, which can be shown to be equivalent; one with an emphasis upon stress and the other upon energy considerations.

In the stress based approach fracture occurs when the stress at the crack tip rises to a sufficient level to break the bonds holding the material together. The expression given by Irwin ^[5] describes the situation

$$\sigma_{ij} = \frac{K}{\sqrt{2\pi r}} f_{ij}(\theta), \quad (1)$$

where σ_{ij} are the components of the stress tensor at a point, K is the stress intensity factor, and r and θ are the polar coordinates of that point. The stress intensity factor relates the magnitude of the stress in the vicinity of a crack to sample geometry and the applied loads. When the stresses are raised to a point of incipient failure then $K = K_C$, the critical stress intensity factor. K_C is geometry independent and as such a measurable material fracture toughness parameter. Tables of values for K are readily available for the most commonly used sample configurations.

The energy based approach developed initially by Griffith ^[6] states that fracture occurs only when there is sufficient energy available to overcome the resistance of the material. This resistance may include surface energy, plastic work or any other energy dissipative process. The energy release rate G is defined as energy U released from the strain field per unit area of crack surface A ; rate in this sense of does not relate to a time derivative

$$G = \frac{dU}{dA}, \quad (2)$$

G like K is dependent upon sample geometry and the applied loads but at the point of incipient failure there is enough stored energy to overcome the resistance to crack

propagation and $G = G_C$ the critical energy release rate. G_C is also geometry independent and as such a measurable material fracture toughness parameter.

At the crack tip there will inevitably exist a region, commonly referred to as the process zone, in which such non-linear phenomena as plasticity and void nucleation and growth occur. This is true for even the most brittle materials. What is of importance is the size of this process zone relative to the dimensions of the sample. When it is sufficiently small, LEFM can still adequately describe the experiment. One way of estimating the size of the process zone is to assume that plasticity occurs when some yield criterion has been met. Assuming that yielding occurs when $\sigma_{yy} = \sigma_{YS}$, where σ_{YS} is the uniaxial tensile yield strength, then by substitution in to (1) obtain

$$r_y = \frac{1}{2\pi} \left(\frac{K}{\sigma_{YS}} \right)^2, \tag{3}$$

where r_y is the process zone radius. In practice, when testing for K_{IC} , the pre-multiplier is increased from $1/2\pi$ to 2.5 by way of a safety factor.

As the lowest values of yield stress occur under the conditions of plain-strain, it is under these conditions that the least amount of dissipative plastic deformation occurs, resulting in the lowest values of K_{IC} and G_{IC} .

3. EXPERIMENTAL

Following ESIS recommendations ^[7], themselves based upon an ASTM standard ^[8], samples were produced within machining tolerance to the dimensions shown in Fig. 1.

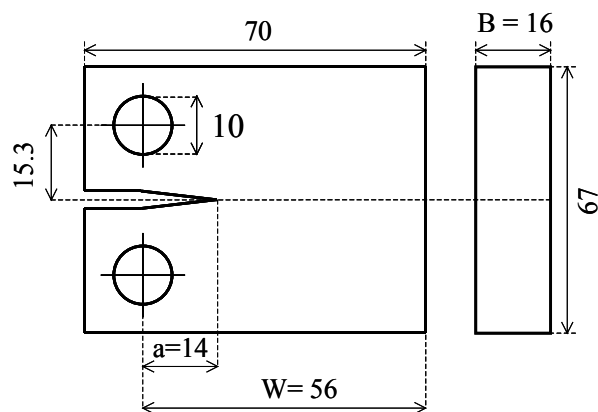


Fig 1. Compact tension geometry with dimintions given in millimeters

The notch was machined with a modified 6" x 3/16" cutting wheel that had been ground down to terminate in a 60° ‘V’. The notches were further sharpened with fresh razor blades. Due to the limited availability of the sugar based PBX simulant only two samples could be made.

A blank sample without a notch was also produced which was used as a calibration sample; this gave data relating to the total system compliance due to loading pin penetration and the non-infinite stiffness of the testing machine.

Single piece brass clevises, shown in Fig. 2, were machined in the to a design that allowed direct attachment to the testing machine and satisfied the requirements of ASTM E399. Silver-steel loading pins are bearing mounted to allow free rotation of the samples

during loading; the bearings are each rated for a static load of 900N and acting in tandem the rig can therefore be safely used for loads of up to 1800N.

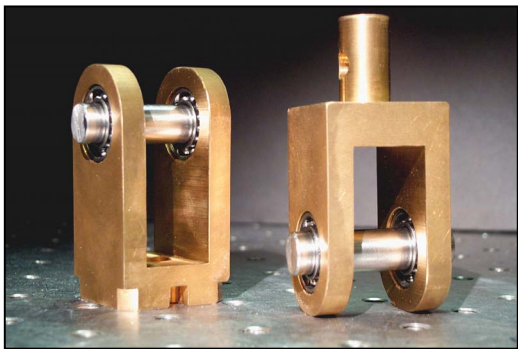


Fig 2. Photograph of clevises for use with the Instron testing machine in loading the compact tension specimens.

The lower clevis (left) bolts directly to the testing machine frame whilst the upper clevis (right) attaches to the load cell via a pin located through the upper shaft. Loading pin parallelism is ensured by the locating slots at the bottom of the lower clevis, and the orientation of the coupling pin on the upper clevis.

The samples were loaded by virtue of a displacement controlled Instron testing machine. It is capable of delivering up to 2 kN of force at a range of speeds, although for this series of experiments a speed of 1 mm/min was used throughout. Displacements and loads were logged on a personal computer.

An electrical circuit was designed incorporating a chain of ten low-resistance metallic strips, which the crack breaks as it propagates, in parallel with 67 Ω resistors. As each metallic strip is broken the total resistance of the circuit rises, and the current flowing through it was monitored by virtue of an oscilloscope that was connected across a 1 kΩ resistor. Figure 3 shows a schematic of the circuit used, each strip has a resistance of approximately 6 Ω and during the experiment the output voltage rose from 0.5 to 3.8 volts.

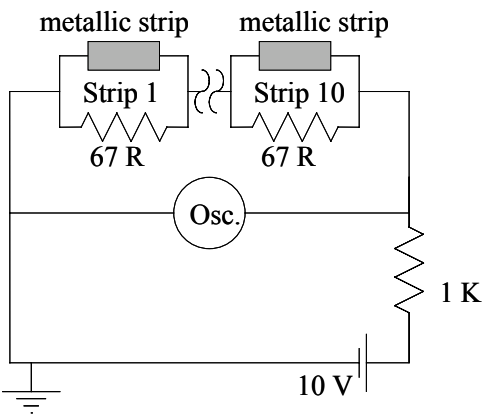


Fig 3. Circuit diagram for measuring crack speed. A series chain is formed from ten metallic strips in parallel with 67 Ω resistors.

The metallic strips were formed by spraying silver-dag through a mask using an artist's airbrush. The mask was formed such that the silver strips were of width 0.7 mm, 30 mm long and of pitch 4 mm. The thickness was measured on an optical microscope to be of the order of 18 μm, and as such would not reinforce the sample in anyway. Previous experiments^[9] have shown that the rise time of the voltage signal is less than the time it takes the crack to cross the strip's width as most of the resistance change does not occur until the rupture of the last segment. The rupture of the first silver strip triggered the oscilloscope; it was set to

capture 10 % pre-trigger so as to record that event. Figure 4 shows a photograph of a prepared sample.

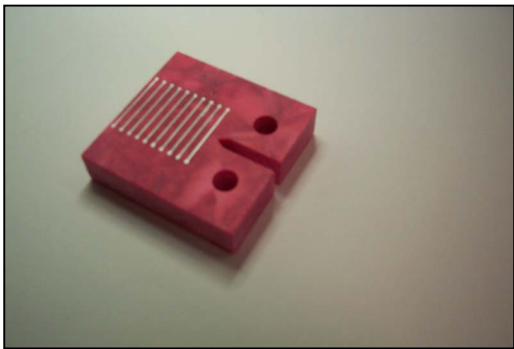


Fig 4. CT specimen with silver strips deposited on to the surface ahead of the crack propogation path.

Wires were attached to each end of the silver strips by ‘gluing’ in place using a small drop of silver-dag.

With the samples held in the clevises the Instron testing machine was load-balanced and the gage-length zeroed. A manually triggered digital camera, CCD array 1300 x 1030 pixels, imaged the event. The tensile loading rate was set at 1 mm/min and the samples were loaded until failure. The calibration sample was tested in the same manner.

4. RESULTS AND DISSCUSION

The experiments were performed on the notched samples and the load-displacement curves obtained. Figure 5 shows the results.

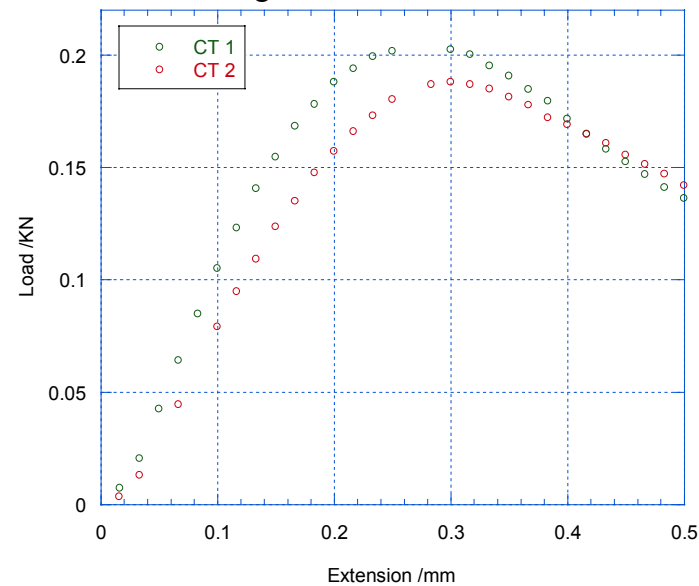


Fig 5. Load-extension curves for the two notched samples CT1 and CT2.

The peak loads and extensions were $P_{MAX_CT1} = 203.5\text{ N}$ at 0.273 mm and $P_{MAX_CT2} = 188.3\text{ N}$ at 0.299 mm . In an ideal case the load would increase linearly from zero and abruptly fall to zero at failure, in practice this is very rarely the case and there is inevitably some degree of non-linearity. This being the case, the initiation load is calculated in the following way; a line of best fit is fitted to the data to find the initial compliance C , this is then increased by a factor of 5 %. Where the line $C+5\%$ intercepts the curve, the load $P_{5\%}$, is taken to be the load at crack initiation. For the data shown in Fig. 5 these values are given in Table 1.

Table 1. Deducing the initiation load $P_{5\%}$

	$C / \text{m N}^{-1}$	$(C + 5 \%) / \text{m N}^{-1}$	$P_{5\%} / \text{N}$
CT1	0.982	1.031	184.5
CT2	1.275	1.342	178.0

At this stage, the procedure is to check that the results lie within LEFM, some flexibility is allowed; up to 10 % non-linearity is permitted i.e. the data must satisfy

$$\frac{P_{MAX}}{P_{5\%}} < 1.1, \quad (4)$$

for the data above this ratio is 1.10 and 1.06 for CT1 and CT2 respectively. Clearly these experiments are only just within the boundaries of LEFM.

The next stage is to calculate the experimental values of the stress intensity factor K_Q using the following relationship:

$$K_Q = f \frac{P_{5\%}}{BW^{1/2}}, \quad (5)$$

where f is the dimensionless constant 4.92 derived from the numerical solution of K_I for this particular geometry of CT sample [7], B and W are sample dimensions indicated in Fig. 1. Using equation (5) to calculate K_Q gives $0.23 \text{ MPa m}^{1/2}$ and $0.24 \text{ MPa m}^{1/2}$ for CT1 and CT2 respectively.

The last stage is to check the size criterion given in equation (3). We require that

$$B, a, (W - a) > 2.5 \left(\frac{K_Q}{\sigma_{YS}} \right)^2. \quad (6)$$

If this condition is met then $K_Q = K_{IC}$ the plain strain value. The ISIS procedure recommends that σ_{YS} be taken either from the uniaxial tensile fracture stress (2 MPa) or else 0.7 times the uniaxial compressive yield stress (5 MPa). These values come from experiments carried out at this laboratory. Using the first value reveals that the smallest dimension ought not to be less than $\sim 35 \text{ mm}$, using the second value not less than $\sim 6 \text{ mm}$. The smallest dimension of the CT sample is the crack length, $a = 14 \text{ mm}$. Clearly the condition is not met if the first estimate of σ_{YS} is satisfied by the second. The differences arise because of the composite nature of the material; under compression the load is borne by the crystalline filler particles, in tension by the polymeric filler. Ideally this condition would be met using both estimates for σ_{YS} . Since the failure is tensile, the most appropriate estimate is the first in which case the condition described in equation (6) was not met. This means samples were not in a state of plane-strain and consequently that measured K_Q is not equal to K_{IC} , rather it will be an over-estimate. Nevertheless the measured value is still useful as it serves as an upper bound to the true critical stress intensity factor and can still be used to validate fracture models for this material.

The energy release rate can be calculated by integrating the load displacement curves to obtain the amount of energy supplied in order to fracture the samples. It is for this reason the unnotched correction-sample was tested. By subtracting the energy supplied to the correction-sample U_{COR} (due to indentation and system compliance), up to the point of failure of each notched sample, from the energy supplied to the notched samples U_Q we

arrive at the energy U due to the presence of the notches, and therefore fracture, alone. Figure 6 shows the difference between the load extension curves for the samples described and table 2 the relevant parameters calculated from these data.

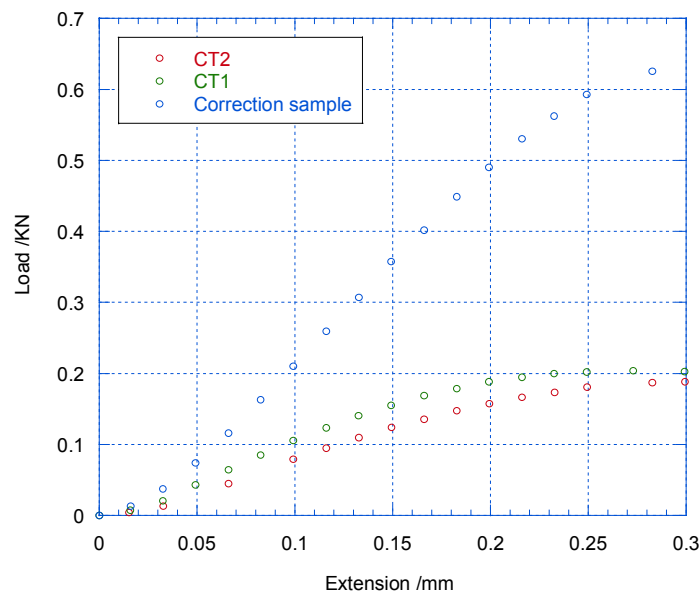


Fig 6. Load extension curves for CT1, CT2 and the unnotched correction sample. Enegies supplied to the samples are found by integration.

Table 2. *Energies supplied to the samples up to $P_{5\%}$.*

Sample	$P_{5\%}$ /N	U_Q /mJ	U_{COR} / mJ	U /mJ
CT1	184.5	18.37	6.70	11.67
CT2	178.0	22.83	6.23	16.60

The energy release rate, G , for each sample can be calculated from

$$G = \frac{U}{BW\phi}, \tag{7}$$

where ϕ is the dimensionless constant 0.199 derived from the numerical solution of for G for this particular geometry of CT sample ^[7]. Using equation (7) the energy release rates are therefore 65.45 Jm⁻² and 93.01 Jm⁻² for samples CT1 and CT2 respectively.

The oscilloscope trace clearly showed when each of the silver strips, illustrated in Fig. 3, broke. Figure 7 shows the raw data obtained from CT2, all the voltage rises expected could be calculated from the measured resistances and are labelled with the exception of the sixth and seventh which ought to have appeared in the region indicated in Fig. 7 by a question mark but which did not.

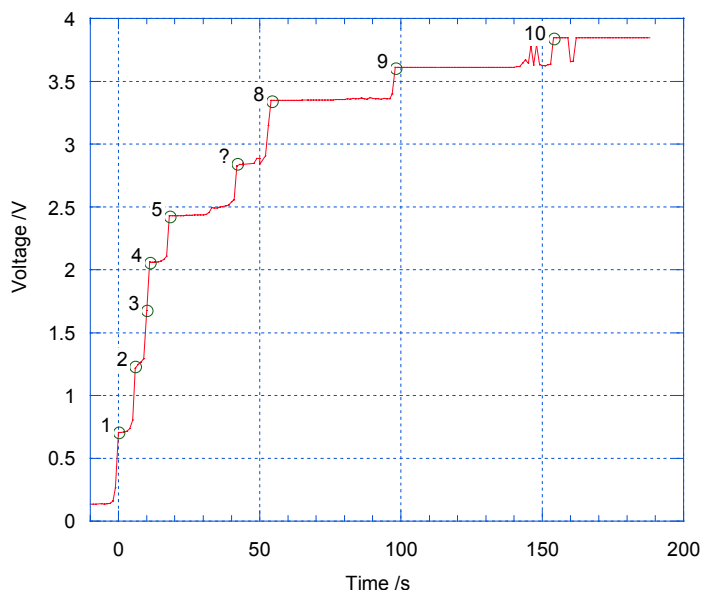


Fig 7. Voltage time trace from the oscilloscope shows when the crack broke the silver strips.

Knowing the inter-strip distance is 4 mm, the crack's speed can be calculated and be seen to fall as it crosses the ligament, from an initial $\sim 1 \text{ mm.s}^{-1}$ to a final $\sim 0.07 \text{ mm.s}^{-1}$. The crack growth is stable. This is likely to be due to the displacement control nature of the loading; once the elastic energy stored in the sample is expended in new crack surface generation more has to be stored through loading before further propagation can occur. The low fracture toughness means that fracture occurs well before any appreciable amount of energy is stored; consequently only small crack advances are possible and growth is stable.

The DICC technique was used to calculate strain fields in the vicinity of the crack tip. Figure 8 shows a result obtained just before the peak load for sample CT2.

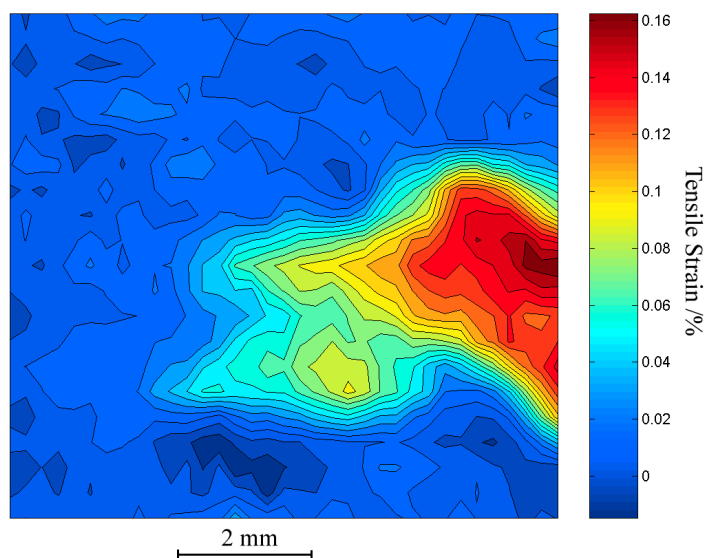


Fig 8. The tensile strain component present in the sample just prior to failure.

Figure 8 shows intense deformation in a very localized region. No crack was visible in the image itself. The maximum tensile strain is of the order 0.16 % which is in agreement with other measurements made on a very similar PBX ^[10]. Quantitative measurements could not be made once the crack began to propagate because there was insufficient spatial resolution in the images to locate the crack-tip.

Figure 9 is a photograph of the sample CT2 after testing and before being removed from the clevises.

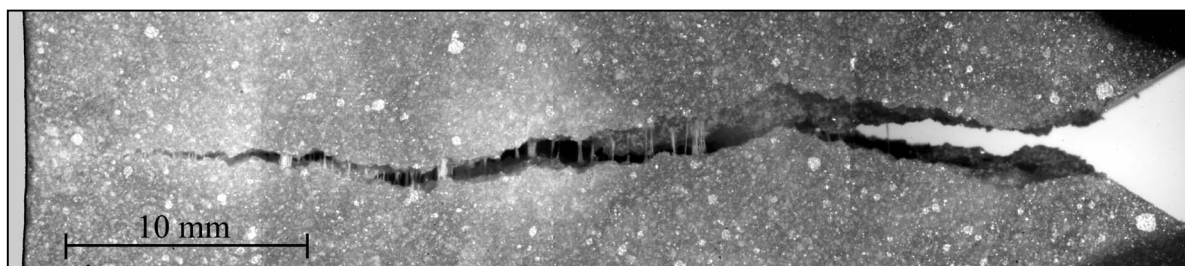


Fig 9. Digital image of the failed sample.

Crack bridging by fibrils of the binder is clearly in evidence in Fig. 9. This is consistent with previous investigations on similar PBXs ^[11,12]. The density of binder fibrils is a maximum at the crack tip and diminishes back along the crack until no stands are seen at all.

Initial failure resulting in crack formation is brittle in nature and occurs at a very low global strain, of the order of $\sim 0.16\%$. Subsequent to crack formation there is crack bridging by the binder fibrils as shown in Fig 9. Further deformation of the fibrils is a ductile process involving extremely large strains, of the order of several hundred percent within a region localised around the plane of the crack.

What is believed to be happening is that initially the binder debonds from the filler particles ^[13] along a plane that will later form the crack; this process is very ‘stiff’ and accounts for the brittle nature of the material. The reduction in load bearing area in this plane dramatically increases the stress in the remaining binder, which yields, and debonded regions grow into voids, separated by binder which form the fibrils visible in Fig. 9; this process is a ductile one. Further deformation results in void coalescence and fibril thinning until the point at which there is no binder spanning the crack faces, at this point failure is complete.

It is important to note that neither the ductile nature of the binder failure following binder/filler debonding nor the stable crack growth are represented in the calculated energy release rates.

5. CONCLUSIONS

The fracture toughness and energy release rates of two PBS CT samples have been measured to be $0.23 \text{ MPa m}^{1/2}$ and 65.45 Jm^{-2} , and $0.24 \text{ MPa m}^{1/2}$ and 93.01 Jm^{-2} respectively. Comparisons of the dimensions of the samples to the size of the process zone ahead of the crack tip indicate that the samples were not in a state of plane strain, consequently the measured values for K_I and G_I are not the critical values, rather, they will be over-estimates. Nevertheless the values are still of interest as they give upper bounds for the critical values and can still be used in choosing the correct size of sample for future experiments. The calculated energy release rates do not incorporate the observed stable crack growth nor the final ductile breaking of the binder fibrils spanning the sample in the latter stage of failure.

The crack's speed has been measured as it traversed the ligament (W-a). The speed was seen to diminish from an initial 1 mm s^{-1} to a final $\sim 0.07 \text{ mm s}^{-1}$. Crack propagation was stable due to the displacement control method of loading.

Use of the DIC technique has shown localized tensile deformation with failure at approximately $\sim 0.16 \%$ strain.

A possible failure mechanism has been suggested which would explain the initial brittleness followed by ductile behaviour that is observed to occur in the failure of many PBXs.

Future work, providing more material can be sourced, will involve looking toward experiments with larger sample sizes so as to measure the critical values of K_I and G_I , as well as trying to measure more appropriate parameters based upon a non-linear elastic foundations such as Rice's J-integral^[14].

Acknowledgements

The Authors wish to thank AWE Aldermaston and the Engineering and Physical Sciences Research Council (EPSRC) for funding this research, and D. Powel for his invaluable workshop assistance.

REFERENCES

- [1] A.J. KINLOCH and R.A. GLEDHILL: *Propellant Failure: A Fracture-Mechanics Approach*, J.Spacecraft, **Vol. 18**, p.333-337, 1981
- [2] J.E. BALZER, C.R. SIVIOUR, S.M. WALLEY, W.G. PROUD and J.E. FIELD: *Behaviour of Ammonium Perchlorate Based Propellants and a Polymer Bonded Explosive Under Impact Loading*, Proc. R. Soc. Lond. A, in press, 2003
- [3] C.R. SIVIOUR, D.M. WILLIAMSON, S.G. GRANTHAM, S.J.P. PALMER, W.G. PROUD and J.E. FIELD: *Split Hopkinson Pressure Bar Measurements of PBXs*, Proceedings of the APS Topical Conference on Shock Compression in Condensed Matter, Portland, Oregon USA, in press, 2003.
- [4] M. SJÖDAHL: *Electronic Speckle Photography: increased accuracy by non-integral pixel shifting*, Applied Optics, **Vol. 33**, p.6667-6673, 1994
- [5] G.R. IRWIN: *Structural Aspects of Brittle Fracture*, Applied Materials Research, **Vol. 3**, p.65-81, 1964
- [6] A.A. GRIFFITH: *The Phenomena of Rupture and Flow in Solids*, Philosophical Transactions Series A, **Vol. 221**, p.163-198, 1920
- [7] D.R. MOORE, A. PAVAN, J.G. WILLIAMS: *K_C and G_C at Slow Speeds for Polymers, (Fracture Mechanics Testing Methods for Polymers Adhesives and Composites)*,ESIS Publication 28, Oxford, p.11-26, 2001
- [8] *ASTM E399 – 83, Standard Test Method for Plane-Strain Fracture Toughness of Metallic Materials, (Annual Book of ASTM Standards)*, **Vol. 03.01**, 1999.
- [9] K.N.G. FULLER: *The Brittle Fracture of Polymers, (PhD Thesis, Cambridge University)*, p.65-81, 1972
- [10] C. LIU: *Fracture of the PBX 9501 Explosive*, Proceedings of the APS Topical Conference on Shock Compression in Condensed Matter, Portland, Oregon USA, in press, 2003
- [11] P.J. RAE, H.T. GOLDREIN, S.J.P. PALMER, J.E. FIELD and A.L. LEWIS: *Studies of the Failure Mechanics of Polymer-Bonded Explosives by High Resolution Moiré Interferometry and Environmental Scanning Electron Microscopy*, Proceedings of the eleventh international detonation symposium, Snowmass, Colorado USA, p.66-74, 1998
- [12] C.LIU, M.G. STOUT and B.W. ASAY,: *Stress Bridging in a Heterogeneous Material*, Engineering Fracture Mechanics, **Vol. 67**, p.1-20, 2000
- [13] P.J. RAE, S.J.P. PALMER, H.T. GOLDREIN, J.E. FIELD and A.L. LEWIS: *Quasi-static Studies of the Deformation and Failure of PBX 9501*, Proc. R. Soc. Lond. A, **Vol. 458**, p.2227-2242, 2002
- [14] J.R. RICE: *A Path Independent Integral and the Approximate Analysis of Strain Concentration by Notches and Cracks*, ASME J. Applied Mech, **Vol. 35** p.379-386, 1968

ON THE REACTIONS OF 2-(DINITROMETHYLENE) -4,5-IMIDAZOLIDINEDIONE WITH ALKALINE AGENTS *

Shu Yuanjie, Cai Huaqiang, Huanghui and Cheng Bibo

Institute of Chemical Materials CAEP,
621900, Mianyang, Sichuan, China

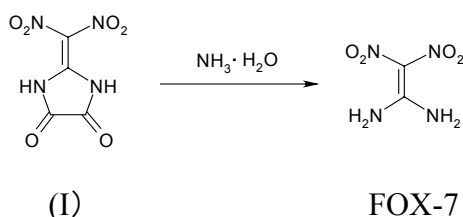
Abstract:

The new preparation methods of 1,1-diamino-2,2-dinitroethylene and 2-dinitromethylene-4,5-imidazolidinedione from 2-methylimidazole were studied. The yield of 2-dinitromethylene-4,5-imidazolidinedione was 20.3% by nitrating 2-methylimidazole in the sulfuric and nitric acid. Under different alkaline conditions, 2-dinitromethylene-4,5-imidazolidinedione can process two different reactions: in the alkalescent conditions, the main product is Fox-7; with alkali conditions, the main product is potassium dinitromethanate. By optimizing reaction conditions, the yield of Fox-7 could be up to 95.3% and for potassium dinitromethanate, it could be 65%.

Keywords: 2-methylimidazole, 2-(dinitromethylene)-4,5-imidazolidione, 1,1-diamino-2,2-dinitroethylene, potassium dinitromethanate

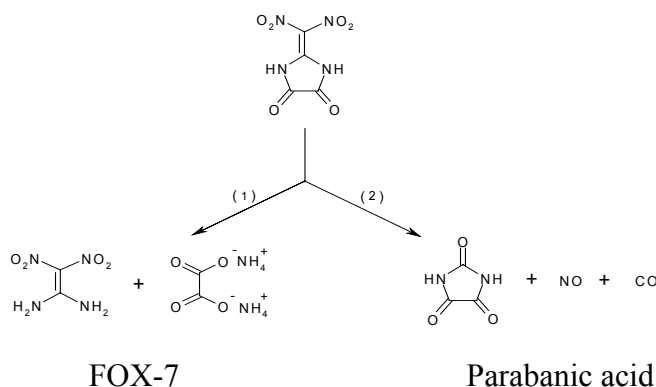
1. INTRODUCTION

2-(dinitromethylene)-4,5-imidazolidione is an important intermediate for preparing Fox-7 (1,1-diamino-2,2-dinitroethylene), which was reported in 1998 for the first time together with Fox-7^[1]



No more reactions have been reported to this day except this reaction. And the chemical properties of (I) are not investigated sufficiently. Our experiments found that in the structure of (I), two amide bonds are reactive and easy to break; the gem-dinitro is unstable and also easy to decompose. Therefore, we regarded that (I) can easily process two different reactions: ring cleavage, losing nitrogen oxides. Such ideas have been proved in the experiments ^[2].

* This project was supported by fund of CAEP (20020540)



We studied the reactions of (I) under different alkaline conditions and found that there are two competitive reactions under the alkaline conditions. The main products of the two reactions are Fox-7 and parabanic acid. When the reactions changed, the yield and ratio of both products vary. By investigating the reaction of (I) in alkali conditions, a simple and convenient procedure for synthesis of potassium dinitromethanate is obtained.

2. EXPERIMENTAL

2.1 Equipment and reaction reagents

Reagents: 2-methylimidazole(c.p.), sulfuric acid(98%, a.c.), fuming nitric acid(1.51 g/cm³), KOH(a.c.), NaOH(a.c.), trifluoroacetic acid(a.c.).

Equipment for analysis: FTIR, Nicolet-800; NMR, Varian INOVA-400 MHz; Magnetic-Mass Spectroscopy, Finnigan MAT-95S etc.

2.2 Preparation of 2-(dinitromethylene)-4,5-imidazolidione(1)

Finely ground 2-methylimidazole 16.5g (0.2mol) was dissolved in sulfuric acid 160 ml(98%) at room temperature with vigorous stirring. Fuming nitric acid (32 ml) was added to the system in 90 min at the same temperature. After 1h a white precipitate formed. Then it was filtrated, collected and washed several times by cold trifluoroacetic acid. 2-(dinitromethylene)-4,5-imidazolidione(1) (8.2g) was obtained after drying at 0°C in vacuum. The yield was found to be about 20.3%. Decomposition temp 240°C (10°C /min DSC); IR. (KBr): 3313 (NH₂), 3226(NH₂), 3169(NH₂), 1805(C=O), 1754(C=O), 1584(NO₂), 1499, 1318(NO₂), 1232, 1176, 758cm⁻¹. ¹H NMR (DMSO-d₆) δ 11.03 ppm; ¹³C NMR (DMSO-d₆) δ 128.71, 154.79, 159.70; MS m/e 202 (M⁺); Anal.Cald for C₄H₂N₄O₆: C, 23.77; H, 1.0; N, 27.72. Found: C, 23. 90; H, 1.23; N, 27.87.Size: standard A4 (297x210mm).

2.3 Preparation of Fox-7

2-(dinitromethylene)-4,5-imidazolidione (2.1g, 0,01mol) was added to KOH solution (5%,10ml) at room temperature with vigorous stirring. The solid dissolved immediately and was kept for several hours. A bright yellow solution formed. At 0~5°C, the crystals were given, filtered and washed for several times by water. The major product formed was Fox-7 (1.41g) (95.3%). Decomposition temp 238°C (7°C /min DSC); IR. (KBr): 3404(NH₂), 3330(NH₂), 3223(NH₂), 1633(NH₂), 1518(NO₂), 1469, 1393 1351(NO₂), 1221, 1166, 1137, 1023, 620, 458 cm⁻¹. ¹H NMR (DMSO-d₆) δ 8. 759 ppm. ¹³C NMR (DMSO-d₆) δ 129.411,

159.040; MS m/e 148 (M^+); Anal.Calc'd for $C_2H_4N_4O_4$: C, 16.22; H, 2.72; N, 37.84. Found: C, 16.09; H, 2.68; N, 37.87.

2.4 Preparation of dinitromethanate

2-(dinitromethylene)-4,5-imidazolidione(2.1g,0.01mol) was treated with water(10ml) at room temperature with vigorous stirring. Then KOH solution (15%,40ml)was added to the system slowly. The solution was heated up to 95°C and kept for 5h. At 10~20°C the yellowish precipitate was separated away from the slurry. The precipitate was then washed for several times and dried to give potassium dinitromethanate (1.4g) (65%). Dec temp. 220°C UV; λ_{max} = 363nm; ϵ = 20800.

3. RESULTS AND DISCUSSION

3.1 Effect of reaction time on the yield of potassium dinitromethanate

It could be seen from table 1 that when the reaction time was over 3 h, there was no FOX-7 and the yield of potassium dinitromethanate was above 80%. Such results demonstrated that the major reaction finished in about 3 h; and in the reaction time of 1h, a little of Fox-7 obtained. These results suggested that the reaction might immediately form Fox-7 firstly, then it decomposed to potassium dinitromethanate. For one hour reaction time, some Fox-7 did not decompose completely, therefore, the yield of potassium dinitromethanate was only 55%; with the prolong of time, the yield of parabanic acid did not change obviously.

Table 1. Effect of reaction time on FOX-7 yield

Reaction time/ h	1	2	3	4
Yield of FOX-7/ %	31	12	0	0
Y. of para.acid / %	3	4	4	3
Y.of dinitromethanate/ %	55	72	81	84

*2-(dinitromethylene)-4,5-imidazolidione(2.1g,0.01mol), T=90°C

3.2 Effect of temperature on reactions

Seen from table 2, temperature had a great effect on reactions. At lower temperature, the yield of fox-7 was relatively high, while parabanic acid and potassium dinitromethanate were both low; with the temperature increased, the yield of Fox-7 lowered, while that of parabanic acid changed little and potassium dinitromethanate increased obviously. Especially, at 90°C the yield of potassium dinitromethanate exceeded 80%. Therefore, lower temperatures might be propitious to ring cleavage reaction to obtain Fox-7; higher temperature might facilitate decomposing of Fox-7 into potassium dinitromethanate , which showed higher yield. At 30~120°C, temperature had little effect on parabanic acid and its yield changed not clearly

Table 2. *Effect of temperature on the reaction*

Reaction temperature/°C	30	60	90	120
Yield of FOX-7/ %	76	41	0	0
Y. of para.acid / %	6	7	6	8
Y.of dinitromethanate/ %	3	15	84	80

*2-(dinitromethylene)-4,5-imidazolidione(0.01mol), KOH 20ml (60%), 3h.

3.3 Effect of alkalescence on reactions

From table 3 it could be seen that the intensity of alkali had a great effect on the components of products. For the reaction of 2-(dinitromethylene)-4,5-imidazolidione (I) with water, parabanic acid was the major product and Fox-7 was by-product, without potassium dinitromethanate. But the reaction of I with ammonia led to form Fox-7, the yield of which was over 90%. In the reaction, the yield of parabanic acid was relatively low and there was little potassium dinitromethanate. While I was treated with NaOH and KOH, the major product was still Fox-7 with lower yield compared with that of treated with ammonia as the ring cleavage agent. At the same time, the yield of parabanic acid increased and there was a small amount of potassium dinitromethanate. Therefore, Fox-7 could be obtained with the highest yield in alkalescent conditions, on the contrary it was easy to produce parabanic acid and potassium dinitromethanate under alkali conditions.

Table 3. *Effect of the kind of alkali on the reaction yield*

Reagent	Concentration. %	Y. OF FOX- 7%	Y. para.acid %	Y.dinitromethanate %
H ₂ O	—	15	76	0
NH ₃	25	91	3	0
NaOH	60	78	7	3
KOH	60	76	6	3

*2-(dinitromethylene)-4,5-imidazolidione(0.01mol), T = 30°C

3.4 Effect of alkali concentration on reaction

The concentration of alkali also affected the components of products. Seen from table 4, the yield of Fox-7 gradually increased with the concentration decreasing of KOH. As the concentration of KOH was 10%, the yield of Fox-7 as the major product was 65% and that of potassium dinitromethanate gradually decreased, only about 18%. The yield of parabanic acid did not change distinctly. It is given from above data that Fox-7 is unstable at the higher concentration of alkali and easy to decompose to potassium dinitromethanate. Therefore, increasing the concentration of alkali is beneficial to the formation of potassium dinitromethanate; Fox-7 is relatively stable and difficult to occur decomposition reaction in lower concentration of alkali, accordingly yield is higher.

Table 4. *Effect of the concentration of alkali on the reaction yield.*

Con. KOH / %	10	30	50	70
Yield of FOX-7 / %	65	25	8	0
Yield of para. acid / %	7	7	5	3
Y.dinitromethanate / %	18	46	71	84

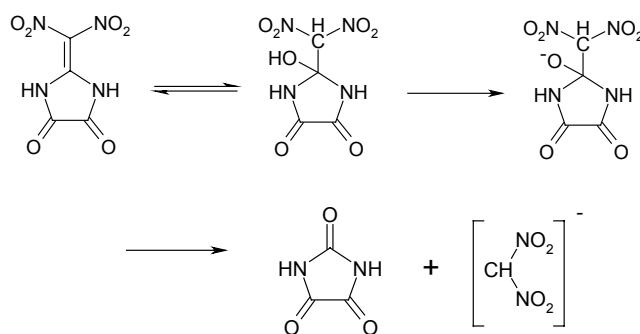
*2-(dinitromethylene)-4,5-imidazolidione(0.01mol), T = 90°, 3h

3.5 Reaction mechanism

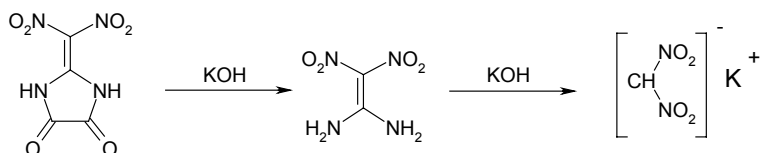
In our previous work [2], we discussed the synthesis mechanism of FOX-7 and parabanic acid in the reaction of ammonia as ring cleavage agent, and the rule is the same with the alkali, such as KOH and NaOH. Therefore, we only discuss the form process of potassium dinitromethanate, another main product.

There may be two potential reaction mechanisms:

One is



the other is



4. CONCLUSION

The products of reactions of 2-(dinitromethylene)-4,5-imidazolidinedione with alkaline agents were characterized and the reaction conditions were optimized. Using KOH as the ring cleavage agent, the total yield of FOX-7 in the optimized conditions is 19.3%, which is higher compared with ammonia ring cleavage method (13.1%) reported in literature. The synthesis mechanisms of intermediates formation in the alkaline ring cleavage method were discussed.

REFERENCES

- [1] LATYPOV, N. V.; BERGMAN, J.; LANGLET, A.; WELLMAR, U.; BEMM, U.: *Tetrahedron*. 54, 11525, 1998
- [2] CAI HUAQIANG; SHU YUANJIE; YU WEIFEI: *Study on synthesis of FOX-7 and its reaction mechanism*, *Acta Chimia Sinica*, V.62, No.3, 295, 2004
- [3] ÖSTMARK, H.; LANGLET, A.; BERGMAN, H.; WINGBORG, N.; WELLMAR, U.; BEMM, U. The 11th International Detonation Symposium, Snowmass, Colorado, pp. 807 ~ 812, 1998
- [4] ANTHONY J.BELLAMY, PATRICK GOEDE, CAMILLA SANDBERG, ET AL.: *Substitution reactions of 1,1-diamino-2,2-dinitroethylene(Fox-7)*, 33rd Int.Annu.Conf. ICT, 2002

MECHANISTIC STUDIES OF DESTRUCTIVE NITRATION OF 2-ALKYL SUBSTITUTED 4,6-DIHYDROXY PYRIMIDINES

A. A. Astratev, D.V. Dashko, A. I. Merzhin and A. I. Stepanov

*Special Design and Construction Bureau SDCB
"Technolog" of the Saint-Petersburg State Institute of Technology
190013, Saint-Petersburg, Moskovskiy pr.26; Russia*

Abstract:

The main stages of destructive nitration of 2-(4-oxo-6-hydroxy-2-pyrimidinylidene) acetic acid in various nitrating mixtures have been identified. The effect of consecutive introduction of nitro groups on the formation of the key intermediate responsible for the generation of 1,1-diamino-2,2-dinitroethylene (DADNE, FOX-7) has been demonstrated. A general scheme of chemical transformations of 2-methyl-4,6-dihydroxypyrimidine under the conditions of acidic nitration has been suggested.

Keywords: *mechanism, nitration, 2-(4-oxo-6-hydroxy-2-pyrimidinylidene) acetic acid, synthesis, DADNE (FOX-7).*

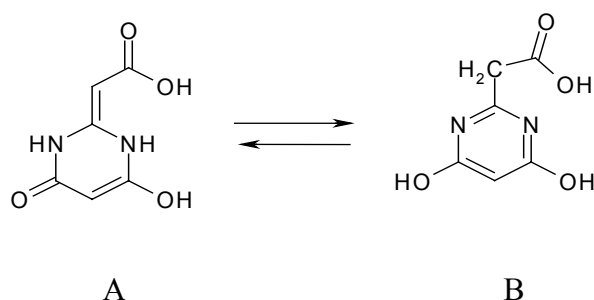
1. INTRODUCTION

Currently a major focus in research into energetic materials is the pursuit of improvements in insensitivity towards external stimuli whilst maintaining or enhancing performance. This goal is consistent with the gradual adoption of insensitive munitions (IM) by defence forces around the world. One of the general approaches toward developing explosive formulations that satisfy IM criteria is to use intrinsically less sensitive ingredients such as 1,3,5-triamino-2,4,6-trinitrobenzene (TATB) which crystal structure features a network of intra- and intermolecular hydrogen bonds. Such network effectively delocalizes the critical stresses within discrete molecular fragments and so prevents or hinders the initial stage of decomposition of nitro compounds, the homolytical rupture of C-NO₂ (N-NO₂) bond. The synthesis of insensitive high explosives possessing a supramolecular network of hydrogen bonds can be carried out both in the series of C-NO₂ and N-NO₂ derivatives, the leading role being played by structures comprising nitro and amino groups in the molecule. Apart from TATB, such structural features are inherent in 1,1-diamino-2,2-dinitroethylene (DADNE) currently known as FOX-7. This compound was first synthesized in SDCB "Technolog" in 1989 ^[1]. More recently in Zelinsky Institute of Organic Chemistry RAS an alternative procedure for DADNE preparation was worked out which was based on the reactions of mono substituted cyanamides with nitro compounds possessing active methylene groups ^[2]. An effective compromise between energetic properties and sensitivity of DADNE has attracted attention of research groups in various countries to this promising insensitive high explosive (IHE). To date a considerable body of works characterizing DADNE as a perspective IHE has been published ^[4-8]. Still the problems relating to the synthesis of DADNE and its analogues remain topical. While for other compounds of similar structure, viz. guanidine and urea, the synthesis of corresponding

nitro derivatives doesn't present any problems and the industrial technologies of their production are realized in many countries, the preparation of nitro derivatives of amidines constitutes a rather intricate problem because of the low reactivity of amidines in direct nitration reactions as distinct from guanidine and urea. At present the main synthetic route to DADNE is based on the generation of intermediates containing dinitroacetamide structural fragments alongside with the readily destroyed moieties arising from substituted nitrogen heterocycles. Such approaches imply a specific protection of the amidine fragment by means of the alteration of its reactivity and stability under the conditions of the nitration reaction. 2-Methylimidazole, its derivatives and derivatives of 2-methyl-4,6-dihydroxypyrimidine were used as starting materials ^[8]. It is noteworthy that the nitration of nitrogen containing heterocyclic compounds often takes place rather ambiguously owing to the accompanying processes of prototropic transformations of such compounds in acid media. The reaction pathway is also affected by the ambident reactivity of such heterocycles. In particular, diazines, despite their rather high basicity, are moderately weak nucleophiles in the reaction of electrophilic substitution. Rationalization of their reactivity is further complicated when the heterocyclic molecule contains substituents capable of prototropic isomerism. Thus, in nitric acid 2-methyl-4-amino-6-hydroxypyrimidine, 2-methyl-4,6-diaminopyrimidine, 2-amino-4,6-dihydroxypyrimidine, 2-methyl-4,6-dihydroxypyrimidine are readily mono nitrated into 5-position of the pyrimidine ring, whereas in mixed acids the nitration of barbituric acid ^[9], 2-amino-, 2-methyl-4,6-dihydroxypyrimidine is accompanied by the formation of corresponding 5,5-dinitro derivatives ^[3]. Even under the conditions of a distinct shortage of nitric acid the main product of 2-methyl-4,6-dihydroxypyrimidine nitration is 2-dinitromethylene-4,6-dihydroxy-5,5-dinitropyrimidine. Still the effect of the successive introduction of the nitro groups into the heterocyclic molecule on the formation of DADNE precursor is currently uncertain.

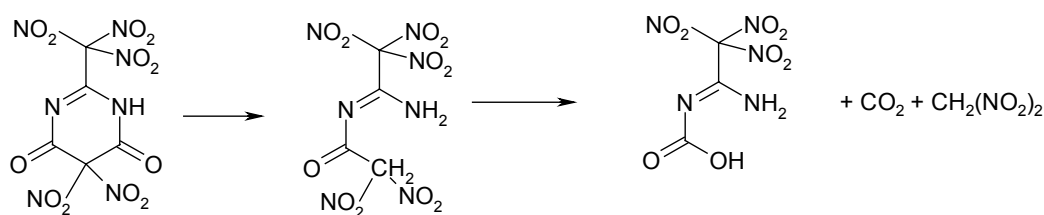
2. RESULTS AND DISCUSSION.

In order to get insight into the mechanism of nitrolysis of dihydroxypyrimidine derivatives, we studied the behavior of another representative in the series of 2-alkyl dihydroxypyrimidines, 2-(4-oxo-6-hydroxy-2-pyrimidinylidene) acetic acid (**1**), in the nitration reaction. As distinct from 2-methyl-4,6-dihydroxypyrimidine, this compound possesses a more active methylene group in 2-position compared to the methyl group in 2-methyl-4,6-dihydroxypyrimidine. Judging by the ¹H NMR spectrum, compound (**1**) exists in CH-form (A).



However, regardless of its tautomeric form, the chemical behavior of compound (**1**) is analogous to that of other 4,6-dihydroxypyrimidines. The most active in electrophilic substitution reactions appears 5-position of the heterocycle. For instance, compound (**1**) is readily brominated forming initially 2-(4-oxo-5-bromo-6-hydroxy-2-pyrimidinylidene) acetic acid (**2**), and eventually dibromoderivative (**3**). Treatment of compound (**1**) with sodium nitrite in acetic acid affords the oxime of 2-(4-oxo-6-hydroxy-2-pyrimidinylidene)

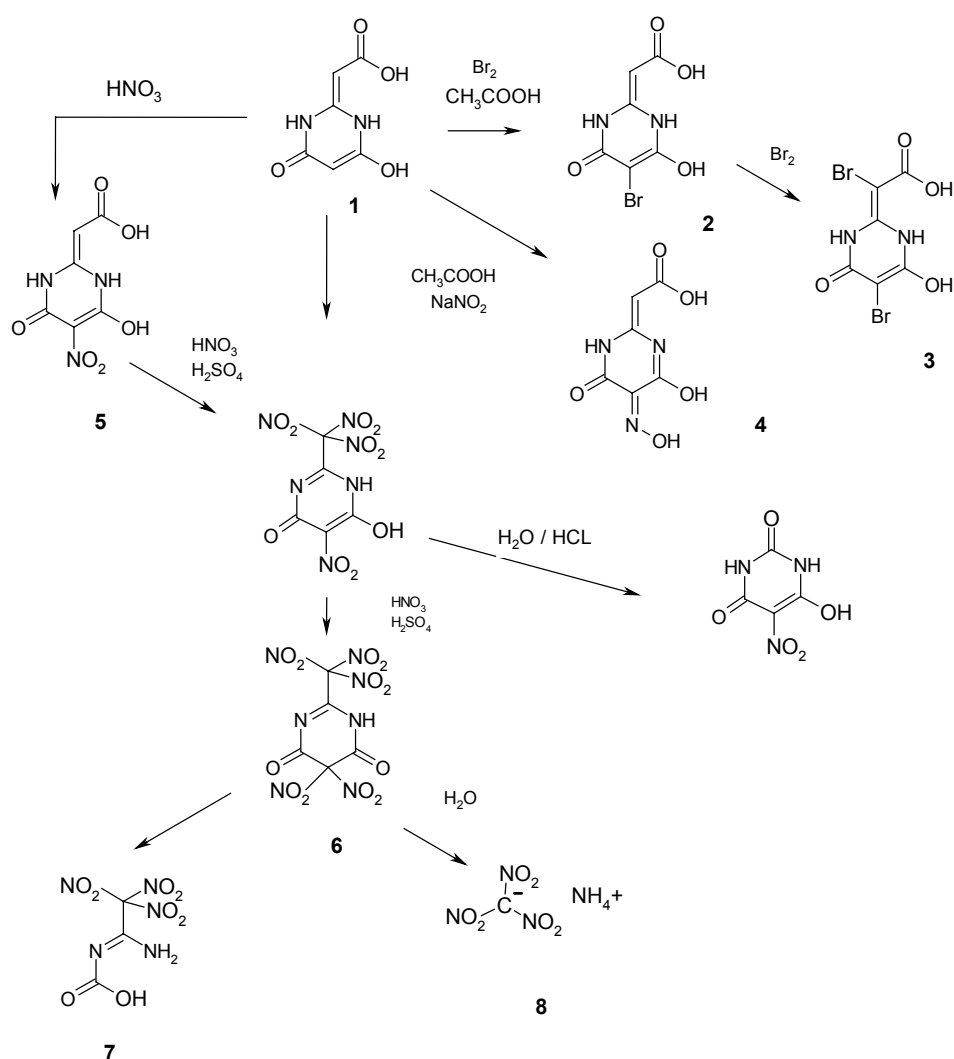
acetic acid (4). The study of compound (1) nitration in various media demonstrated that in nitric acid, like that for mentioned above pyrimidines, the nitration product represents 2-(4-oxo-6-hydroxy-5-nitro-2-pyrimidinylidene) acetic acid (5). The presence of an active methylene group in the molecule of (5) facilitates the nitration process. Thus, after nitration with mixed acid a white crystalline compound was isolated from the reaction mixture, which quickly decomposed in air on the filter. The main product, which was identified after the dissolution of this compound in water, was ammonium trinitromethide (8). In order to avoid its decomposition under the action of atmospheric moisture, the product was kept for 2 weeks in a vacuum-desiccator at room temperature. Based on the data of IR and mass spectra and elemental analyses, the product was identified as 1-amino-1-carbamino-2, 2, 2 - trinitroethane (7). A substantial loss in the mass of the specimen was observed during its storage under reduced pressure. The UV spectrum of sodium hydroxide used as desiccant revealed a characteristic absorption of the dinitromethide anion.



Scheme 1. *Decomposition of 2-trinitromethyl-5, 5-dinitro-4, 6-dihydroxypyrimidine.*

As we reported earlier ^[3], an analogous transformation took place with 2-(dinitromethylene)-4,6-dihydroxy-5, 5-dinitropyrimidine (9).

The results obtained allow us to believe that the nitration of 2-(4-oxo-6-hydroxy-2-pyrimidinylidene) acetic acid under the conditions similar to those for 2- methyl-4, 6-dihydroxypyrimidine most likely results in the formation of 2-trinitromethyl-5, 5-dinitro-4, 6-dihydroxypyrimidine (6).



Scheme 2: Chemical transformations of 2-(4-oxo-6-hydroxy-2-pyrimidinylidene) acetic acid.

The proposed structure of (6) may be supported by comparing its NMR ^{13}C spectrum with that of 2-(dinitromethylene)-4,6-dihydroxy-5, 5-dinitropyrimidine (9) in deuterated 95% sulfuric acid with allowance made for a possible protolytic equilibrium due to the presence of an additional nitro group in the molecule of (6). (See Table 1.)

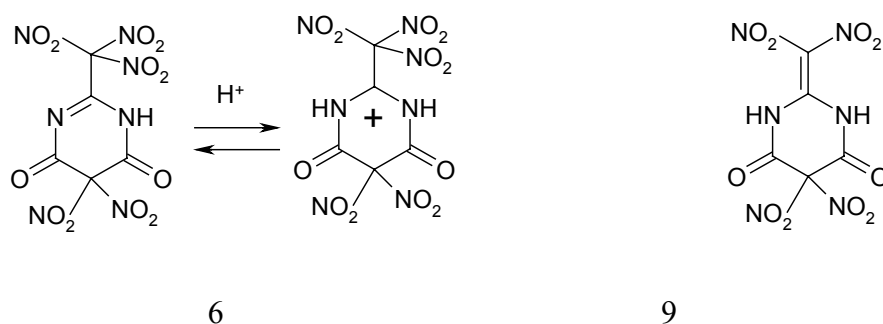


Table 1. Chemical shifts (δ , ppm.) in NMR ^{13}C spectra of compounds (6) and (9).

Compound	N-C-N	-C=(NO ₂) ₂	-C=O	-2- R	Solvent
9	104	113,8	146,7	152,61	D ₂ SO ₄
6	116,6	127,18	153,12	156,7	D ₂ SO ₄

The explicit difference in the course of nitration of compound (1) and the structurally similar 2- methyl-4,6-dihydroxypyrimidine is apparently due to the different sequence of the introduction of nitro groups into the pyrimidine molecule. In the case of (1) and its 5- nitro derivative the nitration proceeds primarily on the exocyclic fragment and after the formation of an electron accepting substituent at 2- position a repeated nitration takes place at 5- position which leads further to the exhausting nitration of the pyrimidine. A similar picture is observed during nitration of barbituric acid and 2- amino-4, 6-dihydroxypyrimidine^[3,9].

So, the nitration of 2-alkyl- and 2-carboxymethyl-4,6-dihydroxypyrimidines proceeds through different intermediates because of the varying sequence of nitro groups introduction into the molecule.

For 2- methyl-4, 6-dihydroxypyrimidine the second stage of nitration takes place on the carbon atom in 5- position, after which the exocyclic moiety is affected. If the situation were opposite, we would observe the sequence analogous to that for the nitration of compound (1) and, as a consequence, DADNE should not appear in the reaction products.

As it was shown by us earlier, the key factor determining the second stage of 2- methyl-4,6-dihydroxypyrimidine nitration, involves its protonation to produce a highly reactive intermediate further nitrated to the 5,5-dinitro derivative. The study of NMR ^{13}C spectra of 2-methyl-5-nitro-4, 6-dihydroxypyrimidine in deuterated 95% sulfuric acid revealed that this compound existed at least into two tautomeric forms, which was evident from the presence of two groups of signals attributed to the carbon atom of the pyrimidine ring. (See Fig. 1)

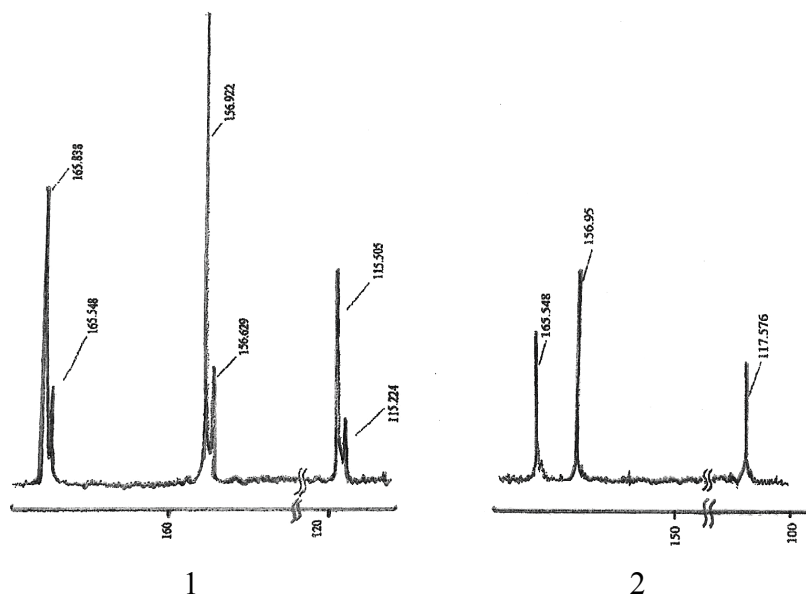


Fig 1. Fragments of NMR ^{13}C spectra of solutions of 2- methyl-5-nitro-4,6-dihydroxypyrimidine in deuterated 95% sulfuric acid (1) and in deuterated 50% sulfuric acid (2).

Judging by the shift of the methyl group signal of 2-methyl-5-nitro-4,6-dihydroxypyrimidine in solutions of sulfuric acid of varying concentrations, the ionization of this compound obeys the acidity function H_a derived for the equilibrium of O-protonation of amides. This compound has the pK_{BH^+} -4.25. The corresponding 4,6-dimethoxy derivative appears to be a Hammett base with pK_{BH^+} -2.2 in terms of the H_o acidity function. As was mentioned above, the similar picture was observed in the nitration of 2-methyl-4-amino-6-hydroxypyrimidine which was protonated also on the nitrogen atom of the pyrimidine ring which was confirmed by the 1H NMR spectrum of its nitrate salt.

Thus, as distinct from 2-methyl- 4,6-dimethoxy-5-nitropyrimidine and 2-methyl-4-amino-6-hydroxypyrimidine which are protonated on the nitrogen atom, 2-methyl-5-nitro-4,6-dihydroxypyrimidine is protonated on the oxygen atom. This results in different modes of nitration of these compounds. So the isomerisation of the O-protonated form leads to the generation of a reactive intermediate readily nitrated to the 5,5-dinitro derivative. When analyzing the possible structures and reactivity of this intermediate, it was established that its further nitration induced the formation of a double bond between the cyclic carbon and a substituent in 2-position. In 1H NMR spectrum of a solution of 2-isopropyl-4,6-dihydroxypyrimidine in concentrated sulfuric acid a methyl group doublet and methine group septet are observed which imply the presence of the isopropyl group. On adding potassium nitrate to this solution, as the 5,5-dinitro derivative forms, the doublet and septet are transformed into a singlet (Fig.2)

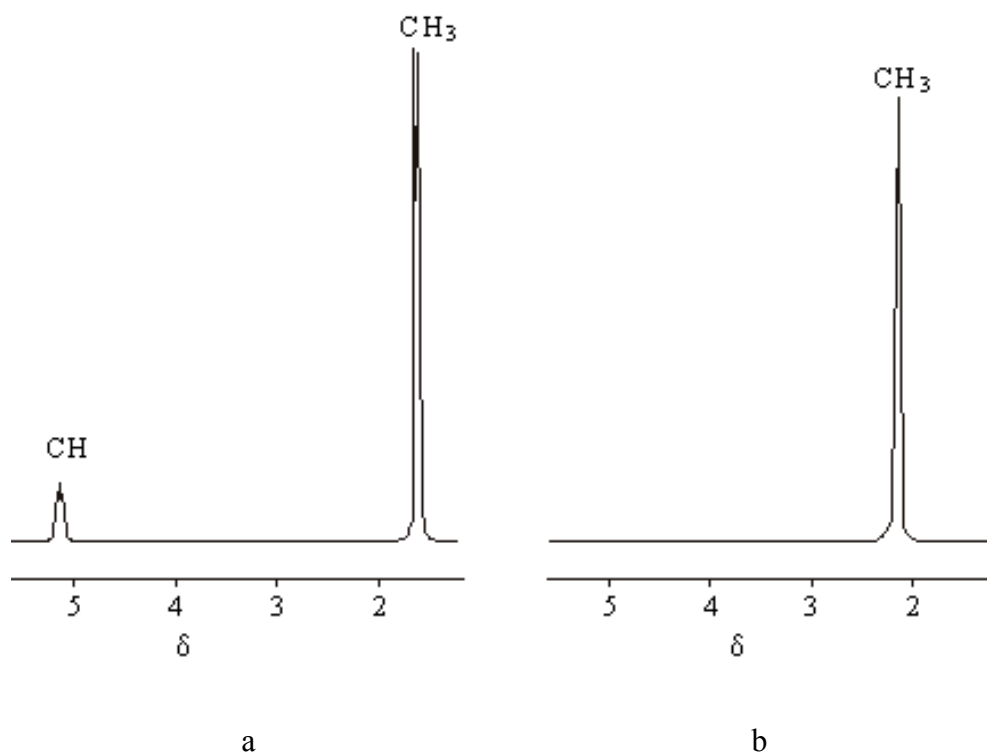
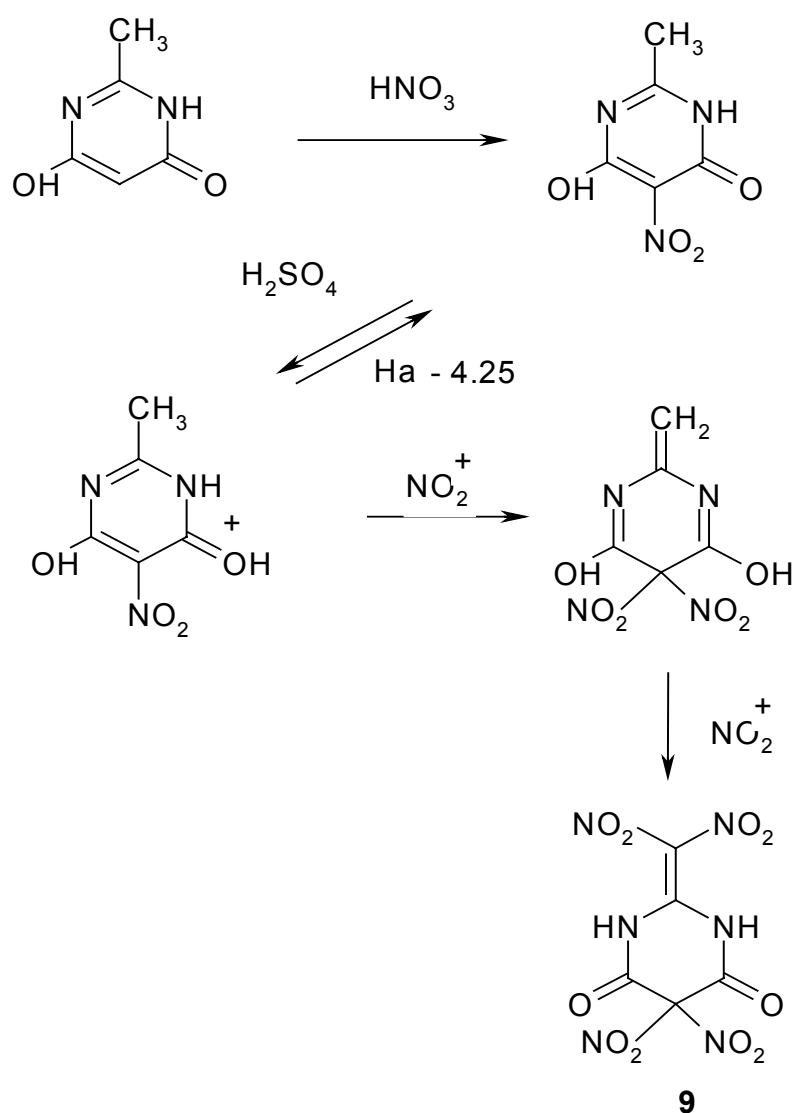


Fig 2. Fragments of 1H NMR spectra of solutions of 2-isopropyl-4,6-dihydroxypyrimidine in 95% sulfuric acid before (a) and after (b) addition of potassium nitrate (δ , ppm.).

This change is apparently a consequence of the formation of a double C=C bond between the substituent and a ring carbon atom due to the rearrangement of the molecule in the course of the second stage of nitration with the formation of a quinoid type structure.

Hence the change in the succession of nitro groups introduction into the dihydroxypyrimidine molecule determines the structure of the key intermediate which eventually produces DADNE. Based on the discussion above, the sequence of chemical transformations leading to the key intermediate responsible for the formation of DADNE, can be depicted by Scheme 3.

The important role of the structure (9) should be stressed. Apparently, it is precisely the presence of the dinitromethylene moiety that determines a definite chemical stability of intermediate (9). Otherwise, in the presence of an ordinary C-C bond at 2-position of (9), the nitration process should have proceeded further until the stage of the trinitromethyl derivative and its decomposition should be similar to that of (6) and barbituric acid ^[9]. In this case the main reaction products should be di- and trinitromethane.



Scheme 3. Nitration of 2-methyl-5-nitro-4,6-dihydroxypyrimidine.

3. CONCLUSION.

The behavior of 2-(4-oxo-6-hydroxy-2-pyrimidinylidene) acetic acid, a close structural analogue of 2- methyl -4,6-dihydroxypyrimidine, in the nitration reaction has been studied and basic differences in the nitration mechanism are shown. The effect of a consecutive order of nitro groups introduction on the generation of the key intermediate responsible for the formation of DADNE has been established. Based on the results obtained, a scheme of the chemical transformations of 2- methyl -4,6-dihydroxypyrimidine in the nitration process is suggested.

ACKNOWLEDGEMENTS

The authors would like to thank the International Science and Technology Center for giving financial support to this project.

REFERENCES.

- [1] USSR Inventor's Certificate № 318468; 1989.
- [2] DOROKHOV V.A., GORDEYEV M.F., BOGDANOV V.S., LAIKHER A.L., KISLYI V.P., SEMENOV V.V.: *A novel synthesis of aminated nitroketenes*, Bull. of Russian Acad. Sci, Ser. Khim. № 11 c. 2660, 1990
- [3] ASTRAT'EV,A; DASHKO,D.; MERSHIN,A; STEPANOV,A. URAZGIL'DEEV, N.: Russian Journal of Organic Chemistry, 37, 729-733, 2001
- [4] LATYPOV,N.V.; BERGMAN, J.; LANGLET, A.;WELLMAR,U.;BEMM,U.: Tetrahedron, 54, 11525-11536, 1998
- [5] BERGMAN, H.; OSTMARK, H; PETTERSSON, A; PETTERSSON, M.-L.; HIIKIO,M.: *Some Initial Properties and Thermal Stability of FOX-7*. Tampa, pp 346-351, 1999
- [6] OSTMARK, H; BERGMAN, H.; BEMM,U.; GOEDE, P.; HOLMGREN,E.; JOHANSSON, M.; LANGLET, A.; LATYPOV,N.V.; PETTERSSON, A.; PETTERSSON, M.-L.; WINGBORG,N.; VORDE,C.; STENMARK, H.; KARLSSON,L.; HIIKIO,M.: *2,2- Dinitro-ethene-1,1-diamine(FOX-7)- Properties, Analysis and Scale Up*: Karlsruhe, 2001
- [7] KARLSOON,S.; OSTMARK, H; ELDSATER, C.; CARLSSON,T.; BERGMAN, H.; WALLIN, S.; PETTERSSON, A.: *Detonation and Properties of FOX-7 and formulations containing FOX-7*; San Diego, pp 5 ,2002
- [8] LOCHERT, I.: "FOX-7- A New Insensitive Explosive" DSTO, 2001
- [9] LANGLET, A.; LATYPOV,N.V.; WELLMAR,U.; BEMM,U; GOEDE , A; BERGMAN, J.; ROMERO, I.: *Nitration of 2-substituted pyrimidine-4,6-diones , structure and reactivity of 5,5-gem-dinitropyrimidine -4,6-diones*; J.Org.Chem., 67, 7833-7838, 2002

SIMULATION STUDY ON ARMOUR-PIERCING EFFECT OF ARMOUR-PIERCING BOMB

Zhou Renbin*, Xie Tiebang* and Xiang Weixiang**

* Huazhong University of Science and Technology, School of Mechanical Science
and Engineering, Wuhan, Hubei, 430074, P.R.China

** Wuhan Ordnance Noncommissioned Officer Academy of PLA,
Department of artillery, Wuhan, Hubei, 430075, P.R.China

Abstract:

Studying the armor-piercing effect of Armour-piercing bomb that attacks aluminum target is essential because the target can be considered the simulation of the actual fight equipment. Based on the hypothesis about building the fraction field, the armor-piercing effect of armor-piercing bomb is analyzed, and the velocity and the intruding depth parameter model of armor-piercing effect are established. Taking a certain armor-piercing bomb as example, the intruding processes of armor-piercing effect are simulated by using the nonlinear finite element analysis program LS-DYNA, while aluminum target simulates the wall of combat equipment in two different conditions. At last, the finite element simulated results are given and analyzed that agree with the experiments.

Keywords: *simulation study, armor-piercing effect, armor-piercing bomb, intrude*

1. INTRODUCTION

It is great important to study the armour-piercing effect of armour-piercing bomb that attacks aluminium target because the target can be considered the simulation of the actual fight equipment^[1,2]. Piercing-piercing bomb impacts the target fleetly with high speed using the huge kinetic energy of pill when the warhead is shoot. Its main damage mechanism is the intruded effect to target. The piercing-piercing effect is the process that piercing-piercing bomb intrudes and destroys the piercing target depending on its pill's huge kinetic energy. It is own mechanism of armor-piercing bomb that attacks the target. The destroy effect includes intrude effect, kill and wound effect. The distributing of fragmental quality and shape of warhead, and the distributing of the fragmental initial velocity and number of interspecies are researched^[3,4]. Based on mechanism analysis of intruding damage of warhead fragments, an intruding damage model of the fragments to ship-borne equipment is established^[5]. The impact and intrude effect is the main analysis in this paper.

2. ARMOR-PIERCING EFFECT

Piercing process of armour is a very complex and unbelievable process. Piercing process of armour and damage force caused by it is different because of the different factors such as type, velocity, hitting angle of piercing-piercing bomb. So, for the damage process that armour-piercing bomb attacks the fight equipment, some hypothesis about building the after-effect fraction field are as following:

The after-effect fraction field is thinking as a point explosion model, all fragments are come from it.

- (1) Distributing of after-effect fragment is a taper area, the angle of cone is about 90°to 110°, the centre line is bisector of inclination between pill and inner armour surface normal.
- (2) The number, quality, velocity and dimension of fragments are distributing approximately and symmetrically according to the centreline of cone.
- (3) Fragments move alone beeline.

2.1 Average initial velocity of fragments

While the incendiary bombs explode, many fragments of different masses, with high speed, will be produced. Within some distance, they are of great damaging effect to structure and equipment. Meanwhile they can cause fire or detonate ammunitions. The initial velocity of fragments is an important parameter in describing the explosion effect of incendiary bombs.

The average initial speeds of fragments are as follows ^[6,7].

$$v_o = \sqrt{2E} \sqrt{\beta / (1 + 0.5\beta)} \quad (1)$$

where, v_o is initial speed; $\sqrt{2E}$ is Gurney constant of the bomb, in this paper, the dynamite is TNT, $\sqrt{2E} = 2370$ m/s; $\beta = C / M_s$ It is the mass rate of the bomb to cartridge case, for 30mm×170mm. Armour-piercing bomb, $\beta = 1/8$.

2.2 Residual velocity of fragments

To calculate the residual velocity of fragments after them piercing a certainty thickness target, the formulation is given as following,

$$v_r = v_c - k(TS)^\alpha m^\beta (\sec \theta_c)^\gamma v_c^\lambda \quad (2)$$

where v_c is velocity when fragment attack the target(m/s) , $k, \alpha, \beta, \gamma, \lambda$ are the coefficients about the material characteristic of target, m is quality of fragments(g), S is landing area of fragments(cm²) , T is thickness of target(m), is landing angle(rad) .

According to the experimental data, when the residual velocity of fragments is 0, the landing velocity is the utmost armour-piercing velocity of fragments, that is,

$$v_c = k_1(T\bar{A})^{\alpha_1} m^{\beta_1} (\sec \theta_c)^{\gamma_1} \quad (3)$$

For aluminium material, the coefficients about the material characteristic of target is that, $k_1=2852$ m/s, $\alpha_1=0.903$, $\beta_1=-0.941$, $\gamma_1=1.098$.

2.3 Distribution of fragments velocity in space

For static dispersion characteristic of fragments, Experiments show that within the dispersion angle Ω , the distribution of the number of fragments is norm. In general, more than 90% of all fragments fall within the angle of Ω . Let $\bar{\varphi}$ be the estimation of the

dispersion angle with norm distribution, σ_φ be the mean squared variance, then the distribution function of fragments in space is,

$$F(\varphi) = \int_0^\varphi f(\varphi) d\varphi = \frac{1}{\sqrt{2\pi}\sigma_\varphi} \int_0^\varphi \exp\left(-\frac{(\varphi - \bar{\varphi})^2}{2\sigma_\varphi^2}\right) d\varphi \quad (4)$$

Where σ_φ can be evaluated according to 90% of the fragments within Ω , $\sigma_\varphi = \Omega/3.3$.

Geometry characteristic of static dispersion characteristic of fragments can be represented as

$$\begin{cases} \varphi_1 = \arctan \frac{d_i/2 + \Delta}{l_1} \\ \varphi_2 = \pi - \arctan \frac{d_i/2 + \Delta}{l_2} \\ \bar{\varphi} = \frac{\varphi_1 + \varphi_2}{2} \\ \Omega = \varphi_2 - \varphi_1 \end{cases} \quad (5)$$

Where, Δ is the maximum expansion distance; l_1, l_2 is the effective length from the mass centre to the head and after-body, respectively. d_i is the inner diameter of the cylinder part of the warhead; φ_1, φ_2 is the dispersion azimuth angles, $\bar{\varphi}$ is the expectation of the dispersion angle.

For dynamic dispersion characteristic of fragments, at the time of explosion, besides the initial speed v_o , there exists a residual speed v_c . The dynamic parameters are marked with “'” on there upper right quarter, then

$$\begin{cases} \varphi'_1 = \arctan \frac{v_o \sin \varphi_1}{v_o \cos \varphi_1 + v_c} \\ \varphi'_2 = \arctan \frac{v_{of} \sin \varphi_2}{v_o \cos \varphi_2 + v_c} \\ \varphi' = \arctan \frac{v_{of} \sin \varphi}{v_o \cos \varphi + v_c} \end{cases} \quad (6)$$

$$v'_o = \sqrt{v_o^2 + v_c^2 + 2v_o v_c \cos \varphi} \quad (7)$$

$$\sigma'_\varphi = (\varphi'_2 - \varphi'_1)/3.3 \quad (8)$$

2.4 Intruding depth of fragments

As the mentioned above, there are many factors influence the armour-piercing effect, just like kinetic energy that pills attack the target, the structure of warhead, the attack angle, mechanical property and thickness of target, and so on. Intruding depth can be calculated by using the following formula.

$$T = D \left[\frac{W v_0'^2 \cos^2 \theta}{\alpha D^3} \right]^{1/\beta} \quad (9)$$

where T is intruding depth(m), D is diameter of pill(m), W is quality of pill(kg), v_0' is attacking velocity(m/s), θ is attacking angle(rad), α , β is constant, according to experience, $\lg \alpha = 6.15$, $\beta = 1.43$.

3. EQUIVALENT TARGETS

Equivalent target, which is to say that, for specific direction and position, the basic element of random shape and material fight equipment can be, described a target that has certain thickness and material to simulate and analyse damage expediently. The thickness of equivalent target is corresponding with thickness of basic element of equipment in given position and direction. If the thickness of basic element of equipment in given position, and direction h_i can be given by radial analysis program, the thickness of equivalent target can be expressed approximately as following,

$$h_{di} = \frac{h_i \sigma_d}{\sigma_t} \quad (10)$$

Where h_i is thickness of basic element of equipment in certain position and direction (m), σ_t is utmost intensity of basic element material (Pa), σ_d is utmost intensity of equivalent target (Pa).

4. SIMULATION MODELS

With respect to limited capacity possibilities there were successfully tested on the whole only 4 testing sets - two were with continuous sensor enclosed to outer circumference, two were with sensor on inner circumference.

The non-linear dynamic finite element program LS-DYNA offers the strong tool to analyse the intruding process of the bombs. In order to study the capability that fight equipment resists damage caused by armour-piercing bomb, using the non-linear dynamic finite element program LS-DYNA, a certain armour-piercing bomb, 30 mm×170 mm, is selected as attacking weapon. The armour-piercing effect of a certain armour-piercing bomb to attack the aluminium target has simulated.

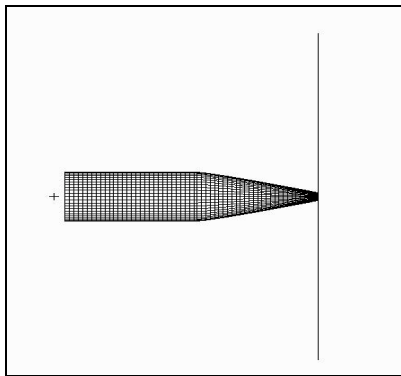


Fig. 1. Operating model one

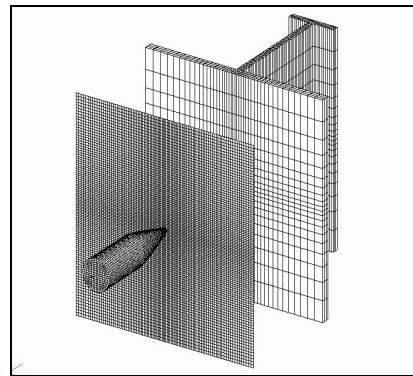


Fig. 2. Operating model two

In order to predigest the calculations, the pill body is thought as a plasmodium equably, the average density of pill body can be gained through total quality dividing total volume; the material parameter can refer the material of general steel [8].

There are two kinds of operating mode that is calculated in this paper. One is that, the bomb intrude aluminium target vertically which the thickness is 4 mm, the other is that, the bomb intrude aluminium targets vertically which includes single aluminium target and T type carriage that thickness are 6 mm and 120 mm × 50 mm × 6.5 mm. The initial velocity is 1080 m/s. Two kinds of operating mode are shown as Fig.1 and Fig.2.

5. CALCULATION RESULTS AND ANALYSIS

Combination of time and continuous method of measurement of the detonation velocity at realised experiments provided many interesting and very useful information. The tests documented and explained several basic aspects of functioning of the FLC. But acquired results at the same time evoked a need at least to possible causes of some surprising discoveries.

5.1 Calculation results

According to the mentioned above, using the empirical formula and the finite element calculating method, the intruding effect of the armour-piercing bomb can be calculated. The armour-piercing effect of 30 mm × 170 mm armour-piercing bomb to attack the aluminium targets in operating model two has simulated as Fig.3.

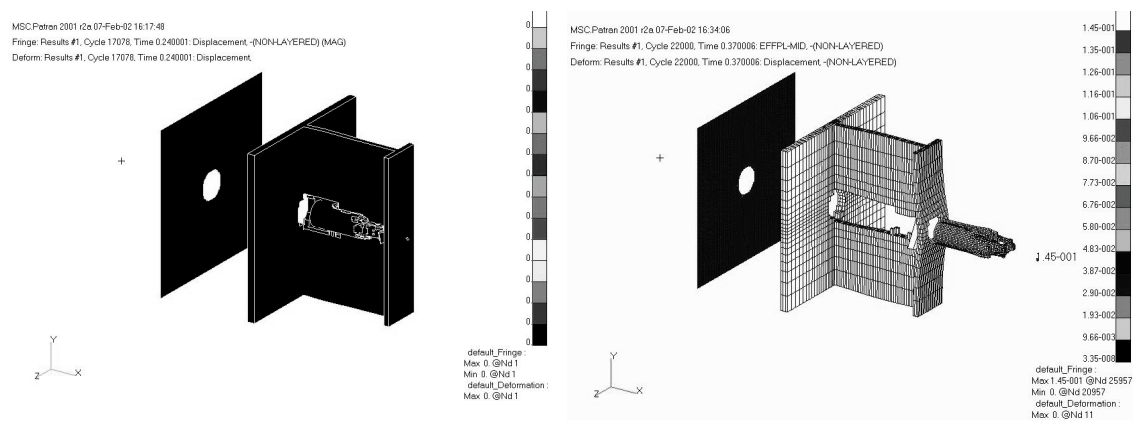


Fig. 3. The armour-piercing effect of operating model two

5.2 Analysis of results

- (1) For model one, the velocity-times curve is shown as Fig.4. There is hardly any baffle effect, for aluminium target that the thickness is 4 mm to pill that the diameter is 30 mm, and there is no obvious plastic deformation when the pill intrude the aluminium target. The crevasse of target is bigger than diameter of pill. The velocity curve of pill shows that a certain range of wave is caused by numerical value surge and distortion surge of intruding process.
- (2) For model two, the velocity-times curve is shown as Fig.5. When the bomb intrudes aluminum targets vertically and constantly, it includes single aluminum target and T types carriage that thickness are 6 mm and 120 mm × 50 mm ×

6.5 mm. The results show that armor-piercing bomb can pierce the assembled aluminum component, and the obvious plasticity distortion can be seen from the body. It can be observed that the intruding process is divided into two parts and the residual velocity of fragments is 980 m/s from the velocity-times curve in operating mode two.

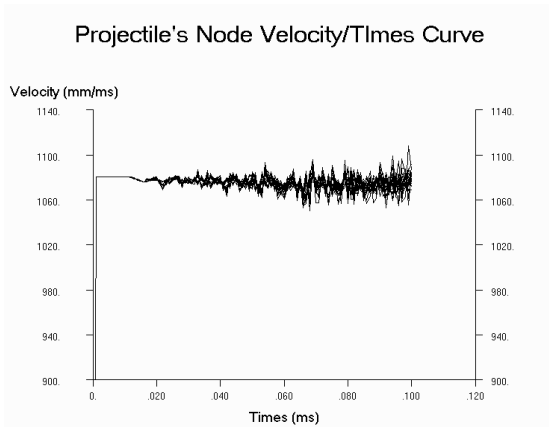


Fig. 4. Velocity-times curve in operating mode one

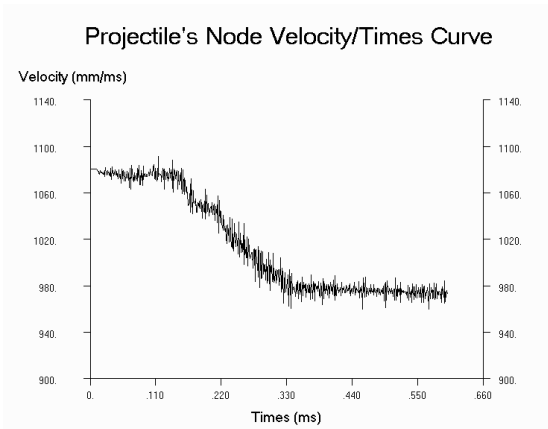


Fig. 5. Velocity-times curve in operating mode two

6. CONCLUSION

In this paper, the subject is concerned chiefly with the study of the armour-piercing effect of the armour-piercing bomb. Based on the hypothesis about building the after-effect fraction field, the finite element calculations of armour-piercing effect of a certain armour-piercing bomb are completed. The results demonstrate that the finite element analyses model presented here is much more reliable and feasible. It is more important to research the armour-piercing effect of armour-piercing bombs; we can get more accurate simulating results that fragments attack to the equipment. It has great significance to improving the survivability for army equipment in wartime.

REFERENCES

- [1] LISA K. ROACH: *A Methodology For Battle Damage Repair (BDR) Analysis*, U.S. Army Research Laboratory, ADA276083, 1994
- [2] WILLIAM R.DAY, PHILLIP A. RIMBLE: *Compilation of Surface Target Vulnerability and Effectiveness Methodologies*. Dooz, Allen and Hamilton, Inc. ADA921078. 1994.05.
- [3] LI TEIPENG: *The Distributing of the Fragmental Initial Velocity and Number of Interspecies*. China: Huadong Institute of Technology, 5-21, 1988
- [4] CAI SHOUJUN: *The Distributing of Fragmental Quality and Shape of Warhead*. China: Huadong Institute of Technology, 4-22, 1988
- [5] ZHOU RENBIN, PU JINYUN AND CHEN YINGCHUN: *Intruding Damage Simulation of Fragments to Ships*, In: Huang Ping, Wang Yajun, Li Shengcai, and Qian Xinming Eds. Progress in safety science and technology (vol.□) Beijing, Science Press. 869-874, 2002
- [6] ZHANG TINGLIANG AND CHEN LIXIN: *Operation Research of Surface-to-Surface TBM*. Beijing: Press of the People's Liberation Army of China, 160-166, 1997
- [7] ZHANG TINGLIANG AND CHEN LIXIN: *Effectiveness Analysis of Surface-to-Surface TBM*. Beijing: National Defense Industry Press, 180-183, 2001
- [8] ZHU XI, JIN TAO AND MEI ZHIYUAN: *The Researches on Capacity of Dandification Resistance of one certain Missile Craft's Structure*. Wuhan: Naval University of Engineering, 5~11,2002

EFFECT OF TNT CHARGES ORIENTATION ON GENERATED AIR BLAST WAVES

-

NUMERICAL SIMULATION USING LS-DYNA

V. Adamík*, J. Vágenknecht**, P. Vávra** and W.A. Trzciński***

* External Consultant of the DTTX on Continuum Dynamics

** Department of Theory and Technology of Explosives
University of Pardubice, 532 10 Pardubice, Czech Republic

*** Military University of Technology, Kaliskiego 2, 00 980 Warsaw, Poland

Abstract

The paper deals with numerical 3D simulation, through the code LS-DYNA, of the effects caused by air blast waves generated by cylindrical TNT charges (the mass of 25g and 50g) which are differently oriented respect to the pressure gauges placed relatively close to the charges (approximately 800 mm and 840 mm from the charges). As the first step for these simulations, the numerical study has been concentrated on the verification of the state equations for TNT and air continuum. It has been concluded that the JWL equation of state and ideal gas equation of state were proper representations for TNT and air respectively. Then, simple formulae for various oriented charges have been developed and verified. These formulae make possible to represent the original cylindrical charges like equivalent 3D ellipsoids (this approach is very important in order to obtain stable computational mesh). The final numerical simulations have been compared with the original experiments performed at Military University of Technology in Warsaw. On the base of this comparison, it has been concluded that the 3D numerical simulations using LS-DYNA have been a very powerful and useful tools.

Keywords: *detonation effect, TNT, orientation of the charge, pressure, air shock wave, numerical simulation, FEM, LS-DYNA*

1. INTRODUCTION

The blast (shock) air wave patterns from the explosion of cylindrical charges are very complex so that the accurate assessment of the blast wave parameters (positive peak overpressure, duration, and the positive impulse) is not a simple task. The problem of experimental determination of blast wave parameters for the nonspherical charges was considered for example in papers ^[6-8]. The process of expansion of detonation products of nonspherical sources was analysed theoretically in works ^[9-10].

This paper is devoted to the problem of 3D numerical simulations of the effects caused by air blast waves generated by cylindrical TNT charges (the mass of 25g and 50g) which are differently oriented respect to the pressure gauges placed relatively close to the charges (approximately 800 mm and 840 mm from the charges).

For the numerical simulations, the 3D dynamic explicit Lagrangian finite element code LS-DYNA ^[1] has been used.

As the first step for these simulations, the numerical study has been concentrated on the

verification of the state equations for TNT and air continuum. It has been concluded that the JWL equation of state (EOS) and ideal gas equation of state were proper equations for TNT and air respectively.

Then, simple formulae for various oriented charges have been developed and verified. These formulae make possible to represent the original cylindrical charges like equivalent 3D ellipsoids (this approach is very important in order to obtain stable computational mesh).

The final numerical simulations performed have been compared with the original experiments performed at Military University of Technology in Warsaw ^[4]. On the base of this comparison, it has been concluded that the 3D numerical simulations using LS-DYNA have been very powerful and useful tools.

In conclusion, the results obtained are summarized and further possible research effort is outlined.

2. NUMERICAL 3D SIMULATIONS

2.1 Computational codes

In this time, several computational 3D codes based on finite element (e.g. LS-DYNA, ABAQUS) or finite difference (e.g. AUTODYN) techniques are available to simulate fast continuum dynamics. These codes can be principally divided into two categories: Lagrangian or Eulerian codes. Advantages and disadvantages of the codes are briefly summarized below:

- Eulerian codes are using the computational mesh that is fixed in the space, it is connected with an external observer. The mesh is not deforming, it remains the same in time. Continuum is flowing across the mesh and therefore it is necessary to evaluate transport terms of the mass, energy, and momentum each computational step. These transport terms usually introduce into the solution errors that are increasing in time. Great problems are connected also with the description of continuum boundary motion (e.g. boundary charge-air). The advantage is nondeformable mesh, the disadvantages are very complex algorithms for transport terms and boundary motion.
- Lagrangian codes are using the computational mesh that is connected with the continuum. Thus, it deforms in time following the continuum deformation. No transport terms are needed, the continuum boundary is moving regularly following the continuum dynamics. Great disadvantage is the fact that the mesh is deforming and its capability deteriorates in time in correct description of the dynamics involved. The solution can be so called rezoning technique but this technique introduces new more regular mesh at certain times and therefore it introduces into the solution similar errors like transport terms above. The best solution is to choose an initial mesh that does not require later rezonings. However, this task is very individual (problem dependent) and very difficult to solve.
- Other important requirement on the simulations is a proper description of continuum dynamic behaviour. For this purpose, most of the 3D codes have quite large possibilities (various equation of state – EOS) and there is not a great problem to describe dynamic behaviour of various continua.

The approach used in this paper was determined by the fact that the authors had for the simulations available the Lagrangian 3D LS-DYNA code without rezoning technique.

Thus, the scope of initial effort was orientated to the problem to find and verify corresponding EOS for TNT and air, and to find proper initial mesh that does not need mesh rezoning.

2.2 Equations of state

On the boundary charge-air, a dramatic pressure decrease occurs. The initial velocity of the boundary and initial air pressure are according ^[2] (for spherical TNT charge and immediate detonation): air blast wave pressure 28.5 MPa, air blast wave velocity 4400 m/s. From the value of the wave pressure it is evident that for the air dynamics, EOS for the ideal gas is appropriate, i.e. (1):

$$p = (\kappa - 1) \cdot \rho / \rho_0 \cdot E \quad (1)$$

where **p** is the pressure, **κ** is isentropic coefficient (**κ** = 1.4), **ρ** is density (**ρ**₀ = 1.225 kg/m³), **E** is internal energy (**E**₀ = 250 kPa).

For description of charge gas products dynamics, there is the JWL (Jones-Wilkins-Lee) EOS available in LS-DYNA. Sometime, there are objections respect to this EOS, see e.g. ^[5], in spite of it the JWL EOS is broadly used and it was used also in this study.

General form of the JWL EOS is as follows (2):

$$p = A \cdot \left(1 - \frac{\omega}{R_1} \cdot \frac{\rho}{\rho_0}\right) \cdot e^{-R_1 \frac{\rho_0}{\rho}} + B \cdot \left(1 - \frac{\omega}{R_2} \cdot \frac{\rho}{\rho_0}\right) \cdot e^{-R_2 \frac{\rho_0}{\rho}} + \omega \cdot E \cdot \frac{\rho}{\rho_0} \quad (2)$$

For TNT, the following parameters are valid ^[3]:

ρ₀ = 1590 kg/m³, **A** = 371.20 GPa, **B** = 3.231 GPa,

R₁ = 4.15, **R**₂ = 0.95, **ω** = 0.30, **E**₀ = 7.0 GPa,

detonation velocity - **D** = 6930 m/s, Chapman-Jouguet pressure - **P**_{CJ} = 21.0 GPa

For the validation of the EOS described above, a numerical 3D simulation was performed for the explosion of a spherical TNT charge with the mass 50g. The following maximum values were obtained at the charge-air boundary: air blast wave pressure 27.4 MPa, air blast wave velocity 4400 m/s. From these values, it is evident that the EOS used describe properly the initial boundary dynamics.

2.3 Numerical 3D simulations

For the validation of numerical simulations regarding the effects of air blast waves on charge surroundings, original experiments performed at Military University of Technology in Warsaw ^[4] have been used. The experiments are described in ^[4], the experimental geometry is introduced in fig.1 and 2.

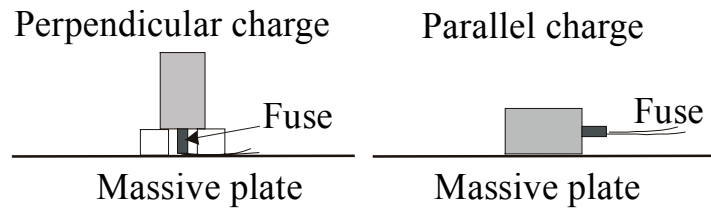


Fig 1. Perpendicular and parallel orientations of the explosive charges

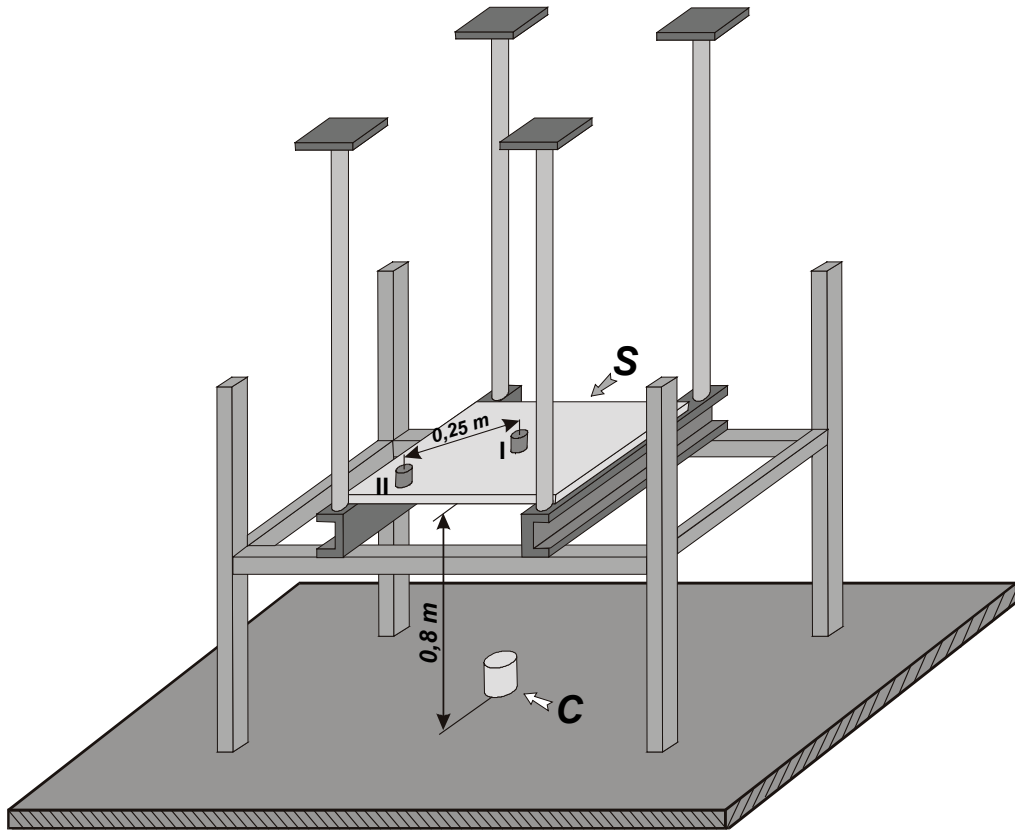


Fig 2. The experimental set-up: *S* –steel plate, *C* –TNT charge, I, II – pressure gauges G1 and G2

For the simulations, the following assumptions have been applied:

- Only one quarter of the system have been modelled due to the symmetry of the problem, this assumption is not exact for the charges with the parallel axis (see fig.1) but according numerical simulations it is quite good
- The steel plate with pressure gauges has been modelled as the ideal rigid wall with possible air sliding without the friction, numerical simulations confirm validity of this assumption
- The original cylindrical charges have been substituted by equivalent ellipsoids with the same mass (see the rules for ellipsoids below) and immediate detonation of the whole charge has been supposed (the validity of this assumption were confirmed by variant calculations)

Initial numerical simulations with the real cylindrical charges have shown that numerical meshes, created by standard finite element technique, very fast degraded (even if the charge edge was modified) especially near boundary charge-air, see fig.3 and 4 as an example. Unrealistic charge expansion is evident and the mesh is not regular near boundary charge-air.

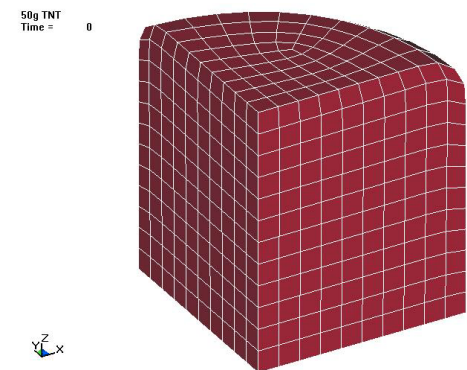


Fig 3. Traditional initial computational mesh for the charge 50g TNT

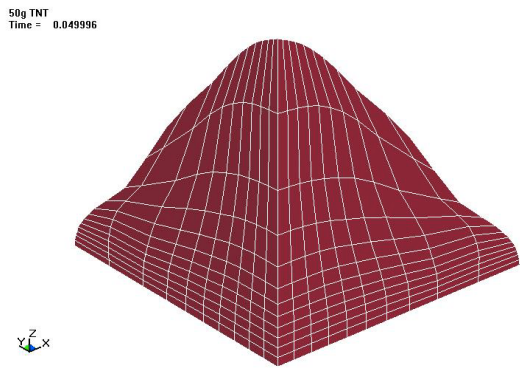


Fig 4. The mesh from Fig.3 at time 0.05 ms, note general form and irregularity at boundary

After a lot of numerical simulations, it was found that the current best solution was to model real cylindrical charges like equivalent ellipsoids with the mesh pattern shown in fig.5. This approach eliminated the charge edges and the mesh remained very regular during the time, see fig.6.

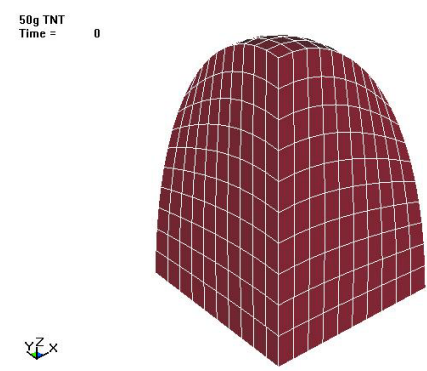


Fig 5. Initial computational mesh for equivalent ellipsoid, 50g TNT

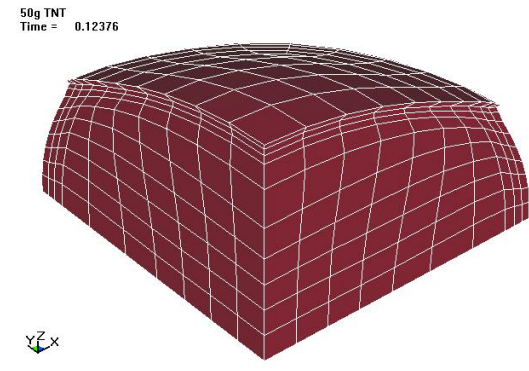


Fig 6. Computational mesh from Fig.5 at time 0.124 ms, note general form and regularity at boundary

For this approach, it was necessary to define the rules for equivalent ellipsoids construction. The following rules were derived and verified:

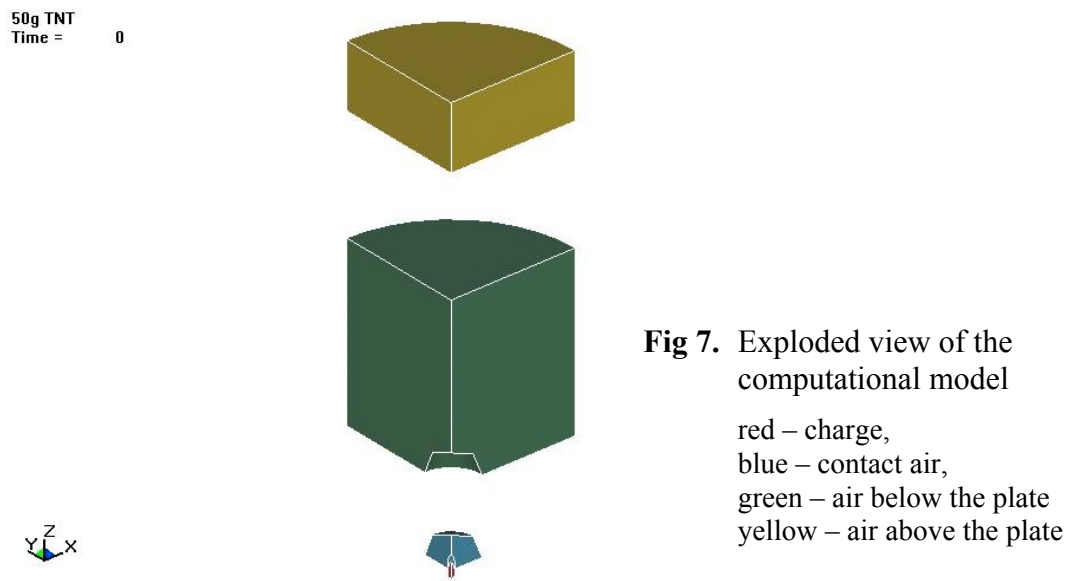
- For perpendicular charges, the ratio of ellipsoid axes is $K1 = H^* / R^*$ where H^* and R^* are fictious charge height and radius. The fictious charge dimensions must be calculated at time when the detonation wave reaches the charge edge. At this time initial charge height H and radius R will be greater and depends on charge-boundary velocity. In our cases we have supposed the velocity 4400 m/s.
- For parallel charges a simple ratio was supposed $K2 = 4R/H$.

By means of these rules, the ratios for various charges were derived, see the summary in Tab.1, for all charges referred in [4].

Table 1. *Dimensions of the charges and ratios for equivalent ellipsoids*

M [g]	R [mm]	H [mm]	K1	K2
10	10	23.2	1.24	1.72
25	15	22.2	1.12	2.70
50	20	25.0	1.07	3.20
75	20	37.3	1.18	2.14

Then finite elements models for the charges of 25g and 50 have been constructed, see as an example fig.7. **For the models, a very important construction regarding the surrounding air has been applied.** Usually, the mesh of the charge and of the contact air zone deteriate in time even if the air blast wave is far enough from the expanding charge. This creates very serious numerical problems in zones which are not of great interest now. The solution adapted was simple one. The surrounding air zone was divided into two zones: first one was the zone of contact air and the second one was the air zone outside. This makes possible to perform the numerical solution in two phases: initial phase with the explosion, generation and propagation of air blast waves up to the time when air waves are quite far from the charge, the second phase when the charge and the contact air zone are deleted and the computation continues only with the dynamics of the air zone outside.



The finite element models for individual charges were identical:

- Total number of elements 49 250,
- Total number of nodes 55 641,
- Total number of boundary conditions 11 131,
- Total number of charge elements 750,
- For all elements, 8-node brick element with one-point integration was used, the elastic hourglass control was applied
- The steel and massive plates were modelled as rigid walls with fluids sliding without friction

2.4 Numerical results

The numerical results obtained for the charges of 25g and 50g are presented briefly below. These results are compared with the experimental results obtained in ^[4]. In fig.8 and 9, the results for 25g TNT are presented. In fig.10 and 11, the results for 50g TNT are summarized.

25g TNT charges

In fig.8, a comparison of numerical and experimental overpressure histories for the gauge G1 is introduced. In fig. 9, a comparison of numerical and experimental overpressure histories for the gauge G2 is presented.

From the figures, it follows that a good agreement has been obtained for the gauge G2. As for the gauge G1, a great discrepancy exists in time history, the maximum overpressure values are in a good agreement.

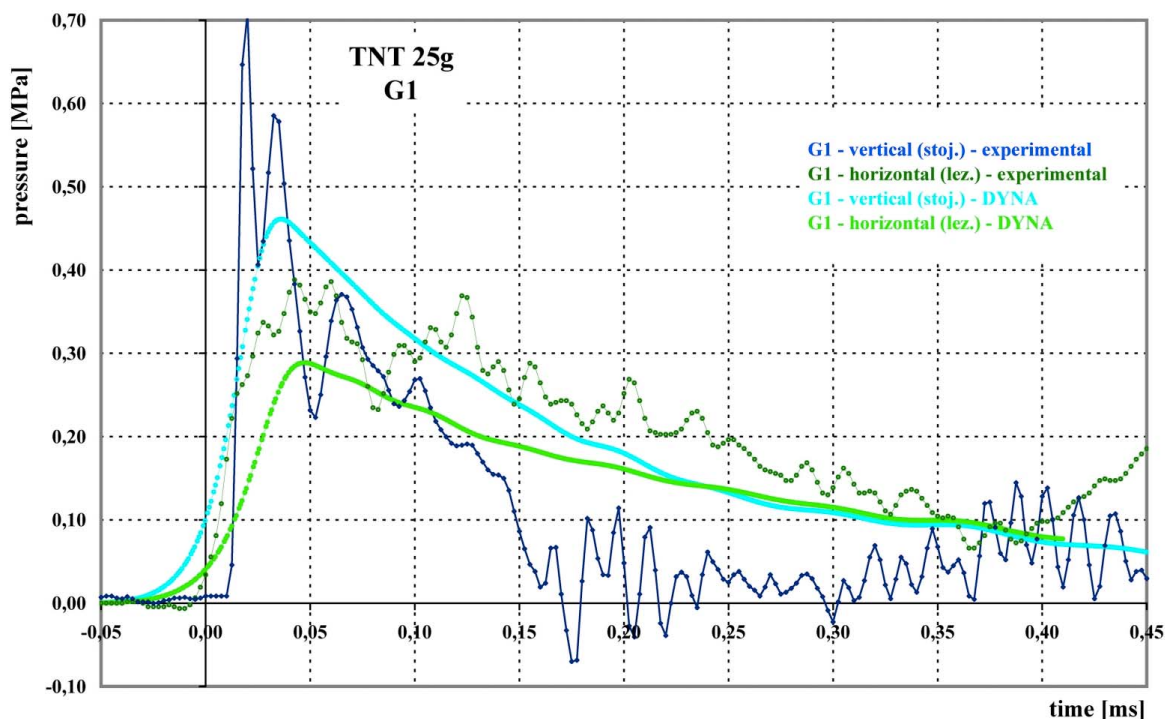


Fig 8. Experimental and calculated overpressure history for charge 25g TNT and gauge G1, stoj. – perpendicular charge, lez. – parallel charge

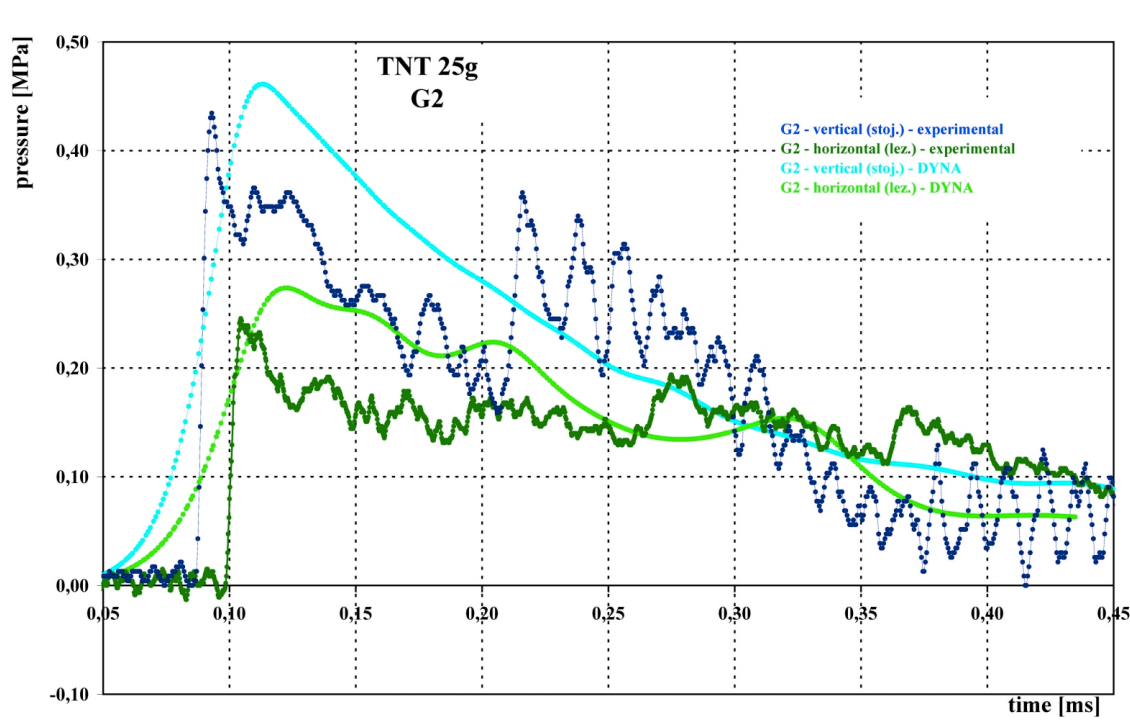


Fig 9. Experimental and calculated overpressure history for charge 25g TNT and gauge G2, stoj. – perpendicular charge, lez. – parallel charge

2.5 50g TNT charges

In fig.10, a comparison of numerical and experimental overpressure histories for the gauge G1 is introduced. In fig.11 a comparison of numerical and experimental overpressure histories for the gauge G2 is presented.

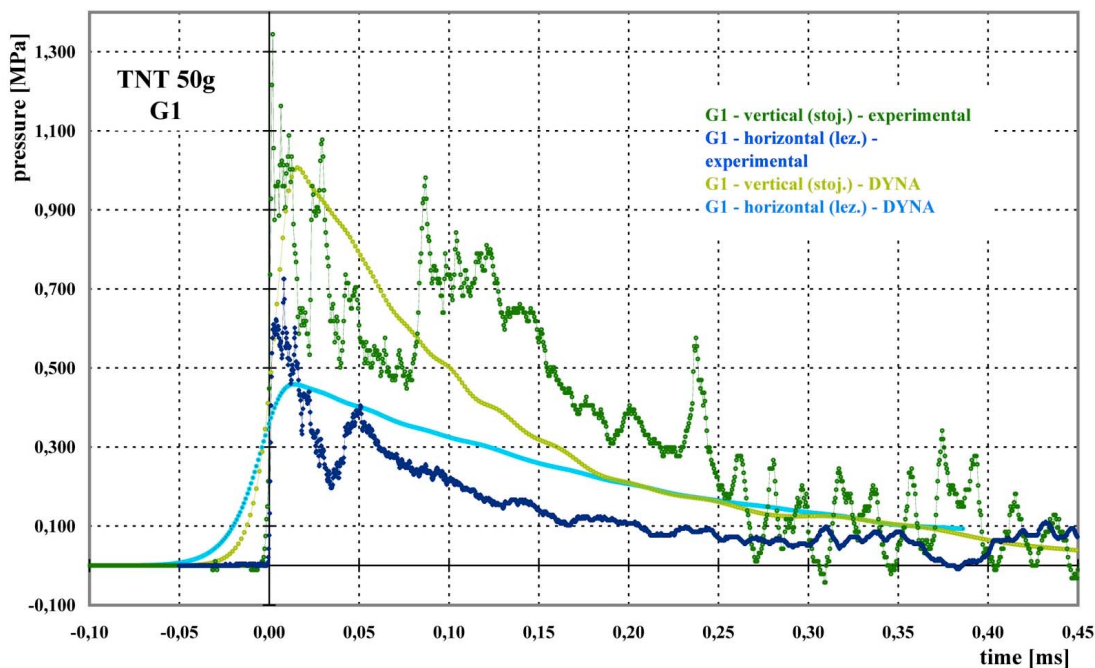


Fig 10. Experimental and calculated overpressure history for charge 50g TNT and gauge G1, stoj. – perpendicular charge, lez. – parallel charge

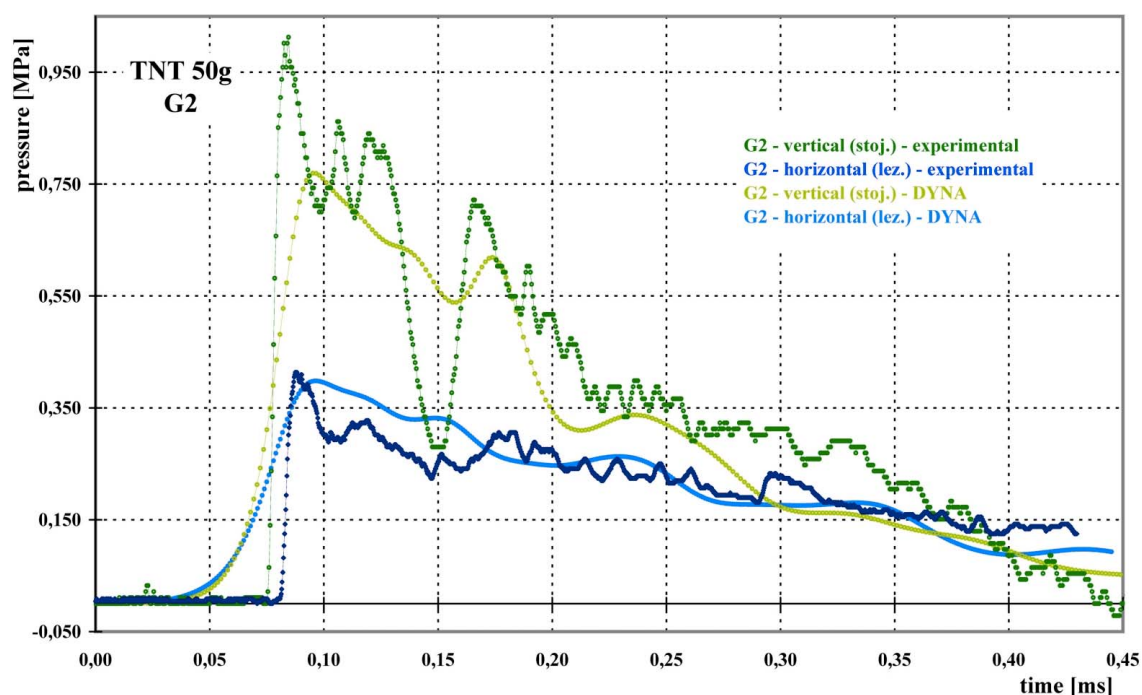


Fig 11. Experimental and calculated overpressure history for charge 50g TNT and gauge G1, stoj. – perpendicular charge, lez. – parallel charge

From the figures, it follows that a good agreement has been obtained for the gauge G2. As for the gauge G1, a great discrepancy exists in time history, the maximum overpressure values are in a good agreement.

The author of the experiments ^[4] have mentioned that the function of piezoelectric gauges PCB Piezotronics, Inc. was influenced by their “nest fixation” within the steel plate. From the comparison above, the authors of the paper presented may judge that the gauges function was not reliable sometime. The greatest discrepancies regard the gauge G1 for parallel charge 50g TNT and the gauge G1 for perpendicular charge 25g TNT. In spite of these facts, it is possible to conclude that numerical 3D simulations performed were very useful and effective. In any case, the simulations presented confirm that the blast waves generated by differently oriented cylindrical TNT charges depends strongly on charges orientation and the numerical results for pressure waves correlate well with observations obtained through the experiments.

3. CONCLUSION

The paper deals with numerical 3D simulation, through the code LS-DYNA, of the effects caused by air blast waves generated by cylindrical TNT charges (the mass of 25g and 50g) which are differently oriented respect to the pressure gauges placed relatively close to the charges (approximately 800 mm and 840 mm from the charges).

Application of the 3D dynamic Lagrangian explicit finite element code LS-DYNA has demonstrated possibilities existing in the field of interest.

The simulations have been compared with the original experiments performed at Military University of Technology in Warsaw. On the base of this comparison, it has been concluded that the 3D numerical simulations using LS-DYNA have been a very powerful and useful tools.

From the simulation presented it follows:

- the simulations confirm that the blast waves generated by differently oriented cylindrical TNT charges depends strongly on charges orientation which was observed through the experiments
- the simulations confirm that for the description of TNT and air dynamics the JWL and ideal gas EOS are faithful , respectively
- 3D numerical simulations of TNT cylindrical charges explosion can be very well substituted by the explosion of equivalent rotating ellipsoids charges
- simple rules for equivalent ellipsoids were derived and numerically verified
- for the numerical simulations, the characteristic element length should be: for the air around 10 mm, for the explosive around 1-2 mm

Further research in the field may be as follows:

- determination of optimal computational mesh for real cylindrical charges without their representation through equivalent ellipsoids
- numerical simulations of various charge orientation with the task to identify physical explanation of observed different effects on generated air blast waves

REFERENCES

- [1] LS-DYNA User's Manual: Nonlinear Dynamic Analysis of Structures, Version 950, Livermore Software Technology Corporation, May 1999
- [2] Fyzika vzryva: TOM 1, Moskva, Fizmatlit, 2002
- [3] DOBRATZ, B.M. AND CRAWFORD, P.C.: LLNL Handbook of Explosives, UCRL-52997, Lawrence Livermore National Laboratory, Change 2, pp. 8-21 - 8-23, 1985
- [4] W.A. TRZCIŃSKI ET AL.: Examination of characteristics of burst wave generated in detonation of crush charge of explosive, Biuletyn WAT, Vol. LII, Nr. 02, 2003
- [5] D.FIŠEROVÁ ET AL.: Systematic study of simulated mine explosions using AUTODYN, Proceeding of the VI. Seminar on New trends in research of energetic materials, University of Pardubice, Faculty of chemical technology, April 22-24, 2003
- [6] W. K. E. HUNTINGTON-THRESHER, I. G. CULLIS: *TNT blast scaling for small charges*, 19th International Symposium of Ballistics, Interlaken, 647-654, 2001
- [7] M. M. ISMAIL, S. G. MURRAY, *Study of the blast wave parameters from small scale explosions*, Propellants, Explosives, Pyrotechnics, **18**, 11-17, 1993
- [8] M. M. ISMAIL, S. G. MURRAY: *Study of the blast waves from the explosion of nonspherical charges*, Propellants, Explosives, Pyrotechnics, **18**, 132-138, 1993
- [9] Л. В. ШУРШАЛОВ: Численное исследование задачи о взрыве цилиндрического заряда конечной длины, ЖВМиМФ, **13**, 4, 1973
- [10] В. В. СЕЛИВАНОВ: Численная оценка влияния формы ВВ на параметры воздушных ударных волн, Физ. Гор. и Взр., **21**, 4, 1985

DETERMINATION OF THE CONSEQUENCES OF POSSIBLE INDUSTRIAL ACCIDENTS

V. Adamík*, B. Janovský** and A. Tkáč***

* External Consultant of the DTTX on Continuum Dynamics, CZ

** Department of Theory and Technology of Explosives,
University of Pardubice, 532 10 Pardubice, Czech Republic

*** Nuclear Power Plants Research Institute,
Okružná 5, 918 64 Trnava, Slovak Republic

Abstract:

The paper is devoted to calculations of the consequences relating to accidental vapour cloud explosions. For this purpose, a general methodology has been developed and applied. The methodology consists of two steps: the first one deals with blast wave characterization – Multi-Energy method has been used, the second one deals with the propagation of the generated blast wave in surrounding air and wave-building interaction – the LS-DYNA code has been applied. The methodology has been applied to a case of unconfined non-obstructed hydrogen cloud explosion in site. An example of the application is presented in the paper. The methodology presented can be used both to determine the consequences of an accidental vapour cloud explosions for risk analysis purpose and at the same time also as an optimization design tool which enables to minimize consequences of possible explosions taking into account various plant layouts.

Keywords: LS-Dyna, gas explosion, consequence analysis, Multi-Energy

1. INTRODUCTION

When a cloud of flammable vapour burns, the combustion may give rise to an overpressure or it may not. If there is no overpressure, the event is a vapour cloud fire, or flash fire, and if there is overpressure, it is a vapour cloud explosion. A vapour cloud explosion is one of the most serious hazards in the process industries. Vapour cloud explosions do occasionally occur and they tend to be very destructive.

In 1974 Flixborough ^[1] in the UK a large escape of cyclohexane from a temporary pipe on a train of reactors gave rise to a vapour cloud, which exploded with a TNT equivalent of some 16 t. The explosion demolished much of the works and killed 28 people, and fire burned for over a week. This incident was particularly influential in the development of major hazard controls in the UK and the European Community.

It is well known that it is more effective to prevent the accident than mitigate its consequences. However, it is possible to locate and lay out a plant so that injuries and damage are minimised if an explosion occurs. Strengthening of important building in the

process plant is another way how to protect the people and technology. It is always necessary to know the size of the blast load and its interaction with the building.

This paper presents a methodology of the blast load calculation during vapour cloud explosion. Two particular methods are used for calculation. The amplitude of blast wave is calculated using the Multi-Energy method ^[2, 3, 4, 5] and the wave propagation and the interaction of the blast wave with objects is assessed by LS-DYNA code. Short description of both methods is presented in the following paragraphs. An example of the application of the presented methodology is described in the second part of this paper.

2. MULTI-ENERGY METHOD – THE FIRST METHODOLOGY STEP

Experimental research during the last decade showed clearly that deflagrative combustion generates blast only in those parts of quiescent vapour cloud, which are sufficiently obstructed and/or partly confined ^[2, 3]. The conclusion that a partially confined and/or obstructed environment offers appropriate conditions for deflagrative explosive combustion has found general acceptance today. However, other parts of the cloud – parts, which are already in turbulent motion at the moment of ignition – may develop explosive, blast generating combustion as well. The remaining parts of the flammable vapour-air mixture in the cloud burn out slowly, without significant contribution to the blast.

Contradictory to conventional modelling methods in which a vapour cloud explosion is regarded as an entity, in Multi-Energy concept a vapour cloud explosion is rather defined as a number of sub-explosions corresponding to the various sources of blast in the cloud. This concept is illustrated in Fig 1.

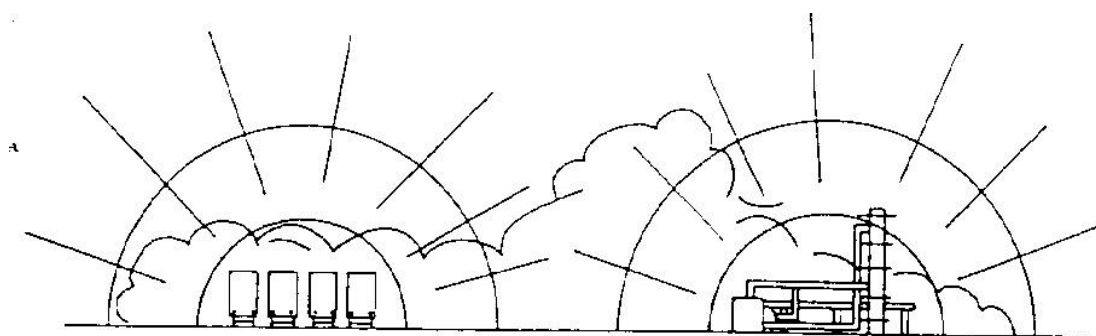


Fig 1. Vapour cloud containing two blast generating obstructed regions ^[2]

Generally, blast effects from vapour cloud explosions are directional. Such an effect, however, cannot be modelled without a detailed numerical simulation of phenomena. An easy-to-apply method, on the other hand, requires a simplified approach according to which blast effects are represented in an idealized, symmetric way. An idealised gas explosion blast model was generated by computation and is represented in Fig 2. Steady flame speed gas explosions were numerically simulated with the BLAST-code ^[6].

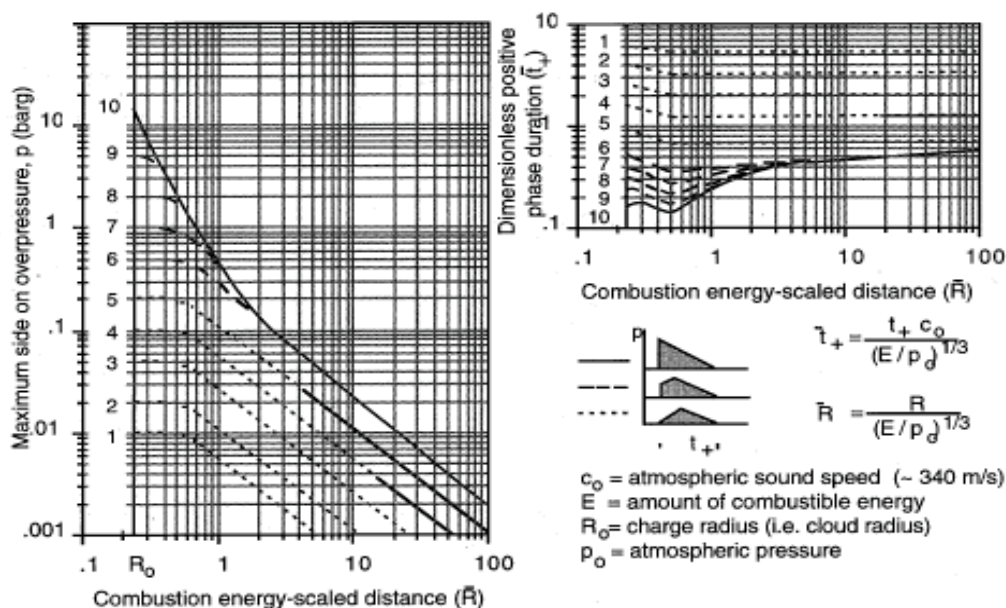


Fig 2. Multi-Energy blast chart [2]

The blast charts were composed for vapour cloud explosions having a combustion energy E_v of 3.5 MJ.m^{-3} which is the combustion energy for most hydrocarbon mixtures at stoichiometric concentration with air. Only the most significant blast-wave parameters such as the side-on peak overpressure ($\Delta \bar{P}_s$) and positive phase duration (\bar{t}^*) of the blast-wave are represented dependent on the distance to the blast centre for a hemi-spherical fuel-air charge radius r_0 on the earth's surface. The data are fully nondimensionalised, with charge energy (E) and parameters characterising the state of the ambient atmosphere: pressure (P_0) and speed of sound (c_0). This way of scaling (Sachs' scaling) takes into account the influence of atmospheric conditions and the blast parameters can be read off in any consistent set of units.

Initial conditions in the cloud, which are obstacle density, parallel plane confinement and ignition strength, are represented by initial blast strength. This initial blast strength is indicated by a number ranging from 1, for very low, up to 10, for detonative strength. The initial blast strength number is indicated in the charts at the location of the charge radius.

In addition, Fig 2 gives a rough indication of the blast wave shape, which corresponds to the characteristic behaviour of a gas explosion blast. Pressure waves, produced by fuel-air charges of low strength, show acoustic overpressure decay behaviour and constant positive phase duration. On the other hand, shock waves in the vicinity of a charge of high initial strength exhibit more rapid overpressure decay and a substantial increase in positive phase duration. Eventually, the high strength blast develops a behaviour approximating acoustic decay in the far field. Another significant feature is that, at a distance larger than about 10 charge radii from the centre, a fuel-air charge blast is more or less independent of initial strength for values of 6 (strong deflagration) and above.

Categorization of the initial blast strength is expressed in a matrix in Table 1, which gives the Multi-Energy method strength class numbers corresponding to the various combinations of the boundary and initial conditions.

Table 1. *Initial blast strength index*

Blast strength category	Ignition energy		Obstruction			Parallel plane confinement	Multi-Energy unconfined	Class	
	Low	High	High	Low	No				
	(L)	(H)	(H)	(L)	(N)	(C)	(U)		
1	L	H	H	L	N	C	U	7-10	
2		H	H						
3			H					C	5-7
4		H	L			C		5-7	
5	L	H	H	L	N	C	U	4-6	
6		H						4-6	
7									4-5
8		H						N	4-5
9	L	H	L	L	N	C	U	3-5	
10	L							2-3	
11	L					N		C	1-2
12	L					N			U

In the application of the Multi-Energy concept, a particular vapour cloud explosion hazard is not determined primarily by the fuel-air mixture itself but rather by the environment into which it disperses. The environment constitutes the boundary conditions for the combustion process. If a release of fuel is anticipated somewhere, the explosion hazard assessment can be limited to an investigation of the environment's potential for generating blast.

The Multi-Energy method was incorporated into some software codes, e.g. Breeze Haz Professional (Trinity Consultants, USA) ^[7].

3. LS-DYNA – THE SECOND METHODOLOGY STEP

LS-DYNA is the explicit dynamic Lagrangian finite element 3D code ^[8]. From the Multi-Energy method described above, the characteristics of the generated blast wave are known. The LS-DYNA code then must numerically simulate the wave propagation within the surrounding air continuum and at the same time has to evaluate the interaction of the wave with the important in-site buildings.

The solution of these problems by presented methodology is as follows.

The source of the explosion is represented by the pressure source surface on which the time history of the pressure wave is known from the Multi-Energy method. On this surface, the obtained pressure history is applied. The surrounding air is represented by a defined air zone within that the important buildings must be modelled.

The defined finite air zone (usually its dimensions are of about hundreds meters, but this is problem dependent) is divided into brick finite elements – 8-node element with one-point integration. The in-site buildings are usually represented by the building walls and roofs. The walls and roofs are modelled like rigid shell elements on which the surrounding air is acting.

The propagation, reflection, and superpositions of the pressure waves are automatically computed by the code. For high pressure (blast or shock waves) waves, the von Neumann and Richtmyer pseudoviscosities are applied. For low pressure waves these pseudoviscosities are not used because they represent system additional dissipation mechanism.

The interaction among the pressure waves and individual buildings is solved by means of the contact algorithm No. 2 of LS-DYNA. The main results of the analysis are total dynamic forces acting on building walls and roofs. These time histories can be used consequently for evaluation of the capability of the individual building to withstand the load. But this analysis is beyond the scope of this paper.

4. EXAMPLE

The volume and the location of the flammable vapour cloud must be known or assumed before the Multi-Energy method application. Source term models and dispersion models may be applied for this purpose. Furthermore, the lay out, or at least a rough impression of the build-up area where the cloud is located, must be available in order to determine the location, the number and the volume of the obstructed regions within the cloud. Then, the blast charts belonging to the Multi-Energy method can be applied to obtain values for the most important blast parameters. These parameters are used as an input into the LS-Dyna code.

In this example the most serious case is supposed. Therefore, the release rate and dispersion of the cloud is not calculated. It is assumed that hydrogen is stored in the 50 m³ vertical storage tank under pressure 4,5 MPa and all amount of hydrogen is immediately released during the accident. Concentration profile inside the cloud is neglected and stoichiometric mixture is assumed. The initial conditions are summarized in Table 2.

Table 2. *Initial conditions*

Amount of H2 in the cloud (Nm3)	2250
Weight of H2 (kg)	189,2
Volume of the stoichiometric mixture hydrogen/air (m3)	7500
Radius of the spherical hydrogen/air cloud (m)	12,1
Energetic content of the cloud (MJ)	2271,322

The initial blast strength index must be then determined. It is suitable to use the Table 1 to determined initial blast strength in the proposed example. It is supposed that ignition source with low energy ignites the cloud. No obstructions and no parallel plane confinement are presented in the cloud.

These conditions fulfill the blast strength category 11 according to the Table 1 therefore initial blast strength category 1 or 2 should be used. Hydrogen is highly reactive, so initial blast strength category 3 were used in order to be conservative.

Combustion energy-scaled distance \bar{R} is calculated according to equation

$$\bar{R} = \frac{R}{(E / p_0)^{1/3}} \tag{1}$$

and Dimensionless positive phase duration \bar{t}_+ is calculated according to equation

$$\bar{t}_+ = \frac{t_+ c_0}{(E / p_0)^{1/3}} \tag{2}$$

where R is charge radius, E is amount of combustible energy, p_0 is atmospheric pressure and c_0 is atmospheric sound speed ($\sim 340 \text{ m.s}^{-1}$).

Triangular shape is supposed because the blast wave could be characterized as pressure wave. The maximum overpressure is reached in time t_{\max} , which is half of the Positive phase duration.

Results of the calculations are written in Table 3.

Table 3. *Multi-Energy calculation results, Initial blast strength 3*

Object	Distance (m)	ΔP_{\max} (kPa)	Positive phase duration (ms)	t_{\max} (ms)
DGS	86	2,5	358	179
PE	160	1,3	358	179
SHN	165	1,2	358	179
BPP	175	1,2	358	179
VK	220	0,9	358	179
S	246	0,8	358	179

These data were input into the LS-Dyna calculations.

5. LS-DYNA MODEL

The solution of this example has been performed for an air zone with dimensions $350 \times 400 \times 200 \text{ m}$. Five buildings were placed into the zone: DGS, BPP, HVB, PE, S, see Fig 3.

The pressure blast source was supposed to have semispherical surface for this example. From this surface the blast waves is propagating into the surrounding air. The time history of the blast wave has a triangular shape, and it was derived by the approach above.

For the air dynamics the following state equation was used:

$$p = (\kappa - 1) \rho E \tag{3}$$

where:

p is pressure (initial value $p_0 = 1,0 \times 10^5 \text{ Pa}$), ρ is air density ($\rho_0 = 1,225 \text{ kg/m}^3$), E is internal energy ($E_0 = 2,5 \times 10^5 \text{ J/kg}$) and $\kappa = 1,4$.

Note: The simulations were performed in SI system units.

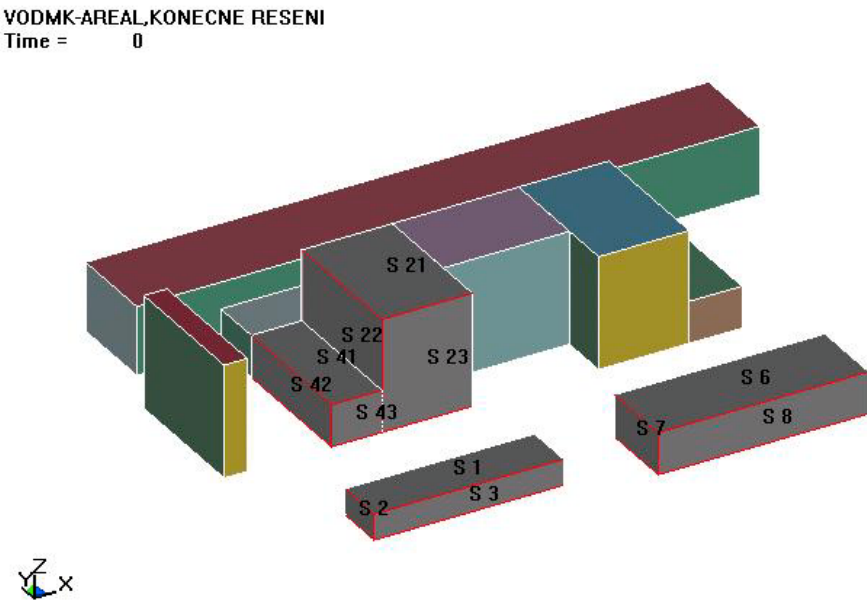


Fig 3. Buildings DGS with walls S2 and S3, roof S1

The parameters of the computational model were:

Total number of nodes: **381437**

Total number of brick elements: **362155**

Total numbers of shell elements: **50**

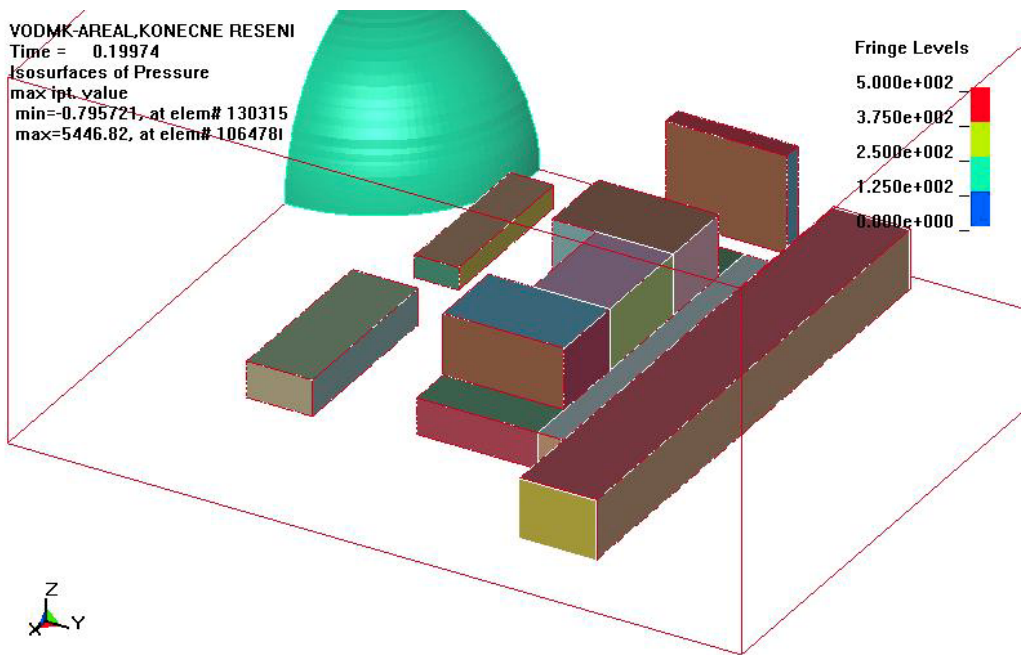


Fig 4. Pressure wave at 0,2 s

Fig 3 illustrates the computational zone with the in-site buildings. In Fig 4-8 the propagation of the pressure wave within the system is presented at times 0,2, 0,5, 0,8, 1,1, 1,5 s.

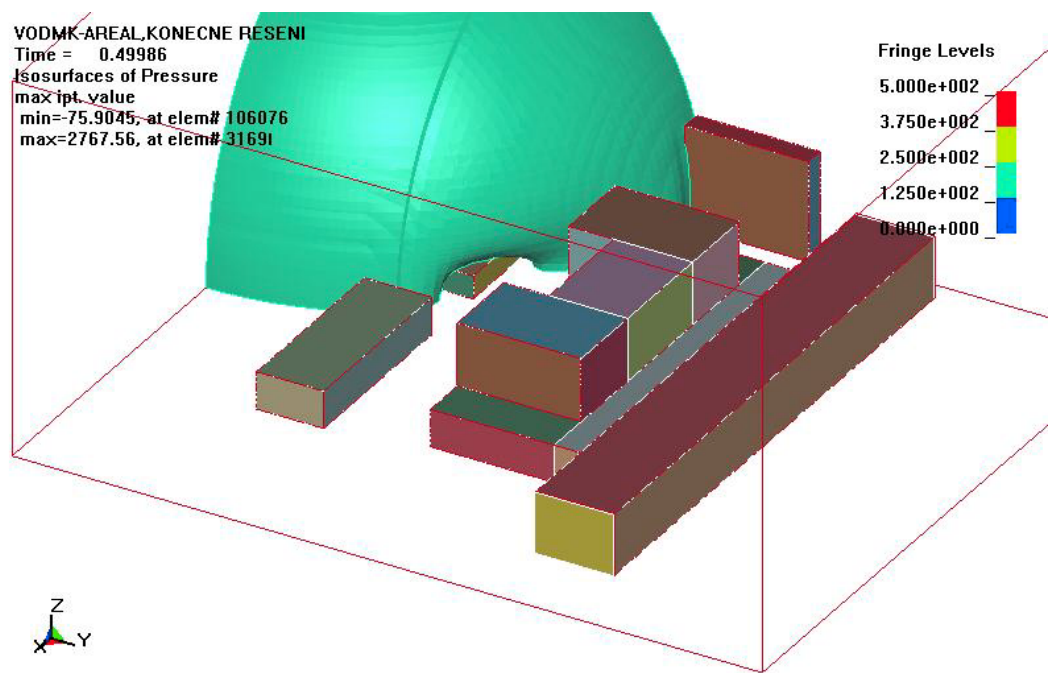


Fig 5. Pressure wave at 0,5 s

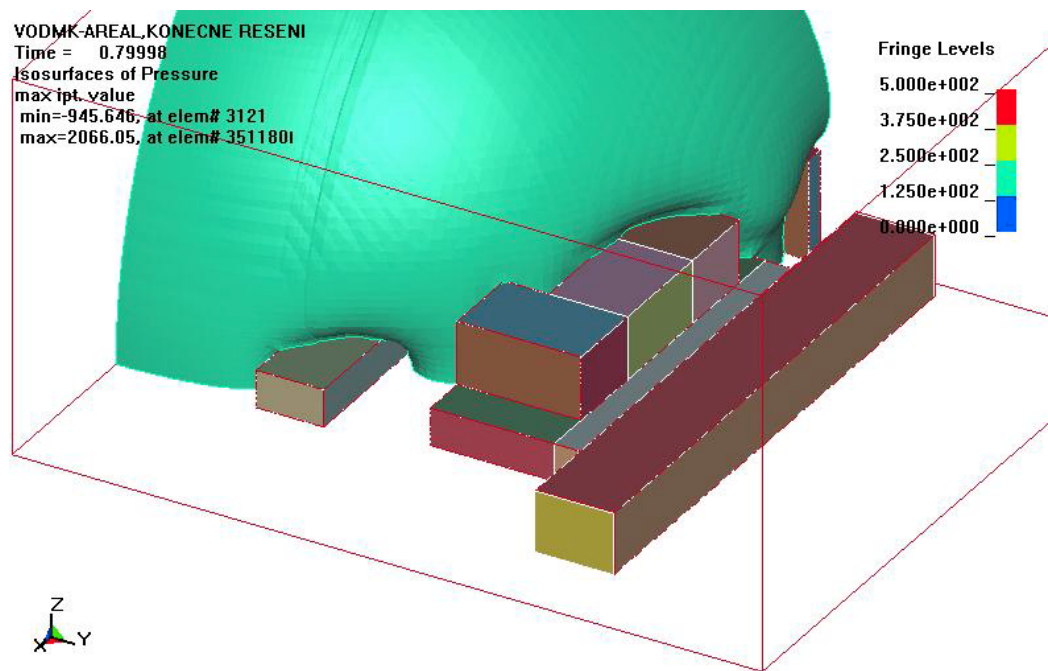


Fig 6. Pressure wave at 0,8 s

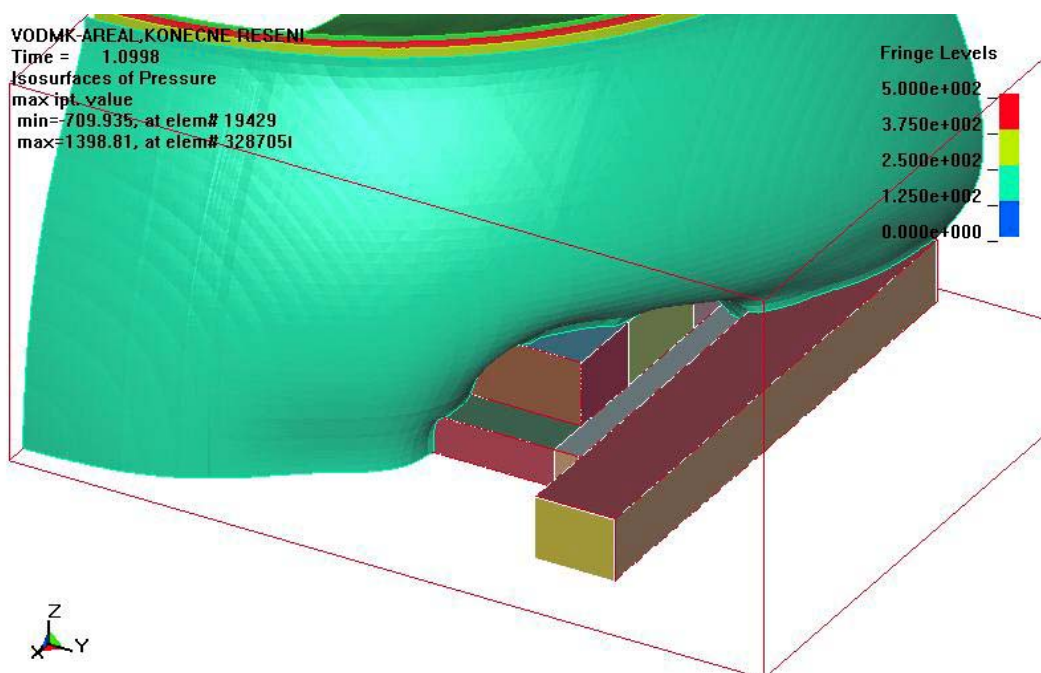


Fig 7. Pressure wave at 1,1 s

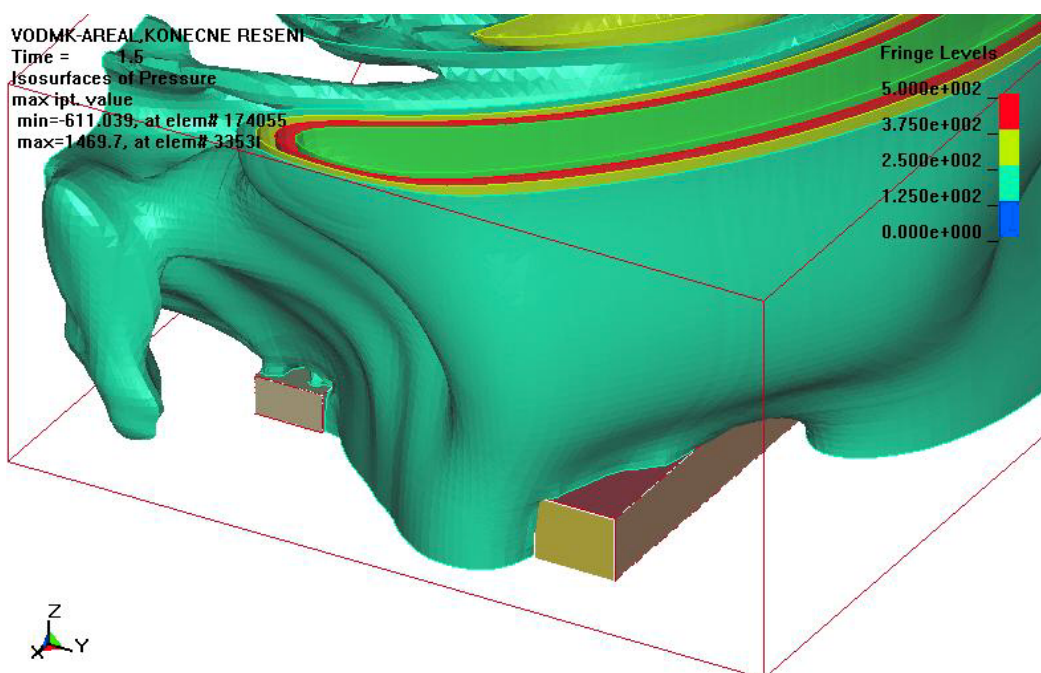


Fig 8. Pressure wave at 1,5 s

As an example, the building DGS is characterized, see Fig 3, by dimensions below. The object was modeled like a hexahedron with the walls and roof:

roof S1: $90 \times 24,0$ m, area $A = 2160 \text{ m}^2$

wall S2: $24 \times 12,3$ m, area $A = 295.2 \text{ m}^2$

wall S3: $90 \times 12,3$ m, area $A = 1107 \text{ m}^2$

In Fig 9, time history of the load function is presented for walls and roof, the corresponding maximum values are $F_{\max} = 2,5453 \cdot 10^6 \text{ N}$, $3,9018 \cdot 10^5 \text{ N}$, $1,6571 \cdot 10^6 \text{ N}$.

Maximum load pressure is respectively $p_z = 1,18 \text{ kPa}$, $1,32 \text{ kPa}$, $1,50 \text{ kPa}$. These values can be compared with limiting pressure values (including the dynamic load factor) and proper safety safeguards can be realized if needed. This analysis is outside the scope of the methodology.

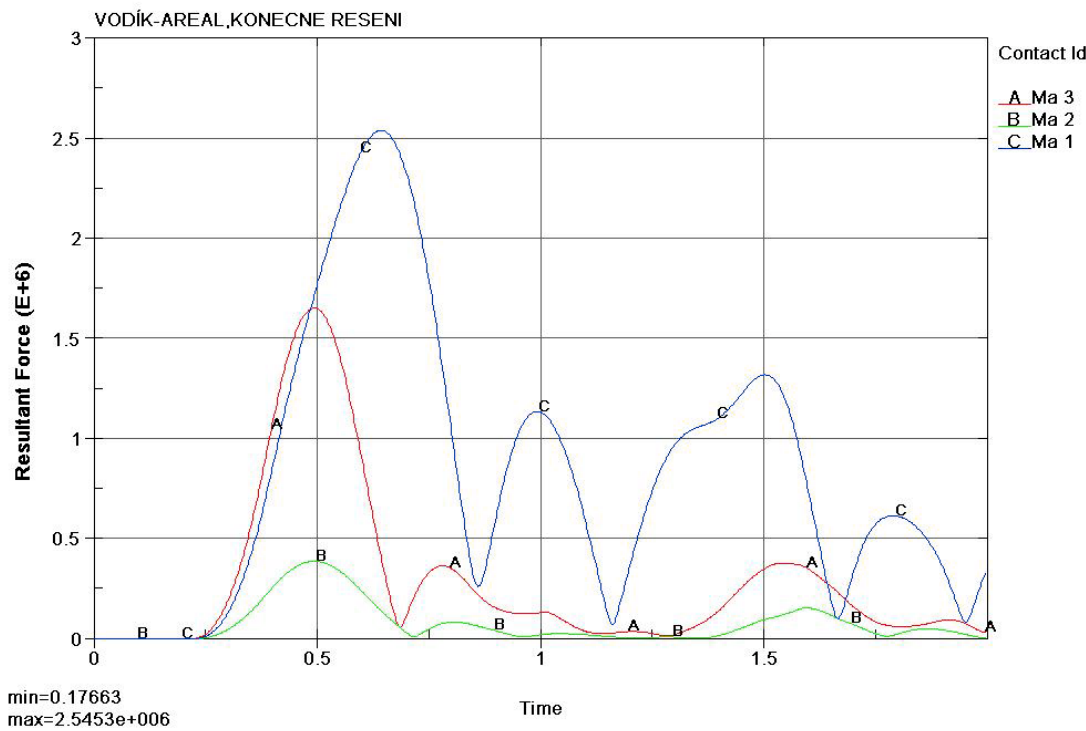


Fig 9. DGS building – load history for walls S2(B) and S3(A), and roof S1(C)

6. CONCLUSIONS

The paper is devoted to calculations of the consequences relating to accidental vapour cloud explosions. For this purpose, a general methodology has been developed and applied. The methodology consists of two steps:

- the first one deals with blast wave characterization – Multi-Energy method has been used,
- the second one deals with the propagation of the generated blast wave in surrounding air and wave-building interaction – the LS-DYNA code has been applied.

The methodology has been applied to a case of unconfined non-obstructed hydrogen cloud explosion in site. An example of the application is presented in the paper.

The methodology presented can be used both to determine the consequences of an accidental vapour cloud explosions for risk analysis purpose and at the same time also as an optimization design tool which enables to minimize consequences of possible explosions taking into account various plant lay-outs.

REFERENCES

- [1] KLETZ, T.: *Learning from accidents*, Butterworth-Heinemann, Oxford, 1994
- [2] *Guidelines for Evaluating the Characteristics of Vapour Cloud Explosions, Flash Fires, and BLEVEs*, Center for Chemical Process Safety of the AIChE, New York, 1994
- [3] *Methods for the calculation of physical effects Resulting from releases of hazardous materials (liquids and gases)*; CPR 14E, Yellow book; Sdu Uitgevers, The Hague, 3rd Edition, 1997
- [4] EGGEN, J.B.M.M.: *GAME: development of guidance for the application of the multi-energy method*, TNO Prins Maurits Laboratory for the Health and Safety Executive, Report 202/1998, 1998
- [5] MERCX, W.P.M., VAN DEN BERG, A.C., VAN LEEUWEN, D.: *Application of correlations to quantify the source strength of vapour cloud explosions in realistic situations. Final report for the project: "GAMES"*, TNO report PML 1998-C53, 1998
- [6] VAN DEN BERG, A.C.: *BLAST – a 1-D variable flame speed blast simulation code using a „Flux-Corrected Transport“ algorithm*, Prins Maurits Laboratory, TNO report No. PML 1980-162, (1980).
- [7] *BREEZE HAZ, User's Guide for the BREEZE HAZ PROFESSIONAL software package*, Trinity Consultants, Dallas, 1999
- [8] *LS-DYNA User's Manual, Nonlinear Dynamic Analysis of Structures, Version 950*, Livermore Software Technology Corporation, May 1999

TOPOGRAPHY OF REACTION ORIGATION OF SILVER AZIDE EXPLOSION DECOMPOSITION UNDER INITIATION BY ELECTRON ACCELERATOR PULSE¹

B.P. Aduiev*, V.P. Filin**, E.V. Tupitsin*, G.M. Belokurov*,
D.E. Aluker* and A.S. Pashpekin*

Kemerovo State University, 650043, Kemerovo, Russia

* Russian Federal Nuclear Center

All-Russia Research Institute of Technical Physics (RFNC-VNIITF)
456770, PO Box 245, Snezhinsk, Chelyabinsk region, Russia

Abstract:

The silver azide pre-explosive luminescence origination by electron pulse initiation in nidi and subsequent broadening of the luminescence ranges overlapping finally the whole sample. Hence, the origination nidi of the reaction are not caused by the local heating and they are not the hot spots in the true sense of the word.

Keywords: *pre-explosive luminescence, discrete centres, initiation, electron pulse*

In ^[1] pre-explosion luminescence of silver azide has been found by registrations under the pulse initiation during the induction time, i.d. in some interval between the initiation pulse and the decomposition onset (to be more exact deformation) of a sample in the process of the explosion decomposition.

In ^[2, 3] pre-explosion luminescence kinetics was shown to present that of initial stages of explosion decomposition chain reaction and, therefore, may be used for its “visualization”.

This finding was used to study the topography of the chain reaction origination of explosion decomposition for silver azide by laser initiation ^[4]

Pre-explosion luminescence (and consequently a chain reaction as well) appeared to be originated in the separate points (nidi) by laser initiation of highly ideal whisker crystals of silver azide.

Within several tens of nanoseconds the nidi grow and being overlapped form continuous luminescent range. One should point out that the control of both the laser beam homogeneity and a perfectness of the crystals does not enable us to account for the fact that the detected nidi are due to the beam inhomogeneity or the sample macro defects.

In ^[5] two possible causes of a nidum appearance were considered:

1. The point defect aggregation having a high absorption coefficient of laser radiation and providing in this connection excitation inhomogeneity (initiation). Such a probability is analysed in ^[6] for an extreme case of fully opaque (black) microinclusions. Here we really deal with a classical model of hot spots ^[7, 8].

¹ The work is supported by ISTC (project No. 2180).

2. The laser radiation absorption is homogeneous in the sample but there are some microareas (nidi) where the chain reaction initiation is facilitated for that or some reason.

In ^[3] some arguments are brought forward in favour of the fact that the nidi may be dislocations in the vicinity of which the band gap width greatly decreases. It is evident that to justify the choice between these probabilities it is necessary to carry out an experiment where the excitation homogeneity would be guaranteed, it being the task of our investigation.

A source of initiating pulse was heavy current pulse electron accelerator (a mean energy of accelerated electrons 300 keV, current density in the beam 10^3 A, duration of a pulse half-height 3–20 ns, beam inhomogeneity over a sample area less than 5%). The whisker crystals of silver azide of $100 \times 100 \times 1000 \mu\text{m}$ in size were used as samples.

An accelerated electron pass ($\sim 500 \mu\text{m}$) considerably exceeds the transverse sizes of the sample and it provides the homogeneity of the sample initiation if one takes into account the physical regularities for the initial radiation processes in condensed media ^[9].

An enlarged sample image was projected on an entrance window of streak-camera by means of an optical system, working in the time-sweep regime. The space resolution of the technique is $\sim 50 \mu\text{m}$.

As a whole, both the equipment and measurement technique applied were identical having the only distinction which is principal for the given research: electron accelerator was used as an initiation source, the latter providing the guaranteed homogeneity of the sample excitation.

Fig.1 presents the data for a number of samples.

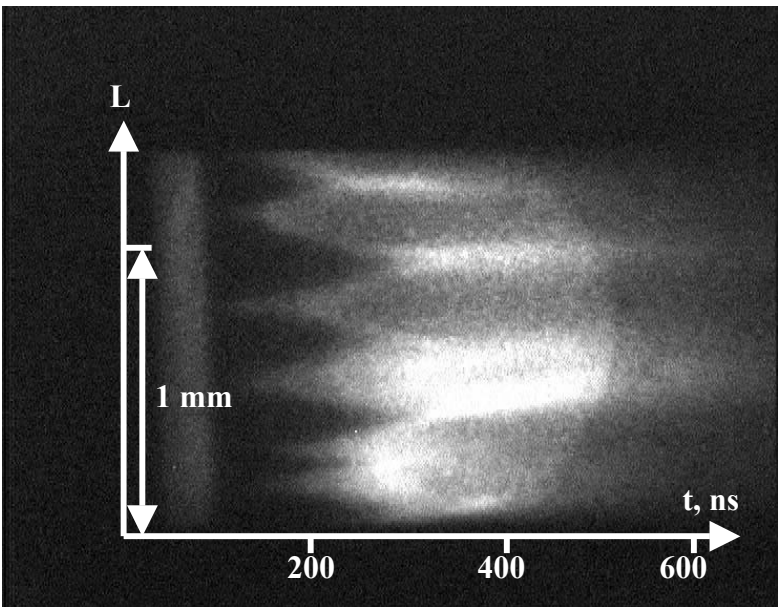


Fig 1. Time dependence of pre-explosive luminescence distribution through the length of the silver azide crystal by electron pulse initiation.

This situation is seen to be similar to that of the laser initiation ^[4,5]: the luminescence origination in nidi and subsequent broadening of the luminescence ranges overlapping finally the whole sample.

Taking the initiation homogeneity into consideration one should make an unambiguous conclusion: a nidum nature of the reaction origination of explosion decomposition is not caused by the energy absorption inhomogeneity of initiating pulse in the sample but it is of deeper causes.

It is due to the accelerator application that enables us to make one more seriously important conclusion.

Both the initiating pulse parameters and the radiation excitation homogeneity ^[9] do not result to the sample heating (in the local points as well!) enough for initiating thermal explosion decomposition reaction.

Hence, the origination nidi of the reaction are not caused by the local heating and they are not the hot points in the true sense of the word.

In summary, one should note that having found angular divergence of luminescence cones (see fig.1) one can estimate the reaction propagation rate over the sample as in articles ^[4,5]. When studied 20 samples the averaged value is in good agreement with the data obtained by laser initiation^[4].

REFERENCES

- [1] B.P. ADUEV, E.D. ALUKER, G.M. BELOKUROV, ET AL.: *Pre-explosive Conductivity of Silver Azide*, Vol. 3, **No. 3**, p.203-204, 1995
- [2] B. P. ADUEV, E. D. ALUKER, G. M. BELOKUROV AND ALL: *Explosive Decomposition of Heavy Metal Azides*, Journal of Experimental and Theoretical Physics, Vol. 89, **No. 5**, p.906-915, 1999
- [3] M.M. KUKLJA, B.P. ADUEV, E.D. ALUKER, ET AL.: *The Role of Electronic Excitations in Explosive Decomposition of Solids*, Journal Of Applied Physics, Vol. 89, **No. 7**, p. 4156- 4166, 2001
- [4] E.D. ALUKER, B. P. ADUEV, A. G. KRECHETOV, ET AL.: *Space-time Characteristics of Pre-detonation Luminescence Origin in Heavy Metal Azides*, In Proceedings VI Seminar New Trend in Research of Energetic Materials, Pardubice, Czech Republic, p. 12- 17, 2003
- [5] E.D. ALUKER, B. P. ADUEV, A. G. KRECHETOV, ET AL.: *Dynamic Topography of Silver Azide Pre-explosive Luminescence*, Combustion, Explosion, and Shock Waves, Vol. 14, **No. 4**, p. 86-91, 1978
- [6] E.I. ALEXANDROV, A. G. VOZNYUK.: *Lead Azide Initiation by laser pulse*, Combustion, Explosion, and Shock Waves, Vol. 39, **No. 5**, p. 105-108, 2003
- [7] F.P. BOWDEN, A. D. YOFFE. *Fast Reaction in Solids*, Butterworths Scientific Publications, London, 1958
- [8] J. E. FIELD: *High Speed Photography at the Cavendish Laboratory, Cambridge, (High Speed Photography and Photonics, S. F. Ray, Eds.)*, Focal Press, London, p.301-304, 1997.
- [9] *High Energy Electronics of Solid State*, (D. I. Vaysburd, Eds.), Nauka, Novosibirsk, 1982 (in Russian)

SPECTRAL-KINETIC CHARACTERISTIC OF PETN LUMINESCENCE UNDER INITIATION BY ELECTRON BEAM¹

B.P. Aduiev*, G.M. Belokurov*, N.V. Garmasheva, S.S. Grechin*,
E.V. Tupitsin*, and V.N. Shvayko****

* Kemerovo State University, 650043, Kemerovo, Russia

** Russian Federal Nuclear Center

** All-Russia Research Institute of Technical Physics (RFNC-VNIITF)
456770, PO Box 245, Snezhinsk, Chelyabinsk region, Russia

Abstract:

Spectral-kinetic characteristics of PETN single crystal explosive luminescence under initiation by a high-strength electron beam have been studied. It has been shown that spectra of radioluminescence arisen from the effect of an electron beam and spectrum of the following explosive luminescence coincide. The spectrum of pre-explosive glow has been found to be of luminescent nature. Linear spectrum of explosion products has been registered. It can be associated with molecular nitrogen luminescence.

Keywords: PETN, explosive luminescence, spectral-kinetic characteristics

A great deal of experimental information concerning physical-chemical processes taking place under explosion decomposition of heavy metal azides has been accumulated using heavy current electron beams and powerful laser pulses in connection with the method of pulse optical spectrometry with high time resolution.

The materials investigated belong to a wide class of initiating explosive substances. The similar experiments have not been performed up to now as applied to the secondary explosive substances which are analogous to PETN. The laser pulse exposure to the PETN free surface is not known to result in the explosion initiation at highly large magnitudes of excitation intensity ^[3].

In the research given to initiate PETN the electron beams of the pulse duration 20 ns, effective values of electrons 0,25 MeV and the current density in a beam $> 10^3$ A/cm² have been applied.

The PETN single crystals 3x4x0.5 mm size have been used as the object of investigation.

Spectra of explosion luminescence were measured employing an experimental installation consisting of UCP-51 spectrograph and FER-7 streak-camera ^[2]. The installation makes it possible to make measurements of luminescence spectra with high time resolution in a wide spectral range when a single sample was exploded.

¹ The work is supported by ISTC (project No. 2180).

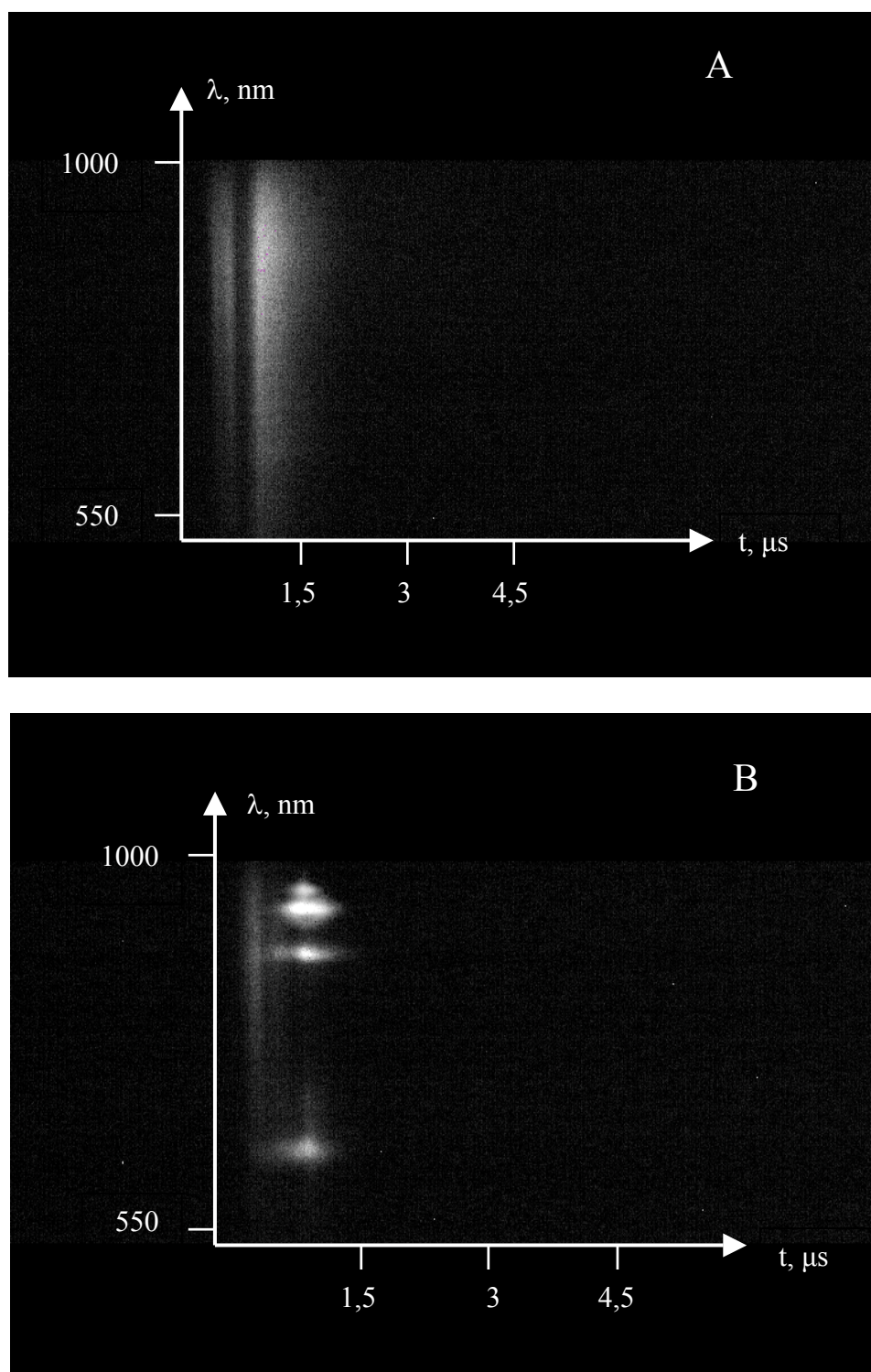


Fig 1. Time sweep of single PETN crystal explosion luminescence registered from output screen of streak-camera
 A – crystal is fixed around the edges
 B – crystal fixed on a substrate

Fig.1 presents explosion luminescence spectra of the PETN single crystals recorded by the output screen of the streak-camera.

In the case shown in Fig.1a. the crystal was fixed around the edges and placed at angle 45° with respect to the electron beam and optical axis of measuring circuit. As seen in the Fig.1, First the spectrum observed appears to be continuous one and second, at the onset the first relatively short luminescence is observed followed by more long-continued luminescence.

If one places the barrier as a transparent film before the crystal, there appears both the continuous and line spectra (Fig.1b). If the crystal is fixed on the metal substrate with its back surface with respect to the electron beam, one can see the same spectra.

Fig.2 shows the explosion luminescence kinetics with the wavelength $\lambda=770\text{nm}$ produced by the treatment of the data presented in Fig.1. The rise front of the first luminescence component corresponds to the electron beam pulse duration of 20 ns. Fig.3 gives luminescence spectra at some instant of time corresponding to luminescence maxima which are shown in Fig.2 with spectral sensitivity of the recording system taking into account.

The results obtained are interpreted as follows. First component of the continuous luminescence can be identified as radioluminescence arisen from an excitation pulse. The second component is associated with the crystal luminescence appearing due to the explosion decomposition development.

The line spectrum is attributed to the products arising as a result of explosion. The latter are scattered out of sight of the optical system and they are possible to be observed when there is a mechanical barriers (a film or a metal substrate). The lines noticed can be referred to molecular nitrogen luminescence [4].

The second component of the continuous spectrum is difficult to be interpreted. We have tried to answer the question if the luminescence is related to the heat radiation appearing as a result of heating during explosion decomposition. If the luminescence seems to be a heat radiation, one can apply the Wien displacement law $\lambda_{\text{max}}T=B$ and define its temperature. In our case $\lambda_{\text{max}}=850\text{nm}$ (Fig.3), hence, $T=3440\text{K}$. Further, using the Planck's formula the radiation spectrum of a black body has been estimated and shown in fig.3 (solid line). As seen in fig.3, the luminescence spectrum measured experimentally cannot be approximated as the heat radiation.

It should be noted that the radioluminescence spectra, spectrum of the first component and explosive luminescence spectrum actually coincide.

Thus, the luminescence observed should be treated as PETN crystal luminescence appearing during explosion decomposition development.

One can suppose that the luminescence kinetics represents that of explosion decomposition for PETN crystals. Additional investigations are necessary to find out both the reaction mechanism of explosion decomposition and luminescence nature.

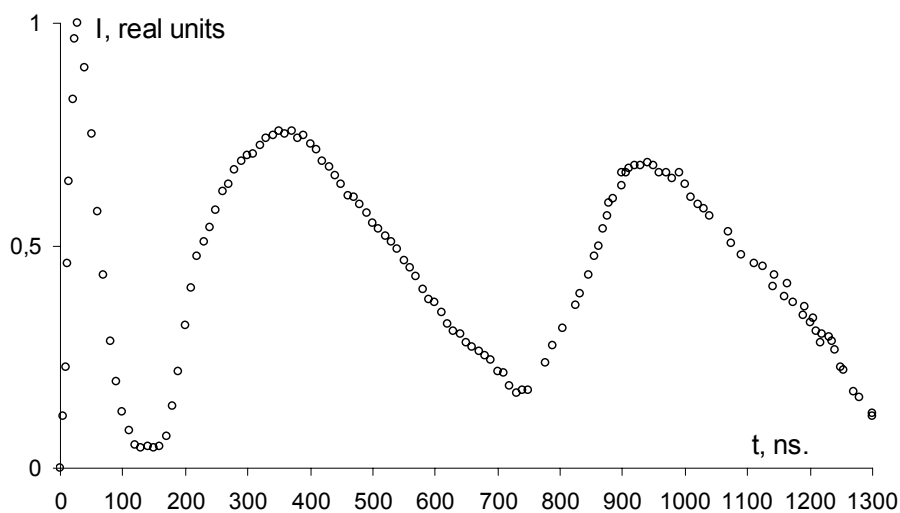


Fig 2. Kinetics of PETN explosive luminescence

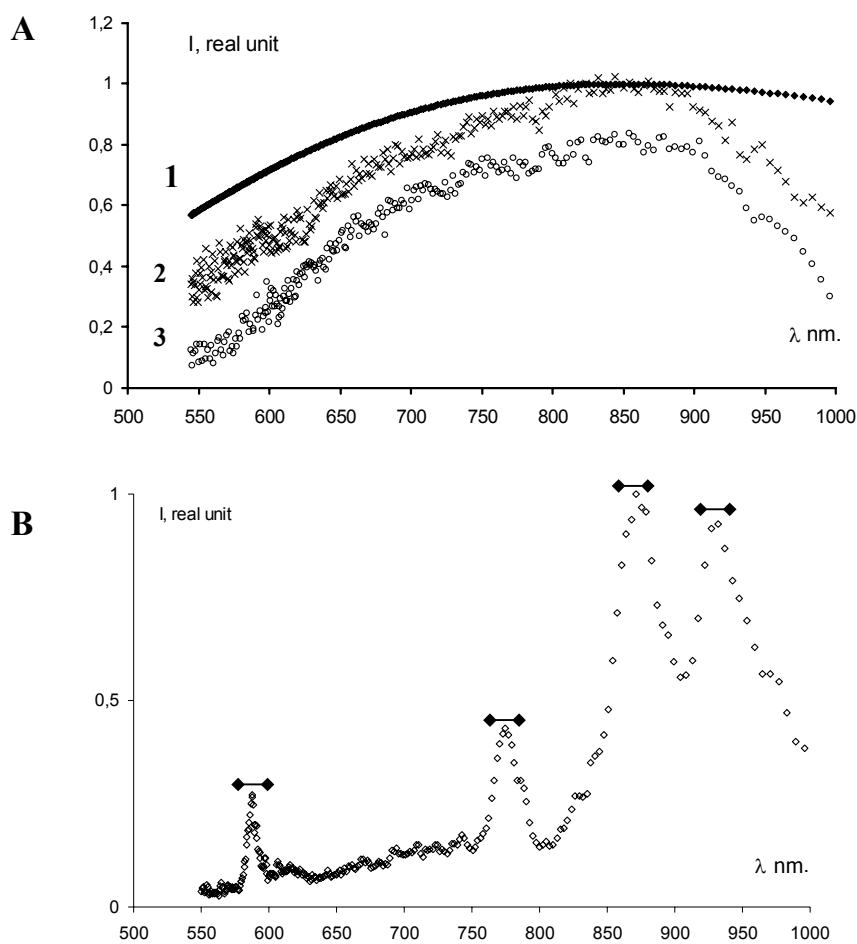


Fig 3. PETN explosive luminescence spectra.

A –PETN single crystal explosive luminescence spectrum

1 – radioluminescence

2 – pre-explosive luminescence

3 – the spectrum calculated for black body at $T = 3440\text{ K}$

B – the spectrum of PETN explosion products

REFERENCES

- [1] B. P. ADUEV, E. D. ALUKER, G. M. BELOKUROV, ET AL: *Explosive Decomposition of Heavy Metal Azides*, Journal of Experimental and Theoretical Physics, Vol. 89, **No. 5**, p.906-915, 1999
- [2] B. P. ADUEV, E. D. ALUKER, G. M. BELOKUROV, ET AL: *Predvzryvnye yavleniya v azidakh tyazhelykh metallov*, CEI “Khim mash”, Moskva, p. 116, 2002 (in Russian)
- [3] A. A. BRISH, I. A. GALLEEV, B. P. ZAICEV, ET AL, *Detonation Imitation of Condensed Explosive by Laser Radiation*, Combustion, Explosion, and Shock Waves, Vol.2, **No. 3**, p.132-133,1966
- [4] R. W. B. PEARSE AND A.G. GAYDON: *The Identification of Molecular Spectra*, London, 1941

THE EXPLOSION PARAMETERS OF BENZOYL AND CYCLOHEXANONE PEROXIDES

N.I. Akinin*, S.V. Arinina*, G.D. Kozak*, I.N. Ponomarev**

* Mendelev University of Chemical Technology
125047, Miusskaja sq. 9, Moscow, Russia

** Joint-stock company "POLION-P"
125047, Miusskaja sq. 9, Moscow, Russia

Abstract:

The ultimate objective of the work was to investigate the ability to heat explosion, burning and detonation of some organic peroxides. The main attention was paid in previous work to investigation of cumene hydroperoxide (CH). The properties of benzoyl peroxide (BP), and cyclohexanone peroxide (CHP) were collected and analyzed in this work. The explanation of the investigation results focused on identifying the most probable occurring chemical reactions at decomposition, heat explosion, burning and on reaction thermochemistry data. The data of investigation in couple with literature materials characterize net cyclohexanone peroxide, cumene hydroperoxide, and benzoyl peroxide as weak explosive, which are able to burning, low velocity detonation, and heat explosion. The results of investigation update the information concerning to explosion characteristics of CHP, CH, and BP and they could be used to achieve accident prevention goal on the plant facilities at its production, processing treatment, and transportation.

Keywords: explosion, hazard, peroxide, burning, detonation

1. INTRODUCTION

The explosion hazard of typical explosives is estimated at experimental and calculating investigation of some parameters. It is important to know the parameters and intensity of heat explosion of the substance, ability to burning without access for air, and ability to detonation. Such approach is necessary condition of industrial safety in the branch of manufacture and treatment of explosives. Peroxides are not applied as explosives, but they find an extensive application as initiator of polymerization, they have a peroxide group -O-O-, which is explosiphore one, and could provide them explosiveness^[1]. There were great number of incidents with CH and much more with BP described in literature, and some of them thoroughly investigated. Considerable portion of these incidents had fatal consequences.

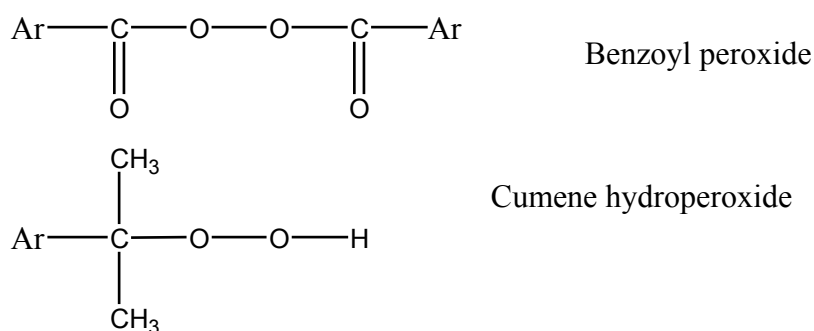
The mechanism of polymerization with peroxides applying has a chain character, foundation of which is Chain Reaction Theory of academician N.N. Semenov. With this respect the branch of chemistry of polymerization close connects with Theory of Explosives, one section of which deals with chain acceleration of chemical reaction.

We used the complex investigation methodology, which had been created, in Mendeleev University of Chemical Technology for explosion hazard estimating of typical explosive system. The methodology included calculation of the explosion parameters: heat of explosion, detonation velocity etc., and experimental measuring of some parameters velocities of burning and detonation, temperature of decomposition beginning, etc. [2-5].

The main attention was paid to benzoyl peroxide (BP) and cyclohexanone peroxide (CHP); bearing in mind that explosion hazard of cumene hydroperoxide (CH) was investigated and discussed in previous work [6].

Typically, the first step in hazard evaluation of substances was a literature searches. We used the searches: scientific and technical literature [7-13], International Chemical Safety Cards (ICSC, Internet), Database of National Institute of Standards and Technology (NIST, Internet), Hazardous Chemical Database (HCD, Internet).

BP and CH are derivatives of benzene, represented by the chemical formulas:



Their properties were collected and presented in work [6]

Cyclohexanone peroxide according to the data of literature [12] can exist in some isomeric modifications (Table 1).

BP and CH has long been recognized as unstable chemical and explosive. International chemical safety cards characterize CH and BP as combustible and explosive substances.

Neither explosion properties nor even enthalpy of formation (ΔH_f) of cyclohexanone peroxide were found in literature. Meanwhile the value of ΔH_f is necessary to compute explosive parameters. The enthalpies of formation of CHP isomers were calculated by means of two methods: taking account deposits of chemical bonds [14], and with the applying the package of computer programs ChemOffice, which used quantum chemical methods of calculation [15]. The results of calculation according the both of methods were close each to another for every isomer; the average values of ΔH_f are collected in Table 1.

The computer code SD [16] was used to calculate the detonation parameters of peroxides under investigation, and modified method [14,17] was used to estimate its explosion temperature at constant pressure. The reaction products according the both of methods were determined by reactions equilibrium including hydrogen, carbon, and products of its oxidation. The calculating parameters of peroxides are: explosion heat - Q, detonation temperature - T_D , detonation velocity - D, temperature of explosion (at P = 10 MPa) - T_p . Calculated principle products are: condense carbon, CH₄, CO₂, CO, H₂O, H₂.

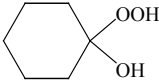
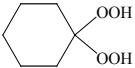
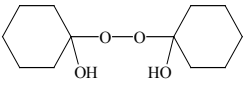
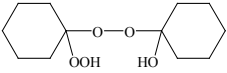
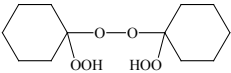
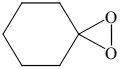
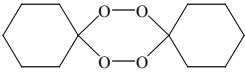
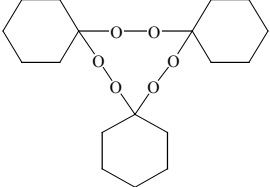
2. EXPERIMENTAL

We had at our disposal the commercial grade product CH, which are named in Russia “Hyperiz”. The product was certificated according technical conditions of Russia № 38.402-62-121-90 and contained net cumene hydroperoxide not less than 89%.

The commercial grade product of cyclohexanone peroxide, solidifyer for encapsulator (technical conditions of Russia 2257 – 036 – 18563945 – 2001), was at our disposal.

BP of laboratory preparing was given in our disposal as water suspension. BP was separated from water, it was twice washed out with alcohol, and then drying of BP was carried out at room temperature (without heating) to constancy of mass. Dry BP had the melting point coincided with literature data $t_m=103\text{ }^{\circ}\text{C}$.

Table 1. . *Structure and some properties of the Cyclohexanone peroxide isomers*

№	Structure of isomer	Melting point, °C	ΔH_f^{gas} , kJ/mol ^{*)}
I		-	-409.2
II		-	-332.6
III		69 – 71	-652.3
IV		78	-573.6
V		82 – 83	-497.5
VI		70 – 72	-149.0
VII		127 – 129	-339.3
VIII		93	-586.2

^{*)} Average values of ΔH_f^{gas} were calculated in this work.

The commercial grade products on base CH and CHP were analyzed by mean of spectrum analysis. Content of CH in Hyperiz complied with demands of technical conditions.

According to spectrum analysis of the commercial grade products on base CHP is solution CHP (33%) in inert component (composition is presented in Table 2). Isomer CHP-V according to analysis is the main part of peroxide component in solidifyer Table 3.

Table 2. *Content of solidifyer on a base CHP*

Substance	CHP	Cyclohexanone	Dimethylphtalate	Diethylenglycole
Content, % mass.	33	6	23	38

Table 3. *Content of CHP isomers in peroxide component of solidifyer*

CHP isomers (see Table 1)	I	II	III	IY	Y	YI	YII	YII
Content, % mole	32		5	13	50	-	-	-

Decomposition of peroxides under heating was investigated in glass laboratory apparatus, consisting from two test-tubs, one of them (d=13 mm) was put into another (d = 30 mm). The substance under investigation (m=0.3-1 g) was placed into inner test-tube and was heated by electric spiral, which was wound on the external test-tube. The temperature of the sample was measured by thermocouple device, which registered the curve temperature vs. time. The working thermocouple was protected by the mean of quartz capillary. The velocity of heating (20-50 degrees/min) was regulated by mean of tension current on the spiral ^[6].

Burning of CH was investigated in the bomb of constant pressure in atmosphere of nitrogen over the pressure range 24 to 36 MPa. The same micro-thermocouple methodology as in work ^[9] was applied for measuring the temperature profile at burning of CH. The burning rate versus pressure was measured by the mean of drum photo-register device in passing through light, because the own luminescence of CH burning was too weak to be registered.

Induction period of heat explosion versus initial temperature was investigated in inertial aluminum thermostat in the range of temperature from 100 to 150 °C for BP and some experiments with CH were carried out at 266 °C.

Investigations of detonation ability of CH and BP were carried out in steel tubes of 10 mm inner diameter, 13mm wall thickness, length l=250 mm, and 9 radial holes d=2 mm were drilled in wall ^[6]. The pressed pellets of phlegmatized RDX (d=12 mm, m=2 g, density $\rho=1.67-1.68 \text{ g/cm}^3$) were used as powerful initiator. The high velocity detonation (3-7 km/s) destroyed the steel tube on fragments. The low (1.5-2 km/s) velocity detonation (LVD) didn't crash the tubes.

Russian streak camera GFR-3 was employed to measure detonation velocity. The luminosity at detonation of BP and CH was too weak for registration by means of photography, and “to develop” the process propagation on streak camera record we used the same technique, as in work ^[6]. Small amount (~0.02 g) of lead azide was promptly placed into each hole on paraffin plug, and then the holes were glued up with a scotch. Luminosity of lead azide flashes fixing in streak camera record helped to judge about a stability of process, and to measure its velocity. Foundation of the registration method is thoroughly described in work ^[6].

3. CALCULATION AND EXPERIMENTAL RESULTS

Results of calculation of explosion parameters are collected in Table 4. One can see that CHP has the largest value of Q, its heat explosion is comparable with Q of threenitrotoluene. A destructive effect of explosion depends on this parameter ^[1], and production of solidifyer, containing CHP, in the form of dilute solution in inert component seem the well-founded step. Calculated heat of explosion of mixture CHP-V with diethilene glycol 50/50 gave negligible value, Q=630 kJ/kg. Explosives having such a small heat of explosion are unknown. So one can conclude that commercial grade solidifyer containing 33% of CHP and having still less Q value is nonexplosive liquid. Commercial grade solidifyer containing 33% of CHP was heated in glass thermostat (m=5 g). Decomposition of CHP began at t=100 °C, the bubbles of gases evolved, and growth of the temperature accelerated but heat of peroxide decomposition is spent on heating and boiling of inert solvent, and temperature of substance under investigation did not exceed t=210 °C (Fig. 1). There were not explosion or appearance of the flame. When all peroxide decomposed boiling and evolving stopped and lowering of temperature began.

Table 4. Calculating explosion parameters of peroxides under investigation at density $\rho = 1.1 \text{ g/cm}^3$

Peroxide	Q, MJ/kg	D, km/s	P, GPa	T _D , K	T _p , °C At P=10 Mpa
CHP-V	3.97	5.19	6.32	2039	1024
CH	3.14	4.40	4.10	1682	918
BP	2.37	2.96	1.89	1609	970

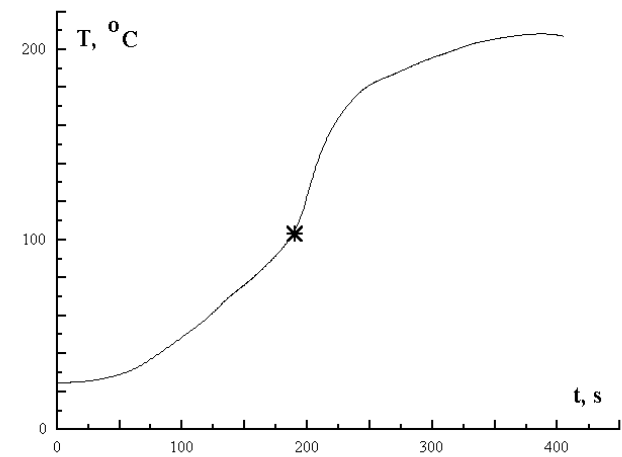


Fig 1. The temperature versus time curve at heating and decomposition of commercial grade solidifyer, containing 33% of CHP.

There were no any visible qualitative changes during approximately linearly law of CH heating ($m=1$ g) in glass thermostat. The moment of very beginning of decomposition (140-160 °C) coincided with acceleration of temperature increasing. Gasification (pseudo-boiling) intensified at self-heating of CH, the droplets of a decomposition products condensed on the wall of test-tube and flew down. At decomposition passing primary colorless substance became a light-brown one. A flame has never appeared at CH decomposition under these conditions ^[6].

Heat explosion of BP was investigated at mass $m=0.3-0.5$ g and velocity of heating 28-23 deg/min. Heat explosion was accompanied by flash and sound effect. There was explosion, destroyed glass apparatus in the run at $m=0.5$ g and velocity of heating 15 deg/min, the intensity of heat explosion in this experiment was high though small mass of BP. The results are shown in Table 5.

The dependence of heat explosion induction period of BP vs. inverse temperature was measured ($m=1$ g) (Fig. 2). The activation energy was calculated taking into consideration these data $E_{BP} = 122$ kJ/mol, this value practically coincides with data of literature. Heat explosion of CH in some experiments at $t=168$ °C was accompanied with flame appearance.

Table 5. *Experimental results of BP behavior at heating*

M, r	Velocity of heating, deg/min	Beginning of decomposition		T_{flash} °C	Result
		T, °C	t, min		
0.3	28	91	3.1	120	Flash
0.5	23	92	3.2	106	Flash
0.5	15	96	5.5	125	Explosion

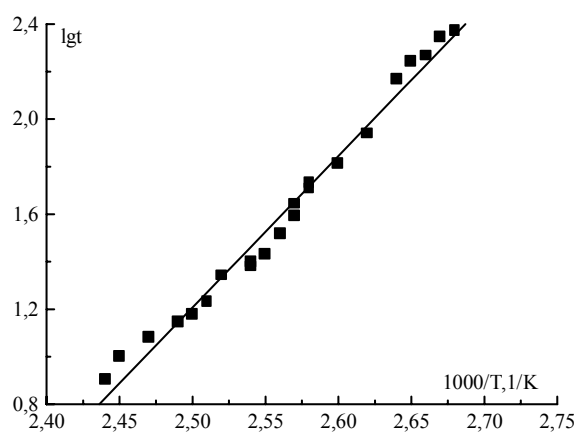


Fig 2. The dependence induction period of heat explosion of BP vs. inverse temperature

Burning of BP had been thoroughly investigated over the pressure range 0.02 to 40 MPa in the work ^[9]. Not only burning law (velocity vs. pressure) of BP was measured, but temperature of burning, and dependence of burning rate from initial temperature were experimentally investigated.

Stable burning of CH propagated in quartz glasses by a diameter of 12 mm at pressure $p=24$ MPa and higher ^[6]. The wolfram-rhenium micro-thermocouples (W+20% Re and W+5% Re, thickness of wires was 50 and after rolling was 20 micrometers) were used to register the profile of temperature at burning of CH. The maximum of temperature $T_m=555^{\circ}\text{C}$ was found to situate practically on the burning surface.

The burning laws (u , mm/s vs. pressure) of BP and CH are compared in Fig.3.

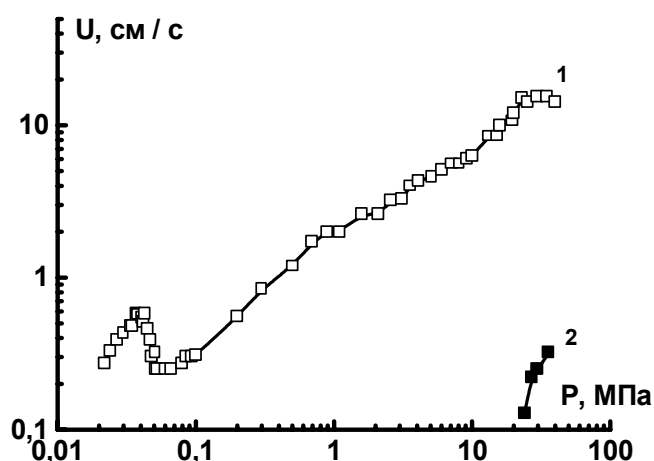


Fig 3. Velocity of burning vs. pressure: 1- BP ^[9], 2 - CH

At the powerful and less powerful initiating ($P_{in}\sim 30$ GPa and $P_{in}=18.2$ GPa) of CH detonation process propagated with constant velocity 1.87 and 1.97 km/s correspondingly. At the lower initiating pressure (4.3 and 1.5 GPa) low velocity detonation damped to the end of tube, the slope of a lines connecting points-flashes of lead azide in a records diminished to the bottom of tube. The streak camera records are shown in wok ^[6].

Investigation of ability to detonation of BP was carried out in the same tubes. Results are collected in Table 6. In powder-like BP charge (density $\rho=0.4-0.57$ g/cm³) at powerful initiating ($P_{in}\sim 30$ GPa) the explosion process propagated along the full length of tubes, but at the beginning of the charge, near initiator, the velocity was higher, and to the its middle diminished to value ~ 1 km/s and became stationary one. If for initiation of explosion process the standard detonator № 8 was applied the velocity was constant along the full length of tubes ($D=0.8$ km/s).

Explosion process propagated in charge (pressed pellets of BP) at density 1.3 g/cm³ at powerful initiation, velocity of process changed from 2.19 to 1.76 km/s along the length of the charge. The explosion process was not initiated by the standard detonator № 8 in pressed BP.

Explosion process propagated in suspension of BP in water at density 1.09 g/cm³ at powerful initiation, velocity of process to the end of charge was stable $D=1.2$ km/s.

Table 6. *BP explosion process velocity of in steel tubes*

Density ρ , g/cm ³	Length of tube, mm	Initiation	D, km/s
0,4	240	Powerful	1.28→0.70
0.57		Powerful	1.77→1.00
0.57		Cap № 8	0.80
1.3		Cap № 8	No initiation
1.3	72	Powerful	2.19→1.76

4. DISCUSSION

The decomposition reactions occurring in CH according to literature ^[11] are (1) and (2). Both of the reactions are characterized by release of energy.



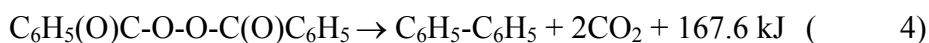
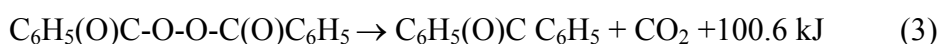
The decomposition rate constant of CH is $K=0.0108 \text{ hour}^{-1}$, activation energy is $E=100 \text{ kJ/mol}$ ^[8]. Pre-exponential factor was estimated taking into consideration these data: $B=K/e^{-E/RT} \approx 10^8 \text{ s}^{-1}$.

The sample of CH by several grams weight at heating decomposed with temperature arising and self-acceleration but without appearance of flame in the laboratory experiments at linear low of heating. An intensity of heat explosion is well known to depend on mass of explosives under heating. The incidents occurring at some facilities involving CH, described in literature ^[10,11], e.g. at hot streaming of vessels contained the leavings of CH, make this assumption objective. Heat explosion of CH in some experiments at high temperature, as it was marked above, was accompanied with flame appearance.

Heat explosion of BP is very intensive even at $m=0.5 \text{ g}$.

High explosion hazard of BP probably connects with its high ability to burning and high intensity of heat explosion. BP burns faster than nitrocompounds, as it was marked in work ^[9], and it able to burn in wider diapason of pressure than they and CH (Fig. 3).

We didn't observe the any amount of carbon or gases created at CH burning in bomb of constant pressure, the quartz glass to the end of burning was filled up by light brown liquid. The experimentally measured temperature of burning was sufficiently lower than computed temperature T_p . These facts testify to leading reaction occurs in condensed phase. The same conclusion was made earlier at investigation of benzoyl peroxide burning. The decomposition reactions (3) and (4) surmised to proceed at burning of BP ^[9].



If the proposed model is true, one could assume that overall reactions occurring at burning of CH are the same ones at the decomposition, i.e. reactions (1) and (2). The reaction temperature was calculated at heat capacity $c=2.1$ kJ/kg K. At heats of reactions (1) and (2), estimation gave the temperatures correspondingly: $T_1=720^{\circ}\text{C}$ and $T_2=477^{\circ}\text{C}$. One may conclude that occurring of exothermic reactions (1) and (2) can ultimately increase the temperature to 555°C , which was fixed at burning experimentally.

The burning of CH was found to propagate at pressure $P\geq 24$ MPa. However, luminosity of flame was too weak to be registered by mean of photography, it could be explained taking into consideration the low temperature of burning and absence of carbon, water, and carbon dioxide in principle burning products. These products could provide to the flames intensive self-luminosity but they are not created as a result of reaction (1) and (2).

BP and CH detonation was observed to propagate in steel tubes as low velocity explosion process $D\approx 1\text{--}2$ km/s. The minimal shock wave pressure to initiate the stable low velocity detonation of CH was $P_{\text{in}}=18.2$ GPa, at $P_{\text{in}}=4.3$ GPa the process damped.

It is clear that inflammability of BP diminishes when it covered with water at storage and transportation, but one must bear in mind that shock wave can initiate explosion process in such suspension.

One must note that detonation pressure at velocity $D\approx 1\text{--}2$ km/s is approximately $P\approx 0.5\text{--}1$ GPa, in other words, shock wave generating by such explosion process or by heat explosion of large amount of peroxides can cause rather high destruction effect.

5. CONCLUSION

The data of investigation in couple with literature materials characterize cumene hydroperoxide and benzoyl peroxide as weak explosive, which are able to burning, low velocity detonation, and heat explosion. The results of our investigation update the information concerning to explosion characteristics of CH and BP and they could be used to achieve accident prevention goal on the plant facilities at its production, processing treatment, and transportation. Dilution of peroxides with inert solvents lowers its explosion properties and reduces its explosion hazard as it was shown in the example of commercial grade solidifier containing 33% of CHP.

It is necessary to note that decomposition of cumene hydroperoxide (exothermic reaction 1) in technological process of acetone and phenol production^[8] is carried out at excess of final product – acetone, which are added before beginning of process. Heat of reaction (1) consumes on boiling and rectification of this final product, and temperature of reaction proceeding never reaches to the heat explosion point of CH.

ACKNOWLEDGMENT

Post-graduate student E.I. Aleshkina and students: I.A. Burtseva and A.V. Muratova took part in carrying out some of the experiments and calculation.

We are grateful to Russian Foundation of Basic Research (RFBR) for partial financial support. (Grant №01-03-32610-a).

REFERENCES

- [1] K.K. ANDREEV, A.F. BELYAEV: *Teoriya vzryvchatykh veshchestv* (Rus.). M.: Oborongiz, 595, 1960
- [2] B.N. KONDRIKOV, G. D. KOZAK, V. M. RAIKOVA. et al.: *Explosion hazard of some liquid nitrocompounds*, Khim. Prom., №. 5, 26, 1990
- [3] G.D. KOZAK, V.M. RAIKOVA: *Energetic characteristics of amonium peroxocompounds of niobium and tantalum*, Trans. of the 26-th Int. ICT Conference, Karlsruhe, FRG, 290, 1995
- [4] G.D. KOZAK, V.M. RAIKOVA: Khim. Prom.: *Explosion hazard of amonium peroxocompounds of niobium and tantalum*, № 2, 15, 1992
- [5] G.D. KOZAK, B.N. KONDRIKOV: *The peculiarities of detonation of nitrobenzene and of propargyl alcohol*, Combustion, Explosion and Shock Waves, V. 35, № 1, 80, 1999
- [6] G.D. KOZAK, N.I. AKININ, V.M. RAIKOVA, S.V. ARININA: *Explosion hazard of some organic peroxides*. Proc. of The 6-th seminar New trends in research of energetic materials, Univ. Pardubice, CSR, 173-182, 2003
- [7] D. STALL, E. WESTRAM, H. ZINKE: *Khimicheskaya termodinamika organicheskikh soedineniy* (transl. into Rus.). M.: Mir, 312, 1971
- [8] B.D. KRUSHALOV, B.I. GOLOVANENKO: *Sovmestnoe Poluchenie fenola i atsetona* (Rus.), M.: Goskhimizdat, 87, 1963
- [9] A.E. FOGELZANG, V.YA. ADZHEMYAN, A.YU. PIMENOV, A.R. SAKLANTII, T.V. DORONINA: *Investigation of burning of benzoyl peroxide*, Voprosy Teorii Cond. Vzryvchatykh System (Rus.). M.: Mendeleev Institute of Chemical Technology, V. 112, 67, 1980
- [10] B.V. BESCHASTNOV: *Avarii v khimicheskikh proizvodstvakh i mery ikh preduprezhdeniya* (Rus.). M.: Khimiya, 445, 1991
- [11] B.V. BESCHASTNOV: *Promyshlennyye vzrivi. Otsenka i preduprezhdenie* (Rus.). M.: Khimiya, 387, 1991
- [12] V.L. ANTONOVSKII: *Organicheskie perekisnye initsiatory* (Rus.). M.: Khimiya, 230, 1972
- [13] V.C. MARSSHALL: *Osnovnye opasnosti khimicheskikh proizvodstv* (trans. Into Rus. from Engl.), M.: Mir, 671, 1989
- [14] B.N. KONDRIKOV: *Chemical Thermodynamics of Combustion and Explosion* (Rus.), Text-book. M.: Mendeleev Institute of Chem. Technology, 80, 1980
- [15] V.I. MINKIN, B.YA. SIMKIN, R.M. MINYAEV: *The Theory of molecules construction*, Rostov-na-Donu. Fenix, 1997
- [16] A.I. SUMIN, V.N. GAMEZO, B.N. KONDRIKOV, V.M. RAIKOVA: *Shock and detonation general kinetics and thermodynamics in reactive systems computer package*, Trans. of 11th Detonation Symposium (Int.), 30-35, 1998
- [17] B.N. KONDRIKOV, G.D. KOZAK, V.N. SHAPOVAL: *Problems Book on Combustion and Explosion* (Rus.). M.: Mendeleev Institute of Chem. Technology, 48, 1981

AN EXPERIMENTAL CHECKING OF A DIVACANCY MODEL OF INICIATING HEAVY METAL AZIDES¹

E.D. Aluker*, A.G. Krechetov*, A.Yu. Mitrofanov*, B.G. Loboiko**,
D.R. Nurmuhametov* and E.V Tupitsin*

* Kemerovo State University, 650043, Kemerovo, Russia

** Russian Federal Nuclear Center
All-Russia Research Institute of Technical Physics (RFNC-VNIITF)
456770, PO Box 245, Snezhinsk, Chelyabinsk region, Russia

Abstract:

Main results are adduced of an experimental checking of a divacancy model of initiating heavy metal azides. The analysis result shows that a divacancy model of initiating heavy metal azides quantitatively do agree with available theoretical data.

Keywords: *heavy metal azides, chain reaction, initiation, model, divacancy*

In ^[1] a model of heavy metal azide initiating has been proposed where initiating pulse result in recharging divacancies being a reaction center. From an uniform standpoint this model accounted for a number of well-known experimental data:

- spontaneous explosions under synthesis ^[3,4];
- availability of initiation threshold ^[3,4];
- a vibrational nature of postprocesses under the threshold excitation ^[6].

However, the most favourable support in favour of any original model is that it predicts some novel phenomena or regularities and their subsequent experimental detection. It became the objective of the research given.

1. SOME PECULIARITIES OF CHAIN REACTION KINETICS.

A proposed model favours in predicting original characteristics of chain reaction kinetics. According to the model ^[1] one can observe the following: in a certain range of initiation energies the rate of the reaction build-up increases with the energy of initiating pulse, however, the values of the rates on the plateau coincide.

The results of experimental observation of this kind of kinetics (using pre-explosion conduction as an example) are shown in fig.1.

¹ The work is supported by ISTC (project No. 2180).

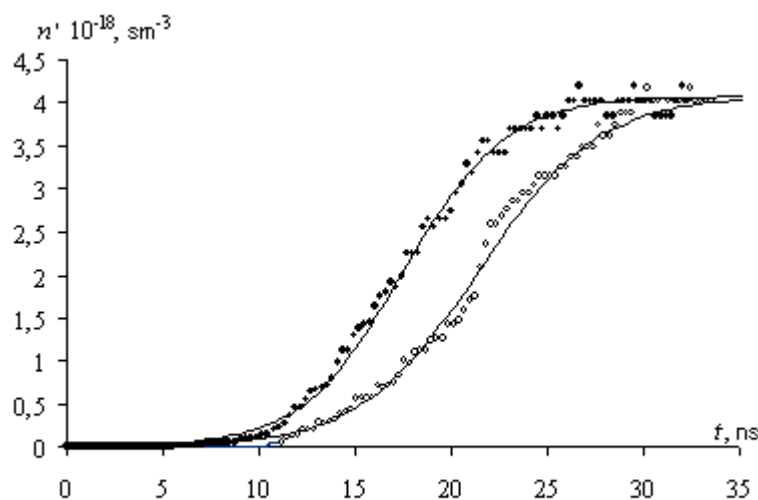


Fig 1. Change kinetics of free carrier charge concentration for silver azide at a variety of initiation energies ($E_2 > E_1$). (n is estimated from experimental data using kinetics of pre-explosion conduction).

2. RADIOLUMINESCENCE

In the model presented ^[1] the two reactions are available that can be accompanied by luminescence:



where V_c^- and V_a^+ are cation and anion vacancies; F is anion vacancy which trapped an electron (the SO – called F-centre).

The reaction (1) is the radiation electron trapping by divacancy, this being the version of the SO-called “trapping” luminescence that has been observed in alkali halide crystals in the earlier studies of Zazubovich (see ^[7]).

The reaction (2) is the radiation recombination of hole with electron localized on divacancy, the latter being the version of the well-known hole recombination luminescence ^[8].

In the context of the model studied luminescence (in case of its detection) has to possess two characteristics.

1. Intensity of the trapped luminescence ($h\nu_1$) must be proportional to the concentration of neutral divacancies but that of the recombination luminescence + to that of divacancies which trapped an electron.

The ordinary effect of previous irradiation of the sample is the generation of free electrons and their localization on divacancies, it should cause decreasing the neutral divacancy concentration and increasing the concentration of the charged ones. More complicated effects are available (the formation of aggregate centers, coagulates, etc.), therefore the dose dependences of both trapped ($h\nu_1$) and recombination ($h\nu_2$) luminescence appear to be contrary ($h\nu_1$ decrease and $h\nu_2$ increase with the dose).

2. In AgN_3 crystal lattice a couple of divacancy orientations can exist, the distance between partners being as high as $2,56\text{\AA}$ and $2,79\text{\AA}$, respectively ^[5]. As a result, spectra of both the trapped ($h\nu_1$) and recombination ($h\nu_2$) luminescence can consist of the two more or less separated bands which correspond to various divacancy orientations.

Moreover, while changing the temperature of the sample one can expect the intensity to be redistributed between the bands which are due to the thermally-activated reorientation of divacancies.

To detect the proposed luminescence we studied in detail AgN_3 radioluminescence excited by electron accelerator pulse ^[9]. The major data of our investigation (in the aspect of our interest) are seen in fig.2. The temperature range given in this figure is caused by the fact that the band $h\nu_1 \leq 1,5\text{ev}$ is succeeded in isolating successfully only at the room temperature are quenched and reliably registered at low temperatures. From the pointstand of the expected results of our model the data shown in fig.2. enable us to relate certainly the band with the maximum $< 1,5\text{ev}$ to the trapped luminescence ($h\nu_1$) and those with maxima $1,65\text{ev}$ and $1,87\text{ev}$ to the hole recombination luminescence on divacancies of various orientation.

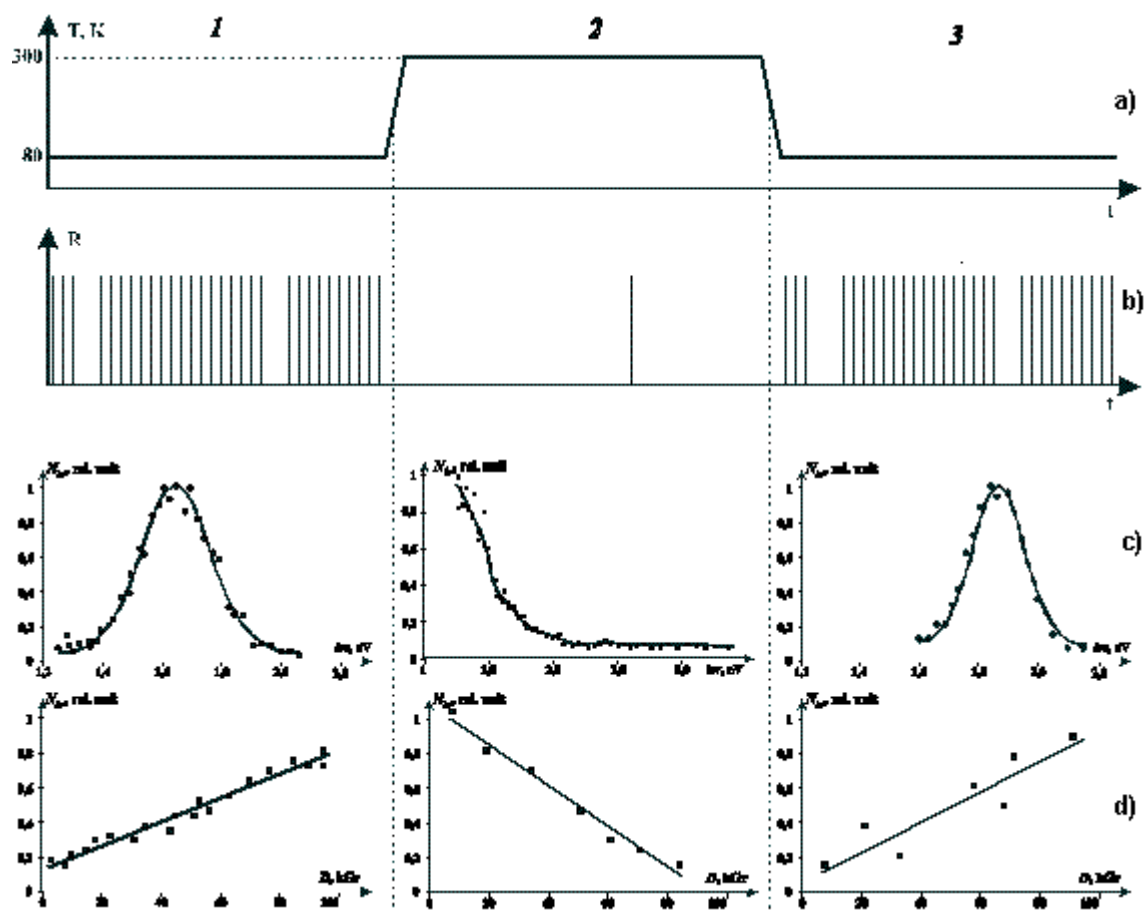


Fig 2. Effect of radiation treatment at 80K and annealing up to 300K on AgN_3 radioluminescence (under the threshold excitation)
a – temperature regime for the experiment²;
b – an irradiation regime (vertical lines are the accelerator pulse);
c – normalized luminescence spectra for the steps 1,2,3;
d – dose dependences of bands $1,65<1,5\text{ev}$ and $1,87\text{ev}$

² The temperature regime was chosen taking into account $1,65\text{ev}$ and $1,87\text{ev}$ band quenching at 300K while a weak band $<1,5\text{ev}$ can be reliably separated only at 300K (when the bands are quenched!).

The similar bands are observed in the first peak which exists when initiating the previously irradiated sample in the above threshold regime (Fig.3)

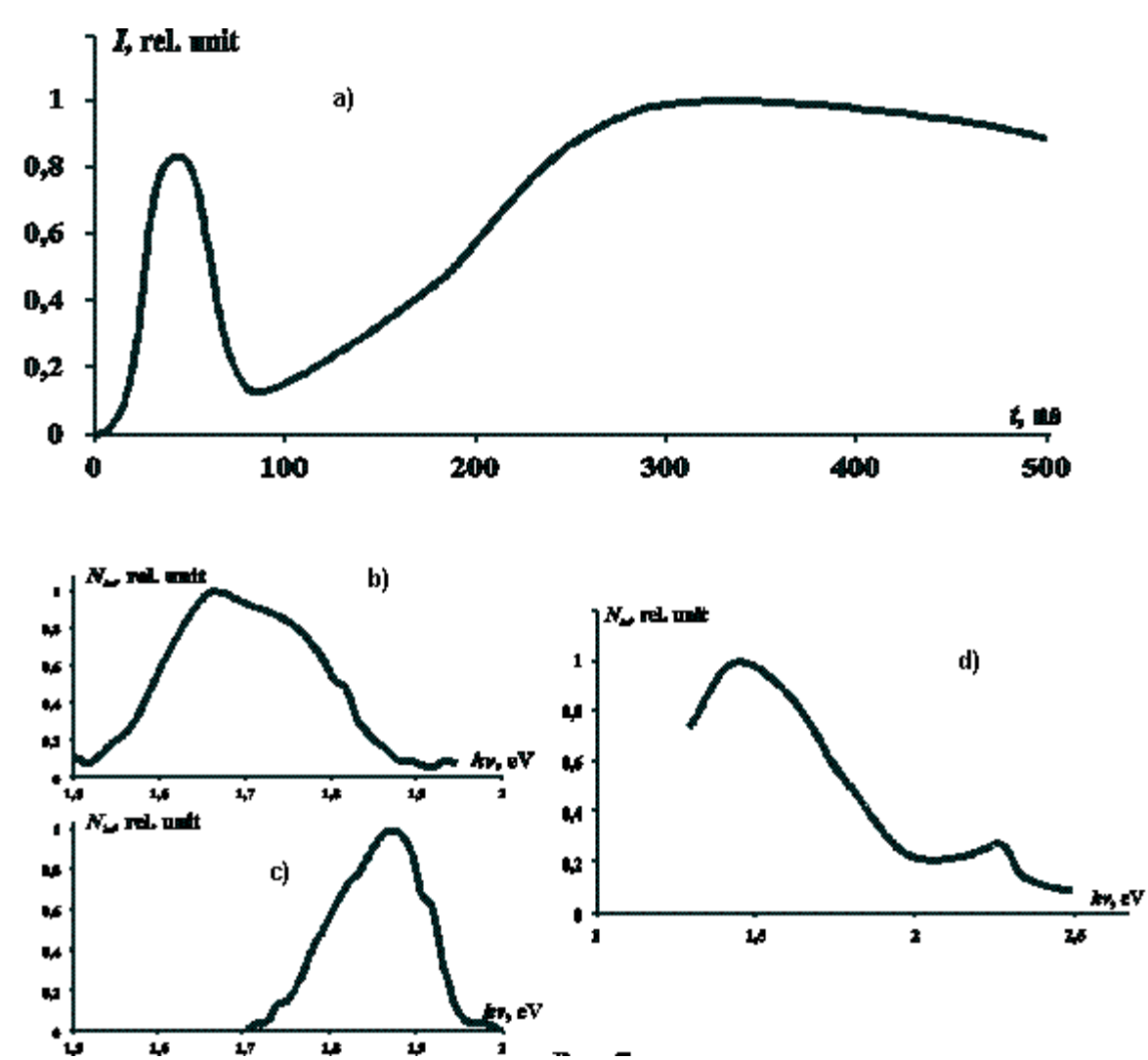


Fig 3. Luminescence of previously irradiated AgN₃ at 300K (the above threshold excitation).
a – luminescence kinetics at $h\nu=1,75\text{eV}$;
b – luminescence spectrum at $t=40\text{nc}$ (previous irradiation at 80K);
c - luminescence spectrum at $t=40\text{nc}$ (previous irradiation at 300K);
d - luminescence spectrum at $t=30\text{nc}$.

The presented data may be considered as a principal argument in favour of a divacancy model of HMA initiation. In conclusion, we would like to pay attention to the extremely important fact, namely, the model predicted makes it possible to control the sample sensitivity.

According to ^[1] initiation energy threshold essentially depends on the concentration of divacancy concentration one can handle the sample sensitivity. Such a control can be performed by means of routine method of solid state physics (irradiation, illumination, thermal treatment, etc.) at present the corresponding experiments are carried out.

REFERENCES

- [1] B. P. ADUEV., E. D. ALUKER, A. G. KRECHETOV: *Pre-detonation Phenomena in Heavy Metal Azides*, In Proceedings VI Seminar New Trend in Research of Energetic Materials, Pardubice, Czech Republic, p. 30-35, 2003
- [2] M.M. KUKLJA, B.P. ADUEV, E.D. ALUKER AND OTHERS: *Role of Electronic Excitations in Explosive Decomposition of Solids*, Journal of Applied Physics, Vol.89, **No. 7**, p. 4156 –4166, 2000
- [3] V. I. FISTUL: *Fizika i khimiya tverdogo tela*. Vol.1., Metallurgiya, Moskva, 1995, (in Russian)
- [4] F. KREGER: *Khimiya nesovershennikh kristallov*, Mir, Moskva, 1969, (in Russian)
- [5] V. V. ANTONOV-ROMANOVSKIY: *Kinetika fotoluminescencii kristallofosforov*, Nauka, Moskva, 1966, (in Russian)
- [6] B. P. ADUEV, A. G. KRECHETOV, A. N. DROBCHIK, E. V. TUPUTSIN: *Spektralno-kineticheskie kharakteristiki doporogovoi radioluminescencii azida serebra*, In Proceedings 12th international conference on radiation physics and chemistry of inorganic materials, Tomsk, Russia. p.204-206, 2003 (in Russian)
- [7] E. D. ALUKER, D. YU. LUSIS, S. A. CHERNOV: *Elektronnie vozbuždeniya i radioluminescenciya shelochno-galoidnikh kristallov*, Zinatne, Riga, 1979, (in Russian)
- [8] A. M. STOUNKHEM: *Teoriya defektov v tverdikh telakh*, Mir, Moskva, 1978 (in Russian)
- [9] B. M. KOVALCHUK, G. A. MESYAC, B. N. SEMIN: *Silnotochniy nanosekyndniy yskoritel dlya issledovaniya bistroprotekajyshih processov*. Pribori i tekhnika eksperimenta, **No. 4**, p.15-22, 1981, (in Russian)

COMPARATIVE CHARACTERISTICS OF TWO ISOMERIC EXPLOSIVES: 4-NITRO-5-NITRIMINO-1H-1,2,4-TRIAZOLE AND 3-NITRO-5-NITRIMINO-1,4H-1,2,4-TRIAZOLE

A.M. Astachov, V.A. Revenko and E.S. Buka

Siberian State Technological University,
Prosp. Mira 82, 660049 Krasnoyarsk, Russia

Abstract:

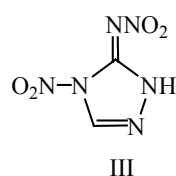
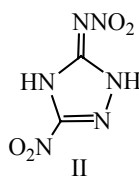
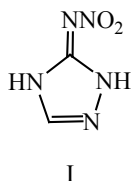
The comparative estimation of properties of two isomeric nitroderivatives of 1,2,4-triazole – 4-nitro-5-nitrimino-1H-1,2,4-triazole and 3-nitro-5-nitrimino-1,4H-1,2,4-triazole, is realized. In contrast to the C-nitrocompound, the N-nitrocompound has higher heat of formation, and as a consequence, the higher explosive characteristics. On the other hand, N-nitrocompound has lower thermal stability and higher impact sensitivity in comparison with C-nitrocompound.

Keywords: high explosives, 1,2,4-triazoles, nitrimines, nitrocompounds

1. INTRODUCTION

It was recently shown that the compounds known as 3(5)-nitramino-1,2,4-triazoles are actually nitrimines and not primary nitramines^[1]. Some works have been devoted to explosive properties of 5-nitrimino-1,4H-1,2,4-triazole (I) {3(5)-nitramino-1,2,4-triazole, NITRA, 3-NRTZ}^[2-5]. This compound is attractive due to its accessibility and low cost, but has relatively moderate detonation parameters. An introduction of additional nitrogroup into the molecule of compound (I) allows to improve the oxygen balance and increase energetic characteristics.

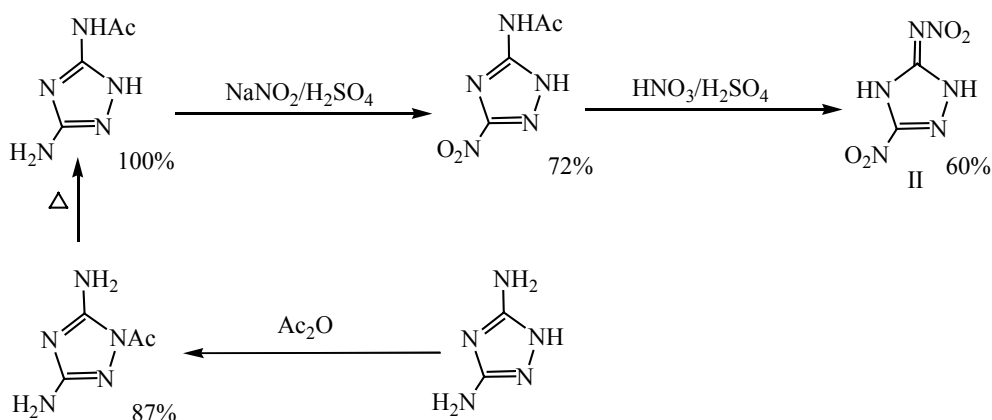
C-nitroderivative of (I) – 3-nitro-5-nitrimino-1,4H-1,2,4-triazole (II) is known^[6], but this compound has been named 3-nitro-5-nitramino-1H-1,2,4-triazole in this work. We have recently synthesized the N-nitroderivative: 4-nitro-5-nitrimino-1H-1,2,4-triazole (III)^[7]. The compound (III) is interesting because of presence of the dinitroguanyl explosophoric fragment. Structure and properties of 1,2-dinitroguanidine and some of its derivatives have been considered in the literature earlier^[8-11].



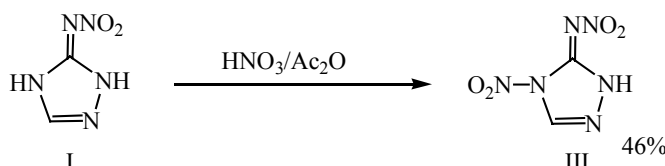
In this paper we consider the influence of the introduction of additional nitrogroup into the molecule of (I) and compare energetic properties of two analogous by the element composition ($C_2H_2N_6O_4$) isomeric high explosives, (II) and (III).

2. SYNTHESIS

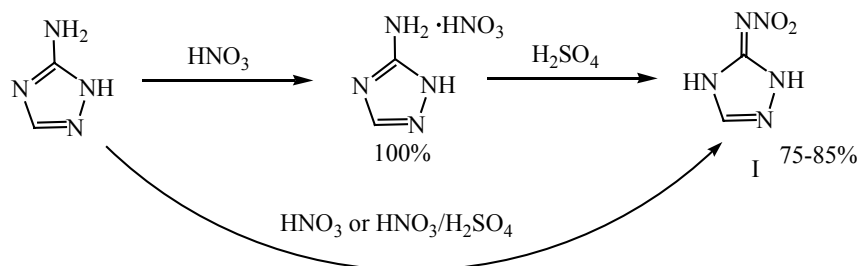
Compound (II) was synthesized from the guanozole (3,5-diamino-1,2,4-triazole) as described previously [16]:



Compound (III) was synthesized by the compound (I) N-nitration [17]:



The initial compound (I) obtaining methods are well known [2-4, 12-15]:



Compound (III) undergoes a slow decomposition during the storage under the room temperature. Therefore the experiments with this compound were carried out just after the synthesis.

3. EXPLOSION TEMPERATURE TEST

Sensitivity to explosion by heat was determined as the temperature of flash and time to explosion delay. The known method is used [16-18]. The sample of explosive (10 mg) is placed in a №8 detonator shell, and the lower end of this shell is plunged into a bath of molten Wood's metal at a measured temperature (T). The time required to cause explosion or flashing is noted with a stop watch. Each experiment was repeated ten times and mean τ values are fixed. Then the similar operation is repeated with another temperature. The specified method allows most simply to find activation parameters of thermal decomposition of explosive compounds. However, the accuracy of definition of activation parameters using such way is, usually, low. Concerning the physical meaning, the given test is close to the test ODTX (one-dimensional time to explosion) [19, 20], but requires essentially smaller mass of explosive and has less complicated equipment.

The temperature – time to explosion curves for compounds (I–III) is shown in Fig. 1. The flash of compounds (II, III) was accompanied by the appearance of a flame and a violent sound. Compound (I) decomposed with soft sound and without a flame.

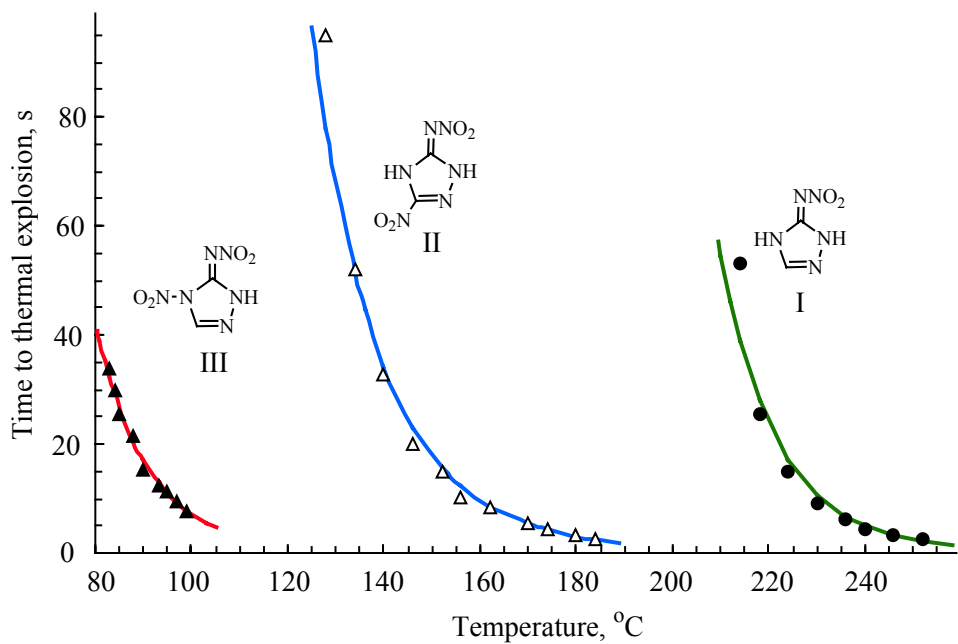


Fig 1. Relationship between the temperature and time to explosion for compounds (I–III)

To find activation parameters from relationship of temperature – time to explosion, data processing in coordinates $\ln \tau = f(1/T)$, shown in Fig. 2, were applied.

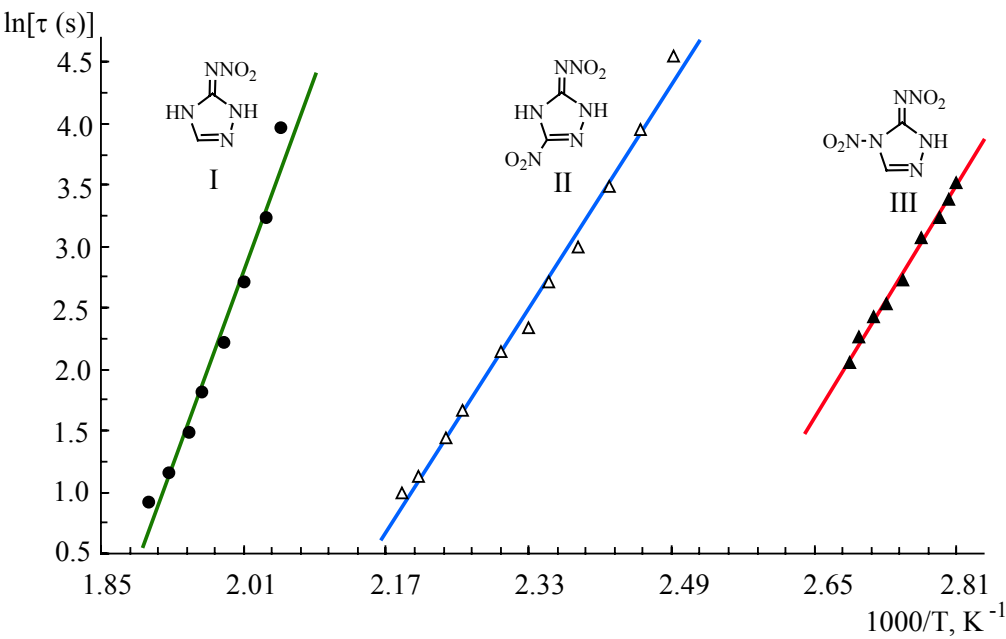


Fig 2. Plot of $\ln \tau$ vs $1/T$ for compounds (I–III)

This relationship can be expressed by the following equations:

$$\ln \tau = -37.21 + 19910.5/T, \quad R = 0.9870, \quad \text{for compound (I)}$$

$$\ln \tau = -24.02 + 11384.4/T, \quad R = 0.9961, \quad \text{for compound (II)}$$

$$\ln \tau = -29.48 + 11734.4/T, \quad R = 0.9947, \quad \text{for compound (III)}$$

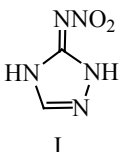
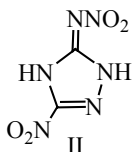
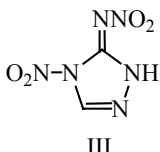
From this equations the values of energy of activation (E_a) and pre-exponential factor (A) are found. The calculation is based on the following expression:

$$\tau = \{c_p RT^2 / (Q_{\text{expl.}} E_a A)\} \exp(E_a/RT),$$

where c_p – heat capacity (we used approximate values for heat capacity organic explosives $c_p = 1.25 \text{ J/(g}\cdot\text{K)}$); R – ideal gas constant, $8.314 \text{ J/(mol}\cdot\text{K)}$; $Q_{\text{expl.}}$ – heat decomposition reaction (J/g), identical with heat of explosion (calculated in the chapter 5).

Calculated activation parameters of thermal explosion are represented in the Table 1.

Table 1. Activation parameters of thermal explosion of compounds (I–III).

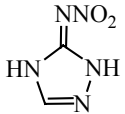
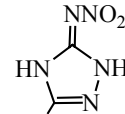
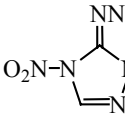
			
	I	II	III
$T_{\text{expl.}}(\tau = 5 \text{ c}), ^\circ\text{C}$	240	171	104
$\Delta T, ^\circ\text{C}$	218–252	128–184	83–99
$E_a, \text{ kJ/mol}$	165.5	94.6	97.6
$\Delta \lg A$	13.69–13.75	7.96–8.07	10.16–10.20
average $\lg A$	13.72	8.01	10.18

The values of activation parameters of compound (I) obtained were close to the results of much more accurate manometric measurements of thermal decomposition this compound in a solid phase ($E_a = 159.5 \text{ kJ/mol}$, $\lg A = 13.68$)^[21]. Such data do not exist for compounds (II, III). The energy of activation of (II, III) is less significant, than for (I). Rather close values of energy of activation of (II, III), probably, testify to the similar mechanism of their thermal decomposition.

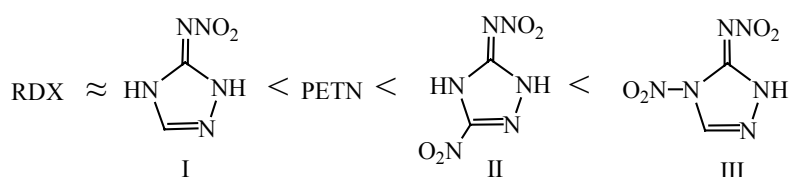
4. IMPACT SENSITIVITY

Sensitivity to impact of (I–III) was investigated with K-44-II drop-weight impact machine^[17]. Conditions of experiments: 5 kg weight drop hammer; the sample of explosive is placed in the plunger assembly №1, consisting of two steel rollers by Soviet state standard 4545-48 (roller diameter 10 mm and height 12 mm)^[16]; samples weight is 30 mg for (I, II) and 10 mg for (III). In conditions of impact tests explosive performance of (III) occurs in the form of detonation and with sample weight 30 mg there is a mechanical damage of plunger assembly. The results of tests are collected in Table 2, the curves of sensitivity are shown in Fig. 3. Each point was obtained by results of 25 trials. For comparison the data for PETN are given.

Table 2. *Impact sensitivity of compounds (I–III).*

Load level (drop height) H, cm	Explosion probability f , %			
	 I	 II	 III	PETN
4			24	
5		0		
6		9	44	
7			68	
8		36		
9			84	
10		44		
11			92	0
12		60		8
13	0		92	
14	8		96	24
15		88		68
16	16			84
17		100	100	
18	28			100
20	32			
22	48			
24	60			
26	68			
28	92			
30	100			

From the data obtained it follows that the sensitivity of (I) approximately corresponds RDX and increases with introduction of additional nitrogroup into the molecule. The more powerful N-nitroisomer (III) is also more sensitive, in comparison with C-nitroderivative (II):



The sensitivity of (I) was determined with the help of fallhammer BAM test (1 kg, $H_0 = 66.3$ cm, $E_0 = 6.5$ J, 1 explosion from 6 trials) earlier^[2–4]. For RDX energy $E_0 = 4.5–6.5$ J^[2–4] also is obtained in the same conditions.

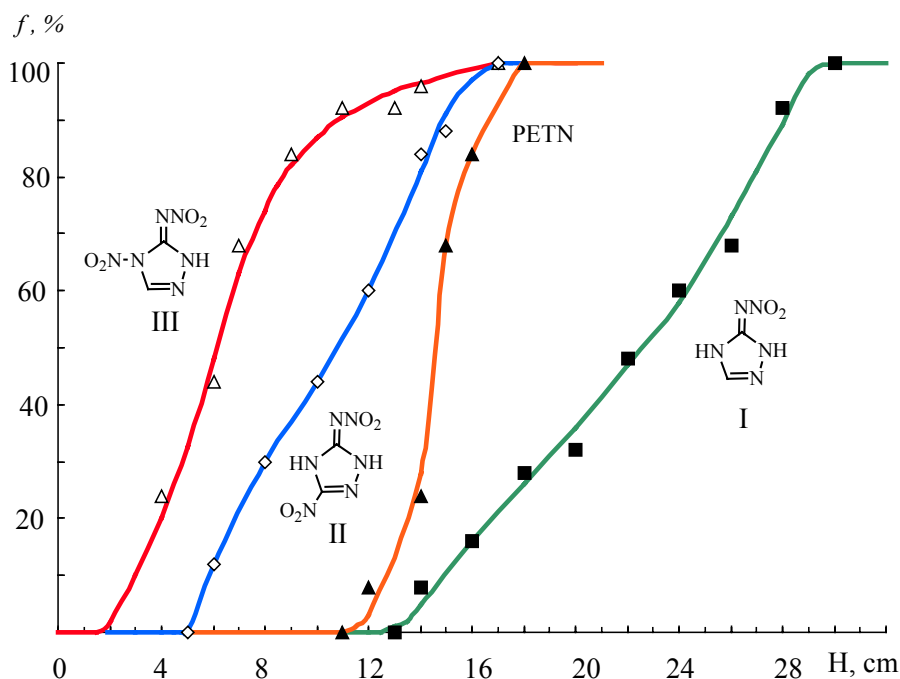


Fig 3. Explosion probability (f) for compounds (I–III) vs drop height of load (H); for comparison the data for PETN are given.

To estimate critical parameters of initiation by impact^[22] we have tried to use a numerical method^[23] and activation parameters of thermal decomposition obtained by us (chapter 3 in this paper). Calculated values of P_{cr} of (I) are close to those for RDX ($P_{cr} = 700$ MPa^[22, 23]). One fails to receive reasonable values for compounds (II, III), probably, owing to low accuracy of activation parameters of thermal decomposition.

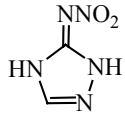
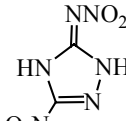
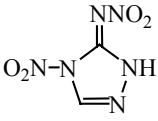
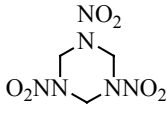
5. ENERGETIC AND DETONATION PARAMETERS

Energetic and detonation parameters of (I), (II) and (III) were estimated using thermodynamic method with BKW equation of state^[24, 25] at various sets of parameters (BKW-RDX, -R, -RR, -C) and, also, by simple correlation methods^[5, 25]. Table 3 shows averaged values obtained by the above mentioned methods. Experimental values of detonation parameters for RDX^[26] are shown in Table 3 for comparison.

The calculation was performed at maximum density of compounds. The condensed carbon formed by detonation was taken into consideration in diamond (BKW-RDX, -R, -C) and ultra fine diamond (BKW-RR) phases. The experiment and thermodynamic calculation shows that diamond phase is preferable in Chapman-Jouguet point for high density explosives^[27]. The standard heat of formation of (I, II) was found from experimentally determined calorimetric heats of combustion. The values for crystal density and heat of formation of (III) is predicted^[7].

From Table 3 data it follows that the compound (II) is comparable to RDX by detonation parameters and the compound (III) surpasses the latter.

Table 3. Some energetic and detonation parameters of compounds (I–III).

				
	I	II	III	RDX
Brutto-formula	C ₂ H ₃ N ₅ O ₂	C ₂ H ₂ N ₆ O ₄	C ₂ H ₂ N ₆ O ₄	C ₃ H ₆ N ₆ O ₆
Molecular weight	129.08	174.08	174.08	222.12
Oxygen balance, %	−43.4	−9.2	−9.2	−21.6
ΔH _f ⁰ , kJ/mol	+112.4 ^[5] +112.5 ^[28] +93.9 ^[2–4]	+84.7 ^[5]	+191 ^[7]	+61.5
ρ ₀ , g/cm ³	1.83 ^[2–4]	1.87 ^[5]	1.87 ^[7]	1.80
Q _{expl.} , MJ/kg	4.42 ^{±2.6%}	5.28 ^{±0.8%}	5.87 ^{±0.8%}	5.40 ^{1.70 g/cm3}
V ₀ , m ³ /kg	0.738 ^{±0.4%}	0.708 ^{±1.3%}	0.709 ^{±1.7%}	0.762 ^{1.70 g/cm3}
D, km/s	8.38 ^{±3.7%}	8.82 ^{±2.6%}	9.01 ^{±2.7%}	8.77
P _{CJ} , GPa	29.4 ^{±5.8%}	34.4 ^{±3.6%}	36.1 ^{±4.2%}	36.1
T _{CJ} , K	1844 ^{a)} –3274 ^{b)}	2207 ^{a)} –4011 ^{b)}	2565 ^{a)} –4342 ^{b)}	3520
γ	3.39 ^{±11.0%}	3.22 ^{±5.8%}	3.18 ^{±4.9%}	2.83

Notes: a) BKW-RDX; b) BKW-C.

6. CONCLUSION

The introduction of the second nitrogroup into the molecule of 5-nitrimino-1,4H-1,2,4-triazole (I) improves oxygen balance and, as a consequence, heat of explosion. In a combination with greater density of (II, III) it results in increase of detonation parameters in comparison with compound (I). The comparison two of isomeric nitroderivatives (II, III) has shown, that in contrast to the C-nitrocompound (II), the N-nitrocompound (III) has higher heat of formation and, as a consequence, the higher explosive characteristics. On the other hand, N-nitrocompound (III) has lower thermal stability and higher impact sensitivity in comparison with C-nitrocompound (II).

Unfortunately, both of compounds (II) and (III), despite of the rather high energetic characteristics have low level of thermal stability and high level of sensitive to impact. This obstructed their practical application. Being the most powerful of the considered compounds, the compound (III) is the most impact sensitive and least thermostable dangerous explosive.

REFERENCES

- [1] A. M. ASTACHOV, A. D. VASILIEV, M. S. MOLOKEEV, V. A. REVENKO, L. A. KRUGLYAKOVA, AND R. S. STEPANOV: *Structure of nitramino-1,2,4-triazoles: nitramines or nitrimines?* Proc. 34th Int. Annual Conf. ICT "Energetic Materials – Reactions of Propellants, Explosives and Pyrotechnics", Karlsruhe, Germany, p. 52/1–13, 2003
- [2] H. H. LICHT, AND H. RITTER: *New energetic materials from triazoles and tetrazines*. J. Energetic Mat. Vol. 12. **No. 4**, p.223–235, 1994
- [3] H. H. LICHT, S. BRAUN, M. SCHÄFER, B. WANDERS, AND H. RITTER: *Nitrotriazole: chemische struktur und explosive eigenschaften*. Proc. 29th Int. Annual Conf. ICT "Energetic Materials – Production, Processing and Charakterization", Karlsruhe, Germany, p. 47/1–15, 1998
- [4] H. H. LICHT: *Performance and sensitivity of explosives*. Propellants, Explosives, Pyrotechnics. Vol. 25. **No. 3**, p. 126–132, 2000
- [5] A. M. ASTACHOV, V. I. VLASENKO, AND E. S. BUKA: *Estimation of energetic characteristic some nitrimines*. Proc. All-Russia Scientific and Techn. Annual Conf. "Modern Problems of Technical Chemistry", Vol. 1., Kazan, Russia, p. 249–253, 2002 (In Russian)
- [6] M. S. PEVZNER, N. V. GLADKOVA, AND T. A. KRAVCHENKO: *5-Amino-3-nitro-1,2,4-triazole and 5-nitramino-3-nitro-1,2,4-triazole*. Russ. J. Org. Chem. Vol. 32. **No. 8**, p. 1230–1233, 1996 (In Russian)
- [7] A. M. ASTACHOV, V. A. REVENKO, AND E. S. BUKA: *4-Nitro-5-nitrimino-1H-1,2,4-triazole: synthesis and properties*. Proc. All-Russia Scientific and Techn. Annual Conf. "Modern Problems of Technical Chemistry", Kazan, Russia, p. 209–210, 2003 (In Russian)
- [8] A. A. ASTRATIEV, D. V. DASHKO, AND L. L. KUZNETSOV: *Synthesis and some properties of 1,2-dinitroguanidine*. Russ. J. Org. Chem. Vol. 39. **No. 4**, p. 537–548, 2003 (In Russian)
- [9] A. D. VASILIEV, A. M. ASTACHOV, M. S. MOLOKEEV, L. A. KRUGLYAKOVA, AND R. S. STEPANOV: *1,2-Dinitroguanidine*. Acta Cryst. C59. p. o550–o552, 2003
- [10] A. M. ASTACHOV, A. D. VASILIEV, M. S. MOLOKEEV, L. A. KRUGLYAKOVA, AND R. S. STEPANOV: *1,2-Dinitroguanidines: structure – property relationships*. Proc. 5th Int. Seminar "New Trends in Research of Energetic Materials", Pardubice, Czech Republic, p. 28–40, 2002
- [11] A. D. VASILIEV, A. M. ASTACHOV, M. S. MOLOKEEV, L. A. KRUGLYAKOVA, AND R. S. STEPANOV: *2-Nitrimino-1-nitroimidazolidine*. Acta Cryst. C59. p. o499–o501, 2003
- [12] G. I. CHIPEN, V. YA. GREENSTEIN, AND R. P. PREIMAN: *Derivatives of aminoguanidines and their transformations. II. Derivatives of nitramino- and diaminoguanidines and their transformations*. Russ. J. General Chem. Vol. 32. **No. 2**, p. 454–459, 1962 (In Russian)
- [13] G. I. CHIPEN: *3-Nitramino-1,2,4-triazole. In the collect. – Method of synthesis of chemical reactive and preparations*. Vol. 14. Moscow, p. 77–79, 1966 (In Russian)
- [14] C.-F. KRÖGER, AND R. MIETCHEN: *Zur nitrierung von 1,2,4-triazolen*. Z. Chem. Bd. 9. **No. 10**, s. 378–379, 1969
- [15] M. S. PEVZNER, T. N. KULIBABINA, N. A. POVAROVA AND L. V. KILINA: *Heterocycle nitrocompounds. XXV. Nitration of 5-amino-1,2,4-triazole and 5-acetamido-1,2,4-triazole by acetylnitrate and nitronium salt*. Khim. Geterotsikl. Soedin. (Chem. Heterocycle Compounds). **No. 8**, p. 1132–1135, 1979 (In Russian)
- [16] K. K. ANDREEV, AND A. F. BELYAEV: *Theory of explosives*, Oborongiz, Moscow, 1960 (In Russian)
- [17] S. G. ANDREEV, A. V. BABKIN, F. A. BAUM ET. AL.: *Physics of explosion, Vol. 1 (Edited by L. P. Orlenko – third edition)*, Fizmatlit, Moscow, 2002 (In Russian)
- [18] A. I. GOLBINDER: *Laboratory works on a course in the theory of explosives*, Rosvuzizdat, Moscow, 1963 (In Russian)

- [19] E. CATALANO, D. L. ORNELLAS, E. WRENN, E. L. LEE, J. MALTON, AND R. R. MCGUIRE: *The thermal decomposition and reaction of confined explosive*. Proc. Sixth Int. Symp. on Detonation, Coronado, CA, USA, p. 214–224, 1976
- [20] T. D. TRAN, R. L. SIMPSON, J. MAIENSCHIN, AND C. TARVER: *Thermal decomposition of trinitrotoluene (TNT) with a new one-dimensional time to explosion (ODTX) apparatus*. Proc. 32nd Int. Annual Conf. ICT "Energetic Materials – Ignition, Combustion and Detonation", Karlsruhe, Germany, p. 25/1–18, 2001
- [21] A. M. ASTACHOV: *Thermal decomposition of the primary nitramines in a condensed phase*, Ph.D thesis, Siberian State Technological University, Krasnoyarsk, 1999 (In Russian)
- [22] G. T. AFANASIEV, AND V. K. BOBOLEV: *Initiation of solid explosives by impact*, Nauka, Moscow, 1968 (In Russian)
- [23] A. V. DUBOVIK: *Calculation of impact sensitivity parameters of solid explosives*. Dokl. Acad. Nauk USSR (Doklady Chemistry USSR). Vol. 286. **No. 2**, p. 377–380, 1986 (In Russian)
- [24] C. L. MADER: *Numerical modeling of explosives and propellants (second edition)*, CRC Press, Boca Raton, 1998
- [25] V. I. PEPEKIN, AND S. A. GUBIN: *Methods of calculation of detonation parameters of explosives*. Khim. Fizika (Chem. Phys. Report). Vol. 22. **No. 9**, p. 72–97, 2003 (In Russian)
- [26] M. F. GOGULYA, AND M. A. BRAZHNIKOV: *Temperature of detonation products of the condensed explosive. 1. The solid explosives*. Khim. Fizika (Chem. Phys. Report). Vol. 13. **No. 1**, p. 52–63, 1994 (In Russian)
- [27] V. V. ODINTSOV, S. A. GUBIN, V. I. PEPEKIN, AND L. N. AKIMOVA: *The form and size of diamond crystals definition behind a detonation wave in the condensed explosives*. Khim. Fizika (Chem. Phys. Report). Vol. 10. **No. 5**, p. 687–695, 1991 (In Russian)
- [28] M. M. WILLIAMS, W. S. MCEVAN, AND R. A. HENRY: *The heats of combustion of substituted triazoles, tetrazoles and related high nitrogen compounds*. J. Phys. Chem. Vol. 61. **No. 3**, p. 261–267, 1957 (In Russian)

APPLICATION OF TLC FOR AN ANALYSIS OF INITIATING EXPLOSIVES

J. Błądek, R. Kowalczyk and S. Cudziło

Institute of Chemistry, Military University of Technology,
Kaliskiego 2, 00-908 Warsaw, PL

Abstract:

Instrumental TLC was used for analyses of initiating explosives (IHE). A chromatographic system suitable for analyte separation and method of densitometric determination of some IHE complexes with ditizone were proposed. A linear dependence of densitometric peak areas A on the analyte mass c in the chromatographic band was obtained (Hg: $A = 33202c - 1406$ and Pb: $A = 42643c - 83$). A limit detection (Hg: 7.15 and Pb: 1.25 ng in the chromatographic band) and maximal range of linear measurements (Hg: 120 and Pb: 20 ng) was determined. The method developed was used to analyze chosen IHE in electrolytes.

Keywords: *initiating explosives, densitometry, TLC analyses*

1. INTRODUCTION

The need for disposal of duds, blinds, and useless (obsolete) ammunition grows almost simultaneously with the development of weapons systems. Up to recent days these tasks were conducted in open field, by destroying mentioned kinds of ammunition with the explosive method. Unfortunately this process is not safe, economical and friendly for the environment. That is why researches are being conducted in many laboratories aiming at development of techniques for not explosive weapons disposal. The most difficult stage of such a procedure is disarming of a fuse. In Military University of Technology (MUT), many efforts were made to develop methods for electrochemical decomposition of casings of percussion caps and fuses in order to release the initiating high explosives (IHE). Thus there was a need to develop analytical methods for these chemicals, allowing the evaluation of their behavior in electrolytes. Joining this research we made an effort to apply to this end the instrumental thin layer chromatography (TLC).

2. EXPERIMENTAL

The application of thin layer chromatography in analyses connected with army needs is relatively wide. TLC techniques are used to determine toxic warfare agents, assess chemical stability of powders and so on. Unfortunately publications concerning analyses of initiating high explosives are extremely rare, definitely more attention is paid to analyses of high explosives [1, 2, 3] and powders [4]. In this research we made an effort to analyze those IHE using TLC. TLC was used as an analytical method and as a technique of sample preparation for thermal analysis. The set of research included: (i) – selection of chromatographic systems, (ii) – development of methods of visualization, (iii) – determination of quantitative relations and measuring errors in densitometric measurements of concentration of tetrazene, lead azide, mercury fulminate and lead trinitroresorcinate and (iv) determination of the mentioned analytes in chosen electrolytes, i.e. development of an extraction method and assessment of recoveries.

Apparatus and materials. Applicator LINOMAT IV (CAMAG); horizontal chromatographic chamber DS; densitometer CS-9000 (SHIMADZU); differential scanning calorimeter (SHIMADZU); chromatoplates with silica gel 60 F₂₅₄ HPLC (MERCK, catalog number 5548) or silica gel with chemically bounded octadecyl (MERCK catalog number 5559); organic solvents (J. T. Backer, MERCK); initiating explosive standards (Department of Explosives MUT).

Chromatographic separation. Mercury fulminate, lead trinitroresorcinate, tetrazene and lead azide were chosen for investigations. In order to obtain standard solutions, the first three analytes were dissolved in ethyl acetate while lead azide (this compound is practically insoluble in most of organic solvents) was dissolved in sodium acetate. Solvents with concentration of 10 ng/μl, which next were placed (20 μl; spraying technique, band width 5 mm) on the start line of chromatoplates. Chromatograms were developed in horizontal chamber DS. Lead trinitroresorcinate (product with distinct yellow colour) was visualised directly in visible light, while mercury fulminate and tetrazene after conducting colour reactions with proper reagents. Those were: 10% water solution of sodium sulfide (with mercury fulminate it creates product with strong black tint) and saturated methyl solution of NN-dimethyl-*p*-phenylenediamine (with tetrazene it creates red-orange reaction product). Lead azide was visualised by fluorescence quenching. The best separation was gained on silica gel in the case of three-step elution with diminished distance z_f : step I: methanol/acetonitrile/dichloromethane 4/3/1 (v/v; $z_f = 8$ cm); step II: methanol/acetonitrile: (v/v; $z_f = 7$ cm); methanol/dichloromethane 2:3 (v/v; $z_f = 6$ cm). After development of chromatograms and removing the remainder of mobile phase, chromatoplates were scanned using light with wavelength appropriate for each analyte.

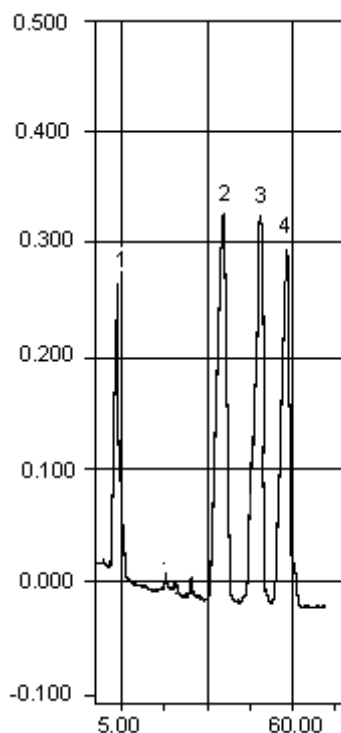


Fig 1. Separation of explosives: 1 – lead azide, 2 – lead trinitroresorcinate, 3 – tetrazene, 4 – mercury fulminate, abscissa – distance of elution, ordinate – absorbance

The obtained good separation of analytes was used for their purification. To this end, the described above experiments were repeated using silica gel plates preparative chromatoplates. On the start lines of such chromatoplates (10×20 cm), solutions of the analytes were sprayed in the form of 10-mm bands using spraying technique. After development of the chromatograms, analytes were removed from the plates along with absorbent, and then the mixture was put into extraction columns. Analytes were eluted and after evaporating of the eluent, pure samples of the IHE were obtained.

Analytical application. These experiments were conducted in order to develop an efficient method for IHE determination in electrolytes. Tests were carried out using 65% solution of HNO_3 (this electrolyte has the most favourable parameters as it comes to the decomposition (digestion) of percussion caps and fuses). Three IHE were chose for the tests. i.e. mercury fulminate, lead trinitroresorcinate and lead azide. These compounds decompose in concentrated nitric acid, and therefore the subject of these analyses were ions of lead and mercury.

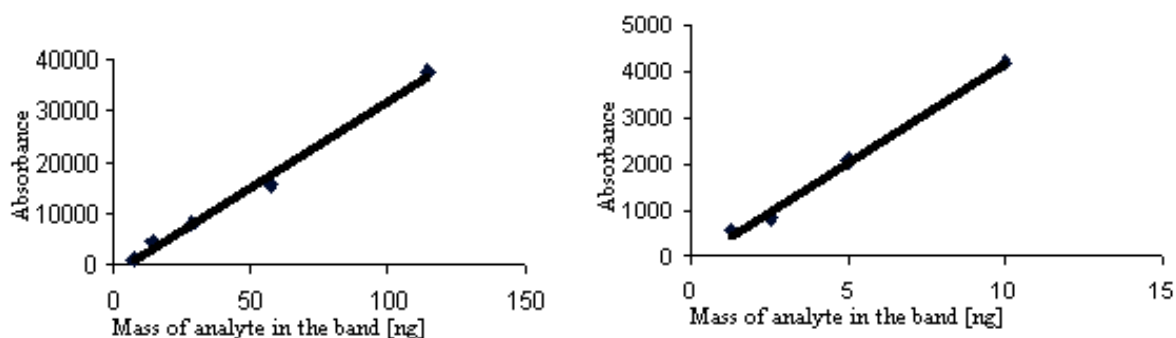


Fig 2. Calibration curves obtained in densitometric measurements for Hg (left side) and Pb (right side) complexes with ditizone

Known amount of lead and mercury were put into the electrolyte (samples of 1 ml in volume) and next – after reducing pH to the value of 7 using ammonia – the samples were extracted with 0,001% solution of ditizone, 5ml in volume. The obtained extract was put directly on the chromatoplates. A good separation of complexes of Hg and Pb with ditizone were obtained in the fallowing chromatographic system: stationary phase silica gel, mobile phase: dichloromethane/carbon tetrachloride 1/2 (v/v). The R_F values in this chromatographic system are: mercury-ditizone complex – 0.3; lead-ditizone complex – 0.5. The maximum of absorption of the complexes occurs at 470 and 500 nm, respectively. These λ_{max} values were used for standardization curve measurements. Their results showed that the dependence of changes of densitometric signal on the concentration of analytes in chromatographic bands is linear in relatively wide range of the analyte concentrations (Fig. 2).

3. CONCLUSION

Today, the need for detection and determination of IHE poses an important analytic problem. The conducted tests were an attempt to determine analytic parameters of these compounds. The obtained results enables us to state that quite a lot of information can be gained using TLC method. It can be used to analyze many organic and inorganic compounds. Especially good results were obtained when the decomposition products of IHE were the subject of analyses. Limit detection at a level of nanogrammes and linearity of calibration curves within wide range of concentrations confirms the possibility of application of TLC for quantitative analyses of initiating explosives.

Acknowledgment:

This research was supported by the State Committee of Scientific Research through Military University of Technology, Grant PBS 700.

REFERENCES

- [1] J. YINON, S. ZITRIN: *Modern methods and applications in analysis of explosives*, Wiley & Sons, 1993
- [2] M. SUČESKA: *Test Methods for Explosives*, Springer, New York, 1995
- [3] A. S. CUMMING, K.P. PARK: *The analysis of trace levels of explosives by gas chromatography/mass spectrometry*, Proc. 1st Int. Symposium on Analysis and Detection of Explosives, FBI Academy, Quantico, VA, pp. 259-265
- [4] J. BŁĄDEK, M. MISZCZAK, M. ŚLIWAKOWSKI: Application of Liquid-Crystalline Detectors to the Quantitation of Propellants' Stabilizers by Thin-Layer Chromatography. *Chem. Anal.*, 38, 339, 1993

APPLICATION OF CARBONACEOUS PRODUCTS OF HALOGENOCARBONS REDUCTION FOR SOLID PHASE EXTRACTION

J. Bładek, A. Arciszewska, S. Cudziło and W. Kiciński

Institute of Chemistry, Military University of Technology,
Kaliskiego 2, 00–908 Warsaw, PL

Abstract:

The possibility of application of carbon materials sensitized in self-propagating heat waves for solid phase extraction (SPE) is presented. Extraction cartridges with the materials were prepared, and samples of water contaminated with pesticides (PDs) and polycyclic aromatic hydrocarbons (PAHs) were analyzed. Modern TLC equipment was used for analyses. Chromatographic systems and analytical parameters of PDs and PAHs were defined and these results were used to determine some retention and elution characteristics of the tested materials. Recovery and measuring errors were estimated (the recovery equaled ca. 50 % and the SD was below 6 %). It was shown that some of the examined materials can be applied as adsorbents for SPE. They are especially good for extraction of analytes with comparatively high polarity.

Keywords: carbon materials, extraction, TLC, pesticides, PAHs

1. INTRODUCTION

Carbonaceous materials sensitized in combustion waves of mixtures of different reductants (e.g. Mg, Al, Zr, Ti, Si, B, CaSi₂, FeSi, NaN₃) with organic compounds of fluorine or chlorine (such as PTFE, C₁₂F₁₀, C₆Cl₆, C₂Cl₆) contain turbostratic graphite, single-crystals of silicon carbide and other crystalline phases, like B₄C, B₁₃C₂, Si, Fe₃Si, and so on^[1,2]. Some of the combustion products are characterized by unique structural and surface properties^[3,4]. For example, they include silicon carbide nanofibers sheathed with amorphous SiO₂ layer and crystallized carbon nanoparticles with hollow cores. The composition and structure of the materials suggest that they are likely to be useful for many analytical applications. In the present work an attempt was undertaken to use some of them as adsorbents in solid phase extraction (SPE).

SPE is a method of sample preparation. As a first approach, it can be described as a simple chromatographic process with liquid media as the mobile phase and the adsorbent as the stationary phase. The method is applied for isolation of analytes from liquid matrixes, particularly from water. During the first step of extraction, the analytes are retained by the adsorbent and then in the end step they are eluted with a small amount (several ml) of organic solvents. Sample preparation plays the major role in analysis, as the complexity of samples makes direct analysis impossible. In particular samples this step is often the limiting factor of the analysis. Variety of surface properties of adsorbents and solvents makes it possible to exploit SPE commonly. The method is quite simple, economical and very efficient, especially in the case of analyses at a level of nanograms^[5]. As a column packing chemical bonded silica gel, ion exchangers and resins are most often used in SPE. In our investigations carbonaceous materials sensitized in combustion wave were applied as adsorbents.

2. EXPERIMENTAL

The effectiveness of extraction of pesticides (PDs) and polycyclic aromatic hydrocarbons (PAHs) from water was evaluated. The set of investigations included: (i) – development of a method for analysis of traces of PDs and PAHs using instrumental thin layer chromatography (this part of research constituted in selection of a chromatographic system allowing separation of the analytes from other matrix components as well as selection of a method of their visualization and qualitative analysis), (ii) – specification of the principles of extraction column preparation, and (iii) – characterization of retention and elution properties of the tested carbonaceous materials during extraction of the analytes from water.

Analytical parameters of the PDs and PAHs. Four PDs (fenuron, carbaryl, phenchlorfos and DDT) and three PAHs (benzo(a)pyrene, pyrene and anthracene) were selected for the tests. Standard solutions of the analytes were sprayed (applicator LINOMAT IV) on the start line of chromatoplates. The chromatograms were developed in classical (ascending) chromatographic chamber using organic solvents. The effectiveness of separation was assessed by observation of fluorescence (PAHs) or on the basis of fluorescence quenching (PDs). The best separation conditions were gained in the case of the following chromatographic systems:

- PDs: normal phase system – stationary phase: high performance silica gel (Merck, cat. no 5548), mobile phase carbon tetrachloride:acetonitrile 5:0.5 (v/v) or methyl chloride:chloroform 1:0.9 (v/v).
- PAHs: reversible phase system – stationary phase: high performance silica gel with chemical bonded octadecyl (RP C-18, Merck, cat. no 5559), mobile phase: methanol.

Table 1. *Analytical parameters for the tested pesticides*

Analyte	λ_{\max} [nm]	Calibration curve			
		$A = f(c)^*$	Correlation coefficient	Detection limit [μg]	Max. range of linearity [μg]
Fenuron	262	$2165.9 \cdot c + 8270$	0.984	1.0	10
Carbaryl	222	$2099.5 \cdot c + 6085$	0.981	0.8	12
Phenchlorfos	205	$6410.3 \cdot c + 237$	0.998	0.5	10
DDT	220	$14936.0 \cdot c + 345$	0.997	0.2	5

* c – the mass of analyte in the chromatographic band [μg], A – absorbance, the surface area of the densitometric peak

The qualitative analyses were carried out using densitometric technique (densitometer CS-9000 SHIMADZU). First, the wavelengths λ_{\max} corresponding to the maximum of adsorption of UV radiation by the PDs and the maximum of fluorescence excitation of the PAHs were determined. Then the chromatographs obtained for standard solutions with different analyte concentrations were scanned using light with wavelength appropriate for each analyte. In this way a dependence of the surface area of the densitometric peak (absorbance) A on the mass of the analyte in the chromatographic band c was determined. The obtained set of analytical parameters is collected in Tabs 1 and 2.

Table 2. Analytical parameters for the tested PAHs

Analyte	λ_{\max} [nm]	Calibration curve			
		$A = f(c)^*$	Correlation coefficient	Detection limits [ng]	Max. range of linearity [ng]
Benzo(a)pyrene	320	$3605.4 \cdot c + 771$	0.999	2.0	20
Pyrene	300	$354.3 \cdot c + 1987$	0.985	15	100
Anthracene	340	$343.7 \cdot c + 703$	0.999	10	80

* c – mass of the analyte in the chromatographic band, A – absorbance, the surface area of the densitometric peak

Preparation of extraction cartridges. The flow of a liquid matrix through an extraction column during SPE process is a classical example of transport of a liquid through a porous beds. According to Leva's equation [6], resistance of the flow Δp depends on the bed height L , grain equivalent diameter d_e , linear flow velocity u (calculated for a column without packing), density of the liquid ρ , and parameters characterizing grain shape φ and bed porosity ε :

$$\Delta p = \lambda \frac{L}{d_e} \frac{\rho \cdot u^2}{2} \left(\frac{(1 - \varepsilon)^{3-n}}{\varepsilon^3} \varphi^{3-n} \right) \quad (1)$$

where: λ - coefficient of flow resistance, n – parameter of the flow pattern.

In the SPE processes, the most effective retention of an analyte is achieved during the laminar matrix flow ($n = 1$), with a volumetric flow velocity less than 1 l/h. The average height of bed usually equals 8÷10 mm, and the sub-atmospheric pressure should not be higher than 400 hPa (safe value, recommended in the service manual of SPE set). Taking into considerations values of the parameters, the minimum grain diameter was calculated as $d_e = 0.12$ mm. This was the basis for selection of the samples that could be used as column packing. The condition was fulfilled by combustion products of the following mixtures (composition expressed in weight percent):

NaN ₃ /PTFE = 62.2/37.8,	NaN ₃ /C ₆ Cl ₆ = 47.8/52.2,
NaN ₃ /C ₆ Cl ₆ = 57.8/42.2 with 20% of ferrocene),	NaN ₃ /SPCW = 55.0/45.0,
CaSi ₂ /PTFE = 22.8/77.2,	CaSi ₂ /PTFE = 27.8/72.2,
CaSi ₂ /PTFE = 47.8/52.2,	CaSi ₂ /C ₆ Cl ₆ = 16.85/83.15,
CaSi ₂ /C ₆ Cl ₆ = 46.85/53.15,	CaSi ₂ /SPCW = 43.2/56.8,
Si/PTFE = 56.0/44.0,	Si/PTFE = 26.0/74.0,
B/PTFE = 22.6/77.4,	

where PTFE – polytetrafluoroethene, SPCW – chlorinated polyvinyl chloride.

The combustion products of the mixtures were sieved and grains with diameters above 0.12 mm were stirred with water. The suspensions obtained were put directly into polyethylene containers with capacity of 3 ml and filtered off at a pressure of 400 hPa. After drying out with a nitrogen stream, the beds were washed with methanol and heksane and used as the extraction columns for the retention tests.

Retention parameters of the tested materials. Samples of water (250 ml) were contaminated with known amount of the tested PDs or PAHs, and then, after solvation the matrix with methanol, the analytes were extracted using a SPE set (T. J. Baker). The

operations included: (i) – initial washing of the bed with alternately a polar and a non-polar solvents, (ii) – passing the tested samples through the columns with volume flow velocity of ca. 1 l/h, (iii) – washing of the adsorbent with pure water and drying with nitrogen, (iv) – elution of the analytes with three 1-ml portions of methylene chloride. The scheme of extraction is shown in Fig.1.

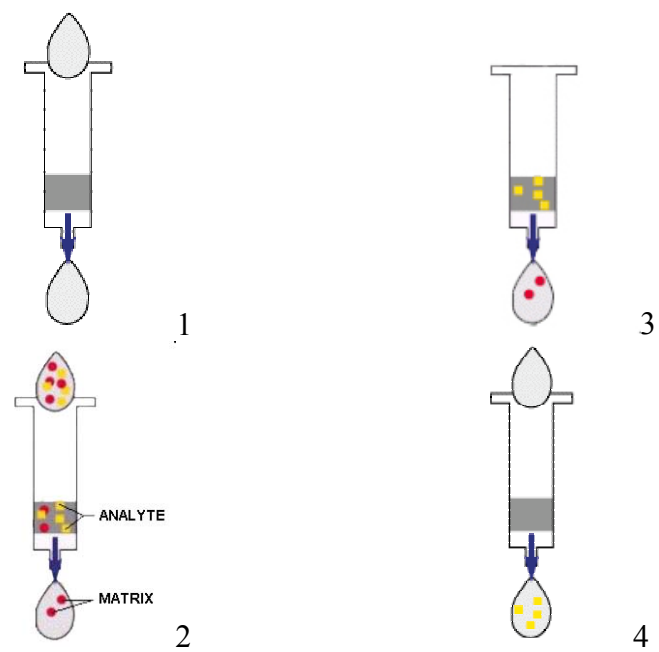


Fig 1. Scheme of the solid phase extraction: 1 – washing columns with polar and non-polar solvents, alternately, 2 – passing the samples through the column (analyte retention), 3 – washing of adsorbent with water and drying in nitrogen stream, 4 – elution of the analyte

The solutions obtained after elution were combined, concentrated to the volume of 100 µl and analyzed using TLC. The concentrated solutions were placed on the start line of chromatoplates (50 µl for PDs and 20 µl for PAHs, spraying technique). The chromatograms were developed and the contents of analytes was determined by the method of internal standard. The conditions for separation and determinations were the same as during measurements of the analytical parameters.

Table 3. Recovery of PDs

Combustion products of:	Carbaryl		Fenuron		DDT		Phenclorfos	
	Recov.*	SD**	Recov.	SD	Recov.	SD	Recov.	SD
CaSi ₂ /PTFE=22.8/77.2	76	5.0	26	4.2	26	4.3	80	4.3
CaSi ₂ /C ₆ Cl ₆ =16.85/83.15	58	4.0	46	5.1	66	4.5	57	5.0
CaSi ₂ /C ₂ Cl ₆ =39.6/80.4	23	4.0	15	4.7	< 5	-	< 5	-
Si /C ₆ Cl ₆ =56.0/44.0	60	4.6	31	4.7	< 5	-	< 5	-
NaN ₃ /SPCW = 55.0/45.0	50	4.2	29	4.3	18	4.4	27	3.9
NaN ₃ /C ₆ Cl ₆ = 47.8/52.2	35	5.1	19	5.2	25	4.8	35	4.2
NaN ₃ /PTFE=62.2/37.8	59	4.8	33	4.4	< 5	-	< 5	-

* – an average value from 5 experimental results, ** – standard deviation

Results of the determinations were used for calculations of the recoveries of the analytes (recovery is a ratio of the analyte mass recovered from the sample to the initial mass of the analyte in the sample). Results of the calculations are collected in Tabs 3 and 4.

Table 5. *Recovery of PAHs*

Combustion products of	Benzo(a)pyrene		Pyrene		Anthracene	
	Recov.	SD	Recov.	SD	Recov.	SD
NaN ₃ /C ₆ Cl ₆ =57.7/42.3*	< 5	-	60	4.5	42	4.7
CaSi ₂ /C ₆ Cl ₆ =46.85/53.15	< 5	-	42	5.1	37	4.3
Si/PTFE=56.0/74.0	8	4.1	51	4.6	21	4.3
NaN ₃ /PTFE=62.2/37.8	13	4.7	39	4.2	25	4.4

* – with an additive of 20% ferrocene

3. DISCUSSION

In the SPE technique, different adsorbents are used (e.g. silica gel, silica gel with chemically bounded phases, ion exchangers, and so on). However, efforts are being made to find new adsorbents with possibly specific retention properties. Active carbons are seldom used for SPE, because of too large specific surface area and consequently unfavorable elution properties. The carbonaceous materials sensitized in combustion wave are characterized by comparatively small specific surface area (ca. 200 m²/g ^[4]) and this justify further investigations aiming at their application as adsorbents in the SPE.

The obtained results indicate that the recoveries of the tested analytes are relatively low (in comparison with other SPE absorbents). Nevertheless, this characteristic does not seem to limit the applicability of the tested materials. In the case of SPE the recovery value (if only at the level of a few dozen percent) has less meaning than the standard deviation, indicating the reproducibility of the analysis. This fact implies that the materials can be used to extract analytes from water samples.

It should be also underlined that the instrumental TLC, used for characterization of the elution and retention parameters of the tested materials, is a reliable and reproducible analytical method, especially useful for qualitative analyses of a big set of samples.

Acknowledgment:

This research was supported by the State Committee of Scientific Research through Military University of Technology, Grant PBS 700.

REFERENCES

- [1] S. CUDZIŁO, A. HUCZKO, W. KICIŃSKI: *Synteza materiałów węglowych i ceramicznych w fali spalania i badanie ich właściwości*, Biul. WAT, **LII**, p. 145, 2003
- [2] A. HUCZKO, H. LANGE, G. CHOJECKI, S. CUDZIŁO, Y. QIU ZHU, H. W. KROTO, D. R. M. WALTON: *Synthesis of novel nanostructures by metal-polytetrafluoroethene thermolysis*, J. Phys. Chem. B, 107, p. 32519, 2003
- [3] S. CUDZIŁO: *Analiza procesu spalania mieszanin reduktor-politetrafluoroeten*, WAT, Warszawa 2003
- [4] S. CUDZIŁO, W. KICIŃSKI, J. BŁĄDEK, A. ARCISZEWSKA, A. HUCZKO: *Characterization of the carbonaceous products of halogenocarbons reduction in combustion wave*, This Proceedings..
- [5] J. BŁĄDEK, M. ŚLIWAKOWSKI: Entry: *Phenols*. Article: *Solid-Phase Extraction*, In: *Encyclopedia of Separation Science*, Ed.: I. WILSON, C. COOKE, C. POOLE, Academic Press Ltd., pp. 3776-3783, London 2000
- [6] D. CIBOROWSKI: *Inżynieria chemiczna. Inżynieria procesowa*, WNT, Warszawa, 1991

THE EXAMINATION OF CHOSEN BALLISTIC PARAMETERS OF IGNITER CHARGE BKNO_3 FOR IGNITERS OF SOLID PROPELLANT ROCKET MOTORS

M. Cieřlikowska, M. Moskalewicz and T. Wolszakiewicz

Institute of Organic Industrial Chemistry, Annopol 6, 03 – 236 Warsaw, Poland

Abstract

The preliminary results of pyrostatic investigations of ignition tablets BKNO_3 were prestented. The investigations were performed in especially designed for this purpose rocket engine with established constant loading density. The time of burning and dynamics of process were estimated.

Keyword: *igniter charge, solid propellant, pyrogenic*

1. INTRODUCTION

The most of modern solid propellant rocket motors uses the pyrogenic way of igniter, which is based on supporting of stream of heat during the determined time to burning area of propellant grain. Typically the igniter is a micro-motor, in which combustion products gives the necessary heat for initialisation of main propellant grain of rocket motor.

Pyrogen way of ignition causes that it is possible to predict the magnitude of heat stream and time of it's effect on the main propellant grain.

The basic source of ignition is the heat forming in the chamber of combustion from the combustion of igniter charge. This charge is formed as a different shape i.e.: granules, tablets and blocks, depends on the size of main motor. The most often encountered igniter charge is a mass based on the mixture of pure boron and potassium nitrate. This mass is an efficient source of heat, it is applicable for conversion and remains stable. It's common application lead to establishing the standard for material and it's shape and one of them is MIL – P - 46994B.

The ballistic properties of this mass were examined to determine burning rate law and burning rate in open and closed volume.

Dynamics of pressure course is ascribed by first derivative of measured pressure in a time unit. It can be determined for any time range. The dynamics of pressure growth characterizing the beginning of combustion and dynamics of pressure fall characterizing of processes of finish burning after BKNO_3 tablets combustion ^[3,4] were examined. The experiments were carried out in constant conditions and the critical diameter of nozzle was changed.

2. THE DESCRIPTION OF EQUIPMENT

The micro-motor of the rocket to determine the ballistic parameters was built according to figure 1. This motor has the constant density of loading $\Delta = 0.3 \text{ g/cm}^3$, the constant diaphragm which made possible partial combustion in closed volume and a nozzle with

changeable critical diameter of flow. The conditions of sample preparation was presented in Table 1.

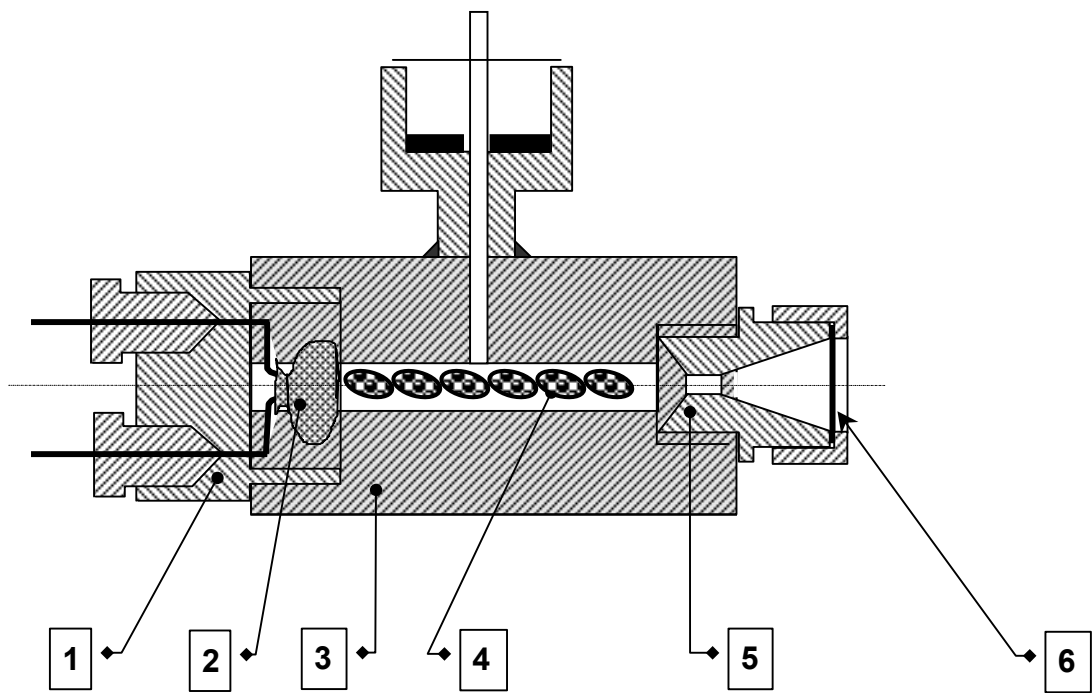


Fig 1. Case of micro-motor design symbols:
 1 - igniter hardware, 2 - primer, 3 - case,
 4 - sample of BKNO₃ pellets, 5 - nozzle,
 6 - alumina diaphragm, 7 - pressure sensor

Table 1.

No of sample	Mass (g)	d _{kr} (mm)	Diaphragm
1	3.6	2.0	Alumina
2	3.6	2.0	Alumina
3	3.6	2.5	Alumina
4	3.6	2.5	Alumina
5	3.6	3.0	Alumina
6	3.6	3.0	Alumina
7	3.6	2.0	Not used
8	3.6	2.5	Not used

The measurements of p(t) for samples was performed using for combustion three tablets type II B bi-convex according to MIL-P-46994B. In every sample the ignition was initiated by electric primer MB2N according to SWW1333. Outlet of nozzle was fenced off by alumina diaphragm with thickness 0.1mm.

To examine this results the method applied for estimation of operation the small rocket motors was used [3,4], according to figure 2.

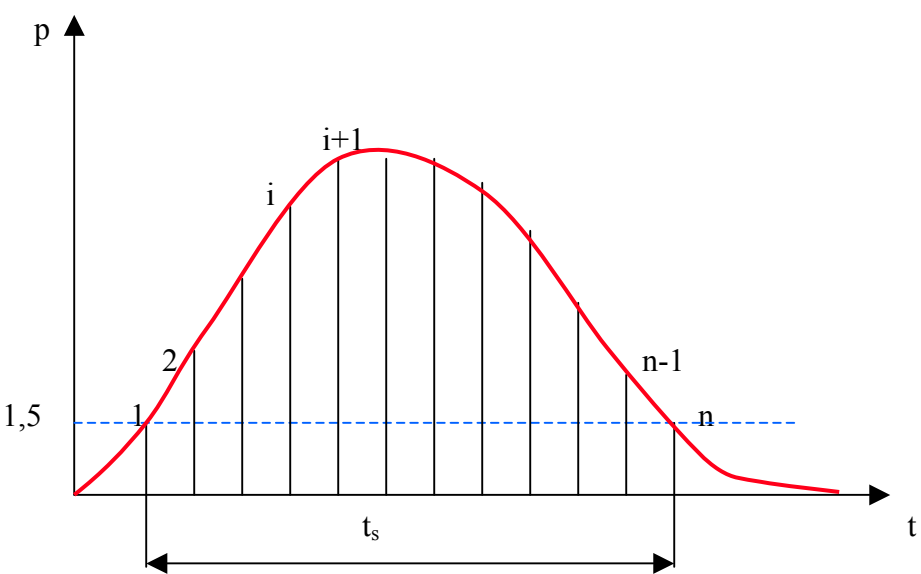


Fig 2. The method of pressure calculation by average route of function p(t)
The average pressure in every sample was determined using the equation :

$$\bar{p} = \frac{\sum_{i=1}^n p_i}{n} \tag{1}$$

where: p_i – pressure at i point
 n – amount of results

The time of combustion of sample t_s was determined as a time between the beginning and the end of course $p(t)$ at the level 0.15 [MPa]. The pressure 0.15 [MPa] established as a beginning pressure for independent combustion of BKNO_3 pellet (in the growing area of the curve) and pure decompression without finish burning in the drop of the curve. This criterion was accepted as preliminary, used in engineering practice [4].

The combustion rate of sample was determined from the equation:

$$\bar{u} = \frac{e}{t_s} \tag{2}$$

where: e – thickness of burning layer established for chosen type of pellet as 1.65 [mm]

For every sample the relation between burning rate and average pressure $\bar{u} = f(\bar{p})$ was established and on this base this dependence was calculated and compared with literature data from [1] for $p = 0.1$ [MPa]

CURVES OF COMBUSTION

The registered curves of combustion was presented in figures 3 ÷ 5.

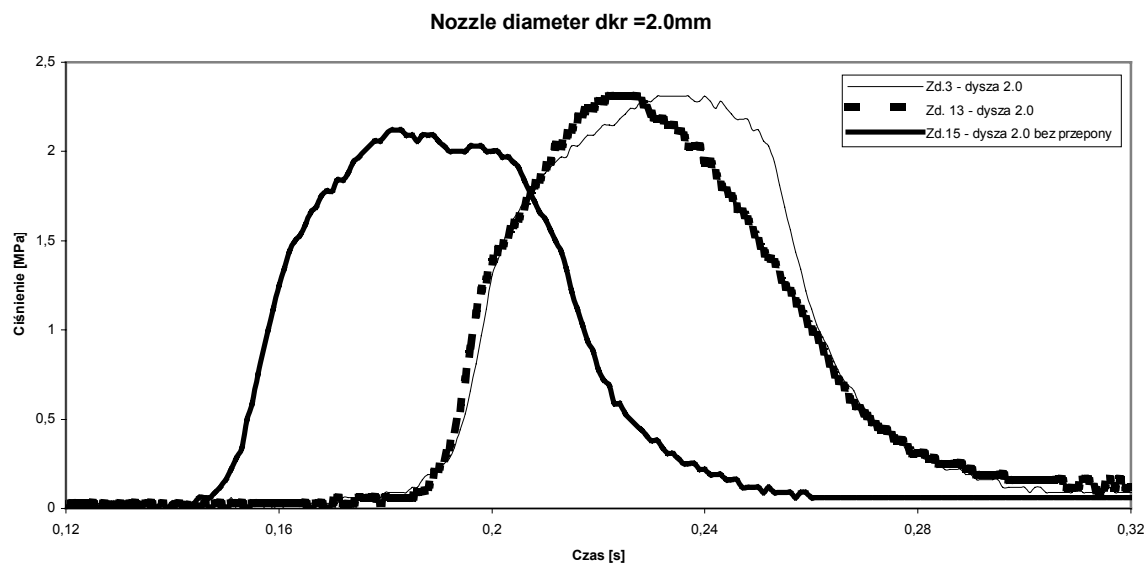


Fig 3. Sample of combustion whit nozzle diameter $d_{kr}=2.0\text{mm}$

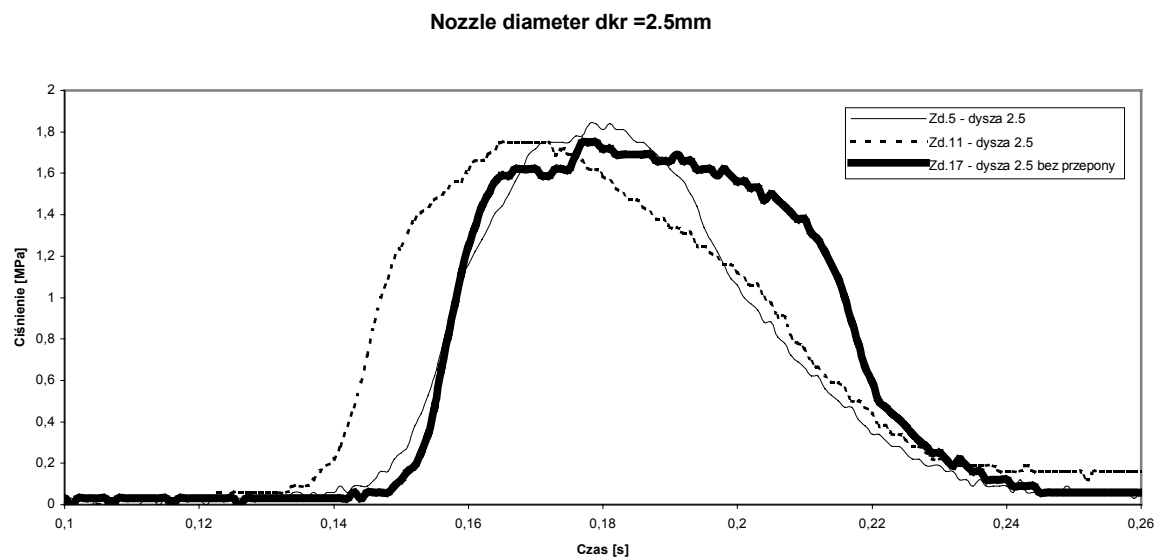


Fig 4. Sample of combustion whit nozzle diameter $d_{kr}=2.5\text{mm}$

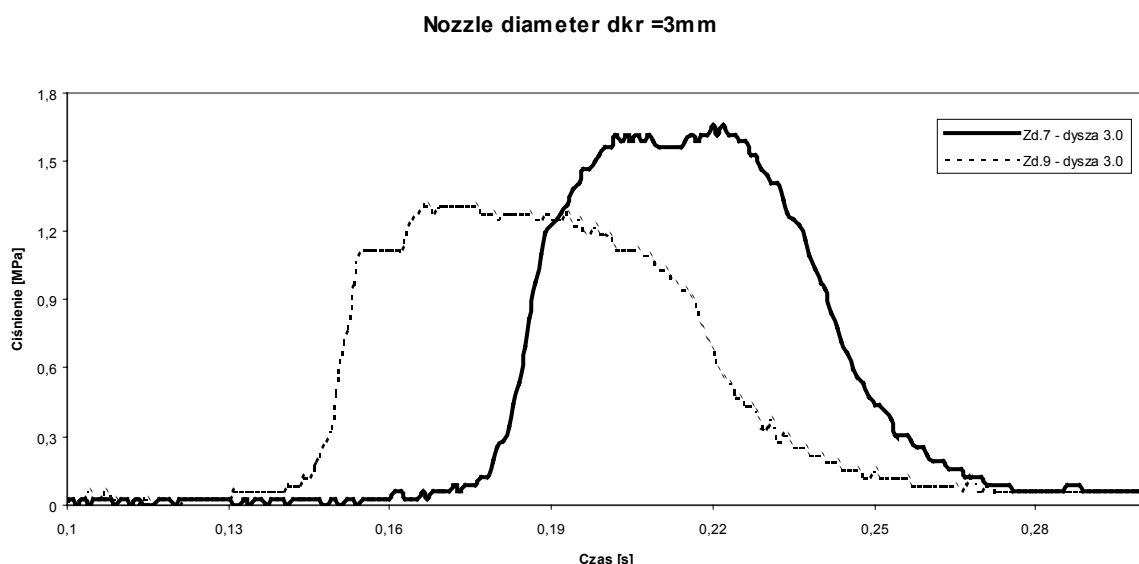


Fig 5. Sample of combustion with nozzle diameter $d_{kr} = 3.0\text{mm}$

We have observed basing on this curves that:

- There is a great similarity of curves courses for the measurements performed in the same conditions of combustion of sample and it proves the repetability of these processes;
- There is no characteristic peaks for samples and it is caused by shape of tablets with two steps of regressivity;
- Dynamics of increase of pressure to the level 1 [MPa] is similar in every sample;
- Dynamics of decrease of pressure from the level 1 [MPa] is similar as in every sample
- Dynamics of growing and decline of pressure depends negligible on critical diameter of nozzle in examined range of dimension d_{kr}

ANALYSIS OF RESULTS

The interpretation of results was made by method described in point 2. Additionally the dynamic of process and relation $p(t)$ in characteristic points i.e. the beginning, in the middle and final phase was presented.

The value of $\frac{+dp_{10}}{dt}$ was determined from the curve (calculated by graphic differentiation) taking into account the values from 0.15 [MPa] to 1 [MPa] in the part of increase of pressure

$\frac{-dp_{10}}{dt}$ and from 1 [MPa] to 0.15 [MPa] in the part of decrease of pressure. The level 1 [MPa] was considered for the estimation of dynamics. For the same periods of time in the curve, the time t_{10}^+ i t_{10}^- was determined. The results were presented in Table 2.

Table 2.

No sample	\bar{p} [atm]	\bar{t} [s]	$\frac{+dp_{10}}{dt}$	t_{10}^+	$\frac{-dp_{10}}{dt}$	t_{10}^-	Burning rate u [mm/s]
1	13.488	0.104	736.36	0.011	279.31	0.029	15.86
2	12.284	0.109	1077.78	0.009	227.03	0.037	15.14
3	10.248	0.084	840.00	0.011	280.00	0.030	19.64
4	10.160	0.101	933.33	0.009	240.00	0.035	16.33
5	10.624	0.086	944.44	0.009	337.50	0.024	19.18
6	9.010	0.099	1062.50	0.008	262.50	0.032	16.66
7	12.946	0.094	1050.00	0.008	322.22	0.027	17.55
8	11.852	0.084	1157.14	0.007	442.10	0.019	19.64

Where:

\bar{p} - average pressure in the registrated curve estimated by metod given in the Figure 2

\bar{t} - average time of combustion estimated by in a level of 0.15 [MPa] according the Figure 2

$\frac{+dp_{10}}{dt}$ - the derivative of pressure growth in the interval of time from 0.15 [MPa] to 1 [MPa] in the area of increase expressed in [atm/s]

t_{10}^+ - time of pressure increase from 0.15 [MPa] to 1 [MPa] expressed in [s]

$\frac{-dp_{10}}{dt}$ - the derivative of pressure decrease in the interval of time from 1 [MPa] to 0.15 [MPa] expressed in [atm/s]

t_{10}^- - time of pressure decrease from 1 [MPa] to 0.15 [MPa] in [s]

u - rate of combustion calculated form the equation ^[2] in [mm/s]

The dependence of $\bar{u} = f\left(\bar{p}\right)$ was counted whit Excel programme as the trends curve which is presented in figure 6.

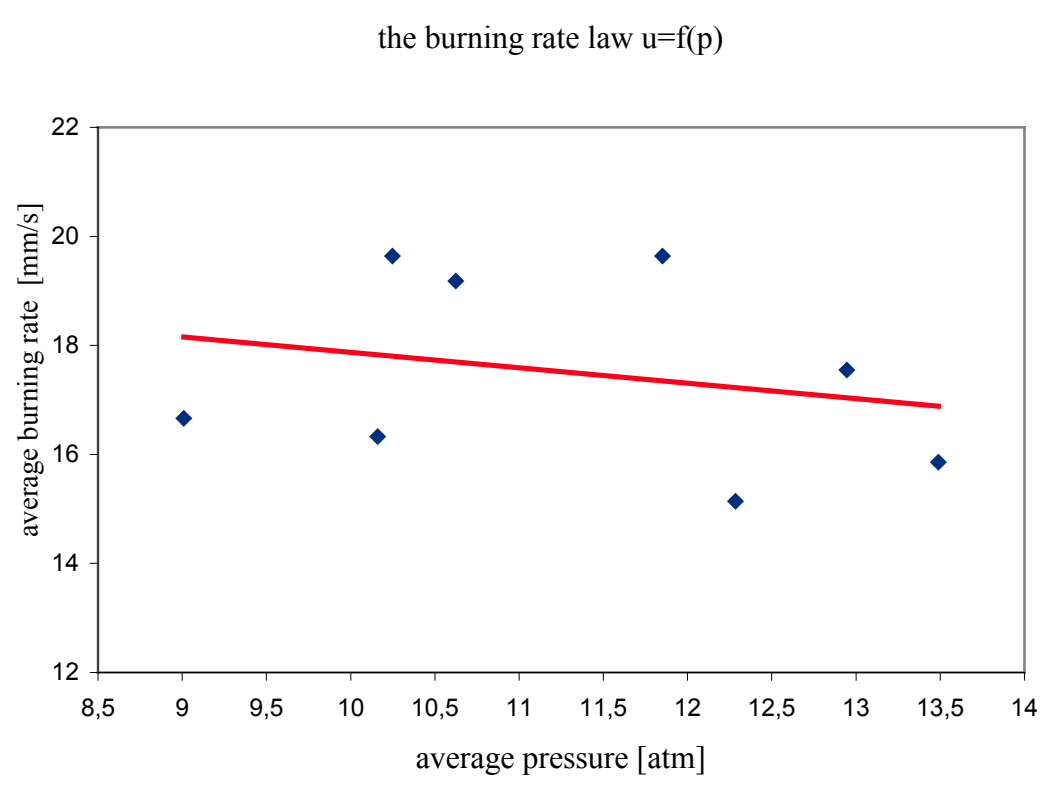


Fig 6. Dependence of burning rate for BKNO₃ tablets as a function of pressure

According Fig.6 was assigned the burning rate law as: $u = -0.2831p + 20.707$

The results allowed to observe the dependence of combustion decrease rate as a function of pressure. In the ranges of examined pressures the dependence is $- 0.28\text{mm/MPa}$.

This experimental value is twice as high as published in literature ^[1] for the pressure 0.1 [MPa].

CONCLUSION

1. The BKNO_3 mass properties cannot be described by typical exponential burning rate law - depending on a pressure;
2. The average measured rate of combustion was from $15.14 \div 19.68$ [mm/s];
3. It cannot be observed in examined system any significant changes in dynamics of increase the pressure till the level of 1MPa and in dynamics of decrease the pressure from 1 [MPa];
4. It can be supposed that the burning rate of this mass is dependent on the rate of products of combustion flow than is susceptible on erosive burning.
5. The examination of mass BKNO_3 properties will be continued.

REFERENCES

- [1] ROBERTSON W.E: IGNITER device for solid rocket motors; Bermite Industries.
- [2] MIL-P-46994B: Pellets, Granules Boron/Potassium Nitrate
- [3] PRISNIAKOW W.F: Dynamika rakietnych dwigatielej twierdого topliwa - Maszynostrojenije, Moskwa, 1984
- [4] DAVENAS A: Solid rocket propulsion technology, Pergamon Press, 1993

SYNTHESIS AND SOME PROPERTIES OF BU-NENA

K. Dudek*, P. Mareček*, J. Skládal* and Z. Jalový**

* Explosia a.s. Research Institute of Industrial Chemistry (VÚPCH),
CZ-532 17, Pardubice-Semtin, Czech Republic

** Department of Theory and Technology of Explosives, University of Pardubice,
CZ-532 10 Pardubice, Czech Republic

Abstract:

Butyl-NENA was synthesized by two-step reaction in laboratory and pilot plant scale. The product was identified by means of ^1H , ^{15}N NMR spectra, IR spectra and elementary analysis. Purity of the sample was determined by HPLC. Evaluated parameters were sensitivity to impact, DTA analysis and acidity of Bu-NENA. The results, especially with regard to utilization of Bu-NENA as a component of propellants and explosives, are discussed.

Keywords: Bu-NENA, synthesis, plasticizer

1. INTRODUCTION

Nitratoethylnitramines, known as NENA-compounds, have recently been discovered to be potentially very useful ingredients in propellants and explosives. This is due to increasing demand for developing less sensitive propellants and explosive compositions.

Alkyl-NENAs were first discovered in the early part of the Second World War by the scientists George Wright and Walter Chute at the University of Toronto [1].

Alkyl-NENAs include both nitrate group and nitramino group. NENA compounds are highly interesting compounds for rocket propellants and LOVA ammunition. Energetic materials, which include alkyl-NENAs, have numerous advantages. Their well known property is the ability to readily plasticize polymers (e.g. nitrocellulose).

In the last years special interest is paid to Bu-NENA. Substitution of Bu-NENA for NG (nitroglycerin) in both propellants and explosives brings along improvement in safety. This type of propellants and explosives meets the present military requirements for advanced ammunition. Bu-NENA has improved thermochemical properties and will be in addition, it is particularly good nitrocellulose plasticizer. Bu-NENA is expected to be use as additives to energetic material.

1.1 Published properties of Bu-NENA

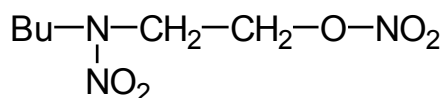
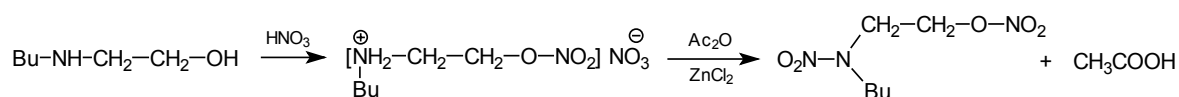


Table 1. *Published properties of Bu-NENA*

Compound	N-(1-butyl)-N-(2-nitroxyethyl)nitramine
Formula index	C ₆ H ₁₃ N ₃ O ₅
Chemical Abstract (CAS)	82486-82-6
Molecular weight [g.mol ⁻¹]	207.2
Oxygen balance (CO ₂ , H ₂ O, N ₂) [%]	-104.3
Melting point [°C]	-9.1 ^[2]
Boiling point [°C]	205 ^[3]
Index of refraction	1.475 ^[2]
Density [g.cm ⁻³]	1.22 ^[2]
Enthalpy of formation [kJ.mol ⁻¹]	-192.46 ^[4] -139.75 ^[4] -192.88 ^[4]

2. EXPERIMENTAL

Bu-NENA was prepared by 2-step reaction by modified procedure mentioned in the paper^[1]. Starting material is commercially available 2-butylaminoethanol. In the first reaction step nitric acid reacts with 2-butylaminoethanol under formation of N-butyl-N-(2-nitroxyethyl)nitrate. This reaction is strongly exothermic. In the second reaction step a solution of acetic anhydride and catalyst (ZnCl₂) reacts with N-butyl-N-(2-nitroxyethyl)nitrate under formation of Bu-NENA and acetic acid.



2.1 Identification, purity and properties of Bu-NENA

Elementary analysis

	C	H	H
Calculated [%]:	34.78	20.29	6.28
Found [%]:	35.01	20.41	6.18

IR spectrum

IR spectra were measured on apparatus IMPACT 410. The sample was scanned in the area 4,000 - 600 cm^{-1} . The results of measurements were compared with STANAG 4583 values (draft July 03) and Shen Qionga^[5] values.

Table 2. IR spectra of Bu-NENA.

Group	Literature ^[5]	Measured values	STANAG (draft)
-NO ₂ (nitrate)	1650 cm^{-1}	1633 cm^{-1}	1625 cm^{-1}
-NO ₂ (nitramine)	1525 cm^{-1}	1514 cm^{-1}	1518 cm^{-1}
-NO ₂ (nitrate)	1280 cm^{-1}	1272 cm^{-1}	1236 cm^{-1}
-O-N (nitrate)	850 cm^{-1}	847 cm^{-1}	842 cm^{-1}

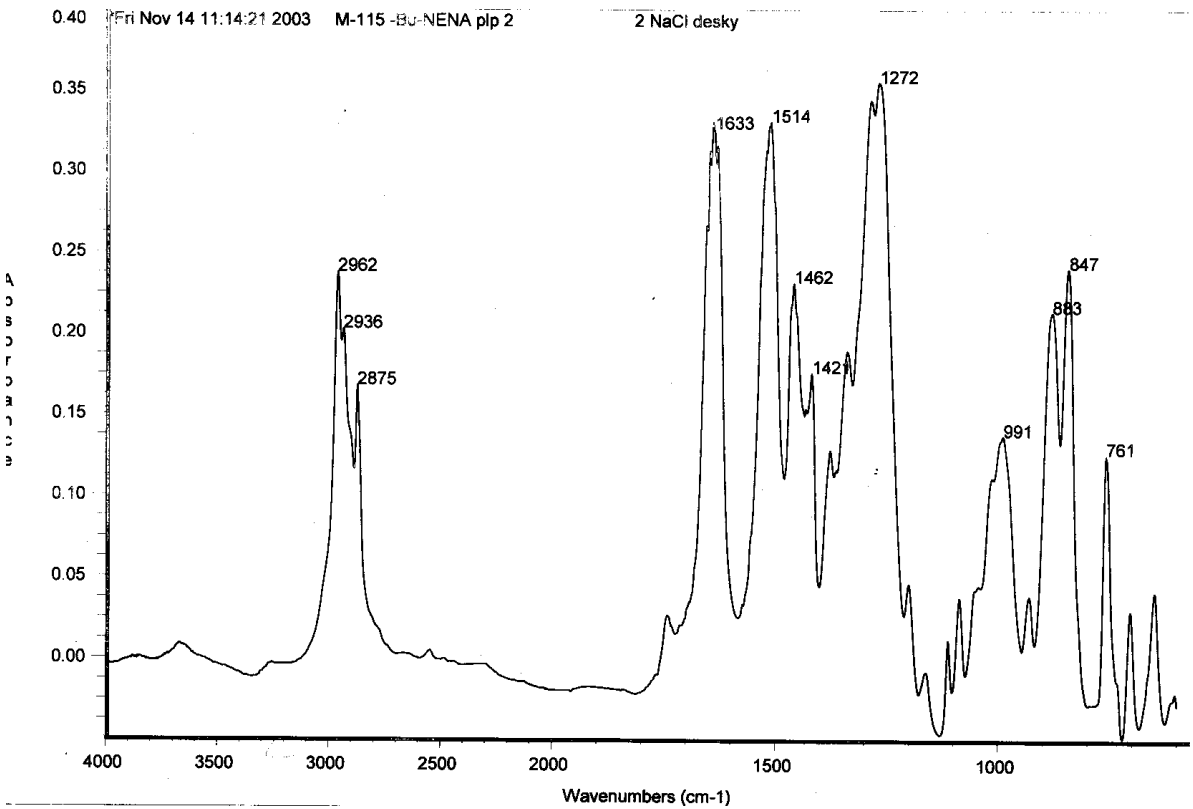


Fig 1. IR spectrum of Bu-NENA (measured values).

NMR spectrum

NMR measurements were carried out at Joint Laboratory of Pardubice University and VÚOS, Pardubice-Rybitví. ¹H and ¹⁵N NMR spectra of Bu-NENA were measured by means of Bruker AMX 360 spectrometer at 25⁰C.

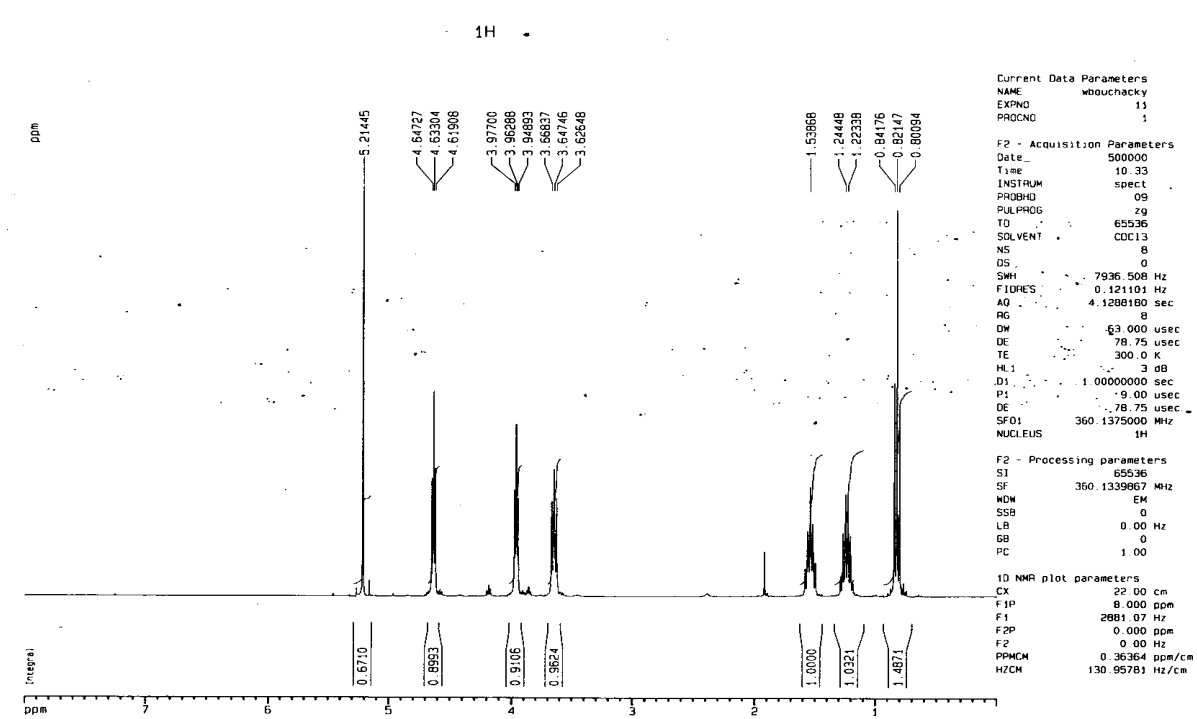


Fig 2. ¹H NMR spectrum of Bu-NENA.

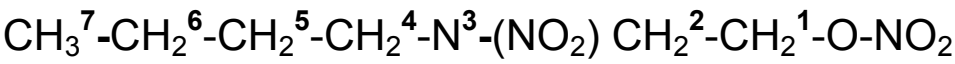


Table 3. Chemical shifts of ¹H NMR spectrum of Bu-NENA.

Shifts (ppm)	Group
0.82	CH ₃ ⁷
1.22	CH ₂ ⁶
1.54	CH ₂ ⁵
3.65	CH ₂ ⁴
3.96	CH ₂ ²
4.63	CH ₂ ¹
5.20	CH ₂ from CH ₂ Cl ₂

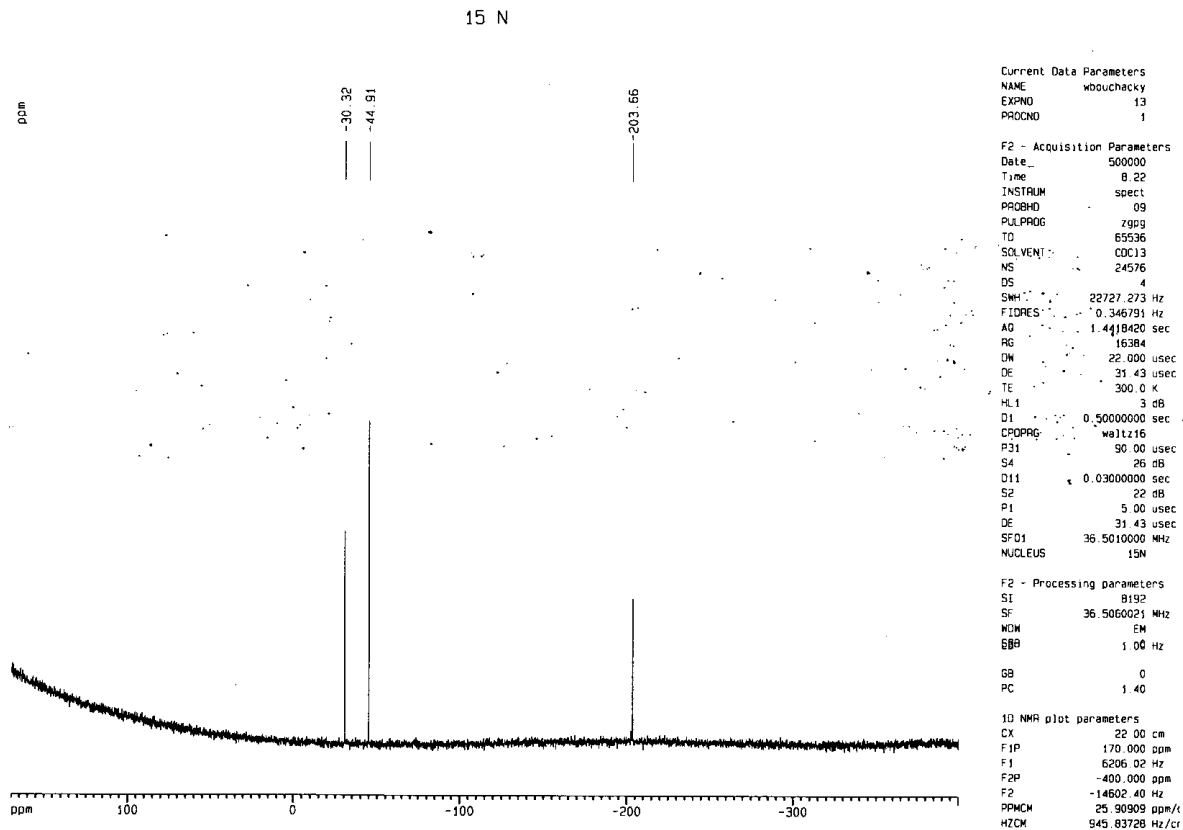


Fig 3. ¹⁵N NMR spectrum of Bu-NENA.

Table 4. Chemical shifts of ¹⁵N NMR spectrum of Bu-NENA.

Shifts (ppm)	Group
-203.7	N-NO ₂
-44.9	O-NO ₂
-30.3	N-NO ₂

Purity

The content of Bu-NENA was determined by using HPLC method.

Column: Separon SGX C18

Mobile phase: Acetonitrile/water 50:50

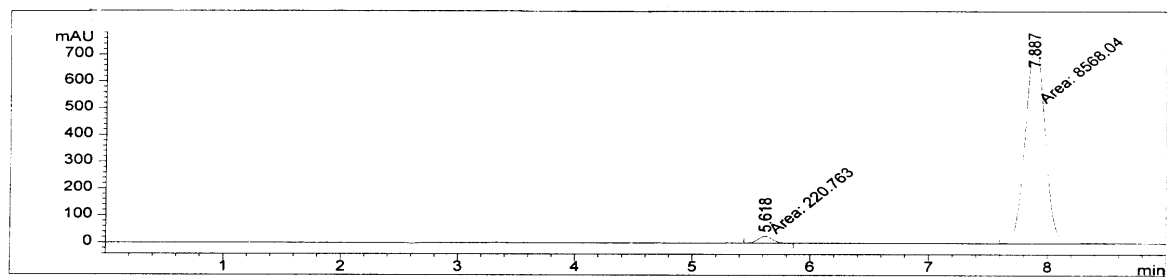
Detector: UV/DAD 240 nm

Flow rate: 1.0 ml/min

Column temperature: 30°C

The first peak in the chromatogram corresponds with N-butyl-N-(2-acetoxyethyl)-nitramine (Bu-AENA).

The second peak in the chromatogram corresponds with N-butyl-N-(2-nitroxyethyl)-nitramine (Bu-NENA).



Peak #	RetTime [min]	Sig	Type	Area [mAU*s]	Height [mAU]	Height %
1	5.618	1	MF	220.76303	25.46175	3.2980
2	7.887	1	MF	8568.04004	746.56976	96.7020
Totals :				8788.80307	772.03152	

Results obtained with enhanced integrator!

Fig 4. HPLC chromatogram of Bu-NENA.

2.2 Some properties of Bu-NENA

DTA

DTA measurement was carried out on apparatus DTA-550 Ex. The sample weight was 50 mg. Heating rate used was 5 °C/min.

DTA thermogram (figure 5) contains one exotherm peak starting at 153°C and with maximum at 191°C.

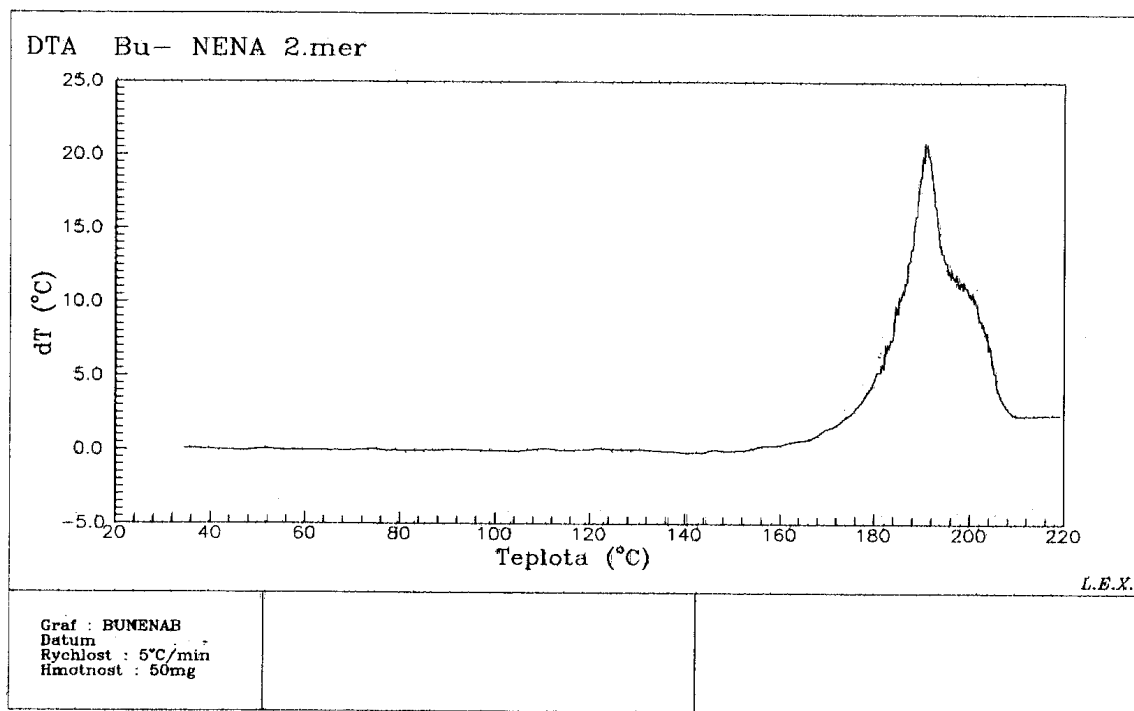


Fig 5. DTA thermogram of Bu-NENA.

Sensitivity to impact of Bu-NENA

Sensitivity to impact was more than 100 cm (5 kg drop-weight BAM apparatus)

Acidity

Bu-NENA was dissolved in acetone and titrated with alcoholic solution of potassium hydroxide (KOH) with bromocresol green as indicator until the solution develops changes the colour to green. Reference solution is used to determine equivalence point.

Calculation:

$$\text{H}_2\text{SO}_4 (\%) = 4,9 * (A - B) * \frac{N}{W} ;$$

Where: A = ml used of KOH in the titration of the sample

B = ml used of KOH in the titration of the blank

W = weight of sample

N = normality of KOH

Result: 0.006 % H₂SO₄

3. CONCLUSION

The synthesis was studied at different reaction conditions. During the research optimal conditions were found with regard to safety, yield, purity and scale up production. Molar ratios of starting compounds and reaction temperatures are in accordance with published values. Bu-NENA was prepared in laboratory scale with the yield 65-69 %, with purity in range 95-97 %. After laboratory research the first pilot-plant experiment was realized.

REFERENCES

- [1] SKJOLD, E.; ET AL.: US Patent 6262301, 2001
- [2] BLOMQUIST, A.T.; FIEDOREK, I.: US Patent 2485855, 1944
- [3] LICHT, H.H.; RITTER, H.: Proceedings of the International Pyrotechnics Seminar, 114-122, 1999
- [4] BATHELT, H.; VOLK, F.; WEINDEL, M.: ICT-Database of Thermochemical Values, version 3, Fraunhofer - Institute für Chemische Technologie, Germany, 2001
- [5] SHEN, Q.: ET AL.: 27th Int. Annu. Conf. ICT, Karlsruhe, 133.1-133.7, 1996

ANALYSIS AFTER COMBUSTION OF PROPELLANTS

A. Eisner*, M. Adam*, K. Ventura*, V. Ježová* and J. Skládal**

* Department of Analytical Chemistry, Faculty of Chemical – Technology,
University of Pardubice, Nám. Čs. Legií 565, Pardubice 532 10, CZ

** Research Institute of Industrial Chemistry, Explosia a.s.,
Pardubice – Semtín 532 17, CZ

Abstract:

The aim of this study is an identification of products after combustion of smokeless powders and solid propellants. In first a sample of smokeless powder was burnt on the clean sand. Than an isolation of compounds from this sand was tried. The accelerated solvent extraction and ultrasonication were used for the isolation of these compounds. Gas chromatography GC 17A with mass spectrometry detector QP505A was used for an identification of compounds.

Keywords: extraction, propellant, GC/MS, accelerated solvent extraction, combustion

1. INTRODUCTION

Old smokeless powders must be liquidated because stabilisator content is low. This smokeless powder is unstable and dangerous for people. The liquidation of smokeless powders could be executed realise with their burning. A knowledge of compounds arising out of smokeless powders is necessary for specification their effect to the environmet.

First step is an isolation of these compounds from sample. The classical ^[1] extraction methods (soxhlet, ultrasonication) and new extraction techniques (accelerated ^[2] solvent extraction, supercritical fluid ^[3] extraction) are used for it.

In principle, accelerated solvent extraction (ASE) is an extraction process taking place in the solid / liquid phase system and being performed at a increased temperature (50-200°C), increased pressure (5-20 MPa) and within a relatively short time interval (max. 20 min.)

In order to perform ASE, the same solvents as for Soxhlet extraction can be used. More over, it is possible to choose even such solvents that are less effective when used in classical techniques. This is due to specially enhanced extraction kinetics of the extraction process in ASE. Very advantageous is that extraction work with ASE can be made under conditions of liquid phase. This allows one to use even mixed solvents, as there is no risk of distilling one component separately.

2. EXPERIMENTAL PART

A sample of propellants was used for these experiments. These contains a nitro-cellulose; a diphenylamine or centralite I as stabiliser; an aromatic nitrotoluene, a nitroglycerine and a nitroguanidine as energetic compound and a phthalates as plasticizers.

Sample of a smokeless powder and propellants (about 5g) were burnt on sand. Before combustion the sand was cleaned in the water eight times and than was dried in an oven (150°C) for 8 hours. The sample of the sand (about 50g) was extracted to 50ml of solvent in ultrasonic bath for 20 minutes, filtered and most of the solvent was evaporated to volume 1 ml.

Also accelerated solvent extraction was used as a comparative extraction technique. After pre-treatment, weight amount of sample was placed into extraction cell with a portion of glass wool on the bottom. Next portion of wool was laid on the surface of the sample and the remaining volume of the cell was filled up with glass balls. After inserting prepared cell into extractor heating oven, the desired value of both temperature and pressure were adjusted by means of extraction solvent.

Two extraction steps were performed when the extract was being entrapped into the same collecting vessel. The conditions for extraction were as follows: weight amount about 15 g of sand and extracted at temperature 110 °C and pressure 10 MPa end extraction time was twice 10 minutes. Acetonitrile was used as a solvent for both extraction methods.

In the next experiments propellants were burnt on a bowl without the sand. A rest of propellant was washed down with 20 ml of an acetonitrile. This extract was evaporated to volume 1ml and it was analyzed.

The extracts obtained were analysed by using of the gas chromatograph GC 17A coupled with mass spectrometry detector QP 5050A (EI, NCI, both Shimadzu) and GC/MS solution data system (Shimadzu). The helium (grade 5.0, Linde) was used as carrier gas. Separations were performed on a 30m x 25µm i.d. capillary column coated with a 0,25 µm film of polymethylsiloxane (DB-5 MS). Split injection 1:10 was used. The column oven was isothermally maintained at 45°C for 5 minutes and than temperature increase for 20°C/min to 280°C which was kept for 5 minutes. The temperature of injector was 220°C and the temperature of interface was 230°C. The identification of compounds was based on the comparison their mass spectrum with the spectrum in the library (NIST 62 and NIST 12, Shimadzu).

3. RESULTS AND DISCUSSION

The propellants, which contained a nitro-cellulose, a diphenylamine, a centralite, an aromatic nitrotoluene, nitroglycerine, a nitroguanidine and a phthalates were burnt on the clean. Next samples from sand were extracted to the acetonitrile and they were analysed with gas chromatography with mass detector. Mass spectrums in the peaks were compared with library. Some of the peaks were identified, but any peaks were not identified with the library. These peaks we will try to identify. We will try to interpret their mass spectrum. The better extraction efficiency results from our experiments for accelerated solvent extraction than ultrasonic extraction. More peaks were found in the extract from accelerated solvent extraction, but the more peaks were not unfortunately identified. Diphenylamine and dibutylphthalate there was found. These compounds are from original propellants. N,N-diethyl-3-methyl-benzamine was identified. It could be any degradation products of the diphenylamine. These compounds were found in both extracts (accelerated solvent extraction and ultrasonic extraction). One of the chromatogram is shown on the figure 1. Aliphatic hydrocarbons (undecane, tridecane and hexadecane), benzene and phthalates were identified in extracts from accelerated solvent extraction.

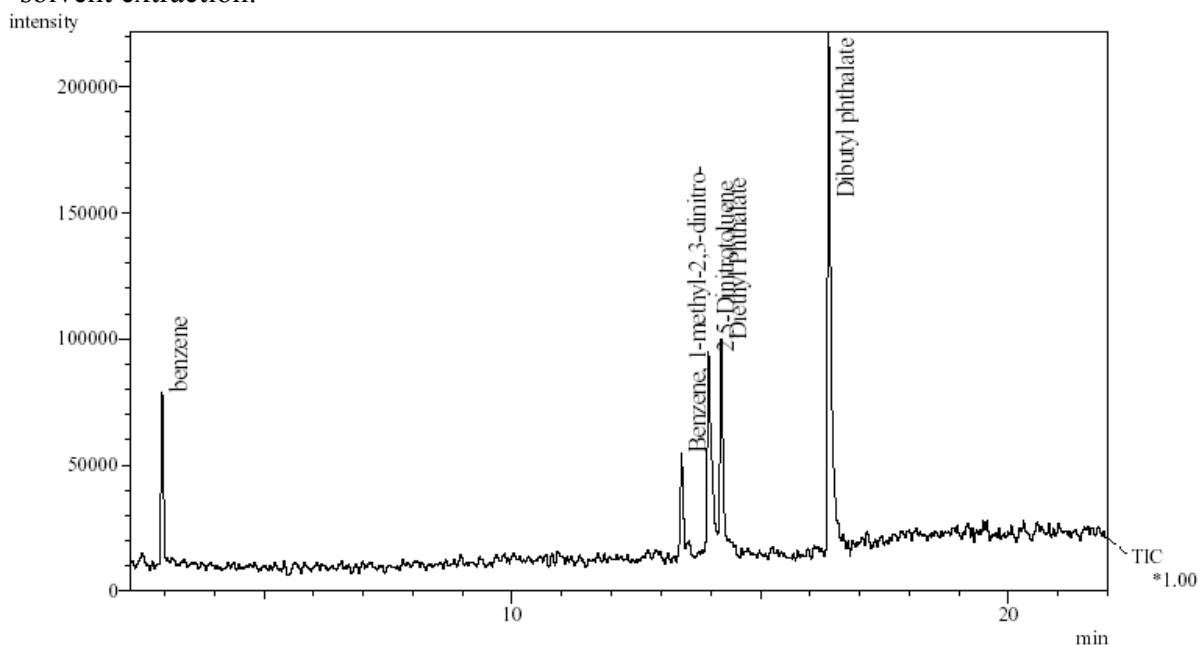


Fig 1. Chromatogram of extract from sand

Because a few peaks were found, we tried to burn 5g of propellant without sand. We burnt it direct on the clear tinny bowl. A rest of propellant was washed down with 20 ml of an acetonitrile. This extract was evaporated to volume 1ml and it was analysed. More compounds were identified in these extracts. Diphenylamine, centralite I, phthalates and 2,4,6-trinitrotoluene come from original propellants. 1,3- and 1,4-dinitrotoluene, toluene, benzene, 1-methyl-2-nitrobenzene, 1-methyl-4-nitrobenzene and N,N-diethyl-3-methyl-benzamine was identified. It could be any degradation products of the compounds, which were in original propellants. One of the chromatogram is shown on the figure 2.

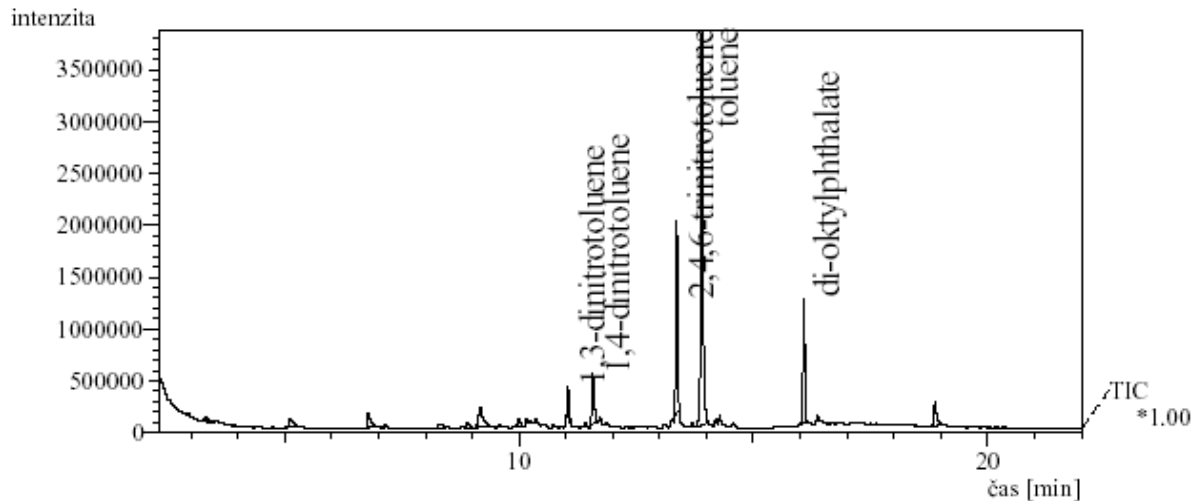


Fig 2. Chromatogram of acetonitrile extract from clear tinny bowl

The nitroglycerine a nitroguanidine were not found in any extracts. These compounds are thermally labile and they completely burn to the carbon dioxide, water and the other gaseous compounds.

4. CONCLUSION

Perform experiments have been confirmed the fact, that accelerated solvent extraction is better then ultrasonic extraction. Almost of the propellants completely burn to the carbon dioxide, water and the other gaseous compounds. We achieved the best results after combustion of propellants on the clear tinny bowl.

Acknowledgement:

Experiments were performed thanks to financial support from the Ministry of Education, Youth and Sports of the Czech Republic (Project MSM 253100002), from the Grant Agency of the Czech Republic (Project 203/02/0023) and from Grant Agency of the Czech Republic (203/02/001).

REFERENCES

- [1] J. ZINON, C. ZITRIN: *Modern methods and applications in analysis of explosives*. ed.: John Wiley & Sons Chichester, 1993
- [2] J.R. DEAN: *Extraction Methods for Environmental Analysis*, John Wiley & Sons, Chichester 1998
- [3] A.A. CLIFFORD: *Solvent Extraction - Supercritical Fluid Extraction*, Encyclopedia of Analytical Science 8, 4724, A.Townshend, editor, Academic press ltd., London 1995

DINITROBIURET AND ITS SALTS

J. Geith, K. Karaghiosoff, T.M. Klapötke, P. Mayer and J. Weigand

Department of Chemistry and Biochemistry, University of Munich,
Butenandtstr. 5-13 (D), D-81377 Munich (Germany)

Abstract:

The work summarizes knowledge about Dinitrobiuret (DNB) - about its important explosives characteristics and parameters. It is focused on preparation, determination of molecular structures and the results of IR-Raman and multinuclear NMR spectroscopic investigations.

Keywords: *dinitrobiuret, DNB, explosives, high energy density materials*

1. INTRODUCTION

In recent years there has been great interest in the development of new solid high-energetic materials. Desired properties for this class of compounds are a halogen-free, nitrogen- and oxygen-rich composition, high density and a large positive heat of formation [1]. Compounds with *N*-bonded nitro groups, such as dinitrourea (DNU) and dinitramide salts are used as explosives and propellants [2, 3, 4]. However a disadvantage of these energetic compounds is their sensibility, which makes them more or less difficult to handle.

Dinitrobiuret (DNB) was synthesized more than 100 years ago [5]. Although known for a long time, surprisingly little is known about its properties. Like dinitrourea DNB also contains *N*-bonded NO₂-groups, but compared to DNU it is much more stable and easier to handle. DNB (**1**) can be readily deprotonated to form stable salts with different cations.

2. EXPERIMENTS AND RESULTS

Here we describe the preparation, molecular structures and the results of IR, Raman and multinuclear NMR spectroscopic investigations of **1** as well as of its K⁺, Ba²⁺ and N₂H₅⁺ salts (**2**). Their possible use as starting materials for the synthesis of new high-performance energetic materials with positive oxygen balance, oxidizing and reducing groups within the same compound, is discussed.

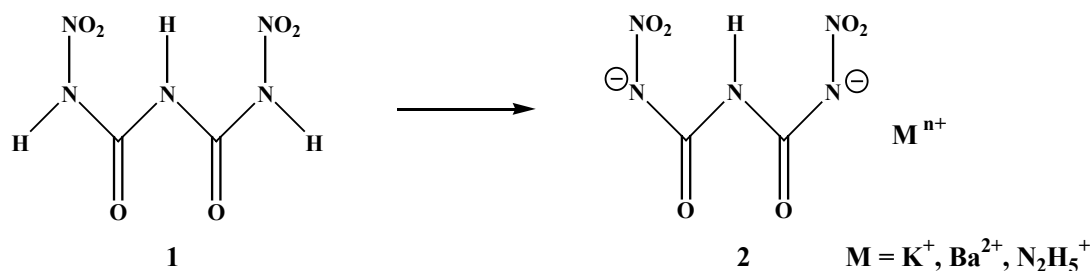


Fig 1. DNB and its salts

DNB was readily prepared by nitration of mononitrobiuret at low temperature with 100% HNO_3 . Salts of **1** were synthesized by an acid-base reaction with metal hydroxides or $\text{N}_2\text{H}_4\cdot\text{H}_2\text{O}$ in alcohols. After recrystallization they were characterized by vibrational spectroscopy and single crystal X-ray diffraction.

Single crystals suitable for X-ray analysis for dinitrobiuret monohydrate, dikalium dinitrobiuretate monohydrate, barium dinitrobiuretate dihydrate and hydrazinium dinitrobiuretate were obtained by evaporation of their solvents (ethanol, water). The observed molecular structures (ORTEP plot) and the packing diagrams for some of these compounds are shown in Figures 2 and 3.

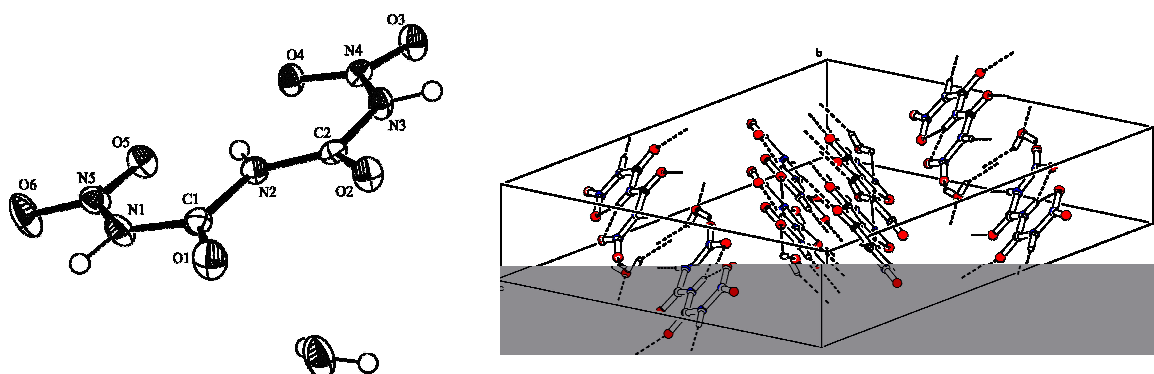


Fig 2. ORTEP plot (50% probability) and packing diagram of dinitrobiuret monohydrate

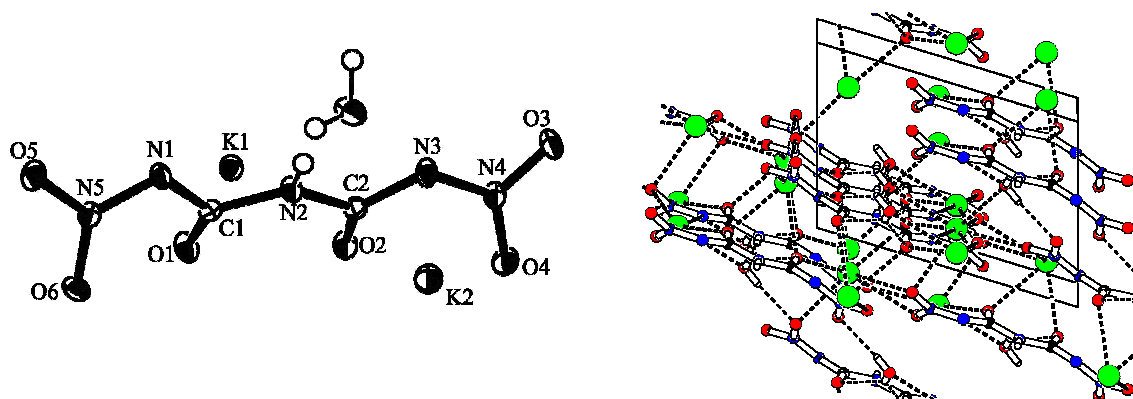


Fig 3. ORTEP plot (50% probability) and packing diagram of dikalium dinitrobiuretate monohydrate

In the crystal of DNB and its salts the biuret-framework is planar with the nitro groups arranged in the same plane.

DND was characterized in detail with ^1H , $^{13}\text{C}\{^1\text{H}\}$, ^{14}N and ^{15}N NMR spectroscopy. In the $^{15}\text{N}\{^1\text{H}\}$ NMR spectra of **1** the different NOE observed for the different nitrogen nuclei in the molecule is related to their structure.

Dinitrobiuret has a high density and a positive oxygen balance (+ 4.1%). It was found to be not sensitive to impact and friction. The heat of combustion ($\Delta H_{\text{comb.}}$) of DNB was determined experimentally using oxygen bomb calorimetry: $\Delta H_{\text{comb.}} = 5195 \pm 200 \text{ kJ kg}^{-1}$. The standard heat of formation (ΔH°_f) of dinitrobiuret was obtained on the basis of quantum chemical computations at the electron-correlated ab initio MP2 (second order Møller-Plesset perturbation theory) level of theory using a correlation consistent double-zeta basis set (cc-pV-DZ): $\Delta H^\circ_f = -353 \text{ kJ mol}^{-1}$.

The detonation velocity (D) and detonation pressure (P) of DNB were calculated using the empirical equations by Kamlet and Jacobs: $D = 8660 \text{ m s}^{-1}$, $P = 33.9 \text{ GPa}$ [6].

3. CONCLUSIONS

Dinitrobiuret is very powerful and promising new explosive with positive oxygen balance (+4.1%), it shows detonation velocity and detonation pressure similar to well established energetic materials such as PETN, RDX or HMX. The crystal structures of dinitrobiuret and some its salts was determined for the first time

Acknowledgment

Financial support of this work by the University of Munich (LMU), the Fonds der Chemischen Industrie and the German Federal Office of Defense Technology and Procurement (BWB, WIWEB) is gratefully acknowledged.

EFFECTS ON ENERGETIC MATERIALS PROCESSED WITH POWER ULTRASOUND

V.I. Grozev*, R.H. Ganev** and Z. S. Grozeva***

* Konstantin Preslavsky University of Shumen,
University str.115, 9712 Shumen, Bulgaria (BG)

** University of Chemical Technology and Metallurgy,
Kliment Ohridski blvd. 8, 1756 Sofia, Bulgaria (BG)

*** Konstantin Preslavsky University of Shumen,
University str. 115, 9712 Shumen, Bulgaria (BG)

Abstract:

We present experimental results derived by the effect of a high power ultrasound on melts of explosives and solutions of propellants. An effect of increase of the speed of formation of crystallisation centers have been identified for 2,4,6-trinitrotoluene and mixtures on its base. We investigated the kinetics of destruction of nitrocellulose in ultrasound field in solution of gunpowders.

Keywords: *ultrasound, explosives, propellants*

1. INTRODUCTION

Ultrasound methods in the production and exploitation of energetic materials can be used in two directions-control and defectoscopy, as well as in treatment in liquid environment. Ultrasonic technique with low intensity is used for measuring the rate of burning of propellants, for control of the structure and the defects of propellant charges ^[1, 2]. Ultrasound treatment with high-power ultrasound is effective in liquid environment and is related to cavitation bubbles formation. The treatment of organic substance melts with powerful ultrasound leads to the increasing of the rate of crystallization, gas-cleaning, intensification of cooling, increasing of density and improving of the casting structure ^[3]. Analogically it could be presumed that the ultrasound processing during the explosive crystallization in the corpus of the ammunition would lead to improvement of the explosive charge quality. Ultrasonic processing of gunpowder solutions leads to destruction of the nitrocellulose macromolecules in single base propellants (SBP) which is of great importance for their utilizations.

The aim of the research is to investigate:

- the possibility of detonation initiation during the processing of melts of 2,4,6-trinitrotoluene (TNT) and mixtures on its base (TRDX-82) in ultrasonic field;
- the influence of the ultrasound on the rate of crystallization centers formation (RCCF) for TNT and TRDX-82;
- kinetics of destruction of nitrocellulose (NC) in ultrasonic field in solution of single base propellants (SBP).

The scientific data of the sensitivity of liquid explosives to the ultrasound initial impulse are inadequate and contradictory. The data for the influence of the ultrasound on the crystallization kinetics of the TNT and TRDX-82 are missing.

2. THE SENSITIVITY OF LIQUID EXPLOSIVES TO ULTRASOUND INITIAL IMPULSE

We study the following theoretical model:

1. During the ultrasound treatment there are generated cavitation bubbles in the explosive melt. When they are closed in the fluid micro-impact waves are spread.
2. We consider each cavitation bubble forms a possible centre of detonation stimulation.
3. The theory of "hot spots" ^[4] is applied to each bubble formed in the melt. According to this theory two conditions are necessary for generating detonation nucleus:
 - the nucleus temperature must be higher than the critical one;
 - the time for the processing of the cavitation micro-impact waves must be longer than the time, needed for the completing the chemical reaction of the explosive decomposition. By calculation and comparing the two values we make a conclusion for the explosive sensitivity.

According to ^[5] the temperature in the cavitation bubble is about 2700⁰C, regardless of the kind of the fluid. The critical temperature for the stimulation of explosive decomposition in the "hot spots" depends on their volume. The radius of the detonation stimulation centre is determined by the volume of micro-impact waves, which is 10⁻⁶m. The critical temperature for decomposing of the explosive at this radius is 400-1000 ⁰C ^[4]. We conclude that the temperature around the closing cavitation bubbles is higher than the critical one for detonation stimulation.

The time, required for completing the chemical reaction in the nucleus of detonation is 10⁻⁶s. The micro-impact waves are generated at the closing of the cavitation bubbles. We determined the period for treatment the micro-impact waves by the following formulas ^[6]:

$$\tau = 3,3 \cdot \Delta t \left(\frac{R_{\min}}{R_{\max}} \right)^{2,5} \quad (1)$$

where Δt - time of closing the cavitation bubble ;

R_{\min} , R_{\max} - minimum and maximum cavitation bubble radius.

For calculation the quantities in the equation 1 we use the formulas:

$$\Delta t = \frac{0,36}{f} \left(1 + \frac{P_0}{P_a} \right) \left[\frac{1}{2,9 \frac{P_0}{P_a} - 3,4 \left(\frac{P_0}{P_a} \right)^2 + 6} \right]^{0,5} \quad (2)$$

$$R_{\min} = \frac{1,2P_v \left(1 - \frac{P_0}{P_a}\right)}{f(P_a \cdot \rho)^{0,5} \left[2,9 \frac{P_0}{P_a} - 3,4 \left(\frac{P_0}{P_a}\right)^2 + \frac{P_v}{P_a} + 0,6 \right]} \quad (3)$$

$$R_{\max} = \frac{\arccos \frac{P_0}{P_a}}{3.14 \cdot f} \sqrt{\frac{P_a}{\rho} \left[\frac{\left(1 - \frac{P_0^2}{P_a^2}\right)^2}{\arccos \frac{P_0}{P_a}} - \frac{P_0}{P_a} \right]} \quad (4)$$

where f -ultrasound frequency, kHz ;
 P_0 -the pressure on the liquid , Pa ;
 P_a -sound pressure, Pa ;
 P_v -pressre on the liquid explosive, Pa ;
 ρ -density of the explosive, g/cm^3 .

The frequency of the used ultrasound generators is 20-22 kHz . The parameters of the ultrasound field and melted explosives are : $P_0/P_a=0,8$, $P_a=25 \cdot 10^{-6} Pa$, $f=20 kHz$, $\rho = 0,98-1,60 g/cm^3$, and $P_v=(1,2-1,5) \cdot 10^2$ by $82^\circ C$.

After substitution in the equation 4, 3, 2, 1 the time, required for the operation on the cavitation bubble we get $(0,4-1,1) \cdot 10^{-9} s$. This time is 1000 times lower than the required for the completing of the explosive reaction. The general conclusion is that in comparing the two conditions, the thermal impulse of the micro-impact waves round the cavitation bubble is lower and detonation is not initiated by treatment with ultrasound.

For the experimental test we treated the TNT and TRDX-82 melts in ultrasound tank with the power of ultrasound generator at 1,2 kW and ultrasound concentrator for 15 minutes. No explosion was observed in all tests. The stimulating of the explosive decomposition is a probable process, which depends on many factors. That's why the result is valid only for the specific conditions of the experiment.

3. KINETICS OF THE EXPLOSIVE MELT CRYSTALLIZATION IN ULTRASOUND FIELD

The rate of crystallization centers formation can be determined experimentally by the following method [7]:

$$Y = \frac{1}{\tau \cdot V} \quad (5)$$

where τ -metastability interval, s ;
 V -volume of the melted explosive, cm^3 .

The metastability interval is described by the curve time-temperature at cooling the melt. The searched interval is determined by staying time at over-cooling temperature (ΔT). The used TNT has been recrystallized to melting temperature 80,0 °C.

The data of the experimental work and statistic calculations of the results are given in fig. 1.

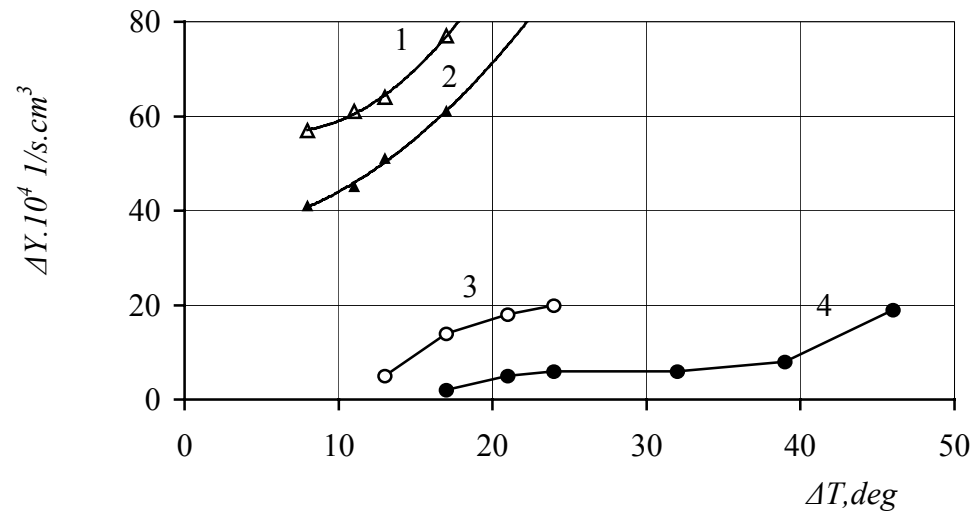


Fig 1. The dependence of the RCCF for treated (1-TRDX-82, 3-TNT) and untreated (2-TRDX-82, 4-TNT) melts with ultrasound

The curves 3 and 4 are described analytically with following equations:

$$Y \cdot 10^4 = -72,499 + 8,3280 \cdot \Delta T - 0,28813 \cdot \Delta T^2 + 0,00327 \cdot \Delta T^3 \tag{6}$$

$$Y \cdot 10^4 = 118,606 - 20,5115 \cdot \Delta T + 1,16776 \cdot \Delta T^2 - 0,0020191 \cdot \Delta T^3 \tag{7}$$

The analysis of this data show that the ultrasound has increased the rate of crystallization. The ultrasound influence is due to its complex stimulating which had resulted in increasing the possibility of generaing crystallization centres.

4. EFFECTS OF ULTRASOUND ON DEGRADATION OF SBP

The molecular weight is a major factor showing the on-going degradation processes in propellants treated with ultrasound. The method of our experimental work is described in [7]. The change of the average viscosimetric molecular weight M_η of nitrocellulose (NC) in the solutions of single base propellants in acetone and in a mixture of ethyl alcohol – diethyl ether after treatment with ultrasound is shown in fig.2.

The observed decrease of the molecular weight of the NC can be explained by mechanical, thermal and chemical influence of ultrasound on the lengths of molecule fragments.. The effects of the used solvents should also be taken into consideration. Hydroxyl and ether groups have a stronger ability to form hydrogen bonds with NC than the

carbonyl groups. A portion of the ultrasonic energy is spend for destruction of the polymer – solvent associates. This portion is larger in the ethyl alcohol-diethyl ether solvent mixture due to formation of a higher number of hydrogen bonds.

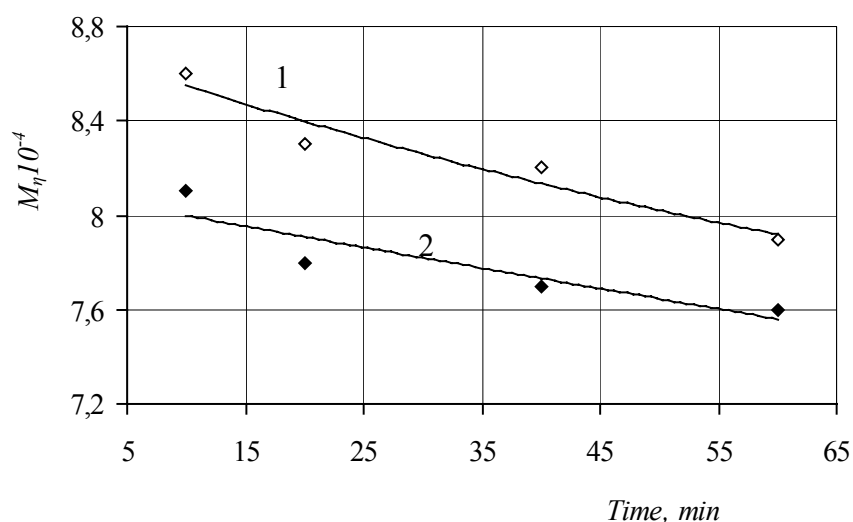


Fig 2. Dependence of molecular weight $M_{\eta} \cdot 10^{-4}$ of NC on time of treatment with ultrasound of solutions of SBP in a mixture of ethyl alcohol-diethyl ether (1) and acetone (2)

The final results show great influence of ultrasound on the properties of propellants and explosives. This fact has to be considered while using ultrasound technologies in the production and exploitation of munitions and their elements.

REFERENCES

- [1] J. STEPANIC, M. SUCESKA and D. SKARE: *Measurements of Energetic Material Dynamic Properties Using Ultrasounds*, Proc. of III. Seminar New Trends in Research of Energetic Naterials, Pardubice, p.195-201, 2000
- [2] T. E. DAYLE, A. D. DEGTYAR, K. P. SORENSEN, M. I. KESLO, and T. A. BERGER: *Ultrasonic Method for Inspektion of the Propellant Grain in the Space Shuttle Rocket Booster*, AIR Conf. Proc., American Institute of Physics, 509, p.1833-1840, 2000
- [3] V. I. GROZEV: *Vlianie na ultrasvuka varhu kristalizaciata na trotil*, Sb. Dokladi na nautchna sesia. VNVAU-VMEI, Gabrovo, p.56-61, 1988 (in Bulgarian)
- [4] F. A. BAUM, K. P. STANJUKOVIC and V. I. SHAHTER: *Fizika vzriva*, FML, Moskva, 1970 (in Russian)
- [5] I. G. POLOCKIJ: *Kavitacia v jidkostah*, Jurnal organicheskoj himii, p.1048-1053, 1947 (in Russian)
- [6] B. A. AGRANAT: *Ultrazvukovaja ochistka*, v sb. Fisicheskie osnovi ultrazvukovoj tehnologii, pod red. L. D. Rosenberga, Nauka, Moskva, 1970 (in Russian)
- [7] V. I. GROZEV: *Kand. disertacia*, VA, Sofia, p.67, 1982 (in Bulgarian)

STUDY ON RING CLEAVAGE AND ADDUCTIVE PROPERTY OF 2-(DINITROMETHYLENE)-4,5-IMIDAZOLIDINEDIONE

Cai Hua-Qiang, Shu Yuan-Jie, Huang Hui and Cheng Bi-Bo

Institute of Chemical Materials, China Academy of Engineering Physics,
621900, Mianyang, China

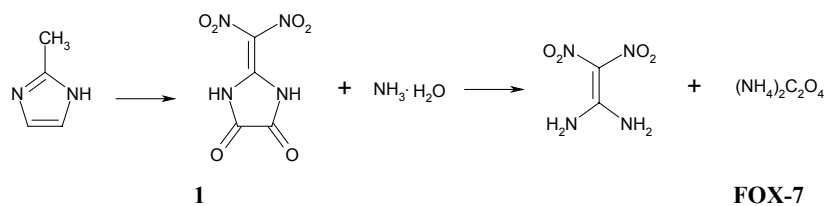
Abstract:

Ring cleavage of 2-(dinitromethylene)-4,5-imidazolidinedione (**1**) was achieved by methanol for the first time and the product was 1,1-diamino-2,2-dinitroethylene (FOX-7). **2**, the first adduct of **1**, was synthesized by the reaction of **1** with methanol in certain conditions and its structure was characterized. Physical and chemical properties of the adduct were studied. Parabanic acid was synthesized by decomposition of **1** in methanol, losing nitrogen oxides and carbon oxides.

Keywords: ring cleavage, adduct, 2-(dinitromethylene)-4,5-imidazolidinedione, methanol, 1,1-diamino-2,2-dinitroethylene, FOX-7

1. INTRODUCTION

Recently, 2-(dinitromethylene)-4,5-imidazolidinedione (**1**) has been reported by Latypov in the synthesis of 1,1-diamino-2,2-dinitroethylene (FOX-7)^[1], Which involved the nitration of 2-methylimidazole with concentration H_2SO_4 and HNO_3 to give **1**. **1** was treated with ammonium hydroxide to yield FOX-7 (Scheme 1).



Scheme 1

But except this reaction, no more new reactions relating to **1** have been reported to this day, so the chemical properties of **1** are not investigated sufficiently. Our experiments have confirmed that **1** has many new reaction characters. In the structure of **1**, double amide bonds are reactive and easy to break, so we have expected that **1** can process ring cleavage by other polar reagent besides ammonium hydroxide, and these have indeed proved to be the case.

It is known that when the adduct of certain compound is formed, characteristics, such as colour, solubility, chemical property and so on may be changed. In molecule **1**, there are unshared electronic pairs in the nitrogen of the amino group, the oxygen of the nitro group and the nitrogen of the ring, which might therefore be expected to combine with acidic hydrogen atoms and to form hydrogen bonds. These assumptions have been conformed by our experiments. By reaction with methanol, **2**, the first adduct compound of **1**, was synthesized and characterized. Physical and chemical properties of this adduct were studied preliminarily.

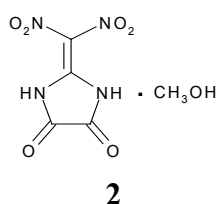
2. DISCUSSION

2.1 Study on reaction reagent

In the reaction of **1** with other compounds, the product pattern was strongly dependent on their polarity. Our preliminary experimental results confirmed that **1** usually only reacted with polar reagent. When **1** was dissolved in acetonitrile, acetone and DMSO solution, it underwent slow decomposition yielding finally parabanic acid, losing nitrogen oxides.

1 was treated with dilute hydrogen chloride to form a mixture at 70°C. When methanol was added, The white solid dissolved immediately to form a buff solution and in a few seconds bright yellow crystals precipitated (88% yield under optimal conditions), spectral analysis proved the product is FOX-7. The major by-product formed was parabanic acid.

But, when **1** was dissolved in methanol at 20°C, the situation was changed. This white solid dissolved immediately and in a few seconds buff crystals precipitated. spectral analysis proved the product was **2**, the methanol adduct of **1**. The major by-product formed was parabanic acid. **2**, now reported for the first time, is the first adduct compound of **1**. However, if **1** was dissolved in other alcohols in the same conditions, for example ethanol, the ring was cleaved and the product was FOX-7.



Methanol possesses a highly polarized hydroxyl, and the acidic hydrogen of it is active. Unshared electronic pairs in the nitrogen or oxygen of **1** are easy to combine with these acidic hydrogen atoms and to form hydrogen bonds, which presents extensive π -conjugation system, so the stability of **1** is enhanced.

2.2 The effect of temperature on yield of the products

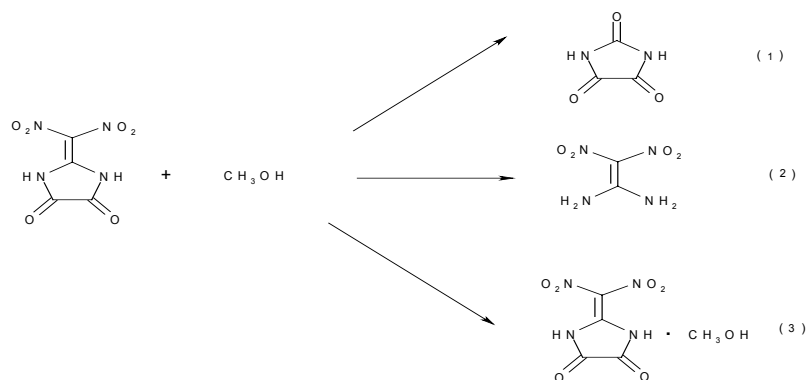
There are many factors affecting the synthesis of FOX-7. temperature is one of the most important factors. Some results are given in Table 1. Experiments indicated that high yields of **2** were achieved between 10-40°C (98% optimum at 20°C). Temperature below 10°C gave a low yield of **2** and the major product formed was parabanic acid (15% yield under optimal conditions at 0°C), while a higher reaction temperature (40-60°C) caused ring cleavage of **1** (FOX-7 is the major by-product and 88% optimum at 60°C) and the yield of **2** was low too.

Table 1. *The effect of temperature on yield of the products*

temperature(°C)			0	20	40	60
yield of the adduct(%)			12	98	80	5
yield of FOX-7(%)			0	0	14	88
yield of parabanic acid(%)			15	0	2	3

Methanol 200ml, 2-(dinitromethylene)-4,5-imidazolidinedione 0.01mol, reaction 30min, Fe and dilute hydrogen chloride (catalytic amounts)

There were three kinds of routes in the reaction of **1** with methanol, so three different products, the adduct, FOX-7 and parabanic acid, were formed respectively (**scheme 2**).



Scheme 2

When the reaction temperature was between 10-40°C, the reaction went along the route 3 primarily and **2** was the major product. If temperature was below 10°C, the route 1 would be the main reaction and the major product was parabanic acid, while if temperature was above 60°C, the route 2 would be the main reaction and the major product was FOX-7. generally more energy was needed in the reaction of ring cleavage, so the route 2 was easy to go when temperature was high (above 60°C), while little energy was needed in the self decomposition of **1**, so the route 1 was easy to go when temperature was low (below 0°C). Forming hydrogen bonds were the essential of making methanol adduct, which needed appropriate energy, so the route 3 was easy to go when temperature was proper (10-40°C).

2.3 Comparison of some properties of 2 with 1

2 is a stable compound. Its properties are different from **1**. **1** is white powder, while **2** is yellow needle crystals. **2** is very poorly soluble in common organic solvents and water, while **1** can readily be dissolved in many polar solvents, such as water, methanol, ethanol, acetonitrile, acetone, DMSO and so on. **1** can be stored for a long time in vacuum, while **2** undergoes slow decomposition yielding finally parabanic acid, a white flake crystal. The chemical properties of **1** are active and can react with many compounds at ambient temperature, while **2** usually do not react with other compounds, but under certain conditions **2** can be also neutralized by aqueous ammonia to form ring cleavage product, FOX-7. **1** is stable thermally and it decomposes at 240°C, while **2** is unstable thermally and it decomposes in about 100°C.

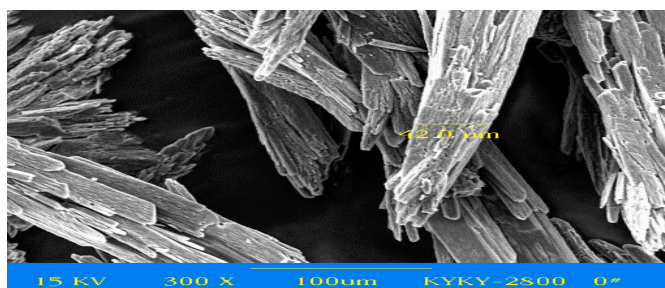


Fig 1. SEM photograph of methanol adduct of **1**

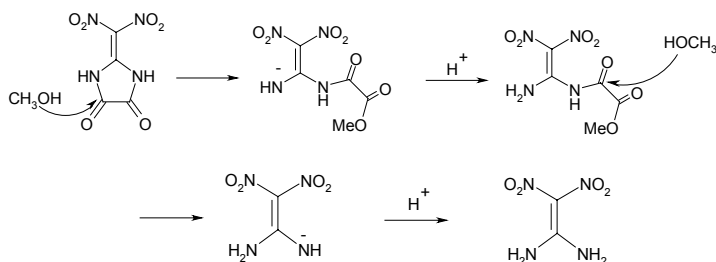
2.4 Comparison of the ring cleavage techniques by methanol with by ammonia.

FOX-7 is a novel and very interesting explosive with high performance and low sensitivity^[2,3,4], but at present the cost of ring cleavage of **1** by aqueous ammonia to FOX-7 is very high. According to our recent investigation we found three main disadvantages^[5]: firstly, **1** need to be separated and purified, and besides, **1** self is an sensitive explosive so it is dangerous in the process of its separation and purification. Secondly, trifluoroacetic acid is used to purify **1**, but it is very expensive, polluted and hard to reclaim. Thirdly, **1** is lost a great deal in the separation and purification process of intermediates.

As mentioned above, FOX-7 was the major product in the reaction of methanol with **1** at high temperature, which was a new method to prepare FOX-7 by ring cleavage and methanol was a new reagent corresponding to aqueous ammonia. More experiments have confirmed that methanol could also react with **1** in sulfuric acid and nitric acid to form FOX-7. In this method raw materials are only 2-methylimidazole, sulfuric acid, nitric acid and methanol, which are easy available. **1** need not be separated and purified, so it was not necessary to use trifluoroacetic acid. The yield of FOX-7 is higher than that of the literature and the cost is low, so the major disadvantages of producing it by aqueous ammonia have been solved and it is a good method for the scale-up of FOX-7.

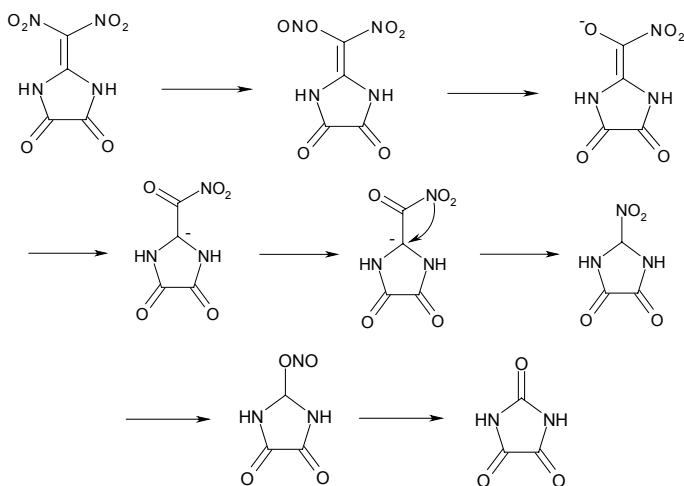
2.5 Reaction mechanism

We have discussed the reaction mechanism of FOX-7 synthesized by ring cleavage of **1** by ammonium hydroxide^[6]. The mechanism of ring cleavage by methanol is similar to it and the only difference is that the nucleophile is the oxygen instead of hydroxyl. The oxygen in methanol attacked at the positive carbon of the carbonylation, with subsequent elimination of double carbonylation, FOX-7 was formed (**Scheme 3**).



Scheme 3

The mechanism of parabanic acid formed are complex and we think that many steps are involved (**Scheme 4**). The key steps are rearrangement of nitro group and elimination of carbon monoxide.



Scheme 4

3. CONCLUSIONS

We have discovered some new reactions of **1**, such as reaction with alcohols. Ring cleavage of **1** to FOX-7 was succeeded by methanol, which was shown to be an easy and accessible route towards it. By complex with methanol, the first adduct of **1**, has been synthesized and characterized. The characters of **1** molecule make it easy to form hydrogen bonds, so other adduct of **1** might therefore be expected to be synthesized in the future. The synthesis of adduct constitute a new research aspect of **1** which make us understood the structure and properties of it deeply and it is important to theoretical research and future applications.

4. EXPERIMENTAL SECTION

NMR spectra were obtained using a Bruker AVANCE 300 MHz spectrometer. Infrared spectra were recorded with a Nicolet 800 FTIR spectrophotometer. Melting points and decomposition temperatures were determined with a Mettler DSC 30. Mass spectra were recorded with Finnigan MAT 95S spectrometer. Elemental analysis were carried out by EA1108 spectrometer.

Caution: All polynitro compounds described in this paper are explosives and proper shielding is strongly recommended.

4.1 Formation of 2-(dinitromethylene)-4,5-imidazolidinedione (**1**)

Finely ground 2-methylimidazole 16.5g (0.2mol) was dissolved in sulfuric acid 160ml (95%) at 19°C with vigorous stirring. At the same temperature nitric acid 32ml (1.51g/cm³) was added over a 90 min period. After 1.5 h a white precipitate was formed, which was collected and washed several times with cold trifluoroacetic acid. The precipitate was dried in vacuum at 0°C. On standing at room temperature for 5 h, 2-(dinitromethylene)-5,5-dinitro-4-imidazolidinedione lost 26.5% of weight and gave 8.4g (20.8%) of 2-(dinitromethylene)-4,5-imidazolidinedione (**1**).

Decomposition temp 240°C (10°C /min DSC); IR. (KBr): 3313 (NH₂), 3226(NH₂), 3169(NH₂), 1805(C=O), 1754(C=O), 1584(NO₂), 1499, 1318(NO₂), 1232, 1176, 758cm⁻¹. ¹H NMR (DMSO-d₆) δ 11.03 ppm; ¹³C NMR (DMSO-d₆) δ 128.71, 154.79, 159.70; MS m/e 202 (M⁺); Anal.Calcd for C₄H₂N₄O₆: C, 23.77; H, 1.0; N, 27.72. Found: C, 23.90; H, 1.23; N, 27.87.

4.2 Formation of the methanol adduct of 2-(dinitromethylene)-4,5-imidazolidinedione (**2**)

2-(dinitromethylene)-4,5-imidazolidinedione (**1**) 2.1g (0.01mol) was dissolved in methanol 200ml at ambient temperature with vigorous stirring. Few finely iron powder and dilute hydrogen chloride were added to the solution. After 30 min, the solution was concentrated and yellow needle crystals precipitated. The precipitate was washed with water and dried at 50°C to give 2.3g (98%) adduct **2**. mp 140.0~140.9°C; IR. (KBr): 3362(NH₂), 3249(NH₂), 1753(C=O), 1734(C=O), 1618(NH₂), 1575(NO₂), 1475, 1323(NO₂), 1230, 1140,

964 cm^{-1} . ^1H NMR (DMSO-d_6) δ 3.69, 8.81, 11.76 ppm; ^{13}C NMR (DMSO-d_6) δ 48.76, 53.55, 100.43, 128.71, 154.93, 159.86; MS m/e 234 (M^+); Anal.Calcd for $\text{C}_5\text{H}_6\text{N}_4\text{O}_7$: C, 25.64; H, 2.56; N, 23.93. Found: C, 25.70; H, 2.64; N, 24.07.

4.3 Ring cleavage of 1 by methanol to 1,1-diamino-2,2-dinitroethylene (FOX-7)

2-(dinitromethylene)-4,5-imidazolidinedione (**1**) 2.1g (0.01mol) was dissolved in methanol at 70°C with vigorous stirring. Few finely iron powder and dilute hydrogen chloride were added to the solution. After 30 min, the solution was concentrated and bright yellow crystals precipitated. The precipitate was washed with water and dried at 50°C to give 1.3g (88%) 1,1-diamino-2,2-dinitroethylene (FOX-7). Decomposition temp 238°C ($7^\circ\text{C}/\text{min}$ DSC); IR. (KBr): 3404(NH_2), 3330(NH_2), 3223(NH_2), 1633(NH_2), 1518(NO_2), 1469, 1393 1351(NO_2), 1221, 1166, 1137, 1023, 620, 458 cm^{-1} . ^1H NMR (DMSO-d_6) δ 8.759 ppm. ^{13}C NMR (DMSO-d_6) δ 129.411, 159.040; MS m/e 148 (M^+); Anal.Calcd for $\text{C}_2\text{H}_4\text{N}_4\text{O}_4$: C, 16.22; H, 2.72; N, 37.84. Found: C, 16.09; H, 2.68; N, 37.87.

4.4 Formation of parabanic acid

2-(dinitromethylene)-4,5-imidazolidinedione (**1**) 2.1g (0.01mol) was dissolved in methanol 200ml at 0°C with vigorous stirring. Few finely iron powder and dilute hydrogen chloride were added to the solution. After 30 min, the solution was concentrated and the solids precipitated. The precipitate proved to be a mixture of parabanic acid and the methanol adduct of 2-(dinitromethylene)-4,5-imidazolidinedione (**2**), which were dissolved in water and the insoluble adduct was filtrated. The filtrate was condensed, then cooling it to 10°C and keeping overnight resulted in the precipitation of 0.17g (15%) of parabanic acid.

Acknowledgements

Project 20020540 was supported by China Academy of Engineering Physics. The authors would like to thank Mrs Xu Ruijuan and Yang Xiulan for Mass spectra and Mrs Wang Lin and Jiang Yan for Infrared spectra measurements.

REFERENCES

- [1] N. V. LATYPOV, J. BERGMAN, A. LANGLET, ET AL: Tetrahedron., , 54, 11525, 1998
- [2] H. ÖSTMARK, A. LANGLET, H. BERGMAN, ET AL: The 11th International Detonation Symposium, Snowmass, Colorado, pp. 807 ~ 812, 1998
- [3] N. MATYUSHIN, G. T.AFANASEV, V. P. LEBEDEV, ET AL: 34th ICT International Annual Conference on Energetic Materials, Karlsruhe, Germany, pp. 119-1 ~ 119-13, 2003
- [4] E. HOLMGREN,; H. CARLSSON, P. GEODE, ET AL: 34th ICT International Annual Conference on Energetic Materials, Karlsruhe, Germany, pp. 107-1 ~ 107-10, 2003
- [5] HUA-QIANG. CAI, WEI-FEI. YU, YE. TIAN, ET AL: China. Energetic Materials, 11(1), 1., 2003
- [6] HUA-QIANG CAI, YUAN-JIE. SHU, WEI-FEI YU, ET AL: Acta Chimia Sinica, 62(3), 295~301, 2004

AGEING INFLUENCE ON STABILITY AND SENSITIVITY OF PETN EXPLOSIVES

M. Chovancová, P. Očko, M. Lazar and A. Pechová

VTSÚ (Military Technical and Testing Institute) Zahorie, 905 24 Senica, SK

Abstract:

In this paper the PETN explosives stability and sensitivity are investigated during their artificial ageing. It was observed their stability was not changed, but sensitivity was changed after ageing. The biggest change was recorded in sensitivity to electrostatic discharge of flegmatized PETN.

Keywords: PETN, Np10, artificial ageing, stability, sensitivity

1. INTRODUCTION

The principal requirement of regular function of ammunition is its qualitative status. It is necessary to investigate during all the time. The reason is due to the ammunition contains explosives, a savoir the matters which have an ability of explosive change. Their lifetime is temporary with row of factors, e.g. chemical composition, chemical purity, conditions of storage, expected application and so on. Baseline physical-chemical characteristics of explosives can be changed in the course of working process, in consequence there are their technical stage, availability and their safety are effected. The knowledge and timely observations of qualitative status ammunition enable to admite in season a row of arrangements that are concentrated on maintenance, increment or innovation of its safety, its reliability and its applicability.

The artificial ageing is one method of qualitative status explosives investigation during their exploitation. It is process of accelerated ageing which simulates natural ageing of explosives in the ammunition system. It is usually done by heating at elevated temperatures, that accelerates physical-chemical processes, which are done in explosive number of years in natural store or exploitative conditions. The scope of artificial ageing is to procure an explosive in short time into the phase, where it will be situated most likely during number of years of natural ageing. This method allows to predict the changes of stability, sensitivity, mechanical and functional properties of explosives.

2. EXPERIMENTAL

For the qualification process of crystal PETN – NpD and PETN with wax – Np10 (90% PETN + 10% wax) it was necessary to investigate the changes of their chemical and thermal stability and sensitivity before, during and after the ageing. It was the scope to sound the negative ageing effect on the present explosives and together on the objective ammunition.

The samples NpD and Np10 was aged artificially at temperature 65°C 6 months in sealed glass tubes. During the ageing the following properties of the samples were investigated:

Table 1.

Property	Test	Methods
Chemical stability	VST	STANAG 4556 STN 29 910
Thermal stability	DTA, temperature of ignition	STANAG 4491
Impact sensitivity	BAM impact test	STANAG 4489
Friction sensitivity	BAM friction test	STANAG 4487
Electrostatic discharge sensitivity	Electrostatic discharge test	STANAG 4490
Shock sensitivity	Small scale GAP test	STANAG 4488

Note:
VST – vacuum stability test
DTA – differential thermal analysis

2.1 Chemical and thermal stability tests

Chemical stability tests were carried by STABIL 16-Ex (made in OZM Research Czech. Rep.) at temperature 100°C 40 hours. Thermal stability tests were carried by use DTA 550-Ex and the apparatus for temperature of ignition (both made in OZM Research) at heating speed 5°C/min. Test results are listed in table 2.

Table 2. *The survey of stability results*

Sample (ageing time in months)	VTS ml	DTA (°C)			Temperature of ignition (°C)
		Melt	Start	Decomp	
NpD (0)	0,9583	140,4	158,0	186,6	191
NpD (1)	0,3875	141,2	157,0	188,3	190
NpD (2)	0,2935	141,8	158,5	188,4	191
NpD (4)	0,4553	145,2	161,5	188,9	194
NpD (6)	0,3720	146,7	163,0	188,2	193

Np10 (0)	1,7205	138,4	154,2	180,0	184
Np10 (1)	1,0125	138,1	155,6	181,0	182
Np10 (2)	1,1655	138,8	155,6	182,5	182,5
Np10 (4)	1,6263	143,8	159,2	187,2	183
Np10 (6)	1,4650	144,0	158,4	185,0	182

Note:

Melt – temperature of melting

Start – beginning of decomposition temperature

Decomp – maximal temperature of thermal decomposition

Temp. of ignit. – temperature of ignition

2.2 Calculation of kinetic parameters

It is possible to calculate some kinetic parameters from VST results by the medium of Arrhenius equation

$$\ln k = \frac{-E}{RT} + \ln A$$

There was needness to measure chemical stability of explosive samples by use a few operating temperatures according to STN 26 910 (Slovak technical specification). VST according to STN spends the rate of evolution of gaseous decomposition products for 20hours from 1 gram of sample as a result. VST according to Stanag 4556 spends as a result the volume of gaseous decomposition products. Measured rates of PETN samples were used for procuration of rate constants $\ln k$ by means of calibration curve which come from published work ^[8]. There was the calibration curve established as a relationship between the rate of evolution of gaseous decomposition products and rate constant of monomolecular decomposition of individual nitro-compositions in work ^[8] and published arrhenius parameters (E_a – activation energy and $\log A$ – preexponential factor) of these stuffs were used. Activation energy E_a and preexp. factor $\log A$ of PETN samples were calculated by used Arrhenius equation. The results of VST according to STN and the kinetic parameters are listed in table 3.

Table 3. *The survey of VST results and calculated kinetic parameters*

Sample	w (ml/g/20)	Pre T (K)	ln(w) (ml/g/s)	ln(k) (s ⁻¹)	E _a (kJ/mol)	log(A) (s ⁻¹)
NpD (0)	0,0356	373,15	-14,5	-21,4	166,414	14,0
	0,0662	383,15	-13,9	-20,0		
NpD (6)	0,0324	373,15	-14,6	-21,5	190,188	17,3
	0,0731	383,15	-13,8	-19,9		
Np10 (0)	0,1404	373,15	-13,1	-18,5	213,971	21,9
	0,3884	383,15	-12,1	-16,7		
Np10 (6)	0,1275	373,15	-13,2	-18,6	202,084	20,2
	0,3630	383,15	-12,2	-16,9		

Note:

w - the rate of evolution of gaseous decomposition products

PETN samples were measured by VST at three working temperature, therefore the thermal relation their lnk could be established. Figure 1 shows this thermal relation lnk of NpD and Np10 before and after ageing. The samples after ageing are marked „ag“. It is showed all thermal relations are linear.

2.3 Stability data evaluation

The achieve results of chemical and thermal stability of investigated explosives and also the calculated values of their E_a and logA made out PETN samples did not change their stability properties during and after artificial ageing. These conclusions are conformable with conclusions of publish work ^[5] include of soft stream of DTA temperature Np10ag to higher values. Thermal stability results suggest thermal decomposition of Np10 has occurred probably any faster than of NpD. It has been due to suppose wax in Np10. It is need confirm these results by TGA and DSC measurements.

2.4 Determinations of sensitiveness

Sensitiveness to impact was determined on the BAM apparatus, in accordance with STANAG 4489. Sensitiveness to friction was determined on the BAM apparatus, in accordance with STANAG 4487. Sensitiveness to electrostatic discharge was determined on the apparatus developed by OZM Research Ltd. in accordance with TP-SHVV-1080-(01)-00-ZH. Sensitiveness to shock wave was determined accordance with STANAG 4488 A – small scale gap test. Small scale gap test was not accomplished with explosive NpD, because testing sample could not be prepared for safety reason. The results of sensitivity tests are in table 4.

Table 4. *Results of sensitivity tests*

Sample	NpD		Np10	
Tests	Virgin	Aged*	Virgin	Aged*
Impact E ₅₀ (J)	4,32	4,2	31,87	20,3
Electric spark E ₅₀ (mJ)	64,78	45,41	164,48	44,03
Friction F ₅₀ (N)	61,5	60,75	153,7	117,71
Small Scale GAP test M ₅₀ (kPa)	-	-	1838	1950 **

* aged 6 month

** aged 2 month (The tests will be continued after 4 and 6 month ageing)

2.5 Results of sensitivity investigation

Sample NpD

Sample NpD is most sensitive explosives. Its sensitiveness to all stimuli increased with ageing. Changes in sensitiveness were not most sensible.

Sample Np10

Sensitiveness of Np10 is increase to impact, electrostatic discharge and friction and in reverse it is decrease to shock wave after ageing. Decrease of sensitiveness to shock wave is most probably subjected by decrease of number hot spots. Hot spots – micro gas bubble was fill by smooth wax during ageing. Tests will be continued after 4 and 6 month ageing. Sensitiveness of Np10 to shock wave will be probably increased on the base results from all sensitiveness tests.

2.6 Relation between DTA results and sensitivity of PETN explosives

The relations between DTA results and sensitivity of explosives to impact and to electrostatic discharge are described in publish works ^[3,10,11]. We have attempted to verify this dependence with our PETN samples. DTA measurements at three rates of heating were evaluated according to Kissinger equation

$$\ln \frac{\phi}{T_m^2} = \frac{E}{R} * \frac{1}{T_m} + A.$$

The evaluation of DTA by Kissinger is situated in figure 2. The slopes of lines from figure 2 were used for establishing of relations between sensitivity of PETN explosives to impact and to electrostatic discharge and DTA results by Kissinger of PETN explosives. Figure 3 and 4 show these dependences are linear. These results very well correspond with results of publish work ^[3]. The values of HMX, RDX, Semtex1A, Comp CHc and C-4 in figure 4 are used from this work. It was confirm the relationships between sensitivity and DTA results of explosives are objective also for PETN explosives and it is possible to do the prediction of explosives sensitivity by means of DTA measurements.

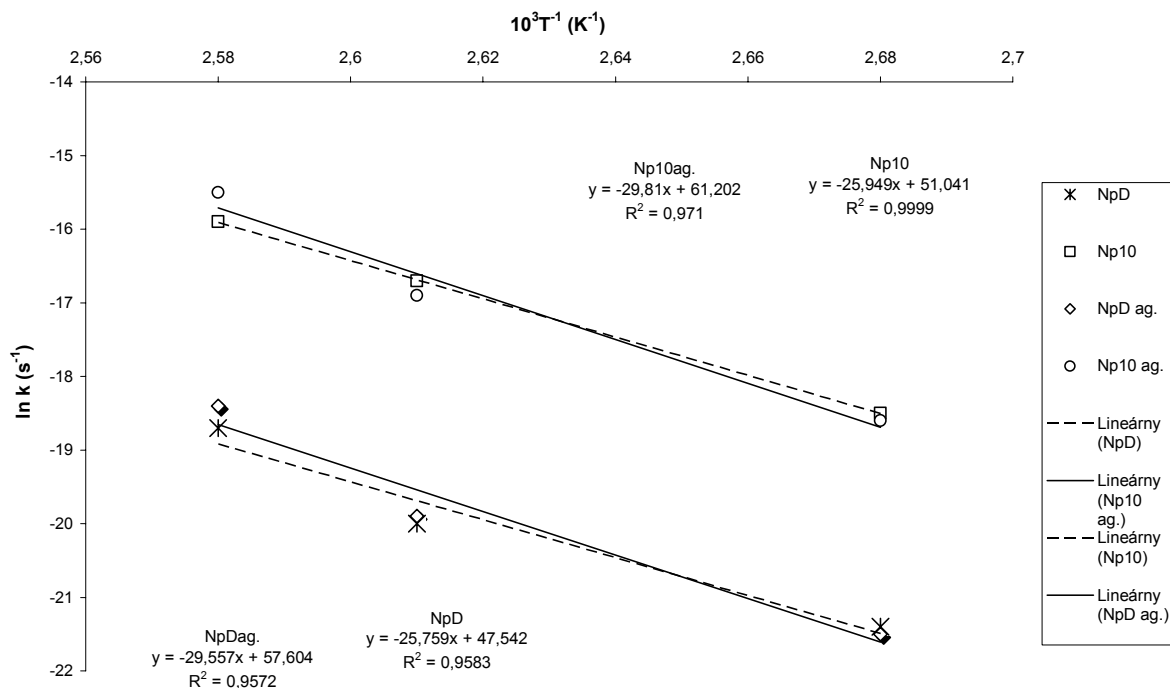


Fig 1. $\ln(k)$ temperature dependence of PETN explosives

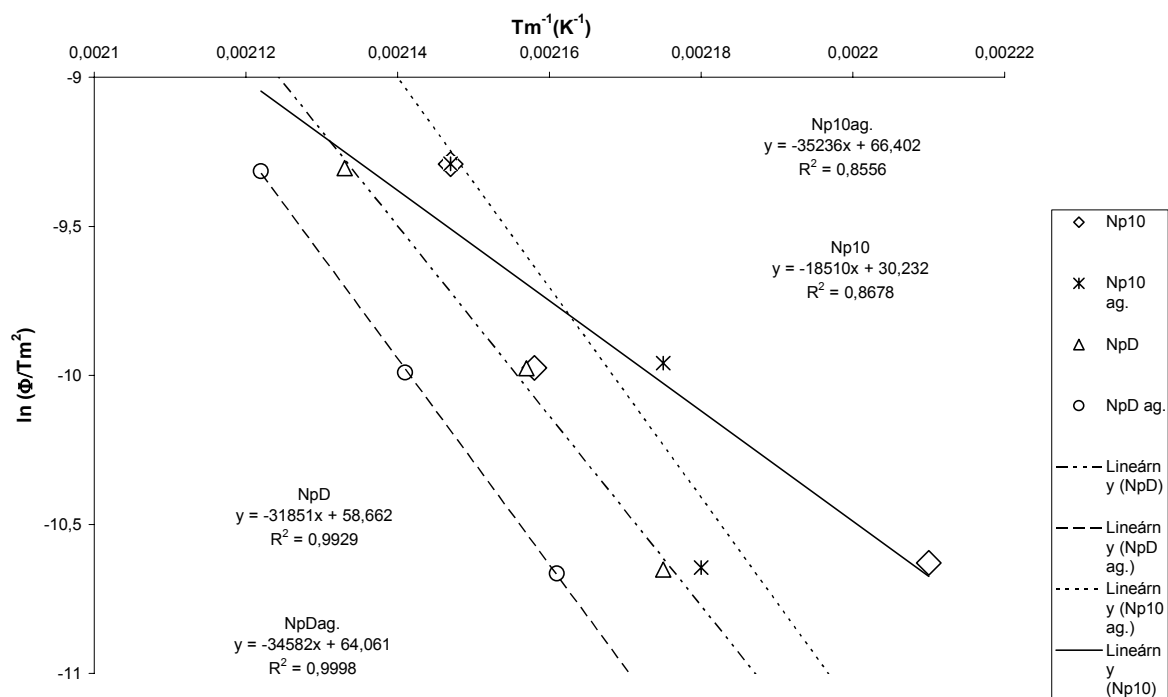


Fig 2. DTA by Kissinger of PETN explosives

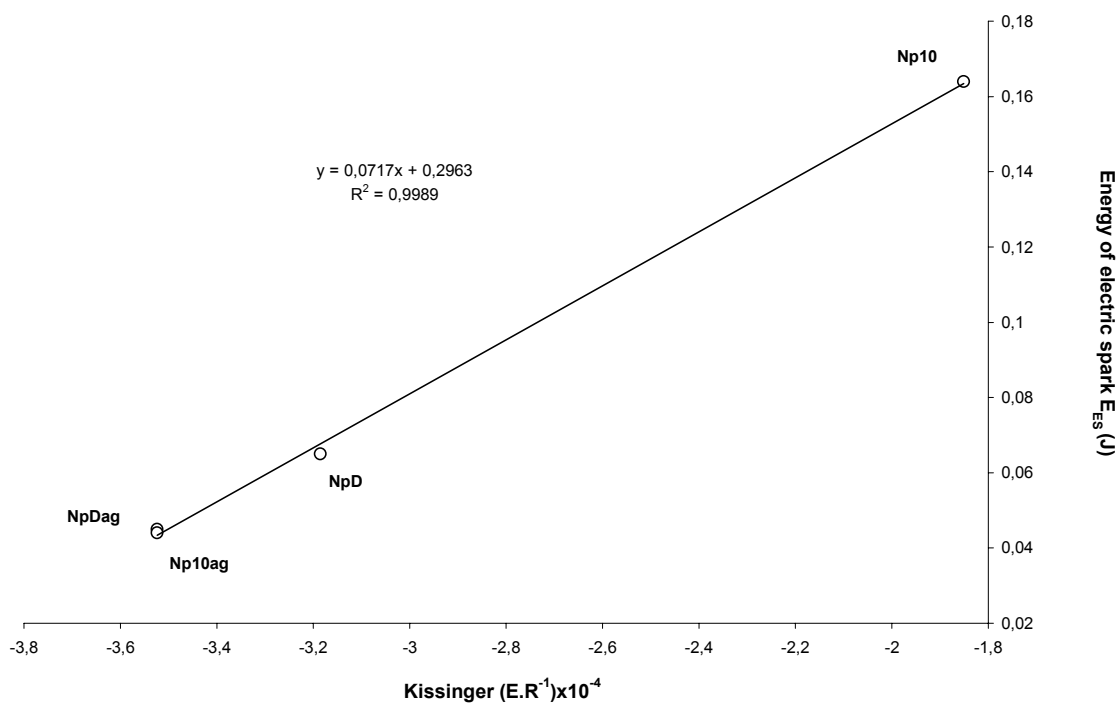


Fig 3. Relationship between Energy of electric spark and slope (ER-1) of Kissinger equation

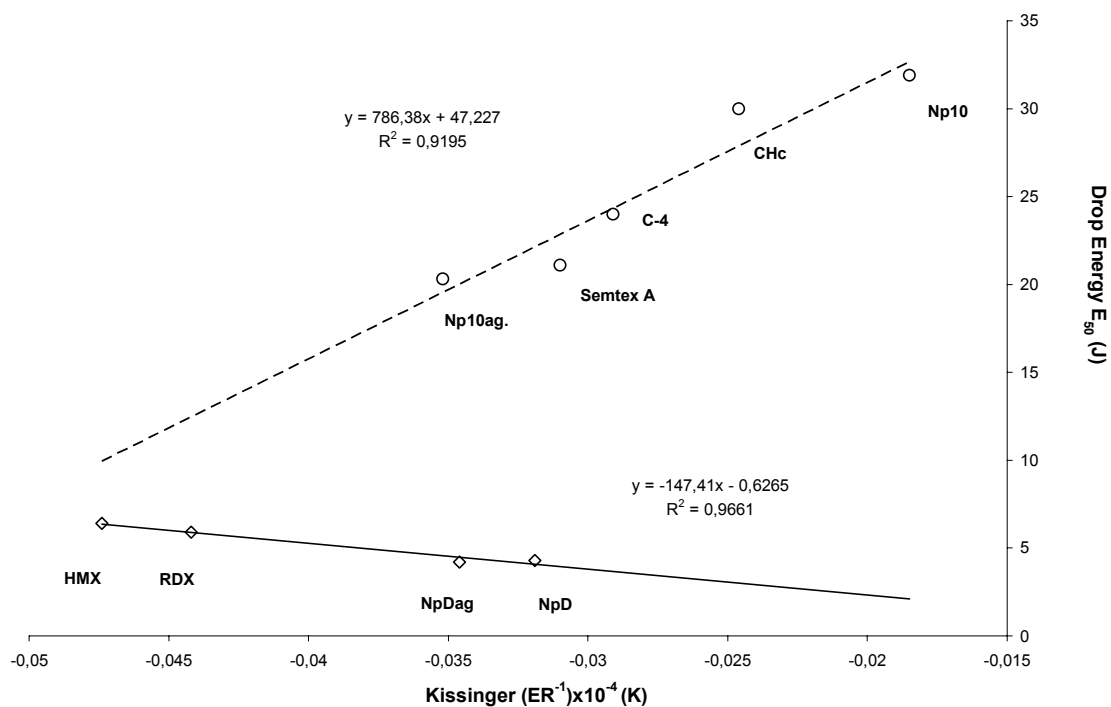


Fig 4. Relationship between impact sensitivity E_{50} and slope (ER-1) of Kissinger equation

3. CONCLUSION

Sensitiveness of observed explosives is increased after ageing, but changes in chemical and thermal stability is negligible. In the case sample NpD, changes of sensitiveness were not most sensible, but in the case sample Np10, changes of sensitiveness were more significant. This increase of sensitiveness is most probably caused by baring of PETN crystals. The negative influence on the results in the case of Np10 can be explained by behaviour of wax with relative low melting temperature.

REFERENCES

- [1] S. BREBERA: Vojenské trhaviny a technologie výroby trhavinových náloží, University of Pardubice, Pardubice 2001 (Dept. Of Theory and Technology of Explosives textbook)
- [2] P. VÁVRA: Teorie výbušin, University of Pardubice, Pardubice 2002 (Dept. Of Theory and Technology of Explosives textbook)
- [3] S. ZEMAN, M. KRUPKA, M. CHOVANCOVÁ, Z. JALOVÝ, M. LAZAR: A description of some explosive characteristics of plastic explosives part III., Proc. of the 3-th seminar New trends in research of energetic materials University of Pardubice, p. 285-296, 2000
- [4] M. KRUPKA: Devices and equipment for testing of energetic materials, Proc. of the 4-th seminar New trends in research of energetic materials University of Pardubice, p. 222-227, 2001
- [5] J. ŠELEŠOVSKÝ, J. PACHMÁN, M. HANUS: Changes in sensitiveness of flegmatized high explosives after artificial aging, Proc. of the 6-th seminar New trends in research of energetic materials University of Pardubice, p.309-321, 2003
- [6] J. STRNAD, J. MAJZLÍK: Determination of electrostatic spark sensitivity of energetic materials, Proc. of the 4-th seminar New trends in research of energetic materials University of Pardubice, p. 303-307, 2001
- [7] M. CHOVANCOVÁ, P. OČKO, J. LOPÚCH, M. LAZAR, A. PECHOVÁ: Chemical and thermal stability of flexible PBXs, Proc. of the 6-th seminar New trends in research of energetic materials University of Pardubice, p. 128-136, 2003
- [8] M. CHOVANCOVÁ: Sledovanie stability plastických trhavín pomocou prístroja Stabil a DTA, License study Thesis, University of Pardubice, 2000
- [9] GURDIP SINGH AND PREM FELIX S: Thermolysis of plastic bonded explosive, Proc. of the 5-th seminar New trends in research of energetic materials University of Pardubice, p. 68-76, 2002
- [10] S. ZEMAN, J. KOČÍ: Electric Spark Sensitivity of Polynitro Compounds.Part IV. A Relation to Thermal Decomposition Parameters. HanNeng CaiLiao 8, 2000
- [11] D. SKINNER, D. OLSON AND A. BLOCK-BOLTEN: Electrostatic Discharge Ignition of Energetic Materials, Propellants, Explos., Pyrotech, 23, 34-42, 1997
- [12] STN 26 910
- [13] AOP-7
- [14] STANAG 4556, 4491, 4489, 4487, 4490, 4488

EXPLOSIVE TYPE SELECTION WITH RESPECT TO THE VENTILATION CYCLE DURATION

B. Janković, D. Vrkljan and Z. Ester

Faculty of Mining, Geology and Petroleum Engineering, Pierottijeva 6, 10-000 Zagreb, Croatia

Abstract:

Extensive measurements of the ambient air quality have been conducted in the past years during excavation of road tunnels situated on the mountainous sections of the future Croatian highway Zagreb – Split. The objective of these measurements was to estimate the worker exposure to toxic gases. Since conventional mining methods have been used for excavation of the tunnels (drilling and blasting), as well as various types of explosives and initial systems, the impact on the workplace environment by toxic gases produced from blasting was also examined. In order to reduce the amount of toxicants in the workplace atmosphere, the field method for selection of the most appropriate types of explosives in the blast charge was developed.

Keywords: *blasting, imission, toxic gases*

1. INTRODUCTION

In tunnelling, various environmental impacts are a matter of concern when blasting is selected for doing the excavation job. Their negative effects are always characterized by the increase of costs and excavation times. One of the most important is production of dust and toxic gases, which creates ventilation problems and potential health hazard for employees, as well as delays in the excavation cycles. The importance of low toxic gases generation rapidly grows with the length of the tunnel excavation, and it is a major factor that weights ventilation parameters and, consequently, the excavation costs.

In the year of 2002, Civil engineering institute of Croatia engaged Department of Mining and Geotechnical Engineering (DMGE) on Faculty of Mining, Geology and Petroleum Engineering to supervise mining operations, such as blasting and ventilation, during excavation of “Mala Kapela” and “Grič” tunnels. Later on, several contractors on future tunnels: “Brinje” and “Brezik” requested workplace environment monitoring regarding air quality and ventilation efficiency. It was early observed that the ventilation cycle duration following blasting on all sites that was participated in this survey depends not only by ventilation parameters, but also of types of explosives used. Considering that fact, it was desirable to make selection of the types of explosives that should have good balance between efficiency on rock fragmentation and toxic gases quantity produced by the detonation of the blast charge.

This paper describes a field method used to determine the most appropriate types of explosives in the blast charge for use in underground excavations by measuring toxic gases imission in the workplace atmosphere during blasting operations. The ventilation cycle duration of blasting operation in underground excavations depends on reentry period following blasting, in which toxic gases produced by blasting have to be diluted to

concentrations acceptable by the law. Keeping that in mind, the appropriate types of explosives would have minimal dilution time needed after detonation, which means that the ventilation cycle duration with utilization of appropriate types of explosives would also be minimal.

2. IMISSION MEASUREMENTS

The actual measurements took place on-site, in vicinity of the rock face. To provide same conditions for number of testing with different types of explosives in the blast charge, the analysis instrument was placed on the predetermined distance from rock face, so the surrounding temperature and pressure (except of detonation) remains constant during sampling interval. Secondly, amount of fresh air supplied by ventilation was regulated in the same manner. In the case when significant fluctuation of atmospheric pressure was observed, the measurements were terminated.

The total amount of all utilized types of explosives in the blast charge was kept constant, with the standard deviation of 6 kg.

2.1 Analysis instrument

To meet demands for monitoring the concentrations of airborne pollutants in a tunnel excavation, and to ensure that the workplace atmosphere provides a safe environment free from levels of toxicants that would create a hazard to health, DMGE acquired appropriate instrument for the detection and measurement of expected gases. The expected gases were gases resulting from blasting and diesel exhaust.

It is well known that the detonation of commercial explosives creates the same gases found from burning fuel. The presence of carbon and nitrogen in commercial explosives makes it likely that carbon monoxide, carbon dioxide and nitrogen oxides will be produced from a blast.

Acquired analysis instrument is capable of continuously indicating fractions of a part per million for 3 toxic gases (electrochemical sensors for CO and NO_x), CO₂ can be measured in percentage of the value by infrared sensor. The instrument is equipped with sampling pump with constant flow accuracy.

3. METHOD IMPLEMENTATION

After the optimal technological parameters of blasting with one set of explosives in the blast charge have been achieved, the measurements were preformed minimal three times with utilization of the established amounts and types of explosives. Imiission measurements of produced toxic gases were recorded. The same procedure was applied after the types or component amounts of explosives in the blast charge were changed.

The appropriate types of explosives for considered underground excavation were determined by comparison of the ventilation cycle durations, where explosives of choice were explosives utilized in blasting operation with minimal ventilation cycle duration.

4. RESULTS

The obtained results of measured concentrations of carbon and nitrous oxides from "Mala Kapela" site are shown, as an example in Fig. 1. The explosive utilized for blasting was bulk emulsion "Elmulex P", prepared and loaded into the blastholes by mobile facility.

The information on rock categorization, geology, supplied air, ventilation duct distance from rock face, and explosive consumption is provided in Table 1.

Shown on Fig. 2. are results from the same location, but this time the explosive utilized for blasting was nitro gelatin "Goma II ECO" and emulsion "Elmulexal" for cut and stopping blastholes, both loaded and placed on the market in tube type cartridges.

For contour blastholes in both cases were used emulsion-type explosive "Elmulex" in cartridges of 25 mm in diameter, as well as non-electric shock tubes system for initiation of explosives.

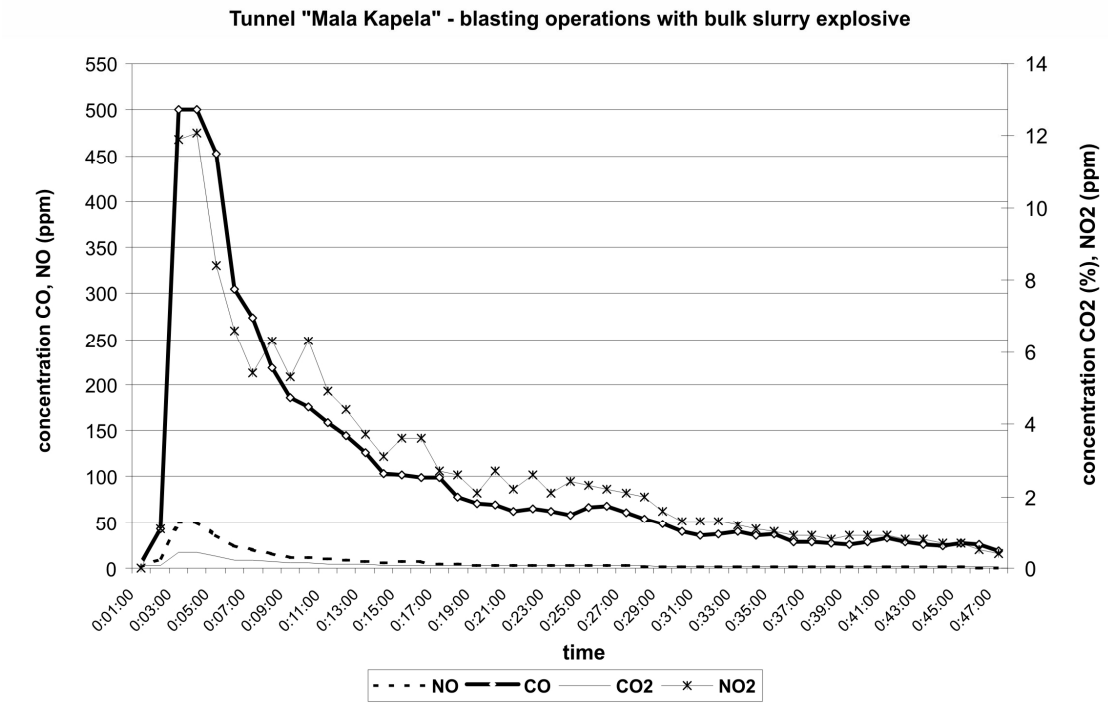


Fig 1. Measurements results with utilization of bulk emulsion explosive

Table 1. Blasting operation data referring to bulk emulsion explosive utilization

Site	Tunnel "Mala Kapela" - south portal
Location	right tube, 525 m from tunnel portal
Geology	dolomitic limestone / dolomite breccias
Rock categorization	II
Rock face surface	74 m ²
Ventilation duct distance	60 m from rock face
Supplied air quantity	22 m ³ s ⁻¹
Bulk emulsion quantity	
"Elmulex P"	514 kg
Emulsion quantity in cartridges	
"Elmulex" Φ25	12,75 kg
Amount of explosives	526,75 kg
Ventilation cycle duration average	47 min

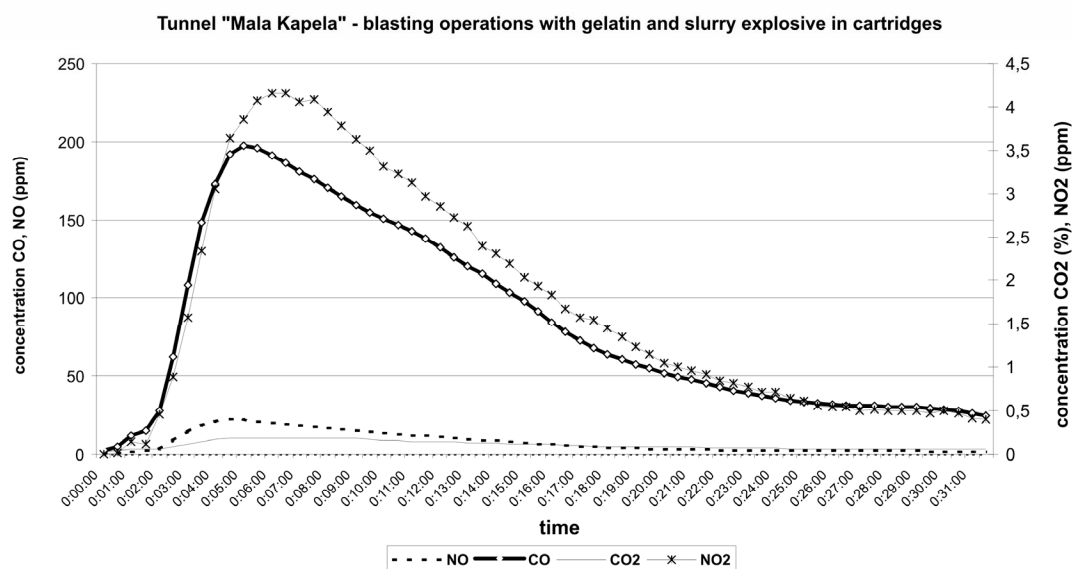


Fig 2. Measurements results with utilization of gelatin and emulsion explosive in cartridges

Table 2. *Blasting operation data referring to gelatin and emulsion explosive utilization*

Site	Tunnel "Mala Kapela" - south portal
Location	right tube, 535 m from tunnel portal
Geology	dolomitic limestone / dolomite breccias
Rock categorization	II
Rock face surface	74 m ²
Ventilation duct distance	62 m from rock face
Supplied air quantity	20 m ³ s ⁻¹
Nitro gelatin quantity	
Goma 2 ECO Φ 40	100 kg
Emulsion quantity in cartridges	
"Elmulex" Φ38	372 kg
"Elmulex" Φ25	51 kg
Amount of explosives	523 kg
Ventilation cycle duration average	31 min

As it can be seen from Table 1 and Table 2, timesavings in ventilation cycle duration with utilization of nitro gelatin and emulsion cartridge explosive types were significant in compare to utilization of on-site produced emulsion explosive.

On the same basis as the example shown, the measurements were continued until appropriate types of explosives for particular excavation were chosen. Additionally, two different sets of explosives in the blast charge for "Mala Kapela" site were considered. The results are shown in Table 3.

Table 3. *Blasting operation data referring to different sets of explosives on "Mala Kapela" site in same geology, rock category and ventilation conditions*

Set 3	Set 4
Nitro gelatin quantity	Nitro gelatin quantity
Danubit Φ 38 208 kg	Goma 2 ECO Φ 40 75 kg
Emulsion quantity in cartridges	Emulsion quantity in cartridges
"Elmulex" Φ 38 264 kg	"Elmulex" Φ 38 400 kg
"Elmulex" Φ 25 51 kg	"Elmulex" Φ 25 51 kg
Total amount of explosives 523 kg	Total amount of explosives 526 kg
Ventilation cycle duration average 36 min	Ventilation cycle duration average 29 min

The best results of blasting were achieved with types and quantities of explosives given in Table 2. Since there weren't significant difference in ventilation cycle duration with the next best result (Set 4) given in Table 3, the chosen types and quantities of explosives were selection from Table 2.

Field measurements were conducted on three more locations but the selection method wasn't implemented. The results are shown in Table 4.

Table 4. *Field measurements of toxic gases imission*

Tunnel	Geology	Rock cat.	Air supply	Surface of r. f.	Explosives	VCD
"Grič"	limestone / limestone breccias / conglomerates and breccias	III	27 m ³ /s	52 m ²	Austrogel G1 Φ 30, 75 kg (gelatine) Lambrex 1 Φ 35, 336 kg (emulsion)	24 min
"Brezik"	sandstones / conglomerates and shale / clay intercalations	IV, V	33 m ³ /s	80 m ²	Goma 2 ECO Φ 40, 154 kg (gelatine)	40 min
"Brinje"	limestone / limestone breccias / conglomerates and breccias	III	42 m ³ /s	52 m ²	Austrogel G1 Φ 30, 125 kg Lambrex 1 Φ 35, (gelatine) 225 kg (emulsion)	13 min

5. CONCLUSION

The factors contributing to the emission of toxic gases during blasting operation, and, consequently, prolongation of the ventilation cycle duration are varied. However the most important found on our investigation are:

1. Oxygen balance. From the measurements results, the blasting operations where were utilization of nitro gelatin explosives dominant, the generation of NO₂ was considerably larger in comparison to blasting with dominant emulsion explosive. On the other hand, much higher peak of CO₂ gases were found in cases where emulsions were dominant component in the blast charge.
2. Measurements results on “Mala Kapela” site (bulk and cartridge type) best describe the importance of the physic-mechanical characteristic of the explosives as homogeneity (density), granular-metric composure, water resistance, packaging and others. Each inconsistence of the explosive’s characteristics with the standardized requirements set forth during its development leads to distortion of the detonation process and to the larger release of toxic gases.
3. The chemical composition, strength, and structure of the rock. When detonating rocks with fissures and cracks, whether filled with clay materials or not, the released toxic gases are substantially larger (“Brezik” site).
4. The technology of the conducted blasting operation and the manner and tools of loading the blastholes. Our investigation suggests that this factor is even more important in regard to toxic gas emissions than the oxygen balance, considered being most significant up till now.

The method for explosives selection described here was successful in determination of types of explosives that are acceptable from environmental and economical standpoint.

In future, the results of these measurements in addition with the laboratory testing may be used to provide data to a computer model development that will reliably predict the expected gases production, and their relevance to excavation plan and ventilation design based on explosive of choice.

REFERENCES

- [1] Z. ESTER: *Method for determination optimal explosive type for tunnel excavation*, Proc. of Science-expert's Symposium, Novigrad, p.373-381, 1994
- [2] M. J. MCPHERSON: *Subsurface Ventilation and Environmental Engineering*, Kluwer Academic Publishers, Dordrecht Hardbound, April 1993

DISSOLVER VER. 1.1 HELPS CENTRAL MINING RESCUE STATION

B. Janovský

Dept. of Theory and Technology of Explosives, University of Pardubice, 532 10 Pardubice, CZ

Abstract:

This paper introduces new software package DisSolver v. 1.1, which was developed under the contract between Czech Mining Authority and University of Pardubice. The package consists of three individual codes – “Výbuchový trojúhelník”, “Následky” and “Vodní zátky”. Code “Výbuchový trojúhelník” solves the problems with explosibility of atmosphere inside the coal mines. Code “Následky” enables the user to calculate the consequences of accidental leaks of natural gas and crude oil during the drilling. Code “Vodní zátky” solves the mathematical model of the water column movement in the gallery as the method of the explosion-proof closing of the seat of fire in the coal mines.

Keywords: *gas explosion, consequence analysis, gas explosibility*

1. INTRODUCTION

Czech Mining Authority enunciated project No. 10/2001 named “Coping with the serious process accidents” under its program of research and development. University of Pardubice won a victory in the public tender for this project. The work had started in July 2001 and was finished in August 2003. The project was jointly solved in cooperation with Research Mining Institute Ostrava-Radvanice and Jan Zigmund, PhD. Software tool which would help to Central Mining Rescue Station (HBZS) solve the accidental situations during the mining of the black coal and drilling of the crude oil and natural gas was the contracted output of this project.

Program goal was fulfilled and program package DisSolver v. 1.1 has been introduced during the final inspection day. The package contains three individual codes:

- “**Výbuchový trojúhelník**” solving the accidents during underground coal mining.
- “**Následky**” solving accidents during drilling of the natural gas and crude oil.
- “**Vodní zátky**” solving the water column movement in the gallery as the method of the explosion-proof closing of the seat of fire in the coal mines.

Short introduction of these individual codes of the DisSolver package will be given in this contribution.

2. “VÝBUCHOVÝ TROJÚHELNÍK”

“Výbuchový trojúhelník” code is the graphical computing system intended for fast assessment of the fuel-air mixture explosibility. According to requirements of the Czech Mining Authority and HBZS the code solves the problems of explosion triangle for both standard and non-standard composition of the coal mine atmosphere. The code is ready for future implementation of the on-line connection with the “Mine Gas Laboratory” (DPL),

which measures the concentration of the standard components of the mine atmosphere. Special procedure for monitoring of the “CO production per liter” was also implemented in the code.

The heart of the code is built of three basic parts:

- 1. Explosion triangle analysis
- 2. Thermodynamic heart of the code
- 3. Inertisation of the fuel-air mixture

Each part of the code represents unique computational solution based on the general physical-chemical patterns, which are described for example in [1, 2, 3, 4, 5, 6, 7].

After running the code user has to choose proper program branch. Basic menu is shown in Fig.1.



Fig 1. Basic menu of the „Výbuchový trojúhelník“ code

2.1 Manual edition of the composition of all combustible (firing) gasses

Selecting this branch, user has to input the composition of the standard combustible mine gases in the data packet (e.g. according to the Table 1). The date and the time is input automatically. Concentration of mixture components could be input by keyboard after clicking on the concentration window. It is also possible to move between the windows by cursors. Concentration of Nitrogen is calculated automatically.

Table 1. *Example of the combustible gases composition*

N ₂	CO ₂	CH ₄	O ₂	CO	H ₂
72,41 %	1,03 %	9,80 %	16,50 %	58 ppm	0,25 %

Input of the data into the next data packet is the same for each measurement. Data packet will be generated automatically when the code will be on-line connected with the DPL. Calculation, explosibility evaluation and explosion triangle plotting are executed immediately after entering each component concentration.

The code also allows the user to propose the inertisation of combustible gases in the mine gallery. This function can be activated through the window “Solver options”. Active inertisation boxes are shown in Fig 2.

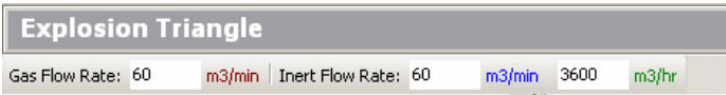


Fig 2. Inertisation boxes enabling to input data necessary for inertisation calculations

If for example the flow rate of gases through the cross-section of the mine is $200 \text{ m}^3 \cdot \text{min}^{-1}$ then user is informed by the code that flow rate $60 \text{ m}^3 \cdot \text{min}^{-1}$ of nitrogen as an inertisation agent is not sufficient to inert the combustible mixture. Warning that it is necessary to decrease the flow rate of the gases through the mine to the value $162 \text{ m}^3 \cdot \text{min}^{-1}$ is displayed immediately in the “Inertisation” window (Fig 3). The value of the inert flow rate ($74 \text{ m}^3 \cdot \text{min}^{-1}$) sufficient for inertisation of the combustible gases in the mine is written in the bubble in the explosion triangle plot (Fig 3).

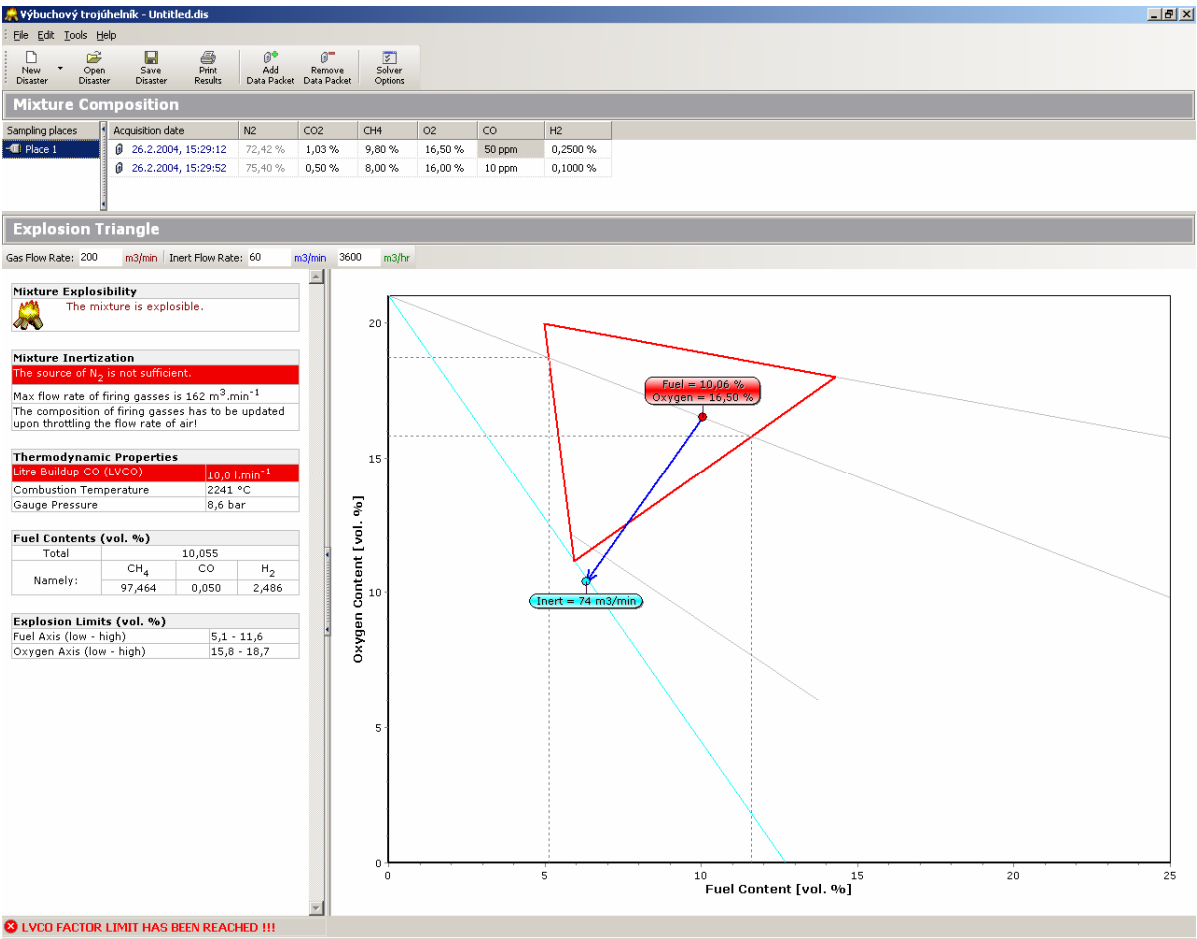


Fig 3. „Výbuchový trojúhelník“ window with active inertisation function

The code controls the flow rate of carbon monoxide. If the value exceeds the critical limit ($10 \text{ l} \cdot \text{min}^{-1}$) then user is warned by flashing red message “LVCO FACTOR HAS BEEN REACHED!!!” in the down left corner of the window (Fig 3).

The results of extended thermodynamic analysis are displayed in the window next to the explosion triangle. But first it is necessary to mark the “Show extended thermodynamic

analysis” in the “Solver Options” window. Structure of displayed results is shown in Fig 4. This option is useful for detailed study of the physico-chemical properties of reacting fuel-air mixture.

Mixture Inertization	
The source of N ₂ is not sufficient.	
Max flow rate of firing gasses is 162 m ³ .min ⁻¹	
The composition of firing gasses has to be updated upon throttling the flow rate of air!	

Thermodynamic Properties	
Litre Buildup CO (LVCO)	11,6 l.min ⁻¹
Combustion Temperature	2241 °C
Gauge Pressure	8,6 bar
Generated Heat (H ₂ O liq.)	2671 kJ.kg ⁻¹
Specific Volume of Products	838 dm ³ .kg ⁻¹
Oxygen Balance	-3,84 %
Combustible Product Content	6,421 vol. %
Specific Heat Ratio	1,2515
Sound Velocity in Products	989 m.s ⁻¹

Combustion Products (vol. %)						
CO ₂	H ₂	CO	H ₂ O	N ₂	O ₂	HCl
6,120	1,987	4,434	17,343	70,116	0,000	0,000

Fuel Contents (vol. %)			
Total	10,056		
Namely:	CH ₄	CO	H ₂
	97,456	0,058	2,486

Explosion Limits (vol. %)	
Fuel Axis (low - high)	5,1 - 11,6
Oxygen Axis (low - high)	15,8 - 18,7

Fig 4. The results of extended thermodynamic analysis

2.2 Manual edit the composition of all combustible components in the gallery environment

“Výbuchový trojúhelník” code makes possible to solve also the situation when mixture of gases consists of gases different from the standard mine combustible gas composition. User can choose the composition of the mixture from the list of the gases, which is displayed in Fig 5. Thermodynamic characteristics are than calculated for the chosen mixture.

Following calculation and command is the same like in the case of the standard mine combustible gas composition.

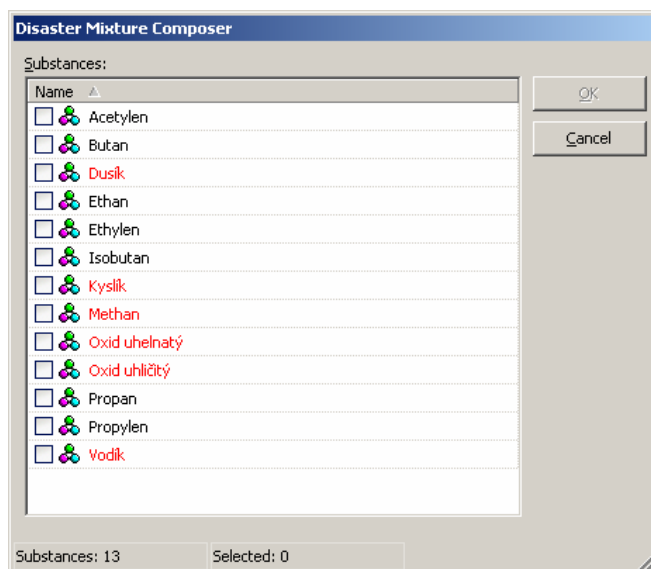


Fig 5. List of the gases, which can be presented in the mine atmosphere

3. “NÁSLEDKY”

“Následky” code is the graphical computing system intended for fast assessment of the accidental natural gas and crude oil release consequences. The code enables the user to find the distances where the specific consequences of thermal radiation and blast wave to people and objects are reached. Three kinds of fires are supposed in the code: jet fire, fireball and pool fire. Vapour cloud explosion is also solved by the code. The code accelerates the routine calculations necessary during the accident fighting, during preventive calculations and training. The command is very simple and user obtains the results in well-arranged numerical form. Every calculation is made immediately after change of any parameter.

Verified methods have been used for particular calculations of physical effects. The methods used are described in theoretical guide of the code ^[8].

This code enables the user to assess the physical effects and consequences of the accidental release of the natural gas and crude oil. The assessment consists of three steps:

- source term calculation;
- physical effects calculation and
- consequence assessment.

Diagram shown in Fig 6 was used for calculation of natural gas release and its consequences. The user inputs the data and chooses particular calculation steps.

Calculation of crude oil release and its consequences is provided according the diagram plotted in Fig 7. The user inputs the data and chooses particular calculation steps.

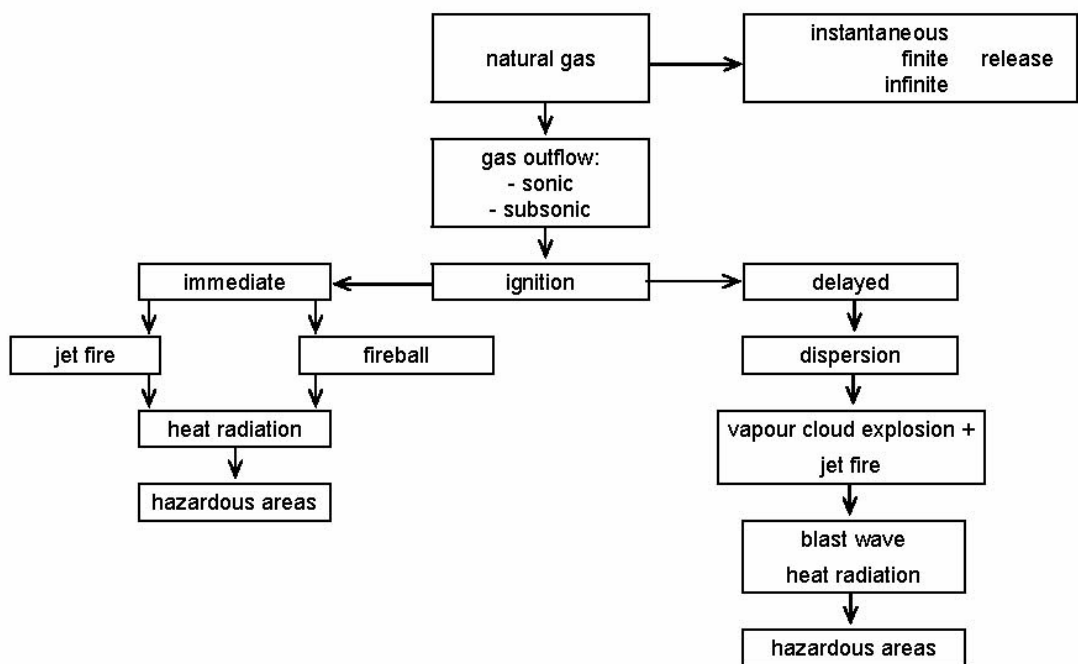


Fig 6. General diagram of natural gas release consequences calculations

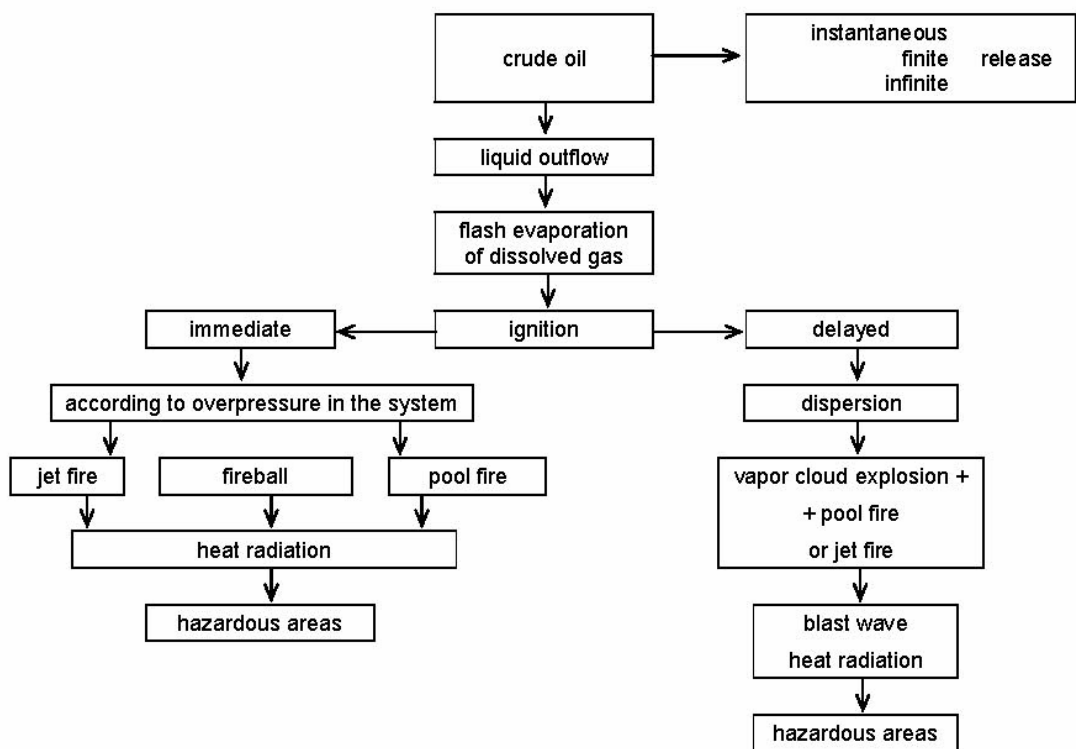


Fig 7. General diagram of crude oil release consequences calculations

After running the code the user has to choose hazardous material involved in the solved situation - crude oil or natural gas.

3.1 Natural gas

User has to select natural gas of proper composition in the database and than basic window showing the results of calculations with default values of initial conditions will appear. This basic window (Fig 8) is divided into three parts:

- Disaster Options;
- Solver Results: Summary and
- Earth (natural) Gas Discharge History.

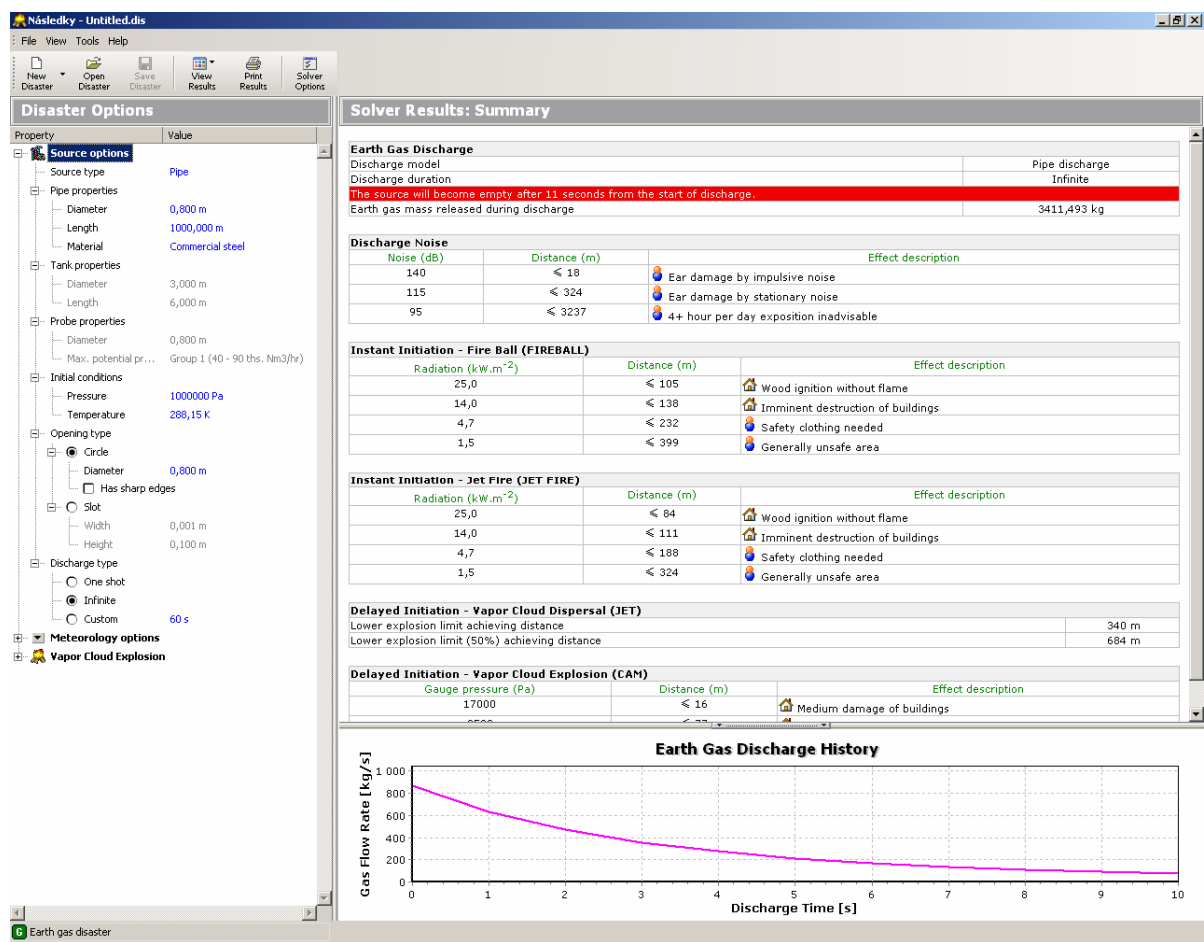


Fig 8. Basic window for natural gas calculations

The window “Disaster Options” offers the change of initial conditions according to user needs. It is possible (necessary) to change default values of following parameters:

- Source type
- Pipe properties
- Tank properties
- Probe properties
- Initial conditions
- Opening type
- Discharge type

There are many models used in the code, which need meteorological data to be specified. This data influences for example density of substance, atmospheric transmissivity for heat radiation calculations, dispersion of substance in atmosphere, etc.

User can choose one of two default meteorological conditions alternatives:

- Consider medium case;
- Consider worst case.

It is also possible to specify each parameter – barometric pressure, ambient temperature, relative humidity, wind velocity, stability class and surface roughness – manually.

The results are presented in matrix form in “Solver results” part of the window. The first matrix contains information about discharge model together with calculated outflow rate.

Individual physical effects are presented in the results window according to ignition time. If immediate ignition is supposed than only fireball and jet fire is supposed. Distances of critical heat radiation levels are displayed. Value of critical heat radiation level is written in the first column, distance, where this level is reached, is written in the second column and description of the characteristic damage is written in the third column.

If delayed ignition is supposed then dispersed material forms the cloud, which can explode after ignition and generate the blast wave causing damages to surrounding. Jet fire develops after the vapour cloud explosion. It is supposed that it is not possible to ignite the cloud if concentration of the combustible material is lower than 50 % of lower explosibility limit therefore distance where this important concentration is reached is also displayed. Distance where lower explosibility limit is reached is also written in this part of the matrix. The same form of results displaying as have been used for heat radiation is used also for consequences of vapour cloud explosion.

“Solver Results: Summary” is shown automatically after running the code, but only the most important characteristic consequences of physical effects are displayed. However, the code offers calculation of many more characteristic damages. After choosing the required physical effects extended results window will appear (e.g. “Solver Results: Vapour Cloud Explosion”, Fig 9). Structure of the results is the same like in the Summary window - three columns where gauge overpressures, distances and characteristic damages are written. Dissipation of gauge pressure with distance from the source is also displayed in the window. Moving the mouse along the curve in the graph the values of distance and actual gauge pressure are shown next to the mouse pointer. The gauge pressure in specific distance or distance for specific gauge pressure can be obtained directly typing the distance or pressure in the proper box at the bottom of the window. The result is displayed immediately.

3.2 Crude oil

Program branch solving the release of crude oil is mostly the same as the branch for natural gas. At the beginning it is necessary to choose proper crude oil type from the database and input the amount of dissolved gas. The only difference in the program branch is calculation of crude oil pool fire consequences instead of calculation of noise level during outflow of natural gas.

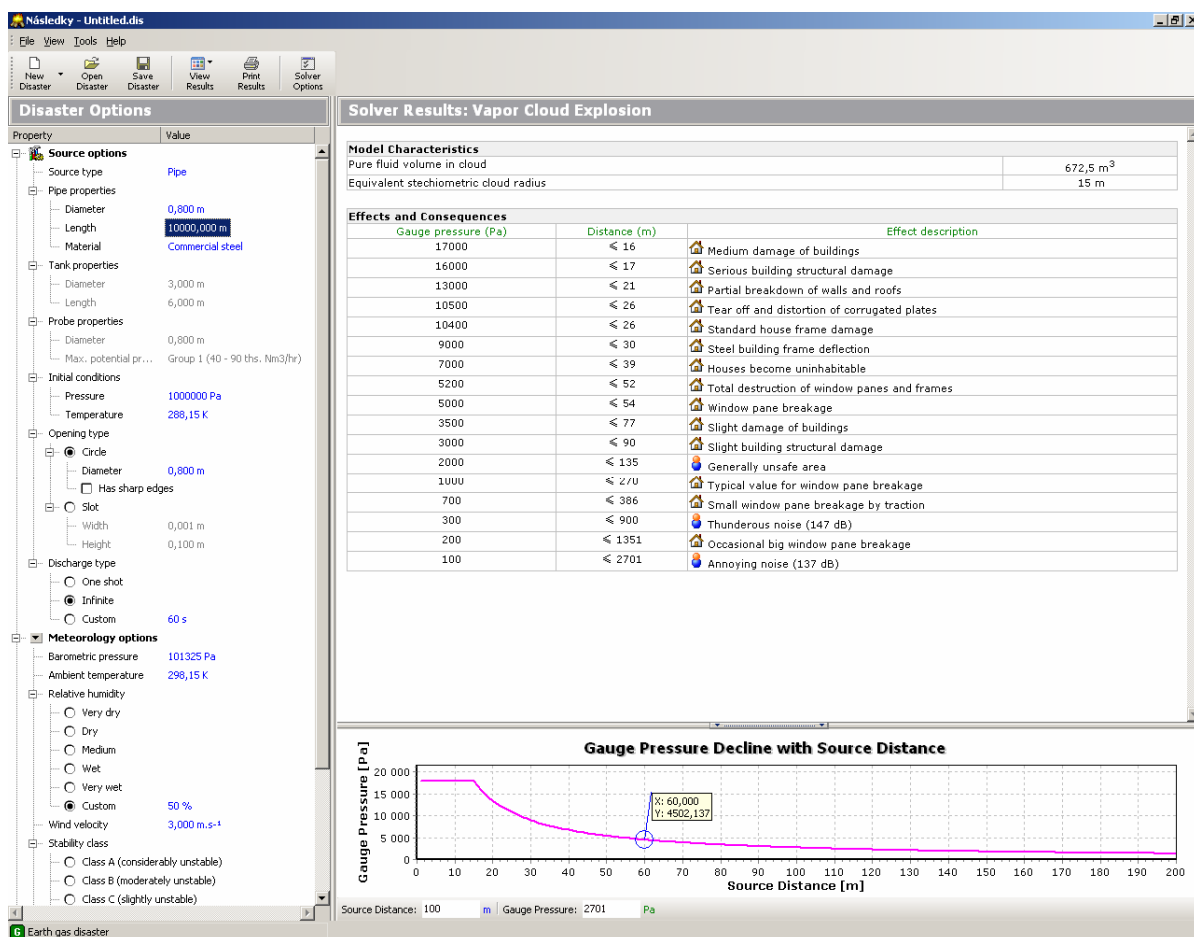


Fig 9. Window of extended results of natural gas cloud explosion

4. “VODNÍ ZÁTKY”

During the project solution a new request to resolve the problem of explosion-proof seat of fire closure by water plug raised. Hence, the third code “Vodní zátky” has been developed.

Numerical solution of differential equation set of water column movement was evolved for more accurate determination of water plug vibration. Blast wave load is supposed to be the cause for the vibration. Set of differential equations is solved by Runge-Kutt method. Solution enables the user to follow behavior of series of variables together with transient states during the water plug movement. Critical length of submergence together with the length on the border of overshoot is found by special procedure.

Based on the defined criteria for explosion-proof water plug it is given the possibility to submergence a mine gallery with interchanging slope in case of incident situation.

The use of water plugs is shown in Fig 10. The alternatives are given by the wind direction and geometrical configuration of the gallery.

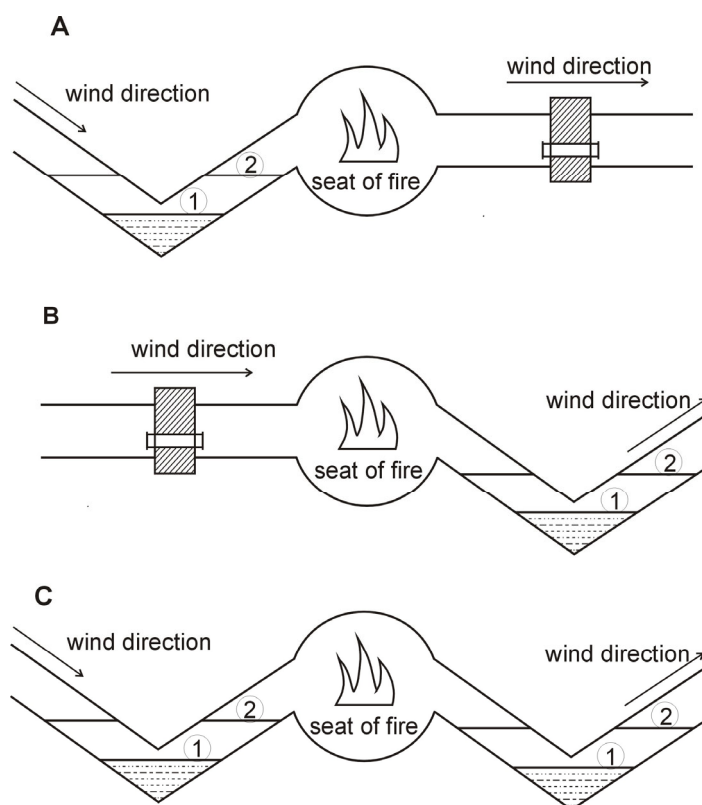


Fig 10. Demonstration of water plug use

Tactical principles of seat of fire closure were treated according to above demonstrated alternatives of water plug use and they are included in the Central Mining Rescue Station Ostrava Instruction No. 1/2003 for building of explosion-proof dams.

Use of the code is simple and consists of two steps. First, the data necessary for the calculation of water plug movement are input in proper box and in the second step after click on the “Řešení” box the code is executed. The results are presented in both written and graphical form. Window of the “Vodní zátky” code is shown in Fig 11.

Parameters and data are input by keyboard into proper boxes. Input data could be divided into following groups:

- Text for locality identification – mine identification, bed identification, gallery identification, date of calculation;
- Input data for calculation – cross-section area of the gallery, gallery height in the lowest point, angle in the direction of expected explosion, angle in the adit direction;
- Completion data – length of the horizontal part of the water plug, available amount of water.

5. CONCLUSIONS

During the project of Czech Mining Authority No. 10/2001 named “Coping with the serious process accidents” in its program of research and development “Increase of safety level of work in the mines and elimination of the hazard from the methane release from the closed mines” program package DisSolver v. 1.1 has been introduced. The package contains three individual codes: “Výbuchový trojúhelník”, “Následky” and “Vodní zátky”.

Czech Mining Authority based in Prague as exclusive owner officially taken the software package at the final inspection day. The process of package implementation in the activities of Integrated Emergency System and Central Mining Rescue Service in Ostrava and Hodonín is in the progress at present day.

User guide for the “Vodní zátky” code became a base for the chapter Water Plugs of the Instruction No. 1/2003 for building of explosion-proof dams published by Central Mining Rescue Station in Ostrava.

REFERENCES

- [1] HAAR, L., SHENKER, S., H.: *Equation of State for Dense Gases*. Journal of Chemical Physics, Vol. 55, str. 4951 – 4958, 1971
- [2] NOVÁK, J., P., MALIJEVSKÝ, A., ŠOBR, J., MATOUŠ, J.: *Plyny a plynné směsi*. Academia, Praha, 1972
- [3] MOORE, J., W.: *Fyzikální chemie*. SNTL, Praha, 1979
- [4] SCHUTZ, A.: Některé aspekty důsledného přechodu na jednotky soustavy SI v chemii. Chemické listy, 70, 1976
- [5] STULL, D., R., AT ALL: *JANAF Thermochemical Tables*. Dow Chemical Co, Midland-Michigan, US Government Printing Office, Washington, D.C., 1967
- [6] ŠINDELÁŘ, V., SMRŽ L.: *Nová soustava jednotek*. SPN, Praha 1968
- [7] MAKARIUS R.: *Inertizace při důlních požárech*. SNTL, Praha, 1993
- [8] JANOVSKEÝ, B., KRUPKA, M.: *Následky - Teoretický manuál programu*; Český báňský úřad, 2003

EXPANSION OF METALLIC TUBES DRIVEN BY HEAD-ON GRAZING DETONATION

Chen Jun and Sun Chengwei

Laboratory for Shock Wave and Detonation Research, Southwest Institute of Fluid, CAEP,
PO Box 919-103, Mian Yang, Sichuan 621900, P.R.China

Abstract:

Since the pressure gradient abruptly increase in the detonation products undergoing a head-on collision of two detonation waves propagating in the cylindrical charge embedded in a metallic tube, the movement of tube wall driven by which will be of particular pattern. The data of expansion, deformation and fracture of the tube are obtained in the experiments with diagnostics of pulsed x-ray shadowgraphy and high-speed photography. A 2-D elastic plastic hydrodynamic Lagrangian code TTD2C has been compiled during this work and succeeded in simulating the head-on collision of two detonation waves and the resulting products flow, also the expansion process of metallic tubes driven by it. The calculated and measured results agree well with each other. The result shows that the fracture time advanced because of the head-on collision.

Keywords: *grazing detonation, head-on collision, metallic tubes*

1. INTRODUCTION

The detonation product's expansion movement driving plate, cylinder and sphere shell is an important problem in the field of investigation of material dynamic characteristics at high strain rates. It is fundamental to the design of cannon, bomb and missile warhead. The history of detonation driving begins with the study of Gurney^[1]. He gets the fragment's velocity with some assumptions in order to calculate the fragment's initial velocity. Chengwei Sun^[2] uses the instantaneous modified detonation-driving model and gets the analytical result of max velocity for grazing detonation-driving plate. He also gets the differential equation of grazing detonation driving plate, long metallic tube, and short cylindrical shell for divergent and convergent movements. Many have studied the phenomenon of one-point initiation problem^[3,4]. But the studies on expansion movement under head-on collision are still limited.

The expanding fracture under detonation load inside of axial symmetrical shell is one of the most typical problems. G.I. Taylor first brings forward the compression and tension criteria on expansion of shells^[5]. It is suggested that radial crack propagates only in area of hoop tension stress not of compressive stress and the hoop stress equals zero at the tip of the crack. So there exists a mid-surface at the cross section of the shell where hoop stress and strain equal zero. When detonation waves arrive, the mid-surface lie at the outer surface of the shell. With the expanding of the shell, the mid-surface moves inward. When the mid-surface moves to the interior interface, the shell is considered completed fracture.

In this paper, we use the experiment methods of pulse x-ray shadowgraphy and high-speed photography to measure the expanding, deforming and fracture process. At the same time, using the two-dimensional Lagrange hydrodynamic code, the interaction of detonation waves and the detonation driving process have been investigated in this paper.

2. EXPERIMENT SET AND EXPERIMENT METHOD

The experiment set is schematically illustrated in Figure 1 and 2. Figure 1 is used for pulsed x-ray shadowgraphy and Figure 2 is for high-speed photography. In these experiments, steel 45 is used as the shell materials. The detonators are initiated simultaneously. The design parameters of the experiment set-up are listed in table 1.

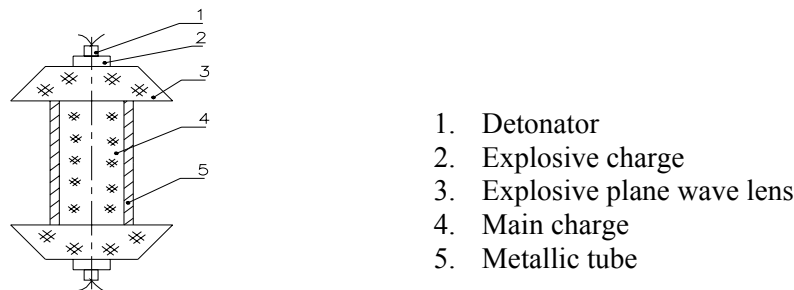


Fig 1. Experimental set up 1

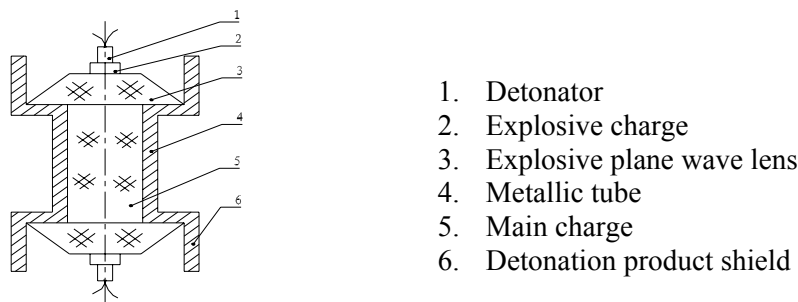


Fig 2. Experimental set up 2

The x-ray shadowgraphy and high-speed photography are used to observe the expansion process. The lay out of x-ray and photography are showed in Figure 3 and 4.

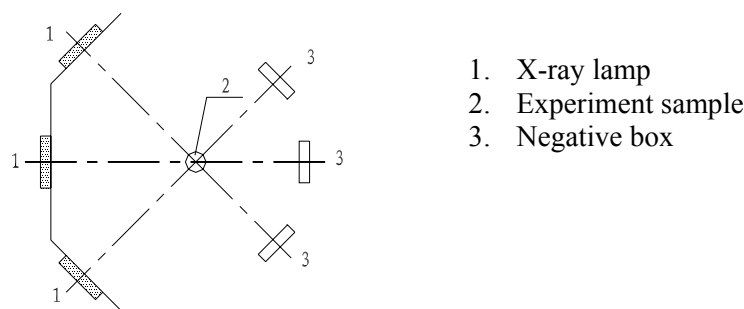


Fig 3. X-ray experiment diagram

For high-speed photography, Xe lamp has low cost, simple power system, suitable spectrum range and high luminosity. In this measurement system, we use flash power control the luminosity and pulse distance. Aluminum foil reflector box can be used as background light source and project light source from normal face. In order to distinguish the deforming process more clearly, the high sensitive colorful negatives are used.

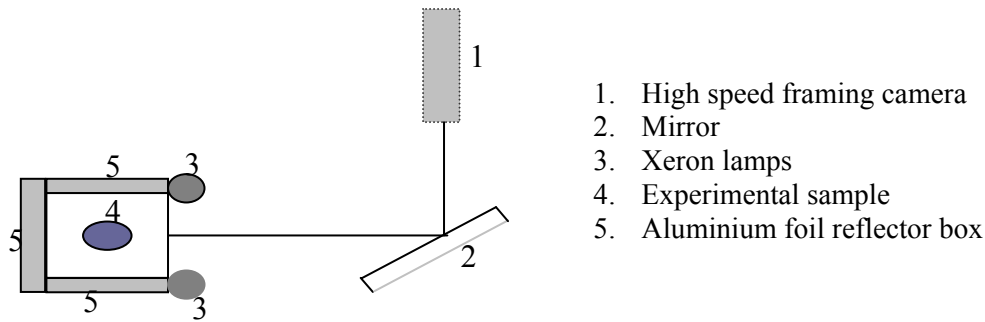


Fig 4. High-speed photography diagram

Table 1. *Experimental Assemblies*

Shot No	Explosive Charge	Thickness of Tube mm	Type of Experimental Setup	Diagnostics
1	JOB-9003 ϕ 25.4×75mm	3	1	X-ray
2	JOB-9003 ϕ 25.4×75mm	3	1	X-ray
3	JB-9014 ϕ 50×153mm	5	1	X-ray
4	JB-9014 ϕ 50×153mm	5	1	X-ray
5	JOB-9003 ϕ 25.4×75mm	3	2	High-speed photography
6	JOB-9003 ϕ 25.4×75mm	4	2	High-speed photography

3. NUMERICAL CALCULATIONS

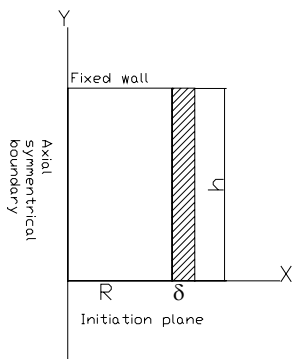


Fig 5. Numerical simulation model

R means the radius of the main explosive charge, δ means the thickness of the metallic tube, h is the half height of the tube. If considering the symmetry of the model and saving the calculating time, the quarter of the model is used. Free boundary at the outer surface and the initiation plane are used.

In the Lagrange coordinate system, Y is the symmetrical coordinate. The slip interface between the explosive and metallic tube is used. The initiation time is taken as the initial time. JWL EOS is used for detonation products.

Table 2. *Parameters of JWL EOS*

Explosive	ρ (g/cm ³)	A (100GPa)	B (100GPa)	C (100GPa)	R ₁	R ₂	ω
JOB9003	1.85	8.4204	0.2181	0.0075	4.6	1.35	0.28
JB9014	1.88	5.4563	0.0852	0.0125	4.2	1.62	0.47

4. RESULTS AND DISCUSSIONS

The mean expanding velocity for shot 1 and 2 is 0.18 ± 0.03 cm/ μ s at the head-on position from the fitting curve of Figure 6. While the mean expanding velocity for shot 3 and 4 is 0.16 ± 0.07 cm/ μ s. The velocity is only considered as the outer surface’s velocity.

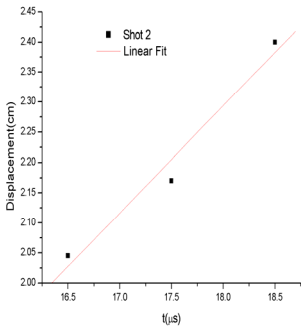


Fig 6. Displacement history at head-on collision point of Shot 2

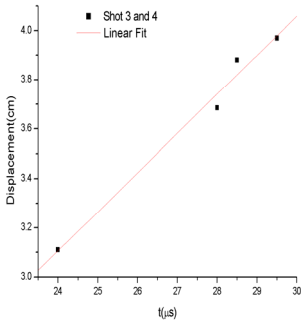


Fig 7. Displacement history at head-on collision point of Shot 3 and 4

Before head-on collision, the metallic tube’s expanding process is similar to one point initiation. After head-on collision, the middle part of the shell has a swelling part and expands quickly. The swelling part exists until the metallic fractured. The fracture time of shot 5 is 24.0 μ s and that of shot 6 is 25.6 μ s from the results of the high-speed photography.

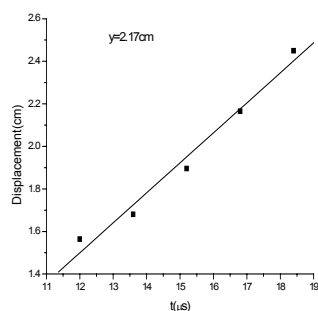


Fig 8. Displacement history at non-head-on collision point of Shot 5

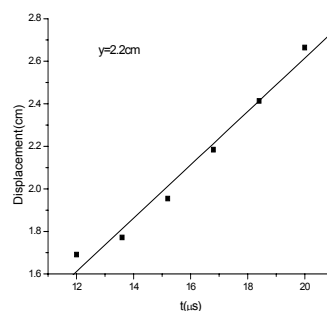


Fig 9. Displacement history at non-head-on collision point of Shot 6

In shot 5, 2.17 cm from the initiation plane is taken as the characteristic station and 2.20 cm of shot 6 is taken. The mean expanding velocity for shot 5 is 0.14 ± 0.01 cm/ μ s at 2.17cm from the fitting curve of Figure 8. While the mean expanding velocity for shot 6 is 0.13 ± 0.01 cm/ μ s at 2.20 cm from the fitting curve of Figure 9. Because the tube of shot 6 is 1 cm thicker than that of shot 5, its mean expanding velocity is a little smaller.

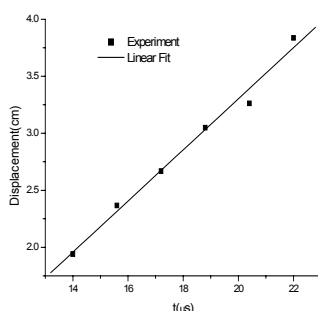


Fig 10. Displacement history at head-on collision point of shot 5

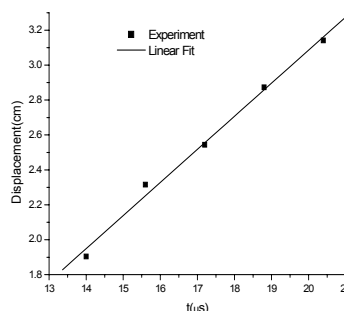


Fig 11. Displacement history at head-on collision point of shot 6

The mean expanding velocity for shot 5 is 0.22 ± 0.01 cm/ μ s (about 1.59 times compared with 2.17 cm) at the position of head-on collision from the fitting curve of Figure 10. While the mean expanding velocity for shot 6 is 0.19 ± 0.01 cm/ μ s (about 1.51 times compared with 2.20 cm) at the head-on collision from the fitting curve of Figure 11. Before head-on collision (at the position of one quarter from the initiation plane, about 1.88 cm, 1.88 cm, 3.83 cm, and 3.83 cm for shot 1, 2, 3 and 4), when the detonation product reaches CJ pressure, the pressure decreases because of the rarefaction waves. After head-on collision, the detonation product pressure goes up immediately because of the interaction of the two detonation waves, the amplitude is about 2 times of CJ pressure, and then it decreases. Figure 12 and 13 shows that after head-on collision for shot 1 and 2, the radial velocity's discrepancy at the axial distance of 1.88cm and 3.75 cm from the initiation plane is about 1.5 times. So this discrepancy drives the head-on collision part move more quickly than non-head-on collision part. From calculations, the non-head-on collision's mean expanding velocity is 0.15 cm/ μ s while it is 0.14 cm/ μ s from the high-speed photography experiment. The experiment result is in accordance with the numerical calculation. The same result appears in shot 3 and 4 at the position of 3.83 cm and 7.65 cm from the initiation plane. The

work ability of JB9014 explosive is much lower than JOB9003, so the shell's radial velocity is smaller at the same load condition.

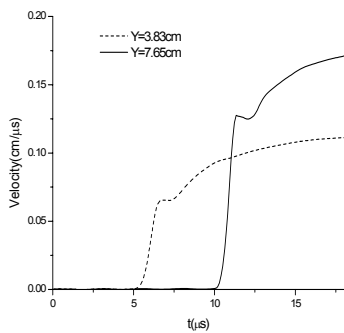


Fig 12. Expanding velocity histories of outer wall at different axial position of shot 3 and 4

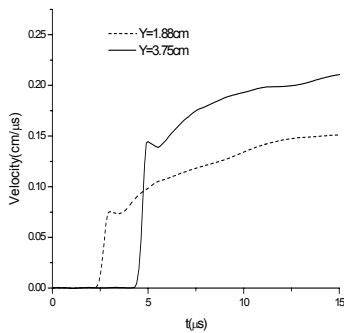


Fig 13. Expanding velocity histories of outer wall at different axial position of shot 1 and 2

From the expanding radial velocity history of the metallic tube, at the beginning of the deforming process, the radial expanding of the shell is quicker. With the weakening of the work ability of the detonation products, the expanding acceleration dies down gradually.

According to Taylor’s criteria, when the mid-surface moves to the interior interface, the shell is considered completed fracture. So from the hoop stress history in figure 14, 15, 16, 17, we can get the completed fracture time. These results are listed in Table 3. Relative fracture means the fracture time from the arrival of the detonation waves. The head-on collision of the two detonation waves makes the metallic tube’s fracture time advanced. Because the limited experiment conditions, the fracture time’ observation is still awaited.

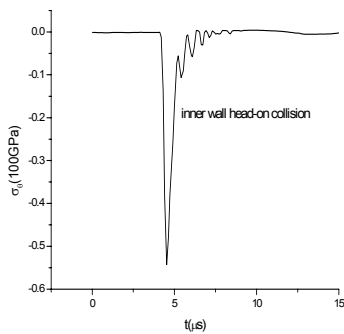


Fig 14. Hoop stress history of inner wall at head-on collision point of shot 1 and 2

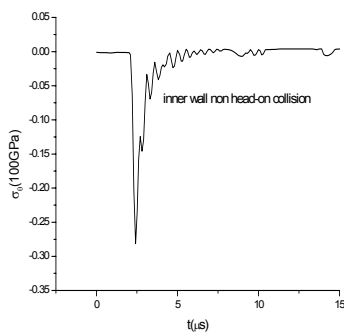


Fig 15. Hoop stress history of inner wall at non-head-on collision point of shot 1 and 2

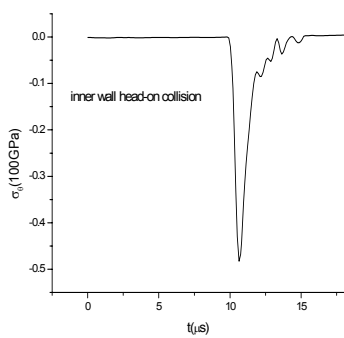


Fig 16. Hoop stress history of inner wall at head-on collision point of shot 3 and 4

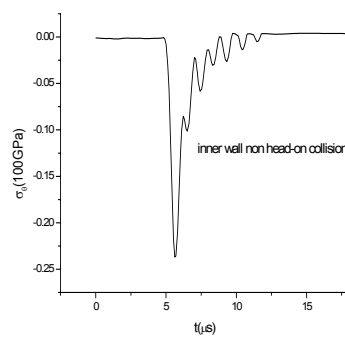


Fig 17. Hoop stress history of inner wall at non-head-on collision point of shot 3 and 4

Table 3. Fracture Time for Shot 1, 2, 3, and 4

Shot No	Fracture Time for Head-on Position (μs)	Fracture Time for Non-Head-on Position (μs)	Relative Fracture Time for Head-on Position (μs)	Relative Fracture Time for Non-Head-on Position (μs)
1 and 2	9.0	12.0	5.1	9.5
3 and 4	16	13.0	5.0	7.5

5. CONCLUSIONS

1) The pressure and pressure gradient increase after the head-on collision of the two detonation waves. The mean expanding velocity of the head-on collision position increases about one and half times compared to the non-head-on characteristic collision position. The relative fracture time for head-on collision also advances obviously.

2) With Taylor’s fracture criteria, the completed fracture time and the relative fracture time of different positions for the metallic tube can be obtained.

3) This Lagrange hydrodynamic code can simulate the expansion movement of the metallic tube precisely. The results of the calculation agree well with the experiment results.

REFERENCES

- [1] GURNEY R.W.: *The Initial Velocity of Fragments from Bombs, Shells and Grenades*, BRL Report 450,1943
- [2] SUN CHENGWEI, ET AL.: *Detonation Physics of Application*, Military Defense Technology Publishing, 2000
- [3] FENG JIAPO, ET AL.: Chinese Journal of High Pressure Physics, 2(2), 1988
- [4] CHEN DANIAN, ET AL.: Explosion and Shock Waves, (1): 27, 1987
- [5] TAYLOR G.I.: Science Paper of Sir Taylor G. I. III(44), Cambridge University Press, London, 387:97, 1963

NONAERATIONS SENSIBILIZATION OF EMULSIVE EXPLOSIVES

I.L. Kovalenko*, V.P. Kuprin** and A.V. Kuprin***

* Faculty of inorganic chemistry, Ukrainian state university of chemical technology,
Gagarin av. 8, 49005 Dnepropetrovsk, UA

** Faculty of physical chemistry, Ukrainian state university of chemical technology,
Gagarin av. 8, 49005 Dnepropetrovsk, UA

*** ECCOM Ltd, Serova str. 15/26, 49070 Dnepropetrovsk, UA

Abstract:

The opportunity of reception bull water-tight (4100-4400 kJ/kg) emulsive explosives such as "water in oil" is shown on the basis of solution of nitrocalcites and ammonium at the expense of sensibilization by the solid high-energy additives. The sensibilization of emulsive explosives is carried out at the expense of the addition of powders of metals and alloys with high hardness, melting point and capacity to react with light-end products of detonating. The responsive efficient explosive is prepared out without padding aeration, introducing of microspheres and explosive reagents.

Keywords: *emulsion, explosive, sensibilization, silicon-containing of materials, ammonium saltpetre*

1. INTRODUCTION

Explosive materials, which one will used for mining encroached massifs of mines of Ukraine and Russia represent trotyl-containing fusion cakes of inorganic nitrates. High temperature of applying, poor water resistance and content of a toxic trotyl, makes such systems dangerous and unsafe in industrial use.

As demonstrate the world tendencies of progressing of explosive materials for mining, alternative of a trotyl are the emulsive explosives, which one have a high level of safety, both in cooking, and in applying.

The compositions and technology creations of emulsion explosive substances on based of nontrotyl emulsive composition^[1] in USUCT were designed.

2. EMULSIVE MATRIX OF EXPLOSIVE SUBSTANCES

The emulsive composition represents a revertive emulsion of solution of inorganic oxidant in a hydrocarbonaceous phase. As oxidant utilised binary concentrations (83-85 %) water solution of calcium and ammonium saltpetre of eutectic composition. The nitrate of lime in composition of a dispersed phase promotes stabilizing emulsive system, prevents

hydrolysis of ammonium saltpetre and is a considerable radiant of bound oxygen. Besides temperature of crystallization of a dispersed phase compounds 338-341K, that allows to plot an emulsion at low temperatures.

For stabilizing an emulsion used oxyethylic surface-active substance (SAS) of animal and plant origin with C14-C16 of a vegetative and animal genesis, which one provide high adsorption on interphase boundary "oil - water". The high stabilizing operating is provided also with geometry of a molecule SAS - part of a molecule, which one is laied out in oil to a phase in view of dual ionic bed has the size more $6 \cdot 10^{-10}$ m, and the proportion hydrophilic and lypophilic of parts SAS (GLB) lays in limits 3-6 on a Griffins scale ^[2,3].

Composition and the concentration limits of reductants of an emulsive matrix allow to receive microemulsion with the size of particles in dispersed phase are 30-40 nm (fig.1) even by single-stage emulgation in reactor with propeller and turbine mixing. The designed emulsion is high-concentration (contain of a dispersed phase 91-92 %), physically stable and water-resistant heterogeneous system, which one is assorted as an in explosive material and does not contain toxic materials.

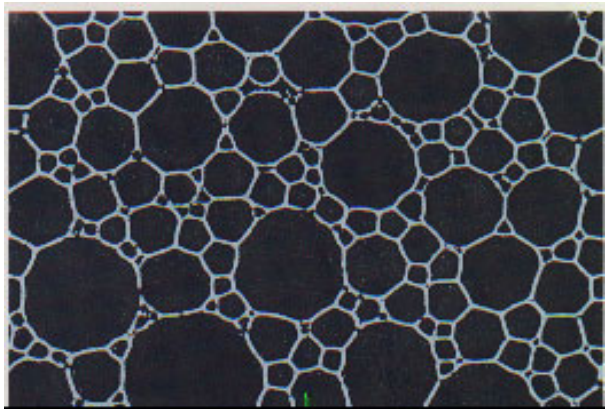


Fig 1. Pattern of an emulsion under an electronic microscope

Such emulsion is a good basis for making secure in haul and applying, high performance nontrotyl of emulsive explosives for encroached rocks. However, low responsiveness to a detonating impulse and small values of energy of explosive (2800 kJ/kg) require reliable sensitization of an emulsion.

Table 1. Basic characteristics of an emulsive matrix

Index	Value
Design energy of detonating, kJ/kg	2800 -3000
Density (T=343 K), kg/m ³	1450 – 1650
Dynamic viscosity (313K), Pa·s	3,00-4,00
Physical stability	30 day
Losses of mass under bed of water in 24 hours, kg/m ²	less than 0,15
Temperature: gravitational segregations, K	363
to a beginning of exothermic destruction, K	163

3. SENSIBILIZATION OF EMULSIVE MATRIX

Applying of conventional methods aerations of sensitization: use gas generating reagents and gas-filled of microspheres has given in making low-current (2800-3000 $\kappa\text{J/kg}$) explosives with relative brisance 0,6 (measurement standard - grammonit 79/21, which one contains 21 % of a trotyl).

By results of studies and thermodynamic calculations was proposed nonaerations an expedient of sensitization of revertive emulsions, which one is based on use of powdery inorganic materials, which one have high hardness and melting point.

The sensitizing operating of such materials is instituted by presence in an emulsion solid particles irregular-shaped with high melting point ^[4], which one promote concentration of energy of shock on acute angles particles, and at the expense of intensive internal friction in heterogeneous system can form the multiple centres of local heating, which one provide an inconvertible detonation on the dodge " of calorific detonating ".

As such sensitizers the powders of ferrosilicon (FS-65) and silicon carbide utilised, which one not only provide an inconvertible detonation of an emulsive matrix on the dodge "of ardent dots", but also import the essential contribution to theoretical operation of detonating.

As a matter of fact, from the point of view of existing submissions about a detonation ^[5], the solid additives, inlet into an emulsive matrix, are inert. They it is pleased are inertial and do not enlist interplay with reductants of explosive mixture directly in a detonation surge, i.e. up to a plain of Chepman-Guge. However these materials are capable to react with explosion products behind a plain of Chepman-Guge, essentially increasing theoretical operation of detonating at the expense of secondary exothermal reactions with steam and oxides of nitrogen. As demonstrate thermodynamic calculations, such reacting spontaneously proceed in temperature range 298-598K.

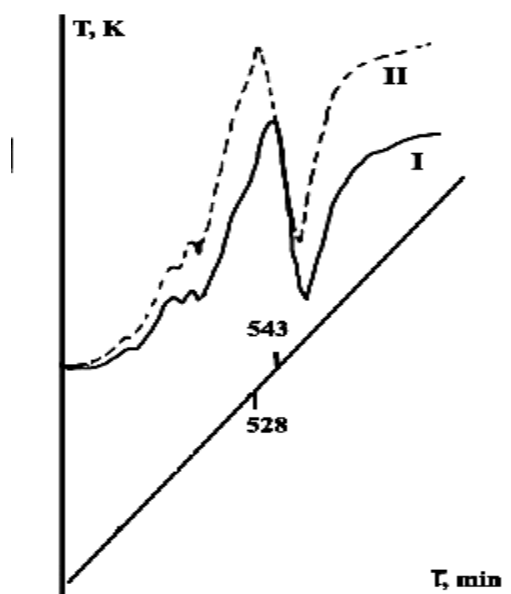


Fig 2. Thermogram of destructions:
I- ammonium saltpetre; II- ammonium saltpetre at the presence of ferrosilicon of a fraction 215-350 microns

Besides as demonstrate differential-thermal analyse the inlet additives influence on dynamics of disintegrating of ammonium saltpetre (fig. 2), dislodging temperature of explosive disintegrating of saltpetre in area of lower temperatures. As in studied temperature range (up to 700K) there is no chemical interplay to ammonium saltpetre, it is possible to speak about catalytic influencing silicon-containing of materials: ferrosilicon and silicon carbide on dynamics of disintegrating of nitrate of ammonium - one of the basic reductants of emulsive explosive.

On the basis of the held studies the emulsive explosives of the mark Ukrainit-HP, sensitized by a powder of ferrosilicon of the mark FS-65 (tab.2) are created.

Table 2. *Basic characteristics of explosive Ukrainit-HP-1*

Index	Value
Oxygen balance, %	-0,05÷-0,40
Energy of explosive, kJ/kg	4100-4400
Light-end products of explosive, m ³ /kg	0,721-0,750
Extreme diameter of detonating in a steel shell, mm	120-150
Speed of a detonation, m\с	4300-4400
Relative work capacity (measurement standard grammonit 79/21)	1,2-1,4
Relative brisance (measurement standard - grammonit 79/21)	0,8-0,95
Losses of mass under bed of water in 24 hours, kg/m ³	0,1-0,2

The utilised expedient of sensitization low-power of emulsive matrix allows to provide good responsiveness of a material to detonation impulse, inconvertible propagation of a detonation and high work capacity at the expense of particular interplay silicon-containing of materials with reductants of heterogeneous system. The responsive efficient explosive is prepared out without padding aeration, introducing of microspheres and explosive reagents.

The obtained explosives of the mark Ukrainit-HP-1 are competitive both on technical and production characteristics, and under the price, and also the safety of reversion, and are capable to exchange trotyl-containing explosive materials used by mines for mining of encroached massifs.

REFERENCES

[1] KRUSIN R.S., KUPRIN V.P.: Emulsion explosive substace, Patent UA 17369 A- № 96020539; 14.02.96;15.04.97

[2] Emulsion, Leningrad, 1975

[3] KACHWEIT M.: Microemulsoin, Annu. Repts Progr. Chem., №95, p. 89-115, 1999

[4] BAUM F.A., STANYKOVICH K.P., SHECHTER B.I.: Physics of detonating, Moscow,1959

[5] DUBNOV L.V, BACHAREVICH N.S., ROMANOV I.A.: Industrial explosives, Moscow, Entrails, 1987

THE CONDENSED EXPLOSIVE SYSTEMS CAPABLE OF PROPAGATING DETONATION IN THE SPIN-PULSATING REGIME

G.D. Kozak^{*} and Z. Lin^{**}

^{*} Mendelev University of Chemical Technology
Miusskaya Sq.9, Moscow, 125190

^{**} Beijing Institute of Technology,
P O Box 327, Beijing 100081, China

Abstract:

Quite distinct inhomogeneity of the detonation front was found earlier at detonation of cast charges TNT/RDX and TNT/PETN. The ultimate objective of this work is to extend the number of explosive systems capable of propagating detonation in the spin-pulsating regime and to generalize the results. Cast TNT/DINA, TNT/TETRYL DNT/PETN and pressed HMX/paraffin charges were investigated. Systems, detonating with low (1~3 MHz) frequency spin pulsation at some content of sensitizer (C_s), have approximately the same calculated detonation parameters: $D_J \approx 7.3$ -7.4 km/s, $Q_V \approx 5.4$ MJ/kg. The compositions TNT/DINA with $C_s > 25\%$, which detonate without spin pulsation, have calculated values Q_V and D_J higher than that named above. Q_V and D_J of itself DINA sufficiently higher than 5.4 MJ/kg and 7.3~7.4 km/s, correspondingly, and spin pulsation at detonation of charges of liquid Dina were not observed.

Keywords: *detonation, pulsation, heat explosion, velocity*

1. INTRODUCTION

Quite distinct inhomogeneity of the detonation front was found earlier at detonation of cast charges: TNT/RDX, TNT/PETN^[1,2] at content of sensitizer $C_s=12$ -15%, and liquids: Nitromethane, solution of DNT in DINA^[2,3]. This regime was registered by means of streak camera records and by means of cooper witness plates. Some of the records and photos of witness plates are shown in Fig. 1.



Fig 1. The streak camera record and photo of witness plate at spin detonation of charge of TNT/PETN 87/13, d=12 mm

There is no any inhomogeneity of luminosity at detonation of mixtures on TNT base if a content of sensitizer exceeded 20%. (Fig. 2.).

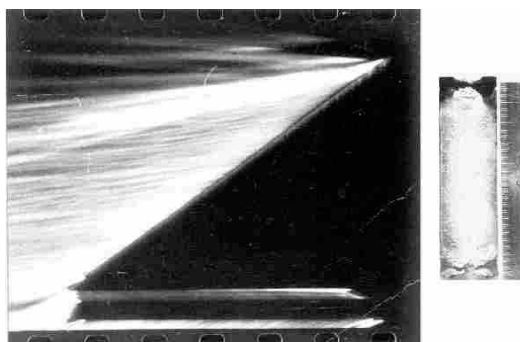


Fig 2. The streak camera record and photo of witness plate at detonation of charge of TNT/RDX 50/50, $d=12$ mm

Waves of reaction absence are seen in streak camera records of detonation of transparent liquids, which were made from the side of bottom of charge (Fig. 3).



Fig 3. The photo of witness plate and streak camera records at spin detonation of charge of Nitromethane (tracing confinement, $d = 17$ mm). Shooting are made simultaneously from the wall side of the charge (sloping white line), and from the side of its bottom by means of placed under it mirror at angle 45° to it axis (lower part of picture).

The mechanism of spin detonation consists of consecutive propagation of damping wave along the lateral surface of a charge, reinitiating of detonation and propagation of super compressed detonation wave in the thin subsurface layer of explosive capable of a propagating detonation in the spin-pulsating regime ^[1]. The stamp of spin detonation on straightened cooper tube witness plate, inside those the cast charge of TNT/RDX 85/15 has been placed, is shown in Fig. 4. The slopping line on the surface of witness plate is the stamp of spin wave.

One can see that the process of super compressed detonation propagated along spiral trajectory. Cast TNT/DINA, DNT/PETN and pressed HMX-paraffin charges were investigated in this respect in work ^[4]. The ultimate objective of this work is to extend the number of explosive systems capable of propagating detonation in the spin-pulsating regime, and to generalize the results of these investigations.



Fig 4. The stamp of spin detonation on straightened cooper tube witness plate, inside those the cast charge of TNT/RDX 85/15 has been placed,

2. EXPERIMENTAL

The experiments were carried out with cast charges on a base of commercial grade TNT and DNT whereas RDX, TETRYL, PETN, and DINA were applied as sensitizers. Some of the runs were carried out with double base propellant NB and pressed charges of mixtures HMX/Paraffin. The methodology of carrying out of experiments was the same as in work ^[1,2]. In a few words it consist from next operations. Cast charges were obtained by pouring of melted mixtures into glass tubes and extracting of castings from the tubes. The dependence of failure detonation diameter (d_f) versus content of sensitizer (C_s) for each mixture under investigation was measured by the method of “go-no-go”, with the exception of the mixture TNT/TETRYL, that was investigated only at 15-30% sensitizer content in charges of 12-14 mm diameter.

The charges were fastened to a copper or brass witness-plate so that a ~5 mm clearance took place between cylinder surface and the plate. The pressed pellets of phlegmatized RDX ($d=12$ mm, $m=2$ g, density $\rho=1.67-1.68$ g/cm³) were used as booster. Russian streak cameras GFR-3 and SFR-2 were employed to register the luminosity of detonation and to measure detonation velocity (D_e). Sometimes, the mirror installed at 45° angle to the charge axis under the bottom of charge was used. This set up permitted to fix the luminosity in the clearance between the charge and the witness-plate one can see it in bottom part of photos in Figs 1-2.

3. RESULTS

The dependencies d_f versus C_s of explosive systems under investigation are compared in Fig.5. The spin regime of detonation was fixed for TNT/RDX, TNT/PETN, TNT/DINA, and TNT/ TETRYL. The first three dependencies are similar to each other, small plateaus are observed on smooth curves. Narrow dents or furrows of 1-2 mm wide and 0.5-1 deep at a 45-60° angle to the charge axis covered the surface of copper or brass witness-plate over which the charge was fixed at the sensitizer content coinciding with plateau region. The traces of light irradiated by the detonation front on the streak camera records were also rather inhomogeneous (Fig.1). The distance between narrows on the witness-plate corresponded to distance between traces on streak-camera records (step of pulsation – h, mm) in every experiment.

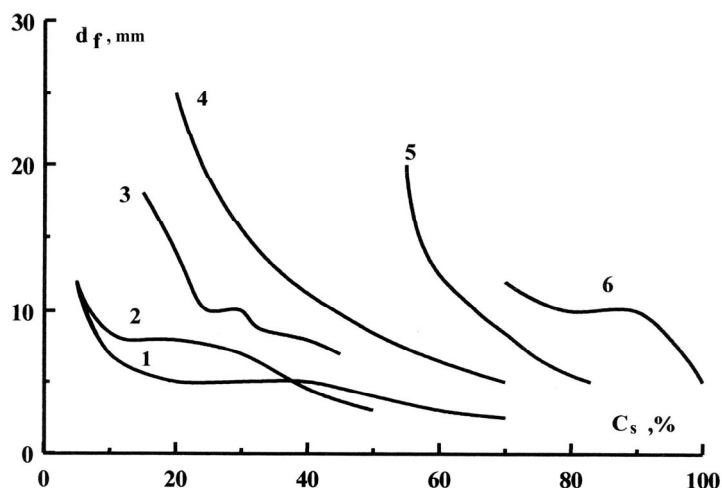


Fig 5. The dependencies d_f versus content of sensitizer (C_s). 1 – TNT/PETN, 2 – TNT/RDX, 3 – TNT/DINA, 4 – DNT/ PETN, 5 – Paraffin/HMX, 6 – DNT/DINA.

The TNT/RDX and TNT/PETN curves are similar one to another, whereas TNT/DINA curve disposes appreciably higher. In other words, DINA is less effective sensitizer of TNT then RDX and PETN are. The thorough description of investigation of frequency of fluctuation ($f = D_e/h$) and as well as calculation of kinetic parameters of the reactions at TNT/RDX spin detonation are contained in the works ^[1,2]. The same low frequency pulsating (2-3 MHz) is observed in the course of experiments on TNT/DINA (Fig. 6) and TNT/TETRYL spin detonation.

Experimental detonation velocity at spin detonation of all of systems studied are very close to calculated one by the method ^[5], however, sometimes it is a little bit greater than that calculated value. It is demonstrated in Fig 7 for TNT/DINA cast charges. When detonation propagates without pulsation (at a large content of sensitizer) the calculated detonation velocity is, as a rule, greater than the experimental one for all of the systems under investigation.

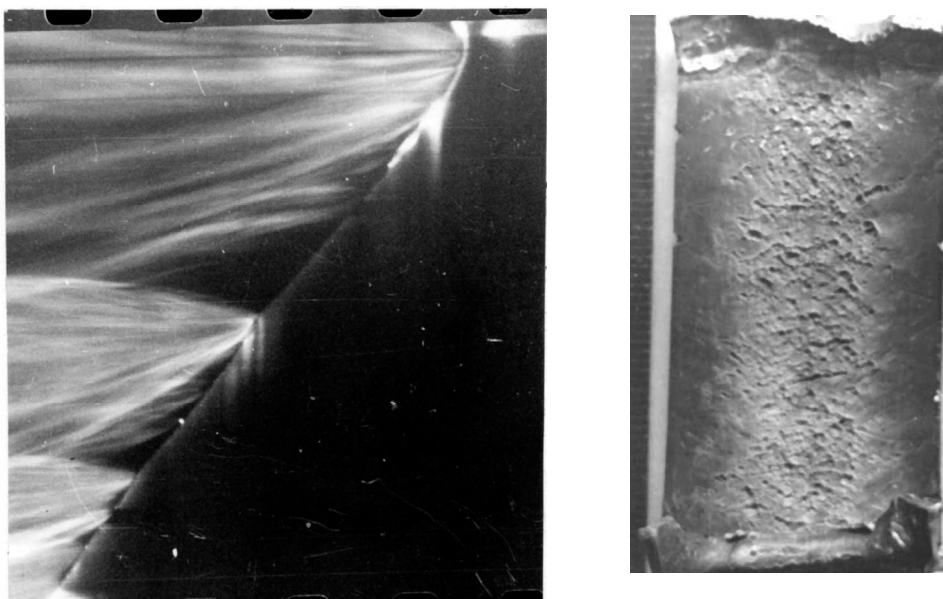


Fig 6. The streak-camera record (a) at spin detonation of TNT/DINA 80/20 ($d=15.5$ mm) the photograph of witness-plate (b) at spin detonation of TNT/TETRYL 85/15 ($d=12$ mm) cast charges

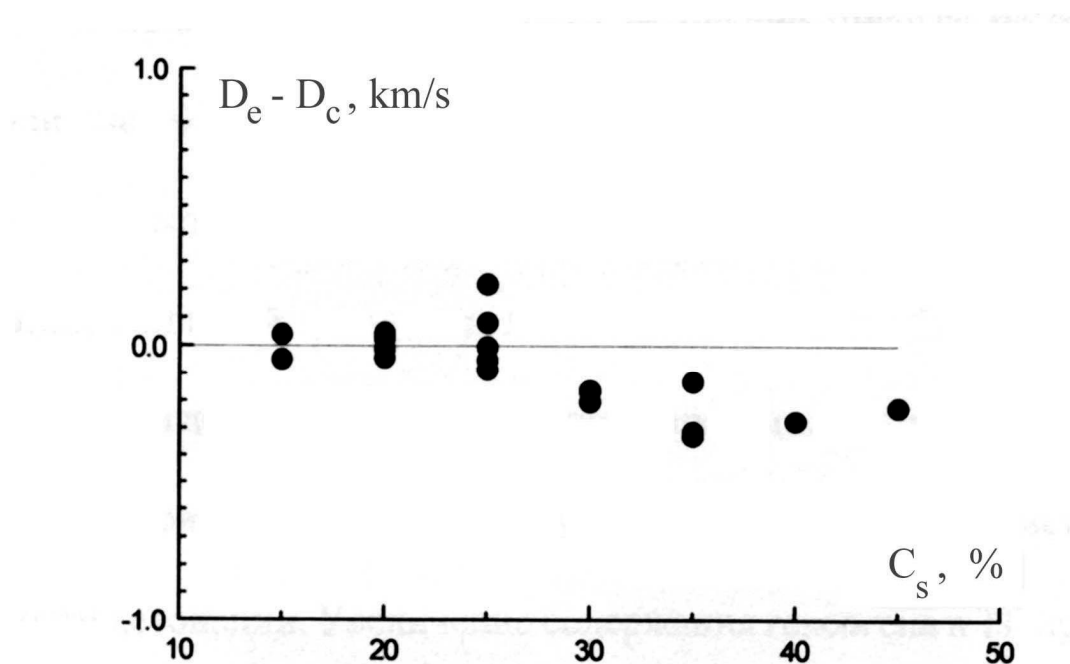


Fig 7. Difference between experimental (D_e) and calculated (D_c) detonation velocity vs. Dina content of TNT-DINA cast charges. Low frequency spin detonation propagated at $C_s \leq 25\%$.

The spin detonation of DNT/PETN cast charges was observed only at 52.5% PETN content in the mixture, the frequency of pulsation sharply decreased from $f=7$ MHz to 3 MHz between the $C_s=52\%$ and $C_s=52.5\%$ (Fig 8).

The pulsating detonation of pressed HMX-Paraffin mixtures are not observed.

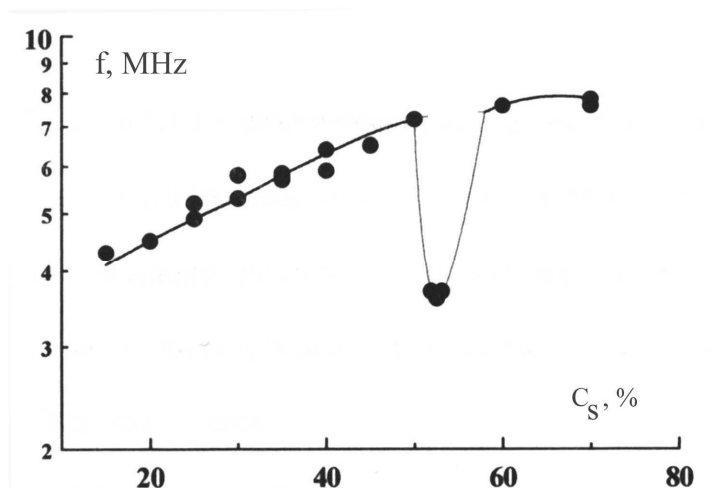


Fig 8. Frequency of pulsation versus PETN content at detonation of cast DNT-PETN charges.

4. DISCUSSION

To explain the discrepancy between TNT-RDX and TNT-DINA $d_f(C_N)$ dependencies the calculated detonation velocity (D_J) and pressure (P_{CJ}) vs. C_N were analyzed and shock-heating temperature (T_S) and pressure (P_3) temperature (T_3) in the reaction zone defining the process of reinitiating of detonation wave in the zone of instability according A.N. Dremin's failure diameter theory ^[6,7] were calculated. The results of calculation are represented in Table 1.

The mixtures, containing 20, 30, and 40% of RDX in the TNT/RDX mixtures have detonation pressure on 1.3, 1, and 2.7 GPa higher than corresponding compositions of TNT/DINA. Similar situation is noted at comparison of the P_3 values. Correspondingly, values T_3 for mixtures TNT/RDX are on 60-100 degrees higher than of TNT/DINA. Bearing in mind the exponential dependence of the reaction velocity vs. temperature, such difference can explain the detonation proceeding in TNT/RDX mixtures at lower diameter.

The technological factors could influence on the specific of $d_f(C_N)$ curves location could cause. Conditions of crystallization of TNT/RDX mixtures (suspension) probably essentially differ from them of TNT/DINA solution.

Calculation detonation parameters: velocity (D_J) and heat (Q_V) of detonation was carried out within the framework of the SD computer code ^[5], the results are collected in Table 2.

One can note that systems: TNT/RDX, TNT/PETN, double propellant NB, TNT/DINA, TNT/TETRYL, and DNT/DINA, detonating with low (1-3 MHz) frequency spin pulsation, have approximately the same calculated detonation parameters: $D_J = 7.3-7.4$ km/s, $Q_V = 5.4$ MJ/kg. The compositions TNT/DINA with $C_S > 25\%$, which detonate without spin pulsation, have calculated values Q_V and D_J higher than that named above. Q_V and D_J of itself DINA sufficiently higher than 5.4 MJ/kg and 7.3-7.4 km/s, correspondingly, and spin pulsation at detonation of charges of liquid Dina were not observed.

Table 1. *Shock-heating temperature (T_S), pressure (P_3), and temperature (T_3) of TNT mixtures with DINA and RDX.*

System	P_{CJ} , GPa	P_3 , GPa	T_S , K	T_3 , K
TNT	19.7	12.3	1523	1063
TNT-DINA 80/20	21.22	13.3	1622	1123
TNT-RDX 80/20	22.48	14.4	1706	1190
TNT-DINA 70/30	21.99	13.7	1673	1147
TNT-RDX 70/30	23.97	15.0	1806	1227
TNT-DINA 60/40	22.76	14.2	1724	1178
TNT-RDX 60/40	25.44	15.9	1906	1282

Table 2. *Step and frequency of pulsation, calculated detonation velocity (D_c) and heat of explosion of systems under investigation*

System	Experimental parameters				Calc. parameters	
	ρ , g/cm ³	d_f , mm	h , mm	f , MHz	D_c , km/c	Q_v , MJ/kg
TNT-RDX 87.5/12.5	1.62	8	~3	~1.8	7.37	5.40
TNT-RDX 85/15	1.62	8	~3	~1.8	7.41	5.42
TNT-PETN 87/13	1.61	7	3-4	-2	7.28	5.40
Propellant NB	1.56	~9 ^{*)}	3	2.5	7.40	5.39
DNT-DINA 30/70	1.50	12.5	>10	~1	7.29	5.40
DINA (melt)	1.50	4.5	<1	>7.5	7.59	5.76
TNT-DINA 85/15	1.612	18	3.4	2.1	7.327	5.38
TNT-DINA 80/20	1.60	14	3.4	2.1	7.324	5.4
TNT-DINA 75/25	1.61	95	3.2→1.4	2.1→5.3	7.410	5.43
TNT-DINA 70/30	1.58	9.5	1.4	5.2	7.332	5.44
TNT-DINA 65/35	1.564	7.8	1.4	5.2	7.312	5.46
TNT-DINA 60/40	1.605	7.5	1.4	5.4	7.524	5.51
TNT-DINA 55/45	1.62	5.5	1.4	5.4	7.629	5.55
TNT-TETRYL 70/30	1.66	-	2.1	3	7.48	5.47
TNT-TETRYL 80/20	1.65	-	3	2.3	7.42	5.42

^{*)} at $T=60^\circ\text{C}$

The heat of explosion of Paraffin/HMX mixtures at $C_S=55-80\%$ does not attain the value of 5.4 MJ/kg and, although at $C_N = 70-75\%$ $D_J = 7.8-7.4$ km/s, pulsating of detonation were not fixed.

As it was noted above, the spin pulsation in DNT/PETN system was registered at $C_{PETN}=52.5\%$. The heat of explosion equals 5.4 MJ/kg and $D_J = 7.3$ km/s just at this composition. DNT is more inert component than TNT and deceleration of decreasing d_f of the curve 4 (Fig. 5) at C_S arising is not observed at weak spin pulsating.

5. CONCLUSION.

Thus the number of cast explosive systems able to detonate in spin regime extended. Detonation velocity and heat of explosion of them were calculated and found to be the same for all the systems, detonated in low frequency (1-3 MHz) spin regime: $D_J = 7.3-7.4$ km/s and $Q_V = 5.4$ MJ/kg.

Acknowledgment

We wish to thank Russian Foundation of Basic Research (RFBR) for partial financial support of this work (Grant 01-03-32610a).

We would like to thank professor B.N.Kondrikov for helpful remarks and discussions.

Our students: P. Boiko, N. Rasshchupkina, H. Kanbar, and E. Sharapova took part in carrying out the experiments.

REFERENCES

- [1] G.D.KOZAK, B.N.KONDRIKOV, V.B.OBLOMSKY: *Spin detonation in solid substances*, Comb., Expl. & Shock Waves, v.25, № 4, 88-93, 1989
- [2] V.B. OBLOMSKY: *Non-ideal detonation of homogeneous and porous explosives*. Cand. Sci. (Ph. D.) Thesis. Mendeleev University of Chemical Technology, Moscow, 1988
- [3] G.D. KOZAK, B.N. KONDRIKOV, V.B. OBLOMSKY: *Spin wave and attenuation of liquid explosive detonation*, Combustion, Explosion, and Shock Waves, vol.28, No.2, pp. 195-199, March-April, 1992
- [4] ZHOU LIN: *Surface phenomena at detonation of condensed explosives*, Cand. Sci. (Ph. D.) Thesis. Mendeleev University of Chemical Technology, Moscow, 2000
- [5] B.N. KONDRIKOV, A.I. SUMIN: Equation of state of gases at a high pressure, Comb., Expl. & Shock Waves, v.23, № 1, 114-123, 1987
- [6] A.N. DREMIN: DAN SSSR, V.147, pp. 870-873 (Russ.), 1962
- [7] A.N. DREMIN AND V.S. TROFIMOV: PMTF. No 1, pp. 126-131, 1964 (Russ.)

DETONATION ABILITY OF SOLUTIONS OF AROMATIC NITROCOMPOUNDS IN NITRIC ACID

G.D. Kozak, V.M. Raikova and V.V. Potapov

Mendeleev University of Chemical Technology
125047, Miusskaja sq. 9, Moscow, Russia

Abstract:

The ultimate objective of our work was to measure the failure detonation diameters of solutions of nitro derivative of toluene: TNT, DNT and MNT, and of nitro derivative of benzene: TNB, DNB and MNB in strong nitric acid at oxygen balance $A=0\%$. They were measured by means of technique of parallel-plate cells. The cells were glued from glass photo plates, each of them had the constant thickness (1.1-1.4 mm). The clearance of cells was made by means of placing teflone sheets between sides of glass plates. Equivalent failure diameter of detonation of the solution of TNT and TNB was $d_f=0.10$ mm, of DNT and DNB - $d_f=0.18$ and 0.15 mm, and of MNT and MNB - $d_f=0.6$ and 0.2 mm, correspondingly. Simultaneously the detonation parameters of the solutions investigated were calculated by means of SD computer code at experimentally measured densities of solutions. Distinction of d_f values was explained by discrepancy of its calculated detonation parameters.

Keywords: detonation, nitric acid, nitrocompounds

1. INTRODUCTION

The mixtures containing the strong nitric acid (NA) and organic compounds are known to be the reaction mixtures of some nitration processes. The investigation of detonation ability of these mixtures is the important part of the complex estimation of explosion hazard of the nitrocompounds manufacturing.

The dependencies of failure detonation diameter (d_f) of solution of di- (DNT) and trinitrotoluene (TNT) in NA on its content (C_N) were investigated in references [1,2]. d_f of these systems at oxygen balance $A=0\%$ were found to be extremely small ($d_f<1$ mm), and it was impossible to measure its exact value by means of the method "go-no go" in glass tubes. At $A<0\%$ and $A>0\%$ the $d_f(C_N)$ curve were defined.

The precise method of measuring d_f less than 1 mm was elaborated in works [3,4]. And d_f of solutions of TNT, DNT, and mononitrotoluene (MNT) in strong nitric acid were measured, at $A=0\%$ [4]. They were equal to 0.1, 0.18, and 0.6 correspondingly. The dependencies d_f versus NA (anhydride, i.e. 100% HNO_3) content (C_N) are shown in Fig. 1. Detonation abilities of solutions of mono- (MNB), di- (DNB), and trinitrobenzene (TNB) in strong nitric acid are investigated near oxygen balance $A=0\%$ in this work.

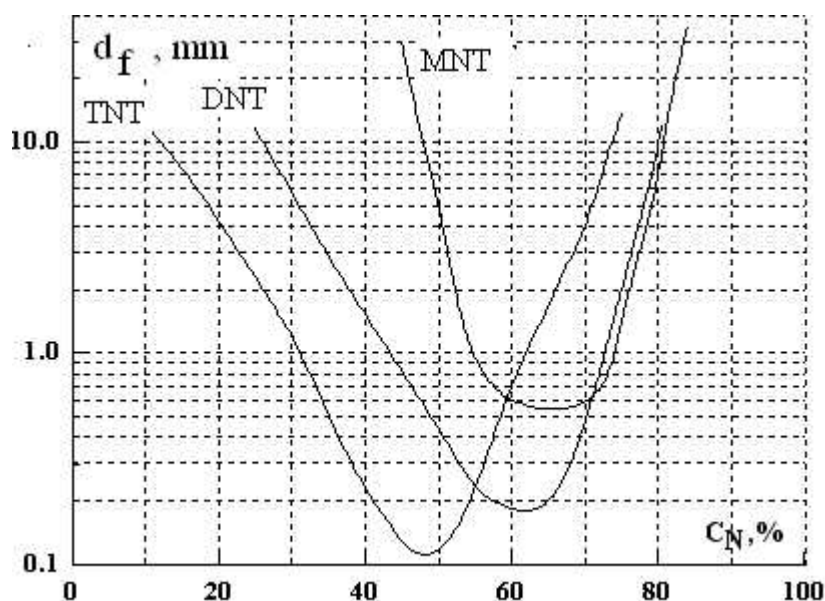


Fig 1. The dependencies d_f of solutions of nitrotoluenes in strong NA versus NA (anhydride) content (C_N)

2. EXPERIMENTAL

2,4-DNB and MNB were commercial grade products, the melting point of DNB was $T_m = 89^\circ\text{C}$. TNB was synthesized in the Laboratory, and was recrystallized, $T_m = 123^\circ\text{C}$. The strong NA (“chemically grade”), which had a concentration $C_N=94-98\%$, was used for preparation of the solutions. Concentration of NA changes continuously at storage, and it was controlled before preparation of every solution.

The methodology of investigation based on the technique using parallel-plate cells which had been proposed in reference ^[5] for measurement of d_f of methylnitrate ($d_f \approx 2$ mm), but it was improved to measurement of $d_f < 1$ mm.

The walls of cells were cut out from glass photography plates (the emulsion was removed preliminary). One of the walls was some longer and wider than another one. The thin Teflon films or strips of glass were placed between walls in left, right and bottom side of vessel, and then the walls were glued together by means of water glass. The thickness of each photography plates (δ) is known to be strictly constant in any direction and it allowed to measure the thickness of clearance (d) between walls of the vessel within an accuracy of 0.01 mm. From plate to plate δ varied in the limits of 1.1-1.4 mm. The values of d in the experiments were changed in the limits of 0.05 to 1.50 mm. The width and the length of the layer of a liquid in the vessel were $H=25-30$ mm and $L=75-80$ mm, correspondingly. Thus the ratio L/d in some experiments on the order of magnitude was 10^3 and never was less than 50. The widening of channel in the top of the vessel was made by means of gluing together of two triangular and one rectangular glass sheets and longer wall of vessel to provide normal initiation of detonation. The photo of cell is shown in Fig. 2. The pellets ($d=5$ mm) of pressed phlegmatized HMX protected by means of polyethylene film were used as boosters. Propagation or failure of detonation were registered by means of brass witness-tube (diameter of the tube is 6 mm) which was placed between wide side of the vessel and the heavy steel plate. The character of deformation of tube specified detonation, attenuation, or absence of detonation ^[3,4].

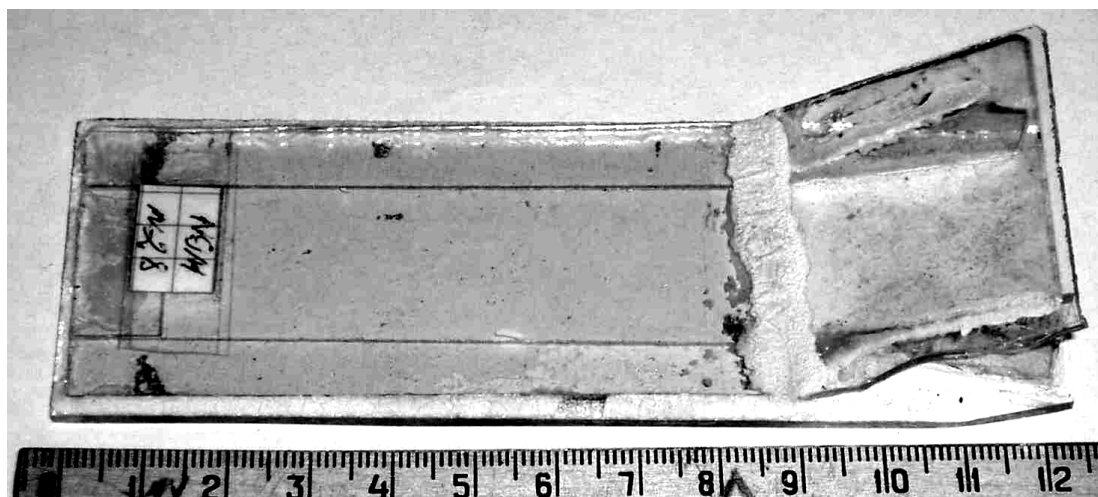


Fig 2. The photo of glass cell

3. RESULTS

The dependencies of density on composition of solutions on base of nitrotoluenes were measured by means of picnometer. The data are presented in Fig. 3, the points signify the results of measurements, dash lines are results of calculation according to the rule of specific volumes additivity.

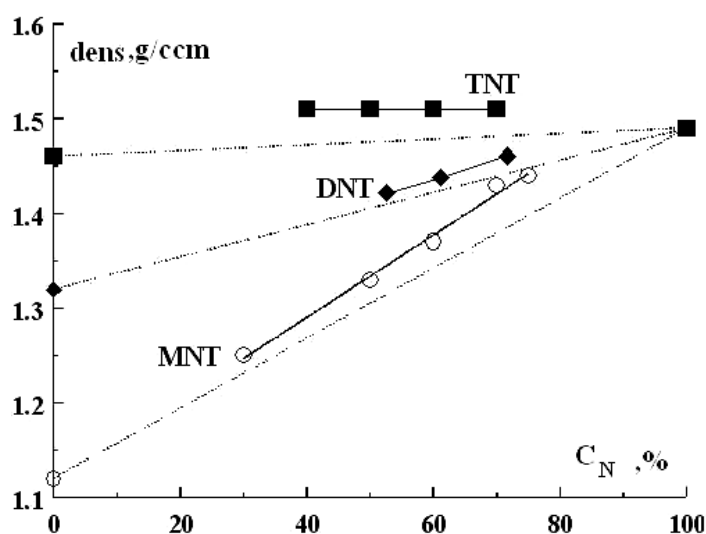
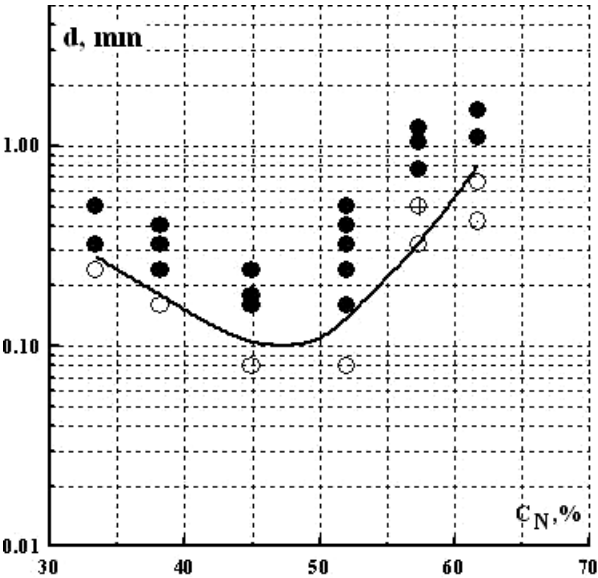


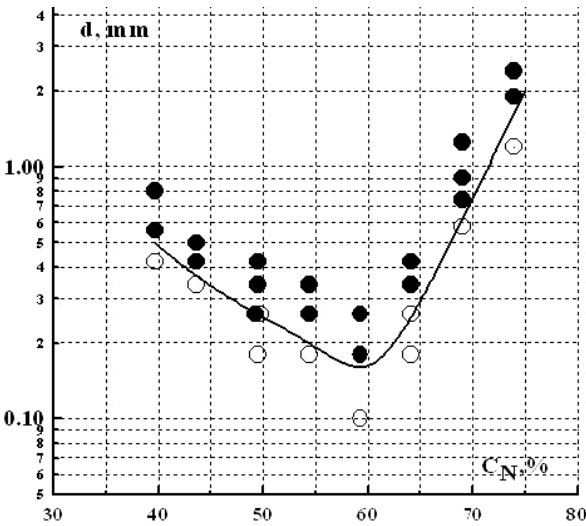
Fig 3. The dependencies of density on composition of solutions on base of nitrotoluenes measured by means of picnometer (points) results of calculation according to the rule of specific volumes additivity (dash lines)

The results of the experiments with solution of TNB, DNB, and MNB in NA are shown in Figs.4a, 4b, 4c, correspondingly. Dark points signify propagation of detonation, open points are failure of detonation, and crosses are damping of detonation. Equivalent diameter $d_f = 4 F/P$ (where S is cross section and P is perimeter of a charge) is used as ordinate (as and in Fig. 1). The content of nitric acid (anhydride) in solution is used as abscise. The lines dividing arias of dark and open points are $d_f(C_N)$ dependencies.

a



b



c

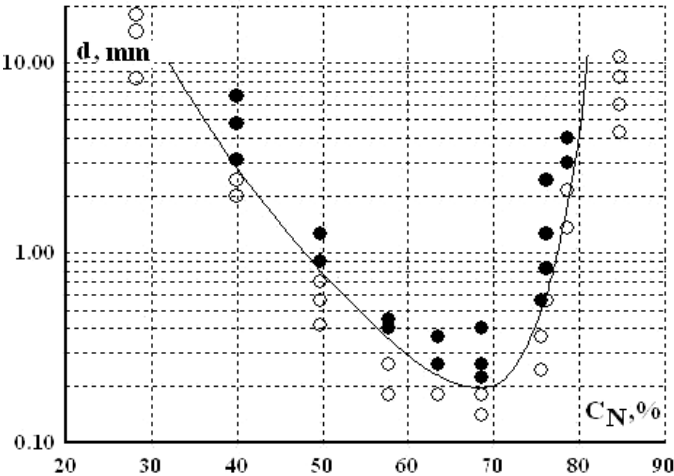


Fig 4. The results of failure diameter measurement of TNB (a), DNB (b), and MNB (c) solutions in strong nitric acid

The curves $d_f(C_N)$ in Figs.4a –4c are similar each other. The values of d_f^{\min} for the solutions of TNB, DNB, and MNB in NA are 0.10, 0.15, and 0.2 correspondingly.

4. DISCUSSION

The comparison of detonation ability of systems under investigation is given in Fig.5a and fig. 5b in coordinates A- d_f . One can see that solutions have the minimal failure detonation diameter d_f^{\min} at A=0%, but for TNT and TNB-systems its are approximately half as much then d_f^{\min} of DNT and DNB solutions and some (2-6) times less then d_f^{\min} of MNT and MNB solutions.

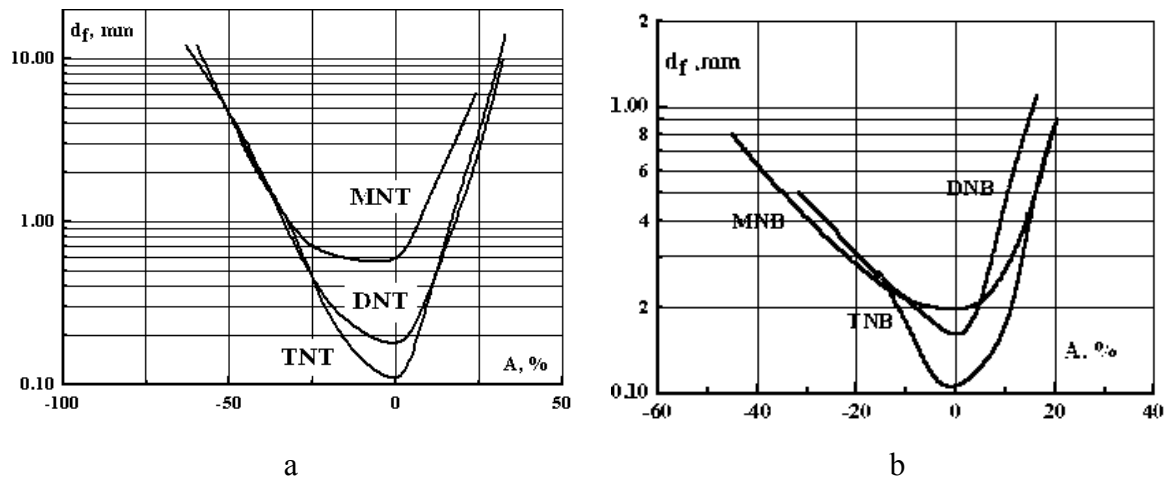


Fig 5. Detonation ability of nitrocompounds solution in NA vs. oxygen balance.

Densities of solutions on a base of nitrobenzenes were not measured experimentally and they were calculated according to the rule of specific volumes additivity and were used in detonation parameters calculation process. As one can see in Fig. 3, difference between calculated and measured density in case of nitrotoluenes systems is not too large. Detonation parameters of solutions were calculated by means of SD computer code ^[6] and some of them (Q_v - heat, D - velocity, P_J - pressure, and T_D - temperature of detonation) for systems having A=0% are collected in Table 1. Contents of nitrocompounds (fuel) in the solution of strong nitric acid, which was applied as dissolvent for every solution preparation, are also presented in Table 1.

As it was shown in works ^[1,2], the dependencies of detonation parameters vs. oxygen balance had maximums at A=0%. Solutions in Table 1 are arranged in ascending order of d_f . As the main goal of this work was description of the methodology of carrying out the experiments and obtaining values of d_f , we only remark here that growth d_f follows the tendency of T_D , Q , and P_J values reduction.

Detailed generalization of this results according to Dremine theory of detonation failure diameter ^[7] based on conception of pulsating reaction zone reinitiating of detonation in this zone near the limit of detonation propagation proceeds is carried out in work ^[8] which is reporting in this seminar.

Table 1. *The detonation parameters of the solution of nitrocompounds (fuel) in strong nitric acid, at A=0%*

d _f , mm	Fuel		D, km/s	Q, MJ/kg	P, GPa	T _D , K
	name	Content, % mass				
0.1	TNT	45.0	7.24	6.0	18.9	4560
0.1	TNB	51.9	7.14	6.2	18.3	4820
0.15	DNB	39.5	6.93	6.0	16.6	4630
0.18	DNT	34.7	6.89	5.9	16.1	4410
0.2	MNB	26.9	6.83	5.8	15.6	4290
0.6	MNT	25	6.6	5.7	14.4	4220

ACKNOWLEDGMENT

We are grateful to Russian Foundation of Basic Research (RFBR) for partial financial support. (Grant №01-03-32610-a).

Our students: L.E. Sazonova and I.S. Maltseva took part in carrying out of the experiments.

REFERENCES

- [1] RAIKOVA V.M., KONDRIKOV B.N., KOZAK G.D.: *The experimental investigation of detonation of solution on base of the nitric acid*, Comb., Expl. And Shock Waves, '1, p.84, 1998
- [2] RAIKOVA V.M., KONDRIKOV B.N., KOZAK G.D.: *Detonation of mixtures on base of the strong nitric aci*, Energetic materials - technology, manufacturing and processing, Proc. 27th Int Annual Conference of ICT, Karlsruhe, FRG, 59-1, 25-28 June 1996
- [3] KOZAK G.D., RAIKOVA V.M., POTAPOV V.V.: *Measurement of Detonation Failure Diameter in Thin Layers of an Explosive Solution*, Combustion, Explosion and Shock Waves v.35, №5, p. 568-569, 1999
- [4] G.D.KOZAK, V.M.RAIKOVA, AND V.V.POTAPOV: *The failure thickness of detonation of solutions on the base of strong nitric aci.*, Trans. of The 30-th International Annual Conference of ICT, Karlsruhe FRG, pp. 96-1 – 97-75 June 29 – July 2, 1999
- [5] KURBANGALLINA R. CH.: *Some data dealing with the ability of methylnitrate detonation*, The collected articles "Physics of explosion", issue 4, p. 112, 1955
- [6] A.I.SUMIN, V.N.GAMEZO, B.N.KONDRIKOV, V.M.RAIKOVA: *Shock and detonation general kinetics and thermodynamics in reactive systems computer package*, 11th Detonation Symposium, Snowmass, Colorado, Paper Summaries, 321 - 324, 1998
- [7] DREMIN A.N., TROFIMOV V.: *Calculation of the failure diameters of liquid explosives*, J. Appl. Mechanics and Technical Physics (Rus.), N1, p.126, 1964
- [8] RAIKOVA V.M., LIKHOLATOV E.A.: *The chemical kinetic at detonation of aromatic nitrocompounds - nitric acid mixtures*, Proc. of The 7th seminar "New trends in research of energetic materials", Univ. Pardubice, CR, April, 2004

FAULT TREE ANALYSIS IN THE PROCESS SAFETY INCIDENT INVESTIGATION

R. Kuracina, B. Janovský and M. Ferjenčík

Department of Theory and Technology of Explosives, University of Pardubice, Czech Republic

Abstract:

This contribution is focused on methods for incidents investigation and its application in chemical industry. It contains a literal retrieval focused on basic principles of incident investigation and in practice section using one of the basic investigation techniques – Fault Tree Analysis. System evaluation of gelatination of nitrocellulose oriented to fire in object is the result of this work. “Minimal cut sets” (MCS) was obtained from the basic events probability of the constructed fault tree. Probability of incidents was then determined from MCS causes and corrective actions were recommended. In final part of this contribution, benefits and deficiencies of this systematic incident investigation was compared with traditional investigation with commission.

Keywords: *fault tree analysis, incident investigation, FTA accident analysis, incident investigation techniques*

1. INTRODUCTION

The systematic approach to evaluation of incidents is not often used in Czech Republic. Confidence to other types of incidents evaluation used by commission dominates in Czech Republic. Therefore the first section of this contribution is focused on investigation techniques, on investigation access and on positive and negative aspects of techniques. The second section is focused on practical use of accident investigation technique.

The contribution follows new and effective approach to finding causes of incidents and removing reasons of events. New investigation approach has several properties that are preferable in investigation process and during design of a technology. This approach identifies and decreases the hazard of incidents in the technology during its following operation.

Evaluation of new incident investigation approach in regard to investigation used up to now and evaluation of the positive and negative aspects of this investigation approach are the results of this contribution. The quality of the results given by used technique of accident investigation and the process of investigation were compared with the process of conventional investigation commission.

The most important benefit of systematic investigation approach compared with the “commission investigation” is that systematic approach takes into account and evaluates properties of the whole system and the complex incident evaluation is the result.

Systematic investigation approach of incident evaluation has its undisputed benefits and therefore is used for incident evaluation in European Union so it is important to explore this section of loss prevention in the process industries in Czech Republic too.

2. INVESTIGATION TECHNIQUES

2.1 Introduction

Incident investigation is important section of process safety management (PSM). Knowledge “what goes wrong” and “why goes something wrong” can avoid the repetition of events by changes in operation procedures, project facilities or operators training.

“Process safety management” represents the use of management systems for identification, understanding and control of the process hazards to prevent injuries and incidents. “Process safety” can be understood as dynamic system concerning technologies, materials, people and equipment. PSM program ensures that right constructed equipment is operated and maintained in safety state.

The term “incident” is defined as accident with real negative consequence and the term “accident” is generally defined as unplanned event with potential for undesirable consequences. Naturally, accidents also involve “near-miss” events, which can be understood as nearly accident.

2.2 Investigation techniques and approach

Three basic problems appear during systematic incident investigation: incident cause investigation, appropriate investigation technique selection and application of available technique for process safety incident investigation (PSII).

PSII can profit from systematic approach. Structured approach to PSII usually represents direct implementation of process safety management and ensures consistent and accurate investigation effort. There is not any technique applicable to any kind of incident, therefore incident investigator has to use assessments and make adaptations to enhance PSII and contribute to solution why and how accident occur.

Three approaches for incident investigation exist: type 1 is a traditional investigation based on informal control, type 2 based on committee, which use expert opinion for credible resolution and measures and type 3 is multiple-cause, system oriented incident investigation.

This contribution is focused on type 3 of investigation approach.

2.3 Cause theories of incidents

Classic accident theory is **Cause theory** ^[1], which significantly influences real PSII. Author of this method defined five dominating causes: origin and social background, error or people, hazardous activity, hazardous conditions and injury.

2.4 Human factor in incident cause

Permanent searching of basic causes in the background of the accident is basic rule of modern PSII. If for example human factor has been identified, the investigation process must continue in this error basic cause search. Human factor plays important role in incident causes and is the axiom of the systematic incident investigation. The term “human factor” describes individual elements of design, maintenance, operations and management. These factors can influence the ability of people to affect the environment safely.

Human factor is described by “Skills – Rules – Knowledge” model, which was developed as the frame for human factor classification. This model divides mental procedures into three levels of execution.

Conventional ability of observations, hand-eye coordination and skill control are on the lower level. Rules performed by routine way are on the second level. Finally, procedures based on knowledge as diagnostics, determination and planning are on the highest level.

2.5 Incident investigation techniques

Some analytical techniques for the incident investigation based on general anatomy of incident, incident theory, human factor theory and views from practice PSII have been certified and realized. All available techniques are used for three intentions: to collect accident information, to support description of incident cause and hypothesis development for further expert exploration and to support evaluation of corrective actions. Three analytical approaches of type 3 investigation exist: deductive, inductive and morphological.

Deductive approach includes consideration starting from general and going to characteristic. Deductive analysis tries to determine, which modes of system, equipments, operational and organizational modes have contribution to error. Incident investigation is typical application of deductive approach ^[2] and Fault Tree Analysis is basic example.

Inductive approach involves logic thought from individual cause to general conclusions. This approach determine, what error or initiation event occurred during system operation. HAZOP is typical example of inductive technique.

Morphological approach to analytical accident investigation is based on the study of existing system structure. Morphological approach is directly focused on potential hazardous equipments. This kind of investigation is controlled by the system design and by the operator's experiences with system management.

2.6 Review of techniques

2.6.1. Deductive techniques

Fault Tree Analysis (FTA), Management Oversight and Risk Tree (MORT), Causal Tree Method (CTM), Multiple-Cause, Systems-Oriented Incident Investigation Technique (MCSOII)

2.6.2. Inductive techniques

Accident Anatomy Method (AAM), Action Error Analysis (AEA), Cause-Effect Logic Diagram (CELD), Hazard and Operability Analysis (HAZOP)

2.6.3. Morphological techniques

Accident Evolution and Barrier (AEB), Work Safety Analysis (WSA)

2.6.4. Other non-systems oriented techniques

Change Evaluation/Analysis (CE/A), Human Performance Enhancement System (HPES), Multilinear Events Sequencing (MES), Human Reliability Analysis Event Tree Technique (HRA), Sequentially Timed Events Plot (STEP), Systematic Cause Analysis Technique (SCAT), Technique of Operation Review (TOR), TapRooT™ Incident Investigation System

3. FAULT TREE ANALYSIS

3.1 Introduction

Fault Tree Analysis (FTA) is deductive technique focused on specific incident or system failure and provides a method for identification of event cause. FTA is a graphical model that illustrates combinations of equipment failures and human errors that can result in the main failure of the system of interest, called top event [3, 4, 5, 6, 7, 8]. The strength of FTA as a qualitative tool is in its ability to identify the combinations of basic equipment failures and human errors, which can lead to accident. This allows the risk analyst to focus preventive or mitigative measures on significant basic causes to reduce the likelihood of accident.

The purpose of an FTA is to identify combinations of equipment failures and human errors that can result in accident. FTA is well suited for analyses of very large systems.

FTA produces system failure models, which uses Boolean logic gates (AND, OR ...) to describe how equipment failures and human errors can be combined to cause a main system failure. Lists of minimal cut sets can be qualitatively ranked by the number and type of failures (e.g. hardware, procedural ...) in each cut sets. Critical cut sets containing more failures are generally less probable than those containing fewer failures. Evaluation of lists of minimal cut sets reveals system design/operation weakness for which analyst may suggest possible safety improvement alternatives.

Using FTA requires a detailed understanding of how the plant or system operates, detailed process drawings and procedures, and knowledge of component failure modes and their effects. Time and cost requirements for an FTA depend on the complexity of the systems involved in the analysis and the level of resolution of the analysis. Modeling a single top event involving simple process by experienced team could require a day or less. Complex systems and large problems with many potential accident events could require many weeks or months, even with an experienced analysis team.

FTA is a deductive technique, which uses Boolean logic symbols to break down the causes of a top event into basic equipment failures and human errors. The analyst begins with an accident or undesirable event, which means that an immediate cause of the event is identified. Each of immediate causes (called fault events) is further examined in the same manner until the analyst identifies the basic causes of each fault event or reaches the boundary established for the analysis. The resulting fault tree model displays the logical relationships between the basic events and the selected top event.

A fault tree model can be used to generate a list of the failure combinations that can cause the top event. These lists are known as cut sets. A minimal cut set (MCS) is a smallest combination of component failures, which will cause the top event to occur [9, 10] if they all will occur or exist simultaneously.

The fault tree is a graphical representation of the relationships between failures and specific accidents. Some FTA symbols are shown in **Fig 1**.

Faults and failures described in a fault tree can be grouped into primary faults and failures (failure in environment for which operation of component was intended), secondary faults and failures (failure in environment, for which operation of component was not intended) and command faults and failures (operation of component is called a malfunction, because the component function was not desired).

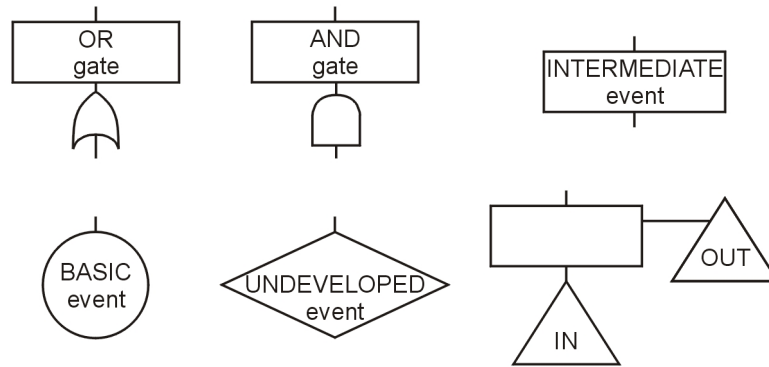


Fig 1. Some FTA symbols

There are many commercially available software programs specifically designed to perform Fault Tree Analysis studies, including **BRAVO**, **CAFTA+PC**, **CARA**, **FaultREASE**, **IRRAS-PC**, **NUSSAR-PC**, **RISKMAN**

3.2 Fault Tree Analysis procedure

There are four steps in analysis procedure: definition of the problem, construction of the fault tree, analysis of the fault tree model qualitatively and documentation of the results.

A top event and boundary conditions for the analysis must be selected to define the problem. These boundary conditions include physical bounds system, level of resolution, initial conditions, neglected events, real conditions and other assumptions.

Fault tree construction begins at the top event and proceeds, level by level, until all fault events have been traced to their basic contributing causes – basic events. The analyst begins with the top event and, for the next level, uses deductive reasoning of causes and effects to determine the immediate, necessary and sufficient error resulting in the top event.

The completed fault tree provides useful information by displaying how failures interact to result in an accident. Minimal cut sets are all combinations of failures, which can result in the fault tree top event and they are logical equivalent to the information displayed in the fault tree.

The fault tree solution method has four steps:

1. unique identification of all gates and basic events, if a basic event appears more than once in the fault tree, it must have the same identifier each time;
2. resolution of all gates into sets of basic events, resolution is displayed in a matrix format manually or with software aid, there are two rules for entering the remaining information into matrix – the OR-gate rule and the AND-gate rule;
3. removal of duplicate events;
4. identification and deletion of all supersets that appear in the other sets of basic events, which are contained in the list of basic events.

Once the list of minimal cut sets for a particular top event is found, the analyst can evaluate the constituent failures to determine the “weak links” in the system. Using the results of this qualitative analysis, fault tree analysts can propose suggestions for improving the safety of the system being studied.

The final step in performing a fault tree analysis is to document the results of the study. This should provide a description of the analyzed system, a discussion of the problem definition, a list of assumptions, fault tree models that were developed, lists of minimal cut sets and evaluation of the significance of the minimal cut sets. In addition, any recommendations that arise from the FTA can be mentioned.

The ranked list of minimal cut sets for a system, based on the top event and the analyzed condition, is the ultimate product of qualitative fault tree analysis. The fault tree model is often used as an effective communication tool with both technical and non-technical decision makers. Based on the numbers and types of failures in the minimal cut sets, the team may recommend improvements that will make the top event less probable.

4. FTA ACCIDENT ANALYSIS

4.1 Introduction

Above described FTA method was used in practical analysis of fire in building B46 (Synthesia a.s. Semtín) for nitrocellulose gelatination ^[11].

Fire probability in every section of the object was generated by fault tree of the whole object and then compared with reality. Then relevant sections of fault tree was used for investigation of the accident in object B 46. All available descriptions of system before and after accident were used.

4.2 Description of object B 46

Object B 46 is bricked, small building with light wooden pressure-relief roof. There are 8 rooms for mixers in whole building, valve chamber and 2 engine rooms. Individual rooms are separated by firewalls. The front pressure-relief wall of the rooms is made by wood. There are 6 mixers installed in rooms No. 1 - 6, rooms No. 7 and 8 are utilized as chambers for fitting workable waste. Non-sparking asphalt floors are in the rooms, xylolite is used for the floor in the valve chamber. Filled ether graduators and equipment for valve ether injection are situated in the valve chamber.

Installed mixers (No. 1 – 6) are powered from separate engine room by transmission and power belts. Mixer is steel-iron tub with capacity of 450 liters and it is equipped with cooling. Two horizontal blenders with double speeds are situated in the mixer tub. The tub is cover by aluminium cover, which is hanged on balance weight. Rubber seal is placed on the contact surface of the cover. Outlet spray cross is mounted at the bottom side of the cover. The cross is connected to ether graduator-tube by rubber hose.

Mixers rooms are connected to central exhaust adsorption system, which is placed in object B 56. This system is controlled by fire detectors above every mixer, which switch off the adsorption system after detection of the fire. A pan in the floor for power belt (permanently) and whole room under the front side of mixer in every room are aspirated.

Electric illumination of the rooms is in non-explosive configuration. Water deluge extinguishers (manually controlled from outdoor) lead into every room. Every mixer is equipped with temperature measuring system. Ether flows to mixer from graduator. Ethanol is dosed into mixer manually from ethanol tank.

4.3 Incident description

The incident in object B 46 (nitrocellulose gelatination) occurred, when the first operator carried away two transport vessels to mixer No. 4. At the same time the works foreman activated ether inlet to mixer and consequently the last operator activated stirring of the mixer. Content of the mixer exploded and burned shortly after the mixer was activated. The water deluge system for mixers no. 4, 5 and 6 was not activated due to licking flames. Central fan of the absorption system was disconnected after the fire rise.

4.4 Object and equipments description after incident

Following state in the mixer room No.5 was found:

The mixer was not visible damaged; the aluminium cover lied on mixer. Aluminium cover was shifted approximately 10 cm to the left. The cover was slightly crushed, but aluminium was not melted. The hanger of the cover was functioned, the mixer content, except small rest, was burned up. The rubber hoses for ether and cooling water inlet was burned up. The power belts burned up and the exhaust absorption system was in partially open position. Aspiration tube from the pan in the floor was partly damaged; the valve of tube was opened. Situation in the room of mixer No. 5 after the fire is shown in **Fig 2**.

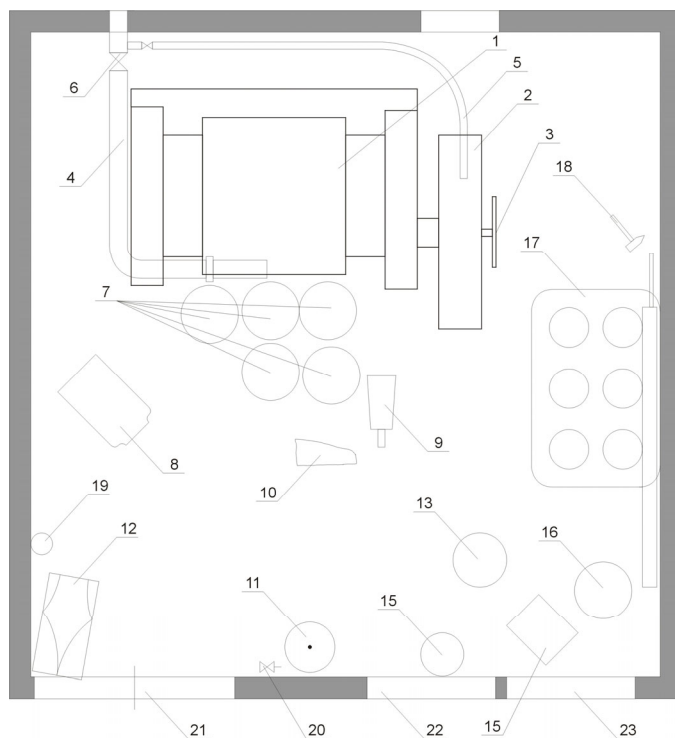


Fig 2. Situation in the room of mixer no.5 after the fire

- 1 – tub of mixer, 2 – cover of power belt, 3 – operating wheel transmission clutch of blenders,
- 4 – aspiration tube from the room, 5 – aspiration tube from a pan in the floor,
- 6 – triple-pole gate of aspiration tube, 7 – transporting containers (5 pieces) prepared for collecting,
- 8 – laying transport container from position 7, – paddle, 10 – the rest of rubber-textile bag,
- 11 – primary place of transport container with wetted ingredients,
- 12 – place of transport container after incident (primary place 11),
- 13 – cover of the transport container after accident (primary place 11),
- 14 – a part of horny content of transport container (primary place 11),
- 15 – bigger part of horny content of transport container, 16 – the rest of transport container,
- 17 – the plate for picking up, 18 – bronze hammer, 19 – balance weight cover of mixer protector,
- 20 – water supply valve, 21 – handling (double) door, 22 – window, 23 – emergency door

4.5 State of the technologic equipments after control

The mixer with equipment was not visually damaged. The indoor walls of mixer was covered by the layer of ash, this layer was moped from the front blender; this track corresponded with the operation of the blender. The distance between the mixer wall and the blender was 15 mm and the distance between the blender and the bottom of the mixer was 10 mm. These distances corresponded with prescribed distances.

The electric grounding of aluminium cover was not found during the inspection of the mixer and even the rest of the grounding was not found. The socket of the blenders and the felt packing on the blenders was all right. The gearbox of the blenders was not damaged. The inlet tube and the aspiration tube had no defect. Any strange element with ability to produce the spark was not found in the tub of the mixer and in the rest of the nitrocellulose.

4.6 Definition of the problem for Fault Tree Analysis

- top event – fire in object B 46 during normal operation
- undeveloped events – wiring failure
- material boundaries – according to definition of the system
- configuration of system – normal operation of mixers with nitrocellulose and solvents
- level of resolution – according to definition of the system
- other assumptions – the sabotage is not included in the analysis

4.7 Fault tree

The fault tree model was based on the available data about incident. Specific conditions of presented system, its shape and configuration, used chemicals and human factor impact was used during the fault tree model development. The top of developed fault tree is displayed in Fig. 3.

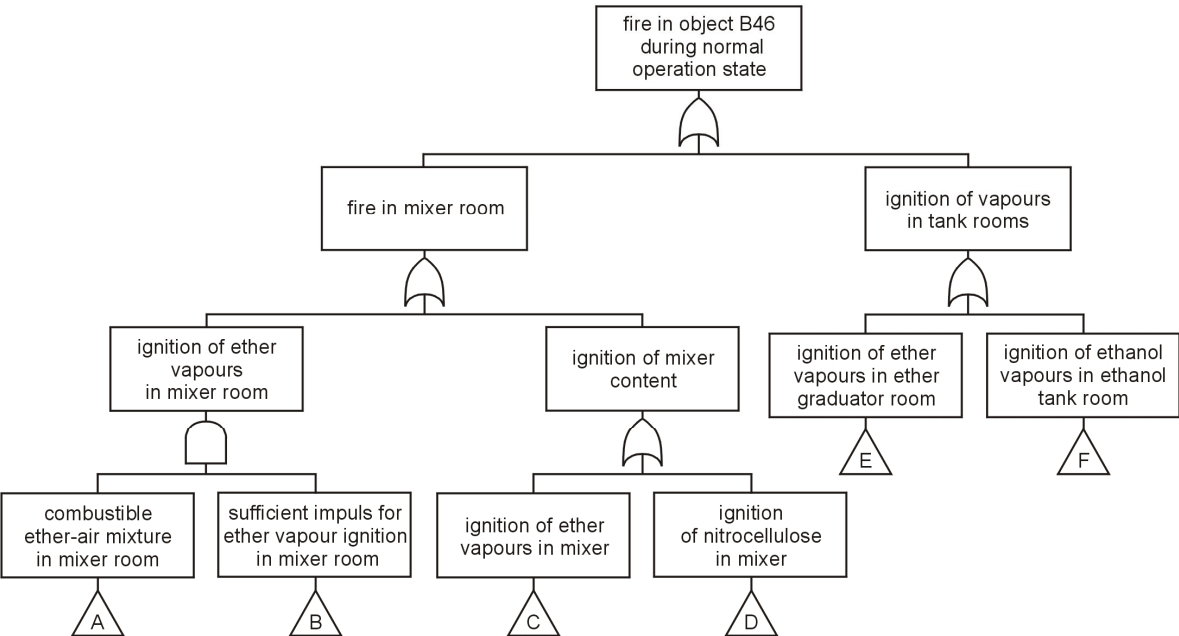


Fig 3. Top tree of analyzed accident

4.8 Events probabilities of A - F transfers

The developed fault tree model with values of individual events probabilities is solved by software FaulTrEASE™ (loaned, version 2.1a by Arthur D. Little) which provides the probabilities of particular sub-trees (**Table 1.**). Probabilities lower than 1.10^{-8} are considered as negligible in the practice, therefore events “ignition of the ether vapours” and “ignition of vapours in the tanks rooms” was not take account in the following incident evaluation.

The ignition of mixer content is the most often cause of fire in object B 46 and its probability is $3,1.10^{-5}$. The frequency “one incident per 3,3 years” is the result from estimated production cycle frequency (10.000/year). As a matter of fact, there were 10 fires during 45 years (1 accident in 4,5 year) in the nitrocellulose gelatination building B 46. This frequency is in good accordance with the frequency obtained from the fault tree with regard to the size of the statistical set of incidents and to estimation of the basic events. This means that probability of the “ignition of the mixer content” corresponds to reality.

Table 1. *Sub-trees probabilities*

	event	transfer	probability
1	ignition of ether vapors in mixer room	A + B	$5,04.10^{-9}$
2	ignition of the mixer content	C + D	$3,14.10^{-5}$
3	ignition of ether vapours in ether graduator room	E	$7,96.10^{-14}$
4	ignition of ethanol vapours in tank room	F	$1,86.10^{-13}$

4.9 Ignition of the mixer content event

Table 2. *MCS with high probability:*

mcs	identific.	basic event	general probability	incident probability
1	33	the mixer filled with the nitrocellulose and ether	0,889	1,000
	40	damaged electric grounding of the cover	$2,000.10^{-5}$	0,900
	41	induction of the static electricity on the cover by outlet of the ether at the filling of the mixer through the outlet spray cross	1,000	1,000
	26	present of the conductive element with ability to discharge of the static electricity	0,833	0,900
	mcs =		$1,482.10^{-5}$	0,810
2	34	insufficiently wet load of the nitrocellulose in the mixer (or section of load)	$1,000.10^{-3}$	0,200
	39	local overheat of nitrocellulose load at pre-crunch	0,010	0,750
	mcs =		$1,000.10^{-5}$	0,150

4.10 Recommendations

Following recommendations can be deduce from minimal cut sets of sub-tree “ignition of mixer content”:

- use conducting rubber in whole object (cover seal of mixer, inlet hoses);
- consequent use of proper operators clothes, clothes which does not induce static electricity;
- use of conducting shoes on conducting floor, provide a replacement for the non-conducting floor with conducting floor;
- consequent grounding of all metal elements in room and its consequent naked wires connection; ensure the resistant grounding of the aluminium cover of the mixer;
- consequent control the content of ethanol in nitrocellulose load; consequent weighing of filled transportation cart and estimation of ethanol content in the “cakes”.

5. CONCLUSIONS

Fault tree and his minimal cut sets were obtained from application of the Fault Tree Analysis to “fire in object B 46” incident. All minimal cut sets of sub-trees “ignition of ether vapours in mixer room” and “ignition of ether/ethanol vapours in tank room” are not very probable therefore the solution of fault tree model was mainly focused on cut sets of sub-tree “ignition of mixer content”.

Most probable cause of a “fire in object B 46” incident is ignition of mixer content. Event frequency of this sub-tree is one incident per 3,3 year. This frequency is in good accordance with real frequency of incidents – 1 incident in 4,5 year. Hence, this section of fault tree model corresponds with reality.

This fault tree analysis indicates that incident cause “static electricity induction in the cover of mixer” is highly probable. The spark was generated after grounding of accumulated static electricity. Than, flammable ether-air mixture in the mixer was ignited by the spark. Ignition of the insufficiently wet nitrocellulose during grinding in the mixer by local overheating is the second possible cause of incident (with lower probability).

“Static electricity induction” was also the conclusion of the classic incident investigation method, but the second possible cause of incident was not considered by commission. This is main lack of commissioning investigation. Commissioning investigation is mainly focused on quick identification of possible cause, but does not evaluate a whole system.

Results of this contribution show that if fault tree model already exists than Fault Tree Analysis is quick technique for incident investigation. FTA application to the system and basic events probability evaluation identify weak sections of the system. Further improvement of the system should be focused on these weak sections. Incident cause can be quickly displayed by systematic evaluation of basic events probabilities.

Probability evaluation of the resulting minimal cut sets is the important benefit of FTA in comparison to classic incident investigation. Probability evaluation accelerates corrective actions of often recurring events. Analyst has to take into account whole system therefore long time is necessary for fault tree model development and that is the handicap of FTA.

This contribution represents the first step in the accident investigation area. This work continues at Department of Theory and Technology of Explosives and other incident investigation method will be applied. Applied methods will be compared and some complex system of accident investigation will be outlined.

REFERENCES

- [1] HEINRICH, H.W.: 1936. *Industrial Accident Prevention*, New York: McGraw–Hill.
- [2] ROBERTS, N.H. ET AL.: 1981. *Fault Tree Handbook*. NUREG–0492. Washington, DC: U.S. Nuclear Regulatory Commission
- [3] *Guidelines for Chemical Process Quantitative Risk Analysis*, Center for Chemical Process Safety, AIChE, New York, 1989
- [4] H.R. GREENBERG AND J.J. KRAMER, EDS.: *Risk Assessment and Risk Management for the Chemical Process Safety Industry* (ISBN 0–422–23438–4), Van Nostrand Reinhold, New York, 1991
- [5] J. STEPHENSON: *System Safety 2000 – A Practical Guide for Planning, Managing, and Conducting System Safety Programs* (ISBN 0–0442–234840–1), Van Nostrand Reinhold, New York, 1991
- [6] L. THEODORE ET. AL.: *Accident and Emergency Management* (ISBN 0–471–61911–6), John Wiley & Sons, Inc., New York, 1989
- [7] F.P. LEES:, *Loss Prevention in the Process Industries*, Vols 1 and 2, Butterworth's, London, 1980
- [8] A.E. GREEN ET. AL.: *High Risk Safety Technology* (ISBN 0–471–10153–2), John Wiley & Sons, Ltd., New York
- [9] J.B. FUSSEL: „*Fault Tree Analysis: Concepts and Techniques*,“ *Generic Techniques in Systems Reliability Assessment*, NATO Advanced Studies Institute, 1976
- [10] W.E. VESELY ET AL.: *Fault Tree Handbook*, NUREG–0492, U.S. Nuclear Regulatory Commission, Washington, DC, 1981
- [11] *Zpráva o vzniku éterových par s následným požárem v objektu B 46*, Východočeské chemické závody Synthsia n.p., Pardubice – Semtín, čj. 309/1300/213

INTERNAL BALLISTIC ANALYSIS OF THE 20 × 102 CARTRIDGE

K. Leinweber and J. Petržílek

Explosia a.s., 532 17, Pardubice - Semtín, CZ

Abstract

Results obtained by two different methods of pressure measurement are discussed. Maximum pressures were measured simultaneously in the cartridge of medium calibre weapon 20 x 102 mm by copper crusher and piezo transducer. Results obtained by different methods were correlated and influence of testing temperature was discussed.

Keywords: crusher, pressure, ammunition

1. INTRODUCTION

Measurement of pressures in weapon chamber during the process of shooting can be achieved by two methods. First of them is the measurement by copper pressure. Pressure of gases inside the cartridge during the shot makes change of the length of copper cylinder (crusher) and such change of dimension is proportional to the maximal pressure inside the cartridge. It means that the result of such measurement is single value which is related to the maximal pressure, but we can not obtain any information about pressure changes during the time. The other method of pressure measurement uses piezo transducer that is connected with ballistic analyser and the result is complete record of pressure built up during the shot. Not only maximum pressure is obtained, but also many other useful information related to the process of propellant burning and projectile movement.

At present time, method of crusher measurement is required in the case of 20x102 mm weapon according to the current specification, but both methods are applied during ballistic testing at the ballistic laboratory of Explosia a.s. Thus, it is possible to perform evaluation between both methods using results obtained during last several years of testing.

2. EXPERIMENTAL

2.1 Cartridge setup

Cartridges consisted of bras case of initial volume circa $W_0=41\text{cm}^3$ primed by electric primer, dummy projectile of weight $q=100\text{ g}$. Smokeless spherical propellant was used as the propelling charge. Ammunition parts of various producers and lots were used.

2.2 Preparation of cartridges before testing

Notch was cut to the rim of the bottom of the case to ensure correct side orientation in the chamber. Two openings were drilled to the case for pressure measurement by both piezo and crusher methods. Both openings were blinded by sticky tape. Prepared cartridges are presented on Figure 1. There is the measuring system chart on the Figure 2.



Fig 1. Types of setups of tested cartridges 20x102 with openings

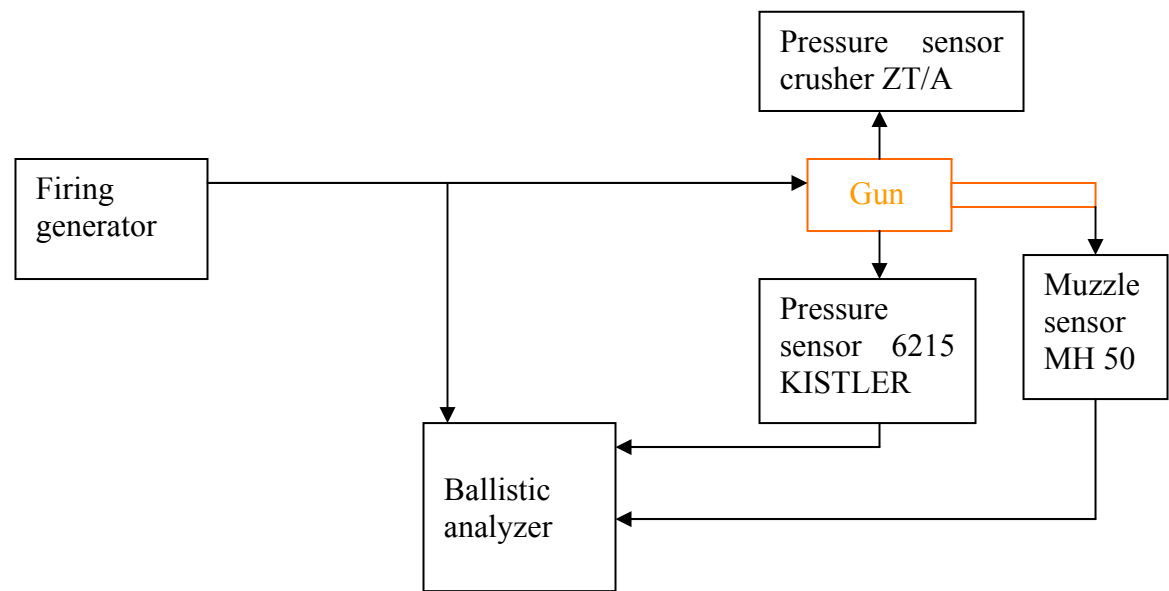


Fig 2. Measuring system chart

2.3 Ballistic testing

Ballistic tests were performed according to the method TP VD-239 57 III using fixed pressure barrel 20x102 mm. The weapon consisted of pressure barrel, receiver. The barrel was equipped by piezo transducer Kistler and pressure measurement ZT/A with copper cylinder. The beginning of the shot was established by the signal from the electrical source of ignition, the end of the shot (time when the projectile leaves the barrel) was established by the signal of transducer MH 50 fitted on the muzzle. Copper crushers were pre-pressed according to the tables by pressures 10 to 30 Kp/cm² lower then measured peak pressures. The setup of pressure transducer and the cartridge are presented on the Figure 3. Signals obtained from transducers were recorded and evaluated by a ballistic analyser (graphical output from the ballistic analyser is presented on the Figure 4), copper crusher was measured by micrometer and consequently, the value of peak pressure was found in the table.

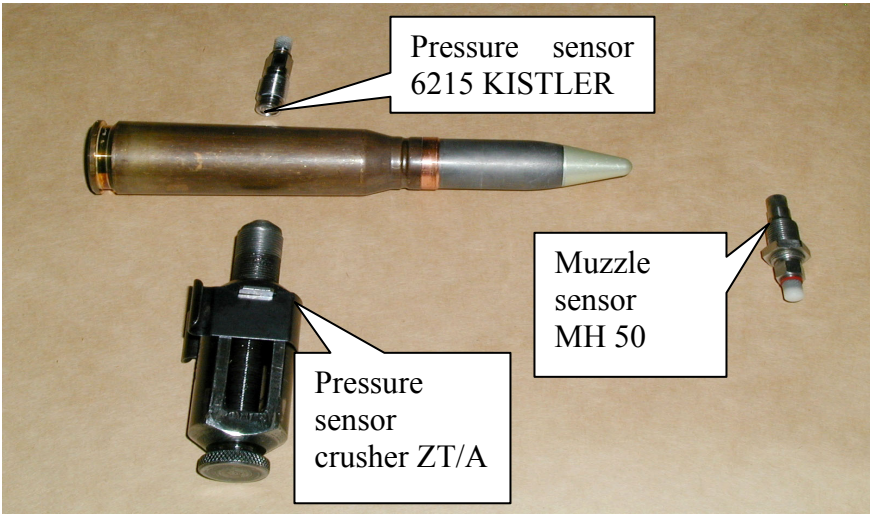


Fig 3. Setup of transducers at shooting

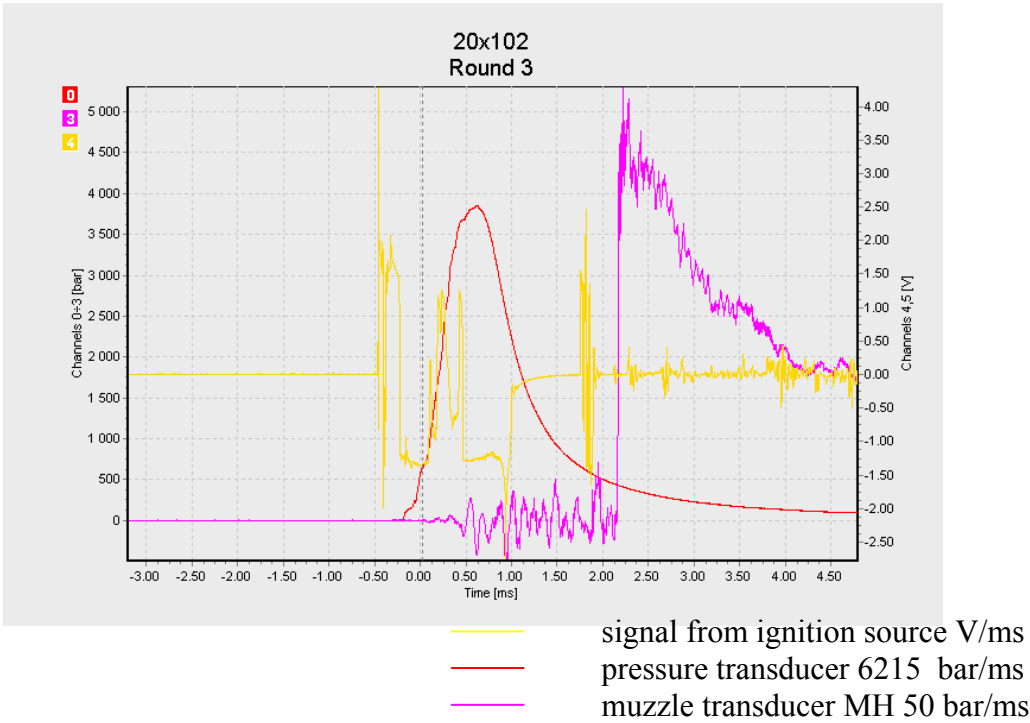


Fig 4. Graphical output from the charge analyser NWM 86E 511-003

3. RESULTS AND DISCUSSION

There was 800 rounds taken into evaluation of correlation between peak pressures obtained by both methods. The piezo peak pressures ranged from 3189 Bar to 5788 Bar. Correlation between results of both measurements is presented graphically at Figure 5. It is clear that there is the linear correlation between both variables, thus the linear regression was applied to the data and peak pressures obtained from piezo curves were explained by results evaluated from copper crusher method. Considering the fact, that the zero pressure should lead to zero pressures measured by both methods, only the linear model without intercept was taken into account in form:

$$P_{\text{piezo}} = a \cdot P_{\text{crusher}},$$

where $P_{crusher}$ and P_{piezo} are the results of peak pressures measured by both methods and parameter a is the slope of the linear dependency. Estimate of the parameter a was established by means of least squares method using the S-PLUS 6.0 statistical pocket. Results of the regression are presented in the Table I. Residual standard deviation is 143 Bar gives us estimation of average precision of model. From the value of the slope, which is 1.1660 ± 0.0015 gives us the estimate of the ratio of $P_{piezo}/P_{crusher}$. From the analysis of residuals (computed as absolute value of the difference P_{piezo} measured – P_{piezo} calculated from regression equation) it was found that residuals follow the normal distribution and 50 % of residuals is less than 94 Bar and maximal residuum was 513 Bar.

The next step of the evaluation was aimed to the question weather there are differences between regression parameters calculated for results obtained at different shooting temperatures. Correlation at different temperatures are plotted at Figure 6 and results of regressions are presented in Table I. There were found small, but statistically significant differences between parameters estimated for different shooting temperatures.

From given results it is clear that there is close linear correlation between results of peak pressures measured by both methods. It is possible to make estimation of pressure measured from the other type with relatively high precision, but still there are some cases where the estimation leads to high differences. Such cases will be studied in near future by more extensive data analysis. As the other explanatory variables could be used parameters computed from the pressure curve (as are slopes of pressure built up, times from ignition to pear pressure and so on). As supportive information about the relevance of pressure measured by different methods could be considered measured velocity of projectile.

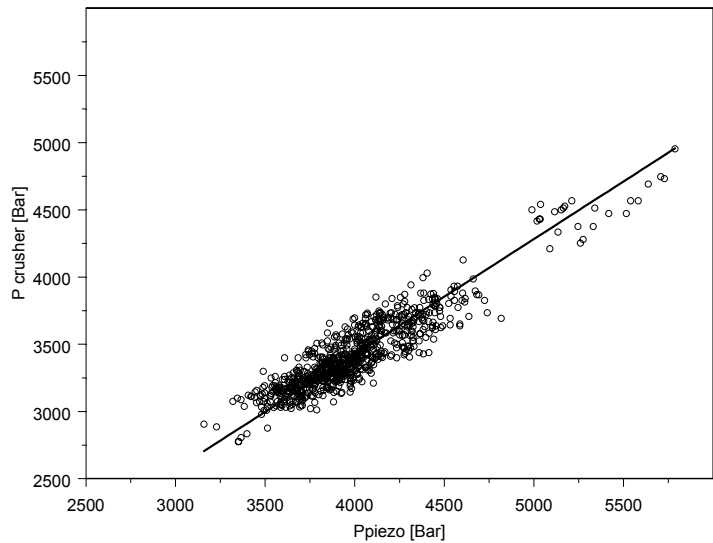


Fig 5. Correlation between peak pressures obtained by piezo and crusher method simultaneously; the line was calculated by linear regression without intercept

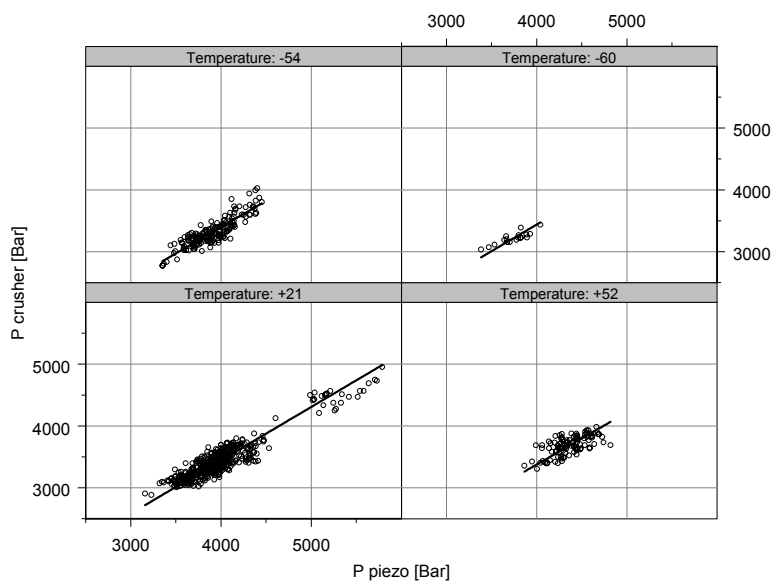


Fig 6. Correlations between peak pressures obtained by piezo and crusher method simultaneously – tests performed at various testing temperatures; the line was calculated by linear regression without intercept

Table 1. *Results of linear regressions*

	N	Slope	Residual standard deviation	Degrees of freedom	Correlation coefficient of linear regression
All	800	1.1660 ± 0.0015	143	799	0.9993
-60 °C	18	1.1620 ± 0.0064	87	17	0.9997
-54 °C	171	1.1756 ± 0.0030	158	170	0.9994
+21 °C	509	1.1593 ± 0.0018	139	508	0.9994
+52 °C	102	1.1827 ± 0.0042	158	101	0.9993

REFERENCES

- [1] ČSN 39 51 05 Testing ammunition
- [2] TP VD-239 57 III.: Procedure ballistic examinations

UNSATURATED POLYESTER INHIBITION SYSTEM FOR DOUBLE BASE PROPELLANTS

M. Lipiński, K. Lipińska, B. Florczak and W. Witkowski

Institute of Industrial Organic Chemistry,
6 Annopol St., 03-236 Warszawa, Poland

Abstract:

Inhibitors are applied to those surfaces of the propellant grain where burning is to be prevented. We investigated inhibition system for double base propellants based on unsaturated polyesters resins. Measurements of the amount of nitroglycerine that migrates into the chosen inhibitors were done using a "sandwich" test. Double base propellant grains were inhibited by a casting technique and statically fired in rocket motor. The nature of P-t profiles suggested that it is potential inhibition system for double base propellants.

Keywords: *double base propellants, inhibitor, nitroglycerine migration*

1. INTRODUCTION

Various methods of coating of propellant grain surface are used in order to prevent surface burning or contact of the grain with its container. Inhibitors are applied to those surfaces of the grain where burning is to be prevented. They consist of plastic materials, which are sometimes charged with inert refractory filler and burn very slowly if at all. Some of the vital requirements of the inhibitor are its chemical compatibility with the propellant, acceptable mechanical properties, low shrinkage and good bonding with the propellant during storage. The major ingredients of double base propellants are nitrocellulose and nitroglycerine. In the case of these propellants the main problem with the choice of inhibitor is the presence of nitroglycerine and its subsequent migration towards inhibitors. This may cause the polymeric material to degrade and delaminate with time. That affects the service life of a solid propellant rocket motor.

At first, cellulose acetate and ethyl cellulose were tried as inhibitors for double base propellants. Nevertheless, cellulose acetate absorbed high amount of nitroglycerine and was stripped off from the propellant surface. Ethyl cellulose has a poor softening point. This led to the search for new types of polymeric materials for their use as inhibitors. A number of polymers have been reported as inhibitors for double base propellants. They include epoxy resins, polyurethanes, silicones, polyester resins and chloropolyesters. It is reported in the literature that unsaturated polyester resins may be used as inhibitors for double base propellants. These resins have a very good strength with double base propellants. The inhibition system based on unsaturated polyesters resins was investigated. We used commercial unsaturated resins and their copolymers with n-butyl methacrylate.

2. EXPERIMENTAL

2.1 Materials

The materials used for its study were as follows.

- Polimal 1602 APyS unsaturated polyester resin (orthoptalic) with reduced styrene emission, containing fillers, having a viscosity at 25°C of 220-280 mPa·s and gel time at 25°C of 15-25 min, was supplied by chemical plant “Organika Sarzyna” (Poland)
- Polimal 1053 AWTP unsaturated polyester resin with reduced styrene emission, having a viscosity at 25°C of 250-350 mPa·s and gel time at 25°C of 15-25 min, was supplied by chemical plant “Organika Sarzyna” (Poland)
- N-butyl methacrylate, purity about 99%, having a density at 20°C of 0,895 g/cm³, boiling point 163°C and solidification point -75°C was supplied by Elf Atochem.
- Luperox GZS , containing methyl ethyl ketone peroxide, which was used for curing, was supplied by Elf Atochem.
- Double base propellants containing 37% of nitroglycerine without any other plasticizers was used for inhibition.

2.2 Method of preparation of specimens

The commercial polyesters were crosslinked alone and as blends with n-butyl methacrylate. All ingredients, as given in Table 1, were mixed by stirring and different test specimens were cast in corresponding molds. The composition was poured under a vacuum to remove any entrapped air. The cured specimens were used for nitroglycerine absorption test.

Table 1. *Compositions of unsaturated resin formulations*

Formulation	Polimal 1602 APyS	Polimal 1053 AWTP	n-butyl methacrylate	Luperox GZS
A	98	-	-	2
B	78	-	20	2
C	-	98	-	2
D	-	73	25	2
E	-	65	33	2

2.3 Nitroglycerine absorption test

The measurements of nitroglycerine sorption can be achieved by liquid absorption methods. That method consists in immersion of polymeric material in liquid nitroglycerine. Then the increase of the material mass with time is measured. The other method, called “sandwich” method consists in preparing a polymeric material block between two propellant blocks – they form a kind of “sandwich”. The prepared set is then stored at elevated temperature and the mass increase of polymeric material is recorded. The described experiments were conducted by “sandwich” method.

The “sandwich” consisted of a propellant block (40 mm × 40 mm × 5 mm), a polymer block (40 mm × 40 mm × 3 mm) and a propellant block. The nitroglycerine migration values were determined by measuring the mass increase of the polymer with time. The test was done at 70°C.

2.4 Inhibition of double base propellants

Inhibition of double base propellant grains was carried out by the casting method in inhibition mold. We used small grain having diameter of 20 mm and their length was 90 mm. The polymeric composition was also poured under a vacuum to remove any entrapped air. The inhibited grains were extracted from the mold after 24 hours. Then the grains were X-rayed to ensure proper bonding between propellant and the inhibitor. The propellant grains were loaded into rocket motors and fired statically, after conditioning at low (−40°C) and hot temperatures (+50°C) following the standard procedure, recording pressure-time profiles.

3. RESULTS

3.1 Nitroglycerine migration towards inhibitor

The results of nitroglycerine absorption tests are presented in Fig. 1 and 2. The points are the average values for triplicate analysis.

Margolin’s formula was used for determining the constant a and constant b .

$$M(t) = \frac{t}{a + bt} + c$$

where:

$M(t)$ (%) of nitroglycerine absorbed at given time, t time in seconds, c (%) plasticizer originally in polymeric material (in that case $c = 0$)

The amount of nitroglycerine absorbed in time infinity can be determined from the following equation.

$$M(\infty) = \frac{1}{b}$$

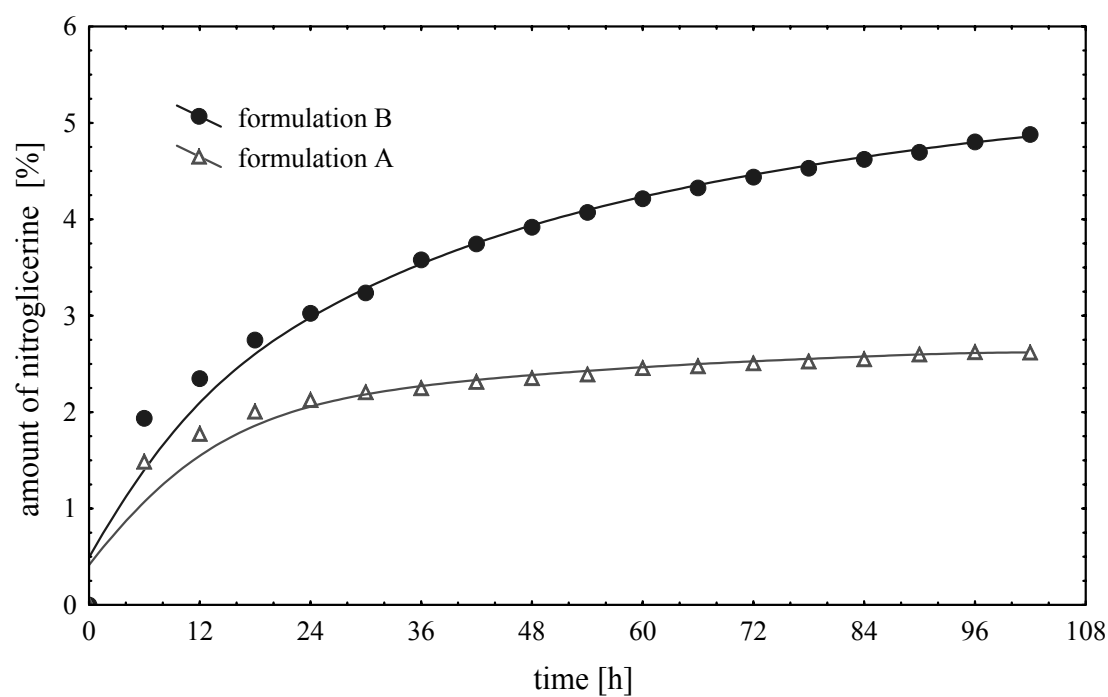


Fig 1. Nitroglycerine migration for A and B formulations

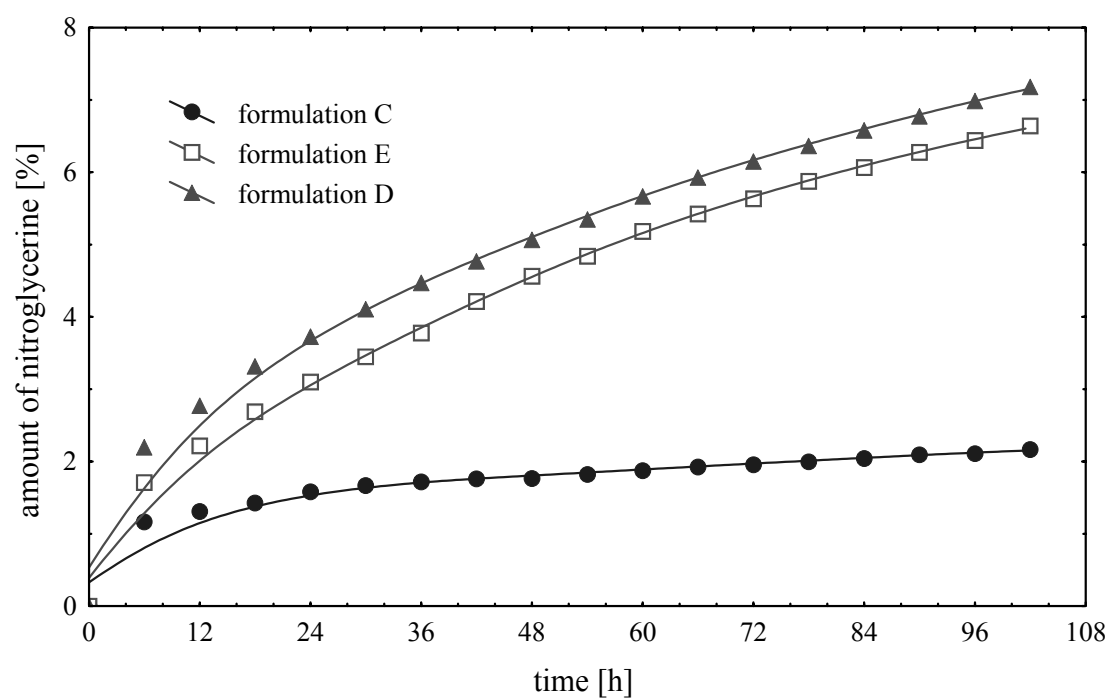


Fig 2. Nitroglycerine migration for C, D and E formulations

The obtained values for a, b and $M(\infty)$ are presented in Table 2. We also determined the amount of nitroglycerine absorbed after storing the specimens at room temperature during three year period (Mc)

Table 2. *Values for sorption curves according to Margolins formula*

Formulation	Constant b	Constant a	$M(\infty)$	Mc
A	0.37	2.20	2.71	2,71
B	0.15	4.31	6.72	5,29
C	0.46	3.63	2.18	2,29
D	0.10	5.22	9.64	8,04
E	0.11	3.73	9.13	9,68

The results of nitroglycerine migration show good compatibility between the values obtained from Margolin’s formula and the values that were experimentally determined. The highest nitroglycerine migration towards inhibitor was observed in the case of formulation E, containing the highest amount of n-butyl methacrylate. Low migration values obtained for formulation A and B results from the fact that there were fillers in these formulations. The nitroglycerine absorption decreases with the increase of filler in unsaturated polyester systems.

3.2 Inhibited grain test

The propellant grains inhibited with formulation D were statically fired in a rocket motor. The P-t profiles are shown in Fig 3 and Fig 4. The static evaluation gave a proper pressure-time curves with the desired performance both at hot and cold temperatures. The pressure-time profiles were satisfactory, flat and neutral, with the small grains having a burning time 12-14 s.

4. CONCLUSIONS

Unsaturated polyester resin systems can be applied as inhibitors for double base propellants. The casting method of propellant grain inhibition seems to the best choice in the case of small grains.

Margolin’s formula can be applied to tested unsaturated polyesters and calculated values of the amount of the nitroglycerine absorbed at time infinity are in agreement with the values experimentally determined after three-year storage.

The nature of P-t profiles suggested that it is potential inhibition system for double base propellants. However, the other mechanical and physical tests should be considered in order to provide a complete picture.

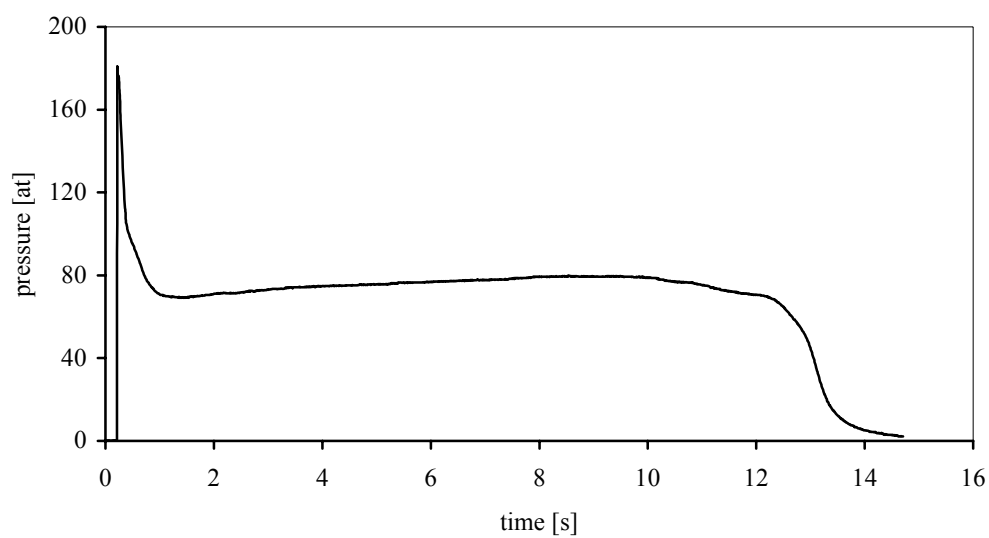


Fig 3. Pressure-time profile at hot (+50°C) temperature

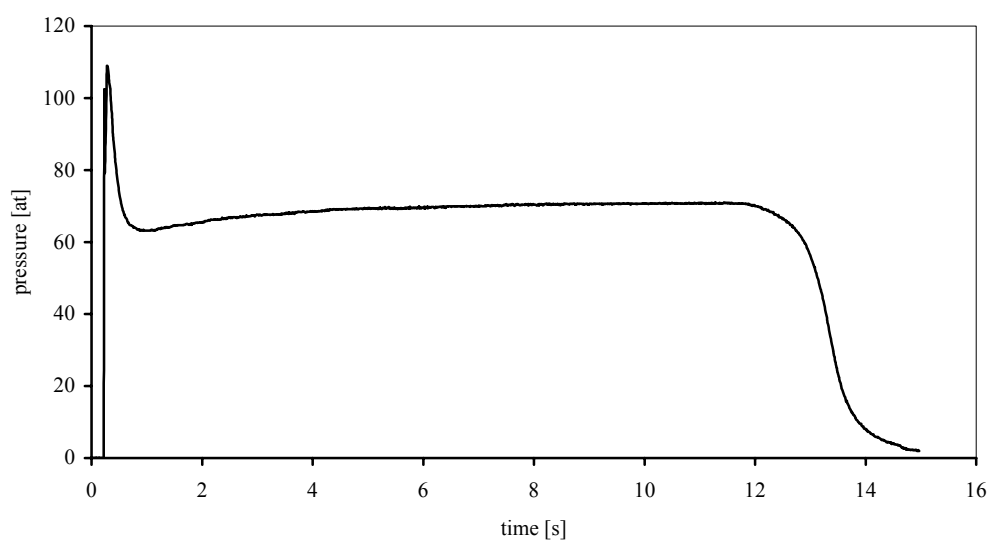


Fig 4. Pressure-time profile at cold (-40°C) temperature

REFERENCES

- [1] J. P. AGRAWAL, Y. KHARE: *Novolac Epoxy Resin – Hydroksy Terminated Adipate Based Inhibition System for Double – Base Propellants*, New Polymeric Materials, **No 3**, p. 167-176, 1994
- [2] J. P. AGRAWAL, K. S. KULKARNI, D. V. WAST, M. P. CHOUK, M. M. MARATHE: *Tereunsaturated Polyesters*, Journal of Materials Science, **No 27**, p. 4577-4581, 1992
- [3] J. P. AGRAWAL, M. P. CHOUK, R. S. SATPUTE, V. C. BHALE: *A Comparative Account of Properties of Novel Unsaturated Polyesters Synthesized by Different Polyestryfication Processes*, Journal of Polymer Science. Part A: Polymer Chemistry, **No 27**, p. 409-421, 1989
- [4] D. C. GUPTA, P. K. DIVEKAR, V. K. PHADKE: *HTPB – Based Polyuretaners for Inhibition of Composite – Modified Double – Base (CMDDB) Propellants*, Journal of Applied Polymer Science, **No 65(2)**, p. 355-363, 1997
- [5] J. P. AGRAWAL, S. VENUGOPALAN, JAVED ATHAR, J. V. SABANE, M. MURALIOLHARAN: *Polisiloksane – Based Inhibition System for Double – Base Rocket Propellants*, Journal of Applied Polymer Science, **No 1**, p. 7-12, 1998
- [6] J. P. AGRAWAL, N. T. AGAWANE, R. P. DIWAKAR, R. CHANDRA: *Nitroglycerine Migration to Various Unsaturated Polyesters and Chloropolyesters Used for Inhibition of Rocket Propellants*, Propellants Explosives Pyrotechnics, **No 24**, 24, 371-378, 1999
- [7] H. F. POTGIETER, R. D. SANDERSON: *NG-Migration into Double Base Propellants*, Journal of Applied Polimer Science, **No 50(10)**, p.. 1761-1772, 1993

SYNTHESIS OF DI(1H-TETRAZOLE-5-YL)AMINE (BTA)

P. Mareček*, K. Dudek* and F. Liška**

* Explosia a.s. Research Institute of Industrial Chemistry (VÚPCH),
CZ-532 17, Pardubice-Semín, Czech Republic

** Institute of Chemical Technology, Faculty of Chemical Technology,
Department of Organic Chemistry, CZ-166 28 Prague, Czech Republic

Abstract:

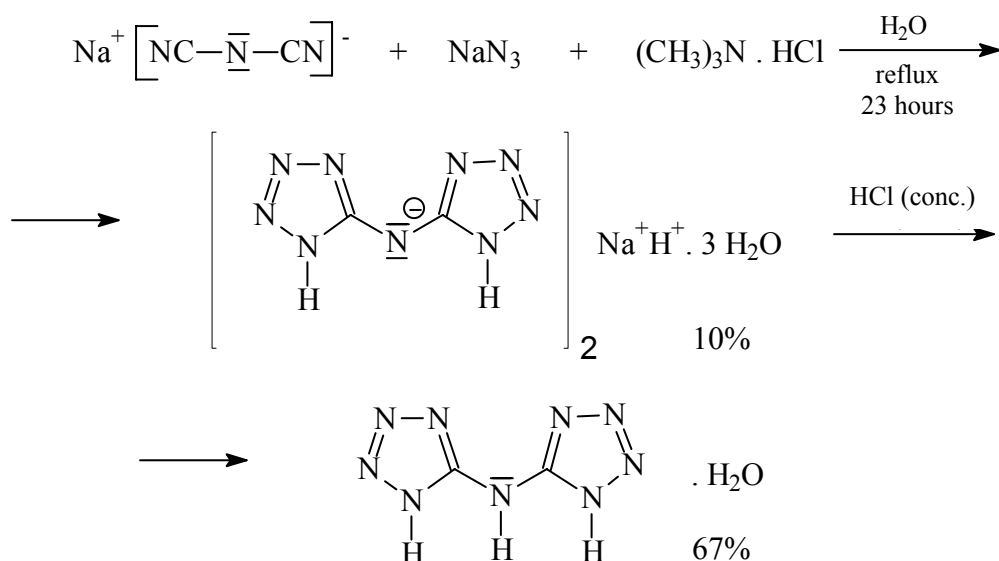
New method of synthesis of di(1H-tetrazole-5-yl)amine is described in the paper. Di(1H-tetrazole-5-yl)amine was synthesized by reaction of sodium azide with sodium dicyanamide in water under presence of zinc chloride as catalyst. This new method eliminates disadvantages of other alternative methods, such as for example: work with expensive and toxic metals, work with excess of volatile and toxic azoimide or work with organic solvents. This synthesis is very simple, safe and provides a good yield.

Keywords: high-nitrogen compound, BTA, 1H-tetrazole

1. INTRODUCTION

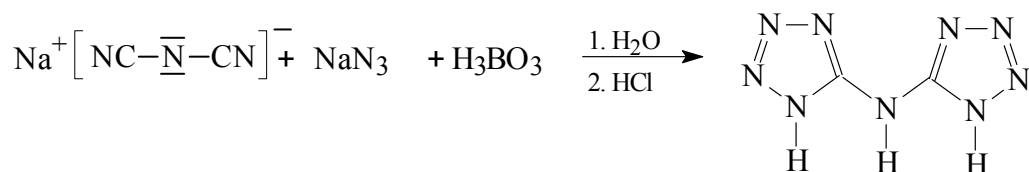
Di(1H-tetrazole-5-yl)amine is high-nitrogen compound, which can be used as component of explosives and gas generators.

Synthesis of di(1H-tetrazole-5-yl)amine consists of addition of azoimide to nitrile group in dicyanamide. The reaction was first described by Norris and Henry ^[1]. Sodium dicyanamide reacts with sodium azide under presence of tetramethyl-ammonium chloride under formation of trihydrate sodium-hydrogen-5,5'-ditetrazolylamide and after acidification by concentrated hydrochloric acid, di(1H-tetrazole-5-yl)amine monohydrate is formed with yield 67%.

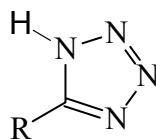
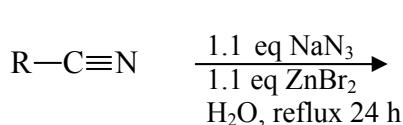


The method described was improved by Highsmith ^[2] from the viewpoint of reaction conditions: pH of reaction mixture, molar ratio of reaction compounds, reaction temperature of mixture, purity of crystalline compound, safety and improved yield. The following compounds have been used to released azoimide from ammonium chloride, dimethylamine hydrochloride, acetic acid, dipotassium hydrogen phosphate potassium dihydrogen phosphate, sodium dihydrogen carbonate and boric acid.

The yield (86.5 %) of di(1H-tetrazole-5-yl)amine was obtained under the following reaction conditions: for liberation of azoimide from sodium azide was used boric acid, molar ratio of boric acid/sodium azide/sodium dicyanamide was 1.650/0.830/0.416 at reaction temperature 95°C.



Optimal procedure for addition sodium azide to nitrile under formation of 1H-tetrazole was published ^[3] in 2001. The mixture of sodium azide, nitrile and zinc salt as catalyst was refluxed with water. The reaction conditions are safe and widely applicable to addition of azoimide to aromatic nitrile and alkanenitrile with activated or nonactivated alkyl group.

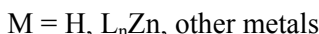


R (yield %): Ph (76%), 2-Py (79%),
4-HOPh (96%), C₇H₁₅ (82%),
Et₂N (72%)

Zinc chloride, bromide and perchlorate were used as catalysts. The role of zinc ion is not exactly known. Zinc ion does not play a role of Lewis acid only. Already at concentration of zinc ion Zn²⁺ 0.03 mol 10 times higher acceleration of reaction was observed and when concentration Zn²⁺ 1.0 mol was used, 300 times higher acceleration was observed.

Proposed mechanism of reaction is two step mechanism, but 2 + 3 addition mechanism can also be used.

We decided to use method the above mentioned for addition sodium azide to sodium dicyanamide.



Desired di(1H-tetrazole-5-yl)amine was prepared by refluxing suspension of zinc salt of di[5-(1H-tetrazole-5-ylamino)-1H-tetrazole-1-id] hydrate in diluted hydrochloric acid for 8 hours at 100 – 110°C. The yield was 67 %.

Elementary analysis: C₂H₃N₉. H₂O (171.1)

calculated: 14.04 % C, 2.94 % H, 73. 67 % N;

found: 13.63 % C, 2.99 % H, 73. 09 % N.

¹³C NMR spectra: 154.8 ppm; 156.9 ppm (C-5, C-5')

3. CONCLUSIONS

The new method of synthesis of di(1H-tetrazole-5-yl)amine was discovered. Di(1H-tetrazole-5-yl)amine was synthesized by reaction of sodium azide with sodium dicyanamide in water under presence of zinc chloride as catalyst.

This method eliminates disadvantages of other alternative methods, such as for example:

- work with expensive and toxic metals
- work with excess of volatile and toxic azoimide
- work with organic solvents

The advantages of this method are:

- this synthesis is very simple
- easy separation of intermediate zinc salt and final product by filtration
- this reaction is safe
- possibility of recovery of zinc chloride
- relatively high yield

REFERENCES

- [1] NORRIS W.P., HENRY R.A.: J. Amer. Chem. Soc., 29, 650, 1964
- [2] HIGHSMITH T.K., HAJIK R.M., WARDLE R.B., LUND G.K., BLAU R.J.: WO 9518802 (1995), US 5468866 (1995); Chem. Abstr., 123,286046, 1995
- [3] DEMKO Z.P., SHARPLESS K.B.: J. Org. Chem., 66, 7945, 2001

CHANGES OF DYNAMIC MECHANIC PROPERTIES OF DOUBLE BASED ROCKET PROPELLANT DURING ARTIFICIAL AGEING

S. Matečić Mušanić, M. Sućeska, M. Rajić Linarić, B. Sanko and R. Čuljak

Brodarski institut–Marine Research & Special Technologies
Av. V. Holjevca 20, 10020 Zagreb, Croatia

Abstract:

Double based rocket propellants are subjected to a chemical ageing, as well as ageing due to physical and physical-chemical processes (migration of low molecular constituents: plasticizers, blasting oil, burning catalysts, degradation of molar mass, etc.). The ageing has significant influence on their relevant properties, including mechanical properties such as tensile strength, storage modulus, loss modulus, tan delta, and temperature of glass transition, etc.

During use these changes can result in dangerous failures, such as rocket motor explosion. Therefore, it is necessary that after some time, temperature, and stress conditions, relevant properties of the propellants are still in the range of acceptable tolerance.

In this work we have studied changes of dynamic mechanic properties (loss modulus, storage modulus, tan delta, etc.) with the artificial ageing at higher temperature (90°C). The results obtained have shown that dynamic mechanical parameters change significantly after ~40 days of ageing. It was found put that the most sensitive parameters on the ageing process are: storage modulus at the room temperature, glass transition temperature, width of peak on loss modulus curve in the glass transition region, and $\tan \delta$ at the glass transition region.

Keywords: *double base rocket propellant, dynamic mechanical properties, storage modulus, loss modulus, tangents delta, glass transition, ageing*

1. INTRODUCTION

The research of ageing process is one of the basic scientific interests in the field of living organisms, construction materials, or energetic materials, such as double-based rocket propellants.

The term "ageing" is connected with change, or degradation of relevant materials properties. A number of parameters can influence degradation of a material properties; such as temperature, time, moisture, atmospheric conditions, stresses produced during production and use of materials, etc.

During the ageing process of the rocket propellants, chemical and mechanical properties change. Consequently, the service lifetime reduces. It is not easy to predict the service lifetime, but because of safety and economic reasons it is one of the main priorities of military science.

It is known [1,2,9-13] that nitrocellulose and other nitric acid esters, which can be ingredients of rocket propellants, are subjected to a slow chemical decomposition even at the room temperatures. The first step of thermal decomposition of nitrocellulose and blasting oil

is NO₂ radical splitting from O-NO₂ group. The released NO₂ can further react with other decomposition products or with propellant ingredients. During this process NO₂ is reduced to NO, N₂O, N, HNO₂ and HNO₃. The presence of HNO₂ and HNO₃ accelerates reactions of the hydrolytic decomposition.

The summary reaction of the thermal decomposition is autocatalytic, and accompanied by the heat generation. The heat released, due to very low propellant conductivity, can accumulate in the propellant grain, and under certain conditions can lead to the propellant self-ignition ^[1, 14].

Apart from ageing, due to chemical reactions, there is also ageing due to physical and physical-chemical processes, such as diffusion, or migration of low molecular constituents like: nitroglycerine, phlegmatizers, plasticizers, etc. ^[2-4] Ageing of the propellants due to chemical reactions, as well as due to physical processes, change mechanical properties, such as tensile strength, modulus of elasticity, morphology, and temperature of glass transition. During use, these changes can result in dangerous failures, such as explosion of rocket motors.

Rocket propellants are also subjected to ageing due to residue stress at rocket grain that can initiate crack formation and crack propagation in the propellant. That residual stress originates in manufacturing process, process of treatment of material and as a consequence of storage conditions. Residual stress that originates during manufacturing can be initiated by ^[1]: rapid cooling of rocket block manufactured by casting processes; stress induced due to different cooling rate between the surface and the inside of the rocket block; different temperature causes different values of coefficient of thermal expansion at the surface and inside of the rocket block, which causes stress at the boundary between the rocket grain and extruder tube, etc.

Because of safety reasons, it is necessary that after some time, temperature, and stress condition, the relevant properties of the propellants be still in range of tolerance. Therefore, it is very important to be able to measure and to quantify relevant properties changes as function of time and temperature.

The dynamic mechanical analysis (DMA) is a very powerful technique for studying viscoelastic properties (loss modulus, storage modulus, tangents delta, temperature of glass transition, etc.), detection of molecular motions, and evaluation of morphology of a material (crystallinity, molecular mass, crosslinking, etc.) ^[4-6, 16].

DMA is measuring technique in which the storage and loss modulus of the sample, subjected to an oscillating load, are separately monitored against the time, temperature, or frequency of oscillation, while the temperature of the sample in a specified atmosphere is programmed. For viscoelastic materials the strain is composed of elastic (stress and strain are in phase) and viscous (stress lags by strain for 90°C) component, in accordance with equation:

$$\sigma = (\sigma_0 \cos \delta) \sin \omega t + (\sigma_0 \sin \delta) \cos \omega t \quad (1)$$

or,

$$\sigma = \varepsilon_0 (E' \sin \omega t + E'' \cos \omega t) \quad (2)$$

where storage modulus (E') is real component, and loss modulus (E'') imaginary components of modulus:

$$E' = \left(\frac{\sigma_0}{\varepsilon_0} \right) \cos \delta, E'' = \left(\frac{\sigma_0}{\varepsilon_0} \right) \sin \delta \quad (3)$$

Damping, or tangents delta ($\tan \delta$) is defined as a ratio between loss and storage modulus:

$$\tan \delta = \frac{E''}{E'} \quad (4)$$

Since the dynamic mechanical properties (such as storage modulus, loss modulus, and damping as functions of time or temperature) are very sensitive to structural changes, this technique is also frequently used to study dynamic mechanical behaviour of rocket propellants. In this work we have studied how the dynamic mechanical properties of a double base rocket propellant change during the accelerated ageing at 90 °C, in order to identify the most sensitive parameter to the ageing process.

2. EXPERIMENTAL

The experiments were carried out using double base rocket propellant of the following chemical composition: 56% of nitrocellulose, 31% of nitroglycerine, 6.5% of dinitrotoluene, 2.5% of centralite I, and 4 % of other additives.

The testing samples for DMA measurements, having rectangular bar shape (50 x 10 x 2.5 mm), were cut from propellant grain. Such samples were subjected to the artificial aging at 90 °C in closed glass probes. The samples for DMA measurements were taken periodically. Total ageing time was 67 days.

Dynamic mechanical measurements were carried out using *TA Instruments* DMA, Model 983. The measuring conditions were:

- heating rate: 2 °C/min.
- frequency of an oscillatory load: 1 Hz
- amplitude of deformation ± 0.2 mm
- length to thickness ratio (L/T): ~10
- temperature range: -120°C to +80°C

3. RESULTS AND DISCUSSION

3.1 Dynamic mechanical properties

The result of DMA analyses for non-aged rocket propellant, or DMA thermogram, obtained at 2°C/min heating rate, 0.2 mm oscillation amplitude, and 1 Hz frequency, are shown in Fig. 1. It follows from Fig. 1 that the storage modulus is almost constant and reaches maximum ($E'=8$ GPa) in the region below glass transition (-120 to -100°C). The transition from glassy to viscoelastic state (onset point on $E'-T$ curve at about -64°C), has as a consequence a drop of the storage modulus four about 6 times (from 8 GPa at -120°C to 1,3 GPa at 25°C). Another distinct change in the storage modulus slope at about 42 °C corresponds to the propellant sample softening.

The loss modulus has a maximum value in the glass transition region. The maximum on $E''-T$ curve, at -26.95°C, is usually taken as the glass transition temperature. At the sample softening region (~ 49.83 °C) the loss modulus value decreases rapidly.

The $\tan \delta$ has local maximum at the glass transition region. The value of $\tan \delta$ increases in the softening region, as a consequence of increased movement of the macromolecules.

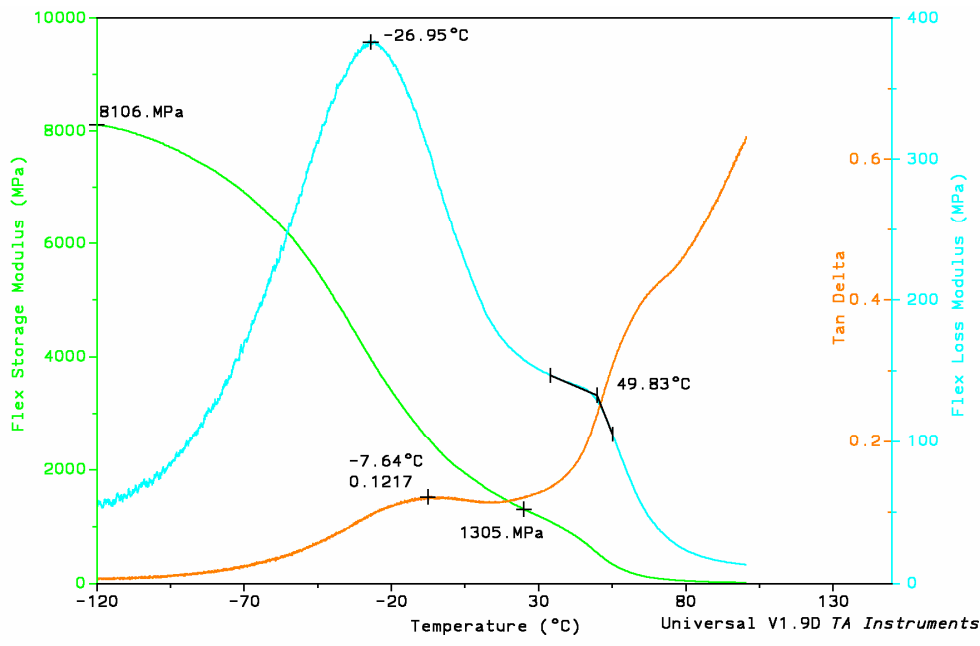


Fig 1. DMA thermogram of studied non-aged rocket propellant

In order to see how dynamic mechanical properties of the propellant studied change with the ageing time at 90 °C, the samples were taken periodically for DMA measurements. The results obtained are analysed below.

Change of storage modulus with aging

Summarised results on the storage modulus behaviour during the ageing time at 90 °C are given in Fig. 2. The figure shows E' - T curves of non-aged propellant, and propellant aged different times at 90°C.

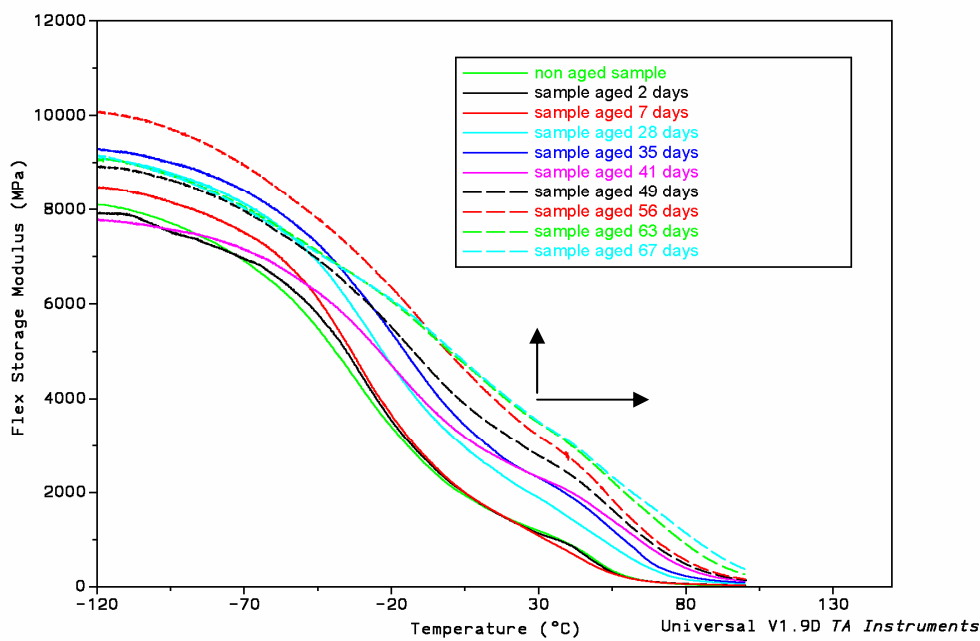


Fig 2. Storage modulus of non-aged propellant and the propellants aged different period of time at 90°C as a function of temperature

It can be seen from Fig. 2 that $E'-T$ curves shift with the ageing time to higher temperatures, as well as to higher values of modulus. In order to quantify these changes in the storage modulus, several characteristic parameters on $E'-T$ curves are analysed: storage modulus at 25 °C, storage modulus at -120 °C, glass transition temperature determined from $E'-T$ curve and softening temperature determined from $E'-T$ curve. The changes of some of these parameters are shown in Figs. 3 and 4.

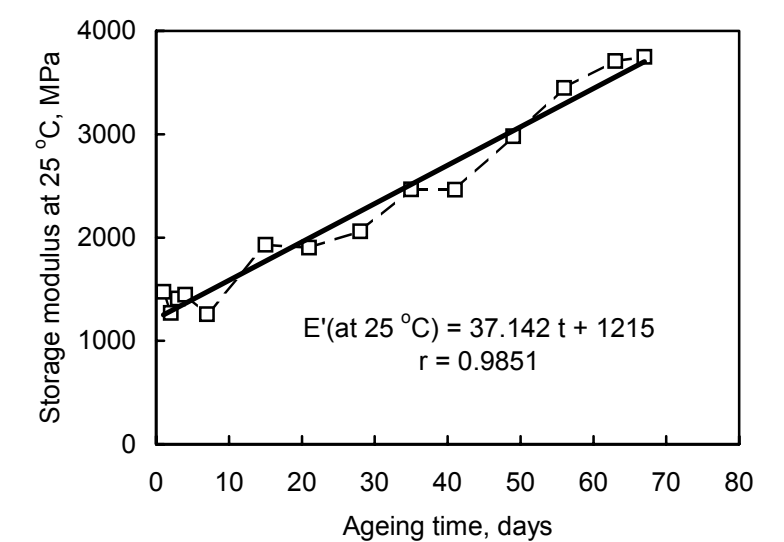


Fig 3. Change of storage modulus at 25 °C with aging time at 90°C

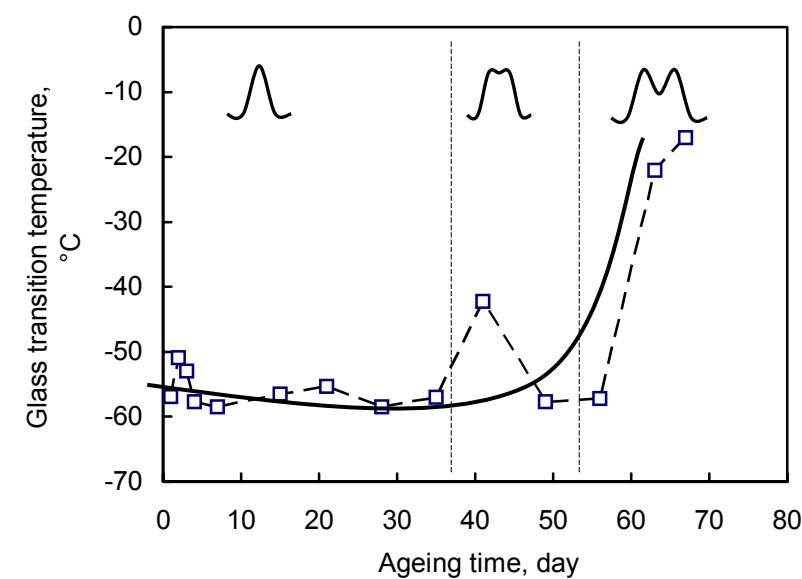


Fig 4. Change of glass transition temperature determined as onset temperature on $E'-T$ curve, with aging time at 90°C

An increase of the storage modulus, especially in range of the room temperatures is connected with decreased flexibility of nitrocellulose macromolecules, what can be result of an increased amount of crystal phase, as well as a decreased amount of plasticizer. The plasticizer migration from the propellant grain interior to the surface, causes a decrease of distances between macromolecules, and an increase of intermolecular forces. These

processes have significant effect on flexibility of the nitrocellulose macromolecule kinetic units.

In order to quantify the changes observed, i.e. to find out which of parameters is the most sensitive to the ageing process, a detailed analyses of several relevant parameters on $E'-T$ curves with the ageing time was performed. The results are presented graphically in Fig. 5.

The degree of change of a parameter, shown in Fig. 5, was calculated using the following equation:

$$y_p = \frac{(P_0 - P_t)}{P_t} 100 \tag{3}$$

where: y_p – degree of change of same parameter, P_0 – parameter value at the beginning of the aging, and P_t – parameter value after some time of aging

Fig. 5 shows that the majority of analysed parameters on $E' - T$ curve do not change significantly with the aging (the changes are within 10%). The exception is the storage modulus at 25°C, which increases significantly and almost linearly with the ageing time. It should be noted that the glass transition temperature determined as onset temperature on $E' - T$ curve changes significantly after ~55 days of ageing.

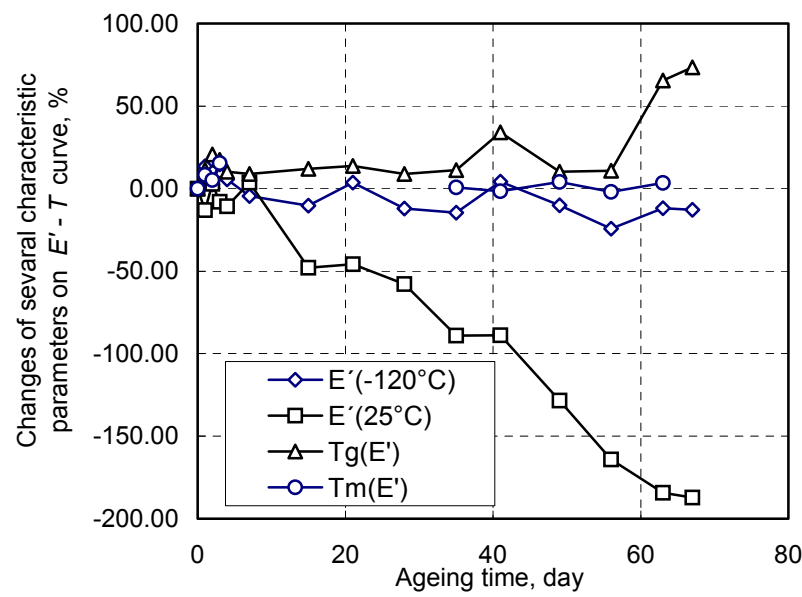


Fig 5. Degree of change (in percents) of some parameters on $E' - T$ curve with ageing time at 90 °C

Change of loss modulus with aging

Summarised results on the loss modulus behaviour, i.e. summarised E'' - T curves of non-aged and aged propellant samples, are given in Fig. 6.

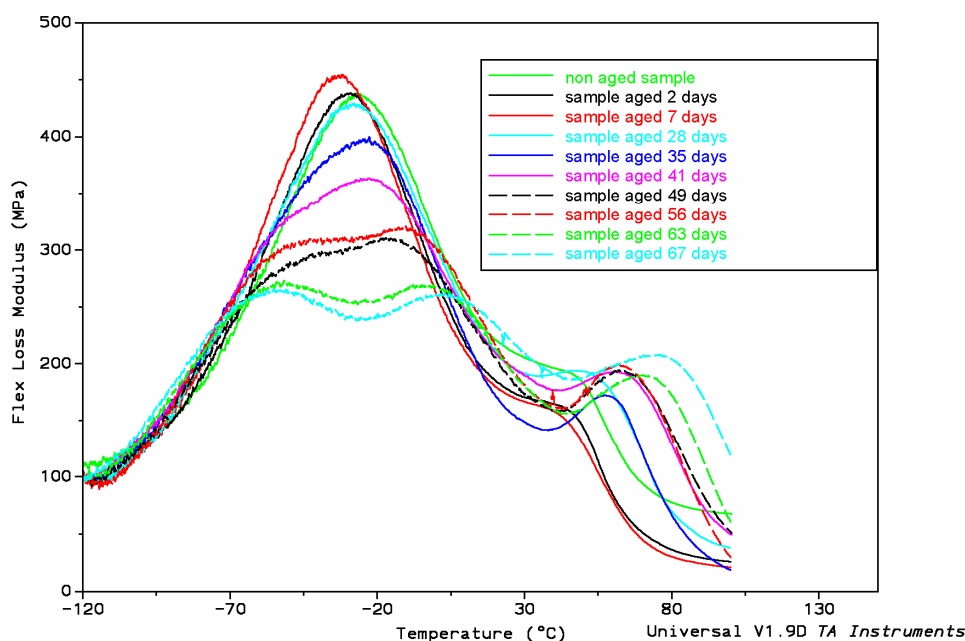


Fig 6. Loss modulus of non-aged propellant and propellants aged different period of time at 90°C, as a function of temperature

It is evident from Fig. 6 that the aging causes significant quantitative and qualitative changes on E'' - T curves of the propellant studied: value of the loss modulus maximum decreases with the ageing, peak width increases, and complete E'' - T curve shifts to higher temperatures.

Significant qualitative changes on E'' - T curve begin after ~28 days of aging at 90°C. After that time of the aging, a gradual splitting of the peak in the glass transition region was observed. The splitting of the main peak into two separate peaks may be consequence of very intensive splitting of nitrocellulose polymer chains. After 56 days of aging, the peak splits completely. The splitting of the peak indicates an increase in the heterogeneity of system.

It is also visible from Fig. 6 that the glass transition temperature (i.e. the peak maximum temperature on E'' - T curve) shifts to higher temperatures. The second peak on the E'' - T curve, at the softening temperature region, becomes much sharper with the ageing time.

The changes of some characteristic parameters on E'' - T curve, such as glass transition temperature, loss modulus at the glass transition temperature, peak width, temperature of second peak at the softening temperature region, etc., with the ageing time are given in Figs. 7 – 11.

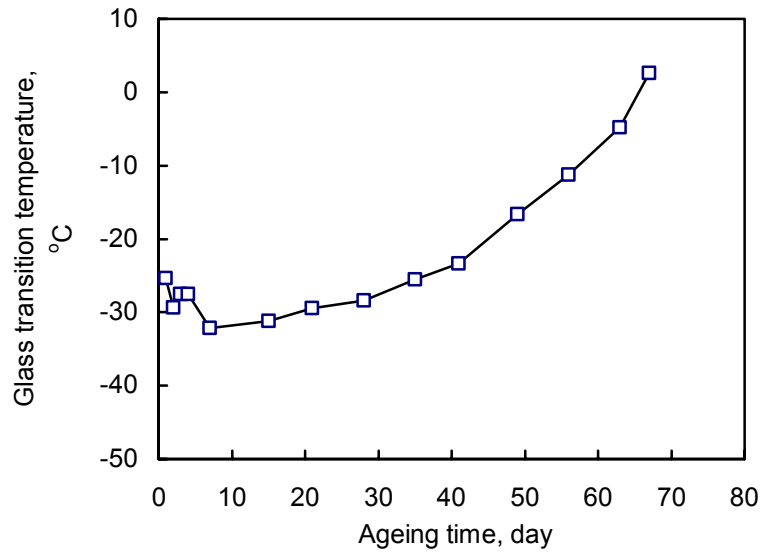


Fig 7. Change of glass transition temperature with the ageing time at 90 °C

It is obvious from Fig. 7 that the aging of propellants has significant effect on the glass transition temperature, i.e. on peak maximum temperature on E'' - T curve. The glass transition temperature shifts with the ageing time to higher temperatures. Such shift indicates a decrease in nitrocellulose macromolecules flexibility. The most important reason for this probably is migration of low molecular ingredients, such as blasting oil and plasticizers, from the propellant grain interior.

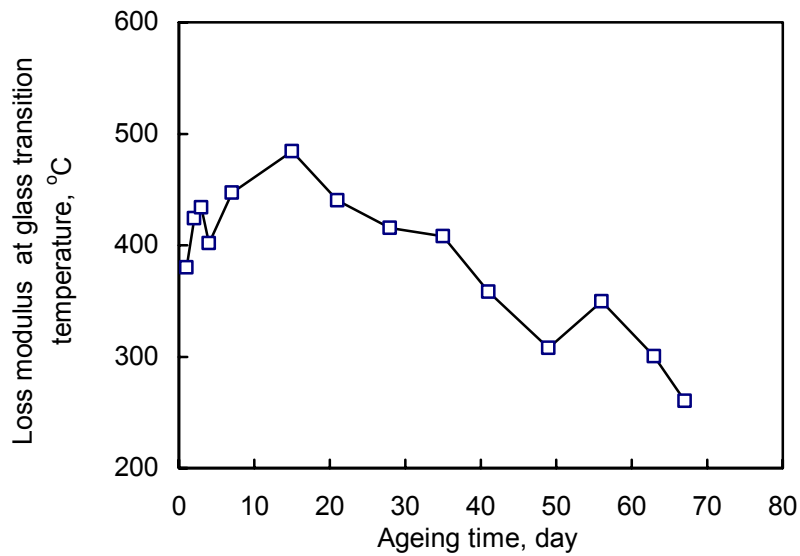


Fig 8. Change of loss modulus at the glass transition temperature (i.e. peak height) with the ageing time at 90 °C

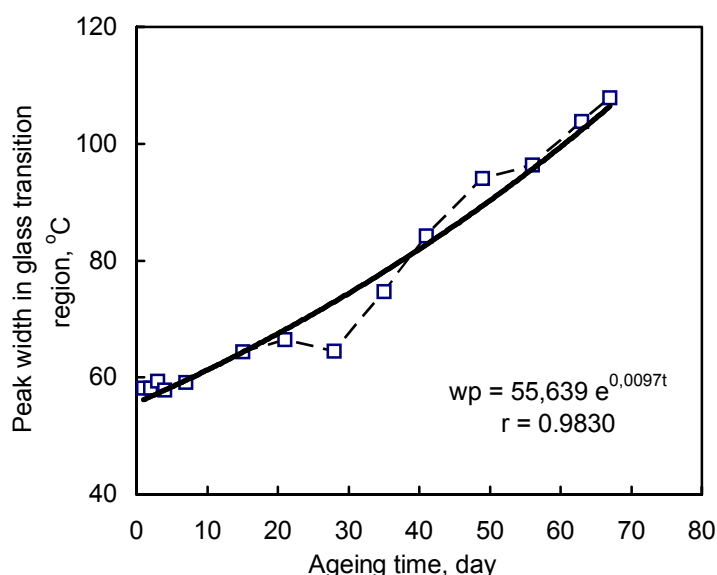


Fig 9. Change of peak width with the ageing time at 90 °C

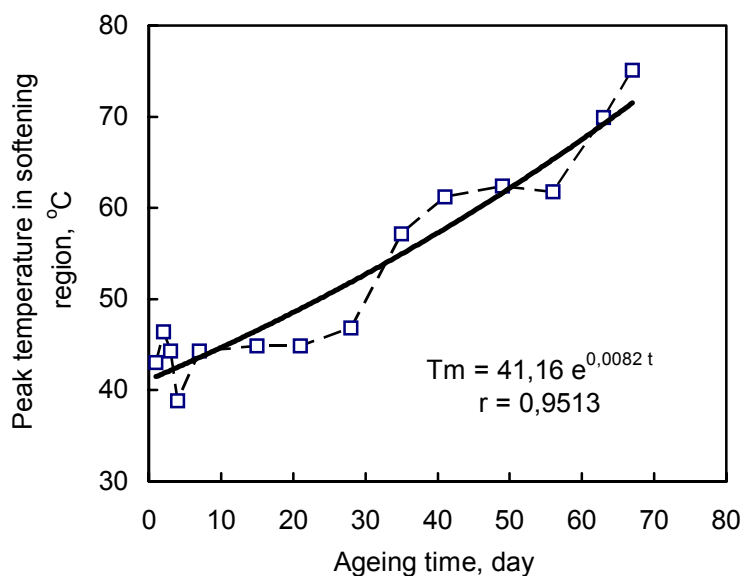


Fig 10. Change of peak temperature in softening region with ageing time at 90 °C

It is visible from Fig. 8 that the peak height, i.e. value of loss modulus at the peak maximum decreases with the ageing time, while at the same time peak width increases (Fig. 9). Figs. 10 and 9 show that peak maximum in the softening temperature region and peak width begin to change more rapidly after 28 days of aging. Total temperature change after 67 days of aging equals in both cases more than 30°C. The shift of the softening temperature to higher temperatures is another indication of decreased flexibility of nitrocellulose kinetic units with the ageing time.

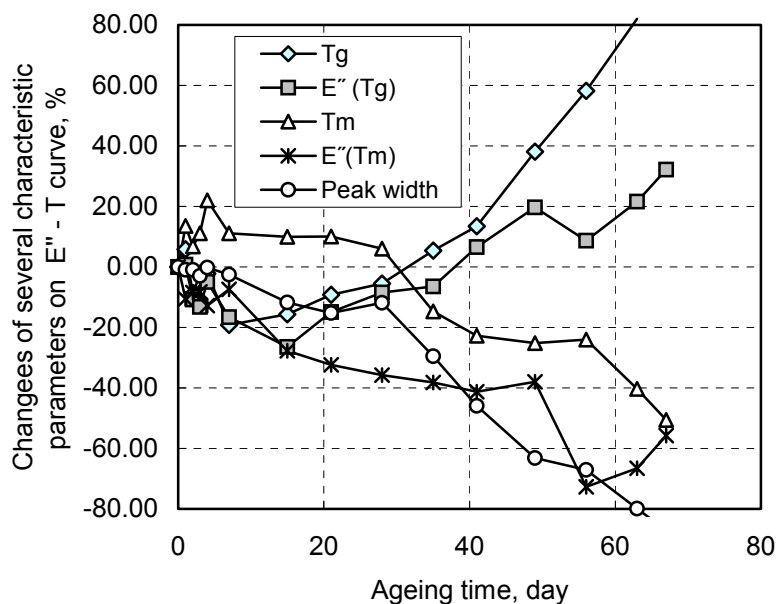


Fig 11. Degree of change (in percents) of some parameters on $E'' - T$ curve with ageing time at 90 °C

Fig. 11 shows that very intensive changes of analysed parameters on curve $E'' - T$ begin after 40 days of aging at 90°C. Fig. 11 shows that the most sensitive parameter on the ageing is glass transition temperature – it changes from ~25 °C for non-aged sample, to ~ 0 °C for sample aged 67 days. The peak height and peak width also change significantly – peak height decreases, while peak width increases with the ageing time.

Change of $\tan\delta$ with aging

The $\tan \delta$ curves as a function of temperature for non-aged propellant and propellants aged different period of time at 90°C are shown summary in Fig. 12.

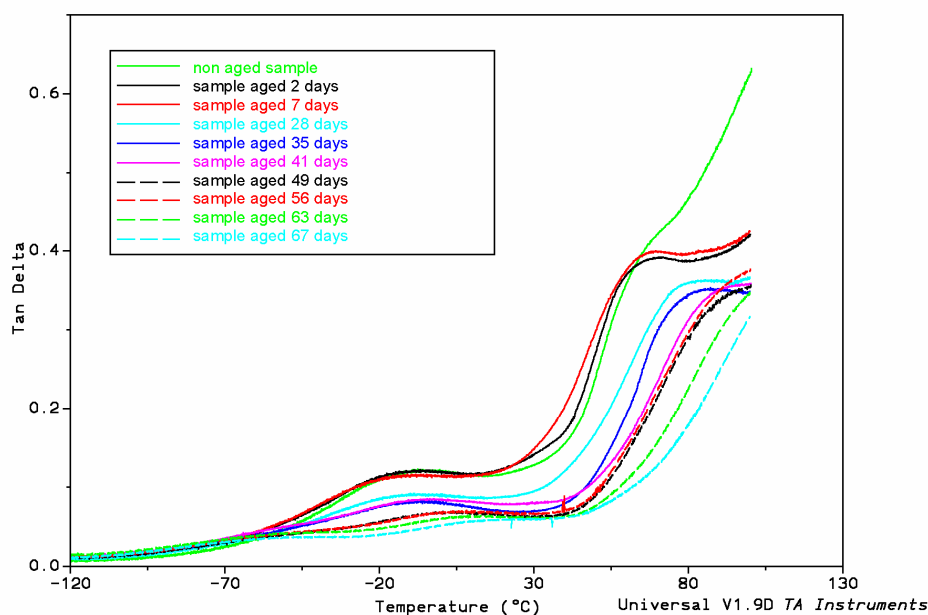


Fig 12. $\tan \delta$ of non-aged propellant and propellants aged different period of time at 90°C, as a function of temperature

Fig. 12 shows that the shape of $\tan \delta$ curves changes considerably with the ageing time at 90 °C. For example, at temperatures below glass transition region the value of $\tan \delta$ remains almost unchanged, while in the glass transition region, viscoelastic region, and in the softening temperature region value of $\tan \delta$ decreases significantly. This means that a viscous component in the propellant structure decreases with the ageing time.

More detailed analysis of changes of characteristic parameters on $\tan \delta$ - T curve, maximum of $\tan \delta$ at the glass transition region, temperature of $\tan \delta$ maximum in the glass transition region, maximum of $\tan \delta$ at the softening temperature region, and temperature of $\tan \delta$ maximum in the softening temperature region, with the ageing time are given in Figs. 13 – 16.

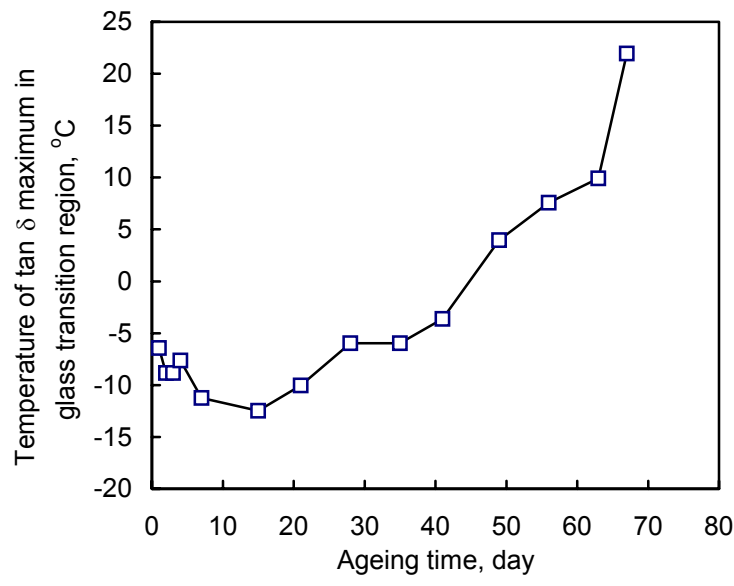


Fig 13. Change of temperature at $\tan \delta$ maximum in glass transition region with ageing time at 90 °C

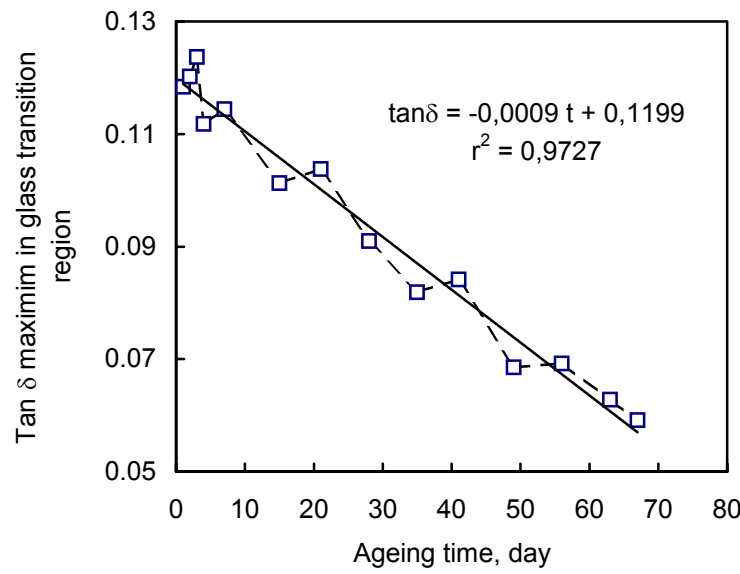


Fig 14. Change of $\tan \delta$ maximum value in glass transition region with ageing time at 90 °C

Fig. 13 shows that the temperature of $\tan \delta$ maximum in the glass transition region has small drop in the earl stage of the ageing, and than increases exponentially with the ageing time. At the same time value of $\tan \delta$ at the peak maximum in glass transition region decreases linearly with the again time (Fig. 14), indicating decrease of viscous component in the propellant samples.

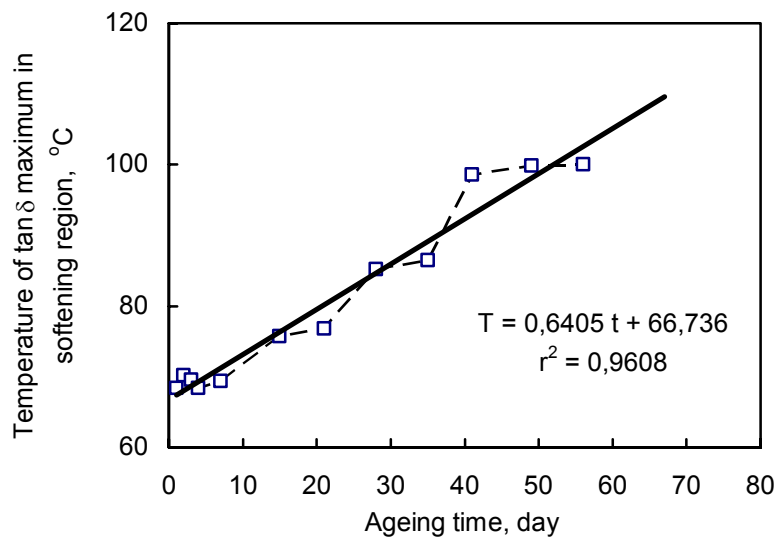


Fig 15. Change of temperature of $\tan \delta$ maximum in softening region with ageing time at 90 °C

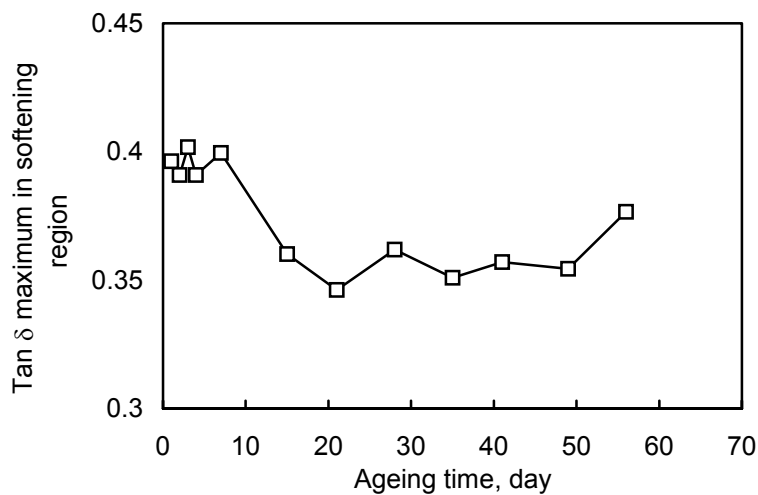


Fig 16. Change of maximum value of $\tan \delta$ in softening temperature region with ageing time at 90 °C

Figs. 15 and 16 show that the temperature of sample softening increases linearly with the ageing time at 90 °C, while value of $\tan \delta$ at that temperature decreases significantly within the first 20 days of ageing and after that time remains almost the same up to 60 days of ageing. Such results can be also connected with decreased amount of viscous component in the propellant with the ageing.

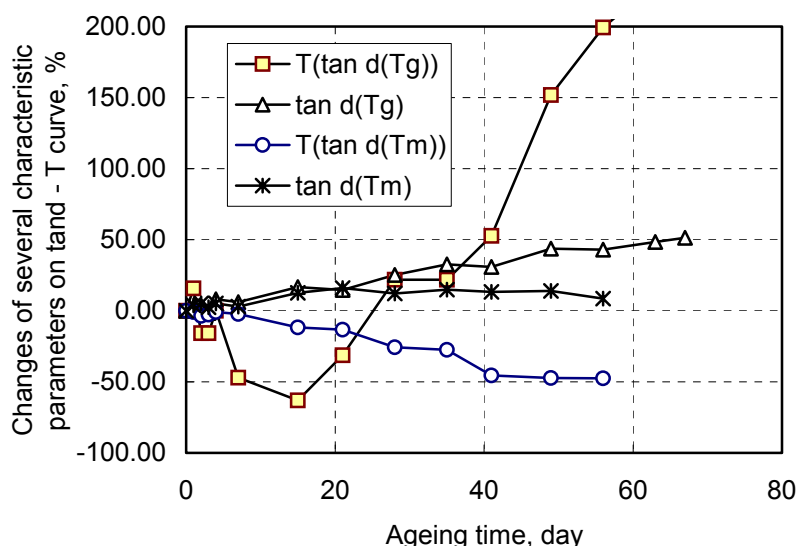


Fig 17. Degree of change (in percents) of some parameters on $\tan \delta$ - T curve with ageing time at 90 °C

Fig. 17 shows that the temperatures of $\tan \delta$ maximum in the glass transition and softening regions change more intensive than value of $\tan \delta$ at these maximum. The most sensitive parameter on $\tan \delta - T$ curve to the ageing process is temperatures of $\tan \delta$ maximum – it begins to change dramatically after 40 days of ageing at 90 °C. Other analysed parameters change less significantly and almost linearly with the ageing time.

4. CONCLUSIONS

The results presented in this paper, which are preliminary results of broader study on dynamic mechanical behaviour of homogeneous rocket propellants during artificial ageing at elevated temperatures, show that the dynamic mechanical properties of studied double base rocket propellant change with ageing time. Also, the results confirm that dynamic mechanical analyser (DMA) can be used to follow and to quantify these changes .

Generally, all DMA curves (storage modulus, loss modulus, and $\tan \sigma$ as functions of temperature) shift to higher temperatures with the ageing time. The most significant qualitative change in DMA thermogram is splitting of peak on E'' - T curve in the glass transition region into two separate peaks after approximately 50 days of ageing.

The shapes and values of some parameters on DMA curves indicates that the ageing causes decreases flexibility (mobility) of nitrocellulose kinetic units, which can be consequence of a decrease in amount of viscous component in the propellant samples (nitroglycerine, plasticizer, etc.). The peak splitting on E'' - T curve in the glass transition region into two separate peaks indicates an intensive degradation of nitrocellulose polymer chain, which have resulted in an increase in system heterogeneity.

It was found out that the most sensitive parameters on the ageing process are: storage modulus at the room temperature, glass transition temperature, and $\tan \sigma$ at the maximum in the glass transition region.

REFERENCES

- [1] M. SUČESKA: *Baruti*, MORH, 1996.
- [2] TAGER: *Physical Chemistry of Polymers*, Mir Publishers, Moscow, 1972
- [3] L. FERRY: *Viscoelastic Properties of Polymers*, John Wiley & Sons, New York, 1961
- [4] T. MURAYAMA: *Dynamic Mechanical Analysis of Polymeric Material*, Elsevier Scientific Publishing Company, Amsterdam, Oxford, New York, 1978)
- [5] CHANG DAE HAN, DOEG MAN BACK AND JINHWAN KIM: *Macromolecules*, 25, 3052-3067, 1992
- [6] W. KEEWIN, W. A. MICKAY, C.F. DIEHL: *Appl. Polym. Sci.*, 56, 947-958, 1995
- [7] J.J. ALCONIS, W. J. MAC KNIGHT, S. MICHEL: *Introd. to Polym. Viscoelasticity*, John Wiley & Sons, New York, 1972
- [8] HALL: *Polymer Materials*, John Wiley & Sons, New York, 1991
- [9] M. A. BOHN: *Kinetic Modeling of the Ageing of Gun and Rocket Propellants for the Improved And Time-Extended prediction of Their Service Lifetime*, Proceed., 1998 Life Time Cycles of Energetic Materials, Fullerton, California, USA, 29 March-1 April, 1998
- [10] M.A. BOHN: *Methods and Kinetic Models for the Lifetime Assessment of Solid Propellants*, Paper 2 on the 87th Symp. Of the Propulsion and Energetics Panel (PEP) of the AGARD, Service Life of Solid Propellant Systems, Athens, Greece, May 6-10, 1996, AGARD-Conference-Proceedings 586 AGARD-CP-586), F-92200 Neuilly sur Seine, France, May 1997
- [11] F. VOLK, G. WUNSCH: *Determination of the Decomposition Behavior of Double Base Propellants at Low Temperature*, *Propell. Expl. Pyrot.* 10, 181, 1985
- [12] A. PFEIL, H.H. KRAUSE, N. EISENREICH: *The Consequences of Beginning Slow Thermal Decomposition on the Molecular Weight of Nitrated Cellulos* , *Thermochim Acta*, 85, 395, 1985
- [13] F. VOLK, M. A. BOHN, G. WUNSCH: *Determination of the Chemical and Mechanical Properties of Double Base Propellants During Aging* , *Propell. Expl. Pyrot.* 12, 81, 1987
- [14] M. A. BOHN, F. VOLK: *Prediction of the Lifetime of Propellants by Stabilizer Consumption and Molar Mass Decrease*, Proceed. ADPA Predictive Technology Symp., June 22-24, Orlando, FL, US-Army ARDEC, Picatinny Arsenal, New Jersey, USA, 1993
- [15] M. A. BOHN: *Systematische Darstellung der Alterung von Rohrwaffentreibmitteln und Raketenfesttreibstoffen*, Paper 109, Proceed. of the 28th Internat. Annual Conference of ICT, Karlsruhe, Germany, Fraunhofer-Institut für Chemische Technologie (ICT), June 24-27, 1997

APPLICATION OF SHEET EXPLOSIVE FOR METAL HARDENING

P. Nesvadba

Explosia a.s., Research Institute of Industrial Chemistry
532 17 Pardubice -Semtín, Czech Republic

Abstract:

This article contains a brief information on application of sheet charges for explosive hardening of metals. The paper defines basic requirements for the properties of the explosives used for explosive metal hardening, resulting from practical applications. At the same time the findings are given here obtained at application of the explosive at hardening of Hadfield steel.

Keywords: *explosive hardening, sheet explosive, Hadfield steel, crossing*

1. INTRODUCTION

At some machinery products explosive hardening by means of shock wave induced by a thin layer of high explosive has been used for several years. It is one of a few methods utilizing construction effects of an explosive and obtaining of materials with better properties, primarily with higher strength and hardness. This method is most widespread at hardening of Hadfield steel casts. This is the case of manganese austenitic steel capable of strong/deep hardening that is used for the parts exposed to strong shocks and wear. One of priorities of explosive hardening is the possibility to harden as to shape more complicated parts. By that this method competes to classical mechanical cold hardening, at which volume changes and wear occur still during the hardening.

2. HARDENING MECHANISM

By detonation of high explosive in intimate contact with metal, the shock wave is induced of high pressure (about 20 GPa) and extremely short duration. Passing through shock wave and reflected waves generate higher or smaller number of defects in the metal crystal lattice (vacancies, dislocations, twinning). In this way the strength and hardness of the metal processed by the passing through shock wave is increased without macro-deformations. The increase in hardness is also adjudged to additional phase-transition of surfeited austenite to ϵ -martensite ^[1]. Despite considerable hardening and increase in hardness, the material is, in addition, capable of retaining relatively high tenacity, even higher than that of conventionally, cold processed steel at the same level of hardening. At manganese (Hadfield) steel the increase in hardness can be measured to the depth of 30 mm in average. On the metal surface the hardness of 350 HB and more can be commonly achieved when compared with the original hardness that, after homogenization, achieves the values about 180 to 200 HB ^[2]. The hardness continuously decreases in the direction to the depth up to the original level of material hardness. Maximum values of hardness vary about 500 HB ^[3].

The mechanism of hardening of austenitic manganese steel has been studied by many authors. The whole of the phenomena has not been quite unambiguously described yet. In the Czech Republic the method has been implemented since the 1960s, but only a few authors have dealt with these problems in detail ^[4].

3. EXPLOSIVES FOR EXPLOSIVE HARDENING OF METALS

3.1 Properties of Explosive for Explosive Hardening of Metals

At present time primarily sheet charges of high explosive are used for explosive hardening of metals. Detonation velocity of these explosives vary about 6,000 to 7,000 m.s⁻¹ and the thicknesses of explosive sheets about 2 to 3 mm. Thickness of explosive layer influences the depth of hardening, the resulting hardness, however, does not vary with explosive layer thickness too much because the shock wave pressure amplitude is almost independent of the explosive layer thickness.^[5] It is not desirable to use greater thicknesses of the charges because of the stress exerted on the Hadfield steel cast processed. Therefore thin sheet charges are applied repeatedly onto one place two to three times. Another reason of multiple hardening is, that, on detonation, the explosive applied onto the metal surface induces gradually alongside the surface slant shock wave that is less effective than perpendicular acting detonation pressure wave.

The casts processed, onto which the explosive is applied, have unprocessed surface after casting or worked by cutting or grinding. Usually the surface of the product designed to be explosive hardened is uneven, rough, with sharp edges and cutting marks which does not facilitate the explosive to adhere. At the same time it is necessary for the explosive to be in close contact with the metal surface without any air cavities and to adhere to the metal surface in all bends and edges. These are the needs why shapeability and adhesivity of sheet explosive is required. Moreover, these properties should be stable within certain temperature range varying from -20° C to +40° C. The casts are commonly processed at ambient temperature and especially in more cold season the shapeability and adhesivity of the explosive deteriorates. Certain solution is processing of the casts in explosion chamber, where adequate temperature range can be guaranteed. Constant thickness of explosive layer applied onto metal surface is taken granted.

From the viewpoint of technician using sheet explosive, the requirements for the properties of the explosive can be summarized into several points:

- stable detonation parameters in thin even layer
- good shapeability and adhesivity and at the same time suitable mechanical strength of the explosive
- possibility to manufacture a sheet charge often of great area dimensions with regard to the thickness of the explosive
- good and safe handling

Composition of the explosive is, in result, a compromise between the requirements taking into consideration application and requirements concerning explosive production technology and the viewpoint of price of the explosive cannot be omitted either. The price of the explosive and costs spent on explosive hardening are reflected in the price of the product and shall be equal to the obtained service life of the product.

3.2 Application of Sheet Charges

Sheet charge is prepared of sheet explosive by forming a suitable shape. The shape results from hardened area geometry. Semi-product for manufacture of the charge are sheet explosives rolled or screw extruded into various formats. The charge is of course applied onto the places that will be exposed to wear at most in future, and that are clean and after finishing. At the same time it is supposed that e.g. Hadfield steel cast is suitably heat treated, does not show any cast defects, especially surface and subsurface flaws. In reverse case these flaws become evident after firing the charge, often they are distinguishable on the metal surface with a naked eye and prevent the product from further processing or use. To certain extent explosive hardening can be considered as certain check of cast quality. In addition, after the first firing of the charge equalization occurs of hardness of metal surface. Differences in hardness before explosive hardening are often given by the manner of working of the cast surface, e.g. by the method of cutting. Still after firing one charge relatively good depth of hardening is achieved. To increase the hardness, the second possibly third charge is consequently applied in the same manner. Extent and the way of hardening depend on particular product of manganese steel.

As to shape more complicated elements it is not possible to avoid joining of several parts forming the charge. These joints are crucial points, because reliable detonation transfer has to be ensured, but no sheet explosive overlaps are allowed. By that the thickness of explosive layer would increase and the effect of explosive would change in comparison with the places covered with one even layer of explosive only. Joints of explosive sheets also appear in the places where the explosive completely covers the edges and ends of the element to limit the effects of reflected voltage surges.^[3]

In the Research Institute of Industrial Chemistry in Pardubice standard hardening is carried out of cast railway crossing frogs of Hadfield steel using the explosive of domestic production – Semtex[®] 10 SE. Figure 1 shows an overview of railway frog and Figure 2 shows application of sheet explosive at hardening of frog point. It is the most often used application of explosive hardening of metals. Occasionally the cast parts of grinding equipment from similar material are explosive hardened.



Fig 1. Overview of frog cast designed for explosive hardening

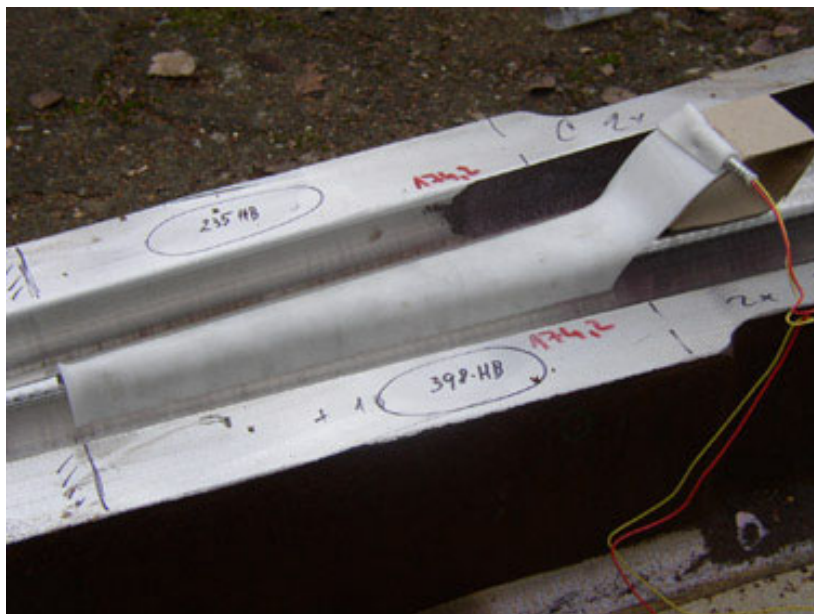


Fig 2. Application of sheet explosive at toe hardening

4. CONCLUSION

The method of explosive hardening by means of sheet explosive is spread in several countries only, with the parameters of explosives and technological procedures themselves being moreless similar. Good results are achieved especially at the most spread application i.e. at explosive hardening of cast railway crossing frogs. This brings economic profit from the viewpoint of increase in wear resistance, i.e. service life of the product. Considering the fact, that each product is designed for particular purposes and Hadfield casts are not always designed for explosive hardening, no mass spread of the application can be expected especially at the thin wall casts, tiny, as to shape more complicated elements, or elements where cutting is used as the final treatment.

The presented hardening method requires a very sophisticated approach at handling with plastic sheet explosives so that desired properties of the product are achieved. In the workplaces of the Research Institute of Industrial Chemistry sheet explosives can be manufactured in such a way that their parameters are adapted to a particular application and the sheet explosive can be manufactured usually by rolling in thicknesses from 0.8 to 10 mm in maximum width of 430 mm and length of 2,000 mm according to thickness of the explosive, possibly, to achieve longer sheets of explosive it is possible for the explosive to be screw extruded. At this way manufactured explosive the thickness/width ratio of the sheet explosive is, however, smaller than at rolled sheets. Composition of the explosive is adapted to the requirements considering both explosive properties and physical properties (strength, shapeability, adhesiveness etc.). To achieve optimum results at explosive hardening of metals is, however, necessary that construction and production technology of the element is suitably prepared for processing by the method of explosive hardening.

REFERENCES

- [1] PÍŠEK F.: Nauka o materiálu I; Nakladatelství ČSAV, Praha, 1957, p. 587
- [2] RYŠ P., CENEK M., MAZANEC K., HRBEK A.: Nauka o materiálu I - Železo a jeho slitiny 4; Nakladatelství ČSAV, Praha, p. 442 - 443, 1975
- [3] BLAZYNSKI T. Z.: *Explosive welding, forming and compaction*; Applied Science, Publishers London and New York, , p. 187 – 188, 1983
- [4] KOTRBATÝ F.: *Zvýšení tvrdosti austenitické manganové oceli detonační tlakovou vlnou*, Sborník VAAZ, Brno, p. 133 - 148 , 1963
- [5] DOHERTY A. E., MYKKANEN J. P.: *Explosive compaction of powdered materials*, Technical paper of American Soc. Tool and Manufacturing Engineers MF 67-115, Michigan, p. 1 – 15, 1967

INFLUENCE OF INSENSITIVE ADDITIVES ON DETONATION PARAMETERS OF PBX

A. Orzechowski*, D. Powal*, A. Maranda** and J. Nowaczewski**

* Institute of Industrial Organic Chemistry, 6 Annopol St, 03-236 Warszawa, PL

** Military University of Technology, 2 Kaliskiego St, 00-908 Warszawa 49, PL

Abstract:

Plastic bonded explosives (PBX) are known as explosives which possess high energy, thermal stability, low insensitivity and good mechanical properties. We investigated plastic explosive based on hexogen. As an additive we used NTO. We researched influence of NTO additives on detonation parameters of plastic explosives. This additive generated the decrease of sensitivity without significant worsening detonation parameters.

Keywords: *insensitive high explosive, plastic explosive*

1. INTRODUCTION

There are a lot of requirements for explosives, which are being used to military and civilian applications. Beside high performance, simple preparation and stability for a long time, very important is the low sensitivity to mechanical stresses. Among insensitive explosives the most significant are c (NTO), nitroguanidine (NQ) 1,3,5-triamine-2,4,6-trinitrobenzene (TATB), dinitroglycouril (DINGU) [1].

We investigated low sensitivity plastic explosives. A major plastic explosive (PE) component decides about explosive properties. Hexogen (RDX), pentrit (PETN) and octogen (HMX) are used very often.

In this work, the influence of NTO additive on detonation parameters of plastic explosives is shown. NTO is commonly accepted as a component of explosive compositions due to its relatively high performance and low sensitivity to mechanical stresses. The samples of mixtures contained NTO/RDX in a different weight ratio. We investigated detonation velocity, blast wave overpressure and blast wave impulse of these samples. The impact sensitivity of these compositions was also evaluated. We made plastic explosives with good sensitivity to mechanical stress without worsening their detonation parameters.

Process for production NTO involves two stages, based on commercially available products [2-5].

- reacting semicarbazide hydrochloride with formic acid,
- nitration triazolone by fuming nitric acid.

The rheological parameters of plastic explosive are decisively influenced by the particle size distribution and the shape of the explosive crystals. Process for production spherical NTO comprising dissolving NTO and cooling solution at a rate of 6 °C per minute [6,7]. NTO is crystalline substance with high density and velocity detonation. Melting point

of 3-nitro-1,2,4-triazol-5-on with decomposition 260°C This explosive is used as a component of thermal resistant mixture. NTO is low sensitive to mechanical stress ^[8]. Critical diameter of NTO is high and depends on its grain size characteristic and compression ratio. The NTO critical diameter is from 13 to 25 mm. ^[9]. Low sensitivity PBX based on HMX, NTO was prepared by A. Becuwe, A. Delclos ^[10].

2. MATERIALS AND METHODS

2.1 Characteristics of explosives

We tested following explosives:

- hexogen (RDX), tamp bulk density 0,86 g/cm³, grain size analysis is presented in Fig.1,
- nitrotriazol (NTO), tamp bulk density 0,90 g/cm³, grain size analysis is presented in Fig.2. Crystals of NTO are shown in Fig.3.

NTO was recrystalizing in order to obtain spherical crystals by dissolving crystals and cooling solution at a rate of 6 °C per minute.

Plastic binder consisted of butadiene-styrene copolymer, dioctyl adipate and oil. Binder composition is given below:

- butadiene-styrene copolymer 30%,
- dioctyladipate 60%,
- oil 10%.

Due to safety and mixing quality the best method was a mixing of wet explosive with butadiene-styrene copolymer water suspension.

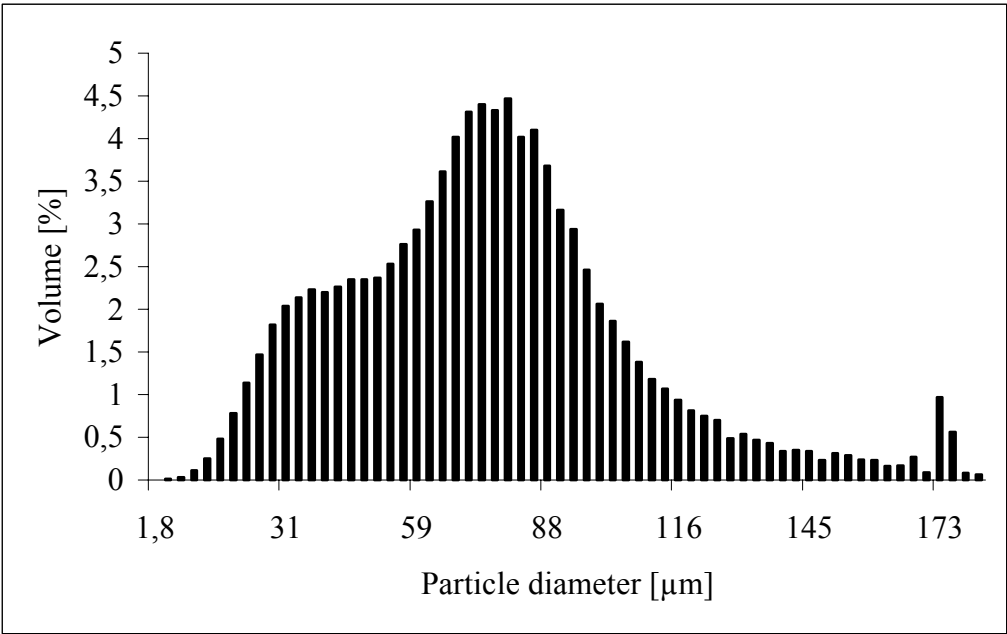


Fig 1. Particle size distribution of RDX

NTO

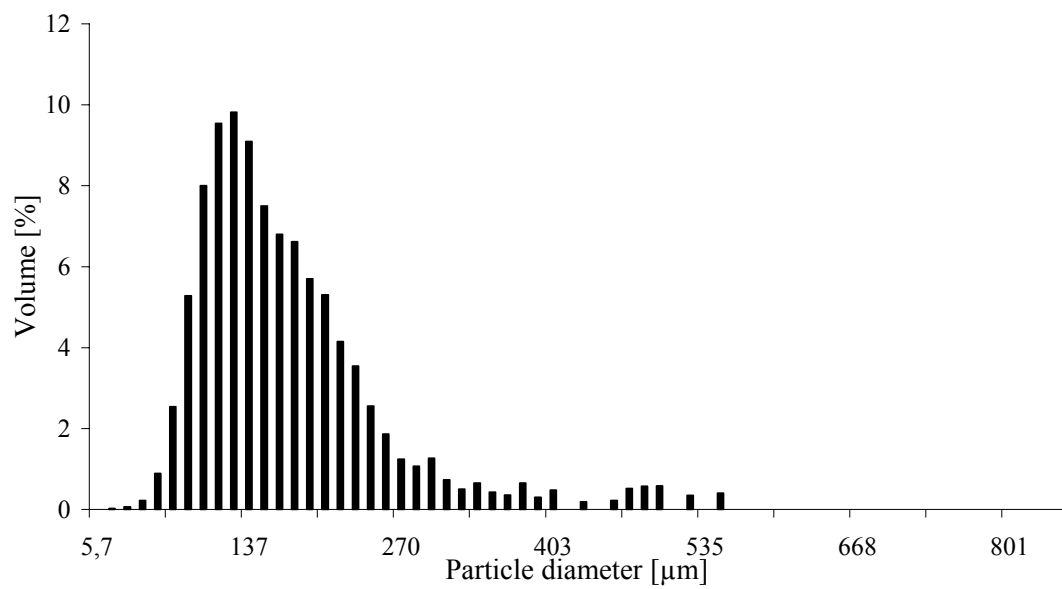


Fig 2. Particle size distribution of NTO

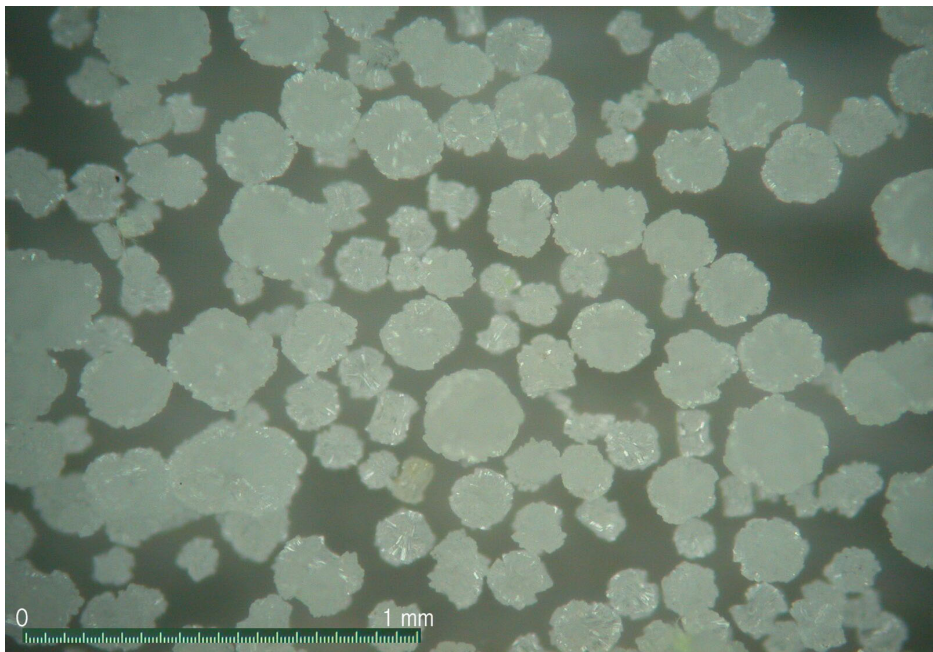


Fig 3. Crystals of NTO

2.2 Detonation velocity measurement

Detonation velocity was determined by the measurement of the time of detonation wave transition through three sections. Sections were 40 mm length. Explosives were placed into PCV pipes (internal diameter 35 mm, external diameter 39 mm, length 170 mm) The mass of explosives was 200 g. Charges was initiated by RDX/TNT boosters. Distance from start charge to first section was 40 mm. The mass of boosters was 16 g. Density and detonation velocities of plastic explosives are shown in Table 1. Additive of NTO decreases detonation velocity of plastic explosive about 200 m/s with increasing content of 20 % NTO. Additive 20 % of NTO slightly decreases detonation velocity about 100 m/s and decreases sensitivity to impact to 34,3 Nm. Samples with 80 % NTO elaborated to steel pipes (35 mm) detonated with velocity 6000 m/s.

Table 1. *Detonation velocities for plastic explosives with additives NTO*

Compositions	Density, g/cm ³	Detonation velocity, m/s	ID, mm	Impact Sensitivity* [Nm]
0 % NTO 100 % RDX	1,42	7420	35	29,4
20 % NTO 80 % RDX	1,45	7200	35	34,3
40 % NTO 60 % RDX	1,46	6960	35	34,3
60 % NTO 40 % RDX	1,49	6760	35	34,3
80 % NTO 20 % RDX	1,52	6000**	35	>49,0
100 % NTO 0 % RDX	1,50	ND	35	>49,0

* min. 1 decomposition at 6 samples

** in steel tubes

ND – not detonated

2.3 Blast wave overpressure

Plastic explosives are commonly used for elongated blasting charges. Both overpressure and blast wave impulse are of great importance during clearing of mines.

We adopted compare the method of measurement of blast wave overpressure generated by explosives ^[11]. We measured the intensity of blast waves generated by the explosion of plastic explosives. We used PCB quartz pressure transducers located in metal stick (Figure 4). Transducers were located 2 m and 3 m from the centre of charges. Transducers and charges were placed 1,5 m above the ground. Explosives were located into PCV pipes (ID 35 mm). The mass of explosives was 200 g. Charges were initiated by RDX/TNT boosters. The mass of boosters was 16 g. Blast overpressure signal for plastic explosive with RDX is presented in Figure 5.

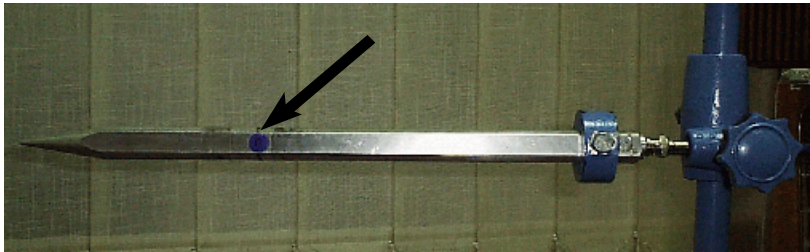


Fig 4. PCB quartz pressure transducers located in metal stick

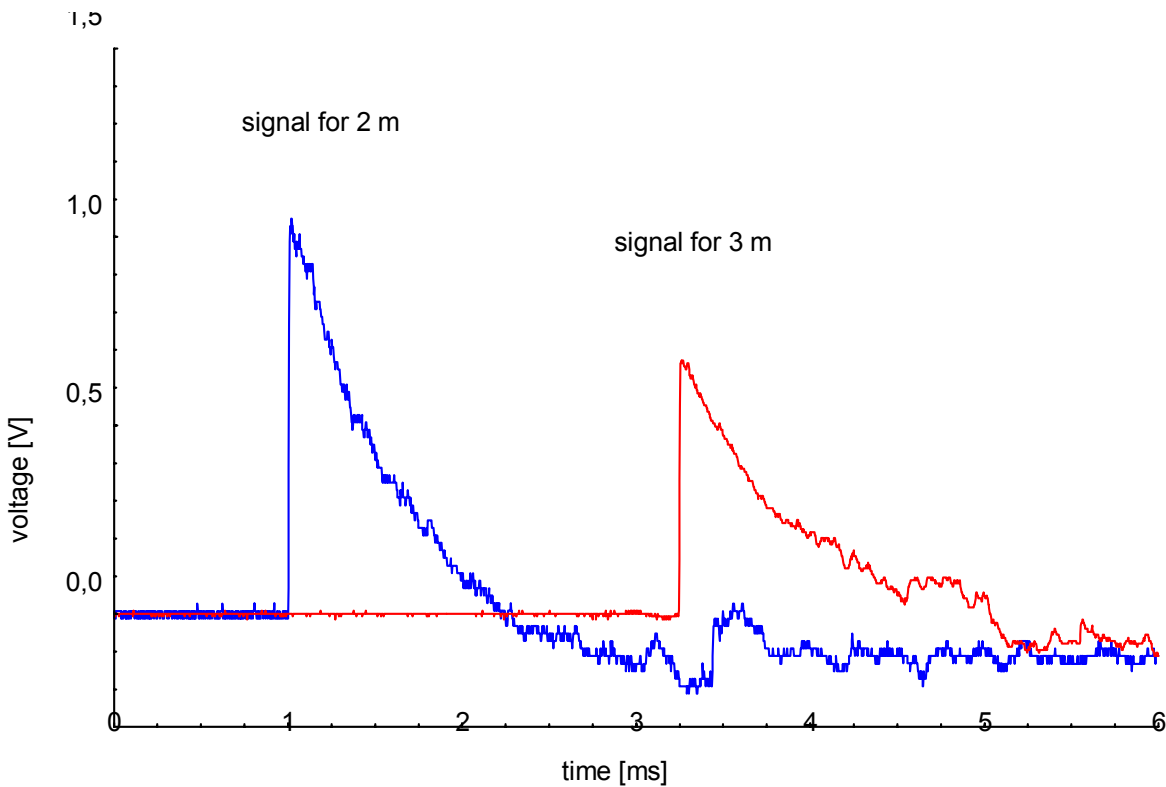


Fig 5. Blast overpressures for plastic explosive containing 84% RDX

Table 5 shows the peak blast overpressures obtained for investigated plastic explosives. Additive of NTO decreases the peak blast overpressure. Additives 20% and 40% NTO slightly decrease blast overpressures of plastic explosive. They were respectively 84,69 kPa, 79,58 kPa for 2 m. Additive 60% NTO decreases peak blast overpressure to 68,40 kPa for 2 m.

Table 2. *The peak blast overpressures for plastic explosive with NTO additives*

Compositions	Density, g/cm ³	Peak overpressures, kPa		Notes
		for 2 m	for 3 m	
0 % NTO 100 % RDX	1,42	86,32	44,48	
20 % NTO 80 % RDX	1,45	84,69	42,11	
40 % NTO 60 % RDX	1,46	79,58	39,11	
60 % NTO 40 % RDX	1,49	68,40	38,55	
80 % NTO 20 % RDX	1,52			Not detonated
100 % NTO 0 % RDX	1,50			Not detonated

2.4 Blast wave impulse

The blast wave impulses generated by plastic explosives were measured. The positive wave impulses correspond with lead block test values [11]. The positive phase impulses were calculated by integrating the blast overpressure signals until a time when the pressure falls below atmospheric pressure. The results are shown in table 3. Additive 20 % and 40 % of NTO slightly decreases positive phase impulse of plastic explosive. The impulses calculated for PE with NTO additives were respectively 39,04 Pa s, 37,91 Pa s for 2 m and 29,97 Pa s, 27,44 Pa s for 3 m. Additive 60 % NTO decreases positive phase impulse to 34,15 Pa s for 2 m.

Table 3. *The peak blast overpressures for plastic explosive with NTO additives*

Compositions	Density, g/cm ³	Positive phase impulse, Pas		Notes
		for 2 m	for 3 m	
0 % NTO 100 %HX	1,42	41,32	31,92	
20 % NTO 80 % HX	1,45	39,04	29,97	
40 % NTO 60 % HX	1,46	37,91	27,44	
60 % NTO 40 % HX	1,49	34,15	25,14	
80 % NTO 20 % HX	1,52			Not detonated
100 % NTO 0 % HX	1,50			Not detonated

3. CONCLUSIONS

Crystalline form and grain size characteristic of used NTO enabled technological processing and ensured for good plasticity.

NTO additives generated the decrease of detonation velocity of plastic explosive. For samples contained 20-60% NTO detonation velocity slightly decreased about 200 m/s with increasing content of 20 % NTO. Sensitivity to impact is the same. Plastic explosive containing 80 % NTO, which were elaborated in steel pipes detonated.

NTO additives decreased peak blast overpressures of plastic explosives. Additive 20 % and 40 % NTO slightly decreased blast overpressures of PE.

NTO additives decreased positive phase impulse of plastic explosives in particular for additives 60 % of NTO.

REFERENCES

- [1] J.P. AGRAWAL: *Recent Trends In High-Energy Materials*, Prog. Energy Combust. Sci., 1998.
- [2] K-Y. LEE, L.B. CHAPMAN, M.D. COBURN, *3-Nitro-1,2,4-triazol-5-one A Less Sensitive Explosive*, J. Energetic Material, 5, 27-33, 1987
- [3] K-Y. LEE, L.B. CHAPMAN, M.D. COBURN: *3-Nitro-1,2,4-triazol-5-one A Less Sensitive Explosive*, US Patent 4733610, 1988
- [4] E.F. ROTHGERY, *Process For The Production of 1,2,4-triazol-5-one*, US Patent 5039816, 1991
- [5] HYUNG SIK KIM, EUN MEE GOH, BANG SAM PARK: *Preparation Method Of 3-Nitro-1,2,4-triazol-5-one By A Process Minimizing Heat Generation During Crystallization*, US Patent 6583293, 2003
- [6] L.B. CHAPMAN: *NTO Development At Los Alamos*, Los Alamos Laboratory, 1989
- [7] S.L. COLLIGNON: *Preparation Of Spheroidal 3-Nitro-1,2,4-triazol-5-one*, Patent USA 4894462, 1990
- [8] BECUWE, A. DELCLOS: *Low-Sensitivity Explosive Compounds for Low Vulnerability Warheads*, Propellants, Explosives, Pyrotechnic, 18, 1-10, 1993
- [9] S. CUDZIŁŁO, A. MARANDA, J. NOWACZEWSKI, R. TRĘBIŃSKI, W.A. TRZCIŃSKI: *Wojskowe Materiały Wybuchowe*, Wyd. Wydział Metalurgii i Inżynierii Materiałowej Politechniki Częstochowskiej, Częstochowa 2000
- [10] BECUWE, A. FRECHE, CH. GAUDIN: *Explosif Composite A Liant Plastiue Polyuretane Charge Au 5-Oxo 3-Nitro 1,2,4- Triazole*, France Patent 2782510, 1990
- [11] K.BUCHALIK, W. WITKOWSKI, R. TRĘBIŃSKI: *Determination o TNT equivalent using the blast wave measurements*, „New Trends In Research Of Energetic Materials Proceedings of the IV Seminar” University of Pardubice, 2001

AN UNDERWATER TEST FOR LWC EMULSION EXPLOSIVES

J. Paszula*, A. Maranda*, B. Gołabek** and J. Kasperski**

* Military University of Technology, 00-908 Warszawa, ul. Kaliskiego 2, Poland

** Blastexpol, Duninów, Poland

Abstract:

In the paper results of some experimental investigations of underwater shock waves parameters generated by explosion of TNT and water-in-oil emulsion explosives are presented. In experiments, the overpressure history in transient shock wave generated by explosion of investigated explosive charges was measured. Moreover numerical evaluation of shock waves energy and bubble energy released during explosion is performed. These calculated parameters could be used as parameters of explosive performance. Comparison of the explosion energy of various kinds of explosives is performed. An influence of aluminium powder on energy released is discussed..

Keywords: *underwater test, emulsion explosives, ability to do work*

1. INTRODUCTION

Many explosives used in blasting industry are accomplished as multi-ingredient mixtures in which the detonation process occurs in a nonideal regime. Differences in physical and chemical characteristics of the components of the mixture results in differences in their reaction susceptibility and overall kinetic mechanisms. In such explosive compositions the chemical reactions in Chapman – Jouguet point, as usually, are still not completed. Some additional reactions continue to proceed in the first stage of expansion of detonation products. As the result, additional energy is liberated after the detonation zone. Therefore, in such explosives the value of detonation velocity which is immediately connected to the detonation energy i.e. energy evolved before the C-J point, cannot be considered as the adequate measure of the energetic performance of the explosives ^[1].

Also other classic methods, like lead block test or ballistic mortar test used for estimation of work capacity do not assure the correct illustration of real energetic potential of nonideal explosives, mainly due to limited mass of samples used in this test probes ^[2, 3, 4]. Performances in underwater explosion test of low water composition (LWC) emulsion explosives as well as TNT were presented.

2. EXPERIMENTAL

2.1 Explosives tested

Emulsion explosives ALAN 1 and ALAN 3 as well as TNT were used in experiments. Base energetic parameters and composition are set up in Table 1.

Table 1. *Composition and energetic parameters of tested explosives*

Parametr MW		Explosives		
		Emulsion explosives		TNT
		ALAN 1	ALAN 3	
Composition [cg/g]	Nitrates	84,26	84,48	-
	Aluminium	2,07	5,00	-
	Water	4,02	3,27	-
	Others	9,65	7,25	-
Mass density, [kg/m ³]		1170	1150	1580 ± 5
Work capacity (Lead block), [cm ³]		-	310	300
Heat of explosion, [kJ/kg]		3640,60	4307,29	4533
Ideal work of explosion, [kJ/kg]		3046,38	3581,13	4500

In Fig. 1 we present exemplary explosives charges. In experiments we used commercial form of emulsion explosives and pressed charges of TNT.



Fig 1. Exemplary explosives charges

2.2 Shock waves overpressure in underwater test

During an underwater explosion appreciable part of explosion energy is following through surrounding water as shock waves. The gas bubble expands due to high internal pressure and temperature generated during explosion. Because of the water inertia, the bubble expands so long, that inner pressure drops below hydrostatic pressure of surrounding water. And then bubble reaches the maximum volume. Difference between hydrostatic and bubble pressure is reason that water starts moving into the centre of the bubble. And the bubble collapses.

We can record of prime shock waves and time of bubble first collapse. These records allow us to calculate shock waves and bubble energy. We used well-known [5] equation to calculate:

- The shock energy:

$$E_s = k_s \int_0^{6,7\theta} p^2(t) dt$$

where: θ - characteristic time; k_s – coefficient.

- The bubble energy:

$$E_b = k_b T_b^3$$

where: T_b - characteristic time; k_b – coefficient.

Time-overpressure distribution in the blast wave generated by investigated explosive charges was measured by pressure gauges of PCB Piezotronics, Inc, Serie 138A. The gauges register overpressure in the transient shock wave, sliding on the working surface of the device. It works as an electromechanical transducer that converts the pressure (ratio of the force acting on the working surface of the active element to magnitude of this surface) into the proportional voltage signal.

The sketch of the experimental set is presented in Fig. 2.

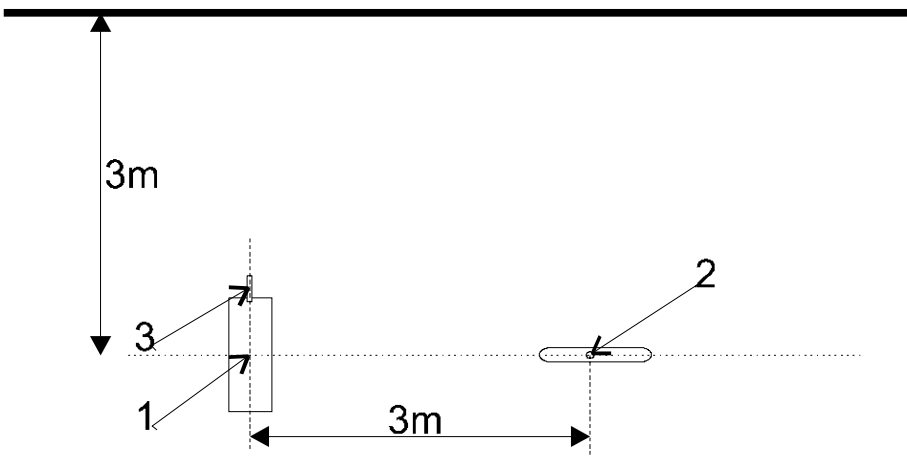


Fig 2. Experimental set up: 1 – explosive charge; 2 – pressure gauge; 3 - detonator

3. RESULTS OF EXPERIMENTS AND DISCUSSION

In the Fig 3 an exemplary registration of overpressure course for ALAN 1 explosive is presented. The charges of 1.0 kg of emulsion explosives and 0.5 kg of pressed TNT were used. The registration is made at the distance and depth of 3 m. Upon the registered overpressure history the maximal pressure value is estimated (see Table 2). In the Fig 4 effect of underwater explosion is presented.

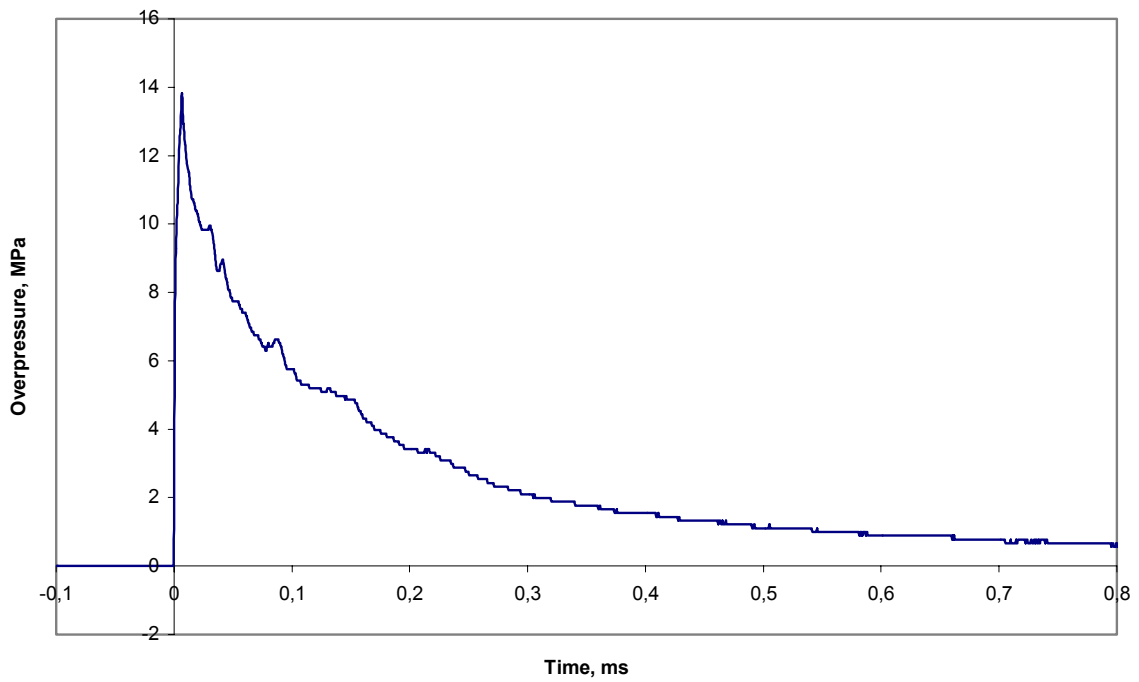


Fig 3. Overpressure vs time diagram for ALAN 1



Fig 4. Effect of underwater explosion of ALAN 1 charge

In the Table 2 the results of overpressure measurements and time of bubble first collapse, as well as calculated value of shock wave and bubble energy for investigated explosives are presented.

Time between primary shock wave and first bubble pulse is base to calculate bubble energy. Time of first bubble pulse record ALAN 1 is presented on Fig 5.

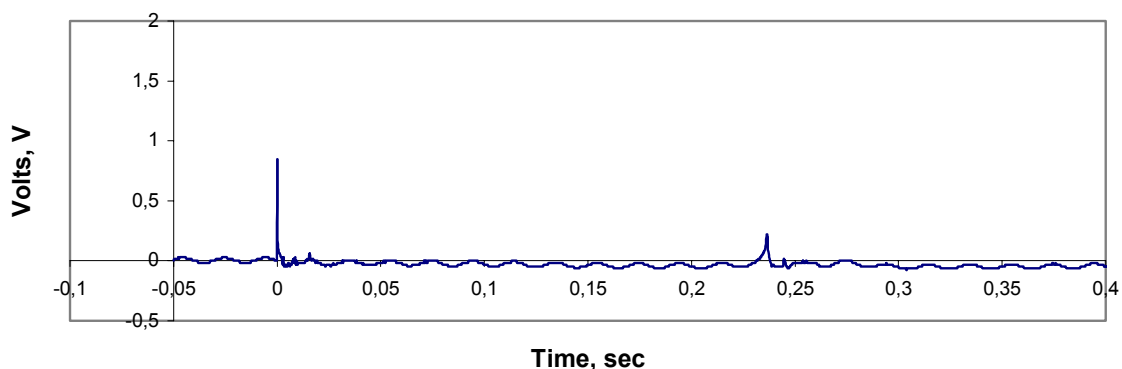


Fig 5. Bubble pulse time period record

Table 2. *Measured underwater shock wave overpressure and calculated parameters with standard deviation for investigated explosives*

MW	Δp_{\max} , MPa	T_b , ms	E_{FU} , MJ/kg	E_b , MJ/kg	A_0 , MJ/kg
TNT	$12,13 \pm 0,77$	184 ± 1	$2,11 \pm 0,11$	1,73	3,84
ALAN 1	$13,19 \pm 0,67$	235 ± 1	$1,42 \pm 0,07$	1,78	3,20
ALAN 3	$13,14 \pm 0,82$	239 ± 1	$1,27 \pm 0,07$	1,87	3,14

As an important factor influencing upon the detonation parameters aluminium particles reaction degree inside the detonation zone can be indicated. In first stage aluminium particles absorb energy and act as an inert additive. The process of aluminium activation occurs on behalf of energy liberated in other chemical reactions. Absorption of energy evolved in parallel chemical reactions aluminium alters the kinetic of this process. Therefore, aluminium lowers detonation parameters, in particular the detonation velocity.

The main output of energy produced in reactions of aluminium combustion occurs after the as the C-J point. The liberated energy influences the process of expansion of detonation products. Due to relatively large energy efficiency of aluminium oxidation the energy liberated in aluminium combustion can bring a considerable contribution to the work capacity of expanding gases. Therefore, value of explosion work (A_0 – as a sum of shock wave energy and bubble energy) can be an important indicator of energetic performance of explosive charge. The comparison of overpressure magnitude attained in underwater shock wave of considered explosives are depicted in Fig 6 and 7.

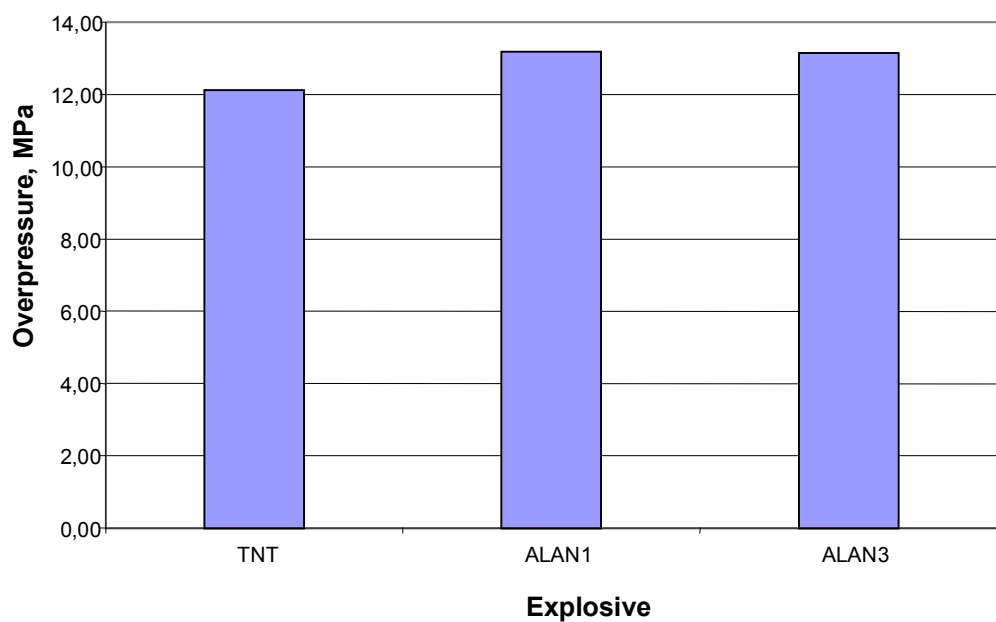


Fig 6. Maximum underwater shock wave overpressure

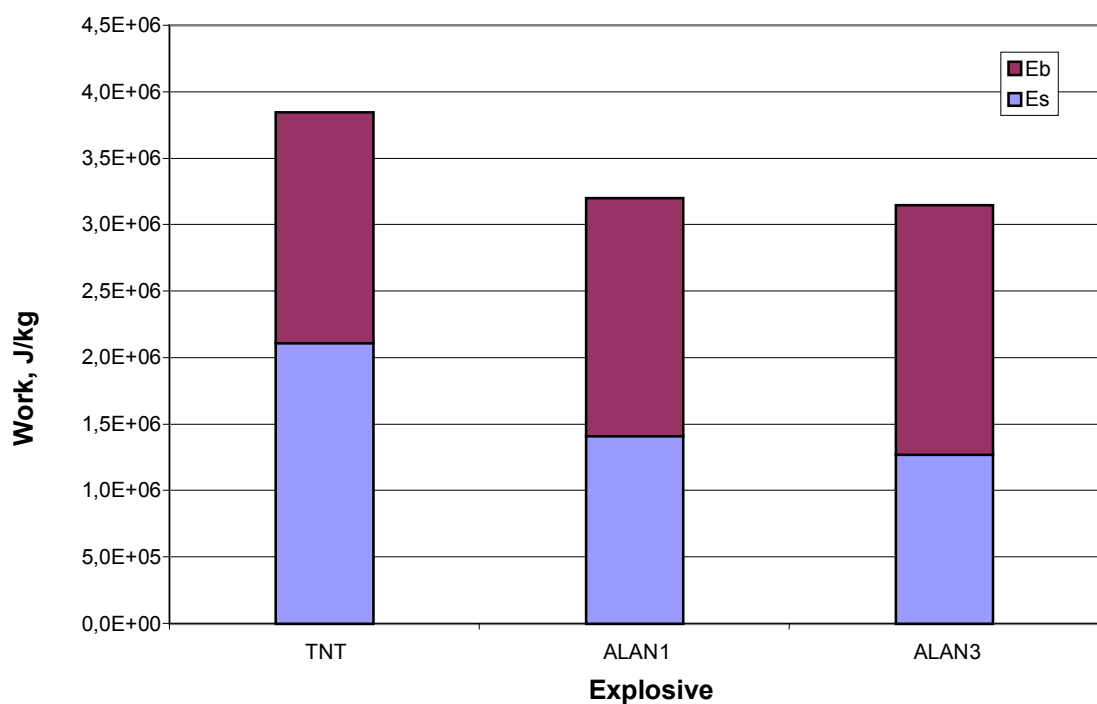


Fig 7. Explosion work for tested explosives

As can be seen, the values of maximum overpressure for emulsion explosive are nearly equal despite higher detonation parameters of ALAN 1. However, ALAN 3 has higher heat of explosion (see table 1). In Fig 7 we can see, that greater addition of aluminum powder in ALAN 3 caused the greater share of bubble energy in explosion work than ALAN 3. Therefore one can conclude that the value of underwater explosion work is a useful characteristic of the working potential of nonideal explosives.

4. CONCLUSIONS

In the paper analysis of underwater explosion parameters of mining explosives are performed. Emulsion explosives of water-in-oil type and TNT were investigated. Values of maximal overpressure magnitude in underwater shock wave generated by explosion of investigated explosive as well as time of first bubble collapse are considered.

Explosive characteristics of heterogeneous explosive mixtures, like emulsion explosives are considered. An attention is paid to the influence of additional energy output, which can proceed after the detonation zone. In this case, the detonation velocity cannot be the measure of the global explosion energy as it is strictly coupled with the energy liberated before the C-J point, through the detonative adiabat. The additional energy that is produced during expansion of detonation products will enhance intensity of loading wave generated in material surrounding the explosive charge. Therefore, by measuring the underwater shock wave intensity and the time of bubble first collapse, we can calculate a work of expansion of tested explosives. So, a more integral characteristic of energy output occurring in explosion could be obtained.

In the paper, experimental measurements as well as numerical evaluation of blast field produced by explosive charges is performed. As can be seen from obtained results, in the case of aluminized explosives when the detonation velocity is lowered due to inertial effects of aluminum particles in the first stage of the detonation process, the value of blast overpressure can give a more realistic estimation of the energy performance.

The proposed method can be used as the optional characteristic of the explosive performance. However, the more comprehensive methodic should be elaborated, to introduce this approach as the criterion for estimation energetical efficiency of explosives.

Acknowledgements

This research is supported by the State Committee of Scientific Research of Poland, Grant 5 T12A 033 23

REFERENCES

- [1] D. L. ORNELLAS: *Calorimetric determinations of the heat and products of detonation for explosives: October 1961 to April 1982*. Report UCRL – 52821, Lawrence Livermore National Laboratory
- [2] P-A. PERSSON, R. HOLMBERG, J. LEE: *Rock Blasting and explosives engineering*, Ch. 4, Boca Raton, Florida, 1994
- [3] P. WOLLERT-JOHANSEN, *Underwater testing of slurry explosives*, Prop. Expl. Pyrot., 5, No. 2/3.
- [4] P.V. SATYAVRATAN, R. VEDAM, *Some aspects of underwater testing method*, Prop. Expl. Pyrot., 5, 62-66, 1980
- [5] G. BJARNHOLT, R. HOLMBERG, *Explosive expansion works in underwater detonations*, Proceedings Sixth Symposium (International) on Detonation, Coronado, California, August 24 – 27, 1976

PREDICTION OF THERMODYNAMIC CONDITIONS FOR NITROESTER VAPOR CONDENSATION ON THE SURFACES OF PROCESS APPARATUS DURING THE PRODUCTION OF ENERGETIC MATERIALS

D.V. Pleshakov and Y.M. Lotmentsev

Mendeleev University, Department of Chemical Engineering,
125047 Miusskaya pl.9, Moscow, Russia

Abstract:

A calculation procedure has been developed for finding thermodynamic conditions under which nitroglycerine, diethylene glycol dinitrate, and triethylene glycol dinitrate vapors are condensed on the surfaces of process apparatus during the production of energetic materials. Temperature – (plasticizer content in dry air) diagrams have been calculated and mapped. The diagrams allow one to estimate the condensation temperature of supersaturated nitroester vapor and to calculate the condensate weight. A procedure has been proposed for measuring the partial saturated vapor pressure of a plasticizer under the production conditions.

Keywords: *nitroester, prediction of thermodynamic condition for condensation, energetic material*

1. INTRODUCTION

Esters of polyatomic alcohols and nitric acid, such as nitroglycerine (NG), diethylene glycol dinitrate (DEGDN), and triethylene glycol dinitrate (TEGDN), are components of various energetic materials. Nitroesters are employed for plasticizing cellulose nitrates in the design of double-base gun powders and propellants and for plasticizing synthetic polymers in the production of mixed solid propellants. NG, DEGDN, and TEGDN are known to be powerful explosives with high impact and friction sensitivities. Therefore, plasticizer separation from energetic materials is undesirable. Nitroester drops can appear when the components of gun powders or propellants have poor thermodynamic affinity or when supersaturated plasticizer vapor is condensed on the surface of process apparatus. The thermodynamic affinity of nitroesters to cellulose nitrates and synthetic polymers has been discussed in ^[1-3]. Our goal in this work was to predict whether NG, DEGDN, and TEGDN vapor could condense on the surface of process apparatus and to estimate the condensation temperature and condensate weight. To this end, temperature - (plasticizer content of dry air) diagrams have been designed. A procedure has also been developed for measuring the partial vapor pressure of nitroesters under process conditions.

2. RESULTS AND DISCUSSION

To design temperature - (plasticizer content of dry air) diagram, one must know the plasticizer saturated vapor pressure as a function of temperature. Saturated vapor pressures of NG, DEGDN, and TEGDN were measured in ^[1, 2] by means of static and gas-

chromatography dynamic methods. The results of these measurements are compiled in Table 1.

Table 1. The saturated vapor pressure of nitroesters

Temperature, °C	Saturated vapor pressure, Pa		
	NG	DEGDN	TEGDN
15	0.033	0.24	0.023
20	0.058	0.39	0.040
25	0.10	0.60	0.067
30	0.17	0.92	0.11
35	0.28	1.38	0.18
40	0.49	2.16	0.31
45	0.69	2.89	0.47
50	1.16	4.26	0.69
55	1.99	6.49	0.99
60	2.86	9.03	1.72

The saturated vapor pressure versus temperature curves were fitted to the following equations:

$$\text{for NG, } \ln p^0 = 29.62 - \frac{9518}{T} \tag{1}$$

$$\text{for DEGDN, } \ln p^0 = 25.31 - \frac{7699}{T} \tag{2}$$

$$\text{for TEGDN, } \ln p^0 = 28.19 - \frac{9210}{T} \tag{3}$$

Here, T is temperature in Kelvin degrees.

An enthalpy versus water content diagram for moist air (Mollier’s diagram) ^[4] was chosen to be a propotype for temperature - (plasticizer content of dry air) diagrams. Temperature t (°C) is related to the plasticizer content (kg/kg dry air) through

$$x = \frac{M}{M_{air}} \frac{\varphi p^0(t)}{P_{air} - \varphi p^0(t)} \tag{4}$$

Here, M is the plasticizer molecular mass; M_{air} is the molecular mass of dry air, equal to 0.029 kg/mol; $p^0(t)$ is the saturated vapor pressure of a plasticizer calculated from eqs. (1) - (3); and P_{air} is air pressure. Our calculations were made for the atmospheric pressure of $P_{air} = 745 \text{ mmHg} = 99\,325 \text{ Pa}$ (taken as a year-average value for the central regions of Russia and Europe ^[4]) and for working pressure of $P_{air} = 10 \text{ mmHg} = 1333.12 \text{ Pa}$ (this is the residual air pressure in an apparatus at blending of the components of an energetic material). For φ , an expression holds:

$$\varphi = \frac{p}{p^0} \tag{5}$$

where p is the partial vapor pressure of the plasticizer. Thus, φ is an analogue of the relative humidity of moist air.

Figures 1 - 6 present the temperature - (plasticizer content of dry air) diagrams for NG, DEGDN, and TEGDN calculated from eqs. (1) - (5). φ ranges from 0 to 100%; temperature, from 15 to 60 °C. $\varphi = \text{const}$ lines form a bundle of diverging lines radiating from one point (not shown) with coordinates $x = 0$ and $t = -273.15$ °C (0 K). Line $\varphi = 100\%$ corresponds to the saturated plasticizer vapor at a chosen temperature. This line is the lower boundary of the working area of the diagram; this working area describes the state of dry air unsaturated with a plasticizer. The area of the diagram lying under line $\varphi = 100\%$ refers to plasticizer-supersaturated air and is of no practical interest.

Figures 7 and 8 show the partial vapor pressures of nitroesters as a function of their air content. The diagrams were calculated from

$$p = \frac{P_{air}x}{\frac{M}{M_{air}} + x} \quad (6)$$

For the efficacy of use of these diagrams, one needs a procedure for determining the plasticizer partial vapor pressure under process conditions, i.e., in the volume of blenders, containers, pipings, and other process apparatus.

The experimental determination of nitroester partial vapor pressures under production conditions is based on the same principles as the dynamic gas-chromatographic determination [2]. The measurement procedure involves two major stages: gas extraction and chromatographic analysis. The gas extraction stage is schematized in Fig. 9. Air and plasticizer vapor are pumped put from the volume of an apparatus (e.g., a blender) by means of a vacuum pump. A gas mixture passes through a chromatographic column. During passage, plasticizer vapor is sorbed in the head of the column and is retained there during the entire gas extraction period.

When gas extraction is over (its duration is recorded with a stopwatch), chromatographic analysis starts. The column is mounted in the thermostat of a chromatograph, a carrier gas is admitted to the column, and temperature is raised to 140 – 150 °C. The plasticizer that has been sorbed during extraction leaves the column and is detected with a flame-ionization detector. To process the chromatograms, a calibration curve that relates the signal area to the plasticizer weight is used.

The concentration and partial vapor pressure of the nitroesters in the volume of process apparatus are calculated from

$$c = \frac{mT_R}{w\tau T_E} \left(1 + \frac{P_2 - P_1}{P_1} \right) \quad (7)$$

$$p = \frac{c}{M} RT_E \quad (8)$$

Here m is the plasticizer weight calculated from the surface area of a chromatographic peak, w is the output of a vacuum pump, τ is the gas extraction duration, T_R is the temperature of the working room, T_E is the temperature inside an apparatus, M is the

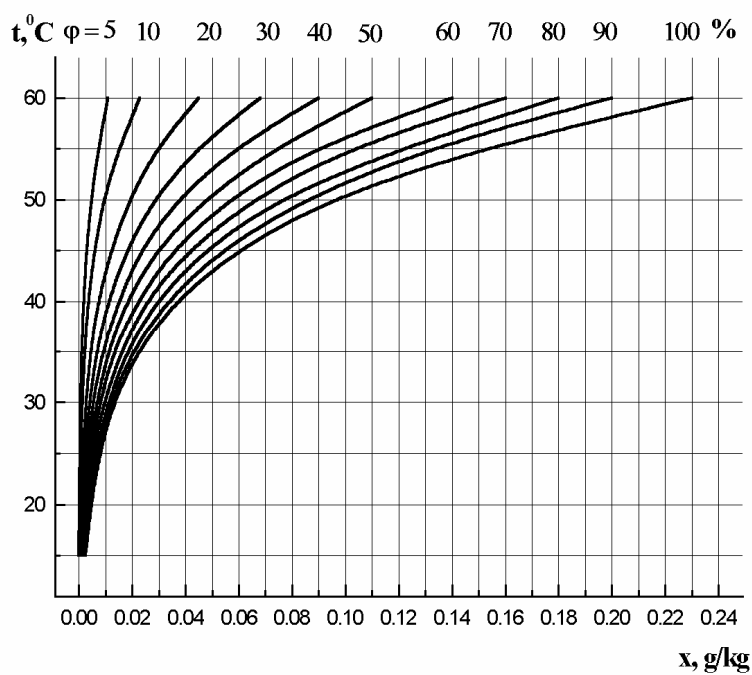


Fig. 1. Temperature vs. NG concentration in dry air diagram
 $P_{air} = 745 \text{ mmHg} = 99\,325 \text{ Pa}$.

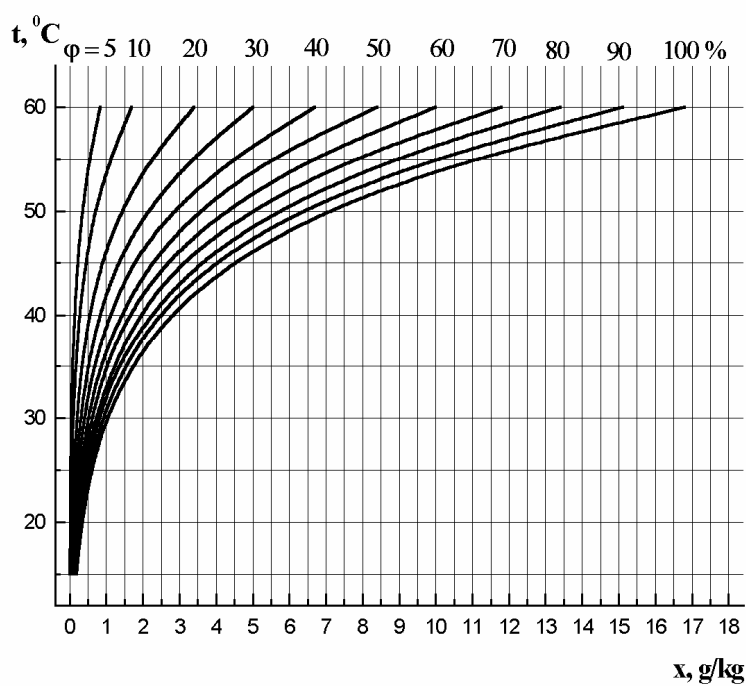


Fig. 2. Temperature vs. NG concentration in dry air diagram
 $P_{air} = 10 \text{ mmHg} = 1333.22 \text{ Pa}$

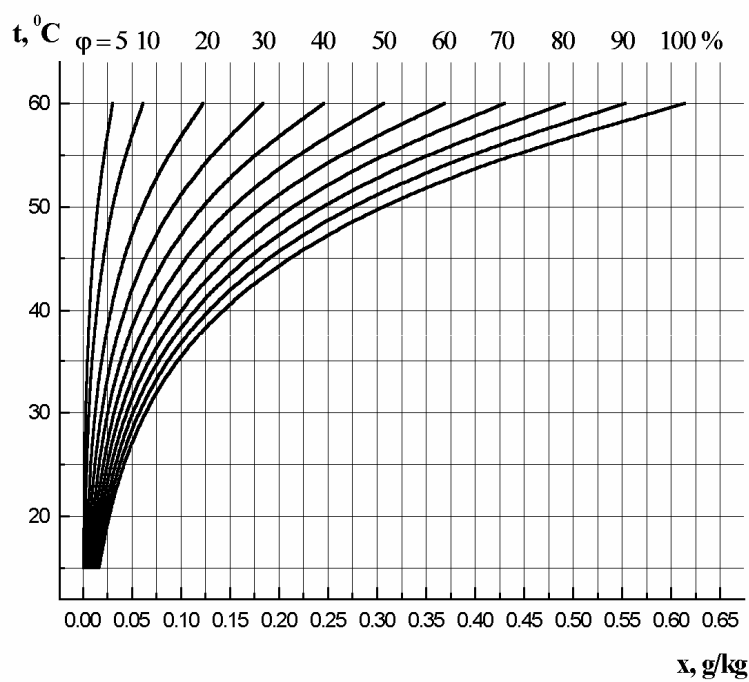


Fig. 3. Temperature vs. DEGDN concentration in dry air diagram
 $P_{air} = 745 \text{ mmHg} = 99\,325 \text{ Pa}$

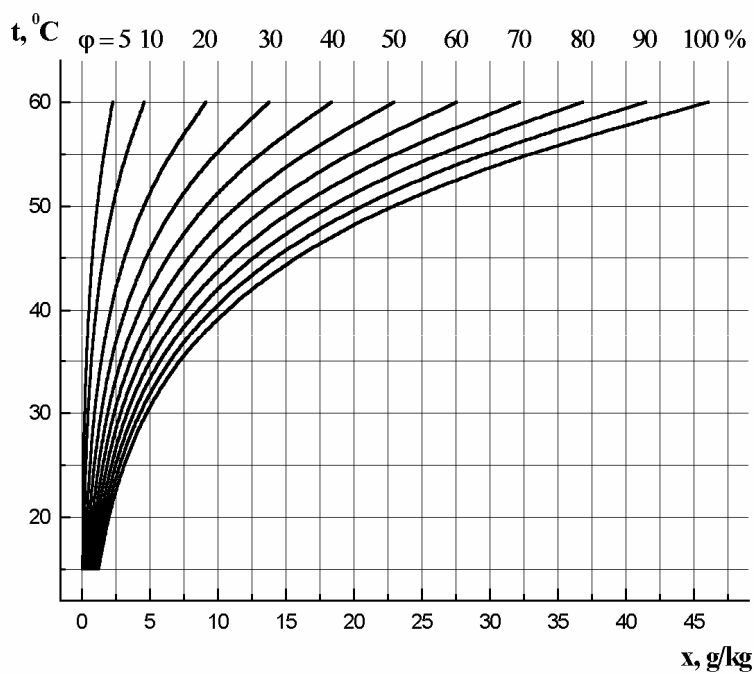


Fig. 4. Temperature vs. DEGDN concentration in dry air diagram
 $P_{air} = 10 \text{ mmHg} = 1333.22 \text{ Pa}$

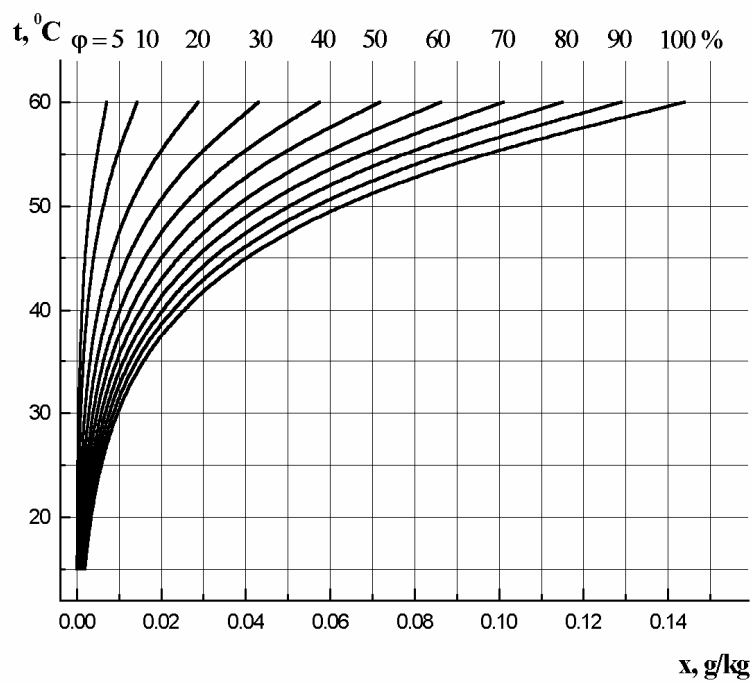


Fig. 5. Temperature vs. TEGDN concentration in dry air diagram
 $P_{air} = 745 \text{ mmHg} = 99\,325 \text{ Pa}$

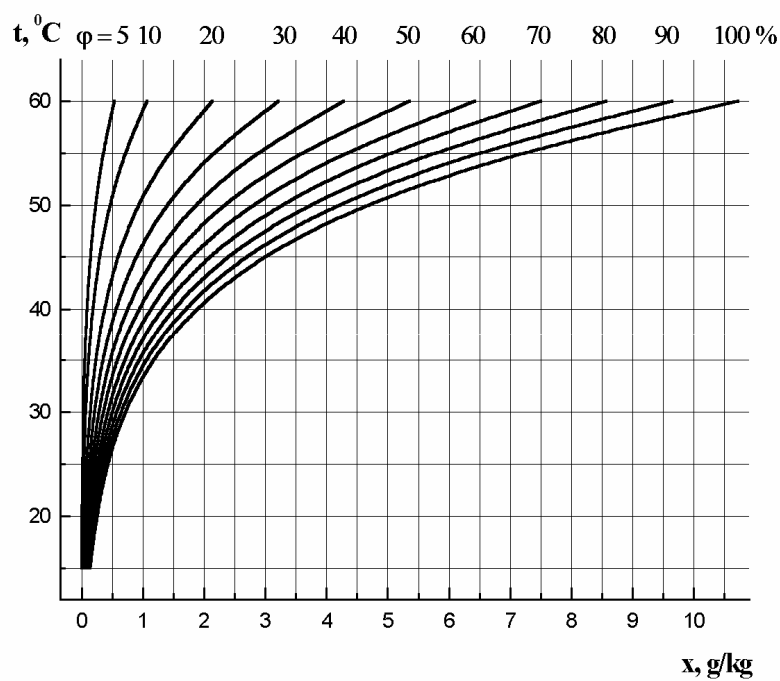


Fig. 6. Temperature vs. TEGDN concentration in dry air diagram
 $P_{air} = 10 \text{ mmHg} = 1333.22 \text{ Pa}$.

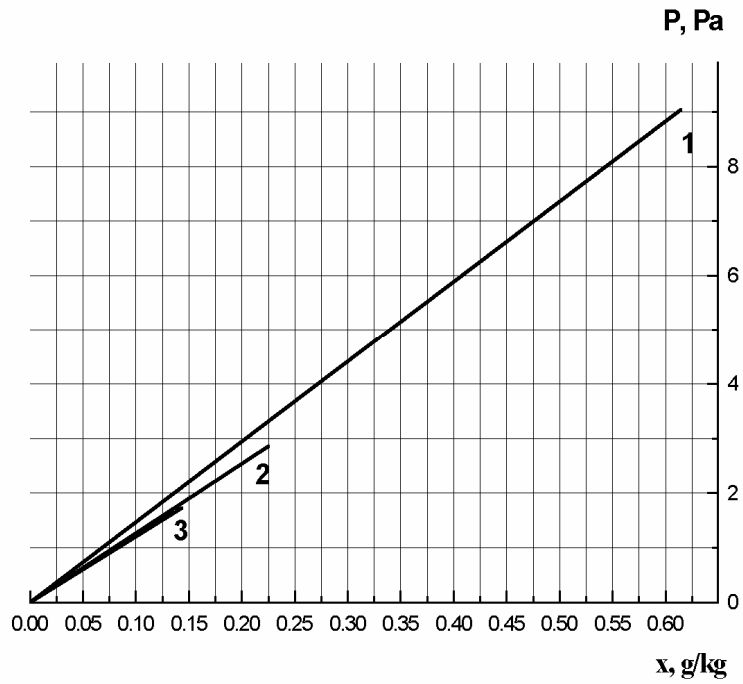


Fig. 7. Partial pressure vs. concentration in dry air plots for DEGDN (1), NG (2), and TEGDN (3). $P_{air} = 745 \text{ mmHg} = 99\,325 \text{ Pa}$

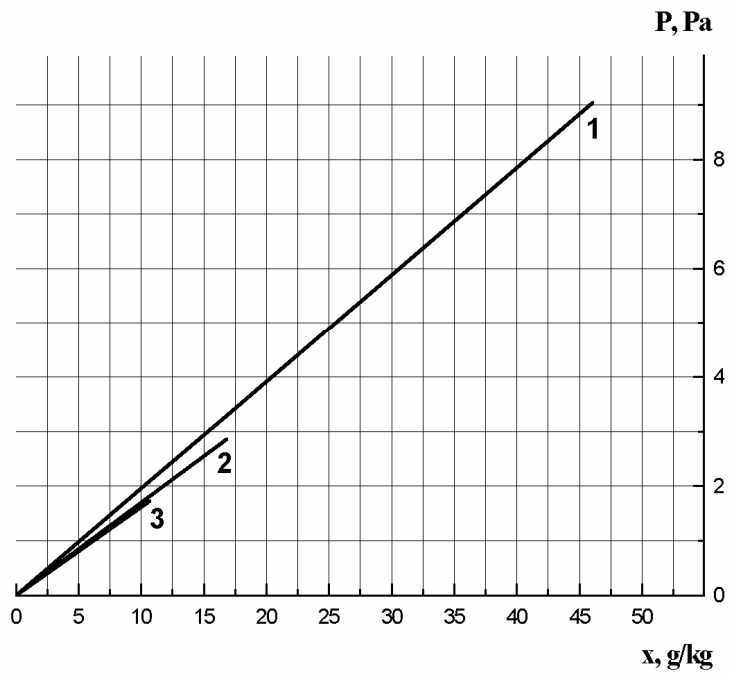


Fig. 8. Partial pressure vs. concentration in dry air plots for DEGDN (1), NG (2), and TEGDN (3). $P_{air} = 10 \text{ mmHg} = 1333.22 \text{ Pa}$

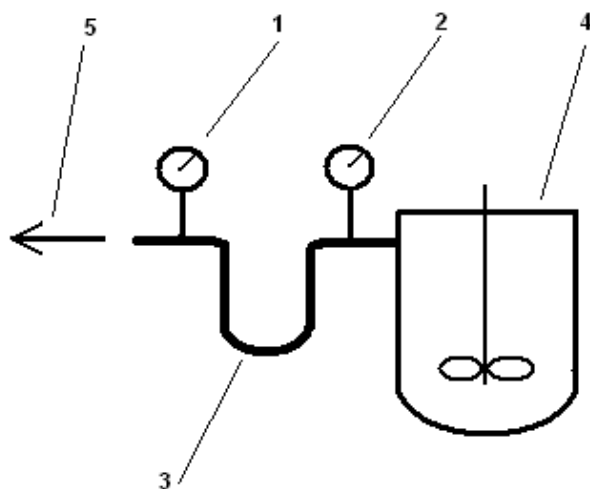


Fig. 9. Schematics of gas extraction. Notation: (1, 2) pressure gages, (3) chromatographic column, (4) blender, and (5) vacuum line

molecular mass of the plasticizer, and P_1 and P_2 are the readings of pressure gages 1 and 2 (Fig. 9).

Once the plasticizer partial vapor pressure has been measured, one can determine x from the curves plotted in Figs. 7 and 8 and find a point on the diagram (Figs. 1 - 6) to characterize the state of the system. After this, designing a straight line parallel to the temperature axis until it meets curve $\varphi = 100\%$, one finds the plasticizer condensation temperature T^* . If the temperature of the system drops below T^* (e.g., down to T^{**}), the ester condensate weight is easily found from

$$m_c = (x^* - x^{**}) \frac{P_{air} V_E}{RT_E} M_{air} \quad (9)$$

where V_E is the volume of the apparatus (e.g., a blender or container), and x^* and x^{**} are the abscissas of curve $\varphi = 100\%$ at ordinates T^* and T^{**} .

The ester condensate weight in a vacuum piping is calculated from an analogue of the above equation:

$$m_c = (x^* - x^{**}) \frac{P_{air} w \tau}{RT_E} M_{air} \quad (10)$$

Here, τ is the operation time of a vacuum pump, and T^{**} corresponds to the temperature of a cold portion of the piping where plasticizer vapor condenses.

3. CONCLUSION

In this work we have calculated and plotted temperature - (plasticizer content of dry air) diagrams for nitroglycerine, diethylene glycol dinitrate, and triethylene glycol dinitrate. The calculations referred to the atmospheric pressure of $P_{air} = 745 \text{ mmHg} = 99\,325 \text{ Pa}$ and working air pressure $P_{air} = 10 \text{ mmHg} = 1333.22 \text{ Pa}$ in the temperature range 15 - 60 °C.

We have developed a procedure for measuring partial vapor pressure for nitroesters in the free volume of a process apparatus. This procedure and the temperature versus plasticizer concentration of dry air diagrams allow one to ascertain whether nitroester vapor could condense on the surfaces of process apparatus, to determine the condensation temperature, and to calculate the condensate weight.

REFERENCES

- [1] YU.M. LOTMENTSEV AND D.V. PLESHAKOV: *Phase State of Nitrocellulose Plasticized with Trinitroglycerin*, Propellant, Explosives, Pyrotechnics, vol. 22, p. 203-206, 1997
- [2] D.V. PLESHAKOV, YU.M. LOTMENTSEV, SHAO ZIQIANG, N.N. KONDAKOVA AND A.V. LUKASHEV: *Solvation Effects and Thermodynamics of Plasticization of Cellulose Nitrate*, Polymer Science, A, vol. 41, no. 3, p. 364-370, 1999
- [3] D.V. PLESHAKOV, YU.M. LOTMENTSEV, N.N. KONDAKOVA, T.A. BESTUZHEVA, E.A. BUTENKO, I.N. KOLESNIKOV AND E.V. ZHURAVLEV: *Thermodynamic Stability of Polyurethane Binders*, Proc. of International Autumn Seminar on Propellants, Explosives and Pyrotechnics, Guilin, China, p. 156-160
- [4] A.G. KASATKIN: *Osnovnyie protsessyi i apparaty khimicheskoy tekhnologii* (Fundamental Processes and Apparatuses of Chemical Technology), Moscow: Khimiya, p. 586-590, 1973

STUDY OF ELECTRON DENSITY OF MOLECULES, INTERMOLECULAR FORCES AND IMPACT SENSITIVITY OF EXPLOSIVES

Miroslav Pospíšil* and Pavel Vávra**

* Charles University, Faculty of Mathematics and Physics,
Ke Karlovu 3, 12116 Prague 2, Czech Republic

** University of Pardubice, Department of Theory and Technology of Explosives,
Studentská 95, 53210 Pardubice, Czech Republic

Abstract:

The electron densities for the selective set of twenty explosives with composition C-H-N-O were calculated (i) for individual molecules and (ii) for molecules placed in crystal cell. Indirect linearity of absolute difference of charges for bonds C-NO₂, N-NO₂ and O-NO₂ versus the length of the bond was founded in both cases. The influence of non-covalent hydrogen bonds for distinctly decreasing of the impact sensitivity was confirmed. On the base of results from experimental methods such as the impact sensitivity and theoretical methods such as molecular mechanics and molecular density calculations for selected set of twenty explosives the possibilities of prediction for impact sensitivity of new energetic materials are discussed.

Keywords: *Impact sensitivity, electron density, energetic materials,
molecular mechanics and hydrogen bond*

1. INTRODUCTION

The research of the structure-properties relationship for the energetic materials is an object of permanent interest. The reason is to create a strategy for the prediction of parameters new (still not ready) energetic materials (EM) with high-energy content and acceptable stability and impact sensitivity. The authors of excellent review^[1] quote well-known linear relation between energy of decomposition and the impact sensitivity. This linear relation pays generally also for detonation energy^[2] apart from several exemptions. It is very probable, that the van der Waals intermolecular forces and especially non-covalent hydrogen bonds have big influence for the impact sensitivity of energetic material crystal cells.^[3]

The definitions and practical methods for determination of the impact sensitivity are in the center of wide debate now. The results of drop hammer test are the most used criterion for the determination of the impact sensitivity of investigated energetic materials because of the most data are disposal. But for many objective reasons, which we can only agree with, this test is very often criticized.

In this work the values of drop hammer test are used (drop h_{50} for 2.5 kg hammer), but the values are differentiate only as higher or lower impact sensitivity, when the criterion for dividing line is drop $h_{50} \sim 50$ cm. The aim of this work was describe the influence of partial charge distribution of the bonds C-NO₂, N-NO₂ and O-NO₂ versus the impact sensitivity of

(i) individual molecules and (ii) molecules placed in crystal cell. In case of molecules in crystal cell the significant influence of van der Waals and non-covalent Hydrogen bonds was indicated.

2. CALCULATION

The NO₂ groups in tested selected set of twenty explosives are connected to carbon, nitrogen and oxygen in different groups. Two different bonds are also included in one molecule in several cases (C-NO₂ and N-NO₂ or O-NO₂ and N-NO₂). The structure parameters of presented energetic materials are determined from X-ray or neutron crystal structure analysis (references cited in table 1). The results of calculated detonation energy (E_D) per volume cell ^[5] and the results of determined drop **h**₅₀ ^[6] are listed in table 1.

Table 1. *Basic parameters of selected explosives*

Number	EM	ρ	H _f	P	D	E _D	h	Ref.
		g.cm ³	kcal.mol ⁻¹	GPa	km.s ⁻¹	kJ.cm ⁻³	cm	
1	HNIW	2,03	99,2	43,99	9,620	9,684	23	7
2	HMX	1,90	17,8	38,08	9,119	8,858	26	8
3	BTNEN	1,96	-175,9	39,08	9,157	8,861	5	9
4	BTNEU	1,86	-71,7	36,57	8,993	8,657	17	10
5	TNAZ	1,84	3,0	36,08	8,960	8,614	21	11
6	RDX	1,80	14,7	34,24	8,786	8,321	24	12
7	PETN	1,77	-129,0	33,13	8,686	8,157	12	13
8	DADNE	1,88	-32,0	33,60	8,591	7,889	120	14
9	DINA	1,67	-74,0	28,54	8,208	7,348	23	15
10	BDNPN	1,73	-65,3	29,30	8,226	7,343	29	16
11	NG	1,59	-118,7	27,07	8,121	7,224	10	17
12	DNI	1,76	4,9	27,50	7,926	6,806	100	18
13	TATB	1,94	-33,3	29,34	7,958	6,710	320	19
14	NQ	1,77	-22,0	27,01	7,843	6,650	177	20
15	TE	1,73	8,0	26,29	7,792	6,590	32	21
16	DATB	1,84	-23,6	26,78	7,719	6,394	320	22
17	TNA	1,77	-18,0	24,90	7,530	6,131	177	23
18	HNS	1,74	16,1	22,97	7,270	5,731	54	24
19	TNB	1,68	-24,6	21,97	7,189	5,631	100	25
20	TNT	1,65	-18,0	20,54	6,991	5,336	160	26

The calculation of molecular density for individual molecules was carried out in WinMOPACv2.0, method AM1. The molecular density for molecules placed in crystal structure was carried out in *Cerius*² modeling environment ^[27], method charge equilibrium approach (Qeq) ^[28]. The crystal structures were built in *Crystal Builder module* on the basis of published X-ray and neutron diffraction data. These structures were not anyway changed after the building during the calculation. The total crystal energy of these selected energetic materials was determined in *Minimizer module* using the universal force field (UFF) ^[29]. The parameters in the universal force field characterize all atoms in the periodic table. The value of total crystal energy and its valence and non-bond energy components were determined. The valence components are bond, angle, torsion and inversion energy terms and non-bond

components are van der Waals and Coulomb energy terms. Van der Waals energy terms are calculated with well-known Lenard-Jones potential functional form ^[30] and Coulomb energy terms are calculated on the base Coulomb principle. The hydrogen bond energy terms are calculated as a part of non-bond energy terms ^[27, 31]. The calculated values are presented in the table 2 for different bond groups.

Table 2. *Selected properties for investigated set of explosives*

	delta $\Delta 1$	Bond length	Impact sensitivity	Ew/Z	Es/Z	Ew+Ec/Z	delta $\Delta 2$
	e	pm	cm	kcal/mol	kcal/mol	kcal/mol	e
Nitramines	N-NO₂						
HNIW	0,965	142,4	23	47,6	150,175	-83,25	0,4397
HMX	0,921	137,3	26	37,85	-60,2	-145,95	0,4397
BTNEN	0,999	137,5	5	33,975	234	45,425	0,5469
TNAZ	0,845	135,1	21	-0,225	162,2	-37,788	0,4886
RDX	0,852	139,8	24	31,8	79,15	-60,188	0,4403
DINA	0,925	135,7	23	8,7	54,775	-59,925	0,4368
BDNPN	1,018	136,7	29	22,5	155,2	-27,6	0,509
<u>NQ</u>	0,958	133,5	177	35,444	-4,288	-83,063	0,3724
TE	0,904	134,8	32	16,2	41,45	-103,525	0,4667
Nitroalifates	C-NO₂						
BTNEN	0,686	154,4	5	33,975	234	45,425	0,2702
BTNEU	0,692	153	17	20,55	187,8	42,3	0,3158
TNAZ	0,682	151,7	21	-0,225	162,2	-37,788	0,1115
<u>DADNE</u>	1,124	142,6	120	25,75	89,875	-12,5	0,2611
BDNPN	0,594	153	29	22,5	155,2	-27,6	0,085
O-nitrates	O-NO₂						
PETN	0,926	140,4	12	8,95	293,1	-94,35	0,8062
DINA	0,906	140,5	23	8,7	54,775	-59,925	0,7306
Ng	0,893	141,4	10	6,9	201,75	-15,7	0,7136
Nitroaromates	C-NO₂						
TE	0,697	149,7	32	16,2	41,45	-103,525	0,0104
<u>TATB</u>	1,009	142,2	320	376,9	480,75	356,05	0,1524
<u>DNI</u>	0,747	147,1	100	56,425	162,838	80,388	0,3208
<u>DATB</u>	0,899	151	320	135,1	214,6	100,7	0,0647
<u>TNA</u>	0,819	147,4	170	56,775	84,825	0,375	0,0384
HNS	0,716	147,1	54	32,025	28,425	-107,65	0,0453
<u>TNB</u>	0,728	149,3	100	14,706	5,213	-63,056	0,0059
TNT	0,73	147,4	160	4,613	48,188	-55,3	0,0486

Note: Underline EM contain non-covalent Hydrogen bonds.

ABBREVIATIONS:

HNIW – 2,4,6,8,10,12-hexanitro-2,4,6,8,10,12-hexaazatetracyclo [5.5.0.0^{5,9}.0^{3,11}]dodecane
HMX – 1,3,5,7-tetranitro-1,3,5,7-tetraazacyclooctane
BTNEN – di (2,2,2-trinitroethyl) nitramine
BTNEU – di (2,2,2-trinitroethyl) urea
TNAZ – 1,3,3-trinitroazetidine
RDX – 1,3,5-trinitro-1,3,5-triazacyclohexane
PETN – pentaerythritol tetranitrate
DADNE – 1,1-diamino-2,2-dinitroethene
DINA – di (2-nitratoethyl) nitramine
BDNPN – di (2,2-dinitropropyl) nitramine
Ng – glycerine trinitrate
DNI – 2,4-dinitroimidazole
TATB – 1,3,5-triamino-2,4,6-trinitrobenzene
NQ - nitroguanidine
TE – N-methyl-2,4,6,N-tetranitroaniline
DATB – 1,3-diamino-2,4,6-trinitrobenzene
TNA – 1-amino-2,4,6-trinitrobenzene
HNS – 2,2',4,4',6,6'-hexanitrostilbene
TNB – 1,3,5-trinitrobenzene
TNT – 2,4,6-trinitrotoluene

3. DISCUSSION

As we can see in table 1, high value of detonation energy E_D corresponds with low value of drop h_{50} . The exemptions exist for two types of energetic materials: DADNE and TE. Low impact sensitivity in case of DADNE was discussed earlier because of DADNE contains non-covalent hydrogen bonds. Values between difference partial charges ($\Delta 1$) for individual molecule calculated in WinMOPACv20, method AM1 and difference partial charges ($\Delta 2$) for molecules in crystal structure calculated in program *Cerius*², method Qeq are numerically various but each group is calculated in relative similar range. These results give hope that for new, still not ready EM, is possible to use the value of $\Delta 1$ for X-NO₂ bonds without knowledge of molecule structure in crystal.

Fact, that some EM contains nitro-groups connected to different atoms, can show reason for their high impact sensitivity (BTNEN, BDNPN, etc.). On the other hand the role of non-covalent hydrogen bonds was confirmed because of their existence in crystal dramatically decrease the impact sensitivity and of course other parameters such as density, melting temperature etc. are influenced.

The values of van der Waals energies E_W , exactly their proportion for individual molecule E_W/Z , have not direct influence for the impact sensitivity of selected investigated EM, when crystals have not contained non-covalent hydrogen bonds. In the case of crystals with non-covalent hydrogen bonds energy E_W/Z decrease the impact sensitivity because of the hydrogen bond energy is included as a part of E_W/Z .

4. CONCLUSION

Presented results show using of accessible programs for qualitative prediction of impact sensitivity for new, still not ready EM. The strong influence of non-covalent hydrogen bonds for decreasing of impact sensitivity for investigated set of EM was shown especially in cases of crystals with molecules contain amine- and nitro-group together. The hydrogen bond connection between oxygen and carbon can also enact a role in decreasing of impact sensitivity. These relations can be more specify with knowledge of results for higher number of EM based on X-ray and neutron diffraction analysis.

Acknowledgement

The authors thank the GACR (Project 203/02/0436) and Dr. Fabry for help with finding crystal structures from database. The authors are also very indebted to prof. Nepraš from Department of Technology Organic Materials, University Pardubice for calculations in program WinMOPACv20.

REFERENCES

- [1] L. E. FRIED: *Design and synthesis of energetic materials*, Annu. Rev. Mater. Res., **31**, p.291-321, 2001
- [2] P. VÁVRA: *Study about energy of explosives*, Proc. 3rd Seminar „New trends in research of EM“, Univ. Pardubice p.223-227, CZ, 2000
- [3] P. VÁVRA and M. POSPÍŠIL: *Effect of intermolecular forces on some properties of explosives II. Influence of non-covalent hydrogen bond*, Proc. 6th Seminar „New trends in research of EM“, Univ. Pardubice, p.473-481, CZ, 2003
- [4] D. D. DLOTT: *Fast molecular processes in energetic materials*, Energetic Materials, part 2, Elsevier, p.125-191, 2003
- [5] P. VÁVRA, M. POSPÍŠIL and J. REPÁKOVÁ: *Effect of intermolecular forces on some properties of explosives*, Proc. 5th Seminar „New trends in research of EM“, Univ. Pardubice, p. 357-368, CZ, 2002
- [6] C. B. STORM, J. R. STINE and J. F. KRAMER: *Chemistry and Physics of EM*, Kluwer, p. 605, 1990
- [7] O. U. YUXIANG et al.: *Synthesis and crystal structure of β -hexanitrohexaazaisowurtzitane*, Science in China series B, **42**, p. 217-224, 1999
- [8] C. S. CHOI and H. P. BOUTIN: *A Study of the Crystal structure of β -Cyclotetramethylene Tetranitramine by Neutron Diffraction*, Acta Cryst., **B 26**, p.1235-1240, 1970

- [9] L. O. ATOVMYAN et al., „*Kristaličeskaja i molekuljarnaja struktura dvuch modifikacij bis-(2,2,2-trinitroetil)nitramina*“, *Ž. Strukt. Chim.*, **21**, p.135-141, 1980
- [10] M. D. LIND: *Crystal Structure of N,N'-bis-(β,β,β -trinitroethyl)urea*, *Acta Cryst.*, **B 26**, 590-596, 1970
- [11] T. G. ARCHIBALD, R. GILARDI, K. BAUM and C. GEORGE: *Synthesis and X-ray Crystal Structure of 1,3,3 Trinitroazetidine*, *J. Org. Chem.*, **55**, p.2920-2924, 1990
- [12] C. S. CHOI and E. PRINCE: *The Crystal Structure of Cyclotrimethylene-trinitramine*, *Acta Cryst.*, **B 28**, p.2857-2862, 1972
- [13] H. H. CADY and A. C. LARSON: *Pentaerythritol Tetranitrate II: Crystal Structure and Transformation to PETN I; an Algorithm for Refinement of Crystal Structures with Poor Data*, *Acta Cryst.*, **B 31**, p.1864-1869, 1975
- [14] U. BEMM and H. ÖSTMARK: *1,1-Diamino-2,2-dinitroethylene: Novel Energetic Material with Infinite Layers in Two Dimensions*, *Acta Cryst.*, **C 54**, p.1997-1999, 1998.
- [15] J. HALFPENNY and R. W. SMALL : *The Structure of 2,2'-Dinitroxydiethylnitramine (DINA)*, *Acta Cryst.*, **B 34**, p.3452-3454, 1978
- [16] A. J. BRACUTI: *Crystal structure of bis(2,2-dinitropropyl)-nitramine (BDNPN)*, *J. Chem. Cryst.*, **27**, p.67-70, 1997
- [17] A. A. ESPENBETOV, M. Y. ANTIPIN and Y. T. STRUCHKOV: *Structure of 1,2,3-Propanetriol Trinitrate (β Modification), $C_3H_5N_3O_9$* , *Acta Cryst.*, **C 40**, p.2096-2098, 1984.
- [18] A. J. BRACUTI: *Crystal structure of 2,4-dinitroimidazole (24DNI)*, *J. Chem. Cryst.*, **25**, 625-627, 1995
- [19] H. H. CADY and A. C. LARSON: *The Crystal Structure of 1,3,5-Triamino-2,4,6-trinitrobenzene*, *Acta Cryst.*, **18**, p.485-496, 1965
- [20] A. J. BRACUTI: *Crystal structure refinement of nitroguanidine*, *J. Chem. Cryst.*, **29**, 671-676, 1999
- [21] H. H. CADY: *The Crystal Structure of N-Methyl-N,2,4,6-tetranitroaniline (Tetryl)*, *Acta Cryst.*, **23**, p.601-609, 1967
- [22] J. R. HOLDEN: *The Structure of 1,3-Diamino-2,4,6-trinitrobenzene, Form I*, *Acta Cryst.*, **22**, p.545-550, 1967
- [23] J. R. HOLDEN, C. DICKINSON and C. M. BOCK: *The Crystal Structure of 2,4,6-Trinitroaniline*, *J. Phys. Chem.*, **76**, p.3597-3602, 1972
- [24] F. GERARD and A. HARDY: *Structure de l'Hexanitro-2,2',4,4',6,6' Stilbene, HNS, et Comparaison avec le Trinitro - 2,4,6 Toluene, TNT*, *Acta Cryst.*, **C 44**, p.1283-1287, 1988.
- [25] C. S. CHOI and J. E. ABEL: *The Crystal Structure of 1,3,5-Trinitrobenzene by Neutron Diffraction*, *Acta Cryst.*, **B 28**, p.193-201, 1972
- [26] W. R. CARPER, L. P. DAVIS and M. W. EXTINE: *Molecular Structure of 2,4,6-Trinitrotoluene*, *J. Phys. Chem.*, **86**, p.459-462, 1982
- [27] *Cerius² documentation*, June 2000, San Diego: Molecular Simulations Inc., 2000
- [28] A. K. RAPPÉ and W. A. III. GODARD: *Charge Equilibration for Molecular Dynamics Simulations*, *J. Phys. Chem.*, **95**, 3358-3363, 1991
- [29] A. K. RAPPÉ, C. J. CASEWIT, K. S. COLWELL, W. A. III. GODDARD and W. M. SKIFF: *UFF, a Full Periodic Table Force Field for Molecular Mechanics and Molecular Dynamics Simulations*, *J. Amer. Chem. Soc.*, **114**, 10024-10035, 1992
- [30] J. E. LENNARD-JONES: *On the Forces between Atoms and Ions*, *Proc. of the Royal Society of London, series A*, **109**, No. 752, 584-597, 1925
- [31] P. COMBA and T. W. HAMBLEY: *Molecular Modeling of Inorganic Compounds*, Weinheim, New York, Basel, Cambridge, Tokyo, VCH, 1995

SPHERICAL NITROGUANIDINE AS COMPONENT OF HIGH EXPLOSIVES

D. Powala*, A. Orzechowski*, A. Maranda** and J. Nowaczewski**

* Institute of Industrial Organic Chemistry, 6 Annopol St, 03-236 Warszawa, PL

** Military University of Technology, 2 Kaliskiego St, 00-908 Warszawa 49, PL

Abstract:

Researches on nitroguanidine (NGU) crystallization were conducted in order to obtain spherical crystals. We investigated plastic bonded explosive based on hexogen with NGU as an additive. Nitroguanidine, as a component of PBX generated the decrease of sensitivity to mechanical stress without worsening other parameters.

Keywords: *spherical nitroguanidine, insensitive high explosive*

1. INTRODOCTION

Growth of terrorist threats and military technology development causes the necessity of new insensitive explosives elaboration. A major component of high energetic material usable form, which decides on explosive properties, is the explosive itself. Hexogen, pentrit, octogen are commonly used high explosives. They are characterized by high explosive energy and low sensitivity to external stress. The increase of resistance to mechanical, electrical and thermal stresses, without worsening other parameters, is realized by the addition of such explosives like nitroguanidine (NGU), 3-nitro-1,2,4-triazol-5-one (NTO) or 1,3,5-triamino-2,4,6-trinitrobenzene (TATB) [1-3].

Attention has been focused on the explosive properties of nitroguanidine since the beginning of the last century. Though, this explosive did not find any practical application [4].

Nitroguanidine obtained the great importance as the component of propellants, which decreases the erosion. Now, interest with nitroguanidine grows up for the sake of its low sensitivity to mechanical stress.

Among the explosives of low sensitivity to external stress, nitroguanidine is inexpensive and easy to synthesize. The important problem is to obtain the suitable form of crystals. This crystalline form should be providing an effective utilization of nitroguanidine as an individual explosive or component of explosive mixtures.

This paper describes the results of investigation of nitroguanidine crystallization in order to attain spherical crystals. Such the form of nitroguanidine was obtained, and plastic bonded explosives (PBX) containing spherical NGU were made.

We tested sensitivity to mechanical stresses of two kinds of plastic bonded explosives. The first kind of PBX contained the nitroguanidine after crystallization from water - such the crystals of NGU have not spherical shape. The second kind of PBX contained the spherical crystals of nitroguanidine. The influence of the crystal form on mechanical stresses was researched.

2. MATERIALS AND METHODS

2.1 Properties of nitroguanidine

Nitroguanidine is white crystalline substance, it exists in two crystalline forms α (thin needles), β (elongated plates). The water solubility of these forms is different. At 25°C and 100°C the solubility of the α form is 4,4 g/dm³ and 82,5 g/dm³. Between these temperatures the β form appears to be more soluble. The solubility of nitroguanidine in popular organic solvents i.e. acetone, methyl and ethyl alcohols, ethyl acetate, ether, carbon tetrachloride, toluene, is limited. The melting point of nitroguanidine is 246°C [4,5].

After crystallization of nitroguanidine from water we obtained crystals in the form of needles. Bulk density of this NGU type is about 0,2 g/cm³, therefore the α form did not find any practical applications as an individual explosive or a component of explosive mixtures. Crystals of NGU after crystallization from water are shown in Fig. 1. The methods of NGU crystallizations are described [6,7].



Fig 1. NGU crystals obtained after crystallization from water

2.2 Methods

In order to obtain the desirable crystalline form of nitroguanidine we carried out several experiments of crystallization. As solvents we used ethylene glycol, and N,N-dimethylformamide. The solubility (in 20°C) of nitroguanidine in these solvents is shown below:

Ethylene glycol	1,1%	N,N-dimethylformamide	12,2%
-----------------	------	-----------------------	-------

Example 1

The mixture consisted of nitroguanidine and ethylene glycol in weight ratio 1:22 was gradually heated to 95°C. The mixture was stirred about 1000 rpm. Then the solution was gradually cooled to 20°C (cooling rate 3°C/min). Then, the solution was leaved for twenty four hours (without stirring). Next, the nitroguanidine was filtered and washed with acetone.

Example 2

The mixture consisted of nitroguanidine and N,N-dimethylformamide in weight ratio 1:4 was gradually heated to 85°C. The mixture was stirred about 1000 rpm. Then the solution was gradually cooled to 5°C (cooling rate 20°C/min). Then, the solution was stirred for two hours. Next, the nitroguanidine was filtered and washed with acetone.

Then we tested sensitivity to impact and friction of plastic bonded explosives based on needle and spherical form of nitroguanidine. The impact sensitivity of explosives was investigated using the drop weight apparatus. The friction sensitivity of explosives was investigated by Peters apparatus.

The samples of PBX consisted of an explosive and a binder. As an explosive component we used mixture of hexogene and nitroguanidine in a different proportion. The plastic binder consisted of butadiene-styrene copolymer, dioctyl adipate and oil.

3. RESULTS

3.1 Nitroguanidine crystallization

The process of nitroguanidine crystallization from its solution in ethylene glycol produced the final product in the form of oblong plates. This shape of crystals is better to any practical applications than the needle form of NGU, which can be obtained after crystallization of nitroguanidine from water. Grain size analysis is presented in Fig. 2 and crystals of NGU are shown in Fig. 3. Because spherical form of crystal is the best to effective utilization of explosive, therefore we carried out crystallization of nitroguanidine from N,N-dimethylformamide.

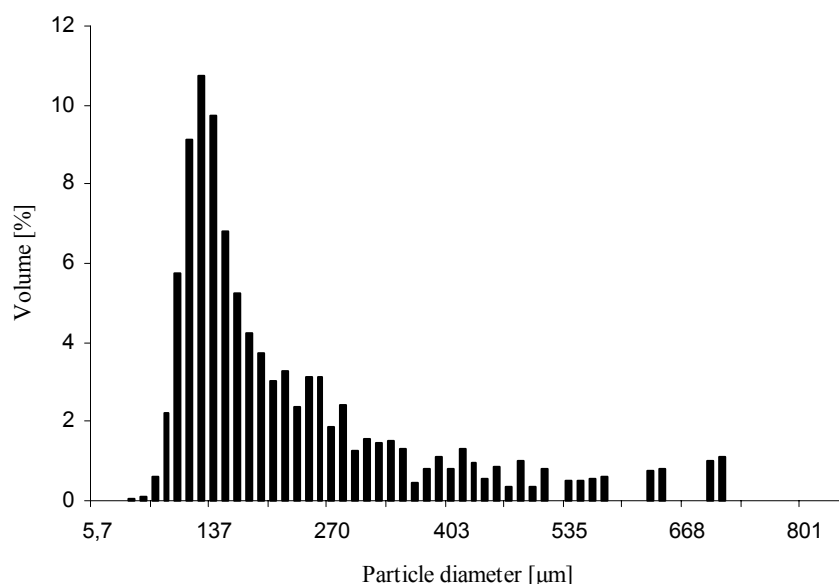


Fig 2. Particle size distribution of NGU after crystallization from ethylene glycol

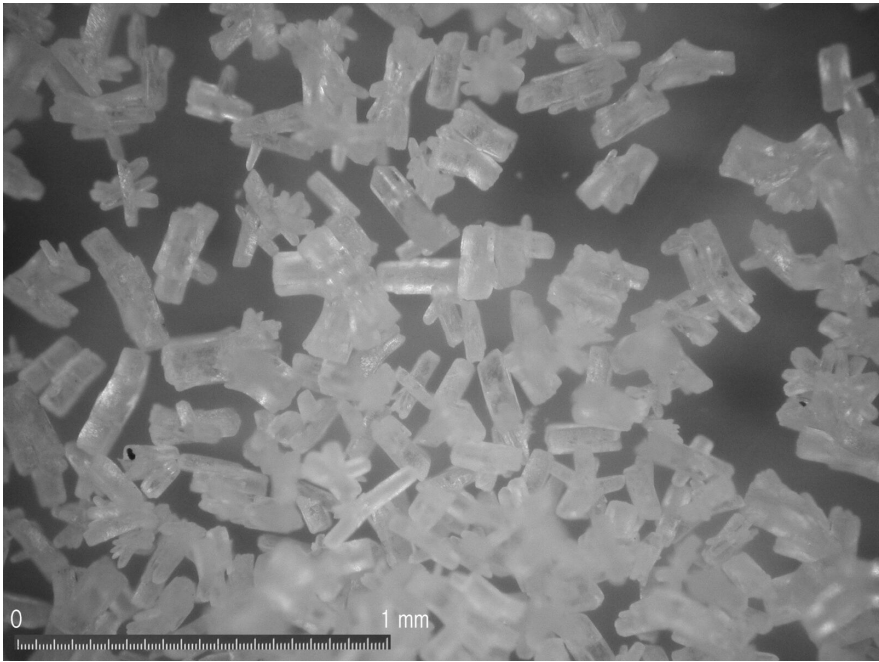


Fig 3. Crystals of NGU after crystallization from ethylene glycol

The crystallization of nitroguanidine from its solution in N,N-dimethylformamide produced the final product in the form of spherical crystals. The particle size distribution of them is shown in Fig. 4 and the shape of crystals is presented in Fig. 5.

The spherical crystals were obtained, and that is why bulk density of NGU increased. Bulk density of NGU after crystallization from water and N,N-dimethylformamide is shown below:

Bulk density of NGU after crystallization from water	0,17 g/cm ³
Bulk density of NGU after crystallization from N,N-dimethylformamide	0,59 g/cm ³

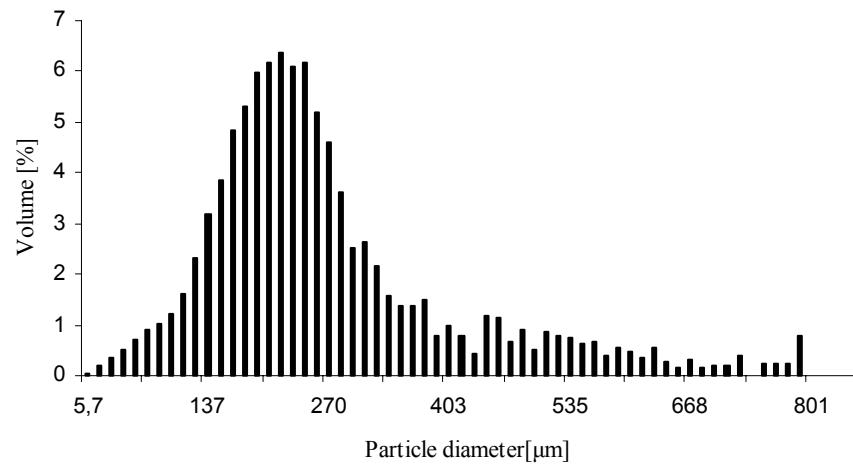


Fig 4. Particle size distribution NGU after crystallization from N,N-dimethylformamide

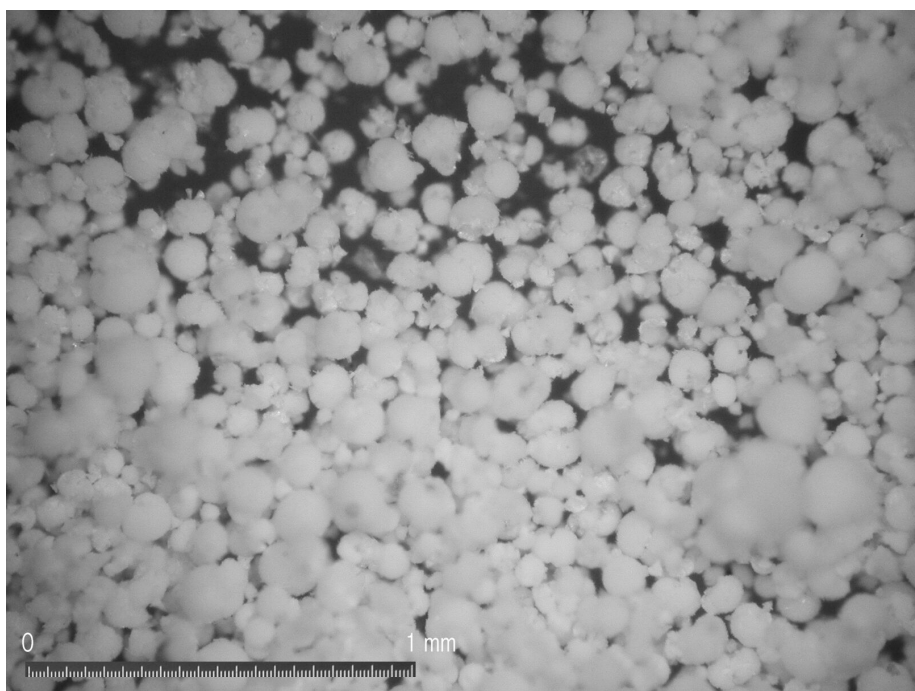


Fig 5. Crystals of NGU after crystallization from N,N-dimethylformamide

3.2 PBX containing needle form of nitroguanidine

Samples of PBX containing needle crystals of NGU were made. The explosive content was 84% with a different quantity of NGU increasing with the decrease of RDX amount. The content of the binder was the same for all samples, and its composition is shown below:

butadiene-styrenecopolymer	30 %
dioctyl adipate	60%
oil	10%

Density of PBX is presented in Tab. 1. The results of impact sensitivity test and friction sensitivity test are shown in Tab. 2.

The density of these samples decreases with growth of nitroguanidine content.

Additive of nitroguanidine reduces the sensitivity of sample to impact. The PBX of 60 % NGU content causes the decrease of sensitivity to impact from 29,4 to 34,3 Nm. For the content of 80 % NGU the sensitivity to impact is 49,1 Nm. The lowest sensitivity value was obtained for the samples of 100 % nitroguanidine as explosive component.

There are no evident changes in sensitivity to friction for all the samples.

Table 1. *Density of PBX containing needle form of NGU*

Content 84 % Explosive 16 % Binder	Density [g/cm ³]
0 % NGU, 100 % RDX	1,43
20% NGU, 80 % RDX	1,30
40 % NGU, 60 % RDX	1,24
60 % NGU, 40 % RDX	1,14
80 % NGU, 20 % RDX	1,08
100 % NGU, 0 % RDX	0,94

Table 2. *Sensitivity to impact and friction PBX containing needle form of NGU*

Content 84 % Explosive 16 % Binder	Impact Sensitivity* [Nm]	Impact Sensitivity** [Nm]	Friction Sensitivity* [N]	Friction Sensitivity** [N]
0 % NGU, 100 % RDX	29,4	24,5	>353	≥353
20% NGU, 80 % RDX	29,4	24,5	>353	≥353
40 % NGU, 60 % RDX	29,4	24,5	>353	≥353
60 % NGU, 40 % RDX	34,3	29,4	>353	≥353
80 % NGU, 20 % RDX	49,1	39,2	>353	≥353
100 % NGU, 0 % RDX	>49,1	≥49,1	>353	≥353

* min. 1 decomposition at 6 samples

** no decomposition at 6 samples

3.3 PBX containing spherical form of nitroguanidine

Density of PBX is presented in Tab. 3. The results of impact sensitivity test and friction sensitivity test are shown in Tab. 4.

The density of samples containing the spherical crystals falls with growth of nitroguanidine content.

The results of researches show the decrease of sensitivity to impact with the increase of nitroguanidine content. The PBX of 60 % NGU content causes the decrease of sensitivity to impact from 29,4 to 34,3 Nm. For the content of 80 % NGU the sensitivity to impact is 49,1 Nm. The lowest sensitivity value was obtained for the samples of 100 % nitroguanidine as explosive component.

There are no evident changes in sensitivity to friction for all the samples.

Table 3. *Density of PBX containing spherical form of NGU*

Content 84 % Explosive 16 % Binder	Density [g/cm ³]
0 % NGU, 100 % RDX	1,43
20% NGU, 80 % RDX	1,41
40 % NGU, 60 % RDX	1,36
60 % NGU, 40 % RDX	1,25
80 % NGU, 20 % RDX	1,20
100 % NGU, 0 % RDX	1,11

Table 4. *Sensitivity to impact and friction PBX containing spherical form of NGU*

Content 84 % Explosive 16 % Binder	Impact Sensitivity* [Nm]	Impact Sensitivity** [Nm]	Friction Sensitivity* [N]	Friction Sensitivity** [N]
0 % NGU, 100 % RDX	29,4	24,5	>353	≥353
20% NGU, 80 % RDX	34,3	29,4	>353	≥353
40 % NGU, 60 % RDX	34,3	29,4	>353	≥353
60 % NGU, 40 % RDX	34,3	29,4	>353	≥353
80 % NGU, 20 % RDX	49,1	39,2	>353	≥353
100 % NGU, 0 % RDX	>49,1	≥49,1	>353	≥353

* min. 1 decomposition at 6 samples

** no decomposition at 6 samples

4. SUMMARY

The process of nitroguanidine crystallization from its solution in N,N-dimethylformamide allowed to obtain the spherical form crystals of product. The treble increase of bulk density of nitroguanidine was obtained.

The growth of nitroguanidine contents generated the decrease of sensitivity to impact of PBX. There was no influence of the crystalline form of nitroguanidine and its content in PBX formulation on sensitivity to friction of investigated PBX. The spherical crystals of NGU allowed to obtain the growth of PBX densities.

The comparison of PBX formulation containing two types of nitroguanidine crystals showed that the PBX containing 20% - 40% of spherical crystalline NGU had lower sensitivity to impact than corresponding PBX based on needle crystalline NGU. For the needle form of nitroguanidine crystals the reduction of PBX sensitivity to impact was obtained in the case of 60% of NGU content.

REFERENCES

- [1] J.P. AGRAWAL: *Recent Trends In High-Energy Materials*, Prog. Energy Combust. Sci., 1998
- [2] A. BECUWE, A. DELCLOS: *Low-Sensitivity Explosive Compounds for Low Vulnerability Warheads*, Propellants, Explosives, Pyrotechnic, 18, 1-10, 1993
- [3] Y. TANG: *The effect of NQ and TATB to the Insensitivity of HMX*, Proc. of 33nd International Annual Conference of ICT, Karlsruhe, Germany, 2002
- [4] T.URBAŃSKI: *Chemistry and Technology of Explosives*, Warszawa, 1965
- [5] A. MARANDA, S. CUDZIŁO, J. NOWACZEWSKI, A. PAPLIŃSKI: *Podstawy chemii materiałów wybuchowych*, WAT Warszawa, 1997
- [6] U.S. Patent: nr. 4967000, 1990
- [7] U.S. Patent: nr. 4544769, 1985

THE CHEMICAL KINETIC AT DETONATION OF AROMATIC NITROCOMPOUNDS – NITRIC ACID MIXTURES

V.M. Raikova and E.A. Likholatov

Mendeleev University of Chemical Technology,
Miusskaya sq. 9, Moscow A-47, Russia

Abstract:

Detonation failure diameter d_f of mixtures of six aromatic Nitrocompounds with nitric acid has been examined in the framework of A.Dremin theory. Shock and detonation parameters as well as characteristics (P_3 , T_3 and τ_3) of the reaction zone to determine reinitiation of detonation wave at low diameters of the charge were calculated by means of SGKR computer package. According to our calculations maximum of T_3 values was fixed at the concentrations of nitric acid corresponding to the minimum of d_f . Effective values of kinetic parameters of reaction between nitric acid and Nitrocompounds are defined.

Keywords: *detonation, kinetic, failure, nitric acid, nitrocompound*

1. INTRODUCTION

Liquid mixtures of nitric acid (NA) with organic substances are used in technology of Nitrocompounds and related substances. Detonation failure diameter data of the solutions of Nitrocompounds in strong nitric acid were reported in ^[1-3].

The failure and reinitiating of the chemical reaction at detonation occur in the so-called zone three according to the Failure diameter theory of Dremin ^[4, 5], which is the foundation for calculation of the temperature (T_3), pressure (p_3) reaction time (τ_3) in this zone. Earlier this theory has been used to calculate the d_f values of liquid substances: nitromethane, trinitrotoluene, and nitroesters ^[6-9]. Later the kinetic parameters of detonation reactions in sulfuric acid solutions of NM and TNT have been defined ^[10]. The kinetic parameters of detonation reactions in mixtures of ethyleneglycoldinitrate (NGL) and nitroglycerine (NG) with diethyleneglycoldinitrate (DGDN), propylnitrate (PN), methanol have been calculated in ^[11,12]. All the results were explained in the light of homogeneous thermal explosion theory for monomolecular reaction. The results of the calculations revealed that values of $E=140-160$ kJ/mol and $\lg k_0= 13,5-14,5$ (s^{-1}) at detonation of the systems based on nitroesters was closed to the data obtained previously in the course of investigation of slow decomposition of these substances.

The kinetics and mechanisms of chemical reactions in detonation wave of NGL, DGDN, and acetic anhydride solutions (ACA) in nitric acid have been studied in works ^[13, 14]. In all of these cases formation and consequent decomposition of a complex or a compound between NA and fuel were assumed to be the leading chemical processes in detonation wave. Composition of the complex in the case of NGL is $[2NGL \cdot HNO_3]$ and in the case of DGDN is $[DGDN \cdot HNO_3]$. The system of ACA-NA comprises more complicated case in chemical sense. A compound produced at a reaction between ACA and NA is supposed to

have slightly indefinite composition, at least in the limits of the concentrations of the ACA-NA mixtures investigated, from $\frac{3}{4}$ to $\frac{1}{4}$. Most probable it is acetylnitrate and the kinetic constants of the decomposition reaction derived from the experimental data corresponding to velocity of decomposition of the substance in detonation wave.

The main purpose of this work is to estimate overall kinetic parameters of reactions in detonation wave of aromatic Nitrocompounds solutions in NA. Detonation failure diameter data of Nitrobenzene (NB), 1,3-Dinitrobenzene (DNB), 1,3,5 -trinitrobenzene (TNB), para-Nitrotoluene (MNT), 2,4-Dinitrotoluene (DNT) and 2,4,6-Trinitrotoluene (TNT) solutions in NA are reported in this seminar ^[15].

Shock and detonation parameters as well as characteristics of the reaction zone defining the process of reinitiating of detonation wave in the zone of instability were calculated by means of SGKR computer Code (Shock and Detonation General Kinetic and Thermodynamics in Reactive Systems computer package) developed in our Laboratory previously ^[16].

It was proposed that decomposition of NA solutions in detonation wave included only one bimolecular reaction. The effective values of kinetic parameters of detonation reactions in every solution were defined.

2. RESULTS OF CALCULATION

The detonation parameters: velocity (D), pressure (p_{cj}) and explosion heat (Q_v) of mixtures were computed by means of the Steady State Detonation (SD) Code ^[16]. Shock parameters and characteristics (pressure P_3 , temperature T_3 and reaction time τ_3) of the reaction zone defining the process of reinitiating of detonation wave in the zone of instability were calculated by means of SWDK Code ^[11]. Input data in this case were experimental dependencies $d_f(C_{NA})$ of the mixtures and the results of calculations by means of the SD Codes.

The pressure p_3 arises with increasing of the pressure p_{cj} (Fig 1). The correlation between p_{cj} and p_3 is found to be a general linear function for all the systems under investigation:

$$p_3 = 0.49 p_{cj} + 1.392 \quad (1)$$

The T_3 value is defined by shock temperature dependence $T(p)$ at the correspondent value of p_3 for every mixture. The dependencies T_3 versus concentration of NA in solutions are shown in Fig.2. According to calculation maximum of T_3 values was fixed at the concentrations of the NA corresponding to point d_f^{\min} .

A shape of calculated dependencies $\tau_3(C_{NA})$ (Fig 3) is similar to a shape of experimental curves $d_f(C_{NA})$ of NA mixtures with aromatic nitrocompounds. Calculated dependencies $d_f(\tau_3)$ of all mixtures under investigation are described by the general linear function:

$$d_f = 33.64 \tau_3 - 0.0163 \quad (2)$$

where d_f in mm, τ_3 in mcs.

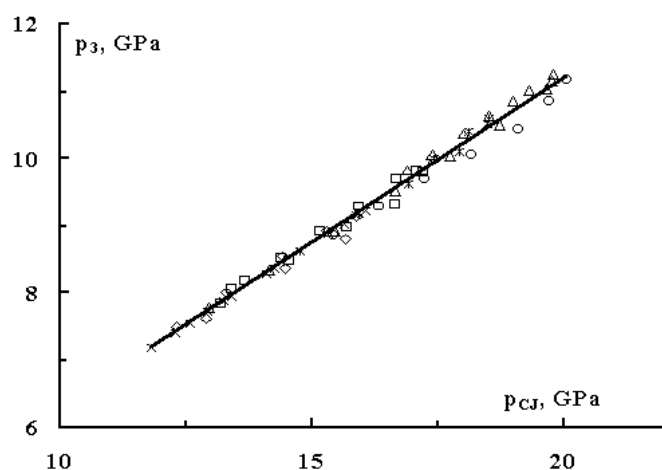


Fig 1. The calculated pressure p_3 vs. p_{cj} for solutions on the base nitric acid. Line corresponds to general eq. (1).

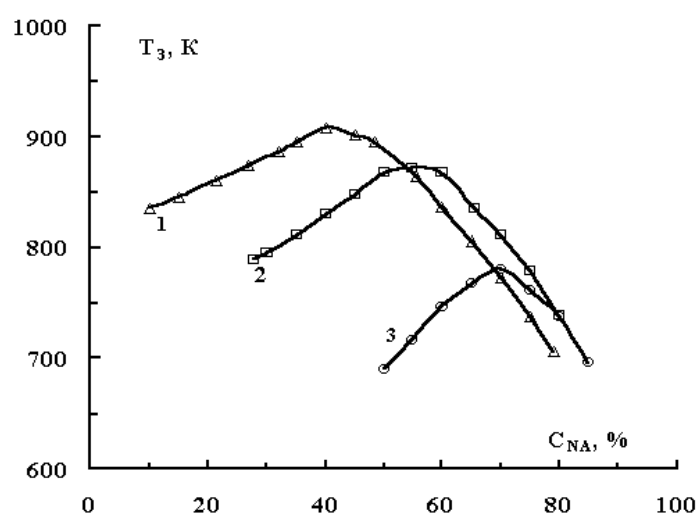


Fig 2. The dependencies of temperature T_3 vs. C_{NA} for mixtures NA-TNT (1), NA-DNT(2) and NA-MNT (3).

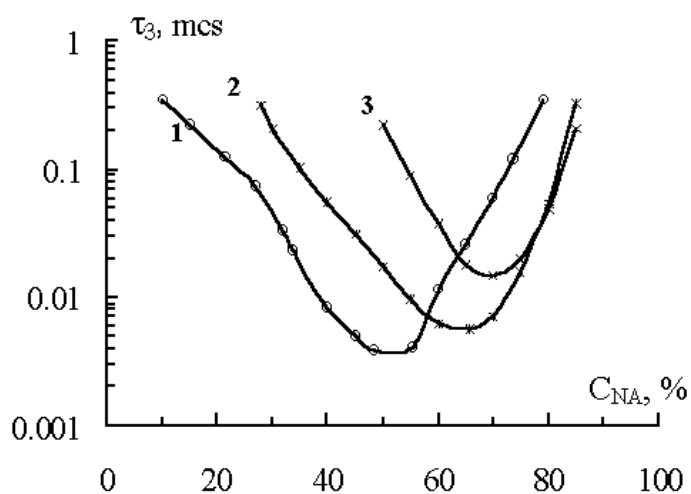


Fig 3. The dependencies of reaction time τ_3 vs. C_{NA} for mixtures NA-TNT (1), NA-DNT (2) and NA-MNT (3).

The experimental data of d_f^{\min} and calculated values of, p_3 , T_3 and τ_3 for all systems under investigation are collected in Table 1. The data of Table 1 show a common tendency: decrease of experimental d_f^{\min} values coincides with a rise of calculated T_3 values correspondingly to increasing of number of groups NO_2 in molecule.

Table 1. *The failure detonation diameter (d_f^{\min}) and characteristics of the reaction zone defining the process of reinitiation of detonation wave (p_3 , T_3 , τ_3) of NA-Nitrocompound mixtures*

Nitrocompound	d_f^{\min} , mm	p_3 , GPa	T_3 , K	τ_3 , mcs
NB	0,18	9	820	0,0060
DNB	0,16	10,52	871	0,0056
TNB	0,10	10,10	899	0,0031
MNT	0,49	9,14	780	0,0150
DNT	0,18	9,33	836	0,0056
TNT	0,12	10,75	880	0,0040

Bimolecular reaction between NA and Nitrocompound was supposed to be most probable at detonation of NA solutions. The interrelation of τ_3 , T_3 and chemical kinetics for bimolecular reaction should be described with the equation:

$$\tau_3 = \frac{c_v \cdot R \cdot T_3^2 C_{nc}}{Q_v \cdot E_a \cdot k_0 C_{nc} C_N} \exp(E_a / RT_3) \tag{3}$$

where E_a is activation energy, k_0 is pre-exponent factor, c_v is specific heat of solution, C_{nc} and C_N are concentrations of Nitrocompound and HNO_3 in solution, mol/l, R is universal gas constant.

Equation (3) could be transformed into another expression:

$$\ln Z = \ln A + \frac{E_a}{RT_3} \tag{4}$$

where

$$Z = \tau_3 Q_v C_{nc} / T_3^2 c_v, \quad A = R / (E_a k_0)$$

Calculated values of Z and T_3 of NA mixtures with aromatic Nitrocompounds are plotted in Arrhenius coordinates (Fig.4). Points were fitted by a linear function. The slop of these lines gives activation energy E_a . Calculated kinetic parameters of detonation reactions in NA solutions are represented in Table.2.

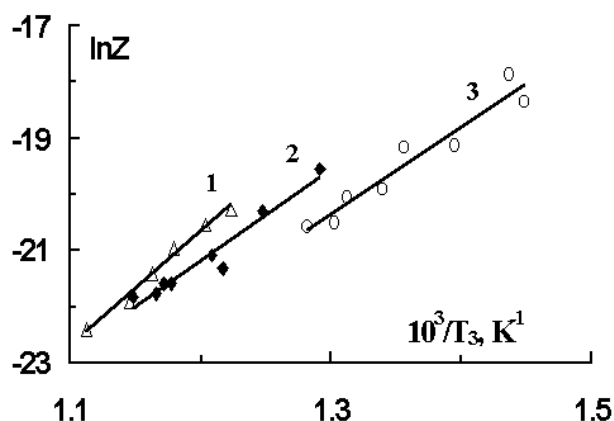


Fig 4. Treatment of experimental data d_f of mixtures NA-TNB (1), NA-TNT (2), and NA-MNT (3) in Arrhenius coordinates.

Table 2. *Calculated kinetic parameters of detonation reactions in NA-Nitrocompound solutions*

Nitrocompound	$\Delta C_{NA}, \%$	Kinetic parameters	
		$E_a, \text{ kJ/mol}$	$\log k_0, \text{ l/(mol}\cdot\text{s)}$
NB	42-80	~ 100	11,6
DNB	40-75	135	13,5
TNB	50-65	169	15,2
MNT	50-85	128	13,4
DNT	65-85	127	13,2
TNT	49-79	132	13,2

3. DISCUSSION

Comparison experimental d_f data of NA solutions shown, that composition of Nitrocompound influences on the value d_f^{\min} . Our calculations explain this fact. Increase in the number of groups NO_2 in molecule leads to rise of shock temperature T_3 on reaction zone and decrease reaction time and d_f .

The dependencies $d_f(C_{NA})$ for mixtures containing 40-50% NA and more are described by second order kinetic equation. The activation energy of decomposition of the mixtures NA with MNT, DNT, TNT and DNB is about $E_a = 130 \text{ kJ/mol}$, and the pre-exponent factor is about $k_0 = 10^{13} \text{ sec}^{-1}$. The activation energy of reaction between NA and NB in detonation wave is $E_a \approx 100 \text{ kJ/mol}$ and the pre-exponent factor is $k_0 \approx 10^{12} \text{ s}^{-1}$. The highest value of E_a (170 kJ/mol) for mixture NA with TNB was found.

Comparison of the kinetic constants vs. $1/T_3$ for all systems under investigation are shown in Fig.5. The dependencies $k(1/T)$ for mixtures NA with NB, MNT and DNT are closed with each other. The constants of reaction rate for mixtures NA with DNB and TNT are more, than foregoing. The least values of reaction rate constant for mixture NA-TNB was found.

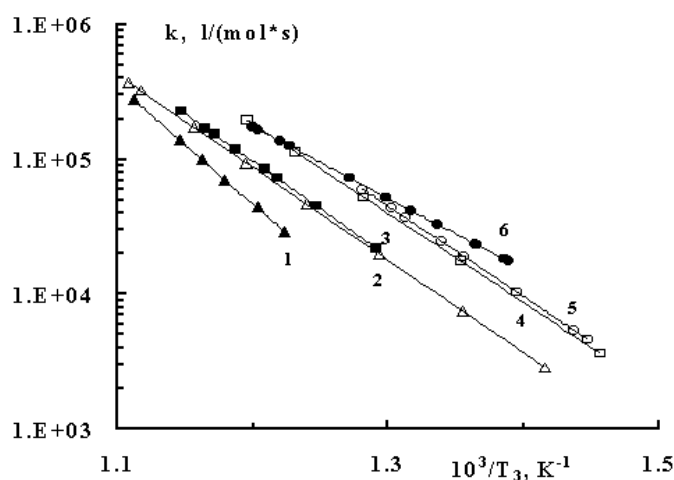


Fig 5. The dependencies of kinetic constants vs. $1/T_3$ for mixtures NA-TNB (1), NA-TNT (2), NA-DNB (3), NA-DNT (4), NA-MNT (5) and NA-NB (6).

4. CONCLUSIONS

Detonation reactions in the mixtures of nitric acid with six aromatic Nitrocompounds were considered in terms of A. Dremin's theory by means of the SGKR computer Code. According to our calculations maximum of T_3 values was fixed at the concentrations of nitric acid corresponding to the d_f minimum. All the results are explained in the light of homogeneous thermal explosion theory for bimolecular reaction. Effective values of kinetic parameters of reaction between nitric acid and Nitrocompounds are defined. There is shown, that constant of reaction rate in detonation wave decreases correspondingly to increase in the number of groups NO_2 in molecule.

Acknowledgements

We thank professor B.N. Kondrikov for helpful discussions and Russian Foundation of Basic Research (RFBR) for partial financial support of this work (Grant № 01-03-32610-a).

REFERENCES

- [1] V.M. RAIKOVA, B.N. KONDRIKOV, G.D. KOZAK: *Experimental investigation of detonation of nitric acid solutions*, Comb., Expl., and Shock Waves, 1998, v. 34, № 1, p.p.77-84
- [2] G.D. KOZAK, V.M. RAIKOVA, V.V. POTAPOV: *Measurement of detonation failure diameter in thin layers of an explosive solution*, Combustion, explosion and shock waves v.35, №5, 1999, p. 568-569
- [3] G.D. KOZAK, V.M. RAIKOVA, V.V. POTAPOV: *The failure thickness of detonation of solutions on the base of strong nitric acid*. Trans. of the 30-th international annual conference. FGR, p.96-1 – 96-7
- [4] A.N. DREMIN: *The failure detonation diameter of liquid explosives*, DAN SSSR, v.147, p. 870-873, 1962 (Russ.)
- [5] A.N. DREMIN, V.S. TROFIMOV: *Calculation of failure detonation diameter of liquid explosives*, PMTF, №1, p. 126-131, 1964 (Russ.)
- [6] J. WENIG, F.W. PETRONE: *The failure diameter theory of Dremine*, 5th Symposium (Int.) on Detonation, Pasadena, Ca. Aug. 18-21, p. 99-104, 1970
- [7] C.N. TARVER, R. SHAW, M. COWPERTHWAIT: *Detonation failure diameter structure of four liquid nitroalkanes*, J. Chem. Phys. V.64, N6, p.2666-2673
- [8] V.N. GAMEZO, B.N. KONDRIKOV: *Calculation of kinetic constants for decomposition of nitromethane and TNT from data on dependence of failure diameter on initial temperature*. Proc of IV Conf. (USSR) on Detonation, Telavi. v.1, p. 111-117, 1988 (Russ.)
- [9] V.N. GAMEZO, B.N. KONDRIKOV AND G.D. KOZAK: *Dependence of detonation failure diameter of nitroesters on initial temperature*, Chemical Physics (Russia), v.12, № 5, p. 719-722, 1993
- [10] B.N. KONDRIKOV, V.N. GAMEZO, G.D. KOZAK AND S.M. KHOROSHEV: *Sulfuric acid influence on the nitrocompounds detonation reactions*, J. de Physique IV, Colloque C4, supplément au J. de Physique III., v. 5, p. C4-395 - C4-405, 1995
- [11] V.M. RAIKOVA, G.D. KOZAK, E.A. LIKHOLATOV: *The chemical kinetics at detonation of nitroester solution*, Proc. of the 6th seminar “New trends in research of energetic materials”, Univ. Pardubice, CSR, pp. 284-293, 2003
- [12] V.M. RAIKOVA, G.D. KOZAK, E.A. LIKHOLATOV: *The failure diameter of detonation of nitrocompounds solutions*. Trans. of the 34th International Annual Conference of ICT, Karlsruhe, FRG, 27 –30 June, pp.117-1 –117-10, 2003
- [13] V.M. RAIKOVA, A. HALAK, B.N. KONDRIKOV: *Chemical kinetics at detonation of organic compounds – nitric acid mixtures*, Proc. of the 30th Int. Annual Conf. of ICT, Karlsruhe, FRG, p. 95-1 – 95-12, June 29 - July 2 1999
- [14] V.M. RAIKOVA, B.N. KONDRIKOV, A. HALAK: *Kinetics of chemical reactions at detonation of mixtures of organic compounds with nitric acid*, Combustion, Explosion and Shock Waves, v.37, № 3, p. 106-114, 2001
- [15] G.D. KOZAK, V.M. RAIKOVA, V.V. POTAPOV: *Detonation ability of solutions of aromatic nitrocompounds in nitric acid*. Proc. of the 7th seminar “New trends in research of energetic materials”, Univ. Pardubice, CSR, 2004
- [16] A.I. SUMIN, V.N. GAMEZO, B.N. KONDRIKOV, V.M. RAIKOVA: *Shock and detonation general kinetics and thermodynamics in reactive systems computer package*, Trans. of the 11-th (Int.) Detonation Symp., Snowmass, Colorado, USA. August 31-September 4, 1998. Bookcomp, Ampersand, p. 30-35, 2000

INITIAL STAGE DECOMPOSITION KINETICS OF NITROCELLULOSE PROPELLANT

M. Rajić Linarić, M. Sućeska, S. Matečić Mušanić and R. Čuljak

Brodarski institut–Marine Research & Special Technologies
Av. V. Holjevca 20, 10020 Zagreb, Croatia

Abstract:

A thermal decomposition reaction in nitrocellulose, which is the basic component of homogeneous propellants, limits the safe use and safe storage time of propellants. Under certain conditions the decomposition may lead to the well-known phenomenon of self-ignition.

In order to be able predict the shelf-life and thermal hazard potential of propellants it is of vital importance to know a true decomposition mechanism and true values of kinetic constants.

In this work we have studied decomposition kinetics of nitrocellulose propellant during the initial decomposition stage (up to 2 % mass loss) at elevated temperatures ranging from 80 to 100 °C. The kinetic results were derived from sample mass loss-time/temperature. It was found out that the activation energy for this decomposition stage equals 123.4 kJ/mol, and pre-exponential factor $1.78 \cdot 10^6$ 1/s. Also, it was found out, on the basis of the kinetic data obtained, that the reaction rate accelerating factor changes with temperature – from ~3 at 90-100 °C temperature range to about 5.5 at the room temperatures.

Keywords: nitrocellulose propellants, kinetics, decomposition, activation energy

1. INTRODUCTION

Because of the wide use and practical importance of nitrocellulose (NC), its degradation mechanism and kinetics have been the subject of numerous investigations [1-12]. From a practical point of view, the most important reasons for it lie in the fact that the rate of thermal decomposition affects quality and service life of propellants, as well as thermal hazard potential.

Nitrocellulose, like other nitric esters, is sensitive to thermal stress due to the low binding energy of the CO-NO₂ bond (155 - 163 kJ/mol). The CO-NO₂ bonds in nitric ester can be split easily thermally (thermolysis) even at moderately high temperatures (> 40 °C). For comparison, the typical values of C-H bonds are 414 kJ/mol, and of C-C bond 344 kJ/mol [12].

The homolytic splitting of CO-NO₂ bond produces the very reactive NO₂ radicals, a strong oxidising agent. It reacts with the cellulose backbone of the nitrocellulose, resulting in an opening of the anhydridoglucopyranose ring. The oxidative-radical consecutive reactions and splitting off of stable molecular units separate the polymer chain through the decomposition of at least one chain element, resulting in NC molar mass decrease.

A simplified reaction scheme of NC decomposition may contain two reaction paths: one is the thermolysis of CONO₂ groups, which means a homolytic cleavage of the CO-NO₂

bond in which two radicals are formed with an activation energy of about 160 – 170 kJ/mol, and the other path is the hydrolysis of CONO₂ groups, which has an activation energy of about 100 kJ/mol^[12].

The degradation process may be slowed down through the chemical trapping of the NO/NO₂ molecules by adding a stabiliser. Diphenylamine (DPA) is normally used as a stabiliser for nitrocellulose propellants. It prevents the decomposition of NC by chemically bonding with the autocatalytically effective NO₂ and HNO₃ – reaction products of the NC decomposition. The reaction of DPA with NO₂ forms consecutive products of DPA, which have stabilising effect too, and are named secondary stabilisers. The important ones are: N-NO-DPA, 2-NO₂-DPA, 4-NO₂-DPA, and dinitrated products -2NO₂-DPA.

A number of investigators have stressed that a true decomposition mechanism and true kinetic constants should be known in order to be able to predict with required accuracy the shelf-life and thermal hazard potential of any explosive material^[2-9]. The application of an inaccurate decomposition model and inaccurate values of Arrhenius kinetic constants in the calculation of the thermal hazard potential of an explosive may result in highly uncertain and unusable data on critical conditions of the self-ignition and on the shelf-life^[13-18].

In order to determine Arrhenius kinetic constants as accurately as possible various experimental techniques and testing conditions have been used by different investigators. Also, various kinetic approaches and data treatment procedures have been applied, resulting sometimes in considerable disagreement in the values of the kinetic parameters for NC propellants reported in literature – from about 120 to 210 kJ/mol^[11-12].

In this work we have studied kinetics of the initial stage decomposition stage of nitrocellulose propellant under elevated temperature conditions (80 – 100 °C).

2. EXPERIMENTAL

Experiments were carried out using nitrocellulose propellant samples. The samples of nitrocellulose propellant were cut to small grains having mass less than 5 mg. Then, the samples weighing 10 g were put in glass vessels having volume of 100 cm³, and subjected to five different elevated temperatures: 80, 85, 90, 95 and 100 °C.

The samples were taken periodically and weighted in order to follow changes in sample mass as a function of time and temperatures.

3. RESULTS AND DISCUSSION

The change in mass of nitrocellulose samples after predetermined period of heating at different temperatures was recorded every day. Table 1 shows loss in samples mass data as a function of temperature and time.

It should be noted that the heating of samples was terminated after an appearance of the red-brown fumes indicating beginning of intensive autocatalytic reactions. For example, it occurs after 7 days at 100 °C, after 15 days at 90 °C, etc.

Table 1. *Mass loss of nitrocellulose propellant samples at 80, 85, 90, 95 and 100 °C*

Time, days	Mass loss, %				
	100 °C	95 °C	90 °C	85 °C	80 °C
1/24 (1 h)	0.66	0.47	0.23	0.15	0.07
1	1.1684	0.7608	0.5394	0.4790	0.3940
2	1.3353	1.1394	0.9652	0.6800	0.5330
3	1.5282	1.2902	1.0682	0.8390	0.7500
4	1.6531	1.4437	1.1683	0.8910	0.7860
5	1.7711	1.5134	1.2787	1.0090	0.8270
6	1.8780	1.5917	1.3408	1.0590	0.8450
7	2.0150	1.6997	1.4326	1.1180	0.8970
8		1.7465	1.4886	1.1580	0.9350
9		1.7854	1.5392	1.2120	0.9650
10		1.8052	1.6080	1.2540	1.0290
11		1.8539	1.6519	1.2830	1.0691
12		1.8813	1.6995	1.3450	1.0971
13		1.9170	1.7118	1.3590	1.1121
14		1.9544	1.7347	1.3910	1.1511
15		1.9878	1.7806	1.4040	1.1801
16			1.8055	1.4170	1.1881
17				1.4290	1.2121
18				1.4480	1.2251
19				1.4630	1.2321
20				1.4720	1.2481
21					1.2611
22					1.2631
23					1.2671
24					1.2921
25					1.2981
26					1.3031
27					1.3111
28					1.3191
29					1.3281
30					1.3331
31					1.3531

The results given in Table 1 are presented graphically as a function of time in Fig. 1.

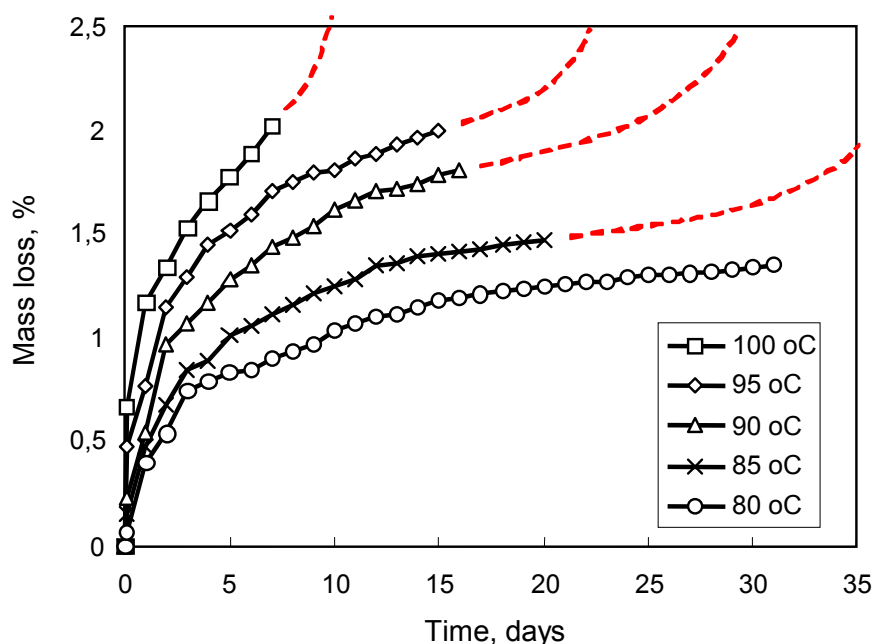


Fig 1. Sample mass loss as a function of time at different temperatures (dashed line indicates an expected trend in sample mass loss)

The shapes of isothermal curves given in Fig. 1 are typical for initial decomposition stage for many solid state reactions – high reaction rate at the beginning, an induction period followed by an accelerated stage ^[19].

After 60 minutes of heating at 100 °C, or two days at 80 °C, the sample mass loss was ~0.6 %. This mass loss is due to the water and residual solvent evaporation. After that period an almost linear increase of sample mass loss is visible. The sample mass loss during this period of heating corresponds probably to the liberation of low molecular mass decomposition product of NC, with no autocatalysis.

The red-brown fumes observed after that period (e.g. after 7 days at 100 °C) confirm the beginning of intensive autocatalytic reactions - indicated in the Fig. 1 by dashed lines. The heating of samples was terminated after appearance of the red-brown fumes and samples were taken out of thermal unit.

The sample mass loss up to 2 % corresponds to the initial stage of decomposition during which low molecular decomposition product of NC liberates, with no autocatalysis. This period is very important from practical point of view because very intensive reactions of stabiliser depletion take place during this period. An autocatalytic decomposition begins after that period, i.e. after depletion of all original stabiliser and its stabilising nitro-derivatives (Fig. 2).

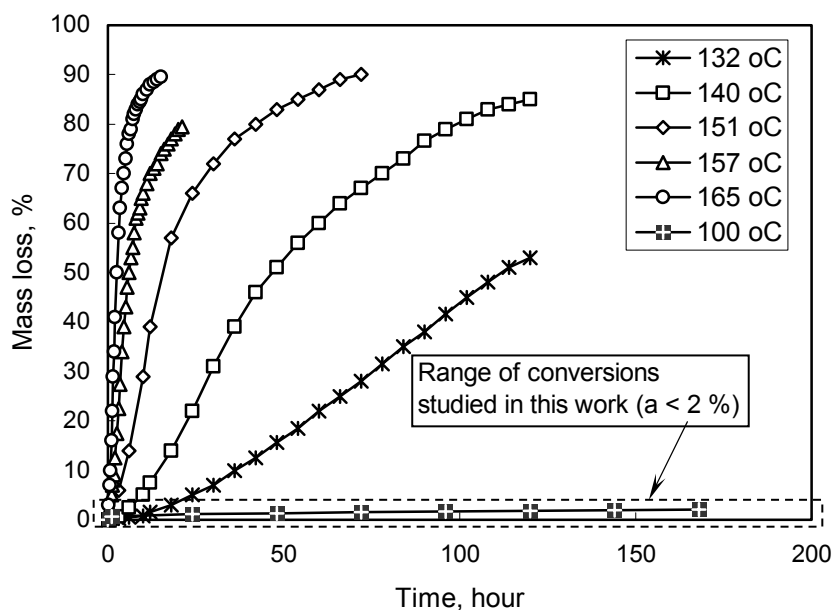


Fig 2. NC propellants conversion vs. time curves at different temperatures (data for temperatures above 100 °C are taken from Isler and Kayser^[1])

In order to derive kinetic constants (k , E , and A) the results given in Fig. 1 are treated in the following way. The conversion-time curves ($\alpha = f(t)$) for each temperature are obtained applying the following equation:

$$\alpha = \frac{m_i - m_t}{m_i} \quad (1)$$

where m_i is initial sample mass and m_t sample mass at time t .

It was found out by the non-linear regression analysis that the conversion-time data may be described the best by the power law kinetic model given by the following equation:

$$\alpha^{\frac{1}{m}} = kt \quad (2)$$

differential form of which is:

$$\frac{d\alpha}{dt} = m \cdot k \cdot \alpha^{\left(\frac{m-1}{m}\right)} \quad (3)$$

where k is the temperature-dependent reaction rate constant, t is time, α is conversion, $d\alpha/dt$ is rate of conversion, and m is constant.

It was calculated by the non-linear curve fitting that the mean value of constant m in Eq. (2) and Eq. (3) equals: $\bar{m} = 0.326 \pm 0.012$. The same value of the constant m indicates that reactions take place according to the same mechanism in the temperature range studied. The rate constants at different temperatures, obtained by the non-linear curve fitting procedure of experimentally obtained data in accordance with Eq. 2, are given in Table 2.

Table 2. Calculated values of rate constants at different temperatures

Temperature, °C	k , 1/s	r	$\ln k$	$1000/T$ 1/K
80	$1.054 \cdot 10^{-12}$	0.9764	-27.579	0.002832
85	$1.621 \cdot 10^{-12}$	0.9892	-27.148	0.002792
90	$3.398 \cdot 10^{-12}$	0.9960	-26.408	0.002754
95	$5.079 \cdot 10^{-12}$	0.9830	-26.006	0.002716
100	$1.001 \cdot 10^{-11}$	0.9965	-25.327	0.002680

The activation energy and pre-exponential factor are calculated from the rate constant-reciprocal temperature dependence, according to the Arrhenius equation (Fig. 3):

$$k = Ae^{\frac{-E}{RT}} \quad (4)$$

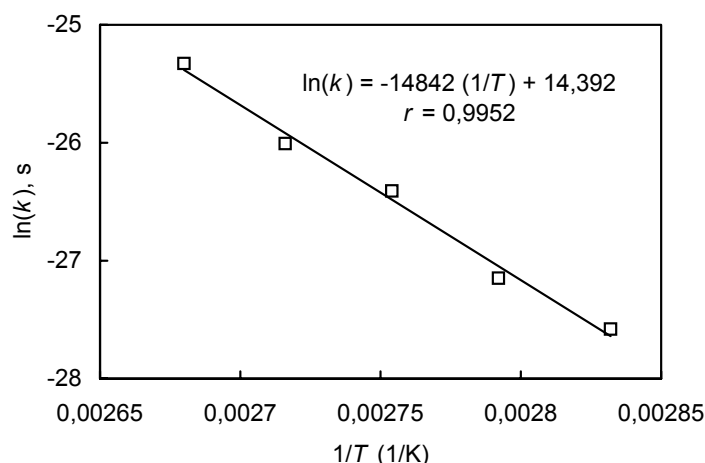


Fig 3. Logarithm of rate constant vs. reciprocal temperature (Arrhenius plot)

From the slope of $\ln(k)$ -($1/T$) line given in Fig. 3, the activation energy was calculated to be 123.39 kJ/mol, and pre-exponential factor $1.78 \cdot 10^6$ 1/s.

The obtained value of the activation energy is very close to some values reported in literature that refer also to the initial stage of decomposition (e.g. to values obtained microcalorimetrically [20]), and at the same time is considerably lower then and 210 kJ/mol [12]. This difference in the activation energies indicates that decomposition mechanism is not the same in the initial stage and acceleratory stage of decomposition.

Taking that an autocatalytic decomposition of NC propellant begins after 2% of mass loss (as follows from our experimental data), the kinetic constants obtained can be used to predict times to reach an autocatalytic decomposition at lower temperatures. By substituting $\alpha = 0.02$, and $m = 0.326$ into Eq. 2, the following equation was derived to calculate times at which sample mass loss will be 2% ($t_{0.02}$):

$$\left(0.02^{\frac{1}{0.326}}\right) \frac{1}{k} = t_{0.02} \quad (5)$$

The results of calculations are given in Fig. 4. It follows from Fig. 4 that the time necessary to reach 2% of mass loss equals 42 years at 40 °C, 204 years at 30 °C, etc.

The kinetic results obtained were used also for the calculation of the reaction rate accelerating factor (α_{10}) as a ratio between reaction rates at 2% mass loss for two temperatures that differ for 10 degrees (Eq. 3):

$$\alpha_{10} = \frac{0.326k_2 0.02^{\left(\frac{0.326-1}{0.326}\right)}}{0.326k_1 0.02^{\left(\frac{0.326-1}{0.326}\right)}} = \frac{k_2}{k_1} \tag{6}$$

where k_1 and k_2 are the rate constants at temperatures T_2 and T_1 . The values of the accelerating factor as a function of temperature are given in Fig. 4.

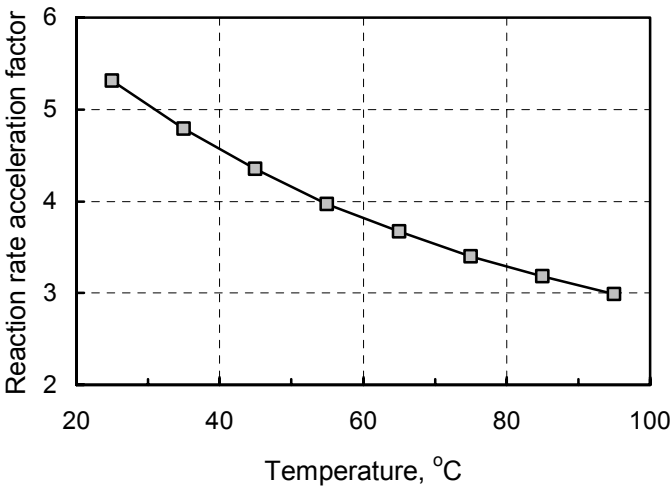


Fig 4. Reaction rate acceleration factor as a function of temperature

It follows from Fig. 4 that accelerating factor changes with temperature: from about 3 to about 5.5 at the room temperatures.

The times to reach 2% of mass loss at different temperatures are also calculated applying frequently used equation:

$$t_1 = t_2 \alpha_{10}^{\left(\frac{T_2-T_1}{10}\right)}, \tag{7}$$

where t_2 is the time necessary to reach 0.02 conversion (or any other) at temperature T_2 , and t_1 is the time to reach the same conversion at temperature T_1 . The results of calculations are presented in Fig. 5, along with the times calculated by Eq. 5.

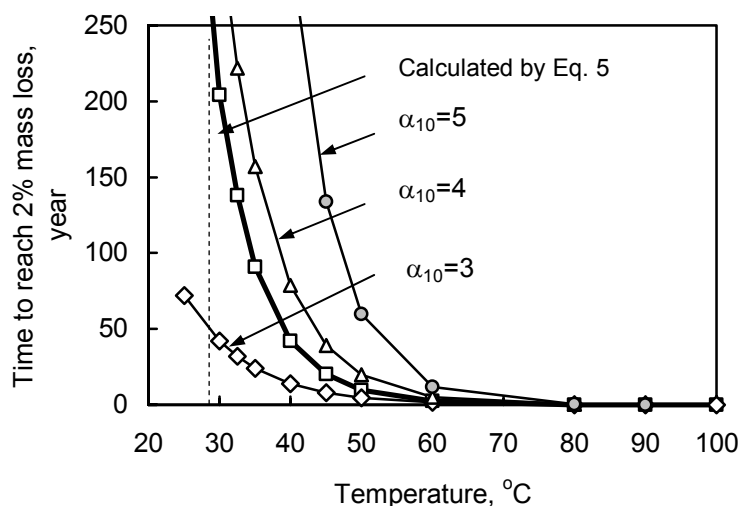


Fig 5. Calculated times to reach 2 % mass loss as a function of temperature

Fig. 5 illustrates that the calculated times to reach 2% mass loss at lower temperatures depend strongly on equation applied (Eq. 5 and Eq. 7), as well as on the value of the accelerating factor in Eq. 7. The difference in the calculated times increases at lower temperatures. This means that the prediction of NC propellant behaviour at the room temperatures on the basis kinetic results obtained at higher temperatures (in this case 80-100 °C) may lead to very uncertain data. This refers particularly to data calculated by Eq. 7.

4. CONCLUSIONS

The results presented in the paper have shown that the activation energy calculated for initial stage of NC propellant decomposition on the basis mass loss-time data equals 123.39 kJ/mol. This value is considerably lower than usually reported values (170 – 210 kJ/mol), but close to values obtained by microcalorimetric measurements (120-130 kJ/mol).

It was calculated on the basis of kinetic model and values of kinetic constants that the reaction rate accelerating factor changes with temperature – from about 3 at high temperatures (90 – 100 °C) to about 5.5 at the room temperatures. This may lead to very uncertain calculated times to reach the same degree of conversions at lower temperatures.

REFERENCES

- [1] ISLER, J., KAYSER, D.: Proceedings of the Sixth Symposium on Chemical Problems Connected with Stability of Explosives, Kungälv, Sweden, 217-237, 1982
- [2] ISLER, J.: Propell. Explos. Pyrotech. 11, pp.40-44, 1986
- [3] VOLK, F., BOHN, WUNCH, M. A. G Propell. Explos. Pyrotech. 12, pp. 81-87, 1986
- [4] KIMURA, J. Propell. Explos. Pyrotech. 13, 8-12, 1988
- [5] BERGENS, A., NYGARD, B. Proceedings of the Ninth Symposium on Chemical Problems Connected with Stability of Explosives. Margretetorp. Sweden. 1992
- [6] BOHN, M. A., VOLK, F. Propell. Explos. Pyrotech. 17 pp. 171-178, 1992
- [7] MISZEZAK, A., BLADEK, J. Proceedings of the Ninth Symposium on Chemical Problems Connected with Stability of Explosives. Margretetorp. Sweden. 1992
- [8] BOHN, M. A. Propell. Explos. Pyrotech. 19 pp. 266-269, 1994
- [9] BOHN, M. A., EISENREICH, N. Propell. Explos. Pyrotech. 22 pp. 125-136, 1997
- [10] SUĆESKA, M. Baruti. MORH. Zagreb. 1996.
- [11] RAJIĆ, M., SUĆESKA, M. High Temperatures-High Pressures 32 pp. 171-178, 2000.
- [12] BOHN, M. A.: Kinetic modelling of the ageing of gun and rocket propellants for the improved and time-extended prediction of their service lifetime, Proc. of 1998 Life Cycles of Energetic Materials, Fullerton, California, USAA, pp.1-38 29 March-1 April, 1998
- [13] ISLER, J., KAYSER, D., Correlation between kinetic properties and self-ignition of nitrocellulose, Proc. of 6th Symp. Chem. Probl. Connected Stab. Explos, Kungälv, Sweden, pp. 217 1982
- [14] SUĆESKA, M., *J. Therm. Anal. Cal.*, 68 pp. 865 2002
- [15] SUĆESKA, M., Influence of thermal decomposition kinetic model on results of propellants self-ignition numerical modeling, Proc. of. 5th Seminar "New Trends in Research of Energetic Materials, Pardubice (Czech Republic), pp. 308 2002
- [16] MCQUIRE, R. R., TARVER, C. M., Chemical decomposition models for thermal explosion of confined HMX, RDX, and TNT explosives, Report UCRL-84986, Lawrence Livermore Laboratory, Livermore, 1981.
- [17] TICMANIS, U., PANTEL, G., WILKER, S., KAISER, M., Precision required for parameters in thermal safety simulation, Proc. of 32nd Int. Annual Conference of ICT, Karlsruhe (Germany), July 3 -6, pp.135.1. 2001
- [18] SUĆESKA, M., RAJIĆ, M., Change of critical condition of propellants self-ignition under conditions of artificial ageing at elevated temperature (in Croatian), Report No. 9-2-668, Brodarski institut, Zagreb, 2002.
- [19] BAMFORD, C. H., TIPPER, C. F. H. *Chemical Kinetics*, Amsterdam, Elsevier Scientific Publishing Company, pp. 195-200, 1980
- [20] WILKER, S., PANTEL G., STOTTMEISTER, L: Stability analysis of porous propellants, Proc. of. 6th Seminar "New Trends in Research of Energetic Materials, Pardubice (Czech Republic), pp. 308 2003

DETERMINATION OF THE RELATIVE DENSITY OF MOLTEN EXPLOSIVES

Fritz van Rooyen

National Institute for Explosives Technology (NIXT) South Africa
PO Box 32544, Glenstantia 0010, Pretoria, Republic of South Africa

Abstract:

The Archimedes principle was used for the determination of the relative density of molten TNT. This method proves to be practical, easily conducted and quick, providing reliable results with high precision and sensitivity.

Keywords: *relative density, Archimedes, TNT*

1. INTRODUCTION

Archimedes's principle is frequently used for the determination of the relative density (RD) of solids, a dimensionless parameter. It is a rapid method providing reliable results especially suitable for irregular objects whose volume can not be accurately determined by other means. In the explosives industry it is applied to the determination of the RD of high explosives ^[1], for instance TNT biscuits, the solid samples normally supplied for quality control. During casting processes the relative density of the molten formulations is also a useful parameter. Hydrometers are mostly used for this purpose; however, due to the relative uncertainty of their readings a more accurate method was required. Investigation yielded no reference to the use of the Archimedes technique for measurements at elevated temperatures, hence this study.

2. THEORY

Archimedes's Law deals with the "loss of weight" (W_m), also known as the buoyant force as experienced when an object is suspended in a liquid of lower RD ^[2]. The law states that in this situation the object experiences a loss of weight which is equal to the weight of the volume of liquid displaced by the object.

Since weight is affected by changes in gravity, its relationship to mass must be taken into account. This can be stated as:

$$W_s = M_s g = V \Delta_l g \quad (1)$$

where W_s is the weight of the object, M_s its mass in air, g the gravity acceleration, V the volume of the object, and Δ_l the RD of the liquid.

According to the Archimedes Law the weight of the object immersed in a liquid is expressed by:

$$W'_s = M'_s g = V g (\Delta_s - \Delta_l) \quad (2)$$

where W'_s is the weight of the object in the liquid and ρ_s it's RD. These two equations can now be combined with volume and gravity acceleration cancelling out to give:

$$\Delta_s = \Delta_l / (1 - M'_s / M_s) \quad (3)$$

If the RD of the metal at higher temperatures is known, equation (3) can be used to determine the RD of any liquid at these temperatures, for example molten explosives. Since the composition of the object, which may be a metal or an alloy, as well as its RD at elevated temperatures are mostly unknown, a temperature/density curve must be compiled for the object by measuring its weight loss at a series of temperatures in a liquid whose RD is accurately known at these temperatures. Pure water is an excellent reference in this respect.

3. EXPERIMENTS

3.1 Apparatus:

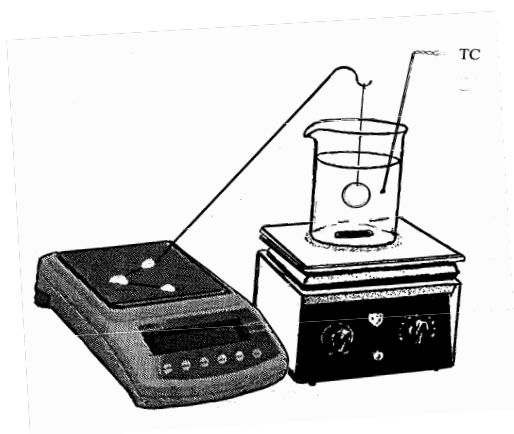


Fig 1. Experimental set-up

A top loading balance capable of weighing to three decimal places was fitted with a stout wire arm as illustrated in the diagram. Prestic was used to firmly fix the triangular base of the wire arm to the balance pan. The object, a 20g mass brass piece as used with older types of balances, was used as a “sinker.” A thin strand of copper wire was tied to the sinker and connected to the hook on the arm in such a way that the sinker was suspended when lowered into the liquid contained in the beaker. Temperatures were measured with a Hanna HI 9053 thermocouple digital temperature meter measuring to 0,1 °C and that was calibrated beforehand.

3.2 Determination of the RD of the sinker

The balance was zeroed after which the suspended sinker was first weighed in air. It was subsequently immersed in a beaker containing deionised water and the mass determined. The results are listed in Table 1.

3.3 Determination of the RD of the sinker at different temperatures.

The sinker was suspended in a beaker containing deionised water that was placed on a hotplate fitted with a magnetic stirrer. After heating to just below the boiling point of the water, the water was allowed to cool slowly, the stirring only interrupted when a mass reading and the temperature were taken. The results are listed in Table 2.

3.4 **Determination of the RD of molten TNT**

About 500g of commercial TNT was melted in a steam-heated double walled vessel to about 95°C and stirred well with a spatula. The sinker was inserted and left for a few minutes to heat up. The melt was then allowed to cool down slowly. At various intervals the stirring was stopped momentarily and the temperature and mass readings taken. At about 81 °C the measurements were stopped since crystallization commenced on the surfaces of the melt and also the copper wire and sinker. These results are listed in Table 2.

3.5 **Determination of the RD of molten RDX / TNT**

About 500 g of Composition B, RDX / TNT (60:40), as used for the filling of shells, was melted in the steam pot and the experiment repeated.

4. **RESULTS**

4.1 **Determination of the RD of the sinker**

Table 1. *Mass of sinker in air and water*

Mass of sinker in air (M _s)	20,133.g
Mass of sinker in water (M' _s)	17,750 g
Temperature of water	20°C
RD of water (Δ _l) at 20°C ^[3]	0,9982

$$\begin{aligned}\Delta_s &= \Delta_l / (1 - M'_s / M_s) \\ &= 0,9982 / (1 - 17,750/20,133) \\ &= 8,431\end{aligned}$$

(3)

4.2 **Determination of the RD of the sinker at different temperatures**

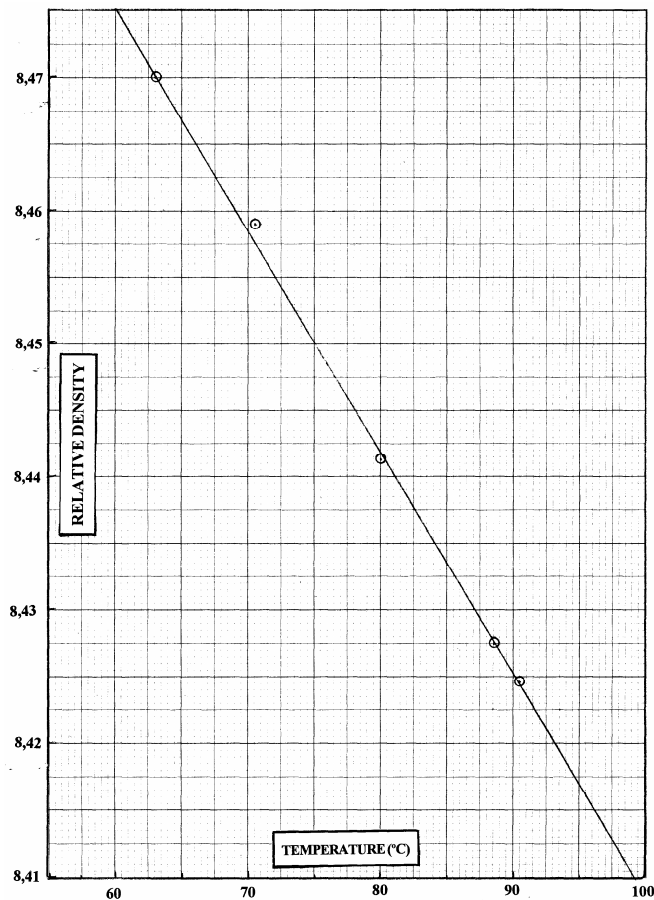
Table 2. *Mass of suspended sinker at elevated temperatures and resultant densities*

°C	90,0	86,0	80,0	70,0	63,0
M' _s	17,827	17,822	17,815	17,810	17,860
Δ _m	2,306	2,311	2,318	2,323	2,333
Δ _l	0,9653	0,9678	0,9718	0,9770	0,9815
Δ _m /Δ _l	2,390	2,388	2,385	2,380	2,377
Δ _s	8,424	8,431	8,442	8,459	8,470

- The 1st row lists the various temperatures where readings were taken.
- The 2nd row lists the mass (M'_s) of the sinker at the various temperatures.
- The 3rd row lists the difference (Δ_m) between the above mass and that of sinker in air (20,133 g).

- The 4th row lists the relative density of water (Δ_l) at the respective temperatures ^[3].
- The 5th row lists the volume of the replaced water and hence the volume of the sinker.
- The 6th row lists the RD of the sinker (Δ_s) at the various temperatures as determined with equation (3).

The RD of the sinker (Δ_s) was now plotted against temperature over the range 60 °C to 100 °C as illustrated in Graph 1. From this graph the RD's of the sinker for all intermediate temperatures as used during experiment 4.3 could be derived.



Graph 1. RD of the sinker at elevated temperatures

4.3 Determination of the RD of molten TNT

Table 3. *Determination of the RD of molten TNT*

°C	92,6	89,5	88,5	86,4	83,1	81,9	80,9
M's	16,682	16,674	16,671	16,673	16,673	16,677	16,678
) _m	3,451	3,459	3,462	3,460	3,460	3,456	3,455
Δ _s	8,420	8,425	8,427	8,430	8,436	8,438	8,440
Δ _l	1,440	1,447	1,449	1,450	1,458	1,449	1,449

- The temperature at which readings were taken is listed in row 1.
- The mass of the sinker (M'_s) at these temperatures are shown in row 2.
- The loss of weight (ρ_m) is shown in the row 3.
- The RD's of the sinker (Δ_s) at the corresponding temperatures as derived from Graph 1, is shown in row four.

The RD of TNT (Δ_t) at the various temperatures as listed in row five is now calculated by means of equation 3 which can be rewritten as:

$$\Delta_t = \Delta_s (1 - M'_s / M_s) \quad (4)$$

4.4 Determination of the RD of RDX / TNT

Since only about 4% of the RDX is dissolved in TNT with the remainder remaining as a suspension, the latter tended to settle on the sinker affecting the loss of weight. Vigorous stirring was required in order to maintain a homogeneous mixture which disallowed accurate reading of the mass.

5. DISCUSSION

Measurements were taken whilst the liquids were cooled, since especially in the case of water, some bubbles arising from dissolved air started to form on the sinker at temperatures as low as 60 °C. This affected the reading.

At the elevated temperatures of between 80 °C and 90 °C as used during casting it was expected that the RD of the molten TNT would change slightly. Over this range, however, it was found that the RD seemed to remain very stable with an average deviation of $1,449 \pm 0,003$ indicating a good precision of 0,2 %.

From Table 3 it is evident that there is virtually no change in ρ_m over this particular temperature range. The slight increase of RD of TNT is compensated for by the slight increase in volume of the sinker, hence the stable values. Due to the presence of a small amount of wax in the commercial TNT used, the value is slightly below that of pure TNT which is listed as 1,47 [4].

6. CONCLUSION

From the results it is evident that the RD of molten solids, for instance TNT, can be measured with great ease and with a sensitivity of four significant figures if a three decimal top-loading balance is used. Non-homogeneous mixtures like Composition B present problems due to the presence of undissolved crystals.

The very low average deviation indicates a precision that is much better than that normally applicable in the explosives industry where the RD of TNT is usually reported to two decimal places only. This implies that a two decimal balance would provide adequate sensitivity.

Acknowledgements

The following affiliations are thanked for the help and facilities provided during the investigation:

- *The Polymer Institute of the Tswane University of Technology, for experiments on molten waxes.*
- *Naschem, a division of Denel, for experiments conducted on explosives.*

REFERENCES

- [1] UK MINISTRY OF DEFENSE: Determination of Density of High Explosives, DEF STAN 13-190/ Issue 1, 29 November 1996.
- [2] J. B. MASON: Physics in the Modern World, Academic Press, New York, pp 217-8, ISBN 0-12-472277-6, 1976.
- [3] R.C. WEAST and M.J. ASTLE: CRC Handbook of Chemistry and Physics, CRC Press, Florida, Table F-11. ISBN 0-8493-0460-8, 1980.
- [4] R. MEYER: *Explosives*, Verlag Chemie, Weinheim/New York, pp 292, ISBN 3-527-25630-X, 1977

COMBUSTION OF DINITRAMIDE SALTS

V.P. Sinditskii, A.I. Levshenkov, V.Yu. Egorshev and V.V. Serushkin

Mendeleev University of Chemical Technology,
9 Miusskaya Square, 125047, Moscow, Russia

Abstract:

Burn rate studies have been carried out on dinitramide salts of common formula of $L_n\text{HN}(\text{NO}_2)_2$ (where $n = 1$ or 2 ; L = methylamine, trimethylamine, tert-butylamine, tetramethylammonium, urea, guanidine, aminoguanidine, triaminoguanidine, ethanolamine, diethanolamine, ethylenediamine, hexamethylenediamine, aniline, 3-nitroaniline, 2-toluidine, benzylamine, phenylhydrazine, morpholine, piperazine, pyridine, 3,5-dimethylpyridine, and 5-aminotetrazole) as well as lithium and barium salts of dinitramide. Most of the salts exhibit either combustion instability (like ADN) or a transition region on their $r_b(p)$ curves. The occurrence of this region depends upon the fuel reactivity and, largely, the surface temperature which is assumed to be dissociation one and dependent on the amine basicity. To disclose combustion mechanism, flame structure of hexamethylenediamine dinitramide (GMDADN) has been investigated with tungsten-rhenium microthermocouples. Besides, burn rate study of GMDADN within a wide initial temperature interval allowed the burning rate temperature sensitivity to be evaluated.

Keywords: Combustion, dinitramide salts, burning rate, temperature profile, temperature sensitivity

1. INTRODUCTION

Ammonium salt of dinitramide (ADN) is currently considered as one of the most promising substitute for the main oxidizer of composite propellants, ammonium perchlorate (AP). Unquestionable advantages of ADN over AP manifest themselves in possibility to produce higher-energy propellant compositions with no HCl in the combustion products, what is very important from ecological standpoint. At present a lot of organic and inorganic derivatives of dinitramide have been synthesized and published^[1,2]. Study of burning behavior of these compounds is believed to allow revealing not only combustion mechanism of dinitramide salts, their place among other energetic materials, but also elucidating combustion peculiarities of ADN-based mixtures if being considered as molecular level model compositions of oxidizer-fuel premixing.

The aim of the present paper was to investigate thoroughly the burning behavior of organic and inorganic salts of dinitramide (DN) and propose a relevant combustion mechanism. The results of earlier investigations on dinitramide salts have been partly presented at some conferences^[3,4].

2. EXPERIMENTAL

Sample Preparation.

Dinitramide salts were prepared by one of the four general pathways:

Scheme I



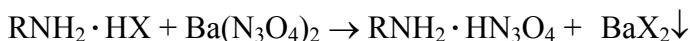
Mixture of ADN with an excess of amine (with or without a solvent) was heated at 60 °C for 4-6 hours under vacuum. The completion of the reaction was determined by the absence of NH_4^+ cation in the reaction mixture. The residuum was washed and recrystallized from a suitable organic solvent.

Scheme II



Equimolar amounts of the reagents in excess of iso-propanol or ethanol were brought to boiling and kept at this temperature until ammonium evolution had stopped. After filtration a major portion of the solution was evaporated, and crystals of dinitramide salt were precipitated upon cooling.

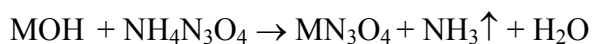
Scheme III



Solid barium dinitramide was dissolved in ethanol and treated with a solution of amine sulfate in aqueous ethanol. After separation of barium sulfate the resulting solution was evaporated until dry followed by recrystallization of the residue.

The metal and tetramethylammonium salts of dinitramidic acid were prepared as following:

Scheme IV



Equimolar amounts of ADN and MOH (M = Li, Ba, Me_4N) in water were heated to boiling and kept for one hour, filtered, and evaporated until dry.

ADN was twice-recrystallized from ethanol and used as the starting material in all the preparation reactions. The only stated impurity was about 0.4 per cent by weight of ammonium nitrate.

Physico-chemical properties of dinitramide salts studied are presented in Table 1.

Burn Rate Measurements. Burn rate measurements were carried out in a window constant pressure bomb of 1.5 liter volume. The pressure range studied was 0.1-36 MPa. A slit camera was used to determine a character of the combustion process as well as burning rate values.

The combustion strands were prepared by compacting the thoroughly comminuted substances in transparent acrylic tubes of 4 or 7 mm i.d. at 150-200 MPa.

Thermocouple Study. Temperature profiles were measured using thin tungsten-rhenium thermocouples embedded in the pressed samples. The thermocouples were welded from 25 μm diameter tungsten—5% rhenium and tungsten—20% rhenium wires and rolled in bands to obtain 5-7 μm bead size. A Tektronix TDS-210 digital oscilloscope was used to record the thermocouple signal. Calculations of adiabatic combustion temperatures were performed using the computer code REAL ^[5].

Table 1. *Preparation methods and physical properties of dinitramide salts*

Compound	Preparation method	Density of pressed strand, g/cc	Melting point °C	Ignition point °C	Enthalpy of formation (calc.), kJ/mol	Ref.
Aminoguanidine dinitramide	II	1.63	87-88	205	-48	[1]
5-Aminotetrazole dinitramide	III	1.87	83-86	170	201	[3]
Aniline dinitramide	III	1.52	95-97	182	39	[1]
Benzylamine dinitramide	I	1.44	59-61	-	-19	[3]
<i>Tret</i> -Butylamine dinitramide	I	1.32	87-89	-	-267	This work
Diethanolamine dinitramide	I	1.55	75-78	198	-598	[3]
3,5-Dimethylpyridine dinitramide	III	1.41	70-73	-	19	[3]
Ethanolamine dinitramide	I	1.53	37-39	175	-335	[3]
Ethylenediamine bisdinitramide	I	1.78	129-131	174	-209	[1]
Guanidine dinitramide	II	1.53	133-136	-	-168	[1]
Hexamethylenediamine bisdinitramide	I	1.40	89-90	192	-154	[3]
Methylamine dinitramide	I	1.53	43-45	177	-121	[1]
Morpholine dinitramide	I	1.49	82-84	180	-226	[3]
m-Nitroaniline dinitramide	III	1.61	101-103	195	-9	[3]
Phenylhydrazine dinitramide	III	1.45	93-95	206	+151	This work
Piperazine dinitramide	I	1.47	200-205	-	-124	This work
Piperazine bisdinitramide	I	1.50	212-214	215	-236	[3]
Pyridinium dinitramide	III	1.53	89-91	-	+35	This work
Tetramethylammonium dinitramide	IV	1.22	234-238	-	-191	[1]
o-Toluidine dinitramide	III	1.43	70-71	178	+6	[3]
Triaminoguanidine dinitramide	III	1.56	88-90	210	+168	[1]
Trimethylamine dinitramide	I	1.28	128-130	-	-90	[1]
Urea dinitramide	III	1.70	96-98	-	-346	[1]
Barium bisdinitramide	IV	2.70	-	-	-525	[2]
Lithium dinitramide	IV	1.96	164-169	-	-238	[2]

3. RESULTS AND DISCUSSION

One of peculiarities of dinitramide-anion is known to be the unique reaction of its transformation to form nitrate-anion and N_2O .^[6,7,8] Because of this exothermic reaction takes place, the studied inorganic dinitramide salts, barium and lithium, proved to be capable of self-sustained burning, although they did not contain any combustible elements. Combustion of these salts (Fig 1) is accompanied by formation of large amounts of condensed products as smoke and solid residue.

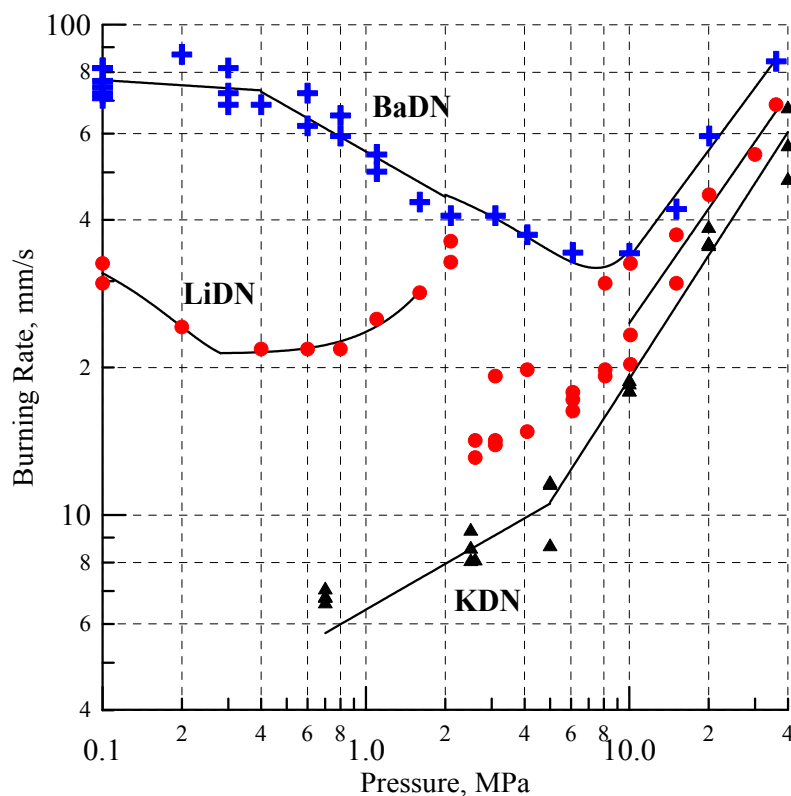


Fig 1. Effect of pressure on the burning rate of inorganic salts of dinitramide

At low pressures, the combustion occurs without luminous flame, which however appears as pressure grows. Both barium and lithium salts demonstrate rather high burning rates in the low-pressure region, decreasing with pressure. The lithium salts has probably a region of unstable burning characterized by a large scatter of data points. The combustion products of barium dinitramide were found to contain mainly barium nitrate and partially barium nitrite and oxide. At high pressures, a contribution of the gas-phase exothermic decomposition of N_2O to the heat balance probably increases, making for stable burning again. Fig 1 presents also burn rate data for potassium dinitramide obtained earlier by A.P.Glazkova at Chemical Physics Institute (Moscow).

Combustion of the organic salts under investigation at low pressures (less than 1-2 MPa) is generally also accompanied by copious fumes and solid residues with no visible flame observed. As the pressure increases, a luminous flame appears several millimeters above the surface, becoming more pronounced at pressures above 10-15 MPa. The condensed combustion products collected after burning at low pressure were analyzed to contain nitrate anion in the composition. In particular, the condensed combustion products of guanidine dinitramide, which unlike other salts were free from resinous impurities, were identified with IR spectroscopy as guanidine nitrate.

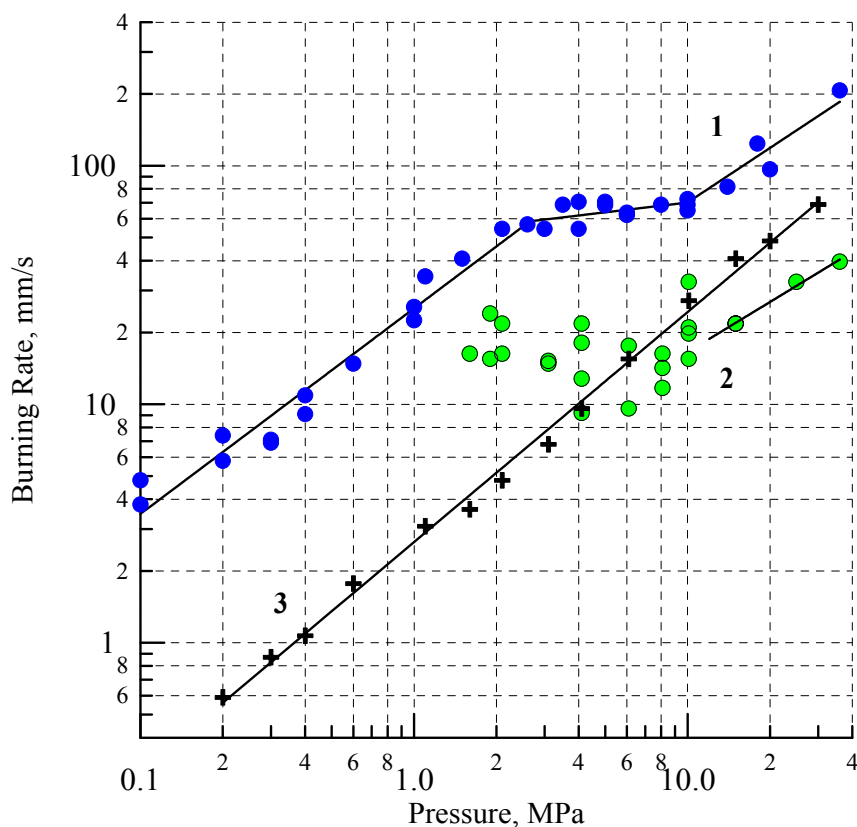


Fig 2. Effect of pressure on the burning rate of dinitramide salts of ethylenediamine (1), ethanolamine (2), and m-nitroaniline (3)

All the salts studied can be divided into 3 main groups according to their burning characteristics (Fig 2): (1) dinitramide salts which show a transition region characterized by the reduced pressure exponent on the $r_b(p)$ curve in the medium pressure range. This is the most commonly encountered group which includes dinitramide salts of amines of both high and low basicity; (2) salts which burning rate-pressure dependence includes a region of combustion instability, characterized by a significant scatter of burning rates in parallel tests. These are salts of amines of high basicity, such as benzylamine and ethanolamine. Methylamine dinitramide can be probably placed into this group as well, although its transition region is difficult to distinguish, because the salt is incapable of burning at all in the low-pressure region; (3) salts which demonstrate stable combustion, showing invariant pressure exponent through the whole pressure range. These includes salts of amines of the least basicity: 5-aminotetrazol and m-nitroaniline.

Fig 2 demonstrates burn rate characteristics for representatives of each group: ethylenediamine dinitramide (1st group), ethanolamine dinitramide (2nd group) and m-nitroaniline dinitramide (3rd group).

To disclose the combustion mechanism, the flame structure of hexamethylenediamine bisdinitramide (GMDADN) has been investigated with tungsten-rhenium microthermocouples. As in the case of ADN, GMDADN shows a local maximum on the burning rate vs. pressure dependence, situated at pressure lower than that of ADN burning rate maximum (Fig 3).

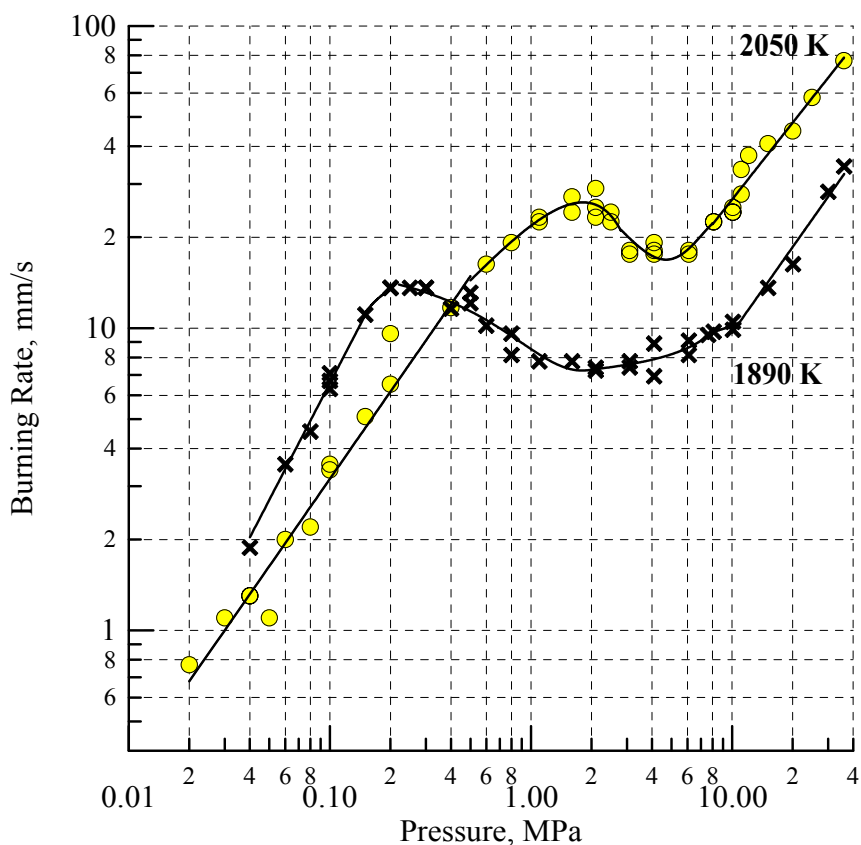


Fig 3. Effect of pressure on the burning rate of dinitramide salts of hexamethylenediamine (crosses) and ammonium (points). Figures are calculated adiabatic combustion temperature

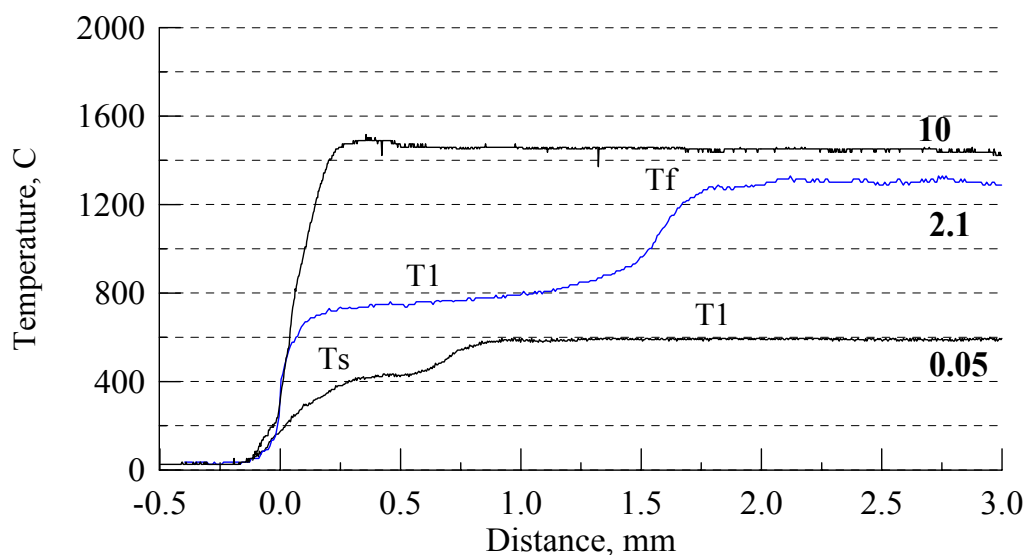


Fig 4. Temperature profiles of GMDADN at 0.05, 2.1 and 10 MPa

Temperature profiles have been measured with thin thermocouples at pressures of 0.05, 0.1, 0.25, 2.1, and 10 MPa, that is before the local burning rate maximum, at the maximum, and after it. The typical profiles are presented in Fig 4.

Table 2. Surface temperature (T_s), first flame temperature (T_1), and maximum flame temperature (T_f) for combustion of GMDADN

Pressure, MPa	T_s , K	T_1 , K	T_f , K
0.05	710±10	860±15	-
0.1	730±15	907±15	-
0.25	765±15	940±15	-
2.1	-	1020±45	1600±35
10.0	-	-	1700±20

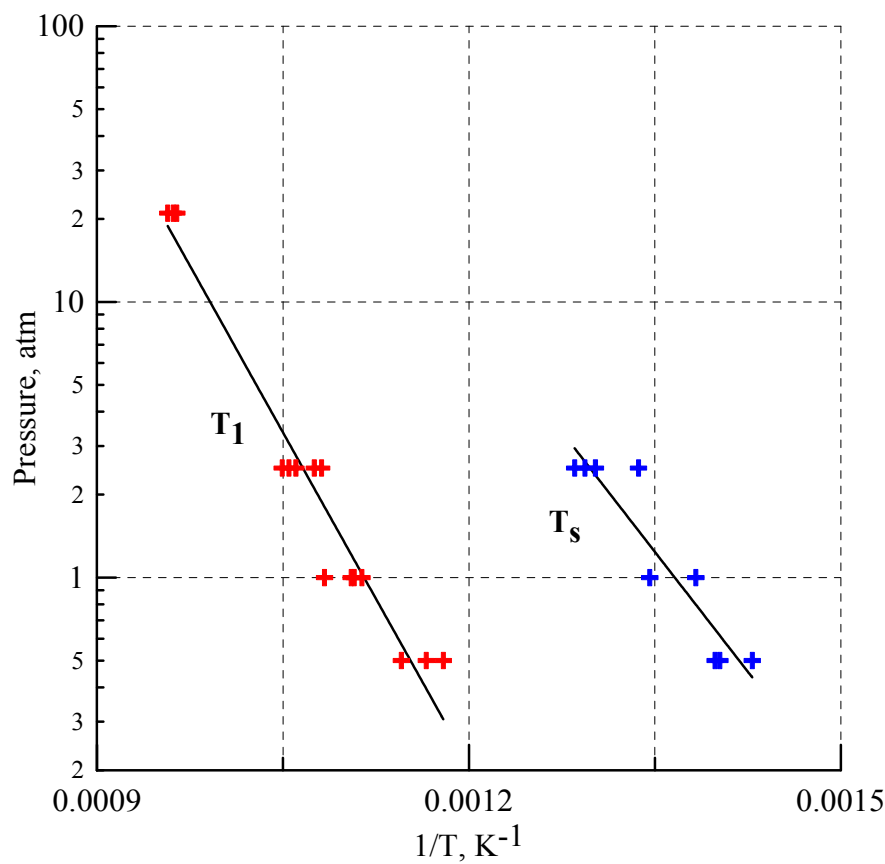


Fig 5. The plot of pressure against reciprocal characteristic temperatures of GMDADN

Temperature profiles of GMDADN reveal characteristic features at low pressures: just above the surface, the temperature is kept constant and equal to the surface temperature for some time and then increases by ~ 200 K in a stepwise manner. The gas flame appears at pressures above 2 MPa. Characteristic temperatures in the combustion wave of GMDADN: the surface temperature (T_s), the temperature above the surface (T_1), and temperature of the final flame (T_f), are presented in Table 2 and Fig 5.

In the previous ADN combustion studies ^[9,10] it was proposed that the temperature of the combustion surface corresponded to the temperature of dissociation of ammonium nitrate formed in the condensed phase, and the temperature T_1 was controlled dissociation reaction of ammonium dinitramide. Using the same approach for GMDADN, the heats of dissociation of nitrate and dinitramide salts have been calculated from the slopes of the curves constructed in the corresponding coordinates $\lg P-1/T_s$ and $\lg P-1/T_1$ to give values of 80 and 111 kcal/mole, respectively. These figures are in a good agreement with heats calculated as a difference

between heats of formation of solid GMDA nitrate and dinitramide and gaseous products of their dissociation, 89 and 104 kcal/mole, respectively.

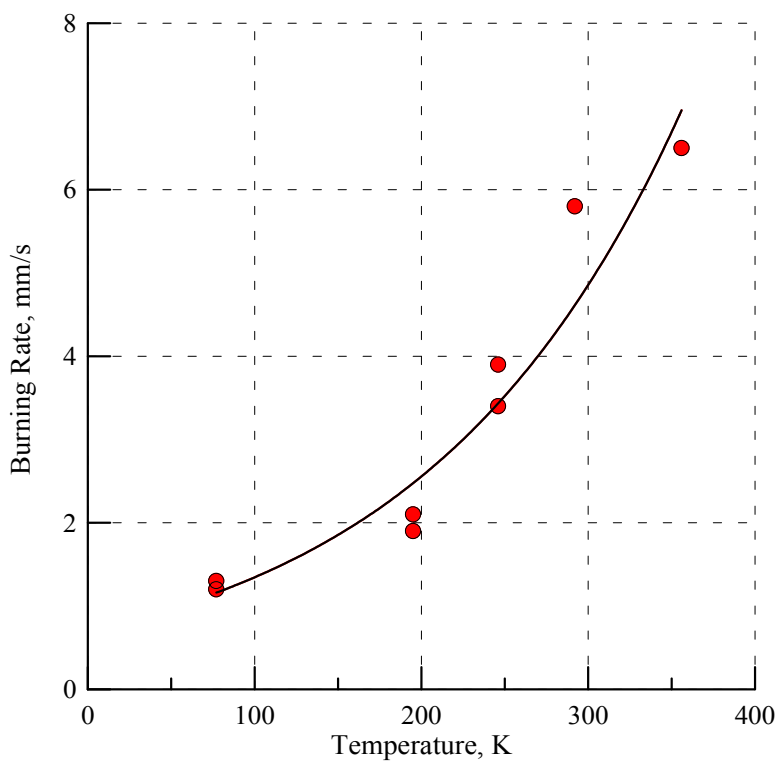


Fig 6. Effect of initial temperature on the burning rate of GMDADN at 0.1 MPa

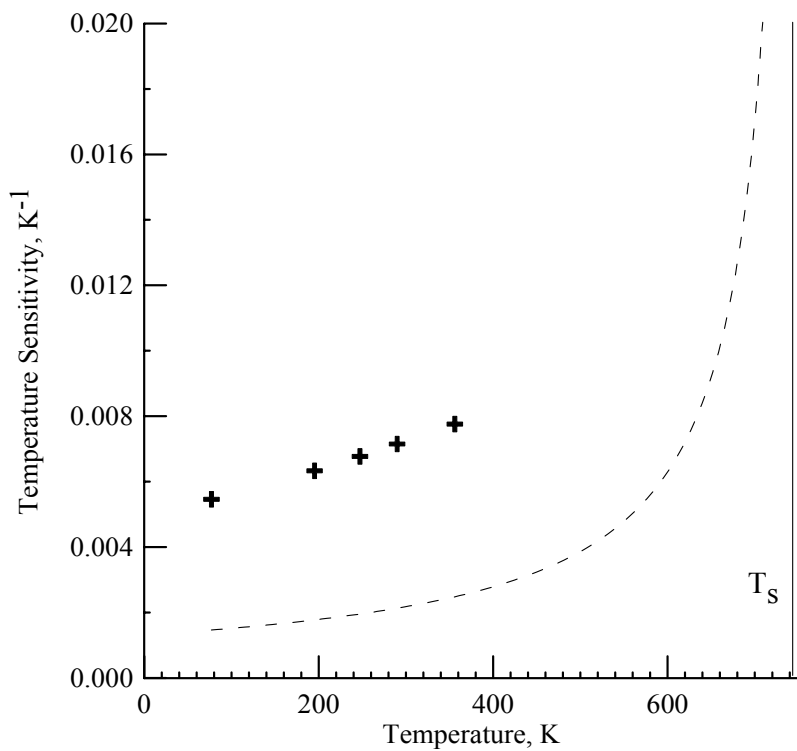


Fig 7. Comparison of the experimental temperature sensitivity of GMDADN (crosses) at 0.1 MPa with calculated one (dashed line)

It is interesting to note that the surface temperatures of GMDADN and ADN measured at the pressures corresponding to the burn rate local maximums are close together (~725 K). Since heat effects of the GMDADN and ADN decomposition in the condensed phase are close also, the similarity between surface temperatures supports the early conclusion,^[11] that the reason for combustion instability is the same: a deficit in the reaction heat for heating-up the solid to the surface temperature and subsequent dissociation.

GMDADN is capable of self-sustained burning at atmospheric pressure even at temperature of liquid nitrogen (77 K), allowing burning rate-initial temperature dependence to be measured in a wide temperature interval (77-383 K) (Fig 6). The burning rate of the salt measured at low temperatures demonstrates rather significant data scatter, which is characteristic for combustion with the leading role of the condensed phase reactions.

Burning rate temperature sensitivity of GMDADN (σ) at atmospheric pressure has been calculated from the experimental data. It increases from $4 \cdot 10^{-3}$ to $8 \cdot 10^{-3} \text{ K}^{-1}$ as the initial temperature grows from 77 to 353 K. These values are several times more than the theoretical ones evaluated from the combustion model based on the dominant role of condensed phase chemistry (Fig 7):

$$\sigma = \frac{1}{T_s - T_0 + L_m / c_p}$$

This may be indicative of the thermal instability of combustion as a reason for the occurrence of the local maximum on the burning rate vs. pressure curve, as was the case of ADN.

These observations allow considering all the dinitramide salts including ADN as having similar combustion mechanism. At low pressures, the reaction of dinitramide salt decomposition to form N_2O and corresponding nitrate plays a dominant role in combustion. As pressure increases, there comes a point when the heat of the reaction is no longer sufficient for heating-up the solid to the surface temperature and subsequent dissociation, while exothermic redox reactions in the gas have yet to be faster and closer to the surface to contribute noticeably to the condensed phase heat balance. This causes a large share of dinitramide salts to exhibit either a transition region or combustion instability area at these pressures. The occurrence of this region depends upon the fuel reactivity and, largely, the surface temperature, which is assumed to be dissociation one and dependent on the amine basicity. Salts of low-basicity amines generally have lower dissociation temperatures, with the result that the balance between heat required and evolved in the condensed phase is unaffected by the increasing pressure. At pressures above 10 MPa a contribution of gas-phase redox reactions gets dominant, bringing about the combustion temperature to the first place.

4. CONCLUSION

A specific region on the burning rate vs. pressure dependence, characterized by either reduced pressure exponent or combustion instability has been found to be a peculiar feature of the combustion of most of the dinitramide salts. All the salts including ADN have been concluded to have a common combustion mechanism which involves the condensed-phase reaction to form N_2O and the corresponding nitrate. This reaction determines the burning rate at low pressures.

REFERENCES

- [1] O.A. LUKJANOV, A.R. AGEVNIN, A.A. LEJCHENKO, N.M. SEREGINA and V.A. TARTAKOVSKY: *Dinitramide and Its Salts. 6. Dinitramide Salts with Amine Bases*, Izvestiya RAN, Ser. Khim., No 1, pp.113-117, 1995
- [2] O.A. LUKJANOV, Y.V.KONNOVA, T.A.KLIMOVA, A.A. LEJCHENKO and V.A.TARTAKOVSKY: *Dinitramide and Its Salts. 3. Dinitramide Salts with Metals*”, Izvestiya RAN, Ser. Khim., No 9, pp.1546-1549, 1994
- [3] V.P. SINDITSKII, A.E. FOGELZANG, A.I. LEVSHENKOV, V.Y. EGORSHEV and V.V. SERUSHKIN: *Combustion Behavior of Dinitramide Salts*, AIAA Paper 98-0808, pp.1-6, 1998
- [4] V.P. SINDITSKII, A.I. LEVSHENKOV, V.Y. EGORSHEV, V.V. SERUSHKIN: *Combustion of Dinitramide Salts*, Proc. Int. Workshop on Unsteady Combustion and Interior Ballistics, Saint-Petersburg, June 26-30, 2000, pp.75-78
- [5] G.V. BELOV: *Thermodynamic Analysis of Combustion Products at High Temperature and Pressure*, Propellants, Explosives, Pyrotechnics, Vol. 23, pp. 86-89, 1998
- [6] S. VYAZOVKIN and C.A. WIGHT: *Ammonium Dinitramide: Kinetics and Mechanism of Thermal Decomposition*, J. Phys. Chem. A, Vol.101, pp.5653-5658, 1997
- [7] T.P. RUSSELL, G.J. PIERMARINI, S. BLOCK and P.J. MILLER: *Pressure, Temperature Reaction Phase Diagram for Ammonium Dinitramide*, J. Phys. Chem. A, Vol.100, pp.3248-3251, 1996
- [8] A.N. PAVLOV and G.M.NAZIN: *Decomposition Mechanism of Dinitramide Onium Salts*, Russ. Chem.Bull., Vol. 46, No. 11, pp.1848-1850, 1997
- [9] A.E. FOGELZANG, V.P. SINDITSKII, V.Y. EGORSHEV, A.I.LEVSHENKOV, V.V.SERUSHKIN, and V.I. KOLESOV: *Combustion Behavior and Flame Structure of Ammonium Dinitramide*, Proc. 28th Inter. Annual Conference of ICT, Karlsruhe, FRG, 24-27 June 1997, paper 90, pp.1-14
- [10] V.P. SINDITSKII, A.E. FOGELZANG, V.Y. EGORSHEV, A.I.LEVSHENKOV, V.V. SERUSHKIN and V.I. KOLESOV: *Combustion Peculiarities of ADN and ADN-based Mixtures (Combustion of Energetic Materials, edited by K. K.Kuo, L.T. DeLuca)*, Begell House Inc., New York, 2002, pp.502-512
- [11] V.P.SINDITSKII, V.Yu.EGORSHEV, V.V.SERUSHKIN, A.I.LEVSHENKOV: *Chemical Peculiarities of Combustion of Solid Propellant Oxidizers*, Proc 8th Inter. Workshop on ROCKET PROPULSION: PRESENT AND FUTURE, Pozzuoli, Italy, 16-20 June 2002, pp. 34-1- 34-20

DETERMINATION OF CHEMICAL STABILITY OF GUNPOWDERS BY QUALITATIVE AND QUANTITATIVE METHODS

R. Smileski, O. Popovski and J. Naumoski

Military Academy "General Mihailo Apostolski" Skopje, Republic of Macedonia

Abstract:

This work presents the results from the analyses made on monobasic gunpowder, which consists of two types of stabilizers (diphenylamine and centralit I) with total mass of representation of about 1,3%.

The content of the residual stabilizer of gunpowder treated at different temperature and at different length of time was determined by using two quantitative methods.. By processing and comparing the results gained at raised temperature an attempt was made to foresee the time of stability of the gunpowder in normal conditions of storing.

As quantitative methods in this case The Hansen test and liquid chromatography (HPLC) were applied According to the first method the gunpowder was treated at 110 °C in the period from 0 to 72 h, and the results were validated by using pH - meter.

The second method was used to determine the content of the residual stabilizer at the same gunpowder treated at 110°C as long as the content of the active stabilized does not go below 50% m/m from the starting one.

Keywords: *gunpowder, chemical stability, stabilizer*

1. INTRODUCTION

The compressive explosive materials, which include all types of gunpowder, contain one or more *nitro esters*, dealt in the stability as a science and practice of the chemical mechanical and ballistics evolution of the homogenous gunpowder and propulsives ^[1, 2].

All these explosive materials are related by two basic properties: sensitivity to external exposure influences, i.e. the capacity of explosive materials to react to external conditions; and the stability of the explosive materials which is expressed in their capability to retain their initial qualities (chemical, mechanical and physical, ballistic and others) within certain limits and in the foreseen period for their use. The stability is analyzed according to the safety of the explosive materials whether they are incorporated into particular systems or are kept separately ^[3].

The chemical stability of explosive materials implies their capability to remain stable after their insertion into ammunition, at temperatures from -30 to +60 °C, and remain unaltered for a number of years, i. e. not to be subject to the process of chemical decomposition. However, the esters especially the nitroesters are not stabile and are subject to spontaneous self degradation (decomposition). The rate of decomposition increases by increasing the temperature while the kinetics goes according to the known Arrhenius law. So the nitrocellulose as basic component of the gunpowder shows signs of thermal degradation. This decomposition of nitrocellulose is a complex process which is thought to be catalyzed by the byproducts of the decomposition itself, especially by the reactive nitrogen oxides ^[4].

The most frequent method for stabilization of the nitrocellulose gunpowder is adding of the diphenylamine, which reacts, with the products of the decomposition when nitrated derivatives of diphenylamine are created. However the stabilization of the intracellular gunpowder can be performed by adding a mixture of two stabilizers (ex. Diphenylamine and centralit) in certain proportion. The nitro cellular gunpowder used in the ammunition are mostly made with the content of the stabilizer from 1% to 1,5% ^[4].

Because the stabilizer as the main acceptor of the nitrogen oxides is closely related with the decomposition of the nitrocellulose, it is thought that the content of the remaining stabilizer is an adequate indicator for determiniing the evolution of the gunpowder. For these reasons monitoring of the content of the stabilizer in the gunpowder is performed depending on the time of storage of the ammunition in which the respective gunpowder had been inserted. When the amount of stabilizer in the gunpowder mass is reduced below 50%, the gunpowder is thought to be chemically unstable and as such, not suitable for further use ^[6].

The mechanism of the diphenylamine reaction with the products of the denitration of the nitrocellulose occurs by substitution of the hydrogen atoms of diphenylamine with the nitroso-gasses of the nitrocellulose, during which N-nitrosodiphenylamine is formed and then in the subsequent stages of substitution several intermediary products are formed – diphenylamine derivatives (fig. 1) ^[7] which are also thought to have a stabilizing effect.

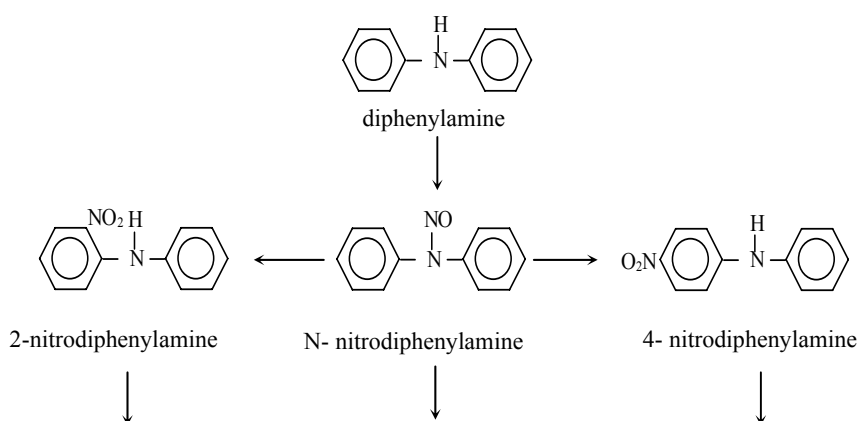


Fig 1. Diphenylamine reaction mechanism

The data from the determination of the total content of stabilizer (diphenylamine, centralit and its derivatives) serve to predict the time of safe storage of the gunpowder, which requires the use of exceptionally quick and accurate instruments and methods. Classical methods do not fulfill these criteria, because the examinations take long (several days), and the gunpowder is treated at higher temperatures which results in its accelerated aging and decomposition according to mechanisms which are still not sufficiently clear.

Gas chromatography has been used for a long time as a leading method in the determination of stabilizer content in gunpowders. Although this method is sufficiently quick it still has certain drawbacks which make it unsuitable for this purpose, i.e. the substances that are analyzed before being entered into the gas chromatography column need to be transformed into gas phase, which causes partial or complete decomposition of the thermally unstable compounds ^[8]. In this manner thermally unstable derivative of diphenylamine, N-nitrosodiphenylamine, is decomposed to diphenylamine ^[9] which prevents the determination of the actual content of diphenylamine and its derivatives.

More recently, a solution was found with the use of the high-pressure reversible liquid-phase chromatography which enables determination at much lower temperatures.

2. EXPERIMENTAL

In this case a monobasic gunpowder with initial content of the stabilizer of about 1,3% is examined. It is determined that a mixture of diphenylamine and centralit I is used as a stabilizer, in a content of about 0,7% and 0,5%, accordingly. The analyses are made by using the classical Hansen method and the liquid chromatography (HPLC).

Before the beginning of the treatment at the given temperature for extraction of the damp, the gunpowder was treated at 80 °C in a period of four hours. The analyses by the Hansen method are carried out by using a suitable thermo block in which the gunpowder was treated at temperature of 110 °C, and then in the test tube with gunpowder a distilled water with pH 5,5 was added and after the intensive mixing with duration of 3 - 5 minutes the pH of the solution was measured. The analyses with liquid chromatography are carried out by using a liquid chromatograph of the company Varian with UV detector and column RP C8 with dimensions 4,6 x 250 mm (stationed phase Bondesil with size of the particles of 5 µm).

The procedure of work is standardized with standard [10].

The thermally treated samples of gunpowder are first diluted with a solvent (dichloromethane solvent) and left for an appropriate time period in order to extract the stabilizer from the gunpowder. After this, with the aid of a microliter syringe, an assay of 2 µl was taken from the solution for analysis. Standard Merck solvents were used for this purpose.

All measurements were performed at room temperatures, at a wave length of 254 nm. The ratio of the solvents in the liquid phase was 60% acetonitrile and 40% water, with a 1 ml/min flow. Every experiment was repeated several times, with the aim to prove the reproducibility and the accuracy of the results.

3. RESULTS AND DISCUSSION

According to the Hansen method the gunpowder is considered as chemically stable if after eight hours of treatment at 110 °C the value of pH doesn't go below 3,30. So, in our case it is a case of a stable gunpowder because the pH value is bigger than 3,30 and after 72 hours (Table 1). Most probably because of the strong base influence of the diphenylamine, pH of the solution increases from 5,5 to 6,10 at the beginning which brings to gaining nonrealistic results for evaluation of the stability. Also, from these results the mechanism of the reaction and the structure of the real stabilizer can not be determined as well as the future course and speed of the gunpowder degradation can not be predicted too.

The results of the examination of the stability by using the liquid chromatography are shown as chromatograms (fig. 2 and 3).

The presence of diphenylamine in the analyzed gunpowder is evident from the chromatograms and centralit, (peak 1) which appear at approximately 12 min. i.e. 13 minutes. Beside the basic stabilizers diphenylamine and centralit, the presence of their derivatives is also obvious: 4-nitrodiphenylamine (peak 3), N-nitrosodiphenylamine (peak 4), and 2-nitrodiphenylamine (peak 5), formed according to the reaction of diphenylamine with the separated NO and NO₂ gasses, (fig.1) and N-nitroso-N-ethylanilin (peak 6).

Table 1. Gunpowder treatment at 110 °C

No.	Time of treatment [h]	pH
1.	2	6,10
2.	4	6,05
3.	6	5,73
4.	8	5,60
5.	10	5,05
6.	12	4,53
7.	24	3,65
8.	48	3,48
9.	72	3,43

Quantitatively the presence of diphenylamine and its derivatives is determined from the surface of the peaks. Reference peaks had been obtained for this purpose. The quantitative analyses show that the content of the total stabilizer in the gunpowder is bigger than 50% m/m after 24 hours treatment at the given temperature (Table 2), while after 48 hours is about 40% m/m. The results on figure 4 show obvious thermal instability of the diphenylamine and centralit derivatives. That instability results into recurrent reaction, especially in the period from 8 to 24 hours.

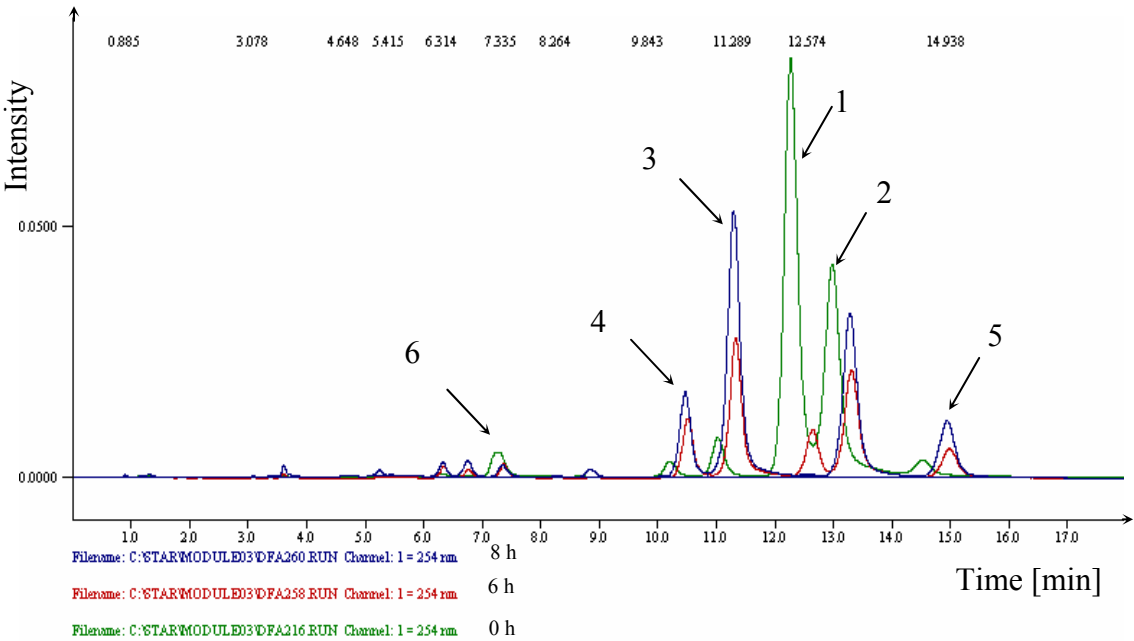


Fig 2. Chromatogram of diphenylamine ,centralit I and their derivatives from 0 to 8 h treatment na 110 °C
1 - DPA (diphenylamine); 2 - centralit I; 3 - N-nitroso-DPA; 4 - 4-nitro-DPA; 5 - 2-nitro-DPA; 6 - N-nitroso-N-ethylanilin

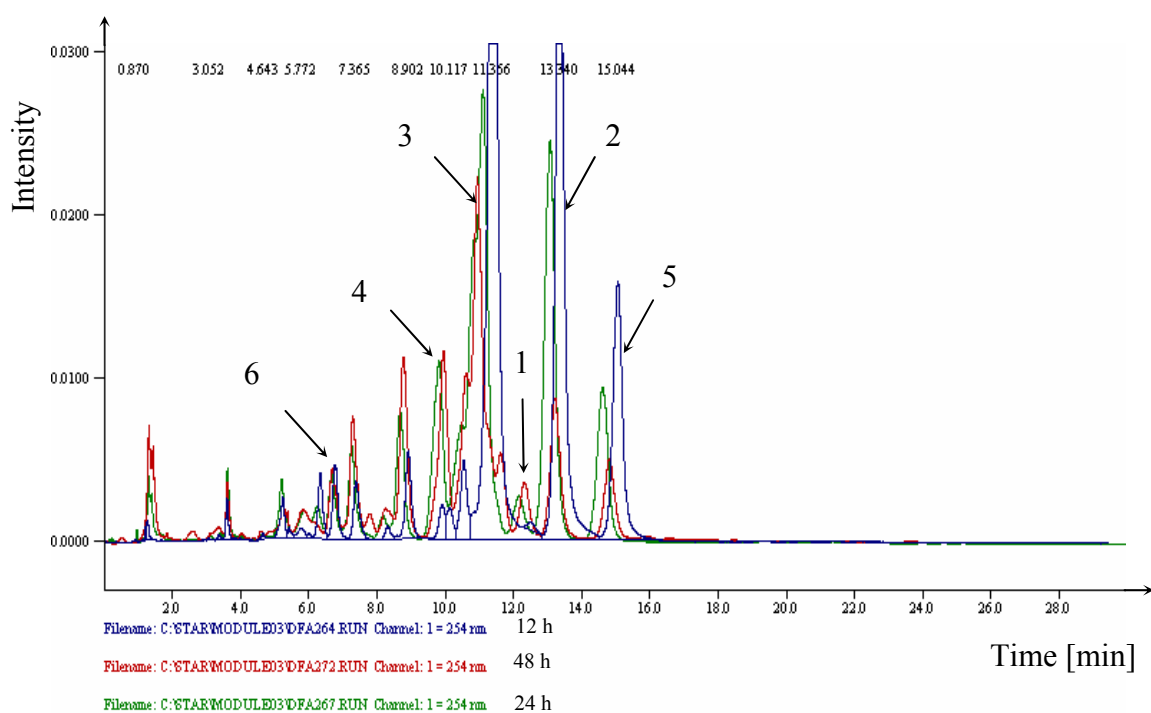


Fig 3. Chromatogram of diphenylamine, centralit I and their derivatives from 10 to 48 hrs treatment at 110 °C
 1 - DPA (diphenylamine); 2 - centralit I; 3 - N-nitroso-DPA; 4 - 4-nitro-DPA;
 5 - 2-nitro-DPA; 6 - N-nitroso-N-ethylanilin

Table 2. Content of the stabilizer after treatment of the gunpowder from 0 to 72 hrs at temperature of 110 °C

Time of treatment [h]	DPA [%m/m]	Centra-lit [%m/m]	N-NDPA [%m/m]	2-NDPA [%m/m]	4-NDPA [%m/m]	2-Ncentr. [%m/m]	Total stabil. [%m/m]
0	0,69	0,52	0,05	0,01	0,02	0,01	1,30
2	0,39	0,36	0,13	0,03	0,02	0,01	0,94
4	0,33	0,29	0,25	0,05	0,04	0,01	0,92
6	0,16	0,28	0,27	0,04	0,05	0,01	0,81
8	0,00	0,33	0,40	0,04	0,05	0,01	0,83
10	0,00	0,36	0,52	0,05	0,02	0,00	0,95
12	0,00	0,40	0,64	0,05	0,01	0,00	1,10
24	0,00	0,36	0,55	0,04	0,03	0,02	1,00
48	0,05	0,12	0,32	0,02	0,04	0,02	0,57
72	0,05	0,02	0,28	0,01	0,05	0,02	0,43

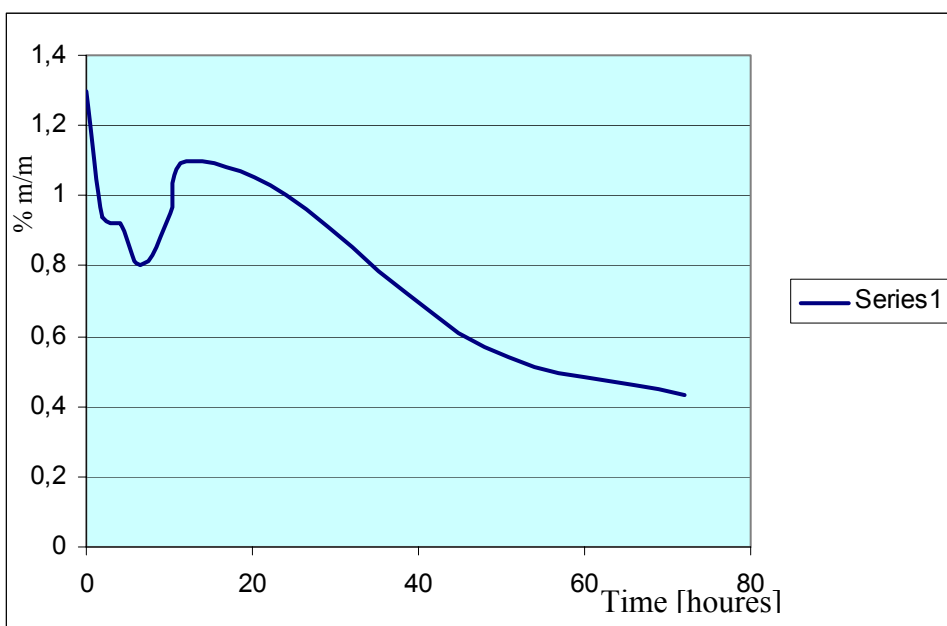


Fig 4. Diagram of the loss of the stabilizer in the gunpowder at treatment of 110 °C

If the gained results for the speed of the loss of the stabilizer in the gunpowder are replaced in the form ^[1]:

$$D_{50}(20^{\circ}\text{C}) = \frac{d_{50}(T) \cdot \gamma_{10}^{\frac{T-20}{10}}}{365}$$

where:

- $D_{50}(20^{\circ}\text{C})$ - Time during which the gunpowder spent half of the stabilizer at storage temperature $T = 20^{\circ}\text{C}$;
- γ_{10} - coefficient (factor of accelerating the degradation reaction for 10 K);
- $d_{50}(T)$ - time during which the gunpowder spend half of the stabilizer at temperature of treatment $T = 110^{\circ}\text{C}$,

then the following is gained:

$$D_{50}(20^{\circ}\text{C}) = \frac{1,7 \cdot 2,5^{\frac{110-20}{10}}}{365} = 17,8 \text{ years}$$

This would mean that the examined gunpowder will be chemically stable in the next 18 years. Still, this result should be taken with a dose of reserve, because it doesn't include the effect of the mass and the surrounding of the gunpowder bullets.

4. CONCLUSION

1. The classical methods including the Hansen method do not give a real picture of the condition of the chemical stability of the gunpowder, but only initial conclusion that at the moment of the examination it is stabile or non stabile.
2. Different then the previous method the liquid chromatography enables gaining real data for the condition of the gunpowder and the stabilizer into it. Because of the relatively high temperature of treatment and the instability of the derivatives of the basic stabilizer, certain mistakes are possible but they do not have big influence over the final evaluation of the chemical stability of the gunpowder.
3. The results gained by using the liquid chromatography can be used with a dose of reserve ,to predict the time during which the gunpowder would be stabile.

REFERENCES

- [1] M. HRISTOVSKI: *Eksplozivne materije – rečnik*, NIU Vojska, Beograd, 1994
- [2] R. Q. SMILESKEI: *Municija i eksplozivni materii - teoretski osnovi*, Maring, Skopje, 1998
- [3] D. PAVLOVIC, A. DUULO: *Osnovi konstrukcije artileriskog naoruzanja*, SSNO, Beograd, 1983
- [4] A. BERGENS, R. DANIELSSON: *Decomposition of Difenyamine in nitrocellulose based propellants – I*, Talanta, 1995, Vol.42. No. 2. pp. 171-183
- [5] MICHAEL P. O'KEEF: *Modern Applications of Chemistry*, Department of Chemistry, UN Military Academy, 1995
- [6] Standard SNO 8069/91, *Pracenje hemijske stabilnosti baruta i raketnih goriva*
- [7] A. BERGENS: *Decomposition of Difenyamine in nitrocellulose based propellants – II*, Talanta, 1995, Vol.42. No. 2. pp. 185-196,
- [8] LJ. JELISAVAC, M. FILIPOVIC, S. STOILJKOVIC: *Odredjivanje sadrzaja difenilamina i njegovih mono-derivata u jednobaznim barutima metodom reversno-fazne tecne-hromatografije pod visokim pritiskom*, Zbornik radova, str. 123-132, Tara, 2001
- [9] A. SOPRANETTI, H.U. REICH: *Possibilities and limitations of HPLC for the characterization of stabilizers and their daughter products in comparison with gas-chromatography*, Proc. Sym. Chem. Probl. Connected Stabil. Explo., Bastad, No. 5, pp. 163-177, 1979
- [10] Standard SNO 8069/91: *Pracenje hemijske stabilnosti baruta i raketnih goriva*

DETERMINATION OF EXPLOSIVE PROPERTIES

R. Špášová

Explosia a. s., Research Institute for Industrial Chemistry,
Safety Engineering Laboratory, 532 17 Pardubice-Semtín, CZ

Abstract:

This paper informs about testing of explosiveness of chemical substances according Ministry of Environment Decree which becomes valid to the date of entering the Treaty of Accession of Czech Republic to European Union into force.

Keywords: *explosive properties, shocks sensitivity, friction sensitivity*

1. INTRODUCTION

There is a number of strict standards and directives for explosives what put great demands on safety precautions for their production, storage and transport. Their implementation comes from exhaustive knowledge of all their dangerous properties.

However, even materials of non-explosive characteristics can paradoxically be as dangerous as explosives but they can behave like explosives for specific conditions. These materials can be treated and stored with no limits nevertheless they are relatively less dangerous than explosives because of their less sensitivity to different stimulants and less explosive effect.

According to the act 356/2003 ^[1] about chemical substances and chemical preparations and the amending some others act the chemical substances and preparations are solid, liquid, pasty or gelatinous and can react exothermally even without access of air-oxygen. They are quickly gas-evolving and in partially bounded space and in defined test conditions they detonate, burn rapidly or they explode after warming-up.

To the date of entering the Treaty of Accession of Czech republic to EU into force becomes valid Ministry of Environment Decree which for chemical substances and preparations there are methods for testing of physico-chemical properties, explosive properties and properties dangerous for environment. On the same day there is cancelled the Decree No.299/1998 and No.316/1998 in which the method for explosibility detection of chemical substances and preparations is determined.

For explosibility detection of materials due to the Decree mentioned above there will be the method A 14 named "Determination of explosives properties".

According to this method the explosive material is considered as the chemical substance or preparation what can explode by heat influence or from the aspect of explosive possibility is impact-sensitive or friction-sensitive in the instrument introduced in that Decree or is more sensitive to impact or friction than 1,3-dinitrobenzene in an alternative instrument. Such method is not used for determination if the material is able to explode in any conditions.

The material must be examined in these tests:

- test of thermal sensitivity,
- test of mechanical sensitivity with respect to shock,
- test of mechanical sensitivity with respect to friction.

2. DESCRIPTION OF METHOD

2.1 Test of thermal sensitivity

This test is used to determine the sensitiveness of solid and liquid substances to the effect of intense heat under high confinement.

The method involves heating the substance in a steel tube closed by orifice plates with differing diameters of hole to determine whether the substance is liable to explode under conditions of intense heat and defined confinement.

The apparatus consists of a non-reusable steel tube with its reusable closing device (figure 1) installed in a heating and protective device. The tube is deep drawn from sheet steel of suitable quality. The open end of the tube is flanged. The closing plate with an orifice through which the gases from the decomposition of the test substance escape is made from heat-resisting chrome steel and is available with the following diameter holes: 1,0 – 1,5 – 2,0 – 2,5 – 3,0 – 5,0 – 8,0 – 12,0 – 20,0 mm [3].

Heating is provided by propane, from an industrial cylinder fitted with a pressure regulator, via a flow meter and distributed by a manifold to the four burners. The gas pressure is regulated to give a heating rate of $3,3 \pm 0,3$ K/s when measured by the calibration procedure [2].

The tube is suspended between two rods placed through holes drilled in opposite walls of the box. The arrangement of the burners is given in figure 2.

Normally substances are tested as received, although in certain cases it may be necessary to test the substance after crushing it. A tared tube is filled of the substance and the substance tamped with 80 N force so that the tube is filled to a level 15 mm from the top.

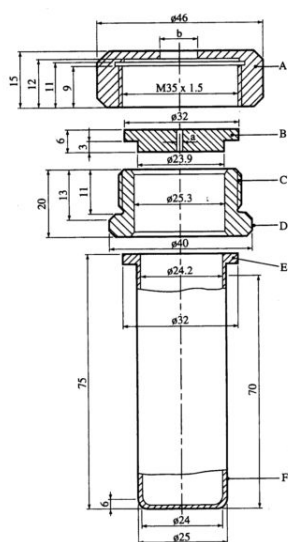


Fig 1. Steel tube and accessories

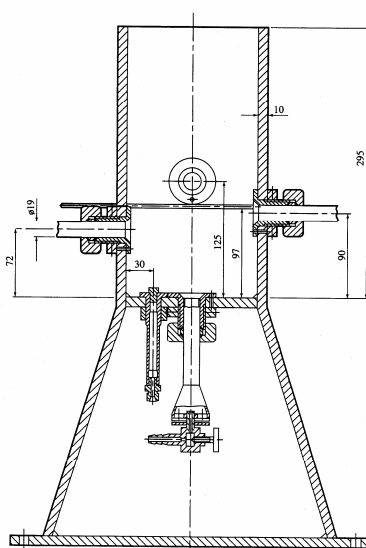


Fig 2. Heating and protective device

Liquids and gels are loaded into the tube to the height of 60 mm taking particular care with gels to prevent the formation of voids. The threaded collar is slipped onto the tube from below, the appropriate orifice plate is inserted and the nut tightened by hand.

Each test is performed until either the tube is fragmented or the tube has been heated for five minutes. A test resulting in the fragmentation of the tube into three or more pieces, which in some cases may be connected to each other by narrow strips of metal as illustrated in figure 3, is evaluated as giving an explosion. A test resulting in fewer fragments or no fragmentation is regarded as not giving an explosion.

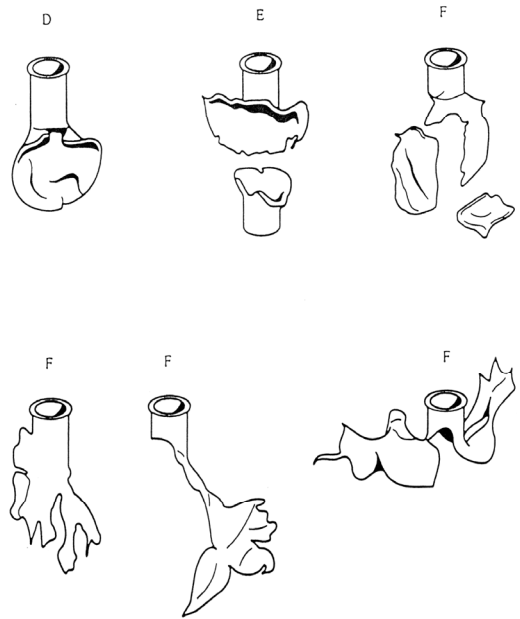


Fig 3. Example of fragmentation (**D,E** No explosion; **F** Explosion)

Series of three test with 6,0 mm diameter orifice plate is first performed and if no explosions are obtained, a second series of three tests is performed with a 2,0 mm diameter orifice plate. If an explosion occurs during either test series then no further tests are required.

The test result is considered positive if an explosion occurs in either of the above series of tests ^[3].

2.2 Test of mechanical sensitivity with respect to shock

The test is used to measure the sensitiveness of solids and liquids to drop-weight impact.

The essential parts of the fallhammer are the cast steel block with base, the anvil, the column, the guides, the drop weights with release device and the impact device (figure 4). A steel anvil is screwed onto the steel block and cast base. The support, into which is fixed the column is bolted to the back of the steel block. The two guides which are fixed to the column by means of three cross-pieces are fitted with a toothed rack to limit the rebound of the drop weight and a movable graduated scale for adjusting the height of the fall. The drop weight release mechanism is adjustable between the guides and is clamped to them by the operation of the lever nut on two jaws. The apparatus is fixed onto a concrete block by means of four anchoring screws secured in the concrete, so that the base is in contact with the concrete over its whole area and the guides are exactly vertical ^[2].

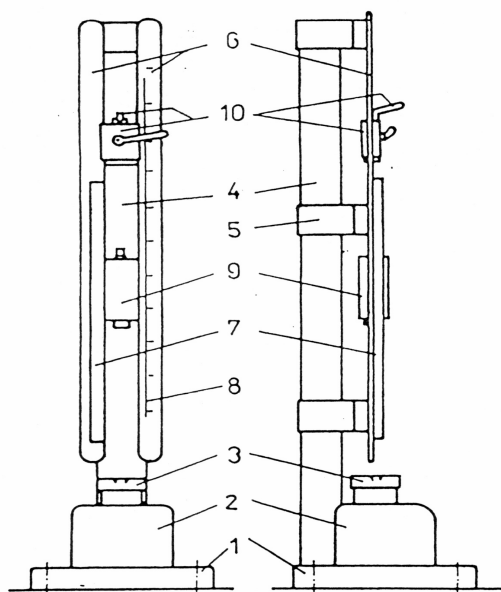


Fig 4. Shock test apparatus (1-base, 2-anvil, 3-steel block, 4-column, 5-medio cross-member, 6-2 guides, 7-toothed rack, 8-graduate scale)

Four drop weights are available with the following masses 1,00 kg, 2,00 kg, 5,00 kg and 10,00 kg. Each drop weight is provided with two locating grooves holding it between the guides as it drops, a suspension spigot, a removable cylindrical striking head and a rebound catch which are screwed on to the drop weight.

The 1 kg-drop weight has a heavy steel centre fitted with the striking head. The 2 kg, 5kg and 10 kg drop weights are of massive and compact steel.

The sample of the substance under test is enclosed in an impact device consisting of two co-axial steel cylinders, one above the other in a hollow cylindrical steel guide ring.

The impact device is placed on an intermediate anvil and centred by a locating ring with a ring of vent-holes to permit the escape of gases.

For solid substances, other than paste-like or gel-types, the following points should be observed:

- a) substances in powdered form are sieved (sieve mesh 0,5 mm), all that passes through the sieve is used for the test,
- b) substances which have been compressed, cast or otherwise consolidated are broken into small pieces and sieved, the fraction passing a 1,0 mm sieve and retained on a 0,5 mm sieve is used for the test,
- c) substances which are transported only in the form of charges are tested in the form of discs with of volume of 40 mm³.

For substances in powdered form, a sample is taken with a cylindrical measure of 40 mm³ capacity. For paste-like or gel-type substances, a cylindrical tube of the same capacity is inserted into the substance and after levelling off the surplus, the sample is removed from the tube by means of a wooden rod. For liquid substances, a fine-drawn popette of 40 mm³ capacity is used.

The substance is placed in the open impact device, which is already in the locating ring in the intermediate anvil, and for powders or paste-like or gel-type substances, the upper steel cylinder is gently pressed until it touches the sample without flattening it.

A series of six tests are performed dropping the 10 kg mass from 0,40 m (40J). If an explosion is obtained during the six tests at 40 J, a further series of 6 tests, dropping a 5 kg mass from 0,15 m (7,5 J), must be performed [3].

Table 1. Test of mechanical sensitivity with respect to friction

The method involves subjecting solid or pasty substances to friction between standard surfaces under specified conditions of load and relative motion.

The friction apparatus consists of a cast steel base plate on which is mounted the friction device (figure 5). This consists of a fixed porcelain peg and moving porcelain plate, the porcelain plate is held in a carriage which runs in two guides. The carriage is connected to an electric motor via a connecting rod, an eccentric cam and suitable gearing such that the porcelain plate is moved, once only, back and forth beneath the porcelain peg for a distance of 10 mm. The porcelain peg may be loaded with, for example, 120 or 360 newtons.

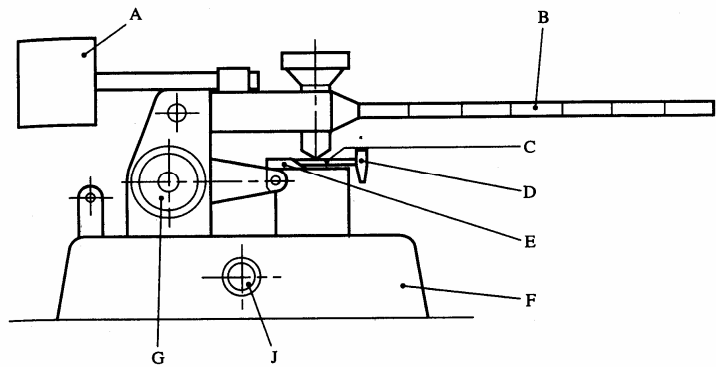


Fig 5. Friction sensitivity apparatus (A-counterweight, B-loading arm, C-porcelain plate, D-peg-holder, E-movable carriage, F-steel base, G-wheel for setting carriage at starting position, J-switch)

The flat porcelain plates are made from white technical porcelain and have the dimensions 25 mm x 25 mm x 5 mm. The cylindrical porcelain peg is also made of white technical porcelain and is 15 mm long, has a diameter of 10 mm and roughened spherical end surfaces with a radius of curvature of 10 mm (figure 6).

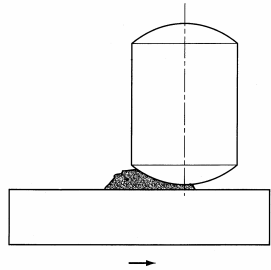


Fig 6. Starting position of peg on sample

The sample volume should be 10 mm³ or a volume to suit any alternative apparatus.

Solid substances are tested in the dry state and prepared as follows:

- a) powdered substances are sieved (sieve size 0,5 mm); all that has passed through the sieve is used for testing;
- b) pressed, cast or otherwise condensed substances are broken into small pieces and sieved; the sieve fraction < 0,5 mm diameter is used for testing.

Substance normally supplied as pastes should be tested in the dry state where possible. If the substance cannot be prepared in the dry state, the paste (following removal of the maximum possible amount of diluent) is tested as a 0,5 mm thick, 2 mm wide, 10 mm long film, prepared with a former.

The porcelain peg is brought onto the sample under test and the load applied. When carrying out the test, the sponge marks of the porcelain plate must lie transversely to the direction of the movement. Care must be taken that the peg rests on the sample, that sufficient test material lies under the peg and also that the plate moves correctly under the peg. For pasty substances, a 0,5 mm thick gauge with a 2 x 10 mm slot is used to apply the substance to the plate. The porcelain plate has to move 10 mm forwards and backwards under the porcelain peg in a time of 0,44 seconds. Each part of the surface of the plate and peg must only be used once; the two ends of each peg will serve for two trials and the two surfaces of a plate will each serve for three trials.

A series of six tests are performed with a 360 N loading. If a positive event is obtained during these six tests, a further series of six test must be performed with a 120 N loading.

The test result is considered positive if an explosion (crepitation and/or a report or bursting into flame are equivalent to explosion) occurs at least once in any of the tests with the specified friction apparatus or satisfies criteria in an alternative friction test ^[3].

3. CONCLUSION

The purpose of this paper was to inform you about the methods of testing of explosiveness of chemical substances according Ministry of Environment Decree which becomes valid to the date of entering the Treaty of Accession of Czech republic to the European Union into force.

REFERENCES

- [1] Act 356/2003 on Chemical Substances and Chemical Preparations and Amending Some Other Act
- [2] Recommendations on the transport of Dangerous Goods, Manual of Test and Criteria, third revised edition, United Nations, New York and Geneva, 1999
- [3] The regulations of Department of Environment, Method A 14: Determination of explosives properties

GEMINAL DINITROCOMPOUNDS THERMAL DECOMPOSITION UNDER NON-ISOTHERMAL CONDITIONS

R.S. Stepanov, L.A. Kruglyakova and A.M. Astachov

Siberian State Technological University
660049, Krasnoyarsk, prosp. Mira 82, Russia

Abstract:

Depending on geminal trinitrocompounds structure, their thermal decomposition proceeds in one or two stages. It is a complex process that includes evaporation, destruction, secondary oxidation-reduction reactions, and autocatalysis. It is shown that thermal sensitivity is tied with temperature of initial decomposition. The steric effect of α -substituent at geminal dinitrogroup significantly influences both decomposition rate constant and decomposition's characteristic temperature. Corresponding quantitative correlations confirm it.

Keywords: *thermal decomposition, geminal trinitrocompounds, kinetics, characteristic temperatures, steric effect*

1. INTRODUCTION

Thermal decomposition and differential-thermal analysis of the wide range of geminal dinitrocompounds, containing $-CONH-$, $-NH-$, $-N-NO_2$, $-H_2COCH_2-$ and other groups, was studied in continuation of [1]. The studies were conducted to determine the influence of chemical structure on decomposition's rate and characteristic temperatures.

2. EXPERIMENTAL

Decomposition and thermal analysis was conducted using derivatograph in the temperature range of 20 to 500°C. The heating rates used were 2.5 °C/min, 5 °C/min, and 10°C/min. None of the heating rates used had any effect on decomposition characteristic temperatures within margin of error. Therefore, all experiments were conducted at heating rate of 2.5°C/min using the sample mass of 0.05 grams. The results of the thermo gravimetric experiment were processed using smoothing splines [2] that guaranteed Arrhenius parameters reliable determination.

3. RESULTS AND DISCUSSION

Thermal decomposition for the majority of polynitrocompounds proceeds in one or two stages, depending on their structure, and is accompanied by exoeffect (Fig.1). If polynitrocompound's molecule contains benzene ring, the loss of mass in such a compound occurs in two stages. The second stage is not accompanied by exothermal effect. This fact leads to a conclusion that no decomposition occurs at this stage but rather evaporation of the aromatic residue forming in the process of decomposition.

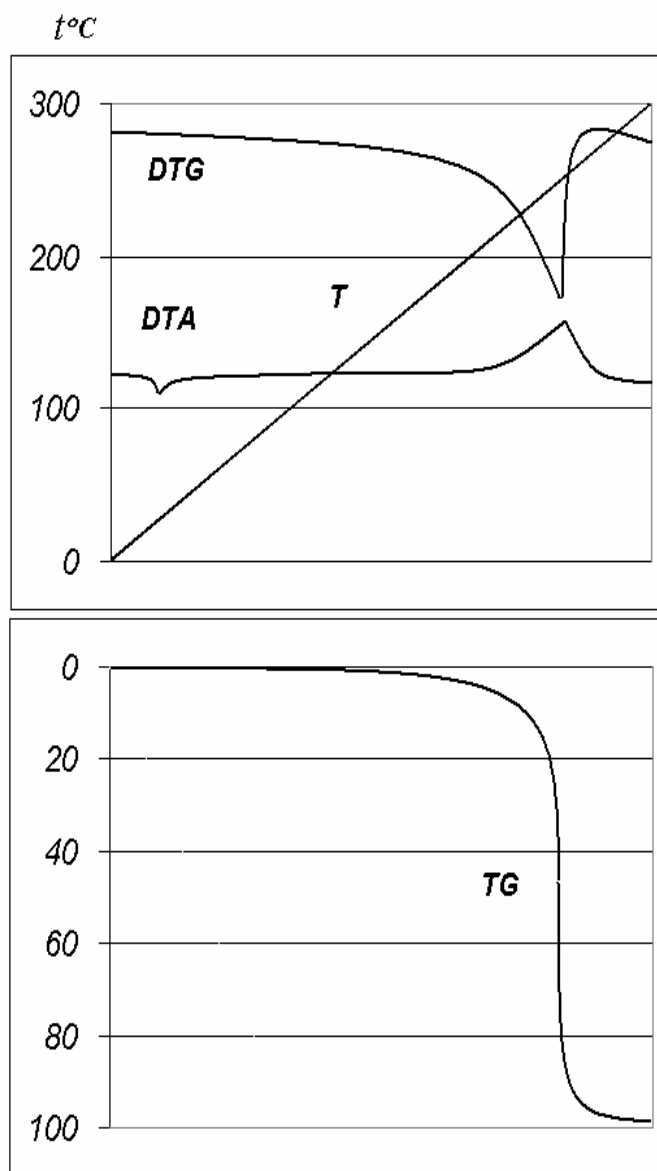


Fig 1. Thermogram for $[H_3CC(NO_2)_2CH_2O]_2CH_2$

Thus, for instance, the main condensed product of decomposition for 2,2-dinitroethyl- and 2,2-dinitropropylbenzamides is benzoic acid. Benzoic acid formation during the process of decomposition was proven by both IR-spectral method and element analysis. Calculation of activation energy on the second stage of decomposition for these polynitrocompounds yielded, correspondingly, $E=45.2$ kJ/mol (10.8 kcal/mol) and 48.6 kJ/mol (11.6 kcal/mol). According to ^[3], benzoic acid evaporation enthalpy is 12.1 kcal/mol, which correlates nicely with the values reported above. For the majority of polynitrocompounds, the endothermic peak (Fig.1) precedes the loss of mass. This peak implies phase transition from crystalline structure to liquid phase. Therefore, thermal decomposition of polynitrocompounds occurs in liquid phase. The only exception is 2,2-dinitroethylbenzamid that begins decomposing before phase transition occurs. Decomposition activation parameters and characteristic temperatures are shown in Table 1.

The Table's data analysis shows that decomposition rate constants are about 1.5-2 orders of magnitude greater than those obtained for thermal decomposition of geminal

dinitrocompounds in liquid phase under static conditions ^[4]. Probably, there are two main reasons for this discrepancy: autocatalysis and partial substance's evaporation. In addition, compensatory effect occurs during decomposition as well (Fig.2).

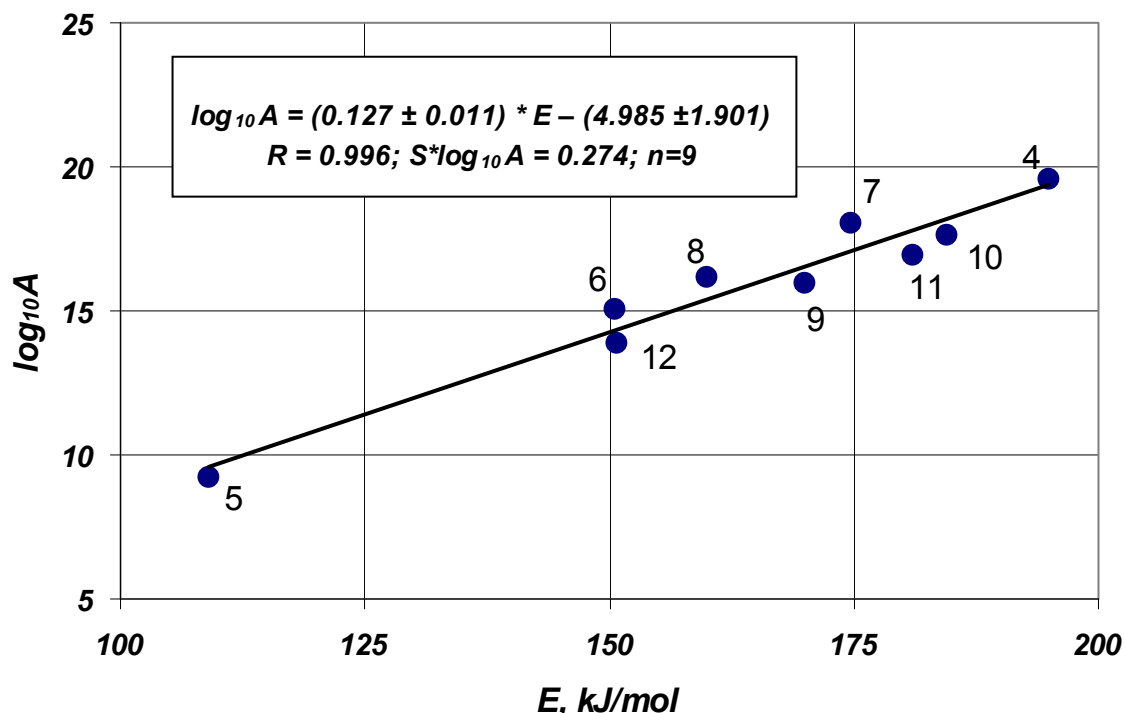


Fig 2. Dependence $\lg A = F(E)$ for nitrocompounds. Points numbers correspond to compounds numbering in Table 1.

It may be formalized as follows:

$$\log_{10}A = (0.127 \pm 0.011) * E - (4.985 \pm 1.901) \quad (1)$$

$$R = 0.996; S*\log_{10}A = 0.274; n=9$$

Reactionary ability of geminal dinitrogroup changes about two orders of magnitude depending on structural factors. Substituted 1,3-dioxanes (compounds 9-11 in Table 1) have the lowest reactionary ability of geminal dinitrogroup while bromdinitroacetal (compound 7) has the highest. One can see from Table 1 that both α - and β -substituents influence geminal dinitrogroup decomposition rate constant. However, α -substituents exert greater influence no matter whether they are electron donors or acceptors. The main factor is the volume of α -substituent. The greater is volume, the higher is decomposition rate constant. The steric factor's influence on hemolytic decomposition of the geminal dinitrogroup by the $C-NO_2$ bond was noted for decomposition both in gaseous phase ^[5] and in liquid phase ^[4]. One may expect all structural effects (except steric effect) to be constant for compounds with general formula $[RC(NO_2)_2CH_2O]_2$ (I). For such compounds the following correlation was found for substituent R (Fig.3) with steric constants E_s :

$$\log_{10} K_{160} = -(0.379 \pm 0.031) E_s - (4.270 \pm 0.081) \quad (2)$$

$$R = 0.990; S_y = 0.067; n=5$$

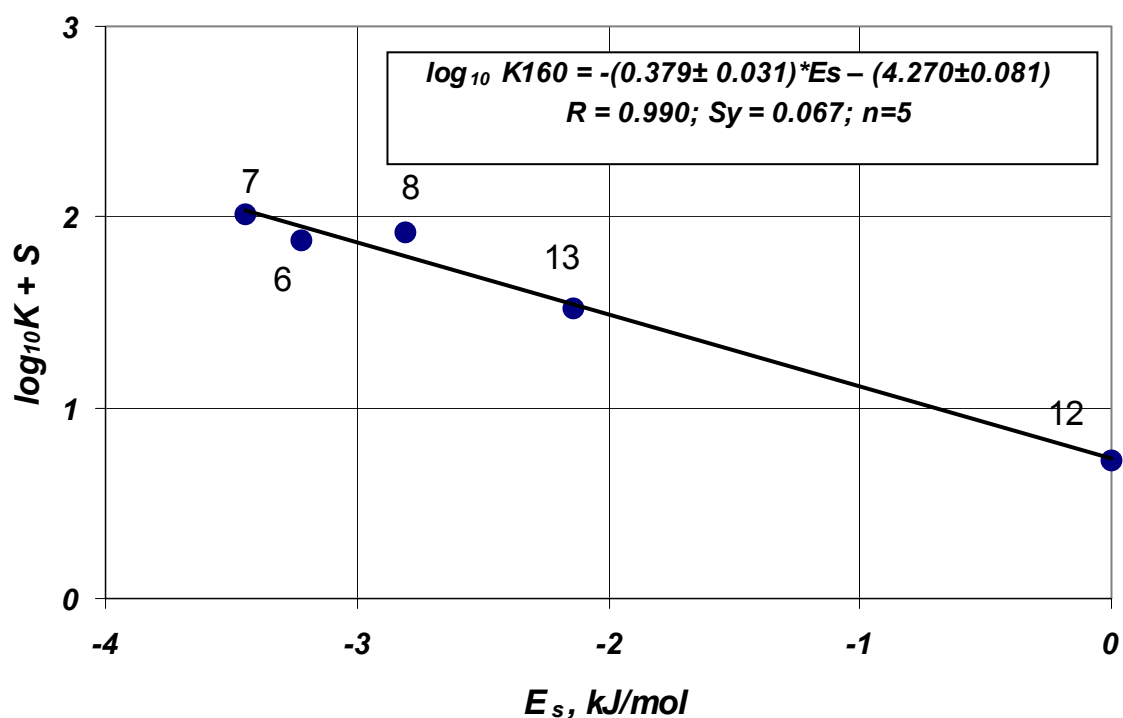


Fig 3. Dependence $\log_{10}K=F(E_s)$ for compounds with general formula $[RC(NO_2)_2CH_2O]_2$. Points numbers correspond to compounds numbering in Table 1

The absolute value of reaction constant ($r = 0.379$) is small compared with one reported in ^[6] because the process of substance's evaporation contributes disproportionately to the total rate of substance's loss of mass. Nevertheless, dependence (2) allows estimating reactionary ability for those of compounds (I) that are proposed for usage.

The temperature of intensive decomposition (T_{max}) at the maximum of exothermal peak serves as a criterion to estimate thermal sensitivity. Interdependence exists between thermal sensitivity and temperature in the beginning of decomposition (T_b) (Fig.4). This interdependence is described by equation

$$T_{max} = 1.194 * T_b \quad (3)$$

$$R=0.983$$

Equation (3) allows estimating not only thermal sensitivity but also how much time substance can withstand thermal impulse of constant intensity before decomposition begins. One can see from Table 1 that T_b grows with compound number, starting from 112°C for compound 1 to 218°C for compound 14. Correspondingly, the time of constant impulse's impact on substance grows from 36.8 up to 79.2 minutes. Since thermal capacity and thermal conductivity are virtually the same for all the compounds, one may conclude that chemical structure and reactionary ability during decomposition are the main factors for compounds sensitivity to thermal wave. Solving Arrhenius equation for T_{max} and T_b through simple transformations, one may relate $T_{max}(K_{max})$ with $T_b(K_b)$ as follows:

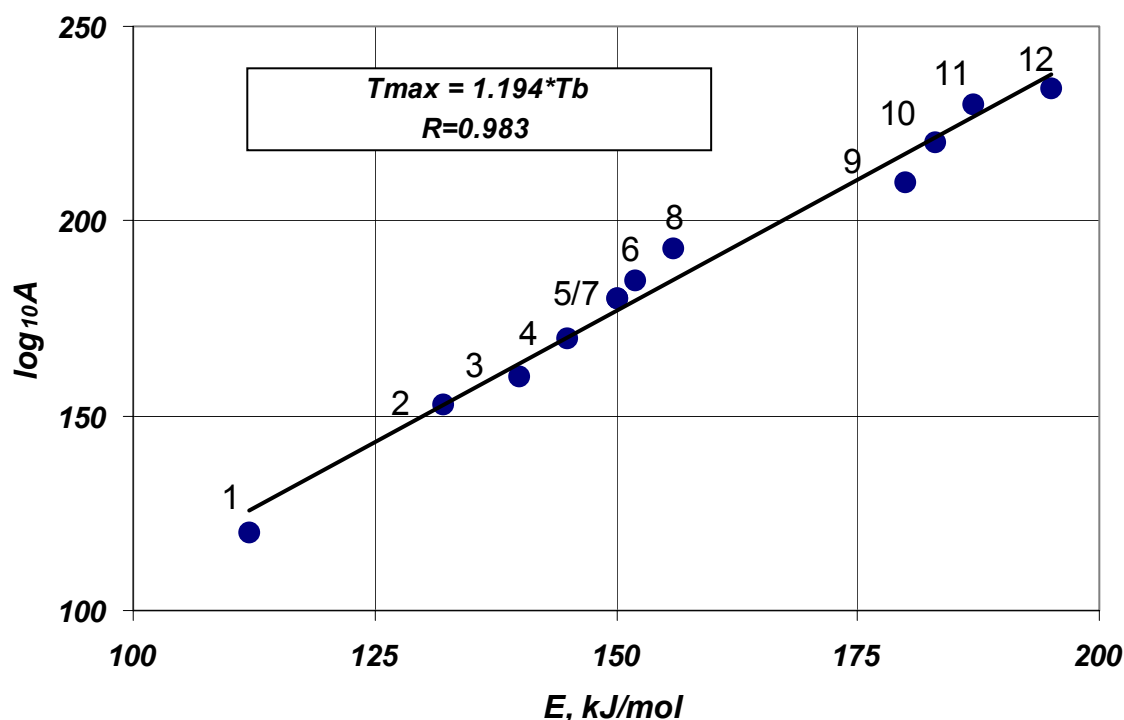


Fig 4. Dependence $T_{max}=F(T_b)$ for nitrocompounds. Points numbers correspond to compounds numbering in Table 1

$$T_{max} = [1 + \log(K_{max}/K_b) / (E/(R*T_b) - \log(K_{max}/K_b))] * T_b \quad (4)$$

Where E is decomposition's activation energy, R is a Universal Gas Constant, and K_{max} and K_b are decomposition rate constants at T_{max} and T_b , accordingly. Assuming reasonable values for activation energy and solving equations (3) and (4) together, one may estimate T_b , T_{max} , and $\Delta T = T_{max} - T_b$ for those dinitrocompounds that were not studied directly.

One may conclude that both T_{max} and decomposition rate constant are fundamental characteristics in modern chemical kinetics. So it is logical to relate $T_{max}(T_b)$ with substituents steric constants E_s for compounds (I). Corresponding data are shown in Fig.5. One can see that all the data points may be approximated satisfactorily with straight lines and are described by corresponding regression equations:

$$T_{max} = (15.195 \pm 1.302) * E_s + (232.701 \pm 27.144) \quad (5)$$

$$R = 0.989; S_y = 2.823; n=5$$

$$T_b = (13.765 \pm 0.711) * E_s + (194.724 \pm 11.035) \quad (6)$$

$$R=0.995; S_y = 2.541; n=6$$

Equations (5), (6) may be used to predict thermal sensitivity and thermostability for those geminal dinitrocompounds with general formula (I) that were not studied directly.

Decomposition time was determined in the temperature interval of $\Delta T = T_{\max} - T_b$ while heating with 2.5°C per minute (Table 1). Note that decomposition time of compounds (I) increases from 3.2 minutes (compound 1) to 17.2 minutes (compound 11) with increase in ΔT . This means thermal sensitivity and thermostability for structurally different compounds change symbatically in accordance with equations (3) and (4).

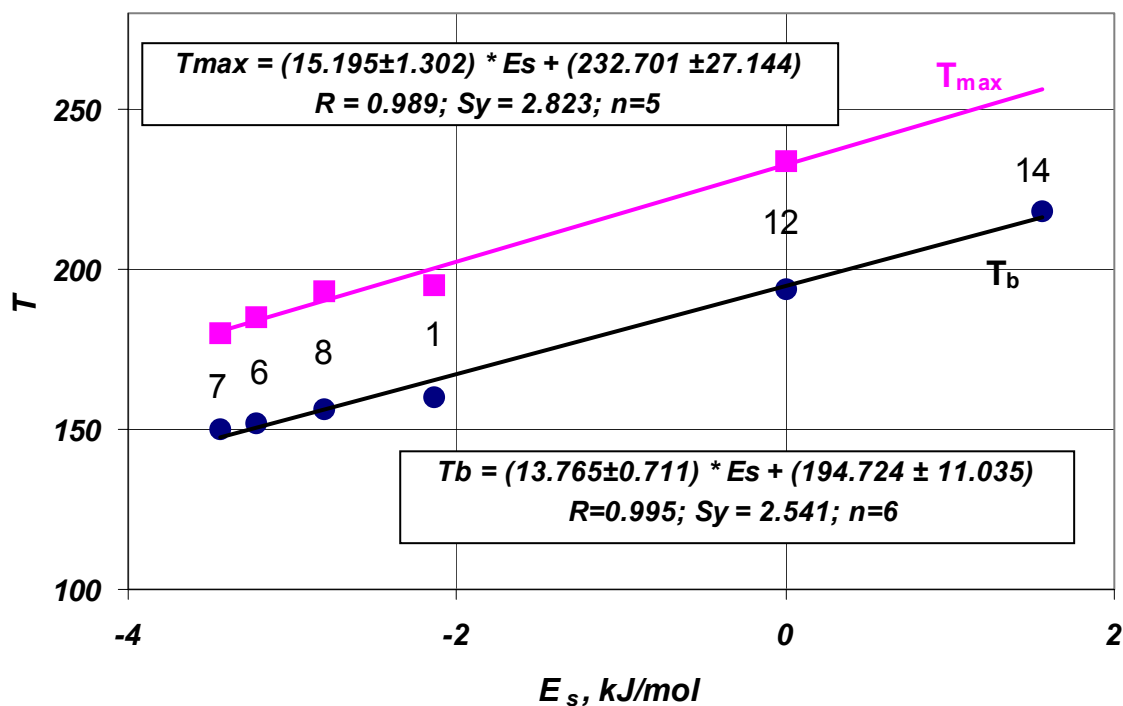


Fig 5. Dependence $T_b = F(E_s)$ and $T_{\max} = F(E_s)$ for compounds with general formula $[RC(NO_2)_2CH_2O]_2$. Points numbers correspond to compounds numbering in Table 1

High thermal sensitivity and low thermostability of compounds 1-3 (see Table 1), containing $B-NH$ - or $-CONH$ - groups, may not be explained within framework of radical decomposition mechanism through break in $C-NO_2$ bond. Similarly to β -trinitroethylamines and amides, decomposition of these compounds proceeds through primary heterocyclic break of $C-C$ bond with dinitroanion and carbonyl-immonium cation formation [1].

Compounds 4,5 (Table 1) that contain $=N-NO_2$ group, show lower thermal sensitivity and higher thermostability compared with compounds 1-3. However, they are more sensitive and less stable than compounds 9-12. The reason for this is both electronic and steric interaction between $-C(NO_2)_2$ - and $=N-NO_2$ groups.

4. CONCLUSION

We found that decomposition of geminal dinitrocompounds proceeds homolitically with $C-NO_2$ bond break or heterolitically with $C-C$ bond break depending on compounds structure. Heterolitic pre-dissociation via bond $C-C$ strongly increases thermal sensitivity and decreases thermostability. The latter circumstance excludes such compounds from practical use.

REFERENCES

- [1] R. S. STEPANOV, L. A. KRUGLYAKOVA, A. M. ASTACHOV: *Geminal Trinitrocompounds Thermal Decomposition under non-Isothermic Conditions*, Proc. of Sixth Seminar "New Trends in Research of Energetic Materials", Univ. of Pardubice, Czech Republic, p.362-366, 2003
- [2] A. M. ASTACHOV, A. A. NEFEDOV, L. A. KRUGLYAKOVA, R. S. STEPANOV: *Raschet Kineticheskikh Parametrov Termicheskogo Razlozheniya s Ispol'zovaniem Sglazhivayuschiy Kubicheskikh Splainov*, Proc. of Int. Siberian Conf. "Methods and Spline-Functions", Novosibirsk, Sobolev Institute of Mathematics, SO RAN, Russia, pp.9-11, 2001 (in Russian)
- [3] D. STULL, E. WESTMAN, G. SINKE: *The Chemical Thermodynamics of Organic Compounds*, Wiley & Sons, New York-London-Sydney-Toronto, 1969
- [4] G. M. NAZIN, W. G. PROKUDIN, G. B. MANELIS: *Thermostability of the High-Energy Compounds*, Russian Chem. Bulletin, Vol.2, p.231-234, 2000
- [5] W. N. SHAN'KO, R. S. STEPANOV, B. W. GIDASPOV: *O Primenenii Korrelyacionnykh Uravnenii k Reakcii Termicheskogo Razlozheniya Polynitroalkanov*, Proc. of Conf. on Scientific Research Results, Section of Organic Chemistry, Siberian State Tech. Univ., Russia, p.41, 1971 (in Russian)
- [6] R. S. STEPANOV, A. M. ASTACHOV, L. A. KRUGLYAKOVA, O. A. GOLUBTSOVA: *Kinetika i Mehanizm Termicheskogo Razlozheniya Nekotorykh Proizvodnykh 5-dinitrometil-2-metiltetrazola*, Russian J. of General Chemistry, Vol. 70, Issue 6, p.999-1001, 2000 (in Russian)

Table 1. Characteristic temperatures, times, and Arrhenius parameters for the first stage of thermal decomposition for geminal dinitrocompounds. Steric constants for the substituents. T_m – melting temperature, T_b – temperature at the beginning of decomposition, T_{max} – temperature at exothermic peak maximum, $\Delta T = T_{max} - T_b$, t_b – time for temperature to rise from 20°C to T_b , t_{max} – time of decomposition from T_b to T_{max}

#	Compound	T_m , °C	T_b , °C	T_{max} , °C	ΔT , °C	t_b , min	T_{max} , min	E , kJ/mol	$\log A$	K_{160}^* $10^5 s^{-1}$	E_s
1	$HC(NO_2)_2CH_2NH(CO)C_6H_5$		112	120	8	36.8	3.2				
2	$H_3CC(NO_2)_2CH_2NH(CO)C_6H_5$	132	132	153	21	44.8	8.4				
3	$H_3CC(NO_2)_2CH_2NHC_6H_5$	53	140	160	20	48.0	8.0				
4	$HCC(NO_2)_2CH_2N(NO_2)CH_2CH_2COOH$	128	145	170	25	50.0	10.0	194.8	19.60	13.6	
5	$H_3CC(NO_2)_2CH_2N(NO_2)CH_3$	69	150	180	30	52.0	12.0	108.0	9.25	13.4	
6	$[H_3CC(NO_2)_2CH_2N(NO_2)CH_2O]_2CH_2$	113	152	185	33	52.8	13.2	150.6	15.05	76.0	-3.22
7	$[BrC(NO_2)_2CH_2O]_2CH_2$	41	150	180	30	52.0	12.0	174.6	18.06	103.4	-3.44
8	$[ClC(NO_2)_2CH_2O]_2CH_2$	Liquid	156	193	37	54.4	14.8	160.0	16.20	83.3	-2.81
9	$(O_2N)_2C \begin{matrix} \diagup CH_2O \\ \diagdown CH_2O \end{matrix} > CH_2$	34	180	210	30	64.0	12.0	170.0	15.94	2.8	
10	$(O_2N)_2C \begin{matrix} \diagup CH_2O \\ \diagdown CH_2O \end{matrix} CH - CH_2CH_2C(NO_2)_2CH_3$	120	183	220	37	65.2	14.8	184.4	17.61	2.6	
11	$(O_2N)_2C \begin{matrix} \diagup CH_2O \\ \diagdown CH_2O \end{matrix} CH - C_6H_4NO_2$	144	187	230	43	66.8	17.2	181.0	16.96	1.4	
12	$[H_3CC(NO_2)_2CH_2N(NO_2)CH_2O]_2CH_2$	35	194	234	40	69.6	16.0	150.8	13.89	5.3	0
13	$[(O_2N)_3CCH_2O]_2CH_2^*$	66	160	195	35	56.0	14.0	180.2	18.22	33.0	-2.14
14	$[FC(NO_2)_2CH_2O]_2CH_2^{**}$	Liquid	218			79.2	evaporation				+1.56

* Data from [5]

** Data from [1]

DETONATION PERFORMANCES OF LOW-SENSITIVITY NTO/HMX EXPLOSIVES

W. A. Trzciński and L. Szymańczyk

Military University of Technology,
Kaliskiego 2, 00 908 Warsaw, Poland

Abstract:

Detonating performances of new explosive compositions containing NTO and HMX are investigated in this work. Detonation velocity, pressure and energy of the mixtures tested and acceleration ability and equation of state of their detonation products are determined. Shock and impact sensitivity is evaluated in the gap test and heavy hammer test.

The compositions investigated can be considered as a suitable insensitive explosive to replace TNT/RDX mixtures in munitions applications.

Keywords: *insensitive munitions, detonation performance*

1. INTRODUCTION

New TNT/RDX/NTD formulations were successfully manufactured and characterized in Ref. [1]. Detonation performance and energetic characteristics of these mixtures were comparable with those of TNT/RDX (40/60) composition. The shock and impact sensitivity of tested formulations was lower than the sensitivity of the TNT/RDX mixture.

In this work, an attempt is undertaken to obtain low sensitivity mixture of NTO and HMX of detonation and energetic performances higher than the composition TNT/RDX 40/60. To select the composition contents the results of thermochemical calculations of detonation parameters are used. For two chosen mixtures the detonation and energetic characteristics are determined. Shock and impact sensitivity of the compositions is also evaluated.

2. COMPOSITIONS

Theoretical estimation of detonation characteristics of NTO/HMX mixtures was performed by the use of the thermochemical code CHEETAH [2]. The detonation velocity was calculated as a function of the mass contents of NTO. It was assumed that the density of the mixtures was 95 % of the theoretical maximal density. The dependence of the detonation velocity D on the contents of NTO x_{NTO} is shown in Fig. 1.

The detonation parameters of TNT/RDX 40/60 mixture (hereafter denoted by CB) are assumed to correspond to the parameters of Comp. B. The detonation velocity of CB is 7830 m/s [1]. From the curve presented in Fig. 1 it follows that for tested contents of NTO in the NTO/HMX mixtures, calculated detonation velocity is higher than that of CB. The composition NTO/HMX 30/70 and the composition NTO/HMX 50/50 were chosen for further investigations.

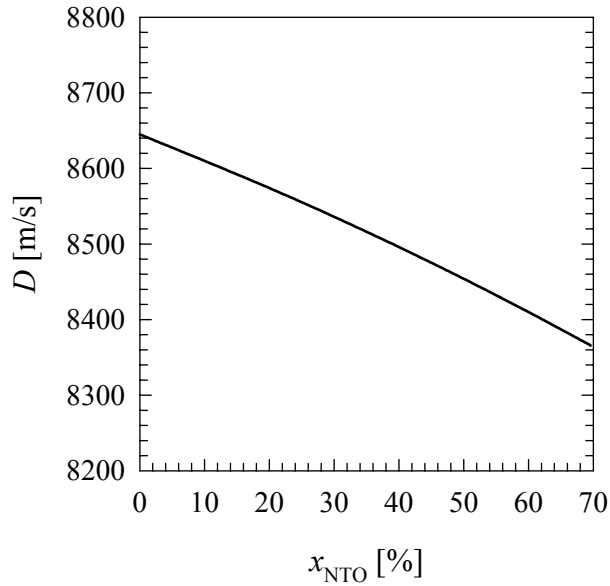


Fig 1. Dependence of the detonation velocity of NTO/HMX mixtures on the contents of NTO

The procedure of preparing the compositions was as follow. NTO was dissolved in water and HMX phlegmatised by Viton was added to the solution. The mixture was frozen with continuous mixing and finally the granulated product was obtained. In reality, the mixture NTO/HMX/Viton 30/66.5/3.5 (denoted by KH30) and the mixture NTO/HMX/Viton 50/47.5/2.5 (denoted by KH50) were tested.

3. DETONATION PERFORMANCE

3.1 Detonation pressure and velocity

To determine the detonation pressure of the mixtures, a variant of the aquarium test was applied ^[3]. In this method, profiles of an oblique shock wave propagating in a cylindrical layer of water during detonation of a cylindrical charge of an explosive tested is recorded with a X-ray set. The experimental profiles are then compared with results of numerical modelling of the expansion process which are in a form of relation between the position of the front of oblique shock wave in water and the exponent of isentrope (γ) of detonation products. The value of γ corresponding to the solution that overlaps the experimental profile is accepted as the exponent sought. The detonation pressure is calculated according to the following equation:

$$p_{\text{CJ}} = \frac{\rho_0 D^2}{\gamma + 1} \quad (1)$$

where p_{CJ} denotes the detonation pressure and ρ_0 is a density of the explosive tested.

The scheme of the experimental arrangement, used in the aquarium test, is shown in Fig. 2. A cylindrical charge of 25 mm in diameter and 250 mm in length was placed inside a PCV tube with an inner diameter of 71 mm and wall thickness of 2 mm. The tube was filled with water. Short-circuit sensors were located in the charge to measure detonation velocity.

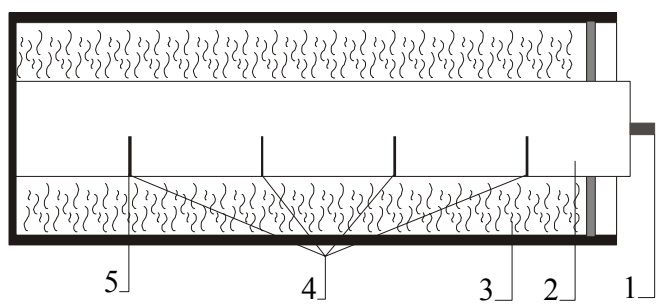


Fig 2. Water test –experimental arrangement: 1 – booster, 2 –charge tested, 3 – water, 4 – sensor to measure detonation velocity, 5 – sensor to trigger the X-ray set

The density and detonation velocity of the mixtures used in the water test and the results are given in Tab. 1. The exponent of isentrope of detonation products was determined by comparison of measured and calculated positions of the shock wave front in a plane section located at a distance of one charge radius from the front of detonation wave. The detonation pressure was calculated from the Eq. (1). Table 1 also contains some theoretical values of the parameters (with an index t) calculated with the thermochemical code CHEETAH.

Table 1. Experimental and calculated detonation properties of the mixtures tested

Explosive	ρ_0 [kg/m ³]	D [m/s]	γ	p_{CJ}	D_t	γ_t	$p_{CJ,t}$
CB - [1]	1674	7830	2.97	25.85	7810	3.02	25.40
KH30	1810	8580	3.20	31.7	8517	3.26	30.82
KH50	1825	8450	3.24	30.9	8475	3.32	30.32

From the results obtained it follows that the detonation parameters of the compositions KH30 and KH50 are significantly higher than those of CB.

3.2 Cylinder test

The cylinder test results were the basis for determination of acceleration abilities and energetic characteristics of the detonation products of mixtures investigated. The process of acceleration of a copper tube by detonation products was recorded with the impulse X-ray apparatus. The tube was 300 mm long with internal diameter of 25 mm and wall thickness of 2.5 mm. The results of the test are presented in Fig. 3. in the form of the dependence of the radius of external surface of the tube on the axis co-ordinate x . To determine the radial velocity of the copper tube, the data obtained from the cylinder test were recalculated by the use of the method described in Ref. ^[4]. The detonation velocities measured in the cooper tube were 8600 and 8480 m/s for KH30 and KH50, respectively.

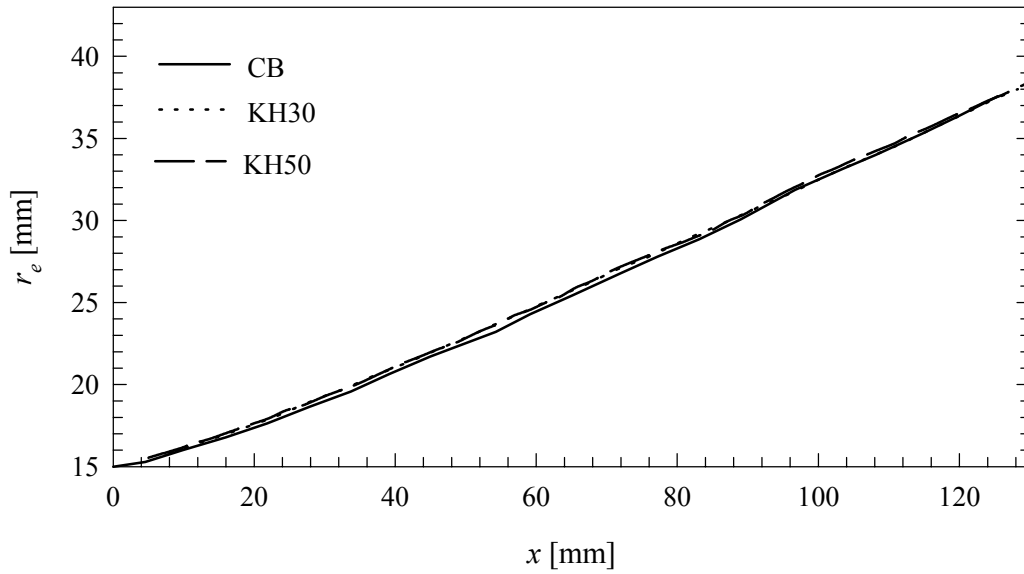


Fig 3. Dependence of the external radius of the tube on the axis co-ordinate

3.3 Gurney and detonation energy

The acceleration ability of explosive can be described by so-called Gurney energy. For cylindrical envelopes the Gurney energy is expressed by the following relation

$$E_G = \left(\mu + \frac{1}{2} \right) \frac{u_L^2}{2} \quad (2)$$

where u_L is the velocity of the tube and μ denotes the ratio of tube mass to explosive mass.

Results of the cylinder test enable us to analyze the dependence of the Gurney energy, described by formulae (2), on the degree of tube expansion. This dependence also describes the acceleration ability of the explosive. The relationship between the Gurney energy and the relative volume of detonation products for the mixtures tested is given in Fig. 4.

The results of cylinder test can also be used to estimate the detonation energy. In Ref. ^[4] it was shown that there was a correlation between the velocity of driven tube at the infinite volume of the detonation products and the detonation energy of an explosive. The relation can be written as follows

$$\frac{e_0}{e_0^s} = \frac{\left(\mu + \frac{1}{2} \right)}{\left(\mu^s + \frac{1}{2} \right)} \left(\frac{u_L}{u_L^s} \right)^2 \quad (3)$$

where e_0 and e_0^s are the detonation energy of a given explosive and a standard explosive, respectively u_L and u_L^s denote the tube velocity determined at the infinitive volume of detonation products of the explosives. These velocities were estimated by the method described in Ref. ^[4]. Using phlegmatized RDX as a standard explosive the detonation

energies of the explosive tested was calculated from (3). The values obtained are given in Table 2.

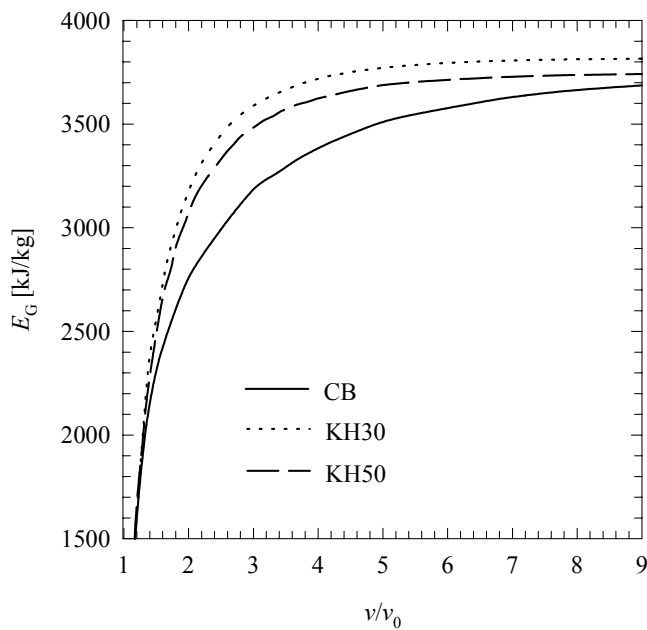


Fig 4. Acceleration ability of the explosive tested

Table 2. Detonation energies estimated of the basis of cylinder test data

Explosive	e_0 [kJ/kg]	$E_0 = e_0 \rho_0$ [MPa]
RDX _{ph}	5263	8.7
CB [1]	5126	8.6
KH30	5125	9.3
KH50	5000	9.1

From the Fig. 4 it follows that the Gurney energy of compositions with NTO are higher that those of TNT/RDX mixture but from Table 2 it follows that the values of detonation energy per unit mass are comparable.

3.4 Isentropes of the detonation products

So-called effective exponent of isentrope is determined on the basis of the real isentrope of the detonation products. It can be estimated from results of the cylinder test. In Ref. ^[5] the effective exponent is determined by comparison of the experimental profile of the copper tube with that obtained from numerical modelling of the expansion process. The detonation products, driving the tube, are described by the constant- γ equation of state. This method was applied in the present work to estimate the effective exponent of isentrope for detonation products of explosive tested. The values of γ are as follows: $\gamma = 3.15$ and 3.15 for KH30 and KH50, respectively.

In reality, the exponent of the isentrope greatly changes during the expansion of the detonation products – from a value of about 3 at the Chapman-Jouguet point to approximately 1.2 at low pressure. Therefore the physical properties of the expanding

gaseous detonation products are more precisely described by the isentrope which was proposed by Jones, Wilkins and Lee. Cylinder test results are commonly employed in most methods of determination of the JWL constants. In one of them ^[6], some connections between JWL coefficient are used. Using the model described in Ref. ^[7], as well as the values of detonation velocity, detonation pressure and detonation energy of the explosive tested, the constant of the JWL isentrope were estimated. Results of calculations are given in Table 3.

Table 3. *The detonation pressure and the constants of JWL isentrope for the detonation products of explosives tested*

Explosive	p_{CJ} [GPa]	A [GPa]	B [GPa]	C [GPa]	R_1	R_2	ω
KH30	31.9	1322.215	25.15556	0.933113	5.36	1.46	0.31
KH50	31.0	1386.098	25.34411	0.897686	5.46	1.46	0.31

Fig. 5 displays how different JWL and constant- γ isentropes for the explosives investigated are.

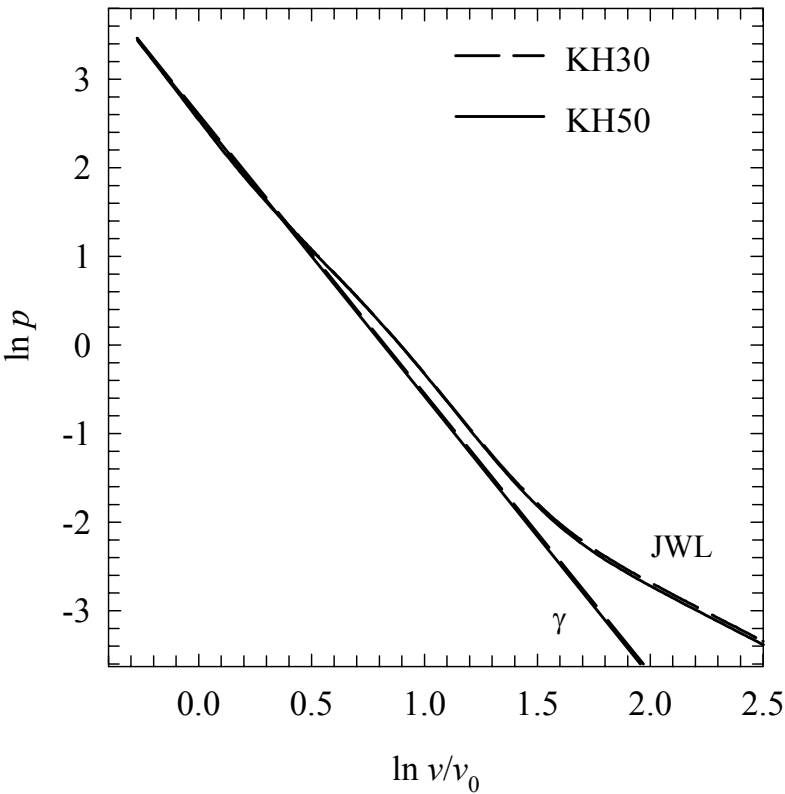


Fig 5. The constnat- γ and JWL isentropes for detonation products of explosives tested

3.5 Expansion work

After determining an isentrope, the expansion work of detonation products can be calculated from the equation:

$$W(v) = -e_c + \int_{v_{CJ}}^v p_i dv \tag{4}$$

where p_i is the pressure on the isentrope starting from the CJ point, and $e_c = (p_{CJ} - p_0)(v_0 - v_{CJ})/2$ is the energy of compression of the explosive at the detonation front.

Dependence of the expansion work on the relative volume of the detonation products of the explosives tested is shown in Fig. 6.

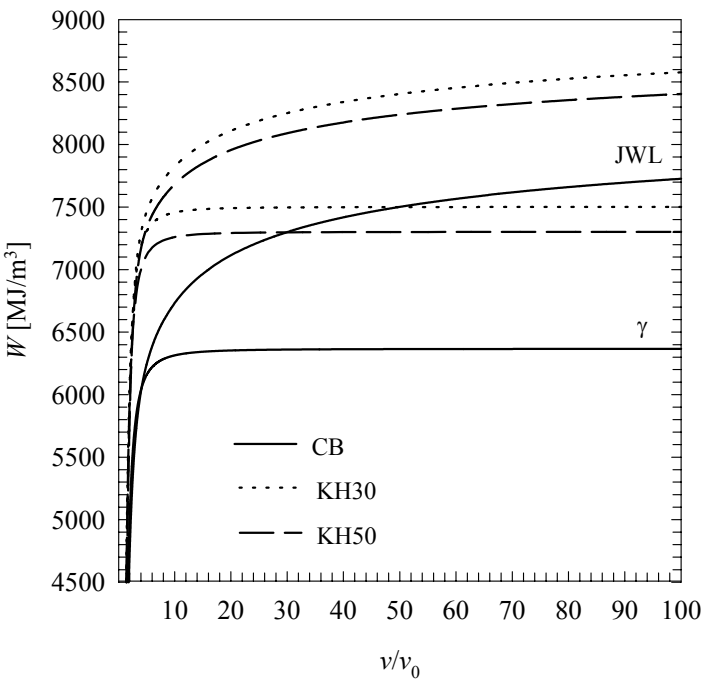


Fig 6. Expansion work as a function of the relative volume of detonation products

4. SENSITIVITY TO MECHANICAL STIMULI

4.1 Gap test

The gap test enables the determination of the shock sensitivity of explosives. The charge configuration used in experiments is shown in Fig. 7. The explosive tested was placed inside a cooper tube similar to that used in cylinder test. A booster made of phlegmatized RDX served as a shock wave generator. From shot to shot, the length of plexiglass attenuator was changer with 1-mm step. The highest and the lowest gap values were appointed for which the complete detonation and failure of explosion process were observed. The complete detonation of explosive charge was indicated when a clean hole was cut in the steel witness plate.

The shock sensitivity of explosive tested as the usual gap results in the form “detonation – no detonation” is presented in Fig. 8. Only one trial was performed for the composition

KH30. It is more sensitive than the composition CB. However, the sensitivity of the mixture KH50 is lower than that of composition CB.

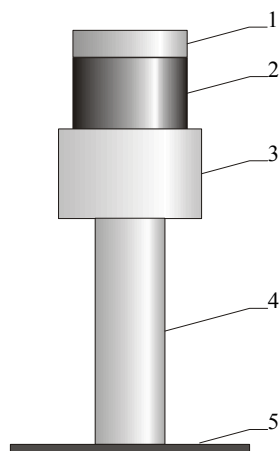


Fig 7. Scheme of the charge configuration to determine the shock sensitivity:

- 1 – detonator and holder,
- 2 – booster, 3 – plexiglass gap,
- 4 - explosive tested in cooper tube,
- 5 – witness plate

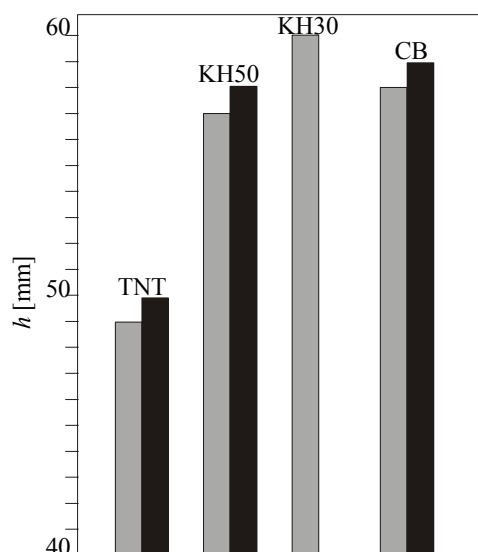


Fig 8. Thickness of plexiglass gap for complete and incomplete detonation in the explosive tested

4.2 Hammer test

For the impact sensitivity determination a fallhammer apparatus was used. A 0.03 g sample of explosive tested was placed in a piston device. The weight of hammer applied was 5 kg. For each drop height 10 trials were conducted. The minimum drop height at which 10 initiations occurred was 9, 20 and 22 cm for compositions CB, KH30 and KH50, respectively. It means that NTO admixture decreases significantly the impact sensitivity of HMX mixtures.

5. SUMMARY

New NTO/HMX formulations were successfully manufactured and characterized. Detonation performance and energetic characteristics of these mixtures are higher than those of TNT/RDX 40/60 composition. The shock and impact sensitivity of formulation NTO/HMX/Viton 50/47.5/2.5 is lower than the sensitivity of the TNT/RDX mixture. Manufactured composition can be considered as a suitable main charge filling to substitute for existing TNT/RDX compositions.

REFERENCES

- [1] W. A. TRZCIŃSKI, L. SZYMAŃCZYK, S. CUDZIŁO: *Detonation characteristics of low-sensitivity NTO-based explosives*, 6th International Seminar “New Trends in research of energetic Materials”, Pardubice 2003
- [2] L. E. FRIED: *CHEETAH 1.39 – User’s Manual*, Lawrence Livermore National Laboratory 1996
- [3] W. A. TRZCINSKI, S. CUDZIŁO, L. SZYMAŃCZYK: *Determination of the Detonation Pressure From a Water test*, Engineering Transactions, **49**, 4, 2001
- [4] W. A. TRZCIŃSKI: *Application of the Cylinder Test for determining Energetic Characteristics of Explosives*, J. Techn. Phys., **42**, 2, 2001
- [5] S. CUDZIŁO, R. TRĘBIŃSKI, W. TRZCIŃSKI: *Determination of the effective exponent of isentrope for the detonation products of high explosives*, Chem. Phys. Reports, 1997, Vol. 16(9), p. 1719-1732
- [6] R. TRĘBIŃSKI, W. A. TRZCIŃSKI: *Determination of an expansion isentrope for detonation products of condensed explosives*, J. Techn. Phys., **40**, 4, 1999
- [7] R. TRĘBIŃSKI, W. A. TRZCIŃSKI: *Modelling of the process of driving a cylindrical tube by the detonation products described by the JWL equation of state*, J. Techn. Phys., **38**, 4, 1997

TRACE ANALYSIS OF EXPLOSIVES BY LC-MSD TECHNIQUE

R. Varga*, P. Ulbrich**, M. Koložvári** and M. Fuknová**

* Department of Theory and Technology of Explosives, University of Pardubice,
532 10 Pardubice, Czech Republic

** Institute of Forensic Science of the Slovak Police Corps,
Sklabinská 1, Bratislava 812 72, Slovak Republic

Abstract:

The aim of this work is the determination of LOD of explosive compounds using Agilent 1100 series LS-MSD system with the atmospheric pressure chemical ionization (APCI) source.

At the analysis of explosive compounds LC-MSD with IONSCAN M 400 (Barringer Inc.), a detector of explosives and drugs, and with the gas chromatography with electron capture detector (agilent Technologies) were compared.

Keywords: trace analysis, explosive, LC-APCI/MS, GC-ECD, IONSCAN

1. INTRODUCTION

In recent years, mass spectrometric detection is increasingly used in LC and GC to improve selectivity and structural identification of unknown organic compounds and also in complicated mixtures ^[1].

The combination of HPLC and atmospheric pressure ionization (API) MS is suitable for the investigation of thermolabile, and polar substances, like various explosives, forensic relevant substances in trace levels ^[2]. Atmospheric pressure chemical ionization (APCI) technique results in protonated molecules with little or no fragmentation. Therefore, fragmentation is needed to get the additional ions necessary for the identification of compounds ^[3]. Several application of LC-APCI/MS to the analysis of explosives and explosive residues are described by André Schreiber et al. ^[2], Xiaoming Zhao et al. ^[4, 5] and D.A. Cassada et al. ^[6].

GC-MS and LC-MS plays an important role in post explosion analysis, possibly by being complementary to each other ^[7]. Except of LC-MS also another methods for rapid and rigorous identification of trace amounts of explosives exist ^[8]. One of the following methods can be used in post explosion analysis of organic high explosives (TNT, RDX, PETN etc.) : ion mobility spectrometry (IMS), gas chromatography with electrone capture detector (GC-ECD) etc. ^[9].

Analysis of nitrate ester explosives by GC can be problematic due to their thermal instability and/or sorption in the analytical system ^[10]. The problem of the thermal instability of the explosive at LC is eliminated because the analysis takes place at room temperature and the formation of active sites on the column from dirty samples is not as great problem as in gas chromatography ^[7]. The ECD is especially selective to compounds containing electronegative atoms (nitro groups) whereas it is insensitive to hydrocarbons ^[11].

There are described different applications of GC-ECD in the field of analysis of common explosives and their post explosion residues ^[12, 13].

Ion mobility spectrometry has become the most successful and widely used technology for the detection of trace levels of nitro-organic explosives. The usability of IMS in the detection of explosives in post-blast residues is reported by Tricia L. Buxton et al. ^[14] and R.G.Eving et al. ^[15].

2. EXPERIMENTAL SECTION

2.1 Used Materials

In this work the following explosives were tested:

- technical dinitrotoluene (structure 1; DNT)
- technical 2,4,6 – trinitrotoluene (structure 2; TNT)
- pentaerythrytol tetranitrate (structure 3; PETN)
- hexahydro-1,3,5-triazine (structure 4; RDX)

From the view of criminalistic expert's report technical DNT and separated isomers of 2,4- and 2,6-DNT are interesting as components of industrial explosives and smokeless powder. TNT is interesting as the basic military explosive, often used component of military and industrial explosive mixtures and as a component of homogenous propellants as well as some pyrotechnical compositions. For the criminalistic investigation, PETN has had a great significance for his abundance as a primarily component of plastic explosives manufactured in Czech Republic, flegmatizers, igniting composition and primacords. RDX can be also very important in the forensic analysis due to its application as a component of military explosives, industrial initiating charges and special detonating fuses or detonators ^[1]. The structures of tested explosives are shown on the Fig. 1.

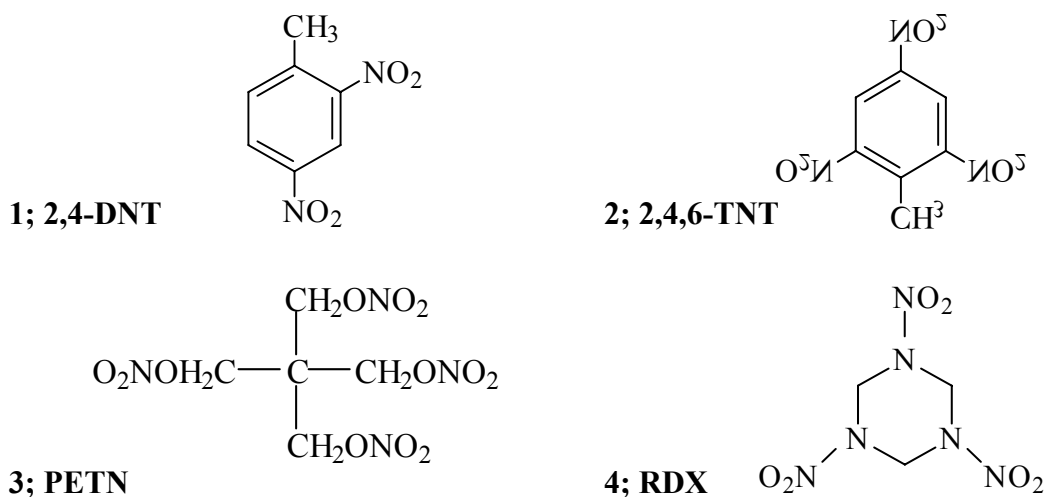


Fig 1. Chemical structures of investigated explosives

2.2 Liquid chromatography-mass spectrometry (LC-MS) conditions

All analyses were performed by means of Agilent 1100 series LC-MSD system with the atmospheric pressure chemical ionization (APCI) source, in the negative-ion mode. The used chromatographic and mass spectrometric conditions are shown below.

Chromatographic conditions:

Column:	Zorbax Eclipse XDB-C8; 4,6 x 150 mm; 5 μm (Agilent Technologies)
Mobil phase:	Methanol/water; 70:30, v/v, with addition of ammonium chloride and formic acid
Flow rate:	1 ml/min
Injection vol.:	20 μl

MS conditions:

Source:	APCI
Mode:	SCAN and SIM
Ionization polarity:	Negative
Capillary voltage:	3000 V
Nebulizer:	60 psi
Vaporizer temp:	300 $^{\circ}\text{C}$
Dry gas flow:	5 l/min
Drying gas temp:	330 $^{\circ}\text{C}$
Fragmentor:	30 V

2.3 Ion mobility spectrometry (IMS)

The ion mobility spectrometer (IMS) of explosives and drugs used in this work was a Barringer Ionscan M 400 (Barringer Instruments, Inc.). All explosive plasmagrams were obtained in negative-ion mode. The carrier and drift gases were Air/air at atmospheric pressure. The drift flow was $353\text{ cm}^3\text{ min}^{-1}$ with a $224\text{ cm}^3\text{ min}^{-1}$ sample flow. The inlet temperature and drift tube temperature were constant during the experiment at 236 and 108 $^{\circ}\text{C}$, respectively. The desorber heater was held constant at 220 $^{\circ}\text{C}$ for the detection of explosives. The prepared standards of explosives were deposited on fiberglass IMS sample filters and the filters were then placed in the IONSCAN for insertion into the IMS. It isn't suitable for the analysis of ethylene glycol dinitrate. Total time of analysis was 6,6 s.

2.4 Gas Chromatograph with Electron Capture Detector (GC-ECD)

The standards of explosives (TNT, DNT, RDX and PETN) were analyzed on a Hewlett Packard 5890 II chromatograph, using a capillary column HP-5 of 5 m length, 0.53 mm inner diameter, and 0.88 μm film thickness. An electron capture detector (ECD) was used for the detection, and the carrier gas was nitrogen of 20 kPa overpressure. The sample (1 μl) was injected directly (on-column), the injector temperature being 70 $^{\circ}\text{C}$. The temperature regime was as follows: the column was kept at 70 $^{\circ}\text{C}$ for 1 min, whereupon the temperature was increased at a rate of 15 $^{\circ}\text{C}/\text{min}$ to 150 $^{\circ}\text{C}$, and 5 $^{\circ}\text{C}/\text{min}$ to 230 $^{\circ}\text{C}$, and this final temperature was kept for 8 min.

3. RESULTS AND DISCUSSION

Stock solutions of individual explosives (DNT, TNT, PETN and RDX) were made in methanol p.a. Standard mixtures were prepared by diluting the stock solution to a final concentration as necessary.

3.1 LC-APCI/MS analysis of explosives

First the scan negative-ion APCI mass spectra of all explosives were measured in order to find out the limits of detection (LOD) of DNT, TNT, PETN and RDX and major ions occurring in these spectra, too. Then three major ions, which were selected in scan mode, were followed in Selected Ion Monitoring (SIM) APCI mass spectra at lower concentrations. This method was used to compare the sensitivity both of these methods. In SIM mode limits of detection were not searched.

The full scan negative-ion APCI mass spectra of the DNT contain three major ions at m/z 181, 182 and 183. The ion at m/z 182 was the molecular ion $[M]^-$. DNT also creates intensive peaks of deprotonated $[M-H]^-$ and protonated molecular ions $[M+H]^-$ at m/z 181 and 183, respectively. Method detection limit of DNT was 3 ppm (Fig. 2A). APCI mass spectrum of DNT in SIM mode is shown on the Fig. 2 B. The sensitivity of MS detector was increased using SIM mode in the analysis of DNT (0,2 ppm). Fig. 2C shows the APCI mass chromatograms of DNT and its individual ions in SIM mode.

The mass spectra of TNT were all characterized by the molecular ions $[M]^-$ at m/z 227. The typical ions of TNT are deprotonated molecular ions $[M-H]^-$ at m/z 226. The m/z 227 of TNT produced major fragment ions $[M-NO]^-$ at m/z 197, which is caused by the loss of 30 mass units ($-NO$). Limit of detection for TNT was 1 ppm (Fig. 3A). The sample of TNT with the concentration of 0,2 ppm was detected in SIM mode (Fig. 3B). Fig. 3C shows the negative ion APCI mass chromatograms of TNT and its individual ions in SIM mode.

At the identification of PETN and RDX ammonium chloride as an additive was used. Except for two nitroaromatic explosives (DNT, TNT), which had $[M]^-$ and $[M-H]^-$ ions as the top ions, the other tested explosives (PETN and RDX) especially formed adduct ions $[M+Cl]^-$.

PETN produced predominant ions at m/z 351 and 353. These ions are attributed to the ^{35}Cl and ^{37}Cl isotope peaks for $[M+Cl]^-$. The ratio of ^{35}Cl and ^{37}Cl isotopes is 75,53:24,47 and that's why the relative abundance of adduct ions in mass spectra will be approximately in the rate of 3:1. The mass spectra of PETN obtained also the other ions. The most important of them was ion $[M-H]^-$ at m/z 315. The molecular ions at m/z 316 failed in spectra of PETN. The ion at m/z 378 originated probably by thermal decomposition of molecules of PETN owing to the high temperature (300 °C) to $-ONO_2$ (NO_3) and was accompanied by autoionization to $[M+NO_3]^-$ (378). Mass spectrum of PETN was also characterized by the presence of two fragment ions at m/z 304 $[M-HNO_2+^{35}Cl]^-$ and 306 $[M-HNO_2+^{37}Cl]^-$. Ammonium chloride produced good sensitivity of adduct ion formation. LOD of PETN in full scan mode was 12 ppm (Fig. 4A). After having selected three top ions obtained from scan mass spectra of PETN, SIM method at lower concentration was tested. Fig. 4B and 4C show APCI mass chromatogram of PETN and its mass spectrum in SIM mode.

With the addition of NH_4Cl , $[M+Cl]^-$ ions dominated in the mass spectra of RDX. The mass spectrum shows (Fig. 5B) ions $[M+^{35}Cl]^-$ and $[M+^{37}Cl]^-$ at m/z 257 and 259. In mass spectra of RDX molecular ions at m/z 222 weren't present. Adduct ions at m/z 258, 260, 267 and 268 were $[M+^{35}Cl+H]^-$, $[M+^{37}Cl+H]^-$, $[M+NO_2-H]^-$ and $[M+NO_2]^-$.

The LOD for RDX under full scan conditions was found 3 ppm (Fig. 5A).

Table 1 includes retention times, mass spectral ions and limits of detection of investigated explosives in LC-APCI/MS.

Table 1. Mass spectral ions and LOD of tested explosives with addition of NH_4Cl

Explosive	M_r	Retention time (min)	Major ions with NH_4Cl	LOD (mg/l)
DNT	182	3,34	$[\text{M}]^-$, $[\text{M}-\text{H}]^-$, $[\text{M}+\text{H}]^-$	3
TNT	227	2,90	$[\text{M}]^-$, $[\text{M}-\text{H}]^-$, $[\text{M}-\text{NO}]^-$	1
PETN	316	4,25	$[\text{M}-\text{H}]^-$, $[\text{M}+^{35}\text{Cl}]^-$, $[\text{M}+^{37}\text{Cl}]^-$	12
RDX	222	2,05	$[\text{M}+^{35}\text{Cl}]^-$, $[\text{M}+^{37}\text{Cl}]^-$	3

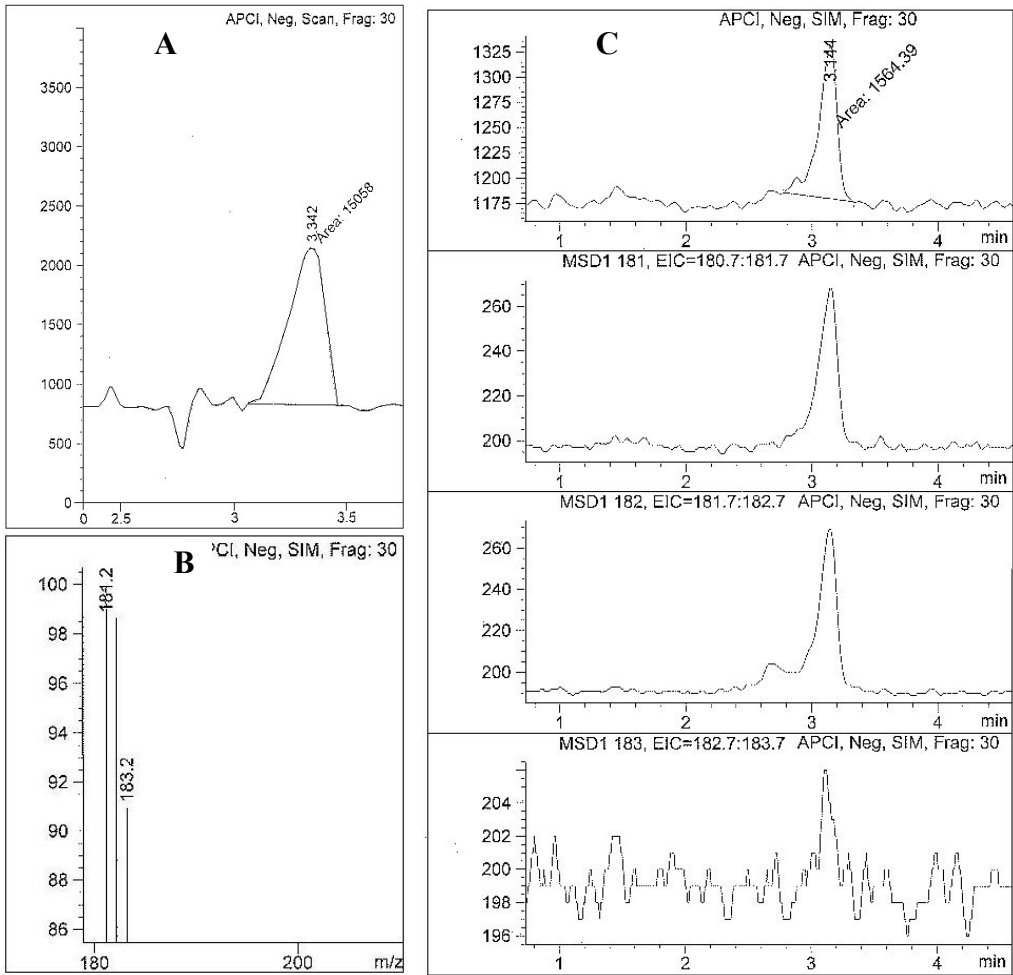


Fig 2. Negative ion APCI mass chromatogram of 3 ppm DNT in SCAN mode (A), its mass spectrum in SIM (B) and APCI mass chromatogram of 0,2 ppm DNT with its individual ions at m/z 181, 182 and 183 (C)

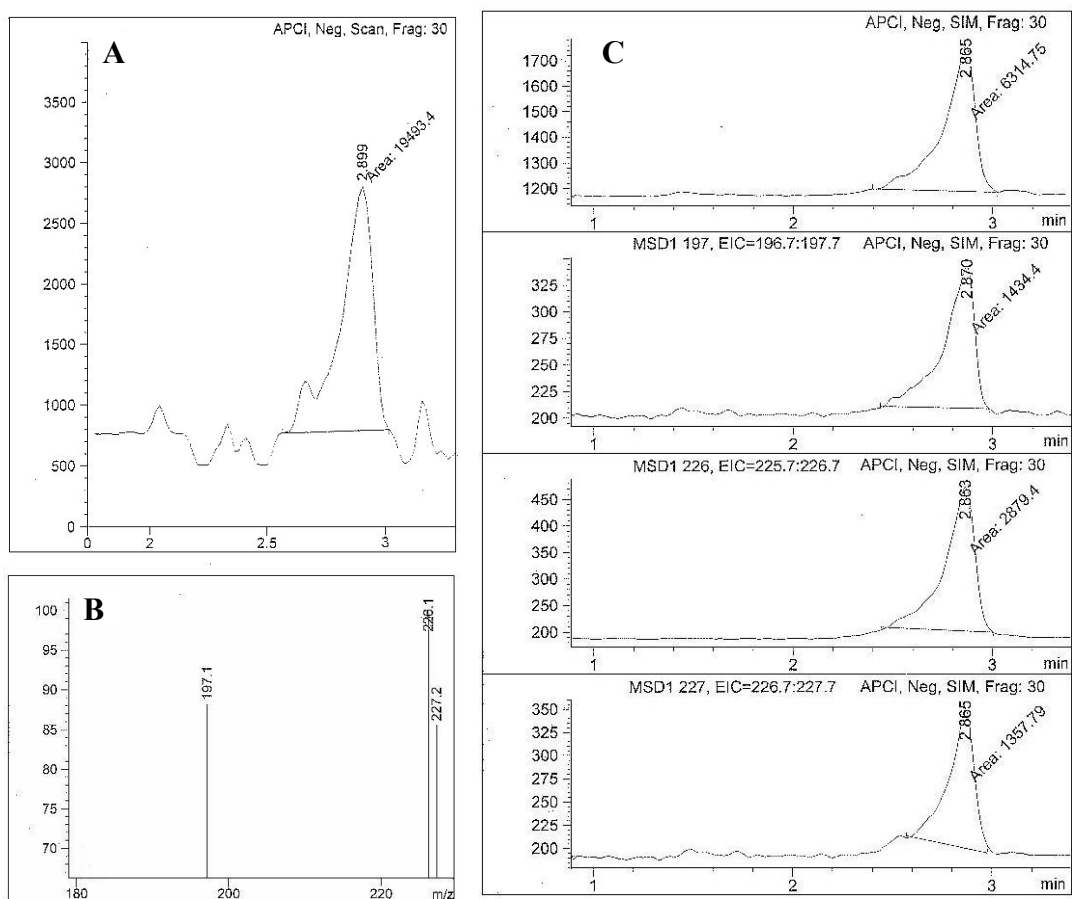


Fig 3. Negative ion APCI mass chromatogram of 1 ppm TNT in SCAN mode (A), its mass spectrum in SIM (B) and APCI mass chromatogram of 0,2 ppm TNT with its major ions at m/z 197, 226 and 227 (C)

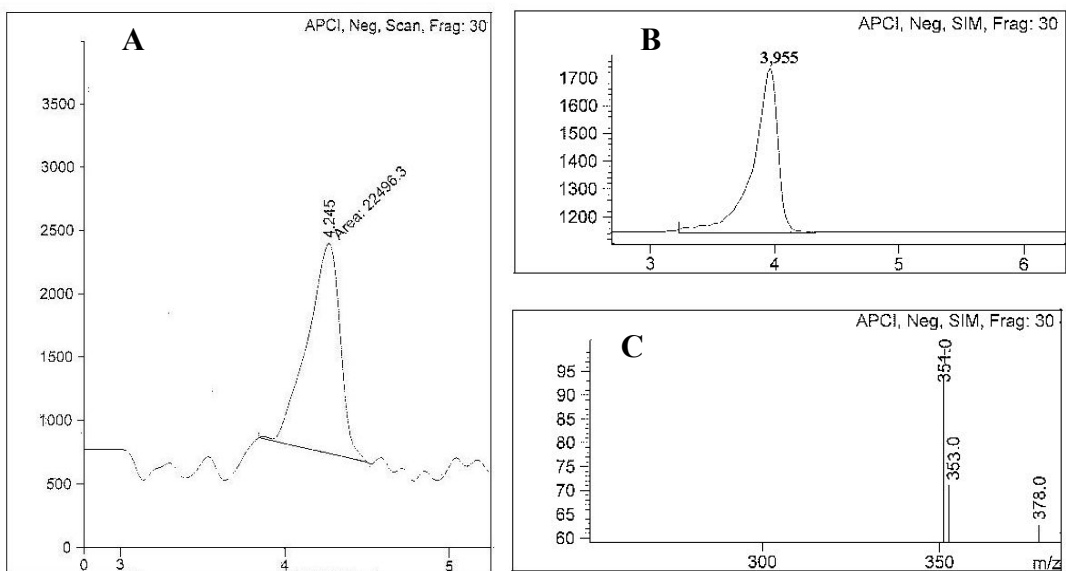


Fig 4. Negative ion mass chromatogram of 12 ppm PETN in SCAN mode (A) and 3 ppm PETN in SIM mode (B) and its mass spectrum with addition of NH_4Cl (C).

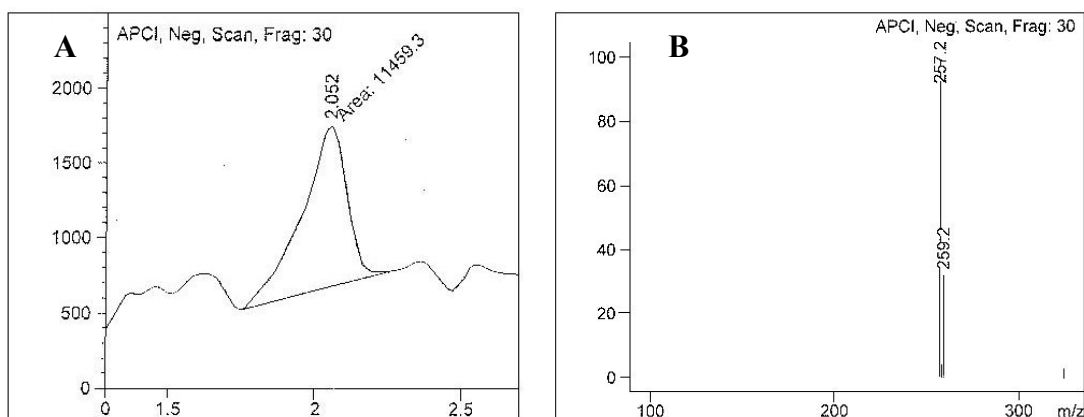


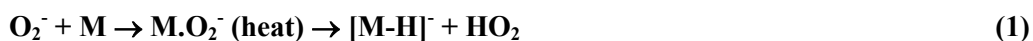
Fig 5. Negative ion mass chromatogram of 3 ppm RDX in SCAN mode (A) and its mass spectrum with addition of NH_4Cl (B)

3.2 Detection of explosives by means of ion mobility spectrometry (IMS)

There was determined the sensitivity of IMS in analysis of series of explosives (DNT, TNT, PETN and RDX). Fig. 6 shows the chromatograms obtained by the IONSCAN M 400 for mixture of explosive samples (1 ppm (A) and 3 ppm (B) of each explosive).

Ionscan Model 400 couldn't detect DNT which is connected with the options of analysis conditions by manufacturer. $[\text{TNT-H}]^-$ with the reduced mobility $K_0 = 1,45 \text{ cm}^2 \cdot \text{V}^{-1} \cdot \text{s}^{-1}$ was the characteristic ion for TNT plasmagram.

The reactant ions in air and at negative polarity are hydrated O_2^- . Ions O_2^- cause proton abstraction of molecules to $[\text{M-H}]^-$ according to the Equation 1.



Mass identification of TNT and other explosives weren't performed, identification of TNT ions was obtained on the basis of literature ^[14, 15].

At concentration 3 ppm in explosive mixture all investigated explosives were detected. Mobility spectra of PETN contained two ions at $K_0 = 1,15 \text{ cm}^2 \cdot \text{V}^{-1} \cdot \text{s}^{-1}$ (PETN-C) and $K_0 = 1,10 \text{ cm}^2 \cdot \text{V}^{-1} \cdot \text{s}^{-1}$ (PETN-N). In cases of RDX, its mobility spectra contained also two ions at $K_0 = 1,39 \text{ cm}^2 \cdot \text{V}^{-1} \cdot \text{s}^{-1}$ (RDX-C) and $K_0 = 1,31 \text{ cm}^2 \cdot \text{V}^{-1} \cdot \text{s}^{-1}$ (RDX-N or RDX- NO_3). Results from IMS analyses of standard solutions (TNT, PETN and RDX) and their typical ions are included in Tab. 2.

Table 2. Summary of IMS response to TNT, PETN and RDX

Explosive	Channel	Amount (mg/l)	K ₀ (cm ² .V ⁻¹ .s ⁻¹)	Drift time (ms)	Typical ion
TNT	TNT	3	1,45	13,03	[TNT-H] ⁻
PETN	PETN-N	1	1,10	17,08	U
	PETN-C		1,15	16,39	U
RDX	RDX-N/NO ₃	1	1,31	14,35	U
	RDX-C		1,39	13,57	U

Notice: U – unidentified

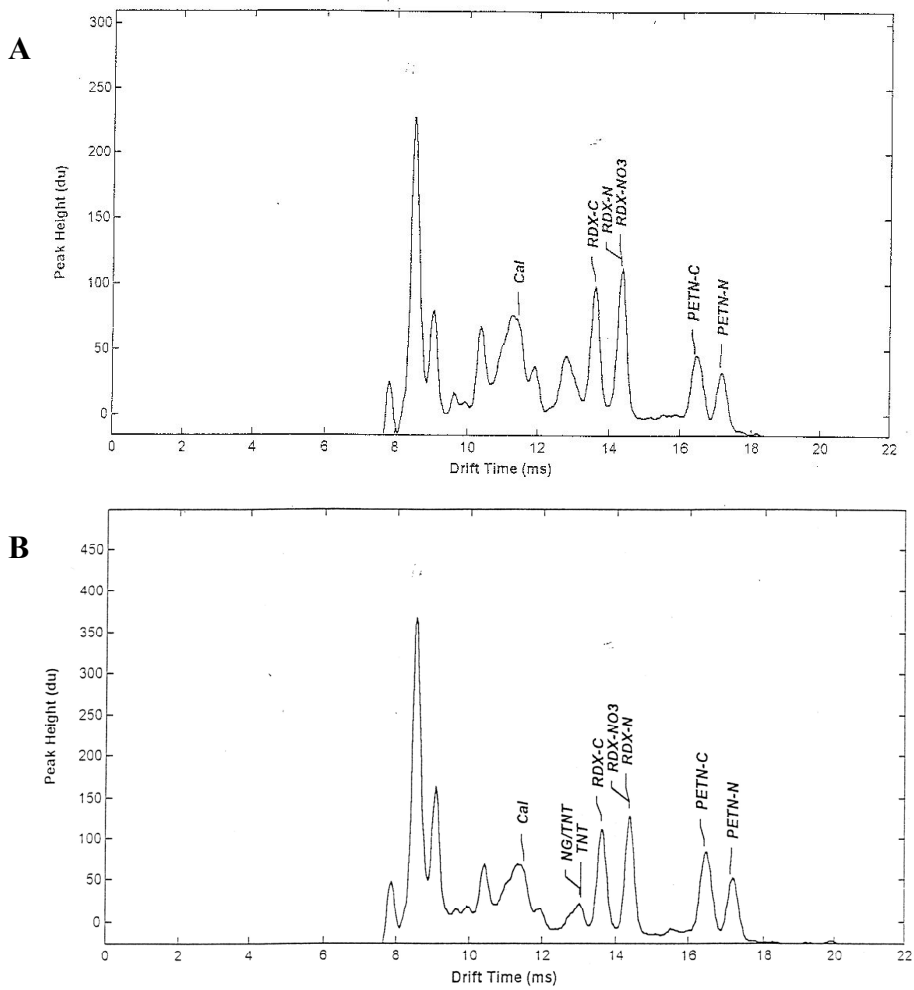


Fig 6. Negative ion spectra of TNT, RDX and PETN for mixture of each explosives (A -1 ppm and B-3 ppm) obtained by using IONSCAN

3.3 Sensitivity of GC-ECD in analysis of explosives

We measured standard of explosives (technical DNT, technical TNT, PETN and RDX) by means of GC-ECD in order to determine the sensitivity of electron capture detector in combination with gas chromatography. Limits of detection (LOD) were determined by evaluation of obtained response of individual explosives. Practically LOD presents an indicated value of concentration, at which the peak height is three-times higher than a noise of the basic line. Determination of LOD at LC-APCI/MS was also based on this rule.

The results of measurements are summarized in Table 3. Retention times for the chosen types of explosives were 3,607 min (2,6-DNT), 4,141 min (2,4-DNT), 4,564 min (3,4-DNT), 5,509 min (TNT), 6,223 min (PETN) and 6,674 min (RDX). Fig. 7 shows the chromatogram obtained by the GC-ECD technique for mixture of explosives (1 ppm of each explosive).

Table 3. The detection limits for the investigated explosives

Explosive	Limit of detection (mg/l)
DNT	0,1
TNT	0,05
PETN	0,5
RDX	0,5

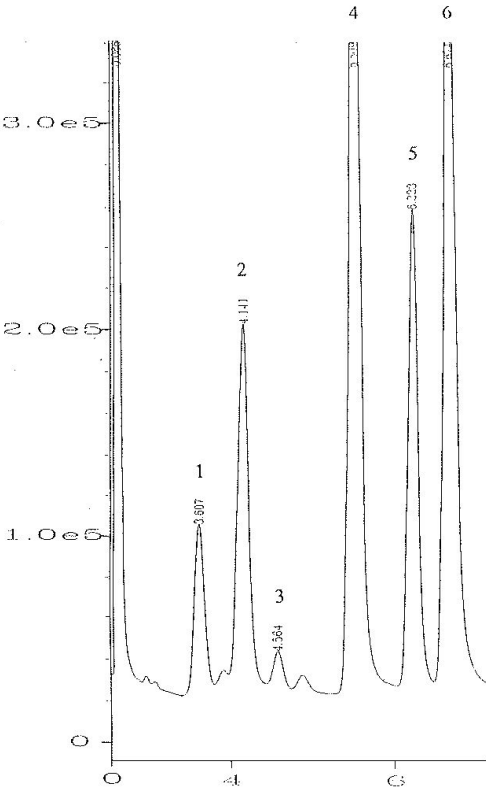


Fig 7. GC-ECD chromatogram of explosive mixtures (1 ppm of each explosive)
Peaks: (1) 2,6-DNT, (2) 2,4-DNT, (3) 3,4-DNT, (4) 2,4,6-TNT, (5) PETN and (6) RDX

The GC-ECD chromatograms of technical TNT and DNT included three good recognizable peaks of DNT, namely 2,6-, 2,4- and 3,4-isomers. The presence of isomeric mixture of DNT is typical for industrially produced explosives.

4. CONCLUSION

The aim of this work were the applications of LC-APCI/MS technique in trace analysis of common explosives and the comparison of the sensitivity of this technique with GC-ECD technique and IMS technique. There were also made library of the characteristic mass spectrum with atmospheric pressure chemical ionization (APCI) for DNT, TNT, PETN and RDX. It was made due to their use in analysis of post explosion residues.

The analyses of standard mixtures showed that the LOD of LC-APCI/MS technique for explosive compounds is at intervals 1 – 12 ppm. There was also used method of “Selected Ion Monitoring” (SIM), which allowed us to increase the sensitivity of LC/MS four to fifteen times in the analyses of investigated explosives, whereas their LOD weren’t searched in this method. Very low limit of detection of SIM method offers considerable possibilities everywhere, where it is necessary to solve problems of qualitative and quantitative analysis of explosives in low till trace concentrations.

The conclusions resulting from the measured standards showed that Ionscan can be used to the orientation identification of organic explosives. Low limits of detection at TNT, PETN and RDX were provided by chemical ionization at atmospheric pressure in negative ion mode. IMS gives low LOD and short times of analyses (6,6 s). This single method is on the other hand insufficient to the confirmation of results from the analysis of explosive residues, it is necessary to use other methods (GC-ECD or LC/MS etc.).

The electron capture detector in combination with gas chromatograph (GC-ECD) provided good results in the analysis of two nitroaromates (DNT, TNT), crystal nitroester (PETN) and nitramine (RDX). GC-ECD technique is more sensitive than the LC-APCI/MS technique in full scan mode. The ECD seemed to have been suitable for the trace analyses of explosives and explosive residues due to its high sensitivity. The advantage of LC-APCI/MS technique is an identification facility of post-explosion residues on the basis of mass spectrum in complicated matrix.

Acknowledgement

The authors would like to thank to the management of Institute of Criminology of Police Forces of the Slovak Republic in Bratislava for making possible and supporting the realization of this work in the Institute.

REFERENCES

- [1] R. VARGA: *Supplement to the analysis of explosive residues*, Thesis, University of Pardubice, 2002
- [2] ANDRÉ SCHREIBER, JÜRGEN EFER AND WERNER ENGEWALD: *Application of spectral libraries for high-performance liquid chromatography-atmospheric pressure ionization mass spectrometry to the analysis of pesticide and explosive residues in environmental samples*, Vol. 869, Journal of Chromatography A, 411-425, 2000
- [3] P.G.M. KIENHUIS AND R.B. GEERDINK: *A mass spectral library based on chemical ionization and collision-induced dissociation*, Vol. 974, Journal of Chromatography A, 161-168, 2002.
- [4] XIAOMING ZHAO AND JEHUDA YINON: *Identification of nitrate ester explosives by liquid chromatography-electrospray ionization and atmospheric pressure chemical ionization mass spectrometry*, Vol. 977, Journal of Chromatography A, 59-68, 2002
- [5] XIAOMING ZHAO AND JEHUDA YINON: *Characterization and origin identification of 2,4,6-trinitrotoluene through its by-product isomers by liquid chromatography-atmospheric pressure chemical ionization mass spectrometry*, Vol. 946, Journal of Chromatography A, 125-132, 2002
- [6] D.A. CASSANDA, S.J. MONSON, D.D. SNOW AND R.F. SPALDING: *Sensitive determination of RDX, nitroso-RDX metabolites, and other munitions in ground water by solid-phase extraction and isotope dilution liquid chromatography-atmospheric pressure chemical ionization mass spectrometry*, Vol. 844, Journal of Chromatography A, 87-95, 1999
- [7] ALEXANDER BEVERIDGE: *Forensic investigation of explosions*, 1 Gunpowder Square, London: Taylor & Francis Ltd., 1998
- [8] C.S. EVANS, R. SLEEMAN, J. LUKE AND J. KELLEY: *A rapid and efficient mass spectrometric method for the analysis of explosives*, Rapid Commun. Mass Spectrom. **16**, 1883-1891, 2002.
- [9] R. VARGA AND P. ULBRICH: *Trace analysis of post explosion residues of industrial explosives by means of GC-ECD and IC*, Proc. 6 th Seminar of New Trends in Research of Energetic Materials, University of Pardubice, Pardubice, Czech Republic, 461-472, 2003
- [10] Y. MCAVOY, K. DOST, D.C. JONES, M.D. COLE, M.W. GEORGE AND G.DAVIDSON: *A preliminary study of the analysis of explosives using packed-column supercritical fluid chromatography with atmospheric pressure chemical ionization mass spectrometric detection*, Vol. 99, Forensic Science International, 123-141, 1999
- [11] J. YINON AND S. ZITRIN: *Modern Methods and Applications in Analysis of Explosives*, Chichester, England: John Wiley & Sons Ltd., 1996
- [12] MARIANNE E. WALSH: *Determination of nitroaromatic, nitramine, and nitrate ester explosives in soil by gas chromatography and an electron capture detector*, Talanta **54**, 427-438, 2001.
- [13] STÉPHANE CALDERARA, DOMINIQUE GARDEBAS AND FABIENNE MARTINEZ: *Solid phase micro extraction coupled with on column GC/ECD for the post-blast analysis of organic explosives*, Vol. 137, Forensic Science International, 6-12, 2003
- [14] TRICIA L. BUXTON AND PETER DE B. HARRINGTON: *Rapid multivariate curve resolution applied to identification of explosives by ion mobility spectrometry*, Vol. 434, Analytica Chimica Acta, 269-282, 2001
- [15] R. G. EWING, D.A. ATKINSON, G.A. EICEMAN AND G.J. EWING: *A critical review of ion mobility spectrometry for the detection of explosives and explosive related compounds*, Talanta **54**, 515-529, 2001

LIFE-CYCLE-ANALYSIS AND “GREEN” ENERGETIC MATERIALS

J. Vávra* and P. Vávra **

* Department of Economy and Management of Chemical and Food Industry
Faculty of Chemical Technology, University of Pardubice
53210 Pardubice, Czech Republic

** Department of Theory and Technology of Explosives
Faculty of Chemical Technology, University of Pardubice
53210 Pardubice, Czech Republic

Abstract:

This paper mentioned the main requirements on “green” energetic materials and the priorities in specific programs in R&D. In this connection with these new requirements are principles of Life-Cycle-Analysis (LCA) and Life-Cycle-Costs (LCC) applicated. Possible use of these methods for costs reduction of new GEM during whole GEM's lifetime is discussed.

Keywords: *life-cycle-assessment, life-cycle-analysis, life-cycle-cost, „green“ energetic materials (GEM)*

1. INTRODUCTION

Research and development (R&D) of new energetic materials (EMs) has been concentrating on several areas in the last two decades. The main requirement still dominating is increase in volume energy. Another requirement, especially concerning the products of explosion transformation, is environmental friendliness. Due to a number of unexpected incidents, induced by action of outer impulses, there emerged a pressure to produce insensitive EMs meeting the requirement for low vulnerability ammunition (LOVA, IM). In the last decade, R&D projects have been appearing and dealt with that are generally referred to as green energetic materials (GEMs). These projects are basically oriented to removal or at least substantial restriction of occurrence of toxic and harmful substances within the whole lifetime of EM, from their production to their liquidation. The above-mentioned requirements are complemented by the problem of production costs of these materials: from the said requirements it clearly follows that the substances fulfilling (or almost fulfilling) all the criteria will be distinctly more expensive than classic EMs in the time period of their introducing into general use. However, this does not mean that after a period of 20-25 years (presumed length of military application) they will be destroyed or depreciated, because the stability of most individual EMs reaches up to hundreds of years. In the following text we will try to give the relevant factors affecting the price of GEMs in the course of their lifetime.

2. THE MAIN REQUIREMENTS FOR GEMs AND PRICE

The main characteristics of GEMs were specified ^[1] in the following way:

- minimizing of use and liberation of toxic materials throughout their lifetime
- content of easily identifiable level at which they still can act as EMs
- they must be easily disarmed and reused

Also their potential benefits were specified:

- minimisation of unexpected incidents
- a reduced cost and reduced influence on the environment
- bio-degradation in the environment
- easy dismantling and resource recovery

There of course also exists the requirement of high performance or high content of usable energy per volume unit.

In particular projects ^[2] the abovementioned general requirements are specified by outlining clear priorities, such as:

- elimination of organic solvents from the production and disarming operations (e.g. by application of liquid or supercritical CO₂)
- elimination of emissions of hydrochloric acid
- elimination of liquidation of EMs by combustion or detonation
- orientation of R&D to energetic thermoplastic elastomers (TPE) and easily hydrolysed EMs
- recycling of components of GEMs
- development of environmental cost predicting methods

All GEM products (propellants and high explosives) should exhibit the so-called R³ characteristics (recover, recycle, reuse). The present approach to prediction of new EMs was presented in an excellent review ^[3] focused on prediction of stability and sensitivity of new structures. This approach results in both acceleration of R&D and decrease in costs. Another example that can be given is working out of the multi-step synthesis of trinitroazetidine ^[4] (TNAZ) in which the amount of wastes was lowered from 15.7 kg to 3.7kg (per 1 kg product).

3. LCA METHOD (LCC)

In order to find out all possible impacts on the environment it is necessary to provide an evaluation and life cycle analysis (LCA) of existing EM and potential GEM products. The LCA method is a systematic analysis serving for estimation of impacts on the environment and human health within the whole lifetime from procurement of the starting materials for production till the end of lifetime and/or final application ^[5]. Generally, the following life phases can be identified for each product: Raw material procurement, manufacturing, distribution, consumer use, and post-consumer use (see Fig. 1).



Fig 1. Life cycle phases ^[6]

At the beginning of LCA it has to be specified for what purposes the method is going to be worked out and what its aims should be, which can be represented by generally formulated requirements that the GEM should meet (as those given in Introduction) or by simple lowering of costs ^[7]. The next step consists in determining the individual raw material and energy inputs and solid, liquid and gaseous wastes occurring at the output. Basically this means a qualitative and quantitative expressing of all inputs and outputs, or assembling of primary data and evaluation of their quality, i.e. credibility, reproducibility and transparency. As the system at hand is complex and large, it is suitable to divide it into smaller subsystems and systematically proceed from one subsystem to the next and gather data on effects on the environment (LCA) and financial impacts connected with these effects. The necessary data that quantify these streams are most frequently obtained by direct measurements at the respective sites, calculations, informed guesses and, as the case may be, discussions with experts directly involved in handling with EMs.

Then it is possible to evaluate impacts on the environment and human health, which includes a connection between specified inputs and outputs in each phase of life cycle and the environmental problems and their subsequent financial expression. This step is connected with several problems too serious for the LCA method to be applied without difficulties. If the LCA should be finished in the form providing information about all the inputs and outputs (i.e. inclusive of the indirect or induced ones – the so-called effects of higher orders) it would inevitably require an enormous body of data and additional information, not only from the area of EMs. In this phase it is usual to carry out the so-called standardisation, when the contributions of individual effects in the same category (e.g. air pollution) are reduced to a common denominator by means of conversion coefficients. A suitable standard is chosen for each category, and the equivalent unit is determined to which the values of all quantitatively identical effects should be converted (e.g. particularly for air pollution, this can be represented by 1 kg carbon dioxide). After the standardisation, there usually follows the so-called normalisation, which takes into account relative harmfulness of individual effects for the given locality ^[8].

The last phase of LCA should include the evaluation of impact of EM on the environment, which basically means determination of mutually relative significance of all the partial burdens. The evaluation procedure very often depends on the aim and purpose of a given study.

4. APPLICATIONS OF LCA (LCC) TO GEMs

For purposes of GEMs as defined at the beginning it would be sufficient (for the time being) to focus attention on the life cycle costs (LCC) with precise definition of the system extent in which the costs and revenues are to be estimated. A significant or at least noticeable improvement can be expected even from a relatively simple analysis, as far as it provides information for estimation of LCC within a given period for a defined unit of EM (functional unit). On the basis of such information, it would be possible to evaluate the existing EMs and to find out the life cycle phases in which higher costs are encountered and where these costs must be lowered in the cases of new GEMs.

In our simple study (a sort of pre-LCA) we have not yet defined a functional unit and not yet tried to precisely delimit the limitations of system. We are trying to get the narrowest possible view of the EM with regard to relevancy and credibility of results. We are more interested in evaluation of the most fundamental inputs and outputs in the area of EMs and GEMs. The aim is to specify the impacts in individual phases of lifetime of products and determination of individual acting effects, inclusive of their anticipated impact on LCC. However, we express these impacts only approximately on the basis of informed guess with respect to the broad spectrum of GEMs.

A more clear treatment will perhaps be possible with help of Table 1 (see Appendix 1), representing individual steps from the existing situation till implementation of GEMs, inclusive of the anticipated impacts connected with the transition to applications of GEMs.

As already mentioned above, it is presumed that the costs in the first phases of lifetime of a product will be increased, which is also confirmed by the estimate of per cent increase in the phases of raw materials procurement and production. This has its rationale, taking into account higher costs inevitably connected with necessary R&D on new technologies for procurement of raw materials. The production itself will need R&D on new procedures and technologies and/or modification of the existing equipment, which will result in an increase in investment costs. This financially negative impacts can be somewhat compensated by the overall lower risks connected with application of the new raw materials, which should show higher stabilities (the aspect of risks in handling) as well as lower risks for the environment and human health.

For this increase to be acceptable for the manufacturer and consumer, it will be necessary to state whether the mentioned increase in pre-manufacturing and manufacturing phases will be compensable by costs decrease during later phases of the life cycle. Already the distribution and storage of EMs can bring savings resulting from lower risks and higher stabilities of GEMs. In the application itself of GEMs, these properties (stability and lower risks in handling) positively affect their economy. In addition to that, lowering of waste materials amount considerably lowers the ecological and thus also economical burden. However, on the other hand, we must point out a possible lowering in performance of GEMs. Despite the trends oriented to reaching the highest possible volume energy, the nearest future will probably see results that are, at the most, comparable with the current EMs, and the performance of GEMs will reach that of the existing EMs at the most.

The last phase of life cycle can undoubtedly be connected with the highest economical and ecological profits. Even the simple liquidation by detonation or combustion should bring

savings following from minimisation of liquidation of wastes and lower risk degree. A much higher economical effect is connected with recycling of individual components of GEMs. Already at present, there exist GEMs whose recycling allows obtaining of up to 95% of effective components ^[2], and it is presumed that this situation will further improve. This would possibly compensate, to a large extent, the use of financially less favourable materials, as they can be further economically utilised. However, it must not be forgotten that the development and production of recycling technologies and apparatus will need investment costs, and that the operation itself of such apparatus connected with recycling of the components will also need operation costs. Therefore, it is required that structure of GEMs should make potential recycling easy and financially acceptable. Another financially interesting opportunity is offered by utilisation of current GEMs as raw materials for manufacturing of other products (e.g. fertilisers due to possible bio-degradation). It is understandable that the utilisation of GEMs at the very end of their life cycle should be known as early as the start of R&D on a new GEM and at the moment of planned initial costing at the latest.

At present, research work is ongoing into methods of determination of LCC for newly created GEMs. Since the period of manufacturing and particularly effective utilisation of EMs reaches to 20 or even 30 years, it is necessary to take into account the time factor. However, substantial simplifications are unavoidable, because any predictions within such extensive time periods are very difficult. For instance, such an interesting method was created by MURAT Club under the name Cost Benefit Analyses (CBA) ^[9].

5. CONCLUSION

The requirements to be met by environmental properties of EMs are bringing about changes in all phases of life cycle. As the economical aspect is significant for these changes, it is absolutely necessary to quantify economical and ecological impacts in the individual phases of the life cycle. From this point of view, the LCA and/or LCC methods appear to be suitable tools for such evaluation. In addition, if correctly carried out, they can provide important information concerning the question whether the application of new “Green” EMs will be connected with an increase in prices of these materials or it will be possible to produce such GEMs that will simultaneously offer, besides the environmentally friendliness, also economical advantages, being equally costly as, or even less costly than the existing EMs. We can state that carrying out of LCC analysis inclusive of its evaluation should be one of the tools for deciding to start R&D on newly designed GEMs and, at the same time, the LCC should serve as a control mechanism, which should—in every phase of life cycle—compare the calculated environmental and economical impacts with the achieved ones in order to find out whether the former ones are being really attained.

REFERENCES

- [1] The Keystone Center: *National policy dialogue on military munitions*, Final report, USA, Sept, 2000
- [2] L. NOCK, D. PORADA, G. KING: *Green Energetic Materials (GEM) – A Program Overview*, JANNAF 30th propel. develop. & charact. subcom. meeting, CPIA Publ. 708, Vol. 1, Colorado, pp. 1-12, March 2002
- [3] L.E. FRIED, M.R. MANAA, P.F. PAGOVI, R.L.SIMPSON: *Design and Synthesis of energetic materials*, Annu. Rev. Mater. Res. 2001, **31**, p.291-321, 2001
- [4] M.D. COBURN, M.A.HISKEY, T.G.ARCHIBALD: *Scale-up and waste-minimization of the Los Alamos process for 1,3,3-trinitroazetidine (TNAZ)*, Waste Management, **17**,143, 1997
- [5] S. SCHALTEGGER, R. BURRITT: *Contemporary Environmental Accounting*, Greenleaf Publishing Limited, Sheffield, UK, 2000
- [6] D. M. BOJE: *Green Life Cycle and Accounting Praxis*, web pages: <http://web.nmsu.edu/~dboje/TDgreenlifecycle.html>, October 1999
- [7] Sustainability, SPOLD (Society for the promotion of LCA Development, Business in the Environment: *The LCA Sourcebook*, London, England, 1993
- [8] Ministerstvo životního prostředí: *Posuzování životního cyklu LCA*, Praha, 2003
- [9] P. LAMY, CH. AIRAULT, COL C. LACROIX: *Cost/Benefit Analysis of MURAT Using Club MURAT ACB Software*, 2001 Insensitive Munition & Energetic Materials Technology Symposium, Bordeaux, France, October 2001

APPENDIX 1

Table 1. *Steps from existing EM to GEM and related economic impacts*

Phase of life cycle	The most important EM characteristics	Costs related with characteristics of existing EM	Steps to "Green" EM	Impact related with steps to GEM	Estimated costs (revenues) changes
Raw material procurement	existing resources existing technology plain procurement	lower costs lower costs lower costs	alternative (new) resources -difficult manufacturing -new technology -new procurement method	expensive R&D, costs increasing related with "green" methods of material procurement	cost increasing about 100 - 200 %
Manufacturing	existing technology existing equipment danger manufacturing	lower costs lower costs higher costs related with handling and health protection	new technology new equipment safe manufacturing and handling	investment requirements lower manipulation risks and lower risks for human health	cost increasing about 40-60 % cost decreasing about 80-90 %
Distribution and storage	sensitivity of products - distribution risks - toxicity at long-term storage	higher costs related with: distribution storage security	stable materials	low danger - of debasing (explosion) - for human health	cost decreasing about 30-50 % cost decreasing about 30-50 %
Consumer use	wastes production manipulation risks	decontamination costs manipulation costs	green product lower product performance stable materials	lower wastes production lower performance lower danger for consumers	cost decreasing about 80-90 % cost increasing about 5-10 % cost decreasing about 30-50 %
Post-Consumer use, liquidation, recycling	decontamination liquidation by detonation liquidation by combustion other reusing (sale) etc.	decontamination costs liquidation costs liquidation costs revenues from sales	reusing of materials "safe" material usage material recycling process	simple liquidation reducing material recycling safe disarming utilization of current GEMs (no adaptation needed) new technology and operation costs	cost decreasing about 60-80 % sales revenues (up to 80-90 % of original material costs) cost decreasing about 60-80 % higher revenues about 30-50 % cost increasing about 20-40 %

MODERN PROPELANTS FOR 30 MM AMMUNITION APPLICATIONS

L. Velehradský, J. Petržílek and V. Puš

Explosia a.s., Research Institute for Industrial Chemistry (VÚPCH),
CZ-532 17, Pardubice - Semtín, Czech Republic

Abstract:

This short survey is to provide some important information about new trends in development of propellants for existing modern weapon systems, or, propellants for ammunition for elder weapon systems with improved performance

Keywords: *modern propellant, development, ammunition, weapon*

1. INTRODUCTION

In many cases new possibilities have been searched for, of improvement of ammunition effect in the target, or, improvement of performance of existing weapon systems without their original safety parameters being exceeded.

Improvement in shell parameters (subcalibre or full calibre ammunition) in target, however, can be solved by increasing the propellant energetic content only, or, by better utilization of its energy. Improvement of full calibre shell effect in target (multifunction effect) can be solved by its technical parameters.

Application of new approaches, analysis of ballistic action by means of modern computer technique, study of parameters of ignition and its optimization, however, led to the rise of new types of propellants with specific properties. That trend led to rise of the propellants capable of safe working at loading densities up to 1.0 (Loading density = charge of propellant /case volume).

2. THEORY

In most cases new possibilities of increasing performance parameters of nitrocellulose based propellants are searched for. Therefore, further intensive research and development works proceed at present time with modern, nitrocellulose based propellants.

In this connection, firstly utilized were spherical powders enabling, due to their shape function, construction of high loading density propellant. Their application has, however, a number of limitations that have been neither technically nor technologically mastered so far. Another way that seems to be successful was the way of improving of extruded (seven perforated) powders simultaneously with solving of ignition and further parameters of the cartridge assembly. The first recorded propellants of this type were nitrocellulose powders in cartridges of the former Soviet Union in anti - aircraft weapon systems Šilka 23 x 152 mm ZU, and in the cartridge for infantry vehicle or aircraft gun 30 x 165 mm introduced into armament about 1970. Another technological and technical way is technical solution of Swiss Munition – at present Nitrochemia – company (the member of Rheinmetall, Germany)

that, with state support, developed production technology for double base propellants of EI type (Extruded Impregnated) for applications in high performance ammunition of Oerlikon company. The same technology is used in Vihtavuori company (Finland), the member of NAMMO company at present time, to which Swiss Army sold the licence in the 1990s.

Simultaneously with the above given development, partial research works proceeded in EXPLOSIA a.s., aimed at certain types of these propellants. The activities in this direction have been to map the possibilities to utilize the existing types of propellants (spherical, nitrocellulose) in some of selected ammunition assemblies, to achieve maximum performances with safety criteria being met for the weapon concerned, at prescribed exploitation temperatures (- 54 to + 52 (71) °C). In 1990th Explosia developed its own technology and new types of single base 7 perforated propellant for medium caliber ammunition that were introduced to the customers^[5].

R&D works have never been stopped. These activities also include performance of analysis of existing charges, analysis of possibilities of technological solutions, designing of technical and technological ways to verify the possibility of production of propellants with higher technical parameters and their verification in model and real assembly with the aim of prognosis of possible application. The aim is to verify the possibility of preparation of propelling charge or charges, as well as the possibility to improve performance parameters of nitrocellulose based smokeless powders. Works should also help to define some physical, chemical and technological parameters of powders for modern powder charge, including technological ways of solving, and to verify their general validity at another type of cartridge.

3. EXPERIMENTS

There have been solved problems concerning the optimization of ballistic function of powders with high loading density for cartridge 30x165 mm and cartridge 30x210 mm. The previous works in this field^[1] confirmed the significant influence of the surface layer and its physical parameters on the ignition process and consequently on ballistic parameters and temperature sensitivity of propellants^[2]. Due to the analysis of data from closed vessel proceed in the Pyro702 program^[3] and to calculation made by the program of inner-ballistic^[4] the influence of parameters of ignition process on ballistic performance has been simulated.

In consequence there have been searched for, the technological ways of reaching the desired ignition parameters and the ways of improving the ballistic function of the powder S105-03 in the weapon 2A42 using the 30x165 mm cartridge in combination with the bullet of 235 g of weight, and of the powder S115 in the weapon 30mmPIDvK using the 30x210 mm in combination with the bullet of 435 g of weight.

The testing of samples prepared for the cartridge 30x165 mm with the bullet 235 g was aimed to determine the influence of three types of the surface treatment of the powder S105-03 on its ballistic. Experimental measurement on the testing gauge involved measures of pressure, port pressure, velocity and other important parameters. The results of shooting are displayed in the following Table 1 and Figure 1. Basic parameters of tested samples proceeded by the program Pyro702 are shown in the Table 2.

Table 1. *Basic parameters of the tested samples S105-03 proceeded by the program Pyro702*

Propellant sample	Coating	Pressure P_{\max} [MPa]	Impuls [MPa.ms]	Max. dP/dt [MPa/ms]	Avg dP/dt [MPa/ms]	Max. G [1/MPas]	Avg.G [1/MPas]
S105 R-1027	DNT	252.7	388	128.4	91.4	3.46	3.31
S105-03 SM-8/03	DNT	242.6	396	114.0	79.6	3.30	3.13
S105-03 VU-4-03	Bu-NENA	253.6	303	151.1	110.6	4.08	3.95
S105-03 R-203079	NG+ DNT	255.9	382	120.9	88.1	3.22	3.11

Table 2. *Ballistic parameter of the tested samples S105-03 in cartridge 30x165 mm*

Propellant sample	Charge [g]	Temperature [°C]	Pressure P_{piezo} [bar]	Pressure p_{crusher} [kg/cm ²]	Velocity $V_{7.5}$ [m/s]	Velocity V_5 [m/s]	Action time [ms]
Specification	cca 125	21	-	≤4100	≥1200	-	≤ 7.0
S105 R-1027	125	21	4623	4092	1232	1240	3.45
S105-03 SM-8/03	125	21	4707	4092	1223	1229	3.48
S105-03 VU-4-03	125	21	4512	4008	1227	1233	3.40
S105-03 R-203079	125	21	4636	4303	1204	1210	3.32

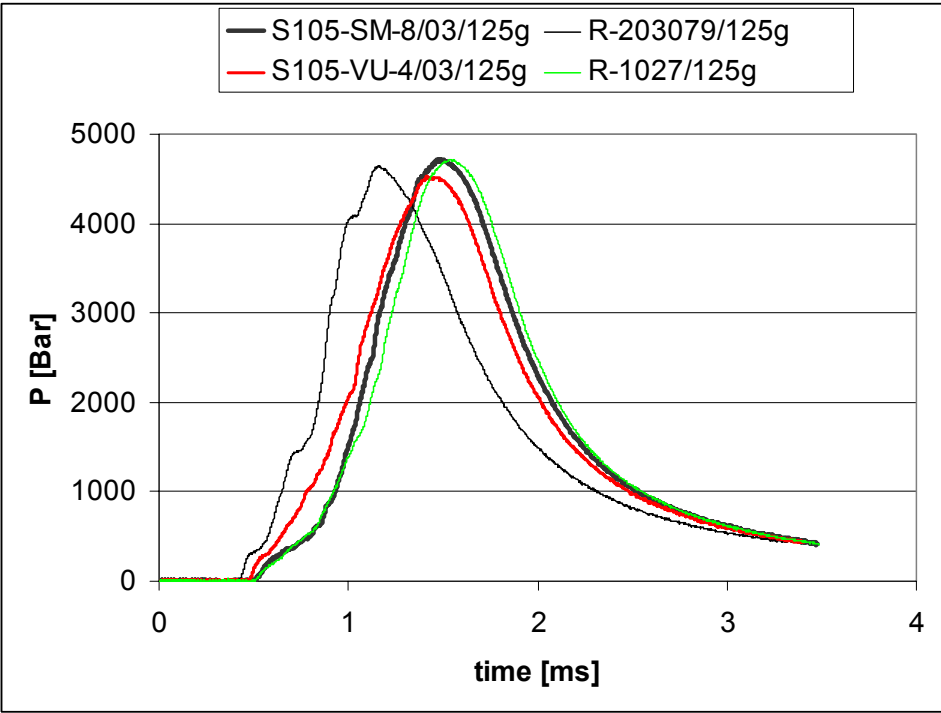


Fig 1. Pressure curve measured for propellant types S105-03 in 30x165 mm cartridge

In the case of the cartridge 30x210 mm, there have been sought the ways of reaching the maximum performance while respecting the pressure limits of the original cartridge using the Explosia’s technology. The results of shooting are displayed in the following Table 4. The basic parameters of the tested samples proceeded by the program Pyro702 are shown in the Table 3.

Table 3. Basic parameters of the tested samples S115 proceeded by the program Pyro702

Propellant sample	Coating	Pressure P _{max.} [MPa]	Impuls [MPa.ms]	Max. dP/dt [MPa/ms]	Avg dP/dt [MPa/ms]	Max. G [1/MPas]	Avg.G [1/MPas]
S115 R-203059	DNT	245.0	563	76.65	59.42	2.40	2.30
S115 R-203060	DNT	240.6	591	65.75	51.43	2.15	2.06
S115 R-203062	DNT	243.1	617	72.94	54.72	2.25	2.15
S115 R-203065	DNT	244.4	579	76.96	58.05	2.36	2.26

Table 4. Ballistic parameter of the tested samples S115 in cartridge 30x210 mm

Propellant sample	Charge [g]	Temperature [°C]	Pressure P _{piezo} [bar]	Pressure P _{crusher} [kg/cm ²]	Velocity V _{7.5} [m/s]	Velocity V ₅ [m/s]	Action time [ms]
Specification 30x210 mm	cca 185	15	-	≤3500	-	995	≤ 7.5
S115 R-203059	195.0	21	4565	4048	1117	1116	≤ 7.5
S115 R-203060	195.0	21	3597	3104	1057	1056	≤ 7.5
S115 R-203062	195.0	21	3781	3268	1078	1077	≤ 7.5
S115 R-203065	195.0	21	4177	3758	1097	1095	≤ 7.5

4. CONCLUSION

The experiments have confirmed the possibility to influence on performance parameters of the powder S105-03 by choosing one of the possible surface treatments. In case of the powder S115 the improvement of its performance by 20 per cent has been reached in the test barrel using the Explosia's technology. The further application of the obtained results will be possible and utilizable when solving the individual problems of new propellants.

REFERENCES

- [1] L. VELEHRADSKÝ, J.PETRŽÍLEK, V.PUŠ, Hnací náplně s vysokou nábojovou hustotou, Grant MPO ČR, Zpráva VÚPCH, 2001
- [2] J. PETRZILEK, L. VALENTA, L.VELEHRADSKY, Temperature sensitivity of small arm propellant, Synthesia a.s., Pardubice-Semtin, CZ, 29th International Annual Conference, Poster Program, 1998
- [3] M. HRDLÍČKA, Program Pyro 702, Explosia a.s., VÚPCH, 2003
- [4] J. PETRŽÍLEK, SW model of Interior Ballistic, Explosia, VÚPCH, 2003
- [5] Product list of Explosia a.s., www.explosia.cz, 2003

DIRECT MONTE – CARLO SIMULATION OF DETONATION PROCESS IN A GAS

Z.A. Walenta*, A. Teodorczyk** and W. Witkowski***

* Institute of Fundamental Technological Research, Polish Academy of Sciences
Swietokrzyska 21, 00-049 Warszawa, Poland

** Institute of Heat Engineering, Warsaw University of Technology
Nowowiejska 25, 00-665 Warszawa, Poland

*** Institute of Industrial Organic Chemistry
Annopol 6, 03-236 Warszawa, Poland

Abstract:

The research on gaseous detonation has recently become a very important issue because of increasing importance of gaseous fuels. We propose to use the Direct Monte – Carlo Simulation technique, which is a very powerful tool for solving complex flow problems. We propose a very simple model of a molecular collision, which makes it possible to increase the thermal energy of a gas, which is similar to the processes in the flame. We show then, that this model can produce the wave, which has the features characteristic for a detonation wave.

Keywords: *detonation, Monte-Carlo simulation*

1. INTRODUCTION

The research on detonation in gases has recently become a very important issue because of increasing importance of gaseous fuels. The urgent technological problem is connected with detonation in pipelines and the necessity of extinguishing it. The devices used for this purpose usually consist of matrices of very narrow channels. Cooling the gas by cold walls of such channels may extinguish the flame and stop detonation.

The Direct Monte – Carlo Simulation (DMCS) technique ^[1] has proven to be an excellent tool for simulating flows in various geometrical configurations – particularly in narrow channels. It offers also a possibility of taking into account the relaxation phenomena and chemical reactions ^[1, 2], these unfortunately increase complexity of the computer programs and the necessary computing times. However, in the case of detonation, considerable simplifications can be made thanks to the fact, that in a detonation wave combustion proceeds at high temperature and at very high speed, therefore all relaxation processes at the molecular level may be disregarded. The only important factor, that remains, is the produced thermal energy.

2. MODEL OF A COMBUSTIBLE GAS

As always in the Monte – Carlo simulations we treat the gas as an ensemble of molecules, which collide with each other and move along straight lines with constant speed between collisions. We assume for simplicity, that all molecules are identical, hard, elastic spheres. We assume, finally, that some of the molecules, uniformly distributed in space, carry certain amount of “internal” energy, the same for each of them. This may be transformed into kinetic energy during collision with another molecule (carrying no energy),

provided that the two colliding molecules approach each other with sufficient (“threshold”) speed. If this is the case, the relative speed of the molecules after collision is increased suitably.

3. DETAILS OF CALCULATION

To check whether the proposed model can actually simulate the detonation wave, several calculation runs for various geometries were performed. We employed the standard DMCS procedure, according to Bird^[1], and the selection of molecules for collisions was performed with the ballot – box scheme, as proposed by Yanitskiy^[3].

The calculations were performed in one- and three-dimensional geometry. In 1-D geometry (plane wave, no walls) the number of molecules was about 5000, in 3-D geometry it ranged from about 3 to 8 million. The calculation area was divided into 1100 cells in 1-D geometry and 1.5 to 4 million cells in 3-D geometry.

The wave was initiated by instant removal of a “diaphragm”, placed at $x = 100$ units of length. The gas in front of the diaphragm contained either 10 or 30 per cent of the molecules carrying “internal “ energy. The energy released in a single collision was such, that the relative velocity of the colliding molecules was increased by the value equal to 10 times the most probable molecular velocity. The temperature of the driver gas (behind the diaphragm) was 10 times higher than that of the driven gas. The pressure was such, that, after the diaphragm removal, the shock wave of Mach number $M_s = 2$ was produced.

4. RESULTS

Figs. 1 – 4 show some selected results of the performed simulations.

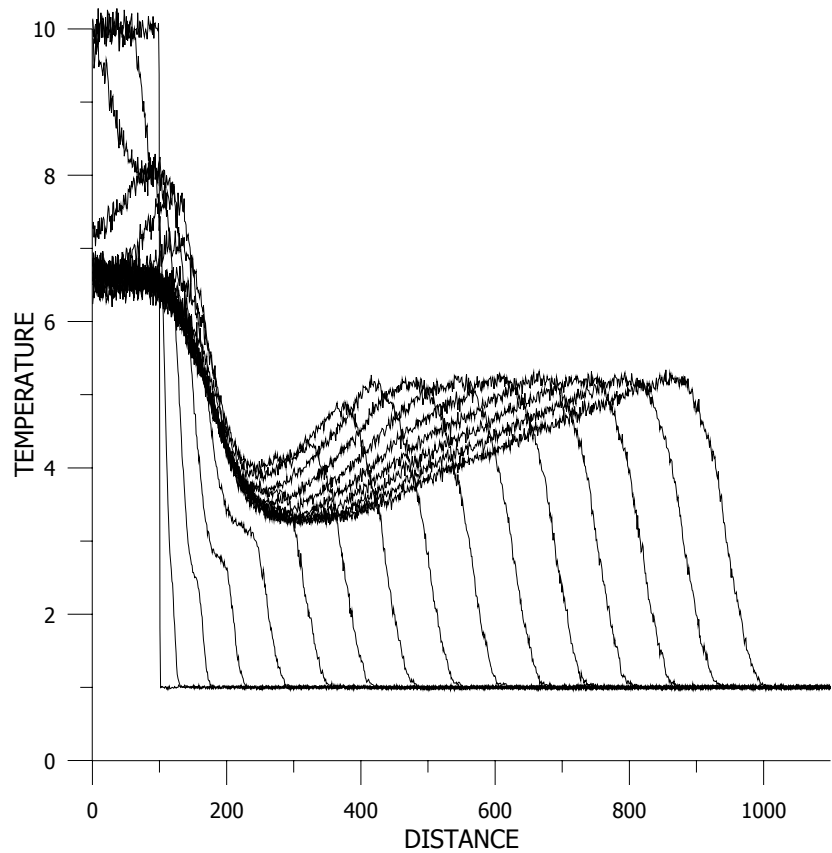


Fig 1. Formation of the plane detonation wave without influence of walls

Fig. 1 shows the simplest case – a plane, perpendicular wave, moving along x – axis in a positive half-space, in a gas containing 10 per cent of the “energetic” molecules. The figure contains diagrams of the gas temperature in terms of distance along the x – axis (measured in mean free paths of the gas molecules) for the initial situation and for 15 subsequent instants, evenly spaced in time. Formation of the primary shock wave after the diaphragm removal is clearly visible. The shock then gradually speeds up, transforming into a detonation wave, which afterwards moves with constant speed and constant intensity, as expected.

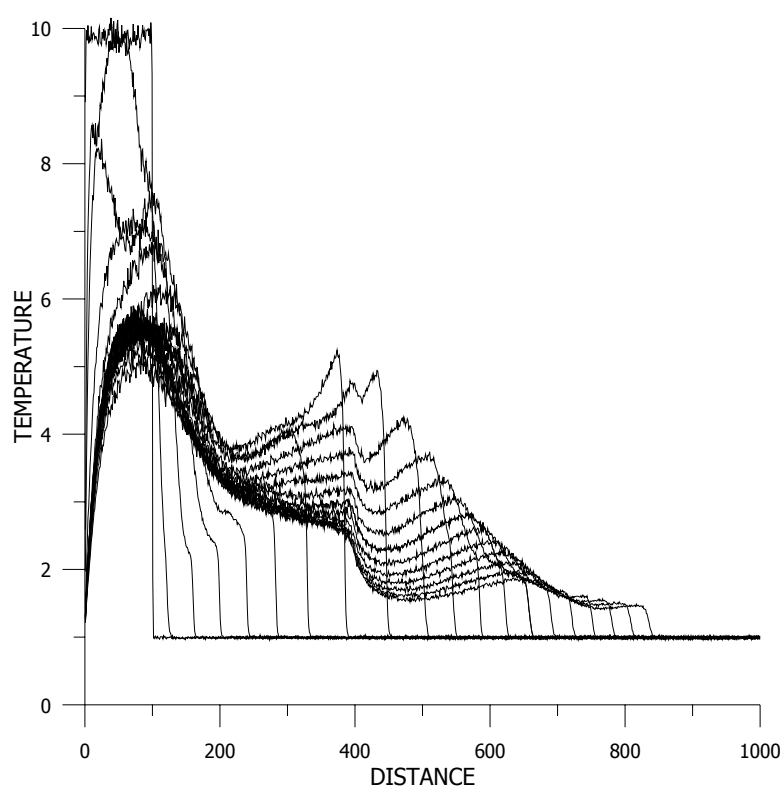


Fig 2. Formation and decay of the detonation wave in a pipe under friction and heat exchange at the walls

Fig. 2 shows similar picture for the wave, moving in a cylindrical pipe in the same gas. The diameter of the pipe is equal to 100 mean free paths. For $x < 400$ the molecules reflect from the walls specularly, i.e. without exchange of tangential momentum, and energy. For $x > 400$ the molecules are reflected diffusely, i.e. after reflection their average energy corresponds to the temperature of the wall, and the average tangential velocity equals zero.

The left part of the picture, up to $x = 400$, looks similarly to that in Fig. 1 – formation of shock and detonation wave is evident. For $x > 400$ however, the walls cool the gas down, below the ignition point, and the shock moves ahead, unsupported by the flame front, getting weaker and weaker.

In Fig. 3 the configuration is the same as in Fig. 2, only the gas contains 30 per cent of the “energetic” molecules. Here, the amount of released energy is so large, that the walls are not able to absorb it. After entering the pipe with rough and heat conducting walls the detonation wave slows down a little bit and decreases its intensity, still it moves steadily forwards. For this kind of gas, to stop detonation it is necessary to have larger ratio of the wall surface to the volume of the pipe – i.e. the pipe of smaller diameter.

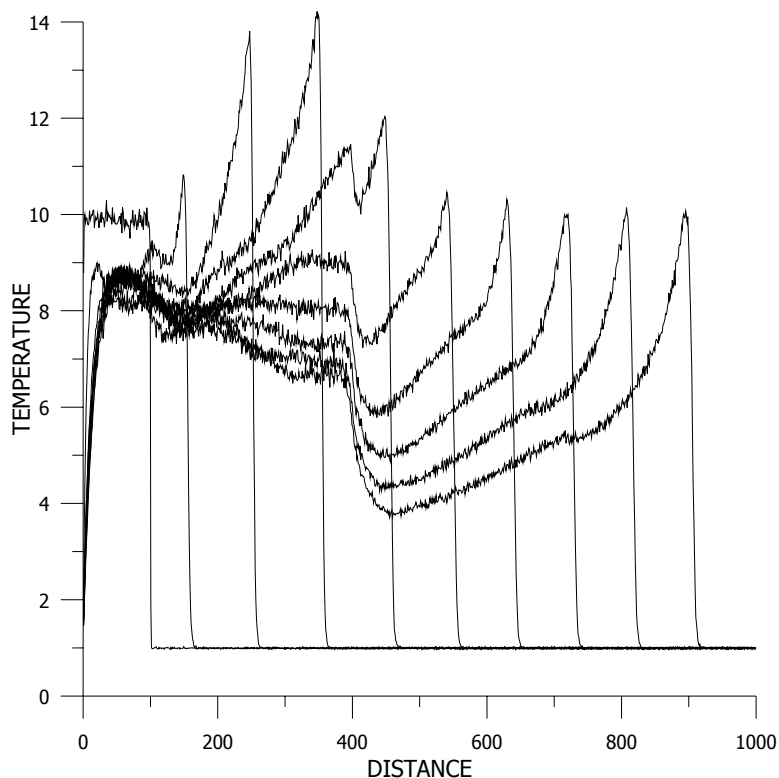


Fig 3. Detonation wave in a highly energetic gas, in a pipe with friction and heat exchange

Fig. 4, which corresponds to the sixth line of Fig. 3, shows the shape of the detonation wave, slightly curved under the influence of the boundary layer. This curvature is evidently rather weak.

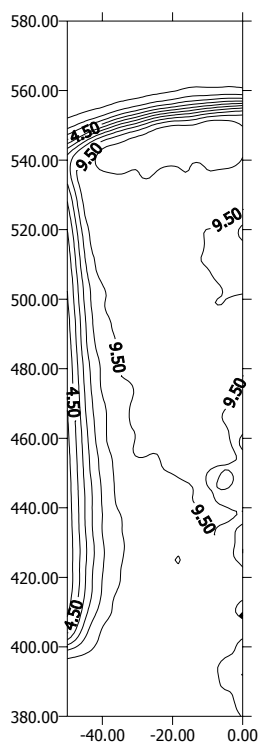


Fig 4. Shape of the detonation wave in a narrow pipe, under the influence of the boundary layer

5. CONCLUSIONS

A method of simulation of the detonation phenomenon, based on the Direct Monte – Carlo Simulation technique has been proposed. This method makes it possible to study detonation in narrow channels and its decay under the influence of wall friction and heat exchange. This method may possibly be used for optimizing the devices stopping detonation in pipes.

Acknowledgements

This research work was supported by the State Committee for Scientific Research (KBN, Poland) under grant No 4T09C 015 22; this support is gratefully acknowledged.

REFERENCES

- [1] G.A. BIRD: *Molecular gas dynamics and the direct simulation of gas flows*, Clarendon Press, Oxford, 1994
- [2] P.S. LARSEN, C. BORGNAKKE: in *Rarefied Gas Dynamics* (ed. M. Becker and M. Fiebig), 1, Paper A7, DFVLR Press, Porz-Wahn, Germany, 1974
- [3] V.E.YANITSKIY, O.M.BELOTSEKOVSKIY: *The statistical method of particles in cells for the solution of problems of the dynamics of a rarefied gas*. Part I, Zh. Vychisl. Mat. Mat. Fiz., 15, 1195-1208; Part II, Zh. Vychisl. Mat. Mat. Fiz., 15, 1553-1567, 1975

SYNTHESIS OF 4,6-DINITROBENZOFUROXAN

V.L. Zbarsky, D. M Stepashkow and N.V. Yudin

Mendeleev University of Chemical Technology,
9 Miusskaya Square, 125047, Moscow, Russia

Abstract:

Problems connected with nitration of benzofuroxan are of specific interest since potassium salt of dinitrobenzofuroxan is considered as promising ecologically pure initiating explosive. In this connection a study has been performed on nitration of benzofuroxan and its mononitroderivatives in nitric and sulfuric- nitric acid mediums. The main reaction products formed in the reaction have been identified.

Keywords: benzofuroxan, 4-nitrobenzofuroxan, 6-nitrobenzofuroxan, 4,6-dinitrobenzofuroxan, nitration, kinetic

1. INTRODUCTION

4,6-Dinitrobenzofuroxan (4,6-DNBF) is an intermediate in preparing of a heavy-metal-free initiating explosive potassium salt of 4,6-DNBF and a low-sensitive high explosive CL-14^[1]. There are several 4,6-DNBF preparation methods nowadays:

1. Direct nitration of benzofuroxan (BF)
2. From 2,4,6-trinitrochlorobenzene to 2,4,6-trinitroazidobenzene followed by its thermal decomposition
3. From 2,4-dinitrochlorobenzene to 2,4-dinitroazidobenzene followed by its nitration and thermal decomposition to 4,6-DNBF

Among the above methods, the first one can be considered as the most promising, because BF can be easily prepared from o-nitroaniline and sodium hypochlorite with nearly quantitative yield.

Nitration of BF to 4,6-DNBF was first realized as early as 1899^[2]. The reaction was most thoroughly considered in the work^[3,4]. In spite of a relative simplicity of the synthesis with concentrated nitric acid or sulfuric-nitric acid mixtures (SNAM), the yield of 4,6-DNBF after recrystallization was relatively low (55-60%)^[5], and the recommended temperature was 0-5 °C that caused a special cooling agent to be used.

2. RESULTS AND DISCUSSION

The present work was aimed at elucidating possible reasons for low 4,6-DNBF yields in the nitration reaction. The first set of experiments involved nitration of BF to 4,6-DNBF in SNAM under different conditions. Variable parameters tested were temperature, the reagent ratio, and the order of reagent mixing, however the yield did never exceed 77%. Dilution of the reaction mixture with water followed by extraction of soluble products showed that the content of organic compounds in the waste acid mixture was very low. To understand the reasons for the lowered yields, a study was undertaken on formation of isomers of mononitro- (NBF) and dinitrobezofuroxans (DNBF) in the reaction as well on the nitration reaction of NBF to DNBF.

On nitration of BF in SNAM in the proportion of 1.2 mole of HNO_3 per one mole of BF, a crude product was obtained, which, according to HPLC analysis, was consisted of five individual substances. Three main compounds were found to be 4-NBF, 6-NBF, and 2,4-DNBF in the proportion of 79:18:3. The share of the remaining two unknown substances was less than 1% by mass of the crude product. The yield of crude mono-NBF was 90% of the theoretical one.

On nitration of BF in the nitric acid of different concentrations, the simultaneous presence *both* the initial BF and 4,6-DNBF among the reaction products was often observed.

At room temperature, the nitration reaction of 4-NBF in the medium of 98% nitric acid did not complete even after holding the mixture for two weeks. The yield of 4,6-DNBF calculated by reacted 4-NBF was 60% only. On nitration in SNAM, the yield depended significantly on the excess of nitric acid: it changed from 71% to 85% when the molar ratio of HNO_3 to 4-NBF was increased from 2 to 5. The yield did not prove to depend on either reaction temperature (in the interval of 20 to 40°C) or the order of reagent mixing, i.e. whether NBF was dissolved in sulfuric acid first followed by addition of nitric acid or vice versa. The product obtained was practically pure 4,6-DNBF (more than 97% of the main compound).

On nitration of 6-NBF with 98% HNO_3 the reaction was completed within 24 hours at room temperature and did not come to the completion at -5°C . The yield of product after evaporation of nitric acid (until constant weight) was 90%, whereas only 50% after subsequent washing with cold water. Nitration with SNAM under different conditions followed by washing with water *yielded* 52-55% of DNBF. The product was analyzed by HPLC to consist of two substances. The main compound was identified as 4,6-DNBF; the other substance was also found in the crude 4,6-DNBF synthesized by direct nitration of BF. To reveal the structure of the second substance chromatomass-spectrometry analyses of the crude product were done, allowing structure of 5,6-DNBF. The following m/z data were obtained: for 4,6-DNBF 228 ($M+2$), 226 (M), 196 ($M-30$), 210 ($M-16$), 180 ($M-46$); for 5,6-DNBF 226 (M), 196 ($M-30$), 210 ($M-16$), 150 ($M-76$).

The content of 5,6-DNBF in crude 4,6-DNBF was estimated from the area of its peak to be around 5%. This substance was not found in the nitration product of 4-NBF.

The content of 5,6-DNBF in the nitration product was *as much as* 30 – 50% in the reaction of 6-NBF with concentrated nitric acid after evaporation without dilution of the reaction mixture by water. The result is in a good agreement with the observation that about 50% of the product can be dissolved in water. It may be expected, therefore, that the activated nitro-group in the 5-position is changeable by hydroxyl to form a readily soluble phenol. The analysis of the water-soluble products has shown the presence of five main

substances and two micro impurities as well as the absence of 4,6- and 5,6-DNBF. Based on mass-spectroscopy analysis data, two of the water-soluble products can be identified as 5-oxy-6-nitrobenzofuroxan (m/z: 197 (M), 167 (M-30), and 5-oxy-4,6-dinitrobenzofuroxan (m/z: 243 (M), 166 (M₂-30), 120 (M-46), 226 (M-17), 196 (M-47), 150 (M-93).

An important part of the research was considered to be evaluation of rate constants of the nitration reaction of BF. The rate constants were measured by using spectrophotometric method with the reacting mass placed directly into a cell at a temperature of 25°C. Decreasing absorption of BF in the area of its absorption maximum (350 nm) was observed, with the data being fairly described by the first-order kinetic equation. It should be noted that BF in the medium of 93.2% H₂SO₄ is in the protonated form, which exhibit the maximum absorption at 312 nm and 385 nm, whereas BF itself has the maximum at 350 nm (in H₂SO₄ of concentration less than 85%). In contrast to BF, UV spectra of 4,6-DNBF are identical in both 80% and 93.2% H₂SO₄, suggesting that 4,6-DNBF remains in the nonprotonated form. We failed to measure the rate of nitration reaction of BF in 93.2% H₂SO₄ in such a manner because of a very short time of the reaction: it was completed in less than 15 seconds (at the ratio HNO₃/BF = 30-300/1, $k_1 > 0.1 \text{ s}^{-1}$). The rate constants have been measured for nitration reaction of BF in 80% and 84% H₂SO₄; the data are presented in Table 1. As seen from the Table, a 4% decrease in the concentration of H₂SO₄ results in decrease in the reaction rate by a factor of 220, confirming an inexpediency of using diluted H₂SO₄ in the nitrating acid mixtures.

H ₂ SO ₄ , %	HNO ₃ /BF Mol/mol	k ₂ l/mol*s
84	15	1,35
84	32	1,31
80	320	0,00594

3. CONCLUSIONS

It has been shown that the consumption of sulfuric acid in the nitration process can be reduced by more than three times as compared with known literature data to amount 8 - 10 grams per 1 gram of BF. The optimal concentration of H₂SO₄ as 92%-94% and consumption of nitric acid as 4-5 moles per 1 mole of BF have been found.

A 12%-18% decrease in the yield of 4,6-DNBF occurs due to red-ox processes during nitration of 4-NBF, resulting in formation of mixture of phenols. Another reason for the decreasing yield is formation of 5,6-DNBF from 6-NBF. It undergoes hydrolysis upon following dilution of the reaction mixture with water, resulting in 10% decrease in the yield of the final product.

4. EXPERIMENTAL

The substances obtained were analyzed by HPLC method on a Millichrom-4 equipped with a chromatographic column Kromasil C-18 using eluent acetonitrile – water - acetic acid in the proportion (by volume) 30:68:2. Time of appearance of BF, 4-NBF, 6-NBF, 4,6-DNBF, and 5,6-DNBF at the fluent feeding rate of 100 $\mu\text{l}/\text{min}$ was 6.5-6.6 min, 10.0-10.3 min, 9.0-9.5 min, and 7.2-7.5 min, respectively.

The extinction coefficients measured with a “Specord M-40” spectrophotometer for are given in Table 2. The measurements were carried out at 260 nm, 320 nm, and 360 nm wave lengths.

wave-length, λ , nm	ϵ , l/(mol • cm)		
	4-NBF	6-NBF	4,6-DNBF
260	3520	12300	10710
320	1713	22430	2170
360	3470	3190	2420

4-NBF and 4,6-DNBF were prepared by nitration of BF followed by recrystallization from acetic acid (m.p.124-144 $^{\circ}\text{C}$ and 174-176 $^{\circ}\text{C}$, respectively). 6-NBF was prepared by two ways: from 2,4-dinitrochlorobenzene (via thermolysis of 2,4-dinitroazidobenzene) and by oxidation of dinitroaniline ¹⁶. The melting point was 70-72 $^{\circ}\text{C}$ after recrystallization from ethanol.

In nitration with nitric acid only, BF was slowly added to the acid cooled to –10 $^{\circ}\text{C}$ keeping temperature below 0 $^{\circ}\text{C}$. After stirring at a given temperature for a specified time, the mixture was poured into ice; the separated product was filtered, washed with cold water and dried under vacuum. In nitration with SNAM, a corresponding benzofuroxan was dissolved in sulfuric or nitric acid at –5 $^{\circ}$ - –10 $^{\circ}\text{C}$ followed by addition of the second acid at 0 $^{\circ}$ - –5 $^{\circ}\text{C}$ and keeping at a given temperature. The product was isolated as described above.

REFERENCES

- [1] Patent USA N 5039812
- [2] DROST P.: Liebiegs Ann. Chem., B. 307. S. 49-69, 1899
- [3] BAILEY A.S., CASE J.R.: Tetrahedron, P. 113 – 131, 1958
- [4] BAILEY A.S., WHEITE J.E.: J. Chem. Soc., N 9. P. 819 - 822, 1966
- [5] NORRIS W.P., SPEAR R.J., READ R.W.: Austral J. Chem., V. 336. N 2. P. 297-309, 1983
- [6] GAUGHRAN R., PICARD J.P., KAUFMAN J.V.R.: J. Am. Chem. Soc., V.76. P. 2233-2236, 1954

APPLICATION POSSIBILITIES OF POLAROGRAPHY IN STUDIES OF CHEMICAL MICRO-MECHANISM OF INITIATION OF POLYNITRO ARENES

S. Zeman and E. Zemanová

Department of Theory & Technology of Explosives,
University of Pardubice, CZ-532 10 Pardubice, Czech Republic

Abstract

The half-wave potentials, $E_{1/2}$, of twenty four polynitro arenes have been determined in aqueous medium buffered at pH 7, the final concentrations of their solutions being 0.5×10^{-4} M and 0.5×10^{-5} M. The ^{13}C NMR chemical shifts of carbon atoms carrying the most reactive nitro groups have been used for specification of the primarily reduced nitro group in the molecule. The found logical relationships between the $E_{1/2}$ values and squares of detonation velocity are of the type of the modified Evans–Polanyi–Semenov equation for energetic materials. It has been stated that the strong dependence of $E_{1/2}$ values on the conditions and way of realisation of the polarographic measurements considerably restrict the application of this method to studies of micro-mechanism of initiation of organic energetic materials.

Keywords: polynitro arenes, polarography, initiation, mechanism

1. INTRODUCTION.

It is well known that nitro groups are centres of heat, impact and detonation reactivity in organic polynitro compounds (see Ref. [1] and references herein). Nitro groups are also responsible for electrochemical reducibility of nitro compounds [2]. This means that there could exist a relationship between the results of polarography and the detonation characteristics of polynitro compounds. For a study of this problem we have chosen polynitro arenes and their derivatives.

2. EXPERIMENTAL

2.1 Polarography of polynitro arenes

A differential pulse polarograph PPA 02 (produced by Labio, Ltd, Prague) was used. This polarograph worked in DPP regime. It was equipped with a 20 ml measuring cell with three-electrode connection: stationary dropping mercury electrode (HMDE) as a working electrode, a platinum wire counter electrode, and a saturated calomel reference electrode. Operation parameters of the polarograph were as follows:

initial potential	100 mV
final potential	−1500 mV
scan rate	$20 \text{ mV} \cdot \text{s}^{-1}$
pulse amplitude	−50 mV
pulse width	100 ms
clock	200 ms
current range	1 μA
offset	7000 mV

In the experiments, 20 ml of the supporting electrolyte (buffer) was pipetted into the electrolytic cell and deoxygenated with nitrogen gas for 3 min. Britton–Robinson buffer (pH 7.00) was used (for preparation see Ref. [3]). The polynitro arenes studied were taken in the form of their 0.1 M solutions in acetone or dimethylformamide. This solution was added to the buffer using a Hamilton micro-syringe to reach two final concentrations: a “higher” one of 0.5×10^{-4} M and a “lower” one of 0.5×10^{-5} M. Then the current-voltage curve was recorded at 20 °C. The half wave potentials, $E_{1/2}$, of the primarily reduced nitro group thus obtained are presented in Table 1.

2.2 The ^{13}C NMR chemical shifts

The ^{13}C NMR chemical shifts of the polynitro arenes studied were taken from Refs. [1,4,5]. These shifts of “bearer atoms” of the most reactive nitro groups are presented in Table 1. The most reactive groups in polynitro arenes are sterically hindered [6], or have a hydrogen atom at γ -position with respect to the group (the so-called trinitrotoluene mechanism of decomposition [7,8]), or their oxygen atom can interact *via* a five-membered transition state with sulphur bridge [9] or the chlorine atom at *ortho*-position to the group (for all the above-mentioned variants see also Ref. [1] and references herein). Positions of carbon atoms, the bearers of such nitro groups, are presented for each compound studied in Table 1, too.

2.3 Detonation velocities

The values of detonation velocities, D , of the polynitro arenes studied were calculated using the known relationships of Kamlet & Jacobs [10] for the maximum theoretical densities of crystals (TMD, i. e. for monocrystal). For compounds with sulphur heteroatom in molecule the D values were taken from Ref. [4] and for STC from Ref. [11]. The D values used are summarised in Table 1.

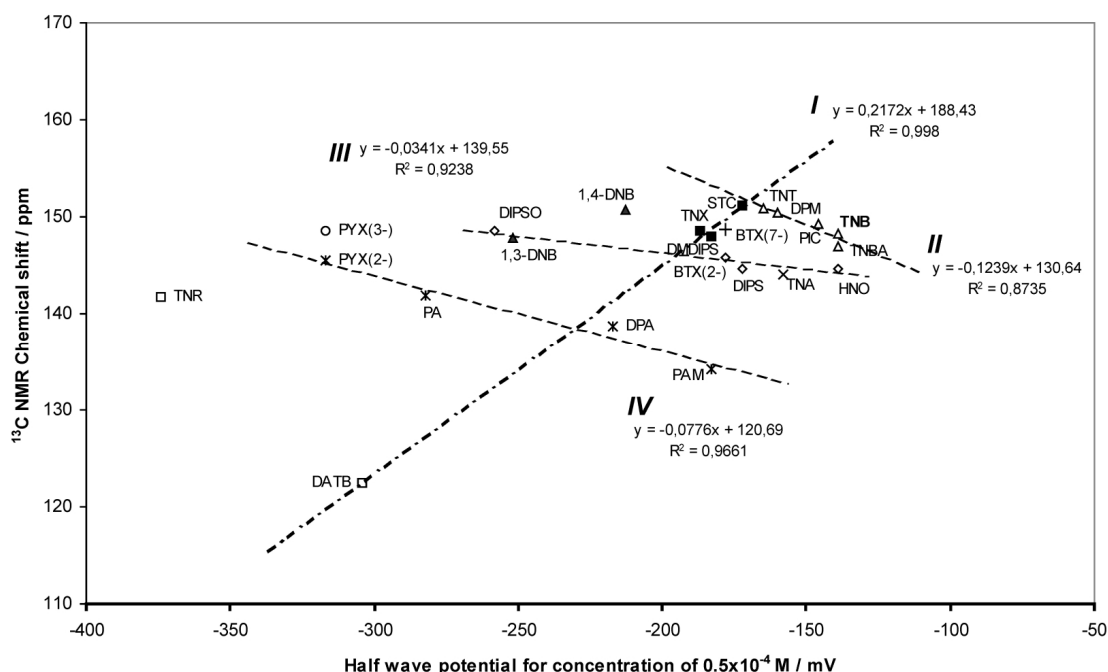


Fig 1. Relationship between the half wave potentials of the primarily reduced nitro groups (for concentration of 0.5×10^{-4} M) and the ^{13}C NMR chemical shifts of the carbon atoms carrying the most reactive nitro groups (the numbers in brackets denote the positions in molecule)

Table 1. Survey of the polynitro arenes studied, their half wave potentials, detonation velocities and ^{13}C NMR chemical shifts of the most reactive positions (in the reaction centres) in their molecules

Chemical name	Code design	^{13}C NMR Chemical shift of the most reactive position in molecule			Half wave potential $E_{1/2}$ in mV for concentration		Detonation velocity D	
		position	δ in ppm	Ref.	0.5×10^{-4} M	0.5×10^{-5} M	km.s^{-1}	Ref.
1,3,5-Trinitrobenzene	TNB	1,3,5-	148.3	1	-139	-113	7.27	a
1-Methyl-2,4,6-trinitrobenzene	TNT	2,6-	150.9	1	-165	-122	7.02	a
1,3-Dimethyl-2,4,6-trinitrobenzene	TNX	2-	148.5	1	-187	-169	6.76	a
2,4,6-Trinitrobenzoic acid	TNBA	2,6-	147.0	5	-139	-118	7.24	a
1-Methoxy-2,4,6-trinitrobenzene	TNA	2,6-	144.0	5	-158	-113	7.05	a
1-Chloro-2,4,6-trinitrobenzene	PIC	2,6-	149.3	5	-146	-114	7.20	26
1,3-Dichloro-2,4,6-trinitrobenzene	STC	2-	151.2	4	-172	-108	6.80	24
1-Methyl-3-hydroxi-2,4,6-trinitrobenzene	TNCr	2-			-291	-261	7.42	a
1-Hydroxy-2,4,6-trinitrobenzene	PA	2,6-	141.9	1	-282	-187	7.57	a
1,3-Dihydroxy-2,4,6-trinitrobenzene	TNR	2-	141.8	1	-374	-327	6.76	a
1-Amino-2,4,6-trinitrobenzene	PAM	2,6-	134.2	1	-183	-135	7.43	a
1,3-Diamino-2,4,6-trinitrobenzene	DATB	2-	122.4	1	-304	-256	7.70	a
2,2',4,4',6,6'-Hexanitrodiphenylamine	DPA	2,2',6,6'-	138.7	1	-217	-122	7.40	a
2,2',4,4',6,6'-Hexanitrooxanilide	HNO	2,2',6,6'-	144.7	1	-183	-87	7.31	a

Table 1 - continued

Chemical name	Code design	¹³ C NMR Chemical shift of the most reactive position in molecule			Half wave potential $E_{1/2}$ in mV for concentration		Detonation velocity D	
		position	δ in ppm	Ref	0.5×10^{-4} M	0.5×10^{-5} M	km.s ⁻¹	Ref.
2,6-bis(2,4,6-Trinitrophenylamino)-3,5-dinitro-pyridine	PYX	2,6-(picryl-)	145.5	1	-317	-218	7.42	a
		3,5-(pyridine)	148.5	1				
2,2',4,4',6,6'-Hexanitrodiphenylmethane	DPM	2,2',6,6'-	150.5	1	-160	-166	7.14	a
2,2',4,4',6,6'-Hexanitrodiphenylsulfide	DIPS	2,2',6,6'-	144.7	1	-192	-190	7,16	4
3,3'-Dimethyl-2,2',4,4',6,6'-hexanitro-diphenylsulfide	DMDIPS	6,6'-	147.9	1	-183	-115	6.70	1
2,2',4,4',6,6'-Hexanitrodiphenylsulfone	DIPSO	2,2',6,6'-	148.5	1	-258	-196	6.77	24
1-(2,4,6-Trinitrophenyl)-5,7-dinitrobenzotriazole	BTX	2,6-(picryl-)	145.8	1	-172	-152	7.34	a
		7-(bezotriazole)	148.7	1				
1,4-Dinitrobenzene	1,4-DNB	1,4-	150.7	1	-213		6.50	a
1,3-Dinitrobenzene	1,3-DNB	1,3-	147.8	1	-252		6.38	a
1-Amino-2,4-dinitrobenzene	2,4-DNAB	2-			-304		6.48	a
1-Amino-2,6-dinitrobenzene	2,6-DNAB	2,6-			-378		6.69	a

Note: a) calculated for TMD according to the Ref [10]

3. DISCUSSION

The course of electrochemical reduction of polynitro arenes strongly depends on pH and concentration of their solution, on the solvent and the surfactants present in the solution, on the electrode potential and the temperature during reduction [2,12]. Solvation also affects results of polarographic measurements [14]. In the present study we have chosen aqueous medium without surfactant additives, buffered at pH 7. In this medium, the final concentration of 10^{-4} M of nitro arene solution is currently used [3,13]; in our case, two final concentrations were adopted, viz. 0.5×10^{-4} M and 0.5×10^{-5} M.

Using the results of ^{13}C NMR spectroscopy, we tried to specify the primarily reduced nitro group in the molecule of polynitro arene. We presumed that the most reactive would be the same nitro groups as those in the case of initiation of the studied substances (see Ref. [1]). Thus Fig. 1 presents the relationship between the $E_{1/2}$ values of the primarily reduced nitro groups and the ^{13}C NMR chemical shifts, δ , of the carbon atoms carrying the most reactive nitro groups in the molecule. In this Figure, straight line *I* corresponds to sterical effect of 1,3-disubstitution in TNB molecule. Straight line *II* includes data for TNB and its monosubstituted derivatives (having a methyl group and therefrom derived substituents, and also chlorine). The group of compounds included in *II* involves poly-nuclear molecules; the BTX molecule with two potential reaction centres in it [1] correlates with this group by the δ value at 2,6-positions of trinitrophenyl group. The data for the second reaction centre of BTX, i.e. at 7-position of benzotriazole grouping, incline to straight line *I*. Group *III* correlates well with the data for 1,3-DNB, and also the data for TNA are close to it. Straight line *IV* corresponds to PAM and its derivatives; logically, the data for PA correlate with it too. The data for the second reaction centre in the PYX molecule [1], i.e. those of 3,5-position of the pyridine grouping, do not correlate with this dependence.

An analogous dependence for the results of measurements carried out with the 0.5×10^{-5} M solutions of polynitro arenes is given in Fig. 2. Group *V* here includes TNR, methyl and chloro derivatives of TNB. Group *VI* includes sterically more hindered derivatives of PAM, but the data of PAM itself do not correlate with it. Logically, group *VII* comprises TNB and its multi-nuclear derivatives, BTX correlating with it by data of its reaction centre at 2,6-positions of trinitrophenyl group. Straight line *VIII* is an analogy to straight line *IV* (Fig. 1). A logical group is *IX*, which includes dinuclear derivatives of TNB. Group *X* is a non-homogeneous set of compounds, being correlated by the data of BTX reaction centre at 7-position of benzotriazole moiety. Again, the data of the second reaction centre in the PYX molecule at 3,5-position of pyridine moiety do not correlate with any of the groups in Fig. 2.

Figure 3 presents the relationship between $E_{1/2}$ values of primarily reduced nitro groups in 0.5×10^{-4} M solution and the square of detonation velocity, D^2 , for the TMD of the polynitro arenes studied. Group *A* includes TNB and its derivatives having substituents interacting with the rest of the molecule by means of induction effects. Hydroxy substituted TNB derivatives form group *A₁* of the compounds. Amino derivatives of TNB (or better still, PAM) constitute group *B* of the compounds. Also PYX and amino derivatives of 1,3-DNB should belong to this group; due to thermochemistry reasons, this is not the case, and the 1,3-DNB derivatives constitute a separate group *B₁*. The data for BTX, in which the trinitrophenyl group is bound to nitrogen atom of benzotriazole moiety, approach the dependence of *B*. Group *C* is logically formed by DIPSO, DIPS and TNB; in the DMDIP molecule, the effect of 3,3'-dimethyl substitution is predominant and, therefore, its data correlate with the straight line *A*.

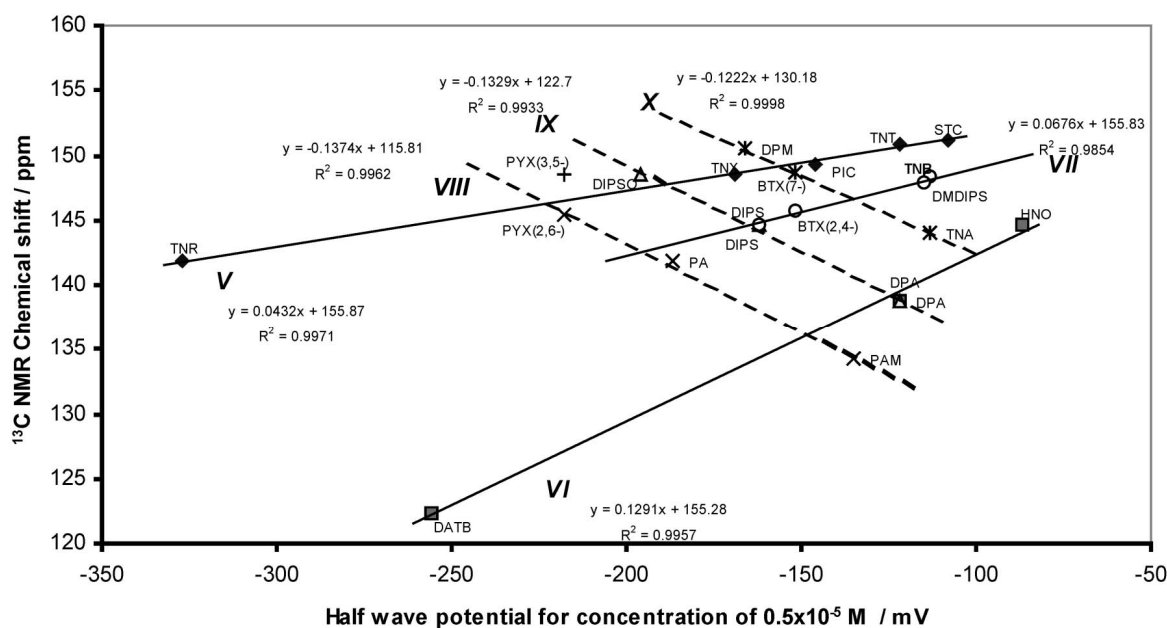


Fig 2. Relationship between the half wave potentials of the primarily reduced nitro groups (for concentration of 0.5×10^{-5} M) and the ^{13}C NMR chemical shifts of the carbon atoms carrying the most reactive nitro groups (the numbers in brackets denote the positions in molecule)

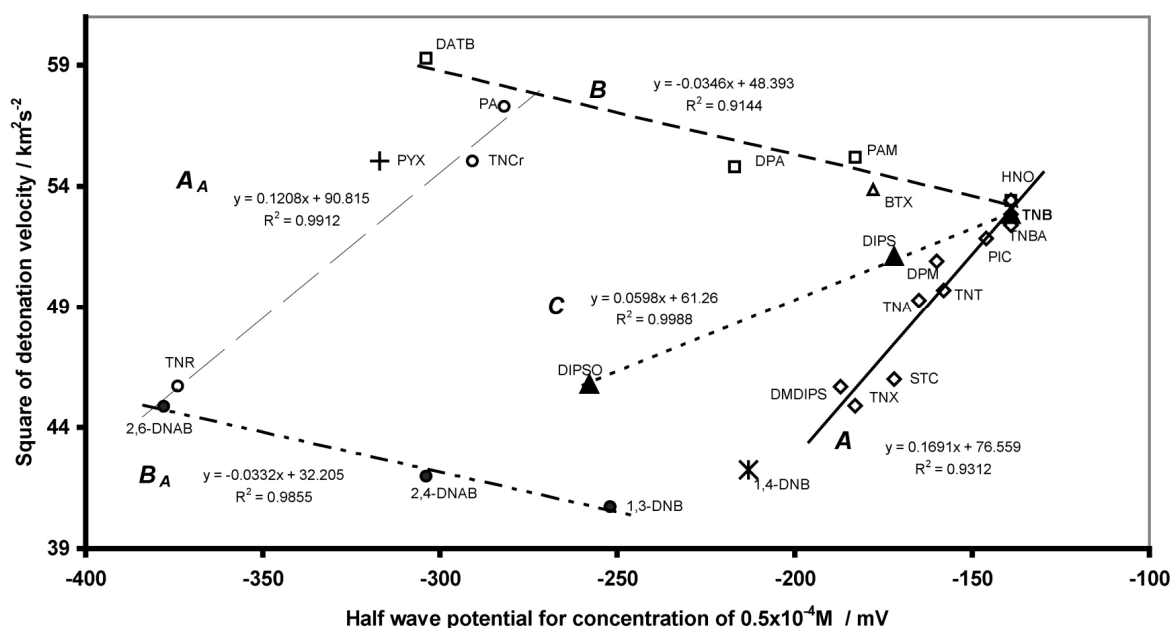


Fig 3. Relationship between half wave potentials of primarily reduced nitro groups in 0.5×10^{-4} M solution and the square of detonation velocity

The ten-fold decrease in final concentration of the polynitro arenes studied also considerably affected the relationship between $E_{1/2}$ and D^2 values (see Fig. 4.). In this case, a new logical dependence was created for the multi-nuclear derivatives (except HNO and DMDIPS). However, the dependence represented by group A in Fig. 3 decomposed. These facts could be interpreted by changes in solvation degree connected with the dilution of final buffered solution of the polynitro arenes examined.

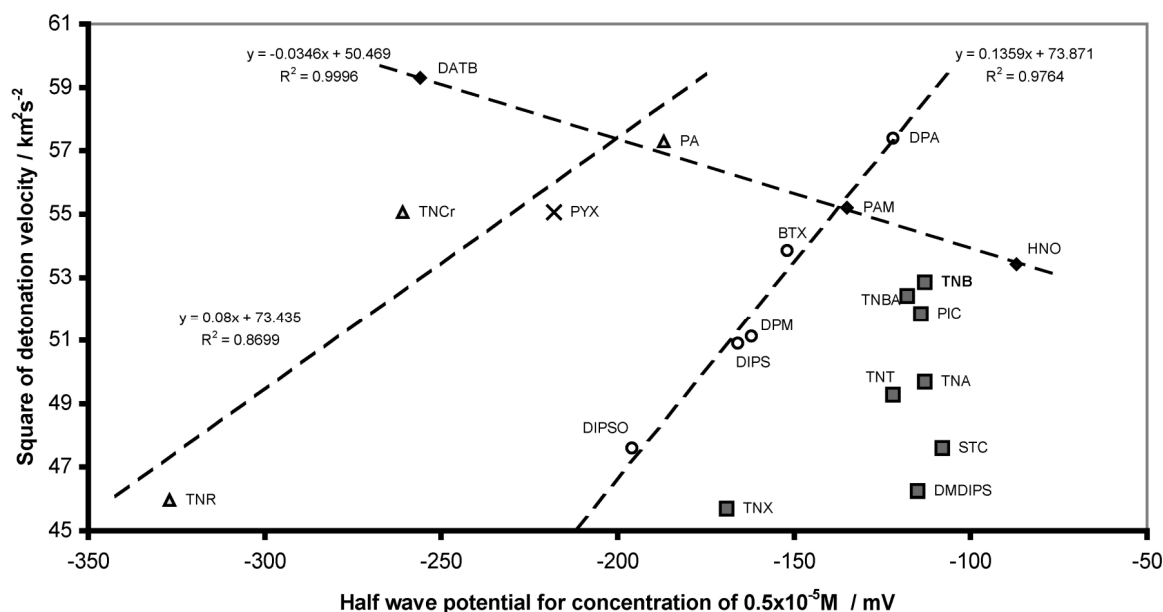


Fig 4. Relationship between half wave potentials of primarily reduced nitro groups in 0.5×10^{-5} M solution and the square of detonation velocity

The dependences in Figs 1, 3 and 4 show a certain similarity of the effects of methyl and chlorine substituents in TNB molecule on the electrochemical reactivity of the resulting derivative. The same similarity also exists in thermal reactivity of polychloro and polymethyl derivatives of TNB [15,16].

The meaning of relationships of the type shown in Figs 3 and 4 can be interpreted as follows: generally, the square of detonation velocity, D^2 , and explosion heat, Q , in the Chapman–Jouget plane are interrelated by definiendum [17, 18]:

$$Q = D^2 \cdot \{2 \cdot (\gamma^2 + 1)\}^{-1} \quad (1)$$

where γ is the polytropy coefficient whose value for high explosives ranges from 2.79 to 3.48 [17]. This means that the relationships in the above-mentioned figures can be expressed as:

$$Q = C_1 \pm a \cdot E_{1/2} \quad (2)$$

which is another form of modified Evans–Polanyi–Semenov equation (E-P-S)

$$E = C \pm \alpha \cdot Q \quad (3)$$

valid for energetic materials [19-25]. In this case the energy, E , can be the activation energy of thermal decomposition [19-21, 23], the slope $E \cdot R^{-1}$ of the Kissinger relationship (in the differential thermal analysis) [24], the energy of electric spark [23] or the charge at nitrogen atom of the most reactive nitro group in the molecule [25]. The last form of E-P-S given above is also physically closest to Eq. (2).

4. CONCLUSIONS

The electrochemical reduction in aqueous medium (the concentration of solution below 10^{-4} M) at pH 7 should primarily attack the same nitro groups as those that react first during initiation of these substances. The values of resulting half-wave potentials, $E_{1/2}$, markedly depend *inter alia* on the solvation of the polynitro compounds studied. It is possible to find logical linear dependences between the $E_{1/2}$ values and squares of detonation velocities of polynitro arenes. These relationships are another form of modified Evans–Polanyi–Semenov equation for energetic materials. The strong dependence of $E_{1/2}$ values on the conditions and way of carrying out the polarographic measurements, along with the very limited solubility of the polynitro compounds studied in media containing water, considerably restrict the application of polarography to studies of chemical micro-mechanism of initiation of organic energetic materials.

REFERENCES

- [1] S. ZEMAN IN: P. POLITZER AND J. S. MURRAY (EDS.): *Energetic Materials, Part 2*, Elsevier B. V., pp. 25-52, 2003
- [2] A. J. FRY, IN S. PATAI (ED.): *Chemistry of Amino, Nitroso and Nitrocompounds and their Derivatives*, Wiley, Chichester, pp. 319-337, 1982
- [3] J. BAREK, M. PUMERA, A. MUCK, M. KADERÁBKOVÁ AND J. ZIMA: *Anal. Chim. Acta* 393, 141, 1999
- [4] S. ZEMAN, V. MLYNÁRIK, I. GOLJER AND M. DIMUN: CS Patent 232 322, Oct. 30th, 1986
- [5] A. LYČKA, V. MACHÁČEK AND J. JIRMAN: *Coll. Czech. Chem. Commun.*, 52, 2946, 1987
- [6] YU. YA. MAKSIMOV AND E. N. KOGUT: *Tr. Mosk. Khim.-Tekhnol. Inst. Mendeleeva*, 104, 30, 1979
- [7] V. G. MATVEEV, V. V. DUBIKHIN AND G. M. NAZIN: *Izv. Akad. Nauk SSSR, Ser. Khim.*, 474, 1978
- [8] G. B. MANELIS, G. M. NAZIN, YU. I. RUBTSOV AND V. A. STRUNIN: *Termicheskoe razlozhenie i gorenije vzryvchatykh veschestv i porokhov (Thermal Decomposition and Combustion of Explosives and Powders)*. Izdat. Nauka, Moscow, 1996
- [9] S. ZEMAN AND M. KRUPKA: *Propellants, Explos., Pyrotech.*, 28, 249, 2003
- [10] M. J. KAMLET AND S. J. JACOBS: *J. Chem. Phys.*, 48, 23, 1968
- [11] S. ZEMAN: *Thermochim. Acta*, 41, 199, 1980
- [12] J. BAREK AND I. ŠVAGROVÁ: *Chem. listy* 84, 1042, 1990
- [13] M. FIELDS, C. VALLE, JR., AND M. KANE: *J. Am. Chem. Soc.* 71, 421, 1949
- [14] P. ZUMAN: *Organická polarografie (Organic Polarography)*, SNTL Praha, 1966
- [15] S. ZEMAN: *Thermochim. Acta* 31, 269, 1979
- [16] S. ZEMAN: *J. Thermal Anal.* 17, 19, 1979
- [17] D. PRICE: *Chem. Revs.*, 59, 801, 1959
- [18] P.-A. PERSSON, R. HOLMBERG AND J. LEE: *Rock Blasting and Explosives Engineering*. CRC Press, Boca Raton, 1994
- [19] S. ZEMAN, M. DIMUN AND Š. TRUCHLIK: *Thermochim. Acta*, 78, 181, 1984
- [20] S. ZEMAN, M. DIMUN, Š. TRUCHLIK AND V. KABÁTOVÁ: *Thermochim. Acta*, 80, 137, 1984
- [21] S. ZEMAN, M. DIMUN, V. KABÁTOVÁ AND Š. TRUCHLIK: *Thermochim. Acta*, 81, 359, 1984
- [22] S. ZEMAN: *J. Energ. Mater.*, 17, 305, 1999
- [23] S. ZEMAN: *Thermochim. Acta*, 384, 137, 2002
- [24] S. ZEMAN, P. KOHLÍČEK AND M. MARANDA: *Thermochim. Acta*, 398, 185, 2003
- [25] S. ZEMAN, R. HUCZALA AND Z. FRIEDL: *J. Energet. Mater.*, 20, 53, 2002
- [26] R. MEYER, J. KÖHLER, A. HOMBURG: *Explosives*, Fifth Ed., Wiley-VCH, Weinheim, 2002

IN SITU MEASUREMENT OF VELOCITY OF DETONATION AND COMPARISON OF HEAVY ANFO PRODUCED IN THE FIELD OF USAGE AND CARTRIDGE EXPLOSIVES

S. Žganec*, E. Zvonimir** and M. Dobrilović**

* Minervo Ltd, Ljubljana, Slovenia

** Faculty of Mining, Geology and Petroleum Engineering,
University of Zagreb, Croatia

Abstract:

This paper describes methods of measuring the velocity of detonation in bore holes loaded with different types of bulk explosive, such as heavy ANFO and cartridge explosives. The explosives are produced at the point of use with mobile equipment. The measurements of the velocity of detonation (VOD) involved bore holes with different diameters. On this basis the interdependence of the VOD and the bore-hole diameter was determined. The VOD measurements, with different blasting parameters, can be used for the selection of the best explosives to be produced at the site, taking into account the geological characteristics of the blasting rock.

Keywords: VOD, measurement, explosives

1. INTRODUCTION

A study of the characteristics of heavy ANFO and cartridge-powder explosives under real conditions was undertaken at the Črni Kal quarry. The explosives were made at the point of use by a mobile unit from the Minervo company. The explosives' velocity of detonation was measured using the continuous method and a Mrel Minitrap instrument.

The mobile unit for the production of explosives at the point of use can make different sorts of explosives, depending on the requirements, with different individual components included in the final explosive product. The explosive products vary from ANFO, reinforced ANFO (reinforced with up to 30% emulsion), emulsion explosive with 70% emulsion, to pure emulsion explosive.

The advantage of this method is in the way the material is transported to the point of use (quarry, road, railway, etc): no explosives are transported, only the individual unexplosive components. Defining the correct proportions of the individual components is crucial when blasting walls with different geological characteristics that require different types of engineering work. MINERVO d.d. Ljubljana is the first company using a mobile unit for the production of such types of explosive in Slovenia as well as in Central Europe.

2. THE USE OF DIFFERENT EXPLOSIVES

2.1 Ammonium-nitrate explosives

Ammonium-nitrate explosives are mixtures of ammonium nitrate (oxidant) and carriers of carbon that can burn. In the past, different fuels were used, such as sawdust, oils, coal dust, etc. Sensitizers, such as TNT, were added to them, and sometimes aluminium powder was also added to increase the power. A detonator (cap-sensitive) is normally sufficient to fire these mixtures. Some of these explosives, also called powder explosives, are less sensitive (non-cap-sensitive) and require a stronger initial charge (booster). Powder explosives are made into charges and, due to their sensitivity, special security measures must be taken during their transport and storage. Because they are not water-resistant, problems can occur during the blasting process. However, their water-resistance can be improved a little by adding hydrophobic substances (e.g. calcium stearin).

2.2 ANFO and reinforced-ANFO explosives

ANFO explosives are a mixture of 94-94.5% ammonium nitrate and 5.5-6% diesel oil. Since the 1970s they have been used on a large scale for surface excavating, in quarries, and for other excavating work. The advantages of these explosives are their ease of use, the possibility to prepare them at the point of use and the fact that they can be machine loaded into bore holes. ANFO explosives can be made into charges of different diameters and weights, but they are rarely used in this form because it would not be economic. More often these explosives are used in bags of 25-30 kg, but the most common and economic method of use is the machine, pneumatic mode using a spiral-containing homogeniser. The advantages of this method are lower energy costs, safety at work, machine loading of bore holes and the complete filling of the bore holes resulting in a larger force. The complete filling of bore holes reduces the need for other means of initiation, as well as sparing the whole working area. Reinforced-ANFO explosives can be reinforced with various supplements, the most common being emulsion explosives in various proportions.

2.3 Emulsion explosives

Emulsion explosives are the most modern commercial explosives. They are, in effect, a reversed version of slurry explosives. In the case of slurry explosives the fuel is dispersed in a water solution of ammonium nitrate, while in the case of emulsion explosives small drops of water solution of ammonium nitrate are dispersed in the fuel. Either a saturated solution or a cooled liquid of ammonium nitrate can be used. The fuel is usually diesel oil, but it can also be mineral oil, wax, etc. The fuel has a large contact surface with the oxidant (ammonium nitrate). In contrast to other explosives, emulsion explosives do not need high-explosive sensitizers for their detonation. Micro gas bubbles are added to the emulsion. The ignition of the initiating explosive causes the compression of the gas bubbles and a high temperature, which leads to the explosion of the emulsion. The density of the emulsion can be regulated with the quantity of added gas bubbles. The force of the explosion can be regulated with the quantity and type of fuel used. The drops of ammonium nitrate are completely surrounded with the fuel and for this reason the emulsion is water-resistant. In terms of handling and storing, emulsion explosives are very safe because they need a strong initiating explosion to detonate them. They can be used in the temperature range between -20° and +35°C. Emulsion explosives can be directly loaded into the bore holes, made into charges of different dimensions, or mixed with ANFO explosive.

3. GEOLOGICAL CHARACTERISTICS OF THE ČRNI KAL QUARRY

The geology of the Črni Kal quarry is relatively simple. The flysch base, covered with alveous and nummulitic limestone, mainly consists of gray-red, or yellow-red, partly limonitized marl, marly clay, and only occasionally sandstone. The contact is folded, and this folding is a consequence of the tectonic mixing of the old Paleocene limestone with the younger, upper Eocene flysch. The alveous and nummulitic limestone covering the flysch is dense, hard, pure and contains a lot of fossil remains. Petrographic analyses have shown that the limestone aggregates contain no bad grains: the limestone is pure and contains less than 1% dolomite. Crevices are found on the surface, and they are mainly parallel. The crevices usually run from north-west to south-east. The surface is of a typical Karst structure showing various Karst characteristics. No source of water is to be found in the quarry area.

4. COMPARISON OF POWDER-EXPLOSIVE CHARGES AND HEAVY ANFO EXPLOSIVES

4.1 Parameters for blasting with powder- explosives charges-amonal

The parameters of boring and blasting (the number of bore holes, the angle of boring, the space between the bore holes, the line of least resistance) for blasting with the charges explosive amonal are as follows:

line of least resistance (w)	3,8 m
space between the bore holes (a)	3,5 m
diameter of a bore hole	76 mm
length of the tap of a vertical bore hole	3.3 m
length of the tap of a horizontal bore hole	2.2 m
height of a level	17.5 m
angle of boring	75°
number of bore holes (n)	38
length of vertical bore holes (v)	17 m
length of horizontal bore holes (dh)	4,5 m
length of all bore holes	817 m
volume of excavated wall (v)	8620 m ³
specific use of explosive /m ³	0.277kg/m ³
effect of a bore hole meter	10,55 m ³ /m
loading per meter of a vertical bore hole	3,29 kg
total amount for vertical bore holes:	2128 kg
horizontal bore holes :	38 x 7 kg of amonal =266 kg
total amount :	2394 kg

4.2 Parameters for blasting with heavy ANFO explosives

The parameters of boring and blasting (the number of bore holes, the angle of boring, the space between the bore holes, the line of least resistance) for blasting with the heavy ANFO explosive are as follows:

line of least resistance (w)	3,8 m
space between the bore holes (a)	3,5 m
diameter of a bore hole	76 mm
length of the tap of a vertical bore hole	3.3 m
length of the tap of a horizontal bore hole	2.2 m
height of a level	17.5 m
angle of boring	75°
number of bore holes (n)	38
length of vertical bore holes (v)	17 m
length of horizontal bore holes (dh)	4,5 m
length of all bore holes	817 m
volume of excavated wall (v)	8620 m ³
specific use of explosive m ³	0.299 kg/m ³
effect of a bore hole meter	10,55 m ³ /m
loading per meter of a vertical bore hole	3,47 kg
total amount for vertical bore holes:	2128 kg
horizontal bore holes :	304 kg of heavy ANFO and 38 x 1 kg of amonal = 342 kg
total amount :	2584 kg

4.3 Used explosives and parameters:

The overall amount of explosive used for blasting with the explosive charges amonal – was 2394 kg, while the amount used for blasting with the heavy ANFO explosive was 2584 kg, consisting of 2546 kg of heavy ANFO and 38 kg of amonal.

The amount of explosive required for blasting with the heavy ANFO increases by 7,9 % if we take into account the use per bore-hole meter.

In both cases the blasting was successful.

5. IN-SITU MEASUREMENTS OF THE VELOCITY OF DETONATION (VOD) WITH THE MREL INSTRUMENT

5.1 Testing of explosives in blastholes

- Measure the continuous VOD in any hole diameter, wet or dry holes, and in any type of rock.
- Measure the continuous VOD in multiple holes per blast.
- Determine whether full detonation, low order detonation or failure occurred, and where in the explosive column it happened.
- Check VOD against manufacturer's specifications in full scale blasting environments.

- Determine the minimum booster size for any explosive by measuring run-up velocities in full scale blasting environments.
- Measure the timing accuracy of detonators in full scale blasting environments.
- Measure the effects of water, drill cuttings, and rocks, etc. trapped within the explosive mass.
- Determine the length of explosive column to use in decking operations to evaluate the effect of stemming and drill cutting dilution, water pick-up, etc. on the explosive run-up requirements.
- Determine the correct length and type of stemming material to be used between decks of explosives to prevent sympathetic detonation of explosive desensitization from occurring.

5.2 Results of measurements

5.2.1. Comparison of blasting with charges explosive amonal and heavy ANFO explosives.

Measurements of the detonation velocity of powder- explosives charges-amonal

The results of the measurements of the detonation velocity of charges explosives amonal are shown in figure 1.

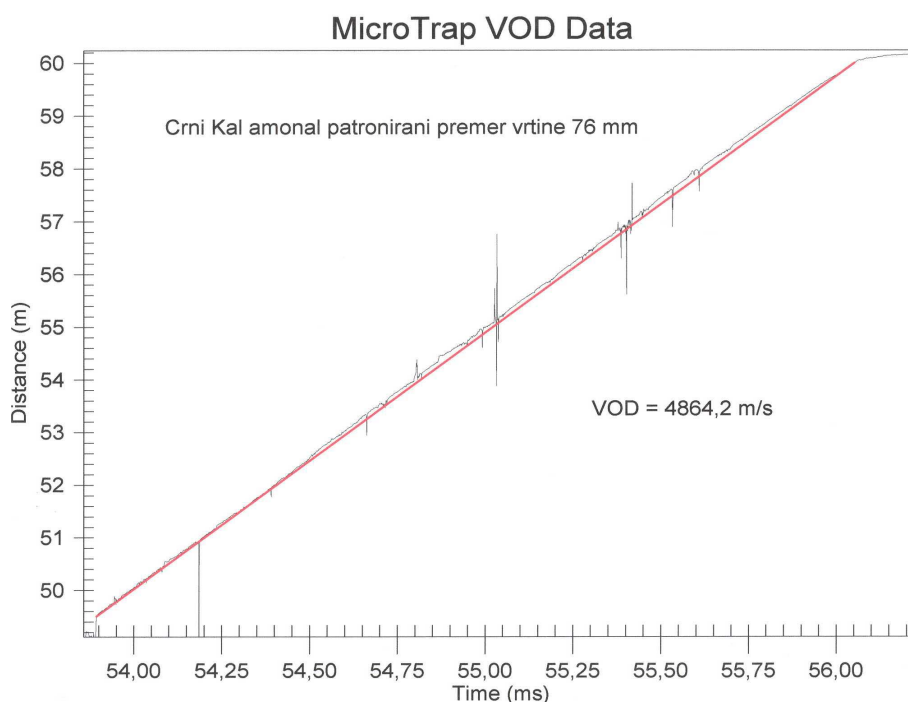


Fig 1. VOD powder- explosives charges-amonal

Measurements of the detonation velocity of heavy ANFO explosives

The results of the measurements of the detonation velocity of heavy ANFO explosives are shown in figure 2.

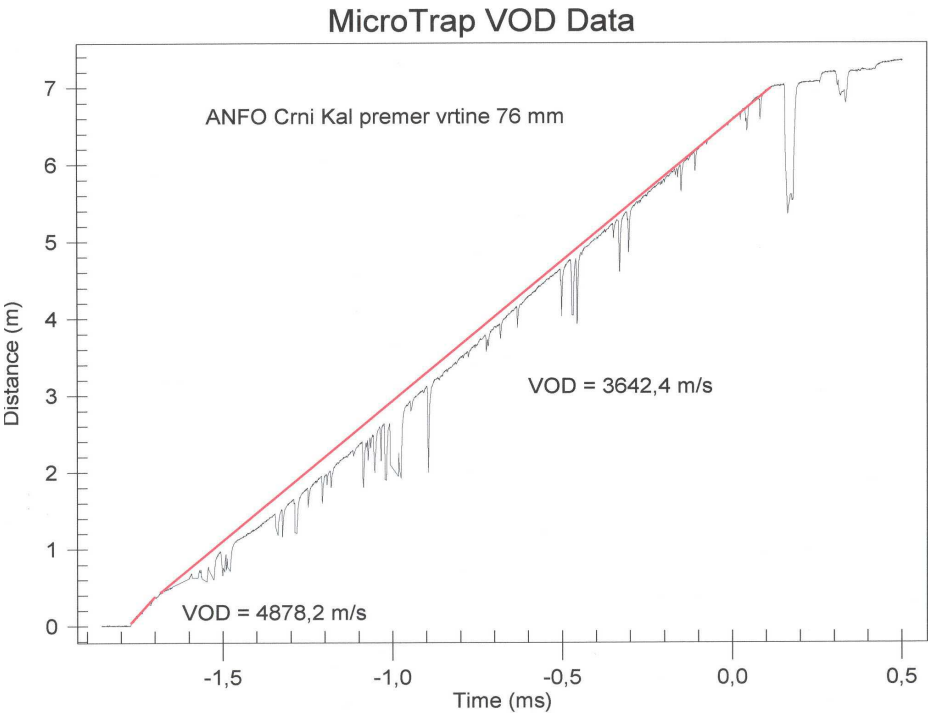


Fig 2. VOD heavy anfo, 10 %emulsion

6. THE MEASUREMENTS OF THE SEISMIC EFFECTS OF BLASTING

Seismic measurements were carried out with the Nomis Seismographs instrument. The measuring location was about 400 m from the blasting point. The measuring location was at the quarry shelter. The results of the measurements relating to the ANFO and heavy explosives are shown in table 1.

Table 1. Results of the measurements

measur. no.	hole depth [m]	explos. charge [kg]	steaming [m]	akustic. comp [dB]	radial comp. [mm/s]	vertical. comp. [mm/s]	transver. comp. [mm/s]	vector sum [mm/s]
1	17,0	56	3,3	117	3,17	2,28	1,77	3,67
2	17,0	59	3,3	116	2,15	0,63	2,66	3,35

7. CONCLUSIONS

In the Črni Kal limestone quarry, various types of explosives were used: plastic, gelignite and powder explosives. As both the explosives and the techniques for their use have developed, so have the modes and parameters of blasting, which means that today explosives that can be made at the point of use represent a significant improvement with regard to safety at work and economics. The mobile unit can make different types of explosives with different individual components included in the final explosive products. These products vary from ANFO, reinforced ANFO (reinforced with up to 30% emulsion), emulsion explosive with 70% emulsion, to pure emulsion explosive. Monitoring the parameters of boring and blasting, the handling of excavated wall mass from loading to crushing, and the measurements of detonation velocity for different explosives enabled us to define the optimum parameters and the most efficient type of explosive. The measurement results of the detonation velocity confirmed that we had selected the most appropriate explosive. In addition, these measurements also enabled us to control the characteristics and the quality of the explosives made at the point of use. From the result of measurements VOD it is found out that the use of heavy ANFO in blast holes under 76 mm is not recommended.

The results of measuring the seismic effects of the blasting proved that seismic effects on the sites remained within the strictest standards and criteria. All the above-mentioned facts and results enabled us to conclude that the use of heavy ANFO explosives is the best solution for the boring and blasting work carried out in the Črni Kal quarry.

REFERENCES

- [1] Design: Minervo Ljubljana: Rudarski projekt za izvajanje del pri izkoriščanju mineralnih surovin in sanaciji kamnoloma , 95, 2002
- [2] Design: Podjetje za vrtanje in miniranje, Ljubljana: Elaborat vrtanje in miniranja, 25, 1995
- [3] Design: Minervo Ljubljana, Priprava razstrelilnih mešanic na mestu uporabe z mobilno enoto "Minervo EC004 3 T", 74, 2000
- [4] Desing: MREL group of Companies, VOD Operations Manual, 72, Canada, 2000
- [5] ESTER Z., VRKLJAN D., DEKOVIĆ Z.: Usporedba učinka miniranja emulzijskih i ANFO, 5/2000
- [6] Eksploziva u laboratoriju i "in situ", 20-22 , Mineral Zaagreb
- [7] KRSNIK J.: Miniranje, Rudarsko-geološko naftni fakultet Zagreb, 187, 1989
- [8] ŽGANEC S., DOBRILLOVIĆ M., ESTER Z.: Drilling and blasting works on a highway construction on the edge of a rock-wall, 2nd World Conference on Explosives & Blasting Technique, Prague, 503-508, 2003